

2015 International Conference on Alternative Energy
in Developing Countries and Emerging Economies
(2015 AEDCEE)

Research Center in Energy and Environment
Thaksin University (Phatthalung Campus)
222 Moo 2, Ban Prao, Pa Payom, Phatthalung, Thailand, 93210



2015 International Conference on Alternative Energy in Developing Countries and Emerging Economies (2015 AEDCEE)

May 28-29, 2015
Sheraton Grande Sukhumvit Hotel
Bangkok, Thailand

- Co-Organized by
- Research and Development Institute, Thaksin University, THAILAND
 - Universite de Moncton, CANADA
 - University of Maryland, USA
 - James Cook University, AUSTRALIA
 - Faculty of Science, Thaksin University, THAILAND
 - Research Center in Energy and Environment, Thaksin University, THAILAND

2015 AEDCEE
2015 International Conference on
Alternative Energy in Developing Countries
and Emerging Economies

May 28-29, 2015
Sheraton Grande Sukhumvit Hotel
Bangkok, Thailand

Research Center in Energy and Environment
Thaksin University (Phatthalung Campus)
222 Moo 2, Ban Prao, Pa Payom, Phatthalung, Thailand 93210

Message from the President of Thaksin University

Welcome to the *Land of Smiles!*

On behalf of Thaksin University, it is an honor, and a pleasure, to welcome all participants to the 2015 International Conference on Alternative Energy in Developing Countries and Emerging Economies.

With climate change concerns growing throughout the world, this third edition of the AEDCEE Conference is more timely than ever. Humanity is rapidly realizing that we collectively need to find and adopt new patterns of energy production and consumption, new methods of transportation, and different types of land use and waste management to reduce our impacts on the environment and to mitigate the risks of climate change.

The 2015 AEDCEE Conference will bring together leaders in the alternative energy industry, academic experts, research sectors and governments to meet, interact, exchange ideas and discuss the state of the art of advanced technology, research and development related to alternative energy sources. Solutions will also be offered in order to respond to the growing demand from developing countries who aspire to achieve environmentally sustainable economic growth.

I join the leadership of the Research and Development Institute, the Faculty of Science, and the Research Center in Energy and Environment of Thaksin University to express our gratitude to our official sponsors, our international institutional partners and our private sector partners for their contributions to the success of this Conference; without your support, this Conference could not be possible.

It is by working collectively and cooperatively that we will move towards the sustainable development of our nations. I trust this Conference will help to take us closer to our goals of implementing alternative energy sources for developing countries and emerging economies to achieve sustainable development, while contributing to mitigate the risks of climate change.

Cordially,

Associate Professor Dr. Wichai Chumni
President, Thaksin University

Message from Co-Organizer (Université de Moncton)

Energy security is an important determinant in the economic development of jurisdictions and the quality of life of people. Over the past two centuries, countries from the North had the privilege to develop using abundant fossil fuel-based energy and, more recently in the time-scale of humanity, nuclear energy. During this period, carbon emissions were not an issue, and nuclear waste was considered, and is still unfortunately considered in many jurisdictions, a problem that we leave for future generations to solve.

In the context of climate change and growing concerns regarding nuclear energy, developing countries and emerging economies must capitalize on the short- and long-term benefits offered by renewable energy sources. This is an opportunity that must not be missed.

The objective of the AEDCEE Conference series is to offer opportunities to disseminate knowledge, and exchange information and best practices, for an efficient development of alternative energy for countries in the South. The strong response from the academic, industry and government communities is an encouraging sign that alternative energy and renewable energy are viable energy options for a more sustainable future.

Once again, it is an honor to work with Thaksin University in the organization of the 2015 AEDCEE Conference.

As in the first two editions of this series, we wish all participants a good and productive Conference, fruitful discussions and new friendships.

Yves Gagnon P.Eng., D.Sc.
Professor
Université de Moncton, Canada

Message from the Co-Chairs

Following most successful first and second editions in 2011, held in Hat Yai, and 2013, held in Bangkok, we are proud to organize and host the 2015 International Conference on Alternative Energy in Developing Countries and Emerging Economies (2015 AEDCEE), held once again in Bangkok, Thailand.

The 2015 AEDCEE Conference is hosting seasoned authors, from countries in the South and in the North, who contribute scientific and technical high quality papers and posters on the various themes of the Conference. We hope the Conference will serve as a guideline for our endeavor regarding alternative energy development and deployment, and that it will influence public policies and technology developments needed to achieve the sustainable development of nations and to mitigate climate change.

We would like to thank the official sponsors of the Conference, namely the National Research Council of Thailand (NRCT), Provincial Electricity Authority (PEA) of Thailand, Electricity Generating Authority of Thailand (EGAT), and the Energy Regulatory Commission (ERC) of Thailand. We also want to recognize our international institutional partners, Université de Moncton (Canada), University of Maryland (USA) and James Cook University (Australia). Finally, but not the least, we offer our most sincere appreciation to our private sector partners who have provided financial contributions that allow us to maintain relatively low registration fees, and thus achieve greater participations from various countries.

But foremost, the success of a Conference relies mainly on the participants. On behalf of Thaksin University, our sponsors and our partners, we are deeply grateful for your participation in the 2015 AEDCEE Conference, and for presenting your great and outstanding research work.

Thank you and Sawasdee,

Asst. Prof. Dr. Pornpun Khemakunasai
Director, Research and
Development Institute
Thaksin University

Asst. Prof. Dr. Sarapee Chairat
Dean, Faculty of Science
Thaksin University

Asst. Prof. Dr. Jompob Waewsak
Director, Research Center in Energy
and Environment
Thaksin University

Keynote Speakers

1. Prof. Ralph Sims
Massey University, New Zealand
2. Dr. Twarath Sutabutr
Deputy Permanent Secretary of the Ministry of Energy, Thailand
3. Prof. Dr. Michael Borowitzka
Murdoch University, Australia
4. Dr. Jun Zhang
International Finance Corporation, World Bank, U.S.A.
5. Prof. Dr. Roland N. Horne
Stanford University, U.S.A.

International Scientific Committee

1. Prof. Dr. Yves Gagnon, Canada
2. Prof. Dr. Michael Borowitzka, Australia
3. Prof. Dr. M. K. Deshmukh, India
4. Prof. Dr. Yves Gagnon, Canada
5. Prof. Dr. Ashwani K. Gupta, USA
6. Prof. Dr. Roland N. Horne, USA
7. Prof. Dr. Kim Hyung-Taek, Korea
8. Prof. Dr. Jongjit Hirunlabh, Thailand
9. Prof. Dr. Samroeng Jakjai, Thailand
10. Prof. Dr. Surapong Jirattananon, Thailand
11. Prof. Dr. Joseph Khedari, Thailand
12. Prof. Dr. Tanongkiat Kiatsiriroj, Thailand
13. Prof. Dr. Christian Masson, Canada
14. Prof. Dr. Anne S. Meyer, Denmark
15. Prof. Dr. Masatoshi Nakamura, Japan
16. Prof. Dr. Yuji Ohya, Japan
17. Prof. Dr. K. S. Ong, Malaysia
18. Prof. Dr. Sebel Z. Ozdogan, Turkey
19. Prof. Dr. Joachim Peinke, Germany
20. Prof. Dr. Christos Pagageorgiou, Greece
21. Prof. Dr. Somsak Panyakaew, Thailand
22. Prof. Dr. Lazzarin Renato, Italy
23. Prof. Dr. Dato Kamarrusaman Sopian, Malaysia
24. Prof. Dr. Somchart Soponronnarit, Thailand
25. Prof. Dr. Eicker Ursala, Germany
26. Prof. Dr. Liqiu Wang, Hong Kong
27. Prof. Dr. Jianzhong Xu, China
28. Assoc. Prof. Dr. Sumate Chairapat, Thailand
29. Assoc. Prof. Dr. Suppachart Chungpaiboonpatana, Thailand
30. Assoc. Prof. Dr. Serm Janjai, Thailand
31. Assoc. Prof. Dr. Vladimir I. Kouprianov, Thailand
32. Assoc. Prof. Dr. Bundit Limmechokchai, Thailand
33. Assoc. Prof. Dr. Rattanachai Pairin, Thailand
34. Assoc. Prof. Dr. Wattanpong Rakwichian, Thailand
35. Assoc. Prof. Dr. Peerapong Teekasakul, Thailand
36. Assoc. Prof. Dr. Supawan Thirawanichakul, Thailand
37. Assoc. Prof. Dr. Yutthana Thirawanichakul, Thailand
38. Assoc. Prof. Dr. Sirichai Thepa, Thailand
39. Assoc. Prof. Gampol Prateepchaikul, Thailand
40. Assoc. Prof. Dr. Abdul Mutalib Leman, Malaysia

Local Scientific Committee

1. Assoc. Prof. Dr. Kulachate Pianthong, UBU
2. Assoc. Prof. Dr. Bunlung Neammanee, KMUTNB
3. Asst. Prof. Dr. Tika Bunnag, RMUTR
4. Asst. Prof. Dr. Sirinuch Chindaruksa, NU
5. Asst. Prof. Dr. Charoenporn Lertsatitthanakorn, KMUTT
6. Asst. Prof. Dr. Naris Pratinthong, KMUTT
7. Asst. Prof. Dr. Sate Sampattakul, CMU
8. Asst. Prof. Dr. Nirundorn Matan, WU
9. Asst. Prof. Dr. Chuleerat Kongruang, WU
10. Asst. Prof. Dr. Kusumal Chaloemyanon, PSU
11. Asst. Prof. Dr. Warit Jawjit, WU
12. Asst. Prof. Dr. Teerayuth Leewijit, PSU
13. Asst. Prof. Dr. Charongpun Musikavong, PSU
14. Asst. Prof. Dr. Nattapol Poomsa-ad, MSU
15. Asst. Prof. Dr. Nipon Ketjoy, NU
16. Asst. Prof. Dr. Somchai Maneewan, NU
17. Asst. Prof. Dr. Surassawadee Kulboon Korkua, WU
18. Dr. Thanunsak Thepaya, PSU
19. Dr. Pisit Maneechote, NU
20. Dr. Montana Rungsiyopas, BUU
21. Dr. Warit Weerapan, PSU
22. Dr. Watsa Khongnakorn, PSU
23. Dr. Kaokanya Sudaprasert, KMUTT
24. Dr. Withaya Puangsombut, RMUTR
25. Dr. Sarocha Charoenvai, RMUTT
26. Dr. Pakorn Ditthakit, WU
27. Dr. Auttapol Golaka, SCG PLC

Program at a Glance

2015 International Conference on Alternative Energy in Developing Countries and Emerging Economies (2015 AEDCEE) May 28-29, 2015 Sheraton Grande Sukhumvit Hotel, Bangkok, Thailand

Wednesday May 27, 2015

Pre-Conference Workshop "Smart Grid for Renewable Energy Integration" Assoc. Prof. Dr. Ahmad Zahedi James Cook University, Australia	
Asoke II	
08:30-09:00	Registration and Coffee
09:00-12:15	Smart Grid for Renewable Energy Integration I and II
12:15-13:15	International Lunch Buffet: Orchid (Lobby)
13:15-16:30	Smart Grid for Renewable Energy Integration III and IV
16:30-16:45	Closing Ceremony

Thursday May 28, 2015

08:00-08:45	Registration and Coffee
08:45-09:00	Welcome Address and Opening of the 2015 AEDCEE Conference (Grand Ballroom I) Asst. Prof. Dr. Sarapee Chairat, Dean of Faculty of Science, Thaksin University, Thailand Prof. Dr. Yves Gagnon, General Co-Chair, University of Moncton, Canada Assoc. Prof. Dr. Wichai Chumni; President of Thaksin University, Thailand
09:00-09:30	Keynote Address: Prof. Dr. Ralph Sims, Massey University, New Zealand (Grand Ballroom I) "Clean Energies Technology: Mitigation of Climate Change"
09:30-10:00	Keynote Address: Dr. Twarath Sutabutr, Deputy Permanent Secretary of the Ministry of Energy, Thailand (Grand Ballroom I) "Current Status and Development of Alternative Energy in Thailand"
10:00-10:30	Coffee and Tea Break
10:30-12:00	Parallel Technical Sessions
12:00-13:00	International Buffet Lunch: Rossini & Basil (1 st Floor)
13:10-13:40	Keynote Address: Prof. Dr. Michael Borowitzka, Murdoch University, Australia (Grand Ballroom I) "The Sustainable Development of Biofuel"
14:45-15:00	Parallel Technical Sessions
15:00-15:30	Coffee and Tea Break
15:30-16:45	Parallel Technical Sessions
16:45-17:15	Poster Session (Grand Ballroom I)
17:30	Bus Transportation from Sheraton Grande Sukhumvit Hotel to Pier (River City) (Instruction in Participant Bag)
19:00-22:00	Grand Pearl Cruise Dinner

Friday May 29, 2015

08:30-09:00	Registration and Coffee
09:00-10:00	Keynote Address: Dr. Jun Zhang, World Bank, USA (Grand Ballroom I) Plenary Discussion: Prof. Dr. Yves Gagnon, University of Moncton, Canada Plenary Chair: Assoc. Prof. Dr. Ahmad Zahedi, James Cook University, Australia "Financing of Renewable Energy Projects"
10:00-10:30	Coffee and Tea Break
10:30-12:00	Parallel Technical Sessions
12:00-13:00	International Buffet Lunch: Rossini & Basil (1 st Floor)
13:10-13:40	Keynote Address: Prof. Dr. Roland Horne, Stanford University, USA (Grand Ballroom I) "World Outlook of Geothermal Energy"
13:45-15:00	Parallel Technical Sessions
15:00-15:30	Coffee and Tea Break
15:30-16:45	Parallel Technical Sessions
17:00-17:30	Closing Ceremony and Best Paper/Best Poster Awards (Grand Ballroom I)

Saturday May 30, 2015

08:00-15:00	Field Trips
08:30-15:00	8 MW Solar Farm: Loxley PLC, Pracheanburi Province
09:00-13:00	The Grand Palace: Cultural Tour, Bangkok

**2015 International Conference on
Alternative Energy in Developing Countries and Emerging Economies
(2015 AEDCEE) May 28-29, 2015
Sheraton Grande Sukhumvit Hotel, Bangkok, Thailand**

Thursday May 28, 2015

Keynote Sessions

Grand Ballroom I	
09:00-09:30	Keynote Address: Prof. Dr. Ralph Sims, Massey University, New Zealand "Clean Energies Technology: Mitigation of Climate Change"
09:30-10:00	Keynote Address: Dr. Twarath Sutabutr, Deputy Permanent Secretary of the Ministry of Energy, Thailand "Current Status and Development of Alternative Energy in Thailand"
10:00-10:30	Coffee and Tea Break

Parallel Technical Sessions

Grand Ballroom I: Combustion and Gasification Technology Chair: Dr. Auttapol Golaka, SCG, Thailand Co-Chair: Asst. Prof. Dr. Jatuporn Kaew-On, Thaksin University, Thailand			
10:30-10:45	GLOBAL AND PULSED RAINBOW REFRACTOMETRY : TOOLS TO IMPROVE LIQUID FUEL COMBUSTION AS WELL AS TO MASTER CO ₂ CAPTURE BY MEA SPRAYS	S. Saengkaew, J. Promvongsa, L. Estel, M. Ouboukhlik, A. Garo and G. Gréhan	France
10:45-11:00	HYDROTHERMAL CARBONIZATION AND GASIFICATION TECHNOLOGY FOR ELECTRICITY PRODUCTION USING BIOMASS	E. Steurer and G. Ardissonne	Germany
11:00-11:15	STATUS OF USING BIOMASS GASIFICATION FOR HEAT AND POWER IN THAILAND	K. Laohalidanond, P. Chaipayong and S. Kerdsuwan	Thailand
11:15-11:30	MUNICIPAL SOLID WASTE CHARACTERISTICS AND GREEN AND CLEAN ENERGY RECOVERY IN ASIAN MEGACITIES	K. Laohalidanond, P. Chaipayong and S. Kerdsuwan	Thailand
11:30-11:45	EVALUATION OF HYDROTHERMAL TREATMENT OF EMPTY FRUIT BUNCH (EFB) FOR SOLID FUEL AND LIQUID ORGANIC FERTILIZER CO-PRODUCTION	A. Nurdiawati, S. Novianti, I. N. Zaini, B. Nakhshinieva, H. Sumida and K. Yoshikawa	Japan
11:45-12:00	APPROACH OF USING CORN RESIDUES AS ALTERNATIVE ENERGY SOURCE FOR POWER PRODUCTION: A CASE STUDY FOR CORN FROM NORTHERN PLAIN AREA OF THAILAND	K. Laohalidanond, and S. Kerdsuwan	Thailand
12:00-13:00	International Buffet Lunch: Rossini & Basil (1 st Floor)		

Asoke I: Bio-Fuel; Ethanol Production Chair: Asst. Prof. Dr. Wichuda Klawej, Thaksin University, Thailand Co-Chair: Dr. Chutima Kaewpiboon, Thaksin University, Thailand			
10:30-10:45	DIRECT PRODUCTION OF BUTANOL-ETHANOL FROM CANE SUGAR FACTORY WASTEWATER (CSFW) AND CELLULOSIC ETHANOL PILOT PLANT WASTEWATER (CEPW) BY CLOSTRIDIUM BEIJERINCKII CG1	J. Comwien, N. Boonvithaya, W. Chulaluksananukul and C. Glinwong	Thailand
10:45-11:00	OPTIMIZATION AND KINETICS MODELLING OF ETHANOL PRODUCTION FROM OIL PALM JUICE IN BATCH FERMENTATION	T. Srimachai, K. Nuithitikul, S. O-Thong, P. Kongjan and K. Panpong	Thailand
11:00-11:15	UTILIZATION OF OIL PALM EMPTY FRUIT BUNCH HYDROLYSATE FOR ETHANOL PRODUCTION BY BAKER'S YEAST AND LOOG-PANG	S. Duangwang and C. Sangwichien	Thailand
11:15-11:30	THE PRODUCTION ETHANOL FROM REUSE LIQUID STILLAGE	A. Choonut, T. Yunu, N. Pichid and K. Sangkharak	Thailand
11:30-11:45	UTILIZATION OF OIL PALM FROND BIOMASS FOR BIOETHANOL PRODUCTION	S. Kumneadklang, C. Niyasom and S. O-Thong	Thailand
11:45-12:00	BIODIESEL PRODUCTION FROM REFINED PALM OIL USING SUPERCRITICAL ETHYL ACETATE IN MICROREACTOR	N. Sootchiewcharn, P. Reubroycharoen and L. Attanatho	Thailand
12:00-13:00	International Buffet Lunch: Rossini & Basil (1 st Floor)		

Thursday May 28, 2015 (cont.)

Parallel Technical Sessions (cont.)

Asoke II: Hydrogen and Fuel Cell Chair: Asst. Prof. Dr. Sompong O-Thong, Thaksin University, Thailand Co-Chair: Asst. Prof. Dr. Chontisa Sukkasem, Thaksin University, Thailand			
10:30-10:45	HYDROGEN PRODUCTION FROM DRY-REFORMING OF BIOGAS OVER Pt/Mg _{1-x} Ni _x O CATALYSTS	F. J. Al-Doghachi, Z. Zainal, M. I. Saiman and Y. H. Taufiq-Yap	Malaysia
10:45-11:00	MODIFICATION OF GREEN CALCIUM OXIDE AND CHARACTERISTICS OF CLEAN ENERGY CATALYSTS	W. Wisajorn, P. Praserthdam, S. Assabumrungrat and S. Soisuwan	Thailand
11:00-11:15	SIMULTANEOUS TREATMENT OF NITROGEN-RICH WASTEWATER AND ELECTRICITY GENERATION USING SINGLE-CHAMBER MICROBIAL FUEL CELLS	V. Sawasdee and N. Pisutpaisal	Thailand
11:15-11:30	INFLUENCE OF INOCULUM PRETREATMENT ON PERFORMANCE OF AIR-CATHODE SINGLE-CHAMBER MFC	P. Tanikkul and N. Pisutpaisal	Thailand
11:30-11:45	EFFECT OF NITROGEN CONCENTRATION ON PERFORMANCE OF SINGLE-CHAMBER MICROBIAL FUEL CELLS	V. Sawasdee and N. Pisutpaisal	Thailand
11:45-12:00	PERFORMANCE OF MEMBRANE-LESS AIR-CATHODE SCMFC IN ELECTRICITY GENERATION FROM DISTILLERY WASTEWATER	P. Tanikkul and N. Pisutpaisal	Thailand
12:00-13:00	International Buffet Lunch: Rossini & Basil (1 st Floor)		

Board Room I: Solar Energy, Dry Sensitized, Solar Cell and Solar-PV Chair: Prof. Dr. R.H.B. Exell, KMUTT, Thailand Co-Chair: Dr. Chontira Saengsubun, Thaksin University, Thailand			
10:30-10:45	POTENTIAL OF SOLAR ENERGY UTILIZATION FOR PROCESS HEATING IN PAPER INDUSTRY IN INDIA : A PRELIMINARY ASSESSMENT	A. K. Sharma, C. Sharma, S. C. Mullick and T. C. Kandpal	India
10:45-11:00	CHLOROPHYLL PIGMENTS AS NATURE BASED DYE FOR DYE-SENSITIZED SOLAR CELL (DSSC)	R. Syafinar, N. Gomesh, M. Irwanto, M. Fraeq, Y.M. Irwan and U. Hashim	Malaysia
11:00-11:15	POTENTIAL OF PURPLE CABBAGE, COFFEE, BLUEBERRY AND TURMERIC AS NATURE BASED DYES FOR DYE SENSITIZED SOLAR CELL (DSSC)	R. Syafinar, N. Gomesh, M. Irwanto, M. Fraeq, Y.M. Irwan and U. Hashim	Malaysia
11:15-11:30	OPTIMAL PHOTOVOLTAIC RESOURCES HARVESTING IN GRID-CONNECTED RESIDENTIAL ROOFTOPS AND IN COMMERCIAL BUILDINGS AND FEED-IN TARIFFS: CASES OF THAILAND	P. Peerapong and B. Limmeechokchai	Thailand
11:30-11:45	SOLAR ROOFTOP INSTALLATION IN THAILAND - A STUDY ON VARIOUS SCENARIOS DISPLAYING POTENTIALS AND LIMITATIONS OF PV SOLAR ROOFTOP INSTALLATION AS A CASE STUDY FOR PATHUM THANI PROVINCE	T. Kullack and S. Chungpaibulpatana	Thailand
11:45-12:00	SIMULATION OF SOLAR AIR CONDITIONING SYSTEM WITH SALINITY GRADIENT SOLAR POND	S. Kanan, J. Dewsbury and G. Lane-Serff	UK
12:00-13:00	International Buffet Lunch: Rossini & Basil (1 st Floor)		

Board Room II: Building Technology Chair: Prof. Dr. Yves Gagnon, University of Moncton, Canada Co-Chair: Dr. Wanphut Se-Chua, KMUTT, Thailand			
10:30-10:45	SYNTHESIS OF NANO-WO ₃ PARTICLES WITH PEG FOR CHROMIC FILM	A. Tasaso and P. Ngaotrakanwivat	Thailand
10:45-11:00	CFD ANALYSIS ON THERMAL COMFORT AND ENERGY CONSUMPTION EFFECTED BY PARTITIONS IN AIR-CONDITIONED BUILDING	P. Aryal and T. Leephakpreeda	Thailand
11:00-11:15	EFFECTS OF AIR SPACE THICKNESS WITHIN THE EXTERNAL WALLS ON DYNAMIC THERMAL BEHAVIOUR OF BUILDING ENVELOPES FOR ENERGY EFFICIENT BUILDING CONSTRUCTION	S. Shaik and A. B. T. Puttaranga Setty	India
11:15-11:30	SUITABLE OPERATING CONDITIONS OF HOT WATER GENERATORS COMBINED WITH CENTRAL AIR PACKAGE UNITS: A CASE STUDY OF TIPCO BUILDING GROUP	C. Jindapeng	Thailand
11:30-11:45	PERFORMANCE ASSESSMENT OF DEDICATED OUTDOOR AIR SYSTEMS FOR OFFICE BUILDING IN THAILAND	N. Inklab, P. Chaiwiwatworakul, S. Chuangchote, P. Rakkwamsuk R. Himmler and S. Chirarattananon	Thailand
11:45-12:00	THERMAL PERFORMANCE ASSESSMENT OF A DOUBLE-PANE WINDOW WITH HORIZONTAL SLATS IN THAILAND	V. Mettanant and P. Chaiwiwatworakul	Thailand
12:00-13:00	International Buffet Lunch: Rossini & Basil (1 st Floor)		

Thursday May 28, 2015 (cont.)

Keynote Session

Grand Ballroom I	
13:10-13:40	Keynote Address: Prof. Dr. Michael Borowitzka, Murdoch University, Australia "The Sustainable Development of Biofuel"

Parallel Technical Sessions

Grand Ballroom I: Bio-Fuel; Biogas Chair: Asst. Prof. Dr. Wichuda Klawej, Thaksin University, Thailand Co-Chair: Dr. Chutima Kaewpiboon, Thaksin University, Thailand			
13:45-14:00	COMPARATIVE PERFORMANCE OF HALOTHIOBACILLUS NEAPOLITANUS AND PARACOCCLUS PANTOTROPHUS IN SULFUR OXIDATION	N. Vikromvarasiri and N. Pisutpaisal	Thailand
14:00-14:15	Ni-Mg-Al HYDROTALCITE FOR IMPROVEMENT OF DARK FERMENTATIVE HYDROGEN PRODUCTION	D. T. H. Le and R. Nitisoravut	Thailand
14:15-14:30	DILUTE ACID PRETREATMENT AT HIGH TEMPERATURE OF OIL PALM TRUNK BIOMASS FOR ENZYMATIC HYDROLYSIS	P. Noparata, P. Prasertsanb, S. O-Thong and X. Pan	Thailand UK
14:30-14:45	EFFECT OF SUBSTRATE AND INTERMEDIATE COMPOUND ON FOAMING IN PALM OIL MILL EFFLUENT (POME) DIGESTION SYSTEM	N. Wongfhad, P. Kongjan and S. O-Thong	Thailand
15:00-15:30	Coffee and Tea Break		

Asoke I: Bio Fuel; Biodiesel Chair: Asst. Prof. Dr. Chontisa Sukkasem, Thaksin University, Thailand Co-Chair: Asst. Prof. Dr. Sompong O-Thong, Thaksin University, Thailand			
13:45-14:00	EFFECTS OF BIOGLYCEROL BASED ADDITIVES ON DIESEL FUEL PROPERTY, ENGINE PERFORMANCE AND EMISSION QUALITY : A REVIEW	P. Mukhopadhyay and R. Chakraborty	India
14:00-14:15	PREPARATION VEGETABLE OIL AS BIODIESEL FEEDSTOCK VIA HETEROGENEOUS CATALYST RE-ESTERIFICATION	S. Jansri	Thailand
14:15-14:30	BIODIESEL PRODUCTION USING LIPASE FROM OIL PALM FRUIT AS A CATALYZT	P. kimtun, O. Choonut, T. Yunu, N. Paichid, S. Klomkloa and K. Sangkharak	Thailand
14:30-14:45	SUFFICIENT ECONOMY FOR ENERGY SECURITY IN WIANG SA JATROPHA COMMUNITY, THAILAND	J. Mungkalasiri, P. Boonkum, R. Wisarnsuwannakorn and W. Thanungkano	Thailand
14:45-15:00	THE DEVELOPMENT OF BIODIESEL PILOT PLANT FOR TEACHING AND LEARNING, RESEARCH, CONSULTATION OF RENEWABLE ENERGY - BIO FUEL	A. M. Leman, I. Baba, W. Sani, M. N. M. Salleh and A. Khalid	Malaysia
15:00-15:30	Coffee and Tea Break		

Thursday May 28, 2015 (cont.)

Parallel Technical Sessions (cont.)

Asoke II: Solar Thermal/PV Technology Chair: Assoc. Prof. Dr. Ahmad Zahedi, James Cook University, Australia Co-Chair: Asst. Prof. Dr. Jompob Waewsak, Thaksin University, Thailand			
13:45-14:00	IDENTIFYING OPTIMAL COMBINATIONS OF DESIGN DNI, SOLAR MULTIPLE AND STORAGE HOURS FOR PARABOLIC TROUGH POWER PLANTS FOR NICHE LOCATIONS IN INDIA	C. Sharma, A. K. Sharma, S. C. Mullick and T. C. Kandpal	India
14:00-14:15	INDOOR TEST PERFORMANCE OF PV PANEL THROUGH WATER COOLING METHOD	Y.M. Irwan, W.Z. Leow, M. Irwanto, Fareq, M, A. R. Amelia, N. Gomeh and I. Safwati	Malaysia
14:15-14:30	PARALLEL FULL CIRCUIT TECHNIQUE FOR POWER CAPACITY OF PHOTOVOLTAIC INVERTER WITHOUT TRANSFORMER	M. Zhafarina, M. Irwanto, A. H. Haziah, M. Fareq, N. Gomeh and Y. M. Irwan	Malaysia
14:30-14:45	STAND-ALONE PHOTOVOLTAIC (SAPV) SYSTEM ASSESSMENT USING PVSYS SOFTWARE	Y.M. Irwan, A.R. Amelia, M. Irwanto, M. Fareq, W.Z. Leow, N. Gomeh and S. Ibrahim	Malaysia
14:45-15:00	ANALYSIS OF FLAT REFLECTOR AS SECONDARY OPTIC FOR FRESNEL LENS FOR ENHANCEMENT OF OPTICAL EFFICIENCY OF CONCENTRATING PHOTOVOLTAICS	N. Patanasemakul, P. Rakkwamsuk, S. Chuangchote, R. Songprakorp and K. Kirtikara	Thailand
15:00-15:30	Coffee and Tea Break		

Board Room I: Energy Policy and Economics Chair: Prof. Dr. Yves Gagnon, University of Moncton, Canada Co-Chair: Dr. Wanphut Se-Chua, KMITL, Thailand			
13:45-14:00	DOES THE USE OF SOLAR AND WIND ENERGY INCREASE RETAIL PRICES IN EUROPE? EVIDENCE FROM EU-27	G. S. Sisodia, I. Soares, P. Ferreira, S. Banerji, D. V. den Poel and M. Kumar	India Belgium Portugal
14:00-14:15	THE STATUS OF ENERGY PRICE MODELLING AND ITS RELEVANCE TO MARKETING IN EMERGING ECONOMIES	G. S. Sisodia, I. Soares, S. Banerji, D. V. den Poel and M. Sahay	India Belgium Portugal
14:15-14:30	AN INVESTIGATION INTO THE CRUDE OIL PRICE PASS-THROUGH TO THE MACROECONOMIC ACTIVITIES OF MALAYSIA	F. Alom	Malaysia
14:30-14:45	ASSESSMENT OF FEED-IN TARIFF POLICY IN THAILAND : IMPACTS ON NATIONAL ELECTRICITY PRICES	P. Pita, B. Limmeechockchai, W. Tia, P. Suktornisiri and P. Limpitpanich	Thailand
14:45-15:00	ROADMAP TO THAILAND'S NATIONALLY APPROPRIATE MITIGATION ACTIONS (NAMAS) 2020: ENERGY SECURITY AND CO-BENEFIT ASPECTS	P. Misila, B. Limmeechockchai and P. Winyuchakrit	Thailand
15:00-15:30	Coffee and Tea Break		

Board Room II: Applied Energy Chair: Asst. Prof. Dr. Jatuporn Kaew-On, Thaksin University, Thailand Co-Chair: Asst. Prof. Dr. Tanate Chaichana, Thaksin University, Thailand			
13:45-14:00	EFFECT OF MANGANESE PROMOTER ON COBALT BASED CATALYSTS SUPPORTED ON MAGNESIA FOR FISCHER-TROPSCH SYNTHESIS	W. Warayanon, S. Tungkamani, H. Sukkathanyawat, M. Phongaksorn, T. Ratana and T. Sornchamni	Thailand
14:00-14:15	PROMOTER EFFECT ON THE PHYSICO-CHEMICAL PROPERTIES OF COBALT BASED CATALYST FOR CO HYDROGENATION	H. Sukkathanyawat, S. Tungkamani, M. Phongaksorn, T. Rattana, B. Yoosuk and P. Narataruksa	Thailand
14:15-14:30	DESIGN EQUATIONS FOR CATALYTIC MICROCHANNEL REACTORS: FISCHER-TROPSCH SYNTHESIS	N. Jermkwan, P. Narataruksa and C. Prapainainar	Thailand
14:30-14:45	TECHNICAL AND ECONOMIC ANALYSIS OF A SMALL BIOMASS PYROLYSIS PLANT	C. Jaroenkhasemmesuk and N. Tippayawong	Thailand
14:45-15:00	THE EFFECT OF FEED LOCATION OF SEMI-BATCH REACTIVE DISTILLATION VIA ESTERIFICATION REACTION OF ACETIC ACID AND METHANOL: SIMULATION STUDY	S. Akkaravathasinp, P. Narataruksa and C. Prapainainar	Thailand
15:00-15:30	Coffee and Tea Break		

Thursday May 28, 2015 (cont.)

Parallel Technical Sessions (cont.)

Grand Ballroom I: Applied Energy Chair: Dr. Pipatpong Wattanawanyoo, Rangsit University, Thailand Co-Chair: Asst. Prof. Dr. Wichuda Klawej, Thaksin University, Thailand			
15:30-15:45	INVESTIGATION OF Al_2O_3 NANOFLUID VISCOSITY FOR WATER/EG MIXTURE BASED	K. A. Hamid, W. H. Azmi, R. Mamat N.A. Usri and G. Najafi	Malaysia Iran
15:45-16:00	A STUDY OF TRANSIENT PERFORMANCE OF A CASCADE HEAT PUMP SYSTEM	P. Nenkaew and C. Tangthieng	Thailand
16:00-16:15	SWIRL FLOW IN A DIFFUSER FITTED WITH HELICAL SCREW-TAPE WITH AND WITHOUT CENTERED ROD	E. S. Shukri and W. Wisnoe	Iraq Malaysia
16:15-16:30	SWIRL FLOW STUDY IN AN ANNULAR DIFFUSER FITTED WITH DIFFERENT GEOMETRICES HUB INSERT	E. S. Shukri, W. Wisnoe and R. Zailani	Iraq Malaysia
16:30-16:45	THERMAL CONDUCTIVITY ENHANCEMENT OF Al_2O_3 NANOFLUID IN ETHYLENE GLYCOL AND WATER MIXTURE	N. A. Usri, W. H. Azmi, R. Mamat, K. A. Hamid and G. Najafi	Malaysia Iran
16:45-17:15	Poster Session (Grand Ballroom I)		
17:30	Bus Transportation from Sheraton Grande Sukhumvit Hotel to Pier (River City) (Instruction in Participant Bag)		
19:00-22:00	Grand Pearl Cruise Dinner		
22:00	Bus Transportation from Pier (River City) to Sheraton Grande Sukhumvit Hotel		

Asoke I: Applied Energy Chair: Asst. Prof. Dr. Jatuporn Kaew-On, Thaksin University, Thailand Co-Chair: Dr. Chontira Saengsubun, Thaksin University, Thailand			
15:30-15:45	HEAT TRANSFER AUGMENTATION OF Al_2O_3 NANOFLUID IN 60:40 WATER TO ETHYLENE GLYCOL MIXTURE	N. A. Usri, W. H. Azmi, R. Mamat, K. A. Hamid and G. Najafi	Malaysia Iran
15:45-16:00	GEOMETRICAL INFLUENCE OF REGENERATOR STACK ON THE PERFORMANCE OF THE STRAIGHT-TUBE THERMOACOUSTIC REFRIGERATOR	N. Maruyama, M. Saito, M. Yamamoto, M. Hirota and Y. Kitaide	Japan
16:00-16:15	EXPERIMENTAL INVESTIGATION ON Al_2O_3 - WATER ETHYLENE GLYCOL MIXTURE NANOFLUID THERMAL CONDITION IN A SINGLE COOLING PLATE FOR PEMFC APPLICATION	I. Zakaria, W. A. N. W. Mohamed, A. M. I. Bin Mamat, R. Saidur and S. F. A. Talib	Malaysia
16:15-16:30	TESTING OF LOW-GRADE HEAT SOURCE ORGANIC RANKINE CYCLE WITH SMALL HOT VAPOR RECIPROCATING ENGINE	W. Darawun, R. Songprakorp, V. Monyakul and S. Thepa	Thailand
16:30-16:45	THERMAL ANALYSIS ON HEAT TRANSFER ENHANCEMENT AND FLUID FLOW FOR LOW CONCENTRATION OF Al_2O_3 WATER - ETHYLENE GLYCOL MIXTURE NANOFLUID IN A SINGLE PEMFC COOLING PLATE	I. Zakaria, W. A. N. W. Mohamed, A. M. I. B. Mamat, R. Saidur, W. H. Azmi, R. Mamat, K. I. Sainan, H. Ismail	Malaysia
16:45-17:15	Poster Session (Grand Ballroom I)		
17:30	Bus Transportation from Sheraton Grande Sukhumvit Hotel to Pier (River City) (Instruction in Participant Bag)		
19:00-22:00	Grand Pearl Cruise Dinner		
22:00	Bus Transportation from Pier (River City) to Sheraton Grande Sukhumvit Hotel		

Asoke II: Wind and Wave Turbine Technology and Wind Farm Chair: Asst. Prof. Dr. Tanate Chaichana, Thaksin University, Thailand Co-Chair: Asst. Prof. Dr. Jompob Waewsak, Thaksin University, Thailand			
15:30-15:45	CFD-BASED POWER ANALYSIS ON LOW SPEED VERTICAL AXIS WIND TURBINES WITH WIND BOOSTER	N. Korprasertsak and T. Leephakpreeda	Thailand
15:45-16:00	EXPERIMENTAL STUDY OF NOVEL WIND BOOSTER FOR LOW SPEED VERTICAL AXIS WIND TURBINE	S. Ngamlarp, N. Korprasertsak and T. Leephakpreeda	Thailand
16:00-16:15	AERODYNAMIC PERFORMANCE TO TURBULENCE AND ITS IMPACTS ON THE POWER CURVE OF WIND TURBINES	S. A. Mathew and B. Ramdas	India
16:15-16:30	DEVELOPMENT OF OFFSHORE WIND FARM LAYOUT OPTIMISATION NUMERICAL MODEL WITH WAKE LOSSES	C. Chantharasenawong, D. Kollasuta and D. Sukawat	Thailand
16:30-16:45	ANALYSIS OF SUITABLE INTERCONNECTION POINTS OF OFFSHORE WIND FARMS IN THE GULF OF THAILAND	P. Ketsamee, K. Chalermyanont and A. Prasertsit	Thailand
16:45-17:00	A PROCESS BASED LCA STUDY FOR A MARINE CURRENT TURBINE	A. Rashedi and T. Khanam	Malaysia UK
16:45-17:15	Poster Session (Grand Ballroom I)		
17:30	Bus Transportation from Sheraton Grande Sukhumvit Hotel to Pier (River City) (Instruction in Participant Bag)		
19:00-22:00	Grand Pearl Cruise Dinner		
22:00	Bus Transportation from Pier (River City) to Sheraton Grande Sukhumvit Hotel		

Thursday May 28, 2015 (cont.)

Parallel Technical Sessions (cont.)

Board Room I: Energy Efficiency Chair: Assoc. Prof. Dr. Ahmad Zahedi, James Cook University, Australia Co-Chair: Dr. Supaluck Amloy, Thaksin University, Thailand			
15:30-15:45	POWER LOSS MINIMIZATION IN RADIAL DISTRIBUTION SYSTEM	K. R. Devabalaji, T. Yuvaraj and K. Ravi	India
15:45-16:00	OPTIMAL PLACEMENT AND SIZING OF DSTATCOM USING HARMONY SEARCH ALGORITHM	T. Yuvaraj, K. Ravi and K. R. Devabalaji	India
16:00-16:15	MERITS AND CHALLENGES OF E-RICKSHAW AS AN ALTERNATIVE FORM OF PUBLIC ROAD TRANSPORT SYSTEM: A CASE STUDY IN WEST BENGAL STATE IN INDIA	D. Majumdar and T. Jash	India
16:15-16:30	ANALYSIS OF ENERGY EFFICIENCY AND BIO-ENERGY IN THE LAND TRANSPORTATION IN LAO P.D.R	S. Phoulavand and B. Limmeechokchai	Thailand Laos
16:30-16:45	CONSTRUCTED WETLAND FOR SEWAGE TREATMENT AND THERMAL TRANSFER REDUCTION	A. Panrare, P. Sohsalam and T. Tondee	Thailand
16:45-17:15	Poster Session (Grand Ballroom I)		
17:30	Bus Transportation from Sheraton Grande Sukhumvit Hotel to Pier (River City) (Instruction in Participant Bag)		
19:00-22:00	Grand Pearl Cruise Dinner		
22:00	Bus Transportation from Pier (River City) to Sheraton Grande Sukhumvit Hotel		

Board Room II: Energy Efficiency, Innovation and Life Cycle Assessment Chair: Dr. Wanphut Se-Chua, KMITL, Thailand Co-Chair: Dr. Warit Werapun, Prince of Songkla University, Thailand			
15:30-15:45	INNOVATIVE SOLUTIONS FOR ENERGY CONSERVATION THROUGH COMMERCIAL AND DOMESTIC DEMAND SIDE MANAGEMENT	D. R. Smith and R. B. Smith	Australia
15:45-16:00	LIFE CYCLE ENVIRONMENTAL IMPACTS OF RENEWABLE ELECTRICITY IN TURKEY: RESERVOIR AND RUN-OF-RIVER HYDRO, WIND AND GEOTHERMAL POWER	B. Atilgan and A. Azapagic	UK
16:00-16:15	URBAN HEAT ISLAND AND HOUSEHOLD ENERGY CONSUMPTION IN BANGKOK, THAILAND	S. D. Arifwidodo and O. Chandrasiri	Thailand
16:15-16:30	THE POTENTIAL OF DEMAND RESPONSE MEASURES OF COMMERCIAL BUILDINGS IN THAILAND	W. Pasom, A. Therdyothin, A. Nathakaranakule, C. Prapanavarat and B. Limmeechokchai	Thailand
16:30-16:45	ENERGY EFFICIENCY ANALYSIS IN AN INTEGRATED BIOMASS GASIFICATION FUEL CELL SYSTEM	W. Paengjuntuek, J. Boonmak and J. Mungkalasiri	Thailand
16:45-17:15	Poster Session (Grand Ballroom I)		
17:30	Bus Transportation from Sheraton Grande Sukhumvit Hotel to Pier (River City) (Instruction in Participant Bag)		
19:00-22:00	Grand Pearl Cruise Dinner		
22:00	Bus Transportation from Pier (River City) to Sheraton Grande Sukhumvit Hotel		

Friday May 29, 2015

Keynote Session

Grand Ballroom I	
09:00-10:00	Keynote Address: Dr. Jun Zhang, World Bank, USA Plenary Discussion: Prof. Dr. Yves Gagnon, University of Moncton, Canada Plenary Chair: Assoc. Prof. Dr. Ahmad Zahedi, James Cook University, Australia "Financing of Renewable Energy Projects"
10:00-10:30	Coffee and Tea Break

Parallel Technical Sessions

Grand Ballroom I: Combustion, Co-Firing and Gasification			
Chair: Assoc. Prof. Dr. Suneerat Fukuda, KMUTT, Thailand Co-Chair: Dr. Auttapol Golaka, SCG, Thailand			
10:30-10:45	THE EFFECT OF MOISTURE CONTENT ON THE CRITICAL MASS FLUX AND PILOTED IGNITION TIME OF PARA RUBBER LITTER	P. Wongchai and W. Tachajapong	Thailand
10:45-11:00	A STUDY ON PHYSICAL AND CHEMICAL CHANGES IN THE BED MATERIAL DURING LONG-TERM COMBUSTION OF OIL PALM RESIDUES IN A FLUIDIZED BED OF ALUMINA SAND	P. Ninduangdee and V. I. Kuprianov	Thailand
11:00-11:15	CO-FIRING OF OIL PALM EMPTY FRUIT BUNCH AND KERNEL SHELL IN A FLUIDIZED-BED COMBUSTOR: OPTIMIZATION OF OPERATING VARIABLES	P. Suheri and V. I. Kuprianov	Thailand
11:15-11:30	DEVELOPMENT OF KINETICS MODELS IN EACH ZONE OF A 10 KG/HR DOWNDRAFT GASIFIER FOR OPTIMIZATION OF OPERATING CONDITIONS BY USING COMPUTATIONAL FLUID DYNAMICS	P. Meenaroch, S. Kerdsuwan and K. Laohalidanond	Thailand
11:30-11:45	OPTIMIZATION OF COMBUSTION BEHAVIOR AND PRODUCER GAS QUALITY FROM RECLAIMED LANDFILL THROUGH HIGHLY DENSIFY RDF-GASIFICATION	S. Chalermcharoenrat, K. Laohalidanond and S. Kerdsuwan	Thailand
11:45-12:00	INFLUENCE OF PLASTIC WASTE OF REFUSE-DERIVED FUEL ON DOWNDRAFT GASIFICATION	C. Kungkajit, G. Prateepchaikul and T. Kaosol	Thailand
12:00-12:15	OPTIMUM EQUIVALENCE RATIO FOR VARIOUS GASIFYING AGENT TEMPERATURE BASED ON THERMODYNAMIC EQUILIBRIUM MODEL	W. Jangsawang, K. Laohalidanond and S. Kerdsuwan	Thailand
12:15-13:00	International Buffet Lunch: Rossini & Basil (1 st Floor)		

Asoke I: Bio Fuel; Bioethanol			
Chair: Asst. Prof. Dr. Wichuda Klawej, Thaksin University, Thailand Co-Chair: Asst. Prof. Dr. Sompong O-Thong, Thaksin University, Thailand			
10:30-10:45	PHYSICO-CHEMICAL AND BIOLOGICAL CHARACTERISTICS OF ENHANCED ANAEROBIC MICROBIAL GRANULATION BY SYNTHETIC AND NATURAL CATIONIC POLYMERS	E. Ariyavongvivat, B. Suraraksa and P. Chaiprasert	Thailand
10:45-11:00	EFFECT OF GRANULE SIZES ON THE PERFORMANCE OF UASB REACTORS FOR CASSAVA WASTEWATER TREATMENT	S. Jijai, G. Srisuwan, S. O-Thong, N. Ismaile and C. Siripatana	Thailand Malaysia
11:00-11:15	OPTIMIZATION OF SUB-CRITICAL WATER PRETREATMENT FOR ENZYMATIC HYDROLYSIS OF SUGARCANE BAGASSE	K. Manorach, A. Poonrisawat, N. Viriya-empikul and N. Laosiripojana	Thailand
11:15-11:30	OPTIMIZING SULFUR OXIDIZING PERFORMANCE OF PARACOCCLUS PANTOTROPHUS ISOLATED FROM LEATHER INDUSTRY WASTEWATER	N. Vikromvarasiri and N. Pisutpaisal	Thailand
11:30-11:45	EFFECT OF MIXING TIME ON ANAEROBIC CO-DIGESTION OF PALM OIL MILL WASTE AND BLOCK RUBBER WASTEWATER	W. Lerdtrattanayawee and T. Kaosol	Thailand
11:45-12:00	DELIGNIFICATION OF ELEPHANT GRASS FOR PRODUCTION OF CELLULOSIC INTERMEDIATE	J. Minmunin, P. Limpitpanich and A. Promwungkwa	Thailand
12:00-13:00	International Buffet Lunch: Rossini & Basil (1 st Floor)		

Friday May 29, 2015 (cont.)

Parallel Technical Sessions (cont.)

Asoke II: Fuel Cell and Energy Storage Chair: Asst. Prof. Dr. Chontisa Sukkasem, Thaksin University, Thailand Co-Chair: Dr. Chutima Kaewpiboon, Thaksin University, Thailand			
10:30-10:45	PROPERTIES OF SILICON DIOXIDE (SiO ₂) IN WATER-ETHYLENE GLYCOL MIXTURE FOR PROTON EXCHANGE MEMBRANE FUEL CELL COOLING APPLICATION	S. F. A. Talib, I. Zakaria, W. H. Azmi, and W.A.N.W. Mohamed	Malaysia
10:45-11:00	DRY METHANE REFORMING PERFORMANCE OF Ni-BASED CATALYST COATED ON STAINLESS STEEL SUBSTRATE	S. Sangsorn, M. Phongakorn, S. Tungkamani, T. Sornchamni and R. Chuvaree	Thailand
11:00-11:15	DEVELOPMENT OF TiO ₂ /TiO ₂ -V ₂ O ₅ COMPOUND WITH PANI FOR ELECTRON STORAGE	W. Boonmeemak, C. Fongsamut and P. Ngotrakanwivat	Thailand
11:15-11:30	EFFECTS OF THE GEOMETRY OF THE AIR FLOWFIELD ON THE PERFORMANCE OF AN OPEN-CATHODE PEMFC-TRANSIENT LOAD OPERATION	S. Kiattamrong and A. Sripakagorn	Thailand
11:30-11:45	ELECTRICITY GENERATION AND SEPTAGE TREATMENT IN MICROBIAL FUEL CELL (MFC) CONSTRUCTED USING EARTHEN MEMBRANE	Cao N. D.T and R. Nitorisavut	Thailand
11:45-12:00	MICROPOROUS ACTIVATED CARBON FROM KOH-ACTIVATION OF RUBBER SEED-SHELLS FOR APPLICATION IN CAPACITOR ELECTRODE	T. Paketanang, A. Artnaseaw P. Wongwicha and M. Thabuot	Thailand
12:00-13:00	International Buffet Lunch: Rossini & Basil (1 st Floor)		

Board Room I: Wind Resource Assessment Chair: Dr. Sajan A. Mathew, NIWE, India Co-Chair: Asst. Prof. Dr. Tanate Chaichana, Thaksin University, Thailand			
10:30-10:45	INVESTIGATION OF OFFSHORE WIND ENERGY POTENTIAL IN THE GULF OF THAILAND	C. Chancham, J. Waewsak, B. Archewaraphruk and Y. Gagnon	Thailand Canada
10:45-11:00	COMPARATIVE STUDY OF FIVE METHODS FOR ESTIMATING WEIBULL PARAMETERS FOR PHANGAN ISLAND, THAILAND	W. Werapun, Y. Tirawanichakul and J. Waewsak	Thailand
11:00-11:15	ASSESSMENT OF WIND ENERGY POTENTIAL IN THE CENTRAL REGION OF THAILAND: AN ECONOMIC ANALYSIS	P. Quan and T. Leephakpreeda	Thailand
11:15-11:30	TERRAIN EVALUATION FOR POWER CURVE MEASUREMENTS OF WIND TURBINES IN VARIANCE TO THE REQUIREMENTS AS PER IEC 61400-12-1	S. A. Mathew and M. Saravanan	India
11:30-11:45	FEASIBILITY OF DEVELOPMENT OF WIND FARMS IN NORTHERN PROVINCE OF SAUDI ARABIA	S. M. Shaahid, L. M. Al-Hadhrani and M. K. Rahman	Saudi Arabia
11:45-12:00	ASSESSMENT OF WIND ENERGY POTENTIAL IN THE CENTRAL REGION OF THAILAND: A WIND ANALYSIS	P. Quan and T. Leephakpreeda	Thailand
12:00-13:00	International Buffet Lunch: Rossini & Basil (1 st Floor)		

Board Room II: Energy Policy; Low Carbon Society Chair: Assoc. Prof. Dr. Navadol Laosiripojana, KMUTT, Thailand Co-Chair: Dr. Supaluck Amloy, Thaksin University, Thailand			
10:30-10:45	THAILAND'S POST-2020 GREENHOUSE GAS EMISSIONS REGIME IN THE ENERGY SECTOR	S. Selvakkumaran, C. Nithitsutibata and B. Limmeechokchai	Thailand
10:45-11:00	LOW CARBON SCENARIOS FOR AN ENERGY IMPORT-DEPENDENT ASIAN COUNTRY: THE CASE STUDY OF SRI LANKA	S. Selvakkumaran, and B. Limmeechokchai	Thailand
11:00-11:15	ENERGY EFFICIENCY IMPROVEMENT AND CO ₂ MITIGATION IN RESIDENTIAL SECTOR: COMPARISON BETWEEN INDONESIA AND THAILAND	T. V. Kusumadewi and B. Limmeechokchai	Thailand
11:15-11:30	ENERGY SAVING POTENTIAL CO ₂ MITIGATION ASSESSMENT USING THE ASIA-PACIFIC INTEGRATED MODEL/ENDUSE IN THAILAND ENERGY SECTORE	P. Chunark and B. Limmeechokchai	Thailand
11:30-11:45	SCENARIO BASED ASSESSMENT OF CO ₂ MITIGATION PATHWAYS: A CASE STUDY IN THAI TRANSPORT SECTOR	P. R. Jayatilaka and B. Limmeechokchai	Thailand
11:45-12:00	ENERGY CONSUMPTION AND GREENHOUSE GAS EMISSION FROM CERAMIC TABLEWARE PRODUCTION: A CASE STUDY IN LAMPANG, THAILAND	P. Riyakad and S. Chiarakorn	Thailand
12:00-13:00	International Buffet Lunch: Rossini & Basil (1 st Floor)		

Friday May 29, 2015 (cont.)

Keynote Session

Grand Ballroom I	
13:10-13:40	Keynote Address: Prof. Dr. Roland Horne, Stanford University, USA "World Outlook of Geothermal Energy"

Parallel Technical Sessions

Grand Ballroom I: Fuel Cell Technology Chair: Assoc. Prof. Dr. Ahmad Zahedi, James Cook University, Australia Co-Chair: Dr. Supaluck Amloy, Thaksin University, Thailand			
13:45-14:00	COMPUTATIONAL MODELLING OF THE FLOW FIELD OF AN ELECTROLYZER SYSTEM USING CFD	A. S. Tijani, D Barra, A. H. Abdol Rahima and K. I. Sainan	Malaysia
14:00-14:15	OPTIMIZATION OF DIRECT COUPLING SOLAR PV PANEL AND ADVANCED ALKALINE ELETROLYZER SYSTEM	A. H. Abdol Rahima, A. S. Tijaniaa, M. Fadhullallah, S. Hanapi and K. I. Sainan	Malaysia
14:15-14:30	EFFECTS OF PROCESSING VARIABLES ON FORMATION OF THIN ELECTROLYTE FILMS FOR SOFCs	D. Wattanasiriwech, A. Srisuwan and S. Wattanasiriwech	Thailand
14:30-14:45	THE SOLID OXIDE FUEL CELL (SOFC) AND GAS TURBINE (GT) HYBRID SYSTEM NUMERICAL MODEL	P. Saisirirat	Thailand
14:45-15:00	APPROACHES FOR REDUCTION OF ELECTRODE POLARIZATION IN ANODE-SUPPORTED SOFCs	M. Meepoh, D. Wattanasiriwech, S. Wattanasiriwech, and P. Ankawattan	Thailand
15:00-15:30	Coffee and Tea Break		

Asoke I: Bio Fuel; Pyrolysis oil and Future Fuel Chair: Assoc. Prof. Dr. Suneerat Fukuda, KMUTT, Thailand Co-Chair: Dr. Auttapol Golaka, SCG, Thailand			
13:45-14:00	EMULSIFICATION OF WATER AND PYROLYSIS OIL	P. Kittipoomwong and M. Narasingha	Thailand
14:00-14:15	EFFECT OF TiO ₂ INCORPORATED WITH Al ₂ O ₃ ON THE HYDRODEOXYGENATION AND HYDRODENITROGENATION OVER CoMo SULFIDE CATALYSTS	T. Rodseanglung, T. Ratana, M. Phongaksorn and S. Tungkamani	Thailand
14:15-14:30	HYDROTREATING OF FREE FATTY ACID AND BIO-OIL MODEL COMPOUNDS : EFFECT OF CATALYST SUPPORT	V. Goodwin, B. Yoosuk, T. Ratana and S. Tungkamani	Thailand
14:30-14:45	CATALYTIC CONVERSION OF PYROLYSIS TAR TO PRODUCE GREEN GASOLINE-RANGE AROMATICS	A. Saad, S. Ratanawilai and C. Tongurai	Thailand
14:45-15:00	THE POTENTIALS OF WATER-IN-DIESEL EMULSIONS AS A FUTURE FUEL	A. H. Nour, A. H. Nour and S. Nurdin	Malaysia
15:00-15:15	THERMOGRAVIMETRIC KINETIC ANALYSIS OF THE PYROLYSIS OF RICE STRAW	N. Kongkaew, W. Pruksakit and S. Patumsawad	Thailand
15:15-15:30	Coffee and Tea Break		

Friday May 29, 2015 (cont.)

Parallel Technical Sessions (cont.)

Asoke II: Solar Heating, Cooling and Electricity Chair: Prof. Dr. R.H.B. Exell, KMUTT, Thailand Co-Chair: Asst. Prof. Dr. Jompob Waewsak, Thaksin University, Thailand			
13:45-14:00	EFFECT OF MASS RECOVERY ON THE PERFORMANCE OF SOLAR ADSORPTION COOLING SYSTEM	K. M. Ariful kabir, K. C. Amanul Alam, M. M. A. Sarkar, R. A. Rouf and B.B. Saha	Bangladesh
14:00-14:15	A PARABOLIC CROSS-SECTIONAL GREENHOUSE TYPE SOLAR DRYER : FIELD EXPERIMENTS AND DISSEMINATION	S. Janjai, P. Pankeaw, R. Wattan, K. Tohsing, Y. Boonrod and A. Sangcharean	Thailand
14:15-14:30	POLYGENERATION SOLAR AIR DRYER	S. K. Deb and B. C. Sarma	India
14:30-14:45	DESIGN AND PRELIMINARY TESTING OF LOW-GRADE HEAT SOURCE ORGANIC RANKINE CYCLE WITH SMALL HOT VAPOR RECIPROCATING ENGINE	W. Darawun, R. Songprakorp, V. Monyakul and S. Thepa	Thailand
14:45-15:00	ENERGY TRANSITIONS FOR THE RURAL COMMUNITY IN KENYA'S CENTRAL HIGHLANDS: SMALL SCALE SOLAR POWERED SYTEMS	H. Ngetha, M. Sasaki, M. Taheri and S. Mathenge	Japan Kenya
15:00-15:15	DESIGN OF LOW POWER WIRELESS POWER TRANSFER BY USING MAGNETIC COIL RESONANT SYSTEM (MCRS) WITH SOLAR ENERGY	M. Fareq, S. Marsitah, M. Fitra, M. Irwanto, H. S. Syafruddin, M. Arinal, Suwarno, N. Gomesh, M. Irwan and T. Hussain	Malaysia Indonesia
15:15-15:30	Coffee and Tea Break		

Board Room I: Energy Policy and Energy Security Chair: Assoc. Prof. Dr. Navadol Laosiripojana, KMUTT, Thailand Co-Chair: Asst. Prof. Dr. Jatuporn Kaew-On, Thaksin University, Thailand			
13:45-14:00	ASSESSING ENERGY SECURITY PERFORMANCE IN THAILAND UNDER DIFFERENT SCENARIOS AND POLICY IMPLICATIONS	A. Phdungsilp	Thailand
14:00-14:15	PROJECTED BUSINESS RISK OF REGULATORY CHANGE ON WIND POWER PROJECT: CASE OF SPAIN	G. S. Sisodia, I. Soares, P. Ferreira, S. Banerji and R. Prasad	Portugal India
14:15-14:30	ENERGY STORAGE: TECHNOLOGY APPLICATIONS AND POLICY OPTIONS	M. Landry and Y. Gagnon	Canada
14:30-14:45	POLICY ASSESSMENT OF POTENTIAL BIODIESEL FEEDSTOCK SUPPLY IN THAILAND	J. Keson, S. Wongsai, A. Ratchaniphont and N. Wongsai	Thailand
14:45-15:00	THE PROSPECT OF BIO-ENERGY FROM SOLID WASTE IN THAILAND: POTENTIAL, POLICY AND BARRIERS	S. Chitapornpan and C. Chiemchaisri	Thailand
15:00-15:30	Coffee and Tea Break		

Board Room II: Applied Energy Chair: Asst. Prof. Dr. Sompong O-Thong, Thaksin University, Thailand Co-Chair: Asst. Prof. Dr. Chontisa Sukkasem, Thaksin University, Thailand			
13:45-14:00	EXPERIMENTAL TEST OF A MINI PEM FUEL CELL VEHICLE ON AN INERTIA DYNMOMETER	S. Hanapi, A. S. Tijani, A. H. A. Rahim and W. A. N. W. Mohamed	Malaysia
14:00-14:15	CRUDE CELLULASE POWDER PRODUCTION BY SOLID STATE FERMENTATION USING CASSAVA RESIDUE AND CO-CULTURED MICROORGANISMS TRICHODERMA REESEI AND SACCHAROMYCES CEREVISIAE	P. Siwarasak, J. Ratanapisit, W. Appamana and S. Thongwic	Thailand
14:15-14:30	EXERGY EFFICIENCY PROFILE OF A 1 kW OPEN CATHODE FUEL CELL WITH PRESSURE AND TEMPERATURE VARIATIONS	S. Hanapi, A. S. Tijani, A. H. A. Rahim and W. A. N. W. Mohamed	Malaysia
14:30-14:45	THE POTENTIAL OF DELIVERING CLEAN LOCALLY AVAILABLE LIMITLESS RICE HUSK ELECTRICTY IN THE CELEBES ISLAND INDONESIA	A. Rachman, U. Rianse, M. Musaruddin and Y. Pasolon	Indonesia
14:45-15:00	ANALYSES OF ENRGY USE AND CO ₂ EMISSIONS IN RESIDENTIAL SECTOR: CASE STUDIES IN THAILAND AND VIETNAM	V. T. H. Thuy and B. Limmeechokchai	Thailand
15:00-15:30	Coffee and Tea Break		

Friday May 29, 2015 (cont.)

Parallel Technical Sessions (cont.)

Grand Ballroom I: Bio Fuel Production Technology Chair: Dr. Auttapol Golaka, SCG, Thailand Co-Chair: Dr. Chutima Kaewpiboon, Thaksin University, Thailand			
15:30-15:45	REMOVAL OF COLOR AND COD FROM LANDFILL LEACHATE BY PHOTOCATALYTIC PROCESS WITH AC/TIO ₂	O. Rojviroon, T. Rojviroon and S. Sirivithayapakorn	Thailand
15:45-16:00	FUEL PROPERTIES OF BIO-PELLETS PRODUCED FROM SELECTED MATERIALS UNDER VARIOUS COMPACTING PRESSURE	T. Unpinit, T. Poblarp, N. Sailoon, P. Wongwicha and M. Thabuot	Thailand
16:00-16:15	PREPARED OF ACTIVATED CARBON FROM MACADAMIA SHELL BY MICROWAVE IRRADIATION ACTIVATION EE	N. Dejang, O. Somprasit and S. Chindaruksa	Thailand
16:15-16:30	THERMOGRAVIMETRIC STUDIES ON OIL PALM EMPTY FRUIT BUNCH AND PALM KERNEL SHELL: TG/DTG ANALYSIS AND MODELING	P. Ninduangdee, V. I. Kuprianov, E. Y. Cha, R. Kaewrath, W. Atthawethworawuth and P. Youngyuen	Thailand
16:30-16:45	ANAEROBIC CO-DIGESTION BIOMETHANATION OF CANNERY SEAFOOD WASTEWATER WITH MICROCYSTIS SP; BLUE GREEN ALGAE WITH/WIHOOUT GLYCEROL WASTE	K. Panpong, K. Nuithitikul, S. O-thong and P. Kongjan	Thailand
17:00-17:30	Closing Ceremony and Best Paper/Best Poster Awards (Grand Ballroom I)		

Asoke I: Wind, Wave and Tidal Resource Assessment and Conversion Technology Chair: Asst. Prof. Dr. Tanate Chaichana, Thaksin University, Thailand Co-Chair: Asst. Prof. Dr. Jatuporn Kaew-On, Thaksin University, Thailand			
15:30-15:45	DEVELOPMENT AND DESIGN OF PIC CONTROLLED FLOAT BUOY WAVE ENERGY CONVERTER SYSTEM	R. M. Anacan and R. G. Garcia	Philippines
15:45-16:00	EXPERIMENTAL INVESTIGATION OF HELICAL TIDAL TURBINE CHARACTERISTICS WITH DIFFERENT TWIST	S. Pongdoang, Y. Tiaple and C. Kayankannavee	Thailand
16:00-16:15	DESIGN, DEVELOPMENT AND EXPERIMENTATION OF DEEP OCEAN WAVE ENERGY CONVERTER SYSTEM	S. Chandrasekaran and B. Raghavi	India
16:15-16:30	EVALUATION OF WIND RESOURCE IN SELECTED LOCATION IN GUJARAT	G. Nagababu, D. Bavishi, S. S. Kachhwaha and V. Savsani	India
16:30-16:45	ECONOMIC EVALUATION OF OFFSHORE WIND POTENTIAL IN WESTERN COAST OF INDIA	G. Nagababu, D. Bavishi and S. S. Kachhwaha	India
16:45-17:00	HYDRO POWER POTENTIAL IN MOZAMBIQUE "CHUA-MANICA"	M. M. Uamusse and K. M. Persson	Sweden Mozambique
17:00-17:30	Closing Ceremony and Best Paper/Best Poster Awards (Grand Ballroom I)		

Asoke II: Sustainable Architecture and Building Technology Chair: Prof. Dr. Elmar Richard Steurer, Neu-Ulm University of Applied Sciences, Germany Co-Chair: Asst. Prof. Fardous Alom, International Islamic University Malaysia, Malaysia			
15:30-15:45	THE DEVELOPMENT OF ENERGY EFFICIENCY ESTIMATION SYSTEM (EES) FOR SUSTAINABLE DEVELOPMENT: A PROPOSED STUDY	Khairunnisa A.R, M. Z. M Yusof, M. N. M Salleh and A. M. Leman	Malaysia
15:45-16:00	THE ENERGY SAVING CALCULATION FOR A RESIDENTIAL SECTOR IN THAILAND WITH TOP-DOWN METHODOLOGY	A. Tiangket, B. Chullabodhi and S. Watechagit	Thailand
16:00-16:15	STUDY OF OPTIMUM INWARD GLASS TILT ANGLE FOR WINDOW GLASS IN DIFFERENT INDIAN LATITUDES TO MINIMUM HEAT GAIN INTO BUILDINGS	K. K. Gorantla and A. B. T. Puttaranga Setty	India
16:15-16:30	RAY TRACING METHOD OF LIGHT THROUGH RECTANGULAR LIGHT PIPE WITH BENDS	T. Taengchum and S. Chirarattanon	Thailand
16:30-16:45	ENERGY CONSUMPTION AND MANAGEMENT IN SUB-URBAN AREA	A. M. Leman, Khairunnisa A.R, M.N.M Salleh, M. F. Zakaria and M. Z. M. Yusof	Malaysia
16:45-17:00	THE ENERGY SAVING IN AIR CONDITION SYSTEM OF THAILAND'S BUILDING AND FACTORIES	W. Thanuanram, N. Auppapong, P. Nupteotrong and D. Buayorm	Thailand
17:00-17:30	Closing Ceremony and Best Paper/Best Poster Awards (Grand Ballroom I)		

Friday May 29, 2015 (cont.)

Parallel Technical Sessions (cont.)

Board Room I: Eco-Friendly Community and Renewable Energy Chair: Dr. Warit Werapun, Prince of Songkla University, Thailand Co-Chair: Dr. Supaluck Amloy, Thaksin University, Thailand			
15:30-15:45	INTEGRATED COMMUNITIES FOR THE SUSTAINABILITY OF RENEWABLE ENERGY APPLICATION: SOLAR WATER PUMPING SYSTEM IN BANYUMENENG VILLAGE GUNUNG KIDUL D.I. YOGYAKARTA	N. S. Wahyuni, S. Wulandari, E. Wulandari, and D. S. Pamuji	Indonesia
15:45-16:00	ECONOMICAL BIODIESEL FUEL SYNTHESIS FROM CASTOR OIL USING MUSSEL SHELL-BASE CATALYST (MS-BC)	S. Nurdin, N. A. Rosnan, N. S. Ghazali, J. Gimbut, A. H. Nour and S. F. Haron	Malaysia
16:00-16:15	SUSTAINABLE DEVELOPMENT AND ECO-FRIENDLY WASTE MANAGEMENT MODELLING FOR LOCAL COMMUNITY	S. Kerdsuwan and K. Laohalidanond	Thailand
16:15-16:30	EFFECT OF APPLIED PRESSURE AND BINDER PROPORTION ON THE FUEL PROPERTIES OF HOLEY BIO-BRIQUETTES	M. Thabuot, T. Pagketanang, K. Panyacharoen, P. Mongkut and P. Wongwicha	Thailand
16:30-16:45	AN INVESTIGATION OF FUEL ECONOMY POTENTIAL OF HYBRID VEHICLE UNDER REAL-WORLD DRIVING CONDITIONS IN BANGKOK	S. Pitanuwat and A. Sripakagorn	Thailand
16:45-17:00	A FIELD OF THE THERMAL COMFORT IN UNIVERSITY BUILDINGS IN THAILAND UNDER AIR CONDITION ROOM	N. Puangmalee, V. Boonyayothin and J. Khedari	Thailand
17:00-17:30	Closing Ceremony and Best Paper/Best Poster Awards (Grand Ballroom I)		

Broad Room II: Energy Efficiency Chair: Assoc. Prof. Dr. Naoki Maruyama, Mie University, Japan Co-Chair: Dr. Chontira Saengsubun, Thaksin University, Thailand			
15:30-15:45	DEVELOPMENT OF VSPP WIND FARM IN SOUTHERN THAILAND	C.A. Kumaresan	India
15:45-16:00	IDENTIFICATION OF DESIGN CRITERIA FOR DISTRICT COOLING DISTRIBUTION NETWORK WITH ICE THERMAL ENERGY STORAGE SYSTEM	G. L. Augusto, A. B. Culaba and A. B. Maglaya	Philippines
16:00-16:15	IDENTIFICATION OF DESIGN CRITERIA FOR CHILLER PLANTS DISTRIBUTION NETWORK IN ALABANG TOWN CENTER	G. L. Augusto and A. B. Culaba	Philippines
16:15-16:30	ORGANIC BULK HETEROJUNCTION SOLAR CELL: PERFORMANCE AND DEGRADATION ANALYSIS	R. P. Tandon	India
16:30-16:45	INFLUENCING FACTORS OF ENERGY USE OF LOW AND MEDIUM INCOME HOUSEHOLDS IN THAILAND	P. Tumm, S. Chirarattanon, P. Rakkwamsuk, P. Chaiwiwatworakul, S. Chuangchote and S. Chiarakorn	Thailand
16:45-17:00	THE ANALYSIS OF THE CYCLICAL IMPACT CHANGES IN THE WORLD, CHINA AND INDIA	J. Vehmas, J. Kaivo-oja and J. Luukkanen	Finland
17:00-17:30	Closing Ceremony and Best Paper/Best Poster Awards (Grand Ballroom I)		

Saturday May 30, 2015

Field Trips

08:00-15:00	Field Trips
08:30-15:00	8 MW Solar Farm: Loxley PLC, Pracheanburi Province
09:00-13:00	The Grand Palace: Cultural Tour, Bangkok

Posters

No.	Grand Ballroom I		
P01	OPTIMIZATION OF FACTORS AFFECTING ACID HYDROLYSIS OF WATER-HYACINTH STEM (EICHHORNIA)	S. Pattra and S. Sittijunda	Thailand
P02	BIOHYDROGEN AND BIOMETHANE PRODUCTION FROM CO-DIGESTION OF PALM OIL MILL EFFLUENT WITH SOLID RESIDUES BY TWO-STAGE SOLID STATE ANAEROBIC DIGESTION	W. Suksong, P. Kongjan and S. O-Thong	Thailand
P03	HYDROGEN AND METHANE PRODUCTION FROM STARCH PROCESSING WASTEWATER BY THERMOPHILIC TWO-STAGE ANAEROBIC DIGESTION	P. Khongkliang, P. Kongjan and S. O-Thong	Thailand
P04	FACTORS AFFECTING ON PROCESS STABILITY OF CONTINUOUS HYDROGEN PRODUCTION FROM PALM OIL MILL EFFLUENT UNDER THERMOPHILIC CONDITION	C. Mamimin, S. Senbat, C. Niyasom and S. O-Thong	Thailand
P05	BIOGAS PRODUCTION FROM BIOMASS RESIDUES OF PALM OIL MILL BY SOLID STATE ANAEROBIC DIGESTION	S. Chaikitkeaw, P. Kongjan and S. O-Thong	Thailand
P06	ETHANOL PRODUCTION FROM DESIZING WASTEWATER USING CO-CULTURE OF BACILLUS SUBTILIS AND SACCHAROMYCES CEREVISIAE	S. Tantipaibulvut, A. Pinisakul, P. Rattanachaisit, K. Klatin, B. Onsrirai and K. Boonyaratsiri	Thailand
P07	LANTHANUM-DOPED STRONTIUM TITANATE FOR TRANSESTERIFICATION OF PALM OIL TO FATTY ACID METHYL ESTERS	P. Sukpanish and C. Ngamcharussrivichai	Thailand
P08	UTILIZATION OF DENDROCALAMUS ASPER BACKER BAMBOO CHARCOAL AND PYROLIGNEOUS ACID	P. Sumanatrakul, P. Kongsune, L. Chotitham and A. Sukto	Thailand
P09	FORECASTING OF CRUDE PALM OIL DEMAND TOWARDS FOOD AND ENERGY SECURITY IN THAILAND	P. Nutongkaew, J. Waewsak, W. Keerativibool, C. Kongruang, T. Chaichana, and Y. Gagnon	Thailand Canada
P10	IDENTIFICATION OF POTENTIAL AREAS FOR THE EXPANSION OF OIL PALM PRODUCTION IN THAILAND	P. Nutongkaew, J. Waewsak, C. Kaewprasert and Y. Gagnon	Thailand Canada
P11	CHARACTERISTICS OF REFUSED DERIVED FUEL-5 FROM THREE SITES IN SOUTHERN THAILAND	P. Nutongkaew, J. Waewsak and Y. Gagnon	Thailand Canada
P12	LIFE CYCLE GHG EMISSIONS OF UTILIZING PALM EMPTY FRUIT BUNCH AS FEEDSTOCK FOR ELECTRICITY PRODUCTION	S. Chanlongphitak, S. Papong, P. Malakul and T. Mungcharoen	Thailand
P13	LIFE-CYCLE GHG EMISSION OF CASSAVA-BASED BIOETHANAL PRODUCTION	T. Namjuncharoen, S. Papong, P. Malakul and T. Mungcharoen	Thailand
P14	SCIENCE TECHNOLOGY AND INNOVATION CHALLENGES OF BIOMASS IMPLEMENTATIONS	S. Chaivongvilan	Thailand
P15	ATTENUATION OF SOLAR RADIATION DUE TO AEROSOLS IN THE ATMOSPHERE OF THAILAND	S. Phokate	Thailand
P16	EFFICIENCY ENHANCEMENT OF ZNO DYE-SENSITIZED SOLAR CELLS BY MODIFYING PHOTOELECTRODE AND COUNTERELECTRODE	K. Hongsith, N. Hongsith, D. Wongratanaphisan, A. Gardchareon, S. Phadungdhithidhada and S. Choopun	Thailand
P17	EFFECT OF ZNO DOUBLE LAYER AS ANTI-REFLECTION COATING LAYER ON DYE-SENSITIZED SOLAR CELLS	E. Chanta, D. Wongratanaphisan, A. Gardchareon, S. Phadungdhithidhada, P. Ruankham and S. Choopun	Thailand
P18	ENHANCEMENT OF ZNO DYE-SENSITIZED SOLAR CELL PERFORMANCE BY MODIFYING PHOTOELECTRODE USING TWO-STEPS ETCHING PROCESS	S. Sutthana, D. Wongratanaphisan, A. Gardchareon, S. Phadungdhithidhada, P. Ruankham and S. Choopun	Thailand

P19	AN EXPERRIMENTAL STUDY OF THERMO-SYPHON SOLAR WATER HEATER IN THAILAND	P. Sae-Jung, T. Krittayanawatch and P. Deedom	Thailand
P20	TECHNO-ECONOMIC ASSESSMENT OF 3-5 kWp SOLAR PHOTOVOLTAIC RESIDENTIAL ROOFTOP SYSTEMS IN SOUTHERN THAILAND	M. Kuasakul, J. Waewsak, C. Kongruang and Y. Gagnon	Thailand Canada
P21	FEASIBILITY OF A 3.5 kWp ROOFTOP RESIDENTIAL SOLAR PHOTOVOLTAIC INSTALLATION IN NAKHON SI THAMARAT PROVINCE, THAILAND	J. Waewsak, M. Kuasakul, C. Kongruang and Y. Gagnon	Thailand Canada
P22	WIND SPEED PROJECTIONS FOR ELECTRICITY APPLICATION OVER THAILAND	S. Ratjiranukool and P. Ratjiranukool	Thailand
P23	GENERATION OF SYNTHETIC WIND SPEEDS USING THE MARKOV ALGORITHM	J. Waewsak, S. Chewamongkolkarn and Y. Gagnon	Thailand Canada
P24	ENERGY YIELD ASSESSMENT OF A PROPOSED 45 MW WIND POWER PLANT IN SOUTHERN THAILAND	J. Waewsak, S. Chewamongkolkarn and Y. Gagnon	Thailand Canada
P25	ENVIRONMENTAL IMPACT ASSESSMENT OF A WIND POWER PLANT: A CASE STUDY FOR NAKHON SI THAMMARAT PROVINCE, THAILAND	J. Waewsak, C. Chancham and Y. Gagnon	Thailand Canada
P26	ON THE ASSESSMENT OF TURBULENCE MODELS FOR WIND FLOW MODELING OVER FLAT, SEMI-COMPLEX, AND COMPLEX TERRAINS	A. Puteh, J. Waewsak, T. Chaichana, N. Dusadee, W. Werapun and Y. Gagnon	Thailand Canada
P27	PERFORMANCE EVALUATION OF CO-AXIS COUNTER-ROTATION WIND TURBINE	T. Chaichana and S. Chaitep	Thailand
P28	THE POSSIBILITY OF USING ELECTRICAL MOTER FOR BOAT PROPULSION SYSTEM	R. Reabroy, Y. Tiaple, S. Pongduang, T. Nantawong and P. Iamraksa	Thailand
P29	THE STUDY OF POWER SYSTEM IN PHOENIX BY LOAD SHEDDING SYSTEM	K. Rattanapanyapan and A. Kaewrawang	Thailand
P30	THE STUDY OF THE EFFECT OF TDeq AND ΔT ON OTTV (CASE STUDY 6 th FLOOR PIENVICHITR BUILDING)	C. Singhpo, N. Pannuchareonwong and C. Benjapiyaporn	Thailand
P31	EFFECT OF CALCINATION TEMPERATURE ON MICROSTRUCTURE AND PHASE FORMATION OF CaCO ₃ PREPARED FROM DONAX SCORTUM SHELLS	S. Kheawmaneail and C. Sangsubun	Thailand
P32	UNDERSHOT WATER WHEEL FOR A SMALL HYDRO-POWER SYSTEM	S. Wiriyumpaiwong and J. Jamradloedluk	Thailand
P33	IMPROVING A GRID-BASED ENRGY EFFICIENCEY BY USING SERVICE SHARING STRATEGIES	B. Punantapong P. Punantapong and I. Punantapong	Thailand
P34	EFFECT OF CHANNEL DESIGN AND OPERATING PARAMETERS ON OPEN-CATHODE PEM FUEL CELL PERFORMANCE: A COMPUTATIONAL STUDY	S. Kreesaeng, B. Chalermisinsuwan and P. Piumsomboon	Thailand
P35	A STUDY OF FINISHED PRODUCT TOM YUM GOONG BY FREEZE-DRYING PROCESS	S. Srisantisuk, P. Thateenaranon and V. Pimpinit	Thailand
P36	THE CONSTRUCTION OF CHARGING BATTERY FOR SMALL ELECTRIC CAR THREE-WHEELER	S. Srisantisuk, P. Anudit and S. Wangsang	Thailand
P37	THE STUDY OF TEST NOZZLE FOR INDUSTRIAL APPLICATIONS	S. Srisantisuk, P. Promma and P. Yooiin	Thailand
P38	THE APPLICATION OF NATURAL DOLOMITIC ROCK AS A HETEROGENEOUS CATALYST IN TRANSESTERIFICATION FOR BIODIESEL SYNTHESIS	A. Buasri, K. Rochanakit, W. Wongvitvichot, U. Masa-ard, and V. Loryuenyong	Thailand
P39	BIOGAS PRODUCTION FROM VEGETABLE WASTE BY USING DOG AND CATTLE MANURE	N. Phetyim, T. Wanthong, P. kannika and A. Supngam	Thailand
P40	PHYSICAL AND THERMAL PROPERTIES OF BRIQUETTE FUELS FROM RICE STRAW AND SUGARCANE LEAVES BY MIXING MOLASSES	P. Jittabut	Thailand
P41	EFFECT OF NANOSILICA ON MECHANICAL AND THERMAL PROPERTIES OF CEMENT COMPOSITE FOR THERMAL ENERGY STORAGE MATERIALS	P. Jittabut	Thailand

P42	WAVE ENERGY POTENTIAL IN THE GULF OF THAILAND	K. Noojeensang, J. Waewsak and Y. Gagnon	Thailand Canada
P43	THERMAL EFFECT OF THERMAL ENERGY STORAGE (TES) TANK FOR SOLAR ENERGY APPLICATION DURING CHARGING CYCLE BASED ON THE GRID SENSITIVITY ANALYSIS	T. Ali, N. Jusoh, R. A. Bakar and K. Kadirgama	Malaysia
P44	LIFE CYCLE ASSESSMENT OF BIODIESEL PRODUCTION FROM USED COOKING OIL BY PYROLYSIS PROCESS	S. Tritanate and P. Reubroycharoen	Thailand
P45	LIQUID PHASE PYROLYSIS OF GIANT LEUCAENA WOOD TO BIO-OIL OVER NiMo/Al ₂ O ₃ CATALYST	P. Wattanaphawong, N. Khuhaudomlap, N. Hinchiranan, P. Kuchontara, K. Kangwansaicho and P. Reubroycharoen	Thailand

List of Session

28 May 2015

10:30-12:00	Combustion and Gasification Technology _____	27
	Bio-Fuel; Ethanol Production _____	41
	Hydrogen and Fuel Cell _____	55
	Solar Energy, Dry Sensitized, Solar Cell and Solar-PV _____	69
	Building Technology _____	83
13:45-15:00	Bio-Fuel; Biogas _____	97
	Bio Fuel; Biodiesel _____	107
	Solar Thermal/PV Technology _____	119
	Energy Policy and Economies _____	131
	Applied Energy _____	143
15:30-16:45	Applied Energy _____	143
	Wind and Wave Turbine Technology and Wind Farm _____	175
	Energy Efficiency _____	189
	Energy Efficiency, Innovation and Life Cycle Assessment _____	201

29 May 2015

10:30-12:00	Combustion, Co-Firing and Gasification _____	213
	Bio Fuel; Bioethanol _____	229
	Fuel Cell and Energy Storage _____	243
	Wind Resource Assessment _____	257
	Energy Policy; Low Carbon Society _____	271
13:45-15:00	Fuel Cell Technology _____	285
	Bio Fuel; Pyrolysis oil and Future Fuel _____	297
	Solar Heating, Cooling and Electricity _____	311
	Energy Policy and Energy Security _____	325
	Applied Energy _____	337
15:30-17:00	Bio Fuel Production Technology _____	349
	Wind, Wave and Tidal Resource Assessment _____	361
	and Conversion Technology	
	Sustainable Architecture and Building Technology _____	375
	Eco-Friendly Community and Renewable Energy _____	389
	Energy Efficiency _____	403

Combustion and Gasification Technology

GLOBAL RAINBOW REFRACTOMETRIES: TOOLS IMPROVE LIQUID FUEL COMBUSTION AS WELL TO MATER CO₂ CAPTURE BY MEA SPRAYS

Sawitree Saengkaew¹, Jantarat Promvongsa¹, Lionel Estel¹, Maria Ouboukhlik¹, Antoine Verdier¹, Bruno Renou¹, Annie Garo¹ and Gérard Gréhan¹

¹UMR CNRS 6614/CORIA, Normandie Université, Université et INSA de Rouen, France

SUMMARY: The efficient and clean use of liquid fuel (fossil or renewable) is a challenge. Among others, a key point is the mastering of the liquid evaporation which control combustion efficiency and pollution emission. The evaporation process acts on the droplet size, temperature and composition. To be able to quantify these parameters, the rainbow refractometry has been developed in several complementary configurations: standard refractometry, global refractometry, 1D refractometry as well as pulsed refractometry (FII). In this paper, the quantification of the evaporation properties of liquid fuels by rainbow refractometry are reported as well as the local characterization of the CO₂ capture by monoethanolamine (MEA) droplets.

Keywords: renewable energy, clean combustion, optical diagnostic, physical properties measurements

INTRODUCTION

Liquid fuel is largely used to produce the energy in a lot of activities: from transportation to local electricity production. Now the essential part of the liquid fuel has a fossil origin but the contribution of renewable fuels is increasing. Each of this renewable fuel, according with its origin, displays different properties (viscosity, density, evaporation rate, etc.). Accordingly, the most essential parameters for combustion optimization must be measured, to permit an optimum adjustment of the engine to the fuel properties.

This paper is devoted to the presentation of rainbow refractometry, which through several configuration permit to measure droplet temperature, composition and evaporation rate with a high accuracy. The paper is organized as follow. The next section recalls the basic of the light scattering at the rainbow angle. Then several experimental configuration based on the properties of the light at the rainbow angle are introduced. Finally exemplifying applications of rainbow setups to characterize droplet heat up, evaporation and CO₂ capture are described. In the conclusion, some perspectives are discussed.

RAINBOW REFRACTOMETRY: CONCEPT AND CONFIGURATIONS

Rainbow refractometry concept

Mathematically, a rainbow corresponds to an extremum of deviation for a ray after a finite number of internal reflections in a droplet. It is characterized by a peak of high intensity easy to identify. Its angular direction essentially depends on the value of the real part of the refractive index while its shape is dependent with the droplet size. As the refractive index is a function of the droplet composition and temperature, the measurement of the characteristic of the light scattered around the rainbow angle is a measurement of the droplet size and refractive index (i.e. of the temperature and composition).

The use of rainbow refractometry to study droplet

has been proposed by Roth et al [1]. Nevertheless, the application of rainbow refractometry on individual particle is difficult because the analysis is perturbed by the ripple structure created by the interference between the light externally reflected and one time internally reflected [2] as well as by the sensitivity of the rainbow to any disturbance from the perfect sphericity.

GLOBAL RAINBOW REFRACTOMETRY CONFIGURATIONS

To resolve these limitations, van Beeck et al introduce the global rainbow configuration [3] where a composite rainbow corresponding to the summation of all the rainbows created by all the droplets in a cloud section is recorded and processed, permitting to measure an average value of the refractive index for section of the cloud understudy. Starting from a critical analysis of the processing strategy, we propose more efficient approaches for the standard rainbow [4] as well as for global [5] rainbow techniques. The approach has been extended to be able to measure an average refractive index by class of size [6] or to measure the evolution of the average refractive index along a line [7].

APPLICATIONS

Droplet Evaporation

To measure accurately droplet evaporation rate nanometric diameter change must be measured. To reach this aim the ripple structure is included in the standard rainbow processing [4]. Moreover, to be able to follow the diameter evolution the 1-D global rainbow configuration is used [7]. As exemplify in figure 1, the 1D-global rainbow permits on one image to record simultaneously the rainbow at several position along a line. In figure 1, the 1D rainbow corresponds to N-Heptane droplet at 20°C injected at 5m/s in air at 20°C. The slope of the ripple fringes is a direct measurement of the evaporation rate. This technique permits to measure nano-metric diameter change on particles as large as 200 µm.

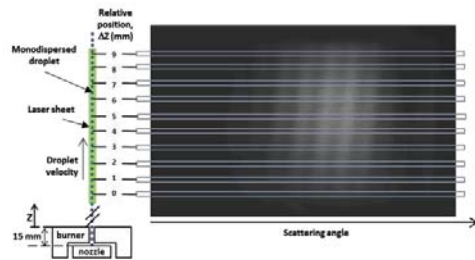


Figure 1. 1D global rainbow measurement.

Table 1 compiles the measured evaporation rate versus the distance from the droplet orifice, exemplifying the sensitivity of the technique.

Table1: evaporation rate of N-heptane droplets versus distance to orifice

Distance from orifice	Evaporation rate (m ² /s)
15 mm	$1.478 \cdot 10^{-9}$
20 mm	$1.391 \cdot 10^{-9}$
25 mm	$1.234 \cdot 10^{-9}$
30 mm	$1.260 \cdot 10^{-9}$
35 mm	$1.182 \cdot 10^{-9}$

In our presentation, application to realistic two phases swired flame will be presented.

CO₂ CAPTURE

Any combustion creates CO₂, to reduce the quantity of CO₂ rejected one of the possibility is to capture it with monoethanolamine (MEA). To increase the exchange area, the MEA can be injected as a spray. When the MEA reacts with the CO₂, carbonate is created, the refractive index value changes. Accordingly, the measurement of the refractive index is a measurement of the chemical extends [8].

In our presentation such a study will be described with a particular attention devoted to the effect of concentration gradient in the droplets.

CONCLUSION

As illustrated by the few examples above, rainbow refractometry is now a mature tool to characterize the thermo-chemical behavior of liquid droplets. Nevertheless, in all these techniques an average quantity is obtained. The extension to the measurement of the properties of each droplet of a cloud section by Fourier Interferometric Imaging (FII) will be the next development.

ACKNOWLEDGMENT

This work has been and is supported by the INTERREG Iva-E3C3 program as well as by the LABEX-EMC3, 3D program

References

- [1] N. Roth, K.Anders, A. Frohn, "Simultaneous Measurement of Temperature and Size of Droplets in the Micrometer Range". *Journal of Laser Application*, **2**, 1990, pp. 37.
- [2] N. Damaschke. "Light scattering theories and their use for single particle characterization". PhD thesis, Technische Universitat Darmstadt, December, 2003.
- [3] J.P.A.J. van Beeck, D. Giannoulis, L. Zimmer, and M.L. Riethmuller. "Global rainbow refractometry for droplet temperature measurement" *Optics Letters*, **24**, 1999, 1996-1698.
- [4] S. Saengkaew, T. Charinpanikul, C. Laurent, Y. Biscos, G. Lavergne, G. Gouesbet, and G. Gréhan. "Processing of individual rainbow signals to study droplets evaporation". *Experiments in Fluids*, **48**, 2010, pp. 111-119.
- [5] S. Saengkaew, "Study of Spray Heat Up: On the development of global rainbow techniques", PhD thesis, October 2005, Rouen University
- [6] S. Saengkaew, V. Bodoc, G. Lavergne and G. Gréhan, "Application of global rainbow technique in sprays with a dependence of the refractive index on droplet size", *Optics Communications*, **286**, 2012, 295-303
- [7] X.C. Wu, H.Y. Jiang, Y.C. Wu, Song, G. Gréhan, S. Saengkaew, L.H. Chen, X. Gao and K.F. Cen, "One-dimensional rainbow thermometry system by using slit apertures". *Optics Letters*, **39(3)**, 2014, pp. 638-641.
- [8] M. Ouboukhlik, S. Saengkaew, M.C. Fournier-Salaun, L. Estel and G. Gréhan, "Local measurement of mass transfer in a reactive spray for CO₂ capture", *The Canadian Journal of chemical Engineering*, **93(2)**, 2015, 419-426

HYDROTHERMAL CARBONIZATION AND GASIFICATION TECHNOLOGY FOR ELECTRICITY PRODUCTION USING BIOMASS

Elmar Steurer¹ and Georg Ardisson¹

¹Neu-Ulm University of Applied Sciences, Germany

SUMMARY: The concept uses agricultural residues as rice husk and rice straw as a renewable energy resource. These rice residues typically exhibit low energy density which limits an economic transportation for electrical power generation. In addition usually combustion does not make sense due to the transportation restrictions and the high contents of ash and dust. To master this challenge, the process of hydrothermal carbonization (HTC) is applied to produce bio coal as a transportable value added product with high energy density and the same caloric value as lignite. The produced bio coal can be transported to gasification units in remote villages to generate electrical base load power for mini-grids in rural communities. Furthermore the usage of the bio coal for gasification has the advantage of a clean gasification process with a very low level of ash and dust pollution. This approach could be the key to a profitable generation of electricity as the HTC carbonization facility produces enough bio coal to achieve economic efficiency while supplying remote gasification units to produce electricity for mini-grids on a reliable and steady level.

Keywords: Rural electrification, biomass, hydrothermal carbonization, gasification, mini-grids

INTRODUCTION BIOMASS PROCESSING BY HYDROTHERMAL CARBONIZATION (HTC)

The HTC conversion provides the following value-added features compared to conventional biomass gasification:

- The efficiency of this carbonization process is 66% according to practical experience undertaken so far.
- The density is increased considerably. Rice straw as a raw material has a low density of 120 kg/m³, whereas, after the HTC carbonization the density increases to 850 kg/m³. The higher density ensures easier handling, storing and transportability.
- Basically any biomass material can be converted into bio coal and nutrient water as by-product within a few hours. The wet biomass material is compressed and heated in a reactor under high pressure of 20 bar and temperatures of 200 degrees (Figure 1). Synthetic bio coal with the quality of lignite is generated after 5-12 hours.
- The HTC technology can be applied to dry as well wet biomass. Thus the energy intensive drying process of all other carbonization procedures is not necessary. Certain humidity is even desired to comply the process requirements. That is a very advantageous feature compared to other carbonization methods. Usually wet biomass is challenging to carbonize due to the high moisture content in the cellular structure affecting this process negatively.

The end product of the HTC procedure is a liquid suspension containing the bio coal particles. The remaining humidity is easy to press out mechanically. Further the excessive energy caused by the exothermal process is used to dry the bio lignite to a humidity level of about 10% which is suitable for gasification purposes.

THE HTC&G CONCEPT - INTEGRATION OF THE HTC TECHNOLOGY WITH GASIFICATION UNITS

Due to its key features – usage of wet biomass and generation of a high-value end product on a large scale - the HTC-carbonization of rice residues and gasification of the produced synthetic bio coal is considered for an integrated approach. This HTC&G concept consists of two components:

On a first stage synthetic bio coal is produced by the hydrothermal carbonization process (HTC technology) in a site with a capacity of 4,000 tons per year to achieve a competitive product with high energy density.

On a second stage the produced synthetic bio coal is used as a fuel in gasification units located in villages alongside to the HTC facility to produce electricity.

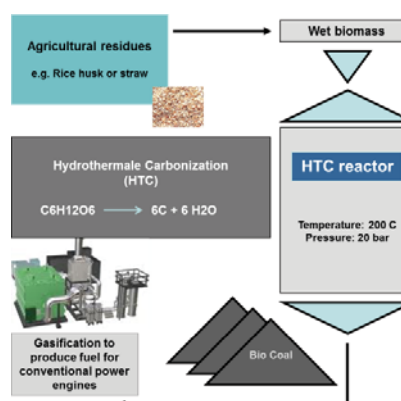


Figure 1. HTC&G carbonization scheme

In such a way the quality of the rice residues as a renewable energy resource is improved to meet the demand of gasification units for rural electrification

purposes. This is the core idea of the proposed two-stage approach (Figure 2). Rice residues transportation is done on the conventional way to supply one HTC carbonization unit. The transportation costs of the produced bio coal to villages for gasification purposes are significantly lower due to the higher density of the produced bio coal.

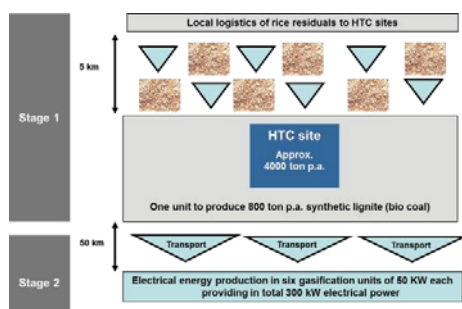


Figure 2. The HTC&G concept for rice residues

BUSINESS VALUATION

The economic rationale depends largely on regional conditions. As an example the business valuation is conducted in the case of the Philippines with following assumptions:

- Total investment costs for the HTC&G facility with a capacity of 4,000 tons of rice residues yearly (16 tons daily) account for USD 1.5 mln, whereas HTC capital requirement amounts to USD 0.9 mln. according to the German company Grenol based on their own experience. The investment costs for the gasification sites of USD 0.6 mln are given by the power price for a conventional gasifier of roughly 2000 USD/kW.
- Yield of 350 tons rice and 250 tons rice residues per km².
- Material costs for rice husk of 1.15 Phil Peso/kg (3 USD-ct/kg).
- Transportation costs for rice residues of 6 USD per ton.
- Labour costs of 14 USD (700 peso) daily for one worker in the HTC site. The required work force is assumed to be three for the HTC site and two workers for each of the assumed six decentralized gasification units.
- Transportation costs for the produced bio coal of 1 USD per km by assuming an average distance of 25 km from the HTC site to the gasification units on average and 8 tons vehicle transport.

Taken together the HTC converts 4,000 tons of rice residues into roughly 800 tons synthetic bio coal. The conversion increases the caloric value by 70%. Gasification of the produced synthetic bio coal generates 1.7 GWh electrical energy per year based on six power stations of 50 kW each assuming 6,000 hours of usage per year and an efficiency rate of 35%. The assumptions lead to total costs of roughly

280,000 USD, whereas depreciation over 20 years amounts to 74,000 USD yearly.

Of specific importance are the levelized costs of electricity (LCOE) split into operating expenditure (OPEX) costs and capacity expenditure (CAPEX) costs. Based on a lifetime of 20 years and a discount rate of 10% the LCOE amounts to 0.22 USD/kWh whereas CAPEX costs are 0.10 USD/kWh and OPEX costs 0.12 USD/kWh. This result makes clear, that the proposed technology provides significant cost advantages compared to the costs of widely used Diesel Gensets as of 0.35 USD/kWh typically. Furthermore the technology is highly competitive from the beginning on as the LCOE of 0.22 USD/kWh is comparable to the electricity tariff of national grids. Based on this LCOE the annual revenues would account for roughly 380,000 USD and a sound profitability in terms of an EBIT of 100,000 USD corresponding to a return of investment (ROI) of 7% could be achieved.

CONCLUSION

This paper introduces a concept to use rice residues for electrical power generation by applying the hydrothermal carbonization technology combined with gasification units (HTC&G concept). The proposed two-step approach takes into account the dispersed availability of biomass and its low energy density as well as the necessity of an economic generation of electricity. The HTC&G concept makes it possible to replace fossil resources of energy economically without subsidies. Unused biomass like rice straw can be used effectively and environmental friendly. Furthermore applying the HTC&G concept on a local level avoids negative environmental effects in terms of transportation efforts and dust pollution of a large scale carbonization. Finally and most remarkable employment for rural people is created. Accordingly there is social and economic benefit using this concept for countries such as Bangla Desh, India, Indonesia, Myanmar, the Philippines, Thailand and Vietnam.

References

- [1] A. Jain. "Design Parameters for a Rice Husk Throatless Gasifier. *Agricultural Engineering International: the CIGR Ejournal*, 8,2006
- [2] S. Ghosh, S. Mahapatra and D. Deka. "Techno-Economic Analysis of Biomass briquetting Technology for Rural Entrepreneurship: A Case Study". *Proceedings of the International Conference on Renewable Energy for Rural Development*. Dhaka, Bangladesh; 2002, pp. 255-257.

STATUS OF USING BIOMASS GASIFICATION FOR HEAT AND POWER IN THAILAND

Krongkaew Laohalidanond¹, Palita Chaiyawong¹, Somrat Kerdsuwan¹

¹ The Waste Incineration Research Centre,
Department of Mechanical and Aerospace Engineering, Faculty of Engineering,
King Mongkut's University Technology North Bangkok, Bangkok, Thailand

SUMMARY: Nowadays the fossil fuel plays a significant role on the global energy supply and demand. Many non-oil producer and agricultural countries have set the target of biomass utilization as alternative energy in their energy policy plan. Gasification is one of the promising technologies to convert biomass to heat and power. However, this technology has faced many challenges, e.g. high capital cost, low energy conversion efficiency, etc. As Thai's government has promoted the using of biomass as alternative energy and has financially supported the use of agricultural residue for heat and power production in 12 pilot projects, this study will review the current status of the gasification technology used in the projects and conduct the performance test in terms of feedstock consumption rate, producer gas yield, heating value of producer gas and thermal efficiency. The feedstock used consists of residues from wood, corncob, palm, etc. 4 projects use producer gas for power generation with the capacity range from 250 to 300 kW_e and 8 projects to produce heat for using in ceramic industry, fertilizer drying, hotel, etc. From the study, the downdraft air gasification technology is suitable for a small scale heat and power production. The heating value of producer gas ranges from 1.89 to 5.89 MJ/Nm³ and the thermal efficiency of 76.96% can be reached.

Keywords: Gasification, Renewable Energy, Heat and Power Production, Performance Evaluation

INTRODUCTION

The global economic and social development relies on the energy available. Vice versa, a security of energy supply in each country will guarantee sustainable development, economic growth and quality of life. As a result of economic growth, urbanization and social development, the world energy demand has increased continuously during the last decades. There are commonly two categories of energy sources: fossil fuels and non-fossil fuels. Fossil fuels include coal, oil, and natural gas which have limited reserves, while non-fossil fuels are hydro, nuclear, biomass and waste, as well as other renewable energy sources, e.g. wind and solar, which are available in nature. Because the utilization of non-fossil energy sources has faced many challenges in terms of high capital expenditure, low energy conversion efficiency, high environmental impacts, and difficulty in the implementation depending on the type of non-fossil energy sources [2-4], nowadays fossil fuel plays a significant role on the global energy supply and demand. The share of non-fossil fuel is still behind the share of fossil fuel, 13.1% of non-fossil fuel in world energy consumption compared to 86.9% of fossil fuel in 2012 [1]. As biomass is the residue derived from agricultural or industry sector which is enormously available in many agro-based countries, it is considered as the main non-fossil fuel source for heat and power production. Many countries, especially non-oil producer countries and agricultural countries have set the target of biomass utilization as alternative energy in their energy policy plan. The European Union (EU) Member States' National Renewable Energy Action Plans (NREAPs) targets to increase the use of solid

biomass and forestry biomass to 36% of the EU renewable energy by 2020 [5]. Likewise, many Asian countries have also boosted the utilization of biomass as a renewable energy source in these countries. The electricity from bioenergy of 6,000 MW, 3,630 MW, 810 MW and 170 MW is targeted in China, Thailand, Indonesia, and the Philippines, respectively. Thai's government has promoted the using of biomass as alternative energy and has financially supported the use of agricultural residue for heat and power production in 12 pilot projects, this study will review the current status of the gasification technology used in the projects and conduct the performance test in terms of feedstock consumption rate, producer gas yield, heating value of producer gas and thermal efficiency.

METHODOLOGY

Current Gasification Technology

The information of gasification technology, feedstock used and designed consumption rate as well as designed capacity for heat and power production of the targeted pilot projects are collected by site surveying and questionnaires.

Performance Test

The performance test begins with the investigation of feedstock properties in terms of proximate and ultimate analysis as well as heating value. The proximate and ultimate analysis is determined according to ASTM and the heating value is measured by bomb calorimeter. The gasification process is continuously run for 30 hr in some pilot projects, in order to determine the feedstock consumption rate, producer gas yield, heating value of producer gas, thermal efficiency of

the gasification process and overall efficiency in case of power production.

RESULTS AND DISCUSSION

Current Gasification Technology

Twelve pilot projects of biomass gasification was proposed and constructed in the different province in Thailand. The feedstock used consists of residues from wood, corncob, palm, and etc. This feedstock is converted to producer gas via a gasification process. The downdraft gasifier is commonly used as the promising technology. However, the updraft gasifier or a plasma torch gasifier is installed in some projects. Four projects use producer gas for power generation with the capacity range from 250 to 300 kW_e and 8 projects to produce heat for using in ceramic industry, fertilizer drying, hotel, etc. Table 1 shows the detail of each pilot project.

Table 1. Detail of each pilot project

No	Province	Feedstock	Feedstock consumption rate (kg/hr)	Energy Production
Pilot projects for power production (kW _e)				
1	Cha Soeng Sao	Wood from fast growing plant	-	250
2	Roi Et	Corn cob	-	300
3	Utharadit	Wood chip	400	260
4	Nakorn Ratchasima	Eucalyptus bark	-	250
Total power production (kW _e)				1,060
Pilot projects for heat production (toe/year)				
5	Kanchanaburi	Wood barks and leaves	50	25
6	Pathum Thani	Wood from fast growing plant	100	84
7	Nhong Kai	Wood chip, mix biomass from corn cob, bagasse, rice straw	100	60
8	Udonthani	Wood chip, mix biomass from corn cob, bagasse, rice straw	100	60
9	Lampang	Agricultural residues in community	380	205
10	Trang	Palm oil empty fruit bunch, rice husk, corn cob, cassava rhizome, wood chip	200	132
11	Chonburi	Corn cob, wood chip	200	115
12	Nakhon Pathom	Coconut shell, coconut fiber	300	192
Total heat production (toe/year)				873

From the performance test, it is found that the actual feedstock consumption is less than the design criteria. The heating value of producer gas from gasification process with steam as gasification agent is slightly higher than that of producer gas from air

gasification, as shown in more detail for some pilot projects in Table 2. In summary, the downdraft air gasification technology is suitable for a small scale heat and power production. The heating value of producer gas ranges from 1.89 to 5.89 MJ/Nm³ and the thermal efficiency of 76.96% can be reached.

Table 2. Performance test of some pilot projects

No	Actual feedstock consumption rate (kg/hr)	Producer gas yield (Nm ³ /hr)	Heating value of producer gas (MJ/Nm ³)	Thermal efficiency (%)	Overall efficiency for power production (%)
1	300	1000	4.0 (air) 5.4 (steam)	78.82 (air)	14.5
5	16.5	137	1.89	-	-
6	75	140	5.04	65.3	-
9	98-262	224.65-409.9	4.53-5.89	36.3-76.96	-
11	84.3	252	5.3	62.59	-

ACKNOWLEDGMENT

The authors would like to thanks the National Innovation Agency (NIA) for financial support, the Waste Incineration Research Center (WIRC) as well as Department of Mechanical and Aerospace Engineering (MAE), Faculty of Engineering, Science and Technology Research Institute, King Mongkut's University of Technology North Bangkok for any kinds of cooperation.

References

- [1] BP Statistical Review of World Energy June 2013, Available online at: <http://www.bp.com/en/global/corporate/about-bp/energy-economics/statistical-review-of-world-energy-2013.html>, Accessed on 12 Jan 2014.
- [2] World Energy Resources 2013 Survey: Summary, World Energy Council, Available online at: http://www.worldenergy.org/wpcontent/uploads/2013/09/Complete_WER_2013_Survey.pdf, Accessed on 12 Jan 2014.
- [3] O. Ozyurt, "Energy issues and renewables for sustainable development in Turkey", *Renewable and Sustainable Energy Reviews*, **14**, pp. 2976–2985, 2010.
- [4] A.J. Waldau, M. Szabó, N. Scarlat and F. M. Ferrario, "Renewable electricity in Europe", *Renewable and Sustainable Energy Reviews*, **15**, 2011, pp. 3703-3716.
- [5] B. Atanasiu, "The role of bioenergy in the National Renewable Energy Action Plans: a first identification of issues and uncertainties", Institute for European Environmental Policy. Available online at: http://www.ieep.eu/assets/753/bioenergy_in_NREAPs.pdf, Accessed on 14 Jan 2014.

MUNICIPAL SOLID WASTE CHARACTERISTICS AND GREEN AND CLEAN ENERGY RECOVERY IN ASIAN MEGACITIES

Krongkaew Laohalidanond¹, Somrat Kerdsuwan¹ and Palita Chaiyawong¹

¹ The Waste Incineration Research Centre,
Department of Mechanical and Aerospace Engineering, Faculty of Engineering,
King Mongkut's University Technology North Bangkok, Bangkok, Thailand

SUMMARY: The population growth, the economic prosperity and the urbanization lead to increase in Municipal Solid Waste (MSW). The higher populated and the higher income countries generated the higher amount of MSW. Not only MSW amount, the MSW composition can also be diverse in different countries. This study will investigate the composition of MSW generated in Bangkok compared to other Megacity of Asian countries, for example, Tokyo, Seoul, Taipei, Singapore and Hong Kong. In addition, the MSW management model integrated with Waste-to-Energy (WtE) will be analysed and compared. With Bangkok as the case study, by the lack of regulations and public participations, there is no MSW separation at sources; hence, MSW generated contains higher organic waste which results in less calorific value of MSW compared to other developed countries. The mixed wet MSW is the main shortcoming of WtE development. As Bangkok is the main MSW producer in Thailand which generates more than one-fourth of domestic MSW, the WtE project is developed in Bangkok as a demonstration plant of WtE. The 500 ton per day incineration plant coupled with power generation unit has been constructed for sustainable MSW disposal and for energy security in Mega city.

Keywords: Municipal Solid Waste, Waste to Energy, MSW Management, Mega-city, Waste's characteristic

INTRODUCTION

Municipal Solid Waste (MSW) is non-hazardous substance generated from routine activities of human life. Sources of MSW can be household, industrial, commercial and institutional sectors, markets, yards and streets [1]. The population growth, the economic prosperity and the urbanization lead to increase in Municipal Solid Waste (MSW). It was estimated that the global MSW amount will increase from 1.3 billion ton in 2012 to 2.2 billion ton in 2025 [2]. Considering the MSW generation rate by countries, it can be remarked that the higher income countries generated the higher amount of MSW per capita, e.g. the lower income countries has an average MSW generation rate of 0.6 kg/capita/day, while the high income countries generate averagely 2.1 kg/day of MSW per capita [2]. This will lead to the different amount of MSW in each country. Not only MSW amount, the MSW composition can also be diverse in different countries depending on the life-style behaviour and the countries' income. The low income countries produce more organic wastes in MSW (approximately 64%-wt. of MSW), in contrast MSW generated from the high income countries contain the less organic waste (28%), as detailed in Table 1 [2]. These physical compositions are the key drivers for decision making of the MSW disposal technology and WtE technology [4].

As Bangkok is the main MSW producer in Thailand which generates more than one-fourth of domestic MSW, this study will investigate the physical and chemical composition of MSW generated in Bangkok compared to other Megacity of Asian countries, for example, Tokyo, Seoul, Taipei, Singapore and Hong Kong. In addition, the MSW management model integrated with Waste-to-Energy

(WtE) will be analysed and compared.

Table 1. The physical composition of MSW by countries' income [2]

Physical composition (%-wt.)	Country's income levels			
	Low income	Lower middle income	Upper middle income	High income
Organic waste	64	59	54	28
Paper	5	9	14	31
Plastic	8	12	11	11
Glass	3	3	5	7
Metal	3	2	3	6
Others	17	15	13	17

METHODOLOGY

Quantity of MSW in Megacity

Bangkok is the capital city of Thailand with the enormous population of approximately 10 million, by which Bangkok can be considered as megacity, similar to Tokyo, Seoul, Taipei, Singapore and Hong Kong. Currently, more than 9,000 ton per day of MSW generated in Bangkok and MSW amount generated in Bangkok will be predicted by Eq. 1.

$$W_{\text{gen}} = \frac{W_{\text{total}}}{P_0} \quad (1)$$

W_{gen} is the waste generation rate per capita, W_{total} represents the total amount of waste generation and P_0 is the population in the current year. The growth in population can be determined by the geometric curve based on the statistical data in last 10 year, as shown in Eq. 2 and the amount of waste generation in next 20 years was also calculated by Eq. 3 [2].

$$P_n = P_0 (1+r)^n \quad (2)$$

$$W_{\text{total},n} = P_n \times W_{\text{gen}} \quad (3)$$

P_n is the population in n^{th} -year; r is the population increasing rate per year.

Physical Characterization of MSW

The physical composition, e.g. organic waste, plastic, paper, textile, etc. of MSW will be investigated by quartering method and compared to other megacity.

WtE Development in Megacity

The suitable WtE for megacity will be selected according to the following criterion:

- Practicability and performance,
- Economics,
- Maturity of technology
- Technological self-reliance,

Thereafter, the conceptual design of prototype scale will be conducted based on the capacity of 500 ton per day.

RESULTS AND DISCUSSION

Quantity of MSW in Megacity

In 2013, there was 9,523 ton per day of MSW generated from registered and non-registered population, as well as excursionists which produce minor amount of MSW. This amount is correspondence to the MSW generation rate of 1.10 kg/day/capita which is almost similar to the MSW generation rate in other megacities, listed in Table 1.

Table 1. MSW generation rate in megacities [5, 6]

Megacity	MSW Generation Rate (kg/day/capita)
Bangkok	1.04-1.18
Hong Kong	1.27-1.36
Seoul	0.95-1.08
Singapore	0.96-1.10
Tokyo	0.77-1.03

The number of MSW will be increased to approximately 10,100 ton per day in the next 20 years, which an increasing rate of 0.3 % each year.

Physical Characterization of MSW in Megacity

Table 2 compares the physical composition of MSW generated in Megacity. From Table 2, it can be seen that the physical composition of MSW generated within Bangkok is almost similar to MSW generated in Hong Kong, where its composition is absolutely different from MSW generated in Seoul, Singapore and Tokyo. This is because of the effective MSW segregation at source in Seoul, Singapore and Tokyo.

WtE Development in Megacity

As the MSW in Megacity consists of more than 80%-wt. of combustible material, the incineration technology is considered as proper WtE technology. Anyway, the shortcoming for Bangkok and Hong Kong is the high organics waste which lead to the high moisture content and the low

heating value. For the conceptual design, the 500 ton per day incineration plant coupled with power generation unit has been constructed for sustainable MSW disposal and for energy security in Bangkok as the prototype model.

Table 2. MSW Characterization in Megacities in %-wt. [6, 7, 8]

Composition	Bangkok	Hong Kong	Seoul	Singapore	Tokyo
Organic waste	49.85	44.0	23.3	27.2	31.3
Paper	8.55	23.0	34.63	21.2	44.5
Plastic	28.49	18.0	16.80	11.5	7.8
Glass	3.74	3.0	11.40	1.0	1.2
Metal	1.43	2.0		14.6	1.2
Textile and other	7.94	10.0	13.87	24.5	14.0
Total	100	100	100	100	100

ACKNOWLEDGMENT

The authors would like to thanks the Bangkok Metropolitan Administration (BMA) for financial support, the Waste Incineration Research Center (WIRC) as well as Department of Mechanical and Aerospace Engineering (MAE), Faculty of Engineering, Science and Technology Research Institute, King Mongkut's University of Technology North Bangkok for any kinds of cooperation.

References

- [1] P. Schübeler, K. Wehrle and J. Christen, "Conceptual Framework for Municipal Solid Waste Management in Low-Income Countries", World Bank, 1996.
- [2] D. Hoornweg, P. Bhada-Tata, "WHAT A WASTE - A Global Review of Solid Waste Management", World Bank, 2012.
- [3] AIT/UNEP, Municipal waste management report: Status-quo and Issues in Southeast and East Asian Countries, 2010.
- [4] World Bank, 1999, Decision Makers' Guide to Municipal Solid Waste Incineration, World Bank.
- [5] Sustainable waste management, Strengthening waste reduction: Is waste charging an option?, Available online at: <http://www.gov.hk/en/residents/government/publication/consultation/docs/2012/MSW.pdf>, Accessed on 22 Jan 2015.
- [6] A.V. Shekdar, "Sustainable solid waste management: An integrated approach for Asian countries", *Waste Management*, **29**, 2009, pp. 1438-1448.
- [7] T. Karak, R. M. Bhagata and Pradip Bhattacharyab, "Municipal waste generation, composition, and management: The world scenario", *Critical Reviews in Environmental Science and Technology*, **42**, 2012, pp. 1509-1630.
- [8] C. Ryu, "Potential of Municipal Solid Waste for Renewable Energy Production and Reduction of Greenhouse Gas Emissions in South Korea", *Journal of the Air & Waste Management Association*, **60**, 2010, pp. 176-183.

EVALUATION OF HYDROTHERMAL TREATMENT OF EMPTY FRUIT BUNCH (EFB) FOR SOLID FUEL AND LIQUID ORGANIC FERTILIZER CO-PRODUCTION

Anissa Nurdiawati¹, Srikandi Novianti¹, Ilman Nuran Zaini¹, Bakhtiyor Nakhshinieva¹, Hiroaki Sumida² and Kunio Yoshikawa¹

¹Department of Environmental Science and Technology, Tokyo Institute of Technology, Japan

²Laboratory of Soil Science, Department of Chemistry and Life Science, Nihon University, Japan

SUMMARY: The hydrothermal treatment (HT) has demonstrated the ability to improve fuel characteristics of biomass. On the other hand, the liquid by-product, which potentially contains solubilized nutrient, is being poorly utilized. This paper presents an investigation of hydrothermal treatment (HT) of EFB on both solid and liquid product characteristics. In this work, the effects of the HT of EFB were investigated at the temperatures of 100, 150, 180 and 220°C with the holding time of 30 minutes. The results showed that HT can increase carbon content, remove up to 55% of ash content from the EFB, lowering potassium and chlorine content to 0.84% and 0.18%, respectively. Moreover, maximum of 37% of nitrogen, 65% of potassium and less than 10% of phosphorus in EFB were dissolved into the liquid product which positively correlated with the HT temperature. These results demonstrate the possibility of employing the HT for obtaining solid fuel as well as nutrient cycling.

Keywords: EFB, HT, co-production, solid fuel, liquid organic fertilizer

INTRODUCTION

The palm oil production is one of Southeast Asia's major agricultural industries. Total global production of palm oil is estimated at over 45 million tons, with Indonesia and Malaysia as major world producers and exporters [1]. However, there is a concern about its environmental impacts since the industry also produces an abundance amount of waste. Empty fruit bunch (EFB) is the major by-product of the palm oil industry which is being acknowledged for energy production. However, raw biomass materials have low bulk density, high moisture content, and low calorific value which limit its ease of use [2]. Therefore, biomass pre-treatment is needed to obtain better solid fuel characteristics of EFB.

The hydrothermal treatment (HT) is known for converting high moisture content solid wastes into dried, uniform, pulverized, and higher energy density solid fuel. However, from HT process of EFB liquid residue was also obtained. To date, the liquid residue is regarded as wastewater, and there is limited investigation on the utilization of this liquid product. It was revealed the HT can transport nutrient components in biomass into a liquid product [3]. This nutrient source can be used as an organic fertilizer. Therefore, this paper deals with the evaluation of solid product as a fuel and liquid residue characterization for liquid organic fertilizer by employing HT.

METHODOLOGY

The experimental apparatus setup consists of a 500 ml batch type autoclave reactor. In this experiment, 20 grams of EFB and distilled water in 1:10 biomass-water ratio was supplied to the reactor. The reactor temperature was set at 100, 150, 180, 220°C, respectively, with the holding time of 30 minutes. Elemental analysis and HHV were

determined for the solid product. Total organic carbon, total NPK, micronutrient, pH, EC measurement and seed germination test was performed for the liquid products.

RESULTS AND DISCUSSION

Fuel properties of solid product

The chemical characteristics of raw and hydrothermally treated EFB are presented in Table 1. HT denotes for the hydrothermally treated sample. Due to increasing carbon content, the HHV is also slightly increased. HT-220 has a heating value which almost equal to low-grade sub-bituminous coal (approximately 20 MJ/kg [4]). From Table 1, it can be seen that ash content was reduced by 55% from 4.9% to 2.25% (dry wt) at HT-180. Table 1 also shows that chlorine and potassium content, which mostly exists in water-soluble form, can be removed up to 73% and 74%, respectively, after HT. High removal of alkali metals can reduce the deposition tendency in the biomass combustion. Higher reaction temperature produces relatively higher HHV especially at HT-220, but considering energy yield, energy requirement and ash content of the product, HT at 180°C seems more favorable for the large-scale production of solid fuel from EFB.

Main nutrient in the liquid product

Primary macronutrients for plant growth, are nitrogen (N), phosphorous (P), and potassium (K). During HT, these elements solubilize into the liquid product. Solubilization ratio defined as the ratio of the initial sample content minus the treated sample content divided by the initial sample content [3].

Table 1. Chemical properties of raw EFB and HT solid products

Element	Weight Percentage (wt%), dry				
	Raw	HT-100	HT-150	HT-180	HT-220
Ash	4.9	4.6	3.4	2.2	4.1
C	43.56	44.07	45.25	46.43	49.98
H	5.34	5.24	5.51	5.57	5.38
N	0.56	0.79	0.59	0.4	0.77
S	0.11	0.08	0.09	0.03	0.09
Cl	0.67	0.23	0.26	0.18	0.5
O (diff)	44.86	44.99	44.9	45.19	39.18
K (%DM)	3.24	1.46	1.48	0.84	0.9
HHVdry (MJ/kg)	16.76	16.81	17.57	18.05	19.65
Energy yield ^a		79%	80%	82%	66%

^a (HHV product x mass yield)/HHV raw

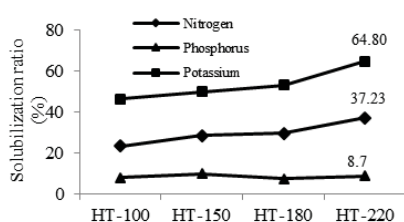


Figure 1. N, P, K solubilization ratios

From Fig. 1. N, P, and K solubilization linearly increased as the reaction temperature was increased, especially for K. However, macronutrients concentration value was still considerably low compared with commercial liquid fertilizer.

Chemical properties of liquid product

The optimum value of pH is ranging from 5.5-8.5 at which plants can best take up nutrients applied to the root and foliage [5]. During HT, the degradation of hemicellulose, cellulose, and extractives produces concentrated sugars and organic acids which dissolved in water. The organic acids produced cause a drop in pH of liquid extract phase as low as 4.1 at HT-220.

The correlation between HT temperature and EC shows an increasing trend. From Table 2, all samples show very high EC which can result in slower plant growth even plant damage.

It can be seen from Table 2 that as the HT temperature increase, more carbon compounds in the liquid phase resulted in higher C/N ratio. Even for HT at the lowest temperature, the C/N ratio is around 20 which indicate that decomposition of organically bound nutrients to an inorganic form will occur at a slower pace.

A phytotoxicity test employing seed

germination index (GI) was used to evaluate phytotoxicity of the liquid product. No germination was found at all liquid HT-220 even after dilution to lower concentration. It might be due to the formation of potentially toxic substances like phenols, furfurals, and their derivatives at treatment temperature high enough for lignin and sugar degradation. Dilution to lower concentration has a tendency to increase the GI which implies the decreasing of harmful effect of liquid HT. Further deeper investigation and improvement of liquid residue performance are still needed prior being applied for the agricultural purpose.

Table 2. Chemical properties of liquid product

Sample	Parameters		
	pH	EC (dSm ⁻¹)	CN Ratio
HT-100	6.6 ± 0.0	5.4 ± 0.0	19.9
HT-150	5.9 ± 0.0	6.2 ± 0.0	18.7
HT-180	5.0 ± 0.0	7.0 ± 0.0	29.9
HT-220	4.1 ± 0.0	9.0 ± 0.0	34.2

CONCLUSION

The hydrothermal treatment experiment for EFB was performed in order to evaluate the characteristics of solid product as fuel and liquid by-product as an organic fertilizer. The reaction temperature was important operating parameters to obtain a usable solid fuel as well as nutrient solubilization to the liquid phase. HT can remove up to 55% of ash and lowering potassium and chlorine to 0.84% and 0.18%, respectively. By considering energy yield, ash content of the product, and energy requirement, HT at 180°C seems more favorable for the large-scale production of solid fuel from EFB. On the other hand, nutrient solubilization linearly increased as the reaction temperature was increased. However, HT conducted at higher than 180°C result in low pH, high EC and C/N ratio which might give poor performance if directly applied to the plant.

References

- [1] World growth, "The economic benefit of palm oil to Indonesia", 2011.
- [2] B. Arias, C. Pevida, J. Feroso, M.G. Plaza, F. Rubiera and J.J. Pis, "Influence of torrefaction on the grindability and reactivity of woody biomass", *Fuel Processing Technology*, **89(2)**, 2008, pp. 169-175.
- [3] X.H. Sun, "Effects of hydrothermal process on the nutrient release of sewage sludge", *Int J Waste Resources*, **3(124)**, 2013.
- [4] American Society for Testing and Materials. In: Part 26 gaseous fuels: coal and coke. Philadelphia (USA): Annual Book of ASTM Standards 1999
- [5] M.E.F. Silva, L.T. Lemos, M.M.S.M. Bastos, O.C. Nunes and A.C. Cunha-Queda, "Recovery of humic like substances from low quality composts", *Bioresour. Technol.* **128**, 2013, pp. 624-632.

APPROACH OF USING CORN RESIDUES AS ALTERNATIVE ENERGY SOURCE FOR POWER PRODUCTION: A CASE STUDY FOR CORN FROM NORTHERN PLAIN AREA OF THAILAND

Krongkaew Laohalidanond¹ and Somrat Kerdsuwan¹

¹ The Waste Incineration Research Centre,
Department of Mechanical and Aerospace Engineering, Faculty of Engineering,
Science and Technology Research Institute,
King Mongkut's University Technology North Bangkok, Thailand

SUMMARY: The whole supply chain management of using corn residue as alternative fuel in agricultural countries will be investigated in this study. Since there are substantial corn residues in the agricultural countries, while corncobs completely utilized as fuels for heat production, corn trash/skin and stem are leftover or burnt on field without energy recovery because they are bulky and non-uniform with high moisture content. In order to use these residues as solid fuel, the pre-treatment is necessary to improve the fuel properties. This pre-treatment are drying, grinding and pelletizing which can be done on field or centralized plant. Regarding to economic analysis including raw material cost, collection cost, transportation cost and pre-treatment cost, the total cost of solid fuel from corn trash/skin and stem is estimated to be 17.6-31.6 US\$ per ton depending on the pelletizing capacity. These bio-pellets can easily be transported and used as feedstock for heating or power generation by direct combustion, co-firing or gasification technology.

Keywords: Municipal Solid Waste, Sustainable Development, MSW Management, Low Income Countries

INTRODUCTION

The world economy is key driver for global primary energy consumption. Although the economic recession during the last recent years resulted in the slow increasing rate of world primary energy consumption, the world primary energy demand, especially crude oil, natural gas and coal, still increases enormously from the last decades. These fuels are fossil fuel which can be diminished in the future. Beyond the fossil fuel diminishment, the utilization of fossil fuel will lead to an increase in carbon dioxide in the atmosphere and the high concentration of carbon dioxide causes the greenhouse effect and consequently, the global warming which becomes the serious problem for human race. One alternative to solve the problem of fossil fuel diminishment and global warming is to use the biomass as substitute fuel. In most of developing countries, there are abundant agricultural residues which can be used as fuel. Corn is the agricultural product which can be grown in many countries throughout the world. It was reported by the International Grain Council [1] that the global corn production in the crop year 2012/13 was accounted for 860.5 million tons and it was increased to 984.3 million tons in crop year 2013/14. It can be evidenced that the corn production is continuously increased for utilization as food, e.g. beverage and alcohol, high fructose corn syrup, starch, cereals, sweeteners, as well as animal feed [2]. The high population of corn leads to a plenty amount of corn residues leftover on field after harvesting. Although corn residues can be leftover on field for fertilizer, the excessive corn residue may reduce soil temperature and delay germination, as well as in case of corn residue

contacts with corn seedling roots, it may have a toxic effect, resulting in the stunting of plants [3]. Hence, the corn residue should be removed from field. The commercial use of corn residues is ethanol production or it can be used as solid fuel for steam and electricity production via combustion and gasification technology [4]. However, corn trash/skin and stem are leftover or burnt on field without energy recovery in some rural region because they are bulky and non-uniform which cause the difficulty in transportation. Considering the fuel property, corn trash/skin and stem contain high moisture content and, consequently, low heating value which is not good property when they are used as fuel. This study will focus on the supply chain management of solid fuel production from corn trash/skin and stem in rural region where is difficultly accessible by mass transportation. Two provinces in Northern Thailand - Nakorn Sawan and Petchchaboon - were used as the model in this study.

METHODOLOGY

Fuel Characteristics of Corn Residues

The sample of corn residues will be taken from source. Then it will be prepared by drying and grinding for analysis. The chemical composition and the heating value are analyzed according to ASTM [3].

Supply Chain Management of Bio-pellet production from Corn Residues

The supply chain management of Bio-pellet production from corn residues covers the collection and transportation of residues until the processing of corn residues into solid bio-fuel.

Cost Estimation of Bio-pellet

Cost estimation will provide the final cost of bio-pellet produced from corn residues. This includes the cost of residues, cost of harvesting and collection, cost of transportation and cost of pellet production. All sub costs can be obtained by interviewing and site surveying.

RESULTS AND DISCUSSION

Fuel Characteristics of Corn Residues

The residues derived from corn cultivation can be separated into corn cob and trash/skin/stem. Corn cob is the residues left over after the removal of corn grains. Corn grains can be removed at cultivation plant by special machine or cobs can be delivered to the corn mills and corn grains can be extracted at mill. Hence, corn cob can be left over both at fields or at corn mills. In contrast to corn cob, trash/skin/stem is always left over at field. From the fuel characterization, corn cob and trash/skin/stem has higher heating value ranges from 15-16 MJ/kg for corn cob and 13-15 MJ/kg for trash/skin/stem. After harvesting for 2 weeks, moisture content of corn cob is less than 10%, where the moisture content of trash/skin/stem varies from 6% to 12%, as shown in Table 1.

Table 1. Fuel Characteristics of Corn Residues

	Petchaboon		Nakom Sawan	
	Trash/ Skin/ Stem	Corn cob	Trash/ Skin/ Stem	Corn cob
Proximate analysis				
Moisture content ¹ (%)	6.12	9.97	11.90	9.94
Volatile matter ² (%)	73.35	83.13	78.85	84.71
Ash ² (%)	7.20	1.98	5.60	2.33
Fixed carbon ² (%)	19.45	14.89	15.55	12.96
Ultimate analysis ² (%)				
Carbon (C)	44.53	44.83	44.65	47.00
Hydrogen (H)	5.88	6.01	6.50	6.55
Oxygen (O)	42.16	47.07	46.18	44.75
Nitrogen (N)	0.17	0.05	2.68	1.66
Sulfur (S)	0.047	0.056	0.027	0.055
HHV (kJ/kg)	14,975	15,073	13,157	16,093

¹ as received basis (after 2 week harvesting)

² dry basis

Supply Chain Management of Bio-pellet Production from Corn Residues

Because the geography of rural area is difficultly accessible which limit the collection by large machines, the manual collection is the most suitable method. By manual collection, trash/skin/stem should be left on field for 1 week until its moisture content can be reduced to 15%. After collection from field, corn trash/skin/stem should be piled up and to facilitate the handling. The most suitable way to transport corn residues is agricultural truck in short distance. Prior to using corn residues as fuel, the processing, e.g. drying, grinding and pelletizing of corn trash/skin and stem is necessary to improve the properties of corn trash/skin and stem to be used

as solid fuel. This processing unit can be install in field or centralized, as shown in Table 2, which include a 100 kg/h for on field processing unit as well as a 1 t/h and 2 t/h for centralized system unit.

Table 2. Detail of Processing Unit for on field processing unit and for centralized system

Detail	2 t/h Unit	1 t/h Unit	100 kg/h Unit
Shredder	50 hp 380 Volts	30 hp 380 Volts	3 hp 220 Volts
Screw Conveyor	3 hp 380 Volts 6 in. wide 6 m long	2 hp 380 Volts 6 in. wide 6 m long	
Pelleting Machine	147 hp 380 Volts	60 hp 380 Volts	10 hp 220 Volts
Size of Bio-pellet	Diameter 6-10 mm 10-30 mm long	Diameter 6-10 mm 10-30 mm long	Diameter 6-10 mm 10-30 mm long
Belt Conveyor	3 hp 380 Volts 50 cm wide 6 m long	3 hp 380 Volts 50 cm wide 6 m long	

Cost Estimation of Bio-pellet

The total production cost of bio-pellet from corn trash/skin/stem depends on the scenarios. For scenario 1 where the 100 kg/h processing unit is located on-field (decentralized), the production cost is 56.8 US\$ per ton. For scenarios 2 and where the 1 t/h and 2 t/h processing unit is established centralized, the production cost is 50.8 US\$ per ton and 49.4 US\$ per ton respectively.

ACKNOWLEDGMENT

The authors would like to thanks the National Research Council of Thailand (NRCT) for financial support, the Waste Incineration Research Center (WIRC) as well as Department of Mechanical and Aerospace Engineering (MAE), King Mongkut's University of Technology North Bangkok for any kinds of cooperation.

References

- [1] International Grain Council, "Supply and Demand of Maize in World Market", Available online at: <http://www.igc.int/en/grainsupdate/sd.aspx?crop=Maize>, accessed on 20 January 2015.
- [2] National Corn Growers Association, "World of Corn 2014", Available online at: <http://ncga.com/upload/files/documents/pdf/woc-2014.pdf>, accessed on 20 January 2015.
- [3] Pioneer Agronomy Science, "Managing Corn Residues in Corn Production", Available online at: http://www.marchutletseeds.ca/uploads/corn_managingcornresidueincornproduction.pdf, accessed on 20 January 2015.
- [4] S. Kim and B. E. Dale, "Global potential bioethanol production from wasted crops and crop residues", *Biomass and Bioenergy*, **26**, pp. 361-375.

Bio-Fuel; Ethanol Production

DIRECT PRODUCTION OF BUTANOL-ETHANOL FROM CANE SUGAR FACTORY WASTEWATER (CSFW) CELLULOSIC ETHANON PILOT PLANT WASTEWATER (CEPW) BY CLOSTRIDIUM BEIJERINCKII CG1

Jantarush Comwien¹, Nassapat Boonvithaya², Warawut Chulaluksananukul³ and Chompunuch Glinwong⁴

¹Environmental Science Interdisciplinary Program, Faculty of Graduate School, Chulalongkorn University, Thailand

²PTT Research and Technology Institute, PTT Public Company Limited, Thailand

³Biofuels by biocatalyst research unit, Faculty of Science, Chulalongkorn University, Thailand

⁴Department of Botany, Faculty of Science, Chulalongkorn University, Thailand

SUMMARY: The ability of *Clostridium beijerinckii* CG1 to utilize sugar from cane sugar factory wastewater (CSFW) and cellulosic ethanol pilot plant wastewater (CEPW) as a renewable carbon sources media to produce acetone-butanol-ethanol (ABE) were investigated. CSFW and CEPW were directly adapted to be culture media for ABE production by *C. beijerinckii* CG1 fermentation in serum bottle (100 ml). The average ABE and butyric acid production from CSFW were reported: acetone 0 g.L⁻¹, butanol 0.3 g.L⁻¹, ethanol 0.3 g.L⁻¹ and butyric acid 0.9 g.L⁻¹ productivity rate whereas production from CEPW are acetone 0 g.L⁻¹, butanol 0.6 g.L⁻¹, ethanol 0.4 g.L⁻¹ and butyric acid 2.5 g.L⁻¹. Evaluate efficiency CSFW productivity rate is 0.06 gL⁻¹h⁻¹ from 50 ml CSFW and CEPW productivity rate is 0.02 gL⁻¹h⁻¹ from 50 ml CEPW. In comparison, In conclusion, CSFW and CEPW can be applied to be appropriated substrate to produce solvents by *C. beijerinckii* CG1 with reasonable concentration without nutrient supplements.

Keywords: Clostridium beijerinckii CG1, Cane sugar factory wastewater (CSFW), Cellulosic ethanol pilot plant wastewater (CEPW), acetone-butanol-ethanol (ABE)

INTRODUCTION

Bioalcohol (eg. butanol, ethanol) are a potential renewable energy at present and future which can be produced efficiently by ABE process. Currently, bioalcohol cannot be competed by petroleum energy because of substrate cost. To develops cost effective bioprocess to produce bioalcohol, this research focus on a new substrate or raw material that are reasonable with reduced food and fuel dilemma.

Industrial wastewaters requires treatment to remove pollutants prior to discharge. Wastewater treatment system is important and the cost of wastewater treatment system in each plants are varied. The method of wastewater treatments are depended on wastewater type and properties. [1] Wastewater contained high organic substances is sophisticated and needs a very specific treatment processes because of its diverse components (such as: mixture of carbohydrate, fat or even polymer and salts). For this reason was not appropriate to use only chemical treatment process but should adapted all physical, chemical and biological treatment process to eliminate most of pollutes. [2] Biological treatment process is one of traditional process combined between aerobic and anaerobic treatment system, which has high efficiency to remove BOD and COD which are critical values the determine wastewater hazard. [3]

Carbohydrate-rich wastewater is one of many kinds of wastewater from food processing industries

[4]. For examples, cassava starch wastewater, vermicelli wastewater, cane sugar industry wastewater and deproteinized whey wastewater. It may contained many monosaccharides and disaccharides sugar (e.g., glucose, mannose, xylose, and arabinose) [5]. In this study, the concept is to combine and consolidate biological wastewater treatment processes with ABE fermentation process together without pretreatment or enzymes digestion processes before. *Clostridium beijerinckii*. is a species which targeted to the objective of research because of its high ABE production with in short periods. Moreover, this bacterium has been reported ability to use various carbon sources [6] and produced endospore for poor environment resistance [7].

Ethanol and butanol was produced from the waste that has been studied many examples, sugar from organic waste (domestic organic waste; DOW) within the country was substrate to produce butanol using *C. acetobutylicum* ATCC824 by dry and wet garbage from country were pretreated and then the concentration of sugar all different ranges 27.7-39.3% (W/W). The result, fermentation by *C. acetobutylicum* ATCC824 be positive without the addition of other nutrients more. Concentration of butanol at 3 g.L⁻¹, butanol productivity rate was 0.03 gL⁻¹h⁻¹ from 100 grams of organic waste [8]. However, still required pretreatment and enzymatic pretreat process are still required to convert wet

garbage to be sugar efficiently. This may effected to the cost of production process.

Both CSFW and CEPW are a kind of carbohydrate-rich wastewater. In this research, the goal is to study potential of CSFW and CEPW as a substrate to produce butanol-ethanol (BE) from consolidated bioprocess designed especially for *C. beijerinckii* CG1.

MEASUREMENT AND METHODOLOGY

Inoculate culture 10% (v/v) of CSFW medium and CEPW medium. *C. beijerinckii* CG1 under anaerobic condition and incubated at 37°C 120 hours in 3 different medium (CSFW, CEPW, and MS medium (glucose 20 g.L⁻¹)). Growth of the bacteria was followed by measuring the absorbance at 600 nm, with 1 mL samples being taken at 0, 24, 48, 72, 96 and 120 hr. ethanol and butanol production were analyzed by gas chromatography.

RESULTS AND DISCUSSION

CSFW and CEPW can be applied to be substrate to produce solvents by *C. beijerinckii* CG1 with reasonable concentration without nutrient supplements.

Illustrations and graphics

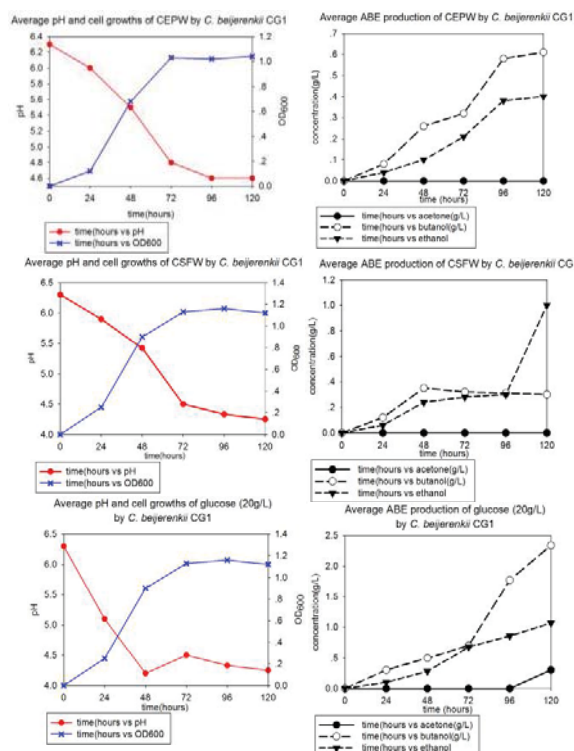


Figure 1. Show average ABE production, cell growths and pH from fermentation by *C. beijerinckii* CG1

ACKNOWLEDGMENT

The authors would like to thank Chulalongkorn University for Research Facility for their financial support and also given to Research Facility.

References

- [1] E. Cristiani-Urbina, A.R. Netzahuatl-Muñoz, F.J. Manriquez-Rojas, C. Juárez-Ramírez, N. Ruiz-Ordaz and J. Galíndez-Mayer, "Batch and fed-batch cultures for the treatment of whey with mixed yeast cultures". *Process Biochemistry*, **35(7)**, 2000, pp. 649-657.
- [2] DSS. Raj and Y. Anjaneyulu. "Evaluation of biokinetic parameters for pharmaceutical wastewaters using aerobic oxidation integrated with chemical treatment". *Process Biochemistry*, **40(1)**, 2005, pp. 165-175.
- [3] M. Afzal, S. Iqbal, S. Rauf and ZM. Khalid. "Characteristics of phenol biodegradation in saline solutions by monocultures of *Pseudomonas aeruginosa* and *Pseudomonas pseudomallei*". *Journal of hazardous materials*, **149(1)**, 2007, pp. 60-66.
- [4] J. Lee. "Identification of multiple cracks in a beam using natural frequencies". *Journal of sound and vibration*, **320(3)**, 2009, pp. 482-490.
- [5] Y. Zhang, B.E. Rittmann, J. Wang, Y. Sheng, J. Yu, H. Shi and Y. Qian. "High-carbohydrate wastewater treatment by IAL-CHS with immobilized *Candida tropicalis*". *Process Biochemistry*, **40(2)**, 2005, pp. 857-863.
- [6] N. Qureshi, T.C. Ezeji, J. Ebener, B.S. Dien, M.A. Cotta and H. P. Blaschek "Butanol production by *Clostridium beijerinckii*. Part I: use of acid and enzyme hydrolyzed corn fiber". *Bioresource technology*, **99(13)**, 2008, pp. 5915-5922.
- [7] NKN. Al-Shorgani, MS. Kalil and WMW. Yusoff. "Biobutanol production from rice bran and de-oiled rice bran by *Clostridium saccharoperbutylacetonicum* N1-4". *Bioprocess and biosystems engineering*, **35(5)**, 2012, 817-826.
- [8] AM. López-Contreras, PA. Claassen, H. Mooibroek and WM. De Vos. "Utilisation of saccharides in extruded domestic organic waste by *Clostridium acetobutylicum* ATCC 824 for production of acetone, butanol and ethanol". *Applied microbiology and biotechnology*, **54(2)**, 2000, pp. 162-167.

OPTIMIZATION AND KINETICS MODELLING OF ETHANOL PRODUCTION FROM OIL PALM JUICE IN BATCH FERMENTATION

Tussanee Srimachai¹, Kamchai Nuithitikul¹, Sompong O-thong^{2,3}, Prawit Kongjan^{4,5} and Kiattisak Panpong^{6,7}

¹School of Engineering and Resources, Walailak University, Thailand

²Department of Biology, Faculty of Science, Thaksin University, Thailand

³Microbial Resource Management Research Unit, Faculty of Science, Thailand

⁴Chemistry Division and ⁵Bio-Mass Conversion to Energy and Chemicals (Bio-MEC) Research Unit, Department of Science,

Faculty of Science and Technology, Prince of Songkla University (PSU), Thailand

⁶Songkhla Rajabhat University (Satun Campus) and ⁷Department of Engineering, Faculty of Industrial Technology, Songkhla Rajabhat University, Thailand

SUMMARY: Ethanol was produced from oil palm frond juice (OPFJ) by using *Saccharomyces cerevisiae* yeast cell. Experiments were operated in batch mode by varying the oil palm age between 3-4, 4-7, 7-10, 10-20 and 20-25 years, respectively. Experimental results showed that OPFJ at 3-4 years gave the highest concentrations of glucose and ethanol as 31.26 and 11.50 g/l, respectively. Ethanol yield was 0.39 g-ethanol/g-glucose, which estimated as 76.47% of the theoretical yield (0.51 g-ethanol/g-glucose). Additionally, the Monod and modified Gompertz equations were used to describe the kinetics of product formation and kinetics of substrate utilization. The estimated values of the kinetic parameter in Monod and modified Gompertz equations of OPFJ at 3-4 years were evaluated: maximum specific growth rate (μ_{max}) was 0.29 g/g-VSS.hr, saturation concentration (K_s) 47.05 g/l, maximum ethanol concentration (P_m) 11.50 g/l, maximum ethanol production rate ($r_{p,m}$) 0.24 g./l.hr and lag phase 0.12 hr. Both models fitted well to experimental data, which had the high regression coefficient values ($R^2 > 0.95$).

Keywords: Ethanol production, Oil palm frond juice, Kinetic modelling, Batch Fermentation

INTRODUCTION

The primary energy from petroleum-derived fuel is expensive and becomes running out because of the increasing energy demand. Thus, it is necessary to find the alternative energy such as ethanol which is produced from agricultural and agro-industrial wastes. Currently, ethanol is mainly produced from starch and sugar as raw materials. However, the use of starch and sugar based materials for ethanol production has led to a “food vs. fuels” conflict [1]. Therefore, using lignocellulosic materials is promising due to the big available quantity, low prices and no rapacious land for plantation of humans. Lignocellulosic materials such as corn stalk, oil palm biomass, rice straw, bagass can be used to produce ethanol. Lignocellulosic material is a complex carbohydrate polymer containing cellulose (40-50%), hemicellulose (25-35%) and lignin (15-20%). However, the main problem in ethanol production by using lignocellulosic materials as a feedstock is the poor hydrolysis and high cost of cellulolytic enzymes [2]. Additionally, the ethanol production of untreated lignocellulose has low yield due to the resistance of high crystalline cellulose to enzymatic hydrolysis [1]. For these reasons, the ethanol production from lignocellulosic feedstocks requires a pretreatment step to open up the structure and reduce the crystallinity of lignocelluloses [3]. It is accepted that the pretreatment process is a “key process” of the ethanol production from lignocelluloses [4].

Oil palm frond (OPF) is a sustainable agriculture waste because it is a main waste material during the harvest of fresh fruit bunch. In 2010, about 7 million tons of OPF were generated in Thailand [5]. OPF is consisted of high carbohydrates in the form of simple sugars which can be used as a raw material in ethanol production. However, using high temperature and pressure and cellulose enzymes to convert OPF to sugars has high cost. Currently, renewable sugars can be simply obtained from OPF by pressing the fresh OPF to obtain the oil palm frond juice (OPFJ). This can save the cost in using OPF as a feedstock to produce ethanol.

METHODOLOGY

Firstly, Analyzed composition of oil palm frond juice (OPFJ) such as glucose, fructose, sucrose, protein and total nitrogen etc. By studying the potential of oil palm frond juice in ethanol production at different oil palm age between 3-4, 5-7, 7-10, 10-20 and 20-25 years, respectively. Then, OPFJ was introduced into the ethanol fermentation process, which 10% (v/v) of *S. cerevisiae* and 1% (v/v) yeast extract were added in this process. After that, the mixture was incubated at 37 °C (Room temperature) with shaking at 150 rpm for 24 hours and samples were collected for analysis at 0, 12, 24, 36, 48, 60, 72 and 96 hours to analyze reducing sugar and ethanol. Finally, the kinetic parameters of anaerobic bacteria in ethanol and biogas production were determined using the

Modified Gompertz and Monod model, which expressed the behavior of the produced formation and microbial growth. This experimental method was shown in Figure 1.

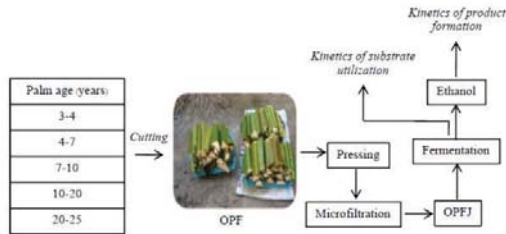


Figure 1. Process of ethanol production from OPFJ in batch fermentation

RESULTS AND DISCUSSION

The initial compositions of OPFJ were shown in Table 1. Figure 2 showed ethanol production from fermentation process by *S. cerevisiae* cultivated in OPFJ, which studied at different oil palm age. The trend of glucose utilization by *S. cerevisiae* was presented in Figure 2.

The kinetic parameters estimated for the product formation and microbial growth were summarized in Table 2.

Table 1. Initial composition of OPFJ

Oil palm age (years)	Volume of OPFJ (ml/kg OPF)	Glucose (g/l)	Fructose (g/l)	Sucrose (g/L)	Protein (g/L)	Total nitrogen (mg/L)	pH
3-4	550	31.26	4.69	2.81	3.75	0.47	4.43
4-7	450	24.43	3.66	2.20	2.93	0.35	4.23
7-10	400	20.43	3.06	1.84	2.45	0.31	4.41
10-20	350	10.87	1.63	0.98	1.30	0.16	4.32
20-25	300	6.67	1.02	0.09	0.80	0.11	4.56

Table 2. Comparison in the parameters of Modified Gompertz and Monod equations

Media	Modified Gompertz			Monod		Reference
	P_m (g/l)	$r_{p,m}$ (g/L.hr)	t_L (hr)	μ_{max} (g/g.VSS.hr)	K_s (g/l)	
OPF juice (3-4Y)	11.50	0.24	0.12	0.29	47.05	This study
OPF juice (4-7Y)	8.80	0.18	0.58	0.26	45.37	This study
OPF juice (7-10Y)	7.50	0.16	0.65	0.24	38.02	This study
OPF juice (10-20Y)	3.79	0.08	0.77	0.15	10.21	This study
OPF juice (20-25Y)	2.34	0.05	0.85	0.11	1.82	This study
Sugar beet juice	73.31	4.39	1.04	-	-	[6]
Whey	-	-	-	0.32	10.50	[7]
Xylose	-	-	-	0.23	1.67	[8]

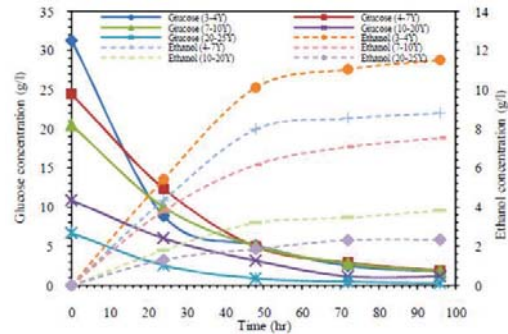


Figure 2. Glucose utilization and ethanol production of OPFJ

ACKNOWLEDGEMENT

I would like to thank the Office of the Higher Education Commission (OHEC) for support the funding in this research. This research project would not have been possible without extensive assistance of the staff from the Microbial Management Research Unit (MRM-TSU), Faculty of Science, Thaksin University, Thailand.

References

[1] M. Shafiel, M.M. Kabir, H. Zilouei, I.H. Horvath and K. Karimi. "Techno-economical study of biogas production improved by steam explosion pretreatment", *Bioresource Technology*, **148**, 2013, pp. 53-60.

[2] M.J. Taherzadeh and K. Karimi. "Enzyme-based hydrolysis processes for ethanol from lignocellulosic materials: a review", *Bioresources*, **2**, 2007, pp. 707-738.

[3] M. Taherzadeh, K. Karimi, K. "Pretreatment of lignocellulosic wastes to improve ethanol and biogas production: a review", *Int. J. Mol. Sci.* **9**, 2008a, pp. 1621-1651.

[4] B. Yang & C.E. Wyman. "Pretreatment: the key to unlocking low-cost cellulosic ethanol", *Biofuels. Bioprod. Biorefin.*, **2**, 2008, pp. 26-40.

[5] T. Vitidsant, N. Laosiripojana & P. Reubroycharoen. "Position paper on biofuel development in Thailand" *Bangkok*, 2010, pp.168.

[6] J.M. Dodic, D.G ucurovic, S.N. Dodic, J.A. Grahovac, S.D Popov and N.M. Nedejkovic. "Kinetic modelling of batch ethanol production from sugar beet raw juice", *Applied Energy*, **99**, 2012, pp.192-197.

[7] D. Ariyanti and H. Hadiyanto. "Ethanol Production from Whey by *Kluyveromyces maxianus* in Batch Fermentation System: Kinetics Parameters Estimation", *Bulletin of Chemical Reaction Energy & Catalysis*, **77(3)**, 2013, pp. 1798-184.

[8] D. Farias, R.R. de Andrade and F. Maugeri-Filho. "Kinetic Modelling of Ethanol Production by *Scheffersomyces stipitis* from Xylose", *Appl Biochem Biotechnol*, **172**, 2014, pp. 361-379.

UTILIZATION OF OIL PALM EMPTY FRUIT BUNCH HYDROLYSATE FOR ETHANOL PRODUCTION BY BAKER'S YEAST AND LOOG-PANG

Sairudee Duangwang¹ and Chayanoot Sangwichien¹

¹Department of Chemical Engineering, Faculty of Engineering, Prince of Songkla University, Thailand

SUMMARY: Oil palm empty fruit bunch is a potential source of glucose which can serve as a promising raw material for production of ethanol. Ethanol production was investigated by using separation hydrolysis and fermentation process (SHF), in which yeast from Loog-Pang (a Thai traditional fermentation starter culture) and baker's yeast were used as biocatalyst. After alkali pretreatment with 15% NaOH for 40 min at 130°C, Cellulose was analyzed to be 61.94% (on dry weight basis). Glucose was 33.45 g/l after cellulose was hydrolyzed by 7% H₂SO₄ at 119 °C for 110 min. The resulting aqueous phase rich in glucose was fermented by yeast from baker's yeast to produce ethanol with the concentration of 8.49 g/l with is 56 times higher than Loog-Pang as yeast. Therefore, implementation of oil palm empty fruit bunch for the development of alternative source of energy could be an effective approach and key enable to the billion-ton biofuel vision.

Keywords: oil palm empty fruit bunch, Loog-Pang, baker's yeast, ethanol, Separation Hydrolysis and Fermentation

INTRODUCTION

Ethanol is widely used as a partial gasoline replacement in US and other parts of the world. It can also be used in a variety of cooking, heating, and lighting appliances. Fuel ethanol is produced from corn which has been used in gasohol or oxygenated fuels since 1980. Ethanol is blended directly with gasoline in a mix of 10% ethanol and 90% gasoline is called gasohol [1].

Oil palm empty fruit bunch are agricultural residues and lignocellulosic biomass, it is a less expensive source of carbon which can be used for production of ethanol. [1].

Ethanol is a renewable energy resource produced through fermentation of simple sugars by yeasts, *Saccharomyces cerevisiae* is the most widely used for ethanol fermentation. Species of Baker's yeast is *Saccharomyces cerevisiae*, which is the same species commonly used in alcoholic fermentation. The folk wisdom in Thailand used Loog-pang as a starter for alcoholic fermentation. Loog-pang is a Thai term for dry form of fermentation starter for production of traditional fermented products from starchy raw materials. These starters are apparently mixed cultures of molds, yeasts and bacteria grown on rice or other cereals. In certain localities native herbs were added. *Saccharomycopsis fibuligera* is a common yeast species found in loog-pang.

The target of the present investigation was to determine amount of ethanol with fermentation of different yeast.

MATERIALS AND METHODS

Raw material

Oil palm empty fruit bunch (OPEFB) fiber was collected from local palm oil, sun-dried and ground to a particle size <1 mm.

Alkali pretreatment

OPEFB was soaked in NaOH (15% w/v) with a OPEFB:NaOH ratio of 1:10 (w/v). The alkaline treated OPEFB was heated at 130°C for 40 min; filtered and neutralized by extensive washing. The dried product of OPEFB was then determined by the AOAC method.

Acid hydrolysis

Acid hydrolysis of OPEFB biomass was carried out in 125 ml Erlenmeyer flasks by 7% w/v of H₂SO₄ at 119 °C for 110 min. The filtrate was then analyzed for determination of glucose. Glucose in the acid hydrolysate was analyzed by High Performance Liquid Chromatograph (HPLC, SHIMADZU) using SUPELCOSIL LC-NH₂ column and RI detector. Aqueous acetonitrile (75%) was used as mobile phase with flow rate of 1.5 ml/min and oven temperature was maintained at 50 °C.

Fermentation

The ethanol production from the hydrolysates obtained after acid hydrolysis was investigated. The fermentation was carried out in 125 ml Erlenmeyer flasks containing 15 ml of fermentation media incubated at 30°C in a rotary shaker at 150 rpm for 5 days. Fermentation was inoculated with different yeast (Loog-Pang and baker's yeast) for ethanol production at different levels varying from 1- 2 g/flask. Aliquots were withdrawn every 24 h for the analysis of sugar and ethanol determination.

Ethanol was estimated by gas chromatography (GC) with an HP-FFAP polyethylene glycol column (30 m X 0.25 mm) at 120°C, flame ionization detectors (FID) at 250°C and injector at 150°C. The carrier gas was helium; flow rate of 2 ml/min.

RESULTS AND DISCUSSION

Compositions of OPEFB

The composition of this material was analyzed

according to the AOAC method. The results of an analysis were based on a 105 °C, dry weight of the composition of OPEFB. The composition of OPEFB was determined to be 52.6% cellulose, 37.3% hemicellulose, 9.5% lignin and 0.6% other. The results agree well with the recent analysis data reported by Umikalsom et al. [2].

Sugar formation

The cellulose was converted to reducing sugar by hydrolysis. It was found that the hydrolysate contained glucose of 33.45 g/l. The results from recent analysis data reported by Rahman et al. [3] show hydrolysis of untreated OPEFB under optimized conditions and the best results of glucose obtained were 7.61 g/l when hydrolyzing acid used was 6% under operating temperature of 130 °C and time period of reaction was 90 min. From this investigation indicated that pretreated OPEFB gave higher amount of glucose than untreated OPEFB.

Ethanol production

The experimental results in Figure 1 shows clearly that the amount of ethanol by baker's yeast is higher than Loog-Pang about 56 times. The amount of ethanol by baker's yeast is in the range of 6.23 to 8.49 g/l, while the amount of ethanol by Loog-Pang in the range of 0.05 to 0.21 g/l because of 1.5 g of Loog-Pang have several types of yeast for the fermentation of ethanol, as a result in the minimum amount of ethanol. In Loog-Pang, there are both yeast and mold, Genus of mold such as *Mucor sp.*, *Amylomyces rouxii* and *Rhizopus oryzae*, there are fungus that are more helpful than harmful. Fungus officiate to produce Amylase enzyme from degrade starch to sugar. Yeast such as *Saccharomyces sp.*, It use to ferment sugar into alcohol. However, it is rare yeast in Loog-Pang.

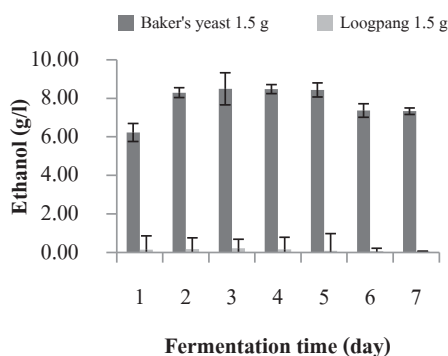


Figure 1. Ethanol yielded from fermentation with baker's yeast compared with Loog-Pang

According to the fermentation by baker's yeast has higher total ethanol than Loog-Pang. Therefore, the effect of time and amount of yeast were investigated by adding baker's yeast 1.0, 1.5 and 2 g for fermentation.

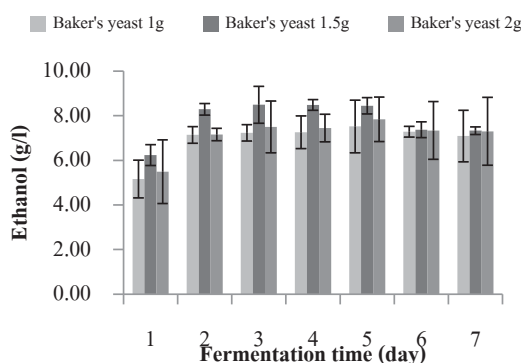


Figure 2. Ethanol yielded from fermentation with baker's yeast

As shown in Figure 2, varying the amount of yeast for fermentation from 1.0, 1.5 to 2.0 g, the results show that 1.5 g yeast can produce the highest ethanol. And the fermentation time of 5 days gave the highest amount of ethanol for all case. However, it was slightly different compared to the 3 days fermentation. Thus, the 3 days fermentation is a suitable time according to economics aspects.

CONCLUSION

Ethanol productions from OPEFB using separation hydrolysis and fermentation process (SHF) were investigated as following. Optimum fermentation condition was for 3 days fermentation by 1.5 g of baker's yeast. Ethanol production was obtained 8.49 g/l. In hydrolysis process can be use enzyme to convert cellulose into sugar for higher ethanol yield and environmentally friendly.

ACKNOWLEDGMENT

The author was granted additional supports from the Prince of Songkla University (PSU) Graduate School Research Support Funding and also a scholarship from PSU.

References

- [1] N.C. Nzelibe and C.U. Okafoagu, "Optimization of ethanol production from *Garcinia kola* (bitter kola) pulp agrowaste", *African Journal of Biotechnology*, **6** (17), 2007, pp. 2033-2037.
- [2] M.S. Umikalsom et al., "The treatment of oil palm empty fruit bunch for subsequent as substrate for cellulose production by *Chaetomium globosum*", *Bioresour Technol*, **62**, 1997, pp. 1-9.
- [3] S.H.A. Rahman J.P. Choudhury, A.L. Ahmad, A.H. Kamaruddin, "Optimization studies on acid hydrolysis of oil palm empty fruit bunch fiber for production of xylose", *Bioresour Technol*, **98**, 2007, pp. 554-559.

different microorganism including *S. cerevisiae* and *E. aerogenes*. The mix-culture of *S. cerevisiae* and *E. aerogenes* for ethanol production from stillage was also evaluated. All experiments were operated at 35°C and 100 rpm for 96 hours.

Analytical methods

The released reducing sugars were measured by the DNS method using D-glucose as a standard followed by Miller method [7]. Analysis of ethanol by dichromate oxidation method followed by Amerine and Oung [6]. The total solids (TS), volatile solids (VS), total soluble solids (TSS), chemical oxygen demand (COD) were determined according to standard methods [8].

The qualitative analysis of reducing sugars and volatile fatty acids were analyzed by high-performance liquid chromatography and gas chromatography.

RESULTS AND DISCUSSION

Characterization of liquid stillage

Liquid stillage an effluent after ethanol recovery was collected and characterized. The stillage was acidic (pH 4.3-4.8) with TS at 17,307 mg/L, VS at 14,400 mg/L, TSS at 9.0 mg/L and COD at 20,900 mg/L. Moreover, the liquid stillage contained reducing sugars (fructose and glucose) and volatile fatty acids including acetic acid, propionic acid and butyric acid. 1.484 g/L of reducing sugar was found in raw stillage.

The production of ethanol from liquid stillage

250 mL of stillage was utilized as substrate for ethanol production. The experiments were done using different glucose concentrations [10, 20, 40 and control (raw material, no glucose addition)] and different microorganism including *S. cerevisiae* and *E. aerogenes*. The mix-culture of *S. cerevisiae* and *E. aerogenes* for ethanol production from stillage was also evaluated. The mix-culture between *S. cerevisiae* and *E. aerogenes* yield the highest ethanol (1.762 g ethanol/ g sugar) after 72 h of cultivation with the stillage supplemented with non-glucose addition (Table 1).

Mix-culture fermentation is more efficient than single culture fermentation because the microbial community structure is optimizing. Therefore, it can improve ethanol production. Mixed culture fermentation is presence of high microbial diversity, which offers increased adaptation capacity for higher alcohols production [9].

Table 1 The production of sugar and ethanol with different culture by simultaneous and saccharification fermentation (SSF) using raw liquid stillage as substrate after 72 h of cultivation

Culture	Sugar (g/L)	Ethanol (%)	Yield (gethanol/g sugar)
<i>S. cerevisiae</i>	0.694	1.975	1.331
<i>E. aerogenes</i>	0.430	0.861	0.580
Mix-culture	0.641	2.615	1.762

CONCLUSION

A simple and realistic process for re-use stillage after ethanol recovery was presented in this study. Raw stillage showed the possible ability to utilize as substrate for ethanol production due to it contained reducing sugar (1.484 g/L) and volatile fatty acid. Raw stillage with no glucose addition gave the highest ethanol yield (1.762 g ethanol/ g sugar) after 72 h from mix-culture of *E. aerogenes* and *S. cerevisiae*.

ACKNOWLEDGEMENT

The author would like to thank Research and Development, Graduated School and Department of Chemistry, Thaksin University for financial support.

References

- [1] T.L.T. Nguyen and S.H. Gheewala, "Fossil energy, environmental and cost performance of ethanol in Thailand", *J. Clean. Prod.* **16**, 2008, pp. 1814-1821.
- [2] T. Roukas, "Ethanol production from non-sterilized beet molasses by free and immobilized *Saccharomyces cerevisiae* cells using fed-batch culture", *J. Food Eng.* **27**, 1996, pp.87-96.
- [3] S. Zafar and M. Owais, "Ethanol production from crude whey by *Kluyveromyces marxianus*. Biochem", *Eng. J.* **27**, 2006, pp.295-298.
- [4] M.L. Rasmussen et al., "Water reclamation and value-added animal feed from corn-ethanol stillage by fungal processing", *Bioresource Technology.* **151**, 2014, pp.284-290.
- [5] A. Choonut, M. Saejong, K. Sangkharak, "The Production of Ethanol and Hydrogen from Pineapple Peel by *Saccharomyces cerevisiae* and *Enterobacter aerogenes*", *Energy Procedia.* **52**, 2014, pp.242-249.
- [6] M.A. Amerine and C.S. Ough "Wine and must analysis", *John Wiley & Son, New York.* 1974.
- [7] G.L. Miller "Use of dinitrosalicylic acid reagent for determination of reducing sugar", *Anal Chem* **31(3)**, 1959, pp.426-428.
- [8] APHA, AWWA and AWEF 1998. Standard Methods for the Examination of Water and Wastewater. Washington D.C. United States of America.
- [9] A. Singla, D. Verma, B. Lal, P. Sarma. "Enrichment and optimization of anaerobic bacterial mixed culture for conversion of syngas to ethanol", *Bioresource Technology.* **172**, 2014, pp.41-49.

UTILIZATION OF OIL PALM FROND BIOMASS FOR BIOETHANOL PRODUCTION

Sureeporn Kumneadklang^{1,3}, Chaisit Niyasom^{2,3}, and Sompong O-Thong^{2,3}

¹ Biotechnology Program, Faculty of Science, Thaksin University, Thailand

² Department of Biology, Faculty of Science, Thaksin University, Thailand

³ Microbial Resource Management Research Unit, Faculty of Science, Thaksin University, Thailand

SUMMARY: Included process producing ethanol from oil palm frond (OPF) by simultaneous saccharification and *Saccharomyces cerevisiae* fermentation. The solid fraction of oil palm frond (20% TS) was pretreated by 2% H₂SO₄, 2% NaOH and 2% NaOH in H₂O₂ presoaking. Pretreatment of solids fraction from oil palm frond at 20% TS by presoaking in 2% H₂SO₄, 2% NaOH and 2% NaOH in H₂O₂ was contain 37, 42 and 49% of cellulose, respectively. Treated oil palm solid fraction was sequentially simultaneous saccharification by enzyme Cellic CTec2 hydrolysis and ethanol fermentation by *Saccharomyces cerevisiae* TISTR5048. Sugar concentration in cellulose hydrolysis of 2% H₂SO₄, 2% NaOH and 2% NaOH in H₂O₂ presoaking was 45.72, 55.73 and 56.94 g/l, respectively. Ethanol of 2% H₂SO₄, 2% NaOH and 2% NaOH in H₂O₂ presoaking was 14.50, 15.00 and 17.20 g/L, respectively. 2% NaOH in H₂O₂ presoaking was the best pretreatment with 82.11% of total solids recovery and containing of cellulose (56.94%), hemicelluloses (30.07%) and lignin (20.00%) and enzyme digestion was 37.59 %

Keywords: Ethanol production, Oil palm frond

INTRODUCTION

Energy consumption has increased steadily as the world population has grown and more countries has become industrialized. The fossil fuels, such as crude oil, coal and natural gas have been the major resources to meet the increased energy demand. However, they are gradually being depleted to extinction because they are not renewable. Moreover, serious environmental and ecological problems have been aroused during their exploitation and use. Therefore, there is great interest in exploring alternative energy sources to maintain the sustainable growth of society [1]. Fuel ethanol production from lignocellulosic biomass is emerging as one of the most important technologies for sustainable production of renewable transportation fuels. Ethanol has a higher octane rating than gasoline and produces fewer emissions, therefore being widely recognized as a substitute and/or additive to gasoline [2]. In terms of chemical composition, the biomass oil palm predominantly contains cellulose (40-50%), hemicelluloses (20-35%) lignin (16-29%) [3]. However, the ethanol production from lignocellulosic materials consists the third main process; the first, size reduction and pretreatment for delignification are necessary to release cellulose and hemicellulose is for hydrolysis; the second, hydrolysis of cellulose and hemicellulose uses enzyme or other method to produce the glucose, xylose, arabinose, galactose, manose; the third, fermentation of reducing sugar to produce the ethanol.

Oil palm frond (OPF) is a sustainable agriculture waste because it is a many waste material due to be cut off during has a harvesting of fresh fruit bunch (FFB) resulting OPF is on value or zero waste. The OPF is cut every time (about 20 days/time) when has a harvest of palm fruits which will be left palm in palm groove as fertilizer for palms only. So, if the use of OPF produced ethanol can be increased the value of OPF and a new raw material to produce ethanol in the future [4]

This research aimed to optimized the conditions for the pretreatment of lignocellulosic materials from Oil palm frond (OPF) to produced cellulose and cellulose hydrolysate by enzymatic hydrolysis for ethanol production.

METHODOLOGY

Oil palm frond (OPF) was obtained from Krabi province plantation area. Whole OPF was chopped by tree chopper and squeeze for recovery oil palm sap juice. Solid fraction from squeeze process was use for ethanol production. 20%Solid fraction of OPF treated by chemical such as 2% H₂SO₄, 2% NaOH and 2% NaOH in H₂O₂ presoaking. Treated oil palm solid fraction was saccharified by cellulase enzyme hydrolysis (Enz.Cellic CTec2) and sequentially simultaneous ethanol fermentation by *Saccharomyces cerevisiae* TISTR5048

RESULTS AND DISCUSSION

Table 1 Chemical composition of Oil palm frond (OPF)

Chemical pretreated	Composition of OPF		
	%cellulose	%hemi-cellulose	% lignin
2% (v/v) H ₂ SO ₄	37.24	32.76	30.00
2%(w/v) NaOH	42.32	29.68	28.00
2% (w/v) NaOH in H ₂ O ₂	49.93	30.07	20.00
raw OPF	41.94	36.06	22.00

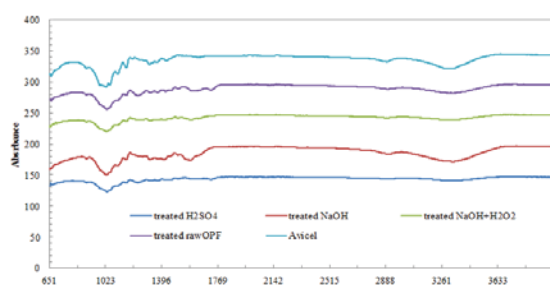


Figure 1. FTIR spectra of avicel, raw OPF, 2% H₂SO₄ treated OPF, 2% NaOH treated OPF and 2% NaOH in H₂O₂ treated OPF

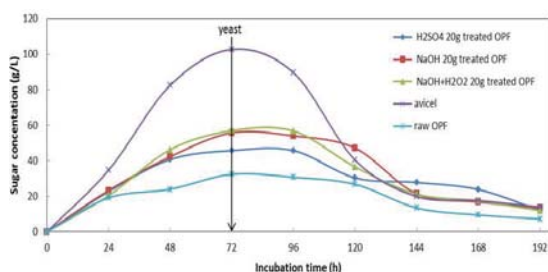


Figure 2. Sugar concentration of enzymatic hydrolysis

Table 2 enzyme digestion stability

material	condition	Sugar concentration (g/L)	enzyme digestion (%)
Oil palm frond	2%(v/v) H ₂ SO ₄	45.73	30.18
	2%(w/v) NaOH	55.74	36.79
	2%(w/v) NaOH in H ₂ O ₂	56.95	37.59
	raw OPF	32.44	21.41

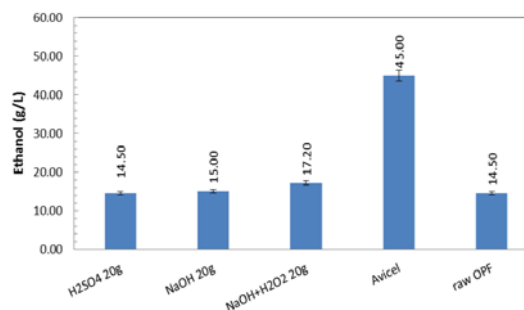


Figure 3 Ethanol production by *Saccharomyces cerevisiae* at 192 hour fermentation.

ACKNOWLEDGEMENT

I would like to thank Faculty of Science Thaksin university and Microbial Resource Management Research Unit at Thaksin university, with the support instrumental and assistance the conduct of research.

References

- [1] S. Zhu, Y. Wu, Z. Yu, C.Z. Wang, F. Yu and S. Jin. "Production of ethanol from microwave-assisted alkali pretreatment wheat straw". *Proc Biochem.* **41**, 2006, pp. 869-873.
- [2] R.K. Sukumaran, R.R. Singhania, G.M. Mathew and A. Pandey. "Cellulase production using biomass feed stock and its application in lignocellulose saccharification for bio-ethanol production". *Renewable Energy.* **34**, 2009, pp. 421-424.
- [3] T. Khunrong, V. Punsuvon, P. Vaithanomsat, and C. Pomchaitaward. "Production of ethanol from pulp obtained by steam explosion pretreatment of oil palm trunk". *Energy sources.* **33**, 2011, pp. 221-228.
- [4] T. Srimachai, V. Thonglimp and S. O-Thong. "Ethanol and Methane Production from Oil Palm Frond by Two stage SSF," *Energy Procedia,* **52**, 2014, pp. 352 - 361.

BIODIESEL PRODUCTION FROM REFINED PALM OIL USING SUPERCRITICAL ETHYL ACETATE IN MICROREACTOR

Nanthana Sootchiewcharn¹, Prasert Reubroycharoen¹ and Lalita Attanatho²

¹Department of Petrochemical and Polymer Science,
Faculty of Science, Chulalongkorn University, Thailand
²Energy Technology Department, Thailand Institute of Scientific
Technological Research, Thailand

SUMMARY: This research investigated the production of Fatty Acid Methyl Ester (FAME) and Fatty Acid Ethyl Ester (FAEE) from vegetable oil with methyl acetate and ethyl acetate at supercritical conditions in microreactor. The experiments were carried out in a microreactor at the reaction temperature in the range of 330 and 370°C with pressure of 200 bar and oil to solvent molar ratio of 1:50. Results showed that the higher ester yield was obtained when using methyl acetate as a reactant compared to ethyl acetate. In addition, the thermal decomposition of fatty acid chains during the supercritical transesterification of vegetable oil in microreactor was observed at the reaction conditions used in this work.

Keywords: biodiesel, transesterification, microreactor, supercritical, methyl acetate, ethyl acetate, thermal decomposition

INTRODUCTION

Biodiesel is the alternative fuel derived from vegetable oil and fat by transesterification reaction. During the transesterification, triglyceride reacts with methanol or ethanol to produce ester as a main product and glycerol as a by-product. The excess amount of glycerol that will be produced from biodiesel industry in the future might have to manage a waste product. To solve this problem, the researcher has focus on the glycerol free process for producing biodiesel. Transesterification process of vegetable oil with methyl or ethyl acetate with give Fatty Acid Methyl Ester (FAME) or Fatty Acid Ethyl Ester (FAEE) as products and triacetin as by-product instead of glycerol (Figure 1). Triacetin has more value than glycerol and can also be used as additive in biodiesel fuel [1].

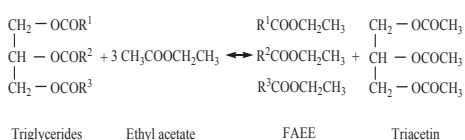


Figure 1. Reaction stoichiometry between triglyceride and ethyl acetate to produce FAEE and triacetin

For the choice of feedstock, Jatropha oil seems to be the good choice due to the contribution of non-food oil. However, palm oil is the most commonly used biodiesel feedstock in Thailand. So, the comparison between Jatropha oil and palm oil was investigated in this research.

Currently, there are various methods for biodiesel production but most of them required the long residence time to achieve the reasonable biodiesel yield. To avoid this problem, the use of microreactor technology is one of the interest methods. Microreactor was defined as miniaturized reaction systems that have small dimensions less than 1 mm [2]. Due to the small dimensions, the

high surface to volume ratio of microreactor was observed, that make excellent mass and heat transfer, shorter residence time, short molecular diffusion distance and better process control than macro-reactor system. Moreover, another advantage of microreactor systems is that the production capacity could be increased by numbering up method by connecting microreactors in series. In comparison, the conventional reactor requires scale up size of each reactor unit which change the quality of reactor.

Presently, there are limited research works concerning transesterification process. Thus, the objective of this study was to investigate the effect of solvent type (i.e. methyl and ethyl acetate) on transesterification process at various reaction conditions. In addition, the comparison of two types of vegetable oil feedstocks (i.e. Jatropha oil and refined palm oil) also presented in this work.

MATERIALS AND METHODS

Crude Jatropha oil from Bioenergy Development Co., Ltd. (Thailand) and Refined palm oil from Patum Vegetable Oil Co., Ltd (Thailand) were used as oil feedstock for this study. Methyl acetate (99%) was purchased from Merck and Ethyl acetate (99.8%) was purchased from RCI Labscan. Triolein (99%), methyl oleate (98%) and ethyl oleate (98%) were purchased from Sigma-Aldrich for using as the GC standards for triglycerides FAME and FAEE analysis. Triacetin (99%) was purchased from Applichem.

The transesterification process of vegetable oil was carried out using methyl acetate and ethyl acetate in microreactor made of stainless steel tubing (316L 1/16 in. x 0.03 in.) with the capacity of 6.94 mL. The reactants were mix at oil to solvent molar ratio of 1:50 and then fed into the reaction system by high pressure liquid pump. The tubular

microreactor was placed in a furnace with controlled temperature and monitored by two thermocouples. The reaction temperature was controlled in the range of 330°C and 370°C and the reaction times in the range of 3 and 20 minute. The ester compositions of product were determined by gas chromatography.

RESULTS AND DISCUSSION

The ester composition of liquid product in the interesterification process of Jatropha oil with methyl and ethyl acetate at oil to solvent molar ratio of 1:50, temperature of 350°C, pressure 200 bar and residence time of 10 min are shown in Table 1. It can be seen that the ester content in liquid product when using methyl acetate as solvent was higher than when using ethyl acetate. At this reaction condition, ester content of 30.8% was obtained when using ethyl acetate as solvent whereas using methyl acetate as solvent, the ester was 36.8%.

Table 1. Composition of ester in liquid products obtained from Jatropha oil when using methyl acetate and ethyl acetate at molar ratio of 1:50, temperature of 350°C, pressure 200 bar and residence time of 10 min

Solvent	Ester composition (wt%)	Total composition (wt%)
Methyl acetate	36.8	83.7
Ethyl acetate	30.8	74.8

The comparison of FAEE content in liquid product obtained from supercritical ethyl acetate biodiesel production using Jatropha oil and refined palm oil as raw materials, at temperature of 350°C, pressure of 200 bars and residence time of 10 min was reported in table 2. The FAEE contents were 30.8 wt% and 52.3 wt% when using Jatropha oil and refined palm oil as raw materials, respectively. The total composition reported in Table 1 is defined as a total identified compositions in the product which including FAEE, fatty acid, triacetin, mono-glycerides, di-glycerides and tri-glycerides. The total composition of the product obtained when using Jatropha oil was only 74.8 wt%.

Table 2. FAEE composition of liquid products obtained from Jatropha oil and Refined palm oil with supercritical ethyl acetate at temperature of 350°C, pressure of 200 bar and residence time of 10 min

Oil	FAEE composition (wt%)	Total composition (wt%)
Jatropha	30.8	74.8
Refined palm	52.3	91.1

Jatropha oil has a higher degree of un-saturation compared to palm oil as shown in Figure 2. Thus, the low total identified composition of Jatropha biodiesel product was probably due to the thermal decomposition of unsaturated part of reactants, reaction intermediates and product in supercritical Jatropha oil biodiesel production [3].

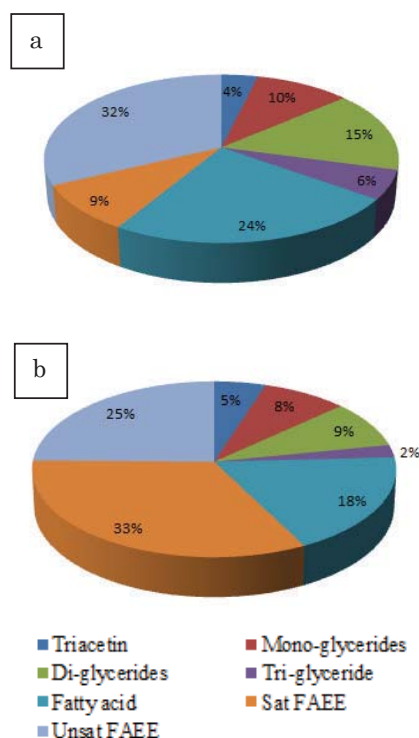


Figure 2. Fatty acid composition of a) Jatropha oil and b) Refined palm oil

ACKNOWLEDGMENT

The authors would like to acknowledge Thailand Institute of Scientific and Technological Research for the financial support

References

- [1] K. T. Tan, K. T. Lee and A. R. Mohamed, "A glycerol-free process to produce biodiesel by supercritical methyl acetate technology. An optimization study via Response Surface Methodology", *Bioresource Technology*. **101**, 2010, pp 965-969.
- [2] S. Hejda, M. Drhova, J. Kristal, D. Buzek, P. Krystynik and P. Kluson, "Microreactor as efficient tool for light induced oxidation reactions", *Chemical Engineering Journal*. **255**, 2014, pp.178-184.
- [3] S. Hawash, N. Kamal, F. Zaher, O. Kenawi and G. El Diwani, "Biodiesel fuel from Jatropha oil via non-catalytic supercritical methanol transesterification", *Fuel*. **88**, 2009, pp.579-582.

Hydrogen and Fuel Cell

HYDROGEN PRODUCTION FROM DRY-REFORMING OF BIOGAS OVER Pt/Mg_{1-x}Ni_xO CATALYSTS

Faris Jassim Al-Doghachi^{1,2}, Zulkarnain Zainal^{1,2}, Mohd Izham Saiman^{1,2}, Zaidi Embong³, Yun Hin and Taufiq-Yap^{1,2}.

¹Catalysis Science and Technology Research Centre, Faculty of Science, University Putra Malaysia, Malaysia.

²Department of Chemistry, Faculty of Science, University Putra Malaysia, Malaysia

³Department of Science, Faculty of Science, Technology and Human Development, University, Malaysia

SUMMARY: Incorporation of NiO onto MgO exhibited a notable conversion when compared to MgO alone, while the addition of Pt to MgO-NiO as a promoter has augmented the conversion of CO₂ up to 99%. CH₄ to CO₂ gases at 2:1 ratio has produced the highest conversion as compared to that obtained by 1:1 ratio. Hence, as a result of this process, the carbon deposition is reduced and consequently the life time of the catalyst has improved.

Keywords: Synthesis gas, H₂ production, Dry-Reforming of biogas, MgO-NiO catalysts

INTRODUCTION

Palm oil biomass is the most abundant bio-renewable resource in Malaysia and Indonesia with great potential for sustainable production of chemicals and fuels. Effluents from palm oil mills also known as palm oil mill effluent (POME) is always regarded as a highly polluting wastewater. Anaerobic digestion is widely adopted in the oil palm industry as a primary treatment for POME. At many palm-oil mills this process is already in place to meet water quality standards for industrial effluent. The biogas, however, is flared off. Biogas contains two greenhouse gases (GHG) *i.e.* about 60-70 % methane (CH₄) and 30-40 % carbon dioxide (CO₂) and also trace amount of hydrogen sulphide, (H₂S). (Chin *et al.*, 2013; Poh *et al.*, 2009). Dry reforming of methane (DRM) has received great attention due to its environmental benefits from utilizing these two greenhouse gases and producing highly valuable synthesis gas (syngas, H₂ and CO) as a feedstock.

METHODOLOGY

Pt/Mg_{1-x}Ni_xO catalysts, where x = 0, 0.03, 0.07, and 0.15 with 1 wt% Pt for each, were prepared by the co-precipitation method from aqueous solution of Ni (NO₃)₂.6H₂O and Mg (NO₃)₂.6H₂O using K₂CO₃. After being filtered and washed with hot water, the precipitate was dried at 120°C for 12 h, and then pre-calcined in air at 500°C for 5 h. Following that, they were pressed into disks at 600 kg/m², and calcined in air at 1150°C for 20 h. The synthesized catalysts were analyzed by XRD, BET surface area and TEM. Crystalline structures of the samples were investigated using X-ray diffraction (XRD) with a Shimadzu XRD-6000 diffractometer. The surface area, pore volume and pore size diameter of the samples were determined using N₂ adsorption-desorption technique with a Thermo Finnigan Sorptomatic Instrument, model 1900. The coke formation of the used catalysts was examined by temperature programmed oxidation (TPO) using

a Thermo Finnigan TPD/R/O 1100 Instrument.

The catalytic evaluation for dry reforming of biogas was performed in a continuous flow system using a fixed bed stainless steel micro-reactor. The reactor was connected to a mass flow gas controller and an online gas chromatograph (GC) (Agilent 6890N; G 1540N). Prior to reaction, approximately 0.02 g catalyst was reduced by flowing 5% H₂/Ar (30 ml/min) from 100 to 700 °C and holding for 3 h. The reforming reaction was performed by flowing a gas mixture consisting of CH₄:CO₂ = 2:1, at a rate of 30 ml/min from 700 to 900 °C at 10 °C/min, then holding for 200 h.

RESULTS AND DISCUSSION

The XRD patterns of the catalysts showed that the crystal system for the catalysts was in cubic phase and this was confirmed by the TEM image (Figure 1). Figure 2 shows the most active catalyst in the dry reforming of biogas. The reaction was carried out for 200 h at 900°C and revealed that the catalyst gave > 95% conversion for both CO₂ and CH₄. The order of conversion of CO₂ and CH₄ is as follows:

Pt/Mg_{0.85}Ni_{0.15}O > Pt/Mg_{0.93}Ni_{0.07}O > Pt/Mg_{0.97}Ni_{0.03}O > Pt/MgO with a CH₄:CO₂ mole ratio of 2:1. Pt/Mg_{0.85}Ni_{0.15}O displayed the best resistance to the deactivation by carbon formation and formed high selectivity of H₂ and CO. Both pores of supporter and doping metal played a vital role in the conversion process as indicated by the BET results. Temperature programmed oxidation (TPO) of the used catalyst showed no significant coke deposition on the surface of this catalyst which may due to the presence of Pt nanoparticles located on the MgO-NiO solid solution. Dry reforming of biogas reaction was also carried out with the presence of low concentrations of oxygen flow (1.25%) and showed an enhancement in the conversion of CH₄. This oxygen reacts with CH₄ to produce CO and H₂O Eq.(1), and finally the steam reacts with the deposited carbon to give syngas Eq.(2).

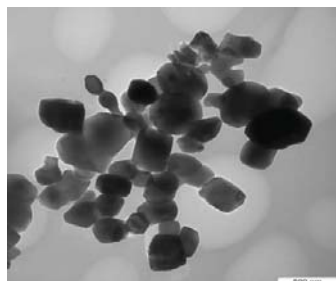
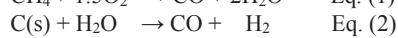
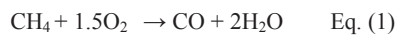


Figure 1. TEM image for Pt/Mg_{0.85}Ni_{0.15}O

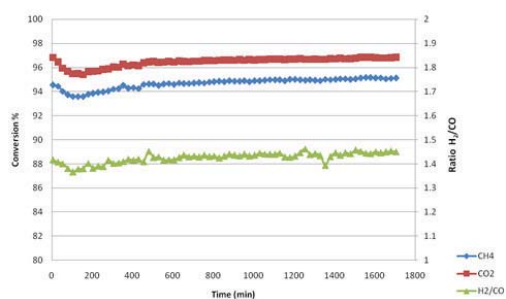


Figure 2. Stability tests of CH₄ and CO₂ conversions and H₂/CO ratio over Pt/Mg_{0.85}Ni_{0.15}O catalysts as a function of time (reaction temperature at 900 °C)

References

- [1] M.J. Chin, P.E. Poh, B.T. Tey, E.S. Chan and K.L. Chin. Biogas from palm oil mill effluent (POME): Opportunities and challenges from Malaysia's perspective. *Renewable and Sustainable Energy Reviews*, **26**, 2013, pp. 717-726.
- [2] P. Poh and M. Chong. Development of anaerobic digestion methods for palm oil mill effluent (POME) treatment, *Bioresour Technol*, **100**(1), 2009, pp. 1-9.

MODIFICATION OF GREEN CALCIUM OXIDE AND CHARACTERISTICS OF CLEAN ENERGY CATALYSTS

Wilasinee Wisajjorn¹, Piyasan Praserttham², Suttichai Assabumrungrat² and Soipatta Soisuwan¹

¹Department of Chemical Engineering, Faculty of Engineering, Burapha University, Thailand

²Center of Excellence in Catalysis and Catalytic Reaction Engineering, Department of Chemical Engineering, Faculty of Engineering, Chulalongkorn University, Thailand

SUMMARY: The additional calcium oxide was designated at 10% by wt in copper-based catalysts. Prior to the catalyst preparation, calcium oxide was prepared by firing natural calcium carbonate (calcite) at 850 °C according to the decomposition temperature obtained from thermogravimetric analysis. The modification of basic strength was accomplished by additional $\text{Ti}(\text{OC}_2\text{H}_5)_4$ or KMnO_4 at 1% weight to calcium carbonate and then they were calcinated at same temperature. CO_2 Temperature Programmed Desorption (CO_2 -TPD) was carried out to investigate the ability to adsorb CO_2 molecules representing the number of basic sites for all calcium oxide. Besides CO_2 TPD, crystalline structure was identified by X-ray diffraction and surface area of all CaO was determined by N_2 physisorption. The copper-based catalysts were prepared with 10% weight CaO or modified CaO. The H_2 temperature programmed reduction was carried out by thermogravimetric analysis under inert gas atmosphere in comparison with the result obtained under 5% H_2 in inert. Addition of calcium oxide into copper-based catalyst gave significant effect on the reduction behaviors.

Keywords: methanol synthesis, modified CaO, copper-based catalysts, CO_2 -TPD and H_2 -TPR

INTRODUCTION

Carbon dioxide is the most well known green house gas effecting on global environment more seriously. The increment of carbon dioxide was mostly from fossil fuel combustion in transportations, electrical power plants and industries which are essentially important for human demand. Although so many energy policies have been launched, the elimination of energy consumption seems ineffective due to highly increasing population. The utilization of carbon dioxide has been recently emerged as interesting topics as it is a chemical source of carbon which can turn to beneficial chemicals via catalytic reactions. The carbon dioxide can directly change to methanol and then dimethylether (DME) or dimethylcarbonate (DMC) which is a starting material for chemical industries. The catalytic material which has been widely used to synthesize methanol is CuO-ZnO catalyst. Up to date, effective condition to produce 98% methanol conversion in industries is operated at high pressure (>atmospheric pressure) and low temperature. Several researches revealed basic surface of the catalyst favoring methanol selection, however methanol synthesis carried out over the catalysts modified by lanthanum, fluorine, zirconium to obtain different basic species was clearly dependent on basic strength. To insist these results, calcium oxide was thus chosen as additive to copper based catalysts in our experiment since it possesses high basic strength.

EXPERIMENTS

Materials Preparation

Calcite calcium carbonate (CaCO_3) of oyster shells was employed as starting material to produce calcium oxide and modified calcium oxide. The starting material was mechanically crushed and

sieve to equivalent mesh size from μm to μm , and then calcination under flowing oxygen 30 ml/min ramping to 850 °C for 2 hours. The ramping rate was 5°C/min. Two precursors, i.e. potassium permanganate (KMnO_4) or titanium ethoxide ($\text{Ti}(\text{OC}_2\text{H}_5)_4$), were designated to obtain 1% content of Ti or Mn in the resulting calcium oxide. The Mn precursor was dissolved in distilled water, whereas Ti precursor was sonicated randomly in ethanol to attain suspension of Ti-based fine particles. The resulting solution/suspension was slightly impregnated into calcium carbonate and then dried at 100°C and calcination at 850 °C for 2 hours. The names of these resulting materials are CaO, CaO/ KMnO_4 and CaO/ TiO_2 , respectively. Additional CaO or modified CaO to copper-based catalyst support (zirconium dioxide, Tosoh ZrO_2) was at 10% by weight in physically mixing support of Tosoh ZrO_2 and as-prepared calcium oxide. The copper-based catalysts were prepared by incipient wetness impregnation at designated 10% copper content in the catalysts. The nomenclatures of these catalysts are Cu/ ZrO_2 /CaO, Cu/ ZrO_2 /CaO/ KMnO_4 and Cu/ ZrO_2 /CaO/ TiO_2 .

Materials Characterization

The as-prepared calcium oxide materials were characterized by means of X-ray diffraction, N_2 -physisorption and CO_2 -Temperature Programmed Desorption (CO_2 -TPD). We aim to test the catalysts for CO_2 hydrogenation, thus the copper-based catalysts were characterized by means of H_2 Temperature Programmed Reduction (H_2 -TPR) to describe the reduction behavior. The H_2 -TPR profiles were obtained by Thermogravimetric Analysis (TGA). 10 mg of the catalysts was placed on alumina crucible in the TGA furnace. Testing 10 mg catalyst was carried out

under N₂ atmosphere and the equivalent testing was carried out under mixture of hydrogen in nitrogen (5% H₂ in N₂). The Furnace temperature was ramped to 800 °C with heating rate 10 °C/min. The decomposition rate under both atmospheres was calculated as following.

$$\text{decomposition rate} = \frac{1}{w_i} \frac{\partial w}{\partial t} \quad (1)$$

where w_i is initial weight of the catalyst 10 mg and $\frac{\partial w}{\partial t}$ is the change of catalyst weight at intervals. The rate of hydrogen consumption tends to apparently correspond to weight decomposition rate while no significant loss of weight under nitrogen atmosphere. The consumption of hydrogen used to reduce the catalysts can be calculated by a net different area of weight decomposition between under inert atmosphere and %5 hydrogen in inert related to the area corresponding to amount of hydrogen consumed in reduction of 10-mg copper (II) oxide.

RESULTS AND DISCUSSION

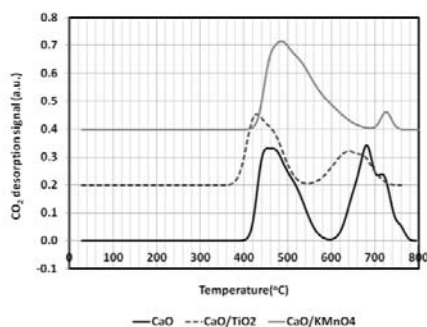


Figure 1. CO₂ Temperature programmed desorption of as-synthesized CaO, CaO/TiO₂ and CaO/KMnO₄

The carbon dioxide temperature programmed desorption profiles were performed in Figure 1. The amount of carbon dioxide adsorbed on calcium dioxide represents the number of basic sites that can chemically bond to form carbonate species. The amount of carbon dioxide desorption increases while compared with our previous results [1]. This is probably due to prolonging the CO₂ saturation for 6 hours. The significant effect of calcium oxide on reduction behaviors exhibits in Figure 2. The decomposition of copper-based catalysts composed of calcium oxide was found at 400°C under nitrogen atmosphere or inert gas, possibly suggesting the unstable compound of calcium species, whereas the most stable only ZrO₂-supported copper catalyst exhibited under nitrogen atmosphere (gray line in Figure 3). The hydrogen reduction of copper species took a place at 300 °C for Cu/ZrO₂, while the copper

species may react at higher temperature while consisting in calcium oxide-modified catalysts. The calcium oxide seems to retard the hydrogen reduction plausibly owing to a formation of copper-calcium compound. However, copper species is likely to be more stable under KMnO₄ and TiO₂ modification. Although copper-based catalyst modified by calcium oxide is incomparable with Cu/ZrO₂ in term of hydrogen reduction, the amount of carbon dioxide desorption, especially at medium temperature is more pronounce.

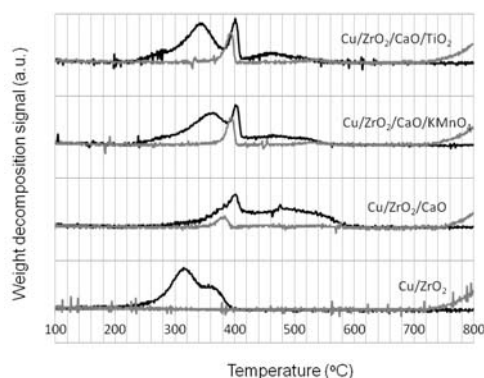


Figure 2. H₂ Temperature Programmed Reduction profiles of copper based catalysts in our experiment

CONCLUSION

Addition of calcium oxide to copper-based catalysts clearly modified the basic strength and the number of basic sites; however, the modification of calcium oxide inhibits hydrogen reduction leading to higher reducing temperature and possibly lower active metal site dispersion.

ACKNOWLEDGEMENT

The authors would like to kindly give their gratitude to Faculty of Engineering, Burapha University for grant No. 23/2556.

Reference

- [1] S. Soisuwan, J. Phommachant, W. Wisaijorn and P. Praserttham, "The Characteristics of green calcium oxide derived from aquatic materials" *Procedia Chemistry*, **9**, 2014, pp. 53-61.

SIMULTANEOUS TREATMENT OF NITROGEN-RICH WASTEWATER AND ELECTRICITY GENERATION USING SINGLE-CHAMBER MICROBIAL FUEL CELL

Vanatpornratt Sawasdee¹ and Nipon Pisutpaisal^{1,2,3,4}

¹The Joint Graduate School of Energy and Environment (JGSEE) King Mongkut's University of Technology Thonburi, Tungkru, Thailand

²Department of Agro-Industrial, Food and Environmental Technology, Faculty of Applied Science, King Mongkut's University of Technology North Bangkok, Thailand

³The Biosensor and Bioelectronics Technology Centre, King Mongkut's University of Technology North Bangkok, Thailand

⁴The Research and Technology Center for Renewable Products and Energy, King Mongkut's University of Technology North Bangkok, Thailand.

SUMMARY: Simultaneous electricity generation and combined carbon and nitrogen removal in wastewater using microbial fuel cells are an intriguing process. The generation of electricity from nitrogen-rich wastewater was examined using single chamber air cathode microbial fuel cells (SCMFCs). SCMFCs were fed with an artificial wastewater containing the initial chemical oxygen demand (COD): nitrogen (N) ratio of 4:1, and operated under mesophilic batch mode. Performance of SCMFCs with external resistances 1,000 Ω and COD concentration 500, 1000, and 2,500 mg L⁻¹ based on maximum power density and current output was compared. The SCMFCs with COD concentration 1,000 mg L⁻¹ gained higher maximum power density and current output by 0.252 mA and 101.92 mW/m², respectively. The COD and ammonium removal in 1,000 mg L⁻¹ condition was 79.0 and 97.9%, respectively. The findings suggested that MFC is a potential technology to treat carbon and nitrogen pollutants in wastewater, and recover electric energy at the same time.

Keywords: single chamber microbial fuel cells, nitrogen-rich wastewater, power density, current

INTRODUCTION

Microbial fuel cell (MFC) is a bio-electrochemical system that directly captures the electrons produced by microbial catabolism. The main application for MFC includes wastewater treatment and generating electricity. A variety of substrates such as: marine sediments, anaerobic digested sludge, food, municipal, slaughterhouse and domestic wastewater [1] can be used as feedstocks in MFCs.

Nitrogen-rich wastewater is an interesting feedstock for generating electricity in MFC, since, many form of organic and inorganic nitrogens can be utilized by microorganisms. MFC generates energy in form of electricity through the oxidation-reduction in the microorganisms. The purpose of this study was examined the effect of COD and ammonium concentration with a fixed COD:N ratio of 4: 1 on electricity generation using SCMFCs.

MATERIAL AND METHOD

SCMFCs

The single chamber air-cathode MFC consisted of an anode and cathode placed on opposite sides in acrylic material cylindrical chamber 4 cm long by 3 cm in diameter (empty bed volume of 28 mL, anode and cathode projected surface area 12.57 cm²).

Setup and operation of MFC

The MFCs were enriched with active microorganisms, obtained from a full-scale up flow anaerobic sludge blanket (UASB), Eiamburapa Industry

Thailand, at the anode. AW with COD concentration 500 mg L⁻¹ was fed to the MFCs in semi-batch mode and open circuit condition until the MFCs reached steady state. When the enrichment was stable, the condition was switch to closed circuit condition. MFC tests were conducted using a single chamber device operated with 1000 Ω external resistance to create a close circuit. SC-MFC was using different substrates concentration with COD: N ratio 4: 1. The COD concentrations were created 500, 1,000, and 2,500 mg L⁻¹. The experiments were operated at temperature 37 °C, and initial pH 7.

RESULT AND DISCUSSION

Electricity generation

The effect of COD and ammonia concentration on the electricity generation was showed in Fig 1. The highest power density was obtained at organic loading of 1,000 mg COD/L. The maximum current and power density were 0.252 mA and 101.92 mW/m², respectively. Electricity generation using 0.018 mM NH₄Cl was comparable to previous report [2] using 0.024 mM NH₄Cl. The previously report [2], was generating electricity 0.068 mA, it was lower than current (0.252 mA) in this study. The suitable concentration of COD and ammonium for SC-MFC was 1,000 mg L⁻¹ due to the highest production and treatment efficiency.

Pollution Removal

The pollution removal efficiency was increased with COD concentration 1,000 mg L⁻¹. The

average of COD removal efficiency was 69.0, 79.0 and 58.0% when operated COD concentration of 500 to 2,500 mg L⁻¹, respectively. The percentage of ammonium removal was approximately 97.9-98.2% (Fig 2). The removal nitrogen processes are assimilation and dissimilation. The dissimilation (nitrification and denitrification) was decomposing organic and inorganic matter convert to energy and assimilation deals with the synthesis of proteins or nucleic acids use for new cells. The nitrification was convert ammonia-N to nitrite and nitrate, and some of ammonia-N was used into cell by assimilation process. Thus, SCMFCs are able to simultaneous electricity generation and pollutant removal in nitrogen-rich wastewater.

Illustrations and graphics

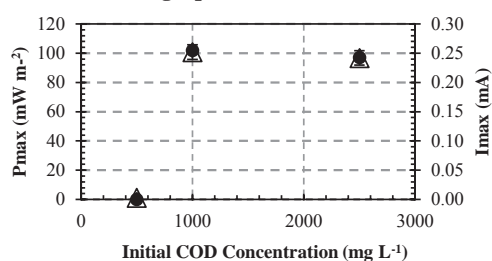


Figure 1. Maximum power output at COD concentration 500, 1,000 and 2,500 mg L⁻¹ (●). Maximum current output at COD concentration 500, 1,000 and 2,500 mg L⁻¹ (△). Symbols and histograms represent mean values of triplicate experiments, and error bars represent one standard deviation.

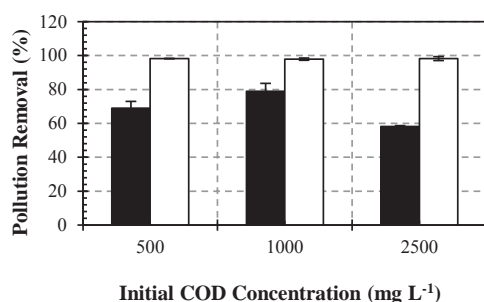


Figure 2. Treatment efficiency of pollution removal (ammonium remove, □ COD remove ■). Histograms represent mean values of triplicate experiments, error bars represent one standard deviation

ACKNOWLEDGMENT

The authors would like to express gratitude to the Joint Graduate School of Energy and Environment (JGSEE), King Mongkut's University of Technology Thonburi, Thailand for the financial support (grant no. JGSEE/THESIS/225).

References

- [1] B. Min, JR. Kim, SE. Oh, JM. Regan, and BE. Logan. "Electricity generation from swine wastewater using microbial fuel cells", *Water Research*. **39**, 2005, pp. 4961–4968.
- [2] Z. He, J. Kan, Y. Wang, Y. Huang, F. Mansfeld, and KH. Nealsen. "Electricity production coupled to ammonium in a microbial fuel cell", *Environ. Sci. Technol.* **43**, 2009, pp. 3391-3397.
- [3] D.R. Bond and D.R. Lovley. "Electricity production by *Geobacter sulfurreducens* attached to electrodes", *Applied and Environ Microbiology*. **69**, 2003, pp 1548– 1555.
- [4] A.P. Crystal, "Microbial Fuel Cell Operation and use with Anaerobic Digestion for Power Production from Dairy Manure", *Cornell University*, 2007.
- [5] GS. Jadhav, andMM. Ghangrekar. Improving "Performance of MFC by Design Alteration and Adding Cathodic Electrolytes", *Appl Biochem Biotechnol.* **151**, 2008, pp. 319–332.
- [6] APHA Standard, Methods for the Examination of Water and Wastewater, 21st ed., Washington, DC, USA: American Public Health Association, American Water Works Association, Water Environment Federation, 2005.
- [7] BE. Logan, and JM. Regan. "Electricity-producing bacterial communities in microbial fuel cells", *TRENDS in Microbiology*. **14**, 2006, pp. 12.

INFLUENCE OF INOCULUM PRETREATMENT ON PERFORMANCE OF AIR-CATHODE SINGLE-CHAMBER MFC

Pinanong Tanikkul¹ and Nipon Pisutpaisal^{1,2,3,4}

¹The Joint Graduate School of Energy and Environment (JGSEE),
King Mongkut's University of Technology Thonburi, Thailand

²Department of Ago-Industrial, Food and Environmental Technology, Faculty of Applied Science,
King Mongkut's University of Technology North Bangkok, Thailand

³The Biosensor and Bioelectronics Technology Centre,
King Mongkut's University of Technology North Bangkok, Thailand

⁴The Research and Technology Center for Renewable Products and Energy,
King Mongkut's University of Technology North Bangkok, Thailand

SUMMARY: Air-cathode SCMFCs using the heat pretreated seed inoculation showed that the shorter period of biofilm formation with the maximum current output after 25 days inoculation when compared to the non-heat pretreated seed inoculation (45 days). The results showed that the high performance of the heat pretreated seed inoculation in term of a peak of voltage and current generation, except the high COD and reducing sugar removal. The better voltammogram in oxidation and reduction peaks of the heat pretreated seed anode biofilm using cyclic voltammetry techniques. The current densities increased with increases of wastewater concentrations and obtained maximum value was 7.37 mA m⁻² of 3,000 mg COD L⁻¹ of the heat pretreated seed inoculation. The results indicated that the wastewater can be used as a substrate to produce electricity and can be treated in air-cathode SCMFCs. In addition, the current outputs and wastewater concentrations displayed a linear correlation in the concentration range of 500 to 3,000 mg COD L⁻¹ ($r^2=0.96$).

Keywords: microbial fuel cell, air-cathode MFC, single-chamber MFC, heat pretreated seed, bioelectricity

INTRODUCTION

Recently, world energy consumption has increased which the main energy source is mostly dependent on fossil fuels, lead to limited fossil energy sources and unsustainable [1]. Therefore, the search of alternative fuels are becoming more and more attractive to reduce dependence on fossil fuels and decreasing storage of fossil fuels [1]. Microbial fuel cells (MFCs), is an ideal and promising technology in recent years which biodegrade renewable materials to electricity directly by using microorganism as a biocatalyst [2]. Microorganisms in anode chamber oxidize energy stored in organic matters to produce protons and electrons through anaerobic condition. The electrons are transferred to anode surface and then from external circuit to cathode. The protons diffuse via the membrane into the cathode chamber, where they combine with an electron acceptor and produce water [1].

The air-cathode, single-chamber MFC has been developed due to high power output versus a two-chamber, low operating costs, and a simple structure [3, 4]. Therefore, this study focused on the startup experiment by using the non-heat pretreated seed compare to the heat pretreated seed as inoculums to enrichment of biofilm and produced bioelectricity along with wastewater treatment in air-cathode SCMFC. In addition, the work was evaluated the relationship between wastewater concentrations with the current output.

METHODOLOGY

Air-cathode SCMFCs were made of acrylic cylindrical chamber (4 cm long, 3 cm diameter and

28 mL working volume) [5]. The anode and the cathode were made of carbon cloth (surface area = 7 cm²) and titanium wire was connected the electrodes.

Anaerobic mixed cultures were obtained from a full-scale up-flow anaerobic sludge blanket (UASB) starch-processing wastewater treatment plant. The seed was heat pretreated to inhibit the methane producing bacteria prior to use [6] and the original seed (non-heat pretreated) was used as the control experiments.

Synthetic wastewater containing glucose as the carbon source was used in this experiment. The heat and the non-heat pretreated seeds were inoculated in the air-cathode SCMFCs with synthetic wastewater in separated reactors under open circuit voltage (OCV) fed batch mode operation. After that, the air-cathode SCMFCs were acclimated with 1,000 mg COD L⁻¹ of synthetic wastewater under 1,000Ω R_{ext}. The impact of wastewater loading on the current output was investigated under varying wastewater in a step wise (125 to 4,000 mg COD L⁻¹). The pH of the wastewater was controlled to 7.0 by using phosphate buffer solution and air-cathode SCMFCs were operated at 37°C.

The characteristics of oxidation and reduction reactions on the anode surface at the start and the end of each part operation were measured by using the cyclic voltammetry (CV) technique. The voltage output was automatically recorded by a multimeter. The current and power were calculated using the Ohms law as previously described [7]. PH, ORP, chemical oxygen demand (COD), reducing sugar, total solid and volatile fatty acids of the influent and the effluent were analyzed.

RESULTS AND DISCUSSION

The air-cathode SCMFCs were inoculated with the heat pretreated seed showed a stable voltage after 25 days acclimated with 1,000 mg COD L⁻¹ under 1,000Ω R_{ext}. In addition to a shorter biofilm enrichment and the high current output of the heat pretreated seed were observed when compared to the non-heat pretreated seed (45 days acclimation). However, this acclimation proved the microbial ability of degrading substrate in term of the COD and reducing sugar removal more than 90 and 99%, respectively. The electrochemical activity of the non-heat pretreated seed biofilm on anode surface showed the redox peaks are quite low when compared to the heat pretreated seed biofilm showed the redox peaks with the highest current was 0.038 mA for the forward scan and -0.31 mA for the reverse scan (Figure. 1). This indicated that the microbial activities in the SCMFCs were different.

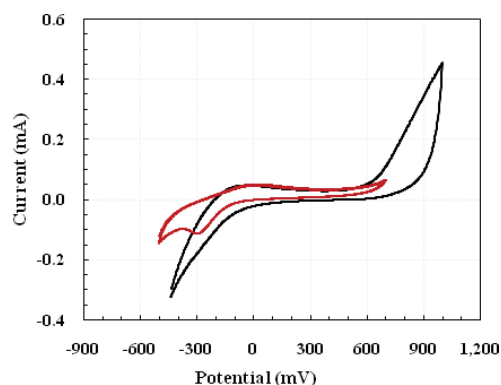


Figure 1. Cyclic voltammograms of anode surface biofilm of the non-heat pretreated seed (red line) and the heat pretreated seed (black line) after inoculation at a scan rate of 20 mV s⁻¹

The air-cathode SCMFCs were operated with varies the wastewater concentrations to observe the effect of organic loading on current output. The results showed the current densities were increased with the wastewater concentrations. However, the current densities values of the heat pretreated seed were higher than the non-heat pretreated seed in all tests (Figure. 2), demonstrating that the voltage and current generation were depended on the wastewater loading and the type of microbial seed. While, the COD removal of the heat pretreated seed was obtained up to 90% and higher than the non-heat pretreated seed.

ACKNOWLEDGMENT

The authors are grateful to Thailand Research Fund through the Royal Golden Jubilee Ph.D. Program (Grant No.PHD/0322/2552) and the Joint Graduate School of Energy and Environment (JGSEE), King Mongkut's University of

Technology Thonburi for financial support.

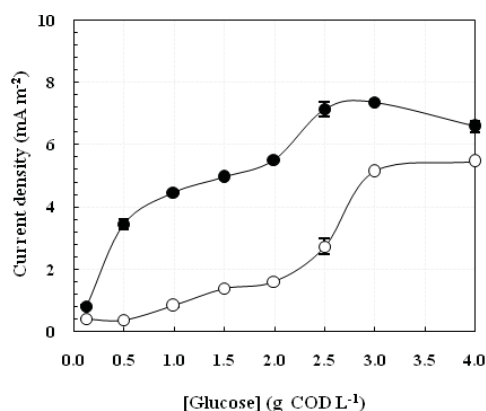


Figure 2. Relationship between current densities with COD values of the heat pretreated seed (●) and the non-heat pretreated seed (○) inoculation at 50Ω

References

- [1] M. Rahimnejad, A.A. Ghoreyshi, G. Najafpour and T. Jafary., "Power generation from organic substrate in batch and continuous flow microbial fuel cell operations", *Applied Energy*. 2011, pp.3999-4004.
- [2] A. Kaur, Hitesh C. Boghani, Iain Michie, Richard M. Dinsdale, Alan J. Guwy, Giuliano and C. Premier, "Inhibition of methane production in microbial fuel cells: Operating strategies which select electrogens over methanogens", *Bioresource Technology*. **173**, 2014, pp.75-81.
- [3] N. Lu, Shun-gui Zhou, Li Zhuang, Jin-tao Zhang and Jin-ren Ni, "Electricity generation from starch processing wastewater using microbial fuel cell technology", *Biochemical Engineering Journal*. **43**, 2009, pp.246-251.
- [4] H. Liu, Cheng S and Logan BE, "Production of Electricity from Acetate or Butyrate Using a Single-Chamber Microbial Fuel Cell", *Environmental science Technology*. **39**, 2006, pp.658-662.
- [5] H. Liu and B. E. Logan. "Electricity Generation Using an Air-Cathode Single Chamber Microbial Fuel Cell in the Presence and Absence of a Proton Exchange Membrane", *Environ. Sci. Technol.* **38**, 2004, pp. 4040-4046.
- [6] H. P. Fang, Chenlin Li and Tong Zhang, "Acidophilic biohydrogen production from rice slurry", *International Journal of Hydrogen Energy*. **31**, 2006, pp.683-692.
- [7] G. S. Jadhav and M. M. Ghangrekar. "Performance of microbial fuel cell subjected to variation in pH, temperature, externalload and substrate concentration", *Bioresource Technology*. **100**, 2009, pp.717-723.

EFFECT OF NITROGEN CONCENTRATION ON PERFORMANCE OF SINGLE-CHAMBER MICROBIAL FUEL CELLS

Vanatpornratt Sawasdee¹ and Nipon Pisutpaisal^{1,2,3,4}

¹The Joint Graduate School of Energy and Environment (JGSEE) King Mongkut's University of Technology Thonburi, Thailand

²Department of Agro-Industrial, Food and Environmental Technology, Faculty of Applied Science, King Mongkut's University of Technology North Bangkok, Thailand

³The Biosensor and Bioelectronics Technology Centre, King Mongkut's University of Technology North Bangkok, Thailand

⁴The Research and Technology Center for Renewable Products and Energy, King Mongkut's University of Technology North Bangkok, Thailand.

SUMMARY: The nitrogen removal in wastewater using single chamber microbial fuel cells is an interesting process. The nitrogen removal from nitrogen wastewater was examined using single chamber air cathode microbial fuel cells (SC-MFCs). SC-MFCs were fed with synthetic wastewater containing the initial chemical oxygen demand (COD) 1,000 mg L⁻¹ and nitrogen (N) 125, 250, 625, and 875 mg-N L⁻¹, respectively and operated under mesophilic batch mode. Performance of SC-MFCs with external resistances 1,000 Ω was based on maximum power density, COD and nitrogen removal. The SC-MFCs with ammonia-N concentration 625 mg-N L⁻¹ gained higher maximum power density by 160 mW m⁻². The ammonium removal was 58 %. The suggested that SC-MFCs is a potential technology with highest of ammonia-N concentration that microorganism accept is 625 mg-N L⁻¹ to simultaneous to nitrogen removal, COD removal and electricity generation.

Keywords: single chamber microbial fuel cells, nitrogen removal, synthetic wastewater, external resistance, power density

INTRODUCTION

The nitrogen wastewater treatment technology is an important process to remove nutrient pollutant. The nitrogen wastewater is a major impact due to its primary role to the impact on eutrophication of water bodies and on human and animal health [1]. The removal of nitrogen in the wastewater is difficult in one process. There are two reactions in nitrogen removal; nitrification is oxic ammonia oxidation, and denitrification is anoxic nitrate reduction. It is require to multiple reactor used for nitrogen wastewater treatment with oxic and anoxic condition. While the SC-MFCs can be simultaneously generate electricity and treat nitrogen in the wastewater. The nitrogen removal in SC-MFCs can be occur nitrification and denitrification in one reactor.

SC-MFCs are interesting for nitrogen wastewater treatment in one process. This process is lower operation cost than other process that requires more than one process. In this study, the limitation of ammonia-N for nitrogen removal and generating electricity were investigated.

MATERIAL AND METHOD

SC-MFCs configuration and operation

The experiments were using air- cathode single chamber microbial fuel cell constructed as a previous describes, (Liu and Logan, 2004). SC-MFCs were operated in close circuit condition (electricity generation) to investigate the effect of power, current, and nitrogen removal in fixed COD concentration and vary ammonia-N concentration. SC-MFCs were operated in batch mode with

temperature 37 °C and pH was 7.

Synthetic wastewater

The synthetic wastewater for SC-MFC modify from Jadhav and Ghangre, (2008) [2]. The synthetic wastewater had fixed COD concentration 1000 mg L⁻¹ and varied ammonia-N concentration 125, 250, 625, and 875 mg-N L⁻¹, respectively. Synthetic wastewater was autoclaved at 121 °C for 15 minutes before use.

Analytical procedures

The pH, ammonia-N, COD, ORP, nitrite-N and nitrate-N were analyzed during the test. There were analyzed according to APHA Standard Method [3].

RESULT AND DISCUSSION

SC-MFCs performance

The carbon source of SC-MFCs was fixed 1,000 mg L⁻¹. The effect of ammonia-N concentration in the system was shown in Fig 1. The limit of power density with ammonia-N was limiting in ammonia-N concentration 875 mg-N L⁻¹. The high ammonia-N wastewater was limit power density because it was occur nitrogen wastewater treatment (nitrification and de-nitrification) in system. The requirement of de-nitrification reaction was electron to occur reaction.

Ammonia-N removal

The milligram of ammonia-N and percentage of ammonia-N removal was shown in Fig 2. The highest percentage of ammonia-N removal was detected in ammonia-N concentration 825 mg-N L⁻¹

was 72% of batch test. The percentage of ammonia-N removal of concentration 125, 250, and 625 mg- NL⁻¹ was 50 to 58% that lower than 825 mg- NL⁻¹. The way of ammonia-N removal was assimilation and dissimilation. The dissimilation is nitrification and de-nitrification. The conversion of nitrogen removal is based on autotrophic nitrification and heterotrophic denitrification [4]. This research successful demonstrated simultaneous nitrogen removal process and electricity generation in SC-MFCs. The best performance of SC-MFCs to nitrogen removal was ammonia-N concentration 625 mg-N L⁻¹.

“Performance of MFC by Design Alteration and Adding Cathodic Electrolytes”, *Apply Biochem Biotechnol.* **151**, 2008, pp. 319–332.

[3] APHA Standard, Methods for the Examination of Water and Wastewater, 21st ed., Washington, DC, USA: American Public Health Association, American Water Works Association, Water Environment Federation, 2005.

[4] K. Than and P. A. Ajit. “Novel microbial nitrogen removal process”, *Biotechnology Advance.* **22**, 2004, pp. 519-532.

Illustrations and graphics

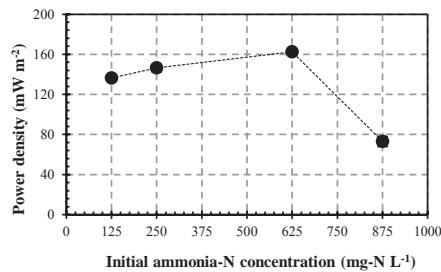


Figure 1. Power density in varying initial ammonia-N concentration

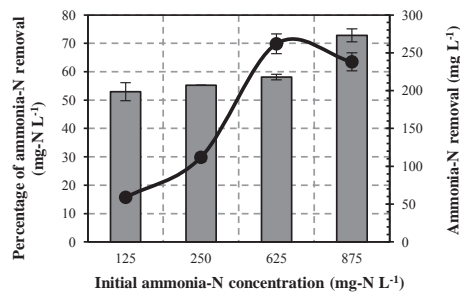


Figure 2. The percentage of ammonia-N removal Ammonia-N removal in varying initial ammonia-N concentration

ACKNOWLEDGMENT

The authors would like to express gratitude to the Joint Graduate School of Energy and Environment (JGSEE), King Mongkut's University of Technology Thonburi, Thailand for the financial support (grant no. JGSEE/THESIS/225).

References

- [1] X. Yong, Y. Zheng, S. Wu, Z.H. Yang and F. Zhao, “Nitrogen recovery from wastewater using microbial fuel cells”, *Front Environment Science Engineer.* 2014, pp.1-7.
- [2] GS. Jadhav, and MM. Ghangrekar. Improving

PERFORMANCE OF MEMBRANE-LESS AIR-CATHODE SCMFC IN ELECTRICITY GENERATION FROM DISTILLERY WASTEWATER

Pinanong Tanikkul¹ and Nipon Pisutpaisal^{1,2,3,4}

¹The Joint Graduate School of Energy and Environment (JGSEE),
King Mongkut's University of Technology Thonburi, Thailand

²Department of Ago-Industrial, Food and Environmental Technology, Faculty of Applied Science,
King Mongkut's University of Technology North Bangkok, Thailand

³The Biosensor and Bioelectronics Technology Centre,
King Mongkut's University of Technology North Bangkok, Thailand

⁴The Research and Technology Center for Renewable Products and Energy,
King Mongkut's University of Technology North Bangkok, Thailand

SUMMARY: Distillery wastewater contains high organic compounds and nutrients suitable for microorganisms in anaerobic processes. The bioelectricity production and the performance of the membrane-less, air-cathode SCMFCs were studied with varying the distillery wastewater concentrations in the range of 125 to 3,000 mg COD L⁻¹ in batch mode under mesophilic condition (37°C). The voltage and current outputs increased with increase distillery wastewater concentration (0.005-0.055 mA). Greater soluble chemical oxygen demand (CODs) removal (29.5-56.7%) and reducing sugar in all batch concentration tested. Results indicated that the distillery wastewater can be produced bioelectricity and can be treated using the air-cathode SCMFCs.

Keywords: microbial fuel cell, membrane-less MFC, bioelectricity, distillery wastewater, wastewater treatment

INTRODUCTION

Microbial fuel cells (MFC) have been developed and can generate electricity directly from almost renewable material or wastewater by using microorganisms through anaerobic condition [1]. However, the amounts of current generation are depending on the types of MFCs and the sources of the substrates [2]. The air-cathode, single-chamber MFC without membrane has been developed to increase mass transfer to the cathode versus a two-chamber, reduced operating costs, and a simplified design [3, 4]. However, membrane-less air-cathode SCMFC was increased oxygen diffusion into the anode chamber, but an aerobic biofilm on the cathode surface can be help removes any oxygen that diffuses into the chamber [4].

Previous studies have focused on the MFCs to generate electricity couple with treating wastewaters, such as food processing [2], swine [5], paper recycling [6], and starch processing [3]. Thailand is the largest source of industrial and agricultural waste and wastewaters which are different characteristics and compositions. The molasses from distillery wastewater in Thailand has been rapidly expanded, and thus generates a large amount of highly polluting. The raw distillery wastewater has very high levels of chemical oxygen demand (COD) [7]. However, for the high level of COD in distillery wastewater which can be used as a source of energy for the bioelectricity production.

This study focused on current generation and the treatment of distillery wastewater in membrane-less, air-cathode SCMFCs under batch mode. In addition, the work was evaluated the relationship between distillery wastewater concentrations with the current output from

air-cathode SCMFC.

METHODOLOGY

Membrane-less, air-cathode, single-chamber MFCs were made of acrylic cylindrical chamber as previously described [8]. The anode and the cathode were made of carbon cloth (surface area = 7 cm²) and titanium wire was connected the electrodes. The air-cathode SCMFCs were enriched with the heat pretreated seed as an inoculums and the synthetic wastewater in previous studied.

The raw distillery wastewater was collected from the primary clarifier effluent of alcohol production which sugar cane molasses was used as the raw material. The distillery wastewater was diluted to the given concentrations from 125 to 3,000 mg COD L⁻¹ and the pH of the dilution was adjusted to 7.0 by using phosphate buffer solution before being fed into the air-cathode SCMFCs without additions of any other nutrient or trace metal. The air-cathode SCMFCs were operated at mesophilic condition (37°C) and fix external resistance in batch mode.

The voltage output was automatically recorded by a multimeter. The current and power were calculated using the Ohms law, as previously described [9]. The liquid sample was collected to analyze for pH, ORP, chemical oxygen demand (COD), reducing sugar and total solid (TS) according to the standard method. Gas composition and volatile fatty acids (VFAs) was measured by using GC.

RESULTS AND DISCUSSION

The air-cathode SCMFCs were operated with varying the distillery wastewater concentrations in the batch mode. The results showed the voltage

generation and maximum current outputs remained increased in the proportion to different distillery wastewater concentration (Figure 1). There is a good evidence for the effect of distillery wastewater on current generation. While, the calibration of maximum current outputs versus wastewater concentrations was obtained up 1,500 mg COD L⁻¹ ($r^2=0.99$). These results are demonstrating wastewater concentration in a low ranging good correlation.

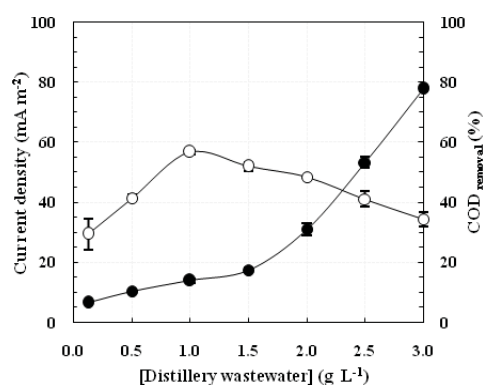


Figure 1. Maximum current outputs (●) and COD removal (%) (○) with distillery wastewater concentrations of 125 to 3,000 mg COD L⁻¹ at 50Ω.

During the operation, the pH of solution decreased (6.2-6.5) from the initial pH after about 12-24 hr operation. Afterwards, the pH of solution reached to 6.7-6.9, when the voltage dropped after a long period operation. This indicated that the protons in solution were removed via the cathode reaction where they combined with oxygen from the air to produce water.

The ORP values in the anode chamber were between -170 to -250 mV when the wastewater concentrations increased. However, SCMFCs without a PEM, the oxygen can diffuse into the anode chamber. Although, in this experiment showed that low ORP values but little change in values after a long period cycle operation. Therefore, concluded that the system operated under anaerobic conditions.

Figure 1 shows the maximum current output increase when the distillery wastewater concentrations increased but the COD removal efficiency decreased. The results indicated that COD removal efficiency was obtained with increasing the wastewater concentrations from 125 to 1,000 mg COD L⁻¹ (30-57%). The CE increased with the wastewater concentration increase of 2.9% at the highest concentration tested. However, the solids are not produced in all batches concentration tested. While, the solids are reduced in all batches concentration tested (5-35%).

ACKNOWLEDGMENT

The authors are grateful to Thailand Research Fund through the Royal Golden Jubilee Ph.D. Program (Grant No.PHD/0322/2552) and the Joint Graduate School of Energy and Environment (JGSEE), King Mongkut's University of Technology Thonburi for financial support.

References

- [1] D. Pant, G.V. Bogaert, L. Diels and K. Vanbroekhoven, "Production A review of the substrates used in microbial fuel cells (MFCs) for sustainable energy production", *Bioresour Technol.* **101**, 2010, pp.1533-1543.
- [2] S. E. Oh and B. E. Logan. "Hydrogen and electricity production from a food processing wastewater using fermentation and microbial fuel cell technologies", *Water Research.* **39**, 2005, pp. 4673-4682.
- [3] N. Lu, S. Zhou, L. Zhuang, J. Zhang and J. Ni, "Electricity generation from starch processing wastewater using microbial fuel cell technology", *Biochemical Engineering Journal.* **43**, 2009, pp.246-251.
- [4] H. Liu, S. Cheng and B.E. Logan, "Production of Electricity from Acetate or Butyrate Using a Single-Chamber Microbial Fuel Cell", *Environmental Science Technology.* **39**, 2006, pp.658-662.
- [5] B. Min, J.R. Kim, S.E. Oh, J. M. Regan and B.E. Logan, "Electricity generation from swine wastewater using microbial fuel cells", *Water Research.* **39**, 2005, pp. 4961-4968.
- [6] L. Huang and B. E. Logan. "Electricity generation and treatment of paper recycling wastewater using a microbial fuel cell", *Applied Microbiology Biotechnology.* **80**, 2008, pp. 349-355.
- [7] P. T. Ha, T.K. Lee, B.E. Rittmann, J. Park and I.S. Chang, "Treatment of Alcohol Distillery Wastewater Using a Bacteroidetes-Dominant Thermophilic Microbial Fuel Cell", *Environ. Sci. Technol.* **46**, 2012, pp. 3022-3030.
- [8] H. Liu and B. E. Logan. "Electricity Generation Using an Air-Cathode Single Chamber Microbial Fuel Cell in the Presence and Absence of a Proton Exchange Membrane", *Environ. Sci. Technol.* **38**, 2004, pp. 4040-4046.
- [9] G. S. Jadhav and M. M. Ghangrekar. "Performance of microbial fuel cell subjected to variation in pH, temperature, externalload and substrate concentration", *Bioresour Technol.* **100**, 2009, pp.717-723.

Solar Energy, Dry Sensitized, Solar Cell and Solar-PV

POTENTIAL OF SOLAR ENERGY UTILIZATION FOR PROCESS HEATING IN PAPER INDUSTRY IN INDIA: A PRELIMINARY ASSESSMENT

Ashish K.Sharma¹, Chandan Sharma¹, Subhash C. Mullick¹ and Tara C. Kandpal¹

¹Centre for Energy Studies Indian Institute of Technology, Delhi Hauz Khas, India

SUMMARY: This paper presents the results of a preliminary analysis towards the potential estimation of solar process heating in paper industry in India. Beside the possibility of using solar energy to provide required temperatures and pressures for process heating other limiting issues such as the possibility of cogeneration in paper mills, solar resource availability at the location of use are also included in the analysis. Firstly, state wise geographical locations of clusters of paper mills having threshold value of DNI 1700 kWh/m²/annum have been identified and to estimate the potential of use of solar energy in process heating two different modalities have been used. In the first approach, collector area required that to meet entire process heating requirement of the paper mills (ignoring the losses in the storage) at the identified locations in the country was estimated. In the second approach a parabolic trough based Solar Industrial Process Heating (SIPH) system that is supported with an auxiliary backup has been considered and based on the hourly energy demand, a design value of DNI of 800 W/m² and applicable values of annual average ambient temperature the collector area required to meet the process heating demand at identified locations has been estimated. In the first case, the SIPH potential in terms of the storage collector area, has been estimated as 3.17 million m² whereas in the second case the required collector area has been estimated as 0.84 million m². Finally using the hourly solar radiation data for the identified locations, the annual energy delivery is estimated at 3.75 PJ per annum with the annual solar fraction being in the range of 0.23-0.28.

Keywords: Solar Industrial Process Heating, Potential Estimation, Paper Industry.

INTRODUCTION

Realistic assessment of potential of solar energy for process heating in paper industry and identification of niche areas (locations, solar resource availability) is critically important for designing and implanting the appropriate policies and promotional measures. In the context of India, a study carried out by GIZ considered paper industry and has estimated a potential of 1.88 PJ per annum [1]. However, the study was limited to low temperature process heat applications such as hot water generation and boiler feed water heating only. It did not consider (i) the use of solar energy to meet process heating demand (through steam generation) at higher temperatures, (ii) solar resource availability at different locations having paper industries and (iii) the possibility of cogeneration etc.

In view of the above, this paper presents the results of a preliminary analysis towards the potential estimation of solar process heating in paper industry in India. Beside the possibility of using solar energy to provide required temperatures and pressures for process heating other limiting issues such as the possibility of cogeneration in Paper mills, solar resource availability at the location of use are also included in the analysis

METHODOLOGY

To begin with, detailed study of paper industry in India is carried out and data for various aspects such as (i) geographical locations of paper mills in the country (ii) raw materials used in paper production (iii) annual production (iv) specific

energy requirement of process heating per tonne of paper produced etc. have been collected [2,3]. Using the data collected, geographical locations of clusters of paper mills with threshold value of Direct Normal Irradiance (DNI) 1900 kWh/m²/annum have been identified and annual paper production and corresponding thermal energy requirement at each location have been estimated. Of course, depending upon the minimum acceptable (threshold) value of annual DNI, the list of locations available for SIPH would change.

Further, at identified locations, performance of parabolic trough concentrator based SIPH systems (with and without storage options) has been assessed. Finally, based on the location wise performance of these systems, estimations for potential of solar process heating in term of useful energy delivery (PJ/annum) and corresponding collectors area requirement (million m²) in paper industry in India have been made.

RESULTS AND DISCUSSION

Since in most of the paper mills in the country satisfaction of process heating demand happens with the supply of steam at a temperature of approximately 300°C, only concentrating solar collector (parabolic trough) have been considered for producing the steam. Thus availability of adequate solar resource - Direct Normal Irradiance (DNI) at the locations of these clusters has been used as one of the criteria for potential estimation. At six locations of the identified clusters (Coimbatore, Tezpur, West Godavari, Erode, Madurai, Udumaleet and Kolkata) the annual DNI is less than 1900 kWh/m²/annum and

hence the same have not been included in the potential estimation.

As per the currently available estimates, a total of 1.64 million tonnes per annum of paper is produced at the identified locations with good DNI availability. Since the large size paper mills that are using cogeneration to produce both electricity and process heat would not be suitable candidates for SIPH in the initial phase. In the remaining paper mills, taking the specific energy requirement of process heating (in GJ/tonne of paper produced) a theoretical potential of 14.2 PJ/annum has been estimated.

Results of paper production and thermal energy requirement at few identified locations of clusters of paper mills in India are presented in the Table 1.

Table1. Annual thermal energy required at locations of paper mill clusters

Location	Paper Production (tonnes per annum)	Thermal energy required (PJ/annum)
Kashipur	208	2.27
Ludhiana	176	1.44
Meerut	114	0.94
Nagpur	230	1.80
Vapi	383	2.98

Based on the location wise performance of SIPH system the required collector area has been estimated as 3.17 million m² and the same should meet the entire demand ignoring the losses in storage system.

Results for collector area estimations at few identified locations of clusters of paper mills in India are presented in the Figure 1.

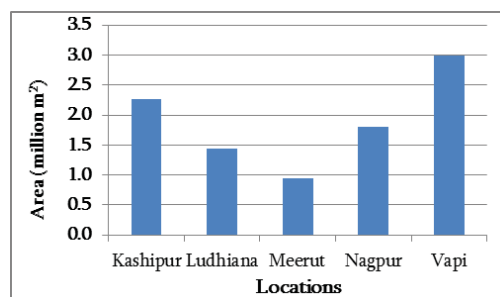


Figure1. Required solar collector area (SIPH system with Storage)

In order to consider the practical feasibility of using a Solar Industrial Process Heating System without storage and a design DNI of 800W/m², the required collector area and useful energy delivered have been estimated as 0.84 million m² and 3.75 PJ/annum respectively.

Finally using the hourly solar radiation data for the identified locations, performance of SIPH system in term of actual energy delivered and the annual solar fraction have been estimated. Estimated results at some identified locations are presented in the Table 2.

Table 2. Collector area requirement and performance of SIPH systems (without storage)

Location	Collector area (thousand m ²)	Energy delivered (GJ/annum)	S.F.
Kashipur	144	628542	0.28
Ludhiana	95	390420	0.27
Meerut	97	401969	0.26
Nagpur	113	411358	0.23
Vapi	187	67478	0.23

Estimated value of solar fraction is varying in the range of (0.23-0.28). As expected, the hourly DNI availability has a direct effect on the solar fraction and annual energy delivery thus necessitating the need for a proper solar resource assessment prior to the installation of SIPH systems in the locations of paper mills.

References

- [1] GIZ. Identification of Industrial Sectors Promising for Commercialization of Solar Energy in India.2012; Accessed at: http://mnre.gov.in/filezmanager/UserFiles/_ComSolar.pdf
- [2] IARMPA. In paper directory of Indian paper manufacturers & allied industry 9th Edition 2011.
- [3] Schumacher K and Sathaye J. India's Pulp and Paper Industry: Productivity and Efficiency. July 1999. Accessed at <http://india.lbl.gov/sites/default/files/41843.pdf>

CHLOROPHYLL PIGMENTS AS NATURE BASED DYE FOR DYE-SENSITIZED SOLAR CELL (DSSC)

R. Syafinar¹, N. Gomesh¹, M. Irwanto¹, M. Fareq¹, Y.M. Irwan¹ and U. Hashim²

¹Centre of Excellence for Renewable Energy (CERE), School of Electrical Systems Engineering, Universiti Malaysia, Malaysia

²Institute of Nano Electronic Engineering (INEE), Universiti Malaysia, Malaysia

SUMMARY: Dye-sensitized solar cell (DSSC) was a third generation of solar cell which promotes simple fabrication, low cost and environmental friendly compared to silicon based solar cells. The usage of natural based dye is proposed as an alternative to chemical synthetic dye. Natural dye from chlorophyll group which is from spinach was used as a photo sensitizer to fabricate titanium dioxide (anatase) nanoparticle based DSSC. Doctor blade method is applied in fabricating the DSSC with the thickness of 10 μm of TiO_2 film. The UV-Vis absorption spectroscopy is used to see the capability of the dyes in absorbing photon from sunlight and it is proven that chlorophyll dyes can absorb photon in the wavelength of visible light spectrum (400-700 nm). The photoelectrochemical parameter for solar cell by using chlorophyll from spinach, which extracted with ethanol solvent showed the open circuit voltage (V_{oc}) as much as 440 mV, current short circuit (I_{sc}) is about 0.35 mA and fill factor (FF) was about 0.49%.

Keywords: dye sensitized solar cell, natural based dye, chlorophyll, spinach, titanium dioxide

INTRODUCTION

DSSC employ ruthenium (II) polypyridinic complex as a sensitizer of wide band gap semiconductor but due to costly and complicated in sensitizing the complexes also containing heavy metal and producing environmental polluting, other method is replacing it using natural dyes from fruits, plants and leaves which offered cost efficiency, non-toxicity and complete biodegradation. Natural dyes play a key role in harvesting sunlight and transferring solar energy into electrical energy [1-4].

Chlorophyll has the ability to absorb light from red, blue and violet wavelengths and obtains its color by reflecting the green wavelength. The strong absorption peaks in the visible region located at 420 nm and 660 nm wavelengths that can be used as a natural sensitizer in the visible light range [5]. The photoelectric conversion efficiency (η) based on chlorophyll pigments has been reported by other researchers such as H. Chang et al., reported that by using spinach as a natural based sensitizer, the photoelectrical performance showed open circuit voltage (V_{oc}) as much as 550 mV, current short circuit (I_{sc}) is about 0.46 mA and fill factor (FF) was about 51% [6]. H. Chang et al., also reported that by using wormwood as a chlorophyll dye for DSSC resulted open circuit voltage (V_{oc}) as much as 0.585V, current short circuit (I_{sc}) is about 1.96 mA, fill factor (FF) was about 47% and conversion efficiency is 0.538 % [7].

In this paper, chlorophyll pigments were extracted from spinach. These extracted dyes were characterized by UV-Vis Spectrophotometer to see the absorption spectra. The photoelectrochemical parameters of DSSC were also investigated.

CHARACTERIZATION AND MEASUREMENTS

The absorption spectra of the dyes were performed using Evolution 201 UV-Vis Spectrophotometer. Characterization equipment for measuring the performance of solar cells by using solar simulator 100 mW/m^2 Ketley 2450, SMU unit and Data Logger. The I-V curves were obtained using kick-start software. The short circuit current I_{sc} and the open circuit voltage V_{oc} were determined from the I-V curve. The fill factor FF (Eq. (1)), the efficiency η (Eq. (2)), were calculated using the following relations:

$$FF = \frac{I_{max}V_{max}}{I_{sc}V_{oc}} \quad (1)$$

$$\eta = \frac{FF \times (V_{oc} \times I_{sc})}{P_{in}} \quad (2)$$

RESULT AND DISCUSSION

Photovoltaic tests of DSSC use spinach's dye by using different solvents as sensitizers were performed by measuring the current density-voltage (I-V) current under irradiation with white light (100 mW/cm^2). As shown in Table 1, the highest fill factor was by using Spinach extracted with ethanol having 0.49% compared to Spinach extracted with water and Spinach's flower extracted with water. Higher interaction between the dye and TiO_2 particle will produce good charge-transfer performance and improving the fill factor [6].

Table 1. Photoelectrochemical parameters for DSSC

Types of dyes	V_{oc} (mV)	I_{sc} (mA)	Fill Factor, FF (%)
Spinach extracted with ethanol	440	0.35	0.49
Spinach extracted with water	384	0.32	0.36
Spinach's flower extracted with water	356	0.26	0.31

Absorption spectra

The high absorption peak when extracted the spinach with ethanol with an absorption range of 600-700 nm and peak absorbance at 610 nm shown in Fig.1 below. The band gap which is the photon energy of TiO₂ is related to the wavelength range absorbed and the band gap decreases with increasing absorption wavelength [8].

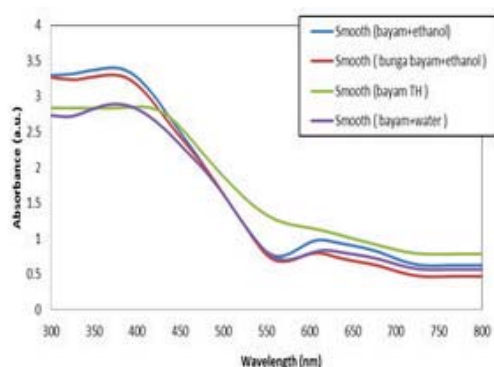


Figure 1: Absorption spectra of Spinach's dye

CONCLUSION

Chlorophyll pigments can be used as a dye sensitizer in DSSC because of its ability in absorbing photon from sunlight and having light harvesting invisible light spectrum and it was proven by testing its observed rate using UV-Vis spectrophotometer. However, the efficiency of DSSC in the range of 1-2% lowers than synthetic dyes. But chlorophyll pigment was cheaper, can be disposed easily and easily extracted compared to synthetic dyes.

References

- [1] A. S. Polo and N.Y.M. Iha, "Blue sensitizers for solar cells: Natural dyes from Clafate and Jaboticaba", *Solar Energy Materials & Solar Cells*. **90**, 2006, pp. 1936-1944.
- [2] K. Sinha, P.D. Saha and S. Datta, "Extraction of

natural dye from petals of Flame of forest (*Butea monosperma*) flower: Process optimization using response surface methodology (RSM)", *Dyes and Pigments*. **94**, 2012, pp. 212-216.

[3] S.A.M Al-Ba'thi, I. Alaei and I. Sopyan, "Natural Photosensitizers for Dye Sensitized Solar Cells", *National Journal of Renewable Energy Research*. **3**, 2013.

[4] M.S. Abdel-Latif, T.M. El-Agez, S.A. Taya, A.Y. Batniji and H.S. El-Ghamri, "Plant Seeds-Based Dye-Sensitized Solar Cells", *Material Sciences and Application*. **4**, 2013, pp. 516-520.

[5] M.A.M. Al-Alwani, A.B. Mohamad, A.A.H. Kadhum and N.A. Ludin, "Effect of solvents on the extraction of natural pigments and adsorption onto TiO₂ for dye-sensitized solar cell applications", *Spectrochimica Acta Part A: Molecular and Biomolecular Spectroscopy*. **138**, 2015, pp.130-137.

[6] H. Chang, H.M. Wu, T.L. Chen, K.D. Huang, C.S. Jwo and Y.J. Lo, "Dye-sensitized solar cell using natural dyes extracted from spinach and ipomea", *Journal of Alloys and Compounds*. **495**, 2010, pp. 606-610.

[7] H. Chang, M-J Kao, T-L Chen, C-H Chen, K-C Cho and X-R Lai, "Characterization of Natural Dye Extracted from Wormwood and Purple Cabbage for Dye-Sensitization Solar Cells", *International Journal of Photoenergy*, **2013**, Article ID 159502, 8 pages.

[8] S. Ananth, P. Vivek, T. Arumanayagam and P. Murugakoothan, "Natural dye extract of lawsonia inermis seed as photo sensitizer for titanium dioxide based dye sensitized solar cells", *Spectrochimica Acta Part A: Molecular and Biomolecular Spectroscopy*. **128**, 2014, pp.420-426.

POTENTIAL OF PURPLE CABBAGE, COFFEE, BLUEBERRY AND TURMERIC AS NATURE BASED DYES FOR DYE SENSITIZED SOLAR CELL (DSSC)

R. Syafinar¹, N. Gomesh¹, M. Irwanto¹, M. Fareq¹, Y.M. Irwan¹ and U. Hashim²

¹Centre of Excellence for Renewable Energy (CERE), School of Electrical Systems Engineering, Universiti Malaysia Perlis (UniMAP), Taman Pengkalan Indah, Jalan Pengkalam Assam, 01000, Kangar, Perlis, Malaysia

²Institute of Nano Electronic Engineering (INEE), Universiti Malaysia Perlis (UniMAP), Taman Pertiwi Indah, Seriab

SUMMARY: Natural dyes extracted from purple cabbage, coffee, blueberry and turmeric were analyzed to see the ability of the natural sources as sensitizer for dye sensitized solar cells (DSSC). The dyes were extracted by using an ultrasonic extraction method with setting up the temperature, time and frequency with 30 °C, 30 minutes and 37 Hz, respectively. UV-Vis spectrophotometer is used to measure the absorbance rate of the dyes in visible light spectrum. From the result, the broadest spectrum of the extracted dye was cocktail dyes from purple cabbage with peak absorbance of 550 nm and having lowest photon energy compare to other dyes only 1.85 eV. From the result obtained, cocktail dyes from purple cabbage and blueberry have good potential into developing high efficiency nature based DSSC.

Keywords: natural dyes, ultrasonic, extraction, spectrum, photon energy, purple cabbage, coffee, blueberry and turmeric

INTRODUCTION

Dye sensitized solar cell (DSSC) are devices which convert visible light into electrical energy based on sensitization of wide band gap semiconductor. The typical configuration of DSSC consists of nanocrystalline titanium dioxide (TiO₂), dye molecule, an electrolyte contained iodide/triiodide (I⁻/I₃⁻) and counter electrode act as catalyst in DSSC. Dye sensitizer is important in absorbing sunlight and transforms it into electrical energy. So far, synthetic inorganic compounds dyes such as Ruthenium (II) complexes with carboxylated polypyridyl ligands are used as sensitizers in DSSC [1] and conversion efficiency so far achieved in 11%-12% [2]. But due to expensive and hard to synthesize, nature based dye from fruits and leaves have been chosen as dye sensitizer because of low cost, abundant in resources and safe material. Several dyes contained suitable pigments for developing a good efficiency were by using carotenoids, anthocyanins and chlorophyll. So far, H. Zhou reported the highest efficiency for nature based dye when using mangosteen pericarp as sensitizer as much as 1.17% [2].

In this paper, four types of natural dye were extracted from purple cabbage, blueberry, coffee and turmeric. These extracted dyes were characterized by UV-Vis Spectrophotometer to see the absorption spectra. Additionally, cocktail dyes from the combination of purple cabbage and blueberry as well as coffee with turmeric were also investigated. The photon energy of each dyes and absorption coefficient was studied.

CHARACTERIZATION AND MEASUREMENTS

The absorption spectra of the dyes were performed using Evolution 201 UV-Vis Spectrophotometer. UV-Vis spectrophotometer is

used to measure the absorbance rate in visible light spectrum. The determination of the band gap of dye absorbed by TiO₂ surface is calculated by using the formula in (Eq. (1)). Where h is the planck's constant, ν is the frequency, λ is the wavelength and c is the speed. The numerical values of the symbols are $h = 6.63 \times 10^{-34}$ Js, $c = 3.0 \times 10^8$ m/s, $1\text{eV} = 1.60 \times 10^{-19}$ J and E stands for photon energy.

$$E = h\nu \quad (1)$$

$$= \frac{hc}{\lambda}$$

The absorption coefficient of the respective wavelengths is obtained by the division of the absorbance with the wavelength shown in (Eq. (2)) using K boltzman constant;

$$\text{Absorption coefficient} = \frac{4\pi K}{\text{wavelength}(\lambda)} \quad (2)$$

RESULT AND DISCUSSION

The absorption spectrum of dye sensitizers

Fig. 8 show the suitable extract solvent for each dye. From this absorbance graph, all pigments can absorb light photons and lead to production of excited electrons which allows the TiO₂ conduction band with acceptable performance to increase the conversion efficiency of dye-sensitized solar cell [3]. Dyes which contained anthocyanin pigment have enough hydroxyl groups to bind with TiO₂ tightly and being able to inject electrons into the TiO₂ conduction band when excited with visible light [4].

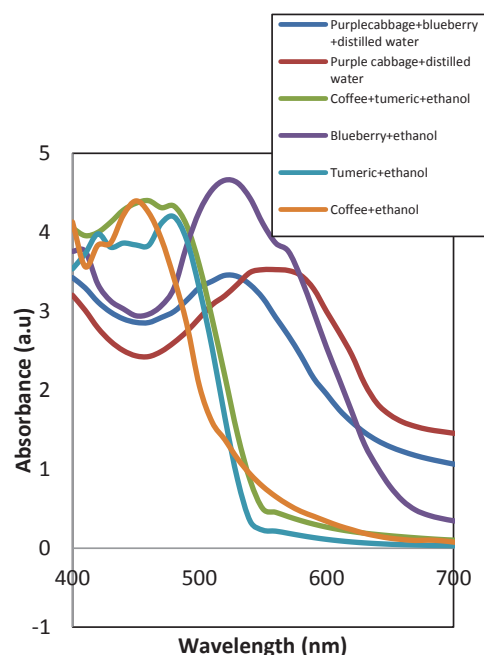


Figure 1. Suitable extraction solvents for each dye

Bandgap, photon energy and absorption coefficient of the dyes

Table 1 demonstrates the ethanol and distilled water as extract solvents for each dye. For purple cabbage, turmeric and cocktail dyes (coffee and turmeric), the suitable extract solvent to extract pigment and colorant by using distilled water, with photon energy of 1.94 eV, 1.84 eV and 1.81 eV. Ethanol as extract solvent were suitable for blueberry, cocktail dyes (purple cabbage and blueberry) and coffee having photon energy as much as 1.86 eV, 1.85 eV and 2.04 eV.

Table 1: Photon energy and absorption coefficient (α) of the dyes

Dyes	Extract solvent	Peak Absorbance (nm)	Absorption range (nm)	Photon energy (eV)	Absorption coefficient (α) $M^{-1}m^{-1}$
Purple cabbage	Ethanol	550	500-600	1.97	1.72
	Distilled water	550	500-600	1.94	1.69
Blueberry	Ethanol	520	500-600	1.86	1.62
	Distilled water	520	500-600	2.00	1.75
Cocktail dyes Purple Cabbage and Blueberry	Ethanol	550	500-600	1.85	1.62
	Distilled water	530	500-600	2.04	1.78
Coffee	Ethanol	450	400-550	2.04	1.78

Turmeric	Distilled water	480	400-550	2.07	1.81
	Ethanol	480	400-550	2.30	2.00
Cocktail dyes Coffee and turmeric	Distilled water	480	400-550	2.11	1.84
	Ethanol	450	400-550	2.26	1.96
	Distilled water	450	400-550	2.07	1.81

CONCLUSION

Natural dyes have been used as an alternative to chemical synthetic dyes because of the abundance of resources, easily extracted, low cost and safe material. Natural dyes such as purple cabbage, blueberry, turmeric and coffee have been extracted to see the potential of using any dyes for sensitizer in dye sensitized solar cell (DSSC). The absorbance of the dyes has been measured and analyzed to see the ability of the dyes to absorb photons in the visible light spectrum. From the absorbance and the photon energy result, cocktail dyes from purple cabbage and blueberry have much potential in developing high efficiency of DSSC based on natural dye.

References

- [1] G. Calogero and G. D. Marco, "Red Sicilian orange and purple eggplant fruits as natural sensitizers for dye-sensitized solar cells", *Solar Energy Materials & Solar Cells* **92**, 2008, pp.1341-1346.
- [2] H. Zhou, L. Wu, Y. Gao and T. Ma, "Dye-sensitized solar cells using 20 natural dyes as sensitizers", *Journal of Photochemistry and Photobiology A: Chemistry* **219**, 2011, pp.188-194.
- [3] M.A.M. Al-Alwani, A.B. Mohamad, A.A.H. Kadhum and N.A. Ludin, "Effect of solvents on the extraction of natural pigments and adsorption onto TiO_2 for dye-sensitized solar cell applications", *Spectrochimica Acta Part A: Molecular and Biomolecular Spectroscopy* **138**, 2015, pp.130-137.
- [4] C.Y. Chen and B.D. Hsu, "Performance enhancement of dye-sensitized solar cells based on anthocyanin by carbohydrates", *Solar energy* **108**, 2014, pp.403-411.

OPTIMAL PHOTOVOLTAIC RESOURCES HARVESTING IN GRID-CONNECTED RESIDENTIAL ROOFTOPS AND IN COMMERCIAL BUILDINGS AND FEED-IN TARIFFS: CASES OF THAILAND

Prachuab Peerapong¹, and Bundit Limmeechokchai¹

¹Sirindhorn International Institute of Technology
Thammasat University, Thailand

SUMMARY: Photovoltaic (PV) has recently undergone impressive growth and substantial cost decreases. Basically wafer-based crystalline-Si PV technologies have the advantage of higher module efficiency as compared to thin-film PV, but thin-film PV has the advantages of lower production cost. This paper tries to investigate solar resources assessment with many types of solar panels available in markets. A single-crystal silicon (mono-Si) or polycrystalline (poly-Si) have been dominant for solar rooftop and in commercial buildings installation in the past years. However until recently thin-film PV modules both amorphous silicon (a-Si) and other non-silicon thin films technology have been advance efficiency developments with low cost. The competition of crystalline and thin film solar panel technologies drives the cost significantly decreased and helps the solar investors for a good financial profit return for a shorter time. This study by satellite-derived data, Solar GIS pvPlanner software shows that the highest output is in a-Si, CdTe and followed by CIS, and c-Si PV modules for the locations considered in this study. The average energy output of amorphous panels in residential solar rooftop installed in Bangkok has the highest values of 1,503 kWh/kWp. And the average energy output of amorphous panels in commercial building installed in Chonburi province has the highest values of 1,601 kWh/kWp. The optimal inclination angle is 15° south direction in both areas. Finally, the economic assessment of solar panels is also investigated for the feasibility investment by RETScreen model.

Keywords: Photovoltaics resources, residential, commercial building, economics, optimal solar harvesting

INTRODUCTION

Solar energy potential in Thailand was investigated. Geographical distribution of solar radiation was studied as shown in Figure 1 [1]. It was found that 45% of the total areas of the country receive annual solar radiation in the range of 17-18 MJ/m².day, while there are only a few percentages of the areas with low solar radiation (less than 15 MJ/m².day).

Under the Renewable and Alternative Energy Development Plan for 25 percent of final energy consumption in 10 years (AEDP 2012-2021), The government of Thailand has planed that the electricity generated by solar power will be 2,000 MW.

Solar rooftop and solar PV installation in commercial buildings are promising because they would not consume a large portions of land, such as in the utility solar installation or solar farm. Thai government hope that the installation in the first phase of solar rooftops will be 200 MW after 2013.

SOLAR RESOURCES ASSESSMENT METHODOLOGY

This study is to investigate the electricity output generated in different types of solar panels (crystalline-Si and thin film), and compared the results to the actual data collection by site visiting. The cases in this study divided into: 1.) Large scale solar rooftop 2.) Small scale solar PV installaton in commercial buildings. The selected sites are located at two specific areas: in Bangkok (13° 45' 49.15" N,

100° 32' 22.97" E), and in Chonburi province (13° 13' 30.83" N, 100° 56' 15.94" E).

The SolarGIS PvPlanner tool is used in this study. The SolarGIS is based on using statistically aggregated solar and temperature data stored in with a time step of 15 minutes collected from 1994-2011 [2].

Simplified input parameters enable to consider key characteristics of a PV system, such as its position, geometry, type and mounting of modules, efficiency of inverter and assumed losses in DC and AC sections. The model calculates reflectance losses at the surface of PV modules and losses due to irradiance and temperature characteristic operating performance of modules in a site-specific climate conditions. The other system losses, mainly at the DC and AC sections are to be set by a user.

RESULTS AND DISCUSSION

This paper compares energy collected from monthly average daily global horizontal irradiation (GHI) of two locations against satellite-derived data from the commercially available software. The best dataset for locations in Thailand was selected as that with the lowest root mean square error. Energy output prediction from Solar GIS pvPlanner software [2]. The software was validated using measured performance data for a PV system. The software was then used to evaluate the energy generated by PV systems with optimally inclined PV modules. This paper therefore assesses the energy generation potential of PV systems with crystalline silicon (c-Si), amorphous silicon (a-Si), copper indium selenide (CIS or CIGS) and cadmium

telluride (CdTe) PV modules in different locations in Thailand.

Table 1 shows satellite-derived annual average daily GHI available in Solar GIS for different locations in Thailand. Solar irradiation varies between 4.79 kWh/m² per day in Bangkok (central region) and 5.06 kWh/m² per day in Chonburi province (eastern region). The annual average ambient air temperature varies between 27.2 °C in Chonburi and 27.5 °C in Bangkok. The optimal inclination angle is 15° south direction in both areas, the solar azimuth in Chonburi province as shown in Figure 2.

Energy output assessment

Predicting the energy output from a PV system is a matter of combining the characteristics of the major components, that is, the PV array and the inverter with local irradiation and temperature-data. Energy output prediction using Solar GIS’s pvPlanner tool was validated using measured data reported. The pvPlanner tool was therefore used to model the energy output from the PV systems assuming: 97.5% inverter efficiency, 5.5% DC losses, 1.5% AC losses and 99% availability.

It is seen in Table 2-3 that the energy outputs in solar rooftop, solar PV in commercial buildings are comparable. The highest output is in a-Si, CdTe and followed by CIS, and c-Si PV modules for two locations considered in this study. The average energy output has the lowest values of 1,341, for c-Si in Bangkok area and 1,440 kWh/kWp in Chonburi province and highest values of 1,503, 1,601 kWh/kWp in Bangkok, Chonburi respectively for a-Si PV modules. Considering that the Solar GIS dataset can also estimate average energy outputs and average annual electricity production as nearly as compared to the collected data from site visiting.

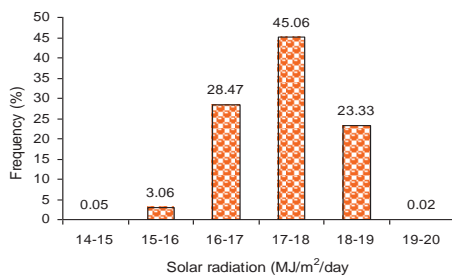


Figure 1. Solar radiation in Thailand.

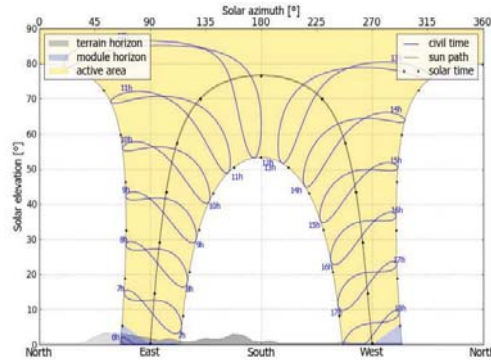


Figure 2. Solar azimuth (°) in Chonburi province

Table 1. Temps and solar irradiation under this study

Location	Ambient Temperatures (°C)	Solar irradiation (kWh/m ² .d)
Bangkok	27.5	4.79
Chonburi	27.2	5.06

Table 2. Residential 11 kW Solar rooftop

Solar panels	Energy output (kWh/kWp)	Performance ratio (%)
c-Si	1,341	74.5
a-Si	1,503	83.5
CIS	1,367	75.9
CdTe	1,479	82.2

Table 3. Commercial buildings 66 kW Solar rooftop

Solar panels	Energy output (kWh/kWp)	Performance ratio (%)
c-Si	1,440	74.6
a-Si	1,601	84.3
CIS	1,466	77.2
CdTe	1,579	83.1

ACKNOWLEDGMENT

Authors would like to thank the GeoModel solar who provides SolarGIS software for this study, the Joint Graduate School of Energy and Environment for scholarship fund, and also the Sirindhorn International Institute of Technology, Thammasat University for the utility availability support.

References

[1] Department of Alternative Energy Development and Efficiency (DEDE), Ministry of Energy, Solar Radiation Maps from Satellite Data for Thailand, 2010.
 [2] Solargis. info/pvplanner 2013. Available on <http://www.solargis.info/pvplanner>.

SOLAR ROOFTOP INSTALLATION IN THAILAND-A CASE STUDY ON VARIOUS SCENARIOS DISPLAYING POTENTIALS AND LIMITATIONS OF PV SOLAR ROOFTOP INSTALLATION FOR PATHUM THANI PROVINCE

Tobias Kullack¹ and Supachart Chungpaibulpatana¹

¹School of Manufacturing Systems and Mechanical Engineering, Sirindhorn International

¹Institute of Technology, Thammasat University, Thailand

SUMMARY: The solar rooftop scheme and the ongoing discussions to install solar on private business, schools and public establishment might challenge the grid and the grid operator needs to take several measurements to be able to implement a high share of renewable energies, especially when generated by Solar Power. Hence possible impacts and the total share of electricity produced by solar rooftop installations in an hourly resolution are being simulated and discussed.

Keywords: Solar Potential Rooftop Thailand, Hourly Simulation, Renewable Energy Scenario, Solar Potential, Solar Rooftop Impact Thailand

INTRODUCTION

The renewable energy implementation and development is being discussed widely in Thailand with its 20-Year Energy Efficiency Development Plan (2011 - 2030) [1] and additionally the 10-Year Alternative Energy Development Plan 2012 - 2021 (AEDP 2012 – 2021) [2], which is targeting on increasing the share of renewable energy and alternative energy uses by 25 percent instead of fossil fuels within the next 10 years. Furthermore with the Energy Regulatory Commission (ERC) Rules and Regulation on Thailand's Solar Rooftop Program to support 100 MW private and 100 MW commercial solar rooftop installation [3] and in addition the newly discussion on the National Reform Council (NRC) to support the installation of 500 MW of solar rooftop installations in 5 years might have an impact on the actual grid. Meanwhile discussions are ongoing that the ERC would devise new regulations allowing members of the public, state organizations and private businesses to install solar on rooftops without having to seek permission.

This paper will review the impact on the installation of PV Solar on rooftops in Pathum Thani up to 200 MW. Therefore an hourly simulation for Pathum Thani province with PVsyst is conducted and the hourly simulated output over one year is compared to the actual consumption of Pathum Thani according to EGAT substation Sai Noi. Limitation and the actual share of electricity feed back to the grid has been evaluated and analyzed. Further the rooftop potential of schools and educational establishments will be estimated and the impact of installing PV Solar on such is simulated and compared to the actual consumption over 1 year to display the potential and technical limitations.

METHODOLOGY

The actual solar radiation data of Pathum Thani province are used to simulate the output of various systems with PVsyst simulation tool in an hour resolution over 1 year for 2012. The available rooftop areas are measured by using a map and estimation of available area. The simulation, including a sensitivity analysis, displaying the P50, P75 and P90 value for the production are being compared to the actual consumption according to EGAT substation Sai Noi. As a reference year, the year 2012 has been selected. Further this paper will simulate several scenarios and focus on the respective grid capacity. Hence systems with a total volume of 100 MW connected to the Low Tension (LT) Distribution and line as well as systems up to 100 MW connected to the Medium Voltage (MV) Distribution line will be simulated and compared.

RESULTS AND DISCUSSION

The paper shows the impact and potential of solar rooftop installation in Pathum Thani province. It further shows the clearly the possible impacts of such installation without clear defined restrictions on maximum installed capacity. The research clearly displays the needs of grid improvements such as smart grid development if such a target with a high solar share wants to be achieved. Several scenarios have to be simulated and each LT and MV Grid has to be inspected and the maximum peak loads and load fluctuation has to be evaluated and an exact plan has to be implemented to ensure sufficient and stable supply.

ACKNOWLEDGMENT

This work is supported by Sirindhorn International Institute of Technology in form of a Scholarship

References

- [1]http://www.thai-german-cooperation.info/download/20130618_1_eedp_tipakorn_ee_action.pdf
- [2]http://www.dede.go.th/dede/images/stories/dede_aedp_2012_2021.pdf
- [3]<http://weben.dede.go.th/webmax/content/thailand-implements-photovoltaic-support-programme-and-increases-renewable-energy-targets>

SIMULATION OF SOLAR AIR CONDITIONING SYSTEM WITH SALINITY GRADIENT SOLAR POND

Safwan Kanan¹, Jonathan Dewsbury¹ and Gregory F. Lane-Serff¹

School of Mechanical, Aerospace and Civil Engineering
Faculty of Engineering and Physical Sciences
The University of Manchester, M13 9PL, Manchester, UK

SUMMARY: In hot dry climates, due to the high demand for space air conditioning during summer and the abundance of solar radiation, solar air conditioning is a promising approaches to reduce the energy consumption and negative environmental impact of buildings. Solar cooling systems have used various types of collectors to drive chillers. In this paper, a salinity gradient solar pond is suggested as a collector to drive an absorption chiller, to provide cool air for a house during hot and dry weather. A coupled simulation between MATLAB and TRNSYS has been used to solve the problem. MATLAB code was written to solve the governing equations for the salinity gradient solar pond and the ground underneath it. TRNSYS software was used to model the solar cooling system including the absorption chiller and building. The weather data used was for Baghdad in Iraq. It was found that the salinity gradient solar pond could be used to drive the absorption chiller and produce cool air for a single family house during the summer period. Different solar pond areas were tested with the same chiller capacity. It was found that a solar pond area of approximately 400 m² was required to provide satisfactory cooling for a typical house with a floor area of approximately 125 m².

Keywords: Salinity gradient solar pond, solar cooling, solar thermal energy, TRNSYS simulation.

INTRODUCTION

Air conditioning of residential and commercial buildings is essential in hot and dry weather such as Iraq. Conventional air conditioning system used electricity is one of usual solutions to provide thermal comfort. The electricity consumption for air-conditioning in Saudi Arabia which is dominated by hot desert climate exceeds 70% of the total electricity consumption during the summer months [1]. This issue caused people to seek alternate cheaper renewable energy source for operations of buildings.

One of the attractive way is to use solar air conditioning when solar thermal energy can be used to drive absorption chiller. The main component of the complete solar cooling system is the solar thermal collectors to produce heat from available radiation. Different type of collectors have used in solar cooling system such as: flat plate solar collector and evacuated tube collector.

In this paper, a novel salinity gradient solar pond has been suggested as a collector to drive an absorption chiller to provide cool air for a house under hot and dry weather conditions. The solar pond is described as an artificial large body of water reservoir that collects and stores solar thermal energy. It is about 1 to 3 meters deep, and the bottom of the pond is usually painted black. The solar radiation landing on the surface of the pond penetrates the liquid and falls on the blackened bottom which is thereby heated. If the liquid is homogeneous which means no density gradient, convection currents will be set up and the heated liquid being lighter will travel towards the surface and dissipate its heat to the atmosphere. In a solar pond these convection currents are prevented by having a concentration gradient of salt, the solution's concentration and density being highest at

the bottom and lowest at the top. Typically ponds are composed of three zones as shown in Fig (1). The first zone is Upper Convective Zone (UCZ), which has low salt concentration. The second zone is Non-Convective Zone (NCZ) or (insulation layer), which has salt density increasing with depth. Hot water in one layer of NCZ cannot rise because of its high relative density (due to its salt content) and water above is lighter (low density). Similarly, water cannot fall because the water below it has a higher salt content and is heavier (high density). Therefore convection motions are hindered and heat transfer from the hot third zone, Lower Convective Zone (LCZ) or (storage layer) to the cold UCZ can only happen through conduction. The heat extracted from the LCZ layer could be used to drive an absorption chiller.

The basic remaining components of complete solar cooling system are absorption chiller to produce chilled water, wet type cooling tower to reject heat to the ambient, fan and cooling coil for distribute cool air inside building, heat exchanger between solar pond and absorption chiller, pumps to regulate the flow rate and controller for the automatic operation of the complete solar cooling system.

MATHEMATICAL MODELLING

The governing equations of heat transfer for salinity gradient solar pond and ground underneath it are solved numerically to determine the temperature distributions within the pond and the ground. Finite difference method is used to solve the one dimensional heat equations for pond and ground. An explicit method is involved to generating solution for the governing equations. MATLAB code was written to solve these equations. The most

important output from the code is LCZ temperature which is used to drive the absorption chiller. The solar air conditioning system model is developed within TRNSYS simulation environment. Calling MATLAB code in TRNSYS is suggested to run the coupling simulation for the pond and the rest of the solar air conditioning system as can be seen as Fig2. The simulation was run with a single effect vapour absorption chiller with rated capacity of 7 TR after cooling demand for a single house was calculated for a typical working summer day. Different solar pond areas were tested with the same chiller capacity.

RESULTS AND DISCUSSION

The coupled simulation was run for one and two years with different solar pond areas. A parameters were chosen depends on available data from manufacturers. Solar pond and results of absorption chiller were validated with experiments and manufacturer data respectively. It was found that a solar pond area of approximately 400 m² was required to provide satisfactory cooling for a typical house with a floor area of approximately 125 m².

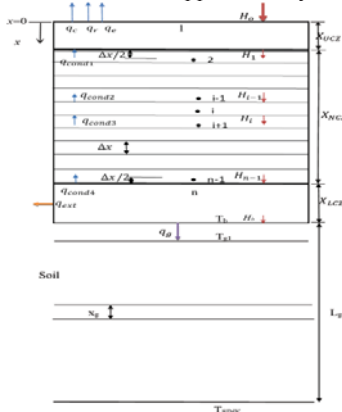


Figure 1. Solar pond and ground mathematical model

Figure 3. shows the chilled water outlet temperature for different solar pond areas for two years simulation time. With 250 m² pond area, the chilled water outlet temperature does not stabilise at the set point (7°C) even in the second year. With 400 m² or more pond area, the chilled water outlet temperature stabilises at the 7°C set point temperature by the end of first summer and during the summer in the second year. 400 m² is therefore suggested as a suitable pond area for this 125 m² single family house.

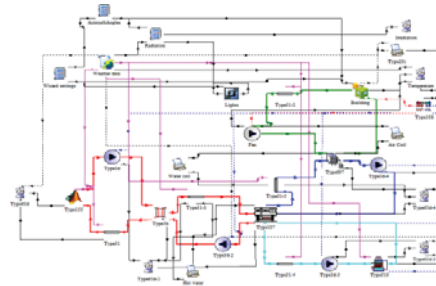


Figure 2. Complete TRNSYS simulation model

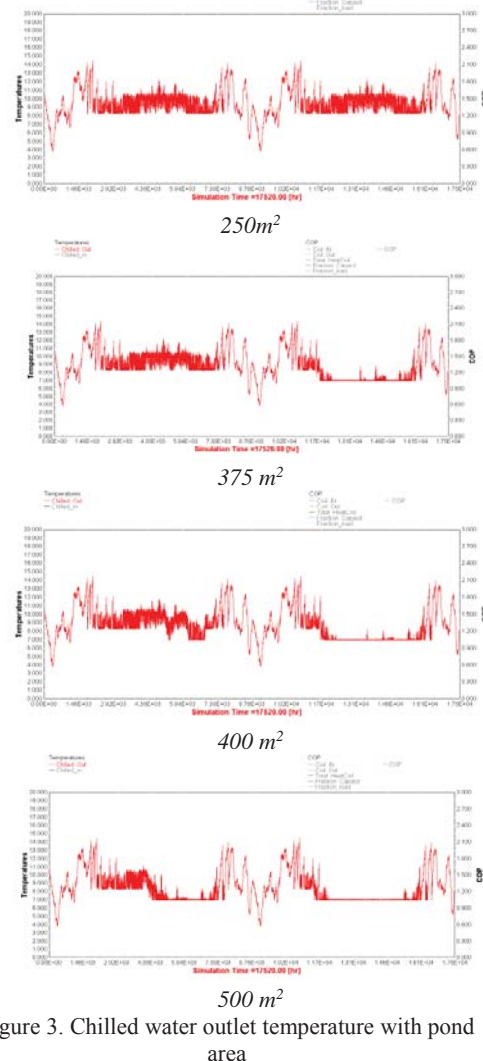


Figure 3. Chilled water outlet temperature with pond area

References

[1] Al-Mogbel, P. Ruch, A. Al-Rihaili, S. Al-Ajlan, P. Gantenbein, A. Witzig and B. Michel, "The potential of solar adsorption air conditioning in Saudi Arabia" *Proceedings of 5th international Conference solar air conditioning*, 2013, Germany.

Building Technology

SYNTHESIS OF NANO-WO₃ PARTICLES WITH PEG FOR CHROMIC FILM

Atiphol Tasaso¹ and Pailin Ngaotrananwiwat¹

¹Department of Chemical Engineering, Faculty of Engineering, Burapha University

SUMMARY: Transparent WO₃ films were successively prepared by sol-gel casting method. Their optical and structural properties were studied at various molecular weight of PEG containing in the film as a dispersing agent. The color contrast (ΔC) during film exposed to UV light represents the optical property. The WO₃ film contained PEG (MW 2,000) exhibited the optimal photochromic performance which ΔC between colored and bleached state was 70. This optical property of WO₃ films is promising higher color contrast and it is an important candidate for smart window application. Moreover, the structural properties of WO₃ films were analyzed with thermogravimetric analysis (TGA), gas sorption analysis (BET), scanning electron microscope and energy dispersive X-ray spectrometer (SEM-EDX).

Keywords: WO₃, chromic material, PEG, smart window

INTRODUCTION

The global forecasting demand of glass have been rising to 9.2 billion square meters in 2015 particularly the use of glass in architecture due to its advantages i.e., allowing the light enter to the building, seeing the outside scenery. However, glass is not able to control the excessive light and heat through the building. This causes the energy consumption increasing which leads to global warming.

To address the problem, smart glass is the promising technology that can adjust its transmittance with external stimulation i.e., light for photochromic smart glass, heat for thermochromic smart glass and electrical for electrochromic smart glass. These leads to the reduction of light and heat from outdoor.

The main component of smart glass is chromic material such as vanadium dioxide (VO₂), titanium dioxide (TiO₂), tungsten oxide (WO₃). Among the chromic material, WO₃ is one of the most intensively investigated because of high coloration, high stability.

Recently, Laura Meda et.al.[1] synthesized WO₃ nanoparticles by variation of dispersing agent and molecular weight of the organic dispersing agent. It showed that polyethylene glycol (PEG) is the promising dispersing agent and molecular weight of PEG effect to electrochemical property. Thus, this work focused on coloration of WO₃ nano-particle film synthesized by sol-gel method with the variation of molecular weight of PEG.

EXPERIMENTS

Film preparation

The synthesized route of WO₃ nanoparticles was inspired by N. Naseri et.al.[2]. Dissolve Na₂WO₄·2H₂O precursor in DI water. Then, HNO₃ was added drop wise to the solution to obtain a greenish yellow precipitation. Then, the obtained particle was rinsed with DI water for several times before dissolving the particle with 2 ml H₂O₂ and stirred to obtain a transparent solution. Aging the solution with ethanol for 2 days. Added the certain

amount of PEG with the various molecular weights (MW 1000, 2000, 10000, 20000). The resulting precursor was coated on an indium tin oxide coated glass plate (3x3 cm.) by casting technique. The film was dried in inert gas condition under humidity control (20%RH).

Measurement

Optical property of WO₃ film was investigated after UV irradiation with the intensity of 5 mW/cm². Color contrast(ΔC) was monitored by UV-vis spectrophotometer for color in terms of CIE lab scale in the transmittance mode. The results can be calculated from equation(1):

$$\Delta C = \sqrt{(\Delta L^*)^2 + (\Delta a^*)^2 + (\Delta b^*)^2} \quad (1)$$

where ΔC is color contrast of the corresponding film during UV irradiation. L^* refers to the transparency index while a^* and b^* refer to the chroma indexes.

RESULTS AND DISCUSSION

The WO₃ films consisting of the equimolar amount of PEG with various molecular weight were prepared. In order to clarify the effect of PEG molecular weight on the coloration of WO₃, thermal gravitation analysis (TGA) was used to quantify the amount of WO₃ in the film. After heating up the film to 600°C in N₂ condition, the remaining weight was defined as the amount of WO₃ in the film, while film containing only PEG was totally decomposed. It can be seen that amount of WO₃ containing in the films are identical as shown in Table 1.

The time-dependent coloration of WO₃ film was studied as shown in figure 1. The color contrast (ΔC) increased with increasing UV irradiation time in the initial period and became saturated after 1-hr irradiation. The appearance color of the film changed from transparent to dark blue. Thus, the coloration ability of WO₃ film was defined in terms of the initial coloration rate calculated after 1-min irradiation and maximum coloration of film determined after 1-hr

irradiation.

Table 1. WO₃ content in the films with various PEG molecular weight characterized by TGA.

PEG molecular weight	WO ₃ weight (mg)	SD
-	0.113	0.008
1000	0.125	0.013
2000	0.121	0.017
10000	0.126	0.017
20000	0.150	0.020

All color contrast of WO₃ films with various PEG molecular weight had the same trends as shown in figure 1.

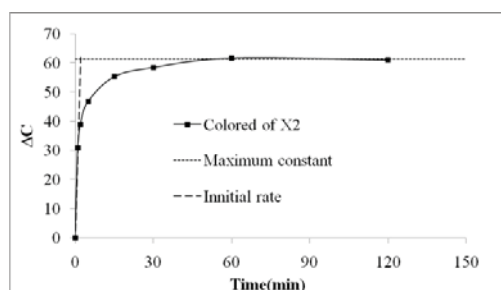


Figure 1. time-dependent coloration of WO₃ film containing PEG molecular weight of 10000

The dependent of initial coloration rate and maximum coloration of WO₃ film on PEG molecular weight was illustrated in Figure 2. It can be seen that the coloration ability of WO₃ film was significant enhanced by adding the PEG in the film. Moreover, the larger molecular weight of PEG the lower the coloration ability of WO₃ film was observed.

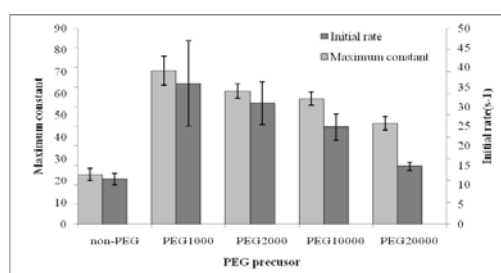


Figure 2. Effect of PEG molecular weight on initial coloration rate and maximum coloration of WO₃ film

Furthermore, the WO₃ film containing of PEG molecular weight of 1000 exhibited the highest maximum coloration and initial coloration rate of 70.58 and 66.6 s⁻¹, respectively. This might be that PEG assisted the WO₃ particles dispersion in the film [3]. These leads to the ease of electrons and

intercalated cations transfer to WO₃ particles so as to the coloration enhancement. However, the larger molecular weight of PEG suppressed the coloration ability. The structural measurements of WO₃ films are ongoing in order to get more information to explain the enhancement of coloration ability.

CONCLUSIONS

Synthesized WO₃ particles with PEG molecular weight of 1000 exhibited the highest maximum coloration and initial coloration rate which are 2.8-times and 3-times higher than those of WO₃ film without PEG addition. Coloration ability of synthesized WO₃ film is a good candidate for smart window technology.

ACKNOWLEDGEMENT

This work has been supported by the Nanotechnology Center (NANOTEC), NSTDA, Ministry of Science and Technology, Thailand through its program of the Center of Excellence Network.

References

- [1] L. Meda, G. Tozzola, A. Tacca, G. Marra, S. Caramori, V. Cristino and C.A. Bignozzi, "Photo-electrochemical properties of nanostructured WO₃ prepared with different organic dispersing agents", *Solar Energy Materials & Solar Cells*. **94**, 2010, pp. 788-796.
- [2] N. Naseri, S. Yousefzadeh, E. Daryaei and A.Z. Moshfegh, "Photoresponse and H₂ production of topographically controlled PEG assisted sol gel WO₃ nanocrystalline thin films", *International journal of hydrogen energy*. **36**, 2011, pp. 13461-13472.
- [3] A.R. Oliveira, B. B. Carvalho, H. S. Mansur and M. M. Pereira "Synthesis and characterization of bioactive glass particles using an ultrasound-assisted sol-gel process: Engineering the morphology and size of sonogels via a polyethylene glycol dispersing agent", *Materials Letters*. **133**, 2014, pp. 44-48.

CFD ANALYSIS ON THERMAL COMFORT AND ENERGY CONSUMPTION EFFECTED BY PARTITIONS IN AIR-CONDITIONED BUILDING

Pradip Aryal¹ and Thananchai Leephakpreeda¹

¹School of Manufacturing Systems and Mechanical Engineering, Sirindhorn International Institute of Technology, Thammasat University, Thailand

SUMMARY: This paper presents a CFD analysis on thermal comfort and energy consumption effected by partitions in an air-conditioned building. CFD experiments are carried out to simulate variables of indoor air before/after installation or removal of partitions. Accordingly, the Predicted Mean Vote (PMV) is determined as an indicator of thermal comfort while cooling load of make-up air is calculated for energy consumption. Some simulated results are validated by measurements with good agreement where a case study is conducted in an air-conditioned space of a library. With the proposed methodology, it can be recommended in a case study that the significant effects of partition on thermal comfort are observed in regions where occupants feel warmer and in regions where occupants feel uncomfortably cool after installing the partition while the energy consumption increases by 24%. Without modification of the air-conditioning units, the installation of the partition at the desired location is not encouraged regarding to occupant's comfort and energy consumption.

Keywords: partition, thermal comfort, PMV, energy consumption, CFD

INTRODUCTION

Nowadays, people spend more than 90% of their living time in building [1]. It is challenging for design engineer to quantitatively justify decision-making process in installation or removal of partition within such indoor-air conditioned environments since there are great interacting effects of partitions towards occupant's thermal comfort and building energy consumption. Generally, the simultaneous attainment of comfortable indoor environment and efficient energy consumption is not an easy task [2]. In a scenario of partitioning, the conditioned space without proper indoor design poses a great threat not only to occupant's comfort but also to energy consumption of building. Thus, it is of significance to qualitatively study interacting effects of partitions in the air-conditioned space on thermal comfort, and energy consumption when the partitions are installed in or removed from the air-conditioned space.

In this study, behaviors of indoor air is numerically investigated by CFD experiments using SolidworksTM Flow Simulation augmented with HVAC module, which reasonably predicts thermal comfort variables and is compelling with powerful visualization capabilities.

METHODOLOGY

CFD experiments are carried out for studying occupants' thermal comfort and energy consumption of air-conditioned building. Proposed by Fanger [3], the Predicted Mean Vote (PMV) is widely used as thermal comfort index. It is calculated by Eq. (1) by using a heat-balanced equation of six variables: air temperature (T), air velocity (v), relative humidity (RH), mean radiant temperature (MRT), clothing insulation (Clo), and metabolic activity (Met). It can

be physically interpreted by thermal sensation on a PMV scale as given in Table 1.

$$PMV = f(T, v, RH, MRT, Clo, Met) \quad (1)$$

Table 1. Thermal sensation on PMV scale

Cold	Cool	Slightly cool	Neutral	Slightly warm	Warm	Hot
-3	-2	-1	0	1	2	3

Energy consumption can be related to cooling/heating load of an air-conditioning unit. It is calculated as total change in enthalpy of air \dot{Q} as written in Eq. (2).

$$\dot{Q} = \sum \dot{m}_o h_o - \sum \dot{m}_i h_i \quad (2)$$

where \dot{m}_o is the mass flow rate at each return duct, \dot{m}_i is the mass flow rate at each supply duct, h_o is the enthalpy of air at each return duct, h_i is the enthalpy of air at each supply duct.

To investigate a case study of effects on thermal comfort and energy consumption, an installation of a partition is advised to be considered for a purpose of usage for a library at Sirindhorn International Institute of Technology, Thammasat University. The library of 700 m² is suitably facilitated by a central air conditioning system with thirty-eight ceiling-type diffusers. In this study, the air-conditioned space is occupied by 21 students and staffs under daily maximum loading capacity around 2 P.M. In this study, values of Clo and Met are 0.5

clo (student uniform) and 1.2 Met (Sedentary activity), respectively, when the experiment is taken. Other variables are determined by CFD analysis.

RESULTS AND DISCUSSION

The variables of indoor air, obtained using the CFD tool, are applied in Eq. (1) and Eq. (2) to generate contours of PMV and to calculate energy consumption in making up air, respectively. Simulated results of PMV distribution are reported in the occupied zone at the height of 1.1 m above ground level. The values of PMV for two cases before/after installation of a partition are shown in Fig. 1 and Fig. 2, respectively. The partition at the mid location is to separate the air-conditioned space into a reading area at the left side and a resting area at the right side.

PMV distribution, in case of a library without partition, has neutral thermal sensation for major region on the reading area, including where students are seated. Few adjacent areas between students have slightly cool thermal sensation with values around -0.7. The resting area of library mostly has slightly cool and cool thermal sensation due to absence of occupants. The simulation result for this case has also been verified by taking measurements of temperature, velocity and relative humidity at different locations throughout the library.

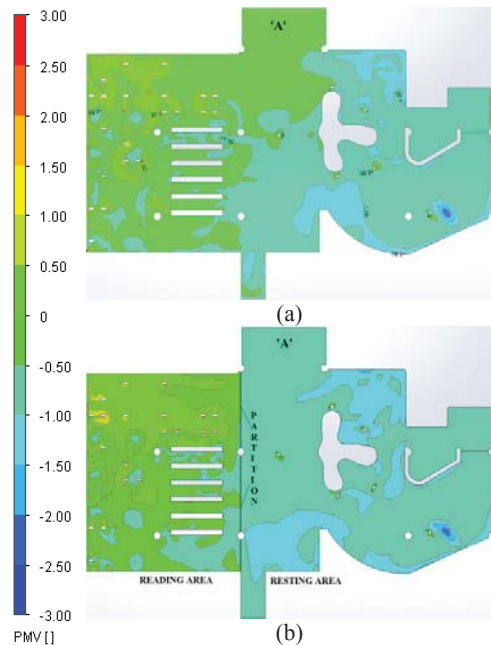


Figure 1. PMV distribution (a) without partition and (b) with partition

After installation of the partition, overall PMV in reading area has marginally increased but still

remain below the threshold limit of thermal neutrality in most of the region except in the nearby premises of students where the PMV has significantly increased to the values around 0.7- 0.8, as a result the students are likely to feel slight warm. In the resting side, there is overall decrement in the value of PMV, the most notable effect is observed in a rectangular region named ‘A’ where the sensation has been changed from neutral to slightly cool. Furthermore, the region with cool sensation has also increased in fewer regions around the corner on the resting side of library.

Table 2. Energy consumption for making up air

Cases	Energy Consumption (kW)
Before installing partition	10.23
After installing partition	12.73

Thus, the energy consumption is higher by 24% after installing the partition. Thermal comfort and energy consumption can subsequently be improved by adjusting supply air temperature and the relative location of diffuser supply and return vent. While installing partition in a current scenario is not encouraged, the detail study of indoor designing and flexibility of the location of partition with the aid of CFD tool can be performed before taking any physical changes in library.

ACKNOWLEDGMENT

The author acknowledges the EFS scholarship provided by Sirindhorn International Institute of Technology, Thammasat University.

References

[1] A. Woodcock and A. Custovic, “ABC of allergies: Avoiding exposure to indoor allergens”. Vol. **316**, 1988, pp. 1075.
 [2] G. Ye, C. Yang, Y. Chen and Y. Lib, “A new approach for measuring predicted mean vote (PMV) and standard effective temperature (SET*)”, *Building and Environment*. **38(1)**, 2003, pp. 33-44
 [3] PO. Fanger, “Calculation of thermal comfort, Introduction of a basic comfort equation”, *ASHRAE transaction*. **73(2)**, 1967, pp. 4-1

EFFECTS OF AIR SPACE THICKNESS WITHIN THE EXTERNAL WALLS ON DYNAMIC THERMAL BEHAVIOUR OF BUILDING ENVELOPES FOR ENERGY EFFICIENT BUILDING CONSTRUCTION

Saboor Shaik¹ and Ashok Babu Talanki Puttaranga setty¹

¹National Institute of Technology Karnataka,
Mechanical Engineering Department, Karnataka, India

SUMMARY: This paper presents the comprehensive investigation of the effect divided air space thickness within the wall on unsteady heat transfer characteristics such as, thermal transmittance, thermal admittance, decrement factor and time lag of five building material walls for energy efficient building enclosure design. The five building material composite walls such as, laterite stone, mud brick, cellular concrete, dense concrete and cinder concrete were studied. A computer simulation program was developed to compute unsteady heat transfer characteristics using the cyclic admittance procedure. From the results, it is observed that the decrement factor decreases and time lag increases with the increase in the divided air space thickness within the composite wall for all building materials. Dense concrete and cellular concrete were observed to be the energy efficient from the lowest decrement factor and the highest time lag perspective, respectively among thirty configurations of the composite walls. Dense concrete decrement factor decreases by 43.73% and Cellular concrete time lag increases by 12.96% for 0.02 m air space thickness compared to the conventional composite wall without air space.

Keywords: energy efficient building envelopes, decrement factor, time lag, air space thickness, admittance

INTRODUCTION

The building sector is responsible for about 33% of power consumption in India, with the commercial sector and residential sector accounting for 8% and 25%, respectively. Building envelopes or enclosures such as, floors, outer walls and roofs are important elements of the buildings to build a comfortable indoor environment. These envelopes are exposed to various climatic conditions. An appropriate design of building enclosures helps in providing desired comfort with least possible power consumption. The study of unsteady thermal characteristics of the walls plays significant role in the design of energy efficient walls. Previously, Thermo physical property changes and thickness of a wall material of a building on time lag and decrement factor using the crank Nicolson method were reported [1]. Wall's insulation thickness and position on time lag and decrement factor were also studied in detail by many researchers. The present study presents the effect of divided air space thickness within the external walls on unsteady thermal response characteristics such as, admittance, transmittance, decrement factor and time lag using the cyclic response admittance method for energy efficient building enclosure design.

ADMITTANCE METHODOLOGY

The admittance procedure is used to calculate unsteady state parameter values using matrices to simplify the temperature and energy cycles for a composite building fabric element that is subjected to sinusoidal temperature variations at the sol-air node. The wall subjected to one dimensional heat flow is given by the diffusion equation

$$\frac{\partial^2 T(X,t)}{\partial X^2} = \frac{\rho C_p}{k} \frac{\partial T(X,t)}{\partial t} \quad (1)$$

For a composite wall, the matrices of each of the

layers can be multiplied together to give the relation between inside and outside of the walls and it is as follows [2, 3]

$$\begin{bmatrix} \theta_i \\ q_i \end{bmatrix} = \begin{bmatrix} e_1 & e_2 \\ e_3 & e_4 \end{bmatrix} \begin{bmatrix} \theta_e \\ q_e \end{bmatrix} \quad (2)$$

Thermal Admittance, (Y) is the amount of energy leaving the internal surface of the element into the room per unit degree of temperature swing.

$$y_i = \left(\frac{q_i}{\theta_i} \right)_{T_{e=0}} = -\frac{e_1}{e_2} \text{ and } Y = |y_i| \quad (3)$$

The decrement Factor (f) is the ratio of the peak heat flow out of the outer surface of the fabric per unit degree of outside temperature swing to the steady state heat flow through the fabric per unit degree of temperature difference between the inside and outside environmental temperatures.

$$f_c = -\frac{1}{Ue_2} \text{ and } f = |f_c| \quad (4)$$

Decrement delay (ϕ) is the time lag between the timing of the internal temperature peak and the peak heat flow out of the external surface.

$$\phi = \frac{12}{\pi} \arctan \left(\frac{Im(f_c)}{Re(f_c)} \right) \quad (5)$$

RESULTS AND CONCLUSIONS

The five building materials such as laterite stone (BM-1), mud brick (BM-2), cellular concrete (BM-3), dense concrete (BM-4) and cinder concrete (BM-5) were considered for the study.

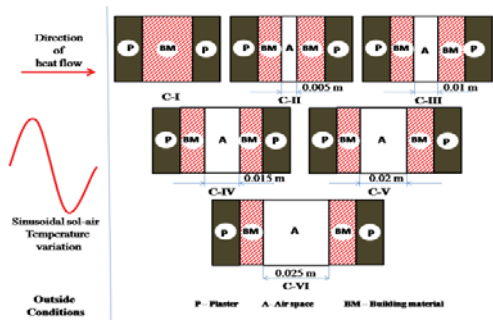


Figure 1. Configuration of composite walls with different air spaces

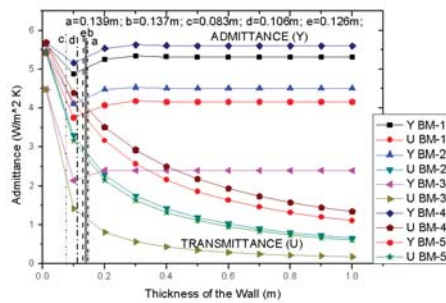


Figure 2. Thermal transmittance and admittance of homogeneous building materials as a function of thickness

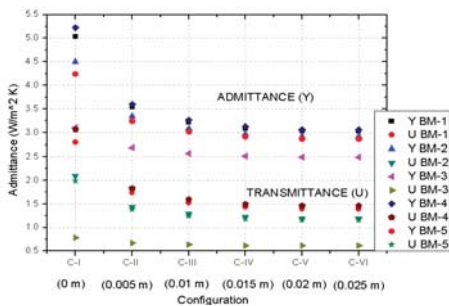


Figure 3. Effect of air space thickness on thermal transmittance and admittance of composite walls

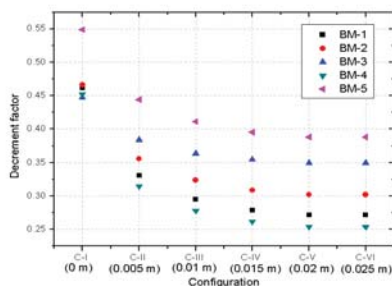


Figure 4. Effect of air space thickness on decrement factor of composite walls

Figure.1 shows the different configurations of the walls with different air space thicknesses and Fig. 3 shows that both admittance and transmittance values decrease with the increase in the air space thickness from 0.005 m to 0.02 m.

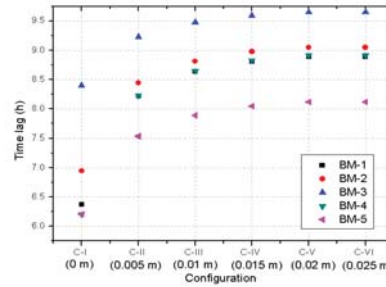


Figure 5. Effect of air space thickness on time lag of composite walls

From the results, it is observed that cellular concrete has the least optimum fabric thickness (0.083 m) as shown in Fig.2. And they are the best materials from lowest decrement factor (0.497 at 0.2 m) and highest time lag (5.31 h at 0.2m) perspective among five studied homogeneous building materials.

From Fig 4, it is clear that decrement factor decreases with the increase in the divided air space thickness within the composite wall for all building materials. Dense concrete (BM-4) was observed to be the energy efficient from the lowest decrement factor point of view among five studied building materials. Dense concrete decrement factor decreases by 43.73% for 0.02 m air space thickness compared to the conventional composite wall without air space.

Fig 5 showed that time lag increases with the increase in the divided air space thickness within the composite wall for all building materials. Cellular concrete (BM-3) was observed to be the energy efficient from highest time lag perspective among five studied building materials. Cellular concrete time lag increases by 12.96% for 0.02 m air space thickness compared to the conventional composite wall without air space.

The results of the study help in designing energy efficient building enclosures.

References

[1] H. Asan, and Y.S. Sancaktar, "Effects of Wall's thermo physical properties on time lag and decrement factor". *Energy and Buildings* **28**(2), 1998, pp.159-166.
 [2] CIBSE, *CIBSE Environmental Design Guide-A*. 7th ed., chartered Institution of Building services engineers, London, 2006, pp 3.1-3.8.
 [3] M.G. Davies, *Building Heat Transfer*, John-Wiley & sons Ltd. 2004, pp. 335-351.

SUITABLE OPERATING CONDITIONS OF HOT WATER GENERATORS COMBINED WITH CENTRAL AIR PACKAGE UNITS: A CASE STUDY OF TIPCO BUILDING GROUP

Chalermporn Jindapeng¹

¹ Master of Engineering (Energy and Environmental Technology Management)
Department of Chemical, Faculty of Engineering Thammasat University

SUMMARY: The main objective in the study of the suitable operating conditions of hot water generators combined with central air package units: a case study of Tipco Building Group was to analyze the suitable operating conditions and energy-related costs in each operating condition of hot water generators combined with central air package units, which resulted in water cooled package

Thermal energy from vapor form refrigerants at high pressures and temperatures was exchanged with thermal energy of the water in the swimming pool that required suitable temperature control for users with the use of plate heat exchangers before refrigerants could enter the condenser in its function to change the status of vapor form refrigerants at high pressures and temperatures to liquid form at high pressures and temperatures. Thus, if this was used to replace heat pumps, it could reduce the electrical energy that was used to make hot water and reduce the cost of the electrical energy of air package units, including the increased efficacy of air package units.

Of the analyses of the suitable operating conditions by means of the study of the elements involved with actual measurements from the system that had been installed at the Tipco Building Group, hot water generators were combined with air package units, which resulted in water cooled packages with a cooling capacity of 75 ton. Plate heat exchangers were used in the transfer of thermal energy from refrigerants to one set of water with a heat exchanger area of 1.5 m², which was used to increase the temperature of swimming pool water that has a capacity of 240 m³. From experimental results, it was discovered after continuous temperature measurements in the swimming pool every 15 minutes that swimming pool water temperature increased by 0.78 °C, 0.75 °C, 0.74 °C, and 0.71 °C. The rates of flow of hot water through the heat exchangers were equal to 14, 16, 18, and 20 litres per minute respectively, where the swimming pool water's temperature was at a constant value and when the rate of flow of hot water increased, this caused hot water temperatures to decrease and the coefficient of performance of the air package units to increase from 5.9 to 6.3, 6.7, 6.9, and 7.6 while the rates of flow of hot water were equal to 14, 16, 18, and 20 litres per minute respectively. As for the cooling systems, there were no changes and the system's cooling functions were normal, as the cooling systems were able to continuously transfer incoming heat for the swimming pool water, which resulted in a constant pressure in the cooling system that allowed its cooling functions to work normally.

Keywords: Central Air Package Units, Hot Water Generators, Heat Exchange

INTRODUCTION

Thailand is a hot country. The average temperature of the world becomes hotter because of Greenhouse Effect. So, electricity consumption in air-conditioners in office buildings, hotels, hospitals, etc. has increased over times. However, the electric current in hotels is also used for boiling water such as to increase the water temperature in swimming pool, and the need of energy becomes more increasing. The procedure to decrease the energy using for hot water generation or warmer water in swimming pool are to generate hot water with Air-Conditioning System, Air Package Unit to exchange the temperature between heat ventilator with cooler water in swimming pool to increase the water temperature, and to decrease the rate of Condenser Water Pump and ventilating fan (Cooling Tower).

Cooler generator or air-conditioners' performance was indicated by Coefficient of Performance (COP). COP is the proportion of absorbed heat from refrigerated space per the heat from compressor 1,2. By considering the circle of

refrigeration, the absorbed heat from Refrigerated space including the Heat of Compression must be removed from refrigerated system by heat ventilation at Condenser. The types of condenser will be called by ventilating materials. The heat from big refrigerated system will be ventilated by Water-cooled condensing unit, the ventilated heat can be reused in form of warm or hot water by using water to be the Condensing medium. The heat absorbed to the water is the circulated energy in form of Heat pump.

The heat for warm water depends on the efficiency of heat exchange machine in hotels, hospitals. The cost is very high comparing to other materials. Because of these causes, seeking for substituted energy to generate hot water is necessary.

This study will study the appropriate status of water heating system with air-conditioning system ventilating by Air Package Unit. The results of the study are to find the appropriate status of water heating system to compare to the investment and expense of all system. The data will be analyzed by

the principles of economy. keyword(s). Each column is 80 mm wide with spacing of 10 mm between columns (total width is 170 mm). All the margins are to be 25 mm including the title page.

SUBMISSION AND NOTIFICATION OF ABSTRACT

If the flowing rate of hot water is increase at a point, the temperature in swimming pool will be stable at once. The information of hot water generation system will be noted to find the appropriate temperature of the water in swimming pool. The data will be collected every 15 minutes. The results found that the water temperature in swimming pool is 0.78 °C, 0.75 °C 0.74 °C , and 0.71 °C increased at the volume of hot water flowing through the machine at 14 ,16 ,18 and 20 liter per minute respectively. The water temperature will be stable once because the heat of air-conditioner is stable. The cooling (highest percentage) is at 60%. From the results, if the rate of flowing hot water is increasing, the temperature will be lower and the standard deviation of the air-condition system will be higher from 5.9 to 6.3 ,6.7, 6.9 and 7.6 at 14 ,16 ,18 and 20 liter per minute. The refrigerating system can generate the cool air as usual because the heat can be continuously ventilated to the swimming pool. The pressure in refrigerated system becomes normal. Meanwhile, the electricity uses is stable, too. The standard deviation of the refrigerating system capability is stable when the flowing of hot water is changed.

References

- [1] S. Thulthaisong and D. Sudphakdee. "Mathematical model of the boiling water system by heat pump by heat re-use in the air-condition system" *Case Study 21th Conference of Mechanical Engineering Network of Thailand*, 2007, pp.75-82.
- [2] A. Chaionant. "Boiling Water with Heat Pump. Thesis of Masters Degree" Master of Mechanical Engineering, Major Energy Technology, School of Technology, Environment and Materials, King Mongkut's University of Technology Thonburi, 2000.

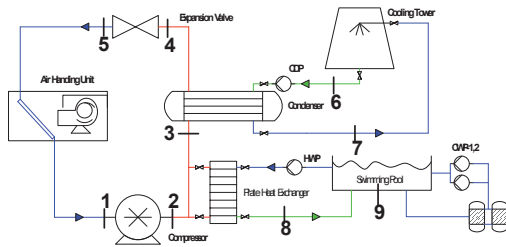


Figure 1. Hot Water Generators Combined with Central Air Package Units

ACKNOWLEDGEMENT

The researcher would like to thank Asst. Prof. Dr. Wanwisa Sakolphap, committee and advisor, who always give the good advice, useful suggestions, along to solve the mistakes until this thesis was successfully finished. Acknowledge Mr. Phanlop Sawanwong, managing director and all officers of Pioneer Preseason Co., Ltd for the kind assistance and support and friends in major of Energy and Environmental Technology Management, Chemical Engineering, Faculty of Engineering, Thammasat University for their kind support.

PERFORMANCE ASSESSMENT OF DEDICATED OUTDOOR AIR SYSTEMS FOR OFFICE BUILDING IN THAILAND

Nontivat Inklab¹, Pipat Chaiwiwatworakul¹, Surawut Chuangchote¹,
Pattana Rakkwamsuk¹ and Surapong Chirarattanon¹

¹The Joint Graduate School of Energy and Environment, King Mongkut's University of Technology Thonburi, Thailand

SUMMARY: Dedicated outdoor air system (DOAS) is a system that supplies the processed outdoor air into air-conditioned space to meet an accepted indoor air quality (IAQ). DOAS can also influence significantly the energy consumption of the air-conditioning system that it is integrated with. In this study, 5 different configurations of DOAS are examined for their application for tropical climate. TRNSYS software is used to model DOAS and then simulate the energy consumption for air-conditioning. From the whole year simulations, the results show that among the selected DOAS configurations, DOAS using a cooling coil integrated with runaround coil and rotary energy wheel can offer the best energy performance.

Keywords: Dedicated outdoor air system, heat recovery, energy simulation, ventilation

INTRODUCTION

Thailand is situated in a tropical region and is subjected to a hot and humid climate. Air-conditioning by cooling is essential for human comfort and nowadays reaches saturation in commercial buildings. In Thailand, the forced convection air-conditioning system is used to control the indoor air at a desired temperature (e.g. 25°C). The cold air is supplied into a room to absorb the thermal loads, and is then returned to mix with the fresh air before it is cooled again at the cooling coil of an air handling unit (AHU). The fresh air is drawn from outside into a building with sufficient amount to maintain a good indoor air quality (IAQ) and to comply with the requirement of the local air ventilation standard [1]. Depending on the system design, the outdoor air may and may not be pre-conditioned before supplying into the buildings [2].

According to the energy reports from more than two thousands commercial buildings in Thailand, the air-conditioning is responsible 50-60% of the total building energy consumption [3]. Energy conservation has undertaken in air-conditioning system to curb the increasing electricity demand of the buildings and the sector as a whole. However, among various measures, it is found that turning-off the ventilation system now become a choice and is implemented in several buildings to reduce the tremendous load from the outdoor air with an expectation of using air infiltration for the ventilation instead. This practice was made with a miss understanding and no concern on the merit of the air ventilation.

A survey result from a research project conducted under a co-funding support from the Thailand Research Fund (TRF) and the Electricity Generating Authority of Thailand (EGAT) show that the quality of the indoor air is quite poor for such buildings deciding to shut off the ventilation system. The measurements indicate the carbon dioxide level exceeding 1,200 ppm.

To address the issue mentioned above, this paper investigates processes for the air ventilation that can meet both the energy efficiency and the acceptable IAQ. The study focuses specifically on the dedicated outdoor air system (DOAS) that is operating with parallel with the air terminal units. An appropriate configuration of the DOAS is identified for Thailand.

DEDICATED OUTDOOR AIR SYSTEM

DOAS is a system that is designed for improving IAQ and delivering precise amount of air ventilation. The equipment for condition air in DOAS system can be divided into 2 parts. The first part is dedicated make-up air unit which bring the fresh outdoor air into the inside space. This includes management of sensible and latent heats of fresh outdoor air and occurred latent heat in the space. Another part of DOAS is AHU which manage occurred sensible heat in the space. A simplified DOAS system is shown in Figure 1. With this system, it assures that air ventilation also meet the standard [4].

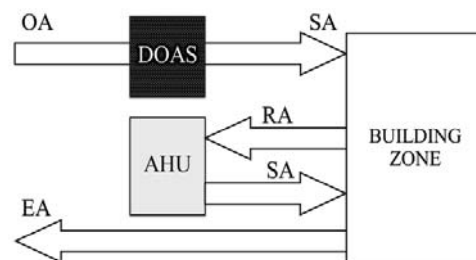


Figure 1. DOAS system.

In the study, 7 systems were considered. These are;

- 1) CON 1 (conventional system,
- 2) CON 1 NO VENT (conventional system with no ventilation,
- 3) CON 2 (cooling coil unit,
- 4) CON 3 (cooling coil integrated with heat recovery run around coil,
- 5) CON 4 (cooling coil integrated with rotary energy wheel,
- 6) CON 5 (cooling coil integrated with rotary energy wheel and sensible wheel, and
- 7) CON 6 (cooling coil integrated with runaround coil and rotary energy wheel.

METHODOLOGY

The systems mentioned above were equipped for office building model in TRNSYS simulation program. The designed condition of an office building model is shown in the Table 1.

Table 1. Designed condition of office building [5].

Designed condition	Dry bulb temperature	Relative humidity
Office	25°C	50%RH

The simulation focused on investigations of cooling load, energy consumption, characteristics, and performances of each DOAS configuration under tropical climate, in order to compare annual cooling loads and evaluate energy saving between conventional air-conditioning system and any DOAS configurations to obtain a suitable DOAS configuration.

The input data used for whole year simulation was meteorological condition data in 2000 from the meteorological station. The weather data was input data for TRYSYS program which was reported in the simulation by 1-h time steps. The internal load was a reclining person, artificial light and equipment.

RESULT AND DISCUSSION

Figure 2 shows results of annual cooling loads between the conventional and DOAS systems. It was found DOAS systems could reduce the cooling load compared with the conventional system (CON 1) in the range of 5-24% and there is no significant between the best performance of DOAS (CON 6) and the conventional system with no ventilation (CON 1 NO VENT). Furthermore, when comparing all cooling loads of DOASs, the lowest average cooling load was found in the case of CON 6, due to the fact that CON 6 has the couple of energy and heat recovery units.

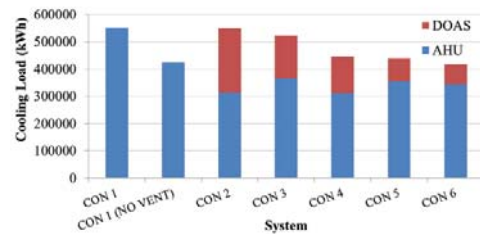


Figure 2. Annual cooling loads of the conventional and all DOAS systems

ACKNOWLEDGMENT

The author would like to thank the Joint Graduate School of Energy and Environment (JGSEE) for the financial support with instruments and a licensed program in this study.

References

- [1] The Engineering Institute of Thailand Under H.M. The King's Patronage, 2013, Ventilation Standard for Ventilation and Air Conditioning Systems.
- [2] W. Morris, "The ABCs of DOAS: Dedicated Outdoor Air Systems", ASHRAE Journal **45**, 2003, pp. 127-129.
- [3] V. Youngcharoen and B. Limmeechokchai, "Energy Analysis of the Commercial Sector in Thailand: Potential Savings of Selected Options in Commercial Buildings", *Proceeding of SEE International Conference*, 2004, pp.496-501.
- [4] S.A. Mumma, "Overview of integrating Dedicated Outdoor Air Systems with Parallel Terminal Systems", ASHRAE Transactions **107**, 2001, pp. 545-552.
- [5] T. Sookchaiya, V. Monyakul and S. Thepa, "A Study and Development of Temperature and Relative Humidity Control System in Hospital Buildings in Thailand", *EDU-COM International Conference*, 2008, pp. 19-21.

THERMAL PERFORMANCE ASSESSMENT OF A DOUBLE-PANE WINDOW WITH HORIZONTAL SLATS IN THAILAND

Vichuda Mettanant¹ and Pipat Chaiwiwatworakul¹

¹Joint Graduate School of Energy and Environment, King Mongkut's University of Technology Thonburi, Bangkok, Thailand

SUMMARY: For buildings in Thailand, heat reflective glasses are used to reduce the solar heat gain from windows to air-conditioning system. However, the glasses highly absorb the solar radiation and eventually causes to the high surface temperature. The people who sit near the window would experience the thermal discomfort with the heat emitted from the glass surface. To address this issue, this paper examines a window equipped with slats enclosed between two glass panes (slat window). In the study, the heat gain and surface temperatures of the slat window were determined. The thermal comfort was assessed in terms of predicted mean vote (PMV). The simulation results show that the slat window, when the slats are tilted to completely shade the beam radiation from entering the window whilst still maximize the exterior view, can reduce 7-60% of the heat gain from the heat reflective glass window. The slat window can also provide the neutral comfort for the whole period of the office hours.

Keywords: slat window, heat reflective glass, thermal comfort, heat gain.

INTRODUCTION

The solar radiation is intense all year round in Thailand. Large commercial buildings are air-conditioned to provide thermal comfort for occupants and the heat reflective glasses with low solar transmittance are used to reduce the cooling load from the solar gain through windows. Since the heat reflective glasses possess high solar absorptance, the glasses accumulate large amount of the solar energy, then arising its surface temperature. This might cause the people who sit close to the windows experience to the thermal discomfort due to the radiative heat from the glass.

The thermal comfort assessments of window have been carried out in different climates. The study of Bessoudo showed that even in cold climate region, the transmitted solar radiation can cause thermal discomfort [1]. In warm climate, the use of heat reflective glass cannot provide good thermal comfort [2, 3]. Due to the low optical transmittance, the glass neglects the opportunity of the use of daylight for interior illumination.

To address this issue, this paper examines a configuration of a window with slats enclosed between two glass panes (slat window). The slats can be tilted to intercept the beam radiation from entering the window. In the study, the heat gain and the surface temperatures of the windows can be simulated for the whole year. The thermal comfort can also be assessed in terms of predicted mean vote (PMV).

METHODOLOGY

In this section, the thermal model of the slat window and assessment of the thermal comfort in terms of PMV are briefly described.

Heat Transfer through the Slat Window

Figure 1 shows the slat window model that consists of two adjacent slats located at the middle

between two glass panes. The slats have a width of W_s and a separation of S_s and are tilted at an angle of ϕ measured with respect to the horizontal direction. The outer glass pane with a thickness of e_o is set apart at a distance of D from the inner glass panes with a thickness of e_i . The distance from the edges of the slats to the surfaces of both outer and inner glass panes is d .

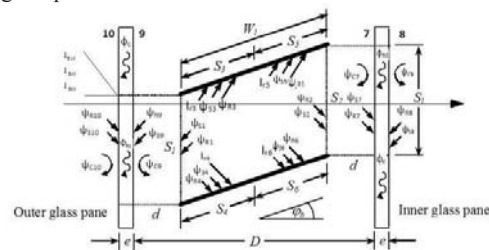


Figure.1. Heat transfer model of the slat window

In the figure, the heat transfer through the slat window (q_w) is analyzed based on mechanisms of radiation exchanges and heat convections. The analysis determines the net radiative energy absorbed (A^s) by the slats and the glasses from the exchanges of the solar (shortwave) and the thermal (longwave) radiations within the air gap of the slat window. The analysis also determines the net energy absorbed due to the heat convection of the air within the gap between either side of the slat edge and the glass pane (A^c).

The energy balances of the whole window system are simultaneously performed in an iterative manner at the slats and the two glass panes by considering the incident solar radiations, the net absorbed energy from the heat exchanges within the air gap, and the heat convection on the glass surfaces by the surrounding air. In the energy balances, the effects of thermal storage and delay in

the temperature and the heat transfer are taken into account as a result of the slat and glass properties.

For the window, the slats can be rotated counterclockwise from the horizontal line at which the slat angle is measured as positive value ($+\phi$). Rotating the slats clockwise from the horizontal line, the angle is measured as negative value ($-\phi$).

Thermal Comfort Assessment

To identify the thermal comfort condition of the people sitting near the window, predicted mean vote (*PMV*) of the ISO Standard 7730 can be used [2-5]. The index categorizes the comfort into 7 levels from +3 for feeling hot to -3 for feeling cold where 0 represents neutral. The *PMV* values used in this study include effect of solar radiation can be calculated as described in [2, 3].

RESULTS

The thermal models described above were used to assess the thermal performance of the slat window in terms of the heat transfer and the thermal comfort condition. In the simulation the window was assumed facing south. The window was 2.8 m wide and 1.5 m high and its sill was 0.85 m above the floor. The properties of the heat reflective glass window and the slat window are summarized in Table 1.

Table 1 Optical properties of the laminated glasses used in the simulations

Description		Heat reflective	The slat window	
			Green-Clear (Outer glass)	Clear-Clear (Inner glass)
Solar range	Transmittance	0.28	0.41	0.75
	Reflectance	0.15	0.05	0.06
	Absorptance	0.57	0.55	0.18
Infrared range	Emittance	0.85	0.85	0.85

Table 2 shows the simulation results for the slat window. The simulation was made for a scheme that the beam radiation is completely intercepted from entering the room during 8:00-17:00. At our location where the latitude and longitude are 14.7°N and 100.5°E, the slats are to be tilted at 30° during November-February, at 10° in March and October and at 0° in the remaining months of the year.

The results show that the slat window can reduce the thermal load from the window by 7-60% of that from the heat reflective glass. The slat window also provides the neutral thermal comfort for the whole period of the office hours 8:00-17:00.

Table 2. Assessment of the heat load and the thermal comfort for slat window

Month	Heat load (W.m ⁻²)	T _{mrt,tot} (°C)		PMV _{tot}		Comfort (%)
		max	mean	max	mean	
Jan.	184.14	36.4	30.3	1.4	0.5	51
Feb.	157.87	34.4	29.2	1.1	0.4	66
Mar.	116.58	30.4	27.5	0.5	0.1	98
Apr.	87.84	28.4	26.7	0.3	0.0	100
May	87.89	27.8	26.5	0.2	0.0	100
Jun.	83.08	27.6	26.6	0.1	0.0	100
Jul.	84.07	28.0	26.6	0.2	0.0	100
Aug.	87.25	28.3	26.7	0.2	0.0	100
Sep.	104.68	29.8	27.2	0.5	0.1	100
Oct.	136.14	32.9	28.2	0.9	0.2	81
Nov.	195.31	36.3	30.8	1.4	0.6	44
Dec.	219.53	37.5	31.8	1.6	0.7	38
Ann.	128.66	37.5	28.2	1.6	0.2	82

CONCLUSION

The performance of the slat window was assessed in terms of heat transmission and thermal comfort. The simulation results shows that the slat window when the slats are tilted to completely shade the beam radiation from entering the window whilst still maximize the exterior view, can reduce 7-60% of the heat gain from the heat reflective glass window. The slat window can also provide the neutral comfort for the whole period of the office hours.

References

- [1] M. Bessoudo, A. Tzempelikos, A.K. Athienitis and R. Zmeureanu, "Indoor thermal environmental conditions near glazed facades with shading devices - Part I: Experiments and building thermal model", *Building and Environment*, **45** (11), 2010, pp. 2506-2516.
- [2] S. Chaiyapinunt, B. Phueakphongsuriya, K. Mongkornsaksit and N. Khomporn, 'Performance rating of glass windows and glass windows with films in aspect of thermal comfort and heat transmission', *Energy and Buildings*, **37**, (7), 2005, pp. 725-738.
- [3] M. C. Singh, S. N. Garg and R. Jha, 'Different glazing systems and their impact on human thermal comfort--Indian scenario', *Building and Environment*, **43**, (10), 2008, pp. 1596-1602.
- [4] G. R. Newsham, 'Manual Control of Window Blinds and Electric Lighting: Implications for Comfort and Energy Consumption', *Indoor Environmental*, **3**, (3), 1994, pp.135-144.
- [5] M. L. Gennusa, A. Nucara, G. Rizzo and G. Scaccianoce, 'The calculation of the mean radiant temperature of a subject exposed to the solar radiation-a generalised algorithm', *Building and Environment*, **40**, (3), 2005, pp. 367-375.

Bio-Fuel; Biogas

COMPARATIVE PERFORMANCE OF HALOTHIOBACILLUS NEAPOLITANUS AND PARACOCCLUS PANTOTROPHUS IN SULFUR OXIDATION

Nunthaphan Vikromvarasiri¹ and Nipon Pisutpaisal^{1,2,3,4}

¹ The Joint Graduate School for Energy and Environment (JGSEE),
King Mongkut's University of Technology Thonburi, Thailand

² Department of Agro-Industrial, Food and Environmental Technology, Faculty of Applied Science,
King Mongkut's University of Technology North Bangkok, Thailand

³ The Biosensor and Bioelectronics Technology Centre,
King Mongkut's University of Technology North Bangkok, Thailand

⁴ The Research and Technology Center for Renewable Products and Energy,
King Mongkut's University of Technology North Bangkok, Thailand

SUMMARY: Hydrogen sulfide (H₂S) is one of the biggest factors limiting the use of biogas, which is related to its properties that can corrosive to internal combustion engines. This study investigated and compared the properties and sulfur oxidizing activities of *Halothiobacillus neapolitanus* (HTN) and *Paracoccus Pantotrophus* (PCP) in their suitable conditions for apply in biotrickling filter to remove hydrogen sulfide in biogas. These bacteria were screened and characterized from different wastewater treatment plants. The results indicated that HTN had higher specific growth rate than PCP. However, the sulfate production rates of HTN and PCP are not significantly different, but HTN can produce higher sulfate concentration, and can tolerant high sulfide and sodium chloride concentration and low pH, which are advantages to apply in biotrickling filter in term of preventing contaminations. This study demonstrated that HTN is better option than PCP for application in the hydrogen sulfide removal in the biogas. However, PCP has challenge to apply for hydrogen sulfide removal in the other conditions such as denitrifying condition.

Keywords: halothiobacillus neapolitanus, paracoccus pantotrophus, thiosulfate, hydrogen sulfide, biogas

INTRODUCTION

Hydrogen sulfide is occurred in biogas production from the degradation of proteins and other sulfur containing compounds present in the organic feed stock during the anaerobic digestion. The hydrogen sulfide concentration depends on the types of material substrates [1]. One of the biggest factors limiting the use of biogas is related to the hydrogen sulfide composition, which is very corrosive to internal combustion engines. Besides, there are reports on health effects to human from hydrogen sulfide [2].

Biotrickling filter process is one of biological process, which is an alternative solution to solve these problems. Chemotrophic bacteria can grow by using inorganic carbon as a carbon source and obtain chemical energy from the oxidation of reduced inorganic compounds such as hydrogen sulfide, elemental sulfur, thiosulfate, etc. Moreover, some of chemotrophs can use both the organic and inorganic carbon as a carbon source and using an inorganic compound as an energy source. These bacteria were called mixotrophic bacteria.

Therefore, this study investigated and compared the properties and sulfur oxidizing activities of HTN (chemotroph) and PCP (mixotroph), which were screened and characterized from different aerobic wastewater treatment plants, in their suitable conditions to apply in biotrickling filter for hydrogen sulfide removal in biogas.

METHODOLOGY

Halothiobacillus neapolitanus NTV01 (HTN) (KJ027464) was screened and purified from activated sludge system collected from a full scale wastewater treatment process of Siriraj Hospital, Bangkok, Thailand. Whereas, *Paracoccus Pantotrophus* NTV02 (PCP) (KJ027465) was isolated and purified from an aerobic wastewater treatment process of leather industry (Ked Prakobkarn Autsahakam Foknang KM. 30 km Co., Ltd., Samut Prakarn province, Thailand).

Thiosulfate mineral nutrient (TMN) contained the following (g/L): 4.0 KH₂PO₄, 4.0 K₂HPO₄, 0.4 NH₄Cl, 0.2 MgCl₂.6H₂O, 0.01 FeSO₄.7H₂O and 10.0 Na₂S₂O₃.5H₂O [3]. In the experiment, HTN and PCP were tested in their optimal pHs and temperatures conditions by shaking at 180 rpm for 120 hours. Liquid samples were periodically collected for analysis of the growth, pH, and sulfate content. Growth of microorganisms was measured with colony forming unit (CFU/mL) by drop plate technique. Sulfate (SO₄) content was determined by turbidimetric method according to standard method.

RESULTS AND DISCUSSION

HTN and PCP were investigated their ability in order to compare advantages and disadvantages of these microbes for applied in biotrickling filter for hydrogen sulfide removal.

HTN is an obligately chemolithoautotrophic

bacterium, which can tolerate and utilize high sulfide concentrations energy sources, and use carbon dioxide as carbon source [4]. PCP can mixotrophically grow by using the mix of organic and inorganic carbon sources (carbon dioxide, glucose, etc.), and it can use sulfide and thiosulfate as energy sources under aerobic conditions [5]. The optimum temperature and pH of these microbes were showed in Table 1. Therefore, HTN was test in pH 7 and at 30 °C, whereas PCP was test in pH 8 and at 37 °C by culture in TMN medium.

The results showed that HTN had higher specific growth rate than PCP (Table 2), but its growth was dropped after 36 hours because pH dropped lower than the pH of its growth range (Figure 1, 2). For the sulfate production, the sulfate production rates of these bacteria are not significantly different, but HTN can produce higher sulfate concentration.

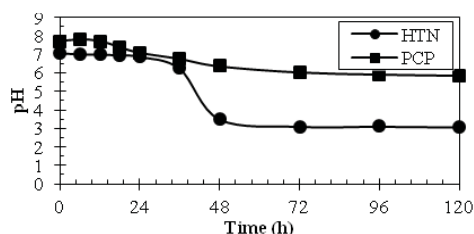


Figure 1. pH of HTN and PCP in TMN medium at optimal conditions. Symbols represent mean values of duplicate experiments; error bars represent one standard deviation

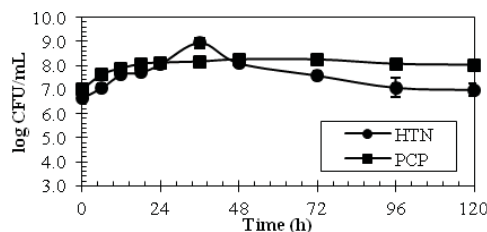


Figure 2. Growth of HTN and PCP in TMN medium at optimal conditions. Symbols represent mean values of duplicate experiments; error bars represent one standard deviation

The previous study reported that HTN can tolerate high concentration of sodium chloride (4 M) [4]. The properties of HTN, which are tolerant high sulfide concentration, low pH and high sodium chloride, are advantage to apply in biotrickling filter in term of preventing contaminations. The study suggested that HTN is better option than PCP for application in biotrickling filter in this condition.

However, PCP might be applied in biotrickling filter for hydrogen sulfide removal in the other conditions such as denitrifying conditions, in which hydrogen sulfide is removed from biogas in

anaerobic condition.

Table 1. Ranges of pH and temperature for *Halothiobacillus neapolitanus* and *Paracoccus Pantotrophus* cultivation [4, 5].

Microbial strains	HTN	PCP
Growth pH range	4.5-8.5	6.5-10.5
Optimum pH	6.9	8
Growth range of Temperature (°C)	8-39	15-42
Optimum temperature (°C)	28-32	37

Table 2. Kinetic parameters of *Halothiobacillus neapolitanus* and *Paracoccus Pantotrophus* at the optimal condition.

Microbial strains	HTN	PCP
Specific growth rate (h ⁻¹)	0.15±0.01	0.14±0.00
The highest growth (CFU/mL)	9.0 x 10 ⁸	1.8 x 10 ⁸
Sulfate production rate (mg/L.h)	147.7±9.8	148.2±21.4
Maximum sulfate concentration (mg/L)	6120.00	5679.60

ACKNOWLEDGEMENT

I gracefully acknowledge the financial support from the Royal Golden Jubilee (RGJ) Scholarship of Thailand Research Fund (TRF, Grant No. PHD/0139/2553), and the Joint Graduate School of Energy and Environment (Grant No. JGSEE 522), King Mongkut's University of Technology Thonburi.

References

- [1] M. Syed, G. Soreanu, P. Falletta, M. Béland., "Removal of hydrogen sulfide from gas streams using biological processes - A review", *Wastewater Technology Centre*, **48**, 2006, pp. 2.1-2.14.
- [2] World Health Organization. Hydrogen sulfide: Human health aspects, International Chemical Assessment Document, 2003, **53**, pp. 13-14.
- [3] N. Vikromvarasiri and N. Pisutpaisal, "Potential Application of *Halothiobacillus neapolitanus* for Hydrogen Sulfide Removal in Biogas", *Energy Procedia*, **61**, 2014, pp. 1219 – 1223.
- [4] D.J. Brenner, N.R. Krieg, J.T. Staley, "Family III *Halothiobacillaceae*. Bergy manual of systematic bacteriology", The Gammaproteobacteria, pp. 58-59.
- [5] D.J. Brenner, N.R. Krieg, J.T. Staley, "Genus XII. *Paracoccus*. Bergy manual of systematic bacteriology", The Alpha-, Beta-, Delta-, and Epsilonproteobacteria, Springer, pp. 197-203.

Ni-Mg-Al HYDROTALCITE FOR IMPROVEMENT OF DARK FERMENTATIVE HYDROGEN PRODUCTION

Diep Thi Hong Le¹ and Rachnarin Nitorisavut¹

¹School of Bio-Chemical Engineering and Technology,
Sirindhorn International Institute of Technology, Thammasat University, Thailand

SUMMARY: Ni-Mg-Al hydrotalcite (HT) was employed to test its potential to enhance biohydrogen production with various doses, from 83 to 417 mg/L. Experiments were carried out at 37 °C using heat-treated anaerobic sludge as inoculum and sucrose as synthetic wastewater in batch tests. X-ray diffraction (XRD) pattern and Fourier transform infrared (FTIR) spectrum were recorded to determine structure and functional groups of HT. As a result, addition of 250 mg/L Ni-Mg-Al HT showed the highest hydrogen yield of 3.37 ± 0.17 mol H₂/mol sucrose, which improved biohydrogen production by 80%. At the end of fermentation process, concentrations of metabolites, including lactic acid, acetic acid, and butyric acid were 160 mg/L, 4661 mg/L, and 5625 mg/L, respectively. Better hydrogen production for addition of 250 mg/L Ni-Mg-Al HT can be attributed to basic property of HT, facilitation of ion Mg²⁺ in electron transfer process and suitable concentration of ion Ni²⁺ as well.

Keywords: biohydrogen, hydrogen yield, dark fermentation, wastewater treatment, hydrotalcite

INTRODUCTION

Hydrogen has been known as a clean and potential energy source because it has no emissions when burnt and contains high energy [1]. Moreover, hydrogen is also an important feedstock of the chemical industry and a necessary element in detoxifying some water pollutants [2]. A number of methods has been applied to produce hydrogen, including thermocatalytic reformation of hydrogen-rich organic compounds, electrolysis of water, and biological processes. Recently, biological systems are getting attention because of its environmental friendliness. Dark fermentation has been considered as a persuasive approach to produce biohydrogen production. However, the most challenging is the low conversion to biohydrogen, nearly 17% [2].

Hydrotalcites (HTs) are unique materials with various practical applications in catalysis, adsorption, pharmaceuticals, photochemistry, and electrochemistry. The general formula is $[M^{2+}_{1-x}M^{3+}_x(OH)_2](A^{n-})_{x/n} \cdot mH_2O$, where M²⁺ can be Mg²⁺, Fe²⁺, Co²⁺, Cu²⁺, Ni²⁺, or Zn²⁺; and M³⁺ can be Al³⁺, Cr³⁺, Co³⁺, Mn³⁺, or Fe³⁺. The interlayer anion Aⁿ⁻ can be Cl⁻, NO₃⁻, CO₃²⁻, or organic anions; x is equal to the molar ratio of M²⁺/(M²⁺ + M³⁺) [3]. Previous studies have been published on the application of HTs for biohydrogen production [4,5]. In this study, Ni-Mg-Al HT was investigated to test its potential in improving biohydrogen production.

METHODOLOGY

The Ni-Mg-Al HT with molar ratio of Ni²⁺/Mg²⁺ = 1:5 and ratio of M²⁺/M³⁺ = 3:1 was synthesized by co-precipitation method. The anaerobic sludge was taken from the bottom portion of an upflow anaerobic sludge blanket (UASB) reactor, which was used to treat brewery wastewater.

Then it was heat-treated at 105 °C for 30 minutes to eliminate activity of methanogenic microorganisms and employed as inoculum in fermentation process. Sucrose solution with concentration of 20 g sucrose/L was used as synthetic wastewater. The nutrients for bacteria were also prepared.

Batch experiments were carried out under mesophilic condition at 37 °C and shaken at 90 rpm using shaking incubator. All experiments were operated in triplicate.

To analyze the structure and determine functional groups of Ni-Mg-Al HT, X-ray diffraction (XRD) pattern and the Fourier transform infrared spectroscopy (FTIR) spectra were collected.

The pH value was measured by a pH meter. Volatile suspended solid (VSS) and total suspended solids (TSS) were determined and proceeded as in the Standard Methods [6]. The components of biogas were analyzed by gas chromatograph (GC) (PerkinElmer, USA). To determine sucrose and VFAs (acetic, butyric and lactic acid) concentrations, at the end of cultivation, mixed liquor samples from each bottle were drawn and filtered through 0.2 μm membrane before being injected into the high performance liquid chromatography (HPLC) (Agilent 1200 infinity Series). Metals release of hydrotalcite (nickel, magnesium, aluminum) was tested by inductively coupled plasma spectrometer (ICP) OES Optima 8000 (PerkinElmer, USA).

The modeling of batch fermentative hydrogen production was based on the following modified Gompertz equation:

$$H = H_{\max} \exp\left\{-\exp\left[\frac{R_m \times e}{H_{\max}}(\lambda - t) + 1\right]\right\} \quad (1)$$

RESULTS AND DISCUSSION

HT characterizations

The XRD pattern of Ni-Mg-Al HT in Figure 1 demonstrates a well-crystallized HT structure through seven peaks for (003), (006), (012), (015), (018), (110) and (113) diffractions. The graph shows general features that are typical of all hydrotalcites: the presence of sharp and intense lines at low values of the 2θ angle, and less intense and generally asymmetric lines at higher angular values [7].

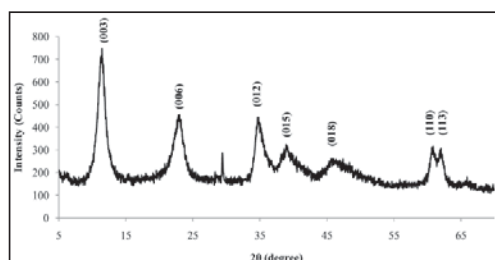


Figure 1. XRD pattern of Ni-Mg-Al HT

Hydrotalcite activity

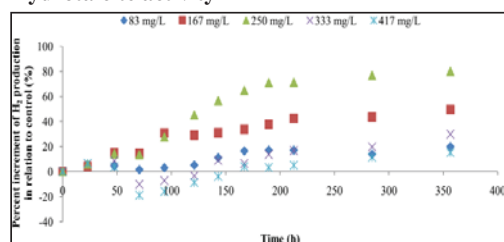


Figure 2. Percent increment of hydrogen production in relation to control of Ni-Mg-Al HT

All doses exhibit higher hydrogen yield compared to control. Among them, 250 mg/L of Ni-Mg-Al HT was considered as optimum dose with hydrogen yield of 3.37 ± 0.17 mol H_2 /mol sucrose, achieved an 80% increase. Similarly, the increase in cumulative hydrogen production from applying different doses of HT was also demonstrated in Figure 2. Table 1 reveals that the modified Gompertz model fit to the experimental data with $R^2 > 0.95$. It is reported that the accumulation of VFAs during fermentation time resulted in a decrease in pH, and inhibited hydrogen production. HT with its nature could keep pH not decrease too much.

As can be seen in Figure 3, metals from HT are released gradually in fermentation process. Magnesium can activate membrane components such as cytochromes for increasing electron transfer

[8]. It is remarkable that nickel is heavy metal, which can inhibit bacteria at high concentration. In this study, suitable Ni^{2+} concentration was also considered as factor which promoted hydrogen production.

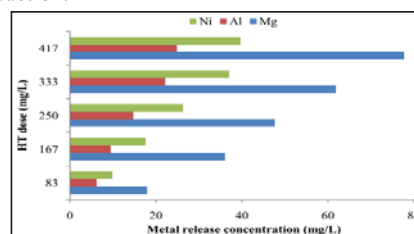


Figure 3. Metal release concentration after fermentation of Ni-Mg-Al

References

- [1] M.D. Bao, H.J. Su, T.W. Tan, "Dark fermentative bio-hydrogen production: Effects of substrate pre-treatment and addition of metal ions or L-cysteine", *Fuel*, **112**, 2013, pp. 38-44.
- [2] H-S. Lee, W.F.J. Vermaas, B.E. Rittmann, "Biological hydrogen production: prospects and challenges", *Trends in Biotechnology*, **28**, 2010, pp. 262-271.
- [3] F. Li, X. Duan, "Applications of layered double hydroxides". *Layered Double Hydroxides Structure and Bonding*, **119**, 2006, pp. 193-223.
- [4] P. Wimonsong, J. Llorca, R. Nitisravut, "Catalytic activity and characterization of Fe-Zn-Mg-Al hydrotalcites in biohydrogen production", *International Journal of Hydrogen Energy*, **38**, 2013, pp. 10284-10292.
- [5] P. Wimonsong, R. Nitisravut, J. Llorca, "Application of Fe-Zn-Mg-Al-O hydrotalcites supported Au as active nano-catalyst for fermentative hydrogen production", *Chemical Engineering Journal*, **253**, 2014, pp. 148-154.
- [6] APHA. Standard methods for the examination of water and wastewater. 19th ed. Washington, DC, USA: American Public Health Association, 1995.
- [7] F. Cavani, F. Trifirò, A. Vaccari, "Hydrotalcite-type anionic clays: Preparation, properties and applications", *Catalysis Today*, **11**, 1991, pp. 173-301.
- [8] P. Sinha, A. Pandey, "An evaluative report and challenges for fermentative biohydrogen production", *International Journal of Hydrogen Energy*, **36**, 2011, pp. 7460-7478.

Table 1. Estimated value of parameters by modified Gompertz Equation and hydrogen yield

Dose (mg/L)	Modified Gompertz model				H_2 yield (mol H_2 /mol sucrose)
	H_{max} (mL H_2)	R_m (mL H_2 /h)	λ (h)	R^2	
0	117.7	0.8	11.02	0.96	1.87 ± 0.16
83	141.9	1.0	6.18	0.99	2.21 ± 0.25
167	177.5	0.9	3.58	0.99	2.87 ± 0.15
250	215.0	1.4	2.59	0.98	3.37 ± 0.17
333	153.4	0.8	3.07	0.98	2.25 ± 0.28
417	136.8	0.8	1.56	0.98	2.03 ± 0.24

DILUTE ACID PRETREATMENT AT HIGH TEMPERATURE OF OIL PALM TRUNK BIOMASS FOR ENZYMATIC HYDROLYSIS

Pongsak Noparat¹, Poonsuk Prasertsan^{2,3}, Sompong O-Thong⁴, and Xuejun Pan⁵

¹ Program in Environmental Science, Faculty of Science and Technology, Rajabhat Suratthani University, Thailand

² Department of Industrial Biotechnology, Faculty of Agro-Industry, Prince of Songkla University, Thailand
³ Palm Oil Products and Technology Research Center (POPTeC), Faculty of Agro-Industry, Prince of Songkla University, Thailand

⁴ Department of Biology, Faculty of Science, Thaksin University, Thailand

⁵ Biological Systems Engineering, University of Wisconsin, United States

SUMMARY: Dilute acid pretreatment of OPT at varying conditions (acid concentration, temperature, and time) indicated that the pretreatment could effectively remove hemicelluloses from OPT, which improved enzymatic digestibility of OPT. Milder pretreatment preserved more hemicelluloses and cellulose in the pretreated OPT, but enzymatic hydrolysability was unsatisfactory because the biomass recalcitrance was not sufficiently removed. Severer pretreatment suffered from low sugar recovery, but the resultant substrate had much better enzymatic digestibility. The results suggested that the pretreatment with 3% H₂SO₄ at 180 °C for 40 min could not only achieve an ~80% enzymatic hydrolysis and but also the highest overall glucose recovery, although the glucose recovery in the pretreatment was low.

Keywords: oil palm trunk; enzymatic hydrolysis; dilute acid pretreatment; cellulosic ethanol

INTRODUCTION

Lignocellulosic materials such as agricultural residues (wheat straw, corncob, and paddy straw), energy crops (switch grass and fast-grow trees), and forest resources have been recognized as renewable feedstocks for industrial applications to produce bioethanol and other biofuels [1]. Oil palm trunk (OPT) is available in large quantity in Southeast Asia and a potential lignocellulosic biomass resource for bioethanol production [2]. One of the technologies for converting the biomass into biofuels is the so-called sugar platform. Specifically, the carbohydrates (cellulose and hemicelluloses) in the biomass are first hydrolyzed into sugars predominantly by enzymes, and then the sugars are biologically fermented to biofuels. Because of the recalcitrance of the biomass caused by the tough physical structure and the presence of hemicelluloses and lignin surrounding cellulose, the biomass has to be pretreated physically and chemically to remove or reduce the recalcitrance before cellulases can efficiently access and satisfactorily hydrolyze cellulose into glucose.

Many methods have been developed and evaluated for biomass pretreatment, such as dilute acid, AFEX, organosolv, steaming, and alkali pretreatment [3]. Among them, dilute acid pretreatment is the most investigated method, and it is also an inexpensive and economically feasible process [4-5]. This study aims to evaluate the dilute acid pretreatment of OPT for enzymatic hydrolysis. The effects of pretreatment conditions including acid concentration, pretreatment temperature, and reaction time on the dissolution of biomass components (cellulose, hemicelluloses, and lignin), sugar yield, formation of fermentation inhibitors, and enzymatic digestibility of the pretreated OPT

will be investigated.

METHODOLOGY

Dilute acid pretreatment was performed at laboratory scale with a microwave reactor manufactured by CEM Corporation (Model MARS, Matthews, NC, USA) with 6 reaction vessels. Each vessel has a total volume of 50 mL. The amount of dry feedstock loaded was 10 g, and dilute acid was added at 1:5 (w/v) solid/liquid ratio. Both the acid and raw material were initially at room temperature. The pretreatment temperature was changed within the range of 160-180 °C; reaction time was from 20 to 40 min; and initial H₂SO₄ concentration was from 1% to 3% (w/w). When the pretreatment was finished, the pretreatment liquor was separated from solid by filtration. The filtrate was analyzed by high performance liquid chromatography (HPLC) to determine the concentration of sugars and inhibitors in the hydrolysate. The mass and moisture content of the solid fraction were measured to determine solid yield, and the solid was stored in a fridge for composition analysis and enzymatic hydrolysis.

Commercial enzymes, cellulase and β -glucosidase, were generously provided by Novozymes North America (Franklinton, NC, USA). The hydrolysis was carried out at 50 °C on a shaking incubator at 200 rpm. Substrate equivalent to 0.8 g cellulose was loaded into a 50-mL falcon tube with 20 mL of 0.05 M sodium acetate buffer (pH 4.8). Approximately 20 μ L of 5 % tetracycline chloride was used to control the growth of microorganisms and prevent consumption of liberated sugars. Cellulase (15 FPU (Filter Paper Unit) per gram cellulose) and β -glucosidase (30CBU (Cellobiase Unit) per gram cellulose) were loaded

into the tube. Hydrolysate was sampled periodically and subjected to glucose analysis [6].

RESULTS AND DISCUSSION

Combined severity (CS) was used to compare different pretreatments, which is a combined factor of pretreatment temperature, time, and acid loading. The results indicated that harsh conditions enhanced the dissolution of biomass components during the pretreatment. For example, the maximum substrate yield was approximately 72.2%, achieved when acid concentration, temperature and time were 1%, 160 °C and 20 min, respectively, which was the mildest condition investigated with the lowest CS of 2.13. On the other hand, the lowest substrate yield (46.8%) was achieved when acid concentration, temperature and time were 3%, 180 °C and 40 min, respectively, which represented the severest condition with the highest CS (3.47) investigated.

In general, severer pretreatment (higher CS) would dissolve more hemicelluloses and cellulose. Severer condition would also cause degradation of the sugars to furfural (FF, from pentoses) and hydroxymethylfurfural (HMF, from hexoses) through dehydration. HMF could be further decomposed to levulinic acid (LA) and formic acid (FA) through rehydration [7].

The 72-h enzymatic hydrolysis profiles of dilute acid pretreated OPT substrates are shown in Figure 1. The substrate pretreated at 1% H₂SO₄, 160 °C, and 20 min showed the lowest cellulose-to-glucose conversion yield of 22% at 72 hour, while the substrate pretreated at 3% H₂SO₄, 180 °C, and 40 min gave the highest cellulose-to-glucose conversion yield of 79%. The substrates pretreated at other conditions had very similar enzymatic digestibility, and their 72-hour cellulose-to-glucose conversion yields fell to 50-56%. In contrast, all hemicelluloses were removed from substrate that was pretreated at the severest condition, which was the predominant reason why this substrate had the best enzymatic digestibility. In addition, the high acid concentration, high temperature and long pretreatment time might have prehydrolyzed (depolymerized) cellulose substrate to certain extent, which certainly enhanced the enzymatic hydrolysis of cellulose. The results suggested that severe condition was necessary for OPT to get a better enzymatic hydrolysis.

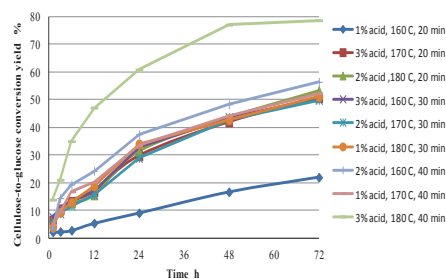


Figure 1. Cellulose-to-glucose conversion yield during the enzymatic hydrolysis of dilute acid pretreated OPT at different conditions

ACKNOWLEDGEMENTS

This work was financially supported by a scholarship from the Office of the Higher Education Commission under the CHE-PhD Scholarship Program. The experiments were conducted in Prof. Pan's laboratory at University of Wisconsin-Madison.

References

- [1] A. T. W. M. Hendriks and G. Zeeman. "Pretreatments to enhance the digestibility of lignocellulosic biomass". *Bioresource Technology*. **100**(1), 2009, pp.10-18.
- [2] K.L. Chin, H'ng PS, L.J. Wong, B.T. Tey and M.T. Paridah. "Production of glucose from oil palm trunk and sawdust of rubberwood and mixed hardwood". *Applied Energy*. **88**, 2011, pp.4222-4228.
- [3] P. Obama, G. Ricochon, L. Muniglia and N. Brosse. "Combination of enzymatic hydrolysis and ethanol organosolv pretreatments: Effect on lignin structures, delignification yields and cellulose-to-glucose conversion". *Bioresource Technology*, **112**, 2012, pp.156-163.
- [4] H. Megawati, W.B. Sediawan, H. Sulistyono and M. Hidayat. "Pseudo-homogeneous kinetic of dilute-acid hydrolysis of rice husk for ethanol production: effect of sugar degradation". *International Journal of Engineering and Applied Sciences*. 2010, pp.64-69.
- [5] R. Katzen and D.J. Schell. "Lignocellulosic feedstock biorefinery: history and plant development for biomass hydrolysis". In: Kamm, B., Gruber, P.R., Kamm, M. (Eds.), *Biorefineries Industrial Processes and Products*. **1**, 2006, pp.129-138.
- [6] X. J. Pan, D. Xie, R. W. Yu, and J. N. Saddler. "The bioconversion of mountain pine beetle-killed lodgepole pine to fuel ethanol using the organosolv process". *Biotechnology and Bioengineering*. **101**, 2008, pp.39-48.
- [7] E. Palmqvist and B. Hahn-Hägerdal. "Fermentation of lignocellulosic hydrolysates, I: inhibition and detoxification". *Bioresource Technology*. **74**(1), 2000, pp. 17-24.

EFFECT OF SUBSTRATE AND INTERMEDIATE COMPOUND ON FOAMING IN PALM OIL MILL EFFLUENT (POME) DIGESTION SYSTEM

Nantharat Wongfhad¹, Prawit Kongjan² and Sompong O-Thang^{1,3}

¹Biotechnology Program, Faculty of Science, Thaksin University, Thailand

²Microbial Resource Management Research Unit, Faculty of Science, Thaksin University, Thailand

³Department of Biology, Faculty of Science, Thaksin University, Thailand

SUMMARY: Anaerobic Digestion (AD) process is a widely applied method for POME management and treatment. AD foaming is one of the major problems that occasionally occur in many biogas plants, since it affects negatively the overall digestion process. POME contains several compounds that can potentially cause foaming during AD. Understanding the effect of substrates and intermediate compounds on foaming tendency and stability could facilitate strategies for foaming prevention and recovery of the process. In this study, the effect of substrates and intermediate compounds on foaming tendency and stability. The results showed that some compound consistent correlation between the effect on foaming stability of POME and POME under AD. In both tests, BSA and gelatine while oil palm decrease foaming stability. However this testing not best way for measure foaming stability during batch AD of POME and foaming problem not effect methane production.

Keywords: biogas, palm oil mill effluent (POME), anaerobic digestion (AD), foaming tendency, foaming stability, intermediate compounds, substrates

INTRODUCTION

AD foaming is one of the major problems that occasionally occur in many biogas plants, since it affects negatively the overall digestion process. Foaming can also result in an inverse solids profile having higher solids concentrations at the top of a digester, creation of dead zones and reduction of the active volume of the digester hence resulting in sludge. So far, there has never been a thorough investigation of a foaming problem in a POME-based digester, which is the main anaerobic digestion used in Thailand. There is a need for investigation of the foaming causes in this system in order to find the method to avoid as well as to resolve the problem. This work aims to investigated substrates and intermediate compounds effect on foaming tendency and stability in POME

METHOD

Preparation of the feedstock and sludge

The POME and anaerobic digester sludge used in this study were collected from 3 palm oil mill plant, in southern of Thailand. POME was stored at the temperature of 4 ° C for later use. Sludge was prepared active in a container closed by lid, there

was a constant production of biogas before being used as the mixed culture.

Physicochemical effect of intermediate compounds on foaming potential.

Design of experiments.

A fractional factorial design of experiments was carried out, and where all the factors involved could be identified with concentrations of different compounds. The influence of a total of 18 factors on different physical and chemical properties of the solutions involving proteins, lipids, carbohydrates, cations and SMP was analyzed. Thus, to run a pure experimental factorial design, 218 experiments should be done. Just 18 of the 262,144 freedom degrees correspond to the main effects.

Experimental set up and operation

To investigate the effect of each compound in a complex mixture, a mixture design of experiments was carried out (Table 2), where all the compounds involved was tested at different concentrations. The foaming tests were initially carried out in both 200 mL of water and POME.

Table 2. Concentrations (g/L) of compounds involved in each test combination.

Res	Protein (g/L)				Lipid (g/L)			Detergent (g/L)		Carbohydrate (g/L)				Trace metal (g/L)			Ammonia (g/L)		SMP (g/L)			
	Factor 1	Factor 2	Factor 3	Factor 4	Factor 5	Factor 6	Factor 7	Factor 8	Factor 9	Factor 10	Factor 11	Factor 12	Factor 13	Factor 14	Factor 15	Factor 16	Factor 17	Factor 18	Factor 19	Factor 20		
1	1	1	1	1	1	1	1	1	1	1	1	1	1	1	1	1	1	1	1	1	1	
2	1	4	4	4	8	1	2	0	4	1	1	0	0	2	2	4	1	1	4	1		
3	1	1	1	4	8	1	2	2	1	1	4	2	2	0	1	4	4	1	4	1		
4	4	1	4	4	2	1	2	2	4	4	1	2	0	2	0	1	1	1	1	4		
6	1	1	1	1	8	4	0	2	4	1	1	2	2	2	4	1	1	1	4	1		
6	1	1	1	1	2	1	0	0	1	1	1	0	0	0	1	1	1	1	1	1		
7	1	4	1	1	2	1	2	2	1	4	4	0	2	2	4	4	1	1	4	1		
8	4	4	4	1	8	1	2	0	1	1	1	2	2	0	4	4	1	4	1	4		
9	1	4	4	1	8	4	0	0	4	4	4	2	0	2	0	1	4	1	1	1		
10	4	4	4	4	2	4	0	2	1	1	1	0	2	2	1	4	1	1	1	1		
11	4	1	4	1	2	1	0	2	4	1	4	2	0	0	2	4	4	4	1	1		
12	4	4	1	4	8	1	0	2	4	4	4	0	2	0	4	1	1	1	1	1		
13	4	4	1	1	8	4	2	2	1	4	1	2	0	2	1	1	4	1	4	1		
14	4	4	1	4	2	4	0	0	1	1	4	2	0	2	0	4	1	4	4	4		
15	1	1	4	4	2	4	2	0	1	4	4	2	2	0	2	4	1	1	1	1		
16	1	4	4	1	2	4	2	2	4	1	4	0	2	0	0	1	1	4	4	4		
17	1	1	4	4	8	4	0	2	1	4	1	0	0	0	4	4	4	4	4	4		
18	1	4	1	4	2	1	0	0	4	4	1	2	2	0	2	1	4	4	4	4		
19	4	1	1	4	8	4	2	0	4	1	4	0	0	2	1	4	1	4	1	4		
20	4	1	1	1	2	4	2	0	4	4	1	0	2	2	4	4	4	4	4	1		

Experimental set up and operation

To investigate the effect of each compound in a complex mixture, a mixture design of experiments was carried out (Table 2). The foaming tests were initially carried out in both 200 mL of pure water POME and POME during AD.

Physicochemical effect of intermediate compounds foaming potential under AD.

The batch digestion investigated the behavior foaming of co-digestion POME and several intermediate compounds in Table 2. Digestion took place in 500 mL serum bottle, was added 160 mL of inoculum POME added 40 mL. All the cases were duplicated. The pH was adjusted to 7.0–7.7 using 5 g/L NaHCO_3 , the bottle was purged with N_2 gas for 3 min, sealed with butyl-rubber septum and aluminum cap, and incubated at 35°C.

Analysis and assay

The foam formation inside the serum bottles was recorded daily. All cumulative biogas production is measured via water displacement method. Methane and carbon dioxide were analyzed by GC-TCD. Total solids (TS) volatile solids (VS) and VFA according to APHA (2005). pH measurements were performed by a digital PHM210 pH meter. Total nitrogen (TKN) was measured Kjeldahl method. The foaming potential of the solutions was determined by the aeration method as described by Boe et al. (2012).

RESULTS AND DISCUSSION

Physicochemical effect of intermediate compounds on foaming potential.

In the water results showed no foaming stability, however POME and water show foaming tendency in Run 3, 4 and 20 showed the highest foaming tendency, the major compound were Na-oleate and Na^{2+} . Almost all testing of POME show highest foaming tendency but Run 1, 2, 8, 12 and 13 show lowest foaming tendency because the main compound were oil palm (Figure 1). The POME had a foaming tendency and stability around 51.67 mL-foam/mL-air min and 3.23 cm^3 . Figure 2 found that Run 8, 10, 11, 12 and 13 increased foaming stability (Figure 2), major compound high protein Ca^{2+} , Mg^{2+} , acetic acid, butyric acid, NH_4^+ and SDS while oil palm (Run 1, 2, 8, 11, 12 and 13) decrease foaming stability (Figure 3).

Physicochemical effect of intermediate compounds foaming potential under AD.

In AD Run 1, 2, 5, 10, 12, 13, 14 and 20 showed the highest foaming stability throughout the AD, found that major compound were BSA, gelatine, oil palm and lactic acid. Run 3, 4, 6, 9, 15, 16, 17, 18 and 19 showed low foaming stability, found that few compound were casein, BSA, NH_4^+ and acetic acid. For Run 7, 8 and 11 showed the

highest foaming tendency in the initial AD. The highest methane production obtains Run 2, 5 and 7 about 11.15, 14.67 and 15.95 $\text{L-CH}_4/\text{L-POME}$.

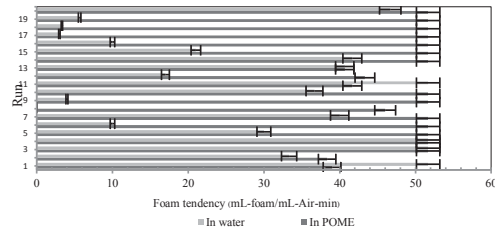


Figure 1. Comparison of foaming tendency between pure water and POME

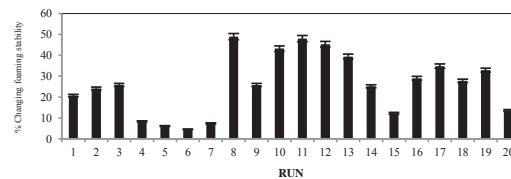


Figure 2. % changing foaming stability of POME

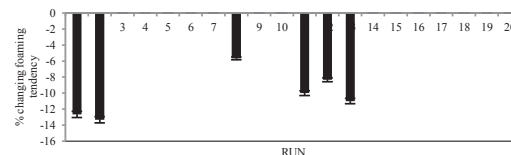


Figure 3. % changing foaming tendency of POME

CONCLUSION

The results showed both testing, BSA and gelatine while oil palm decreases foaming stability. However this testing not best way for measure foaming stability during batch AD of POME. Moreover in Run had major compound BSA, gelatine, oil palm and lactic acid creating foaming stability in bath AD.

ACKNOWLEDGMENT

I would like to thank Royal Golden Jubilee PhD and Research and Development Institute Thaksin University (RDITSU) for financial supports.

References

- [1] W. Barber et al., "Anaerobic digester foaming: causes and solutions", *Water*, **21**, 2005, pp.45–49
- [2] K. Boe, P.G. Kougiaris, F. Pacheco, S. O-Thong, I. Angelidaki, "Effect of substrates and intermediate compounds on foaming in manure digestion systems", *Water Sci. Technol.* **66**, 2012, pp. 2146–2154

Bio Fuel; Biodiesel

EFFECTS OF BIOGLYCEROL BASED ADDITIVES ON DIESEL FULR PROPERTY, ENGINE PERFORMANCE AND EMISSION QUALITY: A REVIEW

Punam Mukhopadhyay¹ and Rajat Chakraborty¹

¹Chemical Engineering DepartmentJadavpur University, India

SUMMARY: Diesel engine emission has been a major contributor of harmful air pollutants viz., nitrogen oxide, hydrocarbon, carbon monoxide, carbon dioxide, particulate matter and smoke emission. To suit stringent emission norms, the polluting components in the fuels need substantial reduction. Blending of bioglycerol based fuel additives in diesel could satisfactorily meet emission norms. Notably, bioglycerol, one of the by-product of biorefineries proved as a prospective resource for sustainable production of valuable bioadditives to help mitigate engine emissions coupled with enhancement of fuel properties. This article presents a comprehensive overview on various glycerol derived fuel additives and the pertinent reaction conditions involved in the production process.

Keywords: engine emission, diesel, glycerol, additive blends

INTRODUCTION

Diesel engines are one of those among the transport related energy use which are popular due to its promising heavy-duty condition compatibility. However, diesel-fuelled engines possess major pitfalls viz., production of NO_x, CO, particulate matter and SO_x which lead to emission restriction issues. In order to reduce the emanations of these harmful gases, several emission reduction systems are used. However, these systems are cost-intensive and cannot be used in long term. Thus, production of such harmful gases can only be mitigated through improvement in the combustion process by adding cleaner fuels (oxygenated additives, biofuels) or fuel additives (FA) [1]. Previously, FAME (Fatty Acid Methyl Ester) was used as FA with diesel; but, it leads to certain confinements. Thus, several studies have been performed to increase the diesel fuel qualities via application of FA [2]. FA from low value glycerol (Gly), a biodiesel by-product has proved to be a promising additive which can upsurge engine performance. However, production of these valuable additives requires adverse reaction conditions making the process economically unattractive. Thus, it is of utmost importance to critically assess the process parameters that can favorably yield the desired additive through economically sustainable pathways. Effort has also been made to understand the effect of this FA on engine emission and performance.

DIESEL FUEL CHARACTERISTICS

Cetane Boosters

The cetane number of a fuel plays an important role in compression ignition (CI) engine. Therefore, fuel having low cetane number (CN) will exhibit long ignition delay, abnormal combustion etc. Thus, many diesel fuel compositions comprises of ignition improvers to improve fuel quality. Triacetin (oxygen content 53.3%), a Gly derived ester serve as an effective replacement when blended with diesel or biodiesel [3]. Table 1 depicts the recent trends in triacetin (TAG) production using various heterogeneous catalysts.

Table1. Recent Developments in Triacetin Production.
#AA: Acetic acid

Catalyst	Reaction Condition	TAG Selectivity	Ref
Heteropoly acid; Bronsted Acid	#AA: Gly 12:1; 60°C; 12h	20%	[4]
Niobiosilicate and mesoporous silicate of SBA-15	AA: Gly 9:1; 150°C; 4h	39 %	[5]

It has been well observed that only higher reaction time and temperature favors triacetin selectivity thus rendering higher operational cost.

Methylation of glycerol with dimethyl sulphate lead to the production of another value added chemical viz., glycerol dimethoxy ethers (GDMEs), and trimethoxy ether (GTME), a new oxygenate additive owing comparable CN like TAG [6]. Mixture of 20 wt. % GDME and 80 wt. % GTME as diesel oxygenate, improves cetane number upto 58 thus rendering less amount of unburnt engine exhausts. However, the reaction time for preparation is quite high making the process uneconomical.

Cold Flow Improver

Diesel fuel, containing n-paraffins produces significant volume of wax in cold climate. FA such as poly-ethers of Gly viz., di-tert-butyl glycerol (DTBG) and tri-tert-butyl glycerol (TTBG) was able to lessen viscosity of biodiesel fuel from 4.12 mm²/s to 4.05 mm²/s [7]. Higher acetyl glycerol viz., diacetate (DAG) and triacetate (TAG) obtained can also serve as cold flow improver. Figure 1 particularizes the effect of TAG addition to biodiesel in terms of cloud point and pour point [8].

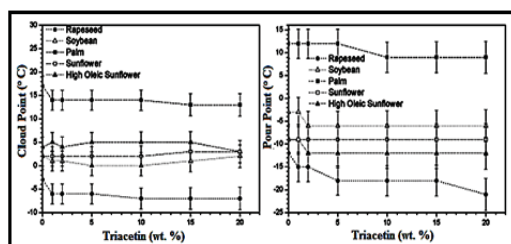


Figure 1. Effect of Triacetin on Biodiesel Quality [8].

Lubricity Improver

Due to environmental restriction on emissions for diesel vehicles desulfurization of fuel incorporates wear in fuel injection equipment. A lubricant lower friction losses and thus increases fuel economy, via reducing exhaust emissions. Knothe & Steidley [9] disclosed that the existence of mono- and diacylglycerols in the range of 100-200 ppm can provide sufficient anti-wear capacity ensuring normal operation of the motor injection system.

EXHAUST GAS EMISSION REDUCER

Smoke Emission Reducer

Smoke emissions are one of the major air pollutants which occur due to improper fuel ignition. It has been established that usage of oxygenated compounds having higher CN produce cleaner burning of diesel fuels. Amongst the Gly based FA a transesterified product of butan-2-one glycerol and methyl hexanoate leads to the production of Gly ketal ester which has been applied as a promising diesel FA [10].

NO_x Mitigator

Oxides of nitrogen emission typically depend on engine performance. Presence of oxygenates in the fuel for reduction of particulates greatly heighten NO_x emission. Fernando et al. [11] recognized thermal NO_x as a major contributor. DAG and TAG were found to decrease NO_x emission thus causing less air pollution [6].

HC and CO emission inhibitor

Several factors are accountable for CO emissions including engine speed, air-fuel ratio, fuel type, injection timing and pressure. It has been proven that blended fuels results in lower CO and HC emission compared to neat fuel [12]. Oprescu et al.

[10] applied their glycerol ketals and glycerol ketal esters in diesel to study emission characteristics in terms of HC and CO (Figure 2).

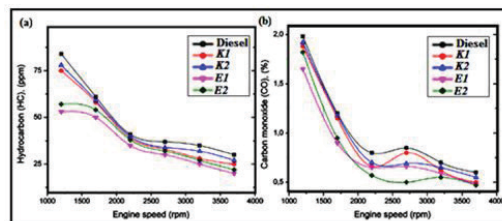


Figure 2. Characteristic curve for a) HC; b) CO emission with variable engine speed [10].

References

- [1] N.I. Tracy, D. Chen, D.W. Crunkleton, G.L. Price, "Hydrogenated monoterpenes as diesel fuel additives", *Fuel*, **88**, 2009, pp 2238–2240.
- [2] M. Gürü, U. Karakaya, D. Altıparmak, A. Alıçylar, "Improvement of diesel fuel properties by using additives", *Energ. Convers. Manage.* **43**, 2002, pp. 1021–1025.
- [3] P.C. Smith, Y. Ngothai, Q. Dzuy-Nguyen, B.K. O'Neill, "Improving the low temperature properties of biodiesel. Methods and Consequences", *Renew. Energy* **35**, 2010, pp. 1145–1151.
- [4] V.L.C. Gonçalves, B.P. Pinto, J.C. Silva, C.J.A. Mota, "Acetylation of glycerol catalyzed by different solid acids", *Catal Today*. **133–135**, 2013, pp. 673–677.
- [5] M. Trejda, K. Stawicka, A. Dubinska, M. Ziolk, "Development of niobium containing acidic catalysts for glycerol esterification", *Catal Today*. **187**, 2012, pp. 129–134.
- [6] J.S. Chang, Y.L. Lawrence, C.S. Chou, T.R. Ling, T.C. Chou, "Methylation of Glycerol with Dimethyl Sulfate To Produce a New Oxygenate Additive for Diesels", *Ind. Eng. Chem. Res.* **51**, 2012, pp. 655–661.
- [7] F. Frusteri, L. Frusteri, C. Cannilla, G. Bonura, "Catalytic etherification of glycerol to produce biofuels over novel spherical silica supported Hyflon catalysts", *Bioresour. Technol.* **118**, 2012, pp. 350–358.
- [8] A. Casas, J. Ruiz, M. Ramos, A. Perez, "Effects of Triacetin on Biodiesel Quality", *Energy Fuels*. **24**, 2010, pp. 4481–4489.
- [9] G. Knothe, K.R. Steidley, "Lubricity of Components of Biodiesel and Petrodiesel. The Origin of Biodiesel Lubricity", *Energy Fuels*. **19**, 2005, pp. 1192–1200.
- [10] E.E. Oprescu, E. Stepan, R.E. Dragomir, A. Radu, P. Rosca, "Synthesis and testing of glycerol ketals as components for diesel fuel", *Fuel Process. Technol.* **110**, 2013, pp. 214–217.
- [11] S. Fernando, C. Hall, S. Jha, "NO_x reduction from biodiesel fuels", *Energy Fuel* **20**, 2006, pp. 376–382.
- [12] J.B. Hirkude, A.S. Padalkar, "Performance and emission analysis of a compression ignition: engine operated on waste fried oil methyl esters", *Appl Energy* **90**, 2012, pp. 68–72.

PREPARATION VEGETABLE OIL AS BIODIESEL FEEDSTOCK VIA HETEROGENEOUS CATALYST RE-ESTERIFICATION

Suechai Jansri¹

¹Major of General Science, Faculty of Education, Chaiyaphum Rajabhat University, Thailand

SUMMARY: The suitable heterogeneous catalyst was investigated for reducing 20 wt% of free fatty acid (FFA) that containing in vegetable oil to less than 3 wt% through re-esterification. There were two groups of heterogeneous catalyst using to reduce FFA: 1) zinc compound: Zn, ZnCl₂, ZnO and ZnSO₄·7H₂O, and 2) Stannum compound: SnCl₄·5H₂O and SnCl₂·2H₂O. The reaction was operated at 150°C under ambient pressure, stirred with 600 rpm and spent retention time around 180 min. The results indicated that ZnO was suitable for reducing free fatty acid via re-esterification process.

Keywords: biodiesel, free fatty acid, re-esterification, vegetable oil

INTRODUCTION

Due to high price of vegetable oil and low free fatty acid (FFA) waste cooking oil, low-cost high FFA vegetable oil was investigated currently to produce biodiesel. Transesterification was the primary process used to generate biodiesel from high FFA vegetable oil. As a result, the low quality of biodiesel was obtained because FFA containing in oil was promoting saponification [1-6]. Therefore, high content of free fatty acid oils could be treated via the enzyme-catalyzed transesterification, acid-catalyzed transesterification, supercritical and two-stage process [1,5, 7]. Limitations of laboratory experiment, the production of biodiesel under ambient pressure and in short time was required. The two-stage process was considered to produce biodiesel.

There are, generally, 2 techniques to produce biodiesel by the two-stage process: 1) saponification followed by transesterification [4, 7] and 2) esterification followed by transesterification [5, 7]. Nevertheless, the latter technique (esterification followed by transesterification) is offered to produce biodiesel from oil containing high FFA, because it requires shorter time and lower production loss than that from the process of saponification followed by transesterification [7]. Although, the second technique had more advantages than the first one, the large amount of methanol (a high toxicity in humans) was consumed. For decreasing methanol consumption rate, re-esterification was used instead of esterification for pretreatment FFA in oil. In this process, FFA was reacted with glycerin to convert into glyceride by using or non catalyst [8-10]. Two groups of catalysts (zinc and Stannum compounds) [9-12] which were required to achieve the re-esterification under the ambient pressure were not comparatively studied. Therefore, the suitable type of catalyst to reduce FFA in oil by re-esterification under atmospheric pressure was investigated.

METHODOLOGY

Beginning of de-acidified process, the oil adding 20 wt% of palmitic acid was weight and heated until the temperature reached 60°C. Then the

compositions of oil were analyzed by thin layer chromatography with flame ionization detector (TLC/FID). At the same time as increasing the temperature of the oil to 150°C, 0.6 wt% of each solid catalyst (Zn, ZnCl₂, ZnO and ZnSO₄·7H₂O, SnCl₄·5H₂O and SnCl₂·2H₂O) [9-12] was dissolved in 50 wt% of 98% commercial grade liquid glycerin (GL) at 100°C. After that, this solution was slowly added in the heated oil. While the solution was heating at 150°C under ambient pressure, the solution was stirred with fixing stirring speed (600 rpm) all the time until the reaction time up to 180 min was reached. One part of the pretreatment oil was centrifuged at 1500 rpm for 15 min. Another one had to be cleaned by hot wet washing (80°C) for 3 times [7]. Finally, the FFA containing in oil was verified.

RESULTS AND DISCUSSION

The characteristics of oil

Prior to discussion the effect of catalysts on FFA reduction, compositions of oil of before and after pretreatment, and adding only GL were explained. The concentration of FFA as shown in Table 1 indicated that after adding GL without catalyst (sample 1.2) into the oil containing high FFA (sample 1.1), the concentration of FFA and TG (triglyceride) decrease. At the same time, the large amount of diglyceride (DG) and monoglyceride (MG) are observed according to Bhosle et al. [8].

Table 1. The compositions of sample

Sample	Sample composition (wt%)			
	TG	FFA	DG	MG
1.1	66.483	19.522	5.747	8.248
1.2	51.034	16.081	10.126	22.759
1.3	9.508	1.915	28.135	60.442

As previously mentions, the reaction between high FFA oil and GL under the catalyst (sample 1.3) also promotes the reducing of FFA and TG, and increasing of DG and MG. The description of typical oil characteristics of re-esterification indicates that besides the re-esterification reaction, TG is also converted to DG and MG by cracking reaction. Although, the creaking reaction promotes the

increasing of DG and MG more than re-esterification, only re-esterification is considered and investigated because of FFA forming soap in transesterification.

The suitable of catalyst

This research focuses on FFA reduction by re-esterification. Although both groups of catalyst, in present, were famous used in high pressure re-esterification, no researcher was compared them under ambient pressure. Therefore, the capability catalyst of converting the FFA into glyceride by re-esterification was investigated. The results after centrifuge as shown in Table 2 indicated that only two catalysts [Zn (sample 2.1) and ZnO (sample 2.2)] can promote the reaction reach the requirement. Moreover, final FFA in re-esterification products which were cleaned up with hot wet washing was also monitored. It was found that no significant differences are found in the two purification technique except for the heterogeneous Zn catalyst re-esterification product.

Table 2. FFA containing in oil by various catalyst

Sample	Catalyst	FFA content	
		Centrifuge (wt%)	Washing (wt%)
2.1	Zn	1.240	N/A
2.2	ZnCl ₂	11.452	11.945
2.3	ZnO	1.416	1.915
2.4	ZnSO ₄ ·7H ₂ O	17.503	14.671
2.5	SnCl ₄ ·5H ₂ O	9.250	7.486
2.6	SnCl ₂ ·2H ₂ O	11.995	12.860

To be more confident, the compositions of all products that purifying by latter technique were considered as shown in Table 3. The results showed that TLC/FID cannot detect the all of composition in the pretreatment product using Zn as a catalyst (sample 3.1). It is possible that during washing the final product, saponification is promoted by Zn catalyst. Therefore, the suitable heterogeneous catalyst for reducing FFA by re-esterification under ambient was ZnO.

Table 3. The compositions of each produce

Sample	catalyst	Composition of oil			
		TG	FFA	DG	MG
3.1	Zn	N/A	N/A	N/A	N/A
3.2	ZnCl ₂	48.555	11.945	16.585	22.915
3.3	ZnO	9.508	1.915	28.135	60.442
3.4	ZnSO ₄ ·7H ₂ O	52.156	14.671	12.085	21.089
3.5	SnCl ₄ ·5H ₂ O	53.606	7.486	9.944	28.965
3.6	SnCl ₂ ·2H ₂ O	67.591	12.860	9.88	9.661

CONCLUSION

ZnO was suitable for reducing FFA around 20 wt% to less than 3 wt% of FFA via re-esterification process under atmospheric pressure by fixing condition at 150°C of reaction temperature, 600 rpm of stirring speed rpm and 180 min of retention time.

ACKNOWLEDGMENT

The author acknowledges Chaiyaphum Rajabhat University Research and Development Institute for providing the research grant.

References

- [1] F. Ma, and M. A. Hanna, "Biodiesel Production: a review", *Bioresource Technology*, **70**, 1998, pp.1-15.
- [2] J.V. Gerpen, L.D. Clements, "Biodiesel Production Technology", *National Renewable Energy Laboratory*, 2004, pp.1-40.
- [3] J.M. Marchetti, V.U. Miguel A.F. Errazu, "Possible methods for biodiesel production", *Renewable & Sustainable Energy Reviews*, **11**(6), 2005, pp. 1300-1311.
- [4] C. Tongurai et al., "Biodiesel production from palm oil (in Thai)", *Songklanakarin J. Sci. Technol.* **23**(suppl.), 2001, pp. 832-841.
- [5] V.B. Veljković, S.H. Lakicevic, O.S. Stamenkovic, Z.B. Todorovic, M.L. Lazic, "Biodiesel production from tobacco (*Nicotiana tabacum L.*) seed oil with a high content of free fatty acids", *Fuel*, **85**(17-18), 2006, pp.2671-2675.
- [6] G. Prateepchaikul et al., "The Reduction of Free Fatty Acid in Mixed Crude Palm Oil via Esterification (in Thai)", *Proceeding of 6th PSU Engineering Conference*, 2008, pp. 387-392.
- [7] S. Jansri and G. Prateepchaikul, "Comparison of Biodiesel Production from High Free Fatty Acid Crude Coconut Oil via Saponification followed by Transesterification or a Two-Stage Process", *Kasetsart Journal (Natural Science)*, **45**(1), 2011, pp.110-119.
- [8] B.M. Bhosle and R. Subramanian, "New Approaches in deacidification of edible oils – a review", *Journal of Food Engineering*, **69**, 2005, pp.481-494.
- [9] P. Felizardo, J. Machado, D. Vergueiro, M. Joana, N. Correia, J.P. Gomes and J.M. Bordado, "Study on the glycerolysis reaction of high free fatty acid oils for use as biodiesel feedstock", *Fuel Processing Technology*, **92**, 2011, pp. 1225-1229.
- [10] G.G. Kombe A.K. Temu, H.M. Rajabu, G.D. Mrema, J. Kandedo and K.T. Lee., "Pre-treatment of high free fatty acids oils by chemical re-esterification for biodiesel production – a review", *Advances in Chemical Engineering and Science*, **3**, 2013, pp. 242-247.
- [11] R.O. Ebebele, A. F. Iyayi and F. K. Hymore, "Deacidification of high acidic rubber seed oil by reesterification with glycerol", *International Journal of the Physical Sciences*, **5**(6), 2010, pp. 841-846.
- [12] A.C. Bhattacharyya and D. K. Bhattacharyya, "Deacidification of high FFA rice bran oil by reesterification and alkali neutralization", *JAOCs*, **64**(1), 1987, pp. 128-131.
- [13] G.G. Kombe, A.K. Temu, H.M. Rajabu, G.D. Mrema and K.T. Lee, "Low temperature glycerolysis as a high FFA pre-treatment method for biodiesel production", *Advances in Chemical Engineering and Science*, **3**, 2013, pp. 248-254.

BIODIESEL PRODUCTION USING LIPASE FROM OIL PALM FRUIT AS A CATALYZT

Pattarawadee kimtun¹, Opas Choonut¹, Tewan Yunu¹, Nisa Paichid¹, Sappasith Klomkloa² and Kanokphorn Sangkharak¹

¹Department of Chemistry, Faculty of Science, Thaksin Univeristy, Thailand

²Department of Food Science and Technology, Faculty of Technology and Community Development, Thaksin University, Thailand

SUMMARY: This study aimed to extract and characterize lipase from oil palm after 0-240 h of harvested. In addition, the application of lipase as a catalyzt for biodiesel production was also evaluated. Lipase was extracted and purified by Tris-base buffer (pH 8.0) followed by the aqueous two phase system (ATPS). The highest protein at 1.96 mg/gat was obtained from oil palm fruit after 0 h of harvested. However, the highest lipase activity at 0.98 Units (1.38 Unit/mg protein) was achieved from palm oil after 120 h of harvested. Afterwards, lipase was taken and purified by ATPS using PEG 1000 under the variation of salts. After purification, lipase activity was increased significantly to 4.76 Unit/mg protein using PEG and NaH₂PO₄. Therefore, purified lipase was utilized as a catalyzt for biodiesel production using transesterification method and the partial properties of biodiesel from lipase were also determined. The biodiesel from lipase had an acid value and free fatty acid content at 0.45 mg/g KOH and 0.21%, respectively. The properties of biodiesel was also compared with commercial biodiesel. Interestingly, the acid value and free fatty acid content of biodiesel from lipase were not significantly different from commercial biodiesel and it was also passed Thailand fuel standard.

Keywords: Lipase; Aqueous two-phase systems, ATPS; Transesterification; biodiesel

INTRODUCTION

Lipase is the enzyme that was a catalyzt in the process of transesterification. Normally, lipase from microbial have been used for biodiesel because of their properites including high temperature resistant and the cheap cost for extraction and purification [1]. However, high lipase activity from palm oil fruit have been also reported. Thailand is a world leading producer of oil palm. Due to the increasing of fuel demand. The research and development for novel lipase have been challenge. Therefore, palm oil is a most suitable source for lipase extraction [2-4].

The objective of this study aimed to extract and characterized lipase from oil palm after 0-240 h after harvested. In addition, the application of lipase as a catalyzt for biodiesel production was also evaluated.

MATERIALS AND METHODS

Extraction of lipase

Oil Palm fruit after 0-240 h of harvested were collected from Phatthalung (Thailand). Lipase was firstly extracted by 50 mM Tris-base buffer (pH 8.0). The extraction was done at the ratio of a oil palm fruit and buffer solution at 1: 2 (w/v). The supernatant was collected by centrifugation at 10,000 rpm for 30 minutes at 4°C. The supernatant was kept at 4°C until used.

Determination of Total protein

The Determination of protein was followed by Lowry method [5].

Determination of lipase activity

The activity of lipase was determined by adding 200 µl samples in 0.1 mM Tris-HCl buffer (pH 8.0) 2.45 ml containing 0.15 M NaCl and 0.5% Triton

X- 100. The determination was operated under 40°C for 5 minutes, then add 50 mM *p*-nitrophenylpalmitate 200µl. The sample was determined for the absorbance at 410 nm compared with *p*-nitrophenol standard curve at concentrations ranging from 0 - 1.0 µg.

Purification of lipase from oil palm fruit using aqueous two-phase systems

For ATPS method, polyethylene glycol (PEG) 1000 was utilized with the variation of salts. Crude enzyme (1 g) was firstly mixed with 5 g of distilled water. The sample was loaded into ATPS system. Lipase was purified in a bottom layer (salt solution). Therefore, purified lipase was collected and characterized.

The Production of biodiesel using lipase as a catalyzt

The purified lipase was mixed with vegetable oil and methanol. The ratio of oil, methanol and lipase is 10: 2: 1. The transesterification was operated under room temperature for 3 h. Therefore, only methyl ester was collected and characterized.

The analytical method

Biodiesel from lipase was chacterized for viscosity, acid value and free fatty acid content. The viscosity was analyzed by the gravity method. In addition, acid value and free fatty acid content were determined by titration method.

RESULTS AND DISCUSSION

The extraction of lipase from oil palm fruit after harvested

The highest protein at 1.96 mg/gat was obtained from oil palm fruit after 0 h of harvested. However, the highest lipase activity at 0.98 Units (1.38

Unit/mg protein) was achieved from palm oil after 120 h of harvested (Table 1).

Table 1 The total amount of protein (mg/g), total amount of lipase (units) and specific lipase activity (unit/mg protein) of extracted lipase from palm oil after 0-240 h of harvested.

Time (hr.)	Total protein (mg/g)	Total lipase (units)	Specific Activity (unit/mg protein)
0	1.96±0.01	0.59	0.30
24	0.98±0.01	0.61	0.63
48	0.86±0.01	0.64	0.75
72	0.81±0.01	0.77	0.95
96	0.76±0.01	0.87	1.15
120	0.71±0.01	0.98	1.38
144	0.68±0.01	0.66	1.06
168	0.61±0.01	0.63	1.03
192	0.56±0.00	0.58	1.03
216	0.51±0.01	0.49	0.96
240	0.46±0.01	0.35	0.76

Afterwards, lipase was taken and purified by ATPS using PEG 1000 under the variation of salts. After purification, lipase activity was increased significantly to 4.76 Unit/mg protein using PEG and NaH₂PO₄ (Table 2).

Table 2 Specific activity of extracted lipase after purified by aqueous two-phase systems with 20% PEG1000 as polymer phase.

Phase transition	VR	KP	KE	Specific activity (units/mg protein)	
				Top	Bottom
20% NaH ₂ PO ₄	1.90	0.84	6.00	4.76	0.37
15% (NH ₄) ₂ SO ₄	1.17	1.08	5.82	3.62	0.53
15% MgSO ₄	2.43	0.61	0.34	3.57	2.48
15% K ₂ HPO ₄	0.92	1.00	1.89	4.05	2.31
15% Na ₃ C ₆ H ₅ O	1.09	0.76	3.28	3.70	0.81
15% Na ₂ SO ₄	0.88	1.02	1.08	4.03	3.29

The production of biodiesel

Analysis viscosity

Therefore, purified lipase was utilized as a catalyst for biodiesel production using transesterification method and the partial properties of biodiesel from lipase were also determined. Biodiesel from lipase was characterized for viscosity, acid value and free fatty acid content. The viscosity was analyzed by the gravity method (Table 3). In addition, the acid value and free fatty acid content were determined by titration method (Table 4). Interestingly, the acid value and free fatty acid content of biodiesel from lipase were not significantly different from commercial biodiesel and it was also passed Thailand fuel standard.

Table 3 The viscosity of biodiesel from lipase compared with commercial biodiesel and oil.

substance	Time (sec)	Relatively viscosities Compared with distilled water
Biodiesel catalyzed by bases	8	1.6
Biodiesel catalyzed by enzymes	14	2.8
Oil (blank)	70	14

Table 4 The acids value and free fatty acids content of biodiesel from lipase compared with Thailand fuel standard.

Fuel property	Limit	Product biodiesel
Acid value (mg/g)	< 0.5	0.45
Free fatty acid (%)	< 3%	0.21

CONCLUSION

Lipase was extracted and characterized from oil palm after 0-240 h of harvested. The highest protein (1.96 mg/gat) and lipase (1.38 units/mg protein) were obtained from oil palm fruit after 0 and 120 h of harvested, respectively. After purification by ATPS, lipase activity was increased significantly to 4.76 Unit/mg proteins. Purified lipase was utilized as a catalyst for biodiesel production and the partial properties of biodiesel from lipase were also determined. The biodiesel from lipase had an acid value and free fatty acid content at 0.45 mg/g KOH and 0.21%, respectively.

ACKNOWLEDGEMENT

The author would like to thank you the Institute of Research and Development, Graduated School and Faculty of Science Thaksin University and The Energy of Policy and Planning office, The ministry of Energy (Thailand) for their financial supported.

References

- [1] F. Hasan, A.A. Shah, A Hameed, "Industrial applications of microbial lipases" *Enzyme Microb Technol.* **39**, 2006, pp. 235–251.
- [2] K. Jaeger and T. Eggert., "Enantioselective biocatalysis optimized by directed evolution," *Curr Opin Biotechnol.* **15**, 2004, pp. 305–313.
- [3] KN. Kilcawleyet, M.G Wilkinson and P.F Fox. "Determination of key enzyme activities in commercial peptidase and lipase preparations from microbial or animal sources," *Enzyme Microbial Technol.* **31**, 2002, pp. 310–320.
- [4] OH. Lowryet, NJ Rosebrough AL. Farr and RJ. Randall. "Protein measurement with the folin–phenol reagents," *Journal of Biological Chemistry.* **193**, 1951, pp. 265–275.
- [5] GC. Terstappenet, AJ. Geerts and MR. Kula. "The use of detergentbased aqueous two-phase systems for the isolation of extracellular proteins: purification of a lipase from *Pseudomonas cepacia*," *Biotechnol Appl Biochem.* **16**, 1992, pp. 228–35.

SUFFICIENT ECONOMY FOR ENERGY SECURITY IN WIANG SA JATROPHA COMMUNITY, THAILAND

Jitti Mungkalasiri¹, Pornpimon Boonkum¹, Ruthairat Wisarnsuwannakorn¹ and Wanwisa Thanungkano¹

¹National Metal and Materials Technology Center, NSTDA, Thailand

SUMMARY: Jatropha has been largely supported over the past five years for use in producing biodiesel and to alleviate the problem of competition for raw materials, between food and energy industry. In addition, jatropha can even be planted in remote locations. Nevertheless, many areas have failed in cultivating jatropha due to problems with low crop yields, harvesting and potentially toxic by-products. Hence, this study analyzed the factors capable of making jatropha a stable product for communities with guidelines for promoting sustainable cultivation by studying the Wiang Sa Cooperative in the province of Nan, which has been successful in growing jatropha. At the core of this success is the application of the sufficiency economy theory in the community context in combination with returning profits to society. The aforementioned work is an excellent model for people in an era of globalization and capitalism.

Keywords: Jatropha; Sufficiency economy theory; Renewable energy

INTRODUCTION

The 11th Edition of the National Economic and Social Development plan (2012-2016) has one purpose of replacing fossil fuels with clean energy and capable of being produced for re-use in the context of Thailand [1]. In order to increase the utilization of alternative and renewable energy, the Thai government's Ministry of Energy has implemented a policy called "Alternative Energy Development Plan (AEDP) 2012-2021," aiming to increase the amount of alternative and renewable energy utilization to 25% of total energy by the year 2021 [2]. For this reason, non-food plants such as algae, jatropha, pongamia, tung oil, canola, rapeseed, have attracted a high degree of interest. Thailand has also considered feasibility and trial planting with promotion of jatropha cultivation as a commercial crop nationwide since 2007. Jatropha is a non-edible crop which can produce high oil content seed, intended for biodiesel production. This tree reaches ages of no less than twenty years. [3] Jatropha can thrive in hot or tropical climates [4]. With the exception of waterlogged lands, Jatropha grows almost anywhere, even on gravelly, sandy and saline soils.

Wiang sa agricultural cooperative

This cooperative is one where trial jatropha cultivation has been carried out in the community from 2007 until today and provides a support (e.g. manual) for the Wiang Sa community to carry out jatropha activities with success sufficiency economy theory applications. The key objective is to secure energy stability for the community toward future self-reliance. Such community development progress is sustainable in terms of economic, social and environmental aspects based on jatropha, the energy crop which has been said to have failed to receive promotion in many places of the world due to economic feasibility. This research was conducted over a two-year period to collect data and obtain an understanding of the community. The data presented

here is actual primary data collected from the local areas. The research team hopes the sharing of ideas and the cooperative's guidelines for success. It will be a good example for promoting alternative energy.

Sufficiency economy

The sufficiency economy theory is a concept created by His Majesty, King Bhumibol, Rama IX as a philosophy indicating a guideline for a certain type of lifestyle [5]. This concept is based on a foundation of Thai culture as a developmental guideline based on a middle-of-the-road approach free from negligence in consideration of moderation, reasonableness, building self-immunity and using knowledge and ethics as a foundation to live upon [6].

STUDY SITE AND SCOPE

Wiang Sa is a district in the province of Nan located in the north of Thailand. The topography is characterized by some flat land and 85% of high mountains with slopes greater than 30 degrees. The average temperature is 26.4 degrees Celsius (10.4 -39.5) and the average rainfall is 1356.2 mm. (1,119.7 mm 1,592 mm). Originally, this cooperative aimed to produce Jatropha biodiesel for local consumption. The Cooperative's job was to harvest jatropha seeds, extract oil and produce biodiesel. After operating for a certain period, the cooperative found large amounts of waste from the production process and the products resulting from biodiesel sales were not cost effective. Thus, attempts have been made to find ways to use the waste as new business opportunities such as charcoal, organic detergent, organic fertilizer, wood vinegar, etc.

RESULTS AND DISCUSSION

Figure 1 shows the business value associated with jatropha. Overall product value increases annually. In 2011, the cooperative earned revenue amounting to over 400,000 baht from the jatropha business, which is much higher in comparison to 2010 and 2009 with values of 150,000 baht and

220,000 baht, respectively.

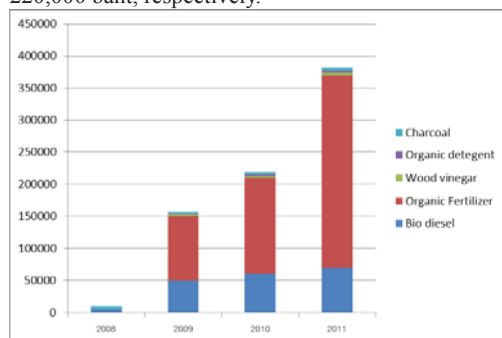


Figure 1. Revenue from Cooperative Goods in Relation to the Jatropha Business 2008-11

When consideration is given to the details, the increase in biodiesel sales can be explained by three main reasons, the improvements in harvest efficiency, the annually increasing production capacity and the sales of used vegetable oil (approximately 40% ratio). Organic fertilizer generates the highest revenue and profits with value exceeding three times biodiesel sales in 2011, and this trend is increasing. In addition, wood vinegar and charcoal are by-products of jatropha oil production that can be used in the community's organic agriculture projects. Ashes from wood vinegar are packed into attractively shaped charcoal briquettes and sold to tourists and hotels. This community also promotes organic agriculture and attempts to cut down daily chemical use.

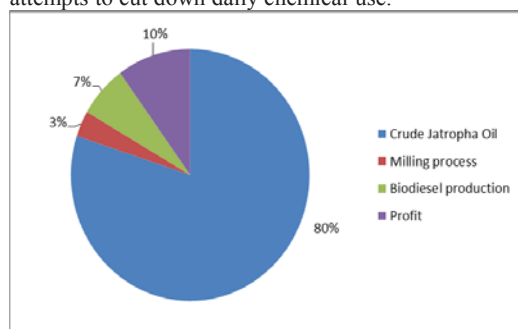


Figure 2. Product value ratios of Jatropha biodiesel

Biodiesel production is divided into four parts (Figure 2). In other words, the primary cost for the products, namely, crude jatropha oil, milling process, biodiesel production and the final part, which is oil profit per liter. However, Wiang-Sa Jatropha biodiesel selling prices are obviously cheaper (10-15%) than market prices sold to cooperative members. In consequence, the cooperative hardly makes any profit from biodiesel sales. In this community, biodiesel B100 has been used for more than the past three years. During the

early days, the community was even concerned about the quality of the biodiesel produced by the cooperative. For this reason, the cooperative has used the aforementioned fuel with the cooperative's two pick-up trucks as a means of building confidence for the community.

The research proposes various options for sustainable development in cooperation with the theory of sufficiency economy which does not focus only on profit. The theory can actually support jatropha plantation with its emphasis on the work of alternative energy in response to local energy demands. This is the way to truly sustainably build energy security for the future.

ACKNOWLEDGMENT

The authors acknowledge the Wiang Sa Cooperative for excellent information and cooperation. This project was financially supported by the National Science and Technology Development Agency (NSTDA), Cluster energy and environment. And also the project "Innovation on Production and Automobile Utilization of Biofuels from Non-Food Biomass in Thailand" implemented under the Science and Technology Research Partnership for Sustainable Development (SATREPS) promoted by Japan International Cooperation Agency (JICA) and Japan Science and Technology Agency (JST).

References

- [1] The eleventh national economic and social development plan (2012-2016). National economic and social development board. Office of the prime minister. Bangkok, Thailand.
- [2] Government of Thailand. Department of Alternative Energy Development and Efficiency, Ministry of Energy. 2011. Alternative Energy Development Plan: AEDP 2012 – 2021. Available at: <http://www.dede.go.th/dede/images/stories/aedp25.pdf> (in Thai) (accessed 05 April 2013)
- [3] WMJ. Achten, L. Verchot, YJ. Franken, E. Mathijs, VP. Singh and R. Aerts. "Jatropha bio-diesel production and use". *Biomass & Bioenergy* **32**, 2008, pp. 1063-84.
- [4] Z. Wang, M Calderon and Y. Lu. "Lifecycle assessment of the economic, environmental and energy performance of Jatropha curcas L. biodiesel in China". *Biomass & Bioenergy*. **35**, 2011, pp. 2893-902.
- [5] Sufficiency economy and the new theory. The Chaipattana Foundation. 2008
- [6] P. mongsawad. "The philosophy of the sufficiency economy: A contribution to the theory of development". *Asia-pacific development journal*. **17(1)**, 2010, pp. 123-143.

THE DEVELOPMENT OF BIODIESEL PILOT PLANT FOR TEACHING AND LEARNING, RESEARCH, CONSULTATION OF RENEWABLE ENERGY – BIO FUEL

A. M. Leman¹, I. Baba¹, W. Sani¹, M. N. M. Salleh² and A. Khalid³

¹Faculty of Engineering Technology, Universiti Tun Hussein Onn Malaysia (UTHM), Malaysia

²Faculty of Computer Science and Information Technology, Universiti Tun Hussein Onn Malaysia (UTHM), Malaysia

³Faculty of Mechanical & Manufacturing Engineering, Universiti Tun Hussein Onn Malaysia (UTHM), Malaysia

SUMMARY: Shortage in the hydrocarbon fuel sources, energy preservation and the future stringent emission regulations have been a formidable challenge to the worldwide industry. The main focus of this paper is to highlight the biodiesel pilot plant development in 9th Malaysia Plan. The purpose and the objective of biodiesel plant such as renewable energy study, human capital, research, training and consultation. The pilot plant was built up in The University Tun Hussein Onn Malaysia and there is a need of future market especially oil and gas related industry. In Malaysia, the Ministry of Energy, Green Technology and Water involved in reducing the CO₂ emissions up to 40% between 2005 and 2020. For that reason, the development Bio-Diesel pilot plant will keep its leading position and relevant alternative fuel to fulfill the characteristics of Low Carbon City Framework and Assessment System (LCCF). Accordingly, the development of diesel car technologies, which is often proposed the reductions of CO₂ emission until 25% than gasoline engine. However, the average world prices for oil palm, corn, and soybeans have risen 136%, 125%, and 107%, respectively, due in large part to both rising global populations and the push for biofuels. Therefore, the alternatives source of fuel is receiving a lot attention especially the application of renewable and sustainability energy from multiple feedstocks of bio-diesel fuel. The development of bio-diesel pilot plant for teaching and learning, research and development, consultation and commercialization was really significant and achieved their objective set-up.

Keywords: Biofuel, renewable energy, Pilot Plant, Training, Oil and Gas

INTRODUCTION

The Department of Plant and Automotive Engineering is one of the prominent departments for the faculty of Mechanical and Manufacturing Engineering was formally established on 1st May 2004. Since its formation, the department has gone through some exhilarating transformation in terms of its staffs, academic programmes and research activities. The ever changing challenges, both locally and globally, will inadvertently drive the department to improve further its academic strength and research capabilities. All the expected improvement will nonetheless contribute to the faculty's aspiration of producing world class academic programmes and technologically competent graduates, in addition to project itself as a renowned research and development establishment. To enhance the knowledge, the decision to set up the team to develop the Biodiesel pilot plant has gone through a few process which is brain storming, technical expert and expenditure preparation.

BIODIESEL PILOT PLANT DEVELOPMENT

The project of the UTHM biodiesel pilot plant began in early 2007 and is expected to be fully operational before end of 2009. Design and construction of the biodiesel plant are complex operations comprising many interrelated activities starting from the feasibility study till the plant handing over. [1-5] This site is selected to utilize the existing steam boiler for heat supply into the process plant.[6-7] The environmental impacts such

effluents of methanol vapor and waste water have been included in the feasibility study. The biodiesel pilot plant is a significant platform especially for conducting research and development in area of alternative energy resources that are plentiful available in Johor. This pilot plant represents the real commercial biodiesel plant however in small scale[8]. Figure 1 to figure 8 shows the plant and the equipment and facilities provided.



Figure 1. Bio-Diesel Pilot Plant [1-4]



Figure 2. Boiler for steam generation [6]



Figure 3. Air Compressor Room [6]



Figure 4. Control Room [7]



Figure 5. Water treatment plant [5]



Figure 6. Chemical storage [7]



Figure 7. Research Laboratory [8]

RESULT AND DISCUSSION

To date capacity of student year 2015 is 130 which is more than 20 training and consultation project has been done under the team lead by Mechanical Engineering Department. The clients are national (ADTEC, IKM, KKTM, POLITEKNIK and related industry. Meanwhile international client including Gazprom, UI, Mercu Buana & IPB.

CONCLUSION

The idea of set-up the bio diesel pilot plant has given an impact especially to enhance a undergraduate student to gain the knowledge and the related industry has utilize this facilities through skill training (boiler man, emergency and response planning, plant operation and instrumentation). In

the research and consultation project, it show the commitment of team members to train post graduate student and be a consultant of a few project that were develop in the country (education and training sector). The objective of bio diesel development has achieve their objective and support the government policy on human capital development and enhance the skill training for sustainable development on oil and gas sector.

ACKNOWLEDGMENT

The authors need to express thank to Education Ministry for funding through FRGS Vot 1216 and Faculty of Engineering Technology, UTHM.

References

- [1] M A Hanna, L. Isom and J. Campbell. "Biodiesel: Current perspective and future", *Journal of Scientific and Industria Research*, 64, 2005, pp. 854-857.
- [2] F.P. Helmus, *Process Plant Design*, 2008, Wiley-VCH.
- [3] N S Nandagopal. "Fundamentals of Process Plant Layout and Piping Design" 2001, IDC-Technologies.
- [4] S.D. Warren. "Process Desi", *Principles*, 1999, John Wiley and Sons, Inc
- [5] J.R. James, W.R. Penney and J. R. Fair "Chemical Process Equipment-Selection and Design", 2005, Elsevier.
- [6] Factory and Machinery Act 1967. Ammendment 2014), MDC Publisher. Kuala Lumpur.
- [7] Occupational Safety and Health 1994. Ammendment 2014, MDC Publisher. Kuala Lumpur.
- [8] G. Towler and R. Sinnott. "Chemical Engineering Design". 2nd edition, 2013, Elsevier.

Solar Thermal/PV Technology

IDENTIFYING OPTIMAL COMBINATIONS OF DESIGN DNI, SOLAR MULTIPLE AND STORAGE HOURS FOR PARABOLIC TROUGH POWER PLANTS FOR NICHE LOCATIONS IN INDIA

Chandan Sharma¹, Ashish K. Sharma¹, Subhash C. Mullick¹ and Tara C. Kandpal¹

¹Centre for Energy Studies,
¹Indian Institute of Technology Delhi, India

SUMMARY: This paper presents results of an analysis undertaken to determine the values of design DNI, solar multiple and hours of thermal storage for least cost of power generation for parabolic trough based solar thermal power plants at 8 niche locations in India. Solar radiation data source of SEC-NREL has been used and annual electricity outputs have been estimated using Systems Advisor Model (SAM). For estimation of levelized unit cost of electricity, benchmark capital cost and other financing conditions suggested by Central Electricity Regulatory Commission (CERC), Government of India have been used. Levelized unit cost of electricity (LUCE) has been found to be minimum for design DNI range of 550-700 W/m² and corresponding range of solar multiple is 1.4-1.6. Results also show that provision of 1 to 3 hours of thermal storage is desirable as it leads to an increase in electricity output with lowering of LUCE as compared to the corresponding values for plants without storage.

Keywords: Solar Thermal Power, Solar Multiple, Design DNI, Levelized Unit Cost of Electricity

INTRODUCTION

Optimal sizing of solar field is one of the important steps in designing a solar thermal power plant that directly affects the electricity output of the power plant and hence its financial feasibility. While an oversized solar field may result in excessive unutilized thermal energy, a plant with undersized solar field shall have low annual capacity utilization factor [1]. Optimal sizing of solar field necessarily involves deciding an appropriate value of design direct normal irradiance (DNI) and also that of Solar Multiple. The solar multiple is defined as the ratio between the thermal power produced by the solar field at the design DNI and the thermal power required by the power block at nominal conditions. Since the solar field of a solar thermal power plant costs approximately 40 to 50 percent of the total cost, an optimal solar field (that ensures operation of the plant at its nominal capacity and at the same time produces electricity at the minimum possible price) is essential for the economic viability of the plant. Besides optimal solar field sizing, provision of adequate hours of thermal storage improves dispatch ability as well as capacity utilization factor [2].

This paper presents results of an analysis undertaken to decide the optimal values of the design DNI, solar multiple as well as the hours of storage in parabolic trough based solar thermal power plants for 8 potential locations in India.

METHODOLOGY

To estimate the annual electricity output and the amount of dumped thermal energy as well as other performance parameters for different values of solar multiple, design DNI and hours of thermal storage, simulations have been carried out using System Advisor Model (SAM), a software

developed by National Renewable Energy Laboratory (NREL), USA. Typical meteorological year (TMY) weather files have been created for the selected locations (Figure 1) and imported into SAM to obtain performance parameters. To create TMY files, solar resource data has been obtained from satellite imagery maps developed by Solar Energy Centre (SEC), Ministry of New and Renewable Energy (MNRE), Government of India in collaboration with NREL, USA. For identifying optimal values of the parameters in consideration, minimum value of the LUCE is used as the criterion. Estimation of LUCE involves inputs in terms of capital cost, operation and maintenance cost and other financing conditions besides annual electricity output. Since capital cost and other related costs embedded in SAM apparently pertain to locations in the United States, the values of the benchmark capital cost and other financing conditions have been obtained from the latest order of the Central Electricity Regulatory Commission (CERC), a key regulator for power sector in India.

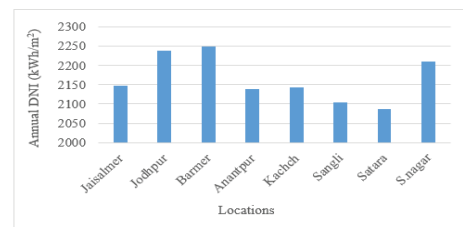


Figure 1. Locations selected and corresponding DNI

RESULTS AND DISCUSSION

For the base case, values of solar multiple and design DNI was assumed as 1.0 and 950 W/m² respectively.

For a design DNI of 950W/m², the solar multiple was varied from 1.0 to 2.0 in steps of 0.1. Alternatively for a pre-decided value of solar multiple (1.0), simulations were carried out for different values of design DNI between 450-950 W/m² in steps of 50 W/m² for all 8 locations considered in the study. An increase in solar multiple and/or decrease in design DNI from the base values defined above, results in lowering of LUCE due to increased thermal output from the solar field resulting in increased thermal energy input to the power block and hence leading to increased electricity output. However, the LUCE again increases with large increase in solar multiple (and/or further decrease in the value of design DNI) as the incremental cost of additional solar field required is not offset by incremental electricity output (as a large amount of collected heat would have to be dumped due to limited capacity of the power block). For the location of Jaisalmer, minimum LUCE of Rs. 11.47/kWh (1US\$ = Rs. 61.41 as on January 23, 2015) has been obtained at a design DNI of 550 W/m² and corresponding annual electricity output is 122 GWh (Figure 2).

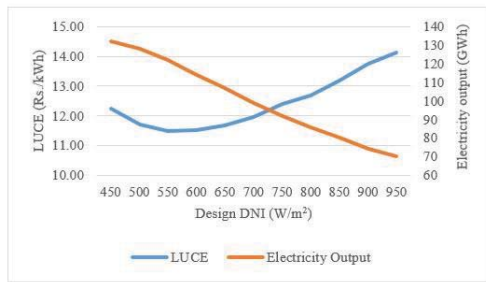


Figure 2. Variation in LUCE and annual electricity output for different values of design DNI

For the location of Jodhpur minimum LUCE of Rs. 11.20/kWh has been obtained at a solar multiple of 1.8 (design DNI fixed at 950W/m²) and annual electricity output is 125 GWh (Figure 3).

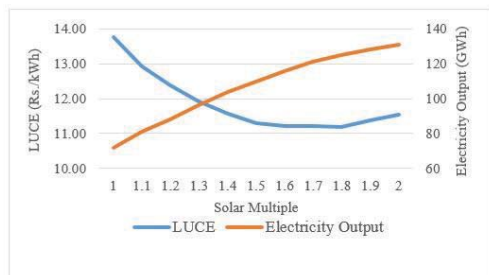


Figure 3. Variation in LUCE and annual electricity output for different values of solar multiple

Similar is the case with the provision of thermal storage (Figure 4). Provision of 1-3 hours of thermal storage facilitates the use of dumped thermal energy

and enables the power block to operate in the no-sunshine hours hence electricity output is increased resulting in decrease in LUCE. However, LUCE again increases with further increase in hours of thermal storage as incremental benefits due to increased electricity output are lower in comparison to the incremental cost of providing thermal storage. Minimum LUCE of Rs. 9.86 /kWh is obtained for 1 hour of thermal storage at the location of Jaisalmer.

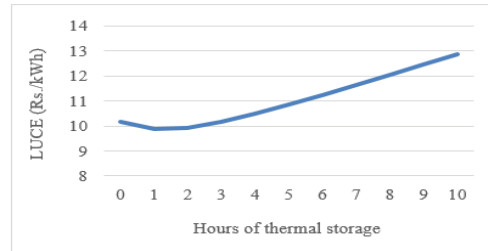


Figure 4. Variation in LUCE with thermal storage

Similar analyses have been undertaken for all the 8 locations in the country having large scale potential for solar thermal power generation and the results obtained have been discussed.

ACKNOWLEDGEMENT

First author would like to thank Technical Education Department, Government of Rajasthan and administration of Government Engineering College Ajmer for allowing to pursue his doctoral research at Indian Institute of Technology Delhi.

References

- [1] S. Izquierdo, C. Montanes, C. Dopazo and N. Fueyo . “Analysis of CSP plants for the definition of energy policies: The influence on electricity cost of solar multiples, capacity factors and energy storage”, *Energy Policy*, **38**, 2010, pp. 6215-6221.
- [2] P. Denholm, YH. Wan, M. Hummon and M. Mehos. “The value of CSP with thermal energy storage in the western United States”, *Energy Procedia*, **49**, 2014, pp.1622-1631.

INDOOR TEST PERFORMANCE OF PV PANEL THROUGH WATER COOLING METHOD

Y.M.Irwan¹, W.Z.Leow¹, M.Irwanto¹, Fareq.M¹, A.R.Ameli¹, N.Gomesh¹ and I.Safwati²

¹Centre of Excellence for Renewable Energy, School of Electrical System Engineering, University Malaysia Perlis (UniMAP), Malaysia.

²Institute of Engineering Mathematics, University Malaysia Perlis, (UniMAP), Malaysia

SUMMARY: The purpose of this paper is discussed about how to increase the electrical efficiency of photovoltaic (PV) panel in indoor test. The performance of PV panel is depends on the environmental factors, which is solar radiation and operating temperature. These environmental factors will be reduced the electrical efficiency of PV panel due to increase in operating temperature of PV panel. The solar simulator is set up on a steel frame is used to lift all of the halogen lamp bulbs. The halogen lamp bulbs act as a natural sunlight. Four sets of average solar radiation at the test surface of solar simulator were measured as 413, 620, 821 and 1016 W/m². DC water pump is used to overcome the problem of low efficiency of PV panel with water flow over the front surface of PV panel. This water cooling mechanism is one way to enhance the efficiency of PV panel for maintaining a low operating temperature during its operation period. The experimental results mentioned that the decrement of operating temperature and increase the power output of the PV panel with water cooling mechanism based on different fixed of solar radiation. The water spraying can be reduced heat on the front surface of the PV panel.

Keywords: PV panel, electrical efficiency, water cooling mechanism, operating temperature, indoor test

INTRODUCTION

PV energy is energy that comes from the sun converts into electricity. Nowadays, PV system is likely recognized and widely using in electric power applications. This is because it can be produced direct current electrical energy without any environmental harm when is exposed to solar radiation.

One of the main obstacles that face the operation of the PV panel is very low PV cell conversion electrical efficiency. The cause of low PV cell conversion electrical efficiency is overheating due to excessive solar radiation and high operating temperatures

To obtain increased electricity efficiency, the PV panel needs to be cooled by removing the excess heat from the cell assembly in some manner. The common solar panel cooling methods are water cooling, air cooling, and heat pipe cooling [1]. Tiwari and Sodha [2] developed a thermal model of an integrated PV/T water cooled system and validated with experimental results. The experimental showed that the maximum thermal energy is caught up the circulating the fluids and it has minimal impact on temperature along with a general thermal efficiency.

Solar simulator is very helpful in the solar energy experimental. This is because many scientists can be simulated the performance of PV panel under controllable indoor test facility. Solar simulators are a supply of light supplying illumination in close proximity to the natural sunlight. With a solar simulator, tests of PV panel performance can be carried out any chosen time, continued for 24 hours a day, and controlled for humidity and the other aspects of a local environment [3]. The type of lamp and the usage time can be affecting the change

of the solar radiation of a general solar simulator light source.

This paper describes the comparison of the performance of the PV panel with and without water cooling mechanism by using solar simulator. The DC water pump is attached on the front side of PV panel to spray water over the surface of PV panel. Moreover, the effect of spraying water over the PV panel on reduces the operating temperature of PV panel and reflection of PV panel. This water cooling mechanism has been used for measured the performance of PV panel for different parameters such as operating temperature, voltage output, current output and power output.

EQUIPMENT SETUP FOR SOLAR SIMULATOR TESTING

The solar simulator is set up on a steel frame with the dimension is 183 cm by 183 cm by 183 cm is used to lift all of the halogen lamp bulbs. This steel frame can be moved horizontally to adjust the solar simulator. Twenty units of halogen lamps with built in reflector is attached on the solar simulator. The lamp bulbs are located in 4 rows consisting of 5 lamp bulbs. All of the lamps can be controlled separately or in grouping, to various total amounts of solar radiation. The solar radiation can be regulated via a combination of amounts of lamp bulbs and height above the target. The center of halogen lamp bulb to another center of halogen lamp bulb spacing is close to 32 cm. The space distance between the PV panels and halogen lamps is approximately 67.3 cm, 82.5 cm, 95 cm and 119.38 cm for testing the various amount of solar radiation, respectively.

RESULTS AND ANALYSIS

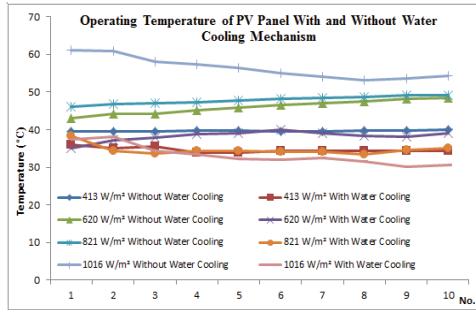


Figure 1. Operating temperature of PV panel with and without water cooling mechanism.

Figure 1 shows the variation of operating temperature of PV panel with and without water cooling mechanism in the different fixed solar radiation.

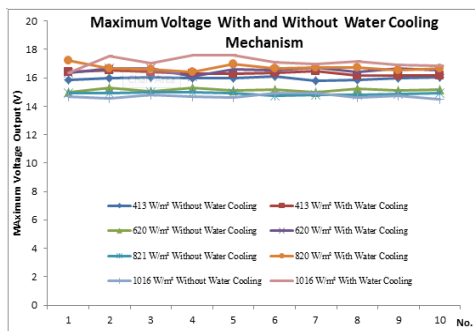


Figure 2. Maximum voltage output of PV panel with and without air cooling mechanism.

Figure 2 illustrates the maximum voltage output of PV panel with and without water cooling mechanism at 413, 620, 821 and 1016 W/m², respectively.

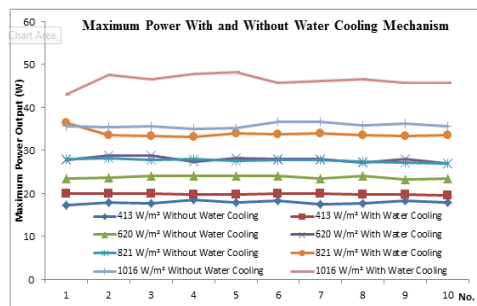


Figure 3. Maximum power output of PV panel with and without water cooling mechanism.

Figure 3 presents the maximum power output of PV panel with and without water cooling

mechanism. In the solar radiation of 413 W/m², the average maximum power output of PV panel with water cooling mechanism is 19.87 W while 17.93 W is the average maximum power output for traditional PV panel. The increment of maximum power output is approximately 9.76 % by using DC water pump. Besides that, 27.97 W, 33.87 W and 46.33 W are the average maximum power output for the PV panel with water cooling mechanism in the 620 W/m², 821 W/m² and 1016 W/m², respectively. Whereas, the average maximum power output of the traditional PV panel in the 620 W/m², 821 W/m² and 1016 W/m² are 23.81 W, 27.71 W and 35.76 W, respectively. The increment of maximum power output is 14.87 %, 18.19 % and 22.81 % in the 620 W/m², 821 W/m² and 1016 W/m², respectively. Thus, the DC water pump was used to cool down the operating temperature in order to enhance performance of PV panel.

CONCLUSION

The solar simulator system with halogen lamp bulbs has been successfully designed and fabricated in this experiment. The main objective of solar simulator is to analysis the performance of PV panel with and without water cooling mechanism in indoor test. Increase in operating temperature of PV panel significantly decreases the electrical yield of PV cells. DC water pump was used to solve this problem. DC water pump will be spray water over PV surface for cooling of PV panel. In the comparison between performance of PV panels with and without water cooling mechanism, water flow over front surface of PV panel can be reduced the operating temperature of PV panel which result in increased the electrical energy efficiency. The experimental results mentioned that the decrement of operating temperature is around 5 - 23 °C increase the power output of the PV panel with air cooling mechanism by 9 - 22 %. The increment of power output will have a significant contribution to the PV system applications. An increase in efficiency of PV panel, investment payback period of the system can reduce and the lifespan of PV panel will also be longer.

References

[1] K. Araki, H. Uozumi, M. Yamaguchi. "A Simple Passively Cooling Structure and Its Heat Analysis for 500x Concentrator PV Module." In: *Proceeding of the 29th IEEE Photovoltaic Specialists Conference*; 2002. pp. 1568-71.
 [2] A. Tiwari, MS. Sodha. "Performance Evaluation of Solar PV/T System: An Experimental Validation". *Solar Energy*, **80**, 2006, pp.751-9.
 [3] M. Shatat, S. Riffat and F Agyenim, "Experimental Testing Method For Solar Light Simulator With An Attached Evacuated Solar Collected", *International Journal of Energy And Environment*, **4**, 2013, pp.219-230

PARALLEL FULL CIRCUIT TECHNIQUE FOR POWER CAPACITY OF PHOTOVOLTAIC INVERTER WITHOUT TRANSFORMER

M. Zhafarina¹, M. Irwanto¹, A. H. Haziah¹, M. Fareq¹, N. Gomesh¹ and Y. M. Irwan¹

¹Centre of Excellent for Renewable Energy, (CERE), School of Electrical System Engineering, University Malaysia Perlis (UniMAP), Malaysia

²Institute of Engineering Mathematics, University Malaysia Perlis, (UniMAP), Malaysia.

SUMMARY: This design Photovoltaic (PV) inverter without transformer is interesting to be designed which consists of power factor correction (PFC) circuit, pulse driver circuit, and full bridge inverter circuit. The pulse driver circuit produce pulse wave. It is easy to create the pulse wave using microcontroller PIC16F628A. The three full bridge inverter circuits is constructed by high switching MOSFET, and connected in parallel, thus the high power capacity of inverter can be obtained.

Keywords: Photovoltaic (Pv) inverter, Pulse Driver and Full Bridge.

INTRODUCTION

PV inverters that have an isolation transformer on the grid side are big in size, therefore making the whole system bulky and hard to install. Topologies that use high frequency transformer in the DC – DC converter have a reduction in the overall efficiency, due to the leakage in the transformer [1][2][3]. A higher efficiency, smaller size and weight and a lower price for the inverter is possible in case the transformer is left out. This PV inverter without transformer is the solutions offer all the advantages, but there are some safety issues due to the solar panel parasitic capacitance [1]. The power factor correction is used to stable the DC voltage which is produced by the PV voltage. The pulse driver circuit is used to produce two pulse waves that are needed to drive the full bridge inverter circuit. The pulse wave is developed by microcontroller PIC16F628A via pulse driver circuit. The full bridge inverter circuit shown in is used to produce an AC waveform that input signal is the two pulse waves from the pulse driver circuit.

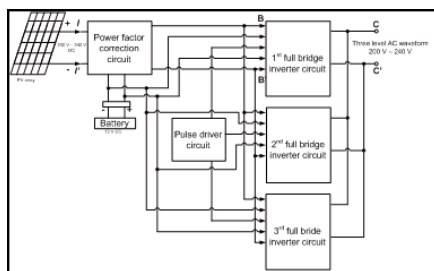


Figure 1. Block diagram of three level single phase photovoltaic inverter without transformer

Parallel operation of the inverter is needed to obtain a high power inverter. When increase the number of paralleled inverters, the high power can be applied. Ideal operation status of the parallel inverter has to be given attention, their output voltage have the same frequency, phase, amplitude and also waveform [4]. In case of parallel inverters,

total load power is summation of each inverter power or total load current is addition of each inverter current as shown in Figure 2. The total load current, i_t is given below:

$$i_t = i_1 + i_2 + \dots + i_n \quad (1)$$

Where:

i_1 = current flow through inverter 1

i_2 = current flow through inverter 2

i_n = current flow through inverter n

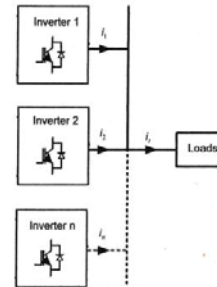


Figure 2. n parallel inverter

POWER FACTOR CORRECTION

The power factor correction is used to stable the DC voltage which is produced by the PV voltage.

PULSE DRIVER CIRCUIT

The pulse driver circuit is used to produce two pulse waves that are needed to drive the full bridge inverter circuit.

FULL BRIDGE INVERTER CIRCUIT

The full bridge inverter circuit shown in is used to produce an AC waveform that input signal is the two pulse waves from the pulse driver circuit.

RESULT AND ANALYSIS

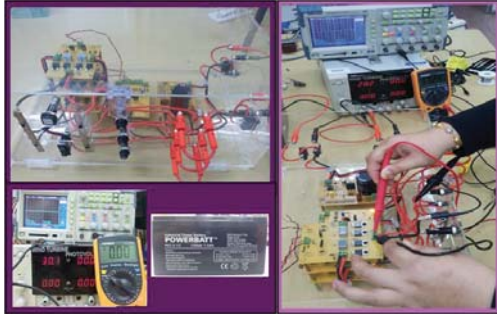


Figure 3: The experimental setup for full bridge inverter circuit.

Figure 3. show the experimental setup for testing the parallel full bridge circuit technique for power capacity of photovoltaic inverter without Transformer.

Figure 4. is the three level single phase inverter waveform from full bridge circuit the voltages in DC input is 20.2 Vdc and converts using full bridge circuit 17.24 Vac.

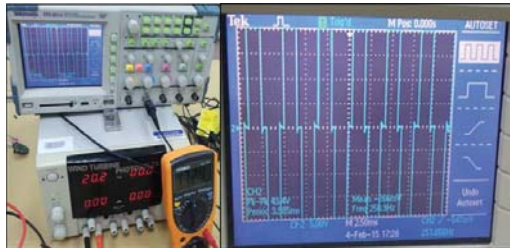


Figure 4. AC output voltage from full bridge circuit.

CONCLUSION

The power capacity for this PV inverter without transformer will increase when the full bridge circuit will added in this project. By paralling the full bridge circuit the total current flow is adds of each inverter circuit.

ACKNOWLEDGMENT

Thank you for Centre of Excellent for Renewable Energy, (CERE), in Kangar, Perlis for providing the equipment to test the circuit.

References

- [1] M. Calais, V. Agelidis; Multilevel converters for single-phase grid connected photovoltaic systems, an overview, *IEEE* 1998.
- [2] M. Calais, J. Myrzik, T. Spooner, V. Agelidis; Inverters for singlephase grid connected photovoltaic systems - an overview; Power Electronics Specialists Conference, *IEEE 33rd Annual*, 4, 2002, pp.23-27
- [3] J. Myrzik, M. Calais; String and module

integrated inverters for single phase grid connected photovoltaic systems - a review; Power Tech Conference Proceedings, *IEEE Bologna*, 2, 2003, pp. 23-26

[4] H. Cai, R. Zhao, H. Yang, Study on Ideal Operation Status of Parallel Inverters, *Journal of Power Electronic*, 23, 2008, pp. 221-233,

[5] W. R. Anis, "Analysis of A Three Level Bridge inverter for photovoltaics, solar cells, 1988, pp. 255-263,

[6] Q. W. Hart, power electronic, Mc Graw-Hill, 2011.

[7] B. Kavidha and K. Rajambal, Transformerless cascaded inverter topology for photovoltaic application, Proceeding of Indian International Conference on Power Electronics, 2006, pp. 328-331,

[8] Y. M. Irwan, W. Z. Leow, M. Irwanto, N. Gomesh, M. R. Mamat and I. Safwati, "A New Technique to Improve The Efficiency of Output Power Solar Panel Using 18F4550 Microcontroller", *Advanced Material Research*, 2014, pp. 31-34, 2014.

[9] B. Ismail, S. Taib, M. Isa, I. Daut, A.M. Saad, F. Fauzy, "Microcontroller Implementation of single phase inverter switching strategies", *International Conference on Control, Instrumentation and Mechatronics Engineering*, 2007, pp.104-107,

STAND-ALONE PHOTOVOLTAIC (SAPV) SYSTEM ASSESSMENT USING PVSYST SOFTWARE

Y.M. Irwan¹, A.R. Amelia¹, M. Irwanto¹, Fareq. M¹, W.Z. Leow¹, N. Gomesh¹ and S. Ibrahim²

¹Centre of Excellence for Renewable Energy, School of Electrical System Engineering, University Malaysia Perlis (UniMAP), Malaysia.

²Institute of Engineering Mathematics, University Malaysia Perlis, (UniMAP), Malaysia

SUMMARY: Photovoltaic simulation tool is important in predicting energy production from the solar system. This paper presents stand-alone photovoltaic (SAPV) system assessment using PVSYST software. The study used simulation software to develop reliable SAPV system as well as predicting the yearly energy output. The simulation of SAPV system configuration is presented using the PVSYST tools software. The total amount of electrical energy generated by PV array that supplied to the load and the various types of power losses are determined. The result obtained the optimal size of SAPV system configuration. Besides, the total energy flow through the whole system is calculated. With PVSYST software, the predicting energy supplied to the load for the whole year can be determined.

Keywords: Stand-Alone Photovoltaic (SAPV), PVSYST software, Photovoltaic (PV), Battery Storage, System Losses

INTRODUCTION

A SAPV system which converts solar into electricity is an independent system that supplies electricity to the load without being connected to the electric grid. The generated power is directly connected to the load but a storage device is needed. A complete working of SAPV system comprises two main parts: PV array and the Balance of System (BOS) component. A PV array is production from combination of PV modules to boost up electrical power. All components in SAPV except PV modules are called BOS such as battery storage, MPPT charge controller and wiring systems [1].

With the robust growth of solar PV application, sizing SAPV system is very important in order to predict the yearly energy production. System designers and installers require reliable tool to predict performance for overall system including total energy production under real conditions [2]. A widely variety of tools exist for the sizing, analysis and optimizing of SAPV system. In this study, the simulations are performed by using PVSYST 6.3.4.

PVSYST is dedicated PC software package for PV system. The process simulation of PVSYST calculates the behavior of the system and all disturbances for each hour of operation of SAPV system. The energy generated depending on meteorological data of site installation. By analyzing the energy resources data, energy production, system configuration and the system losses for installing SAPV system at Centre of Excellence for Renewable Energy (CERE) are discussed.

SAPV DESIGN SPECIFICATION

The sizing parameter for each component is very important to fulfill the system configuration. All components selected based on the energy requirement of the load demand and the potential of meteorological data of site installation. CERE located in Kangar, Perlis lies on 6.43°N latitude and

100.19° E longitude, 4 meter above sea level. The site location has big potential in develop solar system because of high solar radiation level.

SAPV components sizing strongly depending on load demand using by the consumer. All components sizing expected can supply enough energy to the required load. For this study, the lighting system contains 14 LED bulbs with rating power of 18W selected as peak load. All bulbs assumed to be used for 8 hours every day. The average of daily energy required by the loads estimated to be 2.016 kWh/day.

Sizing Components

SAPV component consist four main components which are PV module, battery, charge controller and converter. The PV array should be sized properly to provide enough energy to the loads and for charging the battery. Sizing of PV array can either increased or decreased, according to the mount of requirement load. To receive the maximum amount of solar radiation the PV array needs to be placed at a certain angle. The tilt angle of PV array in this study is 10°.

A SAPV system needs to operate in bad weather (there is not much sunlight) or during the night, thus battery storage is required as for electricity storage. The design principle for sizing the system's battery was to compensate for daily variations in solar radiation and not to act as seasonal energy storage [3]. Choosing batteries for PV systems involves many considerations for balancing energy of the PV system.

A regulator is an essential component of SAPV system. It is used to protect the batteries from overcharge and excessive discharge due to get higher capacity and extend life cycle. With less than desirable voltage, the battery will not operate recharge, with excessive voltage the battery will overheat, causing terminal damage to the battery

cells [4]. The MPPT converter which convert DC mode to AC mode don't operate always at their maximum efficiency. The maximum efficiency can be produced is 96% from their output for this MPPT converter.

RESULTS AND DISCUSSION

SAPV System Configuration

Perlis is blessed with abundant radiation with clear sky. The average daily radiation for the whole day is 4.90 kWh/m².day. Perlis which located in northern part of Peninsular Malaysia has average ambient temperature with 27.8 °C and wind speed about 0.7 m/s. All weather data collected determines the amount of sun energy reached a panel in produced electrical energy.

A reliable SAPV system configuration design as shown in Figure 1. From the PVSYST software simulation, the total battery required is 8 units in order to satisfy the energy requirement. The battery proposed is lead-acid battery with 160 AH battery capacity with nominal voltage for each cell is 12 V. In order to fulfill energy requirement, 8 units of the battery needed. There are 10 units of PV module (UniSolar 64 W) selected in order to satisfy PV array configuration. The PV array must have adequate energy supply to the load and charging battery. The design PV array expected to generate about 640 Wp of nominal power. In PVSYST software, inverter and MPPT charge controller are part of the regulator configurations. The selection nominal voltage for this regulator is 24 V. The selection made depending on system voltage of battery storage. From the simulation, the maximum voltage from PV array limited to 52 V. The regulator can regulate until 640 W of the maximum output power from battery.

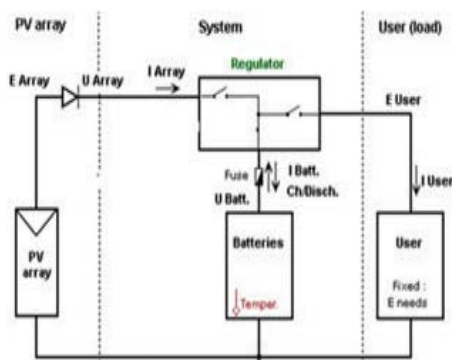


Figure 1. The SAPV system configuration.

Analysis of Energy Production

From PVSYST software, the available solar energy injected to the solar PV array can be determined. PV array did not receive 100% energy from the sun because some of losses. From this simulation, the PV array only generated 841.31 kWh

from 867.62 kWh (sun energy) for the whole year. However the energy produced by PV array is sufficient to meet load requirement for the entire year. The biggest losses for the whole SAPV system occur in PV array production energy. Energy produced from PV array affected by several factor such as ambient temperature, solar incidence, manufacture mismatch and ohmic wiring.

CONCLUSION

In conclude, this paper represents the simulation tools known as PVSYST software due to evaluate the SAPV system. This software enables the designer of PV solar to design the system configuration as well as predicting the energy production generated. The output generated based on the simulation of the sizing system. The system sizing is strongly depending on geographical site location. This study focused on SAPV system which applied to the lighting system for room in CERE building. To fulfill the load demand, 10 units of PV modules with rating power 64 W were selected. Where 8 units of 160 AH batteries used as system storage for the SAPV system. The nominal voltage for each cell of battery is 12V. The simulation result explored sun energy supplied to the PV array sufficiently enough to load user even though there are some losses generated.

ACKNOWLEDGEMENT

The authors thank the Centre of Engineering for Renewable Energy (CERE) in Kangar, Perlis for providing all data used in this study.

References

- [1] N. Idris, A.M. Omar and S. Shaari, "Stand-alone photovoltaic power system application in Malaysia.", *The 4TH International Power Engineering and Optimization Conference (PEOCO2010)*, 2010, pp.23-24
- [2] M. Chikh, A. Mahrane and F. Bouachri, "PVSST 1.0 sizing and simulation tool for PV system.", *Energy Procedia*, **6**, 2011, pp. 75-85.
- [3] E. Tzen, K. Perrakis and P. Baltas, "Design of a stand-alone PV- desalination system for rural areas.", *Desalination*, **119**, 1998, pp. 327-334.
- [4] S. Armstrong, M.E. Glavin and W.G. Hurley, "Comparison battery charging algorithms for stand-alone photovoltaic system.", 2008, IEEE.

ANALYSIS OF FLAT REFLECTOR AS SECONDARY OPTIC FOR FRESNEL LENS FOR ENHANCEMENT OF OPTICAL EFFICIENCY OF COCENTRATING PHOTOVOLTAICS

Nirat Patanasemakul¹, Pattana Rakkwamsuk¹, Surawut Chuangchote², Roongrojana Songprakorp¹ and Krissanapong Kirtikar¹

¹ Division of Energy Technology, School of Energy, Environment and Materials, King Mongkut's University of Technology Thonburi, Thailand

² The Joint Graduate School of Energy and Environment, King Mongkut's University of Technology Thonburi, Thailand

SUMMARY: This work presents a method to increase acceptance angle of Fresnel lens system by adding flat plate reflector as secondary optic element (SOE) at edges of receiver. Two-dimension (2D) ray tracing simulation using MATLAB and the optical characteristics of flat plate reflector are explained. The simulation of a system using Fresnel lens with 14.5 cm diameter and 19 cm focal length is made by varying SOE plate slope from 50 to 80°. The acceptance angle can be increased from 0.5° of a system without SOE to 1° by using a SOE with 65° plate slope and 4 cm height and the optical efficiency is still over 50% at 1.9° incident. By placing a receiver at an off-focal point, the system would have wider acceptance angle of about 1.6° while optical efficiency still maintain considerably high value around 80%

Keywords: Concentrating systems, Fresnel lens, 2D ray tracing, Secondary optic

INTRODUCTION

Concentrating photovoltaics (CPV) uses optical elements, lens or mirrors, to concentrate solar radiation to small area allowing uses of small but high efficiency PV cells. Compound (III-V) PV cells can have energy conversion efficiency as high as 40% under concentration [1]. However, in module operation, the efficiency is usually dropped to around 30%. One of the main reasons is optical loss especially in high concentrating system using Fresnel lens due to narrow acceptance angle which less than 1° [2]. The region where large amount of solar radiation is available, namely equatorial and tropical region, is usually suitable for solar application, but CPV mainly uses direct radiation (beam) to operate. In Thailand, a country in tropical region, about half of solar radiation is diffuse radiation [3] and complete clear sky rarely happen [4]. Even with correct alignment, solar radiation still cannot be completely concentrated on PV cells, making CPV application less favorable.

Secondary optical element (SOE) can be used between primary optical element (POE), Fresnel lens, and PV cells to improve irradiance uniformity on PV cells and acceptance angle of CPV system. P. Benítez [5] presented Fresnel Kohler concentrator as SOE and compared various types of refractive secondary elements. The acceptance angle of system with SOE could be improved to around 1.5° at 625x concentration. K. Araki [6] succeeded in designing CPV module with 35% module efficiency and acceptance angle of 1.1° at 1000x concentration by using 4-segmented Kohler lens as SOE and dome-shaped Fresnel lens. Increasing acceptance angle of concentrating system does not only increase manufacturing or operating tolerance, but also contribute to total energy gain of the system due to circumsolar radiation depending on specific location

as stated by D. Buie [7]. The study of sky distribution in Thailand by S. Chirarattananon [8] indicated that about 60% of the sky can be classified as clear sky condition, albeit not completely clear. This means that most radiation coming from the area around the sun, but cannot properly be concentrated on focal plane, while the sky during rainy season falls into intermediate condition around 40% of the time. From these literatures, it can be seen that increasing acceptance angle could help in improving energy gain of CPV under these conditions.

Adding a SOE in CPV using Fresnel lens to increase acceptance angle could improve usability of CPV in Thailand. In this work, the optical characteristic of Fresnel lens with secondary flat reflectors placing at the edges of receiver was simulated. The slope and height of reflector were varied to find suitable parameters and the optical efficiency was evaluated. This could benefit further experiments of using CPV with secondary reflectors.

METHODOLOGY

The simulation is carried out by generating rays passing through optical systems. It is assumed that there is no loss upon reflection and passing lens. This means that reflectivity was equal to 1 and the optical efficiency of Fresnel lens was 100%. The optical efficiency of system was calculated from the number of rays reached to a receiver.

Two-dimension (2D) ray tracing codes was devised using MATLAB. All rays travel in straight lines and change directions only upon reflection or refraction. The changes of ray directions upon reflection can be found from vector form of reflection law in Eq. (1). The change upon refraction can be found in the similar way as shown in Eq. (2).

$$\vec{r}' = \vec{r} - 2(\vec{n} \cdot \vec{r})\vec{n} \quad (1)$$

$$n'\vec{r} = n\vec{r} + (n'\vec{r}' \cdot \vec{n} - n\vec{r} \cdot \vec{n})\vec{n} \quad (2)$$

where r and n are unit vectors of ray directions and normal vectors of surface, respectively.

Fresnel lens was characterized by focal length f and receive aperture. The facet slope θ_s at the back side of lens could be found from Eq. (3), where ρ is the distance from incident point to the center of lens and n is refractive index of lens material. From these parameters, the normal vector of lens surface at each point from the center could be found.

$$\theta_s = \tan^{-1} \frac{\rho}{n\sqrt{1+(f)^2} - f} \quad (3)$$

The secondary reflector was flat plate reflector characterized by plate slope angle α . Assuming each traveling ray only reflects with the plate once and passes exit aperture, the acceptance angle of plate θ_p depends on distance from exit aperture l and exit aperture size w which could be found from Eqs. (4) and (5), where θ_o is the angle of edge ray to horizontal plane.

$$\theta_o = \tan^{-1} \left(\frac{l}{l+w} \tan \alpha \right) \quad (4)$$

$$\theta_p = 2\alpha - 90 - \theta_o \quad (5)$$

RESULTS AND DISCUSSION

The simulation was based on a system using Fresnel lens with 14.5 cm diameter and 15 cm focal length and 6 mm width receiver at focal point. Secondary reflectors were placed at the edges of receiver. From simulation, this system without SOE has an acceptance angle of 0.5° .

The optical efficiency of the system using SOE with plate slope varied from 50° - 80° is shown in Figure 1. It was found that the acceptance angle of system increased with increasing plate slope to the maximum of 1° using 65° -plate slope. The optical efficiency was more than 50% when incident angle was less than 2° . For 80° -plate slope, the plate blocked incoming rays from lens edge, hence lower optical efficiency ($\sim 60\%$) at small incident angle.

The receiver in a system with SOE can be shifted from a focal point at 19 cm to 18 and 17.5 cm resulting in reducing efficiency at small incident angle (0.5 - 1°) to approximately 95 and 90%, respectively as shown in Figure 2. Anyway, better efficiency was observed at large incident angle, where efficiency is over 90% at 1.5° and over 50% at 2.2° , respectively.

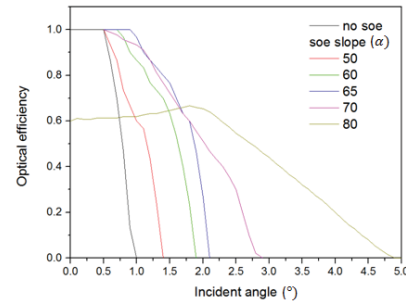


Figure 1. Optical efficiency of Fresnel lens with SOE slopes (α) of 50° , 60° , 70° , 80° and without SOE.

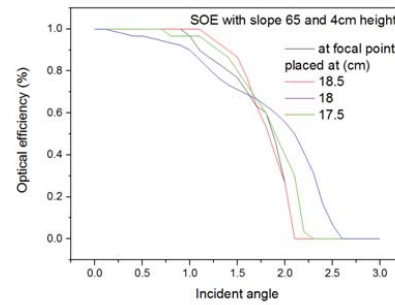


Figure 2. Optical efficiency of Fresnel lens with 65° SOE and a receiver shifted from 19 to 18.5, 18 and 17.5 cm.

References

- [1] R.R. King, A. Boca, W. Hong "Band-gap-engineered architectures for high-efficiency multijunction concentrator solar cells", *Proceeding 24th EUPVSEC*, 2009, 21-25.
- [2] A. Akisawa, M. Hiramatsu, K. Ozaki "Design of dome-shaped non-imaging Fresnel lenses taking chromatic aberration into account", *Solar Energy* **86**, 2012, 877-885.
- [3] R.H.B. Exell, P. Santibuppakul, "New estimates of mean daily diffuse solar radiation in Thailand", *Journal of the Science Society of Thailand*, 1984, **10**, pp. 37-41.
- [4] S. Stephen, G. Warren, Climatic atlas of clouds over land and ocean, URL: www.atmos.washington.edu/CloudMap/ (9/2/2015)
- [5] P. Benítez, J. C. Minano "High performance Fresnel-based photovoltaic", *OPTICS EXPRESS* **A25**, **18**, 2010, pp. A25-A40
- [6] K. Araki, P. Zamora, H. Nagai "Design and development of 35% efficient and 1000x CPV module with sufficient optical alignment Tolerance", *PVSC*, 2012, *38th IEEE*.
- [7] D. Buie, A.G. Monger "The effect of circumsolar radiation on a solar concentrating system", *Solar Energy* **76**, 2004, 181-185.
- [8] S. Chirattananon, P. Chaiwiwatworakul "Distributions of sky luminance and radiance of North Bangkok under standard distributions", *Renewable Energy* **32**, 2007, 1328-1345.

Energy Policy and Economies

DOES THE USE OF SOLAR AND WIND ENERGY INCREASE RETAIL PRICES IN EUROPE? EVIDENCE FROM EU-27

Gyanendra Singh Sisodia¹, Isabel Soares², Paula Ferreira³, Sanjay Banerji⁴, Dirk Van den Poel⁵ and Manish Kumar⁶

¹Amrita School of Business, Coimbatore India; FEP, University of Porto, Portugal; and Department of Marketing, Faculty of Economics, University of Ghent, Belgium

²CEFUP and FEP, University of Porto, Portugal

³DPS, University of Minho, Portugal

⁴Amrita School of Business, Amrita University, Coimbatore, India

⁵Department of Marketing, Faculty of Economics, University of Ghent, Belgium

⁶Self-employed, Ranchi India

SUMMARY: High technology and innovation market risk make renewable electricity generation expensive. On the other hand, green taxes applied to thermal generation also play a significant role in the increasing retail prices, considering that most energy systems are not completely renewable. The academic literature on the relationship between renewable electricity supply and electricity prices to final consumers suggest that a larger share of renewable electricity supply increases the price of electricity to end consumers although wind energy and solar energy have very low marginal costs. This study shows the individual contribution of solar and wind energy generation to the households and industrial electricity retail prices through panel data modeling of EU-27 (1995 to 2011). Random effect modeling was applied to understanding the net effect on prices. Independent variables include regulation perceptions, carbon emissions and levelised costs of electricity generation. The result of this study suggests that energy generation through wind and solar plays a negligible role in determining retail electricity prices to households, whereas in the case of industrial prices, their (solar and wind's) contribution is significant, but the value of the coefficient observed is close to zero.

Keywords: renewable electricity, retail electricity price, panel data, solar energy, wind energy

INTRODUCTION

Renewable energy has been considered as one of the key elements to address climate change issues due to global warming. It is included in the energy policy of major countries [1][2]. This also encourages new economic sectors to reduce the energy dependency on traditional sources [3]. However, generating electricity from renewable sources is still considered to be expensive in comparison to electricity generated through conventional sources. Countries that have succeeded in increasing the renewable energy share have achieved it by introducing efficient and effective support policies. Frameworks such as feed-in-tariff, feed-in premiums, green certificates, etc. offers incentives for generating and supplying renewable energies. Existing literature on renewable energy supports the price increase of electricity in short run. However, the individual effect of electricity generation through solar and wind on retail electricity prices is yet not known in the literature. The purpose of this study is to determine the drivers of electricity prices for households and industries.

Within the mandate of our study, we have asked the following two Research Questions (RQs)-

Research Question 1: Which are the determinants of retail electricity prices for households?

Research Question 2: How does investment in Renewable energy sources affect the retail prices of industrial sector?

DATA AND METHODOLOGY

To address the above research questions, hypotheses were formulated and empirical model with two versions (with two different dependent variables) were developed. Annual data from 1995 to 2011 was used from the World Bank and Eurostat database for EU-27 countries. The World Bank and Eurostat databases are considered to be a reliable source of information. The period chosen was also dictated by the availability of the data on solar and wind energy for the countries in the sample.

The dependent variable that were used are: electricity prices of households and industries (before taxes); whereas, independent variables used are: carbon emissions, levelised cost of electricity generation through wind & solar, electricity generation, renewable electricity generation through wind & solar, annual sunshine hours and regulation perceptions.

A few of the variables that were directly used have random missing values, which was taken care of in the proposed macroeconomic model (see Dragsat, 2009; Wang & Lee, 2013). Thus, we have applied random effect panel data modelling method to address the present study. Finally, results were critically analyzed.

RESULTS AND DISCUSSIONS

The primary consideration for the study is the relevance of independent and dependent variable

identified through the literature and determination of coefficient values and their levels of significance. In our analysis, we observe very high R-squared values for Model version 1 & 2 as 0.91 and 0.86 respectively, which indicates the model fit by 91 and 86 % for electricity prices of households and industries respectively.

In model version 1, wind and solar energies were expected to influence the prices of households. However, it is observed that RES-S play a significant role in determining household electricity prices, but coefficient is not impressive (table 3) and RES-W does not play a significant role in determining household electricity retail prices.

In model version 2, determinants of electricity prices for industry (EPI) are found to be insignificant for LW and LS; CE is negative with a factor of -0.17 and significant at the 1% level.

FINAL NOTES

Through our study, we could say that the electricity prices are influenced by renewable generation in long and short runs (in small or large extents). However, green taxes also raise the final price. Through literature it is observed that in one way or other each of the variable used in the study influence the electricity price.

ACKNOWLEDGMENT

Authors are thankful to: Amrita School of Business Coimbatore, India; FEP, University of Porto, Portugal; and Department of Marketing, University of Ghent for their support in utilizing their research resources. Authors are also thankful to European commission for having given Gyanendra doctoral fellowship to conduct research at University of Porto.

References

- [1] IEA, World Energy Outlook. *International Energy Agency*, Paris. 2012.
- [2] IPCC. "Renewable energy sources and climate change mitigation. Special report of the intergovernmental panel on climate change (Geneva)". 2011
- [3] K. Würzburg, X. Labandeira,, P. Linares. "Renewable generation and electricity prices: Taking stock and new evidence for Germany and Austria". *Energy Economics*.**40**, 2013, pp.159–171.
- [4] Dragset, I. G., 2009. "Analysis of Longitudinal Data with Missing Values. Norwegian University of Science and Technology". Retrieved from <http://www.diva-portal.org/smash/get/diva2:348872/FULLTEXT01.pdf> Dated December 12, 2013.
- [5] W. Wang and L. Lee, "Estimation of spatial panel data models with randomly missing data in the dependent variable", *Regional Science and Urban Economics*.**43**, 2013, pp.521–538.

THE STATUS OF ENERGY PRICE MODELLING AND ITS RELEVANCE TO MARKETING IN EMERGING ECONOMIES

Gyanendra Singh Sisodia^{1*}, Isabel Soares², Sanjay Banerji³, Dirk Van den Poel⁴, Mridula Sahay³

¹Amrita School of Business, Amrita University, Coimbatore, India; and Department of Marketing, Faculty of Economics, Ghent University

²CEFUP and FEP, University of Porto, Portugal

³Amrita School of Business, Amrita University, Coimbatore, India

⁴Department of Marketing, Faculty of Economics, Ghent University

SUMMARY: Investment cost associated to the generation of renewable energy such as wind and solar is generally estimated to be higher. As the wind and solar energy generation do not require any fuel, the marginal cost of electricity generation through renewable energy technologies is very low. Therefore, in the long run, the prices are expected to get reduced, once investment cost is recovered; whereas, in the short run, the expected energy price of electricity increases.

However, the final electricity price depends on several factors such as distribution cost, operating cost, storage cost (if any), load factor, and cost associated to switching of technology for electricity generation through total energy mix. In case of solar and wind energy generation, the technologies have grid priorities, but solar and wind are highly sensitive to weather conditions. Therefore, to make the system efficient, energy system also depends on coal fired plant, gas fired plants, nuclear plants, biomass, hydro, etc. for meeting the energy supply needs. Based on overall capacities, investment costs, energy imports and fuel prices, the final electricity prices are decided. With the current trends in advancement of technologies, and priority for one technology over the other, the prices can still fluctuate in the future.

In the current energy literature, methods available for price forecasting followed the modelling approaches, that use range of variables for forecasting the possible scenarios. These scenarios and forecasting might affect an investment decisions of investors. However, the challenging future scenario in European energy mix addresses the issue of falling electricity price while the renewable energy technologies getting cheaper; which tends to freeze the further investments, unless sufficient government support is available.

The current study aims to explore the various economic forecasting methods presented in the literature for the purpose of energy price modelling, in different contexts such as geographies, oil pricing, demand, supply, marketing, strategy, etc.. The results suggest a large variation in the methodologies being used by scientists to address the issues in different countries. A wide range of variable selection approach has been observed. We aim to propose the utility of dynamic modelling approach that covers the range of relevant variables, by incorporating the possible shortcomings of existing methods. Additionally, our study also aims to present the learning for the purpose of energy marketing in the context of emerging economies, such as India for their energy policy framing.

Keywords: energy price, energy modelling, price forecasting

INTRODUCTION

Across the several developing and developed countries, a larger investment in energy sector has been observed since the last decade. Germany, US, China, Japan and UK were the top investors in the year 2013; whereas India is one of the top 5 countries that invested in solar photovoltaic and wind power generation (REN 21, 2014). For meeting the carbon goals and reducing the energy imports, investment trend in renewable energy technologies is expected to continue for several developing and developed nations. For an instance Belgium, Denmark and Germany have estimated 100% renewable energy share by 2050 (VITO Report 2013; Lund & Manthiesen (2009); Klaus et al. (2010)). The ambitious targets of nations might attract lots of small and large investors to invest in energy projects. Energy market in general is very dynamic and electricity price do not largely vary. Therefore, to an extent, willingness of investors to invest also rely on states' policies and regulations,

apart from just energy prices. To analyse their financial return on investments, investors rely on forecasted electricity prices and statistical tools and techniques. However, the methods and variables to forecast may vary in different studies. Thus, the objective of this article is to present a current review of different tools and techniques used for electricity price forecasting.

METHODOLOGY

We have reviewed current papers (2010-2015) listed in journals available in well recognized databases such as Taylor and Francis, Springer and Elsevier. We have tried to broadly figure out the aspects that articles are describing. Our observations' major focus were methodologies portrayed by researchers. Thus, a chronological listing was prepared and suitable gaps and limitations of methodologies were identified. Finally, we analysed the listed papers and presented our analysis.

FINAL NOTES

Across the literature different methodologies that use range of variables have been addressed in the literature. Nonetheless, each methodology has its own effectiveness and limitation

ACKNOWLEDGMENT

Authors are thankful to European commission for providing doctoral grants to Gyanendra. We are also thankful to Amrita University, University of Porto and Ghent University for providing their resources.

References

- [1] REN 21 (2014). Renewables 2014 global status report. http://www.ren21.net/portals/0/documents/resources/gsr/2014/gsr2014_full%20report_low%20res.pdf 27 March 2015
- [2] T. Klaus, C. Vollmer, K. Werner, H. Lehmann & K. Muschen (2010). Energy Targets 2050: 100% renewable electricity supply. Downloaded <http://www.umweltbundesamt.de/sites/default/files/medien/publikation/add/3997-0.pdf> 27 March 2015
- [3] H. Lund & B. V. Mathiesen. Energy system analysis of 100% renewable energy systems the case of Denmark in years 2030 and 2050, *Energy*. **34**, 2009, pp.524-531
- [4] Vito Report (2013). Towards 100% renewable energy in Belgium by 2050. Downloaded <http://energie.wallonie.be/servlet/Repository/130419-backcasting-finalreport.pdf?ID=28161> 27 March 201

AN INVESTIGATION INTO THE CRUDE OIL PRICE PASS-THROUGH TO THE MACROECONOMIC ACTIVITIES OF MALAYSIA

Fardous Alom¹

¹Department of Economics, Faculty Economics and Management Science, International Islamic University Malaysia, Kuala Lumpur Malaysia

SUMMARY: This study examines the pass-through of crude oil prices (CP) into economic activities of Malaysia including industrial production index (IP), consumer price index (CPI), real effective exchange rate (REER), interest rate (IR) and stock price index (SPI) within the framework of hidden cointegration technique over the quarterly data ranging from 1987 to 2013. The estimated results suggest that positive and negative changes of IP, CPI, REER, IR and SPI do not maintain a long-run association with positive as well as negative changes of real CP. Although the negative changes in CPI, negative changes in IP and negative changes in REER are found to be cointegrated with the positive changes of CP the estimated signs of the error correcting terms do not provide enough evidence to support this provision.

Keywords: crude oil price; economic activities; hidden cointegration; Malaysia

INTRODUCTION

Volatility in the commodity prices particularly CP is a matter of worldwide concern because the volatility adds different types of costs such as production cost, opportunity costs and search costs [1] and consequently generates tensions and uncertainty [2]. The CP shocks that have started in the 1970s attracted the attention of many researchers and it has been observed as one of the many reasons for global economic slowdowns, especially for net oil importing countries [3-5]. A general consensus has been emerged, although not perfectly beyond criticisms, indicating that increases in CP support declining economic activities in the oil importing countries. Converted crude oil or energy regards as an engine for economic activities [6], and so increases in its prices have direct impacts on many economic activities.

A significant body of literature has contributed to the study of oil price-macroeconomic relationships. However, there is a dearth of study in the context of Asian countries in general and Malaysia in particular. Thus the aim set out in the current study is to examine the relationships between oil prices and industrial production, consumer price index, real effective exchange rates, interest rates, and stock price index in Malaysia.

The dearth of studies in the context of Malaysia is one of the main inspirations for the completion of the current study, distinct from the existing studies in several aspects. First, data until 2013 is used which includes all the recent major oil shocks. Inclusion of these recent shocks will enhance understanding of the impacts of CP shocks on economic activities. Second, the study is implemented within the framework of a hidden cointegration and CECM model, which was rarely used in previous studies in general and not used in particular for Malaysia.

DATA AND METHODOLOGY

This study utilizes quarterly CP data along with selected macroeconomic and financial variables including IP, CPI, IR, REER, and SPI for Malaysia over quarter 1, 1987 to Quarter 4, 2013 periods; making a total of 107 observations. The range of data has been chosen based on the availability of data for all required series. As a proxy for world CP, Dubai spot prices measured in US\$ per barrel are used because the Dubai price is more relevant to Asian countries [7]. The prime objective of the study is to examine the relationships between CP and IP, CPI, REER, IR and SPI. Data are collected mainly from the DataStream. The series are seasonally adjusted using US census-X12.

The central objective of this study is to identify the short-run and long-run relationship between crude oil price and macroeconomic variables. With that in mind, both the standard cointegration approach of Engle and Granger [8] and the hidden cointegration approach or Crouching Error Correction model (CECM) provided by Granger and Yoon [9] are used. Both of these methods are used in the same study for more accuracy. The later approach is considered superior to the standard approach because it can capture cointegrating relationships even in a nonlinear data generating process. And even if data series have no cointegration in conventional sense it might be possible to have hidden cointegration in them [9]. Therefore, the aim is to apply both methods to compare the findings as well as using the more sophisticated approach which will enable to identify more accurately whether any relationship exists or not.

RESULTS AND DISCUSSION

First of all, we check the stationary properties of all variables and their components by using ADF and Phillips-Perron (PP) unit root tests. The results of ADF and PP tests present that all logarithmic transformed series and positive and negative

components carry unit roots in levels whereas, they all are stationary at their first differences, implying series are integrated at order 1, $I(1)$. This creates the premises for testing cointegration between series. Next we carry out Engle-Granger cointegration tests but the cointegration tests failed to identify any statistically significant long-run relationships between CP and macroeconomic variables excepting IR. IR is found to maintain a long-run relationship with CP. Since CP and IR are found to have linear relationship we estimate ECM for them. The ECM result shows that the short-term pass through are not statistically significant and the error correcting speed parameter do not have appropriate sign indicating no short or long-run adjustment to equilibrium.

As the standard cointegration procedure failed to identify long-run relations between CP and macroeconomic variables, we proceed with the hidden cointegration approach. The hidden cointegration is similar to the standard cointegration except that we estimate models based on The results show that there are statistically significant relationships, at 10 percent level of significance at most cases, between negative components of CPI and positive components of CP, negative components of IP and positive components of CP and negative components of REER and positive components of CP.

The results suggest that there is indication of possible long-run relationships between negative components of CPI and positive components of CP, negative components of IP and positive components of CP and negative components of REER and positive components of CP. To reveal exact long-run relationships between CP and these stated variables we estimate CECM. Since negative components of CPI seem to be cointegrated with positive components of CP with trend in the equation, we estimate the CECM for this pair of variables. The error correcting terms are statistically significant; however the estimated signs are not appropriate indicating that neither positive components of CP nor negative components of CPI are responsible for the long-run relationships between these two variables. Next we estimate CECM for negative components of IP and positive components of CP without and with trend. In this case also, although the error correcting terms are statistically significant none of them have right sign suggesting the non-responsiveness for the long-run relationships. Same goes with the negative components of REER and positive components of CP. For the first component the error correcting term is statistically significant with wrong sign and for the last part the error correcting term has the right sign but not statistically significant. The above discussion reveals that the changes in CP and the changes in macroeconomic variables do not maintain a long-run relationship.

CONCLUSION

The objective of this paper was to examine the relationship between CP and the economic activities of Malaysia including IP, CPI, REER, IR and SPI within the framework of hidden cointegration technique over the quarterly data ranging from 1987 to 2013. The estimated results suggest that positive and negative changes of IP, CPI, REER, IR and SPI do not maintain a long-run association with positive as well as negative changes of real crude oil prices. Although the negative changes in CPI, negative changes in IP and negative changes in REER are found to be cointegrated with the positive changes of crude oil the estimates signs of the error correcting terms do not support this provision.

ACKNOWLEDGMENT

The author gratefully acknowledges the financial grant from International Islamic University Malaysia, Grant No. EDW A14-117-1544. The author also gratefully acknowledges the valuable review comments from the anonymous reviewers.

References

- [1] RS. Pindyck. "The dynamics of commodity spot and futures markets: a prime". *Energy Journal*, **22**, 2001 pp.1-29.
- [2] R, Blein and R. Longo. Food "price volatility-how to help smallholder farmers manage risk and uncertainty". *Discussion Paper. Rome: IFAD*, 2009.
- [3] JD. Hamilton. "Oil and the macroeconomy since World war II". *Journal of Political Economy*, **91**, 1983, pp.228-48.
- [4] JD. Hamilton. "This is what happened to the oil price-macroeconomy relationship". *Journal of Monetary Economics*, **38**, 1996, pp. 215-20.
- [5] JD. Hamilton. "What Is an oil shock?" *Journal of Econometrics*, **113**, 2003, pp. 363-98.
- [6] S. Paul and RN. Bhattacharya. "Causality between energy consumption and economic growth in India: a note on conflicting results". *Energy Economics*, **26**, 2004, pp.977-83.
- [7] M-H. Liu, D. Margaritis and A. Tourani-Rad. "Is there an asymmetry in the response of diesel and petrol prices to crude oil price changes? Evidence from New Zealand". *Energy Economics*, **32**, 2010, pp. 926-32.
- [8] RF. Engle, CWJ. Granger, RF. Engle and CWJ. Granger. "Cointegration and Error Correction: Representation, Estimation, and Testing. Long-run economic relationships: Readings in cointegration: Advanced Texts in Econometrics Oxford; New York; Toronto and Melbourne: Oxford University" Press, 1991.pp. 81-111.
- [9] CW. Granger and G. Yoon. "Hidden cointegration. Department of Economics Working paper", University of California, Sandiego 2002.
- [10] A. Honarvar. "Asymmetry in retail gasoline and crude oil price movements in the United States: An application of hidden cointegration technique". *Energy Economics*, **31**, 2009, pp.395-402.

ASSESSMENT OF FEED-IN TARIFF POLICY IN THAILAND: IMPACTS ON NATIONAL ELECTRICITY PRICES

Piti Pita¹, Bundit Limmeechockchai^{1*}, Warunee Tia², Pawinee Suksuntornsiri³ and Paiboon Limpitpanich³

¹Sirindhorn International Institute of Technology, Thammasat University, Thailand

²School of Energy and Environment, King Mongkut's University of Technology Thonburi Bangkok, Thailand

³Faculty of Engineering, Burapha University, Thailand

SUMMARY: Thailand, 67% (119,434 GWh) of primary energy resource for electricity generation relies on natural gas. Therefore, it may not be sustainable for the future, due to instability of energy resources. In 2012, government has launched the policy to motivate private sector for investment in electricity generation from renewable energy since 2007. It was called "Adder". Recently, feed-in tariffs (FIT) policy has been announced by the National Energy Board in 2013 to replace adder policy because adder paid on top of the retail electricity price but FITs is a fixed wholesale price. However, both policies subsidize so higher cost of electricity price resulting in inducing higher level of Ft in retail electricity price. So this study assesses impact on fuel adjustment charge (Ft) from Adder and FIT policy during 2010 to 2030 by AEDP25% optimization and PDP2010 rev.3. As a result, in 2030 by optimization case, subsidy for FIT will be about 48,873 million Baht while subsidy for Adders will be about 53,416 million Baht. The FIT will increase average national electricity production cost in Ft mechanism by 0.013 Baht/kWh in 2030 while Adders will increase average national electricity production cost of 0.154 Baht/kWh in 2030. Finally, FIT scheme lowers burden of subsidy than Adder scheme in both short and long terms. Therefore, if government encourages renewable power generation, the proper policy should be offered to compromise the benefit between electricity authority and consumers.

Keywords: Renewable electricity, Feed-in tariffs, adders, Ft, Thailand.,

INTRODUCTION

Electricity is main form of energy consumption in developing countries. In Thailand, 89% of primary energy resource for electricity generation relies on fossil fuels. Therefore, it may not be sustainable for the future, due to instability of energy resources. In 2008 [1], it was also estimated that carbon dioxide (CO₂) emission of 83,370 kton was released to environment because of electricity generation.

To reduce amount of CO₂ emission and to prevent instability of energy resources, Alternative Energy Development Plan (AEDP25%) 2012-2021 [2] has launched the policy to reduce the fossil fuel consumption and to increase energy security in Thailand. Electricity generated by renewable energy are not interesting. This is because of return price of investment is lower than fossil power generation. So, government policymaker has launched the policy for motivate private sector investment in electricity generation generate by renewable energy. It is called "Adder".

Recently, feed-in tariffs (FITs) policy has been announced by the National Energy Board in 2013, hope for replace Adder policy because of Adder paid to top up the retail electricity price but FITs is a fixed wholesale price. However, both policies subsidize high so higher cost of electricity price induces a higher level of Ft in retail electricity price.

So in this study, Assessment of impact on fuel adjustment charge (Ft) from Adder and FITs policy during 2010 to 2030.

METHODOLOGIES

Optimization

This Study use optimization analysis to choose type of renewable energy power plant and use quantities of renewable electricity generation from AEDP25% for short term scenario and PDP2010 rev.3 for long term scenario. Based on the following assumptions.

- Production of electricity from renewable energy will be the cheapest option first.
- Select four potential renewable energy technology (Solar PV, Biomass, Wind Farm and Small Hydro)

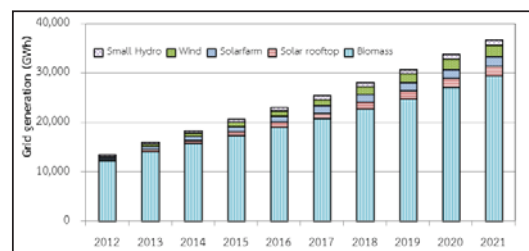


Figure 1. Share grid generation of the selected renewable electricity by AEDP25%

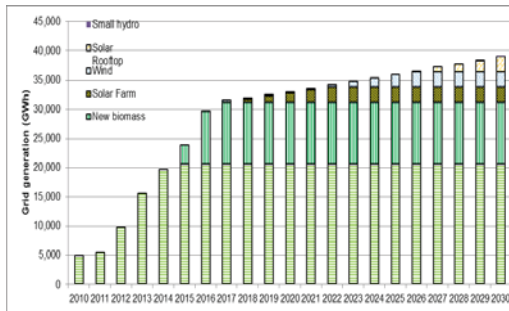


Figure 2. Share grid generation of the selected renewable electricity by Optimization

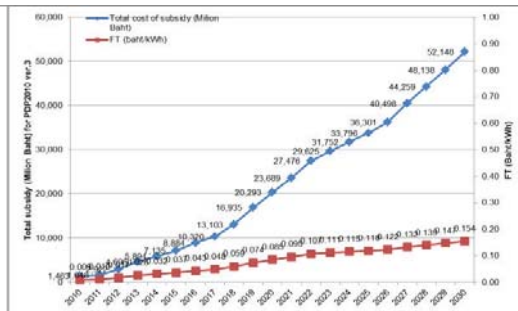


Figure 4. impact from Adder base on optimization by FITs

Fuel Adjustment Charge

$$S_{\text{Adder}} = \text{Renewable electricity} \times \text{Adder} \quad (1)$$

$$S_{\text{FITs}} = \text{Renewable electricity} \times (\text{FITs} - P_{\text{elec}}) \quad (2)$$

Where Adder and FITs are Baht/kWh

RESULTS AND DISCUSSION

Impact on fuel adjustment charge (Ft) from Adder and FITs policy

Under PDP2010, FITs policy lower subsidize burden than Adder policy, subsidize burden by FITs lower than subsidize burden by Adder is 48,873 million baht (Form Adder need money to subsidize 53,416 million baht but 4,543 million baht form FITs), it decreasing annually and the effects of FITs to the Ft, decreasing to 0.013 Baht/kWh in 2030 while the effects of Adder to the Ft, increasing to 0.158 Baht/kWh in 2030

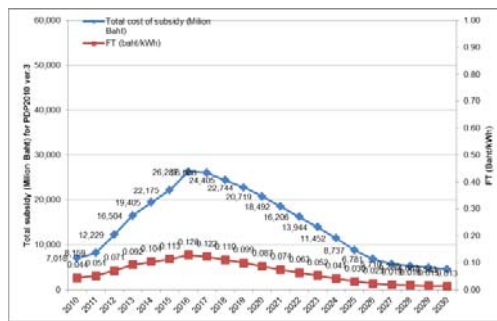


Figure 5. impact from FITs base on optimization by FITs

ACKNOWLEDGMENT

This paper was provided as a partial result of a research project titled “Appropriate Feed-In Tariffs and Macro Economic Impact by Energy Input-Output Analysis”, financially supported by Electricity Generating Authority of Thailand (EGAT) and Thailand Research Fund (TRF) fund. The authors would like to thank Mr Prachuab Peerapong for his assistants in this research project.

References

[1] Department of Alternative Energy Development and Efficiency, “Electric Power in Thailand year 2008,” <http://www.dede.go.th/dede/index.php> [2 Jan 2013], 2012.
 [2] Department of Alternative Energy Development and Efficiency, “The Renewable and Alternative Energy Development Plan for 25 Percent in 10 Year: AEDP 2012-2021,” http://www.eia.gov/forecasts/aeo/er/early_prices.cfm [15July 2012], 2012.

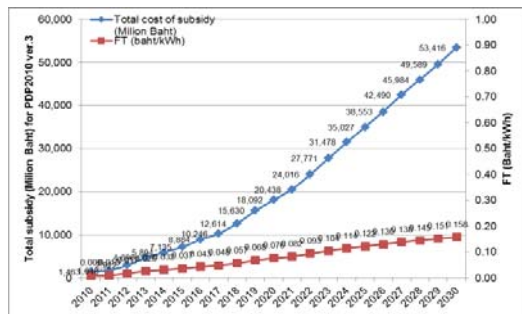


Figure 3. impact from Adder base on optimization by Adder

ROADMAP TO THAILAND'S NATIONALLY APPROPRIATE MITIGATION ACTIONS (NAMAs) 2020: ENERGY SECURITY AND CO-BENEFIT ASPECTS

Pemika Misila¹, Bundit Limmeechockchai¹ and Pornphimol Winyuchakrit¹

¹Sirindhorn International Institute of Technology Thammasat University, Pathumthani, Thailand

SUMMARY: Roadmap to Thailand's NAMAs 2020 presents the pathway for greenhouse gas (GHG) mitigations within 2020. This study proposes estimation of CO₂ countermeasures under 3 plans: the Alternative Energy Development Plan (AEDP) for 25 percent substitution of conventional energy within 10 years, the least cost greenhouse gas mitigation plan by the AIM/Enduse model, and the 20-year Energy Efficiency Development Plan (EEDP) during 2011-2030 and the transportation master plan by the Office of Transport Planning (OTP). This study also considers energy security and co-benefits from the proposed roadmap to reduce CO₂ emissions. Results of energy security and co-benefit analysis are presented. The roadmap to Thailand's NAMA 2020 will not only reduce CO₂ emissions but also increase energy security and several co-benefits, which enhance sustainable energy and environment development.

Keywords: Energy security, Co-benefits, CO₂ mitigation, Thailand's NAMAs

INTRODUCTION

With their concentrated and increasing populations, high levels of economic and cultural activity, cities are critical sites for addressing climate change [1] and greenhouse gas (GHG) emissions. Both climate change problem and GHGs mitigation have been an important issue of discussion in the Conference of the Parties (COP) which is the cooperation of parties to look into countermeasures for reducing GHG emissions, especially carbon dioxide (CO₂) [2].

The Nationally Appropriate Mitigation Actions (NAMAs) was first mentioned in the Thirteenth session on Conference of Parties (COP13) named "Bali Roadmap" [3]. Under the collaboration, NAMAs are classified into two schemes: Domestically Supported NAMAs and Internationally Supported NAMAs. Thailand would prepare its NAMAs plan in order to show an intention of being the support on climate change challenges in South-East Asia. Moreover, in COP20 Thailand pledged its NAMAs on voluntary basis with its GHG mitigation in the range of 7-20% below the business as usual (BAU) case in 2020 through GHG mitigation countermeasure in power generation, industry, buildings, residential and transport sector.

This paper proposes the CO₂ countermeasure roadmap for Thailand's NAMAs under three components: estimate achievement of 1) the Alternative Energy Development Plan for 25 Percent in 10 Years (AEDP 25%), 2) greenhouse gas mitigation plan by the AIM/Enduse model, and 3) The 20-Year Energy Efficiency Development Plan 2011-2030 (EEDP) and transportation master plan by OTP. However, this paper also focuses on the impact of energy security and co-benefits from the proposed CO₂ mitigation countermeasure.

METHODOLOGY

Energy security

Energy security is the availability of energy

sources at reasonable price [4] and the association between national certainty and natural resources for energy consumption in the country. In this study, energy security indices [5] as:

Diversity of Primary Energy Demand (DoPED),

$$\text{DoPED} = \frac{\sum p_i \ln p_i}{\ln T} \quad (1)$$

where p_i is the share of energy resource i to primary energy supply,
 T is the number of energy resource, and
 c_i is the share of imported energy resource i to energy resource i

Non Carbon Based Fuel Portfolio (NCFP),

$$\text{NCFP} = \frac{(\text{Hydro PED}) + (\text{NRE PED})}{\text{Total PED}} \quad (2)$$

Net Gas Import Dependency (NGID),

$$\text{NGID} = \frac{\text{Gas imports in Primary Energy}}{\text{Total Primary Energy}} \quad (3)$$

and Non Carbon Fuel Share (NCFS)

$$\text{NCFS} = \frac{(\text{PE}) + (\text{Energy Generation Mix}) + (\text{FE}) + (\text{Installed Capacity})}{\text{Total PED}} \quad (4)$$

Figure 1 shows energy security indices in four factors: 1) Base Diversity, 2) Gas Security, 3) Sustainability and 4) Vulnerability.

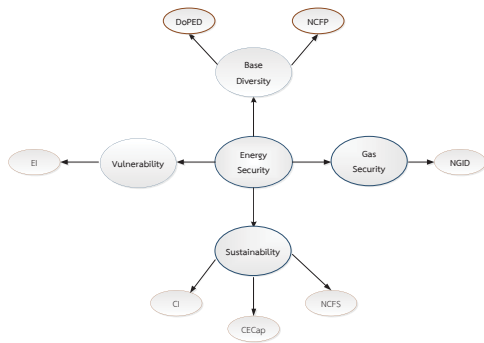


Figure 1. Energy security indices

Co-benefits

The term of co-benefits is the indirect benefit from other effects achieved, apart from main objectives. The co-benefit indices are presented as: Energy Intensity (EI),

$$EI = \frac{\text{Primary energy consumption (toe)}}{\text{GDP (US dollars)}} \quad (5)$$

CO₂ Intensity (CI),

$$CI = \frac{\text{CO}_2 \text{ Emissions (kg - CO}_2\text{)}}{\text{GDP (US dollars)}} \quad (6)$$

and CO₂ Emission per capita (CECap).

$$CECap = \frac{\text{CO}_2 \text{ Emissions (kg - CO}_2\text{)}}{\text{Population (person)}} \quad (7)$$

Figure 2 shows co-benefit indices in three aspects: economic, social and environmental.

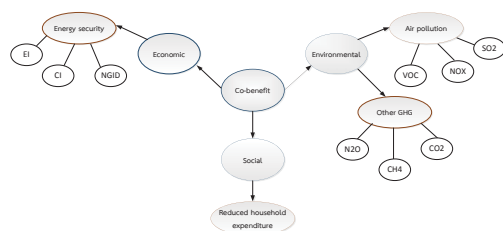


Figure 2. Co-benefits in dimensions

mitigation through promotion of renewable energy generation, through use of ethanol, biodiesel and energy efficiency improvement in power plants under AEDP 25% plan. In terms of least-cost CO₂ mitigation analysis by the AIM/Enduse model and the EEDP, including energy efficiency improvement in lightings, air conditionings and heating system in industries, promotion of the use of bio-fuels: E10, E20, E85, B5 etc. and promotion of hybrid car results in CO₂ mitigation. Results are presented that these three components could reduce CO₂ emissions by 73,087 kt-CO₂ in the 2020NAMA scenario when compared to the 2020BAU scenario. Moreover, energy security and co-benefits are also considered.

Regarding energy security aspect, in the 2020NAMA scenario when compared to the 2020BAU scenario, DoPED, NCEP, NCES and NGID will increase by 0.59%, 123.97%, 27.28% and 4.83%, respectively. The co-benefits in terms of EI, CI and CECap will decrease by 3.72%, 8.98% and 8.98%, respectively. Therefore, this roadmap of Thailand's NAMA 2020 will not only reduce CO₂ emission but also increase energy security and several co-benefits, which enhance sustainable energy and environment development.

ACKNOWLEDGMENT

Authors would like to thank Office of Natural Resources and Environmental Policy and Planning (ONEP) for the supports and comments. However, only the authors are responsible for views expressed in this paper and for any errors.

References

- [1] T. Lee, "Global cities and transnational climate change network". *Global Environmental Politics*, **13(1)**, 2013, pp. 108-127.
- [2] T. Nakata, M. Rodionv, D. Silva and J. Jupesta. "Shift to low carbon society through energy systems design." *Science China. Technological Science*, **53(1)**, 2010, pp. 134-143.
- [3] S. Sharma and D. Desgain. "Understanding the concept of Nationally Appropriate Mitigation Actions". *UNEP Riso Centre, Denmark*, 2013.
- [4] Internation Energy Agency (IEA). "Energy Security". Available: <http://www.iea.org/topics/energysecurity/>
- [5] S. Selvakkumaran, "Assessment of energy Security and the Impacts of IRP: A Case Study of Selected Asian Counties". *M.Sc. Thesis, Sirindhorn International Institute of Technology Thammasat University*, 2011.

RESULTS

Roadmap to Thailand's NAMAs 2020 proposes the measure to promote the reduction of GHG in the 2020NAMA scenario, when compared to the 2020BAU scenario. This paper proposes CO₂

Applied Energy

EFFECT OF MANGANESE PROMOTER ON COBALT BASED CATALYSTS SUPPORTED ON MAGNESIA FOR FISCHER-TROPSCH SYNTHESIS

Watis Warayanon^{1,3}, Sabaithip Tungkamani^{1,3}, Hussanai Sukkathanyawat^{1,2,3}, Monrudee Phongaksorn^{1,3}, Tanakorn Ratana^{1,3} and Thana Sornchamni⁴

¹Department of Industrial Chemistry, Faculty of Applied Science,
King Mongkut's University of Technology North Bangkok, Thailand

²Faculty of Science Energy and Environment,
King Mongkut's University of Technology North Bangkok (Rayong Campus), Thailand

³Research and Development Center for Chemical Engineering Unit Operation and Catalyst Design (RCC),
Science and Technology Research Institute, King Mongkut's University of Technology North Bangkok, Thailand

⁴PTT Research and Technology Institute, PTT Public Company Limited, Thailand

SUMMARY: Fischer-Tropsch synthesis (FTS) is the key performance of the gas-to-liquid (GTL) process. The research is focused on the different between 30 wt.% Co/MgO (30CM) and 30 wt.% Co/Mn/MgO (30CM-Mn). In this work, 30CM catalyst was synthesized by sol-gel method while the 30CM-Mn was prepared by impregnated 30CM with Mn-solution. The effect of Mn promoter on the reducibility and transient CO-hydrogenation were analyzed using H₂-TPR and TPSR, respectively. It was found that the additional of Mn promoter increase the activity of reduction due to the electron donation of Mn promoter. Higher CO-hydrogenation activity at the transient state, resulted from greater pre-adsorbed CO, was obtained when Mn promoter existed. The FTS performance of 30CM and 30CM-Mn were carried out. Mn promoter not only lowered the CH₄ formation but also increased the higher hydrocarbon product selectivity since it lower a hydrogenation rate resulting into increasing long-chain hydrocarbon products.

Keywords: Magnesia, manganese promoter, cobalt based catalyst, Fischer-Tropsch synthesis

INTRODUCTION

Fischer-Tropsch synthesis (FTS) is the key performance of the gas-to-liquid (GTL) process which transforms natural gas into environmental friendly liquid fuel. FTS converts syngas, the mixture of hydrogen (H₂) and carbon monoxide (CO) primarily, to clean hydrocarbon product over solid catalysts. In many practical applications, cobalt-based and iron-based catalysts are the most successfully commercial catalyst as they provided good activity with low cost. Iron-based catalyst has lower active compared with cobalt-based catalyst. Cobalt supported alumina (Co/Al₂O₃) shows high activity and selectivity toward linear paraffin with low activity for water-gas shift reaction. The catalytic activity is depended on the dispersion of active metal. It can be enhanced by a small amount of manganese (Mn) promoter which Mn promoter are mainly composed of metallic cobalt particle dispersed, selectivity to lower molecular weight olefins, decreased methane yield with enhanced propylene formation and increased the electron density of chemisorption site of catalysts [1,3]. Moreover, the catalyst life time is also needed to be improved. To do so, magnesia (MgO) possesses higher resistance towards carbon deposition than Al₂O₃.

The objective of this research is to study the reducibility, transient CO-hydrogenation and FTS activity including selectivity of Co/Mn/MgO compared with Co/MgO catalyst.

EXPERIMENTAL

In this study, 30 wt.% Co/MgO (30CM) catalyst was prepared by sol-gel method. The catalyst was dried and calcined at 450 °C for 4 h. The 30 wt.% Co/Mn/MgO (30CM-Mn) catalyst was prepared by the impregnation of aqueous manganese solution onto 30CM followed by dried and calcined at 450 °C for 4 h.

The chemical properties of catalysts were analyzed reducibility by temperature programmed techniques included H₂-TPR (BELCAT-Basic, Japan) and CO-hydrogenation activity by TPSR (Agilent 6820, USA).

The FTS tests was carried out using a fixed-bed reactor catalysts. Catalysts were in-situ reduced at 750 °C for 24 h under H₂ atmosphere and the catalyst bed was cooled down to the reaction temperature under inert gas afterwards. FTS performed at 200 °C in 80 ml/min flow of syngas (H₂:CO of 2:1) for 24 h. Liquid product was trapped and analyzed by gas chromatography (Agilent 7890A, USA) while gas products were detected by online gas chromatography (Bruker 450-valve, Germany) using FID and TCD detector.

RESULTS AND DISCUSSION

Temperature Programmed Reaction (TPR)

TPR profiles (Figure 1) of cobalt based catalyst show that Co₃O₄ bulk was reduced in two-steps. [2] First peak is assigned to the reduction of Co₃O₄ to CoO and the second peak represents a main reaction of CoO to Co⁰. However, the broad peak observed at high temperature attributed to a reduction peak of interaction between cobalt and support. Compared

to unpromoted catalyst (30CM), the reduction profile of promoted catalyst (30CM-Mn) was shifted to lower temperature as Mn is the structural promoter benefit for increased of small-sized Co-reduction, which assisted of active metal dispersion [4].

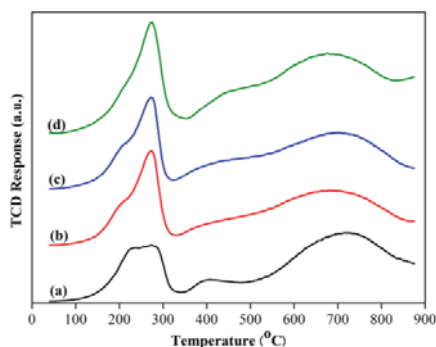


Figure 1. TPR profile of the catalysts (a) 30CM; (b) 30CM-0.25%Mn; (c) 30CM-0.5%Mn; (d) 30CM-1%Mn

Temperature Programmed Surface Reaction (TPSR)

TPSR technique was used to determine catalyst activity of CO-hydrogenation (equation 1) at transient state.



During the test, methane was detected by flame ionization detector depicted as TPSR profile. Figure 2 shows TPSR profiles of unpromoted and promoted cobalt based catalyst. The comparison of temperature at the maximum CO-hydrogenation activity for 30CM-Mn is lower than for 30CM. Likewise, the amount of methane product for 30CM-Mn is greater (Table 1). The results disclosed that Mn promoter significantly improves the CO-hydrogenation activity for transient experiment because Mn promoter raises the amount of pre-adsorbed CO which is a source of C for CH₄ formation.

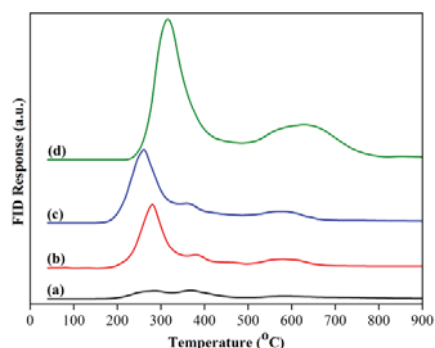


Figure 2. TPSR profile of the catalysts (a) 30CM; (b) 30CM-0.25%Mn; (c) 30CM-0.5%Mn; (d) 30CM-1%Mn

Table 1. CH₄ formation calculated using area under TPSR profiles.

Catalyst	CH ₄ formation (μmol/g _{cat})
30CM	6.04
30CM-0.25%Mn	20.17
30CM-0.5%Mn	30.36
30CM-1%Mn	49.35

Catalytic performance

The results obtained from FTS reaction at 200 °C for 24 h are summarized in Table 2. The appearance of small quantity of Mn decreased the CH₄ formation but increased the higher hydrocarbon product selectivity. The reason is that Mn promoter decreases the hydrogenation rate leading to higher long-chain hydrocarbon produce. [3]

Table 2. FT catalytic performances after 24 h reaction at 1 bar and 200 °C

Catalyst	Selectivity of product (%)				
	CH ₄	C ₂ -C ₄	C ₅ -C ₈	C ₉ -C ₁₅	C ₁₆ -C ₂₄
30CM	33.61	34.25	13.33	14.58	4.28
30CM-0.25%Mn	16.77	25.90	23.39	30.76	3.18
30CM-0.5%Mn	18.89	27.27	19.11	34.73	0.10
30CM-1%Mn	24.33	29.33	12.70	33.26	0.38

ACKNOWLEDGMENT

The authors would like to thank the Research and Development Center for Chemical Engineering Unit Operation and Catalyst Design (RCC), and PTT Research and Technology Institute for instrument and financial support.

References

- [1] A.A. Mirzaei, M. Faizi and R. Habibpour. "Effect of preparation conditions on the catalytic performance of cobalt manganese oxide catalyst for conversion of the synthesis gas to light olefins", *Applied Catalysis A: General*. **306**, 2006, pp.98-107.
- [2] A. Tavasoli, R.M.M. Abbaslou, M. Trepanier and A.K. Dalai, "Fischer-Tropsch synthesis over cobalt catalyst supported on carbon nanotubes in slurry-phase reactor", *Applied Catalysis A: General*. **345**, 2008, pp.134-142.
- [3] F. Morales Carno., "Manganese promotion in titania-supported cobalt Fischer-Tropsch catalysis", *Doctoral Thesis Utrecht University*, 2006.
- [4] Y. Li, X. Qin, T. Wang, L. Ma, L. Chen and N. Tsubaki, "Fischer-Tropsch synthesis from H₂-deficient biosyngas over Mn added Co/SiO₂ catalysts", *Fuel*. **136**, 2014, pp.130-135.

PROMOTER EFFECT ON THE PHYSICOCHEMICAL PROPERTIES OF COBALT BASED CATALYST FOR CO HYDROGENATION

Hussanai Sukkathanyawat^{1,4}, Sabaithip Tungkamani^{1,4}, Monrudee Phongaksorn^{1,4}, Tanakorn Rattana^{1,4}, Phavanee Narataruksa^{2,4} and Boonyawan Yoosuk³

¹ Department of Industrial Chemistry, Faculty of Applied Science, King Mongkut's University of Technology North Bangkok, Thailand

² Department of Chemical Engineering, Faculty of Engineering, King Mongkut's University of Technology North Bangkok, Thailand

³ National Metal and Materials Technology Center (MTEC), National Science and Technology Development Agency (NSTDA), Thailand

⁴ Research and Development Center for Chemical Engineering Unit Operation and Catalyst Design (RCC), King Mongkut's University of Technology North Bangkok, Thailand

SUMMARY: The effects of modification with promoters (Ru, Zr, Mn and K) on the properties of cobalt-based catalyst in CO hydrogenation were investigated by TPSR technique. The catalysts prepared by sol-gel method were characterized by BET, TPR and H₂-TPD. The effect of promoters was observed to have a profound impact on the physicochemical and catalytic properties of catalysts. Addition of Ru, K and Zr promoters to 30Co/MgO (30CM) facilitates the reducibility of catalyst. Mn addition improves the dispersion of metal clusters leading to a decrease in average cobalt crystallite size. Among all catalysts, 30Co-Mn/MgO(30CMM) and 30Co-Ru/MgO(30CRM) demonstrate the high reactivity and the maximum rate for methane formation. This could be attributed to the improvement of carbon monoxide chemisorption on high metal surface area of 30CMM and 30CRM catalyst. The change in physical and chemical properties of catalysts could be elaborated by the structural and electronic effects of promoter.

Keywords: Cobalt, CO hydrogenation, promoter, sol gel, TPSR

INTRODUCTION

Fischer Tropsch synthesis (FTS) has been a topic of interest for production of liquid hydrocarbons from synthesis gas. Iron, cobalt, nickel and ruthenium have been commonly reported to be sufficiently active for Fischer Tropsch synthesis. Because of low cost compared to noble catalyst, iron and cobalt are practical catalyst for application in industrial scale, although they are active under high temperature or high pressure conditions to obtain desired products. Iron based catalysts are important for the formation of heavy hydrocarbon product with the desired olefin and oxygenate content and low CH₄ selectivity, whereas cobalt based catalysts predominantly present high activity and selectivity toward linear paraffin and low water-gas shift reaction [1-2]. For the production of liquid alkane hydrocarbons, cobalt catalysts are suitable for use in this purpose. The activity of cobalt for CO hydrogenation has been reported to depend on the support, preparation method, metal loading, dispersion and promoter [2]. One attempt to develop the catalyst performance in this research is the improvement of the catalyst activity for FTS. Cobalt supported MgO catalyst was well prepared by modified sol gel technique and used as catalysts in this study. The effect of promoter Ru, Zr, Mn and K on the activity of cobalt based catalyst was investigated by transient experiment using temperature programmed surface reaction technique (TPSR).

METHODOLOGY

The effect of promoter (Mn, Ru, K and Zr) on the physicochemical properties was determined by BET, TPR, and H₂-TPD (BELCAT-B, JAPAN). The catalytic activity of cobalt based catalyst was investigated by transient experiment using temperature programmed surface reaction technique (TPSR).

Temperature programmed surface reaction (TPSR) experiment was carried out after catalyst was reduced at 750°C. Before the TPSR was performed on 0.200 g of catalyst packed in the reactor (4.5 mm, i.d.), a flow of 10%CO/He was allowed to the catalyst bed at room temperature for 30 min, following by flushing under He flow. TPSR experiment was studied under the condition of H₂ flow (30 ml/min). Temperature of catalyst surface was increased by temperature programmed from ambient temperature to 800°C with heating rate of 10°C/min. Methane product was detected by FID detector. (Agilent 6820, USA).

RESULTS AND DISCUSSION

One important focus in the development of this research is the improvement of the catalytic activity by addition of promoters and modified sol-gel method. The effect of promoter (Mn, Ru, K and Zr) on catalytic activity performance of 30CM catalysts was observed. Promoter has a great influence on the surface area (Table 1), reducibility (Figure 1) and dispersion (Table 2) of cobalt.

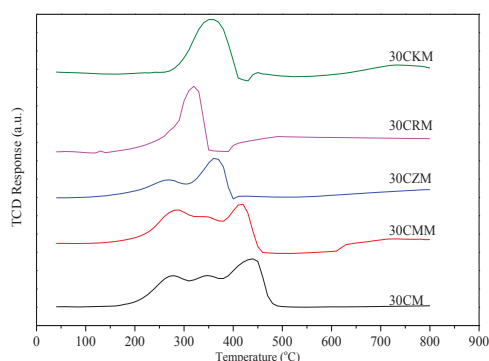


Figure 1. TPR profiles of 30CM, 30CKM, 30CZM, 30CRM and 30CMM catalyst

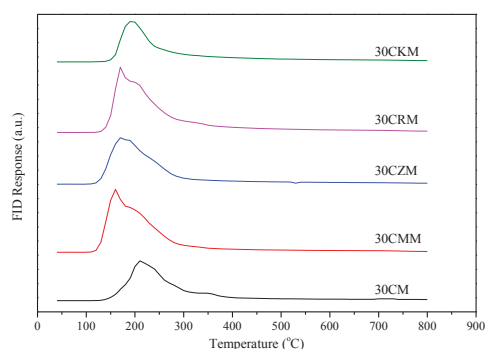


Figure 2. TPSR profiles of 30CM, 30CKM, 30CZM, 30CRM and 30CMM catalysts

TPSR profiles obtained from the hydrogenation of pre-adsorbed CO over 30CM, 30CKM, 30CZM, 30CRM and 30CMM catalyst present in Figure 2. The profile shows that the hydrogenation of pre-adsorbed CO leads to methane formation. TPSR results were summarized in Table 3. The amount of methane on different promoted catalyst decreases in the order of 30CRM > 30CMM > 30CZM > 30CM > 30CKM. The higher of methane formation could be due to an increase surface concentration of active Co metals. Peak temperature (T_{max}), taken as a measure of catalytic activity, shift to lower temperature in the order of 30CM < 30CKM < 30CZM < 30CRM < 30CMM, respectively, indicating an increase in the reactivity of catalyst. It could be concluded that the addition of Ru, Mn and Zr promoters can improve catalytic activity for CO hydrogenation. These findings suggest that Mn induces both structural and electronic promotion effects, resulting in higher metal dispersions and lower temperature for hydrogenation of CO activity of the catalyst [3].

Table 1. Effect of promoter added on physical properties of 30Co/MgO catalysts

Catalyst	Surface Area (m ² /g)	Pore Volume (cm ³ /g)	Average Pore Diameter (nm)
30CM	87.25	0.59	27.18
30CKM	49.26	0.34	27.81
30CZM	74.38	0.43	23.40
30CRM	83.24	0.45	21.74
30CMM	110.09	0.49	17.87

Table 2. %Dispersion, Surface area of Co exposed and crystallite size calculated from H₂-TPD

Catalyst	%Dispersion	Surface area of metal (m ² /g)	Crystallite size (nm)
30CM	6.65	44.97	14.99
30CKM	2.24	15.15	44.49
30CZM	3.35	22.63	29.79
30CRM	4.97	33.63	20.05
30CMM	7.83	52.97	12.73

Table 3. The Activation energies and amount of methane produced over all catalysts obtained from TPSR profiles

Catalyst	Initial Temperature (°C)	T_{max} (°C)	Ea* (kJ/mole)	mol of CH ₄ /g catalyst
30CM	115	211	82.7	9.53×10^{-5}
30CKM	113	199	80.6	8.49×10^{-5}
30CRM	110	182	77.5	1.47×10^{-4}
30CZM	100	187	78.4	1.15×10^{-4}
30CMM	96	172	75.8	1.39×10^{-4}

ACKNOWLEDGMENT

The authors would like to thank the Thailand Graduate Institute of Science and Technology (TGIST) and the National Science and Technology Development Agency (NSTDA) for scholarship and research funding.

References

- [1] Ø. Borg, S. Eri, E.A. Blekkan, S. Storsæter, H. Wigum, E. Rytter and A. Holmen, "Fischer Tropsch synthesis over γ -alumina supported cobalt catalysts: Effect of support variable" *Journal of Catalysis*. **248**, 2007, pp.89-100.
- [2] S. Li, S. Krishnamoorthy, A. Li, G.D. Meitzner and E. Iglesia, "Promoted Iron-Based Catalysts for the Fischer-Tropsch Synthesis: Design, Synthesis, Site Densities, and Catalytic Properties" *Journal of Catalysis*. **206(2)**, 2002, pp. 202-217.
- [3] F. Morales, E.D. Smit, F.M.F. de Groot, T. Visser, and B.M. Weckhuysen, "Effects of manganese oxide promoter on the CO and H₂ adsorption properties of titania-supported cobalt Fischer-Tropsch catalysts" *Journal of Catalysis*. **246(1)**, 2007, pp. 91-99.

DESIGN EQUATIONS FOR CATALYTIC MICROCHANNEL REACTORS: FISCHER-TROPSCH SYNTHESIS

Nutthawoot Jermkwan^{1,2}, Phavane Narataruksa^{1,2} and Chaiwat Prapainainar^{1,2}

¹Department of Chemical Engineering, Faculty of Engineering,
King Mongkut's University of Technology North Bangkok, Thailand

²Research and Development Center for Chemical Unit Operation and Catalyst Design,
Science and Technology Research Institute, King Mongkut's University of Technology North Bangkok, Thailand

SUMMARY: In this work, the design equations for a two-dimensional catalytic microchannel reactor for Fischer-Tropsch synthesis were studied. The main objective of the design procedure was to obtain optimal dimension of height (H) and length (L) responding to Co-Re/ γ -Al₂O₃ catalyst operated with space time of 0.0045 (g_{cat} min)/N cm³. The objective function was created in term of dimensionless number and channel length to height ratio. The channel length was divided into three distinct regions depending on controlled regimes comprising of kinetic controlled, external diffusion controlled and fluid flow rates controlled. The dimensionless of reaction rate was maximized by varying its aspect ratio L/H to obtain the optimal channel length at given channel height with maximum reaction rate. From the study, optimal length of microchannel reactor with the height of 0.5, 0.7 and 1.0 mm were 4.23, 5.01 and 5.98mm respectively.

Keywords: Fischer-Tropsch synthesis, microchannel reactor, design equations

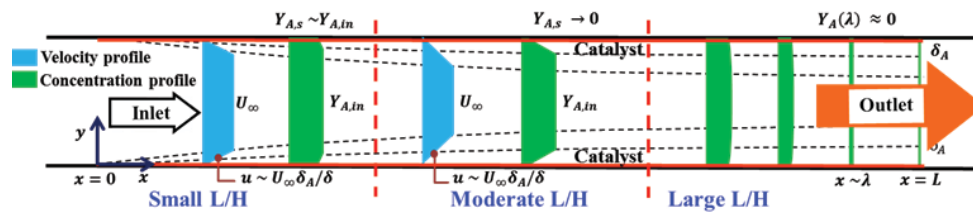


Figure 1. 2-D Model of microchannel reactor with different length [5]

INTRODUCTION

The Fischer-Tropsch synthesis is a well-known process as the catalytic process for the conversion of synthetic gas to fuels. The main products of the process are mixture of hydrocarbons of various molecular weights [1, 2].

Microchannel reactors are micro-scale reactor constructed with a large number of small, parallel channels with enhanced mass transfer properties and intensified heat transfer enabling isothermal operation even of highly exothermic Fischer-Tropsch synthesis compared to conventional fixed bed reactor. In microchannel reactor, high surface area per volume was provided leading to high capacity of active catalyst, much higher specific productivities and low pressure drop [3, 4].

In this study, design equations for catalytic microchannel reactor was studied by considering fluid flow rate, mass transfer and heterogeneous chemical kinetics together with overall reaction rate (R). The aim of this study was to obtain channel length (L) with respect to correlations for length to height ratio, $(L/H)_{opt}$, and maximum objective function, $\tilde{R}_{H,max}$.

METHODOLOGY

Model of micro-channel reactor was two

parallel flat plates with the dimension of H, W, L and δ representing channel height, width, length and coated catalyst thickness, respectively. Channel model with no side-wall effect can be reduced to 2-D model. The channel length can be divided into three regions depending on governing phenomena. These three regimes were on the assumption of constant volume, pressure drop, amount of catalyst and catalyst surface density.

The objective functions were created according to Mathieu-Potvin and Gosselin 2012 [5] as shown in Eq.(1).

$$\tilde{R}_H = \frac{RH^2}{\mu V Y_{CO,in}} \quad (1)$$

Bejan number (Be_H) represents the pressure drop number and this value is limited to the laminar regime. Schmidt number (Sc) represents the behavior of fluid, close to gas or liquid. Catalyst number (Ct_H) represents availability of catalyst surface density [5].

$$Be_H = \frac{\rho \Delta P H^2}{\mu^2}, Sc = \frac{\mu}{\rho D_{CO,S}}, Ct_H = \frac{k_{CO} \Gamma H}{D_{CO,S}} \quad (2)$$

From Figure 1, three regimes were presented. For large L/H, reactor channel was very long.

Reactant was completely converted to product at the end of channel. Global reaction rate was equivalent to mass flow rate of species CO [5]. This assumption leading to objective function depending on Be_H and L/H ratio as show in Eq.(3) [5].

$$\tilde{R}_H \sim \frac{1}{2} Be_H \left(\frac{L}{H} \right)^{-2} \quad (3)$$

For moderate L/H , when channel length was moderate, reaction rate was governed by transport of reactant through boundary layer. Velocity and concentration boundary layers were derived from continuity and species conservation equation to define reaction rate. Therefore, change in CO mole fraction along y -direction was equal to the difference of $Y_{CO,in}$ and $Y_{CO,s}$ over the concentration boundary thickness (δ_{CO}) [5]. Then, objective function can be shown in Eq.(4) [5].

$$\tilde{R}_H \sim 2Sc^{-1/2} Be_H^{1/3} \left(\frac{L}{H} \right)^{-2/3} \quad (4)$$

For small L/H , reaction rate was governed by chemical kinetic of catalyst as diffusion was fast enough to bring reactant to catalyst surface. Concentration of CO at inlet and catalyst surface was nearly equal [5]. Objective function for small L/H can be shown in Eq.(5) [5], which independent of L/H ratio.

$$\tilde{R}_H \sim 2Sc^{-1} Ct_H \quad (5)$$

The input data for prediction of channel length was shown in Table 1. Kinetic data was obtained from Almeida, 2013 [6].

Table 1. Data for channel length prediction at 508 K and 10 atm.

Parameter Description	Value	Ref.
Height of channel [micron]	500, 700,1000	Case study
Amount of catalyst per unit of wall surface [g_{cat}/m^2]	58.575	[6]
Surface reaction rate constant [$mol/g_{cat} s$]	5.54×10^{-4}	[6]
Space time [$g_{cat}min/Nem^3$]	0.0045	[6]

RESULTS AND DISCUSSION

Results were shown in Figure. 2. Behavior of objective function with respects to L/H , which started at very short channel and gradually increases its length. The maximum objective function was on the small L/H line because there was only chemical kinetic effect. Hereafter $\tilde{R}_{H,max}$ decreased as a function of $(L/H)^{-2/3}$ because reactor was limited by diffusion through boundary layers. Optimal design point can be obtained at intersection between small and moderate L/H . For the channel height of 700

micron, optimal length was 5.01 mm obtained at L/H ratio of 7.15. For the channel height of 500 and 1000 micron, optimal length were 4.23 and 5.98 mm, respectively.

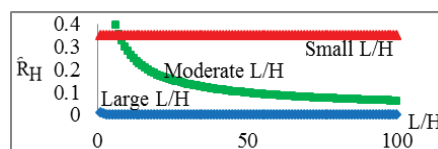


Figure 2. Behavior of the objective function for 700 micron in channel height

CONCLUSIONS

Design of microchannel-reactor for Fischer-Tropsch synthesis in this work provided correlations for determining channel length with respect to correlations for $(L/H)_{opt}$ and $\tilde{R}_{H,max}$. For estimation, channel length were 4.23, 5.01 and 5.98 mm when channel height were 0.5, 0.7 and 1.0 mm, respectively.

ACKNOWLEDGMENT

Thank Graduate College, King Mongkut's University of Technology North Bangkok for the financial support.

References

- [1] S. Chambrey, P. Fongarland, H. Karaca, S. Piché, A. Griboval-Constant, D. Schweich, F. Luck, S. Savin and A.Y. Khodakov, "Fischer-Tropsch synthesis in milli-fixed bed reactor: Comparison with centimetric fixed bed and slurry stirred tank reactors". *Catalysis Today*, **171(1)**, 2011, pp. 201-206.
- [2] R. Myrstad, S. Eri, P. Pfeifer, E. Rytter and A. Holmen, "Fischer-Tropsch synthesis in a microstructured reactor". *Catalysis Today*, **147**, 2009, pp. S301-S304.
- [3] L.C. Almeida, O. Sanz, J. D'olhaberriague, S. Yunes and M. Montes, "Microchannel reactor for Fischer-Tropsch synthesis: Adaptation of a commercial unit for testing microchannel blocks". *Fuel*, 2013, pp. 171-177.
- [4] C. Cao, J. Hu, Shari Li, W. Wilcox and Y. Wang, "Intensified Fischer-Tropsch synthesis process with microchannel catalytic reactors". *Catalysis Today*, **140(3-4)**, 2009, pp. 149-156.
- [5] Mathieu-Potvin, F. and L. Gosselin, "Threshold length for maximal reaction rate in catalytic microchannels". *Chemical Engineering Journal*, 2012, pp. 86-97.
- [6] L.C. Almeida, O. Sanz, D. Merino, G. Arzamendi, L.M. Gandia and M. Montes, "Kinetic analysis and microstructured reactors modeling for the Fischer-Tropsch synthesis over a Co-Re/Al₂O₃ catalyst". *Catalysis Today*, **215**, 2013, pp. 103-111.

TECHNICAL AND ECONOMIC ANALYSIS OF A SMALL BIOMASS PYROLYSIS PLANT

Chawannat Jaroenkhasemmesuk¹ and Nakorn Tippayawong¹

¹Department of Mechanical Engineering, Faculty of Engineering, Chiang Mai University, Thailand

SUMMARY: Bio-oil from pyrolysis of biomass has great potential to be one of the main renewable energy sources. At present, there are only a small number of commercial bio-oil plants because their operation is rather complicated and the return on investment is not attractive. With funding from the government sector, a small biomass pyrolysis plant (capacity of 20-30 liters of bio-oil per day) was built and operated. In this paper, practical stepwise methodologies were presented to technically analyze the production and energy consumption of bio-oil production. Mass and energy balance calculations were carried out to improve process design. An economic analysis was also performed to study the potential of biomass-to-bio-oil conversion costs and viability of commercialization. From the investigation, it was found that the operation cost of crude bio-oil production was about 30-35 Thai baht per liter. Even though the operating cost of the pyrolysis units is excessively high under current situation, the biomass plant still has potential to generate attractive economic return if there are the upgrading process and sustainable policy from the government to subsidize the sale price.

Keywords: bio-oil, thermochemical conversion, feasibility analysis, renewable energy

INTRODUCTION

Bio-oil from pyrolysis is one of a number of renewable energy sources that convert biomass to higher value products. Thai Office of Agricultural Economics (OAE) listed biomasses that have potential to be promoted for energy application. They were fast growing trees or economic trees, (e.g. Eucalyptus, bark, and sawdust), and wood residues. Sawdust from the furniture factory sector was identified to have potential to be a major raw material for Thailand.

With funding from the government, a small biomass pyrolysis plant was built and operated in Phrae, Thailand. Fluidized bed pyrolysis technology was employed at 10 kg/h using sawdust. The base feed cost was 1000 baht/ton. The system was designed to operate at 8-10 h/day. The design of the plant was shown in Fig. 1.

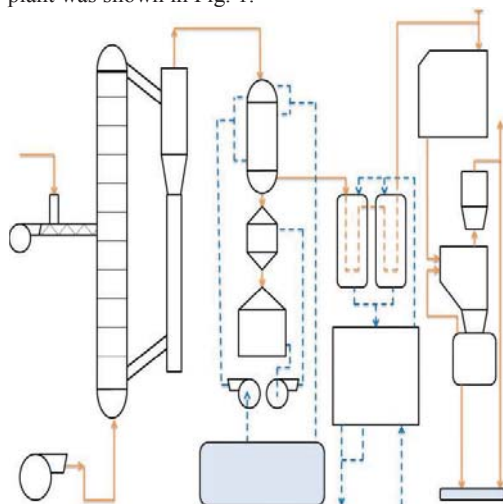


Figure 1. Plant process flow.

Sawdust was fed from the left side of process flow to the pyrolysis reactor, and generated bio-oil

and other products in gas phase. All products moved to various sections to be separated and collected as shown in solid lines. Dotted line shows the cool water loop to condense products.

The objective of this work was to provide a detailed technical and economic analysis of a pyrolysis plant producing 25-35 liters/day of bio-oil. The expected results are the guideline to optimize and improve operation of this plant.

METHODOLOGY

Mass and energy balance were used to technically analyze the production and energy consumption of bio-oil production based on the data from this demonstrated plant.

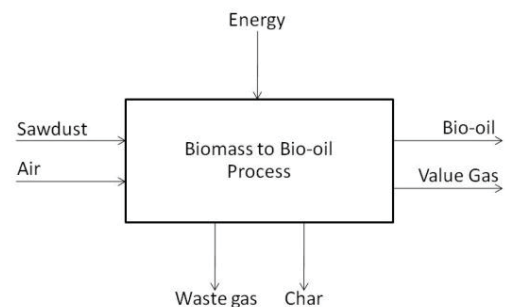


Figure 2. Inputs and outputs at the system boundary

Mass balance is fundamental to the control of processing, particularly in the control of yields of the products. To resolve the mass balance for the biomass to bio-oil plant, the unit operations of the block flow diagram from process in Fig.1 must be defined. Figure 2 shows inputs and outputs at the system boundary [2].

$$m_{stored} = m_{out} - m_{in} \quad (1)$$

Mass flows include raw materials, air, products, wastes gas, char, and stored materials. For energy balance, pyrolysis plant is regarded as a closed system, with total heat equation as

$$\Delta Q = Q_{out} - Q_{in} \quad (2)$$

The energy flows of process include energy of raw material, energy of all products, operation heat, and heat loss [3]. The heat calculation is shown in Fig. 3, based on the technical data from [4].

Operating costs were projected for both variable and fixed operating costs. Variable operating costs were determined from the material and energy balance. The basis for the capital and operating costs as well as the financial calculations were addressed in a low-risk case. Fixed operating costs include maintenance, taxes and insurance. They were forecasted and determined.

Selling costs of crude bio-oil was collected and predicted; based on the previous study due to the lack of data.

RESULT AND DISCUSSION

From mass balance, yields of products from the process were 35-40% as liquid product (30-35% of bio-oil and 5-10% of water), 40-45% as gas products, and 15-25% as char and solid. Yield of bio-oil from other plants and researches was about 50-75%, depending on the raw material and process.

Heat balance was estimated from the heat consumption of the process. It was found that heat losses from bottom to top of the reactor were about 35-43%. This amount of losses may affect directly to the bio-oil yield.

An annual internal rate of 10% was specified for a plant life of 20 years and straight-line depreciation over 10 years. The bio-oil production cost was estimated to be about 30-35 Thai baht per liter.

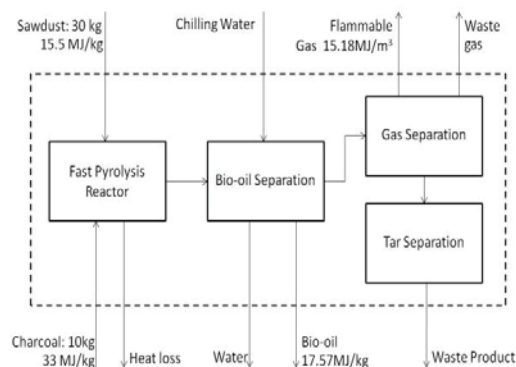


Figure 3. Energy balance diagram.

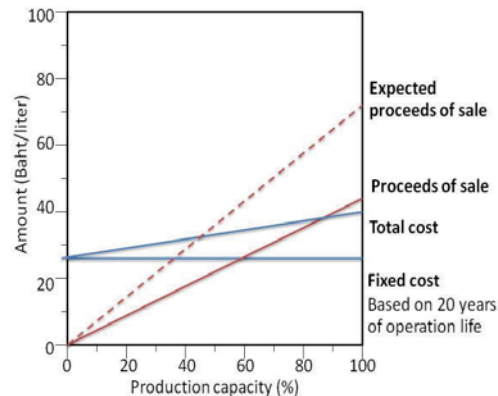


Figure 4. Break-even analysis

There are a number of barriers that must be overcome to generate attractive economic return of this bio-oil plant. First, the amount of heat lost in process to reduce the operation cost, and also product yield improvement should be considered. The bio-oil upgrading process should be established to add more value of bio-oil. Collaborative activities with the government sector should continue with both technology and budget to establish long-term access to this resource. Moreover, for long term development, bio-oil applications in burners, power generation or vehicle and the environmental issues should be studied.

ACKNOWLEDGMENT

Supports from Chiang Mai University and Thailand Research Fund (TRF) via the Research and Researcher for Industry (RRI) program, contract no. PHD56I0041 are acknowledged. Cooperation and assistance from Earth and Sun Alternative Energy Co., Ltd. are appreciated.

References

- [1] Q. Wei, Y. Qu and T. Tan, "Mass and heat balance calculations and economic evaluation of an innovative biomass pyrolysis project", *Frontiers of Chemical Science and Engineering*, **5**(3), 2011, pp. 355-361.
- [2] M. Ringer, V. Putsche and J. Scahill, "Large-scale pyrolysis oil production: a technology assessment and economic analysis", *Technical Report of National Renewable Energy Laboratory/TP-510 -37779*, 2006.
- [3] Mei F. Dudukovic, M. Evans and M.N. Carpenter, "Mass and energy balance for a corn-to-ethanol plant", Master thesis of science, Washington University in St. Louis, 2005.
- [4] S. Sinha, A. Jhalani, M. R. Ravi, A. Ray, "Modeling of pyrolysis in wood: a review" *Solar Energy Society of India Journal*, **10**(1), 2000, pp.41-62.

THE EFFECT OF FEED LOCATION OF SEMI-BATCH REACTIVE DISTILLATION VIA ESTERIFICATION REACTION OF ACETIC ACID AND METHANOL: SIMULATION STUDY

Suputtharagris Akkaravathasinp^{1,2}, Phavanee Narataruksa^{1,2} and Chaiwat Prapainainar^{1,2}

¹Department of Chemical Engineering, Faculty of Engineering,
King Mongkut's University of Technology North Bangkok, Thailand

²Research and Development Center for Chemical Unit Operation and Catalyst Design,
Science and Technology Research Institute, King Mongkut's University of Technology North Bangkok, Thailand

SUMMARY: This paper studied the effect of feed location of semi-batch reactive distillation via esterification reaction of acetic acid and methanol producing methyl acetate using Aspen Batch Distillation model. The reactive distillation model used in this study was developed following a design of an in-house made reactive distillation column which comprised of seven stages including five feed stages containing solid catalyst for the reaction, reboiler and condenser. The main objectives of this batch reactive distillation operation were obtaining high yield of methyl acetate product with 95wt% purity, commercial grade of methyl acetate. The semi-batch distillation operation was charging methanol at reboiler and acetic acid was fed to the column continuously at five different feed stages. From the simulation results, it showed that the feed stage location of acetic acid was the major effect on yield of main product and purity at top stage of the column and we found that the optimum feed stage of acetic acid was stage 5 which gave the maximum yield and purity of methyl acetate at 81.2% by mole and 95.7wt%, respectively.

Keywords: reactive distillation, esterification, aspen batch distillation, simulation

INTRODUCTION

The reactive distillation (RD column) is the combination of reactor and distillation column in a single unit. This unit operation can be operated with two processes occurring at the same time, which are reaction and separation. Reactive distillation column comprises of reactive zone, normally at stripping and/or rectifying zone compared to conventional distillation column. The advantages of reactive distillation can be summarized as follows [1].

- Increase conversion and improved process efficiency and selectivity.
- Reduce the capital investments.
- Save the energy cost for exothermic reaction.
- Avoidance of azeotropic mixture.

The reactive distillation is suitable for equilibrium-limited reactions such as esterification reaction (Eq.1) which is the reaction of methanol with acetic acid to produce methyl acetate that can be used in a wide range of coating and ink resins [2].



From this reaction, acetic acid is reacted with methanol to produce methyl acetate and water and the reaction is reversible. Therefore, conversion of the reaction is limited by the concentration of products. In order to, control the reaction in forward direction, removal of methyl acetate and water from the system is important. Accordingly, separation process will play important role. Reactive distillation can be used in this reaction and separation process. In this case, products and reactants can be separated by distillation process

according to their boiling points.

In this study, effect of feed stage of reactant, acetic acid, was studied in semi-batch reactive distillation using process simulation in order to find optimal feed stage of reactant, where the operation gave high yield of methyl acetate with short operating time and purity of commercial standard.

METHODOLOGY

Semi-batch reactive distillation simulation model was created on Aspen Batch Distillation V7.3 software following a specification of an in-house made column at King Mongkut's University of Technology North Bangkok. The column comprised of seven stages, including reboiler, condenser and reactive zone. The column made from stainless steel 316 with inside diameter and height of 11.43cm and 90cm, respectively. In a simulation model, methanol was charged at the stage seven, reboiler, while acetic acid was fed continuously to the column at stage two to stage six according to the case study. Methyl acetate product was withdrawn from the system at reboiler.

Four specifications were assigned to the model consisting of component specifications, column specifications, reaction data and step operation. The column configuration shows in Figure.1 was created and used for a simulation. The esterification reaction was assigned to occur between stages two to stage six. Reaction data of the esterification reaction used in this study was heterogeneous reaction of acetic acid with methanol proposed by Yu-Ting Tsai, 2011 [3].

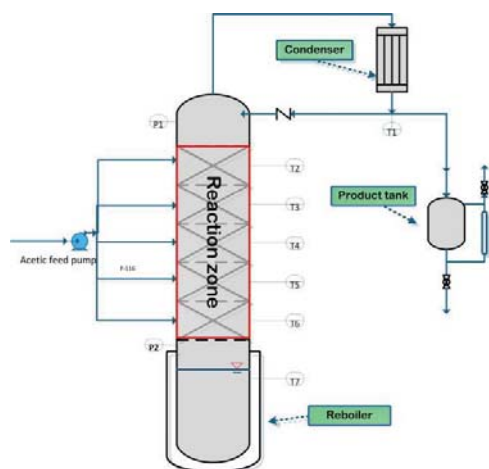


Figure 1. Reactive distillation column model for esterification of acetic acid and methanol

Acetic acid and methanol were fed with 1:1 mole ratio according to stoichiometry giving five liters of methanol charged at reboiler and total acetic acid approximately seven liters fed continuously at the rate of 115ml/min. Temperature of heating media at reboiler was set at 120°C, while at condenser, coolant temperature was set at 20°C. The column was operated with total reflux for 0.5hr, then distilled product was collected continuously at from top stage at product tank with reflux rate of 200mole/hr. The semi-batch reactive distillation process simulation was terminated when amount of methanol in reboiler was lower than 1mol%.

RESULTS AND DISCUSSION

The effect of changing the feed location of acetic acid on methyl acetate yield (total moles of methyl acetate in product tank/mole of acetic acid fed) was shown in Table 1. The feed stage of acetic acid at stage 5 gave the maximum methyl acetate yield at operating time about 0.80 hr.

Table 1. Maximum yield of methyl acetate for case studies.

Feed stage of acetic acid	Operating time (hours)	% Yield by mole
Stage2	0.82	77.48
Stage3	0.81	79.40
Stage4	0.81	80.60
Stage5	0.80	81.21
Stage6	0.79	78.56

Figure 2 showed effect acetic acid feed location on the purity of product as the mass fraction of methyl acetate. From the maximum yield (81.21% mole) and the highest purity (0.96 mass

fraction) of methyl acetate indicate that the optimum feed stage of acetic acid was stage five.

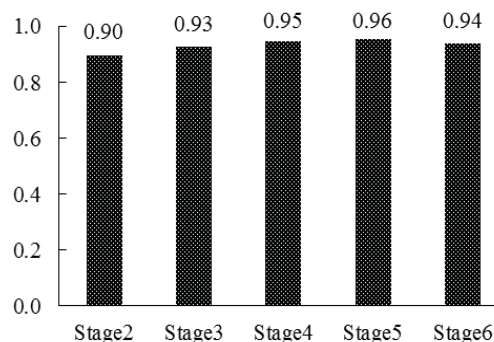


Figure 2. Mass fraction of methyl acetate at product tank

ACKNOWLEDGMENT

The author would like to thank Graduate College and Development Centre for Chemical Engineering Unit Operation and Catalyst Design, King Mongkut's University of Technology North Bangkok for the financial support and their valuable comments.

References

- [1] M.N. Murat, A.R. Mohamed and S. Bhatia, "Modeling of a reactive distillation column: Methyl tertiary butyl ether (MTBE) simulation studies", *IJUM Engineering Journal*, **4**, 2003, pp.13-30.
- [2] <http://www.eastman.com/Pages/ProductHome.aspx?product=71001121>, access on 9th March 2015
- [3] Tsai, Y.-T., H.-m. Lin, et al. "Kinetics behavior of esterification of acetic acid with methanol over Amberlyst 36.", *Chemical Engineering Journal*, **17**, 2011, pp.1367-1372.

INVESTIGATION OF Al_2O_3 NANOFLUID VISCOSITY FOR DIFFERENT WATER/EG MIXTURE BASED

K. AbdulHamid¹, W. H. Azmi¹, Rizalman Mamat¹, N. A. Usri¹ and G Najafib²

¹Faculty of Mechanical Engineering, Universiti Malaysia Pahang, Malaysia

²Department, Tarbiat Modares University, Iran

SUMMARY: Viscosity of Al_2O_3 nanoparticle dispersed in mixture of water and ethylene glycol (EG) were investigated experimentally. The effect of based fluid ratio (water:EG) to nanofluid viscosity was investigated. Nanofluids with volume concentration up to 2.0 % were prepared with 13 nm Al_2O_3 nanoparticles for viscosity measurement. Two-step method were used in preparation of Al_2O_3 nanoparticles suspended in three ratios of water:EG by percent volume which are 40:60, 50:50 and 60:40. The measurements of viscosity were performed using Brookfield LVDV III Ultra Rheometer for working temperature of 30 to 70 °C. Viscosity of nanofluids were observed to be affected by ethylene glycol concentration in the base fluid, nanofluid concentration and temperature. Maximum enhancement of viscosity nanofluid was shown at low temperature with EG concentration at 60 % in base fluid. Viscosity of nanofluid decreases with increases of temperature but increase with nanoparticles concentration and ethylene glycol.

Keywords: nanofluid; aluminium oxide; viscosity; water:EG mixture

INTRODUCTION

In the present study, three mixture ratio of water and ethylene glycol (EG) was prepared by considering the application of using EG in coolant for automotive cooling system. Researches have investigated the effect of different nanomaterials on viscosities.

A study on effect of base fluid and temperature to heat transfer characteristics found that the efficiency of nanofluids improves with increasing in the temperature [1]. The efficiencies are higher for nanofluids suspension mixture base compare to water based. They used SiC nanoparticles dispersed in ethylene glycol-water mixture in volume ratio of 50:50 in their investigation. A study was initiated by Sundar et al. [2] with Fe_3O_4 nanoparticles dispersed in three mixture of ethylene glycol/water ratio (60:40, 40:60 and 20:80). They observed that 1.0 % volume concentration nanofluid in 60:40 EG/W is enhanced by 2.94 % compared to other based fluids. Another mixture base fluid used in investigation is 55:45 (W:EG) [3]. They found that the temperature and volume concentration significantly affect the nanofluid viscosity. Also, the nanofluids exhibit Newtonian behaviors below 45 °C. Aluminium oxide nanofluids in mixture base was studied by Said et al. [4] for ratio of water:EG 40:60. The same behavior notice where the nanofluids exhibits Newtonian behavior for low concentration below 40 °C [3].

The objective of this study is to provide more viscosity data for nanofluids dispersed in various ratio of water-EG mixture. Investigation on this rheological properties is very important to expand the application of nanofluids that use addition of EG in the coolant. The selection of alumina nanoparticle in 13 nm sized is due to its stability period that withstand up to three months.

METHODOLOGY

Nanofluid Preparation

Nanoparticle used in the sample preparation is 13 nm aluminium oxide (Al_2O_3) in powder form. Three mixture ratio of water to ethylene glycol used are 40:60, 50:50 and 60:40 as the base fluid. Two-step method was used in the preparation of nanofluid. Ultrasonication process was employed to help improve the dispersion of nanoparticles in the base fluid.

Viscosity Measurement

Viscosity measurement was done using Brookfield LVDV III Ultra Rheometer. Nanofluid sample was heated at temperature range 30 to 70 °C and measured for its viscosity. Figure 1 shows the arrangement of sample nanofluid in rheometer during measurement.

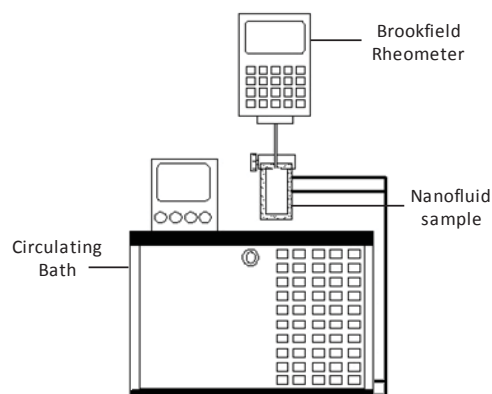


Figure 1. Viscosity measurement

RESULTS AND DISCUSSION

The measurement of nanofluid is initially started with base fluid. Figure 2 shows the distribution of base fluid measurement data, compared to ASHRAE Handbook [5]. Previous studies that use the same procedure are Kulkarni et al. [6] and Vajjha et al. [7].

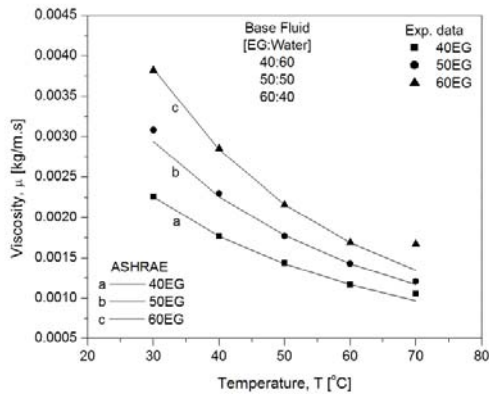


Figure 2. Benchmark test for various mixture base fluid

The results from the measurement of nanofluids in three different base fluids indicate the same trends of viscosity as follow. The viscosity of nanofluids are higher than the base fluid. As the concentration increase, the viscosity also increases. However, the viscosity decreases as the temperature increase. Figure 3 represent the viscosity of Al_2O_3 nanofluid at concentration 1.0 % in all three base fluids.

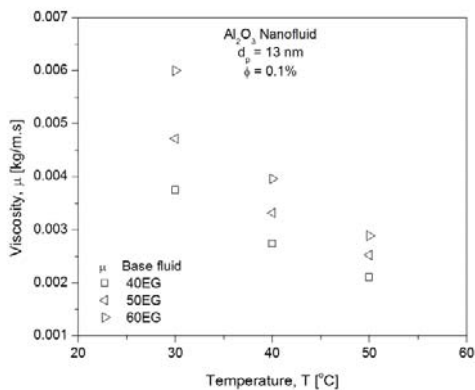


Figure 3. Comparison of nanofluid viscosity at 1.0 % concentration for three base fluids

ACKNOWLEDGMENT

The authors would like to be obliged to Universiti Malaysia Pahang for providing laboratory facilities and financial assistance under project no. RDU1403110.

References

- [1] E.V. Timofeeva, W. Yu, D.M. France, D. Singh, J.L. Routbort, "Base fluid and temperature effects on the heat transfer characteristics of SiC in ethylene glycol/H₂O and H₂O nanofluids", *Journal of Applied Physics*. **109**, 2011, pp. 14914-014914-5.
- [2] L. Syam Sundar, E. Venkata Ramana, M.K. Singh, A.C.M. De Sousa, "Viscosity of low volume concentrations of magnetic Fe₃O₄ nanoparticles dispersed in ethylene glycol and water mixture", *Chemical Physics Letters*. **554**, 2012, pp. 236-242.
- [3] W. Yu, H. Xie, Y. Li, L. Chen, Q. Wang, "Experimental investigation on the heat transfer properties of Al₂O₃ nanofluids using the mixture of ethylene glycol and water as base fluid", *Powder Technology*. **230**, 2012, pp. 14-19.
- [4] Z. Said, M.H. Sajid, M.A. Alim, R. Saidur, N.A. Rahim, "Experimental investigation of the thermophysical properties of Al₂O₃-nanofluid and its effect on a flat plate solar collector" *International Communications in Heat and Mass Transfer*. **48**, 2013, pp. 99-107.
- [5] *ASHRAE Handbook 2009 - Fundamentals* (SI Edition). American Society of Heating, Refrigerating and Air-Conditioning Engineers, Inc. 2009.
- [6] D.P. Kulkarni, P.K. Namburu, H. Ed Bargar, D.K. Das, "Convective Heat Transfer and Fluid Dynamic Characteristics of SiO₂ Ethylene Glycol/Water Nanofluid" *Heat Transfer Engineering*. **29**, 2008, pp. 1027-1035.
- [7] R.S. Vajjha, D.K. Das, D.P. Kulkarni, "Development of new correlations for convective heat transfer and friction factor in turbulent regime for nanofluids" *International Journal of Heat and Mass Transfer*. **53**, 2010, pp. 460-4618.

A STUDY OF TRANSIENT PERFORMANCE OF A CASCADE HEAT PUMP SYSTEM

Piman Nenkaw¹ and Chittin Tangthieng¹

¹Department of Mechanical, Faculty of Engineering, Chulalongkorn University, Thailand

SUMMARY: This paper presents transient state of a cascade heat pump system. The cascade system consists of 2 cycles as follow; Low temperature cycle provided chilled water to received heat from cooling room and high temperature cycle recovered condensation heat to make hot water. Moreover, hot water was reheated consecutively and then affected to cascade heat pump system to vary operating point. When experiment began, hot water temperature rose continuously. And then, as water temperature came into water cool condenser increased, condensing pressure of high temperature cycle was also increased. But the others pressure process was almost constant all the time. So compressor power of heat pump cycle also increased. On the other hand compressor power of refrigeration cycle was constant as mention. Cooling load and condensation heat increased dramatically at the first time, and then cooling load slightly decreased but condensation heat increased continuously. Results show that changing in high temperature cycle did not influence to low temperature cycle.

Keywords: cascade heat pump system, transient state, hot water, chilled water, water cool condenser

INTRODUCTION

Energy crisis such as increment of energy demand, global warming and climate change from energy overconsumption is one of the most advertent topics nowadays. Recovery energy from operating system is a way that reduces intensity of those problems. A sample of system that can recover energy is refrigeration system. Refrigeration system often leaves waste heat from cooling location to ambient. Refrigerating system that reuses waste heat might be called heat pump.

Most building usually needs both heating and cooling. So if waste heat from refrigeration system is recovered to be used, it will save cost and increases energy efficiency. The easy and interesting way is to make hot water from recovery system. Because buildings such as home, hospital and hotel often need both cooling and heating especially countries around equator like Thailand, making hot water from condenser heat instead of heater can reduce energy consumption and increase refrigeration system efficiency. Shuangquan et al. [1] modified home air conditioner to make hot water by condenser heat. This system was run along with normal system that generated hot water from heater. After 1 year experiment, COP of new system was 10% and 90% more than old system in winter and summer respectively. Furthermore, energy cost for all year round was 31.1% less than old system.

However maximum hot water is limited due to the fact that condenser heat was depended on cooling load and condensing temperature. So, it should use more than 1 cycle to make hotter water. Cascade refrigeration system or cascade heat pump is a cooperate system that two cycles refrigeration system operate together in series. So condenser heat is boosted up to higher temperature and water can reach higher temperature. But there are many disadvantages of cascade system such as higher compressor power, complex system and few experimental studies. Bhattacharyya et al. [2]

studied cascade system performance and analyzed parameters that effected to system. From study found that system performance was dependent on evaporating temperature of low temperature cycle, condensing temperature of high temperature cycle and temperature differentiation of high and low cycle in cascade heat exchanger. COP of low temperature cycle was directly proportional to evaporating temperature and COP of high temperature cycle was indirectly proportional to condensing temperature. In addition, effects of one cycle didn't influence to another cycle. Jung et al. [3] compared performance between heat pump system and cascaded heat pump system. From experiment, hot water temperature form cascade system was higher than heat pump system. Furthermore, effects of changing operating temperature of one cycle did not influence to another cycle.

The objective of this paper is to study transient performance of a cascade heat pump by experiment. Working conditions of system were varied all the time by hot water. This paper shows how system was changed by varying both hot water flow rate and temperature.

PROTOTYPE OF CASCADE HEAT PUMP

Fig.1 shows a configuration of prototype of cascade heat pump. Prototype was composed of 4 cycles: chilled water cycle, R-22 low temperature cycle, R-134a high temperature cycle and hot water cycle. Chilled water took heat from cooling room and transfer to low temperature cycle at evaporator. Then, heat was transferred to high temperature cycle through cascade heat exchanger. Finally, heat was transferred to hot water cycle at water cool condenser. This paper considers only transient state. Water from hot water storage tank was pumped through hot water pump to receive heat at condenser and came back to hot water tank. Then, hot water cycle continued pumping water, so water

temperature in tank was raised continuously and system had operated until limit of system because of elevated working pressure and discharge compressor temperature. And then, varied hot water flow rate from 4 L/min to 16 L/min to test how system working was changed.

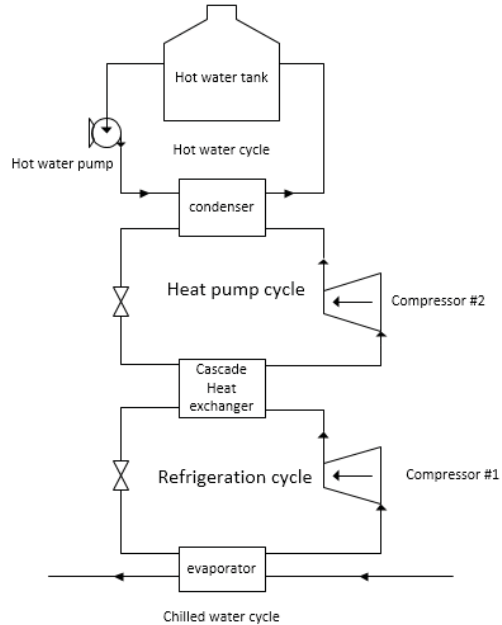


Figure 1. configuration of cascade heat pump

RESULT AND DISCUSSION

At beginning, water temperature in hot water tank slightly rose and then rose consecutively at constant rate. So it affected to cascade heat pump system that operating point was changed as follow. At every hot flow rate, cooling load, condensation heat, R22-compressor power and R134a-compressor power varied as shown in fig.2. Cooling load and condensation heat dramatically rose at the beginning. Then cooling load reached max value and decreased slowly, but condensation heat continued a bit increasing. R22-compressor power varied at the first time, and then was almost constant all the time. R134a-compressor power increased slightly as same as condensation heat.

Moreover, Pressure of refrigerant in each process shows in fig.3. Condensing pressure of high temperature cycle rapidly increased in the beginning, and then almost constantly increased. But evaporating pressure decreased and then slightly increased. Condensing pressure of low temperature cycle varied around a constant value and then almost constant at operating pressure. Evaporating pressure decreased and then constant like as high pressure.

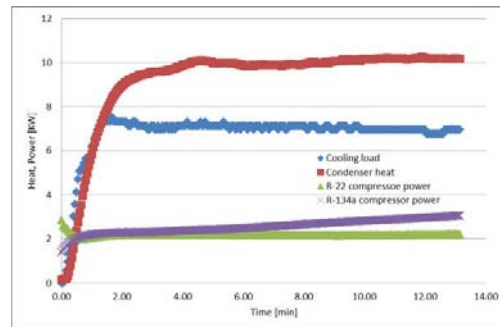


Figure 2. Cooling load, condenser heat, R22-compressor power and R-134a compressor power vs. time

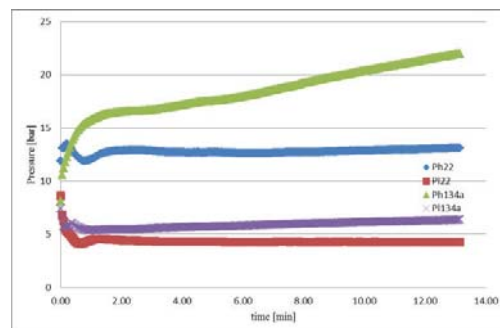


Figure 3. Pressure of each process in cascade heat pump of hot water flow rate 4L/min vs. time

As describe in fig. 2 and 3 can conclude that when heat pump system operated and was influenced by changing of hot water at condenser, the effect didn't impact to low temperature cycle. So, cooling load was almost constant.

ACKNOWLEDGEMENT

The authors would like to thanks faculty of engineering, Chulalongkorn University for their supporting financial and laboratory.

Reference

- [1] S. Shuangquan, S. Wenxing, L. Xianting, M. Jie. "A new inverter heat pump operated all year round with domestic hot water", *Energy Conversion and Management*, **45**, 2004, pp. 2255-2268.
- [2] S. Bhattacharyya, A. Garai and J. Sarkar, "Thermodynamic analysis and optimization of a novel N₂O-CO₂ Cascade system for refrigeration and heating", *International Journal of Refrigeration*, **32**, 2009, pp. 1077-1084.
- [3] H.W. Jung, H. Kang, W. J. Yoon and Y. Kim "Performance comparison between a single-state and a cascade multifunctional heat pump for both air heating and hot water supply", *International Journal of Refrigeration*, **36**, 2013, pp. 1431-1441.

SWIRL FLOW IN A DIFFUSER FITTED WITH HELICAL SCREW-TAPE WITH AND WITHOUT CENTERED ROD

Ehan Sabah Shukri¹ and Wirachman Wisnoe²

¹Middle Technical University, Baghdad, Iraq
Institute of Technology Baghdad
Faculty of Machinery and Equipment, Baghdad, Iraq
²Universiti Teknologi MARA
Faculty of Mechanical Engineering, Selangor, Malaysia

SUMMARY: Temperature performance investigation in a conical diffuser fitted with helical tape with and without centered rod is studied numerically. A helical tape is inserted in the diffuser to create swirl flow that helps to increase the thermal rate with Reynolds number 4.2×10^4 . Three pitch ratios ($P/L = 0.153, 0.230$ and 0.307) for the helical tape with and without centered rod are simulated and compared. The geometry of the diffuser and the inlet condition for both arrangements are kept constant. Numerical findings of these simulations are that the helical tape inserts without centered rod perform significantly better than the helical tape inserts with centered rod through the diffuser.

Keywords: CFD, diffuser, helical tape, heat transfer, pitch ratio

INTRODUCTION

Device with divergent area called diffuser. It can be seen in many fluid applications. It maximizes static pressure recovery while minimizing total pressure loss along the direction of the flow by converting Kinetic energy into pressure energy. It is widely used in gas turbines, pumps, fans, wind tunnels, etc. Different methods are used to increase the heat transfer rate through the force convection include swirl generators. These types of generators create circular and helical motion that can force the heat to distribute in different directions. Swirl can be created by different methods such as helical screw-tape [1, 2] and helical tape [3, 4].

The principle of heat transfer enhancement in the core flow of tube with helical screw-tape inserts was studied by Zhang et al. [1]. The aim was to improve the temperature uniformity and to reduce the flow resistance. The simulation results showed that the average overall heat transfer coefficients in circular plain tubes were enhanced with helical screw-tape of different widths by as much as 212-351%. Eiamsa-Ard and Promvong [2] investigated the enhancement of heat transfer in a double tube heat exchanger fitted with helical screw tape with and without core-rod. It was found that the full-length helical tape with core-rod enhanced heat transfer rate at about 10% better than that without core rod but considerably higher friction loss. Gül et al. [3] found that an increase of heat transfer rate up to 20% could be achieved by the insertion of a short helical tape placed at the entrance of a circular tube.

This work presents numerically the effect of helical tape with and without centered rod on the temperature performance.

NUMERICAL METHODOLOGY

Diffuser with helical tape geometry with / without centered rod

The diffuser and the helical tape with centered

rod geometries represented in Figure 1. The tested diffuser has 48 mm inlet diameter, 145 mm outlet diameter and 140 mm length. The helical tape inserts has the geometric dimensions of ($W = 20$ mm) with centered rod diameter ($d = 5$ mm), and thickness of ($t = 1$ mm). The test was conducted with three different pitches ($P = 20, 30$, and 40 mm). The helical tape geometries are the same the only difference that there is no centered rod. Three different pitch ratios ($P/L = 0.153, 0.230$ and 0.307) are simulated for both arrangements.

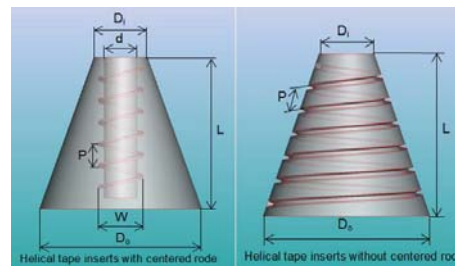


Figure 1. Helical tape inserts with and without centered rod

Computational model

The numerical analyses were performed in three dimensional domains applying standard $k-\epsilon$ model as a turbulence model.

Standard $k-\epsilon$ turbulence model is allowed to predict the heat transfer and fluid flow characteristics.

Heat source

For this study, a spherical heat source of 10 kW with the radius of 0.005 m is put in the diffuser at the beginning of the helical tape inserts. The unsymmetrical location is purposely chosen in order to better observe the swirling motion.

RESULTS AND DISCUSSIONS

Heat transfer is numerically obtained for a diffuser fitted with helical tape with and without centered rod. Results will be discussed for one cutting section along the radial direction of a diffuser at the outlet to investigate the temperature performance.

Effect of different helical tape pitch on temperature performance

Results are respectively shown in Figures 2, 3 and 4. For one cutting sections (outlet section), mentioned figures reveal the effect of different helical tape pitches on the heat transfer rate for temperature range from 450 K (dark blue) to 3500 K (red).

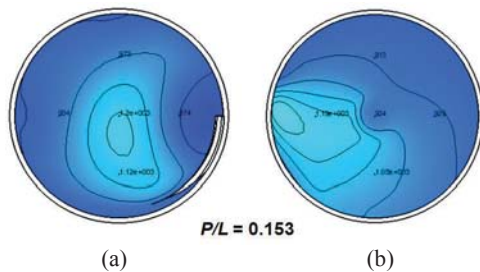


Figure 2. Temperature distribution in a diffuser fitted with (a) helical tape, (b) helical tape with centered rod for pitch ratio = 0.153

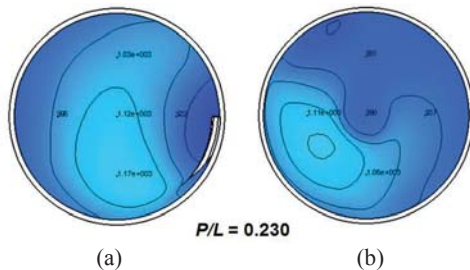


Figure 3. Temperature distribution in a diffuser fitted with (a) helical tape, (b) helical tape with centered rod for pitch ratio = 0.230

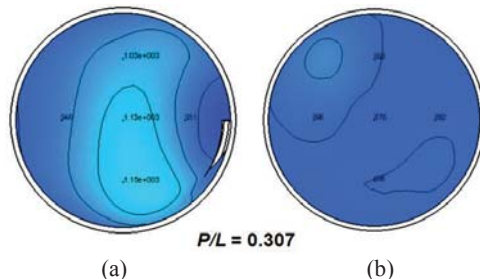


Figure 4. Temperature distribution in a diffuser fitted with (a) helical tape, (b) helical tape with centered rod for pitch ratio = 0.307

From figures 2, 3 and 4 can be observed that temperature will distributed in different direction during the flow. This distribution is due to the helical tape insertion.

Temperature will distribute almost in the same way and same rate in the helical tape without centered rod for the three pitches as shown in (a) for three Figures (2, 3 and 4). Results of diffuser fitted with helical tape with centered rod indicate that temperature will not uniformly distributed as shown in (b) for the three Figures (2, 3 and 4).

CONCLUSION

In the propose study conclusion has been made according to numerical simulation results for two different geometric helical tape positions. They include simulation results of temperature distribution in a diffuser fitted to a helical tape with and without centered rod for different pitch ratios. Therefore the following conclusions can be made from the numerical simulation study:

1) The results show clearly that temperature distribution depend on the existence of the helical tape. Since the temperature will follow helical and circular motion due to the present of helical tape insert.

2) Helical tape without centered rod inserts show temperature distribution but no changes in values have been indicated.

3) Helical tape with centered rod inserts observes ununiformed temperature distribution.

References

- [1] X. Zhang Z. Liu and W. Liu, "Numerical studies on heat transfer and friction factor characteristics of a tube fitted with helical screw-tape without core-rod inserts", *International Journal of Heat and Mass Transfer*. **60**, 2013, pp. 490–498.
- [2] S. Eiamsa-Ard and P. Promvonge, "Heat transfer characteristics in a tube fitted with helical screw-tape with/without core-rod inserts", *International Communications in Heat and Mass Transfer*. **34**, 2007, pp. 176–185.
- [3] H. Gül and D. Evinb, "Heat transfer enhancement in circular tubes using helical swirl generator inserts at the entrance", *International Journal of Thermal Science*. **46**, 2007, pp. 1297-1303.
- [4] E. S. Shukri and W. Wisnoe, "Temperature distribution simulation of divergent fluid flow with helical arrangement", *International Journal of Mechanical, Aerospace, Industrial and Mechatronics Engineering*. **8**, 2014, pp.1469-1472.

SWIRL FLOW STUDY IN AN ANNULAR DIFFUSER FITTED WITH DIFFERENT GEOMETRIC HUB INSERT

Ehan Sabah Shukri¹, Wirachman Wisnoe² and Ramlan Zailani²

¹Middle Technical University, Baghdad, Iraq

Institute of Technology Baghdad

Faculty of Machinery and Equipment, Baghdad, Iraq

²Universiti Teknologi MARA

Faculty of Mechanical Engineering, Selangor, Malaysia

SUMMARY: Influence of swirl flow in an annular diffuser on the temperature distribution is numerically presented. The swirling flow devices consisting of different geometric hubs include pimples hub, helical tape hub and twisted rectangular hub are simulated and compared. The annular diffuser geometries are kept constant with (inner, outer, hub) diameter and length of 48 mm, 140 mm, 30 mm and 140 mm respectively. The numerical simulations for swirl flow have been performed by the different hub arrangements for the Reynolds number 4.2×10^4 and pitch distance ($y = 20$ mm). The analysis is carried out using CFD software with $k-\epsilon$ as a turbulence model. The findings reveal clearly that the three types of hubs will promote the temperature distribution due to the creation of circular and helical motion, however the numerical findings obtain that the best temperature distribution is obtained when the annular diffuser is fitted with pimples hub and helical tape hub.

Keywords: Swirl flow, diffuser, helical tape, height ratio, CFD

INTRODUCTION

Diffusers are divergent flow passages that decelerate a stream of gas or liquid from a high to a low velocity and regain pressure. They play an important role in many fluid machines to convert kinetic energy into pressure energy. They are extensively used in compressors, gas turbines, pumps, fans, wind tunnels, etc. In thermal application heat distribution need to be promoted, such as combustion process. Swirl generators are used for this goal. Due to the importance of internal swirl flow on heat distribution, Sivashanmugam and Suresh [1, 2 and 3] presented a survey on heat transfer enhancement using a circular tube fitted with full-length helical screw element. It was observed that this configuration was very effective for heat transfer enhancement. The heat transfer was augmented without much increase in pressure drop by using spaced helical screw inserts. In a more recent study Zhang et al. [4] who also studied the principle of heat transfer enhancement in the core flow of tube with helical screw-tape inserts confirmed this findings. Eiamsa et al. [5 and 6] studied experimentally different arrangements equipped with twisted tape. The effect of the co-swirl flow and the counter swirl generators through a round tube fitted with helical screw tape and twisted tape has been experimentally tested [5]. The result showed that heat transfer with the combined tapes in counter-swirl arrangement was 3.4% and 10% higher than those in co-swirl arrangement and helical tape alone. Furthermore, he studied the twin counter twisted tapes and twin co twisted tapes as co-swirl flow generators in a test section with four different twist ratios ($y/w = 2.5, 3.0, 3.5$ and 4.0) for Reynolds numbers range between 3700 and 21,000 under uniform heat flux conditions [6].

This work presents numerically the effect of different geometrics hub fitted to an annular diffuser on the temperature distribution. The different geometric hubs are pimples hub, helical tape hub and twisted rectangular hub.

GEOMETRIC MODEL

The simulation studies were conducted with three different hub geometrics inserts clarified in Figure 1 having pitch distance $y = 20$ mm for the Reynolds number 4.2×10^4 .

Annular diffuser geometrics are kept constant with inner diameter, outer diameter, hub diameter and length of 48 mm, 145 mm, 30 mm and 140 mm respectively.

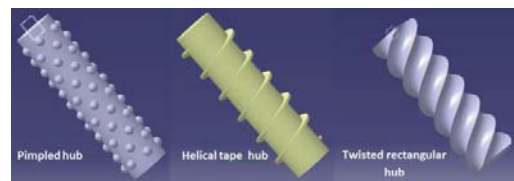


Figure 1. Different hub geometries

NUMERICAL MODEL

Numerical study of temperature distribution inside an annular diffuser equipped with different geometrics hub is performed in the present work. The commercial software Numecca Fine/Open v.3.1 is chosen as the Computational Fluid Dynamics (CFD) tool applying standard $k-\epsilon$ model as a turbulence model for this work.

Heat source

A spherical heat source of 10 kW with the radius of 0.005 m is put in the diffuser at the

beginning of the helical tape inserts. The unsymmetrical location is purposely chosen in order to better observe the swirling motion.

COMPUTATIONAL RESULTS AND DISCUSSIONS

Temperature distribution is numerically performed for an annular diffuser fitted with pimped hub, helical tape hub and twisted rectangular hub. Results discussed for three cutting section along the radial direction of a diffuser includes section 1-1 at 30 mm, section 2-2 at 70 mm and section 3-3 at 110 mm from the inlet as shown in Figure 2.

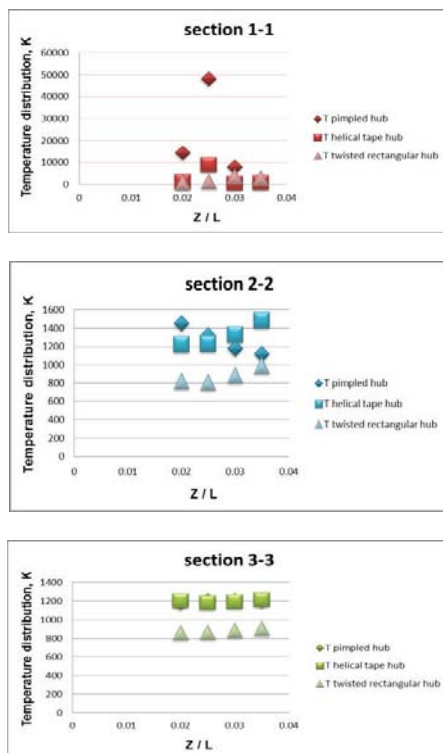


Figure 2. Temperature distribution in three cutting sections

In section 1-1 the temperature started to distribute due to the insertion of the different turbulators. In section 2-2 obtained clearly that the temperature start to distribute uniformly through the section. In section 3-3 near the outlet, temperature shown better distributed in pimped hub and helical tape hub.

Figure 3. reveal the distribution of the temperature near the wall for the three different geometric hubs. It represent the temperature behavior from the inlet until the outlet for three cutting sections.

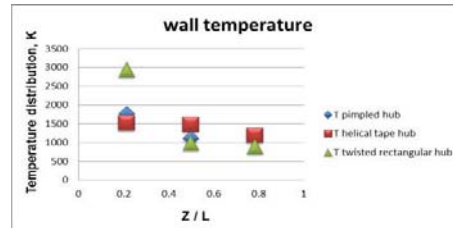


Figure 3. Wall temperature distribution

CONCLUSION

Temperature distribution of different geometric hubs in an annular diffuser were investigated numerically. The simulations were performed for the annular diffuser fitted pimped hub, helical tape hub and twisted rectangular hub. The use of pimped hub and helical tape hub inserts provide significant augmentation of temperature distribution.

References

- [1] P. Sivashanmugam and S. Suresh, "Experimental studies on heat transfer and friction factor characteristics of turbulent flow through a circular tube fitted with regularly spaced helical screw tape inserts", *Applied Thermal Engineering*. **27**, 2007, pp. 1311–1319.
- [2] P. Sivashanmugam and S. Suresh, "Experimental studies on heat transfer and friction factor characteristics of laminar flow through a circular tube fitted with regularly spaced helical screw tape inserts", *Experimental Thermal and Fluid Science*. **31**, 2007, pp.301–308.
- [3] P. Sivashanmugam and S. Suresh, "Experimental studies on heat transfer and friction factor characteristics of turbulent flow through a circular tube fitted with helical screw-tape inserts", *Chemical Engineering and Processing*. **46**, 2007, pp. 1292–1298.
- [4] X. Zhang Z. Liu and W. Liu, "Numerical studies on heat transfer and friction factor characteristics of a tube fitted with helical screw-tape without core-rod inserts", *International Journal of Heat and Mass Transfer*. **60**, 2013, pp. 490–498.
- [5] S. Eiamsa-ard, K. Yongsiri, K. Nanan and C. Tianpong, "Thermo hydraulic of co/counter swirl flow through a round tube fitted with helical screw tape and twisted tape", *Indian Journal of Chemical Technology*. **20**, 2013, pp. 145-155.
- [6] S. Eiamsa-ard, C. Tianpong and P. Eiamsa-ard, "Turbulent heat transfer enhancement by counter/co-swirling flow in a tube fitted with twin twisted tapes", *Experimental Thermal and Fluid Science*. **34**, 2010, pp. 53–62.

THERMAL CONDUCTIVITY ENHANCEMENT OF Al_2O_3 NANOFLUID IN ETHYLENE GLYCOL AND WATER MIXTURE

Nur Ashikin Usri¹, W. H. Azmi¹, Rizalman Mamat¹, K. Abdul Hamid¹ and G. Najafib²

¹Faculty of Mechanical Engineering, Universiti Malaysia Pahang, Malaysia

²Biosystems Engineering Department, Tarbiat Modares University, Iran

SUMMARY: The ability of nanofluids that exhibits enhanced thermal performance is acknowledged by researchers through studies since decades ago. However, the observation of thermal properties for nanofluids in water and ethylene glycol based is not fully explored yet. Hence, this paper presents the thermal conductivity of water and ethylene glycol (EG) based Al_2O_3 nanofluid. The 13 nm sized Al_2O_3 nanoparticles were dispersed into three different volume ratio of water:EG such as 40:60, 50:50 and 60:40 using two-step method. The measurement of thermal conductivity was performed using KD2 Pro Thermal Properties Analyzer at working temperature of 30 to 70 °C for volume concentration 0.5 to 2.0 %. The results indicate that the thermal conductivity increases with the increase of nanofluid concentration and temperature. The measurement data of the nanofluids give maximum enhancement of thermal conductivity at condition 1.5 % volume concentration, temperature of 70 °C and base fluid 60: 40 % (W/EG).

Keywords: nanofluid, aluminium oxide, thermal conductivity enhancement, water:EG mixture

INTRODUCTION

Thermal fluids are vital to remove excess heat from a system or assist heating process in industrial field such as electronic engineering, medical, automotive and HVAC. Thus, thermal conductivity of fluids act as the main properties to be apprehensive in developing an energy efficient heat transfer equipment. Nevertheless, commercialized fluids have low properties i.e. thermal conductivity compare to solids materials. In the early years of 1990's, Masuda et al. [1] introducing suspended nanometer sized particles to the research field and found out that nanometer size particles have higher stability when suspended in conventional fluid than micrometer and millimeter size particles. Research team at Argonne National Laboratory of USA, Choi [2] termed the suspended nanometer size particle as "Nanofluids" conducted investigation of nanofluid thermal ability. As the next generation of thermal fluids, researchers conducted a deeper study on the effective thermal conductivity of nanoparticles suspended in a liquid to understand the nature of nanofluids.

In the first study of combining water and ethylene glycol, Vajjha and Das [3] found out that suspending nanoparticles in the mixture increased thermal conductivity compare to base fluid. This increment is also found by Tadjarodi et al. [4] which conducted measurement for nanoparticles suspended in 60 % of ethylene glycol and 40 % of water by volume percentage.

Hence, this paper intended to measure thermal conductivity of Al_2O_3 nanofluid using three different mixture ratio solutions of water and ethylene glycol as base solution. The experiment is conducted using 13 nm Aluminum Oxide (Al_2O_3) dispersed in 60:40, 50:50 and 40:60 (water: ethylene glycol) mixture base solution. The temperature is varied between 30 to 70 °C using KD2 Pro Thermal Analyzer and controlled water bath.

EXPERIMENTAL SETUP

Preparation of Nanofluid

The Al_2O_3 nanofluid used in the present paper are prepared using two step method which is dispersing 13 nm Al_2O_3 nanopowder in the base fluids. The powder nanoparticles is purchased from Sigma-Aldrich with 99.8 % purity. The density value of Al_2O_3 nanoparticle provided by the manufacturer is 4000 kg/m³. The base fluid is prepared using distilled water and ethylene glycol following designated ratio based by volume percentage which are 40:60, 50:50 and 60:40. Ethylene glycol (EG) has density of 1100 kg/m³ with AR grade (99.5 % purity).

Thermal Conductivity Measurement

There are several technique have been adopted to measure thermal conductivity of nanofluid such as transient hot-wire method (THW), steady-state parallel-plate method and cylindrical cell method [5]. This paper utilized thermal constant analyzer technique to measure thermal conductivity of Al_2O_3 nanoparticles dispersed in different base ratio water to ethylene glycol (60:40, 50:50 and 40:60) as in Figure 1. A KD2 Pro Thermal Property Analyzer manufactured by Decagon Devices, Inc., USA is used to measure the thermal conductivity based on THW theory. The KD2 Pro consists of a handheld controller and 60 mm sensors that is inserted into the test medium. The measurement is conducted under controlled temperature ranging from 30 to 70 °C using a Memmert water bath. The measurements are taken after 5 minutes immersed in the water bath to ensure the temperature is stable. Each readings are taken with 15 minutes interval time until 20 readings to avoid experimental error. The average value is collected after completed one set of data.



Figure 1. Thermal Conductivity measurement setup using thermal constant analyzer technique

RESULT AND DISCUSSION

Before conducting the nanofluids measurement, the experiment setup and method is established by performing measurement for base fluid at different ratio of W:EG (60:40, 50:50, 40:60) in temperature range of 30 to 70 °C. Figure 2 shows the measured thermal conductivities compare to available literature. Thus, the present measurement is in good agreement with both literature with deviation less than 0.1 %

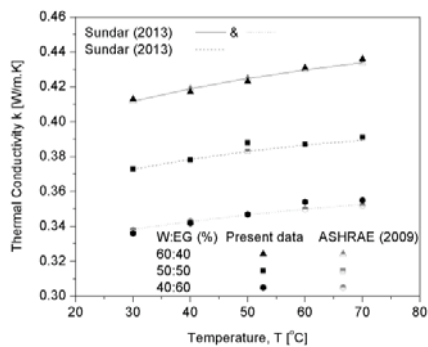


Figure 2. Validation of thermal conductivity measurement for water to ethylene glycol mixture

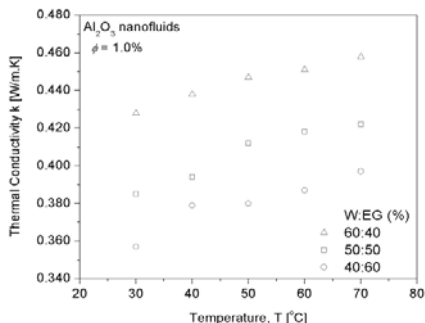


Figure 3. The thermal conductivity of Al₂O₃ nanofluid at 1.0 % in three base fluids

The present data for nanofluids in different base ratio of water (W) to ethylene glycol (EG) propagates higher than base fluids with similar pattern. This shows that suspending nanoparticles in the base fluid enhance the thermal conductivity. Figure 3 display as temperature increase, the thermal conductivity showing an increment pattern.

ACKNOWLEDGMENT

The financial support and laboratory facilities by Universiti Malaysia Pahang under RDU1403110 are gratefully acknowledged.

References

- [1] H. Masuda, A. Ebata, K. Teramae, and N. Hishinuma, "Alteration of Thermal Conductivity and Viscosity of Liquid by Dispersing Ultra Fine Particles", *Netsu Bussei*. **4**, 1993, pp. 227–233.
- [2] U. S. Choi, "Enhancing Thermal Conductivity of Fluids With Nanoparticles, in Developments and Applications of Non-Newtonian Flows". FED-vol. 231/MD-Vol. 66,
- [3] D. A. Siginer and H. P. Wang, Eds., ed New York: "American Society of Mechanical Engineers (ASME)", 1995, pp. 99–105.
- [4] R. S. Vajjha and D. K. Das, "Experimental determination of thermal conductivity of three nanofluids and development of new correlations", *International Journal of Heat and Mass Transfer*. **52**, 2009, pp. 4675-4682.
- [5] Tadjarodi, F. Zabihi, and S. Afshar, "Experimental investigation of thermo-physical properties of platelet mesoporous SBA-15 silica particles dispersed in ethylene glycol and water mixture", *Ceramics International*. **39**, 2013, pp. 7649-7655.
- [6] G. Paul, J. Philip, B. Raj, P. K. Das, and I. Manna, Synthesis, "Characterization and thermal property measurement of nano-Al₉₅Zn₀₅ dispersed nanofluid prepared by a two-step process", *International Journal of Heat and Mass Transfer*. **54**, 2011, pp. 3783-3788.
- [7] ASHRAE Handbook - Fundamentals (SI Edition). Atlanta, GA: American Society of Heating, Refrigerating and Air-Conditioning Engineers, Inc., 2009

HEAT TRANSFER AUGMENTATION OF Al_2O_3 NANOFLUID IN 60:40 WATER TO ETHYLENE GLYCOL MIXTURE

N. A. Usri¹, W. H. Azmi, Rizalman Mamat¹, K. Abdul Hamid¹ and G. Najafib²

¹Faculty of Mechanical Engineering, Universiti Malaysia Pahang, Malaysia

²Biosystems Engineering Department, Tarbiat Modares University, Iran

SUMMARY: Convective coolant play an important part in removing excess heat generated by automotive component to avoid damage and failure of the system. Through recent studies, nanoparticles suspended in base fluid or known as nanofluid have positive effect to heat transfer performance. This paper presents the effect of increment of Alumina nanoparticle dispersed in 60:40 water to ethylene glycol based nanofluids towards heat transfer enhancement. For this purpose, nanofluids are prepared using Aluminium Oxide (Al_2O_3) with average diameter of 13 nm suspended in 60:40 of water to ethylene glycol by volume percentage. The nanofluid is synthesized using two step method and homogenized to lengthen the suspension for volume concentration of 0.2 %, 0.4 % and 0.6 %. The forced convection investigation was conducted at a constant heat flux with Reynolds number less than 20,000 at a constant working temperature of 50 °C. The heat transfer coefficient of nanofluids is compared with the base fluid. It was observed that as nanoparticles suspended in the base fluid is increase, heat transfer coefficient is also higher. The heat transfer augmentation of Al_2O_3 nanofluid at 0.6 % volume concentration is higher than 0.2 % and 0.4 % concentrations.

Keywords: Heat transfer coefficient, nanofluid, aluminium oxide, water:EG mixture.

INTRODUCTION

For the past decades, nanofluids were studied for its superior thermal properties hence been applied in many engineering systems that require cooling systems. The nanofluids are proved to have better stability and rheological properties, higher thermal conductivities with no significant penalty on pressure drop [1-2].

The studies that involved nanofluids in experimental forced convection using EG-water based nanofluids are limited. Kulkarni et al. [3] conducted a research on SiO_2 nanofluid dispersed in 60 % EG and 40 % water for three particles size (20, 50 and 100 nm). The investigation was on the fluid dynamics characteristics and convective heat transfer enhancement under turbulent region ($3000 < \text{Re} < 12000$) for concentration range from 2 % to 10 %. The study demonstrated that the heat transfer coefficient increases as the particle concentration and particle size increases and the effect is more significant for temperature under zero degree. The pressure loss is observed to be increased with the increase in particle concentration. Vajjha and Das [4] conducted a study on three types of nanofluids (Al_2O_3 , CuO and SiO_2) dispersed in 60 % EG and 40 % water for convective heat transfer under turbulent region. The study discussed on effect of particle volume concentration, thermo-physical properties and particle size to the heat transfer performance of the nanofluids. The findings shows that increase in particle concentration contribute to enhancement in heat transfer coefficient.

The objective of present study is to provide the experimental observation of nanofluids heat transfer performance using Al_2O_3 nanofluids in 60:40 water to ethylene glycol mixture.

EXPERIMENTAL SETUP

Preparation of Nanofluid

The nanofluids were prepared by dispersing the nanoparticles in 60:40 ratio of base fluid through proper mixing. The nanoparticle used is Al_2O_3 in powder form which procured from Sigma-Aldrich USA. The fine particles of Al_2O_3 have average particle diameter of 13 nm. Distilled water (W) and ethylene glycol (EG) are used as the based fluid.

Approximately 22 L of the nanofluid is prepared using dilution technique to conduct the heat transfer experiments. The dispersion of pre-calculated mass of Al_2O_3 nanoparticles in mixture base was lengthen using magnetic stirrer and immersed in ultrasonic homogenizer for 2 hours. It was observed stable during the experiment.

Thermophysical Properties

The prepared nanofluids were first measured for their thermal conductivity and viscosity for each concentration using KD2 Pro thermal properties analyzer and Brookfield LV/DV-III Ultra Viscometer. Whereas, the density and specific heat of nanofluid are obtained using classical model solid-liquid mixture relation which commonly used in nanofluid field.

Experimental Equipment

In order to investigate forced convective heat transfer, a fluid loop experimental system is designed as in Figure 1. The experimental system is assemble in consist of a test section with installed heater, a control panel, a collecting tank, a circulating pump, a chiller and bypass valve.

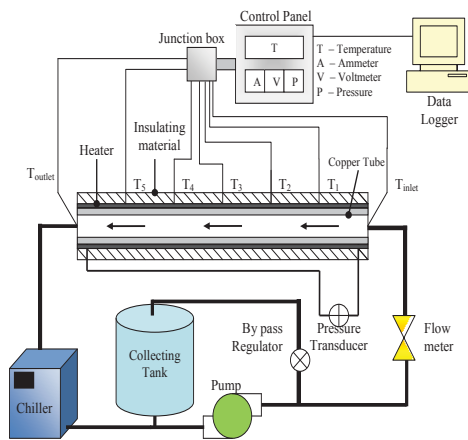


Figure 1. Schematic Diagram of Force Convection

RESULT AND DISCUSSION

The reliability of the experimental setup is established by comparing Nusselt number of distilled water, 40:60, 50:50 and 60:40 ratio (water: ethylene glycol) mixture with single-phase liquid relation by Dittus and Boelter [5] in Eq. (1).

$$Nu = 0.023 Re^{0.8} Pr^{0.4} \tag{1}$$

where, Nu is Nusselt number, Re is the Reynolds number, and Pr is Prandtl number.

Based on good agreement of present experimental data with Eq. (1) shown in Figure 2, experiments are further undertaken with designated base ratio fluid and Al₂O₃ nanofluid in the volume concentration of 0.2 %, 0.4 % and 0.6 % at various flow rates.

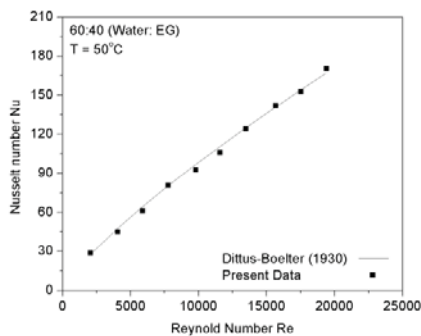


Figure 2. Validation between present data with Dittus-Boelter [5].

The results show that as volume concentration of Alumina suspended in the base fluid increase, the Nusselt number increase. Larger Nusselt number showing higher efficiency of convection process. Therefore, suitable nanofluid volume concentration could be recommended for implementation in

working temperature of 50 °C. Figure 3 shows Nusselt number for Al₂O₃ nanofluid volume concentration 0.2 %.

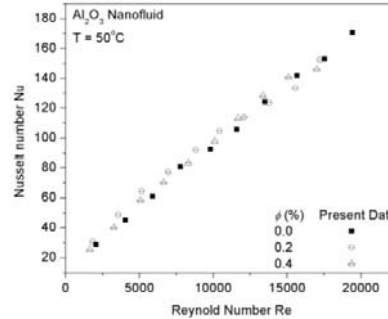


Figure 3. Comparison of Nusselt number between present data with Dittus-Boelter [5] for volume concentration 0.2 %.

ACKNOWLEDGMENT

The financial support and laboratory facilities by Universiti Malaysia Pahang under RDU1403110 are gratefully acknowledged.

References

[1] J.A. Eastman, S.U.S. Choi, S. Li, W. Yu, L.J. Thompson, "Anomalous increased effective thermal conductivities of ethylene glycol-based nanofluids containing copper nanoparticles", *Applied Physics Letters*. **78**, 2011, pp. 718-720.
 [2] W.H. Azmi, K.V. Sharma, P.K. Sarma, R. Mamat, S. Anuar, V. Dharma Rao, "Experimental determination of turbulent forced convection heat transfer and friction factor with SiO₂ nanofluid", *Experimental Thermal and Fluid Science*. **51**, 2013, pp. 103-111.
 [3] D.P. Kulkarni, P.K. Namburu, H. Ed Bargar, D.K. Das, "Convective Heat Transfer and Fluid Dynamic Characteristics of SiO₂ Ethylene Glycol/Water Nanofluid", *Heat Transfer Engineering*. **29**, 2008, pp. 1027-1035.
 [4] R.S. Vajjha, D.K. Das, D.P. Kulkarni, "Development of new correlations for convective heat transfer and friction factor in turbulent regime for nanofluids", *International Journal of Heat and Mass Transfer*. **53**, 2010, pp. 4607-4618
 [5] F. W. Dittus and L. M. K. Boelter, *Heat transfer in automobile radiators of the tubular type*. 2ed: University of California Publications on Engineering, **2**, 1930, pp. 443-461.

GEOMETRICAL INFLUENCE OF REGENERATOR STACK ON THE PERFORMANCE OF THE STRAIGHT-TUBE THERMOACOUSTIC REFRIGERATOR

Naoki Maruyama¹, Mitsunori Saito¹, Mami Yamamoto¹, Masafumi Hirota¹ and Yujiro Kitaide²

¹Division of Mechanical Engineering, Graduate School of Engineering, Mie University, Japan
²Fuji Electric Co., Ltd., Japan

SUMMARY: A thermoacoustic refrigerator using a thermoacoustic phenomenon is introduced in this paper. A straight-tube type system is constructed and experimentally examined. The system consists of a sound source, a resonance tube, and a regenerator stack with a producing temperature gradient in it. A speaker is introduced as the sound source in order to have a steady sound energy. The purpose of this study is to examine the geometrical influence of the regenerator stack inside a thermoacoustic refrigerator on the temperature gradient of gas in the stack. The cell density and the length of the stack are modified to give superior performance. The performance of the refrigerator is evaluated to propose the optimum system configuration and operating conditions.

Keywords: thermoacoustic refrigerator, straight-tube, experiment, regenerator stack, temperature difference

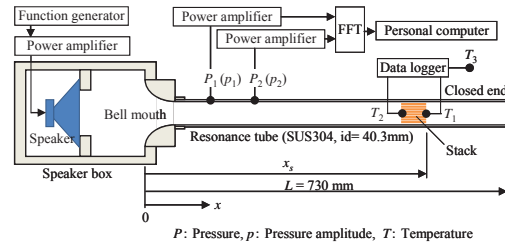
INTRODUCTION

Thermoacoustic energy conversion systems signify energy conversion and heat transport between heat and sound [1, 2]. Advantages of this system include the system not containing refrigerants and moving parts. However, characteristics of the thermoacoustic system are unclear. For the research on the geometrical shape of the regenerator stack specifically, it was found that the cell density and length of the stack provide a great effect on the cooling performance [3, 4]. The purpose of this study is to show the geometrical influence of the regenerator stack inside a thermoacoustic refrigerator on the performance of the system.

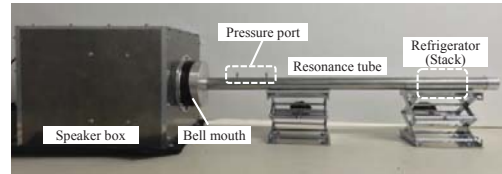
EXPERIMENTAL APPARATUS AND PROCEDURE

Figure 1 shows the thermoacoustic refrigerator employed in this experiment [4, 5]. This system has a simple configuration with a speaker as the sound source, a resonance tube and a refrigerator. A bell mouth is introduced between the speaker and the resonance tube. Air is employed as working gas. Sound is supplied by the speaker, which operates using a function generator with a power amplifier (output: 60 W). The function generator's frequency is set as the resonance wavelength of the resonance tube. Local pressure is measured by a semiconductor transducer attached to the resonance tube. The detected sound pressure is amplified by the power amplifier; then, the pressure profile is presented and recorded by an FFT analyzer.

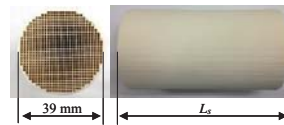
The regenerator stack is constructed by thin ceramic tubes, as shown in Fig. 1(c). The specifications of the stacks used are shown in Table 1. The position of the stack, x_s , is varied along the resonance tube. Both side temperatures (T_1 , T_2) of the stack and ambient temperature (T_3) are evaluated.



(a) Schematic diagram



(b) Photo



(c) Example of regenerator stack ($\rho_s = 400$ cell/in², $L_s = 70$ mm)

Figure 1. Schematic diagram and photos of a thermoacoustic refrigerator

Table 1. Specification of stacks

Material	Ceramic			
	400	600	900	1200
Density: ρ_s (cell/in ²)	400	600	900	1200
Wall thickness (mil)	4.5	3.5	2.5	2.0
Channel radius: r (mm)	0.575	0.472	0.391	0.341
Diameter: D_s (mm)	39			
Length: L_s (mm)	50, 70, 80, 90, 100, 110, 120			

*1 mil = 0.0254 mm

Temperatures are measured and recorded using K-type thermocouples and a data logger, respectively. After achieving a steady state condition, the local temperatures and pressure profiles are measured.

EXPERIMENTAL RESULTS AND DISCUSSION

Progress of local temperatures and pressures for a typical experimental condition are shown in Fig. 2. Temperatures on both sides of the stack change quickly after the sound source is operated. It takes around 400 seconds to achieve a steady state condition. The resonance frequency is $f = 120$ Hz, and it also depends on the resonance tube length. Thus, the resonance tube length should be set to be around 1/4 of a wave length.

Figure 3 shows the temperature difference between the edges of the stack for cell density. The temperature difference is by:

$$\Delta T = T_1 - T_2 \quad (1)$$

which is estimated by averaging the temperatures during the 10 minutes after a steady state condition has been achieved. Temperature difference increases as the stack is set near the closed end. Energy conversion from sound to heat occurs based on the compression and expansion of gas inside the thin tube. Generally, a longer stack has an advantage to have a higher temperature difference. However, it decreases for longer stacks with higher cell density.

Figure 4 shows the temperature difference for stack lengths. ΔT saturates at around 90 - 100 mm in the case of 400 and 600 cell/in². On the other hand, ΔT reaches its maximum at around $L_s = 100$ mm and decreases gradually in the case of 900 and 1200 cell/in². It is considered that the motion of fluid particles in the stack is affected by the molecular viscosity of gas. The energy loss mentioned above grows as the thin ceramic tube of a stack becomes longer. The consumed viscous dissipation energy caused between the gas and wall prevent effective energy conversion.

CONCLUSION

The purpose of this study is to evaluate the performance of the thermoacoustic refrigerator based on the geometrical configuration of regenerator stacks. The characteristics and performance of the refrigerator are evaluated experimentally by the temperature difference between the stack's edges. Temperature difference often increases as the stack length and cell density increase. However, the dissipation of energy by gas viscosity consumes sound energy in the stack. Therefore, the temperature difference between the stack's edges saturated at around $L_s = 100$ mm. As a result, the energy dissipation by friction between fluid particles and stack wall surface becomes larger as the stack density and length become higher and longer than the prescribed values.

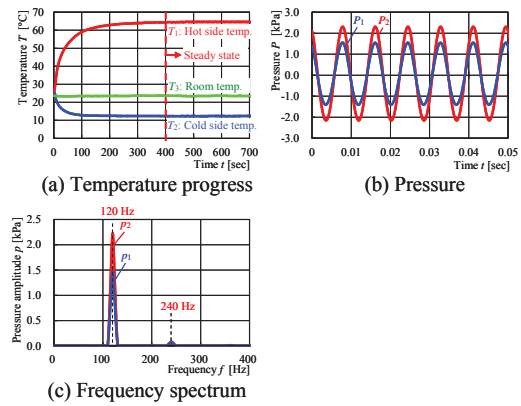


Figure 2. Progress of local temperature and pressures ($x_s/L = 0.95$, $\rho_s = 400$ cell/in², $L_s = 100$ mm)

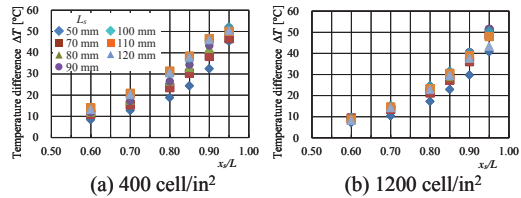


Figure 3. Temperature difference for cell density

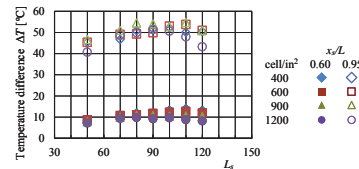


Figure 4. Temperature difference for stack length

References

- [1] G.W. Swift, "Thermoacoustic engines", *J. Acoust. Soc. Am.*, **84**(4), 1988, pp. 1145 - 1180.
- [2] S. Sakamoto and Y. Watanabe, "The experimental studies of thermoacoustic cooler", *Ultrasonics*, **42**, 1999, pp. 53 - 56.
- [3] T. Fujita, et al., "Characteristics of stack in thermoacoustic cooling system (in Japanese)", *IECE Technical Report*, US2005 - 100, 2005, pp. 43 - 48.
- [4] M. Saito, et al., "Geometric Influence of Regenerator Stack on Performance of the Thermoacoustic Refrigerator", *Proc. of The 5th TSME International Conference on Mechanical Engineering*, **13**, 2014, pp.8
- [5] N. Maruyama, Y. Iwasaki, M. Saito, and Y. Kitaide, "Principal characteristics of thermoacoustic refrigerator", *Proc. of The Fifth International Conference on Science, Technology and Innovation for Sustainable Well-Being*, **20**, 2013, pp.6

EXPERIMENTAL INVESTIGATION ON Al_2O_3 - WATER ETHYLENE GLYCOL MIXTURE NANOFLUID THERMAL CONDITION IN A SINGLE COOLING PLATE FOR PEMFC APPLICATION

Irmie Zakaria¹, W.A.N.W Mohamed¹, A.M.I Bin Mamat¹, S.F.A Talib¹, R.Saidur², W.H. Azmi³ and Rizalman Mamat³

¹Faculty of Mechanical Engineering, Universiti Teknologi Mara (UiTM), Shah Alam, Selangor, Malaysia

²Department of Mechanical Engineering, Faculty of Engineering, Universiti Malaya, Kuala Lumpur, Malaysia.

³Faculty of Mechanical Engineering, Universiti Malaysia Pahang, Pekan, Pahang, Malaysia

SUMMARY: Thermal enhancement in applying nanofluid coolant in a single cooling plate with parallel flow mini channels for use in a Proton Exchange Membrane Fuel Cell (PEMFC) is experimentally investigated in this paper. The study focuses on low concentration of Al_2O_3 dispersed in Water - Ethylene Glycol mixtures as coolant in carbon graphite mini channel to mimic a single cooling plate of PEMFC. The experimental study was conducted in a cooling plate size of 220mm x 300mm with 22 parallel mini channels and large fluid distributors. Mini channel dimensions are 100mm x 1mm x 5 mm. A constant heat load of 100W is supplied by a heater pad that represents the artificial heat load of a single cell. Al_2O_3 nanoparticle ranges from 0.1, 0.3 and 0.5 vol % concentration used in this experiment which was then dispersed in 50:50 (water: Ethylene Glycol) mixture. The effect of different flow rates to heat transfer enhancement and fluid flow represented in Re number range of 20 to 140 was observed. Heat transfer is improved up to 15% for 0.5 vol % Al_2O_3 as compared to base fluid. However the pressure drop also increase which result in pumping power increment up to 0.03W.

Keywords: mini channel, nanofluid, heat transfer, PEMFC

INTRODUCTION

The conversion efficiency of a Proton Exchange Membrane Fuel Cell (PEMFC) is contributed by a good thermal management aspect as cell temperature uniformity contributes to the electrochemical reaction efficiency. To allow compact fuel cell designs, the internal cooling plate design and operation requires further improvement to enhance cooling effectiveness. Nanofluid provides higher cooling effect than conventional coolants and is expected to be a promising candidate for PEMFC. Nanofluid in mini channels has been experimentally investigated mostly for electronic heat sink and automotive heat exchangers [1-4]. Nanofluid cooling effects at different nanoparticle fractions to variations in heat sink channel designs, operation and materials are normally reported. Naphon and Nakharinr [2] studied TiO_2 in de-ionized water nanofluid heat transfer characteristic by varying three different channel heights. Sohel et al [5] studied the effect of different flow rates to thermal performance of Al_2O_3 in water at volume fractions range of 0.1 to 0.25 %.

Apart from adoption in mini channel heat sink, nanofluid in an electrically active heat transfer environment such as fuel cell mini channel is a potential area to be explored. However, information on electrical conductivity of nanofluid is still insufficient as compared to other thermo physical properties of nanofluids. Zakaria et al. [6] has established a thermo-electrical conductivity ratio for Al_2O_3 nanofluid in water:EG mixture for PEMFC. Sarojini et al. [7] experimented nanoparticles of

Al_2O_3 , CuO and Cu in distilled water and EG and report that that electrical conductivity increases as the volume concentration increase.

In this study, nanofluid effect on heat transfer and fluid flow on graphite mini channel was investigated for 0.1, 0.3 and 0.5 vol % Al_2O_3 in 50:50 (water: EG) mixture at constant heat flux for Re number range of 20 to 140.

METHODOLOGY

Preparation of nanofluid and thermo physical properties measurement

In this study nanofluid were prepared in 0.1, 0.3 and 0.5 vol % concentrations dispersed in 50:50 (water:EG) mixture. Thermal conductivity was measured using KD2 Pro thermal property analyzer of Decagon Devices, Inc., USA while electrical conductivity was measured using Cyberscan PC-10 conductivity electrode meter.

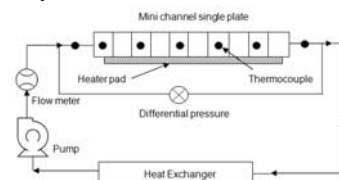
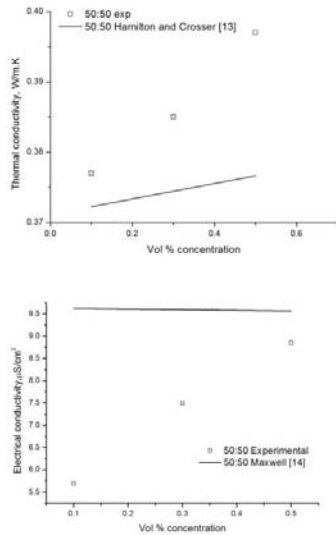


Figure 1. Schematic of mini channel experiment

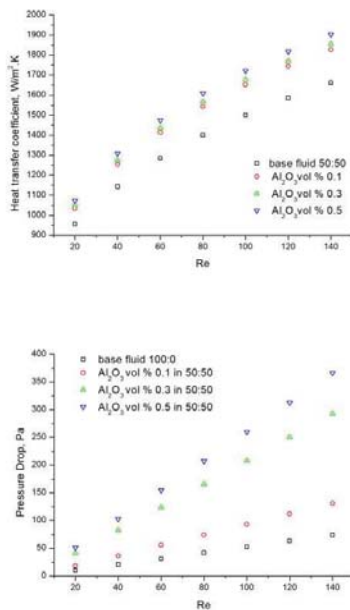
A series of 22 mini channels in a single carbon graphite cooling plate was subjected to a constant heat flux of 100W.

RESULT AND DISCUSSION

Thermo-physical properties of nanofluid



Heat transfer and Fluid flow analysis



CONCLUSION

The result shows that heat transfer coefficient is improved by 15%, 11.6% and 10.3% for 0.5, 0.3 and 0.1 vol % Al₂O₃ in 50:50 (water:EG) as compared to base fluid of 50:50 (water:EG). It is shown that the higher vol % concentration of Al₂O₃ performed better in term of thermal enhancement but at the expense of higher pumping power

required due to increase in pressure drop. Highest pumping power required was at 0.03W for 0.5 vol % Al₂O₃ in 50:50 (water:EG) at Re number 140.

References

- [1] S. S. Khaleduzzaman, R. Saidur, J. Selvaraj, I. M. Mahbubul, M. R. Sohel, and I. M. Shahrul, "Nanofluids for Thermal Performance Improvement in Cooling of Electronic Device " *ADVANCED MATERIALS RESEARCH*, **832**, 2014, pp. 218-223.
- [2] P. Naphon and L. Nakharintr, "Heat transfer of nanofluids in the mini-rectangular fin heat sinks," *International Communications in Heat and Mass Transfer*, **40**, 2013, pp. 25-31,
- [3] B. Ramos-Alvarado, P. Li, H. Liu, and A. Hernandez-Guerrero, "CFD study of liquid-cooled heat sinks with microchannel flow field configurations for electronics, fuel cells, and concentrated solar cells," *Applied Thermal Engineering*, **31**, 2011, pp. 2494-2507,
- [4] M. Keshavarz Moraveji, R. Mohammadi Ardehali, and A. Ijam, "CFD investigation of nanofluid effects (cooling performance and pressure drop) in mini-channel heat sink," *International Communications in Heat and Mass Transfer*, **40**, 2013, pp. 58-66,
- [5] M. R. Sohel, S. S. Khaleduzzaman, R. Saidur, A. Hepbasli, M. F. M. Sabri, and I. M. Mahbubul, "An experimental investigation of heat transfer enhancement of a minichannel heat sink using Al₂O₃-H₂O nanofluid," *International Journal of Heat and Mass Transfer*, **74**, 2014, pp. 164-172,
- [6] I. Zakaria, W. H. Azmi, W. A. N. W. Mohamed, R. Mamat, and G. Najafi, "Experimental Investigation of Thermal Conductivity and Electrical Conductivity of Al₂O₃ Nanofluid in Water - Ethylene Glycol Mixture for Proton Exchange Membrane Fuel Cell Application," *International Communications in Heat and Mass Transfer*, **61**, 2015, pp. 61-68,

TESTING OF LOW-GREDE HEAT SOURCE ORGANIC RANKINE CYCLE WITH SMALL HOT VAPOR RECIPROCATING ENGINE

Wasun Darawun¹, Roongrojana Songprakorp¹, Veerapol Monyakul¹ and Sirichai Thepa¹

¹Division of Energy Technology, School of Energy, Environment and Materials, King Mongkut's University of Technology Thonburi (KMUTT), Thailand

SUMMARY: For testing a recovering low-grade heat source (<100 °C) by the expansion process of the Small Hot Vapor Reciprocating Engine (SHVRE) has never been studied yet. This research focuses on that one for investigating and ORC has been designed for electricity generation not over 500 W. R123 has conducted as working fluid. Testing of ORC has been achieved with the pressure of working fluid not exceeding 7 bars. The results show that the optimal maximum of electric power generation indicates at 5 bars, 270 rpm and 221 W. The tendency of testing ORC compared between R123 and compressed ambient air is agreeable.

Keywords: Organic Rankine Cycle / low-grade heat source / Small Hot Vapor Reciprocating Engine

INTRODUCTION

An organic rankine cycle (ORC) is strongly attended [1-2] and intended to improve the thermal efficiency to convert the renewable energy to the electric power. Particularly low-grade thermal source [1] (<370°C) i.e. industrial processes, biomass, solar energy etc., A recovery of waste heat by using small hot vapor reciprocating engine has never been investigated yet. Feasibility to adapt the rankine cycle and the temperature of heat source does not exceed 100 °C for operating the system is focused. By the expansion process conducts small hot vapor reciprocating engine to achieve conversion of thermal energy in superheated steam in working fluid to the electric power. The optimal maximum of electricity generation that relates with pressure, engine speed and power output is discussed. Additionally, the comparing between R123 and compressed ambient air is also presented.

In a few past decades, turbine expander is popularity and exactly belong to the system that is high electricity generation (>1MW). P.S. Doherty et al. [2] the development of a small-scale system designed at low temperature heat source such as solar energy to generate electricity was described. The system had been designed and operated using n-pentane as the working fluid. The testing of ORC, it delivered 1.5 kW of electricity with 4.3% for thermal efficiency. For getting the advantaged from a phase change of the working fluid (as high energy density), R Bernardello et al [3] established the standard comparing cycles leading to the studied many standard comparing cycles for the reciprocating steam engines. The predicted showed that there were maximum operational points on which depend in some conditions and constructive features. Operating caution of steam engines, the isochoric processes must be aware for they always caused useful energy waste.

DESIGN AND TESTING PROCEDURES

Design of ORC for low-grade energy source, the working fluid is R123 and the maximum electric power generation is not exceeding 500 W. Expander

is modified a compact three-cylinder reciprocating engine as depicted in Table 2. The concept of ideal rankine cycle is adopted for design of ORC. The cycle is the ideal for a vapor power plant of which does not involve any internal irreversibility, i.e. steady state, pressure drop and no heat loss.

Table 1. Hot vapor engine specifications.

Engine specifications	
Engine	3cyl. Daihatsu
Displacement (cm ³)	670
Bore x Stroke (mm)	63 x 72

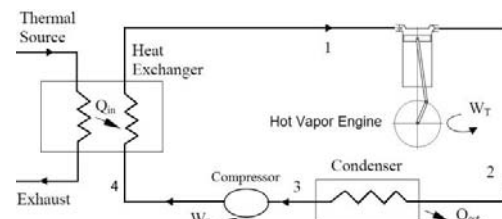


Figure 1. Schematic diagram of ORC system

Sequential stages of the system design start with determining the hot vapor engine (stages 1-2): the expander depressurizes the superheated vapor of working fluid after flows passed this one. Then the vapor becomes at lower pressure P2 and low temperature T2. In order to analyze the cycle (Figure 1) at an expansion stage, it need identify some relationship between the volumes of the cylinder such that the cut-off ratio (ϕ), closure ratio (r_F), volume ratio (ϵ), pressure ratio (r_P) and the specific heat ratio referring the following [3], respectively. Secondly: condenser (stages 2-3), after that: pump (stages 3-4), finally: evaporator (stages 4-1), for calculating such that the condenser load (\dot{Q}_{out}), the work (\dot{W}_p) for recirculating working substance and the quantitative of heat input (\dot{Q}_{in}) can be considered by adapting the first's law of

thermodynamics as well. For depth of details of the procedures, please follow inside the previous paper.

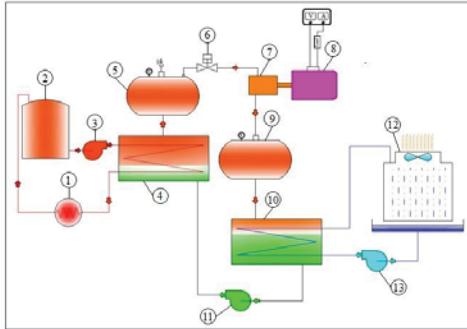


Figure 2. Schematic diagram of preliminary test

EXPERIMENTAL APPARATUS

Figure 2 shows schematic diagram of testing ORC uses R123 as working fluid. To operate the system, working fluid (0.06 kg/s) was heated to superheated vapor and contained the pressure reservoir 200 liters (number 5) while pressure control valve (number 6) was closed until reaching anticipated pressure (7 bars). After that the pressure control valve gradually opened for avoiding difference pressure effect and observed the reciprocating engine for smoothly running. The speed of engine must be stable and then the measurements evaluate the performance of the apparatus as the following: Electricity and engine speed were measured by METRAHit 29S and digital tachometer DT-246L. The mass flow rate of working fluid was measured by calibrated flow meter. After the working fluid come out the condenser, the phase change was accomplished to be saturated liquid. Then it was pumped back to the evaporating process once (number 4).

TESTING RESULTS AND DISCUSSION

The optimal maximum of the ORC testing indicates at about 5 bars (figure 3a), 270 rpm of engine speed and 210 W of electric power output. The electric power trends increasing with raised the engine speed that is depicted by figure 5. A show that is after the critical point of the engine performance, the electricity trends decreasing with increased the engine speed even although the mass flow rates of working fluid increases as elucidated in figure 3b. In the other word, the maximum torque for the reciprocating engine appears at the peak point of conditions. Figure 4 shows Compared work done in a cycle between the compressed air and R123 as a function of the evaporator pressure. The tendency is agreeable whereas the testing of R123 results higher the electric power than the compressed air because the R123 also gets more advantage from phase change of working substance during the expansion process.

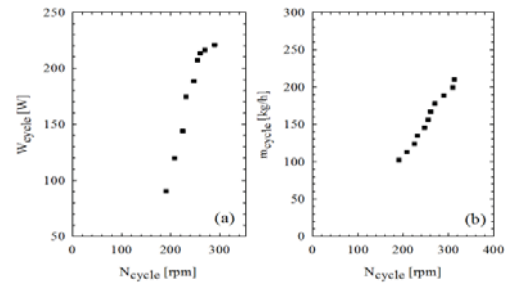


Figure 3. Work done and mass consumption in a cycle of preliminary test

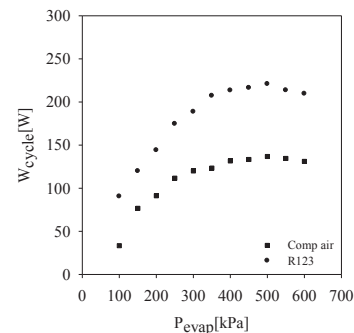


Figure 4. Compared work done in a cycle between compressed air and R123 as a function of the evaporator pressure

CONCLUSIONS

The results show that the optimal maximum of electric power indicates at 5 bars, 270 rpm and 221 W. Testing of ORC compared between R123 and the compressed air trends agreeably.

ACKNOWLEDGEMENT

This research work is supported by the Energy Conservation Promotion Fund, Energy Policy and Planning Office, Ministry of Energy Thailand.

References

- [1] P J Mago, "Performance Analysis of Different Working Fluids for Use in Organic Rankine Cycles", *Power and Energy*, **221**, 2006, pp.255-264
- [2] V.M. Nguyen, P.S. Doherty and S.B. Riffat., 2011, "Development of a prototype low-temperature Rankine cycle electricity generation system", *Applied Thermal Engineering*, **21**, pp. 169–181
- [3] R. Bernardello and J R. Simões-Moreira., "A proposed theoretical standard cycle for a reciprocating steam engine", *Proceeding of Brazilian congress of thermal sciences and engineering*, 2012

THERMAL ANALYSIS ON HEAT TRANSFER ENHANCEMENT AND FLUID FLOW OF LOW CONCENTRATION OF Al_2O_3 WATER - ETHYLENE GLYCOL MIXTURE NANOFLUID IN A SINGLE PEMFC COOLING PLATE

Irnle Zakaria¹, W.A.N.W Mohamed¹, A.M.I Bin Mamat¹, K.I Sainan¹, R.Saidur², W.H. Azmi³
Rizalman Mamat³

¹Faculty of Mechanical Engineering, Universiti Teknologi Mara (UiTM), Selangor, Malaysia

²Department of Mechanical Engineering, Faculty of Engineering, Universiti Malaya, Kuala Lumpur, Malaysia.

³Faculty of Mechanical Engineering, Universiti Malaysia Pahang, Pekan, Pahang, Malaysia

SUMMARY: Numerical analysis of thermal enhancement for a single Proton Exchange Membrane Fuel Cell (PEMFC) cooling plate is presented in this paper. In this study, low concentration of Al_2O_3 in Water - Ethylene Glycol mixtures used as coolant in 220mm x 300mm cooling plate with 22 parallel mini channels of 1 x 5 x 100mm. This cooling plate mimics conventional PEMFC cooling plate which is made of carbon graphite. Large header is added to have an even velocity distribution across all Re number studied. The cooling plate was subjected to a constant heat flux of 100W that represented the artificial heat load of a single cell. Nano particle of Al_2O_3 are at 0.1, 0.3 and 0.5 vol % concentration was dispersed in 50:50 and 60:40(water: Ethylene Glycol) mixtures. The effect of different flow rates to fluid flow and heat transfer enhancement in Re range of 20 to 140 were observed. The result showed that thermal performance has improved by 15%, 11.6% and 10.3% for 0.5, 0.3 and 0.1 vol % Al_2O_3 in 50:50 (water:EG) as compared to base fluid of 50:50 (water:EG). It is shown that the higher vol % concentration of Al_2O_3 the better the thermal enhancement but at the expense of higher pumping power required due to increase in pressure drop. As the concentration level is increased, the pressure drop increases as well.

Keywords: cooling plate, mini channel, nanofluid, heat transfer, PEMFC

INTRODUCTION

Fluid flow and convective heat transfer study in mini channel has received significant attention from researchers due to miniaturization of components design nowadays. Adoptions of mini channel covering from high power densities of electronic devices, fuel cell power sources such as proton exchange membrane fuel cell (PEMFC) and also concentrated solar panels [1]. This miniaturization of cooling channel has increased the heat flux per unit area but with a demerit of higher pressure drop.

Liquid cooling is then enhanced by the dispersion of nano-sized particles with diameter of 1 to 100 nm into the base liquids which results in higher heat transfer coefficient compared to conventional liquids and it is termed as nanofluids [2]. This enhancement is due to the thermal conductivity of nanoparticles which can be either metal or metal oxides with many orders of magnitude higher than the liquid.

Nanofluid in mini channel has been experimentally investigated by researchers mostly for electronic heat sink application. They studied channel with width less than 5mm and made of either copper or aluminium as the heat sink device. TiO_2 in de-ionized water nanofluid has been studied by Naphon and Nakharintr [3] in

term of heat transfer characteristic by varying three different channel heights. Sohel et al [4] on the other hand studied effect of different flow rates to thermal performance of Al_2O_3 in water at volume fractions range of 0.1 to 0.25 %.

Apart from adoption in mini channel heat sink, nanofluid in an electrically active heat transfer environment such as fuel cell mini channel is a potential area to be explored. However, information on electrical conductivity of nanofluid is not much available as compared to other thermo physical properties of nanofluids. Zakaria et al [5] has established a thermo-electrical conductivity (TEC) ratio for Al_2O_3 nanofluid in water:EG mixture for PEMFC and Sarojini et al. [6] have experimented nanoparticles of Al_2O_3 , CuO and Cu in distilled water and EG and discovered that that electrical conductivity increases as the volume concentration increase.

This study numerically investigates the heat transfer and pressure drop characteristic of low concentration of Al_2O_3 ranged from 0.1, 0.3 and 0.5 % vol concentration in 50:50 and 60:40 (water:EG) in a single cooling plate of PEMFC. The nanofluid mixture is selected due to TEC ratio compliance for Al_2O_3 in a PEMFC application.

METHODOLOGY

Mini channel

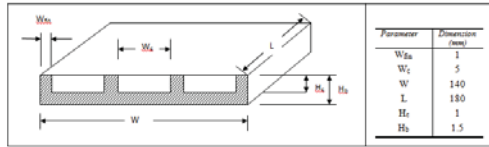
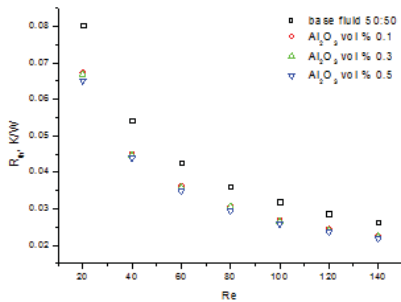
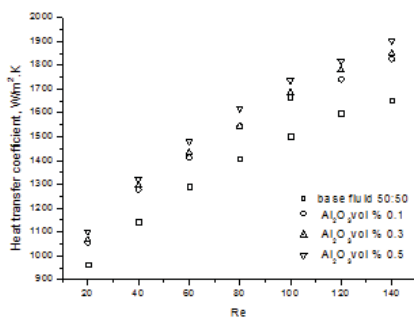


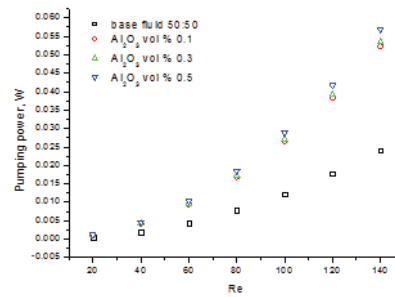
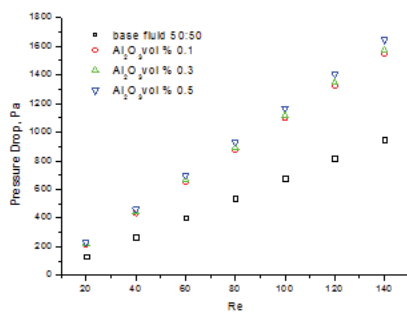
Figure 1. Mini channel dimensions

RESULT AND DISCUSSION

Heat transfer analysis



Fluid flow analysis



CONCLUSION

The result shows that heat transfer coefficient is improved by 15%, 11.6% and 10.3% for 0.5, 0.3 and 0.1 vol % Al_2O_3 in 50:50 (water:EG) as compared to base fluid of 50:50 (water:EG). It is shown that the higher vol % concentration of Al_2O_3 performed better in term of thermal enhancement but at the expense of higher pumping power required due to increase in pressure drop. Highest pumping power required was at 0.03W for 0.5 vol % Al_2O_3 in 50:50 (water:EG) at Re number 140.

References

- [1] B. Ramos-Alvarado, P. Li, H. Liu, and A. Hernandez-Guerrero, "CFD study of liquid-cooled heat sinks with microchannel flow field configurations for electronics, fuel cells, and concentrated solar cells," *Applied Thermal Engineering*, **31**, 2011, pp. 2494-2507,
- [2] S. Lee, S. U. S. Choi, S. Li, and J. A. Eastman, "Measuring Thermal Conductivity of Fluids Containing Oxide Nanoparticles," *Journal of Heat transfer*, **121**, 1999, pp. 280-289,
- [3] P. Naphon and L. Nakharinr, "Heat transfer of nanofluids in the mini-rectangular fin heat sinks," *International Communications in Heat and Mass Transfer*, **40**, 2013, pp. 25-31,
- [4] M. R. Sohel, S. S. Khaleduzzaman, R. Saidur, A. Hepbasli, M. F. M. Sabri, and I. M. Mahbulul, "An experimental investigation of heat transfer enhancement of a minichannel heat sink using Al_2O_3 -H₂O nanofluid," *International Journal of Heat and Mass Transfer*, **74**, 2014, pp. 164-172,
- [5] I. Zakaria, W. H. Azmi, W. A. N. W. Mohamed, R. Mamat, and G. Najafi, "Experimental Investigation of Thermal Conductivity and Electrical Conductivity of Al_2O_3 Nanofluid in Water - Ethylene Glycol Mixture for Proton Exchange Membrane Fuel Cell Application," *International Communications in Heat and Mass Transfer*, **61**, 2015, pp. 61-68,
- [6] K. G. K. Sarojini, S. V. Manoj, P. K. Singh, T. Pradeep, and S. K. Das, "Electrical conductivity of ceramic and metallic nanofluids," *Colloids and Surfaces A: Physicochemical and Engineering Aspects*, **417**, 2013, pp. 39-46,

Wind and Wave Turbine Technology and Wind Farm

CFD-BASED POWER ANALYSIS ON LOW SPEED VERTICAL AXIS WIND TURBINES WITH WIND BOOSTERS.

Natapol Korprasertsak¹ and Thananchai Leephakpreeda²

^{1,2}School of Manufacturing Systems and Mechanical Engineering,
Sirindhorn International Institute of Technology, Thammasat University, Thailand

SUMMARY: This study introduces analysis of effect of wind boosters on power generation from vertical axis wind turbines (VAWTs) for low speed wind by utilizing Computational Fluid Dynamics (CFD). The CFD-based study is selected over real experiments owing to that this method is reliable, fast, and requires low budgets. A wind booster is invented for incorporating with a VAWT in order to not only overcome limitations of harvesting energy with low availability at low wind speed but also enhance performances of a VAWT at higher wind speed. Specifically, a wind booster has numbers of guide vanes installed around a VAWT. All the guide vanes direct wind to impact VAWT blades at effective angles while passages between each guide vane are designed to throttle wind so as to accelerate air flow before impacting VAWT blades. From CFD case studies, guiding and throttling effects of the wind booster are able to increase angular speed of a VAWT which leads to increase in mechanical power generated from a VAWT.

Keywords: low wind speed, wind booster, vertical axis wind turbine, computational fluid dynamics

INTRODUCTION

In Thailand, the average wind speed is relatively low. Therefore, Vertical Axis Wind Turbines (VAWTs) are chosen to be installed because those wind turbines are designed to yield just acceptable performances on mechanical works at not high wind speeds. There are a few relevant researches in attempting to improve performances of VAWTs at low speed conditions. Takao, M., et al [1] developed an air flow controlling device called a "directed guide vane row". Chong, W.T., et al [2] developed omnidirectional guide vanes. Also, Pope, K., et al [3] introduced numerical analysis to determine operating angles of stator vanes for a VAWT. In this study, a wind booster is developed in order to improve angular speed of the VAWT which leads to increase in mechanical power generated from the VAWT. By using specially designed guide vanes, the wind booster can control flow direction and accelerate wind from any directions in order to yield effective impacts to VAWT blades.

METHODOLOGY

Design of wind boosters

The concept for designing a wind booster is to not only guide wind to blades of a VAWT but also increase wind speed before engaging to a VAWT. As shown in Figure 1, guide vanes with curved sided triangle shape are designed to direct air streams to turbine blades properly. To increase wind speed, the guide vanes are arranged to throttle air streams. Since wind can blow to all 360 degree direction of a VAWT, the blades of guide vanes are set up around a VAWT. For CFD case studies, a Savonius-type VAWT and a wind booster are investigated for genuine performances of mechanical behaviors. The material in modeling the VAWT is proposed to be a fiber plastic of 1000 kg/m³.

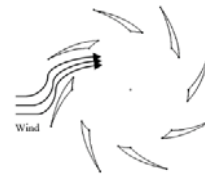


Figure 1. Wind blowing through wind booster.

CFD-based simulation

The experiments are performed with CFD-based simulations by utilizing XFlow™ CFD software [4]. The stand-alone VAWT and the VAWT equipped with the wind booster are tested to investigate different performances on mechanical works. The simulations are divided into 2 cases: 1.) no loading condition and 2.) various loading conditions. In simulations, the wind speed is varied from 1 m/s to 8 m/s for low wind speed conditions. The VAWT is to turn in clockwise direction of the vertical axis under the frictionless rotation. For various loading conditions, external torques are applied to a shaft of the VAWT against the rotation. The wind booster's dimensions are as shown in Figure 2.

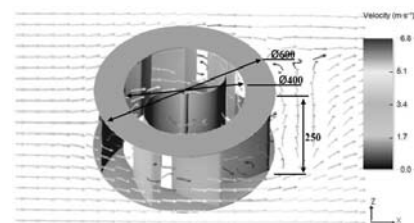


Figure 2. CFD simulation of a VAWT with the wind booster.

RESULTS AND DISCUSSION

No loading condition

Under a no loading condition, the wind booster is capable of increasing angular speeds of the VAWT as shown in Figure 3.

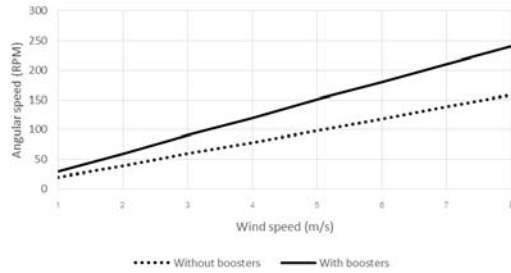


Figure 3. Speed of VAWT against wind speed

Various loading condition

In Figure 4 and Figure 5, the VAWT is operated under load conditions. It can be observed that the higher the external torque is applied, the lower the angular speeds of the VAWT as usual. However, the torques of the VAWT with the wind booster in Figure 5 can be exerted at much higher comparatively.

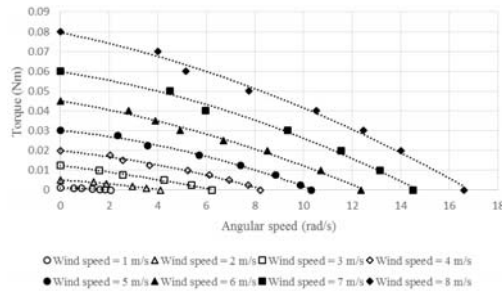


Figure 4. Torques against speeds of VAWT without wind booster

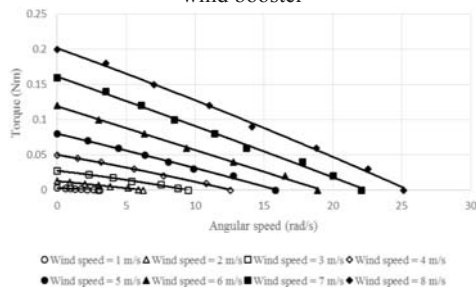


Figure 5. Torques against speeds of VAWT with wind booster.

It can be interpreted that the VAWT with the wind booster is capable of generate higher mechanical powers as shown in Figure 6 and Figure 7.

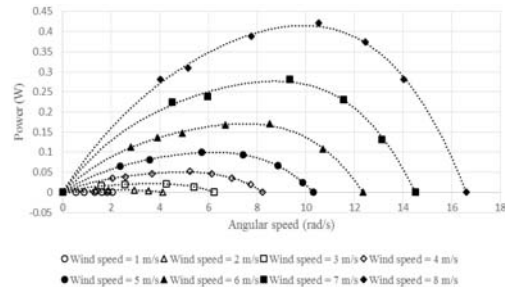


Figure 6. Mechanical powers against speeds of VAWT without wind booster

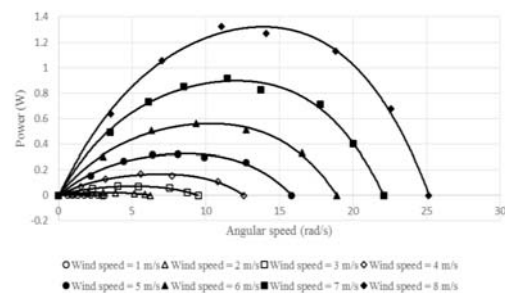


Figure 7. Mechanical powers against speeds of VAWT without wind booster

CONCLUSION

References

[1] M. Takao and H. Takita, "A Straight-Bladed vertical axis wind turbine with a directed guide vane row- effect of guide vane geometry on the performance", *Journal of Thermal Science*, **18**, 2009, pp. 54-57.
 [2] W. T. Chong, S.C. Poh, A. Fazlizan and K.C. Pan, "Vertical axis wind turbine with Omni-Directional-Guide-Vane for urban high-rise buildings", *Journal of Central South University*, **19**, 2012, pp. 727-732.
 [3] K. Pope, V. Rodrigues, R. Doyle, A. Tsopelasa, R. Gravelins, G.F. Naterer and E. Tsang, "Effects of stator vanes on power coefficients of a Zephyr vertical axis wind turbine", *Renewable Energy*, **35**, 2010, pp. 1043-1051.
 [4] "XFlow Next Generation CFD". Available: <http://www.xflowcf.com/> [Accessed: Dec, 2014].

EXPERIMENTAL STUDY OF NOVEL WIND BOOSTER FOR LOW SPEED VERTICAL AXIS WIND TURBINE

Supacheep Ngamlarp¹, Natapol Korprasertsak² and Thananchai Leephakpreeda³

^{1,2,3}School of Manufacturing Systems and Mechanical Engineering,
Sirindhorn International Institute of Technology, Thammasat University, Thailand

SUMMARY: This study introduces experiment of an air flow controlling equipment, which is called “wind booster” in this work. A wind booster is invented for incorporating with a vertical axis wind turbine (VAWT) in order to increase the performance of the VAWT and overcome the limitation of harvesting energy with low availability at low wind speed. A wind booster has several guide vanes installed around a VAWT. The main functions of a wind booster can be divided into 2 parts. The former is “guiding”; the guide vanes direct wind to impact VAWT’s blades at effective angles. The latter is “throttling”; the space between each guide vanes is designed to throttle wind so as to accelerate the air flow before impacting VAWT’s blades. The experimental results show that the guiding and throttling effects of the wind booster are able to increase overall angular velocity of VAWTs at low speed wind.

Keywords: low wind speed, wind booster, vertical axis wind turbine

INTRODUCTION

In many accessible regions of Thailand, average wind speed is generally low. Although VAWTs are designed for mechanically performing well at medium wind speed, they are usually chosen to be suitable for the areas where the wind speed is low as well. Therefore, standalone VAWTs are still unable to generate mechanical power satisfactorily for a best practice, so it is necessary to invent equipment that can improve performance of VAWTs in order to overcome the limitation of harvesting energy at low wind speeds. A wind booster is designed and developed in this study in order to improve efficiency of the VAWT. By the effects of many guide vanes, the wind booster can control wind flow direction and accelerate the speed of upstream wind from any direction in order to make it impact a VAWT’s blades in effective angles.

METHODOLOGY

In this study, we perform experimental study by observing the difference in performance between a standalone VAWT and a VAWT equipped with the designed wind booster at low wind speed conditions of approximately 2 m/s to 7 m/s. Actually, there are other methods which are able to increase power generation of VAWTs, such as creating a larger size turbine. However, the reasons why we select to increase the inlet wind speed and turbine speed over other methods are: 1.) The relationship between wind velocity and wind power is “power \propto velocity³”; therefore, increasing the angular velocity of the turbine can greatly increase the turbine’s power output. 2.) This method does not require a large wind turbine which means savings both in cost and space for installation.

The power available from wind can be obtained by the equation:

$$P = 0.5\rho AV^3 \quad (1)$$

Where P is the power (W), ρ is the air density (kg/m^3), A is the Frontal Area (m^2), and V is the velocity of air (m/s).

Figure 1 shows the wind flow through the space between the guide vanes. The guide vanes control the wind flow to the desired direction and throttle the wind stream to increase the wind speed.

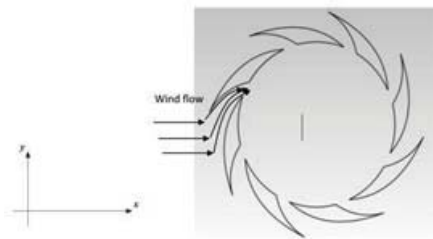


Figure 1. Wind flowing through the wind booster.

Specification of VAWT and booster

The savonius turbine and the wind booster are designed as shown in Figure 2. The material for modelling the turbine is acrylic plastic.

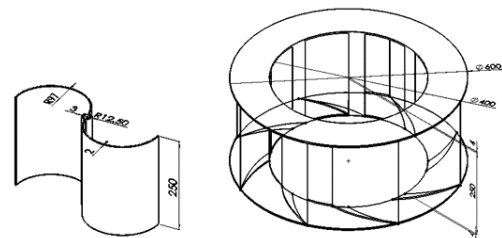


Figure 2. Specification of VAWT and booster

Experiment at setup

In the experiment, the standalone VAWT and the VAWT with wind booster are tested under the

wind of 2-7 m/s which is blown directly from variable speed fan to VAWTs as shown in Figure 3. The wind speed is measured by an anemometer and the VAWTs' angular speed is measured by a tachometer. The measurements of the wind speed are located at the mid front of the wind turbine.



Figure 3. VAWT with wind booster

RESULTS AND DISCUSSION

According to the experimental results as shown in Table 1, the wind booster is significantly able to increase the angular speeds of VAWTs at wind speed of 2-7 m/s. The increment of the angular speeds of wind turbine is graphically shown in Figure 4. The curve of VAWTs' speed with the wind booster is above the curve of turbine speed without the wind booster significantly at various wind speed. This mean the VAWT with the wind booster rotates faster with higher mechanical power than without the wind booster when loads are applied.

Table 1. Comparison of VAWTs' angular speed

Wind speed (m/s)	VAWTs' angular speed (RPM)		Increment (%)
	Without boosters	With boosters	
2	83.8	91.4	19.57
3	87.4	98.6	11.35
4	94.7	108.5	14.57
5	100.1	123.8	23.67
6	110.5	138.3	25.16
7	118.4	146.8	23.99

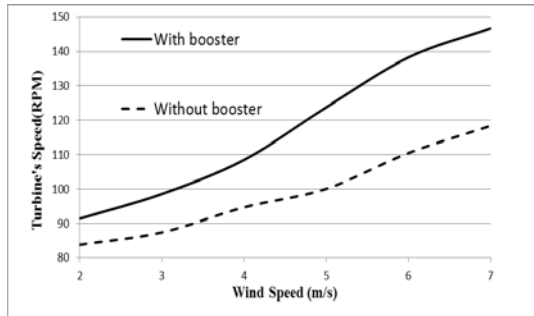


Figure 4. VAWTs' angular speed (RPM) VS Wind speed (m/s).

It should be noted that the percentages of increments can be higher than the results since the fan could not generate the uniform flow of air like atmosphere.

CONCLUSION

For low speed wind, guiding and throttling effects of the wind booster are able to increase overall angular speed or mechanical power of a VAWT.

Reference

[1] M. Takao, H. Kuma, T. Maeda, Y. Kamada, Michiaki Oki and A. Minoda, "A Straight-Bladed vertical axis wind turbine with a directed guide vane row- effect of guide vane geometry on the performance", *Journal of Thermal Science*, **18**, 2009, pp. 54-57.
 [2] W. T. Chong, S. C. Poh, A. Fazlizan and K. C. Pan, "Vertical axis wind turbine with Omni-Directional-Guide-Vane for urban high-rise buildings", *Journal of Central South University*, **19**, 2012, pp. 727-732.
 [3] K. Pope, V. Rodrigues, R. Doyle, A. Tsopelas, R. Gravelsins, G.F. Naterer and E. Tsang, "Effects of stator vanes on power coefficients of a Zephyr vertical axis wind turbine", *Renewable Energy*, **35**, 2010, pp. 1043-1051.
 [4] Y. Ohya and T. Karasudani, "A shrouded wind turbine generating high output power with Wind-lens technology", *Energies*, **3**, 2010, pp. 634-649.

AERODYNAMIC PERFORMANCE TO TURBULENCE AND ITS IMPACTS ON THE POWER CURVE OF WIND TURBINES

Sajan Antony Mathew¹ and Bhukya Ramdas¹

¹National Institute of Wind Energy, India

SUMMARY: The IEC wind turbine design classes are specified in terms of wind speed and turbulence parameters. Turbulence is a complex phenomenon and influences the power curve of a wind turbine. The design calculations using the specific turbulence values of 16%, 14% and 12% for different classes, I(A,B,C), II(A,B,C), III(A,B,C) of wind turbines do face challenges as each site has a range of turbulences. The paper strives firstly to demonstrate the turbulence effects on the power curves of two variable speed pitch regulated wind turbines having different aerodynamic strategies. Secondly the paper strives to investigate the wind turbine performance by presenting the various parametric responses and its impacts on the electrical power of the two wind turbines at different turbulence levels. Thirdly the paper attempts to quantify the impact on the electrical power output of the wind turbines at wind speeds of 6 m/s to 9 m/s and at different turbulence levels.

Keywords: Aerodynamics, Classes, Electrical Power, Turbulence Intensity [TI], Power Performance

INTRODUCTION

The aerodynamic response to turbulence is vital for the optimization of the torque and power characteristics of a variable speed, pitch regulated wind turbine. Wind turbine classes [5] are defined in terms of wind speed and turbulence. It is seen that at many sites, the representative value is different than the mean values of turbulence characteristics for wind turbine classes at 15 m/s. This difference in the turbulence characteristics will alter the power performance and design life time of the deployed wind turbine. This paper has evolved from measurements carried out on two variable speed pitch regulated wind turbines at two wind potential sites in the state of Tamilnadu, India. The methodology for the study initiates with the analysis of the normalized power curves of the wind turbines for turbulence characteristics <10% and >10%, <12% and >12% and <14% and >14% respectively. The variability of the parameters of rotor speed, pitch and electrical power of the two test turbines to the various levels of turbulence have been analysed using the %RSD (Relative Standard Deviation). Further an attempt has been made to analyze the characteristics of the coefficient of power (C_p). The wind speeds which have been analysed are in the range of 6 m/s to 9 m/s where the C_p is higher with turbulence levels <10% and >14% for the two test turbines. Finally the impact on the power has been quantified at different levels of turbulence for the wind speeds 6 m/s to 9 m/s.

SITE

The wind and terrain conditions at both the sites meet the requirements of IEC 61400-12-1 standard. The sector for measurements for both the sites has been defined as per the requirements of the International Standard wherein the sectors are clear from any obstacle wake effects [2] [3] which could impact the power curves of the test turbines. The turbulence level of site 1 is around 12% to 14% compared to site 2 which is around 11% to 12%.

POWER CURVES AT DIFFERENT TURBULENCE LEVELS

The binned power curves of test turbine 1 at turbulence levels <10% and >10%, <12% and >12% and <14% and >14% respectively normalized to standard air density conditions of 1.225 kg/m³ demonstrate that there is a significant difference in the power curve of test turbine 1 for turbulence levels <10% and >10% and the analysis for test turbine 2 demonstrates that there is a large difference in the power curves at turbulence level <14% and >14% vis-à-vis the power curves at turbulence levels <10% and >10% and <12% and >12% for both the test turbines. These differences at different turbulence levels are mainly due to different aerodynamic strategies of test turbines 1 and 2.

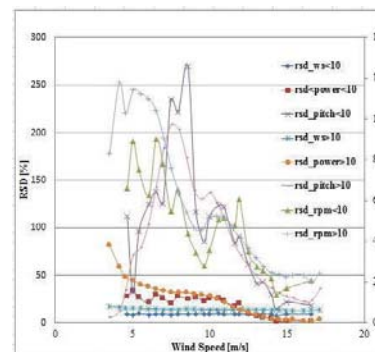


Figure 1. RSD of Wind Speed, Rotor speed, Pitch and Electrical Power at turbulence levels <10% and >10% of test turbine 1

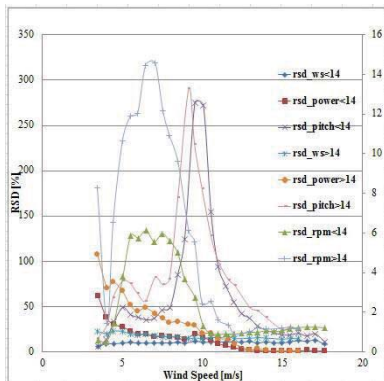


Figure 2. RSD of Wind Speed, Rotor speed, Pitch and Electrical Power at turbulence levels <14% and >14% of test turbine 2

The variability of pitch and the rotor speed resulting in the variability of power is more for turbulence levels <10% and >10% for test turbine 1 and <14% and >14% for test turbine 2 vis-à-vis other turbulence levels as shown in Figure(s) 1 and 2.

IMPACT OF TURBULENCE ON THE ROTOR SPEED, ELECTRICAL POWER AND AERODYNAMIC PITCH SYSTEM

The impact on the power curves for test turbines 1 and 2 has highlighted different aerodynamic responses for different turbulence levels. The aerodynamic control optimization to different turbulence levels ensures maximizing the power as well as reducing impacts of power variation on the grid. The Figure 3 shows the normalized coefficient of power (C_p) for both the turbines. It is seen that the C_p is maximum at wind speeds from 6 m/s to 9 m/s for both the turbines. Therefore it is important to understand that an inadequate aerodynamic response at wind speeds 6 m/s to 9 m/s can lead to significant loss of power.

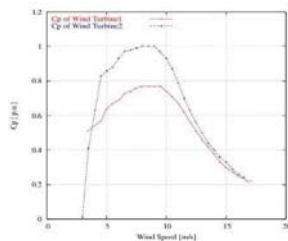


Figure 3. Coefficient of power for test turbines 1 & 2

The Table 1 shows the power loss of the test turbines 1 and 2 for difference turbulence levels for wind speeds from 6 m/s to 9 m/s. The variability of the aerodynamic response in test turbine 1 leading to more loss of power is comparatively more than the variability of the response in test turbine 2.

Table 1. Power loss at wind speeds from 6m/s to 9 m/s

Test turbine 1		
Diff between <10% >10% TI	Diff between <12% >12% TI	Diff between <14% >14% TI
12.54 %	9.59 %	6.67 %
Test turbine 2		
Diff between <10% >10% TI	Diff between <12% >12% TI	Diff between <14% >14% TI
2.4 %	1.5 %	2.0 %

CONCLUSION

The paper has attempted to inform about the impact of different levels of turbulence on the rotor speed, torque and electrical power characteristics. Further the paper has strived to quantify the loss of power at wind speed ranges from 6m/s to 9 m/s where the extraction efficiency is maximum. It is seen from the quantification that the level of % loss of power in the test turbines between different levels of turbulence is significant and there should be strategies to have improved aerodynamic performance to mitigate the impact. The design of effective aerodynamic control would mean efficient pitching and thus lower loss of power. This will assist in optimizing the rotor’s response to the turbulence for improving and optimizing the torque and power characteristics of the wind turbine.

ACKNOWLEDGMENTS

The author(s) wishes to acknowledge the efforts of the project team namely Mr M.Saravanan, Mr A.R. Hasan Ali, Mr Y.Packiyaraj, Mr M.Karrupuchamy and Mr S.Paramasivan for the Power Curve Measurement Campaigns of the test turbines.

References

[1] Wind Turbines- Part 12-1: Power Performance measurements of electricity producing wind turbines. IEC 61400-12-1: First Edition 2005-12,
 [2] S.A. Mathew and B. Ramdas “Wake effects of wind turbines and its impact on Power curve measurements”, *International Science Index*, **10**, pp. 730-735
 [3] F. González-Longatt, P. Wall and V. Terzija, “Wake effect in Wind Farm Performance: Steady State and Dynamic behavior. *Renewable Energy*, **39**, 2012, pp. 329-338
 [4] S. Wharton and J. K Lundquist, “Atmospheric stability affects wind turbine power collection”, *Environ. Res.* **7**, 2012
 [5] Wind Turbines- Part 1: Design Requirements, IEC 61400-01: Third Edition 2005-08

DEVELOPMENT OF OFFSHORE WIND FARM LAYOUT OPTIMIZATION NUMERICAL MODEL WITH WAKE LOSSES

Chawin Chantharasenawong¹, Danai Kollasuta¹ and Dusadee Sukawat²

¹Department of Mechanical Engineering, Faculty of Engineering,
King Mongkut's University of Technology Thonburi, Thailand

²The Joint Graduate School of Energy and Environment,
King Mongkut's University of Technology Thonburi, Thailand

SUMMARY: Offshore wind farm layout optimization is an important design process as poorly designed wind farm will suffer from capacity factor reduction as a result of wake losses. This work presents a numerical wind farm capacity factor calculation model with wake losses, as well as an attempt to perform a simple wind farm layout optimization process. The results suggest that a generic 10km offshore wind farm off the coast of Thailand without wake losses would yield a capacity factor of 44%. A poorly designed wind farm may suffer up to 8% in capacity factor due to wake losses, while a well designed layout suffers only 0.4% drop.

Keywords: offshore wind farm, layout optimization, wake loss

INTRODUCTION

Offshore wind farms are still uncommon in the ASEAN region but it is believed that it will gain popularity in the future. High investments, construction and maintenance costs and most importantly insufficient measured wind speed data are typical problems for countries at the initial stages of harvesting wind energy. This study looks into the next step of the challenges that will be faced. When the wind speed data and approximate offshore wind farm locations can be identified, an appropriate wind farm layout design will need to be achieved. Many factors will influence the wind farm layout designs, such as ship routes, underwater trenches, coral reefs, etc. This research work will focus on the only factor – wake losses. Wake losses are reduction of wind speed immediately downwind of a turbine rotor, which adversely affects the performance of other units of downwind wind turbines. A well-designed wind farm should position its wind turbines to avoid as much wake losses as possible, in order to achieve a maximum Annual Energy Production (AEP).

The primary focus of this research is to develop a reliable capacity factor calculation procedure for an offshore wind farm where wake losses are taken into account. The main advantage of the proposed numerical wind farm AEP model with wake losses over traditional CFD-based software packages is a much smaller computational overhead. The wind farm layout optimization is also attempted in this work but is limited to a simple case with only one parameter.

METHODOLOGY

Offshore wind farm capacity factor

This study will base its calculations on a generic offshore wind farm to be located off the Songkhla coast in the South of Thailand. The following wind speed data at 100m altitude at this location has been generated using WindSim, an industry standard CFD-based software, based on

measured wind speed data from several nearby locations.

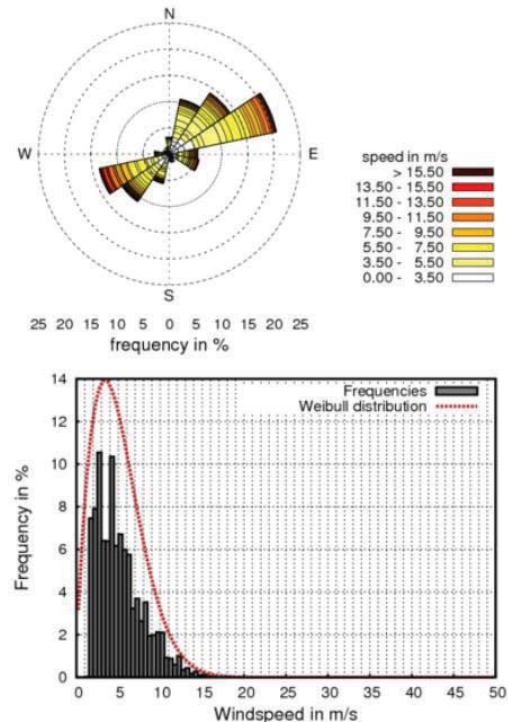


Figure 1. A 16-direction Wind Rose and a combined Weibull distribution at offshore wind farm location

Wind turbine model chosen for this study is the Vestas V126-3.3MW. It is an IEC IIIA wind turbine so it should be suitable for use in a low wind speed region such as Thailand.

Finally, the capacity factors will be computed using the Method of Bins where the wind turbine power curve is combined with the 16-direction annual wind speed frequencies.

Wind farm layout optimization with wake losses

An optimum wind farm layout in this study refers to the layout which generates the maximum AEP. Only wake losses contribute to the performance variation of wind turbines and other non-technical factors such as ship routes and coral reefs are ignored. Wake losses are computed using numerical models proposed by Jensen [1], Husien [2] and Muhamad [3]

A generic offshore wind farm with 10 units of 3.3MW wind turbine with layout shown in Figure 2 is used in this study. Spacing of 7 and 8 times of wind turbine rotor diameter is used.

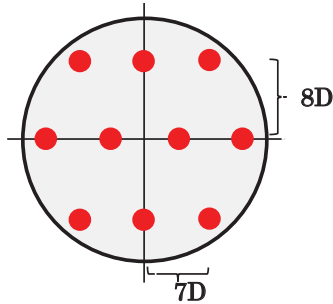


Figure 2. Initial offshore wind farm layout

RESULTS AND DISCUSSIONS

The wind farm in Figure 2 is rotated about the centre while wind turbine spacing remains unchanged. Capacity factor calculations are made at

each rotated position and the findings are presented in Figure 3.

Without wake losses, the wind farm capacity factor is 44.4%. It is found that the wake loss models predict a significant variation of capacity factors between 36.8%-44.0% when the wind farm is rotated around 360 degrees. It shows up to nearly 8% drop in capacity factor if the wind farm layout is badly designed whereas only 0.4% drop is observed in an appropriate the wind farm layout. This result highlights the importance of wind farm layout optimization.

The accuracy of this finding is still unverified by comparing them with CFD simulations, however, the trend should be relatively reliable.

References

- [1] F. González-Longatt, P. Wall, V. Terzija, “Wake effect in wind farm performance: Steady-state and dynamic behavior”, *Renewable Energy*, **39(1)**, 2012, pp. 329-338
- [2] W. Husien, W. El-Osta and E. Dekam, “Effect of the wake behind wind rotor on optimum energy output of wind farms”, *Renewable Energy*, **49**, 2013, pp. 128-132
- [3] M. Ali, J. Matevosyan and J.V. Milanovic, “Probabilistic assessment of wind farm annual energy production”, *Electric Power Systems Research*, **89**, 2012, pp. 70-79

Relation of Capacity Factor and Initial Rotated Angle of Wind Farm Layout 7Dx8D

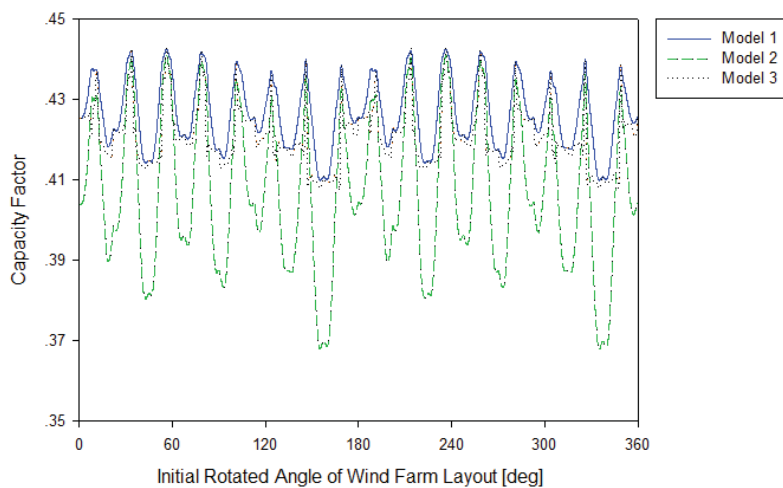


Figure 3. Variations of Capacity Factor of wind farm at each rotated position

ANALYSIS OF SUITABLE INTERCONNECTION POINTS OF OFFSHORE WIND FARMS IN THE GULF OF THAILAND

Phichet Ketsamee¹, Kusumal Chalermyanont¹, and Anuwat Prasertsit¹

¹Department of Electrical Engineering,
Faculty of Engineering, Prince of Songkla University, Thailand

SUMMARY: The off coast of the Gulf of Thailand around Koh Tao and Koh Pha-Ngan have exuberant wind resource, which can develop into the offshore wind farm about 729 MW connected to 115 kV of PEA. Therefore, it is necessary to have technical analysis in order to select suitable connected points. The technical analysis, proposed in this paper consists of power flow and voltage stability. The full-power conversion wind turbine generator and DIGSILENT PowerFactory program will be used for simulating the power system. The simulation results show performances of system before and after wind farm connection. The study results may be used as a reference to develop offshore wind farm in the Gulf of Thailand in the future.

Keywords: the Gulf of Thailand, offshore wind farm, technical analysis, full-power conversion wind turbine generator, DIGSILENT PowerFactory

INTRODUCTION

Currently, electricity power consumption is increasing due to the growth of both the industries and households, while generation system mostly depends on fossil fuels such as oil, natural gas and coal. According to a shortage of these fossil fuels, the price is significantly raised. At the same time, the effects of the fossil fuels on the environment are seriously concerned because of the effect on the global warming. The interest on the renewable energy is highly increased in worldwide.

In Thailand the Alternative Energy Development Plan: AEDP (2012 - 2021) [2] focuses on electricity generation from renewable energies such as wind, solar, water, biomass, biogas and garbage. Especially, wind energy is targeted to be about 1200 MW in 2021 [2]. According to the terrain of Thailand, the offshore wind energy is considered as high potential energy because the installation area is unlimited.

From the results of Assessment of Offshore Wind Energy Potential Pre-Feasibility of Offshore Wind Farm [1], the target area for the offshore wind farm generation is in the Gulf of Thailand around Koh Tao and Koh Pha-Ngan. The average wind speed is about 6.0 to 7.5 m/s and it can install about 729 MW of maximum capacity as shown in Figure 1. The efficiency for the production of electrical energy (capacity factor: CF) is approximately 14.13% to 17.60%. However, the feasibility study is not yet considered to the choice of interconnection points for the offshore wind farms to the grid.

However, the connection of offshore wind farm to the grid will significantly impact the security, stability and quality of grid [3] and according to the journals which has been extracted [4-6], the increasing of connection of wind farm to the grid will have a direct impact to the power flow and voltage stability. Therefore, it is necessary to analyze power flow for checking whether any components might be overloaded during normal operation conditions as well as analyzing voltage

stability in order to study the limits of the power system with the maximum load that the system can be paid prior to voltage collapse.

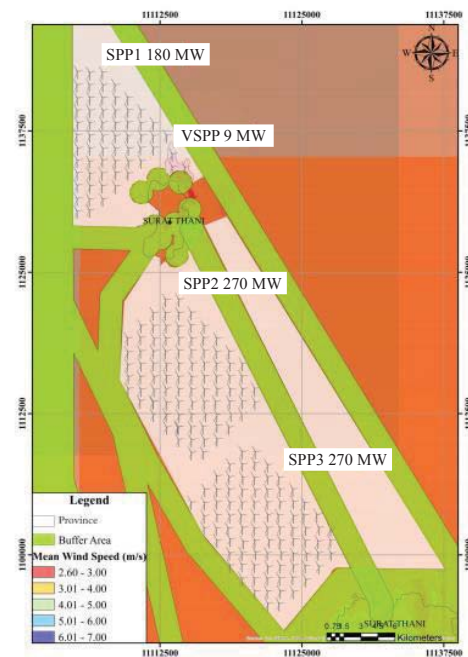


Figure 1. Suitable area that can develop all offshore wind farms in the Gulf of Thailand [1]

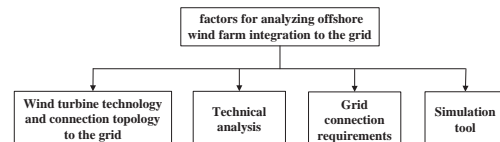


Figure 2. Consideration factors for analyzing offshore wind farm integration to the grid.
This paper presents the power system analysis

of the offshore wind farm grid connection around Koh Tao and Koh Pha-ngan in the distribution system of the PEA with four consideration factors including wind turbine technology and connection topology to the grid, technical analysis, grid connection requirements and simulation tools as shown in Figure 2.

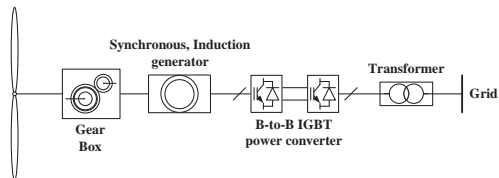


Figure 3. Schematic diagrams of full-power conversion wind turbines [7]

The 720 MW offshore wind farms are modeled with the selection of the full-power conversion wind turbine generator of Vestas V112 model as in Figure 3. The power system analysis to 115-kV grid connection are performed in system power flow and voltage stability in order to select the suitable connected points for the offshore wind farms as shown in Figure 4. The simulation models are analyzed with the DIgSILENT PowerFactory program. The simulation results show performances of system before and after wind farm connection. The study results may be used as a reference to develop offshore wind farm in the Gulf of Thailand in the future.

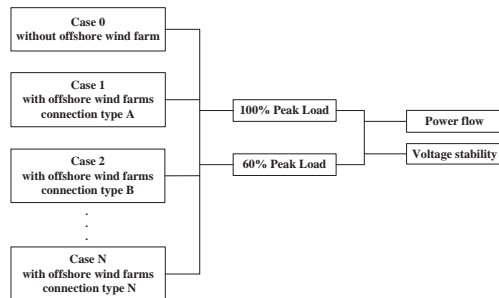


Figure 4. Case study and technical analysis.

ACKNOWLEDGEMENTS

The authors would like to thank the Prince of Songkla University (PSU) and Provincial Electricity Authority (PEA) for providing the research facilities.

References

- [1] Research Center in Energy and Environment (RCEE), Thaksin University, "Assessment of Offshore Wind Energy Potential Pre-Feasibility of Offshore Wind Farm," July 2013.
- [2] Ministry of Energy, "Alternative Energy Development Plan: AEDP (2012 - 2021)," online[.

Available: www.enconfund.go.th/pdf/index/aedp25.pdf. [31 October 2014].

[3] T. R. Ayodele, A. Jimoh, J. L. Munda, and A. J. Tehile, "Challenges of Grid Integration of Wind Power on Power System Grid Integrity: A Review," *International Journal of Renewable Energy Research (IJRER)*, **2**, 2012, pp. 618–626,

[4] R. D. Zamora, M. A. Rosado, "Stability Analysis of Wind Energy Generation in the Electrical System of Puerto Rico," *International Conference on Renewable Energies and Power Quality (ICREPO' 14)*, April 2014.

[5] K. Bhumkittipich, C. Jan-Ngurn, "Study of Voltage Stability for 22kV Power System Connected with Lamtakhong Wind Power Plant, Thailand," *Energy Procedia*, **34**, 2013 pp. 951–963,

[6] N. T. Linh, "Voltage stability Analysis of Grids Connected wind Generators," *4th IEEE Conference on Industrial Electronics and Applications, 2009. ICIEA 2009*, 2009, pp. 2657–2660.

[7] Vestas, "V112-3.0 MW Offshore,"]Online[. Available:www.vestas.com/.../Productbrochure_V112_Offshore_UK. [5 January 2015].

A PROCESS BASED LCA STUDY FOR A MARINE CURRENT TURBINE

Ahmad Rashedi¹, Taslima Khanam²

¹University of Cambridge, United Kingdom

²Universiti Teknologi PETRONAS, Malaysia

SUMMARY: Due to environmental and energy insecurity issues, renewable electricity got enhanced interest in our time. Marine power is one of the promising renewable energy sources in many offshore locations of the world. Accordingly, many research groups are exploring the ways on how to harness more marine power. This article presents life cycle analysis results of a marine current turbine based on *ReCiPe* life cycle impact assessment method. Total 18 life cycle impact categories are calculated with their respective damage categories and single score indicator. Low life cycle impacts carried by this power generation turbine shows high competitiveness of the base technology in global energy scenario from environmental and sustainability perspective.

Keywords: life cycle analysis, marine current turbine, renewable power generation, sustainability, *ReCiPe* impact assessment method.

INTRODUCTION

Marine power is one of the promising renewable technologies which got enhanced interest of the researchers and entrepreneurs in recent days due to many environmental reasons. Amongst these are severe greenhouse gas emission and associated climate change issues that can be dominantly attributed to conventional fossil fuel based power generation technologies. Conversely, a shallow ocean bed of 35-45 m depth with mean-peak current velocity over 2 m/s is sufficient to generate substantial power from ocean current. This potentiality is available in many offshore locations around the world. A few prototype and full scale marine power generation devices have been installed and commissioned accordingly in many European offshore regions; ranging from small scale to farm level output [1].

Although the operational phase of the technology is considered green, the production, manufacturing, transportation, installation and end-of-life period possess significant life cycle impact emission potentiality to the surrounding environment. It is important in this state to conduct an overall life cycle analysis (LCA) study of the marine turbine technology. As of definition, LCA calculates comprehensive life cycle impact of the stand-in technology in every phase of its life cycle under system boundary limit. LCA guidelines are epitomized in life cycle documentations extending from LCA principle and framework to goal, scope definition, inventory analysis and interpretation by *International Standard Organization (ISO)* in ISO 14040 and 14044 standards [2], [3]. Based on these established procedures, the present study evaluates life cycle impact assessment of marine current turbine and presents the results according to different impact categories.

As major journal citation databases affirm, no study earlier focused on life cycle impact assessment of marine current technology according to established LCA methodology. How different

primary, secondary and tertiary manufacturing processes contribute to overall LCA impact is an important issue that left untouched. Additionally, it is significantly important to identify how each and every engineering material contributes to overall marine turbine life cycle. All these novelties are covered in present analysis. The study focuses on *ReCiPe* LCA method for life cycle impact calculation of marine turbine which calculates life cycle inventory results by 18 important indicators [4]. *ReCiPe* uses an environmental damage mechanism as the basis of LCA modeling and it presents results by more impact indicators than most other LCA methods. Another prime reason behind choosing this LCA method stands in its combining both the indicators of *Eco-Indicator 99* and *CML 2001* LCA methods.

LCA SYSTEM MODEL

The recently commissioned marine current turbine plant installed in Strangford Lough (Northern Ireland) site by Marine Current Turbines Ltd (MCT) of UK will be used as the LCA model in this study [1]. This model uses SeaGen turbine with rated capacity of 1.2 MW. SeaGen is virtually an underwater windmill based on two 16 m diameter axial flow rotor which are climbed on a crossbeam on either side of a centrally located tower. The turbine generates 4736 MWh per annum at Strangford Lough site amounting to 94.7 GWh over an assumed 20-year project life. Corresponding material and process inventories of this turbine are collected from a relevant study led by a University of Edinburgh team and from the website of turbine manufacturer [5].

RESULTS AND DISCUSSION

The life cycle emissions of SeaGen turbine according to emission categories are calculated based on 'single score' indicator method with a *functional unit* of 1.2 MW. A 1% *cut-off point* is

introduced only to show the major emissions. Life cycle impact values are additionally shown according to - i) total plant level and ii) by three separate damage categories in Fig. 1. Impact of the three individual end-point damage categories are calculated based on similar unit based mid-point impact categories out of the total eighteen different impact categories. It appears that ‘resource depletion’ damage category carries the highest impact in marine current turbine followed by ‘effect on human health’ and ‘effect on eco-systems’. ‘Effect on eco-system’ carries a negligible value which indicates the marine current turbine doesn’t affect marine eco-systems significantly.

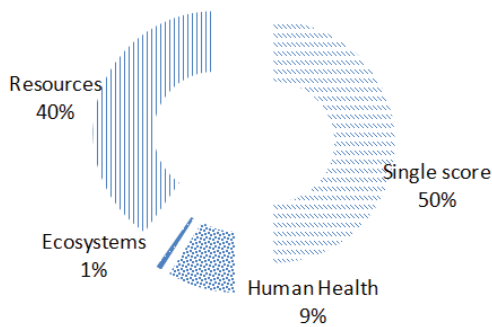


Figure 1. Total LCA impact and impacts relevant to 3 damage categories

Next, life cycle impacts are shown according to various sub-assemblies of marine turbine in Fig. 2. It appears that material based LCA processes carry the highest impact within 3 sub-assemblies.

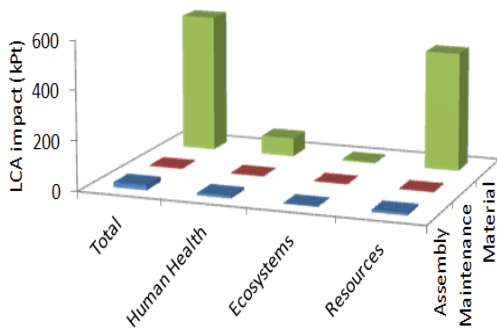


Figure 2. LCA impact comparison by sub-assemblies of SeaGen turbine

This is not uncommon for such a technology where huge amount of materials are needed and all the life cycle processes of these materials are also included in this analysis starting from their extraction from ore to until final disposal state (recycling/land-fill). The unit ‘kPt’, short form of kilo eco-point, in Fig. 2 refers to life cycle impact carried by 1000 average European person over a time-span of 1 year. Henceforward, individual

material based life cycle processes that contributing significantly are evaluated to study their individual life cycle performance. Detailed results are shown in Fig. 3 where steel and copper processes appear to carry the highest impact where cast iron process appears very much impact-savvy.

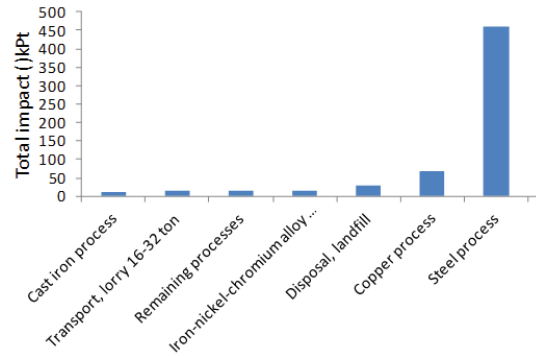


Figure 3. LCA impacts comparison by individual life cycle processes

Based on the findings, more impact-savvy materials need to be introduced in future designs by replacing the high impact carrying ones from *green design perspective*.

CONCLUSION

The life cycle assessment study of marine current turbine shows the 1.2 MW SeaGen turbine carries nearly 590 kPt life cycle impact over its 20 years lifetime. This low impact for a power generation technology appears very promising for such a start-up technology. Nevertheless, there is still scope to further streamline the design with the introduction of new material systems.

References

[1] C.A. Douglas et al., “Lifecycle assessment of the Seagen marine current turbine,” *Proceedings of the Institution of Mechanical Engineers*, 2008, pp. 1-12.
 [2] ISO 14040, “Environmental management—life cycle assessment - principles and framework”, Geneva: International Organisation for Standardisation, 2006.
 [3] ISO 14040, “Environmental management—life cycle assessment – requirements and guidelines”, Geneva: International Organisation for Standardisation, 2006
 [4] <http://www.lcia-recipe.net/> (Accessed 11 Sep 2014).
 [5] <http://www.marineturbines.com/> (Accessed 09 Sep 2014).

Energy Efficiency

POWER LOSS MINIMIZATION IN RADIAL DISTRIBUTION SYSTEM

K.R.Devabalaji¹, K.Ravi¹ and T.Yuvaraj¹

¹School of Electrical Engineering, VIT University, Tamil Nadu, India

SUMMARY: Nowadays the number of consumers in the distribution system is increasing, the electricity demand and the number of capacitor bank placement is also increasing. Improper placement of capacitor bank leads to decrease the benefits of the system. The objective function of the proposed work is to minimize the total power loss of the system while satisfying all the constraints. The Loss Sensitivity Factor (LSF) is implemented to pre-identify the optimal location of the capacitor. An effective biologically inspired algorithm (Bat Algorithm) is proposed to search the optimal size of the capacitor banks. The proposed method has been tested on IEEE 34-bus agriculture distribution system to demonstrate the performance and effectiveness of the technique.

Keywords: Power Loss Minimization, Bat Algorithm, Cumulative Voltage Deviation, Distribution system.

INTRODUCTION

As we move away from the substation the voltage of the radial distribution system will decrease due to lack of reactive power in distribution system. In the distribution system 10-13% of generated power is dissipated as I²R losses [1]. Improper placement of capacitor will lead to reduce the benefits and even it collapse the entire distribution system. The researchers used classical methods to solve optimal location and sizing of the capacitor placement. Genetic algorithm was used to identify the location and sizing of the capacitor units and results were compared. The particle swarm optimization was used to obtain location and sizing for the capacitor bank and their objective is to reduce power losses. Direct search algorithms was implemented to locate and sizing of the capacitor placement in the distribution system. A Non-dominated sorting genetic algorithm was used to find the placement of capacitor in electric radial distribution system. Hybrid SA and heuristics method were introduced for solving the optimal capacitor placement in distribution system in order to minimize power loss reduction. Antunes Chet al. proposed the non-dominated sorting genetic algorithm to solve the optimal capacitor placement in radial distribution system for reactive power compensation. Baran et al introduced mixed integer programming for the capacitor placement. Chis et al had chosen more sensitivity nodes for optimal location and sizing by heuristic search strategies to maximize the net savings. Fuzzy based GA was used to determine the optimal size with the multi objective of minimize the energy cost and enhance voltage profile. Plant growth algorithm had used to allocate the capacitor units to minimize power losses W.F. Mohammad et al introduced the supervisory control and data acquisition system (SCADA) with fuzzy based decision maker to calculate the suitable capacitor required to enhance the power factor according to the measured parameters. Sayyad Nojavan et al proposed mixed integer nonlinear programming approach to determine the location and size of the capacitor to minimize the power losses and increasing the net benefits. All the

authors had tried to minimize the power losses, but failed to minimize the number of compensating location. In the present work, the number of compensating location has been decreased to two and simultaneously achieved better results than that of other existing techniques.

In this paper, Bat algorithm has been proposed to find the optimal size of the capacitor. LSF is used to pre-find the optimal location of the capacitor placement. In this paper, the optimal location followed is slightly different from the existing method. The first and foremost aim of this work has to reduce the total power loss of the system. The proposed method is tested on IEEE 34-bus radial distribution system. The obtained results are compared with the other existing methods which founds to be better than that of other existing techniques.

PROBLEM FORMULATION

Objective function.

The objective function of this work is to minimize power loss of the system and it can be expressed by

$$\text{Min } F = \min(P_{\text{Loss}}) \quad (1)$$

The objective function is subjected to satisfy the equality and inequality constraints.

Loss Sensitivity factor

The loss sensitivity factor is used to identify the location in order to install the capacitor. The node which have highest value of LSF have more chance to install capacitor. Another advantage of using this method leads to reduce the search space for optimization process. It is given by

$$\frac{\partial P_{\text{loss}}(m, n)}{\partial Q_{mn}} = \frac{2Q_{mn}R_{mn}}{|V_m|^2} \quad (2)$$

The LSF values are sorted in descending order for all the lines and the buses which have the higher value has more chance for selecting candidate location to install the capacitor.

BAT ALGORITHM

Bat algorithms can be developed by idealizing

some of the characteristics of bats. The approximated or idealized three rules are given by

1. Each bat utilizes echolocation characteristic to sense distance, and they also ‘know’ the difference between food/prey and background obstacles in some magical way using echolocation property.

2. Each bat flies randomly with velocity V_i position X_i , with a frequency f_{min} varying wavelength λ and loudness A_0 to seek for prey. It has an ability to regulate the frequency (or wavelength) of their emitted pulse and regulate the rate of pulse emission ‘r’ in the range of [0, 1] relying on the proximity of its aim.

3. Even though the loudness can vary in different ways we assume that the loudness varies from a large positive A_0 to a minimum constant value A_{min} .

RESULT AND DISCUSSION

The proposed method is applied to IEEE 34-bus system. The line data and bus data for this system is given in [2]. The total real power of the system is 4636.5 KW and reactive power of the system is 2873.5 KW. The real and reactive power losses of the system without capacitor is 221.29 kW and 65.1 kVAr respectively as shown in table 1. The parameter used for net savings is energy rate $C_e = \$0.06/kWh$, installation cost of capacitor $C_{cl} = \$1000/each\ location$, purchase cost of capacitor $C_c = \$3.0/kVAr$, $T=8760$. The net savings is given by

$$Net\ savings = [(C_e * P_{Loss}^{Cap} * T) - (C_{cl} * N_{BC}) - (C_c * T_c)]$$

Where N_{BC} is the number of compensated buses in the system.

T_c is the total capacitor rating.

P_{Loss}^{Cap} is the total power loss of the system

with capacitor.

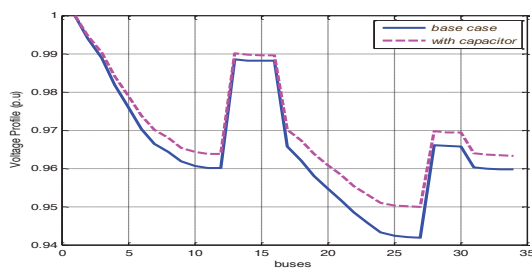


Figure 1. Voltage profile of the IEEE 34-bus system with and without capacitor

Table 1. Simulation result of IEEE 34-bus system

Parameters	PGSA	DE-PS	Proposed method
Size (kVAr) and location	1200(19), 639(22), 200(20).	750(19), 850(22), 150(20), 150(21).	650(10), 1150(25)
P_{loss}	168.7	169.0590	165.9
Net savings (\$)	18522	17751	21711

The DE-PS method, the authors are able to reduce the real power loss to 169.059 kW (CVD of 0.1520) with injecting 1900 kVAr. In the proposed method, the real power loss are reduced to 165.9 kW. The proposed method of location will give better voltage profile, achieved the CVD value to 0 and losses are also decreased effectively with less compensating value when compared with existing technique.

CONCLUSION

In this paper the Bat algorithm has been implemented to test the IEEE 34-bus distribution system. The loss sensitivity factor has been used to pre-identify the optimal location of the capacitor. From the simulation results, it is very clear that the proposed method have achieved better power loss reduction, better net-savings and less compensation location when compared with other existing techniques. Then, this leads to decrease the intake of MVA from grid and it ensures the stability of the system. Hence, the proposed method can able to implement for any kind of distribution system to enhance voltage profile and conclude that the proposed method of capacitor location is suitable to minimize both power loss and

References

[1] Attia A. El-Fergany, “Optimal capacitor allocations using evolutionary algorithms”. *IET Gener. Transm. Distrib*, 7 (6), 2013, pp. 593-601.
 [2] M.Chis, M.M.A. Salama and S. Jayaram “Capacitor placement in distribution system using heuristic search strategies”. *IEE Gener. Transm. Distrib*, 144 (3), 1997, pp. 225-230.

OPTIMAL PLACEMENT AND SIZING OF DSTATCOM USING HARMONY SEARCH ALGORITHM

T. Yuvaraj¹, K. Ravi¹ and K.R.Devabalaji¹

¹VIT University, Vellore 632014, Tamil Nadu, India

SUMMARY: This paper investigates a new approach to find the optimal location and sizing of Distribution STATic COMPensator (DSTATCOM) with an objective function of minimizing the total network power losses. Harmony search algorithm is used to find the optimal location and sizing of DSTATCOM. The proposed work is tested on standard IEEE 33-bus radial distribution systems. The obtained result shows that optimal placement and sizing of DSTATCOM in the radial distribution network effectively reduces the total power losses of the system.

Keywords: Distribution STATic COMPensator (DSTATCOM), Harmony Search Algorithm, Radial distribution Network

INTRODUCTION

In recent years, the distribution networks have received much attention by the power engineers because they play an important role in power system quality and planning. To introduce deregulation in power system, it creates the power quality problems such as voltage fluctuation, voltage sag and voltage instability in the distribution system. These power quality problems lead to power loss increase, slower response time and decreasing of power flow limits. Many researchers approximated that in the distribution side 13% of total generated power is wasted as a loss [1]. From the consumer point of view, the power loss reduction is one of the important issue to improve the overall efficiency of the power delivery [2].

So we need to use highly advanced equipment's for power loss reduction of the distribution network. Such equipment's are capacitor banks, shunt and series reactors, automatic voltage regulator (AVR) or recently developed Distribution network Flexible AC Transmission (DFACTS) such as Distribution Static compensator (DSTATCOM), Unified Power Flow Conditioner (UPQC), and Static Synchronous Series Compensator (SSSC). Compare with other reactive power compensation devices, DSTATCOM has many features, such as low power losses, less harmonic production, high regulatory capability, low cost and compact size. DSTATCOM is a shunt connected Voltage Source Converter (VSC) which has been applied in distribution networks to compensate the bus voltage so as to provide power factor and reactive power control. The DSTATCOM has the capability of providing quick and continuous capacitive and inductive mode compensation. DSTATCOM can inject correct amount of leading or lagging compensating current when it is associated with a specific load so that the total demand meets the specification for utility connection. DSTATCOM is predicted to play significant role in the radial distribution systems due to the increasing power system load. Optimum allocation of DSTATCOM maximize the load ability, power loss minimization,

stability enhancement, reactive power compensation power quality enhancement such as voltage regulation, voltage balancing a flicker suppression system. Based on the literature review, to determine the optimal location and sizing of DSTATCOM has a considerable impact in radial distribution system. In this paper, harmony search algorithm has been proposed to find the optimal location and sizing of the DSTATCOM in the radial distribution network to reduce the total power losses. The proposed method is tested on IEEE 33- bus radial distribution system. The obtained results are compared with the other existing methods which founds to be better than that of other existing methods.

PROBLEM FORMULATION

Objective Function

The objective of DSTATCOM placement in the radial distribution system is to minimize the total power losses while satisfying the equality and inequality constraints. The mathematical formulation of the objective function (F) is given by

$$\text{Minimize}(F) = \text{Min}(P_{\text{TLoss}}) \quad (1)$$

Harmony Search Algorithm

The steps involved in the Harmony search algorithm is

Step 1: Initialize the input data

$NVAR(1)$:The number of variables, i.e. the number of DSTATCOM Placement
$NG(2)$:The number of inequality constraints
$NH(1)$:The number of equality constraints
$Max_{itr}(1000)$:The maximum number of iteration for this problem.
$HMS(6)$:Harmony memory size.
$HMCR(0.9)$:Harmony consideration rate $0 < HMCR < 1$
$PAR_{min}(0.4)$: Minimum pitch adjusting rate
$PAR_{max}(0.9)$:Maximum pitch adjusting rate

BW_{min} (0.0001) :Minimum bandwidth
 BW_{max} (1.0) :Maximum bandwidth

Step 2: Initialize Harmony Memory
 Step 3: Update the member for all result vector in Harmony search Generation of the random number according to minimum and maximum limit.
 Step 4: Test for convergence, finally the algorithm will give the optimal size of the DSTATCOM.
 Hence this steps have to be follow in order to minimize the objective function.

SIMULATION RESULT AND DISCUSSION
IEEE 33-bus test system

To show the effectiveness and performance of proposed method, it has been tested on standard IEEE 33-bus systems. The line voltage, real and reactive loads of the radial distribution networks are 12.66 kV, 3.72 MW and 2.3 MVar, respectively. The proposed method has been programmed and implemented using MATLAB environment to run distribution system load flow, calculate real and reactive power losses and to identify the optimal location and size of DSTATCOM. In this system, the 30th bus is selected for optimal DSTATCOM installation. The voltage profile of the 33-bus with and without DSTATCOM is shown in figure 1. From fig 1, it can be noted that implementation of DSTATCOM in the radial distribution system has improved the voltage profile effectively.

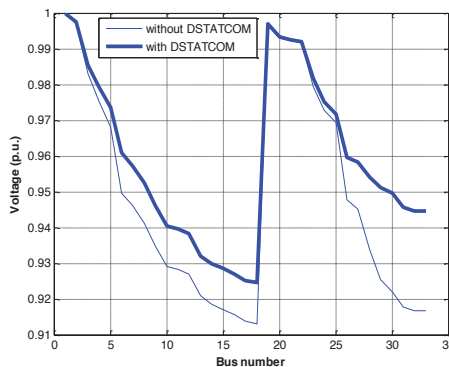


Figure 1. Voltage profile improvement for 33 bus system

Table 1 shows the comparison of real and reactive power losses, locations, optimal size (kVAr) and total annual cost saving for existing and proposed methods. In the proposed method, the real and reactive power losses have been reduced to 143.97kW and 96.47kVAr after installing the DSTATCOM in the system. And also the total annual cost saving is \$ 24,264. The proposed method total power losses reduction and total annual cost saving is high compared to existing Immune

Algorithm method. This shows that the proposed harmony search algorithm based optimization is more effective than the Immune Algorithm based optimization. DSTATCOM.

$$TCS = K_p (T \times P_{TLoss}) - K_p (T \times P_{TLoss}^{with\ DSTATCOM}) - (K_c \times DSTATCOM_{cost, year}) \quad (2)$$

Table 1. Performance analysis of the proposed method after installation of DSTATCOM on 33-bus system

Items	Base case	Immune Algorithm	Proposed Method
Optimal size (kVAr)	-----	962.49	1150
Location	-----	12	30
P_{loss} (kW)	202.67	171.79	144.91
% Reduction in P_{loss}	-----	15.24	28.5
Q_{loss} (kVAr)	135.24	115.26	96.95
% Reduction in Q_{loss}	-----	14.78	28.3
V_{min} (p.u)	0.9131	0.9258	0.9236
Total annual cost saving (\$)	-----	11,130	24,264

Conclusion

This paper presents a new approach to find optimal location and sizing for DSTATCOM in the radial distribution network. The proposed method has been tested on standard IEEE 33-bus system. From simulated results, it can be noted that implementation of DSTATCOM in the radial distribution system has reduced the total power losses effectively which is better than existing IA method. It can be concluded that the proposed harmony search algorithm based technique is very accurate in finding the optimum solutions.

Reference

[1] A. Attia. EI-Fergany.: Optimal capacitor allocations using evolutionary algorithms. IET Gener. Transm. Distrib. Feb(2013) 593-601.
 [2] J. Saeed and V. Behrooz. "Reconfiguration of distribution networks to mitigate utilities power quality Disturbances". *Electr Power Syst Res*, **91**, 2012, 9-17

MERITS AND CHALLENGES OF E-RICKSHAW AS AN ALTERNATIVE FORM OF PUBLIC ROAD TRANSPORT SYSTEM: A CASE STUDY IN WEST BENGAL STATE IN INDIA

Deepanjan Majumdar¹ and Tushar Jash¹

¹School of Energy Studies, Jadavpur University, India

SUMMARY: This study discusses the impact of alternative vehicles in public road transport sector, based on the case study of West Bengal State in India. In recent times, battery operated three wheeled vehicles have emerged in the public road transport sector and have become one of the preferred mode of transport among the commuters. These vehicles are energy efficient than their LPG based counterparts, the auto-rickshaws, and are also environment friendly with a specific energy consumption of 55.1 kJ/passenger-km. But the present technology and the new amendments of the Government of India, especially by regulating the speed of the vehicle, challenges the proper incorporation of such vehicles. The results show the merits of such vehicles over the conventional forms, but again the technical challenges to overcome are also discussed.

Keywords: electric vehicle, specific energy consumption, specific energy cost, road transport

INTRODUCTION

Economic development of a region is accompanied parallel by increase in transportation activities. Especially the urban areas and the surrounding regions experience the maximum percentage of both freight and passenger transport. Road transport sector is again, a major consumer of fossil fuel in form of liquid petroleum and gas. In India, three-wheeled auto-rickshaws play an important role in the public transport sector, and are powered by either CNG (Compressed Natural Gas) or auto LPG (Liquefied Petroleum Gas), commonly known as autogas, depending on the availability.

During the recent years, battery-operated electric rickshaws, also known as e-rickshaws, have gained much popularity. The e-rickshaws being environment friendly has a potential to reduce the carbon footprint due to transport activities. The major drawback in case of e-rickshaws was that they were not legalized as a public mode of transport. Petitions were filed against these vehicles, raising the questions of public safety, transportation permit, proper registration of vehicles and drivers' license. This is because, e-rickshaws did neither match the criteria for the exemption of such legal procedures nor could be provided such permits as they were not included in the vehicles act. The major protests came from the other public vehicles like buses and auto-rickshaws. A study by TERI (The Energy Research Institute, India) under the Government of India had recommended the e-rickshaws to be treated as motor vehicles [1]. Based on this study, during the last parliamentary session, the Government of India has passed new amendments in the Motor Vehicles Act, to ensure the legalization of e-rickshaws, considering the public safety and official registration of these vehicles.

This study has been conducted in major urban and suburban areas of West Bengal State in India, where e-rickshaws have become operational during the last two years. E-rickshaws are three-wheeled electric vehicles (EV) and are capable of ferrying four to five passengers at a time (excluding the driver), like that of the I.C. engine based auto-rickshaws. In these areas, e-rickshaws have become one of the preferred modes of public transport and are claimed to be comfortable by the commuters, than the auto-rickshaws. But again, like the auto-rickshaws, if these vehicles are allowed to ply on thoroughfares, the speed limit of 25kmph of e-rickshaws will likely affect the traffic speed, which will indirectly affect the environment, due to low speed emission of other petroleum based vehicles on road. The objectives of the present study were to discuss the merits of e-rickshaws over their I.C. engine counterparts, their economic and environmental impact, and also the challenges and adverse effects of these vehicles due to the present technology used has been discussed in this study.

METHODOLOGY

E-rickshaws in West Bengal had started operating in major urban areas, townships, and suburbs. The data regarding the operating conditions of these vehicles were collected by conducting a primary survey with formatted questionnaires among the operators and the commuters. The electricity consumption data were measured with energy meters, which were supplied to the operators. The measurements of distance traversed were noted from the odometer readings, maintaining the intervals of battery charging. Each set of data were gathered over a period of one week to check the travel pattern and the proper energy consumption of such vehicles. From

the collected data specific energy consumption for passenger transportation has been estimated. The specific energy cost of transportation has also been estimated, based on the electricity utility tariff of the specific region. In this study two electricity utility tariffs from CESC Ltd and WBSEDCL, were considered for the specific cost estimation. For the e-rickshaw owners, the sole charging hub remained their household sockets as other charging facilities were still not available. The electricity tariff for these household consumers was around INR 6.40/kWh for both the utilities considered. Majority of the grid power supply in West Bengal is based on coal fired thermal power stations. Thus the charging of e-rickshaws is accompanied with emissions from power stations. The environmental impact was calculated from the energy consumption data. The survey has also been extended to other vehicles on road, like auto-rickshaw, bus, and AC bus. These data were compared to that of the e-rickshaw for estimating the merits and the demerits of e-rickshaw.

RESULTS AND DISCUSSION

The e-rickshaws has been found energy efficient than the conventional modes of transports having an average specific energy consumption of 55.1 kJ/passenger-km, whereas the same for the LPG based auto-rickshaw was estimated to be 377.5 kJ/passenger-km, as shown in Figure 1. The specific cost of energy for transportation has been estimated to be INR 0.098 and INR 0.62 per passenger-km for the e-rickshaw and auto-rickshaw, respectively.

The major pollutant due to the combustion of carbon based fuels is carbon dioxide. The specific CO₂ emission for transportation has been estimated

for both e-rickshaw and auto-rickshaw. In general, coal fired thermal power stations in India have been reported to emit 1.281 kg of carbon dioxide per unit of electricity [2]. CO₂ emission from combustion of LPG has been reported at 1.53 kg/litre [3]. The comparative results between e-rickshaws and auto-rickshaws have been shown in Table 1.

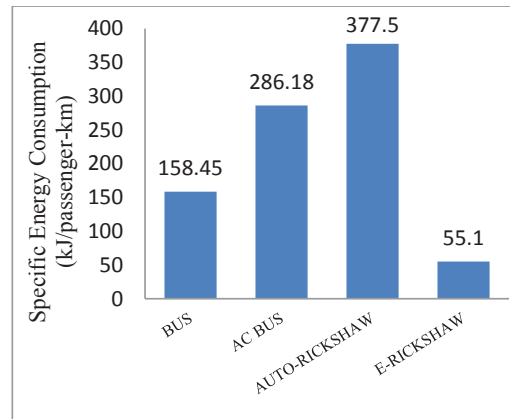


Figure 1. Specific energy consumption of different types of public transport vehicles in West Bengal

According to the amendment, the maximum motor capacity and speed limit of e-rickshaws have been regularized at 2000 W and 25 km/h respectively [4]. Thus the present technology has to meet the standards according to the present day traffic to avoid road congestion, which may lead to pollution problems.

Table 1. Comparative picture of Auto-rickshaws and E-rickshaws

Vehicle	Propulsion Technology	Maximum speed (km/h)	Maximum distance per refuel	Specific Energy Consumption (kJ/passenger-km)	Specific Energy cost (INR/passenger-km)	Specific CO ₂ emission (gm/passenger-km)
Auto-rickshaw	SI engine	60	230–280	377.5	0.62	24.54
E-rickshaw	*BLDC motor	25	80–100	55.1	0.098	19.29

*Brushless DC motor

References

- [1] <http://www.indiatvnews.com/news/india/study-recommendstreatingerickshawasmotorvehicles45352.html>, accessed on January 15, 2015.
 [2] T. Jash, "Renewable Energy And Environment", *Geographical Review of India*. **69** (1), 2007, pp. 20-24.

- [3] <http://www.biomassenergycentre.org.uk/>, accessed on January 27, 2015.

- [4] The Economic Times, "Promulgation of e-rickshaw ordinance gets Cabinet nod", 25, 2014.

ANALYSIS OF ENERGY EFFICIENCY AND BIO-ENERGY IN THE LAND TRANSPORTATION IN LAO P.D.R

Sengsuly Phoualavand¹ and Bundit Limmeechokchai²

¹Sirindhorn International Institute of Technology, Thummasat University, Thailand

²Department of Mechanical Engineering, Faculty of Engineering, National University of Laos, Laos

SUMMARY: land transport is the major mode transportation in the where it has consumed about 96% of total energy consumed in the transport sector. This paper investigates the effectiveness of the policy packages which includes counter measures (CM) relevant to the transport sector, namely 1) fuel switching, 2) electric vehicles 3) hybrid vehicles and 4) plug-in hybrid vehicles to reduce energy consumption and CO₂ emission during 2010-2050. In this study, the Long-rang Energy Alternative Planning (LEAP) model was applied to forecast sector-wise transport demand. Results show that the energy consumption in the transport sector will be increased from 593 ktOE in 2010 to 2,982 ktOE in 2050 while CO₂ emission will be increased from 1,789 kt-CO₂ in 2010 to 8,993 kt-CO₂ in 2050. However, implementation of four mitigation actions will reduce energy consumption by 5% and CO₂ emission by 9% when compared to the BAU scenario.

Keywords: Energy efficiency, Bio-energy, Energy consumption, CO₂ emission, LEAP model, Land transport

INTRODUCTION

In duration of the full national economic development in last decade, Laos has a high economic growth at an annual average growth rate of 8%. Similarly, in 2013 Laos's passenger traffic and the number of registered vehicles increased by about 7 times in comparison with 2000. The significant increase in vehicle volume has caused traffic congestion, air pollution especially, Vientiane capital city and other main cities, as well as import more foreign petroleum to satisfy the rapid increment in fuel demand in the transport sector.

The transport sector is the major energy consuming sector in Laos with a share of 22% of total final energy used in 2010. Being a landlocked country, Laos depends heavily on road transport for transportation. In 2010, road transport accounted for 95% of total passenger travel (passenger-kilometers) and 88% freight movement (ton-kilometer). The remaining passenger and freight traffic were carried through waterways and air transport.

Imported petroleum plays an important role in this sector and is the main energy source responsible for the energy consumption and CO₂ emissions. Since Laos does not have endogenous oil resources to meet the entire demand it is imperative to import petroleum oil from oversea. In 2010, the imported petroleum volume has been accounted for 646 million liters.

To avoid imported oil dependency and CO₂ emissions, bio-energy has been introduced by blending of gasoline with ethanol and diesel with bio-diesel to increase energy security and to reduce environment impacts from GHG emissions.

Additionally, the advanced technology is one of the counter measures proposed by IEA to reduce energy use and GHG emissions and other harmful gas emissions. There are several alternatives exist as advanced technologies which can be selected in both passenger and freight transport. In this study, three types of advanced technologies were considered to

analyze the energy efficiency. They are hybrid, plug-in hybrid and electric vehicles.

This study aims to analysis land transport energy consumption, and discuss about energy saving and CO₂ mitigation potential of implementation of fuel switching and introduction of advanced technologies. The analysis has been conducted using the Long-rang Energy Alternative Planning (LEAP) model with two scenarios; namely Business as Usual (BAU) scenario and counter measure (CM) scenario by considering 2010 as the base year for forecasting sector-wise transport demands up to 2050.

METHODOLOGY

The goal of this study is to investigate the energy consumption and CO₂ emissions in the transport sector under business-as-usual (BAU) scenario and to analysis CO₂ emission reduction and energy saving of four counter measures actions. The estimation of sector-wise transport energy demand and CO₂ emission were performed by using long-rang energy alternative planning model.

Scenario Design:

BAU scenario: This acts as a reference case that helps to estimate and analyze the future energy system performance under various policies and actions. In this scenario, the energy consumption and emission patters will be expressed under the assumption where no new policies or actions will be implemented in the time horizon 2010-2050.

Counter measure (CM) scenario: This scenario was focused on analyzing CO₂ mitigation and energy saving capabilities of potential countermeasures actions for Laos. In this study, two mitigation actions under CM scenario were selected, namely fuel switching action and advanced technology actions.

Fuel switching action: Two alternative fuels were considered in terms of fuel switching action as

gasoline blended with ethanol called gasohol and diesel blended with bio-diesel called bio-diesel. In this study, E10 and E20 (10% and 20% of ethanol blends with gasoline) and B5 and B10 (5% and 10% blends of bio-diesel with diesel) were modeled as alternative fuels with increasing penetrations.

Advanced technology action: To save energy and mitigate CO₂ emission on road transportation, advanced technology is an effective action implemented which can be in the transport sector. In the CM scenario, it has been chosen three advanced technologies for the transport modeling as three actions where all actions are starting in mid-term (2021-2030) with low penetration rates and increase to high in accordance to the price of technology and country's infrastructure

RESULTS AND DISCUSSION

Business as Usual (BAU)

Following the patterns of social-economic development in Lao transport sector. The energy consumption in selected year for the scenarios is given in the Figure 1. As it can be seen, the total energy consumption (TEC) trends under the each scenario have gradually been increased until 2050 with different annual growth rates. The projection shows the energy consumption under the BAU scenario would increase at about ten times from the base year 2010 where it has increased from 593 ktoe to 2982 ktoe in 2050, with annual growth rate of 5%. The significant increase is caused by pick-up and Truck where their energy consumption accounted for 21% and 28% of total energy consumption in the BAU scenario respectively. (see Figure 1)

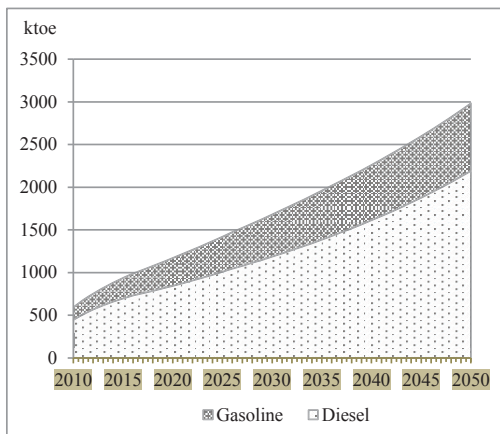


Figure 1. Energy consumption by vehicle types in the BAU scenario

Baseline CO₂ Emission

As it shown in Figure 2, the total CO₂ emission in the road transport in the BAU scenario would increase from 1,789 kt-CO₂ in 2010 to 8,993 kt-CO₂ in 2050 due to increase in energy demand and high fossil fuel use. On the other hand, the results show

potential reduction of CO₂ emissions in the CM scenario when compare to baseline scenario due to implementation of mitigation actions. (see Figure 2)

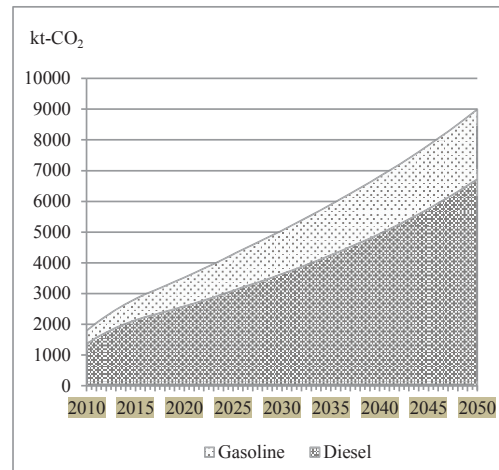


Figure 2. CO₂ emissions in the BAU scenario

ACKNOWLEDGMENT

Authors would like to thank Sirindhorn International Institute of Technology (SIIT), Thammasat University for the provision of "Excellent Foreigner Students (EFS)" scholarship and also would like to thank Stockholm Environment Institute (SEI) to provision of "LEAP" software.

References

- [1]Japan International Cooperation Agency, L.M.o.P.W.a.T., *Basic data collection study on low-emission public transport system in Lao PDR*, 2012, Ministry of Public Works and Transport: Vientiane, Lao PDR.
- [2] J. Javid, R., A. Nejat, and K. Hayhoe, Selection of CO₂ mitigation strategies for road transportation in the United States using a multi-criteria approach. *Renewable and Sustainable Energy Reviews*, **38(0)**, 2014, pp. 960-972.

CONSTRUCTED WETLAND FOR SEWAGE TREATMENT AND THERMAL TRANSFER REDUCTION

Akarat Panrare¹, Prapa Sohsalam² and Tusanee Tondee¹

¹Rattanakosin College for Sustainable Energy and Environment,
Rajamangala University of Technology Rattanakosin, Thailand

²Science and Environmental Technology Program, Faculty of Liberal Arts and Science,
Kasetsart University, Khamphaeng Saen Campus, Thailand

SUMMARY: The studying of thermal transfer reduction through the house by using a nearby constructed wetland was set at Kamphaeng Saen, Nakhon Pathom, Thailand. A model house with 3 x 3 x 2.5 of width x length x ceiling height was established with constructed wetland at west and south of the house. Differential temperature between inside and outside of the house was hourly collected by using thermocouple. The sewage which was produced from this house passed through wetland system and sewage treatment efficiency was also analyzed. The influent and effluent quality was analyzed at condition of plant and no-plant in wetland and hydraulic retention time of 2 and 4 days. The result showed that, the hottest direction and time was west and 4 pm. Plant in constructed wetland resulted to significant thermal transfer reduction which was 3 times compared with no-plant at west. The wastewater treatment efficiency was increase with plant in wetland and increase of HRT.

Keywords: constructed wetland, thermal transfer reduction, sewage treatment.

INTRODUCTION

Nowadays, residential construction was targeted for convenience energy-saving and eco-friendly. Air conditioner was the basic need for housing in tropical country which is the most proportion of household electric power consumption 40% approximately. [1] The reduction of air conditioner usage can be done by architectural design, selection of walls and windows material and the roof system which can prevent heat transfer into the buildings. [2] In an addition, the landscape planning, building orientation design for air ventilation or reducing heat from solar radiation by extend eaves or using sunscreen slats/lath [3,4], Shade garden [5] which commonly used today.

Planting the constructed wetland in high ambient temperature area could reduce the heat transfer to the residential area and has a potential to treating household wastewater. In this study, constructed wetland was used as purpose which mentioned above. Constructed wetland was installed at west and south of the model home and varying hydraulic retention time at 2 and 4 days. The domestic wastewater treating efficiency and thermal transfer reduction performance by constructed wetland were investigated

MATERIAL AND METHODS

Synthetic wastewater and wastewater feeding system

Synthetic wastewater contained BOD 170 mg/L, Suspended solid 100 mg/l and 50 mg/l of ammonia were prepared by mix tapioca flour and urea with nearby water source (canal water). synthetic wastewater was kept in 2 m² storage tank, connected with 0.5 HP pump and adjust flow rate to 6.25 and 12.5 l/day for 2 and 4 days HRT.

Constructed wetland installation

Constructed wetland system was built by square steel tube frame with the dimensions of 2.0 m length, 0.5 m width and 0.7 m height. Cover inner wall with 100 micron HDPE plastic sheet. 0.5 m height of wetland medium was consisted of 40 mm crushed rock. The 1 month growth of *Canna indica L.* (1 m. height in average) was planted with the density of 20 plant/m². The experimental area was set up at Kasetsart University, Kamphaeng Saen Campus, Nakhon Pathom, Thailand. (14.023473N, 99.974945E)

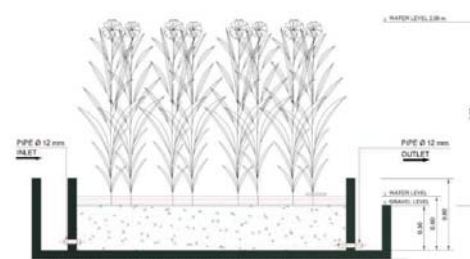


Figure 1. Constructed wetland schematic

Model home

Model building was the size of 9 m³ (3 x 3 m). The height of the ceiling was 2.5 m., the distance from ceiling to roof ridge was 1 m. and long frieze of 50 cm. Model home was raised above the ground surface for 50 cm.

Water quality analysis

Influent and effluent samples of constructed wetland system were collected every 2 days in each set of an experiment (10 days). The wastewater samples were analyzed as standard APHA method (2005) [6]

Statistical analysis

All statistical analyzed were performed using SPSS 16.0 by SPSS Inc. In all cases, significance was defined by $P < 0.05$. Test for significant difference in each condition were tested using a One-way ANOVA with a Duncan's Multiple Range Test (DMRT).

RESULT AND DISCUSSION

Heat transfer reduction by constructed wetland

From 24 hr. average temperature profile of building in 5 different direction. The roof of the building has the highest temperature (44.40 degree Celsius) at 3.30 pm. Inside model home temperature, western and southern direction were received the high amount of heat at 4 pm of the day which was 38.07 and 35.50 degree Celsius, respectively.

Table 1. Building temperature difference.

Conditions	Temperature difference	
	Western	Southern
CW Without Vegetation	1.21 ^a	0.66 ^a
Vegetation, West	3.55 ^b	0.67 ^a
Vegetation, South	1.55 ^a	2.03 ^b
Vegetation, West and South	3.65 ^b	2.29 ^b

The building with combination of western and southern side constructed wetland had the highest temperature difference (3.55 and 2.03 degree Celsius). Which means, the constructed wetland was capable to reduce the heat transfer from the environment to the building in each direction and also reducing the overall heat receives of the building.

Wastewater treatment efficiency

Figure 2 illustrated the concentrations of TSS, BOD, TKN and PO₃ of the wastewater before and after treating by constructed wetland.

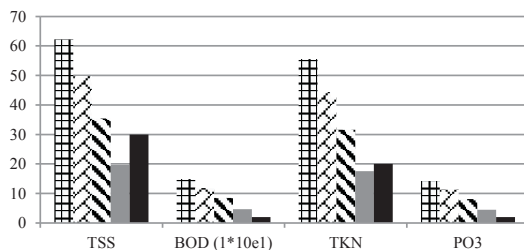


Figure 2. Contaminant concentrations of Constructed Wetland influent and effluent, without vegetation at 2 day HRT (▨), 4 day HRT (▩) and with vegetation at 2 day HRT (■), 4 day HRT (■) and domestic wastewater discharge standard. (■).

From figure 2, CW with vegetation at 4 days HRT had the lowest concentration of all interested contaminant (19.7, 40.7, 17.5 and 4.5 mg/l for TSS, BOD, TKN and PO₃ respectively). CW with vegetation gave higher efficiency and increasing HRT was also provided more removal efficiency.

Compared to domestic wastewater discharge std. from Ministry of natural resource and environment, but only TSS and TKN of CW with vegetation @ 4 day HRT were met the standard. Extending the HRT would proficient reducing BOD and PO₃.

CONCLUSION

This research proved that constructed wetland was capable to reduced housing energy consumption by reducing overall heat transfer from environment (2 – 3 degree Celsius) and also had a capability to remove TSS, BOD, TKN and PO₃ (81.5%, 73.4%, 69.6%, 77.7% of removal efficiency respectively) from wastewater to below domestic wastewater discharge allowance at 4 days HRT or above. Increasing HRT to 6 or 8 may increase the overall treating efficiency to acquired qualified contaminant concentration.

Moreover, Nitrogen and Phosphate in wastewater gave the positive effect to the vegetation as the essential nutrient. Planting the vegetative Constructed Wetland in household not only gave the capability to treating the wastewater, but also reducing the heat received and gave the architectural aesthetics.

References

- [1] C. Surawut, P. Chaiwiwatworakul, S. Chiarakorn, P. Rakkwamsuk and S. Chirarattananon, "Reducing energy consumption cost and greenhouse gas emission for tropical low-income housing: Thailand contribution", *5th International Conference on Sustainable Energy and Environment (SEE 2014)*
- [2] N. Philip and H. Kenneth, "Passive Solar Handbook". *California Energy Resources Conservation*. 1980.
- [3] G. Guohui, "A parametric study of Trombe walls for passive cooling of buildings", *Energy and Buildings*, **27(1)**, 1998, pp. 37–43.
- [4] M.A. Karam, M. Ismail and A.M.A. Rahman, "Passive cooling techniques through reflective and radiative roofs in tropical houses in Southeast Asia: A literature review", *Frontiers of Architectural Research*, **3(3)**, 2014, pp. 283–297.
- [5] H. Akbari, "Shade trees reduce building energy use and CO₂ emissions from power plants", *Environmental Pollution*, **116**, 2002, pp. 119–S126.
- [6] APHA, AWWA, WEF. "Standard methods for the examination of water and wastewater (22nd edition)", Washington, D.C., USA. (2012).

Energy Efficiency, Innovation and Life Cycle Assessment

INNOVATIVE SOLUTIONS FOR ENERGY CONSERVATION THROUGH COMMERCIAL AND DOMESTIC DEMAND SIDE MANAGEMENT

Darryl R. Smith¹ and Robert B. Smith²

¹Redshift Wireless Pty. Ltd., Sydney, Australia

²AEC Consultants Pty. Ltd., Sydney, Australia

SUMMARY: Development of alternative energy sources must go hand in hand with demand management. This is of particular importance in developing countries where energy consumption will continue to increase as the economy becomes more developed and the people more affluent. With the market penetration of mobile communications command and control of heating and cooling systems in commercial and domestic buildings is becoming a viable option. Such solutions are particularly applicable to the existing building stock. Tools are available to achieve the task. All that are needed are the systems and processes to link the mobile device to a smart command and control system which is then able to manage the appliance to achieve energy savings and at the same time show the consumer the savings that have been made. This abstract raises the issues that will be discussed in detail in the final paper together with the energy savings that could result from such an approach.

Keywords: energy demand management, energy conservation, mobile communications, WiFi

INTRODUCTION

Energy demand can be addressed at both on the generation side as well as the demand side. Increasing supply can be achieved by building more power generating facilities, as well as developing renewable and alternative energy sources. Demand can be addressed by requiring Green-rated buildings and energy efficient equipment but retrofitting solutions to existing buildings is a more difficult and costly task.

As communities in the Asian tropical areas become more affluent energy efficient fans are being replaced by power hungry air-conditioning units, in an aging electricity network not designed for such loads. Demand for electricity continues to increase markedly, causing reduction in power availability and reliability.

One key issue that needs to be addressed is the energy consumption of existing commercial and residential buildings. Countries are trying to address demand but are potentially overlooking low cost solutions at the commercial and residential building level. These solutions can be either mandated, voluntary, or community based.

This paper explores some of the issues and possible solutions.

AVAILABILITY OF COMMUNICATION INFRASTRUCTURE

Mobile/Cell Phone penetration

The last decade has brought significant changes with the not only the availability of communications infrastructure, but the cost of access to that communications infrastructure. For instance, by 2013 Thailand had over 90 million active mobile phone subscribers. Even as the government invests in broadband infrastructure, mobile will be a key driver of internet use in Thailand.[1] Since then things have only escalated with widespread acceptance of tablet computers (such as the iPad), and many households

going wireless for not only voice communications but also for Internet access. With ubiquitous communications infrastructure, advanced services have become available.

WiFi connected embedded devices

The past year has brought major changes in the infrastructure for WiFi connected embedded devices. At the start of 2014, for instance, the Spark Core WiFi processor at US\$39 and the Electric Imp at US\$25 were the state of the art in terms of price for prototype development. By the end of 2014, these same modules started to look decidedly expensive with the ESP8266 costing US\$2.70.[2]

Possible way forward

As the communications infrastructure is becoming ubiquitous in developing countries it provides an opportunity to utilize this technology to as a demand management tool for domestic and commercial buildings. The question becomes one as to whether 3G, WiFi or both can be used for command and control.

ENERGY DEMAND MANAGEMENT

There are a number of "rules" that should be followed in developing demand management tools. These "rules" include:

- If the energy savings are obtained with making one off adjustments, making the adjustment manually will probably bring higher savings. For instance, there is little benefit in dynamically adjusting the thermostat on a hot water heater;
- Concentrate on the areas of highest use, and do a simple cost benefit analysis on each area;
- Consider whether replacement is a better option than management. Rather than controlling 50W halogen down lights, replacing these same lights with 3W LED's will probably be cheaper, even without control;
- Plan for the communications infrastructure not to

work, potentially for months at a time;

- Dynamic pricing is an external price signal that can be used to reduce demand; and
- There is a benefit, both environmentally and financially to moving load, even if there are no reductions in consumption.

AREAS OF ENERGY CONSUMPTION IN COMMERCIAL AND DOMESTIC BUILDINGS HVAC – Heating, Ventilation and Air Conditioning

Despite being 200-300% efficient, space heating and cooling using air conditioners and heat pumps can consume significant amounts of energy. Many buildings are being installed with individual split system units rather than centrally controlled units, making central control and monitoring more difficult. Manufacturers are starting to make devices connected, but this is still a premium feature missing from the lower end of the market. It also does nothing for the existing stock of units in the field.

A system on centralizable, retrofittable WiFi devices is proposed as a way to gain energy reduction. Such a system provides savings primarily through enforced timers, temperature range limits and central command and control. Varying the thermostat by 1°C has the potential to reduce energy consumption by up to 15%. Larger variations have the potential for greater savings.

Electric Solar Hot Water Units

Whilst electric solar hot water units use less energy than normal storage hot water units, over the course of a year, their energy consumption is approximately 15% of a similarly sized electric only unit. This energy is used for circulating water through the roof panels and also for boosting the water in the tank when there has not been enough solar activity to sufficiently heat the water. It is the boost heating that has a potential for energy savings.

In hotels, the peak hot water usage is for bathing in the mornings and evenings. The cheapest price for electricity is currently generally overnight; the peak time for solar heating will be during the middle of the day. There is therefore a discontinuity between the times where hot water is consumed, and the best times to heat the hot water.

Electric Hot Water Units

The traditional schemes for Storage Electric Hot Water within Australia are to turn the heating of the water on and off either through a timer, or through tones superimposed on the electricity network. Other countries use a separate control wire from the electricity distributor to turn the Hot Water Heater on and off.

They all fail to a certain extent when Time of Use energy is used for heating water, be it on an Off Peak or general use energy rate. Ideally, when water is heated using electricity on a Time of Use tariff,

customers would like to:

- Decide the maximum rate they would like to pay to heat their hot water;
- Be able to adjust the maximum rate through a simple interface;
- Be able to override the maximum rate for a few hours, once they have used all their available hot water; and
- Provide daily feedback on energy used to heat water to provide a tighter feedback loop.

CONCLUSION

Development of alternative energy sources must go hand in hand with demand management. This is of particular importance in developing countries where energy consumption will continue to increase as the economy becomes more developed and the people more affluent. Whilst new products are likely to incorporate energy saving devices it is difficult mandate retrofitting. On the other hand, the consumer is likely to retrofit a suitable device if it can be shown that there are immediate cost benefits.

Tools are available to achieve the task. All that are needed are the systems and processes to link the mobile device to a smart command and control system which is then able to manage the appliance to achieve energy savings and at the same time show the consumer the savings that have been made.

This abstract raises the issues that will be discussed in detail in the final paper together with the energy savings that could result from such an approach.

References

- [1] Anon., "Mobile Brings More Consumers Online in Thailand: Cheaper smartphones propel internet uptake", *eMarketer*, August 14, 2013, at <http://www.emarketer.com/Article/Mobile-Brings-More-Consumers-Online-Thailand/1010131>, (accessed January 28, 2015).
- [2] C. Gammel, "The Amp Hour Podcast: #232–Impedance Matching with Davidson and Vandembout–Presbytes Pushing Portfolios"⁵, 2015 at <http://www.theamphour.com/232-impedance-matching-with-davidson-and-vandembout-presbytes-pushing-portfolios/> (accessed January 28, 2015).

LIFE CYCLE ENVIRONMENTAL IMPACTS OF RENEWABLE ELECTRICITY IN TURKEY: RESERVOIR AND RUN-OF-RIVER HYDRO, WIND AND GEOTHERMAL POWER

Burcin Atilgan¹ and Adisa Azapagic¹

¹ School of Chemical Engineering and Analytical Science, The University of Manchester, UK

SUMMARY: This paper sets out to estimate for the first time the life cycle environmental impacts of electricity generation from renewables in Turkey. There are 55 reservoir hydropower, 205 run-of-river hydropower, 39 wind and six geothermal power plants in Turkey all of which are considered in this study. The results indicate that wind is the worst option overall, with nine out of 11 impacts higher than for hydropower and geothermal. However, its global warming potential is 88% and 11% lower than for geothermal and large reservoir, respectively. Acidification from geothermal is 281 times higher than for wind power. The majority of the annual impacts from the renewable electricity mix are from hydropower with the exception of acidification which is largely from geothermal electricity.

Keywords: Turkey, renewable energy, life cycle assessment, electricity generation, sustainability

INTRODUCTION

In today's world, energy has an essential role for sustainable development. Providing reliable, clean and affordable energy is important for the economic and social growth of a country. Turkey is a developing country with a rapidly growing economy and population. Like many other countries, it already has difficulties in meeting energy demand as the endogenous fossil energy resources are insufficient, the problem that will only be exacerbated by the growing economy and population. On the other hand, although there is a large potential of renewable energy resources, their current utilization is low. In 2010, the total energy generation in Turkey was 377,894 GWh while the total consumption amounted to 1,270,764 GWh, more than three times higher than the country's generation capacity. This has led to Turkey's dependency on energy imports from other countries so that nearly 70% of the national demand is being met by imported fossil fuels [1].

The electricity demand in Turkey has been growing rapidly, reaching 211,208 GWh in 2010, almost seven-fold higher than in the mid-80s. In 2010, renewables generated 58,018 GWh, contributing 26.4% to the total generation. The most important renewable energy source to generate electricity is hydropower (24.5%) [1]. The high share of fossil fuels in Turkey's electricity mix together with the increasing demand has led to a steady increase in greenhouse gas emissions from the sector, growing by 115% between 1990 and 2010 [2]. It is, therefore, important that Turkey identifies and implements sustainable energy technologies suitable for the country, if climate change and other environmental impacts are to be curbed.

METHODOLOGY

The LCA has been carried out following the ISO 14040/14044 guidelines [3]. The goal of the

study is to estimate the life cycle environmental impacts of electricity generation from renewable sources in Turkey, using 2010 as the base year. Two functional units are considered:

- generation of 1 kWh of electricity by large and small reservoir, run-of-river, wind and geothermal power plants; and
- annual generation of electricity from these power plants, in this case 55,379 GWh generated in 2010.

The scope of the study is from cradle to grave, comprising electricity generation as well as plant construction and decommissioning.

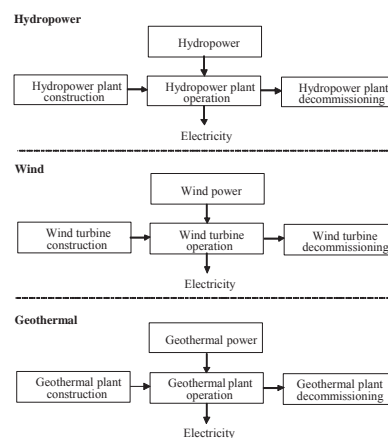


Figure 1. The life cycle stages of renewable electricity

RESULTS AND DISCUSSION

The CML 2001 impact assessment method [4], November 2010 update, has been used to estimate the environmental impacts via GaBi software [5]. The following impacts are considered: abiotic depletion potential (ADP elements and fossil), acidification potential (AP), eutrophication potential

(EP), fresh water aquatic ecotoxicity potential (FAETP), global warming potential (GWP), human toxicity potential (HTP), marine aquatic ecotoxicity potential (MAETP), ozone layer depletion potential (ODP), photochemical ozone creation potential (POCP), also known as summer smog, and terrestrial ecotoxicity potential (TETP).

The results indicate that electricity from onshore wind is the worst option overall, with nine out of 11 impacts higher than for hydroelectricity options and geothermal power. This is due to the impacts from the life cycles of construction materials. However, the GWP of wind power is 88% and 11% lower than for geothermal electricity and large reservoir hydropower, respectively. On the other hand, the acidification potential of geothermal power is around 280 times higher than from wind power because of the air emissions of hydrogen sulphide (99.9%). Overall, geothermal power is the best option for seven impacts (eutrophication, ozone layer depletion, summer smog and all the toxicity categories). Large reservoir hydropower has the lowest depletion of elements and fossil resources as well as acidification. Small reservoir and run-of-river plants are the best and geothermal power worst options for the global warming potential.

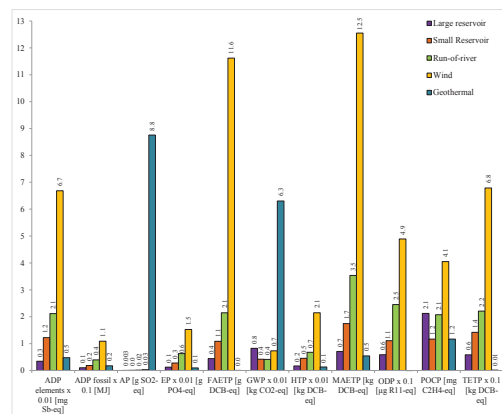


Figure 2. Environmental impacts from renewable electricity sources in Turkey, expressed per kWh

As the results of this study suggest, construction of the power plant is the main contributor to the impacts. Recycling of materials at the end of their useful time instead of landfilling reduces the environmental impacts by up to 40%.

The annual GWP is estimated at 404 kt CO₂-eq., of which large reservoir plants contribute 62.5%, small reservoir 14.3%, geothermal 10%, run-of-river 7.5% and wind 5.3%. By comparison, the total annual GWP from fossil fuel plants in Turkey is estimated at 109 Mt CO₂-eq. [6]. This is 270 times higher than the impact from renewable

electricity, although fossil fuels supply only 2.7 times more electricity (153,190 GWh/year).

The spread of renewable energy sources as an alternative to fossil fuels is important for Turkey to reduce the dependence of import energy, provide security for supply and reduce the environmental impacts from the electricity sector. Therefore, the government should encourage and possibly incentivize increasing the share of renewables in the electricity mix. However, renewable electricity options should be chosen with care. For example, increasing the proportion of geothermal power in the electricity mix would increase some of the life cycle impacts such as acidification and global warming potential.

ACKNOWLEDGEMENTS

This work was funded by the Republic of Turkey Ministry of National Education. This funding is gratefully acknowledged.

References

- [1] EUAS, *Annual Report 2011*, Turkish Electricity Generation Company: Ankara.
- [2] TUIK, *National Greenhouse Gas Inventory Report, 1990-2010*, 2011, Turkish Statistical Institute: Ankara.
- [3] ISO, *Environmental Management - Life Cycle Assessment - Requirements and Guidelines*, 2006a&b, International Organisation for Standardisation: Geneva, Switzerland.
- [4] J.B. Guinée, M. Gorrée, R. Heijungs, G. Huppes, R. Kleijn, A.D. Koning, L.V. Oers, A.W. Sleeswijk, M.A.J. Huijbregts, *Life Cycle Assessment: An Operational Guide to the ISO Standards: Part 2a*, in Ministry of Housing, Spatial Planning and Environment (VROM) and Centre of Environmental Science (CML)2001: The Netherlands.
- [5] PE International, 2013, *GaBi v.6*, Stuttgart, Echterdingen.
- [6] B. Atilgan, and A. Azapagic (2014). Life cycle environmental impacts of electricity from fossil fuels in Turkey. *J Cleaner Prod.* In press. doi:10.1016/j.jclepro.2014.07.046.

URBAN HEAT ISLAND AND HOUSEHOLD ENERGY CONSUMPTION IN BANGKOK, THAILAND

Sigit D. Arifwidodo¹ and Orana Chandrasiri²

¹ Department of Landscape Architecture, Faculty of Architecture, Kasetsart University, Thailand

²International Health Policy Program, Ministry of Public Health, Thailand

SUMMARY: This study focuses on the urban heat island (UHI) development and its impact on household energy consumption. Hourly air temperature data were used to study the characteristics and intensities of UHI in Bangkok area. A survey questionnaire of 400 randomly selected respondents is conducted to explain the relationship between UHI intensity and household energy consumption. Cooling Degree Days (CDD) index was used to establish the correlation between UHI and energy consumption. The result indicates that the presence of urban heat island in Bangkok plays a significant role in residential energy use, directly and indirectly. Energy consumption is found to have association with CDD. The study concludes that combining the concept of UHI mitigation and adaptation planning and energy-efficient housing design will contribute to better solutions for creating a more energy-efficient city.

Keywords: household energy consumption; urban heat island; urban planning; sustainable urban development; cooling degree days

INTRODUCTION

Bangkok has been experiencing high growth of urbanization and industrialization which led to several environmental problems such as air pollution, water pollution, land subsidence as well as the problems from the presence of urban heat island such as temperature rise and high energy consumption. In 2012, the maximum temperature difference between urban and rural area of Bangkok was 7°C, which higher than in the last 10 years. Correspondingly, due to the appearance of urban heat island many problems arise, hence the impacts of urban heat island should be also taken into consideration. In case of Bangkok, the air conditioning load is considered to have the largest share (almost 60%) of electricity use. Therefore, it is important to assess the impact of UHI to household energy consumption from the microclimate perspective.

METHOD

The study defines household energy consumption as the per-square meter of floor electricity consumption assuming that different types of house have the same amount of lighting, appliances and usage pattern. A survey questionnaire of 400 randomly selected respondents is conducted to explain the relationship between UHI intensity and household energy use. Cooling Degree Days (CDD) index was used to establish the correlation between UHI and energy consumption. The study also uses Cooling Degree Days (CDD) to investigate the effect of higher temperature on cooling energy consumption in Bangkok. The CDD profiles from 4 weather stations from 2013-2014, in addition to providing an energy audit database, are used in the OLS regression to examine the sensitivity of electricity consumption.

RESULT

The long-term annual air temperature record in Bangkok from 1980-2013 shows that the temperature had been cooler in cool season and warmer in hot season. Using Bangkok Metropolis weather station as an example, figure 1 shows that the mean maximum and minimum annual air temperature from 1980-2013 was 33 °C and 24 °C respectively, and increasing linearly by 0.95 °C and 1.97 °C. One significant factor affecting this increase is probably the rapid urbanization in Bangkok. The monthly CDD are estimated for the base temperatures 18 °C and 24 °C. The highest number of CDD in 4 areas occurs in April and the lowest in January. 84% of households analyzed in the study have air conditioning (AC) equipment in their housing units.

A survey conducted by the National Statistical Office of Thailand [9] shows that the average energy expenditure is 2,084 THB or 10.9% of the total expenditure with the expenditure on electricity is 607 THB (29.1% of the total energy expenditure). The average electricity expenditure in Bangkok Metropolitan Area is 1,133 THB, higher than other region in the country. The number is slightly different with the result from the survey (854.35 THB for the electricity expenditure). 72% of households in the study has Air Conditioning (AC) equipment in their housing units. There is a positive correlation between income and the number of AC unit owned in the house (two-tailed *t-statistics*, $p < 0.0001$). This is because the higher the income, households tend to have bigger floor area in the house. The floor area of the house is also found to have a positive correlation with the frequency of AC use (two-tailed *t-statistics*, $p < 0.005$). Air Conditioning (AC) equipment ownership is the most fundamental factor in household space cooling consumption. More than 80% of the respondents have AC equipment in their housing units. There is a

positive relationship between the ownership of AC equipment and CDD ($F = 81.569, p < 0.001$). As expected, there is a positive correlation between household energy consumption and CDD. Regressing monthly energy use for space cooling per square meter (E) to CDD resulting in high coefficients of R^2 (adj $R^2 = 0.881$; std error = 1.046; p -value < 0.001). This finding implies that CDD and E values experience change in the same direction. The OLS regression between monthly CDD and monthly electricity consumption (kWh/sq.m) shows that there is a positive correlation (adj. $R^2= 0.841$, Std error = 1.322, p -value < 0.001). The result indicates that the presence of urban heat island in Bangkok plays a significant role in residential energy use, directly and indirectly.

Energy consumption is found to have association with CDD. The study concludes that combining the concept of UHI mitigation and adaptation planning and energy-efficient housing design will contribute to better solutions for creating a more energy-efficient city.

References

- [1] S. Arifwidodo and T. Tanaka. "Development of Bangkok and The Evidence of Urban Heat Island". *Proceeding of International Symposium on Economics and Social Science 2015*. Bangkok: ISESS

THE POTENTIAL OF DEMAND RESPONSE MEASURES OF COMMERCIAL BUILDINGS IN THAILAND

Witchuda Pasom¹, Apichit Therdyothin¹, Adisak Nathakaranakule¹, Cherdchai Prapanavarat² and Bundit Limmeechokchai³

¹School of Energy, Environment and Materials, King Mongkut's University of Technology Thonburi, Thailand

²Department of Electrical Engineering, King Mongkut's University of Technology Thonburi, Thailand

³Department of Mechanical Engineering and Manufacturing Systems, Sirindhorn International Institute of Technology, Thailand

SUMMARY: The aim of this research is to estimate the potential of demand response measures applying to commercial building in Thailand based on the actual testing result from 3 existing buildings in Bangkok. The potential measures can be divided into 2 main categories namely self-generation using existing standby generators and reducing their actual demand using various techniques. The initial estimation point out that the maximum of 2.1 MW can be reduced from these 3 tested building. However, the actual experiment shows that only 1.76 MW can be archived. The difference of the peak reduction mainly comes from not only the in-accurate estimation of the standby generator ability in both capability and durability but also the effect on the comfort condition stability in the building. Therefore, the appropriate estimated level of demand reduction from the building should approximately 83% of technical potential. The final recommendation from the building owner is the building should adopt DR scheme and able to reduced their demand to some extent. However, it depends on the level of benefit offered to the building.

Keywords: Peak demand reduction, Demand side management, Demand response

INTRODUCTION

The energy security of the electricity system is crucial to the development of the national economy for the developing country including Thailand. Especially during the summer when the peak of the system is high and the generating capacity of the country are hardly cope with. Building the new power plant is seemed to unacceptable not only investment cost but also the environment point of view. Therefore, enhancing the behaviors of electricity user like demand response is considered. Many countries found that these measures are acceptable by their customer. Generally this type of measures have lower cost than building new peak power plant [1],[2].

However, this type of measure need participation from numbers of the customers and can affect the daily operation of those customers. Therefore, the measures have to be tested and evaluated for their actual cost of operation and all side effects before applying these schemes to all customers.

RESEARCH METHODOLOGY

In this study, many demand response measures have been actually tested and verified in 3 existing building. The buildings comprise of hospital building and 2 shopping malls. The baseline of electricity using pattern of all major equipment in the building has been collected. These data have been used to estimate the potential of peak demand reduction during the tested period [3]. The electricity consumption data can be used to evaluate the baseline of the building and some specific system to get the actual peak reduction during tested period. (1pm-4pm)

The testing process can be device into 2 main parts.

The first part is monitoring the overall electricity use pattern that will be used to formulate the base line for the test day. The second part is the result of the test day that will be used to compare with the formulated based line to identify the peak reduction.

RESULTS AND DISCUSSION

To formulate the base line for each individual building, we need to monitor the electricity consumption pattern of the building for 10 days prior the test day. In the test day, the overall electricity consumption of the building will be measured together with the various high consume equipment and system. During the test hour, 1 pm. to 4 pm. of the test date, the actual electricity consumption of the building will be compared with the formulated base line to evaluate the real value of the peak reduction. The finding can be summarized as follows.

Hospital

Figure 1 show the electricity consumption pattern of the hospital and the peak reduction during the test hours.

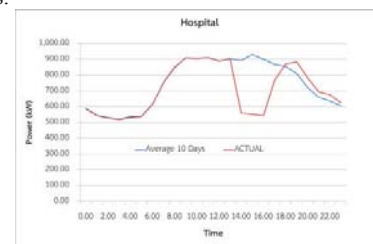


Figure 1. The power reduction from DR tested of the hospital

The graph show that the peak kW of the tested hospital can be reduced 355 kW or 36.5% of peak demand of the building. This is mainly come from the use of standby generator to cut off the building peak and a bit rising the temperature in the building. The rough calculation of the cost of electricity generated by the standby generator is 7.80 baht per kWh base on the price of diesel at 29.99 baht per liter.

Shopping mall 1

The Measures applied to the shopping mall 1 including running the standby generator for 3 hours, limited the door opening of the freezer, set demand limit of the chiller to 80% of maximum demand. These can reduce 318 kW of peak demand or equal to 26.7% of actual demand. The profile of electricity used during the test hours is shown in fig.2. The cost of running standby generator of this building is about 10.0 baht per kWh.

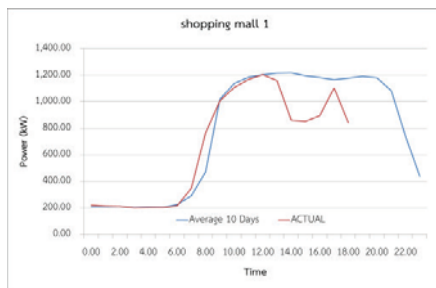


Figure 2. The power reduction from DR tested of the shopping mall 1

Shopping mall 2



Figure 3. The power reduction from DR tested of the shopping mall 2

The measures that applicable for the shopping mall 2 is running of standby generator, shut down one chiller and a storage water pump. The peak of the building can be reducing by 1.09 MW or equivalent to 26.7% of the actual peak demand. The cost of electricity generated is 9.17 baht per kWh

The total peak reduction in these 3 building is 1,759 kW, that 64% is the result of running the

standby generator while others 36% from various peak reduction measures.

Many problems are faced during the testing hour for example, the temperature inside the standby generator room and of the generator itself rising up to the level that considered too dangerous to continue the test. This cause the shopping mall to stop its generator before the test is finish. There are reported of problem about the maximum generating capacity of the generator which found that even the newest one can't run at it rated capacity for 3 hours. Moreover, the running of this exercise show that the utility in the building are not well maintain and prepare enough for this activities

DISCUSSION

Demand respond in Thai building seem to have high potential but main reduction is from running standby generator which have high running cost. Therefore, the cost of applying demand response program in Thailand may face high running cost. In the individual point of view of the building owner, implementing this demand respond may cause some effect on their customer. Therefore, the incentive that they should get must be higher enough.

ACKNOWLEDGMENT

The author would like to thanks to all 3 example buildings and Energy Conservation Laboratory (EnConLab) of King Mongkut's University of Technology Thonburi for their excellent cooperation and the tested data.

References

- [1] M. Parsa Moghaddam, A. Abdollahi, M. Rashidinejad and A. Rashidinejad, "Flexible demand response programs modeling in competitive electricity markets", *Applied Energy*, **88(32)**, 2011, pp. 57-3269.
- [2] P. Faria, Z. Vale, "Demand response in electrical energy supply: An optimal real time pricing approach" *Energy*, **36(8)**, 2011, pp. 5374-5384.
- [3] W. Pasom, A. Therdyothin, A. Nathakarakule, C. Prapanavarat and B. Limmeechokchai, "Potential of demand response in Thailand" *5th International Conference on Sustainable Energy and Environment* 19-21 November 2014, Bangkok, Thailand

ENERGY EFFICIENCY ANALYSIS IN AN INTEGRATED BIOMASS GASIFICATION FUEL CELL SYSTEM

Woranee Paengjuntuek¹, Jirasak Boonmak¹ and Jitti Mungkalasiri²

¹ Chemical Engineering Department, Engineering Faculty, Thammasat University, Thailand

² MTEC, National Science and Technology Development Agency, Thailand

SUMMARY: Biomass gasification for power generation has received considerable attention as a partial substitute for fossil fuels power generation. Gasification is the incomplete combustion that converts a carbon-containing feedstock into syngas including hydrogen, methane, carbon monoxide, carbon dioxide, water and other gaseous hydrocarbons. To increase power efficiency, fuel cell is one of the most suitable ways to combine with biomass gasification especially solid oxide fuel cell (SOFC). SOFC is considered as the most encouraging fuel cell type due to its high power generation efficiency and long term stability. In order to use energy more efficiently, energy analysis should be evaluated. In this study, Aspen plus 7.2 is used to perform an integrated biomass gasification fuel cell (BGFC) system with rice straw feedstock for power generation.

Keywords: biomass gasification, energy efficiency, fuel cell, power generation system

INTRODUCTION

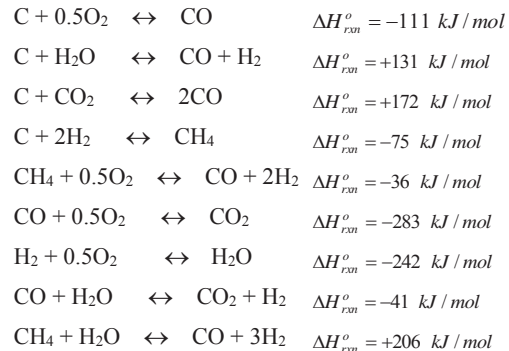
According to the population growth in Thailand, there is not sufficient electricity and also energy consumption. Furthermore, using fossil fuels have negative environmental impacts due to greenhouse gas emissions and air pollution problem. Therefore, biomass is a renewable and sustainable source to produce environmentally friendly energy. Biomass is also considered as the ideal energy source for gradually replacing fossil fuels. Moreover, agricultural residues in Thailand such as rice straw, bagasse, palm empty bunch and cassava rhizome have increased in recent year. Biomass residues can also use for domestic heating and industrial cogeneration. In Thailand, rice straw is one of the main agricultural residues and it is estimated to be about 26 Mt/year. In addition, the capital cost of rice straw power generation is low [1].

Considering environmental issues, biomass gasification for power generation has received considerable attention as a partial substitute for fossil fuels power generation. Because it is more environmentally friendly and it provides a profitable way to dispose wastes. In addition, the energy efficiency of biomass gasification can be greatly enhanced when operating with highly efficient power generation systems, such as solid oxide fuel cell (SOFC). The combined cycle of renewable energy sources and innovative power generation technology are called integrated biomass gasification fuel cell (BGFC) system. Therefore, the purpose of this study is to evaluate an energy efficiency of integrated biomass gasification fuel cell system using rice straw feedstock in order to purpose sustainable way for electricity production in Thailand.

BIOMASS GASIFICATION

Biomass gasification is the conversion of solid fuels (biomass) such as wood, wood-waste, rice straw and agricultural residues into a combustible gas. Combustible gas consists of carbon monoxide (CO), carbon dioxide (CO₂), hydrogen (H₂) and traces of methane (CH₄). This mixture is called producer gas or syngas.

Gasification reactions, series reactions with oxygen and additional gas phase reaction, are



The composition of rice straw is referenced by [2].

FUEL CELL

A fuel cell is an electrochemical energy conversion device which directly converts one part of chemical energy into electrical energy by consuming hydrogen-rich fuel and oxidant. At the cathode, oxygen is reduced by the incoming electrons to produce oxygen anions that are conducted through the electrolyte to the anode where they electrochemically combine with the adsorbed hydrogen to form water and heat as a by-product and release electrons to the external circuit. The electrochemical reactions as follows [3]:

At the anode:



At the cathode:
 $1/2O_2 + 2e^- \rightarrow O^{2-}$
 Overall reaction:
 $H_2 + 1/2O_2 \rightarrow H_2O + \text{Heat} + \text{Electricity}$

205.35	kg rice straw/hr
2.0	air to biomass ratio
1.3	steam to biomass ratio
1000°C	gasifier temperature
1 bar	gasifier pressure
1000°C	fuel cell temperature
5 bar	fuel cell pressure

INTEGRATED BIOMASS GASIFICATION FUEL CELL SYSTEM

Integrated biomass gasification fuel cell system (BGFC) is an alternative way to generate electricity from biomass with less pollution. BGFC system contains 6 main units as shown in Figure 1. These are gasifier, cyclone, heat recovery steam generator (HRSG), gas clean up, steam turbine, and solid oxide fuel cell (SOFC). The system generates electricity from two ways, the turbine unit and SOFC unit, which has different efficiency. The electrical output from fuel cell is predicted by electrochemical model [4].

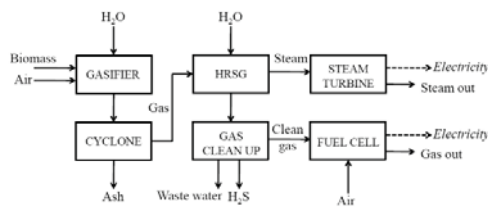


Figure 1. The process flow diagram of BGFC system.

ENERGY ANALYSIS

Energy analysis is based on the first law of thermodynamics, the conservation principle of energy in quantity. The energy efficiency, η , of a system or system components is defined as the ratio of energy output to the energy input of system.

For thermal efficiency

$$\eta_{th} = \frac{\sum Q_{out}}{\dot{m}_{biomass} LHV_{biomass} + \sum Q_{in}} \times 100 \quad (1)$$

For fuel cell efficiency

$$\eta_{fuel\ cell} = \frac{Power_{fuel\ cell}}{\dot{m}_{H_2} LHV_{H_2}} \times 100 \quad (2)$$

For total energy efficiency of BGFC

$$\eta = \frac{Power_{fuel\ cell} + Power_{turbine}}{\dot{m}_{biomass} LHV_{biomass} + \sum Q_{in}} \times 100 \quad (3)$$

RESULTS AND DISCUSSION

The results show that at the optimal operating condition of

The electrical powers generated from steam turbine and SOFC fuel cell are 3.79 and 1391.82 kW, respectively. In addition, the BGFC performance is evaluated in terms of thermal efficiency, eq.(2), electrical efficiency, eq.(3) and total energy efficiency, eq.(3). The results revealed that the BGFC system using rice straw feedstock has 55.2% thermal efficiency, 17.5% fuel cell efficiency and the total energy efficiency is 73.2%.

Nevertheless, the BGFC operation produces large quantities of waste heat and steam. Therefore, energy efficiency of the BGFC system can be improved by recovering the waste heat and unused steam in order to reduce the energy consumption in the system.

ACKNOWLEDGMENT

The author would like to acknowledge the support from Engineering Faculty and Thammasat University Scholarships.

References

- [1] M. K. Delivand, M. Barz, and S. Garivait, "Overall analysis of using rice straw residues for power generation in Thailand-project feasibility and environmental GHG impact assessment", *Journal of Sustainable Energy & Environment Special Issue*, 2011, pp. 39-46.
- [2] J. Sadhukhan, Y. Zhao, N. Shah and N. Nigel, "Performance analysis of integrated biomass gasification fuel cell (BGFC) and biomass gasification combined cycle (BGCC) systems", *Chemical Engineering Science*. **65**, 2010, pp. 1942-1954.
- [3] T. Seitarides, C. Athanasiou and A. Zabaniotou, "Modular biomass gasification-based solid oxide fuel cells (SOFC) for sustainable development", *Renewable and Sustainable Energy Reviews*. **12**, 2008, pp. 1251-1276.
- [4] J. Boonmak and W. Paengjuntuek, "Optimal operation analysis of IGFC system", *Thammasat International Science and Technology*. **19**, 2014, pp. 52-59.

Combustion, Co-Firing and Gasification

THE EFFECT OF MOISTURE CONTENT ON THE CRITICAL MASS FLUX AND PILOTEED IGNITION TIME OF PRRA RUBBER LITTER

Pissanu Wongchai¹ and Watcharapong Tachajapong¹

¹Department of Mechanical Engineering, Faculty of Engineering, Chiang Mai University, Thailand

SUMMARY: An attempt has been made to understand the effect of moisture content on the critical mass flux and ignition time. It is a key component of understanding fire spread on para rubber plantation in the dry season. The critical mass flux was measured under a variety of external radiant heat flux and moisture content of wood. From the experiment, the critical mass flux for piloted ignition increases with moisture content. It was found that the critical mass flux was increased 28.29% from moisture content 0 % to 10% and 35.65 % from moisture content 10% to 15 %. It was also found that the critical mass flux increased, the heat flux would increase for all levels of moisture content. However ignition time decreased, the heat flux would increase for all moisture content also.

Keywords: critical mass flux, moisture content, ignition time, piloted ignition, para rubber litter

INTRODUCTION

Para rubber plantation is the 2nd economically important crops that could make capita income for Thailand. Para rubber plantation will shed leaves during the dry season. The accumulation of Para rubber litter fuel with the hot weather and windy causes a fire spread in the rubber plantation every years.

Ignition of Para rubber litter can be divided into two types; piloted ignition and spontaneous ignition. Spontaneous ignition occurs without external pilot source and is rare because it requires very high radiation source to occur. While piloted ignition is the most prevalent in wild land fires as it occurs by ignition source at the lower temperature and is the mechanism responsible for fire growth [3].

Moisture content is one of the most important factor affect the ignition behavior i.e. (1) it changes the thermal properties of the material (density, thermal conductivity, and specific heat increase), (2) it transfers heat by molecular diffusion, and (3) its evaporation is strongly endothermic [1]. The ignition temperature increase by about 2 °C for each moisture content increase 1 % [2]. Critical mass flux and ignition time of fuel increase if moisture content increases [4].

From previous researches, it can be seen that the moisture content of the fuel affect the critical mass flux and ignition time. So, the intent of this work is to study the effect of critical mass flux on the ignition time and moisture content.

THERMAL MODEL PILOTEED IGNITION

Considering the one dimensional, the energy conservation equation for heat flux is

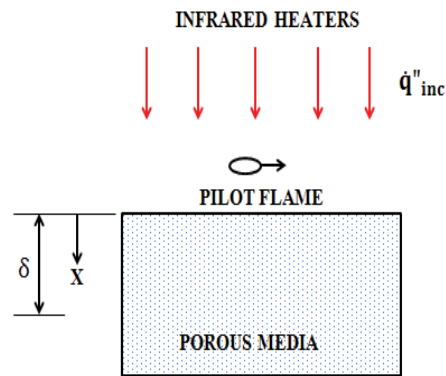


Figure.1 Piloted Ignition of porous media.

$$\alpha_k \rho_k c_{pk} \frac{\partial \bar{T}}{\partial t} = \frac{a_b}{\delta} \dot{q}_{inc} + \frac{2a_b}{\delta} \sigma (T_\infty^4 - \bar{T}^4) + \frac{h_{conv}}{\delta} (T_\infty - \bar{T}) \quad (1)$$

The distribution of temperature in the porous media. The heat flux transmission to material is equal to the heat flux incident combined with the heat loss due to convection and radiation. Ignition will occur when the surface temperature reaches to the piloted ignition temperature.

Although the ignition temperature can be measured by experimental, but it is easier to use equation. The critical heat flux which is the lowest heat flux where the temperature reached T_{ig} after infinitely long exposure duration. The equation for the critical heat flux is thus represented by [3]. Ignition temperatures can be obtained from

$$\dot{q}_{inc,cr}^* = 2\sigma (T_{ig}^4 - T_\infty^4) + \frac{h_{conv}}{a_b} (T_{ig} - T_\infty) \quad (2)$$

EXPERIMENTAL DESIGN

An apparatus was built to measure the critical heat and mass flux of porous media. It consists of burner, infrared heater, sample holder, load cell, and data logger (see Fig 2.).

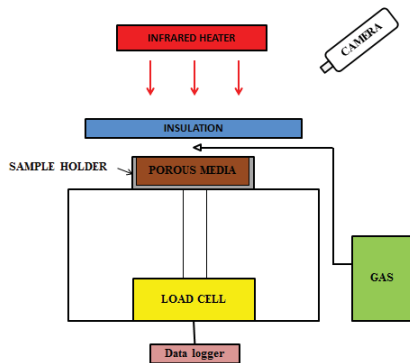


Figure.2 Experiment apparatus

The sample put in holder which placed on top of load cell. The sample is heated from above using an infrared heater capable of producing a uniform heat flux of 0–40 kW/m² over the sample surface. Experiments were performed with moisture content of 0%, 15% and 25% on a dry weight basis. All tests were repeated three times to provide an estimate of the experimental variability.

RUSULTS AND DISCUSSION

Fig. 3 and 4 show the critical mass flux and ignition time for all tests. They were performed with a heat flux of 40 kW/m². It was found that critical mass flux were 2.311 g/s-m² and 3.317 g/s-m², the ignition time 21.4 second and 28.1 second when the moisture content increased 0 – 15 % and 15 – 25 %, respectively. As well as, both test 20 and 30 kW/m² show in the Fig.3 and 4.

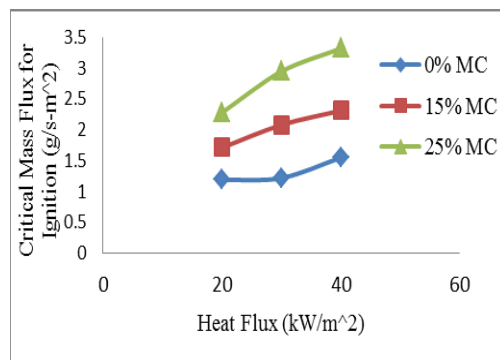


Figure.3 Critical mass flux for piloted ignition

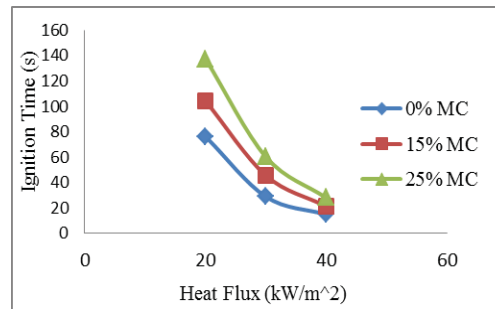


Figure.4 Ignition time for piloted ignition

From fig.3, the critical mass flux increases 3 % every 1 % increased in moisture content. The critical mass flux increased when the heat flux increase for all moisture content. At the time of ignition, the critical mass flux dramatically increases because moisture content in fuel evaporates rapidly within molecular. The moisture content will delay ignition time (see fig.4) because heat flux is difficult to transfers through the porous layer. Therefore it is clear that the critical mass flux increased with incident heat flux. This agrees well with the trend found by Rich et al (2007). The critical mass flux for piloted ignition ranged from about 1.0 – 3.5 g/s-m² (see fig.3), while values reported in the literature ranged from about 0.5 – 5.5 g/s-m² for a range of materials [5].

In conclusion, it was found that the critical mass flux for ignition increased when b the heat flux or moisture content increased. Ignition time also increased when moisture content increased as well.

ACKNOWLEDGMENT

The authors would like to thank my parent and Theerawat Manawan for their invaluable help in building the apparatus.

References

- [1] D.L. Simms, M. Law, "The ignition of wet and dry wood by radiation", *Combustion and Flame*, **11** (5), 1967, pp. 377–388.
- [2] M. Janssens., "Piloted ignition of wood", *Fire and Materials*, **15** (4), 1991, pp. 151–167.
- [3] P. Mindykowski , A. Fuentes, J.L. consalvi, B. Porterie, "Piloted ignition of wildland fuels", *Fire Safety Journal*, **46**, 2011, pp. 34-40.
- [4] S. McAllister, "Critical mass flux for flaming ignition of wet wood", *Fire Safety Journal* **6**, 2013, pp. 200-206.
- [5] D.Rich, C. lautenberger, J.L Torero, J.G Quintiere, C.Fernandez-Pello, "Mass flux of combustible solids at piloted ignition", *proceedings of the Combustion Institute*, **31**, 2007, pp. 2653-2660.

A STUDY ON PHYSICAL AND CHEMICAL CHANGES IN THE BED MATERIAL DURING LONG-TERM COMBUSTION OF OIL PALM RESIDUES IN A FLUIDIZED BED OF ALUMINA SAND

Pichet Ninduangdee¹ and Vladimir I. Kuprianov¹

¹School of Manufacturing Systems and Mechanical Engineering, Sirindhorn International Institute of Technology, Thammasat University, Thailand.

SUMMARY: Empty fruit bunch and palm kernel shell with elevated/high potassium content were burned in a conical fluidized-bed combustor using alumina sand as the bed material to prevent bed agglomeration. During 60-h combustion tests with each biomass fuel, the heat input to the combustor and excess air were constant. The pressure drop across the bed, the bed temperature, and the CO, C_xH_y, and NO emissions were recorded at different time instants. A SEM/EDS analysis was performed to investigate the time-domain changes in alumina grains morphology as well as in elemental composition of grain coatings. Composition of the used/reused bed material and that of PM emitted from the combustor were determined according to the XRF method at different operating times. No features of bed agglomeration were found during these long-term combustion tests. However, physical and chemical properties of the bed material underwent substantial changes with time.

Keywords: Oil palm residues, fluidized-bed combustion, bed agglomeration prevention, bed grains coating

INTRODUCTION

Empty fruit bunch (EFB) and palm kernel shell (PKS) are biomass residues from production of palm oil, both exhibiting great potential as a feedstock for heat and power generation in Thailand.

Though the fluidized-bed combustion has been regarded as the most suitable technology for energy conversion from biomass, bed agglomeration has been reported to be a major operational problem, basically occurred during fluidized-bed combustion of biomasses with elevated/high contents of alkali metal, when using silica/quartz sand as bed material [1]. As reported in studies on burning EFB and PKS with elevated/high potassium content in a fluidized bed of silica sand, these residues have a strong tendency to bed agglomeration and, eventually, fast bed defluidization [2]. To avoid bed agglomeration, some alternative bed materials, such as alumina, dolomite, and limestone, can be employed when firing high-alkali biomass fuels [1,3].

The main focus of this study was to investigate physical and chemical changes in properties of the bed materials during the fluidized-bed combustion of EFB and PKS with the aims: (i) to assess a capability of the bed material to withstand bed agglomeration in long-term operation, and (ii) to understand the mechanisms of interaction between bed grains and biomass ash particles.

MATERIALS AND METHODS

In this study, combustion tests were performed on the fluidized-bed combustor with a cone-shaped bed (*Details regarding the combustor design and geometry, as well as auxiliary equipment, will be provided in the manuscript*). Table 1 summarizes the major properties of EFB and PKS, such as the proximate and ultimate analyses, the composition of fuel ash (as oxides), and the lower heating value of both biomasses. From Table 1, the EFB ash included very high content of potassium (K₂O = 47.21 wt.%),

while it was elevated (K₂O = 8.12 wt.%) in the PKS ash, both indicating a high risk of bed agglomeration if silica sand is used as bed material. Alumina sand (Al₂O₃ = 84.2 wt.%) was therefore used as the bed material in this study to prevent bed agglomeration.

To ensure similar heat input to the combustor (about 200 kW_{th}) during the combustion tests with the selected biomasses, EFB was burned at 40 kg/h, whereas PKS at 45 kg/h. In all the tests, excess air was 40%. During the 60-h test run for firing a biomass, the pressure drop across the bed, the bed

Table 1. Properties of the fuels used in this study

Property	EFB	PKS
<i>Proximate analysis (as pre-dried for EFB, as received for PKS, wt.%)</i>		
Moisture	8.2	5.4
Volatile matter	74.2	71.1
Fixed carbon	12.8	18.8
Ash	4.8	4.7
<i>Ultimate analysis (as pre-dried for EFB, as received for PKS, wt.%)</i>		
C	48.20	48.06
H	6.49	6.38
N	0.47	1.27
O	31.74	34.10
S	0.10	0.09
<i>Fuel ash analysis (as oxides, wt.%)</i>		
SiO ₂	26.21	54.12
Al ₂ O ₃	3.11	3.11
K ₂ O	47.21	8.12
CaO	12.54	23.21
MgO	3.24	2.65
Fe ₂ O ₃	3.21	6.14
P ₂ O ₅	1.21	1.15
LHV (kJ/kg)	18,400	16,300

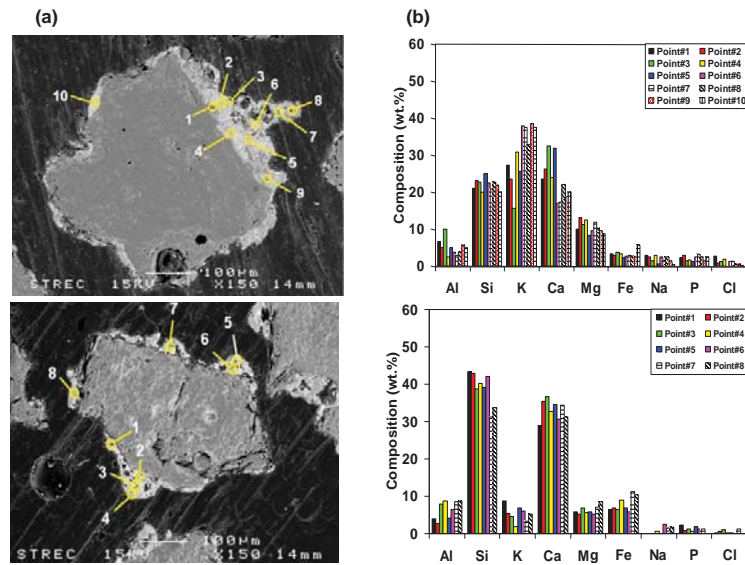


Figure 1. (a) SEM micrographs and (b) EDS spot analysis of individual alumina grains after 60-h tests for burning empty fruit bunch (upper) and palm kernel shell (lower)

temperature, and the gaseous emissions (CO , C_xH_y , and NO) were continuously monitored and recorded.

Apart from this, the used/reused bed material and particulate matter (PM) were sampled at different operating times (20 h, 40 h, and 60 h) and analyzed for their chemical composition using an XRF technique. A SEM-EDS analysis was employed to study the morphology of individual bed particles, as well as to determine an elemental composition of particle coatings. The particle size distribution and the average (volumetric) particle diameter of the bed material were determined by a "Mastersizer 2000".

RESULTS AND DISCUSSION

As revealed by the experimental results, the profiles of the pressure drop across the bed, the bed temperature, and the CO , C_xH_y , and NO emissions exhibited persistent fluctuations with relatively uniform amplitude for the entire testing period (*Graphs showing these profiles will be provided and discussed in the full manuscript*). This evidence can be attributed to a smooth fluidization of the alumina bed. As found by visual inspections after finishing of the 60-h tests for burning an individual biomass, no feature of bed agglomeration were observed in the bed material. Thus, alumina sand can effectively prevent bed agglomeration when firing these problematic oil palm residues.

Figures 1 shows the SEM-EDS analysis at individual points (spots) on a transverse section of individual grains after 60-h tests for burning EFB and PKS (*The SEM-EDS analyses performed after 20-h and 40-h combustion tests will be provided and discussed in the full manuscript*). It can be seen in Figure 1 that a coating of variable thickness was formed on alumina grain surfaces, the appearance and thickness of the coating being affected by the

fuel type. As revealed by the EDS analysis at different points, the coating consisted mainly of ash-related elements with the contents showing an apparent difference between innermost and outermost coating layers (*to be discussed*).

CONCLUSIONS

The use of alumina sand as the bed material can prevent bed agglomeration during combustion of empty fruit bunch and palm kernel shell in a fluidized-bed combustor during its long-term operation. However, morphological characteristics and chemical condition of the bed (alumina grains) undergo substantial changes with time.

ACKNOWLEDGEMENT

The authors wish to acknowledge the financial support from the Thailand Research Fund (Contract No. BRG5680014).

References

- [1] J. Werther, M. Saenger, E.U. Hartge, T. Ogada and Z. Siagi, "Combustion of agricultural residues", *Progress in Energy and Combustion Science*. **26**, 2000, pp. 1–27.
- [2] P. Chaivatamaset, P. Sricharoon, S. Tia, B. Bilitewski, "A prediction of defluidization time in biomass fired fluidized bed combustion", *Applied Thermal Engineering*. **50**, 2013, pp. 722–731.
- [3] P. Ninduangdee and V.I. Kuprianov, "Combustion of oil palm shells in a fluidized-bed combustor using dolomite as the bed material to prevent bed agglomeration", *Energy Procedia*. **52**, 2014, pp. 399–409.

CO-FIRING OF OIL PALM EMPTY FRUIT BUNCH AND KERNEL SHELL IN A FLUIDIZED-BED COMBUSTOR: OPTIMIZATION OF OPERATING VARIABLES

Priatna Suheri¹ and Vladimir I. Kuprianov¹

¹School of Manufacturing Systems and Mechanical Engineering, Sirindhorn International Institute of Technology Thammasat University, Thailand

SUMMARY: Co-combustion of palm kernel shell (primary fuel) and empty fruit bunch (secondary fuel) was studied on a conical fluidized-bed combustor using alumina sand to inhibit bed agglomeration. During the (co-)firing tests, the fuels were injected into the reactor at different levels ensuring constant heat input, while the energy fraction of secondary fuel (EF_2) was ranged from 0 to 0.25 with excess air (EA) of 20–80%. The experimental results showed significant effects of both EF_2 and EA on the CO, C_xH_y , and NO emissions, as well as on combustion efficiency of the combustor. Cost-based optimization aimed at minimizing “external” costs of the biomass–biomass co-combustion was applied to determine the optimal values of EF_2 and EA. Under optimal operating conditions, the combustor can be operated with high (about 99%) combustion efficiency at minimum emission costs, while reducing the NO emission roughly by 50% compared to firing pure palm kernel shell.

Keywords: Fluidized-bed combustor, oil palm residues, co-firing, emission costs, optimization

INTRODUCTION

Presently, the palm oil industry plays an important role in the national economies of most tropical countries around the world. In 2013, total world production of palm oil was 58 million tones. Indonesia is the world’s largest palm oil producer with a production share of 53.4%, followed by Malaysia (32.7%) and Thailand (3.6%) [1].

Palm kernel shell (PKS) and empty fruit bunch (EFB) are oil palm residues exhibiting a substantial potential as a resource of energy for heat and power generation via direct combustion in fluidized-bed systems. However, burning PKS with its elevated fuel N content on its own results in elevated NO emission from a combustion system. Co-firing of PKS and high-moisture (“as-received”) EFB seems to be an effective way to remediate this problem.

This work was aimed at studying the potential of co-combustion of PKS (primary fuel) and EFB (secondary fuel) in a fluidized-bed combustor for the reduction of NO emission compared to burning of PKS on its own. The effects of energy fraction of EFB and excess air on the CO, C_xH_y , and NO emissions and the combustion efficiency of the combustor were the focus of study. A cost-based optimization of the major operating variables for minimizing “external” costs of the biomass–biomass co-combustion was also among the work objectives.

MATERIALS AND METHODS

The experimental tests for the co-combustion of PKS and EFB were performed on a fluidized-bed combustor (FBC) with a cone-shaped bed. (*The experimental setup will be described in the full manuscript*). To prevent bed agglomeration, alumina sand was used as the bed material in this combustor.

In all tests, the heat input to the combustor by the two fuels was fixed at 200 kW_{th}, whereas the energy fraction of secondary fuel (EF_2) was varied from 0 (i.e., when firing pure PKS) to 0.25. The fuel feed rates of the biomasses were therefore varied

depending on EF_2 . For each co-firing option (fixed EF_2), the amount of excess air (EA) was ranged from 20% to 80%. During a test run at fixed EF_2 and EA, temperature, O₂, CO, C_xH_y , and NO were measured along the combustor centerline, as well as at stack. For each run, EA and the combustion efficiency were determined using relevant relations. A cost-based optimization method [2] was applied to determine the optimal values of EF_2 and EA ensuring the minimum “external” costs of the co-combustion. (*Relevant relations and optimization model will be provided in the manuscript*).

RESULTS AND DISCUSSION

Axial profiles of temperature, O₂, CO, C_xH_y (as CH₄), and NO were plotted using data from the tests. As revealed by the experimental results, both EF_2 and EA have significant effects on the CO, C_xH_y , and NO emissions, as well as on the combustion efficiency (*all to be discussed in the manuscript*). The peaks of CO and C_xH_y at a level of secondary fuel (EFB) injection played an important role in the reduction of NO emission from the combustor.

Figures 1 and 2 show the CO and C_xH_y emissions during co-combustion of PKS and EFB at variable EF_2 and EA. Since the CO emission include some part of CO formed in the oxidation of C_xH_y , that CO emission was substantially higher than the C_xH_y emissions for the specified ranges of operating conditions. From Figures 1 and 2, these emissions experienced substantial (opposite) effects from the operating conditions, particularly at relatively low excess air. With higher EF_2 (at fixed EA), both CO and C_xH_y emissions significantly increased, mainly

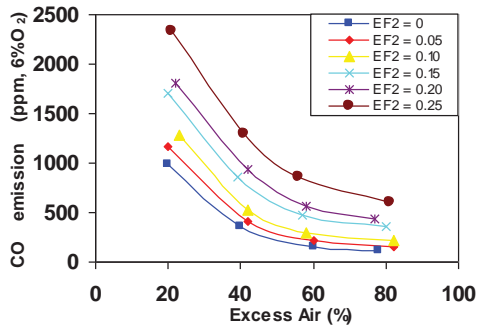


Figure 1. Effects of EF₂ and EA on the CO emission from the co-combustion of PKS and EFB.

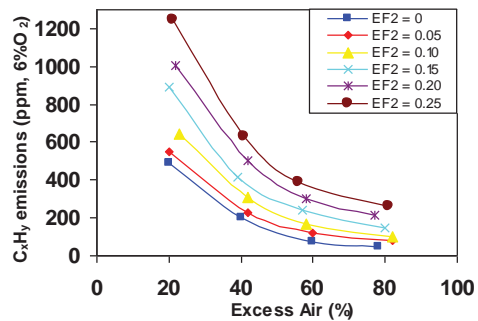


Figure 2. Effects of EF₂ and EA on the C_xH_y emissions from the co-combustion of PKS and EFB.

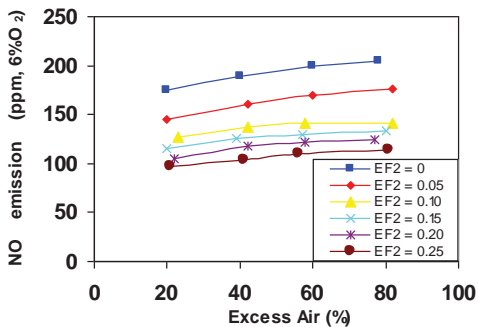


Figure 3. Effects of EF₂ and EA on the NO emission from the co-combustion of PKS and EFB.

due to the increasing impact from injection of EFB (downstream from the conical section). On the contrary, an increase in EA at fixed EF₂ led to the diminishing of these two emissions. Thus, in the co-combustion of PKS and EFB biomasses, EA can be regarded as an effective tool in controlling of the CO and C_xH_y emissions.

Figure 3 shows the NO emission for the ranges of EF₂ and EA. As seen in Fig. 3, an increase in EF₂ at fixed EA apparently led to a substantial reduction of the NO emissions, likely due to the increased CO

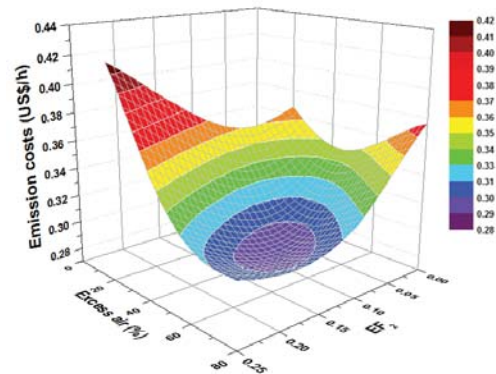


Figure 4. Effects of EF₂ and EA on the emission costs of the conical FBC co-fired with PKS and EFB.

and C_xH_y in the vicinity of secondary fuel injection. However, increasing EA at fixed EF₂ resulted in the higher NO emission, which can be attributed to the fuel-NO formation mechanism.

Figure 4 shows the emission costs (US\$/h) of the co-combustion of PKS and EFB, which were predicted using the mass fluxes of the CO, C_xH_y, and NO emissions, as well as specific "external" costs of the emissions regarded as a fiscal equivalent of emission impacts to the environment and humans.

It can be seen in Figure 4 that the effects of EF₂ and EA on the "external" costs were substantial. With increasing EF₂ at relatively low EA, the "external" costs increased significantly were high, mainly due to the contribution of CO and C_xH_y. However, according to the optimization analysis, these costs were at the minimum when EF₂ was about 0.15, via maintaining EA at near 50% (see Figure 4).

Under these optimal conditions, the major gaseous emissions can be controlled at acceptable levels: 250 ppm for CO and 120 ppm for NO. Both CO and NO emissions are substantially below the emission limits imposed by the Thai environmental legislation: 740 ppm for CO and 205 ppm for NO (as corrected to 6% O₂, on a dry gas basis).

ACKNOWLEDGMENT

The authors wish to acknowledge the financial support from the Thailand Research Fund (Contract No. BRG5680014). Special thanks to Mr. Pichet Ninduandee for his assistance in the experiments.

References

- [1] International Energy Agency, 2012. World Energy Outlook 2013.
- [2] P. Ninduandee and VI. Kuprianov, "Combustion of palm kernel shell in a fluidized bed: Optimization of biomass particle size and operating conditions," *Energy Conversion and Management*, **85**, 2014, pp. 800–808.

DEVELOPMENT OF KINETICS MODELS IN EACH ZONE OF A 10 KG/HR DOWNDRAFT GASIFIER BY USING COMPUTATIONAL FLUID DYNAMICS

Pubet Meenarooh¹, Somrat Kerdsuwan¹ and Krongkaew Laohalidanond¹

¹The Waste Incineration Research Center
Department of Mechanical and Aerospace Engineering,
Faculty of Engineering, King Mongkut's University of Technology North Bangkok, Thailand

SUMMARY: Thermal-chemical conversion of biomass via gasification is widely perceived as a means of renewable energy production, where downdraft gasification is considered as a promising technology for the production of electricity for use in communities. In order to optimize the operating conditions of a downdraft gasification process, mathematical models are commonly used to reduce the time consumption of the process and to reduce the expenditure occurring during the experimental work. This study aims to develop a kinetics model to demonstrate the gasification process in each zone of a 10 kg/hr downdraft gasifier, including drying, pyrolysis, oxidation, and reduction zone. Computational fluid dynamics (CFD) is used to solve the partial differential equations. The Euler-Lagrange approach for dispersed two-phase flows has been applied for simulating the gas-solid transport phenomena inside the gasifier. The results of this study include the effect of air flow rate on the temperature profile along the height of the gasifier and the concentration of producer gas at the gasifier outlet. Model validation has been made with experiments using wood chips as feedstock. The developed model can be used to optimize the running parameters of a downdraft gasifier to archive the optimum cold gas efficiency.

Keywords: Renewable energy, Downdraft gasification, Computational fluid dynamic, Kinetics model

INTRODUCTION

Nowadays, the residual biomass from agricultural products has been increasing significantly and is left without use or is inefficient. For example, after harvesting crops, the waste residue, e.g. wood chips, rice husk, and bagasse, is left unusefully in the field. Studying the properties of this biomass, it has been found that it is high in volatile matter, low sulphur, and ash content, which can be used as an alternative energy source to solve the current energy crisis [1].

The gasification process is a thermal-chemical conversion technology which is suitable for converting biomass into producer gas, consisting of CO, H₂, and CH₄. The advantages of producer gas are as follows: (1) it can be used as fuel in internal combustion engines to generate electricity, and (2) it can be applied in various chemical syntheses. There are many types of gasifier, but this study focuses only on the downdraft gasifier because it can produce low tar producer gas [2] and it can be established within the community for decentralized electricity production. The downdraft gasification process consists of the drying, pyrolysis, oxidation, and reduction zone from top to bottom. The feedstock is fed at the top of the gasifier. The drying zone has a temperature under 200 °C, because of which the moisture in the feedstock is driven off by evaporation into water vapor. The dried feedstock continues to move downward to the pyrolysis zone by gravity. This zone has a temperature ranging from 200 to 600 °C. The products in this regime can be classified into solid (char), liquid (tar), and volatile gas. The gasifying agent was injected at oxidation zone, where the char and volatile gas from

the pyrolysis zone react with the agent. As the reactions in this zone are exothermic, heat is generated and transferred to the other zones in the gasifier. The unburnt char falls down into the reduction zone and reacts with the gases formed from the other zones. As a result, the producer gas is generated and exits the gasifier at the bottom.

Since the reactions occurring in the gasification process are very complex, the operating conditions have influences on both the producer gas quantity and quality. In order to reduce time and expense during the experimental work, mathematic models of the gasification process were developed. The gasification models can be divided into a thermodynamics model and a kinetics model. This study focuses on the kinetics model because the gas-solid transport phenomena and the kinetics reactions between the solid and gas phases in the gasifier will be taken into account. I. Janajreh and M. Al Shrah improved the kinetics model and used 2D-CFD for predicting the temperature distribution in the downdraft gasifier and the evolution of the producer gas [3]. Hui Liu et al. simulated a 3D model of a circulating fluidized-bed reactor using biomass as feedstock and compared various turbulences models and the effect of the water gas shift reaction by choosing models in the FLUENT program [4].

The objective of this study was to develop a kinetics model of a 10 kg/hr lab-scale downdraft gasification process. The gasification models can predict the gas-solid transport phenomena and the kinetics reactions in each zone of the reactor consisting of the pyrolysis, oxidation, and reduction zone. The model results showed the effects of the air

flow rate on the temperature profile along the height of the gasifier and the concentration of producer gas at the outlet. In addition, the model results were compared to the experimental data from a previous study using wood chips as feedstock in a 10 kg/hr lab-scale downdraft gasifier [5].

METHODOLOGY

The schematic and 2D axisymmetric geometry of a lab-scale downdraft gasifier is given in Figure 1. The inner diameter and the height of cylindrical gasifier were 0.268 m and 0.8 m, respectively.

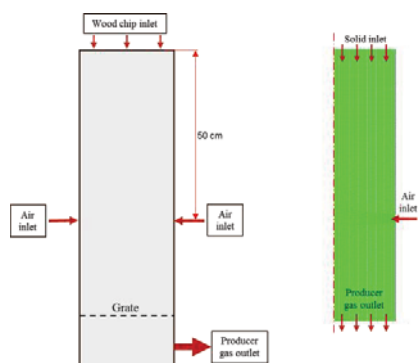


Figure 1. The geometry of the gasifier

The governing equations for continuity, momentum, energy, and the species transport equation were applied to solve for the continuous phase or gas flow. The discrete phase model was applied for wood particles flow. The coupling between the discrete and gas phase was the interphase exchange of mass, momentum, and energy. These terms were added in source terms for the governing equations.

The reaction models, e.g. moisture evaporation, devolatilization, heterogeneous surface reactions, and homogeneous reactions, were the source terms for the governing equations. The moisture evaporation in the drying zone was assumed to be controlled by droplet vaporization, which could be applied when the wood particle temperature reaches the vaporization temperature. The pyrolysis rate of the wood chips was controlled by kinetic reactions, which were described by Arrhenius equations. The quantity of the volatile species was calculated from the ultimate analysis of the wood chips. The pre-exponential factor (A) and the activation energy (E_a) for the reaction rate of the wood chip pyrolysis were 10^8 s^{-1} and $140 \text{ kJ/mol}\cdot\text{K}$, respectively. [6] The wood chips were assumed to be spherical and the reaction kinetics rate was applied to the heterogeneous surface reactions. The gas phase homogeneous reactions involved in this study were CO combustion, H_2 combustion, and the water-gas shift reaction.

The air flow rate was varied from 250 to 450 L/min to predict its effect on the temperature distribution along the gasifier's height and the concentration of the producer gas compositions, which consisted of H_2 , CO, CO_2 , CH_4 , and N_2 at the outlet.

RESULTS AND DISCUSSION

The simulation results showed that the temperature distribution inside the gasifier increased with an increase in the air flow rate. These results can be explained because of the increase of the increase in the char combustion reaction rate and volatile combustion reaction rate.

Regarding the producer gas composition, an increase in air flow rate led to a decrease in CO and H_2 concentration, whereas the CO_2 increased. The reason was the increase in the O_2 concentration in the air introduced into the gasifier, which promoted the char combustion reaction rate and H_2 combustion reaction rate to increase.

ACKNOWLEDGMENT

The authors would like to thank the Development of Machinery and Industrial Equipment (DMIE), Science and Technology Research Institute, for supporting the FLUENT program, and the Waste Incineration Research Center (WIRC) as well as the Department of Mechanical and Aerospace Engineering (MAE), Faculty of Engineering, King Mongkut's University of Technology North Bangkok, for their kind cooperation.

References

- [1] Anjireddy, Bhavanam, R. C. Sastry. "Biomass Gasification Processes in Downdraft Fixed Bed Reactors." *International Journal of Chemical Engineering and Applications*. **6**, 2011, pp.425-433.
- [2] P. Abdul Salam, S. Kumar, Manjula Siriwardhana. "The Status of Biomass Gasification in Thailand and Cambodia" *Energy Environment Partnership*, 2010, pp.6-12.
- [3] I. Janajreh and M. Al Shrah. "Numerical and Experimental Investigation of Downdraft Gasification of Wood Chips." *Energy Conversion and Management*. **65**, 2013, pp.783-792.
- [4] Hui Liu, Ali Elkamel, Ali Lohi and Mazda Biglari. "Computational Fluid Dynamics Modeling of Biomass Gasification in Circulating Fluidized-Bed Reactor Using the Eulerian-Eulerian Approach." *Ind. Eng. Chem. Res.* **52**, 2013, pp.18162-18174
- [5] T. G. Etutul et al., "Effect of Temperature on Tar Behavior during Air Gasification Process", 3rd TSME International Conference on Mechanical Engineering, October 2012, Chiang Rai.
- [7] Colomba Di Blasi. "Dynamic Behaviour of stratified downdraft gasifiers." *Chemical Engineering Science*. **55**, 2000, pp.2931-44.

OPTIMIZATION OF COMBUSTION BEHAVIOR AND PRODUCER GAS QUALITY FROM RECLAIMED LANDFILL THROUGH HIGHLY DENSIFY RDF-GASIFICATION

Somboon Chalermcharoenrat¹, Krongkaew Laohalidanond¹, and Somrat Kerdsuwan¹

¹The Waste Incineration Research Center,
Department of Mechanical and Aerospace Engineering, Faculty of Engineering,
Science and Technology Research Institute,
King Mongkut's University Technology North Bangkok, Thailand

SUMMARY: The growth in population and economy results in the rapid increasing of Municipal Solid Waste (MSW) by higher demand of urban consumptions. It has significant direct impact on environmental pollution in air, water and soil. MSW is generally got rid of by landfill which requires a lot of land space, however, it was considered as a non-sustainable management. After years of landfill, plastic, paper and other non-decomposed materials still remain. In order to provide the land space for supporting the recent waste, the old MSW is needed to be reclaimed to produce RDF (Refuse Derived Fuel). For assuring reclaimed landfill waste compositions, the surrogate RDF consists of plastic (HDPE) and paper (newspaper) at ratio 75:25%-wt. It is prepared by extrusion machine to produced high density RDF-5 which contains density higher than 600 kg/m³. Gasification was the selected technology for producing the producer gas since it can be applied in various purposes and the overall efficiency is higher compare to a conventional incinerator. The experiment was conducted in a laboratory scale downdraft gasifier by feeding surrogate RDF-510 kg/hr with the air flow rate 12, 15 and 18 Nm³/hr, respectively. Charcoal was added as an additive at the same weight of RDF in order to increase the concentration of producer gas. Results show highest CO% and LHV are offered from air flow rate 12 Nm³/hr with 22.02% and 4.39 MJ/Nm³, respectively whereas highest H₂% is obtained from air flow rate 15 Nm³/hr. The experiment results demonstrate densified reclaimed landfill RDF mixing with additive can optimize the combustion behaviour in terms of temperature distribution along the gasifier height and improve the producer gas quality.

Keywords: reclaimed landfill, refuse derived fuel, gasification, renewable energy

INTRODUCTION

Petroleum fossil resources are limited in times and therefore are arraigned in environmental impact. In the same time, the increasing of world population is the crucial problem in energy usage and environmental pollution. Municipal Solid Waste (MSW) is also rapidly increased due to enlargement of natural resources consumption. This causes deficiency in sanitary landfill and the left MSW was disposed in open dumpsite and uncontrolled burned into the atmosphere. For sustainable solution, reclaiming of MSW from dumpsite to recover energy in terms of heat and electricity by thermal conversion should be prudentially considered. Not only reduction the usage of fossil fuels but the land also can be reused for other purposes. Since years of disposal by landfill, the biodegradable waste was decayed and the remaining is mostly plastic, small amount of paper, biomass and other non-degradable compositions. After the process of removing non-combustible compositions, the reclaimed landfill waste which contains some heating value can be supplied as feedstock for heat source of alternative energy.

Gasification is the promising thermal conversion technology in high energy output yield compared to conventional incineration [1]. To be utilized the reclaimed landfill waste as fuel in gasification process, RDF (Refuse Derived Fuel) is

the most proper form of feedstock. RDF-5 can be classified as high densified fuel by compression in several forms of pellets, briquettes and etc. The benefit of compression is not only increase the density but also easy for transportation since the different location of RDF manufacturing machine and the gasifier place [2].

The aim of this research is to study the characteristic of combustion behavior and producer gas production with optimum of the operating conditions by using extruded of RDF-5 from reclaimed waste which is mainly plastic for use as feedstock of gasification. To ensure the uniformity of physical and compositions of RDF, surrogate MSW has produced from extrusion method. It contains of waste plastic (HDPE) and waste newspaper with ratio 75:25 %-wt. for representation as forty years old reclaimed waste [2]. To increase the efficiency of gasification, charcoal is fed in the bottom of gasifier in the same weight of RDF as the additive. In addition, to conduct gasification experiment of feedstock that contains mostly plastic, can cause very high temperature and damage of gasifier. Feeding some biomass or char is benefited to control the overall temperature and to maintain temperature in gas reduction zone. Downdraft gasifier has been deployed in this experiment due to high thermal efficiency and lower tar produced. Producer gas concentration, lower heating value,

distribution of temperature inside gasifier are investigated in this article.

MATERIALS AND EXPERIMENTAL METHODOLOGY

Materials

The feedstock used in this study consists of RDF and charcoal. The extruded RDF-5 is surrogate reclaimed landfill which is made from waste plastic (HDPE) and waste newspaper with ratio of 75:25 %-wt. The RDF has been prepared by screw extrusion machine which is adapted from conventional biomass briquetting machine [4]. The mangrove wood charcoal has been used as the additive to protect plastic melting and to act as obstructer to prevent gas to move down from drying and pyrolysis zone into reduction zone.

Experimental Methodology

The experiments were conducted in a 10 kg/h laboratory scale downdraft gasifier. Air flow rate were set to be 12 Nm³/hr, 15 Nm³/hr and 18 Nm³/hr. After RDF was ignited and then the gasification process started, temperature of combustion zone and reduction zone were reached until constant values. Three samples of producer gas were taken to analyze the producer gas composition and energy recovery from gasification system. All zones of gasification reaction were recorded temperature from the start through the stable condition that gasification took place. Gas samples were analyzed by gas chromatography (GC) model GC-2014 with TCD detector to analyze H₂, CO, CH₄ and CO₂. Producer gas concentrations obtained from GC are used for analysis the lower heating value of the different air flow rate.

RESULTS AND DISCUSSION

Temperature distribution

The results of temperature distribution for downdraft gasification process with feedstock RDF-5 and charcoal show the highest temperature of 12 Nm³/hr which thermocouple T4 reached to 1,049.5 °C. The highest temperature of 15 Nm³/hr which thermocouple T4 reached to 1,062.5 °C. The highest temperature of 18 Nm³/hr which thermocouple T4 reached to 1,181.3 °C.

Effect of Air Flow and Charcoal on Producer Gas Composition

The air flow of the actual air supply indicate the oxygen feed in the combustion zone. The air flow is important factor that effects the combustion behaviour and producer gas quality. The volatile matter and fixed carbon are important factor that effect for thermochemical reaction at reduction zone for producer gas quality.

Table 1. Producer gas composition at difference air flow rate

Air flow rate Nm ³ /hr.	Producer gas composition (%-vol., average)				Lower heating value MJ/Nm ³
	CO	CH ₄	CO ₂	H ₂	
12	20.88	1.85	4.59	10.33	4.41
	21.93	1.37	3.89	9.82	4.32
	22.02	1.35	3.58	10.43	4.39
Average	21.61	1.52	4.02	10.19	4.37
SD.	0.63	0.29	0.52	0.33	0.05
15	17.96	0.95	4.51	10.49	3.74
	18.20	0.57	3.96	8.98	3.47
	16.90	1.38	4.29	11.92	3.91
Average	17.69	0.97	4.25	10.46	3.71
SD.	0.69	0.41	0.28	1.47	0.22
18	16.83	1.45	2.59	10.90	3.82
	19.77	1.11	3.33	9.19	3.88
	21.44	0.86	3.34	8.22	3.90
Average	19.35	1.14	3.09	9.44	3.87
SD.	2.33	0.30	0.43	1.36	0.04

CONCLUSION

The optimum operating condition for high quality of producer gas from reclaimed landfill through highly densify RDF-gasification is at the air flow rate of 12 Nm³/hr. The Producer gas has the low heating value of 4.37 MJ/Nm³.

ACKNOWLEDGMENT

The authors would like to express their grateful to the Waste Incineration Research Center (WIRC), Department of Mechanical and Aerospace Engineering, Faculty of Engineering and Science and Technology Research Center (STRI) of King Mongkut's University of Technology North Bangkok for the facilities support. This research was financially supported by Faculty of Engineering, King Mongkut's University of Technology North Bangkok.

References

- [1] The Waste Incineration Research Center, King Mongkut's University of Technology North Bangkok, 2006, The technology evaluation of energy production from municipal solid waste, JGSEE BM-T-Ws-019
- [2] Somboon Chalermcharoenrat, Nuth Sirirermux, Krongkaew Laohalidanond and Somrat Kerdsuwan. Optimization of the Production of Densified RDF from Reclaimed Landfill without Mixing Binding Agent Using Hydraulic Hot Pressing Machine. The 5th TSME International Conference on Mechanical Engineering (TSME-ICOME 2014).
- [3] Knoef, H.A.M, Handbook Biomass Gasification. 2005, Netherland: BTG biomass

INFLUENCE OF PLASTIC WASTE OF REFUSE-DERIVED FUEL ON DOWNDRAFT GASIFICATION

Chatchai Kungkajit¹, Gumpon Prateepchaikul² and Thaniya Kaosol¹

¹Environmental Engineering Program, Department of Civil Engineering, Thailand

²Department of Mechanical Engineering,
Faculty of Engineering, Prince of Songkla University, Thailand

SUMMARY: The potential of syngas production from unused and used plastic waste Refuse-Derived Fuels (RDFs) by downdraft type fixed bed gasification technology is investigated. It is found that unused and used plastic waste RDFs can be successfully converted to generate the syngas, known as syngas consisting of carbon monoxide, carbon dioxide, hydrocarbon, hydrogen sulfide oxygen and water vapor. The performance of the gasifier is evaluated in terms of composition of syngas, rate of carbon monoxide production. The result can be concluded that the unused plastic RDF produces the syngas as same as the used plastic RDF. The HHV (Higher Heating Value) of the unused and used plastic RDF syngas are 781 and 500 kJ/Nm³, respectively. The unused plastic RDF produces the highest syngas, comparing the HHV of the syngas.

Keywords: HHV, plastic waste, gasification, downdraft, syngas, RDF

INTRODUCTION

Plastic waste is one of Municipal Solid Waste (MSW). Plastic waste contains the lowest liquids by weight. Alternative and sustainable plastic waste disposal methods should be considered in regarding to the environmental and economic awareness. Thermal processes such as gasification are existing technologies to convert plastic waste into syngas and leaving residual solid ash for final disposal. A downdraft type fixed bed gasification system is intended to manage plastic waste because it produces syngas with less tar [1]. The syngas can be used as a fuel for internal combustion engines.

RDFs cover a wide range of waste materials which have been processed to fulfill guidelines, regulatory or industry specifications mainly to achieve a high calorific value. Possible wastes for syngas production include residues from industrial waste, sewage sludge, biomass waste and MSW recycling.

In this paper, a pilot-scale downdraft type fixed bed gasification system with a tar cleaning system has been studied. This research is aiming to convert plastic waste to a syngas using the proposed downdraft type fixed bed gasification system.

MATERIAL AND METHODS

Raw materials

Two types of RDFs made of unused and used plastic wastes each of which palm leaves, were used in the experiments (Figure 1). The raw materials were mixed and pressed then extruded to produce cylindrical shape briquettes with a diameter of 50 mm. The unused and used plastic RDFs were evaluated in the downdraft gasification tests. The initial moisture contents are low.

Experimental setup and procedure

Figure 2 presents the downdraft type fixed bed gasification system used for the experiments. The

total height is 80 cm with a diameter of 12 cm. Three thermocouples were installed along the height. At the central position of the downdraft type fixed bed gasification system, T1, T2 and T3 were installed at the syngas exit, 10 cm above the grate and 30 cm above the grate, respectively. The optimum equivalence ratio (ER) is 0.38 which is the result of our previous study. Air velocity into the downdraft type fixed bed gasification system is 3.25 m/s.



Figure 1. (a) Unused plastic RDF and (b) used plastic RDF

For each RDF, the primary char bed was created first in the gasifier to enable a quick start in the subsequent gasification runs. A batch of 1-kg feedstock was loaded into the downdraft type fixed bed gasification system in each experiment. Before starting the ignition, the level of the feedstock was measured in order to calculate the density of the feedstock and the rate of feedstock consumption.

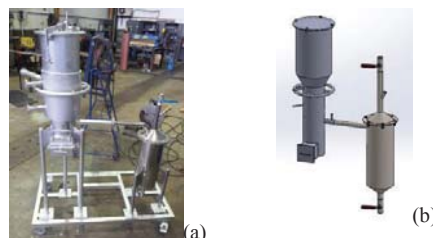


Figure 2. (a) Downdraft type fixed bed gasification system and (b) schematic of downdraft type fixed bed gasification system

The measurements of temperature and the sampling of syngas are carried out at an interval of two minutes. Each experimental run is carried out for 15 to 20 minutes. At the end of the experiment any leftover biomass or char is removed from the downdraft type fixed bed gasification system. The syngas is cleaned in the water. Passing through the cleaning step, the syngas is also cooled and passed into a gas composition analyzer. The syngas included in the analysis are CO, CO₂, HC, O₂, NH₃, CH₄ and H₂S. The oxygen is possible to be indicated during the security check before each run.

RESULTS AND DISCUSSION

Plastic RDF characterizations

The used plastic RDF character is 4.13% moisture content, 62.99% volatile solids, 7.70% fixed carbon and 25.17% ash. The ultimate analysis of used plastic RDF contains 41.88% C, 6.50% H, 24.59% O, 0.78% N, 0.06% S and 5,671 kcal of calorific value. The unused plastic RDF character is 7.18% moisture content, 72.41% volatile solids, 9.24% fixed carbon and 11.16% ash. The ultimate analysis of unused plastic RDF contains 42.86% C, 6.42% H, 20.49% O, 0.77% N, 0.06% S and 5,725 kcal of calorific value.

The properties of used and unused plastic RDFs show similar composition with low levels of moisture content and high levels of calorific value.

Gasification operations

In the present study, the potential of syngas production from used and unused plastic waste RDFs by downdraft type fixed bed gasification system is investigated. The four distinct reaction zones of downdraft type fixed bed gasification system are drying, pyrolysis, oxidation and reduction zones [2]. Figure 3 shows the temperature as a function of operation times for unused and used plastic RDFs. Material balance is carried out to examine the reliability of the results generated in the experimental study. The total mass input includes the plastic RDFs consumption and air. The total mass output comprises of the ash and syngas produced.

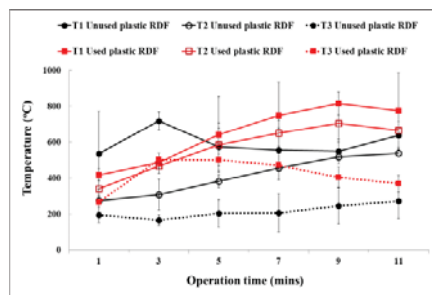


Figure 3. Temperature as function of operation times for unused and used plastic RDFs

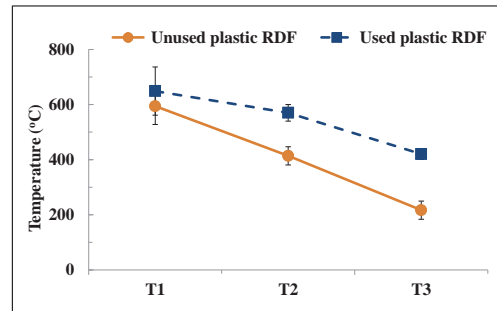


Figure 4. Temperature as function of three thermocouple positions for unused and used plastic RDFs

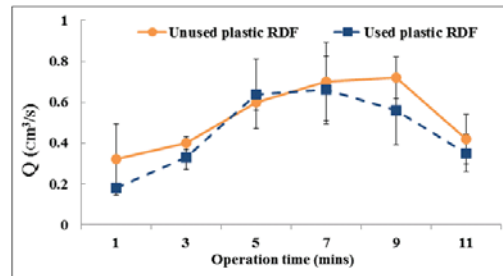


Figure 5. Syngas flow rate as function of operation time for unused and used plastic RDFs.

It is observed that both unused and used plastic RDFs produce the syngas (Table 1 and Figure 5). The HHV of the unused and used plastic RDF syngas are 781 and 500 kJ/Nm³, respectively. The unused plastic RDF produces the highest syngas, comparing with the HHV of the syngas.

Table 1. Syngas compositions under ER= 0.38.

Gas composition (%Vol)	Unused plastic RDF	Used plastic RDF
CO ₂	9.23±2.38	7.63±2.52
O ₂	5.67±2.24	6.89±4.39
H ₂ S	0.16±0.04	0.21±0.09
CO	6.75±1.45	4.32±2.49
HC	0.46±0.18	0.21±0.12

ACKNOWLEDGMENT

The authors would like to acknowledge Prince of Songkla University (ENG 560562S) for providing financial support.

References

- [1] Z.A. Zainal, A. Rifau, G.A. Quadir and K.N. Seetharamu, "Experimental investigation of a downdraft biomass gasifier", *Biomass Bioenergy*, **23**, 2002, pp. 283-289.
- [2] T.B. Reed and A. Das, "Handbook of biomass downdraft gasifier engine systems", *Biomass Energy Foundation Press*, 1988.

OPTIMUM EQUIVALENCE RATIO FOR VARIOUS GASIFYING AGENT TEMPERATURE BASED ON THERMODYNAMIC EQUILIBRIUM MODEL

Woranuch Jangsawang¹, Krongkaew Laohalidanond² and Somrat Kerdsuwan²

¹Sustainable Energy Research Center, Faculty of Industrial Technology,
Phranakorn Rajabhat University, Bangkok, Thailand.

²The Waste Incineration Research Centre,
Department of Mechanical and Aerospace Engineering, Faculty of Engineering,
King Mongkut's University Technology North Bangkok, Bangkok, Thailand, 10800

SUMMARY: This study provides the optimum equivalence ratio of biomass gasification process based on thermodynamic equilibrium model. There are two cases of chemical equilibrium in a gasification process. The first being with excess carbon present in the gasification process while the second one possess excess gasifying agent with all the carbon completely gasified. The simulation results clearly show that under the certain conditions, there must exist a case between these two cases where the carbon is completely gasified without any excess gasifying agent or carbon. This point has been determined from the cross over point between CO₂ and CO. Moreover, the results show that at higher gasifying agent temperatures the trend of CO increases more sharply than that at lower gasifying agent temperatures and vice versa for CO₂. The optimum equivalence ratio becomes less fuel rich with increase in gasification temperatures. At atmospheric pressures the optimum equivalence ratio was found to be 3.0 for gasification temperatures in the range of 600-900 K, while it was 2.0 for gasification temperatures of 1000-1500 K and 1.5 for gasification temperatures of 1600-2500 K.

Keywords: gasification; thermodynamic equilibrium model; gasifying agent temperature; optimization of gasification temperature.

INTRODUCTION

Interest in the use of biomass as sustained fuel continues to grow in many countries around the world [1]. The reason stems from both environmental concerns and sustainable energy availability and recovery. According to the international policies of CO₂ reduction, the positive environmental issue of biomass utilization is the zero net production of greenhouse gases. In contrast to fossil fuels, biomass does not introduce any new carbon into the environment so that a carbon balance is equilibrated [1].

Gasification is thermochemical conversion of solid carbon based material into combustible gaseous product using a gasifying agent. The thermochemical conversion changes the chemical structure of the biomass using high temperatures. Basically, preheating of gasifying agent is to deliver more enthalpy into gasification process, which enhances the thermal decomposition of the gasified solids. The gasifying agent allows quick conversion of the feedstock into clean gas through different heterogeneous reactions. The gasification process requires some gasifying agent. For example, using oxygen partially oxidizes the feedstock, which releases heat as well as the formation of CO, H₂ and CH₄ from solid carbon in the hydrocarbon fuel. The gasifying agents can be air, oxygen, steam or CO₂. The gasification product contains CO₂, CO, H₂, CH₄,

H₂O, trace amount of higher hydrocarbons, inert gases present in the gasifying agent and various contaminants such as particles, ash and tars. Gasification has several advantages over traditional combustion process. It takes place in a low oxygen environment that limits the formation of dioxin and large quantities of SO_x and NO_x. [2]. Gasification is more efficient than combustion because exergy losses due to internal thermal energy exchange are reduced from 14-16% to 5-7% of expended exergy. The losses due to internal thermal energy exchange may be reduced by replacing air with oxygen or alternatively by preheating the air. The gas composition evolved from biomass gasification strongly depends on the gasification process, the gasifying agent, and the feedstock composition. The fraction of different gases could be changed by controlling the gasifying agent properties. It is therefore useful to understand the basic issues behind the choice of agent. In the present study, oxygen is used as the gasifying agent. The equilibrium modeling is used to predict the performance of gasification process under various conditions of gasifying agent. Thermodynamic calculations are carried out to determine the equilibrium composition from a gasification system at constant temperature and pressure. Equilibrium model can predict thermodynamic limits as a guide to process design, evaluation and improvement [3]. Numerical simulations have been conducted using

GASEQ equilibrium code which uses element potential method to minimize the Gibbs free energy of a system to obtain equilibrium composition of the product gas using O₂ as the gasifying agent.

The main objectives of this paper are therefore to analysis the effect of equivalence ratio and gasifying agent temperature on the evolved gas composition using oxygen as the gasifying agent. The simulations assist one to determine the optimum equivalence ratio at any gasifying agent temperature and provide optimum operational conditions for the process control.

EQUILIBRIUM MODELING FOR BIOMASS GASIFICATION

Equilibrium Models

Thermodynamic equilibrium calculations are applied to determine the equilibrium compositions in gasification systems at constant temperature and pressure. The method for calculating equilibrium calculations at a specified temperature is based on the minimization of Gibbs free energy (NASA method). The equilibrium number of moles of species i is x_i ($i = 1$ to nSp). The Gibbs free energy G of the mixture at pressure p is given by:

$$\frac{G}{RT} = \sum_{i=1}^{nSp} \left(\frac{x_i G_i^0}{RT} + x_i \ln \frac{x_i}{\sum x_i} + x_i \ln p \right) \quad (1)$$

G_i^0 is the molar free energy at 1 atmosphere of species i ,

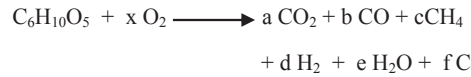
$\sum x_i$ is the total number of moles in the mixture and p is the pressure.

At equilibrium G/RT is at a minimum, subject to the elemental composition being fixed.

Reaction Equilibrium

In the present study non-stoichiometric method is used for equilibrium modeling. The advantage of non-stoichiometric method over stoichiometric method is that no particular reaction mechanism or species are involved. The only inputs are reaction temperature, pressure and an elemental composition of the feedstock, which can readily be obtained from ultimate analysis data. This method is particularly suitable for unclear reaction mechanisms and feed steam such as biomass whose precise chemical conversions are unknown [4]. Cellulose is the most abundant renewable organic molecule in nature and represents the main constituent of wood [2]. Therefore, cellulose, represented by chemical formula of C₆H₁₀O₅, is used as biomass fuel in the present study. Based on the assumption that the gasification

product contain CO₂, CO, H₂, CH₄, H₂O and unburnt carbon, the products from the oxidation of biomass (pure cellulose) with O₂ is described from:



RESULTS AND DISCUSSIONS

1. Effect of Equivalence Ratio on Gasification Product Composition

The simulation results show that there is a cross over point between CO₂ and CO. This point is referred here as the optimum equivalence ratio for the gasification process. As indicated in the results that CO₂ is produced at the equivalence ratio lower than the cross over point. This implies that there is excess gasifying agent present in the gasification process.

2. The Optimum Equivalence Ratio at Various Gasification Temperatures

The simulation results showed that for case of lower gasifying agent temperatures, the amounts of CO produced slowly increases with decrease in the amount of oxidizer while it sharply increases at higher gasification temperatures.

REFERENCES

- [1] W. Jangsawang, A. Klimanek, and A. K. Gupta, "Enhanced Yield of Hydrogen from Wastes Using High Temperature Steam Gasification", *Journal of Energy Resources Technology, Transactions of the ASME*, 2006, Vol. 128, No. 3, pp. 179-185.
- [2] W. Jangsawang, A. K. Gupta, K. Kitagawa, and S. C. Lee, "High Temperature Steam and Air Gasification of Non-Woody Biomass Wastes", *Proc. of the 2nd Joint International Conference on Sustainable Energy and Environment. 2006: SEE 2006*, Bangkok, Thailand, November 21-23, 2006, Paper No. C002, pp. 199-219.
- [3] Q. Yan, L. Guo, and Y. Lu, "Thermodynamic Analysis of Hydrogen Production from Biomass Gasification in Supercritical Water", *Energy Conversion and Management*, 2006, Vol. 47, pp. 1515-1528.
- [4] XT. Li, J. R. Grace, A. P. Watkinson, C. J. Lim, and A. Ergudenler., "Equilibrium Modeling of Gasification: A Free Energy minimization Approach and Its Application to a Circulating fluidized Bed Coal Gasifier", *Fuel*, 2001, Vol. 80, pp. 195-207.

Bio Fuel; Bioethanol

PHYSICO-CHEMICAL AND BIOLOGICAL CHARACTERISTICS OF ENHANCED ANAEROBIC MICROBIAL GRANULATION BY SYNTHETIC AND NATURAL CATIONIC POLYMERS

Ekhnarin Ariyavongvivat¹, Benjaphon Suraraksa² and Pawinee Chairprasert¹

¹Division of Biotechnology, School of Bioresources and Technology,
King Mongkut's University of Technology Thonburi, Thailand

²Excellent Center of Waste Utilization and Management,
National Center for Genetic Engineering and Biotechnology (BIOTEC), Thailand

SUMMARY: This research aimed to investigate the effect of adding cationic polymer on anaerobic microbial granulation. High and medium molecular weight of synthetic polymers (3150 and 8265) and natural polymer (chitosan) were selected to study the effects of dose and type of external polymer on microbial granulation in anaerobic digestion using laboratory-scale jar test. The suitable dose of 3150, 8265 and chitosan was 2.0, 2.0 and 13.0 mg/gVSS, respectively. The bench reactors were operated for a period of 120 days at organic loading rate (OLR) of 0.5-2.0 Kg COD/m³.d. As the results, these cationic polymers enhanced anaerobic granulation in term of granule properties which consists of physical, chemical and biological properties. Size distribution of all reactors increased specially addition of polymer 3150 which provided the granule percentage from 2.74% to 16.40%. Chitosan contributed on increased of extracellular polymeric substances (EPS) production from 20.2 to 50.0 mg/g VSS, and also specific methanogenic activity (SMA) reached to 0.18 g COD/g VSS.d. The experimental results showed that addition polymer 3150 and chitosan gave well productive in term of granule properties. Granule scanning electron microscope (SEM) and fluorescent in situ hybridization (FISH) with confocal laser scanning microscope (CLSM) photographs indicated the accomplishment of granulation by progressively increasing the OLR.

Keywords: Anaerobic granule, Cationic Polymer, CLSM, FISH, SEM

INTRODUCTION

The anaerobic processes can be either conventional free cell processes or attached growth also known as biofilm and granule. Comparing to conventional free cell systems, the bioreactors with immobilized cells show the better results including greatly improved the reactor productivity, smaller reactor vessels and shorter retention times. It is due to higher cell density and high resisted to pH, temperatures and concentrations of toxicants, which are lethal for a free suspended culture.

Anaerobic microbial granulation is considered to be a key parameter for the successful operation of an upflow anaerobic sludge blanket (UASB) reactor and an anaerobic hybrid UASB-fixed film reactor (AHR). It is a natural process under favorable conditions due to the tendency of bacteria to self-immobilize. The granulation is often initiated by adsorption of bacteria to inert material, or with each other due to syntrophic relationship between methanogenic and acetogenic species in mixed consortia. To form granulation, not only pH, temperature, composition and concentration of organic compounds in wastewater, hydrodynamics, microbial ecology and production of extracellular polymeric substance (EPS) by anaerobic bacteria are factors governing granulation but the presence of multivalent cations is also one important factor to accelerate granulation. The cationic polymer additives are generally used to accelerate the granules formation because of positive charges facilitating the formation of microbial granules by formed bridges among negative charges of

anaerobic microorganism. Synthetic cationic polymers with high and medium molecular weight have been used by researchers for acceleration of sludge granulation. Show et al. (2004) used the high molecular weight cationic polymer to accelerate the formation of sludge granules in UASB reactor [1]. Moreover, chitosan as a natural polymer also be used for enhancement of sludge granulation. A study conducted by El-Mamouni et al. (1998) found that the granulation rate of mixed culture in the UASB reactor supplemented with chitosan was faster than that in the UASB reactor supplemented with synthetic cationic polymers [2].

Both of synthetic and natural polymers are effected on the granulation size. The reactor performance and stability is not only depended on the granulation size and quantity of granule but also relies on the quality of granule. Therefore, this research aimed to study effect of cationic polymer additives on microbial granulation and its properties by using high and medium molecular weight of synthetic polymers (3150 and 8265) and natural polymer (chitosan).

EXPERIMENTAL SET UP

Three continuous stirred tank reactor (CSTR) with a working volume of 5 l were used with addition of 3150 (reactor 3150), with addition of 8265 (reactor 8265) and chitosan (reactor chitosan). The initial seed sludge was inoculated in each reactor as 5 g VSS/l. The reactors were start-up with initial OLR 0.5 gCOD/l.d or F/M ratio 0.1 gCOD/gVSS.d at HRT of 4 days and up-flow liquid

velocity of 1 m/h. The polymers were added weekly into the reactor based on the suspended solid (SS) concentration. After reactors reached steady state condition, the organic loading rate (OLR) was increased as a series of steps from 0.5 kg/m³/d to 2.0 kg/m³/d (OLR 0.5 – OLR 2.0) and operating for 4 months. 3150, 8265 and chitosan were added every week in reactor 3150, reactor 8265 and reactor chitosan with the optimum dose of 2, 2 and 13 mg/g SS, respectively. The alkalinity in each reactor was adjusted to 2000 mg CaCO₃/l by the addition of NaHCO₃. All reactors were operated at an ambient temperature and monitored microbial physical, chemical and biological properties.

RESULTS AND DISCUSSION

The percentage of granule size distribution during the experiment. After 4 months operation, the particle size of all reactors less than 0.1 mm was decrease from 72% to 24-36% with OLR 2.0. The granule size population in range over 0.6 mm of reactor 3150, 8265 and chitosan was 16.40%, 3.67% and 6.82%, respectively. Addition with chitosan contributed on increased of EPS production from 20.2 to 50.0 mg/g VSS which was higher than addition with polymer 3150 (42.4 mg/g VSS) and 8265 (39.9 mg/g VSS). Moreover, the reactor addition with chitosan had the highest methanogenic activity and followed by polymer 3150 and 8265 with SMA values of 0.18, 0.16 and 0.13 g COD/g VSS.d, respectively. This result indicated that polymer did not cause any inhibition to methanogenic activity.

The addition of cationic polymers was successfully achieved in reactor 3150 and chitosan. It was found that the addition of 3150 was suitable for flocculation or initial stage of granulation, and chitosan was suitable for long term granulation. The granular size of reactor 3150 and chitosan was bigger in the reactor 8265. The increase of granular size was related to an increase of EPS production. It suggested that addition of polymer 3150 and chitosan could facilitate the formation of granules which did not affect on microbial activity.

ACKNOWLEDGMENT

The authors are grateful to the Thailand Graduate Institute of Science and Technology (TGIST) for the scholarship to Mr. Eknarin Ariyavongvivat. The research facility was supported by Excellent Center of Waste Utilization and Management (ECoWaste), King Mongkut's University of Technology Thonburi.

References

- [1] K.Y. Show, Y. Wang, S.F. Foong and J.H. Tay, "Accelerated start-up and enhanced granulation in upflow anaerobic sludge blanket reactors", *Water Research*, **38**, 2004, pp. 2293 - 2304.
- [2] R. El-Mamouni, R. Leduc, and S.R. Guiot,

"Influence of synthetic and natural polymers on the anaerobic granulation process", *Water Science and Technology*, **38(8-9)**, 1998, pp.341-347.

EFFECT OF GRANULE SIZES ON THE PERFORMANCE OF UASB REACTOR FOR CASSAVA WASTEWATER TREATMENT

Sunwancee Jijai¹, Galaya Srisuwan¹, Sompong O-thong², Norli Ismail³ and Chairat Siripatana¹

¹Renewable Energy Research unit

School of Engineering and Resources, Walailak University, Thailand

²Research Center in Energy and Environment

Department of Biology, Faculty of Science, Thaksin University, Thailand

³School of Industrial Technology, Universiti Sains Malaysia, Malaysia

SUMMARY: The UASB reactors were operated at five different hydraulic retention times (HRTs). The various sizes of granules from three different sources: a cassava factory (CS), a seafood factory (SS), and a palm oil mill (PS), were used as inocula for anaerobic digestion of cassava wastewater. For comparison, the first reactor with only granules from its own source (R1, CS) was treated as control. The other two reactors were inoculated with mixed granules from different sources (R2, CS+SS and R3, CS+PS). As HRT decreased from 5 days to 1 day, the organic removal efficiencies decreased from 91.49 to 43.23 %, 89.36 to 45.13 % and 87.23 to 32.69 % for R1, R2 and R3 respectively (or inversely with increasing OLR). In this study selected mathematical models including Monod, Contois, Grau second-order and Modified Stover-Kicannon kinetic models were applied to determine the substrate removal kinetics of UASB reactors. The results showed that Grau second-order and Modified Stover-Kicannon kinetic models were more suitable than the others for all different sizes of granules.

Keywords: UASB, Cassava wastewater, Monod, Contois, Grau second-order, Modified Stover-Kicannon

INTRODUCTION

Currently, environmental regulatory authorities are setting strict criteria for wastewaters from industries and there is a large potential to convert the waste into energy. In Thailand, a 'Strategic Plan for Renewable Energy Development' has been established since 2003. It aims to increase the share of renewable energy from 6.4%, or 4,237 kilo tons of crude oil equivalent (ktoe) per year in 2008 to 20.3% of the commercial primary energy, or 19,700 ktoe per year, by the year 2022. Although Thailand is an agriculture country with the large volume of potential biogas feed stocks, only two major sources are currently utilized for biogas production: wastewaters from cassava starch factories and pig farms [1].

Many researchers found that wastewater from cassava factory are suitable for anaerobic process such as UASB reactor. The successful treatment in UASB reactor is principally attributed to the formation of anaerobic granules in sludge bed. The granule size is an important parameter directly influences the performance of reactor. Other factors affecting the performance of UASB reactor include temperature, organic loading rate, pH, alkalinity and nutrients etc [2]. The scope of this research is to study the effect of granule sizes on the performance of UASB reactors for cassava wastewater treatment in term of organic removal and biogas potential from different sizes of inocula/granules using kinetic models. The preliminary results in this work could be valuable for design and operation in continuous biogas plants.

MATERIALS AND METHODS

Seed and Wastewater

The granular sludges were collected from three sources: a cassava factory, a seafood factory and a palm oil mill. Cassava wastewater was collected from a cassava factory. It was kept at 0-4 °C until used in the experiments.

Reactors and Analytical Procedures

The three identical laboratory-scale UASB reactors were operated continuously at different five hydraulic retention times (HRTs) of 5, 4, 3, 2 and 1 day with cassava wastewater. The corresponding organic loading rates were 3.76, 4.70, 6.27, 9.40 and 18.80 kg CODm⁻³d⁻¹ respectively.

All analytical procedures were performed in accordance with standard methods for examination of water and wastewater APHA [3]. Gas production were measured daily by using water displacement method (Gas counter) [4]. The methane content was measured using Gas Chromatograph (GC-8A Shimadzu).

The kinetic models selected mathematical models including Monod, Contois, Grau second-order and Modified Stover-Kicannon kinetic models.

RESULTS AND DISCUSSION

Reactors performance

The COD removal efficiency decreased from 91.49 to 43.23 %, 89.36 to 45.13 % and 87.23 to 32.69 % for R1, R2 and R3 respectively with decreasing HRTs. This was because the decreasing of HRT led to shorter residence time, thus lowering the efficiency. Because of the disintegration and wash away of biomass or granules along with the

effluent due to high mixing intensities [5]. This indicated that acidogenesis occurred more rapidly than acitogenesis and methanogenesis, thus the later steps became the rate-limiting steps which dictated the performance of UASB reactors.

Kinetic model

The values of kinetic parameters showed that the Grau second-order and Modified Stover-Kicannon models represented all data better than Monod and Contois models as indicated by the corresponding regression coefficients for three reactors (R1, R2 and R3). These results were similar to the study of Abtahi et al, 2013, Isik and Sponza, 2005 and Mullai et al, 2011[5-7]. It also showed that the sizes of granule had a strong effect on the process performance and substrate removal in the UASB reactors fed with cassava wastewater. The UASB reactor R1 used only granules from cassava factory which had biggest average sizes (1.5-1.7 mm.) gave the highest substrate removal and biogas production.

The kinetic constants in term of the saturated constant (K_s) in Monod model and kinetic parameter (β) in contois models. Whereas high β in UASB-R1 reflected strong negative effect of granule size on the substrate accessibility of microbial cells, K_s in Monod model indirectly showed similar trend albeit with different interpretation. Highest K_s values in UASB-R1 was a combined effect of high cell density (thus high substrate demand) and diffusion-limiting in-granule substrate transport, both were a result of the biggest granule size. The apparent high K_s value is again does not explain high half-substrate consumption rate according to Monod model formulation. So there is no surprise that both Monod and Contois models could not represent the experimental results so well since their basis in model formulation do not directly include diffusion-limiting step into consideration. Consequently, Monod and Contois are fundamentally unsuitable for modeling UASB with granules and some diffusion-limited consideration must be included in the formulation [5-8].

The kinetic value (K_B , R_{max}) in Modified Stover-Kicannon model suggest that the substrate removal rate is strongly affected by the granule size. And the different of kinetic coefficients value because each studies different of initial substrate (S_0) and different of inocula that use in each reactors [6, 8]. The results kinetic values can be used to explained performance of UASB reactors and to predict the effluent COD from UASB reactors. From four kinetic models (Monod, Contois, Grau-second order, Modified Stover-Kicannon model), when compared with data from experiments, Grau-second order and Modified Stover-Kicannon models were more suitable for predicting COD effluent as indicated by higher regression coefficients (higher than 0.98) for all the reactors (R1, R2 and R3)

CONCLUSION

The results of this study showed that sizes of granules highly affected the reactor performance and biogas production in UASB reactors. The COD removal efficiencies and biogas production decreased with decreased HRTs. The experimental data of UASB reactor treating cassava wastewater were in good agreement with the kinetic models particularly Grau second-order and Modified Stover-kicannon models.

ACKNOWLEDGMENT

The authors would like to thank Walailak University and Ministry of Science and Technology of Thailand grant for financial support.

References

- [1] N. Paepatung, A. Nopharatana and W. Songkasiri "Bio-Methane Potential of Biological Solid Material and Agricultural Wastes". *Asian Journal on Energy and Environment*. **10(1)**, 2009, pp. 19-27.
- [2] SA. Habeeb, AABA. Latiff, ZB. Daud, ZA. Ahmad. A review on granules initiation and development inside UASB Reactor and the main factors affecting granules formation process. *International Journal of Energy and Environment*. **2(2)**, 2011, pp. 311-20.
- [3] APHA A, WEF, editor. Standard Method for the Examination of Water and Wastewater. 20 ed. Washington D.C.: *American Public Health Association*; 1999.
- [4] Abdel-Hadi M. A. "Simple apparatus for biogas quality determination". *Misr Journal Of Agricultural Engineering*. **25(3)**, 2008, pp. 1055-1066.
- [5] M. Pandian, Huu-Hao NGO, S. Pazhaniappan. "Substrate Removal Kinetics of an Anaerobic Hybrid Reactor Treating Pharmaceutical Wastewater". *Journal of Water Sustainability*. **1(3)**. 2011, pp. 301-312.
- [6] Abtahi SM AM, Nateghi R, Vosoogh A, Dooranmahalleh MG. Prediction of effluent COD concentration of UASB reactor using kinetic models of monod, contois, second-order Grau and modified stover-kicannon. *Int J Env Health Eng*. **1(8)**, 2013, pp. 1-8.
- [7] M. Işik and DT. Sponza. "Substrate removal kinetics in an upflow anaerobic sludge blanket reactor decolorising simulated textile wastewater". *Process Biochemistry*. **40(3-4)**, 2005, pp. 1189-1198.
- [8] DT. Sponza and A. Uluköy. "Kinetic of carbonaceous substrate in an upflow anaerobic sludge sludge blanket (UASB) reactor treating 2,4 dichlorophenol (2,4 DCP)". *Journal of Environmental Management*. **86(1)**, 2008, pp. 121-131.

OPTIMIZATION OF SUB-CRITICAL WATER PRETREATMENTS FOR ENZYMATIC HYDROLYSIS OF SUGARCANE BAGASSE

Kuncharika Manorach¹, Nawin Viriya-empikul² and Navadol Laosiripojana¹

¹The Joint Graduate School of Energy and Environment (JGSEE),
King Mongkut's University of Technology Thonburi, Thailand

²National Nanotechnology Center (NANOTEC),
National Science and Technology Development Agency, Thailand

SUMMARY: Sugarcane bagasse was pretreated with sub-critical water carried out at several operating conditions; reaction temperature (126.36 °C to 193.64 °C), reaction time (3.18 min to 36.82 min), and bagasse/water ratio (1/4.64 to 1/11.36) in 600 mL autoclave reactor by using central composite design and response surface methodology. This work was aimed to study and identify the optimum conditions to increase the enzymatic digestibility of the cellulose fraction for subsequent sugar conversion. The effects of pretreatment conditions on the solubilization and separation of the components of bagasse, degradation of carbohydrates, morphological structure change of pretreated bagasse in comparison with the raw material, and the formation of degradation products (organic acids and furan aldehydes) were investigated.

Keywords: Sugarcane bagasse, Sub-critical water, Enzymatic hydrolysis

INTRODUCTION

Presently, petroleum resources are the major feedstock for the production of commodity chemicals and fuels. Nevertheless, rapid depletion of these finite resources and the increase in emissions of CO₂ level encouraged a replacement of petroleum with renewable resources such as lignocellulosic biomass, forest biomass, and municipal solid waste. Among various potential large-scale industrial biorefineries, the use of lignocellulose feedstocks is known as one of the most promising approaches particularly in the agricultural-based countries.

Lignocellulosic biomass is mainly composed of cellulose (40-50%), hemicellulose (25-30%), and lignin (15-20%). Cellulose, a linear polymer of glucose molecules linked with β -(1-4)-glycosidic bonds is a major structural component of plant cell walls. Hemicellulose is a branched polymer of different 5-carbon sugars (xylose, arabinose) and 6-carbon sugars (glucose, galactose, and mannose) that linked cellulose and cross-links with lignin. Lignin is an aromatic polymer that composed of p-coumaryl alcohol (H), coniferyl alcohol (G), and sinapyl alcohol (S) forming a layer of the cell walls.

To convert lignocellulosic biomass to biofuels/chemicals, it generally requires: (1) a pretreatment step for cellulose crystallinity reduction by the hydrolysis of hemicellulose and delignification (2) an enzymatic hydrolysis step of cellulose to produce sugar monomers. It has been known that pretreatment of lignocellulosic biomass enhances the product yield and is therefore of great importance for the efficient biorefinery process.

Various pretreatment methods have been developed to change the physical and chemical structures and break down the hemicellulose and lignin shield efficiently. Hydrothermal pretreatment where fiber is heated in water at 150-230 °C, is considered as an attractive method due to a simple

operation, potential on hemicelluloses dissolution, and chemical handling. Moreover, sub-critical water requires little or no chemicals because their particular solvent is water, which is environmentally friendly and cost-effective.

In sugarcane-producing countries like Thailand, there is an abundant opportunity for the use of sugarcane bagasse. In this work, sugarcane bagasse is selected as the efficient feedstock to produce sugar monomers. Sub-critical water pretreatment will be performed under several operating conditions in order to increase biomass digestibility prior to the enzymatic hydrolysis. The optimum pretreatment conditions will be determined based on experimental design studies.

METHODOLOGY

Raw material preparation

Sugarcane bagasse obtained from the PTT Global Chemical Public Company Limited, Thailand was used as the feedstock in this work. The bagasse was dried at 60 °C for 24 h before processing. A portion of the sugarcane bagasse was characterized according to the methodologies of the National Renewable Energy Laboratory [NREL, 2006] followed by high performance liquid chromatography analysis (HPLC) to determine carbohydrate content (mostly cellulose and hemicellulose), acid insoluble lignin (AIL), acid soluble lignin (ASL), and ash content. Both untreated and treated sugarcane bagasse were analyzed and compared.

Experimental procedures

Pretreatment

Sub-critical water pretreatment was performed in a 600 mL autoclave reactor with a heater. Central composite design and response surface methodology were used to optimize the pretreatment conditions; reaction temperature, reaction time, and

biomass/water ratio as shown in table 1. The sugarcane bagasse and de-ionized water were added to the reactor at different bagasse to water ratios. The hydrolysis was carried out in the range of 126.36 °C to 193.64 °C for 3.18 to 36.82 min. When the desired reaction time was reached, the reactor was cooled down by immersing into a cold water bath. Then, the pretreated slurries obtained after sub-critical water pretreatment was separated by filtration. The solid fraction was washed with de-ionized water until pH value became in the range of medium. The sample was dried at 60 °C for 24 h and weighed for calculation of solid recovery before subjecting to enzymatic hydrolysis to evaluate the improvement on biomass digestibility.

Table 1. Range of variables for the central composite design

Variables	Axial point (-1.682)	Low level (-1)	Central level (0)	High level (+1)	Axial point (+1.682)
Temperature (°C)	126.36	140	160	180	193.64
Time (min)	3.18	10	20	30	36.82
Bagasse to water ratio	1/4.64	1/6	1/8	1/10	1/11.36

Enzymatic hydrolysis

The enzymatic assay was provided by the National Center for Genetic Engineering and Biotechnology (Biotech), Thailand. After pretreatment, solid residue (5% of 5 ml total reaction volume) was hydrolyzed with 50 mM of citrate buffer (pH 5). Then, the enzyme (Cellic® CTec2) was added at 10 FPU/g dry treated bagasse. Next, the mixture was incubated at 50 °C, and 200 rpm for 72 h and collected for determination of reducing sugars by DNS methods.

Analytical procedures

Analysis of the solid fraction

The chemical compositions of solid residue were analyzed according to the NREL method followed by HPLC analysis to determine carbohydrate content, acid insoluble lignin, acid soluble lignin, and ash content. Morphological structures of the raw material and pretreated material were characterized using a scanning electron microscope (SEM). CHNOS measurement was employed for the elemental analysis.

Analysis of the liquid fraction

HPLC with refractive index detector (Shimadzu, Japan) was used to analyze the liquid products for free sugars, organic acids, and furan aldehydes. In the hydrolysates, sugars were separated on an Aminex HPX-87H column (Bio-Rad, USA) operating at 45 °C with 5 mM H₂SO₄ as the mobile phase at a flow rate of 0.5 ml/min. UV-Vis was used as quantification tool for solubilized lignin. Biochemical oxygen demand

(BOD) and chemical oxygen demand (COD) were used for wastewater treatment indicators. Total organic carbon (TOC) was used as an indication of biomass at different conditions.

RESULTS AND DISCUSSION

Effect of Bagasse and water to air ratio

Bagasse and water to air ratio of sub-critical water pretreatment was varied at 4/1, 3/2, and 2/3 at 160 °C for 20 min. The compositions of raw and pretreated sugarcane bagasse were analyzed according to the NREL method as shown in table 2. Sub-critical water pretreatment significantly removed hemicellulose from the solid phase with higher content of cellulose. The highest cellulose content is obtained from 2/3 bagasse and water to air ratio as 64.36% and almost the same as those at 4/1 ratio. Enzymatic hydrolysis results showed that the maximum reducing sugars could be obtained at 4/1 ratio that is the optimum bagasse and water to air ratio in the further experiment.

Table 2. The compositions and enzymatic hydrolysis results of raw and pretreated materials [C: Cellulose, H: Hemicellulose, L: Lignin, A: Ash]

Bagasse+ water/air ratio	Compositions of Raw mat. (%)				Compositions of Pretreated mat. (%)				Reducing sugars (mg/g biomass)
	C	H	L	A	C	H	L	A	
4/1					61.21	9.83	28.67	5.15	285.05
3/2	42.29	25.14	22.85	4.32	53.42	15.62	26.90	4.15	241.14
2/3					64.36	4.35	32.49	5.61	276.50

ACKNOWLEDGMENT

The authors would like to thank the PTT Global Chemical Public Company Limited, Thailand for their financial support.

References

- [1] W. Abdelmoez, S. M. Nage, A. Bastawess., "Subcritical water technology for wheat straw hydrolysis to produce value added products", *Journal of Cleaner Production*, **70**, 2014, pp. 68-77.
- [2] C. S. Goh, K. T. Lee and S. Bhatia., "Hot compressed water pretreatment of oil palm fronds to enhance glucose recovery for production of second generation bio-ethanol", *Bioresource Technology*, **101**, 2010, pp. 7362-7367.
- [3] X. Xiao, J. Bian, Ming-Fei Li, Hui Xu, Bin Xiao., "Enhanced enzymatic hydrolysis of bamboo (*Dendrocalamus giganteus* Munro) culm by hydrothermal pretreatment", *Bioresource Technology*, **159**, 2014, pp. 41-47.
- [4] P. Kumar, M. D. Barrett., Methods for Pretreatment of Lignocellulosic Biomass for Efficient Hydrolysis and Biofuel Production, *Industrial & Engineering Chemistry Research*, **48**, 2009, pp. 3713-3729.

OPTIMIZING SULFUR OXIDIZING PERFORMANCE OF PARACOCCLUS PANTOTROPHUS ISOLATED FROM LEATHER INDUSTRY WASTEWATER

Nunthaphan Vikromvarasiri¹ and Nipon Pisutpaisal^{1,2,3,4}

¹ The Joint Graduate School for Energy and Environment (JGSEE),
King Mongkut's University of Technology Thonburi, Thailand

² Department of Agro-Industrial, Food and Environmental Technology, Faculty of Applied Science,
King Mongkut's University of Technology North Bangkok, Thailand

³ The Biosensor and Bioelectronics Technology Centre,
King Mongkut's University of Technology North Bangkok, Thailand

⁴ The Research and Technology Center for Renewable Products and Energy,
King Mongkut's University of Technology North Bangkok, Thailand

SUMMARY: Biogas has been used as alternatives for renewable energy in many applications. Hydrogen sulfide in the biogas is a significant factor to limit its usages. This research focused on using a pure bacterial strain for hydrogen sulfide removal from biogas in a biotrickling filter process. The pure bacterial strain was isolated from leather industry wastewater treatment plant. 16S rDNA sequence showed that the isolated bacterium is closely related to *Paracoccus Pantotrophus*. *P. Pantotrophus* is able to use sulfide and thiosulfate as energy sources for growth under aerobic conditions. The optimum phosphate buffer (26 - 78 mM, pH 8) and thiosulfate concentrations (5 - 20 g/L) were evaluated for microbial growth and sulfur oxidation activity before applying in the biotrickling filter system. The result showed that 52 mM buffer concentration and 10 g/L thiosulfate were suitable for growth and sulfur oxidation activity. The research findings suggest that *P. Pantotrophus* has the potential application in the biotrickling filter process of hydrogen sulfide removal for upgrading biogas quality.

Keywords: paracoccus pantotrophus, thiosulfate, hydrogen sulfide, biogas

INTRODUCTION

Biogas has been accepted to be one of the green alternatives for renewable energy. One of the biggest factors limiting the use of biogas is related to the presence of hydrogen sulfide exerting corrosive to internal combustion engines and equipments. Besides, there are reports on health effects to human from hydrogen sulfide. The biotrickling filter is one of alternative biological techniques of alternative solution.

Chemotrophic bacteria can grow by using inorganic carbon as a carbon source and obtain chemical energy from the oxidation of reduced inorganic compounds such as hydrogen sulfide. Some of these microbes, which were called mixotrophic microorganisms, can heterotrophically grow by using the organic carbon as carbon source and using an inorganic compound as an energy source [1]. Therefore, these microbes have potential to degrade hydrogen sulfide from biogas by applying in biotrickling filter.

This research focuses on the screening and characterizing a pure culture strains capable of hydrogen sulfide removal in biogas from high sulfide source such as waste water from leather industry. The medium was evaluated the optimal buffer (phosphate buffer) and thiosulfate concentrations for microbial growth and sulfur oxidation activity before using in biotrickling filter system.

METHODOLOGY

Mixed cultures obtained from the wastewater treatment plant of leather industry, Samut Prakarn province, Thailand was isolated and purified by repeatedly transferring the cells to fresh medium. The sulfur oxidation ability was tested prior to strain identification by 16S rDNA sequence analysis.

Thiosulfate mineral nutrient (TMN) was used for screening, culturing, and testing the microorganism. This medium contained the following (g/L): 2.0 KH₂PO₄, 2.0 K₂HPO₄, 0.4 NH₄Cl, 0.2 MgCl₂·6H₂O, 0.01 FeSO₄·7H₂O and 8.0 Na₂S₂O₃·5H₂O [2].

Concentration of phosphate and sodium thiosulfate in TMN were varied in order to find the optimum concentration for microbial growth and sulfur oxidizing activity. The buffer concentrations were varied in the range of 26 - 52 mM (pH 8).

The concentrations of sodium thiosulfate were varied in the range of 5-20 g/L at the optimum buffer concentration. Each experiment, *P. Pantotrophus* was cultivated at 37 °C, 180 rpm. The growth was observed by colony forming unit (CFU/ml). Liquid samples were periodically collected for analysis of pH and sulfate content.

RESULTS AND DISCUSSION

Pure culture strain capable of oxidizing thiosulfate was isolated, purified, and identified by 16S rDNA sequence analysis. The results showed that it is closely related to *P. Pantotrophus* NTV02

(99% identity) (KJ027465). *P. Pantotrophus* is mixotrophic bacteria that can use mix of different carbon and energy sources. *P. Pantotrophus* can also grow on sulfide and thiosulfate under aerobic and denitrifying conditions [3]. Therefore, *P. Pantotrophus* is a bacterium that is challenged to use for upgrading the biogas quality in term of hydrogen sulfide removal.

Higher ability to control pH was found in higher buffer concentrations (Fig. 1A), but the growths of the *P. Pantotrophus* are not significant different at all buffer concentrations (Fig 1B). The results of growth founded that the highest growths of 26 mM, 52 mM, and 78 mM buffer are 1.0×10^8 , 1.2×10^8 , and 1.3×10^8 CFU/mL, respectively. Therefore, the higher buffer concentrations have no effect to the growths of the *P. Pantotrophus*.

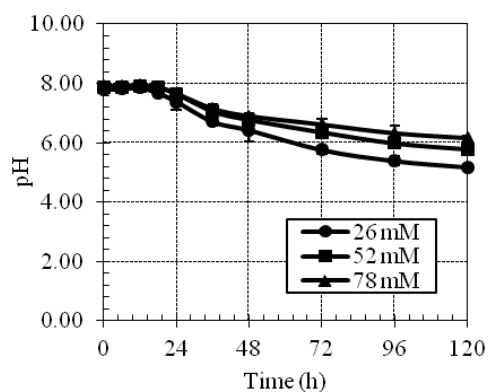
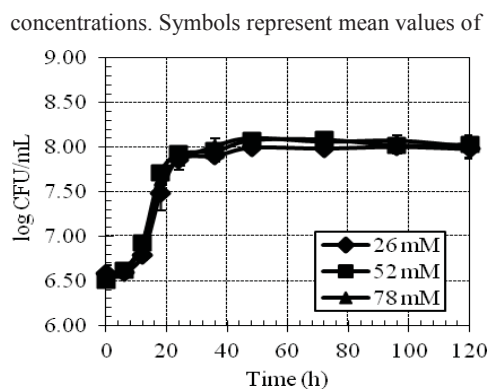


Figure 1. pH of TMN medium during the cultivation of *P. Pantotrophus* with varying buffer



duplicate experiments; error bars represent one standard deviation.

Figure 2. The growth of *P. Pantotrophus* in TMN medium with varying buffer concentrations.

Symbols represent mean values of duplicate experiments; error bars represent one standard deviation

The highest sulfate production rate was found in 52 mM buffer concentration (97.29 ± 3.72 mg/L·h). Therefore, 52 mM buffer concentration is suitable for the growth and sulfur oxidation activity of *P. Pantotrophus* in TMN medium.

The thiosulfate concentrations have effect to the growth and sulfate production of *P. Pantotrophus*. 10 g/L thiosulfate concentration had the highest sulfate production rate. The growth of *P. Pantotrophus* was apparently corresponded with sulfate production.

Maximum sulfur conversion of 66.7% after 36 hours incubation was found at the initial concentration of 10 g/L. Less sulfur conversion was observed at the thiosulfate concentration of 15 and 20 g/L. The results indicated that optimum thiosulfate concentration for *P. Pantotrophus* growth and sulfur oxidation activity is 10 g/L.

ACKNOWLEDGEMENT

I gracefully acknowledge the financial support from the Royal Golden Jubilee (RGJ) Scholarship of Thailand Research Fund (TRF, Grant No. PHD/0139/2553), and the Joint Graduate School of Energy and Environment (Grant No. JGSEE 522), King Mongkut's University of Technology Thonburi. Besides, I would like to thank Ms. Natnaree Promduang and Ms. Sirinun Tungtondee for their assistants.

References

- [1] M. Syed, G. Soreanu, P. Falletta, M. Béland., "Removal of hydrogen sulfide from gas streams using biological processes - A review", *Wastewater Technology Centre*, **48**, 2006, pp. 2.1-2.14.
- [2] Y. Jin, M. Veiga, C. Kennes., "Autotrophic deodorization of hydrogen sulfide in a biotrickling filter", *Journal of Chemical Technology and Biotechnology*, **80**, 2005, pp. 998–1004.
- [3] D.J. Brenner, N.R. Krieg, J.T. Staley, "Genus XII. *Paracoccus*. Bergy manual of systematic bacteriology", Volume Two, Part C, The Alpha-, Beta-, Delta-, and Epsilonproteobacteria, Springer, pp. 197-203.

EFFECT OF MIXING TIME ON ANAEROBIC CO-DIGESTION OF PALM OIL MILL WASTE AND BLOCK RUBBER WASTEWATER

Weerapong Lerdratranataywee¹ and Thaniya Kaosol¹

¹Environmental Engineering Program, Department of Civil Engineering, Faculty of Engineering, Prince of Songkla University, Thailand

SUMMARY: This paper aims to study a biogas production of Anaerobic Continuous Stirred Tank Reactor (An-CSTR) using decanter cake from palm oil mill factory with block rubber wastewater as a co-anaerobic digestion. The objective is to study the effect of mixing time for co-digestion on An-CSTR. The best ratio from previous research is used for the continuous An-CSTR processes. Two different values of Hydraulic Retention Times (HRTs) were used in these studies which were 10 and 30 days. Also, two values of mixing time at 12 and 24 hr/day were used. Both parameters were used in the biogas production in this study. All reactors presented the biogas production. The biogas production from both reactors of 10-day-HRT was similar and the gas production from both reactors of 30-day-HRT was similar. Thus, it can be concluded that the 12 and 24 hr/day of mixing time on An-CSTR processes have no significant effect on the biogas production. The biogas production from 10-day-HRT was higher than that from 30-day-HRT. The best biogas production performance on An-CSTR process of decanter cake and block rubber wastewater was observed from the reactor with 10-day-HRT and 12 hr/day mixing time. The average methane was 441 mL/day.

Keywords: anaerobic digestion, biogas, decanter cake, block rubber wastewater, mixing time

INTRODUCTION

An anaerobic digestion is a widely used technology for converting organic wastes into biogas under an absence of oxygen. Typically, the biogas consists of 55-80% methane, 20-45% carbon dioxide [1]. Therefore, the biogas can be used as a renewable energy source [2]. The renewable energy is one of the most important factors of the global prosperity. It can also reduce the greenhouse gas emissions from fossil fuels.

Agricultural wastes have potential for biogas production. The solid organic matter in biomass can be converted to biogas in anaerobic bio-reactors. However, the completely mixing is required in the bio-translated process in order to achieve the best performance. The mixing operation requires electricity that is directly translated to cost.

In this paper, the biogas production of various mixing times on the continuous An-CSTR processes is compared. The co-digestion between decanter cake and block rubber wastewater is used in this experiment in order to evaluate an energy cost.

MATERIAL AND METHODS

Raw materials

Block Rubber Wastewater (BRW) is obtained from a factory in Songkhla province, Thailand. The BRW contains high amount of COD which is the main environmental problem. Thus, the wastewater treatment is required before discharging the effluent to any receiving water source. The decanter cake (DC) is obtained from a palm oil mill factory in Krabi province, Thailand. The DC contains high amount of COD, TS and TVS. Therefore, the DC can increase the organic substrates in the BRW for biogas production. A seeding in the An-CSTR is the filtrated cow manure.

Experimental setting

The four An-CSTRs are set up in the laboratory scale. The reactors are carried out in 6 L of total volume with 5 L of working volume including interchangeable internal mixing machines. In order to operate An-CSTR in anaerobic condition, all reactors are integrated with gas bags and gas counters (Figure 1).

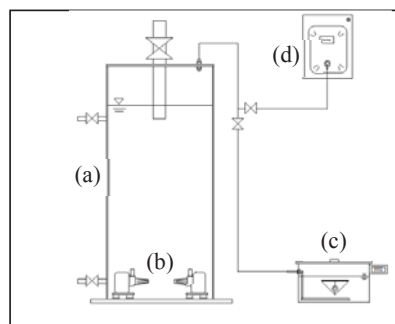


Figure 1. The schematic of the An-CSTR: (a) Anaerobic continuous stirred tank reactor, (b) two mechanical mixers, (c) a gas counter, and (d) a gas bag

In this study, the ratio of 5 g of DC and 200 mL of BRW is used because this ratio was the best ratio from the previous study. The co-material samples contain 7.0 of pH, 1,525 mg/L as CaCO₃ of Alkalinity, 147,661 mg/L of COD, 12,428 mg/L of TS, 8,118 mg/L of TVS and 859 mg/L of TKN. Table 1 shows the experimental setting of all four reactors are labeled R1, R2, R3, and R4. Each of which has different value pair of HRT and mixing time. R1 and R2 use 24 hr/day mixing time with 30-day-HRT and 10-day-HRT, respectively. R3 and

R4 use 12 hr/day mixing time with 30-day-HRT and 10-day-HRT, respectively. The parameters to be analyzed include pH, temperature, COD, TS, TVS, alkalinity, TKN and biogas content. All analytical procedures are performed according APHA [3]. The biogas is analyzed for methane composition using a Gas Chromatography with Thermal Conductivity Detector. The percentage of methane is recorded as the methane content representative.

Table 1. Experimental operations

Reactors	HRT (days)	Mixing time (hr/day)
R1	30	24
R2	10	24
R3	30	12
R4	10	12

The pH and temperature values of each reactor are analyzed daily. The parameters of each reactor are analyzed daily. The other parameters are analyzed every 3 days. The removal efficiency parameters such as COD, TS, TVS and TKN can be calculated. The biogas is collected daily using a gas bag. The biogas production is recorded daily as the volume of biogas produced using a gas counter. The biogas is collected in a gas tube every 4 days for analyzing the biogas composition.

RESULTS AND DISCUSSION

The mesophilic condition of An-CSTRs was between 28°C and 36°C. The pH value was between 6.3 and 7.2 for all 150 days. The startup period rose up in 20 days. The steady state of anaerobic condition observed after 43 days in all reactors. At the steady stage, the average biogas production was 255, 1,000, 269 and 1,012 mL/d, for R1, R2, R3 and R4, respectively. The composition of methane in biogas production ranged from 25.7-43.3, 30.3-57.3, 33.9-49.1 and 33.1-53.5% for R1, R2, R3 and R4, respectively. The daily biogas production at 20-150 days is demonstrated in the figure 2. The average methane production generated is 99, 445, 107 and 441 mL/d, for R1, R2, R3 and R4, respectively.

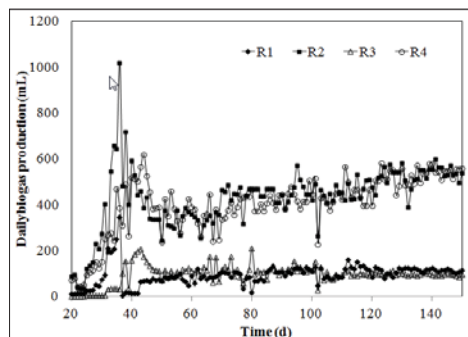


Figure 2. The daily biogas production at 20-150 days.

The observed daily biogas productions of R1 and R3 are similar while R1 and R3 are similar while R1 is operated at 24 hr/day mixing time and R3 is operated at 12 hr/day mixing time. Both R1 and R3 are operated at the same HRT condition of 30 days. The same results are observed from R2 and R4 that are operated at 10-day-HRT and different mixing times. Thus, the mixing time has no significant on the biogas production. Therefore, the mixing operation cost can be reduced by reducing the mixing time.

CONCLUSIONS

This research shows the comparison of biogas and methane productions resulting from 12 and 24 hr/day of mixing time for An-CSTR under 10 and 30 days of HRT. The co-digestion materials are decanter cake from palm oil mill factory and wastewater from block rubber factory. The result showed that the biogas production and anaerobic performance for both mixing times at same HRT showed no significant difference. It can be concluded that the best performance of An-CSTR operation in this study is 12 hr/day of mixing time at 10 days of HRT of co-digestion between decanter cake and block rubber wastewater. The average methane is 441 mL/day and the methane ranged between 33.1-53.5%.

ACKNOWLEDGMENT

The authors would like to thank you the Sustainable Waste Management (SWM) team (ENG-58-2-7-11-0200-S) and the National Research Council of Thailand (NRCT), Thailand (ENG550020S) for their financial support.

References

- [1] V. N. Gunaseelan. "Anaerobic Digestion of Biomass for Methane Production: A Review", *Biomass Bioenergy*. **13**, 1997, pp. 83-114.
- [2] R. E. Speece. "Anaerobic Technology for Industrial Wastewaters". *Archae Press USA*, **22**. 1996.
- [3] APHA, AWWA and WEF. "Standard Methods for the Examination of Water and Wastewater". 22th edition. Washington D.C.: *American Public Health Association*; 2012.
- [4] Metcalf & Eddy, Inc., George Tchobanoglous, Franklin Burton, H. David Stensel. "Wastewater Engineering: Treatment and Reuse". 5th Edition. New York: McGraw-Hill Companies; 2014.

DELIGNIFICATION OF ELEPHANT GRASS FOR PRODUCTION OF CELLULOSIC INTERMEDIATE

Juraut Minmunin¹, Paiboon Limpitpanich² and Anucha Promwungkwa¹

¹Department of Mechanical Engineering, Faculty of Engineering, Chiang Mai University, Thailand

²Department of Mechanical Engineering, Faculty of Engineering, Burapha University, Thailand

SUMMARY: In this work, elephant grass, a species of Napier grass which contains 60.20% cellulose, 23.80% hemicellulose and 8.20% lignin, was tested in laboratory for lignin remover or delignification. Two steps of delignification were performed. Alkali pretreatment was used for determining the best condition of the first delignification. Then, a material from the best condition was tested with ozonolysis process. Five concentrations of NaOH with vary from 0.5 to 10.5 wt.% were used for alkali pretreatment. Ozone flow rate of 5 liters per minute for time from 10 to 30 minutes were used. The optimum condition was 5.5 wt.% NaOH and 30 minutes of ozone flow. At this condition, 93.9 % of lignin was remover and 80.6 % of cellulose was recovered comparing with the untreated one. Lignin to cellulose ratio of the material is 0.0103 which is the lowest.

Keywords: Napier grass, elephant grass, alkali pretreatment, ozone pretreatment, delignification

INTRODUCTION

Due to global energy crisis, an alternative energy has been developed. In Thailand, Ministry of Energy of Thailand implemented the Alternative Energy Development Plan. As addressed by the plan, 25% of total energy consumption in Thailand's economy in 2021 must be substituted by renewable and alternative energy [1]. In transport sector, ethanol which is used for mixing with gasoline must be produced 9 million liters per day in 2021. In 2013, the capability of ethanol production was 4.2 million liters per day, but only 2.9 million liters per day was produced [2]. Now ethanol in Thailand is made from molasses, sugarcane and cassava which are biomass having recalcitrant lignocellulosic structure [2].

Ethanol can be produced by a two-step process. The first stage is to eliminate lignin from biomass which is called delignification. This pretreatment yields a cellulosic intermediate. Then, an enzymatic hydrolysis is used to reactive the intermediate to ethanol in the second step.

Most tropical countries have high potential to grow cellulosic biomass due to their solar radiation, diversity of climatic zones and biodiversity [3]. One of the potential biomass is from Napier grass. It is a high potential energy crop since it yields high plant, but needs low fermentation. In this work, elephant grass, a species of Napier grass, was experimental investigated in laboratory for delignification. Two pretreatments which are alkali and ozone were studied in order to estimate the optimum conditions for production of cellulosic intermediate.

MATERIALS AND METHODS

Materials

Elephant grass used in this study was from Amphoe Hang Chat, Lampang Province, Thailand. The farming area are around 1,200 rai. Its altitude is 1,200 meters above sea level. The grass is utilized for elephant food at The Thai Elephant Conservation Center with a capacity of 500 tones yearly.

For delignification, the grass was cut to a small size less than 1 cm. This grass was washed with distilled water and immediately dried in an air flow. After that, the material was grinded to a particle size less than 1 mm and dried again in an oven at 103 °C for hours to achieve a moisture content of less than 10 wt.%. Then, it was vacuum kept in a sealed plastic bag in desiccator as shown in Figure 1 (left). The material was characterized to determine the contents of cellulose, hemicellulose, and lignin following TAPPI T 203 om-88, T 223 om-88 and T 222 om-88, respectively.



Figure 1. Materials used in this study: before pretreatment (left) and after pretreatment (right)

Alkali pretreatment with NaOH

The first process to delignification from the material was alkali. NaOH solution is one that yields the highest concentration of reducing sugar comparing with others such as dilute acid and steam explosion [3]. NaOH concentrations of 0.5, 3.0, 5.5, 8.0 and 10.5% were used. 30.0 g of material was immersed in the solution and incubated at 70 °C for 2 hours. Then, it was washed with distilled water until neutral PH and dried at 103 – 105 °C for 10 hours. The material was characterized to determine its composition. A material which % lignin is minimum was used for delignification with ozone.

Ozone pretreatment

Before delignification with ozone, a selected material from alkali delignification was dried at 103 – 105 °C for 4 hours. The material was mixed with 160 g of distilled water in a reactor. 5 lit/min by ozone generator (ECONOWATT OZG gas 1000 mg) was flowed into the reactor for 10, 20 and 30 min. Then, it was washed with distilled water and dried at 103 – 105 °C for 10 hours. The material was characterized to determine its composition. A sample of material after delignification is shown in Figure 1 (right).

RESULTS AND DISCUSSION

Composition of sample after pretreatments

Table 1 lists the composition of materials after alkali pretreatment. At 5.5 wt.% NaOH, lignin content is 5.2. At this alkali concentration, 51.4 % of lignin is removed and 76.5 % of cellulose is recovered (see Table 2). This treated material was selected for delignification with ozone. It is noted that the untreated material contains 60.20% cellulose, 23.80% hemicellulose and 8.20% lignin.

Table 3 lists % cellulose, % hemicellulose, % lignin and other of materials after ozone pretreatment. It was found that longer time of ozone pretreatment presents lower % lignin. Table 4 lists the characterization of treated materials after ozone pretreatment. It was found that at 30 minutes of ozone pretreatment, 93.9% of lignin was removed comparing with the untreated material.

Table 1. Composition of elephant grass after alkali pretreatment.

% NaOH (w/w)	Composition (wt.%)			
	Cellulose	Hemicellulose	Lignin	Other
0.5	62.0	24.0	7.8	6.3
3.0	63.2	24.1	7.5	5.2
5.5	65.4	25.5	5.2	3.9
8.0	65.9	24.2	5.3	4.5
10.5	68.5	21.7	6.5	3.3

Table 2. Characterization of elephant grass after alkali pretreatment.

% NaOH (w/w)	% Lignin remover	% Recovery		
		Solid	Cellulose	Hemicellulose
0.5	8.8	96.0	98.9	96.6
3.0	21.0	87.0	91.4	88.2
5.5	51.4	76.5	83.1	81.9
8.0	57.4	66.0	72.3	67.2
10.5	63.5	46.0	52.4	42.0

Table 3. Composition of alkali-treated materials after pretreatment with ozone.

Ozone (min)	Composition (wt.%)			
	Cellulose	Hemicellulose	Lignin	Other
-	65.4	25.5	5.2	3.9
10	69.7	23.2	4.2	2.8
20	74.8	21.4	1.5	2.3
30	76.4	20.5	0.8	2.4

Table 4. Characterization of alkali-treated materials after pretreatment with ozone. (wt.%, based on untreated material.)

Ozone (min)	% Lignin remover	% Recovery		
		Solid	Cellulose	Hemicellulose
-	51.4	76.5	83.1	81.9
10	63.5	71.0	82.3	69.3
20	87.8	65.5	81.5	58.8
30	93.9	63.5	80.6	54.6

Optimum pretreatment conditions

Delignification make the grass sample losing solid materials which are cellulose, hemicellulose, lignin and other. The optimum delignification condition could be one which presents high percent or ratio of cellulose recovery and lignin remover. As shown in Figure 2, the optimum pretreatment condition is 5.5 wt.% NaOH and 30 min ozone. The process gave 93.9 % lignin remover and 80.6 % cellulose recovery. Lignin to cellulose ratio of the material is 0.0103 which is the lowest. Biomass which has the lowest ratio of lignin to cellulose is high potential biomass for ethanol production.

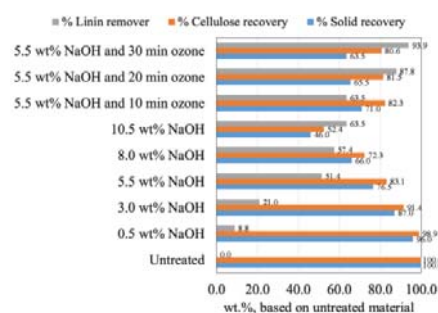


Figure 2. Characterization of elephant grass

ACKNOWLEDGMENT

The authors would like to thank the Energy Policy and Planning Office, Thailand's Ministry of Energy for their financial support.

References

- [1] Ministry of Energy, Thailand, "The Renewable and Alternative Energy Development Plan for 25 Percent in 10 Years (AEDP 2012-2021)", Available HTTP: http://www.dede.go.th/dede/images/stories/dede_aedp_2012_2021.pdf, 2011.
- [2] Bank of Thailand, "Ethanol Situation Report 2013 and tendency to 2014", Available HTTP: http://www.bot.or.th/Thai/EconomicConditions/Thai/Northeast/commodities/Doclib_CommodityYearly/Ethanol%20Yearly%202556.pdf, 2013.
- [3] C. Elian, R. Jorge and R Luis, "Effects of the pretreatment method on enzymatic hydrolysis and ethanol fermentability of the cellulosic fraction from elephant grass", *Fuel*, **118**, 2014, pp.41-47.

Fuel Cell and Energy Storage

PROPERTIES OF SILICON DIOXIDE (SiO₂) IN WATER-ETHYLENE GLYCOL MIXTURE FOR PROTON EXCHANGE MEMBRANE FUEL CELL COOLING APPLICATION

S.F.A.Talib¹, W.H. Azmi², Irnie Zakaria¹, and W.A.N.W. Mohamed¹, A.M.I. Mamat¹, H.Ismail¹, and W.R.W. Daud³

¹Faculty of Mechanical Engineering, Universiti Teknologi MARA, Malaysia

²Faculty of Mechanical Engineering, Universiti Malaysia Pahang, Malaysia

³Fuel Cell Institute, Universiti Kebangsaan Malaysia

SUMMARY: Polymer Electrolyte Membrane Fuel Cells (PEMFC) operation is sensitive to micro electrochemical changes and can only tolerate a small temperature variation for optimal power generation. An effective cooling system is needed to comply with this condition. Nanofluids are perceived as a potential coolant for thermal management in PEMFC application that allows for more compact design. The dispersion of nanofluid in water-ethylene glycol base fluid enhances the thermal conductivity for improved heat transfer. Here, the thermal conductivity, viscosity and electrical conductivity of different Silicon Dioxide (SiO₂) concentrations diluted in Ethylene Glycol/Water (EG/W) mixtures of 40EG, 50EG and 60EG are reported. Highest value of thermal conductivity recorded is the dispersion of nanofluid in 40EG whereas the viscosity of SiO₂ is the highest in 60EG dilution. The electrical conductivity of SiO₂ shows a drastic increment as the volume concentration is increased.

Keywords: nanofluids, PEMFC, thermal conductivity, viscosity, electrical conductivity

INTRODUCTION

Fuel cell is one of the applications that use hydrogen as fuel to generate electricity. Fuel cell is aforesought as potential energy generation device. The hydrogen acts as the fuel for the system and fed to the anode. Ion and electron disassociated from hydrogen is transported through membrane to the cathode and integrated with oxygen to produce water. Electricity is generated by the charge flow.

Fuel cells are classified based on the type of electrolyte used which is Phosphoric Acid Fuel Cell (PAFC), Alkaline Fuel Cell (AFC), Molten Carbonate Fuel Cell (MCFC), Solid-oxide Fuel Cell (SOFC) and Polymer Electrolyte Membrane fuel Cell (PEMFC). SOFC consists of ceramic membrane as electrolyte and carry oxygen ions. SOFCs have high operating temperature and more feasible to stationary application. PEMFCs in contrast consists of polymer membrane as an electrolyte operate at low temperature and feasible to many application due to its high power density

The operating temperature of PEMFC is in the range 30° - 100°C [1]. Thermal management is critical to avoid the membrane of fuel cell dry thus reduce charge transport resistance [1]. Proton migrate to cathode through electro-osmotic drag. High proton conductivity in the membrane is vital to achieve high performance of fuel cell [2]. An effective cooling is required in PEMFC to avoid dehydration and cathode flooding [1].

Nanofluid is a potential coolant for heat transfer application such as fuel cell thermal management and electronic device cooling [3]. The enhanced thermophysical characteristics of suspended nanometer sized particles into base fluids

have been considered in many research and application. Application of nanofluids as coolant is currently a new attempt in fuel cell design approach and lead to compact without affecting the design of cooling system.

The presence of nanoparticles in the base fluid increase the thermal conductivity; an important property in heat transfer. However, nanofluid also exhibit higher viscosity and electrical conductivity as the particle concentration is increased across temperature. High viscosity correlated to the pressure drop and pumping power. A low electrical conductivity of coolant is essential in fuel cell application. Excessive electrical conductivity will lead to shunt current and coolant electrolysis on the device. Therefore, nanofluids need to be characterized in detail to meet the fuel cell operating parameter.

METHODOLOGY

Preparation of nanofluids and thermophysical characterization

The nanofluids are prepared using dilution method. The solution of silicon dioxide (SiO₂) with volume concentration of 13.458% is diluted in base fluid of water-ethylene glycol (WEG) mixture. The concentration of EG used are 40%, 50% and 60%. The volume concentration of SiO₂ prepared are 0.1%, 0.3% and 0.5%. The thermal conductivity is measured using KD2 Pro thermal property analyzer of Decagon Devices, Inc. The viscosity is measured using Brookfield DV-III Ultra Programmable Rheometer connected to a temperature controlled bath and the electrical conductivity is measured using Cyberscan PC-10 conductivity electrode meter.

RESULTS AND DISCUSSION

Thermophysical Properties

The experimental of effective thermal conductivity of SiO₂ in 60EG is compared against the Hamilton and Crosser's model as shown in Figure 1.

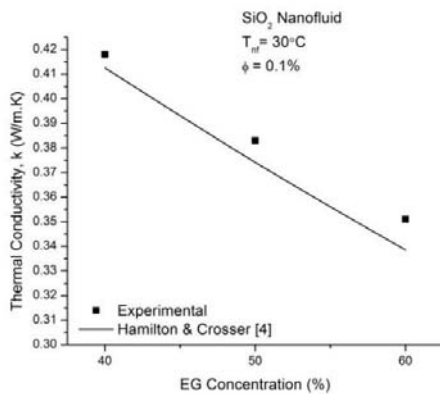


Figure 1. Effective Thermal Conductivity of SiO₂ in 40 EG at 30°C

Figure 1 shows the thermal conductivity of SiO₂ nanofluids agrees with the Hamilton and Crosser model. The thermal conductivity of 0.1% SiO₂ is plotted against EG concentration. The pure EG contains low thermal conductivity as compared to distilled water. The increment of EG concentration in base fluid exhibit lower thermal conductivity of SiO₂ nanofluid.

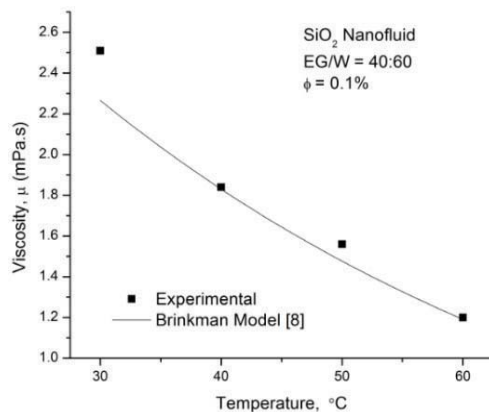


Figure 2. Effective Viscosity of SiO₂ across temperature

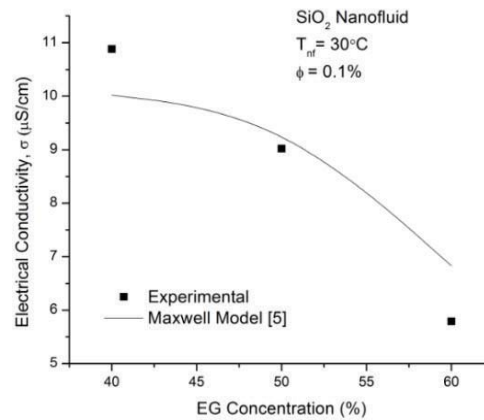


Figure 3. Effective Electrical Conductivity of SiO₂ in 40 EG at 30°C

CONCLUSION

The presence of nanoparticles enhanced the thermophysical properties of base fluids. PEMFC requires coolant that has better heat transfer characteristic in term of thermal conductivity to remove heat from the stack. High concentration of nanoparticles exhibit higher thermal conductivity. However, the viscosity and electrical conductivity also increase consecutively. The viscosity of a fluid is related to the pumping power. The pressure drop in laminar flow is directly proportional to the viscosity. Electrical conductivity also need to be considered as high electrical conductivity can cause the coolant electrolysis and cause electrical leakage in the appliance. Evaluation such as Thermoelectrical Ratio (TEC) established by Zakaria et. al [4] is needed to evaluate the feasibility of nanocoolants in PEMFC.

References

- [1] G. Zhang and S. G. Kandlikar, "A critical review of cooling techniques in proton exchange membrane fuel cell stacks," *International Journal of Hydrogen Energy*, **37**, 2012, pp. 2412-2429.
- [2] Z. Luo, Z. Chang, Y. Zhang, Z. Liu, and J. Li, "Electro-osmotic drag coefficient and proton conductivity in Nafion® membrane for PEMFC," *International Journal of Hydrogen Energy*, **35**, 2010, pp. 3120-3124.
- [3] A. Ijam and R. Saidur, "Nanofluid as a coolant for electronic devices (cooling of electronic devices)," *Applied Thermal Engineering*, **32**, 2012, pp. 76-82.
- [4] Z. Irnie Azlin, M. Zeno, S. Hanapi, and W. M. Wan Ahmad Najmi, "Thermal and Electrical Experimental Characterization of Ethylene Glycol and Water Mixture Coolants for a 400 W Proton Exchange Membrane Fuel," *Applied Mechanics and Materials*, **660**, 2014, pp. 391-396.

DRY METHANE REFORMING PERFORMANCE OF Ni-BASED CATALYST COATED ON STAINLESS STEEL SUBSTRATE

Suntorn Sangsorn^{1,2}, Monrudee Phongaksorn^{1,2}, Sabaithip Tungkamani^{1,2},
Thana Sornchamni³ and Rungroj Chuvaree³

¹Department of Industrial Chemistry, Faculty of Applied Science,
King Mongkut's University of Technology North Bangkok, Thailand

²Research and Development Center for Chemical Engineering Unit Operation and Catalyst Design (RCC),
King Mongkut's University of Technology North Bangkok, Thailand

³PTT Public Company Limited, PTT Research and Technology Institute, Thailand

SUMMARY: In this work, the Ni-based catalysts (10wt.%Ni/Al₂O₃-MgO and 10wt.%Ni/MgO) were synthesized by sol-gel method. Then, each type of catalyst powder was prepared as a pellet and a coated plate where the coated plates were produced using spray coating. The dry methane reforming (DMR) performances of coated plate catalysts were studied and compared with DMR performances of pellet catalysts. As the mass transfer was increased, the methane consumption rate per gram of coated plate catalysts was ten times greater than those of pellet catalysts approximately. The deposition of the carbon was also significantly prevented when the catalyst were constructed as a thin film layer on the plate under our developing condition. Therefore, this coated plate catalysts can be further used for multichannel reactor.

Keywords: Nickel based catalysts, spray coating, dry methane reforming

INTRODUCTION

Syngas or synthesis gas mainly consists of hydrogen and carbon monoxide which are widely used in chemical industries and electricity generation. Syngas also plays a vital role in alternative energy production as it is a reactant for liquid fuel synthesis process (Fischer-Tropsch process). Nonetheless, hydrogen is considered as a direct high efficiency alternative fuel in near future. Syngas can be produced from biomass, biological gas, natural gas or coal through the catalytic reforming processes such as steam reforming, dry reforming, partial oxidation and autothermal reforming with the different metal supported catalyst and reactants. Normally, catalysts for reforming are pelletized Ni based catalysts, packed in a fixed-bed reactor [1]. However, the pellet catalysts have been concerned with a stability issue due to heat and mass transfer limitations, causes of sintering and carbon formation problems. Therefore, researchers have overcome these limitations by employing a new type of reactor, called multichannel reactor, which improves temperature control and mass diffusion. In the coated-wall of multichannel reactor, the physical size of channel in the reactor is decreased and the surface-to-volume ratio is increased. As a result, the relative surface area per fluid volume is high which improves heat and mass transfer performance [2-4]. The requirement for this type of reactor is the proper coating condition and technique to develop thin-film layer of heterogeneous catalyst onto the reactor walls. Recently, the three major techniques; wash coating, spin coating and spray coating, are applied [5]. Advantages of these techniques are high efficiency, low operating temperature, simple installation, simple handling, and simple maintenance.

This research aims to investigate the dry

methane reforming (DMR) performance of our Ni-based supported catalysts coated onto stainless steel plate by spray coating and to compare with DMR performance of the similar catalyst in pellet form under the same reaction condition.

EXPERIMENTAL

10 wt% Ni/Al₂O₃-MgO (10NAM) and 10wt.% Ni/MgO (10NM) were prepared by sol-gel method followed by dried at 60°C for overnight and calcined at 650°C for 4 h. Then, a portion of the 10NAM and 10NM powder was pelletized while the other portion was prepared as a precursor for spray coating via ball mill technique. To produce a coated plate catalyst, a stainless steel (SS 316) with the dimensions of 6.9 mm x 60.0 mm x 4.0 mm was used as a the substrate. After coating process, the coated plate was dried at 60°C for overnight and calcined at 650°C for 4 h.

DMR tests were carried out in a tubular reactor. The pellet catalyst (~200 mg) was packed as a fixed-bed, whereas the coated plate catalyst (~15 mg) was located vertically. Catalysts were reduced in-situ with 30 mL min⁻¹ H₂ at 620°C for 2 h. The reforming was performed at 620°C for 6 h with the mixed flows of CH₄ for 15 mL min⁻¹, CO₂ for 25 mL min⁻¹ and N₂ for 20 mL min⁻¹. The outlet gas was analyzed using an on-line gas chromatograph (Agilent GC7890A) equipped with a thermal conductivity detector (TCD).

RESULTS AND DISCUSSION

Coating surface morphology

The micrographs of 10NAM and 10NM powder are illustrated in Fig. 1(a,b). As seen in the figure, the particle of catalyst powder is different in particle size. Although catalyst particle on the coated plate is more uniform (Fig. 1 (c,d)), the

agglomeration of powder still exists due to the characteristic of spray coating.

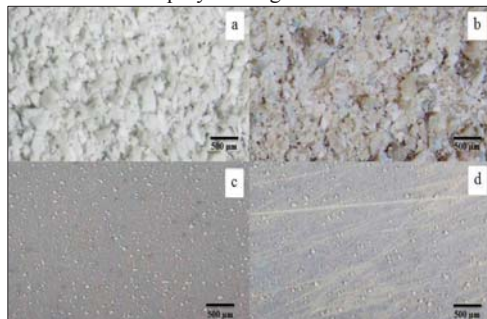


Figure 1. The SEM micrographs of fresh catalysts: (a) 10NAM powder, (b) 10NM powder (c) 10NAM coated plate (10NAMC) and (d) 10NM coated plate (10NMC)

DMR performance

DMR result is presented in Fig. 2. It shows that the methane consumption rate per gram of 10NAM increases from 0.05-0.06 [molCH₄] $g^{-1}min^{-1}$ for pellet (10NAMP) to 0.55-0.98 [molCH₄] $g^{-1}min^{-1}$ for coated plate (10NAMC) and this rate per gram of 10NM increases from 0.04-0.06 [molCH₄] $g^{-1}min^{-1}$ for pellet (10NMP) to 0.49-0.89 [molCH₄] $g^{-1}min^{-1}$ for coated plate (10NMC). The results reveal that the improvement of mass transfer limitation by surface exposition of metal active site enhances methane consumption rate per gram of catalyst for ten times, approximately.

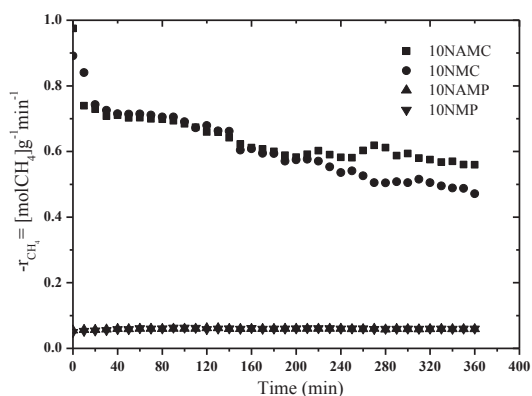


Figure 2. The methane consumption rate per gram of catalyst over 10NAM pellet (10NAMP), 10NM pellet (10NMP), 10NAM coated plate (10NAMC) and 10NM coated plate (10NMC)

SEM micrographs (Fig. 3) of the spent pellet catalyst (10NAMP) and the spent coated plate catalyst (10NAMC) show that the filament carbon were formed on the surface of the spent pellet catalyst (Fig. 3 (a)); whereas, this type of carbon has not grown on the surface of coated plates (Fig. 3 (b)). The reason of carbon deposition on pellet

catalyst could be contributed to the limitation of heat and mass transfer which constructs a hot spot and a rich carbon species area at the same time and place. In contrast, this condition can be eliminated in coated plate catalyst. Thus, the catalyst layer on coated plate developed in our group is sufficiently thin and stable to prevent carbon formation as well as to reach a remarkable activity, simultaneously. Consequently, the coated plate catalyst can be adapted for a coated-wall multichannel reactor.

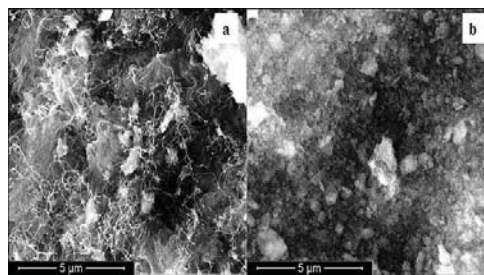


Figure 3. The SEM micrographs of spent catalysts: (a) 10NAMP and (b) 10NAMC

ACKNOWLEDGEMENT

The authors gratefully acknowledge PTT Public Company Limited, Thailand for the financial support, Department of Industrial Chemistry and Research and Development Center for Chemical Engineering Unit Operation and Catalyst Design (RCC) for supporting this research work.

References

- [1] S. Tungkamani, M. Phongakson, P. Narataruksa, T. Sornchamni, N. Kanja-nabat, N. Siri-Nguan, "Developing carbon tolerance catalyst for dry methane reforming", *Chemical Engineering Transition*. **32**, 2013, pp. 745-750.
- [2] J. J. Lerou, A. L. Tonkovich, L. Silva, S. Perry, J. McDaniel, "Microchannel reactor architecture enables greener processes", *Chemical Engineering Science*. **65**, 2010, pp. 380-385.
- [3] C. W. Liu, H. S. Ko, C. Gau, "Microchannel Heat Transfer: Heat Transfer - Theoretical Analysis, Experimental Investigations and Industrial Systems, Prof. Aziz Belmiloudi (Ed.)", *In Tech*, 2011.
- [4] A.K. Avci, D.L. Trimm, M. Karakaya, "Microreactor catalytic combustion for chemicals processing", *Catalysis Today*. **155**, 2010, pp. 66-74.
- [5] V. Hessel, A. Renken, J. Schouten, J. Yoshida "Micro Process Engineering: A Comprehensive Handbook 3 Volume Set", *Wiley-VCH: Weinheim*, Germany, 2009.

DEVELOPMENT OF TiO₂/TiO₂-V₂O₅ COMPOUND WITH PANI FOR ELECTRON STORAGE

Wanchai Bonmeemak¹, Chalermpan Fongsamut² and Pailin Ngaotrakanwivat¹

¹Department of Chemical Engineering, Faculty of Engineering, Burapha University, Thailand

²Department of Electrical Engineering, Faculty of Engineering, Burapha University, Thailand

SUMMARY: The polyaniline (PANI) assembled on TiO₂-V₂O₅ compound (TVC) was prepared by in-situ polymerization method. The TiO₂-TVC and TiO₂-TVC/PANI composite films at TVC/TiO₂ molar ratio of 0.1 deposited on the ITO glass successfully prepared using spin coating technique. The products were characterized by using SEM-EDX, TGA, FTIR and electrochemical technique. The result showed that the energy storage of TiO₂-TVC composite films is 3,062.0 C/mol of TVC (80.3% of maximum capacity) and the maximum energy storage is 3,724.3 C/mol of TVC (97.6% of maximum capacity) for TiO₂/PANI-TVC at 2.2% weight of PANI in TVC/PANI. This result suggests that optimal amount of PANI effect on higher efficiency of energy storage.

Keywords: energy storage, TiO₂, polyaniline and TiO₂-V₂O₅ compound

INTRODUCTION

TiO₂ is known as a photocatalyst which has various remarkable functions including self-cleaning, anti-bacterial, gas sensor, and anti-corrosion. The utilization of TiO₂ is active based on redox reaction of photogenerated electrons and holes that are excited under UV irradiation. However, these applications are workable only under UV light irradiation on TiO₂ surface. The restriction of applications under daylight is an important drawback of TiO₂ which can be eliminated by development of its ability for energy storage. Recently, our group has developed TiO₂-V₂O₅ compound (TVC) that exhibits high capacity of energy storage [1]; however, the coupling TiO₂ and TVC for photo energy storage gave low efficiency possibly owing to distance barrier of charge transferring between exciting photoelectrons and energy storage sink. Therefore, to bridge the gap of transferring these electrons the in-situ conductive polymer has been developed in our present work. PANI (polyaniline) is the most attractive polymer because the preparation is facile and polymeric bulk is inert, stable and insoluble in solvent, especially the polymer exhibits photocatalytic and conductive properties. The optimum amount of additional PANI to TiO₂/TVC electron storage films was investigated in the range of 2.0 to 6.0 wt%. The results and short discussions are as the following.

EXPERIMENTS

Energy storage matter (TVC)

Dissolved titanium (IV) isopropoxide 16.7 ml in to 0.07 M NHO₃ solution and stirred at room temperature (20%RH) for 3 days to obtain clear solution. Purified sol TiO₂ by dialysis in DI water. Mixed 90 mg V₂O₅ in 30 ml sol TiO₂ and subsequently 2 hours ultra-sonicated for well mixing to obtain yellowish slurry. Calcined the yellowish slurry to brown powder at 550°C for 1 hour.

The charge transferring was improved by PANI assembling on TVC by in-situ polymerization method. Mixed TVC 4 g, aniline 0.1 g and (NH₄)₂S₂O₈ 226.7 mg in 0.5 M HCl 100 ml and

stirred for 12 h. Filtrated and washed with ethanol for several times and dried at 80°C for 2 h to obtain TVC/PANI. The amount of PANI consisting in assembled films was adjusted at molar ratio of aniline/(NH₄)₂S₂O₈ increasing to 2, 3 and 4 times.

Film preparation

The TVC coating was prepared by mixing TVC/PANI in 6 ml of DI water and subsequently ultrasonicated for 5 min. After mixing, added 200 mg P25 and re-sonicated to obtain blue-green slurry. This slurry was coated on ITO glass at 3,500 rpm for 20 second and then calcined at 350°C for 1 h. All films were fixed the molar ratio of TiO₂/TVC at 0.1.

Characterization

The actual TVC/TiO₂ mole ratio in the film was evaluated by scanning electron microscope /energy dispersive x-ray spectroscopy (SEM/EDX). The amounts of PANI on TVC/PANI were investigated by thermal gravitation analysis (TGA) under N₂ atmosphere. The electrochemical properties were observed by conventional electrochemical cell. The sample was set as working electrode, while reference cell was Ag/AgCl electrode and counter cell was platinum electrode.

Measurement

Electron capacity of films was measured by using a digital potentiostat. A voltage recorder was used to monitor the open-circuit potential of the coated electrodes. The light source used was a Hg-Xe lamp equipped with a 365 nm band-pass filter. The light intensity was about 5 mW.cm⁻² at the sample surface. After the film was exposed to the light, constant current (1μA) electrochemical discharging was carried out in a 0.1 M NaCl aqueous solution. The cut-off potential was -0.1 V versus Ag/AgCl for the electrochemical discharging. Additional films were observed at maximum capacity by charging the potential to -0.4 V versus Ag/AgCl and discharging at the same condition.

RESULTS AND DISCUSSION

PANI growth on TVC was investigated by FT-IR technique as shown in figure 1. The FT-IR spectra indicate functional group of PANI existing in TVC/PANI. The band at the position higher than 2000 cm^{-1} indicates the typical PANI form. The peaks occurring at 1,538 cm^{-1} and 1,454 cm^{-1} in the spectra of commercial PANI and synthesized PANI correspond to quinone and benzene ring stretching respectively. The band at 1,287 cm^{-1} is ascribed to stretching C-N bond locating in quinonoid structure, whereas a secondary aromatic amine presents C-N bond stretching at 1,214 cm^{-1} . The bands occurring at 1,066 and 1,024 cm^{-1} are assigned to C-H bond existing in aromatic ring and the band around 800-880 cm^{-1} is attributed to a presence of C-H bond locating in 1,4-disubstituted rings [2]. The FT-IR spectra of TVC/PANI composite presents the intrinsic absorption peaks of PANI and the peak shifting to blue visible range ascribing to chemical reaction between TVC and PANI.

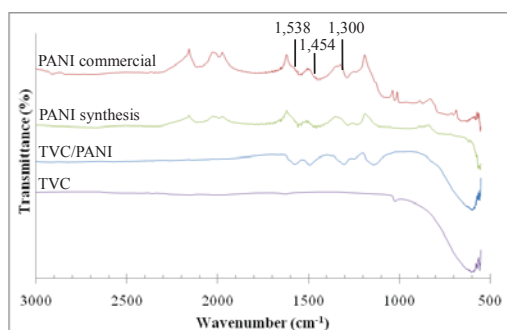


Figure 1 FT-IR spectra of TVC/PANI

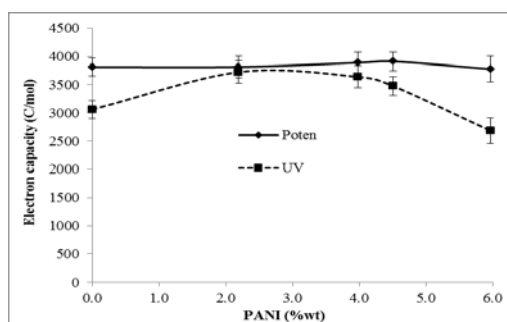


Figure 2 Electron capacity of TiO_2 -TVC/PANI composite films after electrochemical charging (potent) and photo-charging (UV) condition

Electrochemical charge and discharge behavior of TiO_2 -TVC films and TiO_2 -TVC/PANI films were investigated. The TVC undergoes the following redox reactions as shown in equation 1.



TVC- TiO_2 film and TiO_2 -TVC/PANI films were electrochemically charged at -0.4 V versus Ag/AgCl for 3 h and discharged at $1 \mu\text{A}$. The fabricated film with PANI seems to have no effect on the electron capacity because the electron capacities of both films are even at 3,840 C/mol as shown in figure 2.

However, the electron capacity of TVC- TiO_2 film was only 3,062.0 C/mol, which is 80.3% of maximum capacity, after UV irradiating for 3 h. These indicated the distance barrier of charge transferring between TiO_2 and TVC. The energy storage enhancement was accomplished by coupling of PANI and TVC. It can be seen that the TiO_2 /PANI-TVC film composing of PANI in TVC/PANI of 2.2 wt% could store electron up to 3,724.3 C/mol which is 97.6% of maximum capacity. However, the larger amount of PANI suppressed the electron transfer. The structural and physical measurements of films are ongoing.

CONCLUSION

The amount of PANI varied at 2.2, 4.0, 4.5 and 6% by weight in fabricated films facilitates the rate of electron transferring from TiO_2 to TVC and it leads to increase of energy storage efficiency especially from 80.4% to 97.6% for the film composed of 2.2% wt. PANI. This is plausible because of the specific physicochemical properties of TVC/PANI i.e. porosity and conductivity. These optimum properties can encourage the mobility of cations and electrons to TVC.

ACKNOWLEDGEMENT

This work has been supported by the Nanotechnology Center (NANOTEC), NSTDA, Ministry of Science and Technology, Thailand through its program of the Center of Excellence Network.

References

- [1] P. Ngaotrakanwivat, Meeyoo and Vissanu, "TiO₂-V₂O₅ Nanocomposites as alternative energy storage substances", *Journal of nanoscience and nanotechnology*, **12**, 2012, pp. 828-838.
- [2] M. Trchová, I. Sedenkova, E. Tobolkova and J. Stejskal, "FTIR spectroscopic and conductivity study of the thermal degradation of polyaniline films", *Polymer Degradation and Stability*, **86**, 2004, pp. 179-185.

EFFECTS OF THE GEOMETRY OF THE AIR FLOWFIELD ON THE PERFORMANCE OF AN OPEN-CATHODE PEMFC TRANSIENT LOAD OPERATION

Suangrat Kiattamrong^{1,2} and Angkee Sripakagorn^{1,2}

¹Department of Mechanical Engineering, Faculty of Engineering, Chulalongkorn University, Thailand

²Fuel Cell Research Group, Chulalongkorn University, Thailand

SUMMARY: A PEM Fuel Cell (PEMFC) is being proposed as the new clean technology for the automotive application. However, its high capital cost limits its capability to challenge competing technologies. The open-cathode PEMFC was introduced to eradicate this pitfall. For the present work, the single-cell open-cathode PEMFC was fabricated with 100-cm² activation area to study the influence of the geometry of the air flowfield on the performance. Six cathode flowfield plates with different channel configurations were tested and compared under limited amount of air supplied. The load was specified to be transient sinusoidal variations representative of the automotive load profile. The results were compared in the form of the hysteresis loop on the polarization curve. The flowfield with high aspect ratio gave a better performance. On the other hand, the flow area played no significant effect on the performance.

Keywords: PEMFC, transient load, open-cathode, flow channel

INTRODUCTION

Due to the increasing concern on the energy security and climate situation, electric vehicle is being developed continually to replace the conventional automobiles for the past few decades.

Recently, fuel cell vehicle is proposed as another promising option. A proton exchange membrane fuel cell (PEMFC) is outstanding among the other fuel cells technologies which limits in the operating temperature and heavy weight. The performance and the durability of the PEMFC keep improving if not for its high capital cost that put paramount constraint against its future in the automotive application.

To eradicate this pitfall, the open-cathode PEMFC was introduced. The design goals are to increase the system efficiency and reduce the auxiliary system cost. Similar to the typical PEMFC, studies pointed out that air channel configuration plays the important role on the performance for the open-cathode PEMFC. However, in comparison to the typical design, the numbers of the literatures are low and the conclusions are vague.

This study attempted to illustrate the influence of the geometry of the air flowfield on the performance of the open-cathode PEMFC in the limited but sufficient air supply condition for the sake of the compact unit. The specimens were tested under the transient load to reflect automotive operating conditions.





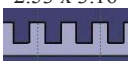

EXPERIMENTAL METHODOLOGY

Test Unit

The single-cell open-cathode PEMFC was fabricated. The active area of the membrane electrolyte membrane (MEA) was 100 cm². The supply of the hydrogen was dead end with the purging valve. The bipolar plates were made of the graphite plates. Six cathode bipolar plates were prepared with the different straight air flowfield

configurations; two aspect ratios and three flow areas (detailed on table 1). Three fans were selected to precisely feed sufficient air to the test cell for the electrochemical process and the transfer of heat produced from the process. The perforated plate was specially placed between the cathode bipolar plate and MEA to protect MEA from the damage caused by the different pressure between the air and the hydrogen channels.

Table 1. Air flowfield configurations.

Flow Area (mm ²)	Aspect Ratio		No. of Channels
	0.80	1.25	
2	1.26 x 1.58 	1.58 x 1.26 	40
5	2.00 x 2.50 	2.50 x 2.00 	25
8	2.53 x 3.16 	3.16 x 2.53 	20

Test Rig

The MEA, bipolar plates and perforated plate with the current collectors and end plates were assembled (in order as depicted in Fig.1) and placed in the test rig with the fan as in Fig.2. The external electric load, data acquisition (DAQ) and hydrogen inlet port were properly connected to the test rig before testing.

Experiment

The single cell was applied with the transient load by the external electric load. The operating temperature and the relative humidity were 25°C and 60-70%, respectively. The load profile was sinusoidal. The load current range of the load was

within 0-30 A and the frequency was 0.1 Hz. The cell voltage was recorded via DAQ.

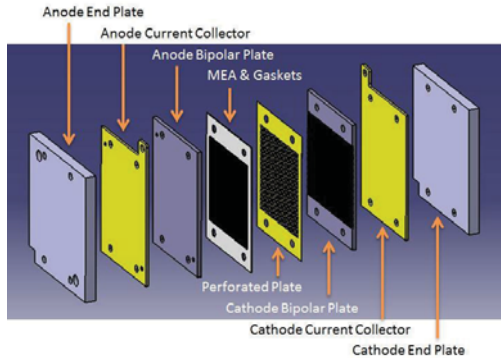


Figure 1. Single-cell open-cathode PEMFC assembly

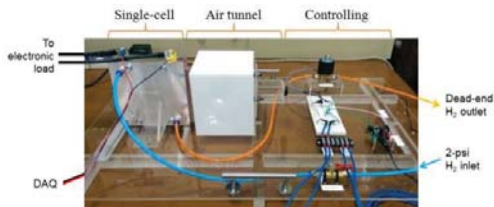


Figure 2. Test rig

RESULTS AND DISCUSSION

The present results confirmed the results from the last study [1]. The performance increases with the high aspect ratio as in Fig.3. By the way, the flow area played no significantly effect on the in Fig.4. So, the wide air channel can reduce the domination of the mass transfer loss at the current density operation and the flow area causes no change on the performance of the open-cathode PEMFC in the case the air is adequately supplied.

Beside the suggestion on the configuration, the study showed the important of the air supply unit of the open-cathode PEMFC. For example, the high performance fan can feed the air through the small channel but the respective high power resulted in the reduced system efficiency and added capital cost. So, in the design step, the acceptable system efficiency should be specified before choosing the fan and the design of the geometry of the air channel.

ACKNOWLEDGMENT

This study cannot be achieved without the financial support from Chula Unisearch and Special Task Force for Activating Research (STAR) and the facilities support from Fuel Cell Research Group of Chulalongkorn University.

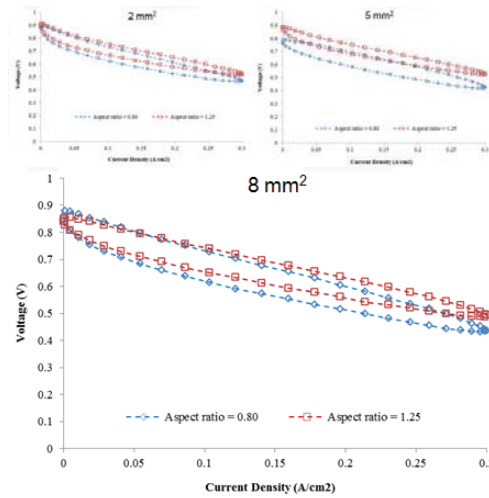


Figure 3. The effect of the aspect ratio on the performance

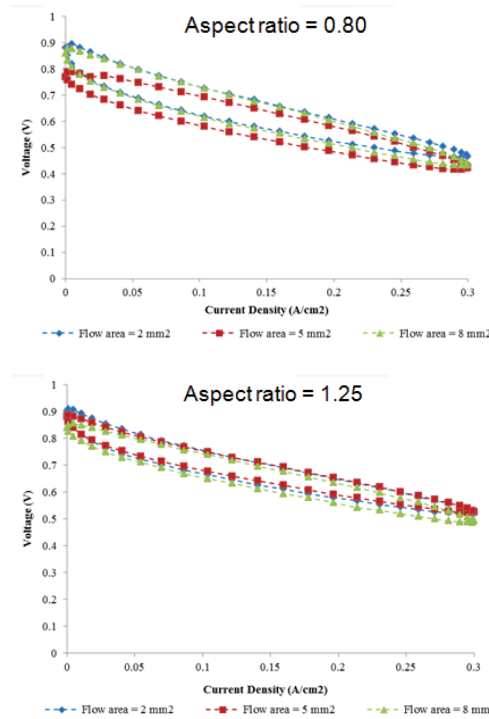


Figure 4. The effect of the flow area on the performance

References

[1] S. Kiattamrong and A. Sripakagorn, "Effects of the Geometry of the Air Flowfield on the Performance of an Open-Cathode PEMFC", *Proceedings of 5th international Conference on Sustainable Energy and Environment (SEE2014)*, 2014, pp. 408-413.

ELECTRICITY GENERATION AND SEPTAGE TREATMENT IN MICROBIAL FUEL CELL (MFC) CONSTRUCTED USING EARTHEN MEMBRANE

Dan Thanh Ngoc Cao¹ and Rachnarin Nitorisavut¹

¹School of Bio-Chemical Engineering of Technology-Sirindhorn International Institute of Technology, Thammasat University-Rangsit Campus, Thailand

SUMMARY: An attempt has been made to construct a low cost Microbial fuel cell (MFC) from the commercially available earthen material without involving any costly membrane. In fact, proper operation of such a device requires that activity at the anodes is not impaired by the ability of the cathode to transfer current to the cathodic electrons acceptor. Therefore, suitable anode/cathode ratios were determined based on MFC performance in both electricity and septage treatment. Those ratios were 4.5, 3, 2.25, 1.8 and 1.5 which was equivalent to the number of anode graphite wires (GWs) of 9 and the cathode graphite wires of 2, 3, 4, 5 and 6, respectively. MFC units were loaded at $0.26 \text{ kgCOD} \cdot \text{m}^{-3} \cdot \text{day}^{-1}$ corresponded to a hydraulic retention time (HRT) of 14h. The maximum power output of $1.11 \pm 0.1 \text{ W} \cdot \text{m}^{-3}$ at an external resistance of 100Ω was generated in MFC unit with ratio of 4.5. Results indicate that for the same anode surface area, the power generation and internal resistance depend on the anode/cathode ratio.

Keywords: carbon graphite wires, anode/cathode ratio, V-shape earthen membrane, internal resistance.

INTRODUCTION

In recent years, the energy crisis has become the most important issue all over the world, which requires scientists and researchers to look for replacement of fossil fuel. For this reason, it is necessary to find out other alternatives and renewable energy sources such as wind, solar and hydropower. Moreover, there is a serious increase in wastewater pollution affecting to human life, especially for people who live in remotes areas.

Microbial fuel cell (MFC) is considered as a promising technology for wastewater treatment and the additional benefit of energy generation[1]. In general, MFC micro-organism in MFC extracts electric current from a wide range of soluble or dissolved complex organic waste and renewable biomass under anaerobic condition. A large number of substrates have been provided as feed such as glucose[2], brewery waste[3], potato processing waste [4], starch industry waste [5], domestic waste [6], etc. Although MFC was proved to have ability of electricity processing combining with wastewater treatment, the scale-up of the MFC still remains as a critical issue. The capital cost to develop such a system have to be concerned due to a key factor in improvement of the MFC technology from laboratory research to real implementation as a sustainable energy sources. On the other hands, membrane component is accounted a large section in budget and internal resistance for whole MFC cell.

In the present study, a MFC is constructed with an earthen membrane in V-shape configuration without using the commercially available expensive membrane. The earthen membrane itself has been applied as the medium for proton exchange membrane and making cathode chamber. Overall, the conclusion is that earthen membrane itself can be applied as a cost-effective membrane in MFC.

METHODOLOGY

Data reported were obtained from two-chambered MFCs reactors. Reactors were constructed in a 3 inch cylindrical PVC pipe with length of 78 cm. An anodic working volume was 2L (Figure 1). V-shaped earthen membrane also functioned as cation exchange membrane (CEM) and cathodic chamber with volume of 500 mL. Carbon graphite wires (GWs) were selected as cathode material due to its high conductivity and high surface area. Electrodes ratio were varied in range of 1.5-4.5 using 2-6 GWs as cathode while anode was for 9 GWs. Duplicated reactors and analyses were performed for each variation.

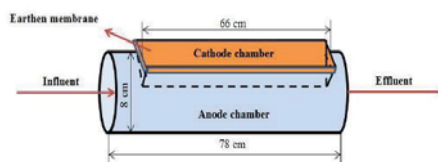


Figure 1. Schematic of MFC using earthen material as proton exchange membrane

Anaerobic sludge was collected from anaerobic digester of Nonthaburi municipality, Thailand. The seed sludge was 1L accounting for half of the total working volume of anode chamber. Open circuit voltage (OCV) and current were measured using electrical meter and data were recorded daily. Influent and effluent COD concentrations were monitored according to Standard Methods [7].

RESULTS AND DISCUSSION

Electricity harvesting

The MFC unit with ratio of 4.5 generated a maximum volumetric power (normalized to the working volume of anode chamber) of $1.11 \pm 0.1 \text{ W} \cdot \text{m}^{-3}$ (at $2.22 \pm 0.1 \text{ A} \cdot \text{m}^{-3}$ and $499 \pm 23 \text{ mV}$) at

100 Ω external resistance (Figure 2). The power generation increased in the MFC with an increase of GWs as cathode. The volumetric power generation in ratio of 4.5 was 1.1, 1.53, 1.82 and 2.15 times higher than that of ratio of 3, 2.25, 1.8 and 1.5, respectively. On the other hand, the internal resistance determined based on polarization curves were 94 ± 2 , 121 ± 18 , 146 ± 29 , 107 ± 21 and 100 ± 2 (Ω) in ratio of 4.5, 3, 2.25, 1.8 and 1.5, respectively.

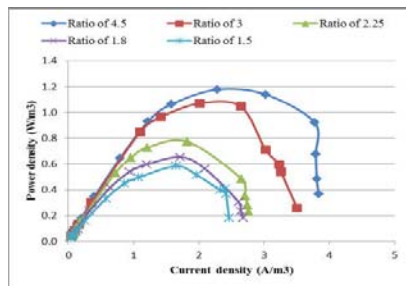


Figure 2. Power curves of MFC with different electrodes ratios at $0.26 \text{ kgCOD} \cdot \text{m}^{-3} \cdot \text{day}^{-1}$

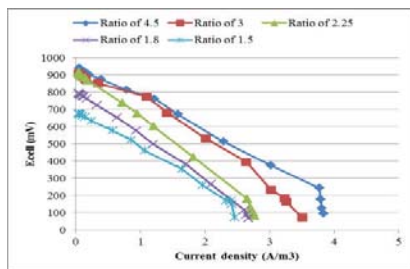


Figure 3. Forward sweep of the polarization curves of the MFC units with different electrode ratios

When a qualitative assessment of the polarization curves was made (Figure 3), a clear shift of the polarization curves at cell voltage below 1000 mV was noted. This phenomenon associated with mass transfer or kinetic limitation was observed during polarization lowered resulted in a less steep descent of the current generation. The MFC units with ratio of 3 and 4.5 appeared to suffer less from this leveling of the current of $3.51 \text{ A} \cdot \text{m}^{-3}$ and $3.84 \text{ A} \cdot \text{m}^{-3}$, respectively.

Septage treatment

Current increased in most of the reactors though the COD removal efficiency was reduced. The amount of biodegradable organic matter in septage might not be stable and the quality depends on the number of toilet users or the dilution ratio of toilet flush to septic tank. Although the highest current of 16.69 ± 1.9 (mA) was generated in MFC unit with ratio of 4.5, the highest COD removal efficiency of 56 ± 9 (%) was observed in unit with

ratio of 1.5 (Figure 4).

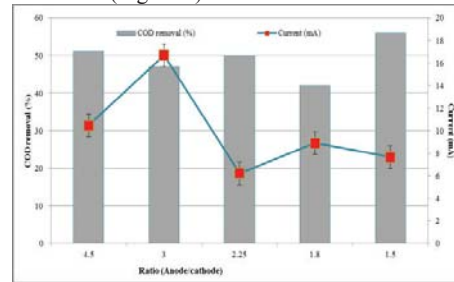


Figure 4. Correlation between current generation (mA) and COD removal (%)

According to that result, an increase of cathode's surface area did not result in an increase of COD removal efficiency.

ACKNOWLEDGMENT

This research was financially supported by Asian Institute of Technology for the development of innovative decentralized wastewater treatment.

References

- [1] B.H. B.E.Logan, R.Rozendal, U.Schroder, J.RG Keller, S.Freguia, P.Aeltermann, W.Verstraete and K.Rabaey. "Microbial fuel cells: methodology and technology", *Environmental Science and Technology*, **40**, 2006, pp. 5181-5192.
- [2] K. Rabaey, G. Lissens, S. Siciliano and W. Verstraete "A microbial fuel cell capable of converting glucose to electricity at high rate and efficiency", *Biotechnology Letters*, **25**, 2003, pp. 1531-1535.
- [3] X. Wang, Y.J. Feng and H. Lee. "Electricity production from beer brewery wastewater using single chamber microbial fuel cell", *Water Sci Technol*, **57**, 2008, pp. 1117-1121.
- [4] I. Durruty, P.S. Bonanni, J.F. González and J.P. Busalmen "Evaluation of potato-processing wastewater treatment in a microbial fuel cell" *Bioresource Technology*, **105**, 2012, pp. 81-87.
- [5] Z.S. Lu Na, Zhuang Li, Zhang Jintao and Ni Jinren. "Electricity generation from starch processing wastewater using microbial fuel cell technology", *Biochemical Engineering Journal*, **43**, 2009, pp. 246-251.
- [6] J. Choi and Y. Ahn "Continuous electricity generation in stacked air cathode microbial fuel cell treating domestic wastewater" *Journal of Environmental Management*, **130**, 2013, pp.146-152.
- [7] APHA. Standard Methods for the Examination of Water and Wastewater, Washington DC, USA: American Public Health Association, 20th ed (1998).

MICROPOROUS ACTIVATED CARBON FROM KOH-ACTIVATION OF RUBBER SEED-SHELLS FOR APPLICATION IN CAPACITOR ELECTRODE

Thanchanok Pagketanang¹, Apichart Artnaseaw¹, Prasong Wongwicha¹ and Mallika Thabuot^{1,2}

¹Department of Chemical Engineering, Faculty of Engineering, KhonKaen University, Thailand

²Center of Knowledge Development of Rubber Tree in Northeast group (KDRN),
KhonKaen University, Thailand

SUMMARY: This study is to prepare the activated carbon from rubber seed-shells by KOH activation. Activated carbons (ACs) for the electrochemical double layer capacitors (EDLCs). Impregnation-Activation Method using 2%wt. of KOH solution as a chemical agent was used. The BET surface area, pore volume and pore size distribution of ACs were characterized using N₂ adsorption technique. The surface morphology was evaluated with SEM. Electrochemical properties of the prepared ACs electrodes have been studied using cyclic voltammetry (CV) in 30%wt. of KOH as electrolyte. All prepared ACs had adsorption isotherm Type I indicating as the pore structure is mainly composed of micropores. Highest specific surface area (620 m²/g) with high iodine number (639.73 mg/g) was obtained from the carbonization at 900°C. The specific capacitance of the microporous ACs sheet electrode reached 63.2 F/g at 1mV/s.

Keywords: chemical activation, rubber seed shells, microporosity, electrochemical double layer, capacitors

INTRODUCTION

Electrochemical double layer capacitor (EDLC) has been received widely attentions because of its characteristics of environmentally friendly, longer lifecycle and high power supply, quickly rechargeable and faster energy transfer [1-3]. Activated carbons (ACs) with high specific surface area with suitable porous texture and surface chemistry are expected to give high electrochemical performance of EDLCs with high energy. KOH activation was reported as a powerful method in developing and controlling the number of micropores with a very similar pore size distribution. The KOH-activated starch AC presented high BET surface area, large pore volume and high capacitance of 238 F/g in 30 wt% KOH aqueous electrolytes [3]. Honeycomb-like morphology AC with high specific surface area showed the specific capacitance reached to 251.1 F/g at 2 mV/s scan rate in the organic electrolyte [1]. From the AC preparation from sunflower seed-shell, impregnation activation method with KOH gave AC with greater capacitive behavior and higher capacitance retention ratio at high drain current than the carbonization activation method did [2]. KOH was used as the activating agent to produce the AC from rubber seed-shell with the majority structure of mesopores [4]. Results showed that the BET surface area, total pore volume and diameter of activated carbon were 1288.52 m²/g, 0.81 cm³/g and 2.49 nm, respectively. However, there has been no reported on its performance in supercapacitor electrode. In this study, we selected rubber seed-shell as the precursors to prepare activated carbon by KOH chemical activation followed by high temperature carbonization. As-prepared ACs electrode has been evaluated by cyclic voltammetry, the influences of pore structure on electrochemical properties were also discussed.

METHODOLOGY

Para rubber seeds were collected at the local garden in Kalasilp Province (Thailand). The rubber seed-shell residue from extraction was separated to be dried. Then it was crushed and screened to particle sizes less than 1 mm. 150g of prepared rubber seed-shell residue was impregnated in 500 ml of 2wt.% of KOH solution for 24 h. The sample was filtered and dried in an air oven at 110°C for 12 h. Then dried sample was carbonized in a horizontal tube furnace, under a flow of N₂ atmosphere at the final temperature of 700, 800 and 900°C. After that, the products were dried in an air oven. The proximate and ultimate analyses of rubber seed-shell and prepared activated carbon were conducted. Pore properties of rubber seed shells-based ACs were characterized by nitrogen adsorption at 77K using ASAP2010V5.03G surface analyzer (Micromeritics, USA). The surface morphology of rubber seed shell-based ACs were examined using scanning electron microscope SEM (Hitachi S-3000N). Selected rubber seed shell-based ACs powders were well mixed with 20%wt. PVDF binders with the help of NMP. Then, this paste was applied with the brush on the glass plates to form the thin layer before drying overnight at 110°C. ACs layers with the thickness of 0.3 mm were cut into sheet electrodes with the effective surface area of 1x1cm². The electrochemical measurements of each as-prepared electrode were performed on R600 workstation (Gamry Instrument, Germany) equipped to a three-electrode test cell in a 30wt.% KOH electrolyte. The CV measurements were conducted at the ambient temperature, the voltage range of -0.2V to 0.2V at different sweep rates ranging from 1, 5, 10 and 20 mV/s were used.

RESULTS AND DISCUSSION

From the proximate and ultimate analyses, rubber seed-shell contains high volatile matter, low

ash content and high amount of carbon. The resultant ACs from carbonization at 700, 800 and 900°C are denoted as AC700, AC800 and AC900, respectively. The volatile content of produced activated carbon decreased with the higher carbonizing temperature. ACs prepared in this study have the majority structure of micropores. Activated carbon has an increase of the microporosity from 80.597 to 93.310 vol.% and the decrease of average pore diameter from 2.165 to 0.950 nm with the increase of surface area from 429 to 620 m²/g when the carbonizing temperature increased from 700 to 900°C. Figure 1 shows all ACs isotherms exhibit type I isotherm curves suggesting the presence of a large number of micropores, with a few exist of mesopores. Figure 2 shows that there are a lot of nano-holes on the ACs surface. Microscopic scale is formed already at the carbonization of 700°C, but AC700 has the rough surface of various pores distributed. In the meanwhile, AC900 was comprised by a large number of pores with a clearly uniform size distribution and ordered pore structure.

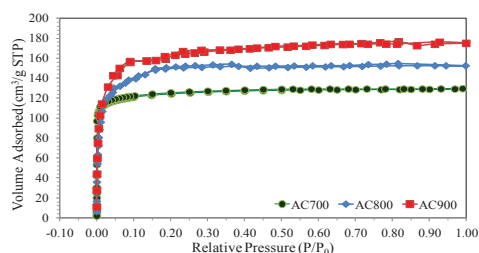


Figure 1. N₂ adsorption/desorption isotherms for prepared ACs.

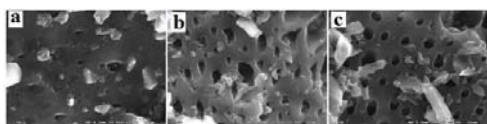


Figure 2. SEM images of prepared ACs at (a) 700°C, (b) 800°C and (c) 900°C.

Under different scan rates of CV measurement, (Figure 3 and Figure 4), the CV of AC700 exhibits clearly deformed asymmetric rectangular shape, which could be described to its small surface area, big average pore size with low microporosity structure. Therefore, less ionic diffusion from bulk electrolyte can access to inner micropore surface when current changes its direction. The CVs plot of AC800 and AC900 are observed as the nearly symmetric rectangular in the potential range of investigation indicating of acceptable capacitive behavior. These shape characteristics caused by the slower reorganization of the double layer as the slower ionic motions in the micropores. The voltammograms became distorted dramatically with the increase of scan rate (Figure not shown here), indicates that activated carbons are not suitable for

quick charge-discharge operation. AC900 has the higher specific capacitance due to its largest surface area and highest microscopic structure. Less electrochemically active surface area of pores being utilized at the higher scan rate resulted to the decrease of specific capacitance values for all three ACs investigated (Figure not shown here). AC900 gave the highest capacitance of 63.2 F/g at the scan rate of 1 mV/s.

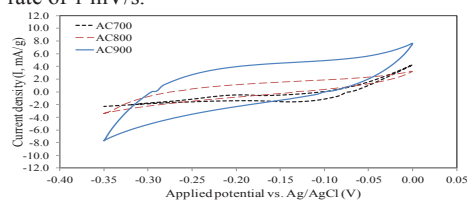


Figure 3. CVs at 10 mV/s for ACs sheet electrode.

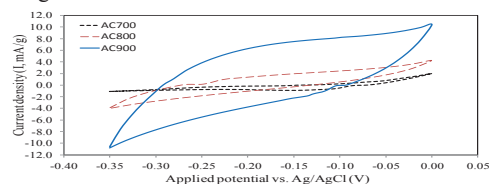


Figure 4. CVs at 20 mV/s for ACs sheet electrode.

These results showed that microporous activated carbons were prepared from rubber seed-shell by impregnation in 30%wt. KOH solution, followed by carbonization. The specific capacitance increases with surface area and microporosity scale, reaching a maximum of 63.2 F/g for a surface area and microporosity proportion of 620 m²/g and 93.31%, respectively.

ACKNOWLEDGMENT

We would like to thank Center of Knowledge Development of Rubber Tree in Northeast group (KDRN), KhonKaen University (Thailand) for the fully funded support to conduct this research.

References

- [1] X. Li, C. Han, X. Chan and C. Shi, "Preparation and performance of straw based activated carbon for supercapacitor in non-aqueous electrolytes", *Microporous and Mesoporous Materials*. **131(1)**, 2010; pp. 303-309.
- [2] X. Li, W. Xing, S. Zhuo, J. Zhou, F. Li, S.Z. Qiao and G.Q. Lu, "Preparation of capacitor's electrode from sunflower seed shell", *Bioresource technology*. **102(2)**, 2011, pp.1118-1123.
- [3] H. Wang, Y. Zhong, Q. Li, J. Yang and Q. Dai, "Cationic starch as a precursor to prepare porous activated carbon for application in supercapacitor electrodes", *Journal of Physics and Chemistry of Solids*. **69(10)**, 2008, pp.2420-2425.
- [4] A. Borhan and A.F. Kamil, "Preparation and Characterization of Activated Carbon from Rubber-seed Shell by Chemical Activation", *Journal of Applied Sciences*. **12(11)**, 2012, pp.1124-1129.

Wind Resource Assessment

INVESTIGATION OF OFFSHORE WIND ENERGY POTENTIAL IN THE GULF OF THAILAND

Chana Chancham¹, Jompob Waewsak¹, Boonlert Archewarahun² and Yves Gagnon³

¹Research Center in Energy and Environment

Department of Physics, Faculty of Science, Thaksin University, Thailand

²Division of Climatology, Thai Meteorological Department, Thailand

³Université de Moncton, Edmundston (NB), Canada

SUMMARY: This paper presents an investigation of the offshore wind energy potential in the Gulf of Thailand using the Weather Research and Forecasting (WRF) system along with the NCEP/NCAR R2 reanalysis climate database. Wind resource maps at 80 m, 100 m, and 120 m agl, at a resolution of 9 km, are developed in order to identify the potential areas for offshore wind farm development. The predicted wind speeds are validated using observed wind speeds from 30 met masts installed along the coastal line of the Gulf of Thailand. Measured-predicted ratios (M/P) and percent mean relative errors (PMRE) are analyzed to validate the wind resource maps. Results show that, for potential areas of development in the Gulf of Thailand, the annual mean wind speeds are in the range of 6-7 m/s. The wind regime in this area is strongly affected by the Northeast (November to February) and Southwest (May to August) monsoons, when high wind speeds occur. The average M/P and PMRE are 0.98 and 7%, respectively. Furthermore, specifically to the Bay of Bangkok, the technical power potential and the energy produced by offshore wind farms are estimated at 5,000 MW and close to 11 GWh/year, respectively.

Keywords: offshore wind energy, wind resource maps, weather research and forecasting, atmospheric modeling

INTRODUCTION

Offshore wind energy is emerging as an interesting alternative renewable energy source for power generation as it has the potential to mitigate climate change, increase energy security and stimulate the global economy. The cumulative installed capacity of offshore wind farms worldwide approached the 5 GW mark in 2013 [1]. However, most of these existing offshore wind farms are in specific locations, such as the Baltic Sea, the North Sea, and China's East Coast.

Based on the experiences around the world, four key factors appear to influence positively the development of offshore wind farms, namely government policies, technological advancements for the grid parity of offshore wind turbine generators, operation and maintenance, and cost reductions [2]. However, the offshore wind resource assessment is the first, and necessary, key step in the development of offshore wind farms.

Consequently, the objective of this paper is to investigate the offshore wind energy potential in the Gulf of Thailand.

METHODOLOGY

Wind resource mapping is an efficient tool in wind farm development, both at the large scale and to identify sites where micro-siting wind resource assessments should be performed in the early stages of wind farm projects. In this work, wind resource maps, at 9 km resolution, for the Gulf of Thailand are developed by means of atmospheric modeling, along with long-term climatic data. The Weather Research and Forecasting (WRF) system, considered a next generation atmospheric model, is

applied under nesting grids on two domains, i.e., 27 km and 9 km, to predict wind speeds and directions over the Gulf of Thailand. The long-term NCEP/NCAR R2 climatic database between 2001 to 2010 is used as WRF's input. The predicted wind speeds are validated using measured wind speeds obtained from 30 met masts installed along the coastal area, as shown in Figure 1.

Measured-predicted ratios (M/P) and percent mean relative errors (PMRE) of the predicted wind speeds are analyzed to display the performance of the model. Further, the technical power potential and the annual energy production are also analyzed in the context of offshore wind farm development.

RESULTS AND DISCUSSION

Figures 2-4 show the annual mean speeds in the Gulf of Thailand at 80 m, 100 m, and 120 m agl, respectively. It can be observed that not only does the average wind speeds increase with elevation, but also the area with high wind speeds. Results show that the M/P is 0.98, while the PMRE is 7%. Finally, the potential area of development is prominent in the Bay of Bangkok, where mean speeds of 6-7 m/s could justify the installation of 5,000 MW of offshore wind farms and produce, at a capacity factor of 25%, close to 11 GWh/year.

ACKNOWLEDGEMENT

The authors gratefully acknowledge the Thailand Research Fund (TRF) and the Electricity Generating Authority of Thailand (EGAT) for their financial support to this research work.

References

- [1] Paraic Higgins and Aoife Foley, "The evolution of offshore wind power in the United Kingdom", *Renewable and Sustainable Energy Reviews*, 37 (2014) 599-612.
- [2] Sandhya Kota, Stephen B. Bayne and Sandeep Nimmagadda, "Offshore wind energy: a comparative analysis of UK, USA and India", *Renewable and Sustainable Energy Reviews*, 41 (2015) 685-694.



Figure 1. Geographical distribution of the met mast installations around the Gulf of Thailand.

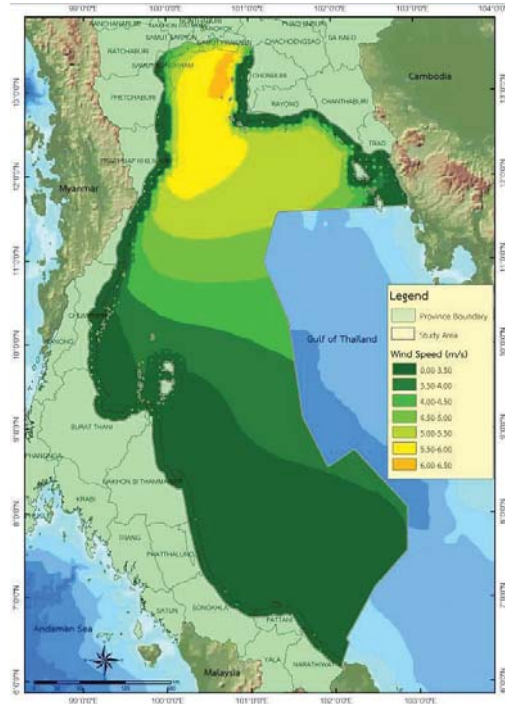


Figure 3. Annual mean speeds at 100 m agl in the Gulf of Thailand.

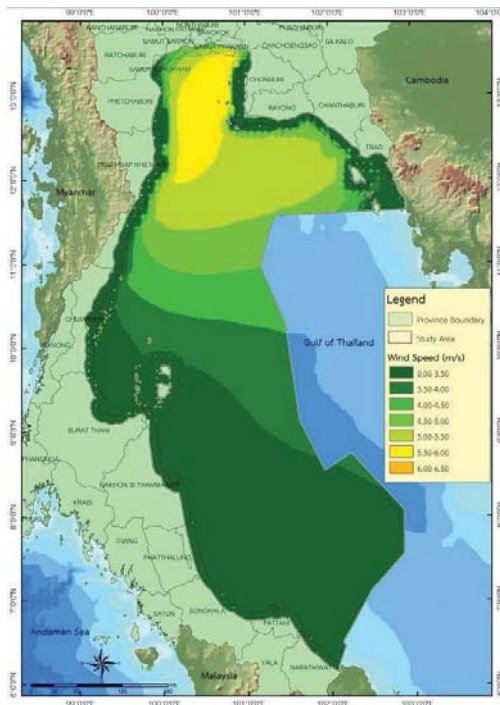


Figure 2. Annual mean speeds at 80 m agl in the Gulf of Thailand.

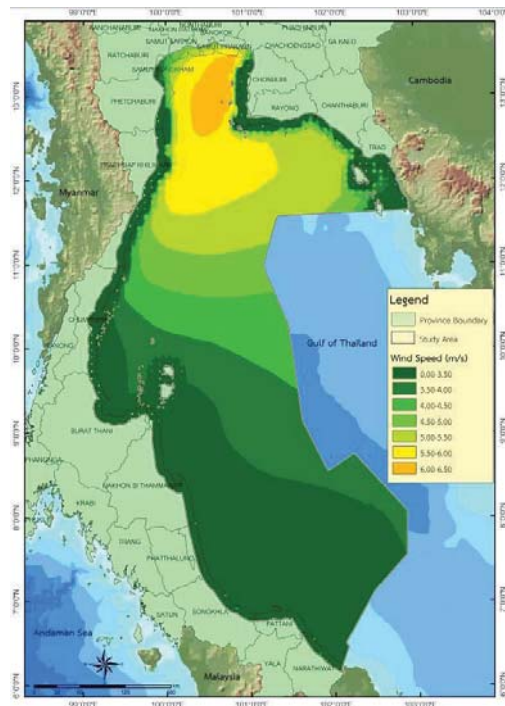


Figure 4. Annual mean speeds at 120 m agl in the Gulf of Thailand.

COMPARATIVE STUDY OF FIVE METHODS FOR ESTIMATING WEIBULL PARAMETERS FOR PHANGAN ISLAND, THAILAND

Warit Werapun¹, Yutthana Tirawanichakul², and Jompob Waewsak³

¹Faculty of Science and Industrial Technology

, Prince of Songkla University, Suratthani Campus, Suratthani, Thailand

²Faculty of Science, Department of Physics, Prince of Songkla University, Hatyai Campus, Thailand

³Research Center in Energy and Environment, Department of Physics, Faculty of Science, Thaksin University, Thailand

SUMMARY: Weibull function distribution has been widely used to represent in wind speed frequency distribution. Two importance parameters are k shape and c scale, which is related on the Weibull function. This research aims to compare five methods for estimating Weibull parameters. The wind speed data since January 2012 to December 2014 was used to analyze with different methods, namely empirical, energy pattern factor, maximum likelihood, modified maximum likelihood and graphical method for estimating k shape and c scale. The goodness of fit was judged by using Kolmogorov-Sminorv test, R^2 and the percent error of wind power density. Based on this data, the energy pattern factor was best for the percent error of power density and highest R^2 . The graphical method was the worst performance in this case.

Keywords: Weibull distribution, wind energy, power density, estimating Weibull parameters

INTRODUCTION

The assessment of wind energy potential is very important step before deciding to install wind turbine or wind farm. Generally a long term meteorological of wind speed data in time series was arranged in wind speed frequency distribution. These data was fit in Weibull function, which is consist of two parameters, k shape and c scale. Many numerical methods for estimating k shape and c scale has been used to fit wind speed frequency distribution. The maximum likelihood method is recommended for use with time series wind data whereas modified maximum likelihood method is recommended for use with wind data in frequency distribution format [1]. The power density method, or sometime is called energy pattern factor method was proposed for estimating Weibull parameters by Akdag and Dinler [2] because it does not require iterative procedure like a maximum likelihood method. However Chang [3] compared six numerical methods for estimating Weibull parameters, it is found that maximum likelihood method performs best follow by modified maximum likelihood method.

This paper aims to compare five numerical methods to suggest which is the most suitable for determining two parameters of Weibull function by using the wind speed data from January 2012 to December 2014 at Phangan Island.

METHOD OF ESTIMATION

The measured wind speed data from January 2012 to December 2014 was used from Phangan station at the height of 120m, which supported by National Research Council of Thailand. The number of wind speed data in 2012 until 2014 was 51289, 27751 and 52413 respectively. It should be note that in 2013 the number of data did not include the wind speed data from May to October because

of the problem of sensor.

The estimation of k shape and C scale of Weibull function was studied using five methods, namely empirical method, energy pattern factor, maximum likelihood, modified maximum likelihood and Graphical method .

In order to consider, which method can be fitted best with the actual wind speed data, so the R^2 and Kolmogorov-Sminorv test were determined. The actual power density was calculated by following equation 1 and the power density from Weibull function can be calculated following equation 2. Where ρ is the air density, T is the time in hour and \bar{v}^3 is the average of wind speed cubes

$$E_a = \frac{1}{2} \rho \bar{v}^3 T \quad (1)$$

$$E_w = \frac{1}{2} \rho C^3 \Gamma \left(1 + \frac{3}{k} \right) T \quad (2)$$

RESULTS AND DISCUSSION

The probability density of wind speed of actual data and four methods in 2012 and 2014 are shown in the figures 1-3, respectively. The Graphical method is the worst performance curve when compared with the actual wind speed data whereas empirical method and energy pattern factor give the probability quite the same curve. The k shape and c scale was shown in the table1. The energy pattern factor method has the lowest percent error of power density and the highest of R^2 of five methods, showing in the table2 and table3.

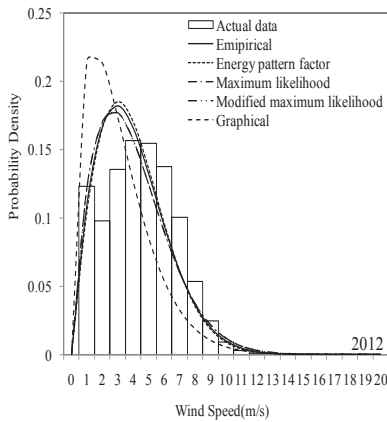


Figure 1. Comparison the actual data and Weibull function with different methods in 2012

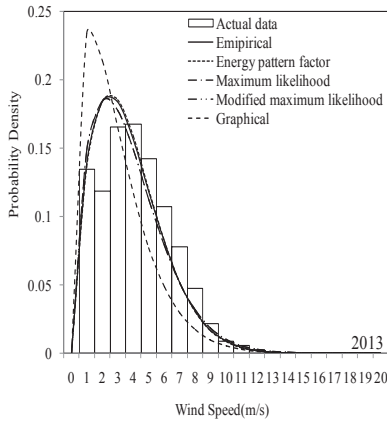


Figure 2. Comparison the actual data and Weibull function with different methods in 2013

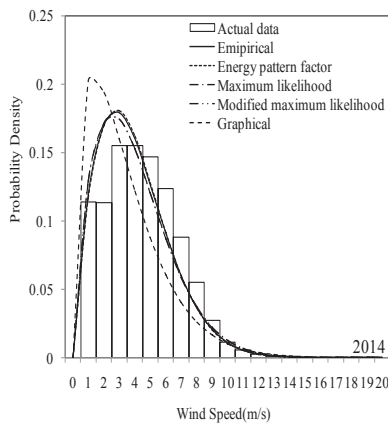


Figure 3. Comparison the actual data and Weibull function with different methods in 2014

Table 1. The estimation results of k and C

Method of Estimation	2012		2013		2014	
	k	C	k	C	k	C
Empirical	1.837	4.465	1.699	4.145	1.763	4.420
Energy pattern factor	1.891	4.470	1.724	4.150	1.787	4.425
Maximum likelihood	1.729	4.419	1.617	4.110	1.677	4.383
Modified maximum likelihood	1.727	4.428	1.618	4.118	1.682	4.396
Graphical	1.428	3.316	1.350	3.124	1.339	3.581

Table 2. The percent error of power density

Method of Estimation	2012	2013	2014
Empirical	2.823	1.581	1.374
Energy pattern factor	0.420	0.143	0.190
Maximum likelihood	8.206	6.921	6.108
Modified maximum likelihood	8.002	7.394	6.633
Graphical	36.751	33.782	12.122

Table 3. The Kolmogorov-Sminorv test and R² of each methods

Statistical Test	Method of Estimation	2012	2013	2014
Kolmogorov-Sminorv	Empirical	0.061	0.049	0.044
	Energy pattern factor	0.066	0.052	0.046
	Maximum likelihood	0.055	0.038	0.038
	Modified maximum likelihood	0.058	0.038	0.036
	Graphical	0.223	0.194	0.163
R-square	Empirical	0.840	0.897	0.912
	Energy pattern factor	0.842	0.900	0.914
	Maximum likelihood	0.825	0.882	0.897
	Modified maximum likelihood	0.826	0.883	0.899
	Graphical	0.559	0.643	0.685

ACKNOWLEDGMENT

The authors would like to thank the National Research Council of Thailand and Prince of Songkla university for financial support.

References

[1] J.V. Seguro and T.W. Lambert, "Modern estimation of the Weibull wind speed distribution for wind energy analysis", *Journal of Wind Engineering and Industrial Aerodynamics*, **8(1)**, 2000, pp. 75-84.
 [2] A. A Seyit and D. Ali, "A new method to estimate Weibull parameters for wind energy applications", *Energy conversion and Management*, **50(7)**2009, pp. 1761-1766.
 [3] C. Pau Tian., "Performance comparison of six numerical methods in estimating Weibull parameters for wind energy application", *Applied Energy*. **88**, 2011, pp.272-282.

ASSESSMENT OF WIND ENERGY POTENTIAL IN THE CENTRAL REGION OF THAILAND: AN ECONOMIC ANALYSIS

Pham Quan¹ and Thananchai Leephakpreeda¹

¹School of Manufacturing Systems and Mechanical Engineering, Sirindhorn International Institute of Technology, Thammasat University, Thailand

SUMMARY: This paper presents the economic analysis which is able to evaluate the possibility for investment of a wind project in Thailand. The effect of adder program is studied. Besides of that, many financial involved indices such as net present value, internal rate of return, benefit-cost ratio, pay-back period as well as generation cost are concerned to evaluate the feasibility of the project. Due to the benefit of exploiting wind energy, selling carbon credits as well as imported crude oils reduction are taken into account. All involved economic parameters in the project are updated. The study is applied at three wind masts in provinces: Ratchaburi, Pathum Thani and Saraburi in the central region of Thailand. A recommended wind turbine of VestasTM 850 kW is applied to those three provinces, which have the low wind speed profile, to evaluate the feasibility of the project in the economic aspect.

Keywords: renewable energy, economic analysis, wind power, wind turbine, Thailand

INTRODUCTION

Wind energy is exploited rapidly these days. The potential of wind power is statistically analyzed by the collected data through years. Then, a certain wind project can be carried out with an economic analysis about the possibility for the investment. Especially, many economic involved parameters such as adder rate are depended on the policies of the government. Therefore, all aspects of the project have to be considered and studied before being applied.

Normally, costs and profits which play main roles in any project are carefully concerned. Firstly, the total project cost to install wind turbines to produce electricity consists of initial investment cost and operation and maintenance cost for running through the whole project. The initial investment cost includes turbine cost and construction cost such as civil work cost, grid connection cost and construction management cost.

The benefits of the project earn mainly from the selling of electricity. In Thailand, the government puts many efforts to reduce the use of oil and natural gas for power generation. The target is to reduce environmental impact as well as global warming which is the main issue nowadays. Every kWh produced by renewable energy resources such as wind energy, solar energy, etc will be added an amount of money to the electricity rate. According to the policy, the adder will be added to the first 7 to 10 years at the rate of 0.117US\$/kWh during the project life [1]. Besides of that, there are benefits from selling of Carbon credits and reduction of imported crude oil.

In generally, net present value (*NPV*), internal rate of return (*IRR*), benefit cost ratio (*B/C*) and payback period (*PBP*) are common economic indices which determine the possibility of the project. Besides of that, generation cost (*GC*) is also a main index which is able to reflect the performance efficiency of wind turbines.

METHODOLOGY

In economic analysis, important indices such as *NPV*, *IRR*, *B/C*, *PBP* and *GC* are studied. *NPV* is defined to be the difference between the present value of cash inflows and outflows. It is used to analyze the profitability of an investment or a project. The project is said to be successful or worthy to be invested when *NPV* is positive. *IRR* is defined to be the discount rate often used in capital budgeting that makes the net present value of all cash flows from a particular project equal to zero. *IRR* is expected to be higher than the minimum loan rate. *B/C* is a ratio attempting to identify the relationship between the cost and benefits of a proposed project. *B/C* is also a criterion for investment decisions at a minimum acceptable rate. In general, the project is expected to get the value of benefits to be more than the cost. *PBP* is simply applied to determine how rapidly in years a project returns initial investment to investors. *GC* is calculated mainly from the total cost of the project to the generated electricity. Finally, the project is reported to be possible and feasible with positive *NPV*, *IRR* higher than minimum loan rate, *B/C* higher than 1, and *PBP* lower than 10 years. In further, the study presents how all economic indices get effected when the rate of adder are able to be increased. On another aspect, the reduction in amount of carbon dioxide and imported crude oil are then calculated to give consideration to how impactful wind projects influence the global warming.

RESULTS AND DISCUSSION

All significant economic parameters are researched under the update circumstance as shown in Table 1. By applying all the parameters to the calculation, main indices are calculated respectively.

Table 1. Numerical values for feasibility study

Parameter	Value
Cost of turbine	1.0 million EUR/1MW
USD exchange rate	31.65 THB/US\$
Euro exchange rate	42.27 THB/US\$
kTOE* per kWh	8.52*10 ⁻⁸ kTOE/kWh
Crude oil cost	110.3 US\$/barrel
Sale rate of carbon credit	8.34 EUR/ton
Sale rate of electricity	3.75 THB/kWh
Adder within first 10 years	0.117 US\$/kWh
Minimum loan rate	7%
Inflation rate	3%
Discount rate	7%
Project life	20 years

*TOE: Ton of Oil Equivalent

It is reported that the annual energy productions produced by recommended wind turbine of Vestas™ 850 kW at the height 120 m are 601, 735 and 1,030 MWh at sites in Ratchaburi (S1), Pathum Thani (S2) and Saraburi (S3) respectively [2]. As a result of taking the electricity production of all sites to analyze the feasibility of the project, all economic indices are calculated under the effect of inflation and adder as shown in Table 2.

Table 2. Economic indices at all sites

Site	GC (US\$/kWh)	NPV (US\$)	IRR (%)	B/C	PBP (years)
S1	0.15	55,953	7.5	1.03	11
S2	0.12	477,613	11.2	1.26	9
S3	0.09	1,405,894	18.3	1.77	7

According to Table 2, site S3 gains the most profit with NPV of 1.4 million US\$, IRR of 18.3%, B/C of 1.77 and PBP of 7 years. Significantly, because of acceptable economic indices all sites are reported to be possible to install the wind turbine of Vestas™ 850 kW. On another aspect, the generation cost at site S3 is lowest of 0.09 US\$/kWh among all sites. Due to the exploitation of wind energy, the reduction in amount of carbon dioxide released to the atmosphere and the number of crude oil barrels imported to the country are calculated as shown in Table 3.

Table 3. Reduction in amount of carbon dioxide and imported crude oil with respective cost.

Site	S1	S2	S3
Amount of imported crude oil (barrel/year)	374	457	641
Cost of imported crude oil (US\$/year)	41,226	50,418	70,653
Amount of CO ₂ (ton/year)	0.84	1.0	1.5
Cost of CO ₂ (US\$/year)	3,481	4,257	5,966
Total cost (US\$/year)	44,707	54,675	76,619

According to Table 3, the amount of 1.5 ton of carbon dioxide per year and 641 barrels of imported crude oil per year with total cost up to 76,619 US\$ could be reduced when wind turbine is installed at site S3. Among all involved parameters, the adder rate which is under the control of country's policy also plays a significant role in the project. Table 4 shows the effect of adder to the project when the government is able to increase the rate of adder to help the investor.

Table 4. Values of NPV, IRR, B/C, and PBP under the effect of adder

Site	Adder	NPV (US\$)	IRR (%)	B/C	PBP (years)
S1	25% Increase	179,321	8.66	1.10	10
	50% Increase	302,688	9.83	1.16	9
S2	25% Increase	628,487	12.53	1.34	8
	50% Increase	779,361	13.95	1.42	8
S3	25% Increase	1,617,323	20.26	1.88	6
	50% Increase	1,828,752	22.22	2.00	6

In accord to Table 4, NPV can be increased up to 179,321 and 320,688 US\$ when adder is increased 25% and 50% respectively at site S1. That means the government can attract investors to generate more wind projects at the low wind speed region by increasing a certain amount of the adder rate.

CONCLUSION

It is possible to install wind turbines in the central region of Thailand which is a low wind speed region. The increase of adder rate has an important role to attract investor to invest more wind projects meanwhile rises up the price of electricity for the customer.

ACKNOWLEDGMENT

The authors would like to thank the National Research Council of Thailand (NRCT) for supporting wind data measurements and Sirindhorn International Institute of Technology for giving opportunities to conduct the research.

References

- [1] T. Sopitsuda, G. Chris, "An assessment of Thailand's feed-in tariff program", *Renewable Energy*, **60**, 2013, pp.439-445.
- [2] P. Quan, "Investigation and assessment on potential of wind energy in the central region of Thailand", *Master Thesis Dissertation*, 2014.

TERRAIN EVALUATION FOR POWER CURVE MEASUREMENTS OF WIND TURBINES IN VARIANCE TO THE REQUIREMENTS AS PER IEC 61400-12-1

Sajan Antony Mathew¹ and M Saravanan¹

¹National Institute of Wind Energy, India

SUMMARY: The terrain evaluation is an important aspect of Site Feasibility Studies for Power Curve Measurements as per the requirements of IEC 61400-12-1. The terrain evaluation is guided by the requirements set in “Annexure B” of the standard IEC 61400-12-1. It is seen that many wind potential sites have variations which do not comply with the requirements and therefore are rejected for the purpose. This paper strives to demonstrate that a non-compliant terrain condition could also be used for the measurement of the power curve of a wind turbine if approached in an alternate manner. The methodology derives its concept from the fact that within the derived sector for measurements, the terrain compliance to the requirements of the IEC standard is a requisite. This would also assist in understanding the terrain condition of a site in line with the requirements of IEC 61400-12-1 and to use the site for measurements which otherwise would have been rejected.

Keywords: Power Performance, Site Feasibility Studies, Annual Energy Production, Terrain, Slopes

INTRODUCTION

The Site Feasibility Studies for Power Curve Measurements assist in the assessment of terrain, obstacles, sector for measurements and wind conditions of a particular site and its compliance to the requirements of IEC 61400-12-1. Therefore, terrains whose slopes and variations do not comply with the requirements of the IEC standard are summarily rejected. This has definitely posed challenges to the conduct of Power Curve Measurements and therefore alternatives should be pursued wherever possible. This paper has evolved from a study carried out for Power Curve Measurements in a non-compliant IEC terrain in Maharashtra, India. The methodology involved terrain evaluation as a part of the Site Feasibility Studies. The preliminary evaluations have been carried out using 90 m resolution SRTM data as well as 30 m resolution ASTER data. The analysis for terrain evaluation using 30 m Aster data has been compared with 1 m site surveyed contour map.

The data which was finally used for the purpose was the 1 m site surveyed contour map. The area for which measurement of height contours has been done is 8 times L over 360 Deg where L is the distance between the test turbine and the meteorological mast. The sector for measurements has been derived as per the requirements of IEC 61400-12-1[1]. The power curve measured and normalised as per the requirements of the IEC standard is compared with the normalised certified power curve of the wind turbine. The certified power curve is a measured power curve on which necessary due diligence has been carried out by accredited agencies and therefore its comparison to the measured power curve concludes the appropriateness of the methodology used in variance to the requirements of the standard IEC 61400-12-1[1].

SITE

The location of the measured turbine in the 1m site surveyed terrain map considered for the study at the site is shown in Figure 1 with the turbine facing the predominant South Western direction. The terrain undulations towards the North Eastern, Eastern and the South Eastern directions can be seen.

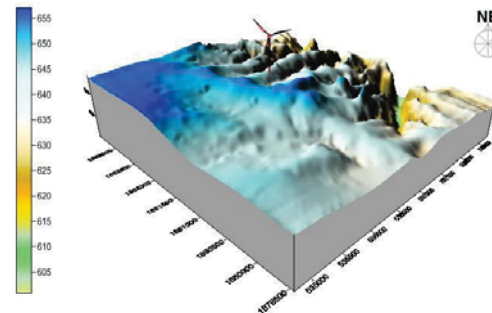


Figure 1. 1m site surveyed terrain map considered for the study at the site

TERRAIN EVALUATION

The preliminary analysis for the terrain has been done with 90 m resolution SRTM data as well as 30 m resolution ASTER data. There are variations seen in the SRTM and ASTER data sets vis-à-vis the 1m site surveyed map. The data from the 1m site surveyed contour map has been filtered for the various sectors and distances (<2L, 2L-4L, 4L-8L). The slopes, minimums, maximums, variations and residuals from the best fit through the test turbine have been evaluated. The slopes and variations of the terrain vis-à-vis the requirements of “Annexure B” of IEC 61400-12-1[1] are shown in Table 1.

Table 1. Terrain conditions

Distance	Sector	Maximum Slope % (IEC)	Measured Slope %	Maximum variation from the plane (IEC)	Measured variation
< 2L	360 degree	< 3	1.10	<0.04 (H+D)	0.06 (H+D)
≥ 2L and < 4L	Inside measurement sector	< 5	1.26	<0.08 (H+D)	0.04 (H+D)
≥ 2L and < 4L	Outside measurement sector	< 10	1.73	Not Applicable	
≥ 4L and < 8L	Inside measurement sector	< 10	1.51	<0.13 (H+D)	0.09 (H+D)

It is seen from Table 1 that the deviation from the requirements does arise from the region <2L in the 360 Deg Sector and it does not meet the terrain requirements of “Annexure B” of IEC 61400-12-1. The evaluation of the terrain with a new criteria for the region <2L inside measurement sector rather than 360 degrees has been carried out wherein all the criteria within the sector for measurements have been met as per the requirements.

POWER CURVE MEASUREMENTS RESULTS AND ITS COMPARISON

In order to understand the impact of the new criteria and its feasibility the comparison of the measured and normalised power curve is carried out with the certified power curve. The sector for measurements is from 152 Deg to 324 Deg and adequate enough to fulfil the required database and analysis for Power Curve Measurements. The criterion for comparison is the uncertainty for each measured bin. The two power curves are comparable to each other as it lies within the uncertainties of the measured power as shown in Figure 2.

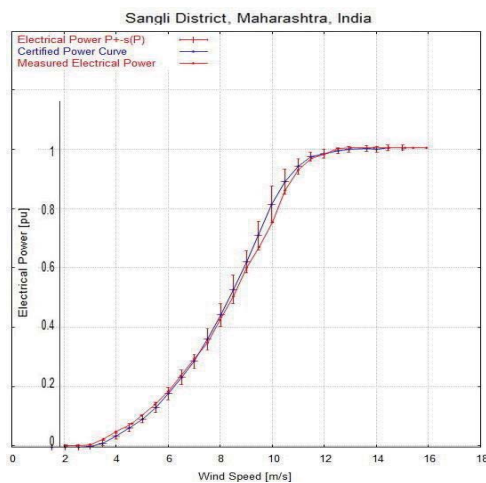


Figure 2. Comparison of power curves normalized to standard air density of 1.225 kg/m³

CONCLUSION

The various facets of the study have evolved through a methodology in which a non-compliant terrain condition has been used for conducting a Power Curve Measurement test in variance to the requirements of “Annexure B” of IEC 61400-12-1[1]. It is seen that by introducing a new criterion, a terrain which otherwise could have been rejected has been used for the power curve measurements. The new criterion has been tested with the comparison of the measured power curve with the certified power curve of the wind turbine. The comparison informs the suitability of using the new criterion for the purpose. The limited difference between the power curves in the range between 7.5 m/s and 12 m/s is solely due to the characteristics of the tested wind turbine and not from the impacts of the terrain condition. The testing of wind turbines due to various issues at sites is evolving and need different approaches to overcome the challenges whenever they come up. This alternate method is definitely one of the various methods which could be used without any impacts on the power performance of wind turbines.

ACKNOWLEDGMENT

The author(s) wishes to acknowledge the efforts of the project team namely, Mr A.R. Hasan Ali, Mr Y.Packiyaraj, Mr M.Karruppuchamy and Mr S.Paramasivan for the Power Curve Measurement Campaigns of the test turbines.

References

- [1] IEC 61400-12-1: *First Edition 2005-12, Wind Turbines- Part 12-1: Power Performance measurements of electricity producing wind turbines.*
- [2] IEC 61400-12-2: *First Edition 2013-03, Wind Turbines- Part 12-2: Power Performance measurements of electricity producing wind turbines on nacelle anemometry.*

FEASIBILITY OF DEVELOPMENT OF WIND FARMS IN NORTHERN PROVINCE OF SAUDI ARABIA

S. M. Shaahid¹, Luai M. Al-Hadhrami¹ and M. K. Rahman¹

¹Center for Engineering Research, King Fahd University of Petroleum & Minerals, Saudi Arabia

SUMMARY: In the present study, the economic feasibility of development of 15 MW wind power plant (wind farm) at Al-Jawf, Northern Province of the Kingdom of Saudi Arabia (K.S.A) has been investigated by analyzing long-term wind speed data. The monthly average wind speeds of Al-Jawf ($29^{\circ} 56' N$, $40^{\circ} 12' E$) range from 3.3 to 4.4 m/s at 10 m height. The wind farms simulated consist of different combinations of 600 kW commercial wind machines (50 m hub-height). NREL's (HOMER Energy's) HOMER software has been employed to perform the techno-economic assessment. The study presents monthly variations of wind speed, cumulative frequency distribution (CFD) profiles of wind speed, monthly and yearly amount of energy generated from the 15 MW wind farm, cost of generating wind-based energy (COE, \$/kWh), capacity factor (%), etc. The CFD indicates that the wind speeds are less than 3 m/s for 47% of the time during the year at Al-Jawf. This implies that wind electric conversion systems (WECS) will produce energy for about 53% of the time during the year. The annual energy produced by 15 MW wind farm has been found to be 20497 MWh. The COE by using 600 kW commercial WECS has been found to be 0.0561 US\$/kWh. With the development of 15 MW wind farm, about 483 tons/year of carbon emissions can be avoided entering into the local atmospheric.

Keywords: Wind speeds; commercial wind machines; wind farms; hub-heights; cost of energy (\$/kWh)

INTRODUCTION

The electricity we use everyday produces air pollution and greenhouse gases with serious consequences on our environment/health both globally and locally. Generating electricity by utilizing wind and other renewable energy technologies can greatly reduce the above damage and will also mitigate or cope-up with the ever increasing cost/uncertainty in supply of oil. Renewable energy (wind/solar) based power system is a nature-friendly option for power production to foster sustainable development challenges.

Literature indicates that wind energy (being free, sustainable, site-dependent, promising, non-polluting) is being rigorously pursued by a number of countries (with average wind speeds in the range of 5 m/s – 10 m/s), in an effort to reduce their dependence on fossil-based non-renewable fuels [1-2]. Cumulative global wind energy capacity reached about 369000 MW as of 2014. The price of generating energy using commercial WECS is in the range of 4 to 5 cents per kWh. The technology of the wind machines has improved remarkably. WECS in the range of 5.0 MW are commercially available [3].

Research related to renewable energy in Saudi Arabia has been subject matter of several earlier studies [4]. In the present study, long-term wind speed data (of the period 1970-1982) of Al-Jawf, (Northern Province of K.S.A.) has been analyzed to assess the techno-economic feasibility of development of wind power plant (wind farm). Long-term data indicates that the monthly average wind speeds vary from 3.3 to 4.4 m/s at 10 m height. Attention has been focused on the feasibility of development of 15 MW wind farm. The wind farms simulated consist of different combinations of 600 kW (50 m hub-height) commercial wind machines.

National Renewable Energy Laboratory's (NREL's) and HOMER Energy's HOMER (Hybrid Optimization Model for Electric Renewables) software has been utilized to carry out the techno-economic analysis of wind farm. HOMER is a recognized computer model for design of renewable wind/solar power systems. The study presents the monthly variations of wind speed, CFD profiles of wind speed (i.e. availability of wind in different wind speed bins), etc. Emphasis has been placed on estimation of monthly/yearly energy generation from the proposed 15 MW wind farm). Attention has also been focused on diurnal power. Furthermore, the study estimates the cost of wind-based electricity (COE, US\$/kWh) and capacity factor of wind power plants for the proposed location by using 600 kW WECS.

BACKGROUND INFORMATION

The K.S.A. is an arid/desert land with long hot summers and short cold winters. The month of March marks the beginning of spring and the transition from winter to summer. K.S.A. has one-fifth of the world's oil reserves, and is the largest oil producer and exporter of total petroleum liquids in the world. The electrical power demand of K.S.A. is increasing at an alarming rate. The demand for electricity is expected to reach about 55,000 MW by 2020. Since, Saudi Arabia has reasonable wind regime, an appreciable fraction of its energy needs may be harnessed from wind energy.

WIND SPEED DATA

The long-term (1970-1982) daily average wind speeds of Al-Jawf are demonstrated in Fig. 1. In general, the monthly average wind speed ranges from 3.3 to 4.4 m/s at 10 m height. It can be depicted from Fig. 1 that wind speed is relatively

higher during the summer months (May to August) as compared to other months (*this is a welcome characteristic because the load is high in summer in this part of the world.*). This implies that WECS (if installed) would produce more energy during summer time. The CFD analysis indicates that the wind speeds are less than 3 m/s for 47% of the time during the year. CFD is a tool or frame of reference to assess the potentiality/reliability of a site

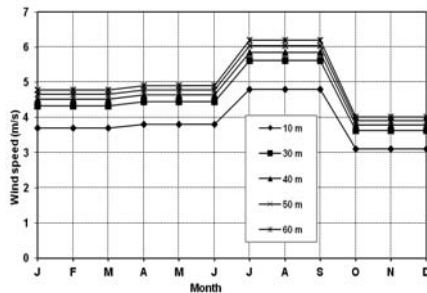


Fig. 1. Monthly average wind speeds (at Al-Jawf, K.S.A.) at different heights

RESULTS AND DISCUSSIONS

Energy generation from wind farms

Figure 2 shows the monthly wind energy generation/yield from 15 MW wind farm (cluster of 600 kW wind machines, 50 m hub-height). It can be noticed that the power generated during summer months (March to June) is greater as compared to other months. This is a favorable characteristic because the load is high during summer months in this part of the world. This indicates that Al-Jawf is a suitable candidate for installation of wind farms. The annual wind energy generated from 15 MW wind farm has been found to be 20497h MWh.

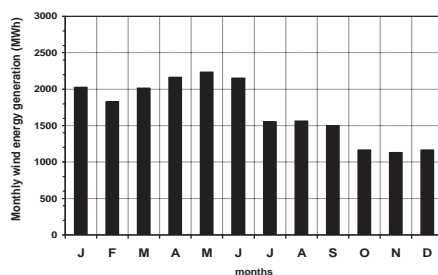


Figure 2. Monthly energy generation from 15 MW wind farm (600 kW machines, hub-height 50 m) at Al-Jawf

Cost of wind based electricity (COE, \$/kWh)

The COE by using 600 kW (50m hub-height) commercial WECS has been found to be 0.0561 US\$/kWh. From investor's point of view, the COE of electricity determines the economic attractiveness of a wind park.

Capacity factor of wind-based power plants

The capacity factor (CF) is given as the ratio of

the actual energy output to the theoretical maximum output, if the machine was running at its rated power during all the 8760 hours of the year. The CF is an important indicator in measuring the productivity of a wind turbine. The CF of wind-based power plant at Al-Jawf has been found to be 16%. (by using 600 kW WECS, 50 m hub-height).

CONCLUSION

The present study has discussed the economic feasibility of development of 15 MW wind farms at Al-Jawf, Northern Province of the K.S.A. Attention has been focused on the monthly/seasonal variations of wind speed, CFD profiles of wind speed, monthly and yearly energy generation from the 15 MW wind farms (50 m hub-height), diurnal power, COE (US\$/kWh), capacity factor (%), etc. The CFD indicates that the wind speeds are less than 3 m/s for 47% of the time during the year. This implies that wind farms (if installed at Al-Jawf) will produce energy for about 53% of the time during the year. The annual energy produced by 15 MW wind farms (50 m hub-height) has been found to be 20497 MWh. The cost of wind-based electricity by using 600 kW (50m hub-height) commercial WECS has been found to be 0.0561 US\$/kWh. This indicates that Al-Jawf is a suitable candidate for harvesting wind power. Attempt has been made to determine the capacity factor (CF) of wind-based power plants, the CF has been found to be 16%. With the development of 15 MW wind farm, about 483 tons/year of carbon emissions can be avoided entering into the local atmosphere].

ACKNOWLEDGEMENT

The authors acknowledge the support of the Research Institute of the King Fahd University of Petroleum and Minerals, Dhahran, Saudi Arabia. The authors extend special thanks to Dr. Tom Lambert and Dr. Peter Lilienthal (NREL and HOMER ENERGY) for their support.

References

- [1] V.J. Dao, N.S. Panchal, S. Faby, V. Sitaram and T.M. Krishnamoorthy. "Assessment of wind energy potential of Trombay Mumbai India" *Energy Convers. Mgmt.* **39(13)**, 1998, pp. 1351-1356.
- [2] H. Mir-Akbar R.B. and David. "Economic feasibility and optimization of an energy storage system for Portland Wind Farm (Victoria, Australia)" *Applied Energy*, **88**, 2011, pp. 2756-2763
- [3] http://www.gwec.net/wp-content/uploads/2015/02/GWEC_GlobalWindStats2014_FINAL_10.2.2015.pdf
- [4] S.M. Shaahid, S.I. El-Amin, S. Rehman, A. Al-Shehri, F. Ahmad, J. Bakashwain, and Luai M. Al-Hadhrami. "Techno-economic potential of retrofitting diesel power systems with hybrid wind-photovoltaic-diesel systems for off-grid electrification of remote villages of Saudi Arabia" *International Journal of Green Energy*, **7**, 2010, pp. 632-646.

ASSESSMENT OF WIND ENERGY POTENTIAL IN THE CENTRAL REGION OF THAILAND: A WIND ANALYSIS

Pham Quan¹ and Thananchai Leephakpreeda¹

¹School of Manufacturing Systems and Mechanical Engineering, Sirindhorn International Institute of Technology, Thammasat University, Thailand

SUMMARY: In this paper, wind energy potential is assessed in the central region of Thailand. Measurements of wind speed and wind direction are recorded with a sampling rate of one minute during a year at three levels of 65 m, 90 m, and 120 m. Three sites of wind masts at Ratchaburi, Pathum Thani, and Saraburi are objectively selected as potential provinces in the central region of Thailand. The WASPTM is implemented to determine statistical values of wind data, wind resources, and power productions according to selected wind turbines. The Weibull distribution functions of all three sites are reported for rationalizing wind energy potential. The wind turbine of BonusTM 1 MW is simulated to generate annual energy productions with low capacity factors in ranges between 0.03 and 0.09. Those results are caused due to the low wind speed region. The small sizes of wind turbines (<1MW) with lower cut-in and rated speed can be recommended such as VestasTM 850 kW, which yields higher capacity factors in ranges between 0.05 and 0.14.

Keywords: Renewable energy, wind resource assessment, wind power, wind farm, wind turbine

INTRODUCTION

The central region of Thailand is a vast area which is a quarter of Thailand. The population in the area is reported to be crowded with a high demand of electricity. Energy is raised up as a significant factor to develop the social and economic status. Nowadays, renewable energy keeps being a hot issue among scientists and engineers. Wind power which is a crucial source of environmental-friendly energy is concerned more and more in Thailand. The amount of installed wind turbines is increasing obviously recent years. One big wind farm is installed at Huay Bong, Nakhon Ratchasima province with the capacity of 207MW which starts a new era of wind power in Thailand [1]. As a result of that, the demand to assess wind potential energy becomes really necessary. Especially, the central region of Thailand which has a large area with easy accessibility to existing power lines is worthy to be concerned. The stability of electricity in the region will be improved if potentials of wind energy can be exploited

In this study, the potential of wind energy in the central region of Thailand at Ratchaburi (S1), Pathum Thani (S2), and Saraburi (S3) provinces are investigated by using one-year measured data of wind at three levels: 65 m, 90 m, and 120 m. The recorded data of the on-site wind is treated as statistical characteristics of wind. Additionally, topographical data such as height variation, roughness and sheltering obstacles are used in develop wind resource map at potential areas. Mapping potential energy helps to find surrounding area, at which wind turbines can generate maximum electricity output. Studies determine wind powers by using WASPTM software, which is well-known commercially available PC program for estimating wind data, wind resources, and power productions. In this study, common and standard wind turbines in the commercial wind turbine market are chosen to

assess the annual energy production at all sites.

The wind potential is assessed by applying wind data to a distribution function. There are so many well-known distribution functions such as Pearson, Chi-2, Johnson, Rayleigh and Weibull functions. Among these, the Weibull distribution function is proved to have high flexibility and simplicity that can fit a wide collection of recorded wind data [2]. WASPTM is also built by applying Weibull distribution function in its program.

METHODOLOGY

In assessing potential on electrical energy production from wind energy, all of performance factors are analytically investigated from measured data of wind around the areas, which are feasible to install wind turbines at desired heights. Physically, a wind speed is a height-dependent variable to be determined for how strong the wind drives blades of a wind turbine.

In this work, a wind map of Thailand is initially investigated for finding accessible areas with high potential of wind energy. Field surveys to those areas are done with observing wind speed at ground level and personally questioning local people about wind potential during a whole year.

Measurement devices are mounted on wind masts for detecting wind speeds and wind directions at heights of 65 m, 90 m, and 120 m. A three-cup anemometer of NRG#40C and a wind vane of NRG#200P are used to measure a wind speed and a wind direction, respectively. The wind speed and the wind direction are recorded by the Nomad 2TM wind data loggers during the whole year 2012 at a sampling rate of 1 minute with averaging values in every ten minutes.

Main steps include wind data collection, generating wind climate, wind energy assessment and wind resource map stimulation. All of steps are worked out by the program WASPTM and its

elemental program. The wind turbine Bonus™ 1MW and Vestas™ 850 kW are applied to assess the wind potential energy at all sites. Figure 1 shows the power production versus the wind speed of two turbines to investigate and study the energy production.

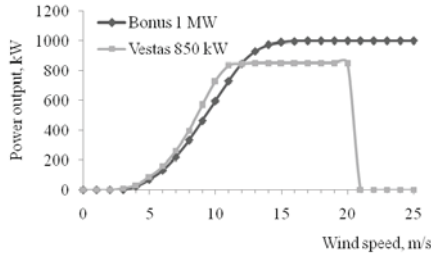


Figure 1. Power curves of wind turbines

RESULTS AND DISCUSSION

Table 1 reports statistical values of annual wind mean speed, and parameters of the Weibull distribution that are the shape parameter *k*, the scale parameter *c*, and the power density at every height for all sites. Accordingly, the probability density functions of wind data at three sites representatively at a height of 120 m are plotted as shown in Figure 2.

Table 1. Mean wind speed, shape parameter *k*, and scale parameter *c*, and average power density

Site	Height (m)	Mean wind speed (m/s)	<i>k</i>	<i>c</i> (m/s)	Power density (W/m ²)
S1	65	3.02	1.42	3.32	35
	90	3.25	1.48	3.59	41
	120	3.65	1.80	4.10	58
S2	65	3.49	2.09	3.94	42
	90	3.92	2.09	4.43	59
	120	4.01	2.10	4.53	70
S3	65	4.15	2.07	4.57	63
	90	4.21	2.11	4.75	69
	120	4.57	2.08	5.16	99

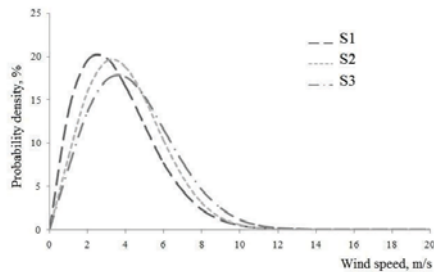


Figure 2. Weibull distributions of wind data for three sites at a height of 120 m.

The data of wind measurement is analyzed by the WASP™ software to determine the annual electricity productions generated by wind turbines. Table 2 shows the average power densities and annual energy productions (*AEP*) with capacity factors (*c_f*) of wind turbines at every height of all sites.

Table 2. Average power density, and power production with capacity factor

Site	Height (m)	Bonus™ 1 MW		Vestas™ 850 kW	
		<i>AEP</i> (MWh)	<i>c_f</i>	<i>AEP</i> (MWh)	<i>c_f</i>
S1	65	255	0.03	349	0.05
	90	338	0.04	450	0.06
	120	465	0.05	601	0.08
S2	65	329	0.04	443	0.06
	90	426	0.05	560	0.08
	120	574	0.07	735	0.10
S3	65	493	0.06	639	0.09
	90	633	0.07	803	0.11
	120	829	0.09	1,030	0.14

According to Table 2, the wind turbine of Vestas™ 850 kW which is a smaller turbine is reported to generate more energy than Bonus™ 1MW at every height of all sites. The reason is mainly from the low wind speed profile which is varied from 3 m/s to 4 m/s for mean wind speed. From the power curve performances in Figure 1, the wind turbine Vestas™ 850 kW has the lower cut-in speed (3 m/s compared to 4 m/s) and lower rated speed (13 m/s compared to 20 m/s).

CONCLUSION

In conclusion, the central region of Thailand is reported to have the low wind speed region. The site S3 has the highest potential compared with sites S1 and S2. A small wind turbine such as Vestas™ 850 kW with a lower cut-in and rated speed is well fitted to the wind profile of the region.

ACKNOWLEDGMENT

The authors would like to thank the National Research Council of Thailand (NRCT) for supporting wind data measurements and Sirindhorn International Institute of Technology for giving opportunities to conduct the research.

References

[1] Mott MacDonald, <https://www.mottmac.com/article/2310/huay-bong-207mw-wind-farm-thailand>; August 17, 2014.
 [2] EK. Akpinar, S. Akpinar, "A statistical analysis of wind speed data used in installation of wind energy conversion systems", *Energy Conversion and Management*. **46**, 2005, pp.515–532.

Energy Policy; Low Carbon Society

THAILAND'S POST-2020 GREENHOUSE GAS EMISSIONS REGIME IN THE ENERGY SECTOR

Sujeetha Selvakkumaran¹, Chontichaprin Nithitsuttibuta¹ and Bundit Limmeechokchai¹

¹Sustainable Energy and Low Carbon Research Unit
Sirindhorn International Institute of Technology, Thammasat University, Thailand

SUMMARY: There has been a call for concerted efforts at enhanced reduction of greenhouse gas (GHG). The Intended Nationally Determined Contributions (INDCs) are to be communicated in 2015 by Parties to the UNFCCC, so as to take actions to reduce the post-2020 global GHG emissions. Energy sector is the majority contributor to the total GHG emissions of Thailand. The objective of this study is to frame a BAU case for the Thai energy sector and to account the total GHG emissions until 2030. The study then assesses the potential mitigation possible in each sub-sector and the possible INDCs and the contributing key technologies. The energy sector is modeled individually as five sub-sectors, namely the power, industry, transport, residential and commercial sectors. The time horizon considered is 2005-2030 and the GHGs covered are CO₂, CH₄ and N₂O. The Asia-Pacific Integrated Model (AIM) Enduse model is used to model the sectors. The BAU case and an INDC scenario are constructed. The INDC scenario includes mitigation technologies for each sub-sector. Results show that a mitigation of 12% is possible in the INDC scenario in 2030, when compared to the BAU case. The majority of mitigation is possible through the transport and power sectors.

Keywords: Intended Nationally Determined Contributions (INDCs), Energy, Thailand, CO₂ mitigation

INTRODUCTION

The Parties to the United Nations Framework Convention on Climate Change (UNFCCC) are negotiating an international agreement for the post-2020 period, to be adopted by 2015, that aims to limit the rise of the global average temperature to below 2°C above pre-industrial levels [1]. As a preparation for the 2015 agreement, a decision was reached at the 19th Conference of Parties (COP19) that countries should communicate their Intended Nationally Determined Contributions (INDCs) in 2015.

According to Thailand's Second National Communication submitted to UNFCCC, in 2000, 60% of the total GHG emissions of Thailand were from the energy and transport (energy combustion) sectors. This sector is the majority emitter of GHGs in Thailand [2]. The Ad-Hoc Working Group on the Durban Platform for Enhanced Action (ADP) postulates that the 2015 agreement and the connected INDCs should, on principle, take into account the common but differentiated responsibilities (CBDR) and respective capabilities (RC) of each participating country [3]. It also reiterates that a rigorous scientific approach should be the basis for such a commitment.

The objective of this paper is to frame a coherent BAU for the energy sector of Thailand and estimate the GHGs. The paper also assesses the mitigation possible in the CM scenario when compared to the BAU case. The chief outcome of the paper is the understanding of the GHG emission regime of Thai energy sector up to 2030, and a reasoned and scientifically arrived at INDC, which also follows the principle of CBDR.

METHODOLOGY

The energy sectors of Thailand are modeled

using AIM Enduse. The AIM Enduse is a recursive dynamic optimization model, based on technology based bottom-up principle [4]. Each sector is modeled separately. The time horizon for the study is 2005 to 2030. This study presents a BAU case, which has frozen efficiency characteristics and maintains the status quo, along with an INDC scenario, which includes counter-measures (CMs).

The future demand for each sub-sector is estimated by using a linear multi-variable regression model. In the case of the industrial sector, the sector is sub-divided into nine sub-sectors and the energy demand is computed separately for each sub-sector. The residential sector demand is estimated by a multi-variable linear regression model which uses the GDP and number of households as the independent variable. Similarly, transport sector demand is estimated by its correlation to the value added in the transport sector and population.

The GDP and population estimates are obtained from [5] and [6] respectively. The past energy data are obtained from official reports [7]. The power generation demand is obtained from [5]. Most of the CMs are obtained again from already existing governmental plans such as [8] and [9] and international technology-focus based reports such as [10].

RESULTS

The overall energy demand, in terms of primary energy demand and final energy demand and the GHG emissions, along with power sector emissions are presented.

Energy demand and GHG emissions

The Figure 1 presents the total primary energy supply (TPES) and the total final energy supply (TFS) of Thailand. The Cumulative Annual Growth Rate (CAGR) of TPES in BAU and INDC are 3.8%

and 3.5%, respectively.

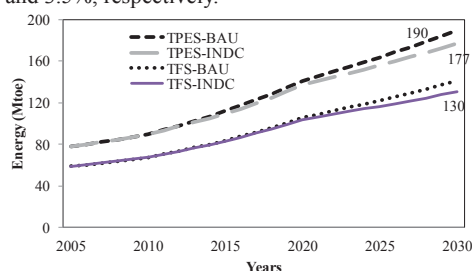


Figure 1. The energy supply in Thailand

This shows that there is a decreasing effect on the energy supply needs in the INDC scenario. Similarly, the CAGR of TFS is 3.8% and 3.3% in the BAU and CM cases, respectively.

Figure 2 shows the GHG emissions in the BAU and INDC scenarios. It can be seen that the total mitigation in 2030 is 60 Mt-CO₂eq, which is 12% lower when compared to the BAU case.

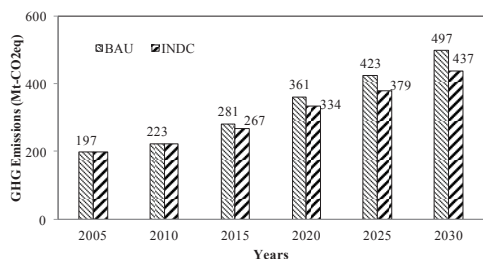


Figure 2. The GHG emissions in Thailand

In terms of contributions of GHG emissions in 2030, the sector with the highest emissions is power sector, contributing 42% and 43%, in the BAU and INDC scenarios, respectively. This is followed by the industrial sector, which contributes 28% of the GHG emissions, in 2030 in both the BAU and INDC scenarios.

Power sector GHG mitigation

Table 1 gives the GHG mitigation in terms of fuel type in the power sector of Thailand. The highest mitigation comes from Natural Gas (NG), which is to be expected as NG has the largest fuel share. But the significant fact to be noted is the contribution from renewables, which in 2030, amounts to 10% of the total mitigation.

Table 1. The GHG mitigation in the power sector.

GHG reductions (kt-CO ₂ eq)	2011	2015	2020	2025	2030
Coal	298	2,163	3,013	3,329	3,664
Lignite	377	1,972	2,067	2,350	2,672
NG	1,220	7,510	9,620	12,062	14,392
Fuel Oil	0	-229	36	40	44
Diesel	1	5	7	8	8
Biogas	-44	-200	-306	-188	-105
Black liquor	-168	1,304	1,459	1,253	995
MSW	-19	-211	-300	-320	-330
Renewables	-42	1,818	2,183	2,214	2,176
Total	1,623	14,132	17,778	20,746	23,516

GHG mitigation in industrial, transport and building sectors

The highest contribution to mitigation from 2010 to 2030, cumulatively, comes from the power sector, which amounts to 291 Mt-CO₂eq, in the CM scenario, when compared to the BAU case.

The contributions from the residential and commercial sectors are not significant, since they predominantly use electricity, which is accounted for in the power sector, and biomass, which is accounted only for CH₄ and N₂O.

CONCLUSION

The INDCs are required from countries in an effort to curb future GHG emissions from spiraling out of control and causing harm to the environment. In Thailand the energy sector dominates the GHG emissions. Results show that a potential mitigation of 12% is possible in the year 2030 in the INDC scenario, when compared to the BAU case. This mitigation is made up of CMs being adopted in each energy sub-sector.

ACKNOWLEDGMENT

The training of National Institute for Environmental Studies (NIES), Japan, and Mizuho Information and Research Institute of Japan are gratefully acknowledged by the authors.

References

- [1] K. Levin, D. Rich, and Y. Dagnet, "Ex-ante clarification, transparency, and understanding of Intended Nationally Determined Mitigation Contributions", WRI Working Paper, *World Resources Institute*, March 2014.
- [2] Office of Natural Resources and Environmental Policy and Planning (ONEP), "Thailand's Second National Communication", Ministry of Natural Resources and Environment, 2010.
- [3] Ad-Hoc Working Group on the Durban Platform for Enhanced Action (ADP), "Parties' views and proposals on the elements for a draft negotiating text", *Non-paper*, July 2014.
- [4] Asia-Pacific Integrated Modeling (AIM) Team "AIM Enduse Manual", *National Institute for Environmental Studies (NIES)*, 2012.
- [5] Electricity Generating Authority of Thailand, "Power Development Plan, Revision 3", EGAT, 2012.
- [6] National Economic and Social Development Board (NESDB), "
- [7] Department of Energy Efficiency and Alternative Energy (DEDE). "Energy Situation of Thailand 2010", DEDE, 2011.
- [8] Department of Energy Efficiency and Alternative Energy (DEDE), "Alternative Energy Development Plan 2012-2021", DEDE, 2012.
- [9] Department of Energy Efficiency and Alternative Energy (DEDE), "Energy Efficiency Development Plan 2012-2030", DEDE, 2012.
- [10] International Energy Agency, "Energy Technology Perspectives", Paris, 2012.

LOW CARBON SCENARIOS FOR AN ENERGY IMPORT-DEPENDENT ASIAN COUNTRY: THE CASE STUDY OF SRI LANKA

Sujeetha Selvakkumaran¹, Bundit Limmeechokchai¹

¹Sustainable Energy and Low Carbon Research Unit (SELC), Sirindhorn International Institute of Technology
Thammasat University, Thailand

SUMMARY: Energy sector of a country is the backbone in which a country's industrial competitiveness is built. It is imperative that a well-functioning energy sector is present to facilitate the growth of a country. That being said, the environmental wellbeing of the country and the entire world is important. The energetic analyses of the power, transport and industrial sectors of Sri Lanka are presented in this paper, along with possible Low Carbon scenarios. The Low Carbon scenarios are assessed for the CO₂ mitigation, energy consumption reduction and also for co-benefits such as energy security and productivity. The Sri Lankan energy sector is modeled using Asia-Pacific Integrated Model AIM/Enduse. Results show that Low Carbon activities in Sri Lanka increase energy security of the country, along with increasing productivity. Mitigations of 41.3%, 25% and 37% are achieved in the most ambitious LCS scenario, when compared to the BAU case in 2050, in the power, industry and transport sectors, respectively.

Keywords: Low Carbon Society, Energy security, Sri Lanka, CO₂ mitigation

INTRODUCTION

The energy sector of a country is vital to the achievement of development-based objectives of a country. The developing countries are at a crossroad as to conflicting objectives. On the one hand they have to aim to be more competitive in terms of economic growth and wellbeing, but on the other hand, they are faced with challenges in procuring energy sources, which aid in propelling them towards economic security. In addition to this, the world, as a whole is waking up to the realization that energy sector and its use and economic growth should be attained sustainably.

Sri Lanka is a South Asian island country, situated in the middle of the Indian Ocean. In 2010, its total energy demand was approximately 8.8 Mtoe, which lead to 13.12 Mt-CO₂ of CO₂ emissions [1]. Sri Lanka is still very much reliant on the agricultural sector of the economy. Yet, Sri Lanka has seen a burgeoning growth in energy demand in the last two decades. From being a hydropower-reliant power sector, Sri Lanka has become reliant on fossil fuel power plants which place a burden on the economy [2]. Sri Lanka is also susceptible to high oil prices as it does not possess any significant reserves of conventional fossil fuels or coal. In addition to this the domestic energy demand is still dominated by conventional biomass use in the rural areas. Ultimately, Sri Lanka is very much dependent on imported fossil fuels, thus making it vulnerable to developmental setbacks [2].

The objective of this paper is to identify the extent of CO₂ mitigation possible through Low Carbon scenarios in Sri Lanka in high-emitting energy sub-sectors and to quantify the co-benefits which accrue through the mitigation.

METHODOLOGY

The power, transport and industrial sectors of Sri Lanka, which account for approximately 80% of

its total CO₂ emissions from the energy sector, are modeled using AIM Enduse. The AIM Enduse is a recursive dynamic optimization model, based on technology based bottom-up principle [3]. Each sector is modeled separately and with the extent of detail, whereby it is close enough to represent the actual system but, not overtly more complicated than necessary. The time horizon for the model is 2010 to 2050.

The power sector is primarily divided into carbon based and non-carbon based generation plants. The industrial sector is divided into nine sub-sectors, with the energy demand of each sub-sector being accounted for separately. The transport sector is divided into freight and passenger travel demand.

The past data have been gathered from governmental publications such as [1] and [4]. The future plans have been gleaned from various governmental sources. For the power sector, the governmental generation expansion plan has been used [5] and for the future of transport sector, ministerial sources [6] have been used. The future energy consumption in each sector has been estimated individually by linear multi-variable regression models, where the independent variables are the value added in each sector, and the population of Sri Lanka.

This study presents a BAU case, which has frozen efficiency characteristics and maintains the status quo, along with three Low Carbon Society (LCS) scenarios with varying degrees of LCS measure implementation. These LCS scenarios are named LCS1, LCS2 and LCS3. LCS1 has lower levels of LCS measures implemented in it, whereas LCS2 has moderately higher levels of LCS measures and LCS3 has very high aspirations of LCS measures.

RESULTS

Each sector results are presented in this section. The CO₂ emissions in terms of each sector, along with the behaviour of energy security are presented for each sector. Energy security is measured along the lines of diversity of primary energy demand (DOPED), oil share (OS), and renewable fuel share (RFS).

Power sector

The Figure 1 presents the CO₂ emissions in the power sector of Sri Lanka. It can be seen that the emissions are very much reduced in the LCS3 scenario. Even though the mitigation is less in LCS1 scenario, both LCS2 and LCS3 scenarios show positive signs in mitigation.

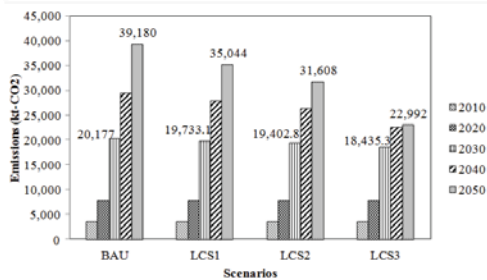


Figure 1. The CO₂ emissions in the power sector

In terms of energy security in the power sector, all the LCS scenarios perform better.

Industrial sector

The Figure 2 presents the CO₂ emissions in the industrial sector of Sri Lanka. The emissions don't reduce drastically in the LCS1 and LCS2 scenarios, as it is to be expected, but there is significant reduction in the LCS3. The reasons for the reduced reduction are that along with the LCS aspirations being low in LCS1 and LCS2 scenarios, the industrial sector is also heavily dependent on conventional biomass, which is accounted as being carbon neutral.

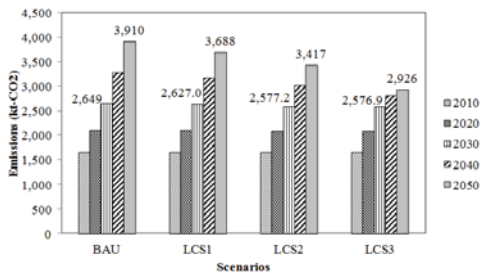


Figure 2. The CO₂ emissions in the industrial sector

Transport sector

As can be seen from Figure 3, the transport sector emissions show a very interesting trend in the future, in the LCS scenarios. The LCS2 and LCS3 scenarios exhibit a peak nature in terms of CO₂

emissions, which is not similar to the power and industrial sectors. The LCS scenarios also show a marked improvement in energy security, when compared to the BAU case

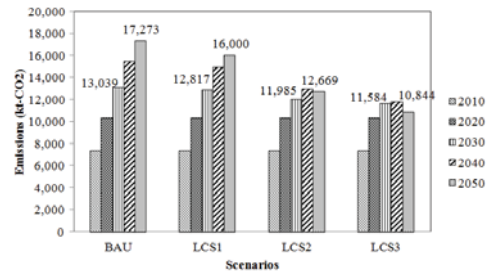


Figure 3. The CO₂ emissions in the transport sector

CONCLUSION

The energy sectors of Sri Lanka are expected to show rapid growth in the coming decades, leading to higher CO₂ emissions, which are detrimental to the general environment. The low carbon activities which may be designed and implemented have a beneficial impact in reducing the CO₂ emissions. As such, the power sector, industrial sector and transport sector all show reduced CO₂ emissions, along with increased energy security and productivity. The LCS3 scenario has higher productivity along with enhanced energy security, in terms of DOPED, RFS and OS.

ACKNOWLEDGMENT

Authors would also like to thank Sri Lanka Sustainable Energy Authority for the provision of data. The research training and guidance of National Institute for Environmental Studies (NIES), Japan is also gratefully acknowledged.

References

- [1] Sri Lanka Sustainable Energy Authority (SLSEA), Sri Lanka Energy Balance 2010, Colombo, 2010.
- [2] S. Selvakkumaran and B. Limmeechokchai, "Energy Security and Co-benefits of energy efficiency improvement in three Asian countries", *Renewable and Sustainable Energy Reviews*, **20**, 2013, pp. 491-503.
- [3] Asia-Pacific Integrated Modeling (AIM) Team "AIM Enduse Manual", *National Institute for Environmental Studies (NIES)*. 2012.
- [4] Central Bank of Sri Lanka, "Sri Lankan Economic and Social Statistics 2010", 2011, CBSL.
- [5] Ceylon Electricity Board (CEB), "Sri Lankan Power Generation Expansion Plan", 2011, Ministry of Power and Energy.
- [6] D. Perera, "Sustainable Transport Initiatives in Sri Lanka", *Presentation at the Ministry of Transport*, 2008, Ministry of Transport.

ENERGY EFFICIENCY IMPROVEMENT AND CO₂ MITIGATION IN RESIDENTIAL SECTOR: COMPARISON BETWEEN INDONESIA AND THAILAND

Tri Vicca Kusumadewi¹ and Bundit Limmeechokchai¹

¹Mechanical Engineering Department, School of Manufacturing System and Mechanical Engineering, Sirindhorn International Institute of Technology, Thammasat University, Thailand

SUMMARY: This paper presents energy efficiency improvement and CO₂ Mitigation in the residential sector between Indonesia and Thailand. The Long-range Energy Alternative Planning (LEAP) model was used to analyze future energy demand and CO₂ emissions during 2010-2050. This study applied the Demand Side Management (DSM) options to reduce CO₂ emissions in the residential sector by implementing energy efficiency improvements such as efficient lighting, cooking, cooling and entertainment devices. The results indicate that in the business as usual (BAU) scenarios between 2010 and 2050, for Indonesia the energy demand will increase from 18147 ktoe in 2010 to 36044 ktoe in 2050. By adopting these scenarios, energy will save by 27.6% of total energy demand in 2050 while cumulative CO₂ emission can be reduced by 16% of overall CO₂ emissions in 2050. For Thailand, the energy demand will increase from 1879.1 ktoe in 2010 to 3167.8 ktoe in 2050. The energy will be save by 15.5% of total energy demand in 2050 and cumulative CO₂ emission can be reduced by 13.36% of overall CO₂ emission in 2050.

Keywords: LEAP model, Energy Efficiency, CO₂ mitigation, Residential Sector

INTRODUCTION

Electricity is a basic energy to supply energy in each sector. The electricity production is undesirable emission and environmental effects. The existence of carbon emissions can lead to climate change. Climate change is a global issue that started to be a topic of conversation in the world since 1992. Law No. 6 1994 was ratified by Indonesia in the convention on climate change. It needs to maintain a stable concentration of greenhouse gases (GHGs) and objective of the convention GHGs in the atmosphere thus ensuring food security and sustainable development [1]. The meeting resulted in the Kyoto Protocol regulating GHGs emissions due to human activities so that its concentration in the atmosphere is stable and does not harm the earth's climate system. This protocol contains an obligation for developed countries called Annex I countries to reduce emissions by 5% from 1990 levels in the year 2008-2012 [2]. While developing countries are entering into the Non-Annex I countries, they are not obliged to reduce emissions as Indonesia and Thailand. In Asia several countries were developed low carbon Asia research projects. The program will be run in accordance with the country regulation for an Asia and national action plan for reducing CO₂. Therefore, the objective of this study is to prepare for the sustainable development in the residential sector which are energy consumption and CO₂ emitting in Indonesia and Thailand. In this study, the LEAP developed by Stockholm Environment Institute is employed to estimate energy demand and CO₂ emissions in addition to assess CO₂ mitigation from four mitigation measures, the option considered includes: (1) efficient lighting devices, (2) efficient cooking devices, (3) efficient cooling devices and (4) efficient entertainment devices.

METHODOLOGY

A study of energy planning and policies is prepared by forecast energy demand in Business as Usual (BAU) case, and calculate supply required to supply energy demand. The power generation optimized with renewable energy power generation. As well as, in residential sector was analyzed efficient improvement appliance services. The methodology for the research study can be best described as follows: (i) Data sources (statistical report, research paper, official government plan, and online database), (ii) Data Collection, (iii) develop energy models for residential, (iv) formulate energy efficiency scenario, (v) result of energy models, and (vi) Evaluation of CO₂.

In the residential sector mitigation, the energy efficiency improvement is replacement of existing energy devices with more efficient ones based on the data currently available on the market. The four mitigation include in the scenario are efficient lighting devices, efficient cooking devices, efficient cooling devices and efficient entertainment devices. The proposed efficient technology are to obtain energy saving and CO₂ mitigation during 2010-2050. Regarding the proposed penetration rate of particular technology as follows:

Lighting system

Lighting is the most important end use to reducing energy use in the residential sector. The options considered include: (i) conventional lighting appliances is fully replaced by year 2030, and (ii) compact Fluorescent Lamp would share 40% and 50% of total lighting within 2030 and 2050, respectively.

Cooking system

Conventional cooking appliances are fully replaced with high efficiency appliance corresponding to particular service type by year 2030.

Cooling system

Refrigerator and Air Conditioner is the target for efficiency improvement, since their electricity use is growing rapidly. The options considered include: (i) improvement of Refrigeration efficiency, and (ii) improvement of Air Conditioning efficiency.

Entertainment g system

Television appliances are fully replaced with high efficiency appliance corresponding to particular service type by year 2030.

RESULT AND DISCUSSION

The result shown in figure 1, in the BAU scenario between 2010 and 2050, in Indonesia the energy demand will increase to 18147.7 ktoe to 36043.6 ktoe, respectively. By adopting these policy strategies, compared with the base year, the energy demand will increase by 50% in 2050. In the energy efficiency scenario the energy will save by 27.6% compared with BAU in 2050. CO₂ emissions shown in fig 2, currency by 12.6 million tons in 2010 and is expected to reach 33.9 million tons in 2050. The CO₂ emission will be increased 2.5 times during 2010-2050. In the energy efficiency scenario, CO₂ emissions will increased by 17%, in 2050, to 28.2 million tons; and, cumulative CO₂ emissions reduction will reach 16% against BAU scenario from 2010-2050.

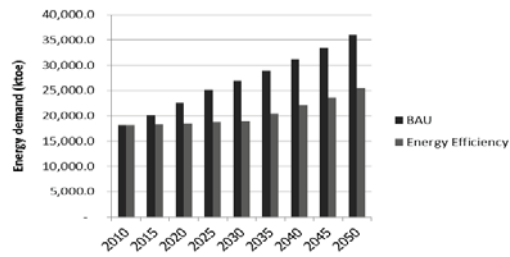


Figure 1. Indonesia energy demand 2010-2050

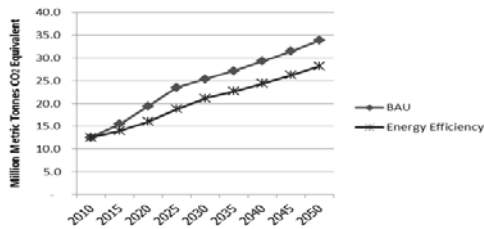


Figure 2. Indonesia CO₂ emissions 2010-2050

Figure 3 shows the Thailand energy demands, in BAU scenario energy demand will be increased by 1879.1 ktoe in 2010 and 3167.8 ktoe in 2050, respectively. In 2050 the energy demand will increase by 41% compared with base year 2010. In the energy efficiency scenario the energy will save by 15.5% compared with BAU in 2050. CO₂

emission emission is 1.9 million tons in 2010 and will be increased by 3.3 million tons in 2050. In the energy efficiency scenario, CO₂ emissions will increased by 16.91%, in 2050, to 2.7 million tons; and, cumulative CO₂ emissions reduction will reach 13.36% against BAU scenario from 2010-2050.

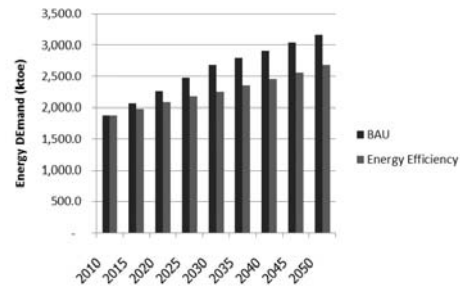


Figure 3. Thailand energy demand (2010-2050)

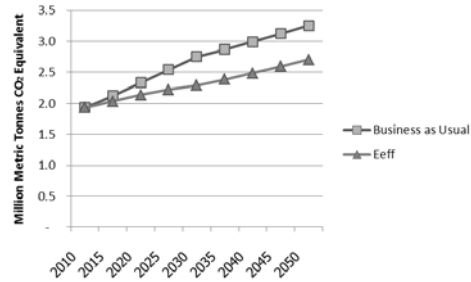


Figure 4. Thailand CO₂ emissions (2010-2050)

Energy demand and CO₂ mitigation between Indonesia and Thailand are different because both countries have total different of population and number of households. Indonesia consumed higher energy than Thailand because of higher population growth at 1.5% per year while Thailand population growth rate is only less than 0.5% per year.

ACKNOWLEDGEMENT

Authors would like to thank Sirindhorn International Institute of Technology, Thammasat University for the scholarship provided.

References

- [1] Indonesia second national communication under the United Nations framework convention on climate change (UNFCCC), Ministry of environment, Republic Indonesia, 2010.
- [2] The United Nations framework convention on climate change (UNFCCC), Kyoto Protocol reference manual: on accounting of emissions and assigned amount, 2008.

ENERGY SAVING POTENTIAL CO₂ MITIGATION ASSESSMENT USING THE ASIA-PACIFIC INTEGRATED MODEL/ENDUSE IN THAILAND ENERGY SECTORE

Puttipong Chunark¹ and Bundit Limmeechokchai¹

¹Sirindhorn International Institute of technology, Thammasat University, Thailand

SUMMARY: As a world has interconnected to the human activities globally, the energy demand is also increasing rapidly. Such activities have also released tremendous amount of GHG emissions, especially CO₂ emissions. Nonetheless, Thailand is classified as Non-Annex I country without commitments for controlling the CO₂ emissions. However, Thailand has started to respond to such commitments. The objective of this study is to give a policy option to a policy maker in climate change issue by using AIM/Enduse model. The AIM/Enduse model is an optimization linear programming approach. There are two scenarios created in this study. The current policy options have been applied in the BAU scenario via four energy demand sectors and energy supply sector. Efficient and advanced technologies have been introduced into the energy system in peak CO₂ scenario. Such a scenario would be expected to meet peak CO₂ emissions between 2035 and 2045.

Keywords: Thai energy sectors, AIM/Enduse, CO₂ emissions scenario, Peak CO₂ emissions, CO₂ mitigation

INTRODUCTION

Climate change is a very important issue nowadays. Various international organizations have focused on the increase of greenhouse gas emissions (GHG) emissions, especially CO₂ emissions. The United Nations Framework Convention on Climate Change (UNFCCC) has convinced developed and invited developing countries to reduce GHG emissions for stabilizing GHG concentration in the biosphere. Moreover, the Intergovernmental Panel on Climate Change (IPCC) Fifth Assessment Report states that "It is very likely that all regions will experience either declines in net benefits or increases in net costs for increases in temperature greater than about 2-3°C" [1].

Thailand is classified as a Non-Annex I country without commitment for controlling the CO₂ emission as a certain level. However, Thailand has started to respond to the international issues for mitigating such emissions. The objective of this study is to provide the policy option for mitigating CO₂ emissions via providing the advanced and efficient technology into the energy system, namely, power sector, industrial sector, residential sector, commercial sector and transport sector. Carbon Capture and Storage (CCS) is an important technology option for cutting down such emissions. Moreover, efficient technologies, high efficient and fuel saving engine in residential, commercial and transport sector are also important for energy-saving and CO₂ mitigation.

METHODOLOGY

The AIM/Enduse model used in this study was developed by National Institute for Environmental Studies, Japan. The AIM/Enduse is based on the cost minimization linear optimization programming approach. This model starts from the flow of energy source, either primary or secondary energy, through the conversion of energy sources by using an energy

technology to serve a final service demand for users or customers. The AIM/Enduse model can be utilized for forecasting the energy demand and CO₂ emissions either in the regional- and country-levels by evaluating the total system cost at an optimal solution [2-4].

There are two scenarios which have been developed in this study, namely, the BAU scenario and peak CO₂ scenario together in the study time horizon of 2005-2050. The current policies, which are implemented for the Thai energy system, have been applied in the BAU scenario. Efficient and advanced technologies have been introduced into the energy system in the peak CO₂ scenario. Such a scenario could give a perspective to a policy maker to fully understand what will happen in the future.

RESULTS

Thailand has currently implemented several energy policies for employing an energy efficient and sustainable development. Thus, in order to examine such policies, the future trend of energy consumption and CO₂ emissions in each energy sector has been proposed under the BAU scenario as follows:

Energy Consumption and CO₂ Emissions

Total energy consumption would increase from 58.8 Mtoe in 2005 to 181.8 Mtoe in 2050 as depicted in Figure 1. According the high energy demand in non-metallic sub-sector, industrial sector has the most energy consumption. The energy consumption in industrial sector would rise from 22.6 Mtoe to 100.3 Mtoe or grow at an annual average growth rate (AAGR) 2.5%. Transport sector also plays an important role for consuming energy in BAU scenario. The energy demand would increase from 23.4 Mtoe to 51.8 Mtoe with AAGR 1.8% between 2005 and 2050. However, the energy demand in residential sector and commercial sector has been slightly increased from 8.9 Mtoe to 19.2

Mtoe and 3.8 Mtoe and 10.5 Mtoe with an AAGR 1.7% and 2.3% between 2005 and 2050, respectively. However, the energy consumption in power sector has not been shown since it has not been accounted for the final energy demand. Therefore, the electricity demand in each energy demand sector has been accounted in the final energy demand.

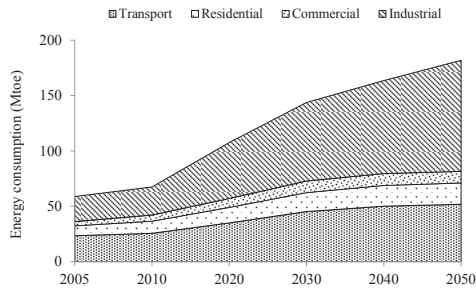


Figure 1. Sectoral Energy consumption in the BAU scenario

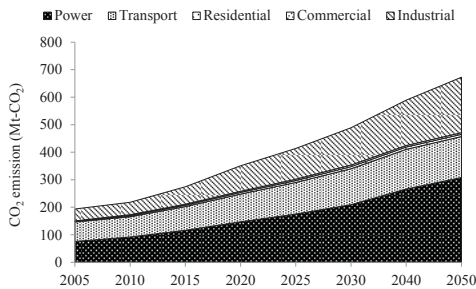


Figure 2. Sectoral CO₂ emissions in the BAU scenario

Total CO₂ emissions would increase from 194 Mt-CO₂ to 672 Mt-CO₂ with an AAGR 2.8% during 2005-2050 as illustrated in Figure 2. Power sector releases the most CO₂ emissions which accounted for 75.5 Mt-CO₂ in 2005 and 307.9 Mt-CO₂ in 2050 according to the usage of natural gas. Although natural gas has lower emission factor than coal and lignite, however, the share of total power plants using natural gas in Thailand is raised simultaneously while following the Power Development Plan and the CO₂ emissions would be 53.1 Mt-CO₂ in 2005 and 196.3 Mt-CO₂ in 2050. Industrial sector is the second largest contributor of CO₂ emissions accounting for 201.5 Mt-CO₂ in 2050.

Potential for Reduction of Energy Consumption and CO₂ Emissions

In this study, advanced technologies and more efficient technologies will be introduced in each energy sector. Mostly, CCS technology can be used for cutting the CO₂ emissions, especially in the

power sector and industrial sector. On the other hand, CCS technology has currently been developed under pilot scales. The implementation of diversified policies, especially the energy efficiency programs in lighting and cooling systems in the residential and commercial sector are also considered to respond to the global issue of conserving the temperature increase to not exceed 2 degree Celsius. The CO₂ emissions will be expected to reach a peak between 2035 and 2045.

ACKNOWLEDGEMENT

The authors would like to acknowledge National Institute for Environmental Studies (NIES), Japan for contributing AIM/Enduse model. The authors would also like to thank Go Hibino, Kazuya Fujiwara and Yuko Motoki from Mizuho Information and Research Institute, Japan for comments, provision and assistant in AIM/Enduse modeling.

References

- [1] IPCC (the Intergovernmental Panel on Climate Change). Climate Change 2014: impacts, adaptation and vulnerability, 2014. Working group II contribution to the Intergovernmental Panel on Climate Change, Fourth Assessment Report, Summary for policymaker.
- [2] Z. Wen et al., Evaluation of energy saving potential in China's cement industry using the Asian-Pacific Integrated Model and the technology promotion policy analysis, *Energy Policy*. **77**, February 2015, pp.227-237, ISSN 0301-4215 (<http://dx.doi.org/10.1016/j.enpol.2014.11.030>)
- [3] M. Kainuma et al., Climate Policy Assessment: Asia-Pacific Integrated Modeling. Springer-Verlag, Tokyo.
- [4] K. Promjiraprawat, P. Winyuchakrit, B. Limmeechokchai, T. Masui, T. Hanaoka and Y. Matsuoka, "CO₂ mitigation potential and marginal abatement costs in Thai residential and building sectors", *Energy and Building*. **80**, 2014, pp. 631-639.

SCENARIO BASED ASSESSMENT OF CO₂ MITIGATION PATHWAYS: A CASE STUDY IN THAI TRANSPORT SECTOR

Pradeep R. Jayatilaka¹ and Bundit Limmeechokchai¹

¹School of Manufacturing Systems and Mechanical Engineering
Sirindhorn International Institute of Technology, Thammasat University, Thailand

SUMMARY: “When to implement actions” and “how much to abate” are two major concerns of policy makers when it comes to policy formulation for CO₂ mitigation. This study investigated the CO₂ mitigation potential in Thailand transport sector under four possible mitigation pathways. Those pathways comprise four mitigation actions and three different time frames as implementation periods (2015, 2025 and 2035 as commencement years). To represent that, along with the BAU case (as reference), four CO₂ countermeasure scenarios were modeled namely L2035, L2025, L2015 and FS. The AIM/Enduse model was used for modeling by taking the planning period of 2010-2050. Results show that L2015 scenario can achieve the highest CO₂ mitigation with 23% cumulative reduction against BAU from 2010-2050. However, due to countermeasure implementation delays (by 10 years in L2025 and by 20 years in L2035), mitigation potentials have dropped by about 25% and 50% in L2025 and L2035, respectively.

Keywords: CO₂ mitigation, transport sector, AIM /Enduse, abatement cost, co-benefits

INTRODUCTION

Global warming due to excessive greenhouse gas emissions is the highest threat faced by the world in this 21st century. Keeping global mean temperature increase below 2 °C (accumulation of 1,150 Gt-CO₂ in atmosphere) [1] when compare to pre-industrial level is the agreed upon target which will result a manageable risk according to forecasts. However, achieving this goal is a greater challenge unless all the nations committed to it.

In regards to this global issue, Thailand, as the second largest energy consumer and CO₂ emitter among ASEAN countries, has an important role to play. In Thailand, when it comes to CO₂ emissions and energy consumption, among set of economic sectors, transport sector receives much more importance since it was responsible for about 28% of CO₂ emissions and has consumed about 35% of total energy used in the country in 2010 [2]. This has further emphasized with high dependency on fossil fuels in the sector and inefficient transport modes.

In recent past, Thai government has developed variety of national development plans such as “20-Year Energy Efficiency Development Plan” and “Alternative Energy Development Plan (AEDP) to improve the sustainability of the energy system and the economy. Focus of them is aligned with the CO₂ mitigation objective since they too aimed to promote efficient technologies, renewable power generation, efficient modes and alternative fuel use in transportation etc. Nevertheless, in the transport sector, yet, significant progress can only be seen in fuel switching from fossil oil to bio-fuels. Moreover, successful implementation of proposed countermeasures depends on variety of factors such as proper investment, public acceptance and availability of technologies. Hence, actual implementation time frames and abatement quantities of those countermeasures are ambiguous. Therefore, in order to retrofit the current plans and

for the development of new strategies, it is required to analyze possible pathways of CO₂ mitigation.

In literature, even though few studies can be found that has analyzed CO₂ emission in Thai transport sector, none has taken into account the time factor of actual implementation of actions. Hence, the objective of this paper is to analyze four likely alternative pathways of CO₂ mitigation in Thai transport sector to check their mitigation potentials and impacts on energy system.

METHODOLOGY

The AIM/Enduse model was used to model Thai transport sector. It is a bottom-up optimization model with detailed technology selection framework [3]. The transport sector was modeled as 16 vehicle categories which comprise 11 passenger and 5 freight transportation categories belonging to land, water and air modes. Planning period was selected as 2010-2050 with base year as 2010.

Fuel switching, penetration of advanced technologies, modal shift and travel demand management (TDM) have been considered as mitigation actions. Since fuel switching action has already been initiated in Thailand successfully, only its penetration has been increased in countermeasure (CM) scenarios. The rest has considered as new actions. Together with the BAU, four CM scenarios have been developed as given below.

- 1) L2015: This models implementation of all the actions from 2015 onwards.
- 2) L2025: This scenario assumes 10 year delay in implementation of new actions
- 3) L2035: This assumes 20 year delay in implementation of new actions
- 4) FS (Fuel Switching only): This examines the mitigation potential of fuel switching action alone if new actions will not be successful.

In addition to investigating peak CO₂ abatements, energy savings and fuel mix changes

under developed scenarios, abatement costs and individual mitigation potentials of considered actions have also been examined. Furthermore, co-benefits of CO₂ mitigation in terms of energy security and local air pollutants have also been analyzed.

RESULTS AND DISCUSSION

CO₂ emission trends under modeled scenarios are presented in Figure 1. As it can be seen, L2015 has the highest abatement potential with 23.1% cumulative reduction of CO₂ emission (840 Mt-CO₂) against the BAU from 2010-2050. Although emission has reduced in other CM scenarios, reduction potential has significantly dropped due to delay in initiation of actions. However, even in FS scenario (only fuel switching action), CO₂ emission has been reduced by 8.8% cumulatively, against the BAU due to higher penetration of bio-fuels.

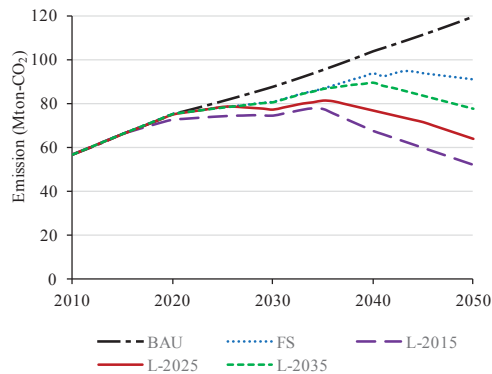


Figure 1. CO₂ emissions in all scenarios

Energy consumptions in all scenarios in the base year and 2050 are given in Figure 2. It clearly shows that, in the CM scenarios, total energy consumption has reduced along with fossil fuel share. When compared with the 2050BAU, even though reduction in energy consumption is low in FS, fuel mix has changed where more penetration can be seen in bio-diesel blends and ethanol blends. The rest of CM scenarios has also followed a similar pattern with more energy saving potentials. However, it is a significant fact that by 2050, in L2015, gasoline, Liquefied Petroleum Gas (LPG) and Compressed Natural Gas (CNG) shares have dropped to insignificant levels while electricity consumption has increased considerably due to penetration of EVs and plug-in hybrids.

Abatement cost calculations show that modal shift and TDM give cost savings along with moderate mitigations where earlier implementation can provide higher mitigations without much change in cost. Furthermore, among efficient technologies, penetration of high efficient Internal Combustion Engine (ICE) vehicles can also give cost saving. In L2035, it has the highest mitigation share. However,

in L2015, highest level of mitigation has been recorded from EVs and plug-in hybrids, although their abatement costs are considerably high. Furthermore, mitigation potential of hybrid vehicles has been increased when it penetrates earlier in time, while its cost of abatement fluctuates around US\$ 45/t-CO₂.

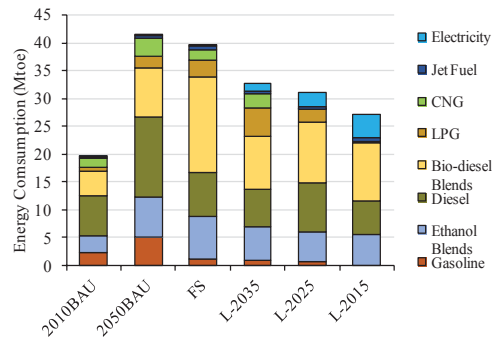


Figure 2. Energy consumption in scenarios in the base year and 2050

Under co-benefit analysis, NO_x, SO₂, CO and PM were selected as air pollutants in this study. Results show that cumulative emissions of all those gases have reduced in all the CM scenarios considered where highest reduction recorded under L2015 as expected. Impact on energy security was analyzed using four indicators namely, diversity of fuel mix, non-carbon based fuel portfolio, energy intensity and CO₂ intensity. Results show that CO₂ mitigation will positively impact with significant level on energy security with respect to all analyzed indicators.

ACKNOWLEDGMENT

Authors would like to thank National Institute for Environment Studies (NIES), Japan and Mizuho Information and Research Institute, Japan for the financial assistance and support received. Authors would also like to acknowledge Sirindhorn International Institute of Technology, Thammasat University for the scholarship provided.

References

- [1] National Research Council, "Climate Change: Evidence, Impacts and Choices", 2012. National Academy of Sciences; Washinton D.C.
- [2] Department of Alternative Energy Development and Efficiency, "Annual Report: Thailand Energy Situation 2011". Ministry of Energy; Bangkok.
- [3] M. Kinuma, Y. Matsuoka and T. Morita, "The AIM/end-use model and its application to forecast Japanese carbon dioxide emissions", *European Journal of Operational Research*. **122**(2), 2000, pp.416-425.

ENERGY CONSUMPTION AND GREENHOUSE GAS EMISSION FROM CERAMIC TABLEWARE PRODUCTION: A CASE STUDY IN LAMPANG, THAILAND

Panatda Riyakad¹ and Siriluk Chiarakorn¹

¹Division of Environmental Technology
School of Energy, Environment and Materials
King Mongkut's University of Technology Thonburi, Thailand

SUMMARY: This paper presents energy consumption and greenhouse gas (GHG) emission from ceramic tableware production in Lampang, Thailand. All data of energy consumption in ceramic production were collected from a small enterprise manufacturing plant and the unit of analysis was 1 kg of product. A scope of study was gate to gate. The amount of GHG emission in a unit kgCO₂e/kg of product was calculated by 2006 IPCC Guidelines for National Greenhouse Gas Inventories method [1] and the emission factors were referred from Thailand Greenhouse Gas Management Organization (TGO) [2] and IPCC databases [3]. The results showed that the total energy consumption from ceramic tableware production was 24.28 MJ/kg of product and almost 98% of total energy consumption was from liquefied petroleum gas (LPG) consumption during firing. The amount of GHG emission was 0.236 kgCO₂e/kg of product. The glost firing was found to be a hotspot of energy consumption and GHG emission.

Keywords: energy consumption, greenhouse gas emission, ceramic tableware, ceramic production, Lampang

INTRODUCTION

In Thailand, Lampang's ceramic tablewares have been well known for long times. The most famous product, "Cham tra kai" a ceramic tableware with a hen design is the signature of Lampang. But nowadays, Lampang ceramic industry has suffered from energy crisis because the cost of energy, i.e. LPG, has been continuously increasing. As a result many small plants have been shutdown. Ceramic production is not only one of industry that consumes high energy but also emits high greenhouse gases (GHG) which causes global warming. However, the database of energy consumption as well as GHG emission from tableware ceramic production has not been available. Therefore, this research aimed to evaluate the energy consumption and GHG emission from ceramic tableware production from a small enterprise manufacturing plant in Lampang, Thailand. The hotspots of energy consumption and GHG emission were identified. The output results could be valuable information for energy conservation and GHG management in ceramic tableware production.

METHODOLOGY

The activities data were collected from a small enterprise manufacturing plant in Lampang, Thailand. The major ceramic tableware production comprised of six processes: forming, drying, biscuit firing, glazing, glost firing and quality checking, which is in a boundary of gate to gate. The selected ceramic tableware product was a stoneware plate (7 inches diameter). The forming process was jiggering method. The material flows in each manufacturing process were analysed, based on the functional unit of 1 kg product. The amount of GHG emission was calculated by IPCC 2006 method. The emission factors were from TGO and IPCC databases. The

GHG emission in a unit of kgCO₂e/kg of product was calculated by Eq. (1).

$$\text{GHG emission} = \sum [\text{Activity data (unit)} \times \text{EF}] \quad (1)$$

where

EF: Emission factor (kgCO₂e/unit)

RESULTS AND DISCUSSION

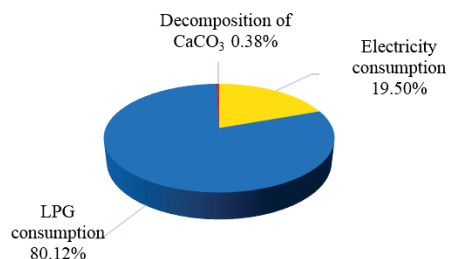


Figure 1. Percentages of GHG emissions divided by sources in ceramic tableware production (gate to gate)

Major energy sources consumed in ceramic tableware production were from electricity and LPG. The total energy consumption of ceramic tableware production was 24.28 MJ/kg of product, contributed by electricity only 1.11% and LPG 98.89%. Glost firing process was determined as a hotspot of energy consumption, accounted for 68.25% of total energy consumption. The GHG emissions from ceramic tableware production were from the consumption of energy (electricity and LPG) and the decomposition of calcium carbonate (CaCO₃) during glost firing. Total GHG emission was 0.236 kgCO₂e/kg of product. From Figure 1, the largest GHG emission was from LPG (80.12%), followed by electricity consumption (19.50%) and decomposition of

calcium carbonate (0.38%). Similar to the energy hotspot, glost firing process was also found to be the hotspot of GHG emission with the largest share of 55.49% of total GHG emission. Thus, the energy conservation and GHG mitigation options for ceramic tableware production should be focused in glost firing process.

ACKNOWLEDGEMENT

The authors would like to express to their gratitude to the National Research Council of Thailand (NRCT) for financial support. The authors would like to thank Chupra Co., Ltd. for their kind collaboration in data collection and field survey. The authors also thank Lampang Ceramic Association (LCA) for their kind collaboration and supports.

Reference

- [1] Intergovernmental Panel on Climate Change (IPCC), *IPCC Guidelines for National Greenhouse Gas Inventories*, 2006, Available online: <http://www.ipcc-nggip.iges.or.jp/public/2006gl/>
- [2] Thailand Greenhouse Gas Management Organization (TGO), *Emission Factor CFP*, 2014, Available online: <http://thaicarbonlabel.tgo.or.th/carbonfootprint/index.php?page=9>.
- [3] L. Hanle et al., "Chapter 2: Mineral Industry Emissions", *IPCC Guidelines for National Greenhouse Gas Inventories*, **3**, 2006, pp.2.35.

Fuel Cell Technology

COMPUTATIONAL MODELLING OF THE FLOW FIELD OF AN ELECTROLYZER SYSTEM USING CFD

Alhassan Salami Tijani¹, Danial Barr¹ and A. H. Abdol Rahim¹

¹Faculty of Mechanical Engineering, Universiti Teknologi MARA
Shah Alam, Selangor, Malaysia

SUMMARY: A bipolar plate is one of the primary components in a Polymer Electrolyte Membrane (PEM) electrolyzer which contributes to its hydrogen production efficiency. Its primary function is to distribute the flow of a fluid, in this case water, evenly over the active area of an electrolyzer cell. A well designed and optimized bipolar plate is required to produce an efficient and cost effective PEM electrolyzer stack. In this paper optimal flow plate design and computer models of several available flow plate designs were constructed, and then run through a numerical simulation to evaluate both the hydrodynamic properties they exhibited, the velocity field and pressure gradients. Results indicate that under the specified conditions, the pressure gradient decreases diagonally along the bipolar plate, from the inlet to the outlet. However, the sharpness, or evenness of the pressure gradient varies depending on the design of the bipolar plate. The velocity fields also follow the same general trend, only that they increase in magnitude as they approach the outlet rather than decrease. However, the magnitude of their velocity in the middle of the plates, especially in some of the designs, such as in the multi-pass serpentine designs, varies randomly within a certain range rather than decreasing or increasing evenly, it is only at the outlet that the velocity gradient becomes more consistent.

Keywords: Hydrodynamic properties, Simulation, PEM Electrolyzers, Hydrogen production

INTRODUCTION

PEM Electrolyzers are essentially inverted fuel cells, where, instead of generating electricity by harnessing the reaction potential of hydrogen and oxygen to form water, it instead consumes energy to split water into hydrogen and oxygen. The main issue with this device is that it's components can be costly, thus requiring that designs be tested rigorously by simulation, before they are actually fabricated. It's cost also hampers the mass manufacture of the device, thus requiring the development of more cost effective designs before this system becomes truly effective.

The hydrodynamic properties of the flow field on the anode side of the electrolyzer stack play an important part in improving the efficiency of the device. A high operating pressure with an even pressure distribution across the reaction surface of the PEM helps to reduce the internal cell resistance, thus reducing the required power output to initiate electrolysis [1]. This also allows for the production of compressed hydrogen gas, thus facilitating storage as noted by Tsiplakides [2]. This is due to the fact that, compressing water consumes much less energy comparing to the energy required for compressing gas state hydrogen as was found by Onda et al [3]. Also of note, is that the gradient of reduction in voltage is the highest between atmospheric pressure and 1 MPa [4] thus, meaning that the pressure threshold for high pressure electrolysis is 1 MPa and above.

In order to achieve such ideal conditions, the design of the flow field is once again of paramount importance. The design in question must maintain the aforementioned fluid flow characteristics so as to minimise turbulence within the flow field.

HYDRODYNAMIC MODEL OF THE BIPOLAR PLATE

A bipolar plate is a structure in a PEM electrolyzer that channels the flow of water over the reactionary surface of the membrane. It is generally constructed out of a metal plate which has grooves machined into it to provide passage for water to flow over the reactionary sites of the membrane. The fluid, in this case, water, is supplied to an inlet and outlet channel machined through the plate, resulting in a flow field. Base on the parameters in Table 1, geometrical models were developed in CATIA which were later imported into ANSYS FLUENT software package for simulation and visualization of their flow patterns. When loaded onto ANSYS, the direction of flow for the fields were determined, with the inlet being relatively close to the origin point while the outlet is on a diagonal opposite of the inlet as illustrated in Figure 1. The models we constructed to similar external dimension, with flow field area or approximately 0.01m².

Table 1: Common parameters of the simulated designs

System Parameters	Values/Properties
Flow field surface area	0.01m ²
Operating pressure	8 MPa or 80 bar
Operating temperature	27°C or 300K
Internal wall condition	No slip, Eulerian

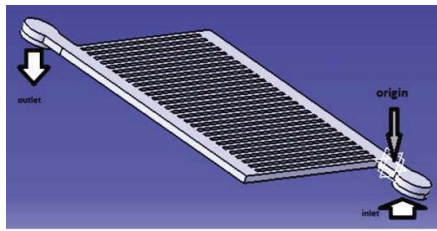


Figure 1. Flow directions into/out of the flow field

RESULT AND DISCUSSION

The general pattern of pressure distribution across the flow field of all the designs appears to be a gradual drop in pressure diagonally across the flow field from the inlet to the outlet as is visible in the Figure 2 (a), (b) and (c). The reason for this drop in pressure can be attributed to several factors, some of them being losses due to drag, or simply due to kinetic losses from in-flow turbulence. However the factors behind the pressure drop are not of as much concern as the effect flow field geometry has on the pressure gradient. Figure 2(d) is an overlay for the pressure gradient of the three designs. The readings were taken along a plane perpendicular to flow direction bisecting the flow field at Z=0.05m. The readings show that the pressure gradient for each design is significantly different, with the parallel flow field displaying the most gradual pressure drop of about 5MPa across the field, while both serpentine variants, that is the single and two-pass fields, record losses of up to 7MPa.

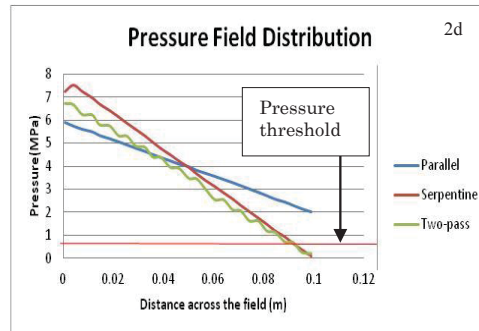
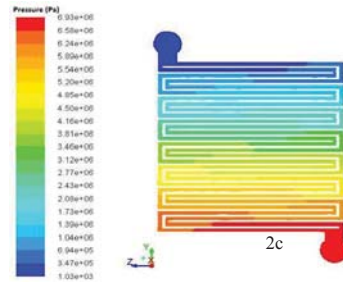
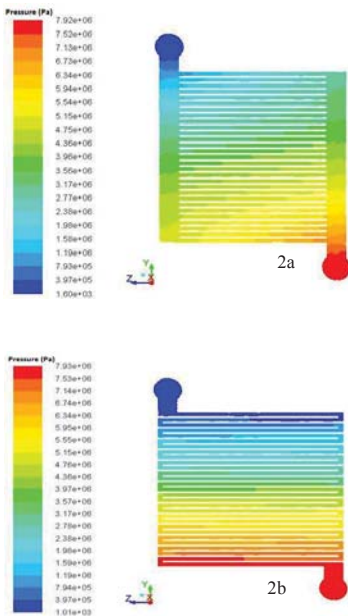


Figure 2. Pressure distribution across the flow fields (a) parallel flow field (b) serpentine flow field single pass (c) serpentine flow field, (d) pressure gradient of the three designs.

References

[1] Ö. F. Selamet, F. Becerikli, M. D. Mat, and Y. Kaplan, "Development and testing of a highly efficient proton exchange membrane (PEM) electrolyzer stack," *International Journal of Hydrogen Energy*, **36**, 2011, pp. 11480-11487.
 [2] D. Tsiplakides. PEM water electrolysis fundamentals. Available: http://research.ncl.ac.uk/sus/hgen/docs/summerschool_2012/PEM_water_electrolysis-Fundamentals_Prof._Tsiplakides.pdf
 [3] K. Onda, T. Kyakuno, K. Hattori, and K. Ito, "Prediction of production power for high-pressure hydrogen by high-pressure water electrolysis," *Journal of Power Sources*, **132**, 2004, pp. 64-70.
 [4] S. K. Mazloomi and N. Sulaiman, "Influencing factors of water electrolysis electrical efficiency," *Renewable and Sustainable Energy Reviews*, **16**, 2012, pp. 4257-4263.



OPTIMIZATION OF DIRECT COUPLING SOLAR PV PANEL AND ADVANCED ALKALINE ELECTROLYZER SYSTEM

A. H. Abdol Rahim¹, Alhassan Salami Tijani¹, Muhammad Fadhulllah¹, S. Hanapi¹ and K.I. Sainan¹

¹Faculty of Mechanical Engineering, Universiti Teknologi MARA
Shah Alam, Selangor, Malaysia

SUMMARY: In this paper, mathematical model and simulation for optimization of direct coupling solar photovoltaic (PV) panel and advanced alkaline electrolyzer is presented. The simulation models related the PV panel and the advanced alkaline electrolyzer are constructed in MATLAB Simulink environment. Results related power-voltage characteristics and the current-voltage characteristics of both systems have been presented. Simulation studies were carried out at different operating temperatures (40, 60 and 80°C) for the advanced alkaline electrolyzer. It was observed that the operating voltage that corresponds to 80°C results in the smallest operating voltage compared to the other two operating temperature. The results show that the difference in operating temperatures did not have any significant effect on Faraday's efficiency of the electrolysis process. However, Faraday's efficiency increases sharply to a maximum of about 98% at current density of 90mA/cm². At solar irradiance of 1000W/m², the PV was observed to produce a maximum power of about 60W. This power was matched against the voltage requirement of the advanced alkaline electrolyzer. The number of cells of the advanced alkaline electrolyzer was varied to give an optimum number of cells that can match the available power from the PV.

Keywords: Matlab Simulink, electrolyzer, mathematical model, direct coupling

INTRODUCTION

Continual use of the conventional energy sources poses threat to the environment. The climate change, pollution, and greenhouse gas emission are among the examples. Shifting to a better alternative energy such as the solar and wind energy system can be a better solution. They are renewable thus do not deplete with time. The advantage of hydrogen is that it may be used as fuel in almost every application powered by fossil fuels today and without harmful emissions [1]. Since it can be used to fuel various applications, hydrogen had been deemed as a promising future energy carrier [1, 2]. Hydrogen gases can be produced by water splitting process or known as electrolysis. Water splitting process requires electricity to flow through electrode and water in order to break their molecule into hydrogen and oxygen.

During the past decade, several methods have been utilized to harvest the hydrogen. However, the only state-of-the-art technique is the advanced water electrolysis. The application of hydrogen as fuel had been made practical since water electrolysis is a mature and commercially available technology which is widely being used for generating hydrogen capacities ranging from few cm³/min to thousands m³/h [3]. The hydrogen produced can be directly feed to be used by fuel-generated applications or stored into storage tanks.

The use of solar PV to generate electricity as the power generator for alkaline electrolyzer ensures an environmental-friendly system. Numerous researchers have been focusing on the direct coupling of the PV and alkaline electrolyzer.

THEORETICAL CONCEPT OF ADVANCED ALKALINE ELECTROLYSIS / TECHNOLOGY

The technology alkaline electrolysis is most widely used for water electrolysis in which the electrolyte is liquid [4, 5]. The major difference between conventional alkaline electrolyzers and advanced alkaline electrolyzers is that, the operational cell voltage has been reduced and the current density increased in advanced alkaline electrolyzers. Typically the new advanced commercial alkaline electrolyzers operate with current densities up to 500 mAcm⁻² and system efficiency near to 83% referred to the higher heating value (HHV) [6].

An alkaline electrolyzer consists mainly of a container, electrolyte, anode cathode and diaphragm. The two main design technology configurations are unipolar (tank) and bipolar (filter press). In the unipolar design the electrodes, anodes and cathodes are alternatively suspended with parallel electrical connection of the individual cells while in the bipolar design the individual cells are linked in series electrically and geometrically.

RESULTS AND DISCUSSION

The Simulation result in Figure 1 shows that as the current input is increased, the cell voltage also increased. The reason behind this phenomenon was merely due to the dissociation of the water molecules into hydrogen and oxygen molecules. As there are more water molecules to be dissociated, the values of V_{cell} will keep increasing according to the current. Thus, when the current is increased, more water molecules are dissociated which means that more voltage needed to overcome the process of splitting the water. Figure 1 also shows that the voltage values

are different according to the operating temperature of the advanced alkaline electrolyzer. Simulation studies are carried out at different level of temperatures which are at 40°C, 60°C and 80°C. At highest temperature which is 80°C, the voltage is much smaller compared to the other two operating temperature.

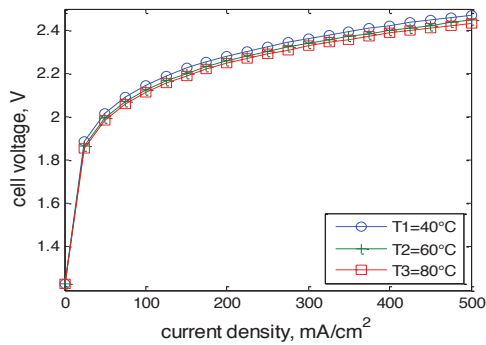


Figure 1. cell voltage against current density

As illustrated in Figure 2, the higher current supplied to the advanced alkaline electrolyzer increases the hydrogen flow rate. This is related to the basic dissociation of water molecules. Whenever there are more current supplied, there are more water dissociation process occurs thus the amount of hydrogen ions which are dissociated are higher.

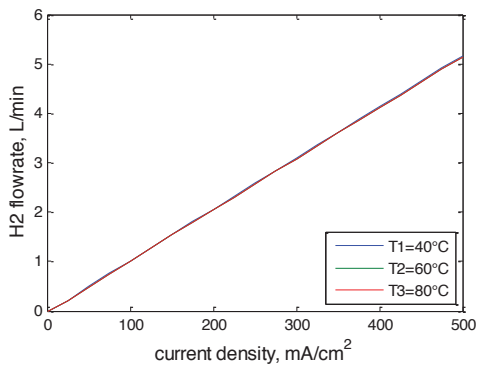


Figure 2. H₂ flowrate against current density

The graph in Figure 3 shows the I-V characteristics of the PV generator simulated at different solar irradiance. Results obtained shows that the current and voltage are affected by the irradiance. At 1000 W/m² solar irradiance, the current produces by the generator are much greater than at lower values of irradiance. This is because of the light-generated current produces by the PV generator increase as the irradiance increase.

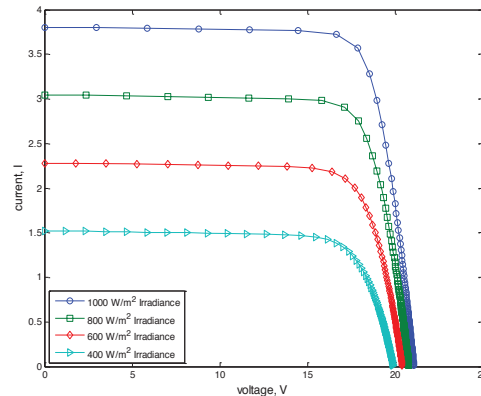


Figure 3. I-V characteristics of PV at different solar irradiation

References

[1] M. Shen, N. Bennett, Y. Ding, and K. Scott, "A concise model for evaluating water electrolysis," *International Journal of Hydrogen Energy*, **36**, 2011, pp. 14335-14341.

[2] T. N. Veziroglu and F. Barbir, "Solar-Hydrogen Energy System: The Choice of the Future," *Environmental Conservation*, **18**, 1991, pp. 304-312.

[3] F. Barbir, "PEM electrolysis for production of hydrogen from renewable energy sources," *Solar Energy*, **78**, 2005, pp. 661-669.

[4] A. H. Abdol Rahim, A. S. Tijani, W. A. N. Wan Mohamed, S. Hanapi, and K. I. Sainan, "An Overview of Hydrogen Production from Renewable Energy Source for Remote Area Application," *Applied Mechanics and Materials*, **699**, 2014, pp. 474-479.

[5] A. S. Tijani, N. A. B. Yusup, and A. H. A. Rahim, "Mathematical Modelling and Simulation Analysis of Advanced Alkaline Electrolyzer System for Hydrogen Production," *Procedia Technology*, **15**, 2014, pp. 799-807.

[6] O. Ulleberg., "Modeling of advanced alkaline electrolyzers: a system simulation approach," *International Journal of Hydrogen Energy*, **28**, 2003, pp. 21-23.

EFFECTS OF PROCESSING VARIABLES ON FORMATION OF THIN ELECTROLYTE FILMS FOR SOFCs

Anuwat Srisuwan¹, Suthee Wattanasiriwech¹, Darunee Wattanasiriwech¹, and Pavadee Ankawattana²

¹Mae Fah Luang University, Chiangrai, Thailand

²National Metal and Materials Technology Center, Thailand

SUMMARY: Effects of processing variables on formation of thin 8YSZ electrolyte films on the porous screen-printed anode/Ni-NiAl₂O₄ support are presented in this paper. The screen-printed support design was Ni-8YSZ functional anode (thickness ~5 μm) on the thick NiO-NiAl₂O₄ (1:1 weight ratio) support. Average pore size and porosity of the anode functional layer was made to be around 1.1 μm and 37% respectively. 8YSZ electrolyte layer was fabricated via an electrophoresis deposition with variations of voltage (10, 20, 30 V) and deposition time (20, 30, 40 s). It was shown that at 10 V for 20 s, the thin layer was only loosely deposited while adjusting the voltage to 20 V resulting in a smooth film surface. Further increasing the voltage to 30 V gave an adverse result. However, these films were not yet densified after co-sintering and reduction in H₂ atmosphere. Further attempt was done by increasing the deposition time to 30 s at 20 V. This resulted in a densely packed microstructure arrangement. Further increasing the deposition time to 40 s gave rise to layer cracking. Electrical performance of the cells was measured at the temperature range of 500-800 °C under H₂/O₂ atmosphere. The highest power density obtained was 70 mW/cm². Impedance spectroscopy analysis indicated the ohmic resistance of 6 Ω·cm² while the total resistance was found to be 49 Ω·cm².

Keywords: solid oxide fuel cells, electrophoresis deposition, impedance spectroscopy, external support

INTRODUCTION

Solid oxide fuel cells (SOFCs) are the electrochemical devices that produce clean electrical energy from chemical energy stored in the fuels, primarily hydrogen and hydrocarbon [1,2]. SOFCs could be used with a variety of fuels and also showed promising conversion efficiency, so a great deal of development research on this type of fuel cell has been undertaken [3,4].

SOFCs configuration is based on sandwiching the dense electrolyte between the anode and cathode whose mixed conduction modes between electronic and ionic are highly required. In the conventional anode support design, a conducting metal, typically Ni, is mixed with the electrolyte powder in order to reduce the thermal stress and also to enhance the ionic conduction. Attempts to use external supports in order to reduce the thickness of the expensive anode, which in turn gave rise to lower polarization of the anode layer were reported [5-6]. Metal such as stainless steel were reported to be a promising external support as it is cheap and does not require complicated fabrication technique [5]. Thermal mismatching between the metal support and the cermet anode layer was the concerns as cyclic operation may result in thermal stress and layer cracking. The use of ceramic support such as alumina was found to result in a dense interlayer which was harmful to gas diffusion to the next layer [6].

Fabrication of dense electrolyte layers could be achieved by many methods such as tape casting, sol-gel, vapor phase, and screen-printing. These methods presented some drawbacks. Electrophoresis deposition was the technique used for fabrications of thin layers using a simple apparatus [7]. Very thin layers with a thickness of less than 10 micrometer

could be fabricated. In this method, stable slurry of the material to be deposited was prepared. Particle size homogeneity of the powder played an important role in controlling microstructure arrangement of the final products [8].

In this paper, the use of an external support was reported. This support was prepared from alumina ceramic mixed with NiO. The powders were mixed in a proportion to form pre-designed conducting Ni/NiAl₂O₄ cermet after firing and reduction in hydrogen. The anode layer was then coated using a screen-printing method. Fabrication of the electrolyte layer using an electrophoresis was studied. Effects of the fabrication conditions, coating time and voltage on the coating layers were examined. Electrical performances of the single cells were measured at the temperature range of 500-800 °C under H₂/O₂ atmosphere.

METHODOLOGY

The designed final weight ratio between NiO and NiAl₂O₄ was 1:1. The weighed NiO and Al₂O₃ powders were mixed in a vibrational mill before uniaxially pressed to form cylindrical supports. The supports were then fired at 1400°C for 1 h before prior to reduction at 750-800 °C in H₂ atmosphere. Phase, microstructure, porosity and electrical conductivity and bending strength of the supports were examined using XRD, SEM, water absorption and 4-point probe methods. For fabrication of the cells, the NiO-8YSZ anode paste was applied on the support pre-fired at 1000 °C using a screen-printing technique. The screen-printed supports were coated with carbon to enhance conductivity before being placed on a copper plate attached in the negative side during the electrophoresis deposition. Stainless steel is used as an inert positive electrode.

The deposition was performed with variations of voltage from 10, 20, 30 V and deposition time of 20, 30, 40 s. Cell performance was measured at the temperature range of 500-800 °C under H₂/O₂ atmosphere. Platinum was used as the cathode and also the current collector. Polarisation of the cells was examined using an impedance spectroscopy (Solartron SI 1260). Cell configuration for performance testing is shown in Figure 1.

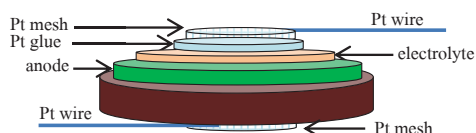


Figure 1. The model picture shows cell configuration for the performance testing.

RESULTS AND DISCUSSION

XRD analysis showed that the fired support contained mixed phases of NiO and Ni₂Al₂O₄ only. After reduction at 750 °C, there appeared reflections according to Ni while NiO peaks were still observed, suggesting that some of the NiO phase had transformed into Ni. Reflections according to the NiO had disappeared after reduction at 800 °C suggested that this condition was suitable to use. This support showed, porosity, flexural strength and conductivity at 800 °C of 32%, 80 MPa and 1300 S·cm⁻¹ respectively. The screen-printed anode layer contained porosity of around 30% after reduction with a layer thickness of 5 μm.

8YSZ electrolyte slurry was deposited onto the bi-layer supports with variations of voltage from 10, 20 and 30 V. It was shown that at 10 V for 20 s, the thin layer was only loosely deposited while adjusting the voltage to 20 V resulting in a smooth film surface. Further increasing the voltage to 30 V gave an adverse result. However, the films were not yet densified after co-sintering and reduction in H₂ atmosphere. The deposition time was then increased to 30 and 40 s. Increasing the deposition time to 30 s at 20 V resulted in a densely packed microstructure arrangement.

Electrical performance of the cells was measured at the temperature range of 500-800 °C under H₂/O₂ atmosphere. The highest power density obtained was 70 mW/cm² (Figure 2). Impedance spectroscopy analysis indicated the ohmic resistance of 6 Ω·cm² while the total resistance was found to be 49 Ω·cm².

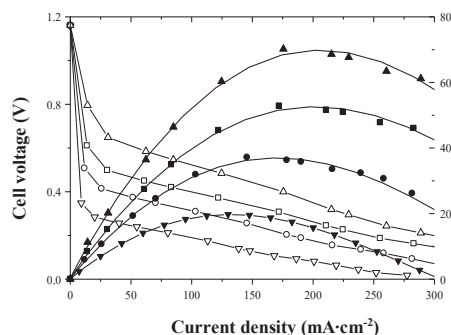


Figure 2. Electrical performance of the cells measured at various temperatures.

ACKNOWLEDGMENT

We are grateful for financial support from Mae Fah Luang University, Thailand and Thailand Graduate Institute of Science and Technology.

References

- [1] S.P.S. Badwal, S. Giddey, C. Munnings, A. Kulkarni, "Review of Progress in High Temperature Solid Oxide Fuel Cells," *Journal of the Australian Ceramics Society*, **50**[1], 2014, 23 – 37.
- [2] S. Park, J. M. Vohs, R.J.Gorte, Direct oxidation of hydrocarbons in a solid oxide fuel cell," *Nature*, **404**(16), 2000, pp265-267.
- [3] T. Talebi, "The role of addition of water to non-aqueous suspensions in electrophoretically deposited YSZ films for SOFCs," *International Journal of Hydrogen Energy*, **35**(17), 2010, pp 9434-9439.
- [4] T. Yamaguchi, S. Shimizu, T. Suzuki, Y. Fujishiro and M. Awano, "Fabrication and evaluation of a novel cathode-supported honeycomb SOFC stack," *Materials Letters*, **63**(29), 2009, pp 2577-2580.
- [5] Y.B. Matus, L.C. De Jonghe, C.P. Jacobson, S.J. Visco, "Metal-supported solid oxide fuel cell membranes for rapid thermal cycling," *Solid State Ionics*, **176**(5-6), 2005, pp 443-449.
- [6] A. Srisuwan, D. wattanasiriwech, S. wattasiriwech, and P. Aungkavattana, "Preparation of NiO-Ni₂Al₂O₃ Composite and Its Feasibility to use as an External Support for SOFC," *Proceedings of 7th International Conference on Materials Science and Technology (MSAT7)*, 7-8 June 2012, Thailand.
- [7] L. Besra, "Electrophoretic deposition on non-conducting substrates: the case of YSZ film on NiO-YSZ composite substrates for solid oxide fuel cell application," *Journal of Power Sources*, **173** 2007, pp 130-136.
- [8] M. Meepho, S.Wattanasiriwech, P. Angkavattana, and D. Wattanasiriwech, "Application of 8YSZ nanopowder synthesized by the modified solvothermal process for anode supported solid oxide fuel cells," *Journal of Nanoscience and Nanotechnology*, **15**(1-5), 2015, pp. 2570-2574.

THE SOLID OXIDE FUEL CELL (SOFC) AND GAS TURBINE (GT) HYBRID SYSTEM NUMERICAL MODEL

Penyarat Saisirirat¹

¹Department of Mechanical Engineering Technology
College of Industrial Technology, King Mongkut's University of Technology North Bangkok, Thailand

SUMMARY: Fuel cells when combined with conventional turbine power plants offer high efficiencies. The feature of certain fuel cells (Solid Oxide Fuel Cell or SOFC, Molten Carbonate Fuel Cell or MCFC), which makes them suitable for hybrid or combined systems, is their high operating temperature. In this work, a detailed thermodynamic model of SOFC and Gas turbine hybrid system is simulated in MATLAB. Few configurations of the combined or hybrid cycles are proposed and analyzed. A comparative study based upon performance parameters, such as SOFC power and turbine inlet temperature is used to select the better configuration. Simple thermodynamic models for the compressor and turbine are used during the configuration selection. The results are compared to the available literature.

Keywords: efficiency, gas turbine, hybrid, model, solid oxide fuel cell

INTRODUCTION

The solid oxide fuel cell (SOFC) power plant is known to be a potential alternative in the electric utility for commercial and industrial sectors. It produces less harmful chemical and acoustic emissions at higher efficiency than the conventional technologies. SOFC operates at temperatures high enough to enable the direct reformation of natural gas to hydrogen, electrochemically producing both electrical power and high-grade waste heat for combined heat and power (CHP) system. It has been demonstrated by simulation technique that SOFC can achieve 50% net electrical efficiencies and have already been considered feasible for integration with multi-MW gas turbine engines [1]. Siemens-Westinghouse Power Corporation developed the first advanced power system, which integrates a SOFC stack with the gas turbine engines. The pressurized (3 atm) system generates 220 kW of electrical power at a net electrical efficiency of 55% [2]. Based on the works in the previous study [3], the author further develops the hybrid SOFC-GT power system model. The emphasis of this study is to reduce the reliance on experimental data for plant performance prediction.

SOFC – GAS TURBINE HYBRID SYSTEM MODELS

In this work, a few configurations of the hybrid system are simulated and their performances are analyzed. Based upon the comparative study, the better configuration is chosen and discussed in detail. The basic parameters that are focused at, in choosing the optimum configuration, are the cycle efficiency and the fuel cell power. The first configuration has been chosen based upon the idea that since combustor exhaust is at high temperature, even the low mass flow rate will be enough to heat the fuel stream to a required temperature. The second configuration is the proposed configuration and the only difference is that here both (fuel and air) the streams are heated by the turbine exhaust.

Both configurations are shown below in figures 1 and 2. For both configurations the compressor, SOFC, turbine and combustor efficiencies are 68.5%, 45%, 88.4% and 100 %, respectively.

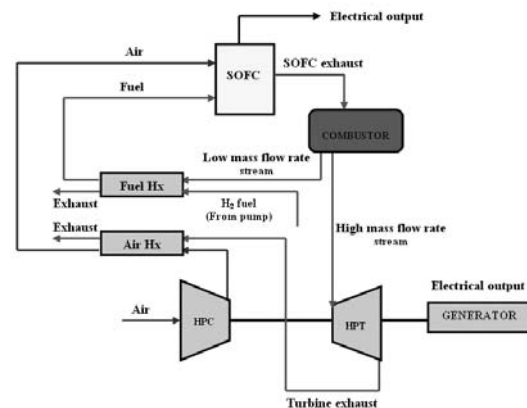


Figure 1. Schematic of the first configuration

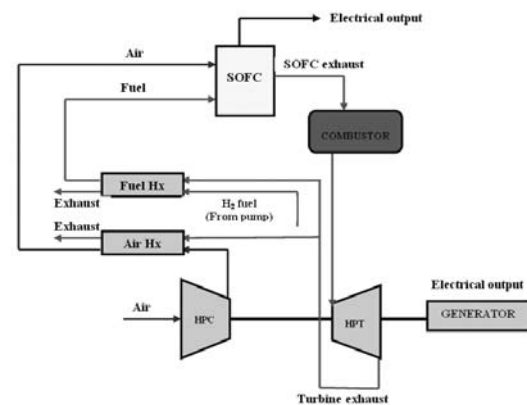


Figure 2. Schematic of the second configuration

A gas turbine cycle is based on the Brayton cycle, which is a simple series of compression,

combustion, and expansion processes. The main components of the cycle are a compressor, a combustor, and a gas turbine. The number of components is not limited to three as the cycle may consist of several compressors and turbines. Gas turbine engines are generally used for power production falling in the range of few kilowatts to several megawatts and offer an electrical efficiency of 30-40%. This can be further improved by adding a topping cycle to achieve efficiencies of up to 60%.

A SOFC stack has been modeled using MATLAB. Other components of the hybrid system like heat exchanger, compressor, gas turbine, and combustor have been modeled using the same simulation tool. All the components have been integrated to form a cogeneration power system and thermodynamic behavior the cycle is being studied. Hydrogen is used as fuel that the composition by mol is 97% H₂ and 3% H₂O. Air composition by mol is 21% O₂ and 79% N₂. The fuel pump power is not included while calculating the cycle efficiency. Pressure losses in the fuel cell, combustor, and piping are negligible. The combustor of the model is based on simple combustion reactions and the complete system is adiabatic. The operating conditions for the cycle components are the compressor pressure ratio and turbine pressure ratio is 2.9. Design temperature and pressure is 25 °C and 1 atm. For SOFC that is a current density equal to 1.00 A/cm² and cell voltage equal to 0.8 volt. It was selected from a polarization curve that was produced in MATLAB.

RESULTS AND DISCUSSION

Table 1. Comparative result for two configurations

	Config. 1	Config. 2
Fuel flow (g/s)	9.62	9.62
Air flow (g/s)	400	400
SOFC temp (°C)	944	832
Turbine Inlet temp (°C)	1136	1166
SOFC power (kW)	359	319
HPT (kW)	104	108
Total power (kW)	463	427
Cycle efficiency (%)	58	53.5
Exhaust temp (°C) (Air HE)	617	605

From table 1, it can be seen that configuration 2 has lower steady state performance and configuration 1 gives the better. Configuration 1 gives 58% cycle efficiency. We can say that the low performance of configuration 2 can be attributed to the low operating temperature of the fuel cell stack, as the SOFC performance is directly proportional to the operating temperature. As we instead from configuration 2 by 1, the operating temperature improves and hence the performance of the fuel cells. The configuration 1 is chosen as the better configuration out of the configurations studied. Due

to the compressed high temperature exhaust from the combustor is expanded in the turbine and low mass flow rate stream is used to heat the fuel before enter to the SOFC, so it is the reason that the SOFC operating temperature is higher than another configuration. The enthalpy of the exhaust leaving the turbine is high enough to give the required preheating to the air stream in the air heat exchanger. The exhaust from the air heat exchanger is released to the ambient. The cycle efficiency obtained in this case is 58% and the power of the fuel cell is around 77.54% of the total power. The turbine inlet temperature is also within the limits (lower than 1477 °C). For further analyzed in is very interesting to study about the performance and characteristics behavior of the configuration 1 when both of the overall heat transfer coefficient and air mass flow rate are changed for supporting that the configuration 1 is the better configuration.

The presented work is an attempt to model the solid oxide fuel cell and gas turbine hybrid system for auxiliary aerospace power is analyzed using a system-level model. The system is designed to produce 440 kW of net electrical power, sized for a typical long-range 300-passenger civil airplane especially at sea level conditions.

CONCLUSIONS

A hybrid solid oxide fuel cell and gas turbine power system models was developed and implemented in MATLAB. Two types of models have been developed based on simple thermodynamic expressions. Some important observations are made during the configuration study. The fuel cell performance is found to be a strong function of operating temperature (which depends upon the preheating of the input streams). The parameters that limit the cycle performance are the SOFC temperature, the turbine inlet temperature, and the exhaust temperature.

References

- [1] A.F. Massardo and F. Lubelli, "Internal reforming solid oxide fuel cell-gas turbine combined cycles (IRSOFC-GT): part A - cell model and cycle thermodynamic analysis", *Journal of Engineering and Gas Turbines Power*. **122**, 2000, pp. 27-35.
- [2] J.H. Hirschenhofer, D.B. Stauffer, R.R. Engleman, and M.G. Klett *Fuel Cell Handbook*, 1998, 4th ed., Parsons Corporation Reading P.A for U.S. Department of Energy, November.
- [3] S.H. Chan, H.K. Ho, and Y. Tian, "Modeling of a simple hybrid solid oxide fuel cell-gas turbine power plant", *Journal of power sources*. **109**, 2002, pp. 111-120.

APPROACHES FOR REDUCTION OF ELECTRODE POLARIZATION IN ANODE-SUPPORTED SOFCs

Malinee Meepoh¹, Darunee Wattanasiriwech¹, Suthee Wattanasiriwech¹ and Pavadee Ankawattana²

¹Mae Fah Luang University, Chiangrai, Thailand

²National Metal and Materials Technology Centre, Thailand

SUMMARY: In this study, yttria stabilised zirconia (8YSZ), NiO-8YSZ, lanthanum strontium cobalt fluorite (LSCF) powders were used as electrolyte, anode and cathode respectively. Electrolyte was deposited on the pre-fired porous anode by an electrophoresis deposition while the cathode layer was deposited using a screen-printing method. Attempts to reduce electrode polarization were performed by two approaches. First, prevention of insulating phase formed between 8YSZ/LSCF interface in order to reduce the interfacial polarization. For this reason, samaria doped ceria (SDC) was thus used as an interlayer in this study. Second, the microstructure of anode support was adjusted so the anode polarization was decreased. Electrochemical characterisation of the cells was performed using an impedance spectroscopy technique. Insertion of the SDC interlayer between the LSCF cathode and YSZ electrolyte was successful in prevention of insulating phase formation. The results showed that the polarization resistance was decreased as compared to the cell without SDC interlayer. The polarization of anode substrate can be minimized by enlarging pore size of anode substrate together with the fine microstructure of anode functional layer.

Keywords: solid oxide fuel cells, electrophoresis deposition, impedance spectroscopy, interlayer

INTRODUCTION

Solid oxide fuel cells (SOFCs) have been proposed to be one of the key energy resources for the future due to their promising efficiency, environmental friendliness, fuel flexibility and low chemical, particulate and noise emission as well as size compaction [1-2]. Operation of cells was based on electrochemical reaction between a fuel and an oxidising agent, principally oxygen resulting in water and electrical power. SOFCs with a porous anode supported design were popular as they showed lower ohmic resistance [3]. In this design, thin electrolyte film was deposited on the pre-fired porous anode and co-fired at electrolyte sintering temperature. The challenge was to maintain porous anode feature while densifying only the electrolyte layer. This cell design somehow was prone to electrolyte cracking during manufacture due to high thermal expansion coefficient of the NiO compared to that of zirconia electrolyte [1]. Manufacturing of this cell design must be of great care. In anode supported design, polarization was governed by electrode polarization as the ohmic losses could be greatly reduced.

Electrophoresis deposition is a technique widely used for fabrication of thin films [4]. It provides many advantages such as short formation time, little restriction in the shape of deposition substrate, suitability for mass production, and ease of thickness control [5].

The use of this technique for fabrication of the thin electrolyte layer of the thickness less than 10 micron was performed in this study. Attempts to reduce electrode polarization of the cells were addressed.

METHODOLOGY

Three different cell designs were studied. They are based on anode support/anode functional layer/electrolyte/ without or with interlayer/cathode and are called cell-A, B and C. Anode support was prepared by mixing NiO and 8YSZ at 50:50 weight ratio. Corn starch was used as pore former at 15 wt% of the solid. The anode support was milled, before pre-sintered at 900 °C for 4 h, for 1 and 24 h to obtain two different microstructures. The anode functional layer had a NiO:8YSZ of 60:40 weight ratio and was fabricated by an EPD method. The 8YSZ suspension was prepared by dispersing 10 g/l powders in ethanol solvent. The 8YSZ electrolyte was then deposited on the functional layer at a constant voltage of 30V for 2 min. Finally, the sample was co-sintered at the same sintering condition of 1400°C for 2 h with a heating rate of 1°C/min. For SDC interlayer, the SDC paste was prepared by mixing SDC powder with terpenol by hand grinding. SDC paste was then screen-printed onto the surface of sintered electrolyte, followed by drying at 60°C and subsequently sintering at 1200°C for 2 h in order to obtain sufficient contact with the electrolyte. The thickness of the sintered SDC interlayer was about 50 µm. To prepare LSCF cathode, LSCF powder ($\text{La}_{0.6}\text{Sr}_{0.4}\text{Fe}_{0.8}\text{Co}_{0.2}\text{O}_3$) was mixed with terpenol by hand grinding to form LSCF cathode paste. LSCF paste was then screen-printed onto the sintered electrolyte or sintered SDC surface, followed by drying at 60°C and subsequently sintering at 1100°C for 2 h in order to obtain sufficient contact with the electrolyte. The thickness of the sintered LSCF cathode was about 40 µm. For cell performance testing, Pt meshes were used as current collectors and attached to the electrodes with Pt paste, followed by sintering at 800°C for 1 h.

The electrochemical performances were measured with hydrogen as fuel and oxygen as the oxidant at 800°C. To distinguish different loss mechanisms, the single cell was characterized using impedance gain/phase analyzer (Solartron 1260). Microstructure and morphology of the fabricated cells before and after the performance tests were examined by a scanning electron microscopy attached with an EDS.

RESULTS AND DISCUSSION

For cell-A, the insulating phase was obviously observed at 8YSZ/LSCF interface. After addition of SDC interlayer in cell-B, no insulating phase was observed in the 8YSZ/SDC interface. The SDC interlayer was relatively porous. It was due to the low sintering temperature of 1200°C which SDC layer could not be fully densified at this temperature. The electrochemical performance of cell-A and cell-B measured at 800 °C under open circuit potential conditions using hydrogen as fuel and air as oxidant. It showed that the power density of cell-B (with SDC interlayer) was higher than that of cell-A (without SDC interlayer). The maximum power densities were 2.1 and 7.4 mW/cm² for cell-A and cell-B, respectively (Figure 1)

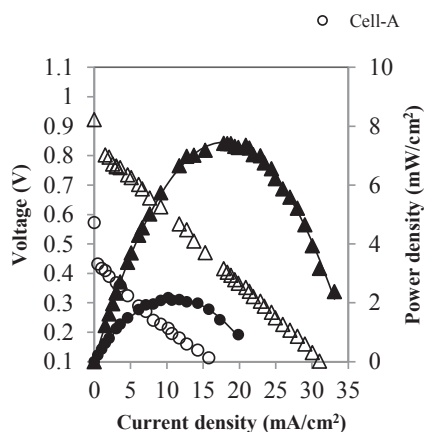


Figure 1. Electrical performances of cell –A and –B.

The electrochemical performance of cell-B and cell-C at 800 °C is shown in Figure 2. It can be seen that a dramatic enhancement in cell performance was achieved for cell-C with large pore size anode substrate. The maximum power density obtained from cell-C was 77 mW/cm².

CONCLUSION

Addition of SDC interlayer between the LSCF cathode and YSZ electrolyte could prevent of formation of SrZrO₃ insulating phases. The results showed that the polarization resistance was decreased compared to the cell without SDC

interlayer. However, thick SDC interlayer exhibited higher ohmic resistance. The polarization of anode substrate can be minimized by enlarging pore size of anode substrate together with the fine microstructure of anode functional layer. A dramatic enhancement in cell performance was achieved for the fuel cell with large pore size anode.

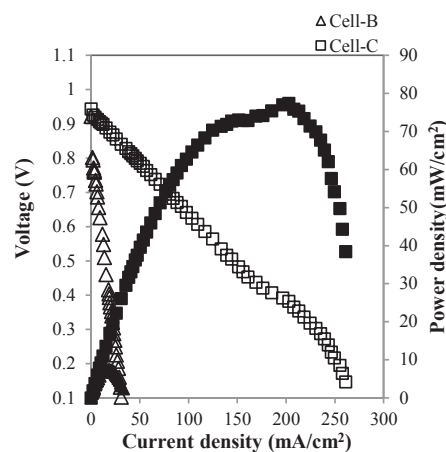


Figure 2. Electrical performances of cell –B and –C.

ACKNOWLEDGMENT

We are grateful for financial support from Mae Fah Luang University, Thailand and Thailand Graduate Institute of Science and Technology

References

- [1] S.P.S. Badwal, S. Giddey, C. Munnings and A. Kulkarni, "Review of Progress in High Temperature Solid Oxide Fuel Cells," *Journal of the Australian Ceramics Society*, **50(1)**, 2014, pp. 23 – 37.
- [2] A. Webe and E. Ivers-Tiffée, "Materials and Concepts for Solid Oxide Fuel Cells (SOFCs) in Stationary and Mobile Applications," *Journal of Power Sources*, **127**, 2004, pp. 273-83.
- [3] S.C. Singhal and K. Kendal, *High-temperature Solid Oxide Fuel Cells: Fundamentals, Design and Applications*: Elsevier, 2003.
- [4] L. Besra, "Electrophoretic deposition on non-conducting substrates: the case of YSZ film on NiO-YSZ composite substrates for solid oxide fuel cell application," *Journal of Power Sources*, **173** 2007, pp. 130–136.
- [5] [8] M. Meepho, S.Wattanasiriwech, P. Angkavatana, and D. Wattanasiriwech, "Application of 8YSZ nanopowder synthesized by the modified solvothermal process for anode supported solid oxide fuel cells," *Journal of Nanoscience and Nanotechnology*, **15(1–5)**, 2015, pp. 2570-2574.

Bio Fuel; Pyrolysis oil and Future Fuel

EMULSIFICATION OF ATER AND PYROLYSIS OIL

Prakorn Kittipoomwong¹ and Monpilai Narasingha¹

¹Chemical Engineering Department, Faculty of Engineering,
King Mongkut's University of Technology North Bangkok, Thailand

SUMMARY: Emulsification of pyrolysis oil produced from recycled HDPE was experimentally investigated. Pyrolysis oil was made from recycled HDPE pellets using a pyrolyzer operated under cascade heating steps and heating rates. Water-in-oil emulsion was produced with ultrasonic mixer and homogenizer using Span80 surfactant as emulsifier. The emulsion stability was assessed by water droplet size and visual observation. Rheological properties were measured to confirm the microstructure change. The emulsion viscosity follows the Einstein equation for a dilute emulsion with water content less than 10%. The ultrasonic mixer was confirmed to be more effective than mechanical homogenizer both in term of smaller water droplet size and lower viscosity. Water-in-oil emulsion was more viscous than its constituting components. A proper droplet size minimization can mitigate the viscous emulsion issue.

Keywords: pyrolysis oil; emulsification; ultrasonic; rheology; emission control

INTRODUCTION

The conversion of waste plastics into fuel by pyrolysis process is a practical approach to resolve the problematic waste management and improve energy sustainability. The pyrolysis process can accept wide ranges of plastics feedstock which substantially reduce labor intensive sorting process. One of the drawbacks impeding the wide spread usage of the pyrolysis oil is the considerable amount of alkenes and nitrogen compounds leading to soot and nitrogen oxide [1]. Emulsification of pyrolysis oil and water can significantly improve NO_x, CO, and soot emission. In addition, the microexplosion phenomena which water droplet vaporized within the emulsion contributes to greater mixing and improves combustion characteristic. A proper emulsification process is indispensable given the immiscible nature between oil and water. The ability to produce fine disperse phase droplet can greatly enhance the fluid properties. In addition, small disperse phase droplet size is less likely to coalescence and exhibits lower viscosity.

In this study, the emulsification of water and pyrolysis oil was experimentally investigated with particular attention to microstructure and the corresponding rheological properties. The average and distribution of water droplet dispersed in pyrolysis oil under various preparing conditions are assessed and compared to the change in measured viscosity.

EXPERIMENTAL METHODS

Pyrolysis oil was produced from recycled HDPE pellets by thermochemical conversions using a batch-type pyrolyzer as illustrated in Figure 1. A 3-liter capacity of 316 stainless steel pyrolyzer is externally heated by an electric furnace operated under cascade heating steps and heating rates [3]. Industrial grade nitrogen gas was fed into pyrolyzer to purge air out of the reactor prior to each run. Pressure relief line is connected through a water tank for safety. The pyrolysis oil was collected from

the main line after passing through a water-cool condenser maintained at about 15°C. The fast pyrolysis process provides 80% product yield using recycled HDPE pellets as a raw material.

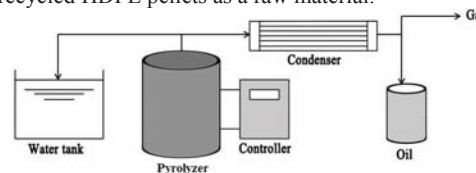


Figure 1. Schematic diagram of pyrolysis process

Water-in-oil (w/o) emulsion was produced with a commercial grade of Sorbitan monooleate (Span 80) as emulsifier [4]. The w/o emulsion were prepared by gradually adding distilled water into the pre-mixed pyrolysis oil and Span80. The surfactant concentration was kept at 2% by volume. The oil and water mixture were emulsified at room temperature by either (1) ultrasonic mixer (Bandelin Sonopuls) operated at 20 kHz (176 watt) or (2) homogenizer (IKA-Ultra-Turrex T50) operated at 4,000 rpm (440 watt). The mixing time is 15 minutes.

The visual characterizations of emulsion were assessed in term of average size and distribution of water droplet. The emulsion microstructure was analyzed by a micrograph taken by microscope (Olympus IX-83ZDC). The micrograph was evaluated by image-analysis software (ImageJ ver. 1.47) to obtain an average and size distribution of water droplet. Also, rheological characterizations of emulsions were assessed in term of kinematic viscosities measured by Ubbelohde capillary viscometer.

RESULTS AND DISCUSSION

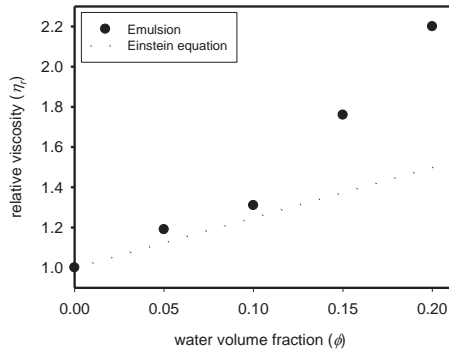
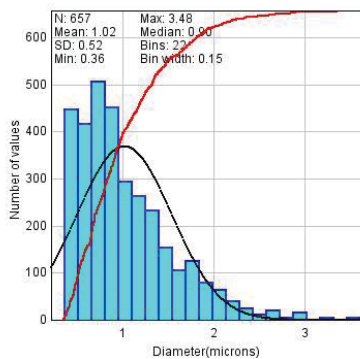


Figure 2. Relationship between water content and emulsion viscosity

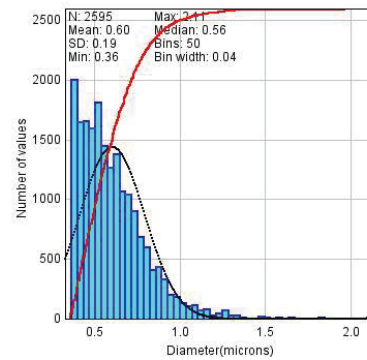
The relative viscosity (η_r) of an infinitely dilute emulsion is given by the Einstein equation:

$$\eta_r = \frac{\eta}{\eta_c} = 1 + 2.5\phi \quad (1)$$

where η and η_c are viscosity of emulsion and continuous phase (pyrolysis oil), respectively and ϕ is the volume fraction of disperse phase (water). In Figure. 2, the effect of water content on emulsion viscosity is demonstrated. The emulsion viscosity exhibits behavior similar to that predicted by Einstein equation up to water volume fraction of 0.1. Also, the viscosity is independent of shear rate as expected for the dilute condition. However, the emulsion viscosity dramatically increases when the water content is increased beyond the dilute limit. The rapid viscous trend is one of the drawbacks which hinder the application of high water content emulsion due to possible complication of subsequent units, e.g. fuel burner or atomizer.



(a) homogenizer



(b) ultrasonic mixer

Figure 3. Water droplet size distribution in $\phi = 0.1$ emulsion prepared by homogenizer and ultrasonic

Emulsification mixing process gives rise to variations in the emulsion microstructure and rheological properties. In Figure 3, the water droplet size distribution is shown for $\phi = 0.1$ emulsion prepared by (a) homogenizer and (b) ultrasonic. The droplet produced by ultrasonic is smaller than that by homogenizer. The viscosity of emulsion prepared by ultrasonic mixer is also found to be lower at the same water content. This confirms the efficient mixing by ultrasonic mixer.

ACKNOWLEDGMENT

The authors are thankful to Mr. Pipat Subsuksunran, Ms. Prachtida Pornprasert and Mr. Nitikorn Pengsawang for their assistance.

References

- [1] B. K.Sharma, B. R. Moser, K. E.Vermillion, K. M.Doll, and N. Rajagopalan, "Production, characterization and fuel properties of alternative diesel fuel from pyrolysis of waste plastic grocery bags", *Fuel Process Technol.*, **122**, 2014, pp. 79-90.
- [2] E. Mura, P. Massoli, C. Josset, K. Loubar, and J. Bellettre, "Study of the micro-explosion temperature of water in oil emulsion droplets during the Leidenfrost effect", *Exp. Therm..Fluid Sci.*, **43**, 2012, pp. 63-70.
- [3] P. Subsuksunran, P. Kittipoomwong, M. Narasingha and W. Soontornrangson "Stability of pyrolysis oil-water emulsion", *Adv. Mat. Res.*, **953-954**, 2014, pp. 1238-1241.
- [4] P. Kittipoomwong and M. Narasingha, "Emulsification of Water and Pyrolysis Oil by Sorbitol Derivative Surfactants", *Appl. Mech. Mater.*, **633-634**, 2014, pp. 537-540.

EFFECT OF TiO₂ INCORPORATED WITH Al₂O₃ ON THE HYDRODEOXYGENATION AND HYDRODENITROGENATION OVER CoMo SULFIDE CATALYSTS

Thirada Rodseanglung^{1,2}, Tanakorn Ratana^{1,2}, Monrudee Phongaksorn^{1,2} and Sabaitip Tungkamani^{1,2}.

¹Department of Industrial Chemistry, Faculty of Applied Science,
King Mongkut's University of Technology North Bangkok, Thailand

²Research and Development Center for Chemical Engineering Unit Operation and Catalyst Design (RCC),
King Mongkut's University of Technology North Bangkok, Thailand

SUMMARY: The influence of TiO₂ incorporation in Al₂O₃ support was investigated in the catalytic activity of hydrodeoxygenation (HDO) and hydrodenitrogenation (HDN) reactions. Alumina–titania supported CoMo sulfide catalysts (mole ratio 1:0, 1:0.25, 1:50, 1:0.75, and 0:1) were prepared by sol-gel method. The CoMo sulfide catalysts were characterized by BET, NH₃-TPD, H₂-TPR, XRD and TEM techniques. Guaiacol and quinoline were used as model compounds in HDO and HDN reactions, respectively. The liquid products were examined by GC-FID and GC-MS. The results suggest that TiO₂ incorporated Al₂O₃ support obviously involves the catalytic activity on the HDO and HDN reactions. The role of the partial incorporation of TiO₂ into Al₂O₃ was discussed.

Keywords: Hydrodenitrogenation, hydrodeoxygenation, sulfide catalysts, Al₂O₃-TiO₂ support, CoMo catalysts.

INTRODUCTION

Bio-oil derived from fast pyrolysis of lignocellulosic biomass contains significantly quantities of several oxygen compounds, mostly in the form of phenolic compounds with some nitrogen compounds. As an alternative transportation fuels, bio-oil upgrading using hydrotreating process is necessary in order to dramatically remove the oxygen content through hydrodeoxygenation (HDO) reaction. The elimination of nitrogen compounds during the hydrotreating process via hydrodenitrogenation (HDN) is also important process because nitrogen compounds poison and deactivate the catalyst. The conventional catalysts for hydrotreating process are CoMo and NiMo supported on Al₂O₃. Al₂O₃ support provides high surface area and high thermal stability [1], however, as mentioned earlier, TiO₂ supported molybdenum catalysts has attracted considerable attention catalysts due to these catalysts exhibit the higher hydrotreating activities compared to Al₂O₃ supported molybdenum catalysts. However, the disadvantages of TiO₂ are low surface area, low thermal stability and poor mechanical property causing negative effect for long-term stability [2].

This work is to study the effect of the incorporating TiO₂ to Al₂O₃ support. The catalytic activities tested by HDO and HDN reaction as a function of TiO₂ content were investigated.

EXPERIMENTAL

The 10%Mo/Al₂O₃-TiO₂ catalysts were prepared by the sol-gel method at varying the molar ratios of Al₂O₃ to TiO₂; 1:0, 1:0.25, 1:0.50, 1:0.75, 1:1, and 0:1. Then, the catalysts were dried at 50 °C for 48 h and calcined at 550°C for 4 h. Afterward, the addition of 3% Co in the catalyst powder by using impregnation method, followed by dried 50 °C for 48 h and calcined at 550°C for 4 h. The 3%Co10%Mo/Al₂O₃-TiO₂ catalysts denoted as 310CMAT(x:y), where (x:y) are

mole ratio (1:0.5,1:0.75 and 1:1), whereas alumina and titania used as support designed as 310CMA and 310CMT, respectively .

The surface area, pore volume and average pore diameter were characterized by N₂ adsorption using BELSORP:MINI II. The reducibility and acidity of catalysts were analyzed by temperature programmed reduction of hydrogen (H₂-TPR) and temperature programmed desorption of ammonia (NH₃-TPD), respectively using BELCAT-B. The phase identification of catalysts was confirmed by X-ray diffraction (XRD) using X-ray diffractometer (Rigaku TTRAX III) . Finally, the morphology of MoS₂ catalysts was evaluated by TEM technique analyzed by JEOL, JEM-2010.

Before the hydrotreatment test, the catalysts were sulfidized in a fixed bed reactor under the H₂S atmosphere. The HDO and HDN activities were carried out in a high temperature and pressure batch reactor (Parr 4848) at 300 °C under hydrogen pressure 50 bar for 2 h. The model compounds used as a feedstock for the catalytic activity testing consist of 5.00 wt.% guaiacol (a model of phenolic compound), 0.30 wt.% quinoline (a model of nitrogen compound) and organic solvent (1,2,3,4-tetrahydronaphthalene and n-hexadecane). The liquid products were analyzed by Agilent 7890 gas chromatograph equipped with the flame ionization (FID) detector and Agilent 5975 gas chromatograph equipped with mass spectrometer (MS) detector.

RESULTS AND DISCUSSION

Catalyst characterization

Textural properties (Table 1) of the synthesized catalysts after calcination exhibit that 310CMA catalyst provides the specific surface area up to 249.32 m²/g with the average pore size of 3.95 nm, while the specific surface area of 310CMT is 67.14 m²/g with the average pore size of 10.62 nm. Surface area of

mixed Al_2O_3 and TiO_2 support decreases with increasing TiO_2 content but the average pore size slightly increases. The reason can be contributed to the incorporation of TiO_2 to the Al_2O_3 support [3].

Table 1. Textural properties of all catalysts

Catalysts	S_{BET} (m^2/g)	Average pore diameter (nm)	Pore volume (cm^3/g)
310CMA	249.32	3.95	0.25
310CMAT(1:0.25)	255.52	4.97	0.32
310CMAT(1:0.5)	231.51	5.15	0.29
310CMAT(1:0.75)	181.51	5.01	0.22
310CMAT(1:1)	198.35	5.61	0.27
310CMT	67.14	10.62	0.18

TPR profile of alumina support (Figure 1a) shows two broad H_2 consumption signals related to octahedral and tetrahedral Mo^{6+} reduction ($\text{Mo}^{6+} \rightarrow \text{Mo}^{4+}$), while TPR profile of titania support (Figure 1f) shows inversely tetrahedral and octahedral Mo^{6+} reduction [4]. Interestingly, the appearance of shoulder signal ca. 500-600 °C for 310CMAT(0:1) and 310CMAT(1:1) catalysts probably relates to $\text{Ti}^{4+} \rightarrow \text{Ti}^{3+}$ surface titania cations reduction [4].

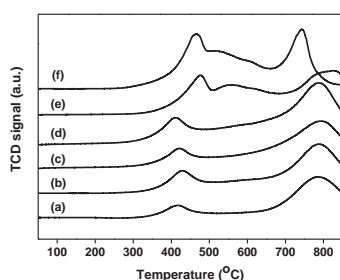


Figure 1. TPR-profiles of (a) 310CMA (b) 310CMAT(1:0.25) (c) 310CMAT(1:0.5) (d) 310CMAT(1:0.75) (e) 310CMAT(1:1) and (f) 310CMT

XRD patterns of three catalysts in Figure 2 observed only diffraction patterns of catalyst support. Alumina and titania supports exhibit the diffraction peaks belonging to the $\gamma\text{-Al}_2\text{O}_3$ and anatase TiO_2 phases, respectively, whereas 310CMAT(1:1) reveals anatase phase with low crystalline. This confirmed the incorporation of TiO_2 to Al_2O_3 .

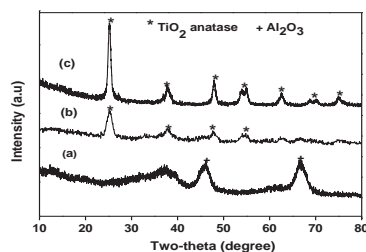


Figure 2. XRD patterns of (a) 310CMT (b) 310CMAT(1:1) and (c) 310CMT.

Catalytic activity test

The catalytic activity of HDO and HDN indicates that the TiO_2 enhances both HDO and HDN activity as shown in Figure 3. Especially, 310CMAT(1:1) gives activity close to 310CMT. From these results, TiO_2 was considered as an electronic promoter in supported CoMo catalysts. The 3d electron in Ti^{3+} formed under the reducing conditions can be transferred through the Mo 3d conduction band, leading to weakening of the Mo-S bond and an increase in the number of coordinately unsaturated metal sites (CUS) [3]. Moreover, it also indicated that TiO_2 also is a promoter for HDN of quinoline, enhancing both the hydrogenation and C-N bond cleavage activities.

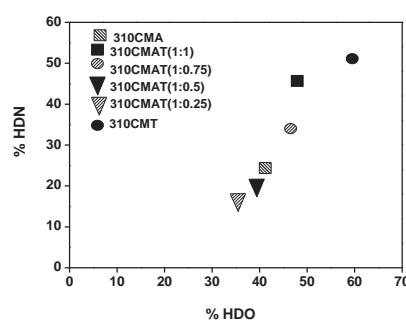


Figure 3. HDO and HDN activity of the all catalysts at 300 °C under H_2 pressure 50 bar for 2h

ACKNOWLEDGEMENT

The authors would like to thank Japan International Cooperation Agency (JICA) and the National Institute of Advanced Industrial Science and Technology (AIST) for training and the financial support.

References

- [1] A. Popov, E. Kondratieva, L. Mariey, J.M. Goupil, J. El Fallah, J.-P. Gilson, A. Travert and F. Maugé, "Bio-oil hydrodeoxygenation: Adsorption of phenolic compounds on sulfided (Co)Mo catalysts", *Journal of Catalysis*, **297**, 2013, pp. 176-186.
- [2] G.M. Dhar, B.N. Srinivas, M.S. Rana, M. Kumar and S.K. Maity, "Mixed oxide supported hydrodesulfurization catalysts—a review", *Catalysis Today*, **86**, 2003, pp. 45-60.
- [3] J. Ramirez, G. Macías, L. Cedeño, A. Gutiérrez-Alejandre, R. Cuevas and P. Castillo, "The role of titania in supported Mo, CoMo, NiMo, and NiW hydrodesulfurization catalysts: analysis of past and new evidences", *Catalysis Today*, **98**, 2004, pp. 19-30.
- [4] J. Xu, K. Sun, L. Zhang, Y. Ren and X. Xu, "A highly efficient and selective catalyst for liquid phase hydrogenation of maleic anhydride to butyric acid", *Catalysis Communications*, **6**, 2005, pp. 462-465.

HYDROTREATING OF FREE FATTY ACID AND BIO-OIL MODEL COMPOUNDS: EFFECT OF CATALYST SUPPORT

Vituruuch Goodwin^{1,2,3}, Boonyawan Yoosuk³, Tanakorn Ratana^{1,2} and Sabaithip Tungkamani^{1,2}

¹Department of Industrial Chemistry, Faculty of Applied Science
King Mongkut's University of Technology North Bangkok, Thailand

²Research and Development Center for Chemical Engineering Unit Operation and Catalyst Design (RCC)
King Mongkut's University of Technology North Bangkok, Thailand

³National Metal and Materials Technology Center (MTEC)
National Science and Technology Development Agency (NSTDA), Thailand

SUMMARY: The effect of catalyst support on catalytic hydrotreating of free fatty acid and guaiacol as model compounds of bio-oil obtained from fast pyrolysis of seed oil cake and lignocellulosic biomass was investigated. Two different sulfide supported catalysts were synthesized and characterized, i.e., molybdenum sulfide on TiO₂ and Al₂O₃ supports. The catalytic performance was studied through catalytic hydrotreating of linoleic acid and guaiacol at 573 K. Hydrotreatment of linoleic acid and guaiacol showed that sulfide catalyst supported on TiO₂ enhanced catalytic activity and hydrodeoxygenation (HDO) pathway while Al₂O₃ supported catalyst preferred hydrogenation pathway. The increment of free fatty acid in mix model compounds from 2.5 wt% to 20wt% hindered catalytic hydrotreating reaction and thus reducing catalytic activity enhancement effect of TiO₂ supported catalyst.

Keywords: Bio-oil upgrading, hydrodeoxygenation, free fatty acid, sulfide catalysts, TiO₂ support

INTRODUCTION

Pyrolysis oil from fast pyrolysis of biomass converts lignocellulosic biomass into biofuel could be a future of alternative fuel. Generally, pyrolysis oil or so called bio-oil contains hundreds of organic compounds including hydrocarbons and oxygen containing compounds such as acids, aldehydes, ketones and phenolics which cause bio-oil to have low heating value and low stability. Thus, upgrading of bio-oil via catalytic hydrotreatment is a crucial process to improve bio-oil fuel properties and stability.

Catalytic hydrotreating process is a promising path to upgrade bio-oil. Besides lignocellulosic biomass, bio-oil can also be obtained from seed oil cake which contains triglycerides and fatty acids. In this study, guaiacol (2-methoxyphenol) was used as a model compound representing lignin derived bio-oil and linoleic acid as a free fatty acid model. Various amount of linoleic acid from 2.5wt% to 20wt% was added to investigate the catalyst performance. The effect of catalyst support on hydrotreatment of bio-oil and fatty acid model was investigate using an unconventional CoMo catalyst supported on TiO₂ which had known for its great electron transfer property and enhancement toward hydrodeoxygenation [1]. The catalytic activity and selectivity affected by support are transcribed with data of reactant conversion and degree of hydrodeoxygenation (%HDO) as different support favors different reaction pathway of hydrotreatment.

EXPERIMENTAL

All catalysts were synthesized via sol-gel method, dried at 318 K for 48 h and calcined in air at 823 K for 4 h. The calcined supported catalysts were then sieved in the range of 250-600 μm and

sulfide with 5%H₂S/H₂ at 673 K for 4 h. just before hydrotreating experiment. All calcined catalysts were characterized for surface area, pore volume and pore diameter according to Brunauer Emmett Teller (BET) technique based on nitrogen adsorption isotherms. Temperature programmed reduction of hydrogen (H₂-TPR) and temperature programmed desorption of ammonia (NH₃-TPD) were conducted in BELCAT B equipment.

The hydrotreating reaction was performed in a Parr batch reactor. Each batch was filled with 20 g of feedstock, which is a mixture of guaiacol, linoleic acid and dodecane as solvent with 0.4 g of sulfide catalyst. Hydrotreating temperature was set at 573 K for 1 h and initial hydrogen pressure of 4 MPa. To investigate the catalytic performance of two catalysts with different support, a set of feedstock with a fixed 5wt% guaiacol and various linoleic acid loading at 2.5, 5, 10 and 20 wt% were hydrotreated. After the reactor was cooled down to room temperature, the liquid product was collected and analyzed by GC-MS and GC-FID.

RESULTS AND DISCUSSION

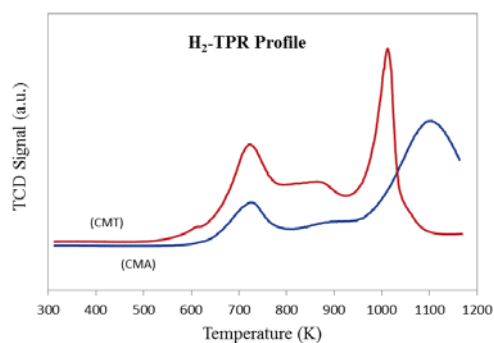
Catalyst characterization

Two calcined catalysts, cobalt molybdenum on TiO₂ designated as CMT and cobalt molybdenum on Al₂O₃ named CMA were characterized by BET technique to determine surface area. The results of BET analysis are shown in Table 1. Catalyst supported on Al₂O₃, CMA, has more surface area at 219.45 m²/g compared to CMT which has lower surface area at 91.07 m²/g. Furthermore, CMA exhibits smaller pore volume with an average pore diameter of 3.86 nm.

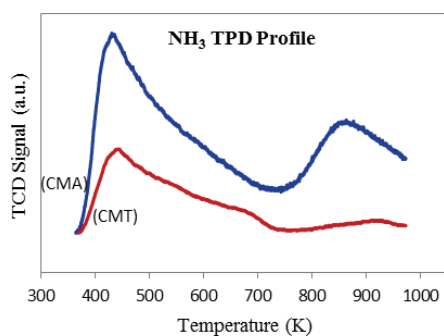
Table 1. Textural properties of supported catalysts

Catalyst	Surface area [m ² /g]	Pore volume [cm ³ /g]	Pore diameter [nm]
CMA	219.45	0.21	3.86
CMT	91.07	0.18	7.89

The result from H₂-TPR profile is used to evaluate catalyst reducibility. CMT catalyst is more reducible than CMA due to lower initial reduction temperature at 573 K with larger H₂ consumption (peak area) as showed in Figure. 1.

Figure 1. H₂-TPR profile of CMT and CMA catalysts

The plot of NH₃ desorption profile is shown in Figure 2. CMA catalyst has two desorption peaks around 473 K and 873 K referred that CMA catalyst contains two different surface acid sites and has high acidity compare to CMT catalyst which shows only one desorption peak near 473 K.

Figure 2. NH₃-TPD profile of CMT and CMA catalysts

Hydrotreatment of guaiacol and linoleic acid

Catalytic hydrotreatment of 5 wt% guaiacol and 2.5 wt% linoleic (reactants : catalyst = 3.75:1) at 573 K is the only reaction with 100% conversion of linoleic acid. CMT catalyst yields more saturated and unsaturated C18 hydrocarbons than C17 hydrocarbons indicated high selectivity toward hydrodeoxygenation (HDO) pathway. This is due to

the effect of TiO₂ support which acts as an electronic promoter to increase MoS₂ (CUS) active sites for hydrodeoxygenation pathway [2, 3]. CMA catalyst yields saturated acid (i.e., stearic acid) and C17-C18 via hydrogenation (HYD) more than through HDO pathway.

Catalytic activity of both catalysts decreases as linoleic acid was added more than 5 wt% to the feedstock. The plot of %conversion and %HDO vs % linoleic acid in feedstock are shown in Figure 3. %HDO of both catalysts is dramatically dropped when linoleic acid increases to 5 wt%, especially on CMT that has low surface area. This may indicates the transport limit due to high reactant : catalyst ratio. It was found that fatty acid methyl ester was formed from esterification process competing with hydrotreating process when linoleic acid increases. Thus, supports with different intrinsic properties play an important role on product selectivity and reaction pathway of hydrotreatment over sulfide catalysts. However, high amount of fatty acid added into feedstock affects both catalysts resulted in reduction of catalytic activity due to transport limit.

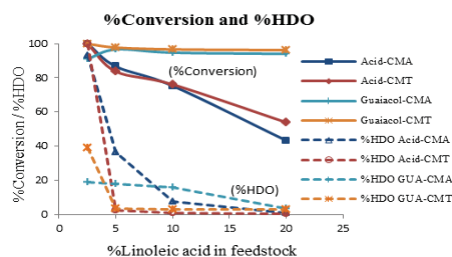


Figure 3. %Conversion of linoleic acid and %HDO at various %linoleic acids loading

ACKNOWLEDGMENT

The authors gratefully acknowledge JICA-SATREPS for the collaboration and support. The authors also thank Thailand Graduate Institute of Science and Technology (TGIST), NSTDA for doctoral financial support.

References

- [1] V.N. Bui, D. Laurenti, P. Delichere, and C Geantet, "Hydrodeoxygenation of guaiacol: Part II: Support effect for CoMoS catalysts on HDO activity and selectivity", *Applied Catalysis B: Environmental*, **101**, 2011, pp.246-255.
- [2] J. Ramirez, G Macias, L Cedeno, A.G. Alejandre, R. Cuevas and P. Castillo, "The role of titania in supported Mo, CoMo, NiMo and NiW hydrodesulfurization catalysts: analysis of past and new evidences", *Catalysis Today*, **98**, 2004, pp. 19-30.
- [3] D. Wang, X Li, E.W. Qian, A Ishihara, and T Kabe, "Elucidation of promotion effect of cobalt and nickel on MO/TiO₂ catalyst using a ³⁵S tracer method", *Applied Catalysis A: General*, **238**, 2003, pp. 109-117.

CATALYTIC CONVERSION OF PYROLYSIS TAR TO PRODUCE GREEN GASOLINE-RANGE AROMATICS

Abdulrahim Saad¹, Sukritthira Ratanawilai¹, and Chakrit Tongurai¹

¹Department of Chemical Engineering, Faculty of Engineering,
Prince of Songkla University, Thailand

SUMMARY: This study was undertaken to generate gasoline-range aromatics from pyrolysis tar derived from rubberwood. Catalytic cracking of the pyrolysis tar was conducted using HZSM-5 catalyst in a dual reactor. The effects of reaction temperature, catalyst weight, and nitrogen flow rate were investigated to determine the yield of organic liquid product (OLP) and the percentage of gasoline aromatics in the OLP. The results showed that the maximum OLP yield was about 28.33 wt%, which was achieved at 536 °C and a catalyst weight of 3.5 g. The maximum percentage of gasoline aromatics was about 54 wt%, which was obtained at 575 °C and a catalyst weight of 5 g. The anticipated components, i.e., benzene, toluene, ethylbenzene, and xylenes (BTEX), were detected in the OLP proving that green gasoline aromatics can be produced from rubberwood pyrolysis tar via zeolite cracking.

Keywords: Pyrolysis tar, zeolite cracking, organic liquid product (OLP), green gasoline-range aromatics

INTRODUCTION

With the global oil crisis of the 1970s and the greenhouse effect, there is increasing interest in exploring renewable energy resources as complement to conventional fossil fuels. Biomass is one of the important sources of renewable energy that is a CO₂ neutral resource; as a result, significant attention has been paid to biomass as an alternative to petroleum fuels [1].

Present-day pyrolysis oil has attracted considerable interest, particularly in fuels production, making it the most suitable material that can compete with the non-renewable fuel resources. However, the direct substitution of pyrolysis oil for petroleum might be limited due to its thermal instability, high viscosity, and high oxygen content. As a result, an upgrading process is required to improve its quality by reducing the oxygen content. Catalytic cracking using HZSM-5 catalyst was found to be useful for upgrading pyrolysis oils [2].

The concern of producing green gasoline, particularly gasoline-range aromatics from pyrolysis oil, has aroused attention in recent years. A handful of previous studies have demonstrated that pyrolysis oil derived from different biomass sources could be converted to gasoline hydrocarbons by catalytic cracking over ZSM5 catalysts [3].

The rubber tree is widely planted in southern Thailand, and has been utilized to a great extent for charcoal production using pyrolysis process. The pyrolysis liquid is an unavoidable by-product obtained during the manufacture of charcoal; over time, the liquid is divided into aqueous and oily layers. The oily layer, more accurately called pyrolysis tar, is a sticky liquid mixture of different oxygenated compounds. On the basis of compositions, pyrolysis tar has the capability to produce green gasoline rich with aromatic chemicals. Additionally, it can add value to the production of charcoal. To the best of authors' knowledge, pyrolysis tar as a by-product from charcoal

production has received limited attention, and no study was conducted to upgrade it to gasoline-range aromatics or organic liquid product (OLP). Thus, this work was carried out with the aim of investigating the potential use of tar for producing green gasoline through catalytic cracking over HZSM-5 catalyst in a dual reactor.

EXPERIMENTAL

Materials

Crude pyrolysis liquid was collected from Phatthalung Province. The liquid had been settled for about two months, after that, a settled tar was separated by decantation. The physiochemical properties of tar were determined. The HZSM-5 catalyst was prepared and characterized.

Experimental Setup and Procedure

Catalytic cracking of pyrolysis tar was conducted in a dual reactor assembly without any catalyst in the first reactor, followed by a second fixed bed reactor loaded with HZSM-5 catalyst. The experiments were operated at atmospheric pressure, a reaction temperature that varied from 400 to 600 °C, a catalyst weight of 1 to 5 g, and a nitrogen flow rate of 3 to 10 mL/min. 15 experiments were designed using Essential Regression and Experimental Design software. The experiments were conducted to determine two quantities (Table 1), i.e., the yield of OLP and the percentage of gasoline aromatics in the OLP. In a typical run, the second reactor was loaded with the catalyst. Both reactors were heated until the desired temperature was attained, after which a syringe pump was used to introduce 15 g of pyrolysis tar into the first reactor at the rate of 1.4 g/min. The products of reaction were cooled and separated into liquid and gaseous products, i.e., OLP, aqueous liquid, and gases.

RESULTS AND DISCUSSION

Product Distribution

It was observed that a significant amount of char was formed in the first reactor, due to the thermal effect on the unstable components of the tar. The yield of char ranged from 20 to 24 wt % over the experimental runs. The amount of aqueous product ranged from about 25 to 33 wt %.

It was essential to investigate the distributions of OLP yield, which ranged from about 10 to 27 wt% over the experimental runs. The yield reached a maximum of 27 wt% at 500 °C with 3 gram catalyst.

Content of Gasoline-Range Aromatics in OLP

The composition of OLP, particularly gasoline-range aromatics (BTEX), was of prime interest. It was found that the percentage of gasoline aromatics in OLP for all runs ranged from about 2 to 52 wt% (Table 1), with a maximum value of about 52 wt% at 600 °C and 3 g of catalyst. The formation of aromatic hydrocarbons supported the hypothesis that the oxygenated compounds in the pyrolysis oil can be converted into aromatic hydrocarbons by dehydroxylation, decarbonylation, and decarboxylation with the HSZM-5 catalyst.

Table 1. Experimental Runs and Results

Runs	Experimental Results	
	OLP yield	Percentage of gasoline aromatics in OLP
1	10.00	2.01
2	18.45	10.10
3	18.30	9.90
4	20.28	29.83
5	15.13	20.88
6	14.98	20.00
7	27.31	40.77
8	27.50	41.53
9	26.90	42.00
10	25.00	49.41
11	24.80	48.29
12	22.65	24.28
13	24.40	52.25
14	24.35	50.65
15	22.00	45.21

Optimization

The main targets in this study were OLP and gasoline aromatics in the OLP. RSM was used to predict the optimum values of the three variables. Essential regression software was used to optimize the conditions, and the results showed that the maximum value of OLP yield was about 28.33 wt% for a temperature of 536 °C and a catalyst weight of 3.5 g as shown in Figure 1. In addition, the maximum percentage of gasoline aromatics was about 54 wt%, which was obtained at 575 °C and a catalyst weight of 5 g. as shown in Figure 2.

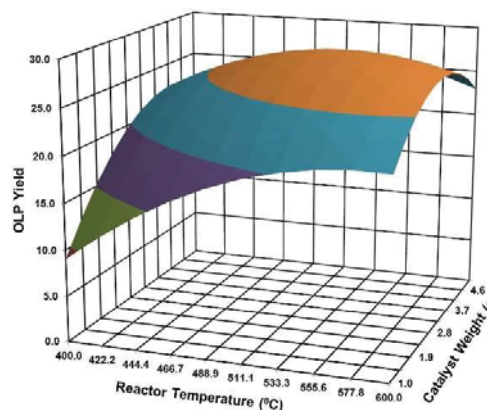


Figure 1. Surface plot of OLP yield as a function of catalyst weight and temperature

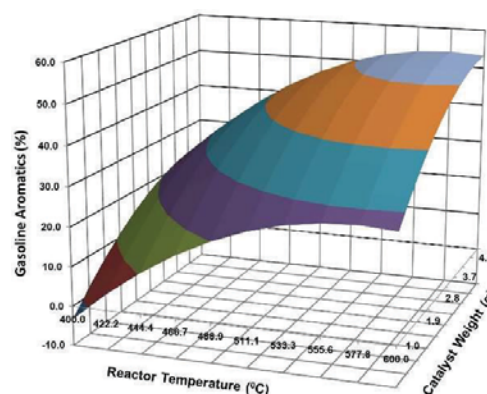


Figure 2. Surface plot of gasoline aromatics (%) in OLP as a function of catalyst weight and temperature

ACKNOWLEDGMENT

The authors sincerely acknowledge the graduate school of Prince of Songkla University for the financial support for this study.

References

- [1] M.F. Demirbas, M. Balat and H. Balat, "Potential contribution of biomass to the sustainable energy development", *Energ. Convers. Managers*, **50**, 2009, pp.1746-1760.
- [2] A.V. Bridgwater and G. Grassi "Biomass pyrolysis liquids: upgrading and utilization", *Elsevier Applied Science*, 1991.
- [3] Adjaye, J.D. and N.N. Bakhshi., "Production of hydrocarbons by catalytic upgrading of a fast pyrolysis bio-oil. Part I: Conversion over various catalysts", *Fuel Processing Technology*, **80**, 1995, pp. 161-183.

THE POTENTIALS OF WATER-IN-DIESEL EMULSIONS AS A FUTURE FUEL

Abdurahman Hamid Nour^{1*}; Azhari Hamid Nour²; Said Nurdin¹

¹Faculty of Chemical and Natural Resources Engineering, University Malaysia Pahang-UMP

²Faculty of Industrial Sciences and Technology, University of Malaysia Pahang-UMP, Malaysia

*Corresponding email: nour2000_99@yahoo.com

SUMMARY: With the increasing energy prices and the drive to reduce CO₂ emissions, universities and industries are challenged to find new technologies in order to reduce energy consumption, to meet legal requirements on emissions, and for cost reduction and increased quality. The presence of water within diesel fuel in the form of water-in-diesel (W/D) emulsion reduces both particulate matter (PM) and nitrous oxide (NO_x), by lowering the combustion temperature and altering the combustion pattern to more completely burn the carbon in the fuel. In this study, emulsion of W/D was prepared by high speed mixing homogenizer and the physical properties (density, viscosity, flash point, surface tension, dynamic viscosity) were investigated. Results show that the emulsions of 5%, 10%, 20% and 30% W/D were stabilized for two months, under the conditions of 2% surfactant, 5000 rpm and 10 minutes of mixing time. Under the same conditions, the stability period was limited to 3 weeks for emulsions with a water concentration of 40%.

Keywords: Water-in-diesel emulsion, stability, combustion, surfactant, emission

INTRODUCTION

When water is present in an immiscible dispersed droplets phase within the continuous oil phase it usually leads to the formation of water-in-oil emulsion (W/O). W/O emulsion is of great interest in several industrial and environmental applications. Some examples of these applications are crude oil spillage [1], pipeline transportation of water in heavy crude oil [2]; [3]. The use of a suitable surfactant can further reduce the surface tension between water and oil, leading to the formation of an emulsion. A water-in-oil emulsion with high emulsification stability has been used in the past as an alternative fuel for combustion equipment such as diesel engines, boilers, incinerators, etc., for fuel economy and pollutant reduction. These goals were accomplished primarily due to the occurrence of the phenomenon of micro-explosions. An emulsion is atomized into many tiny water-in-oil droplets by a fuel nozzle. Because the boiling point of water is lower than that of oil, under the burning condition of high temperature and high pressure, the water droplets enveloped by the oil phase will absorb the enthalpy of reaction to form water vapor with a volume.

In spite of preferable advantages of diesel engines, they are one of the major pollution contributors to present time. Such primary pollutants exhausted from diesel engines are particulate matters (PM), nitrogen oxides (NO_x), Sulphur oxides (SO_x), unburnt hydrocarbon (HC), carbon monoxide (CO), and carbon dioxide [4]. Emulsion of diesel and water are often promoted as being able to overcome the difficulty of simultaneously reducing emissions of both NO_x and PM from the diesel engines [5]. The main mechanism causing the reduction in NO_x emissions seems to be the decrease in the temperature of the combustion products as a result

of vaporization of the liquid water and consequent dilution of the gas phase species. As for PM emissions, the presence of water during the intensive formation of soot particles seems to reduce the rate of formation of soot particles and enhance their burnout by increased concentration of oxidation species such as OH [6]. The aim of the present study is to obtain stable water in diesel emulsion (WiDE) which is stabilized with surfactants, in order to reduce operating costs, emissions and fuel consumptions of any internal-combustion engine. Primary step before using WiDE as a fuel is to characterize their properties as it will influence certain operating parameter of the engine such as injection timing and mixing process [7]. Besides that, it was found that physical and chemical kinetics of the combustion is influenced by the presence of water vapour in fuel [8]. The present study is aiming to investigate the effect of various factors on the stability behavior of W/D emulsions. These factors are the temperature, water concentration, mixer speed, surfactant concentration and surface tension.

METHODOLOGY

Diesel oil samples obtained from Petronas Refinery at Melaka. A detailed procedure for the water-in-diesel (W/D) emulsions preparation and their procedures including the formation of W/D emulsion, their characteristics and methods of preparation are thoroughly described in a previous research by [9]. Here the work merely describes the main experimental steps. The physico-chemical properties of the diesel and W/D emulsions were shown in Tables 1. For preparation of water-in-diesel (W/D) emulsions, the agent in oil method was implemented, that is; the emulsifying agent dissolved in the continuous phase (diesel) and water

added gradually to the mixture (diesel + emulsifying agent). Emulsions were agitated vigorously using a standard three blade propeller at room temperature (25-30 °C). The volume of water settled to the bottom was read from the scale on the beaker with different times. The prepared emulsions were used to check for w/o or o/w emulsions. All emulsions investigated were type of water-in-oil emulsions (oil continuous phase). The surfactant used in this study was Triton X-100 (polyethylene glycol octylphenyl ether), which has a chemical formula of $C_{33}H_{60}O_{10}$. This surfactant is a nonionic hydrophilic surfactant that is suitable for use in the production of both W/O and O/W emulsions.

RESULTS AND DISCUSSION

The most important factor in the preparation of emulsions is the selection of suitable surfactant or blend of surfactants which can satisfactorily emulsify the chosen ingredients at a specific temperature. Emulsification is greatly influenced by hydrophilic-lipophilic balance (HLB) of any surfactant/ emulsifier [10]. Percentage of water in the emulsion, stirring intensity, stirring duration, emulsifying temperature and operational pressure are other parameters of interest that affect the stability of an emulsion. The WiDE prepared for the current study was observed for more than 65 days since it was emulsified and found to be stable for the mentioned period. It was noted that, the larger the amount of water content in the emulsion, the brighter milky emulsion is produced. It is evident that the density of the emulsion increases with increasing in the amount of water in the mixture. This was attributed to the higher density of water that was being added to diesel fuel which is of lower density. Densities for diesel and the five WiDE emulsion samples measured at 20°C to 50°C were plotted in Figure 1.

Table1. Density of diesel and WiDE Emulsions (5%, 10%, 20%, 30% & 40%)

Diesel	Kg/m ³	Kg/m ³	Kg/m ³	Kg/m ³
	at 20 °C	at 30 °C	at 40 °C	at 50 °C
	840	835	828	820
WiDE-5%	848	842	835	828
WiDE-10%	854	849	842	834
WiDE-20%	870	865	858	850
WiDE-30%	877	872	865	857
WiDE-40%	930	925	918	910

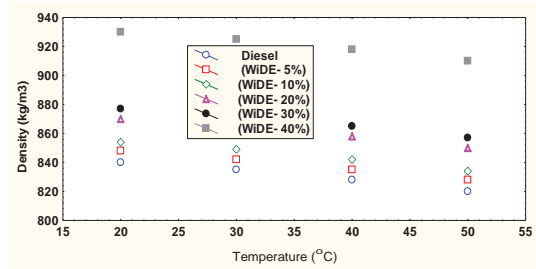


Figure 1. Density of diesel and WiDE emulsions

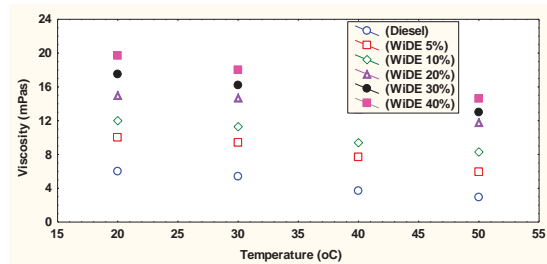


Figure2. Viscosity of diesel and WiDE emulsions

References

- [1] Mingyuan, L.; Christy, A.; Sjoblom, J. (1992). In: Sjoblom, ed. *Emulsions- A Fundamental and Practical Approach*. Dordrecht: Kluwer Academic Publishers V363.
- [2] Pilehvari, A.; Saadevandi, B.; Halvaci, M.; Clark, D. (1988). In: Roco, M. C. ed. *Pipeline transportation of heavy crudes as emulsions*. Proceedings 3rd International Symposium Liquid Solid Flows, ASME V75, New York.
- [3] Carcoana, A. (1992). *Applied Enhanced Oil Recovery*. New Jersey: Prentice-Hall.
- [4] Lin, C.Y.; Wang, K.H. (2003). *Fuel* **82**, 1367–1375.
- [5] Fahd, E. A.; Wenming, Y.; Lee, P.S.; Chou, S.K.; Yap, C.R. (2013). *Appl Energy* **102**, 1042-1049.
- [6] T. Xuan-Thien.; Jamil, G. (2005). 5th Asia Pacific Conference on Combustion, (2005).
- [7] Armas, O.; Ballesteros,R.; Martos, F. J.; Agudelo, J.R.(2005). *Fuel* **84**, 1011–1018 (2005).
- [8] Alahmer, A. (2013). *Energy Conversion and Management* **73**, 361-369 (2013).
- [9]Abdurahman, H. Nour.; Rosli. M.Y; Zulkifly. J. (2006). Study on demulsification of water-in-crude oil emulsions via microwave heating technology. *J. Applied Sci.*, 6: 2060-2066.
- [10] Rosen, M.J. (2004). *Surfactants and interfacial phenomenon*. Wiley; (2004).

THERMOGRAVIMETRIC KINETIC ANALYSIS THE PYROLYSIS OF RICE STRAW

Nithitorn Kongkaew^{1,2}, Witchaya Pruksakit² and Suthum Patumsawad¹

¹Department of Mechanical & Aerospace Engineering, Faculty of Engineering, King Mongkut's University of Technology North Bangkok (KMUTNB), Thailand

²The Joint Graduate School of Energy and Environment (JGSEE), Thailand

SUMMARY: A kinetic of the pyrolysis of rice straw is investigated with thermogravimetric analyzer with non-isothermal methods selected for analyzing solid-state kinetics data is presented. The weight loss was measured by TGA in nitrogen atmosphere. The samples were heated over a range of temperature from 298 K to 973 K with three different heating rates of 5, 10 and 15 K min⁻¹. The results obtained from thermal decomposition process indicate that there are two main stages such as active and passive pyrolysis. In the DTG thermograms the temperature peaks at maximum weight loss rate changed with increasing heating rate. The activation energy and pre-exponential factor obtained by Kissinger method are 172.62 kJ mol⁻¹, 1.456 × 10¹¹ min⁻¹, while, the same average parameters calculated from FWO and KAS methods are 192.66 kJ mol⁻¹, 1.287 × 10²² min⁻¹ and 193.60 kJ mol⁻¹, 6.887 × 10¹⁵ min⁻¹, respectively. Experimental results showed that values of kinetic parameters obtained from three different methods are in good agreement, but KAS and FWO methods are more efficient in the description of the degradation mechanism of solid-state reactions.

Keywords: rice straw, pyrolysis, thermogravimetric analysis, kinetics, isoconversional method

INTRODUCTION

An understanding of biomass pyrolysis can give rise to a development of biomass conversion process. Since pyrolysis is the first step of biomass conversion such as gasification, liquefaction, carbonization and combustion, its sound understanding is significant for the effective use of biomass. For engineering applications, knowledge of the pyrolysis kinetics is essential for predicting the pyrolysis behavior of biomass material as well as designing the suitable reactor design and operating condition which the correctness of the kinetic expression heavily depends upon reliable evaluation of kinetic parameters from the decomposition behavior under different conditions of temperature and/or environment.

The main purpose of this study was to approach the pyrolysis of rice straw by thermogravimetric analysis. Furthermore the present study provides a comparison of selected methods for analyzing non-isothermal solid state kinetic data and investigate the kinetics of thermal decomposition to describe the pyrolysis process. The pyrolysis process was performed by TGA in nitrogen atmosphere and the thermal analysis curves were recorded at several linear heating rates. Three model-free (Kissinger, Flynn-Wall-Ozawa and Kissinger-Akahira-Sunose) non-isothermal methods were used to calculate Arrhenius parameters and to verify which of them allow to detect reaction mechanisms of pyrolysis process. The effect of heating rate on decomposition was also studied.

EXPERIMENTAL AND METHODOLOGY

Experimental

ThermoGravimetric Analysis, TGA was performed using Perkin Elmer, Pyris1 analyzer. To maintain pyrolysis conditions, high purity nitrogen

was used as the carrier gas with 50 ml min⁻¹ of volume flow rate. TGA for drying step had a heating rate of 10 K min⁻¹ for all analysis, while pyrolysis step were performed at three different heating rates: 5, 10 and 15 K min⁻¹. Weight sample was 5-10 mg. The sample was put in a ceramic crucible each time and first dried from laboratory temperature to 378 K and the heated from 378 to 973 K. During the heating, the mass of the rice straw and furnace temperature were record.

Kinetic theory

Kinetic analysis techniques have been classified as either model-fitting (i.e., identification of kinetic reaction model) or isoconversional (i.e., model-free). Modern thermal analysis appears to prefer the use of the latter methods for two main reasons [1]: 1) model-free kinetics is sufficiently flexible to allow for a change of mechanism during the course reaction; 2) mass transfer limitations are reduced by the use of multiple heating rates. By contrast, model fitting kinetic methods generally involve a single heating rate, the disadvantage being that activation energy varies with heating rate due to mass/energy transfer effects. In this study intrinsic reaction rate coefficients are obtained for the pyrolysis of rice straw under differential oxidizing conditions as follows.

$$\frac{d\alpha}{dt} = \frac{A}{\beta} \exp(-E/RT) f(\alpha) \quad (1)$$

Where A is the pre-exponential Arrhenius factor, E the activation energy, R the gas constant and $f(\alpha)$ a function called reaction model which describes the dependence of the reaction rate on the extent of reaction, α . Integrating up to

conversion, α , Eq. (1) gives,

$$\int_0^{\alpha} \frac{d\alpha}{f(\alpha)} = g(\alpha) = \frac{A}{\beta} \int_{T_0}^T \exp(-E/RT) dT \quad (2)$$

Isoconversion methods involve carrying out a series of experiments at different heating rates [2].

Model free: Kissinger method

Kissinger [3] developed a model-free non-isothermal method where is no need to calculate E_a for each conversion value in order to evaluate kinetic parameters. This method allows to obtain the value of activation energy from a plot of $\ln(\beta/T_m^2)$ against $1000/T_m$ for a series of experiments at different heating rates (β), where T_m is the temperature peak of the DTG curve. The equation is the following:

$$\ln\left(\frac{\beta}{T_m^2}\right) = \ln\left(\frac{AR}{E}\right) - \frac{E}{RT_m} \quad (3)$$

The activation energy E_a can be calculated from the slope of the plot which is equal to $-E_a/R$.

Model free: Flynn-Wall-Ozawa (FWO) method

The FWO method [4] allows to obtain apparent activation energy (E_a) from a plot of natural logarithm of heating rates, $\ln \beta_i$ versus $1000/T_{ai}$ which represents the linear relation with a given value of conversion at different heating rates.

$$\ln(\beta_i) = \ln\left(\frac{A_a E_a}{Rg(\alpha)}\right) - 5.331 - 1.052 \frac{E_a}{RT_{ai}} \quad (4)$$

Where $g(\alpha)$ is constant at a given value of conversion. The subscript i and α denotes given value of heating rate and given value of conversion, respectively. The activation energy E_a is calculated from the slope $-1.052E_a/R$.

Model free: Kissinger–Akahira–Sunose (KAS)

The KAS method [5] is based on the following expression:

$$\ln\left(\frac{\beta_i}{T_{ai}^2}\right) = \ln\left(\frac{A_a R}{E_a g(\alpha)}\right) - \frac{E_a}{RT_{ai}} \quad (5)$$

The apparent activation energy can be obtained from a plot of $\ln(\beta_i/T_{ai}^2)$ versus $1000/T_{ai}$ for a given value of conversion, α , where the slope is equal $-E_a/R$.

RESULT AND DISCUSSION

Kinetic analysis

Kissinger plot of $\ln(\beta/T_m^2)$ versus $1000/T_m$ K⁻¹ of pyrolysis process for rice straw shown in Fig. 2. The regression equations and the square of the correlation coefficient (R^2) is also presented. The activation energy (E_a) and pre-exponential factor (A) were derived from the slope and intercept of plotting regression line, respectively. The results obtained from Kissinger method are 172.62 kJ mol⁻¹ and 1.46×10^{11} min⁻¹ for activation energy and pre-exponential factor, respectively.

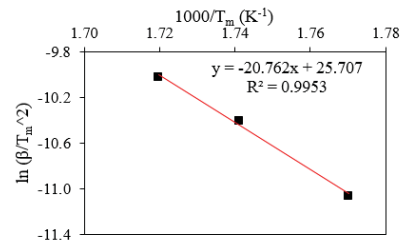


Figure 1. Kissinger plot of rice straw

The kinetic parameters obtained by FWO and KAS methods were calculated according to Eq. (4) and (5), respectively, for a given value of conversion, α . The apparent activation energies were obtained from the slope and pre-exponential factors from the intercept of regression lines and the calculated squares of the correlation coefficients, R^2 , were higher for all cases and were from 0.975 to 0.996.

References

- [1] E. Sima-Ella and T.J. Mays. "Analysis of the oxidation reactivity of carbonaceous materials using thermogravimetric analysis". *J Therm Anal Calorim*, **80**, 2005, pp. 109-113.
- [2] A. Khawam and DR. Flanagan. "Role of isoconversional methods in varying activation energies of solid-state kinetics: II. Nonisothermal kinetic studies" *Thermochim Acta*, 436, 2005, pp. 101-112.
- [3] H. Kissinger. "Variation of peak temperature with heating rate in differential thermal analysis" *J Res Nat Bur Stand*, **57**, 1956, pp. 217-221.
- [4] J. Flynn, and L. Wall. "A quick, direct method for the determination of activation energy from thermogravimetric data" *J Polym Sci Pol Lett*, **4**, 1996, pp. 323-328.
- [5] T. Akahira and T. Sunose. "Joint convention of four electrical institutes" *Sci Technol*, **16**, 1971, pp. 22-3.

Solar Heating, Cooling and Electricity

EFFECT OF MASS RECOVERY ON THE PERFORMANCE OF SOLAR ADSORPTION COOLING SYSTEM

K.M Ariful kabir¹, K.C. Amanul Alam², M. M. A. Sarker¹, Rifat A. Roufb³ and Bidyut B. Saha⁴

¹Bangladesh University of Engineering and Technology (BUET), Bangladesh

²East West University, Bangladesh

³Independent University, Bangladesh, Bangladesh

⁴Interdisciplinary Graduate School of Engineering Sciences, Kyushu University, Japan

SUMMARY: The study investigates the effect of mass recovery process on the performance of a conventional two bed solar adsorption cooling system with direct solar coupling mathematically. In an adsorption refrigeration system, the pressure in adsorber and desorber are different. The mass recovery scheme utilizes this pressure difference to enhance the refrigerant mass circulation. Average Cooling Capacity (ACC) and Coefficient of Performance (COP) were calculated by computer simulation to analyze the influences of operating conditions. The results show that the average cooling capacity of mass recovery system is superior to that of conventional system. It is also seen that mass recovery process enhances the overall performances of solar driven chiller and there is an optimum mass recovery time for an adsorption cooling system with direct solar coupling.

Keywords: Adsorption, mass recovery, solar energy, cooling system

INTRODUCTION

Integrating adsorption cooling systems with solar energy or waste heat can substantially reduce the dependency on fossil fuels making them potential candidates for net zero energy building operation [1,2]. Many researchers studied the adsorption cooling system utilizing solar energy, among them, remarkable studies are made by Anyanwu and Ezekwe [3] for refrigeration system, Sumanthy et al.[4], Clauss et al [5] and Alam et al.[6] for air-conditioning system. Recently, Rouf et al. [7] investigated performance of solar driven adsorption chiller for climatic condition of Dhaka, Bangladesh. Later, Alam et al.[8] introduced heat storage tank to the solar driven adsorption cooling system to extend the working hour beyond sunset. As it was discussed that solar driven air-conditioning has a great potential and mass recovery cycle enhances the performance, therefore, solar driven cooling system with mass recovery process will be very effective. From this context, a two bed conventional adsorption cooling system with mass recovery coupled with solar collector, with silica gel-water pair as adsorbent/adsorbate, is analyzed numerically under the climatic condition of Dhaka, Bangladesh in the present study.

PRINCIPLE AND OPERATIONAL PROCESS OF THE SYSTEM

There are six thermodynamic steps in the cycle, namely, (i) Pre-cooling (ii) Adsorption/Evaporation (iii) Mass recovery with cooling (iv) Pre-heating (v) Desorption/ Condensation and (vi) Mass recovery with heating. The adsorber (SE1/SE2) are alternately connected to the solar collector to heat up the bed during pre-heating and desorption/condensation process and to the cooling tower to cool down the bed during pre-cooling and adsorption/ evaporation process.

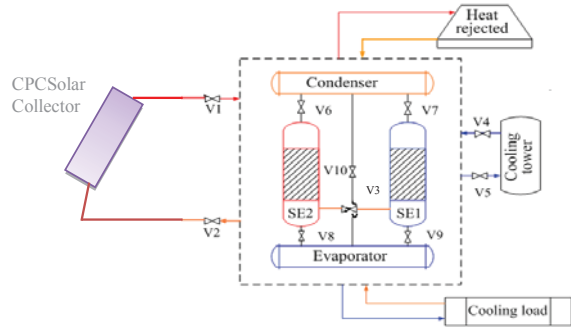


Figure1. Schematic diagram of the solar driven adsorption space cooling system with mass recovery

RESULTS AND DISCUSSIONS

The intension of the present study is to enhance cooling capacity. For the climatic condition of Dhaka at least 14 collectors with 1000s cycle time is needed [7] for the basic adsorption chiller with baser run conditions.

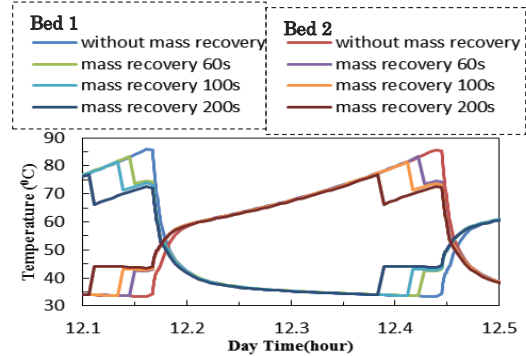


Figure 2. Temperature profile for beds of different mass recovery

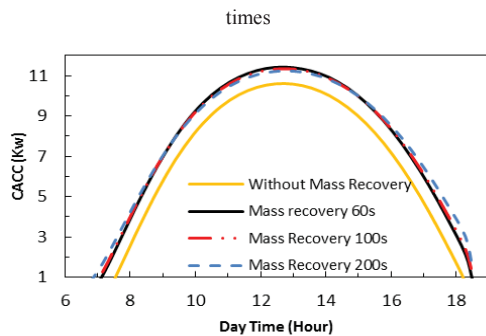


Figure 3. Cooling capacity (kW) of different mass recovery times

The temperature histories of the adsorption chiller with and without mass recovery process are depicted in Fig.2. In case of direct solar coupling with cycle time 1000s, the bed temperature reaches 87°C, however, the temperature rises around 84°C with 60s mass recovery time. The cooling capacities without mass recovery process and with different mass recovery process time are compared in Fig. 3. It is seen that increasing mass recovery process time does not affect the cooling capacity. For the present case the optimum mass recovery process time is 60s.

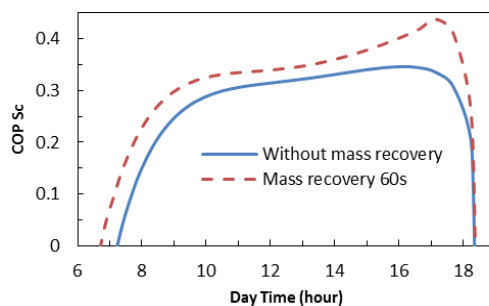


Figure 4. Solar COP in a cycle for mass recover (60s) and without mass recovery

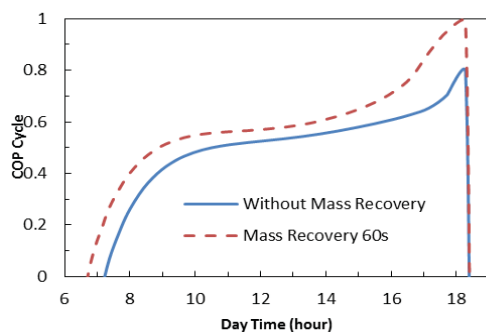


Figure 5. Solar COP in a cycle for mass recover (60s) and without mass recovery

As mass recovery process improve the cooling capacity, therefore, it may be predicted that the

collector area could be reduced by introducing mass recovery process in solar driven cooling system which need a further detail investigation.

The solar COP in cycle (COP_{sc}) and thermal COP in a cycle (COP_{cycle}) are presented respectively in Fig.4 and Fig.5. It is seen that both COP values are improved if mass recovery process is applied. It is also seen that the improvement rate in early morning and late afternoon is higher than those in mid-day.

CONCLUSION

Based on the analysis of the mass recovery process with the solar heat driven adsorption chiller with direct solar coupling, the following concluding remarks can be made for the base run conditions. Mass recover process enhances the performances of the solar driven adsorption chiller. Mass recovery process also enhances the working hour. The optimum mass recovery time is 60s. Maximum Cyclic average cooling capacity with mass recovery is around 11.45 kW at noon while the system produces around 10.5kW without mass recovery process at the same time. Therefore, almost 9% cooling capacity can be achieved by introducing mass recovery

References

- [1] C.Y. Tso, C.Y.H. Chao and S.C. Fu, "Performance analysis of a waste heat driven activated carbon based composite adsorbent-water adsorption chiller using simulation model", *Int.J.Heat Mass Tran*, **55**, 2012, pp. 7596-7610.
- [2] E.E. Anyanwu and C.I. Ezekwe, "Design, construction and test run of a solid adsorption solar refrigerator using activated carbon/methanol as adsorbent/adsorbate pair", *Energy Conversion and Management*, **44(18)**, 2003, pp. 2879-2892.
- [3] K. Sumathy, L. Yong, H. Muller and H. Kerskes, "Performance analysis of a modified two-bed solar-adsorption air-conditioning system", *Int. J. Energ. Res.*, **33**, 2009, pp. 675-686.
- [4] M. Clause, K.C.A. Alam and F. Meunier, "Residential air conditioning and heating by means of enhanced solar collectors coupled to an adsorption system," *Solar Energy*, **82(10)**, 2008, pp. 885-892.
- [5] K.C.A. lam, B.B. Saha and A. Akisawa, "Adsorption cooling driven by solar collector: a case study for Tokyo solar data", *Applied Thermal Engineering*, **50(2)**, 2013, pp. 1603-1609.
- [6] R.A. Rouf, K.C.A. Alam, M.A.H. Khan, T. Ashrafee and M. Anwer, "Solar Adsorption Cooling: A Case Study on the Climatic Condition of Dhaka", *Academy Publisher Journal of Computers*, **8(5)**, 2013, pp.1101-1108.
- [7] K.C.A. Alam, R.A. Rouf, S.B.B. Saha, M.A.H. Khan and F. Meunier. "Autonomous Adsorption Cooling – driven by Heat Storage Collected from Solar Heat", *Journal of Heat Transfer Engineering (under review)*.
- [8] A. Akahira, K.C.A. Alam, K.C. Y. Hamamoto, A. Akisawa and T. Kashiwagi. "Mass recovery adsorption refrigeration cycle-improving cooling capacity", *International Journal of Refrigeration*, **27**, 2004, pp.225-234,

A PARABOLIC CROSS-SECTIONAL GREENHOUSE TYPE SOLAR DRYER: FIELD EXPERIMENTS AND DISSEMINATION

Serm Janjai¹, Prasan Pankaew¹, Rungrat Wattan¹, Korntip Tohsing¹, Yutthasak Boonrod¹
And Anusorn Sangcharoen¹

¹Solar Energy Research Laboratory, Department of Physics,
Faculty of Science, Silpakorn University, Thailand

SUMMARY: A greenhouse type solar dryer was developed. The dryer has a parabolic cross-sectional shape in order to efficiently receive solar radiation and to reduce wind load. This type of dryer has different loading capacities, ranging from 100 kg to 1500 kg for fruits and vegetables. After having tested, several units of this type of dryer were installed for drying various food products in different parts of Thailand. Field experiments were conducted. It was found that the drying time of the products dried in this type of dryer was significantly less than that dried with the natural sun drying and high quality dried products were obtained from these dryers. A Thai government agency has set up a program to disseminate this type of dryer. To date, more than five hundred units of this type of dryer were installed to produce dried products in a commercial scale in Thailand under the government program and private investment.

Keywords: renewable energy, solar dryer, greenhouse type solar dryer

INTRODUCTION

Many agricultural products need to be dried after the harvest for preservation purposes. For a fruit like banana, drying also helps to modify its taste, flavor and texture to meet consumer requirement. In developing countries, natural sun drying method is usually used to dry agricultural products. Although, it is a cheap method, the products being dried are usually subjected to losses due to insects, animals and rain. In general, developing countries are situated in the tropics where solar energy is abundant. As a result, during the past 40 years a number of solar dryers have been developed to utilize solar energy for drying agricultural products [1-3]. However, most of these dryers have a limited loading capacity and are impractical for commercial applications. Having realized these problems, our research group has developed a parabolic cross-sectional greenhouse type solar dryer for drying agricultural products in a commercial scale.

The objective of this paper is to present field experimental results and the dissemination of this type of dryer.

DESCRIPTION OF THE DRYER

The dryer composes of a parabolic roof structure made from polycarbonate sheets on a concrete floor. The parabolic cross-sectional shape helps to receive efficiently solar radiation and reduce wind load. The structure of the dryer is made of galvanized iron bars. Inside the dryer, there are arrays of trays placed on single level raised platforms with passages between the platforms. The polycarbonate sheets protect products from rain, insects and animals. They also help to create the greenhouse effect inside the dryer and to reduce heat losses. Electric fans are placed in the wall opposite to the air inlet to ventilate the dryer. Different sizes of this type of dryer were constructed and tested at

Silpakorn University. The smallest size has a loading capacity of 100 kg of fruits or vegetables while the largest size (Fig. 1) can be used to dry 1,500 kg of ripe banana.



Figure 1. Pictorial view of the dryer a) outside view
b) inside view

FIELD EXPERIMENTS

Several units of this type of dryer were constructed to dry various products in different parts of Thailand. Examples of these products are banana, chili and rice cracker. Field experiments were conducted to dry these products. Solar radiation, drying air temperature, relative humidity and

moisture content of the products were monitored during the drying experiments. The positions of the measurements are depicted in Fig. 2. Example of the drying curves of the products dried in the dryer, as compared to that dried with the natural sun drying are shown in Fig. 3.

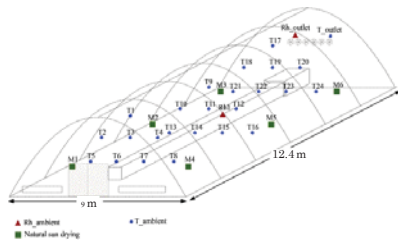


Figure 2. The positions of the measurements. T = temperature, Rh = relative humidity and M = moisture content

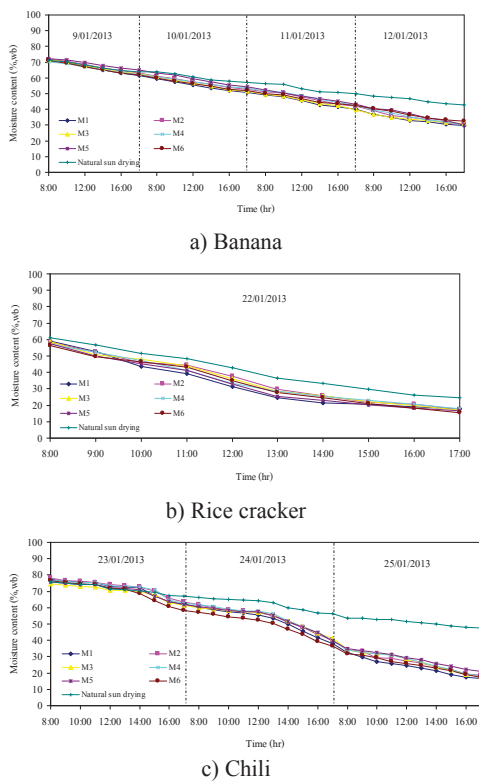


Figure 3. The decrease of moisture content of the product dried in the dryer and that dried with natural sun drying a) banana b) rice cracker and c) chili.

It was found that during 9 am - 4 pm the drying temperature inside the dryer was 5-20 °C higher than ambient air temperature, depending on the time of the day and weather conditions and the drying time

of the products dried in the dryer is significantly less than that dried with natural sun drying. In addition, high quality and products were obtained from the dryer.

DISSEMINATION

As the utilization of this type of dryer helps to save LPG consumption to dry products in small scale food industries, the Department of Alternative Energy Development and Efficiency (DEDE) of Thailand has set up a program to promote the wide-spread use of this type of dryer. According to the program, small-scaled food industries who are selected to join the program will receive subsidy on the initial cost of the dryer. To date more than five hundred units of this type of dryer were installed in Thailand with private investments and subsidy program of DEDE.

CONCLUSION

A parabolic cross-sectional greenhouse type solar dryer has been developed. The dryers have been installed to dry various products and field experiments were carried out to evaluate the performance of these dryers. It was found that the drying time of the products dried in this dryer was significantly shorter than that dried with natural sun drying. More than five hundred units of this type of dryer were installed in Thailand with private investments and subsidy program of DEDE.

ACKNOWLEDGEMENT

The authors would like to thank the Department of Alternative Energy Development and Efficiency for inviting Silpakorn University to carry out this project. The authors also thank the Energy Conservation Promotion Fund for providing the financial support to the project.

References

- [1] A. Fudholi, K. Sopian, M.H. Ruslan, M.A. Alghoul and M.Y. Sulaiman, "Review of solar dryers for agricultural and marine products", *Renewable and Sustainable Energy Reviews*. **14**, 2010, pp. 1-30.
- [2] A. Sharma, C.R. Chen and N.V. Lan, "Solar-energy drying systems: A review", *Renewable and Sustainable Energy Reviews*. **13**, 2009, pp. 1185-1210.
- [3] S. Janjai and B.K. Bala, "Solar drying technology", *Food Energy Reviews*. **4**, 2012, pp.16-54.

POLYGENERATION SOLAR AIR DRYER

Deb Sudip Kumar¹ and Binoy Chandra Sarma²

¹Professor in Mechanical Engineering Department
Assam Engineering College, Guwahati, India

²Research Scholar, Assam Engineering College, Guwahati, India

SUMMARY: Over 85% of industrial dryers are of the convective type with hot air or direct flue gases as the drying medium. Over 99% of the applications involve removal of water. In this study, the performance of a solar air heater with the recovery of the absorbed heat by the metallic concentrator sheet itself besides its normal heat accumulation in the receiver at the focus of the concentrator for generating drying air at a low to medium temperature range is discussed. The system performance through thermal analysis & the performance of a model achieving the required temperature range is also investigate in this study.

Keywords: dryer, polygeneration, moisture, equilibrium, humidity

INTRODUCTION

The flat plate collector used for drying purposes absorbs solar irradiative heat by the exposed collector surface made up of conductive material which is meant for services at a low temperature range below 100°C in an average with the proportionate mass flow rate with that of the collector surface area. Comparatively a low cost thin metallic sheet concentrator having moderate reflectance of around 70% will concentrate solar irradiation at the focus simultaneously with some absorbed solar irradiative heat due to its conductive property. If both accumulations are shared in drying purposes at different temperature ranges, the mass flow rate will increase giving out higher rate of drying effect.

In an indirect method of solar food drying, air is heated in a solar collector which is ducted to the drying chamber to dehydrate the agricultural food product. A temperature gradient followed by a mass transfer of moisture from the inner part of the feed to continue the process. This moisture migration through diffusion due to the vapor–pressure gradient, capillary flow & feed shrinkage pressure can be enhanced though optimum supply of hot air of regulated temperature range determined by the residence time period of drying & its relative humidity. The difference in psychometric properties i.e. partial pressure of water vapor in the air and the partial pressure of the moisture in the product is the driving force for drying.

In this study, the heat generation at the focal point as well as absorbed heat recovered from the concentrator itself has been investigated through the performance of a bench model as referred at Fig.1, the temperature range of which achieved a range to serve the purpose of an indirect solar dryer. This temperature range can be speculated as conducive for drying of a number of agricultural food products enlisted at Table 1.

THERMAL ANALYSIS

The proposed bench model is made up of thin sheet of low cost stainless steel of 70% reflectance

(approx) such that the focal point falls in the aperture plane of the dish concentrator having an aperture diameter of 1040 mm. The rear side is insulated maintaining the requisite space for hot air bounded by the rear surface of the concentrator & the insulating cover as referred in Fig.1



Figure 1. Bench Model of the proposed system

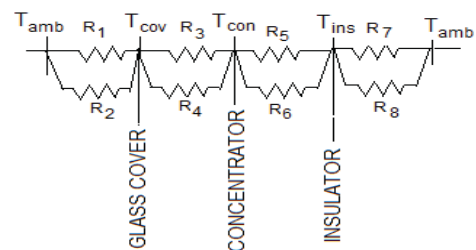


Figure 2. Simplified Thermal Circuit of the Model

The equivalent thermal circuit diagrams at Fig.2 has

been analyzed to achieve the expression for total heat recovered only from the absorption of direct solar irradiation.

This much of heat is an additional source at a

maximum temperature range of 64°C at which drying heat can be supplied to the agricultural food items enlisted in Table 1. The items can be processed further by heat from the receiver at the focal point of the concentrator achieving a maximum of 144°C. At this temperature further processing like pre & post drying processes, washing etc can also be done by hot water.

Accordingly three heat balance equations for the aperture glass cover (Tcov), drying air (Ta) & the rear insulator enclosure (Tins) will yield an expression for the net heat output for the proposed polygeneration system .

Here (as referred in Fig 2)

R = Respective Thermal Resistances due to the Radiative & Convective Heat Transfer Coefficient (W/m².K)⁻¹

T_{amb}=Ambient Temperature(K)

T_{con} =Concentrator Surface Temperature(K)

T_{ins} =Insulating Enclosure Temperature (K)

q_{ha} = Heat carried away by the air from the space in the system above & below the concentrator bounded by the glass cover & the rear insulator cover respectively (J/kg)

I_e = Effective Solar irradiative heat arriving at the concentrator surface (W/m²).

On substitution & rearrangement of the equations we can have an expression as follows which can also be expressed in a further detailed manner using Cramer's rule.

Output = q_{ha} = I_e - U_L(A.Ta -B.Tamb)} Where,

$$A = \left[\left\{ 1 + \frac{2/R_3 + 2/R_4}{1/R_1 + 1/R_2} \right\} \left\{ \frac{1/R_5 + 1/R_6}{1/R_7 + 1/R_8} + 1 \right\} - \left\{ \frac{1/R_5}{1/R_6} \right\} \left(\frac{1/R_1 + 1/R_2 + 1/R_3 + 1/R_4}{1/R_6} \right) \right]$$

$$B = \left[\left\{ \frac{1/R_5 + 1/R_6 + 2/R_7 + 2/R_8}{1/R_1 + 1/R_2} \right\} - \left\{ \frac{1/R_5 + 1/R_6 + 1/R_7 + 1/R_8}{1/R_6} \right\} \right]$$

U_L = Overall System loss coefficient

$$U_L = \frac{[R_1 R_2 R_3 R_4 R_5 R_6 R_7 R_8]}{\left[\frac{1 + (R_3 + R_4)}{(1/R_1 + 1/R_2)} \right] [(1/R_5 + 1/R_6 + 1/R_7 + 1/R_8)(R_1 + R_2)]}$$

The bench model temperature reading plotted as referred Fig 3 envisages the utility of such a system for a large variety of food items enlisted at Table 1.

Earlier such polygeneration systems were studied by Bergene et.al. [1], De Vries et. El. [2] etc primarily on Solar Photo Voltaic Cell with Thermal (CPVT) system.

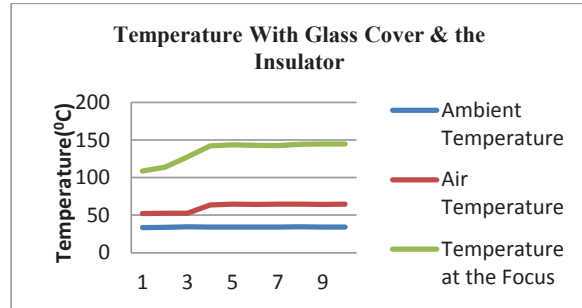


Figure 3.

Table 1. Application sectors

Drying Items	Drying Temperature (°C)	Initial Moisture (%)	Final Moisture (%)
Bananas	70	80	15
Barley	82	20	13
Beets	70	85	14
Cardamom	50	80	10
Cassava	70	62	17
Chilies	40	90	20
Coffee seeds	50	65	11
Copra	40	75	5
French beans	75	70	5
Garlic	55	80	4
Grapes	60	78	18
Oats	82	25	13
Onions	50	85	8
Peanuts	35	50	13
Pepper	55	80	10
Potato	70	85	14
Rice	43	25	12
Rye	25	20	13
Soybeans	67	25	11
Sweet potato	75	75	7
Tea	50	75	5
Wheat	82	20	14

ACKNOWLEDGMENT

This study is supported by the AICTE, MHRD, Govt. of India under Research Promotion Scheme (RPS) for the core topic titled ‘Simulation & Optimization of Solar Hybrid Energy Polygeneration’.

References

[1] T. Bergene and O. M. Lovvik, “Model calculations on a flat plate solar heat collector with integrated solar cells,” *Solar Energy*, **55(6)**, 1995, pp. 453-462.
 [2] D. W. de Vries, *Design of a photovoltaic/thermal combi-panel[Ph.D. thesis]*, Eindhoven Technical University, Netherlands, 1998.

DESIGN AND PRELIMINARY TESTING OF LOW-GRADE HEAT SOURCE ORGANIC RANKINE CYCLE WITH SMALL HOT VAPOR RECIPROCATING ENGINE

Wasun Darawun¹, Roongrojana Songprakorp¹, Veerapol Monyakul¹, Sirichai Thepa¹

¹Division of Energy Technology, School of Energy, Environment and Materials,
King Mongkut's University of Technology Thonburi (KMUTT), Thailand

SUMMARY: This research focuses on the design and preliminary investigating the organic rankine cycle (ORC) by expansion process of working fluid serves as the Small Hot Vapor Reciprocating Engine (SHVRE) which is appropriate for Thailand. For the system design, working fluid is R123 and the electricity generation is imposed not over 500 W. Preliminary testing of ORC has been accomplished with working fluid used as the compressed ambient air not exceeding 7 bars. The results show that the optimal maximum of electric power generation appears at 5 bars, 270 rpm and 137 W, respectively.

Keywords: Organic Rankine Cycle / low-grade heat source / Small Hot Vapor Reciprocating Engine

INTRODUCTION

Nowadays, the organic rankine cycle (ORC) is strongly interested [1-2] to improve the thermal efficiency for recovering waste heat to the electric power. Especially low-grade thermal source [1] (<370°C) i.e. industrial processes, biomass, solar energy etc., Focused on a recovery of waste heat by using a small hot vapor reciprocating engine has never been reported before. This paper deals with feasibility on which adapts the rankine cycle for recovering waste heat and the temperature of heat source does not exceed 100°C. Expansion process uses reciprocating engine for converting thermal energy in superheated steam to the electric power via generator. Pretest uses the compressed air (≤ 7 bars) as working substance. The optimal maximum of electricity generation that relates with pressure, engine speed and power output is discussed.

Many researches use a turbine to convert thermal energy in superheated steam, to mechanical energy and then to the electric power. Turbine expander is exactly suitable for high electricity generation (>1MW) [3]. Lately, the convertor as stirling engine is on-going fascination and researches earnestly. Sripakagorn and Srikam [4] reported the operating prototype at 500°C of heat source temperature and with a low charged pressure of 7 bars used working fluid as the air. The engine produced the maximum power output of 95.4 W at 360 rpm and the thermal efficiency was 9.35% at this maximum power condition. Whereas, the expansion process of working fluid is ideally isothermal. For using a phase change of the working fluid to achieve high energy density, the concept of a reciprocating steam engine is conducted. Takahisa Y, et al [5] proposed a new type of friendly environmental system "ORC" operating with low-grade heat sources. HCFC-123 was working fluid. Investigations were utilized i.e. numerical simulation model and experimental apparatus. The

predicted results showed the optimum operating conditions of water, increasing the turbine inlet temperature resulted high turbine power output. In contrary, when the turbine inlet temperature was as low as possible above the boiling point of working fluid, the best operating conditions for HCFC-123 appeared.

DESIGN AND TESTING PROCEDURES

The criteria of system design, the working fluid is R123 and the electricity generation is imposed not over 500 W. The hot vapor reciprocating engine that is used in this study is modified compact three-cylinder as expressed in Table 2. Design of ORC for low-grade heat source relies on the concept of ideal rankine cycle. The cycle is the ideal for vapor power plants of which does not involve any internal irreversibility [6], i.e. steady state, pressure drop and no heat loss and consists of the following four processes:

- 1-2 isentropic expansion in the reciprocating engine
- 2-3 constant pressure heat rejection in a condenser
- 3-4 isentropic compression in a compressor
- 4-1 constant pressure heat addition in an evaporator

Table 1. Hot vapor engine specifications.

Engine specifications	
Engine	3cyl. Daihatsu
Displacement (cm ³)	670
Bore x Stroke (mm)	63 x 72

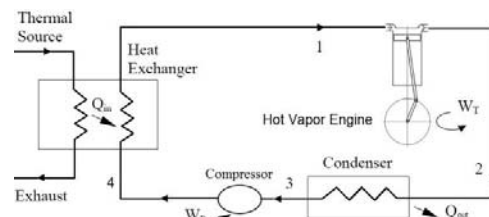


Figure 1. Schematic diagram of ORC system

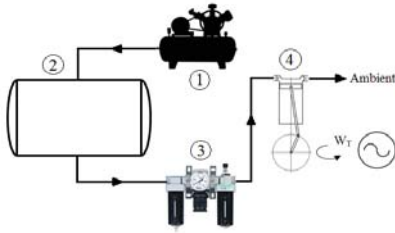


Figure 2. Schematic diagram of preliminary test

Hot vapor engine (stages 1-2)

The superheated working fluid flows into the engine and its pressure is depressurized after the vapor expands. The vapor comes out of the engine at lower pressure P_2 and at low temperature T_2 . In order to analyze the cycle (Figure 1) at an expansion stage, it need identify some relationship between the volumes of the cylinder such as the cut-off ratio (ϕ), closure ratio (r_F), volume ratio (ϵ), pressure ratio (r_P) and the specific heat ratio referring the following [7], respectively.

Thus the mass flow rate of working fluid and work done per cycle is defined by:

$$m_{\text{cycle}} = \frac{V_1 P_{\text{evap}}}{kRT_{\text{evap}}} \left[k(\phi - 1) + 1 - \frac{r_F^k}{r_P} \right] \quad (1)$$

$$W_{\text{cycle}} = P_{\text{evap}} V \left\{ \phi + \frac{1 + \phi(\epsilon - 1)}{(k - 1)(\epsilon - 1)} \right. \\ \left. \left[1 - \frac{1 + \phi(\epsilon - 1)}{\epsilon} \right]^{k-1} \right\} \\ - P_{\text{cond}} V \frac{\epsilon(\epsilon^{k-1} - 1)}{(k - 1)(\epsilon - 1)} \quad (2)$$

Condenser (stages 2-3)

The condenser load (\dot{Q}_{out}) can be calculated from the first's law of thermodynamics as follows equation:

$$\dot{Q}_{\text{out}} = \dot{m}(h_3 - h_2) \quad (3)$$

Pump (stages 3-4)

Compressor circulates working substance the work (\dot{W}_p) of which is calculated by the equation:

$$\dot{W}_p = \dot{m} \frac{P_4 - P_3}{\rho \eta_{\text{comp}}} \quad (4)$$

Evaporator (stages 4-1)

The quantitative of heat input is computed by the following equation:

$$\dot{Q}_{\text{in}} = \dot{m}(h_1 - h_4) \quad (5)$$

Experimental apparatus

The schematic diagram of preliminary testing (Figure 2.), to operating system, the ambient air is compressed and contained the compressed vessel receiver until the pressures reaching 7 bars. Then pressure level of the compressed air is controlled by pneumatic regulator to serve the engine. The speed of engine is stable after that the measurements evaluate the performance of the apparatus.

PRELIMINARY TESTING RESULTS AND DISCUSSION

The optimal maximum of the electric power for the preliminary test appears at about 5 bars, 270 rpm of engine speed and 137 W of electric power output and the tendency shows increasing with raised the engine speed as shown in figure 3a. After the critical point of the engine performance, the tendency decreases with increased the engine speed although the mass flow rates of working fluid increases with raised the engine speed as depicted in figure 3b because decreasing of the reciprocating engine torque appears.

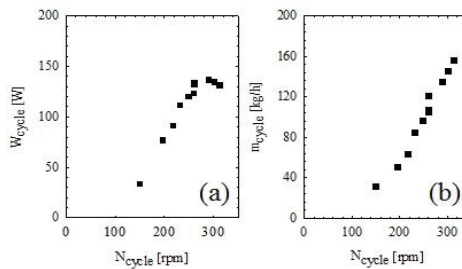


Figure 3. Work done and mass consumption a cycle of preliminary test

CONCLUSIONS

The SHVRE is achieved for operating with the compressed air. And the optimal maximum appears at about 5 bars, 270 rpm and 137 watts.

ACKNOWLEDGEMENT

This research work is supported by the Energy Conservation Promotion Fund, Energy Policy and Planning Office, Ministry of Energy Thailand.

References

- [1] P.J. Mago, "Performance Analysis of Different Working Fluids for Use in Organic Rankine Cycles", *Power and Energy*, **221**, 2006, pp.255-264
- [2] M. Kanoglu, "Energy analysis of a dual-level binary geothermal power plant", *Pergamon Geothermics*, **31**, 2002, pp.709-724
- [3] O.N. Igobo and P.A. Davies., "A high-efficiency solar rankine engine with isothermal expansion", *International Journal of Low-Carbon Technologies*, **0**, 2013, pp.1-7
- [4] A. Sripakagorn and C. Srikam, "Design and performance of a moderate temperature difference Stirling engine", *Renewable Energy*, **36**, 2011, pp.1728-1733
- [5] Y. Takahisa, F. Tomohiko, A. Norio and M. Koichi "Design and testing of the Organic Rankine Cycle", *Energy*, **26**, 2000, pp.239-251
- [6] Y.A. Cengel and M.A. Boles, *Thermodynamics: an engineering approach 6 Edition*, Mc Graw Hill, New York, 2011
- [7] R. Bernardello and J.R. Simões-Moreira., "A proposed theoretical standard cycle for a reciprocating steam engine", *Proceeding of Brazilian congress of thermal sciences and engineering*, 2012

ENERGY TRANSITIONS FOR THE RURAL COMMUNITY IN KENYA'S CENTRAL HIGHLANDS: SMALL SCALE SOLAR POWERED SYTEMS

Harrison Ngetha^{1,2}, Minoru Sasaki¹, Meisam Taheri¹ and Stephen Mathenge²

¹ Department of Mechanical Engineering, Faculty of Engineering,
Gifu University, Japan

² Department of Electrical & Electronic Engineering, School of Engineering,
Dedan Kimathi University of Technology, Kenya

SUMMARY: This paper explores Kenya's central highlands rural community's sources of energy choices' in the last three decades. The paper tracks the changes in sources of energy (firewood, charcoal, kerosene, car battery and dry cells) up to the option of using the solar homes systems. In Kenya, the demand for clean energy for both industrial and domestic activities is on the rise. Currently, the energy for the industries and urban areas is derived largely from petroleum and hydroelectric power. On the other hand, for the low-income earning rural community in the Kenya's central highlands, firewood is however the major source of energy for most domestic activities. Considering that arid and semi-arid regions constitute over 80% of the country, the demand for firewood for instance impacts the natural ecosystems and disrupts the natural nutrient cycling.

Keywords: Kenya's Central highlands, solar energy, wind power, sources of energy, households

INTRODUCTION

The central highlands in Kenya which straddles the equator exhibits one of the best climates in the country of Kenya [Figure 1]. The area receives direct sunlight for the better part of the year. The temperatures vary according to time of the year and day. The warmest to highest temperatures occurs between 9am and noon. The temperatures are moderate, though fluctuating between highs of 29°C in January and lows of 7°C in July, giving a taste of extremes at both ends [Figure 2]. The area has a tropical like climate and has two wet seasons and two dry ones [1]. The major town is Nyeri town which is the Nyeri County headquarters.

A typical rural household in the Kenya's central highland consists of several housing units; the main house, a detached kitchen, usually closer to the main house, the boy's sleeping rooms at a distance from the main house and the domestic animal's shed much closer to the kitchen. In the rural countryside, the educational institutions usually have large tracks of land and the buildings are usually spread out. This kind of land use and building pattern usually possess lots of inefficiencies especially when it comes to lighting. In both cases the pit latrines are a distance away from the main buildings.

From mid-1970 to recent times, the access to the national grid supply of electricity, by the Kenya's population stands at around 44% from 23% in the early 1970's. despite this achievement, reliable electricity is an oxymoron. Blackouts have been a norm especially in the Kenya's central highlands due to inconsistent supply electricity and high demands. Due to this, solar power systems have been implemented, though in small scale basis, in areas where many rural communities may never get access to the national grid. This is because of the high costs involved, which necessitates significant amount of government subsidies [2]. The decline of coffee and tea prices in the world market has really affected the buying capacity of the small scale farmers in the central highlands. Thus, in the Central Kenya highlands, only fewer than 3% of the rural households are linked to the national grid.



Figure 1. Geographical maps of Kenya and the Central highlands (courtesy of world atlas)

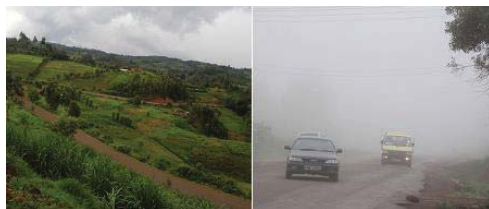


Figure 2. Central Kenya highlands during months of March and July, 2014

ENERGY TRANSITIONS

Firewood & Kerosene

Traditionally, the main sources of energy, for the rural household in Kenya's central highlands are firewood (cooking and heating) and kerosene (lighting). Depending on the economic status of the household, there exists three different types of kerosene lighting devices; the traditional tin lamp

(produced by local artisans), industrially produced wick lanterns and the kerosene pressure lamps [Figure 3].



Figure 3. Tin-wick, Glass and Lantern kerosene lamps

Only a few households (teachers and civil servants) could afford the kerosene pressure lamps. The better endowed households used charcoal for cooking in addition to firewood.

Dry Cells & Car Battery

During the mid-80's~90's, dry cells were used in powering radios and torches. Ordinarily, new dry cells would be used on the torches for some time before being transferred to the radio. The purchase of the kerosene and the dry cells mostly happened once per month after payday.

The television was a luxury item and owning a 'Black & white' TV made one a 'village celebrity'. The color TV was primarily for the local Parish churches, the District and Provincial high schools. The main reason for this is that, only those institutions were connected to national grid system [3]. The rest of the rural folks relied on car batteries to power their TVs. The charging stations at the local shopping centers provided the recharging services. These charging stations were not operated by trained technical personnel, but by the owners of local retail shops or metal-work workshops. The charging systems were old and mostly locally refurbished. The people tasked with repairing and refurbishing the charging systems were the local 'Jua Kali' artisans. This resulted to a reduced life span of the batteries, due to wrong parameter settings of the charging current and voltages.

SOLAR HOME SYSTEMS

As the years went by and the purchasing power of most of the families improved, a 6 ~ 10W solar panel would be purchased to aid in the charging of the car battery used with the TVs. The wiring would be temporary as this was a step by step process of upgrading the solar home system. After buying the solar panel, it was almost inevitable to upgrade the battery from shallow discharge car battery to deep discharge solar battery. However, this was not done when the need arose, but was done either after the 'Tea Bonus' or the 'Coffee Boom' payouts. The entrant of solar panels as an alternative source of energy coincided with improvement in technology

and also the influx of electronics from China which were more affordable to the common 'Mwananchi'.

The initial solar panels that were affordable were physically big and had low power ratings. As the prices dropped, the power rating increased and the physical size reduced, better solar panels became more affordable.

At this juncture, a formal and semi-permanent wiring was done. It was semi-permanent because, the power connections between the TV and the radio were mostly used interchangeably. With time this wiring was done in a neater way, though still allowance for expansion or changes was factored in.

From the year 2000, DC energy saving bulbs came into the market. Prior to the entrant of energy saving bulbs, the rural folk either used the 20~40W incandescent bulbs or resulted to the locally assembled 2-ft fluorescent lighting system. By around 2008, the low power DC energy saver bulbs came in to the major towns in the Central Kenya Highlands. At the same time local institutions and small scale electrical companies started fabricating the 12Vdc to 240Vac inverter systems. This was much more suited to the operating environments of most of the households. And by 2010, most of the system had been upgraded to about 70~100W solar panels systems, a charger controller, an inverter and 75~150Ah deep discharge battery system [Figure 4].



Figure 4. Typical Solar Home System (Panels, Charger controller, Inverter and batteries)

CONCLUSION

As the purchasing power of the rural community in the Kenya's central highlands improves, more household are investing in Solar Home systems. This coupled with advancement in technology for low power devices, is aiding in conserving the environments as well as improving the lives of the rural folks.

References

- [1] P. N. Mbuti, "Hydropower, meteorology and sustainable development in Kenya", *Proceedings of the 4th Kenya Meteorological Society workshop on meteorological research, applications and services, Mombasa, Kenya, 7th – 11th September 1998*.
- [2] Republic of Kenya, "Scaling up renewable energy program", *investment plan for Kenya; 2011*.
- [3] Kenya Power (2010). "Annual Report & Accounts: 2009–2010", *Nairobi: Kenya Power Company (KPC)*.

DESIGN OF LOW POWER WIRELESS POWER TRANSFER BY USING MAGNETIC COIL RESONANT SYSTEM (MCRS) WITH SOLAR ENERGY

M. Fareq¹, S. Marsitah¹, M. Fitra², M. Irwanto², Syafruddin. HS¹, N. Gomesh¹, M. Irwan¹, M. Arinal¹, Suwarno²

¹Centre of Excellent for Renewable Energy (CERE)

School of Electrical System Engineering, Universiti Malaysia Perlis, Malaysia

²Departmen of Electrical, Faculty of Technology Industry, Institut Teknologi Medan, Indonesia

ABSTRACT: The design of low power wireless power transfer is using the concept of Magnetic Coil Resonant System (MCRS). The concept of MCRS is function like an antenna to transfer the power from one point to another point. The project will show the efficiency of the wireless power transfer based on the differences diameter of the coil and also the distance between the transmitter and receiver coil. The solar energy source is used to make this project is green technology.

Keywords: wireless power transfer, magnetic coil resonant system, solar energy source.

INTRODUCTION

Wireless power transfer has been a dream of human beings. Many scientists have researched it uninterruptedly, but very little progress has been made. They have been studied very deeply and used in each daily life, such as electric toothbrushes, cordless home phones and so on. Efficiency of non-contact electromagnetic induction can reach to 80%, but in a very short distance, just in 1cm. Wireless power transfer of resonant coupling can transfer energy in 5cm and its efficiency can get to 40%, which will be a new technology with wider using range. The effect which the coil is highly resonant, any energy placed on coil dies away relatively slowly over very many cycles, but if a second coil is brought near it, the coil can pick up most of the energy before it is lost, even if it is some distance away. [1-2]

This project just used LED as an output or load. Figure 1 below shows the block diagram for the whole project.

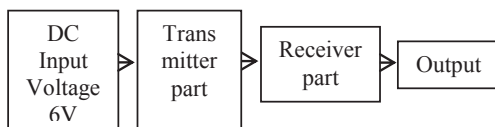


Figure 1. Block Diagram of Wireless Power Transfer

THEORY

Wireless Power Transfer (WPT) is the process where electrical energy is transmitted from a power source to an electrical load across an air gap using induction coils. The receiver coil takes power from the electromagnetic field and converts it into electrical power. [3]

Inductive or magnetic coupling works on the principle of electromagnetism. When a wire is proximity to a magnetic field, it induces a magnetic field in that wire. Transferring energy between wires through a magnetic field is inductive coupling. [4]

TESTING PROCESS

The experimental setup has been studied for the transmitter and receiver circuit. The LED has been used as a load and connected at the receiver part. The source for this process actually used the solar system to give the source to this project, but for the testing used the direct voltage source.

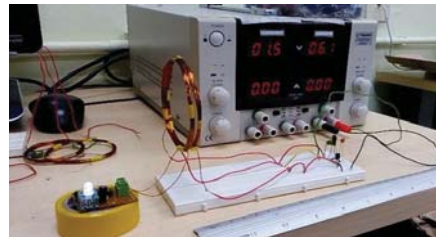


Figure 6. The test done by placing the coil close to each other.

Figure 6 shows the testing of the circuit when both of coils are close together. As shown in the figure above, the LED is lit up clearly and the voltage output at that time also higher.

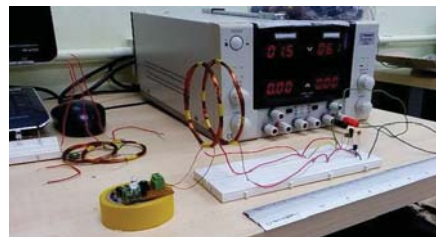


Figure 7. The test, by separating the coil with a distance of 2 cm.

Figure 7 shows the testing process if the coils are having some distance. From figure above the LED is dimmed and almost not light up. Then, the

value of voltage output also decrease. After that, for this testing is repeated again with the different diameter size of the coil to get the data measurement for each coil.

RESULT

An experiment has been conducted to get the efficiency of the power transfer based on the different diameter size of the coil and also the maximum distance that power can transfer by using the different diameter size of the coil. In this experiment, there are 5 different diameter size of the coil, which is started with 6 cm, 7 cm, 8 cm, 9 cm and the biggest size is 10 cm but the number of turns is fixed with 10 turn for both transmitter and receiver coil.

Table 1. Result obtained from the testing.

Diameter (cm)	Distance (cm)	Voltage Output, V_o (V)
6.0	0.0	2.816
	0.5	2.802
	1.0	2.729
	1.5	2.551
7.0	0.0	2.855
	0.5	2.822
	1.0	2.766
	1.5	2.722
8.0	0.0	2.826
	0.5	2.801
	1.0	2.732
	1.5	2.649
9.0	0.0	2.866
	0.5	2.816
	1.0	2.768
	1.5	2.694
10.0	0.0	2.381
	0.5	2.853
	1.0	2.801
	1.5	2.744
	2.0	2.746
	2.0	2.648

Table 1 shows the result of the output voltage with the some distance between the transmitter and receiver coil. The maximum distance is until the LED still can light up which is the power still can transfer to the load.

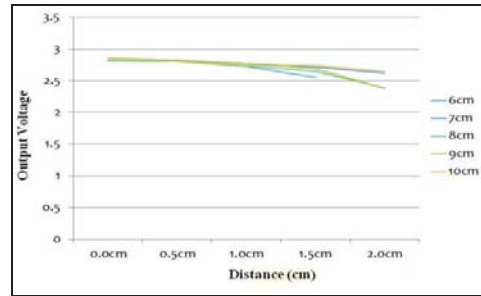


Figure 9. Graph of output voltage vs distance.

Figure 9 shows the graph that has been created according to Table 1. As shown in the graph above, the increasing of the distance between coil, the output voltage will continually constant until at the certain point the voltage output will decrease.

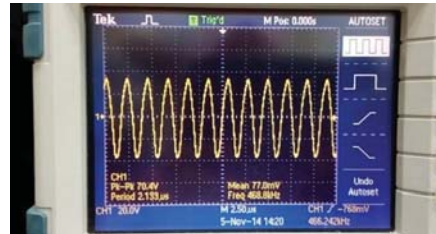


Figure 10. Sinusoidal output waveform for the range of 2 cm.

Figure 10 above shows the output waveform from the oscilloscope. The waveform shows the sinusoidal wave and the amplitude of wave is small because the distance for the transmitter and receiver coil is far in range of 2cm.

CONCLUSIONS

Based on experimental result, the study on wireless power transfer using MCRS has much aspect in terms distance, range of frequency and result show the nearer the distance, the voltage transferred is higher. In this project, the LED is a symbol of bulb that can be used with this prototype. The increasing in the size of diameter coil, the higher power will produce and the slight longer distance that can be wirelessly transfer power.

References

[1] Mystica Augustine Michael Duke, "Wireless Power Transmission", International Journal of Scientific & Engineering Research, Vol.5, Issue 10, October 2014.
 [2] Shishir Shukla, "Wireless Charging", IEEE-CRCE Technobuzz, Vol. 5, Issue 1, pp. 9, September 2011.

Energy Policy and Energy Security

ASSESSING ENERGY SECURITY PERFORMANCE IN THAILAND UNDER DIFFERENT SCENARIOS AND POLICY IMPLICATIONS

Aumnad Phdungsilp¹

¹Department of Industrial Engineering, Faculty of Engineering, Dhurakij Pundit University, Thailand

SUMMARY: Energy security is strongly related to energy and climate policies. Understanding of energy security implications is critically important for shaping policy measures. This study presents the future energy security assessment in Thailand under three energy scenarios. The assessment was based on the use of energy security indicators to track the impact of changes in the energy system under three energy scenarios for the period 2012–2030. These indicators were clustered into four groups, including energy demand, diversification of energy supply resources, environmental dimension, and energy market. The three scenarios were derived from published data. The analysis suggests that Thailand needs to develop specific policy measures to enhance energy security in terms of energy market dimension and to pay more attention in national energy efficiency and total CO₂ emissions to maintain the economic growth.

Keywords: energy scenarios, energy security, Thailand

INTRODUCTION

Many countries consider energy security as equivalent to national security because of its influence on national autonomy and development. Energy security has also integrated into a major part of energy policy. It is generally accepted that energy security is strongly related to other policies as well such as environmental and climate policies. This implies the importance of assessing energy security consequences of energy development pathways. Thailand imports approximately 60% of total primary energy supply in 2013. Oil and natural gas account for 76% of primary energy supply and 68% of total final energy consumption. This high import dependency and low fuel diversity leaves the country vulnerable in terms of energy security.

A number of potential energy development pathways exist to enhance energy security in Thailand, but most of these pathways would entail a considerable commitment in time and funds, thus scientific support would be of great value in facilitating decisions of policy makers. In addition, concerns about climate change have become an additional factor in energy security debate and energy policy decision-making since energy use and conversion are key components for addressing the mitigation of climate change. Direct physical impacts of climate change are likely to impact energy security. The diversification of energy supplies to enhance energy security could have a bearing on the climate protection. Therefore, understanding energy security implications of energy and climate policies is critically important for anticipating the degree of support from all level of the society.

The definition of energy security varies from place to place and time to time. Also, it depends on the purpose of evaluation. Generally, energy security can be defined as how to equitably provide available, affordable, reliable, efficient, environmental friendly, and socially acceptable energy services to end-users [1]. Energy security studies typically focus on the

security of energy supply. A few studies focus on a particular sector (e.g., industrial or power sector) or a specific technology (e.g., nuclear security). Some studies provide a generic approach to evaluate historical energy security based on several indicators or combined into a single indicator. It is, however, little effort to date has assessed the quantify energy security and compared energy security dimensions of different energy pathways, and the policy implications. Moreover, there are a small number of existing energy security assessment studies in Thailand. As a result, the objective of this paper is to assess future Thailand's energy security performance of different energy scenarios. The method used in this study can also be applied for analysis of national energy security in other countries and could be applied for provincial level, if relevant data are available.

METHODOLOGY

There are no standard metrics to assess energy security. Indicators are the most widely used tools to assess energy security. This study follows the assessment framework developed by [2]. It consists of selecting energy security indicators and applies to assess different energy scenarios. In addition, this study analyzes the energy security implications of energy and climate policies. The assessment is based on a combination of quantitative and qualitative analysis. For quantitative analysis, the methodology relies on the use of indicators to track the impacts of changes in the energy system in three energy scenarios. For qualitative method, the policy implications of energy security scenarios are analyzed.

Following common definition of energy security, indicators were identified as selected to quantify energy security. This resulted in nine indicators under four major groups, as shown in Table 1. In fact, many energy security indicators have been proposed and published, however, a small number of indicators can be used for evaluating

energy security under long-term energy scenarios. The indicators were selected based on four criteria: (1) relevant to current energy security concerns; (2) sufficiently apply to energy systems; (3) possible to calculate from available data; and (4) able to provide information for policy analysis. These clustered groups of indicators reflect the energy security of the overall energy system from the generation, conversion and utilization.

Table 1. Clustered groups and indicators for assessment.

Group	Indicator
1. Energy demand	1. Energy intensity
	2. Energy use per capita
	3. Oil use per capita
2. Diversification of energy supply resources	4. Shannon-Wiener Index (SWI)
	5. Non carbon incentive fuel portfolio (NCFP)
3. Environmental dimension	6. Total CO ₂ emissions
	7. CO ₂ emissions per capita
	8. Energy import
4. Energy market	9. Net energy import dependency (NEID)

The energy scenario inputs in this paper are the Business-as-Usual (BAU) [3], the Low Carbon Society (LCS) [4] and the High Economic Growth (HEG) [5]. These energy scenarios provide detailed quantification of developments of the energy system. They enable to apply indicators for assessing and analyzing future energy security performance. Then, data are calculated for each indicator. Due to different units of indicators, data are converted into ordinal values from the raw data of nine indicators. The scoring range is scaled from 1 to 10. Equal weights are given to the indicators. A higher score means a better energy security situation.

RESULTS AND DISCUSSION

This study strongly suggests that energy security analysis should be extended beyond traditional themes of oil or gas supplies to incorporate emergent areas of importance. It will lead to new opportunities in shaping energy policy measures. Figure 1 shows the energy security situation in 2030 for each scenario compared with 2012, as the base year. It reflects how the energy security would improve in four dimensions. A score of 10 presents high energy security performance. The indicators are calculated based on data from the three scenarios for 2030 and compared with data in 2012 to track changes in energy security performance over time (see Figure 2).

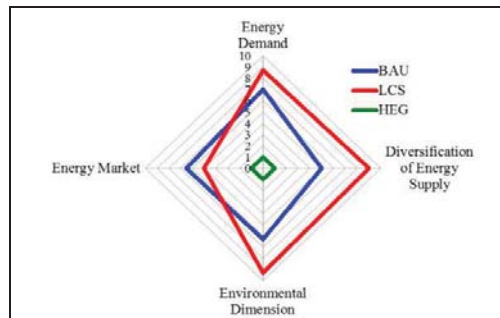


Figure 1. Energy security performance in 2030 of three scenarios

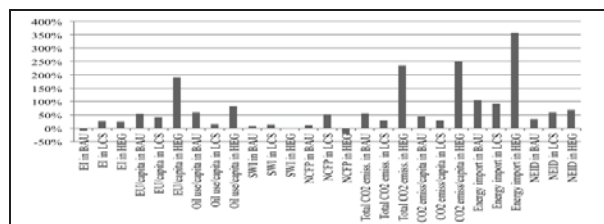


Figure 2. Percentage change of energy security indicators in 2030 compared with 2012 for the three scenarios

The analysis of three scenarios shows that in BAU scenario, there is an improvement in energy security in most dimensions. The LCS scenario shows high potential improvements in three dimensions. In particular, the diversification of energy supply resources shows the highest improvement as compared with other scenarios. The HEG scenario shows a little improvement in all dimensions. This scenario indicates the high energy use per capita, total CO₂ emissions and high energy import.

References

[1] B.K. Sovacool, I. Mukherjee, I.M. Drupady and A.L. D’Agostino, “Evaluating energy security performance from 1990 to 2010 for eighteen countries”, *Energy*. **36**, 2011, pp.5846-5853.
 [2] J. Martchamadol and S. Kumar, “Thailand’s energy security indicators”, *Renewable and Sustainable Energy Reviews*. **16**, 2012, pp.6103-6122.
 [3] Asia Pacific Energy Research Centre (APEREC), APEC Energy Demand and Supply Outlook 5th Edition; 2013.
 [4] B. Limmeechokchai, S. Chungpaibulpatana, R. Nitorisavut, P. Winyuchakrit and A. Pattanapongchai. Low-Carbon Society Vision 2030 Thailand; 2010.
 [5] M. Watcharejyothin and R.M. Shrestha, “Regional energy resource development and energy security under CO₂ emission constraint in the greater Mekong sub-region countries (GMS)”, *Energy Policy*. **37**, 2009, pp.4428-4441.

PROJECTED BUSINESS RISK OF REGULATORY CHANGE ON WIND POWER PROJECT: CASE OF SPAIN

Gyanendra Singh Sisodia¹, Isabel Soares², Paula Ferreira³, Sanjay Banerji⁴, and Rajiv Prasad⁴

¹Amrita School of Business, Amrita University, Coimbatore, India; and FEP, University of Porto, Portugal

²CEFUP & FEP, University of Porto, Portugal

³DPS, University of Minho, Portugal

⁴Amrita School of Business, Amrita University, India

SUMMARY: Regulatory uncertainties have often posed a business risk to renewable energy investors. Energy regulations in Spain were recently revised in June 2014. The objective of this study is to analyze the 50 MW wind power project under revised framework. The project is evaluated using NPV with risk and real options method through Monte Carlo simulations. As a part of this study, five scenarios were evaluated. The base scenario, "Business As Usual (BAU)" consist of recent framework that was into place, just before the new regulation was announced. The other scenarios (including newly introduced framework) were compared to the BAU. We have focused on "delay" option for the current scope. The overall results of the study suggest a negative NPV under the revised framework, with significantly higher delay value. From the results, it is advisable to delay the project. Paper also presents the policy implications under scenarios selected in the papers. Paper also presents the policy implication for developing countries. The paper also served as the learning for developing nations from European Union states.

Keywords: Regulatory uncertainty, business risk, project evaluation, renewable energy support schemes
renewable energy, wind power

INTRODUCTION

The tentative investment requirements for any of the projects may be mostly valid in the context of specific policy under which the investment is made. If the firm perceives the regulatory uncertainties as adversely affecting the firm's profitability, the firm may refrain from investing in such projects [1]. This study is in the context of current regulatory change that Spain has announced in June 2014 for renewable energy projects. According to the revised framework, the regulatory period for the wind power project is reduced from 20 years to 6 years. After, the regulatory period is over, the project can sell wind electricity at market price. World's largest renewable energy company, EDPR1 has estimated a loss of Euros 30 million in operating under revised framework. This study throws light on the business risk associated with medium sized, 50 MW wind power project. In Europe, feed-in tariffs, feed-in premiums, renewable certificates etc. support renewable energies. The major focus of the current study is to put forth the fluctuations in monetary profits due to changing feed-in tariff policy. The main objective of the study is to evaluate the project through traditional methods, NPV given by Fisher (1907) [2] and through the real options approach introduced by Black and Scholes (1973) [3]. The main research question asked through this study is: Given the present policies, is it better to delay or expand the project To address this question, we studied two scenarios: first, the base scenario (the case prior to the enforcement of revised policy) ; second, the scenario after the implementation of revised policy.

¹Please refer edpr.com

DATA AND METHODOLOGY

Data and Assumptions

A 50 MW (39 units of 1.3 MW) wind power project was studied in the current context. Wind towers were considered to be installed at optimal elevation where it can receive optimal wind speed for electricity generation. Factors such as steel cost, site, and labor cost etc. can affect installation cost. Per megawatt installation cost considered in the study ranged from 1.2 and 1.8 million Euros/MWh² with the average of 1.5 million Euros. The assumed cost consists of labor cost and other costs, including official/regulatory formalities. The project is considered to be irreversible in nature (with a life of 25 years), that requires at least 4 years setup period before it can generate electricity, with no salvage value at the maturity of the project.

Cost associated with the leasing of land was estimated to be Euros 1,00,000 per year with an annual increment of 10% after every fifth year. Operations and maintenance cost is estimated to be 13.91 Euros/MWh with fluctuation of 12.51 to 17 Euros per MWh. Staffing and insurance are assumed to be 305,932 Euros per year with the increment of 10% after every fifth year. Present value (PV) factor ranging from 2-5% are considered; in the most likely case PV factor of 2.5% is taken. Assumptions that we have considered were similar to the assumptions that were made by Monjas-Barroso & Balibrea-Iniesta (2013) for evaluating wind power

² The prices range considered were influence from IRENA.Org report downloaded from http://www.irena.org/DocumentDownloads/Publications/RE_Technologies_Cost_Analysis-WIND_POWER.pdf

projects in Denmark, Finland and Portugal [4]. The average market prices of electricity in Spain were obtained from MIBEL3.

Methodology

With the above-mentioned data and assumptions, the project under two scenarios was evaluated through this study. We evaluated the project through NPV (with risk factors) and through a real options approach (with “delay” and “expand” option). We used existing models used in other studies [4][5][6][7] to address our study. Input values with varying risk parameters (under assumptions) were considered for modelling the business risk. For the modelling purpose, a trial version of @Risk software developed by Palisade (2000) was used.

RESULTS

Business risk for medium sized wind power projects was evaluated through this study. The electricity data from Mibel was used. NPV risk was calculated and compared for two projects. Black and Scholes real options model was used to calculate the option to delay and option to expand the project. Under the revised framework, the investment seems risky, and it is better to delay the project. This study leads to further study that leads to framing new policies under which the investors’ return on investments could be safeguarded.

FINAL NOTES

The wind power may still be not competitive with other mainstream sources of power like thermal, nuclear etc. and hence needs greater regulatory support. The reduction in the price protection from 20 years to 6 years in Spain has shown that the new projects post-regulatory change are unviable according to our study. So, developing nations in Europe as well as elsewhere including India who want to promote wind power should learn from Spain's mistake and provide price protection to new wind power plants for the entire project life of 20 - 25 years.

ACKNOWLEDGMENT

Authors are thankful to Amrita School of Business; FEP, University of Porto; University of Minho for providing academic support. Authors are also thankful to European Commission for giving an opportunity to Gyanendra for pursuing doctoral research at University of Porto.

References

[1] K. R. Fabrizio, “The Effect of Regulatory Uncertainty on Investment: Evidence from Renewable Energy Generation” *Journal of Law, Economics, and Organization*. **29**, 2012,

pp.765–798.

[2] I. Fisher, “The Rate of Interest: Its Nature, Determination and Relation to Economic Phenomena”, New York: Macmillan Co.1907.

[3] F. Black, M. Scholes, “The pricing of options and corporate liabilities”, *Journal of Political Economy*, **81**, 1973, pp. 637–659.

[4] M. Monjas-Barroso, and J. Balibrea-Iniesta, “Valuation of projects for power generation with renewable energy: A comparative study based on real regulatory options”, *Energy Policy*, **55**, 2013, pp.335–352.

[5] L. Santos, I. Soares, C. Mendes, and P. Ferreira, “Real Options versus Traditional Methods to assess Renewable Energy Projects”, *Renewable Energy*, **68**, 2014, pp.588–594.

[6] A. Michailidis, K. Mattas, I. Tzouramani and D. Karamouzis. “A Socioeconomic Valuation of an Irrigation System Project Based on Real Option Analysis Approach”, *Water Resources Management*, **23**, 2008, pp.1989–2001.

[7] T.K. Boomsma, N. Meade and S.-E. Fleten. “Renewable energy investments under different support schemes: A real options approach” *European Journal of Operational Research*, **220**, 2012, pp. 225–237.

[8] Palisade Corporation, RISK risk analysis and simulation add-in for microsoft excel: a software package. Version 6, Newfield, NY, 2000.

³ Average electricity price two years (2012 and 2013) were obtained from Mibel data available at <http://www.mercado.ren.pt/>

ENERGY STORAGE: TECHNOLOGY APPLICATIONS AND POLICY OPTIONS

Mathieu Landry¹ and Yves Gagnon¹

¹Université de Moncton, Edmundston (NB), Canada

SUMMARY: This paper presents technology applications and policy options related to energy storage in energy systems or grids. Energy storage technologies are a promising area that could be an important tool to achieve a low-carbon future since they allow for the decoupling of energy supply and demand. Energy storage technologies could potentially be deployed across the supply, transmission and distribution, and demand portions of an energy system or grid. The services they provide are either based on a power application or an energy application and range from long-term seasonal storage to short duration spinning and non-spinning reserve. In terms of energy storage technologies, pumped storage hydropower systems are a mature technology and comprise over 99% of the current total global installed capacity of energy storage technologies which is evaluated at over 141 GW. Finally, policy options should seek to enable compensation for the multiple services performed across the energy system in order to achieve widespread deployment.

Keywords: Energy storage, renewable energy, policy, power grids, thermal grids

INTRODUCTION

Energy storage is a promising technology that could be an important tool to achieve a low-carbon future. Specifically, it allows for the decoupling of energy supply and demand, which can provide a valuable resource to electricity system operators.

The most important drivers for increasing use of energy storage are [1]:

- Improving the efficiency of energy system resources;
- Increasing integration of variable renewable resources (i.e., wind and solar);
- Rising self-consumption and self-production (distributed generation) of energy (electricity, heat/cold);
- Increasing end-use sector electrification (i.e., electric vehicles);
- Increasing energy access (i.e., off-grid electrification); and,
- Growing emphasis on grid stability, reliability and resilience.

By providing services in the energy system, energy storage technologies are valuable tools for operators of energy systems with supply and/or demand variability. While the latter has historically been part of the energy system, the former is an increasing concern as jurisdictions are looking to increase the penetration of variable renewable energy generation on their energy grids.

ENERGY STORAGE TECHNOLOGIES

In this section, a brief overview of energy storage technologies is presented. Energy storage is not limited to one single technology, rather, it encompasses a range of technologies, which include:

- Pumped Storage Hydropower (PSH);
- Underground Thermal Energy Storage (UTES);
- Compressed Air Energy Storage (CAES);
- Pit Storage;
- Molten Salts;

- Batteries;
- Thermochemical Storage;
- Chemical-Hydrogen Storage;
- Flywheels;
- Supercapacitors;
- Superconducting Magnetic Energy Storage (SMES);
- Solid Media Storage;
- Ice Storage;
- Hot- and Cold-Water Storage; and,
- Hydrogen Energy Storage

In terms of location in an energy system or grid, energy storage technologies could potentially be deployed across the supply, transmission and distribution, and demand portions of an energy system or grid as is presented in Figure 1.

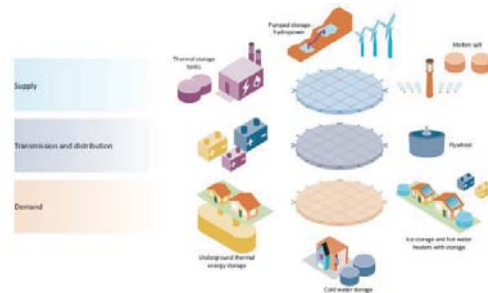


Figure 1. Hypothetical deployment of energy storage technologies in an electric power system [2]

The services provided by energy storage technologies along with potential services provided by the introduction of other energy technologies, such as smart grid technologies, generally determine the best locations for their integration in the energy system. Having said this, because of the nature of the service they provide, thermal storage technologies are generally found either in the supply (thermal storage tanks and molten salts) and demand (hot and cold-water storage) portions of the energy

system.

Current Status of Energy Storage Technologies

Contrary to other energy technologies such as renewables, there is a current lack of widespread and accessible data related to quantifying global energy storage capacities. However, good datasets exist for the United States, Canada, Japan and some regions of Europe in relation to large-scale grid connected electricity storage capacities. From these datasets, it can be estimated that the current global installed capacity of electricity storage technologies is at least 141 GW. For their parts, PSH systems with approximately 140 GW of installed capacity worldwide comprises over 99% of the total global installed capacity of energy storage technologies. Other notable technologies with significant global installed capacity include CAES, various battery and flywheel-based energy storage technologies [1, 3].

In terms of thermal energy storage, global energy storage capacities are not known. However, it can be said that domestic hot water tanks are the most common of these technologies. Other notable technologies widely used are ice and chilled water storage which is commonly used in Australia, the U.S., China and Japan, and underground thermal energy storage (UTES) which is used in many European countries. It is estimated that approximately 1 GW of ice storage has been deployed in the U.S. in order to reduce peak energy consumption for areas that experience high cooling demands [4]; while in Denmark, pit storage is commonly used in district heating networks.

In regards to the current commercial maturity of energy storage technologies, Figure 2 presents the initial capital requirement and technology risks versus the current phase of development of key energy storage technologies.



Figure 2. Current maturity of energy storage technologies [5]

From Figure 2, it can be seen that in terms of current commercial maturity of energy storage technologies, pumped storage hydropower (PSH), pit storage, cold water storage, underground thermal energy storage (UTES) and residential hot water heaters with storage are the technologies which are currently in their commercialization phase, ranked on lowest capital requirement and technology risk.

Of all of these technologies, PSH is the most mature and widespread energy storage technology. It is to be noted that compressed air energy storage (CAES) is still considered to be near the end of the demonstration and deployment phase and thus near commercialization [5].

POLICY OPTIONS

It has been shown that the widespread deployment of energy storage technologies is highly dependent on achieving acceptable cost recovery [1]. To this end, policy options should seek to enable compensation for the multiple services performed by energy storage across the energy system in order to achieve widespread technology deployment.

ACKNOWLEDGEMENT

This work was supported by the New Brunswick Environmental Trust Fund. Initial phases of this work were performed while the second author was a Staff on Loan at the International Energy Agency in Paris, France.

References

[1] International Energy Agency (IEA), “Technology Roadmap: Energy Storage”. Paris, France, **64**, 2014, pp. 14.

[2] Energy Information Administration (EIA), “Energy Storage: Location, Location, Location and Cost”, *Today in Energy*. Washington, DC, United States, 2012.

[3] Electric Power Research Institute (EPRI), “Electrical Energy Storage Technology Options”, Palo Alto (California), US, **170**, 2010.

[4] A. O’Donnell and K-A Adamson, “Thermal Storage for HVAC in Commercial buildings, District Cooling and Heating, Utility and Grid Support Applications, and High-Temperature Storage at CSP Facilities”. Pike Research, New York, United States, 2012.

[5] B. Decourt and R. Debarre, “Electricity Storage: Factbook”. Schlumberger Business Consulting Energy Institute, Paris, France, **98**, 2013.

POLICY ASSESSMENT OF POTENTIAL BIODIESEL FEEDSTOCK SUPPLY IN THAILAND

Jutaporn Keson¹, Sangdao Wongsai¹, Adisorn Ratchaniphont¹ and Noppachai Wongsai¹

¹Andaman Environment and natural Disaster research center (ANED),
Faculty of Technology and Environment, Prince of Songkla University,
Phuket Campus, Thailand

SUMMARY: The Thai government has promoted the Renewable and Alternative Energy Development Plan for 25 Percent in 10 Years (AEDP 2012-2021) to reduce the energy importation. In the present study, we aimed to assess the potential development of alternative source for biodiesel sector. A case study of three provinces, Krabi, Suratthani, and Nakornsrihammarat, was considered to seek for suitable areas for oil palm expansion based on the land suitability guided by the Good Agriculture Practice (GAP) of the nation. We emphasized on the AEDP policy implementation for the restriction of expansion only on the pre-existing croplands, mainly the rubber plantation. Our results indicated that only the land availability and suitability in the three provinces are sufficient for oil palm expansion target as far as any ages of rubber plantation are considered. In the future, we propose to investigate the ages of rubber plantation in order that only the old plantation should be considered as suitable oil palm expansion.

Keywords: renewable energy, GIS, land suitability, oil palm, para rubber,

INTRODUCTION

The majority of energy consumption in Thailand depends on the importation. Crude oil has the highest proportion at 80% of total domestic oil consumption, and the value is over 31 billion US dollars. The Thai government has promoted the Renewable and Alternative Energy Development Plan for 25 Percent in 10 Years (AEDP 2012-2021) to reduce the energy importation, and to take opportunity for the future development of low carbon economy and society [1].

Biodiesel is one of the attractive renewable fuel sources in Thailand, and the main feedstock is obtained from palm oil. The AEDP policy production target is set at 5.97 million liters per day by 2021. Such that 880 thousands hectares of oil palm plantation will be required by 2021. In order to regulate this biodiesel alternative, the government has established the protocol-based strategy of oil palm industry (2004-2029) and has set the national development toward energy security as the most significant part of The 11th National Economic and Social Development Plan (2012-2016). Rubber plantation is chosen as the priority croplands in land transformation to oil palm. This is due to the fact that the yield of rubber plantation in Thailand is much more over the world marketing demand. Therefore, the reduction of replanting this plantation is motivated by the government incentives and subsidies to stimulate land use changes from cash crops to energy crops.

With the aim of policy implementation, oil palm expansion is in consideration with land availability and land suitability guided by the Good Agriculture Practice (GAP) of the Thai agriculture handbook on oil palm plantation. Agriculture is complicated in nature because of the large scale and the dynamic of plantation, and thus using GIS can easily and quickly analyze and update information

both quantitative and qualitative [2]. The aim of this study was to assess the potential development of alternative source for biodiesel sector. We considered the two largest producers of oil palm fresh fruit branch, Krabi and Surat thani provinces, in order to seek for suitable areas for oil palm expansion based on the land suitability guided by the GAP of the nation. Nakornsrihammarat province was selected as an alternative producer to assess the possibility of oil palm expansion in the future. We emphasized on the AEDP policy implementation for the restriction of expansion only on the pre-existing croplands, mainly the rubber plantation.

MATERIAL AND METHOD

Study area

Krabi, Surat thani and Nakornsrihammarat provinces are situated in southern Thailand. The three provinces cover an area of approximately 2,781 thousand hectares. About 90% of oil palm plantations are located in the south of the country because its climatic and landscape conditions are suitable for the growth. Thus, the Thai government has focused on the expansion of oil palm plantation areas in these areas to maximize yield production.

Geographic Information System

Land use classification in 2012 and land suitability for oil palm growth were obtained from the Land Development Department, Ministry of Agriculture and Cooperatives of Thailand. Before performing the GIS analysis, we reclassified land use types into seven categories with a focus on areas that grow rubber and oil palm plantation. These categories were oil palm, para rubber, other agricultures, forest, water body, urban and bare land. Four categories of land suitability were classified as suitable, marginal, not suitable and unclassified. We

defined the suitable area as an area with the potential of producing high yield, the marginal area with the lower yield, the unsuitable area for very low yield (not worth to invest), and the unclassified area mostly on the steep hill or in the forest.

This GIS analysis was based on a raster analysis. A cell size of 100 meters was chosen to ensure that the smallest area of rubber and oil palm will be discovered. A method of converting polygon features to a raster dataset is based on the maximum combined area for a cell assignment. Finally, a map of rubber plantation that is currently situated on lands that in fact are suitable for oil palm was produced.

RESULTS AND DISCUSSION

Although the series of government regulations on the biodiesel development sector have been strategically planned, the achievement of the policy production target is dependent on all stakeholders in the oil palm industries. When focusing on land requirement, a choice of crop made by the land owners is the most important factor in driving the potential of biodiesel feedstock supply under the land limitation. It is noted that the policies have implemented by encouragement not by enforcement. Therefore, at the regional level, local authorities are key success for policy implementation in practices. They are responsible to convey information on government incentives and subsidies to farmers, where appropriate, encourage them to transform their pre-existing crops to oil palm by taking into consideration of land suitability, educate them with the GAP, and monitor the outcomes using a total area of oil palm expansion and yield production per unit area as succession indicators.

Having said that, a basis of knowing in advance from where is the most suitable to where is not worth to grow oil palm is essential for a farmer encouragement process. Incorrect information may affect farmers' life since oil palm is a monoculture plant with a growth cycle of 25 years. Table 1 shows different land use types in 2012 that are currently situated on lands that are suitable for oil palm growth, and Figure 1 illustrates a map of rubber plantation on the potential areas that could be converted to grow oil palm in the future. A total area of rubber in the study area is approximately two folds of that of oil palm. The majority of the oil palm plantations are located on the suitable and marginal suitable lands. In addition, only the land availability and suitability in the three provinces are sufficient for oil palm expansion target giving that any ages of rubber plantation are considered. In the future, we propose to investigate the ages of rubber plantation in order that only the old plantation should be considered as suitable areas for oil palm expansion. Such information will provide an insight of actual land availability and suitability in consideration with the policy regulations, which in

turn, offer a better accuracy of yield estimation.

Table 1. Land suitability of oil palm plantation and its current situation of land cover in 2012 of Krabi, Surat thani and Nakornsrihammarat provinces

Land use	Area (1000 Hectare)			
	Suitable	Marginal	Not suitable	Un-classified
Oil palm	240.4	101.8	52.4	40.2
Para rubber	564.2	119.8	264.7	117.0
Other agricultures	69.1	144.8	57.4	39.8
Forest	30.3	20.1	670.9	15.8
Urban	34.6	36.8	21.9	11.3
Water body	4.2	3.8	10.0	21.1
Others	20.7	40.0	18.3	9.2

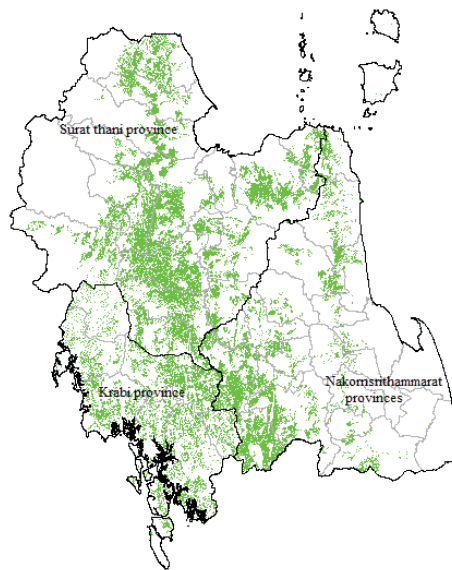


Figure 1. Rubber plantation areas suitable for new oil palm plantation expansion

ACKNOWLEDGMENT

The authors wish to express their gratitude to the Faculty of Technology and Environment, Prince of Songkla University, Phuket Campus, for financial support, and thank to the Land Development Department, Ministry of Agriculture and Cooperatives of Thailand for the data used in this study.

References

- [1] T. Sutabutr, "Alternative Energy Development Plan: AEDP 2012-2021", *International Journal of Renewable Energy*, 7, 2012, pp.1-10.
- [2] P. Borrelli, S. Modugno, P. Panagos, M. Marchetti, B. Schütt and L. Montanarella. "Detection of harvested forest areas in Italy using Landsat imagery", *Applied Geography*, 48, 2014, pp.102-111.

THE PROSPECT OF BIO-ENERGY FROM SOLID WASTE IN THAILAND: POTENTIAL, POLICY AND BARRIERS

Sukhuma Chitapornpan¹ and Chart Chiemchaisri²

¹School of Engineering and Resources, Walailak University, Nakhon Si Thammarat, Thailand

²Department of Environmental Engineering, Faculty of Engineering, Kasetsart University, Thailand

SUMMARY: This paper presents the prospect of bio-energy from solid waste in Thailand. The global warming is the current problem that getting the worldwide attention and speeding up to find the measures for the solutions. Thailand imported more than 60% of energy in each year for commercial use, including 80% of total domestic oil usage which relying on energy import. The Royal Thai Government considers it a foremost mission to lead Thailand through the current global economic crisis towards sustainable growth and increasing quality of life of people. The review on Thai government on the strategic plan on the promotion of alternative energy development for 25% use within 10 years for energy security and measures in reducing in GHGs release, waste scheme, and a roadmap on solid waste management for the whole country were studied. The results shown the estimation of the prospect of bio-energy from municipal solid waste of Thailand in terms of its potential, opportunities and barriers from policies.

Keywords: renewable energy, solid waste, bio-energy, barriers, energy security

INTRODUCTION

Nowadays, solid waste management had become serious environmental problem for many countries in Asia, especially the fast developing economies like Thailand. The amount of waste generation is increasing at a fast rate where the waste collection services are not covering the service areas, in particularly in rural and remote locations, including a large fraction of solid waste stream is managed as open dump landfills. In 2013, the Pollution Control Department (PCD) reported the situation of solid waste that the amount of solid waste generated was 26.77 million tons and only approximately 7.2 million tons (25.7%) were disposed at 466 disposal sites (totally 2490 disposal sites) while the accumulated waste amount of 19.9 million tons were improper managed and accumulated [1]. Thus Thailand government had considered and set a roadmap on solid waste management for the whole country with a systematic management. The critical waste situation areas will undergo a systematic procedure to deal with waste materials in 3 stages; up-stream, mid-stream and down-stream management. Whereas, the areas without a critical waste situation will manage the waste problem following 3 steps; i.e. (1) dispose waste material in a proper landfill to ensure fire control and make disposed waste for the electricity generation in advance, (2) landfill mining of disposed waste materials to be used as refuse derived fuel (RDF) for electricity production by cooperation with the private sector in producing refuse-derived fuel stick for power generation and the disposal of new solid waste, and (3) to enforce the law and regulations on solid waste management in private sector.

From world energy consumption statistic [2] indicates that the world energy consumption had been increasing about 2.59% per year since 1965 to

2013. In 2013, energy consumption of 12,730.4 M toe was three times higher than consumption in 1965 [2]. The increasing in energy demand in Thailand resulting in energy imports more than 60% of energy used commercially, including 80% of total domestic oil usage in each year, and the import portion tends to increase as local petroleum failed to catch up with escalating demand. As Thailand is rich in agricultural products that can be yielded for energy purposes such as biomass, biogas, biodiesel, ethanol, and the by-products from processed food industry, including solid waste from local administrative organization. Thus, these can make Thailand the best potential on alternative energy development and create opportunity to strengthen energy security in the future. The Government of Thailand has currently assigned the Ministry of Energy to set up the 10 Year Alternative Energy Development Plan (AEDP) aiming to create the framework and direction for increasing alternative energy consumption by 25% in 2021 [3, 4]. Thailand statistics of renewable energy consumptions shows in Fig. 1.

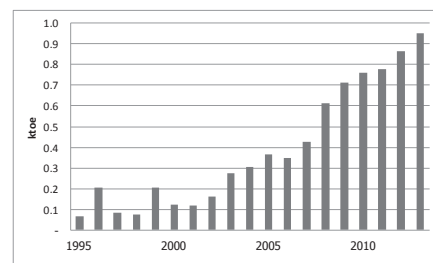


Figure 1. : Statistics of the Thailand's renewable energy 1995-2013[2]

According to AEDP plan in bio-energy, the power generation from waste in small and medium local administrations as well as small communities such as schools, temples, communities, and other agencies had been set up and promoted [3]. The 2021 target is set as 400 MW where a current total capacity is at 65 MW (information on electricity generation in July, 2014).

Therefore, this paper gives general background of the bio-energy program, especially in solid waste management scheme, in Thailand including related national solid waste management schemes and policies. The potential of bio-energy production from solid waste in according to national solid waste management plans is analyzed and discussed. Bio-energy promotion programs in the past and currently situation have been reviewed. Barriers to the promotion of the bio-energy and lessons learnt are also presented together with suggestions for policy change to accelerate the utilization of bio-energy in solid waste management.

RESULTS AND DISCUSSION

In the past, there are various constrains in developing of waste to energy projects for example, the limitation in technology with high investment cost and low returns, limitation of grid system, the protest from publics, limitation in the amending of private sector and local governances and the delayed in permissions process, etc. According to AEDP plan (2012-2021), the bio-energy development in solid waste schemed will be focused on (1) to promote community to collaborate in broaden production and consumption of renewable energy from MSW in the medium and small sizing Local Admin Organizations and to promote and support producing energy from MSW in small communities. In addition, the amending laws and regulations which do not benefit to renewable energy development in producing energy from MSW by all types, especially refuse-derived fuel (RDF) type, then to co-generate heat and power in factory including promoting in oil production derived from plastic waste, the public relations and building up comprehensive knowledge of people in targeted area for establishment of waste to energy system. Furthermore, the research work as mechanism in development of integrated renewable energy industry in study the RDF management would be promoted, including the research and develop on domestic production of incinerator and the small waste to energy system and the development in the standards and appliances for producing oil from plastic waste.

Waste amount are being more severe environmental problem in Thailand because 19.9 million tons of municipal solid waste had been accumulated and improper managed causing pollution problems on surface water, underground water, soil, and illegal waste dumping in improper

area, etc. In 2013, PCD had reported the number of disposal site over country of 2,490 disposal sites, of about 19% (466 disposal sites) of total were properly disposed by sanitary and/or engineering landfill (3%), controlled dump site (15%), large scale incineration (0.08%), waste to energy (WTE) (0.04%), mechanical biological treatment (MBT) (0.12%), integrated solid waste treatment system (0.05%) and small scale incineration (0.3%), which the retained number of 80% (2024 disposal sites) of total operate with improper methods i.e. open dump sites, incineration without air pollution treatment system. These situation cause more seriously environmental problems and solid waste management in local organization to deal with large amount of solid waste themselves.

The current Thai Cabinet had demonstrate the road map for municipal solid waste management to solve the problem of a large number of solid waste accumulated at disposal sites without proper management. The concept of landfill mining and rehabilitation for the combustible materials for RDF production and incineration had been introduce which could increasing in energy production. The overall energy production would be over estimation according to AEDP plan and might effect to the buying and purchasing price in the future.

References

- [1] Pollution Control Department, Ministry of Natural Resources and Environmental, The Pollution Situation Report in 2013. See also: www.pcd.go.th. (in Thai).
- [2] BP, BP Statistical Review of World Energy June 2014. See also: www.bp.com/statisticalreview
- [3] Department of Alternative Energy Development and Efficiency, Ministry of Energy, The Thailand energy situation report in 2013. See also: www.dede.go.th
- [4] Sutabutr T., "Alternative Energy Development Plan: AEDP 2012-2021" *International Journal of Renewable Energy*, **7(1)**, 2012, pp. 1-10. See also: [http://www.sert.nu.ac.th/IIRE/FP_V7N1\(1\).pdf](http://www.sert.nu.ac.th/IIRE/FP_V7N1(1).pdf).

Applied Energy

EXPERIMENTAL TEST OF A PROTOTYPE PEM FUEL CELL VEHICLE ON AN INERTIA DYNAMOMETER

S. Hanapi¹, S. M. H Syed Omar², Alhassan Salami Tijani¹, A. H. Abdol Rahim¹ and W. A. N. Wan Mohamed¹

¹Faculty of Mechanical Engineering, Universiti Teknologi MARA, Malaysia

²Faculty of Electrical Engineering, Universiti Teknologi MARA, Malaysia

SUMMARY: Fuel cell vehicles (FCV) are being seriously viewed as a clean alternative for transportation as it uses hydrogen and emit zero harmful tailpipe emissions. Due to this greater interest, research on FCV at many levels is being performed in all parts of the world. A generic prototype FCV was developed locally as part of a continuous work on understanding the underlying mechanism and optimization of the FCV power train. The 104 kg FCV is driven by a 1.2 kW PEM (proton exchange membrane) fuel cell and 360 W rated power of Brushed DC Maxon motor. This paper reports the simulation, experimental and validation tests of the mini FCV using a custom made inertia dynamometer test bench. This test bench is equipped with data logger that are able to log voltage, current, speed and time. The test bench was designed to simulate actual of vehicle performance parameters such as energy flow, acceleration resistance, rolling resistance and aerodynamic drag. The overall power train efficiency and energy consumption of the FCV was analyzed as a final outcome.

Keywords: PEM fuel cell vehicle, Model, Experimental test, Inertia dynamometer test bench, validation

INTRODUCTION

Internal combustion engines development especially automobiles, is one of the greatest achievements of modern technology. Automobiles have made great contributions to the growth of modern society by satisfying many of its needs for mobility in everyday life. The fast growth of the automotive industry, unlike that of any other industry, has encouraged the progress of human society from a primitive one to a highly developed industrial society. The automotive industry and the other industries that serve it constitute the backbone of the world's economy and employ the greatest share of the working population. However, fossil fuel used by combustion engine vehicles is the major source of harmful air pollutants such as greenhouse effect, regional acidification and climate change. To solve the problem dependence on oil, is to use electric energy for electric vehicles based on different energy sources are being considered such as bio diesel, ethanol, solar and fuel cells which are replacing the traditional non renewable energies.

Thus, electric vehicles have a strong development for different applications such as cars, scooters, bicycle and others. Proton Exchange Membrane (PEM) fuel cells are considered as one of the most alternative fuels, a potential replacement for the conventional internal combustion engine (ICE) in transportation applications [1]. The advantages of PEM fuel cell powered vehicle as a high efficiency, quick start up, low operating temperatures, high current density and zero pollution. Manufacturer form Hyundai who the first company take a challenge when they announced they be the first car manufacturer to commercialize fuel cell electric vehicle (FVEC) in 2012. The first action by supplied 100 units of FCEV to be use as taxis in South Korea [2]. Then, followed by the world largest car maker Toyota Motor Corporation when the manufacturer scheduled for production on 2014 [3]. Many

researcher involves the study in FCEV to find an alternative and great inventions idea that will change the concept of vehicle for the improvement the efficiency, cost, fuel consumption and etc. In order to test the overall performance of the vehicle needed to take a large number of road tests under different circumstances. Taking account of the high cost of real vehicle test, the propose simulation test using test bench was conducted. This paper presents a laboratory test bench using inertia dynamometer test bench. The aim of the studies at this test bench to analyze and validate the test bench with real on road conditions. Different approaches have been reported to study the vehicle behavior based on models of the system and other test using dynamic loads. The method is feasible and cheap but the results obtained depend on the model accuracy to represent the real system. The simulation and experimental obtained results are analyzes based on the energy balance approach.

NUMERICAL MODEL FOR PROTOTYPE PEM FUEL CELL VEHICLE

In order to model the dynamic behavior for prototype PEM fuel cell vehicle on a test bench, knowledge about the physical aspects of the vehicle should be known. Numerical model is based on the prototype PEM fuel cell car. The objectives of the fuel cell vehicle model is to predict the performance of the prototype PEM fuel cell car on the custom made inertia dynamometer platform, and understanding the vehicle acceleration characteristic. The total power of the prototype PEM fuel cell vehicle must be calculated and measured before simulate the performance of the vehicle. The characteristic of the vehicle list in Table 1.

Table 1: Car characteristics

Vehicle parameters	Values
Dimension (LxWxH)	2.7 m x 0.6 m x 0.6 m
Vehicle mass + driver	104 kg
Body material	Carbon fiber, fiber glass, Polyurethane (PU) foam
Front surface area	0.1 m ²
Chassis	Aluminum
Body	Carbon fiber, fiber glass, Polyurethane (PU) foam

Total power of the vehicle also known as total tractive effort, F_{te} . With the design of the car and the target of achieving energy efficiency, calculations of the total power is needed in the beginning. All the mechanical resistance was identified. The motion resistances are given by the sum of rolling resistance, F_{rr} , aerodynamic resistance, F_{ad} , climbing resistance, F_{hc} and acceleration resistance, F_{la} . In this study, assumption for hill climbing force is zero. All the forces are written in equation below:

$$F_{te} = F_{rr} + F_{ad} + F_{la} + F_{hc} \quad (1)$$

$$F_{te} = \mu_{rr}mg + \rho AC_d v^2 + ma + mg\sin\theta \quad (2)$$

where μ_{rr} is rolling coefficient, A is vehicle frontal area, C_d is drag coefficient, m is vehicle mass, ρ is for air density, a is acceleration and $\sin\theta$ is a gradient. The following mechanical features of the prototype car were entered in the model shown as below:

- Drag coefficient, $C_d=0.062$
- Aerodynamic frontal area, $A=0.1 \text{ m}^2$
- Mass, $m=104 \text{ kg}$
- Rolling coefficient of tire (manufacturer's data), $\mu_{rr}=0.0025$
- Traction wheel diameter, $r=0.2425 \text{ m}$



Figure 1: PEM fuel cell prototype vehicle [1] S.

VEHICLE SIMULATION INERTIA TEST BENCH CHARACTERISTICS

Inertia test bench is used to study transient effect of the vehicle inertia on its propulsion system and simulate dynamic power demand changes regarding its mass by using a simple test bench system consisting of a motor connected to a large flywheel.

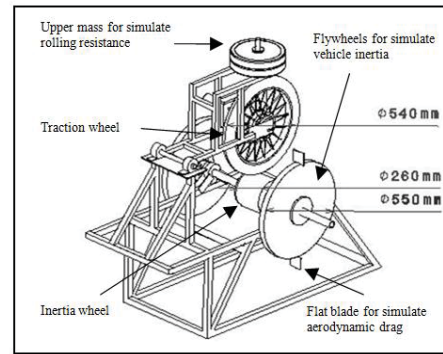


Figure 2. Inertia test bench

The test bench simulate several parameters such as rolling friction, aerodynamic drag coefficients, vehicle mass, wheel radius, real time vehicle speed and wheel torque. In an inertia test bench, the motor test is typically the vehicle's traction motor and flywheel utilized to simulate vehicle inertia. The simulation process used only one motor and connected to a flywheel. It allows for simple and easy test platform. The real overview for the inertia test bench is shown in Figure 2. Flywheel are the combinations of shafts, wheel and pieces of iron wheels. Flywheel used for emulating vehicle inertia effect since the magnitude of the acting torque on the flywheel is proportional to the rate of change of its rotational speed. The equivalent dynamic equation for the test bench can be expressed as:

$$T_m = J_{\text{flywheel}} \times \left(\frac{d\omega}{dt} \right) \quad (3)$$

Where ω is the shaft rotational speed and J_{flywheel} is the rotational inertia of the flywheel connected to the shaft. In order to simulate actual vehicles acceleration on the test bench uses the expression for kinetic energy in the linear and rotational context. The total kinetic energy stored in a moving vehicle is a combination of its translational kinetic energy and its rotational kinetic energy:

$$E = \frac{1}{2}mv^2 + \frac{1}{2}J\omega_w^2 \quad (4)$$

ACKNOWLEDGEMENTS

The authors would like to acknowledge and thank all the authors used as reference in this work.

Reference

- [1] O. Mert, I. Dincer, and Z. Ozelik, "Performance investigation of a transportation PEM fuel cell system," *International Journal of Hydrogen Energy*, 37, 2012, pp. 623-633.

CRUDE CELLULASE POWDER PRODUCTION BY SOLID STATE FERMENTATION USING CASSAVA RESIDUE AND CO-CULTURED MICROORGANISMS TRICHODERMA REESEI AND SACCHAROMYCES CEREVISIAE

Pongsri Siwarasak¹, Juraiwan Ratanapisit¹, Weerinda Appamana¹, Sathaporn Thongwic²

¹Department of Chemical and Materials Engineering, Faculty of Engineering,

²Department of Mechanical Engineering, Faculty of Engineering,
Rajamangala University of Technology Thanyaburi, Thailand

SUMMARY: This research deals with the production of fresh crude cellulase by solid state fermentation (SSF) using cassava residue and the co-cultured microorganisms of *Trichoderma reesei* and *Saccharomyces cerevisiae* under varying conditions. The output from SSF was then dehydrated to derive crude cellulase powder. In the production of fresh crude cellulase, the experiment began with 100g cassava residue and the co-cultured microorganisms in pH5 liquid medium (LM) of 10^7 cell/mL. To find the suitable moisture content for SSF, the ratio of cassava residue (100g) to LM was varied between 1:0.6, 1:0.8 and 1:1w/v, whose sugar concentration was varied between 0.8, 1.6, 2.4 and 3.2%w/w and the co-cultured microorganisms remained constant at 10^7 cell/mL in an incubator at $24\pm 2^\circ\text{C}$ for 7 days. The optimal condition is at 1:1w/v, 3.2%w/w and 6 days of incubation. The fresh crude cellulase with 55%w/w moisture content was subsequently dehydrated and pulverized to produce crude cellulase powder with 12%w/w.

Keywords: *Trichoderma reesei*, *Saccharomyces cerevisiae*, crude cellulase powder, solid state fermentation, cassava residue

INTRODUCTION

An agro-industrial lignocellulosic waste, cassava residue is a solid waste product from the production of tapioca flour and available in great quantity in Thailand. In addition to its abundance, the attractively low cost of lignocellulosic cassava residue makes it an economically viable substrate for bioethanol production. Lignocellulosic-based bioethanol can be produced by fermentation using microorganisms by which cellulose is digested by cellulase to produce glucose. Cellulase is an enzyme which is produced by a fungus, e.g. *Trichoderma reesei*.

This research aims to produce fresh crude cellulase by SSF using cassava residue and co-cultured microorganisms *T. reesei* and *S. cerevisiae* in the specially formulated LM of pH5 under varying conditions. The resultant fresh crude cellulase with 55%w/w moisture content was dehydrated and pulverized for crude cellulase powder with 12%w/w. In addition, the crude powder was applied to dried pineapple peels to produce ethanol using submerged fermentation. It is anticipated that the experimental findings will be of great use to many agricultural countries, including Thailand, in the production of bioethanol from agro-industrial residues.

MATERIALS AND METHODS

Biomass feedstock

The experimental cassava residue was obtained from General Starch Co., Ltd., a food processor located in Thailand's northeastern province of Nakhonratchasima, while Siam Winery Co., Ltd. contributed the fresh pineapple peels.

Liquid medium

The pre-SSF liquid medium (LM) was

specially formulated and consists of 8g urea ($(\text{NH}_4)_2\text{SO}_4$), 15g phosphate-potassium fertilizer (NPK-0-52-34), 1g calcium hydrogen phosphate 2 hydrate ($\text{CaHPO}_4 \cdot 2\text{H}_2\text{O}$), 1g magnesium sulfate 7 hydrate ($\text{MgSO}_4 \cdot 7\text{H}_2\text{O}$), 1L reverse osmosis (RO) water.

Preparation of co-cultured microorganisms

The co-culturing of *T. reesei* and *S. cerevisiae* was carried out by inoculating both strains onto potato dextrose agar (PDA) in one same Petri dish as shown in Fig.1(a) and (b). The incubation period was 5 days at room temperature (30°C).



Figure 1. Co-cultured microorganisms on PDA dish: (a) initial incubation, (b) after five days of incubation

The optimal condition for inoculum starter

The co-cultured microorganisms were inoculated in the four sets of pre-SSF pH5 LM (i.e. those with 10, 20, 30 and 40 g/L sugar concentrations) individually before magnetically stirring for 30 min. The target concentration of co-cultured microorganisms is 10^7 cell/mL. Then, determination of the optimal preparation condition of inoculum starter for SSF was carried out in 1L glass bowls by varying the ratio of sterilized cassava residue (100g) to LM between 1:0.6, 1:0.8 and 1:1w/v. The bowls were covered with wrap film perforated and incubated at $24\pm 2^\circ\text{C}$ for 7 days. Finally, once the optimal preparation condition of

inoculum starter (i.e. 1:1w/v for 6 days) was identified, the production of a larger-scale fresh crude cellulase was carried out in 10L polypropylene (PP) containers (boxes) under the optimal condition. The 10L PP boxes were filled with 625g cassava residue, 125g inoculum starter and 750mL pH5 LM with 30g/L sugar concentration. The mixture has an initial moisture content of 55%w/w and was incubated at 24±2°C for 6 days to produce fresh crude cellulase.

The crude cellulase powder production

To produce crude cellulase powder, approximately 6000g fresh crude cellulase was dehydrated in a hot air oven at 60°C for 10hr to expel moisture from initially 55%w/w to 12%w/w.

RESULTS

Effect of liquid medium volume and sugar concentration on starter inoculum

Fig.2 compares the co-cultured microorganisms growth under the 2.4% and 3.2%w/w sugar concentration conditions. Thus, the condition with 100mL LM, 3.2%w/w sugar concentration and 6 days of incubation is selected as the optimal condition for the preparation of starter inoculum, which has cell growth of 1.13×10⁹ cell/mL.

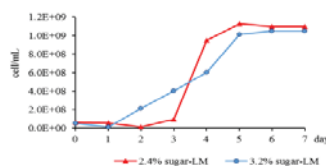


Figure 2 Cell growth relative to incubation time for SSF using 100 g cassava residue mixed with 10mL of pH5 LM containing 2.4% and 3.2%w/w sugar

Cell growth and cellulase activity of fresh crude cellulase

In Fig.3, the maximum cell growth of co-cultured microorganisms is 1.81×10⁹ cell/mL on day 6 of incubation and the cellulase activity profile of fresh crude cellulase, in which the cellulase activity is 8.64 IU/gds on day 5 of incubation. The daily manual collection of samples for enzyme assay affects the cellulase activity due to substrate reduction [2]. Interestingly, the presence of mycelia and spores in the inoculum starter shortens the lag phase and enhance the activity of fresh crude cellulase [2, 3].

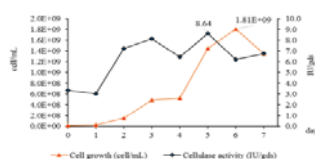


Figure 3 Profile of cell growth and cellulase activity relative to incubation time for SSF

Drying fresh crude cellulase prior to transform into powder form is necessary to prolong the shelf life of co-cultured microorganisms, to minimize the storage requirement, and to increase ease of use. Figs.4 (a)-(b) are the images of fresh crude cellulase and its powder form, respectively. The cellulase activity before and after drying process, as seen in Fig.5.



(a) before drying (b) after drying

Figure 4 The co-cultured microorganisms on cassava residue under SSF: (a) fresh crude cellulase and (b) crude cellulase powder

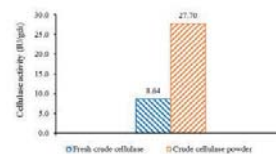


Figure 5 Cellulase activity of crude cellulase before (55%w/w moisture content) and after drying (12%w/w moisture content)

ACKNOWLEDGMENTS

The authors would like to extend deep gratitude to Rajamangala University of Technology Thanyaburi for financial support. Sincere appreciation is extended to Nusara Saramas, Thadapan Yodnoom, Jadsada Thongsiri, and Wassana Jaito for their technical assistance. Moreover, special thanks go to Warapong Vorawareejit for cassava residues.

References

[1] S. Pongsri, N. Kuppithayanant, C. Duangduen and P. Prajanket. "Two Strains Co-culture of *Trichoderma reesei* RT-P1 and *Saccharomyces cerevisiae* RT-P2 and Its production of ethanol from pineapple peel waste." *Proceedings of 2nd Rajamangala University of Technology Thanyaburi International Conference, Bangkok, Thailand 24-26 November, 2010.*

[2] L. Mitchell, H. Goen and C.R. Ralf. "Ethanol from lignocelluloses using crude unprocessed cellulase from solid-state fermentation". *Bioresource Technology*. **101**, 2010, pp. 7083-7087.

[3] S. Haiyan, G. Xiangyang, H. Zhikui and P. Ming. "Cellulase production by *Trichoderma* sp. on apple pomace under solid state fermentation". *African Journal of Biotechnology*. **9(2)**, 2010, pp. 163-166.

EXERGY EFFICIENCY PROFILE OF A 1 KW OPEN CATHODE FUEL CELL WITH PRESSURE AND TEMPERATURE VARIATIONS

S. Hanapi¹, Alhassan Salami Tijani¹, A. H. Abdol Rahim¹ and W. A. N. Wan Mohamed¹

¹Faculty of Mechanical Engineering, Universiti Teknologi MARA, Malaysia

SUMMARY: A proposed electric vehicle using proton exchange membrane (PEM) as clean energy have been attracting due to their high efficiency, high energy density and zero emissions. Standard exergy analysis of a mini urban vehicle powered by a 1 kW Proton Exchange Membrane (PEM) fuel cell engine system has been presented in this manuscript. A sensitivity analysis has been studied in order to evaluate the effect of variable operating temperatures and pressures on the physical exergy and efficiency of a 1 kW PEM fuel cell engine. The calculation of the physical and chemical exergies, mass flow rate and exergy efficiency are performed at temperature ratio (T/T₀) and pressure ratio (P/P₀) ranging from 1 to 1.15 and 1 to 4, respectively. The findings of the exergy analysis reveal that the overall efficiency of the fuel cell system was observed to be 61.3%. The result of the parametric study show that an increase in operating temperature and pressure results in an increase in exergy efficiency of the system.

Keywords: PEM Fuel Cell, Vehicle System, Efficiency, Exergy Analysis, Operating Parameters

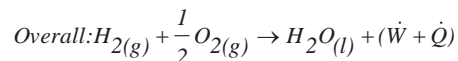
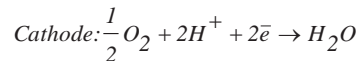
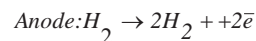
INTRODUCTION

Conventional fuels used in automobiles application are the major problems with increasing global energy consumption and harmful air pollutants. So a movement towards environmentally friendly bring the fuel cells to the forefront. PEM fuel cell is an electrochemical device which converts the chemical energy of hydrogen and oxygen directly and efficiently into electrical energy with heat and water as wastes product. A PEM fuel cell used to power automobiles using hydrogen as a energy source can offer several advantages such as energy efficient, quick start-up, low or zero emissions, low noise and can obtain a power density [1]. The thermodynamics efficiency of the system in PEM fuel cell vehicle has a great importance due to the limited supply of available energy as well as the overall impact on vehicle performance. Understanding of the thermodynamic irreversibilities is helpful to improve their energy performance.

Exergy analysis is one of the tools which represent the amount of energy that may be totally converted to work [2]. In simple words, exergy is a potential or quality of energy [3]. It is possible to make sustainable quality assessment of energy. Exergy is always evaluated with respect to a reference environment. When a thermodynamic system is in equilibrium with the environment or based on condition, the state of the system is called "dead state" [4], in which the temperature and pressure are called "dead state temperature" and "dead state pressure". These are then considered for exergy analysis [5].

Also, the dead state may be arbitrarily selected, while the dead state temperature is often taken to be equal to the environment temperature and dead state pressure is taken as atmospheric pressure [6]. In the PEM fuel cell system, the design is a thin plastic sheet through which hydrogen ions can pass and the membrane coated on both sides with highly dispersed metal alloy particles like platinum that are active

catalysts. Hydrogen is fed to the anode side of the fuel cell where due to the effect of the catalysts, the hydrogen atoms release electrons and become hydrogen ions (protons). The electron move in the form of an electric current that can be utilized before it returns to cathode side of the fuel cell where oxygen is fed. The ions of protons diffuse through the membrane to the cathode and the hydrogen atom is combined and reacted with oxygen to produce water as a product. This is the place where electrical power is produced by the following electrochemical reactions [7]:



SYSTEM DESCRIPTIONS

In order to quantify exergy, a reference or dead state that corresponds to the state of thermodynamic equilibrium with the natural surroundings must be defined. An equilibrium environment in which a substance cannot undergo an energy conversion process to produce net positive work is called as reference state. Also, it is assumed that the intensive properties of the environment are not significantly changed by any process. In the present study the restricted dead state is defined as standard conditions for temperature and pressure (STP) condition (298 K and 1 atm). The exergy efficiency of a PEM fuel cell system shown in Fig 1 is the ratio of the power output \dot{W} to the differences between the exergy of the reactants air and hydrogen and the exergy of the products air and water which can be defined as [8]:

$$\varepsilon = \frac{\text{Electric Output}}{(\text{Exergy})_R + (\text{Exergy})_P} \quad (1)$$

$$\varepsilon = \frac{\dot{W}}{(\dot{E}_{\text{air},R} + \dot{E}_{\text{H}_2,R}) - (\dot{E}_{\text{air},P} + \dot{E}_{\text{H}_2\text{O},P})} \quad (2)$$

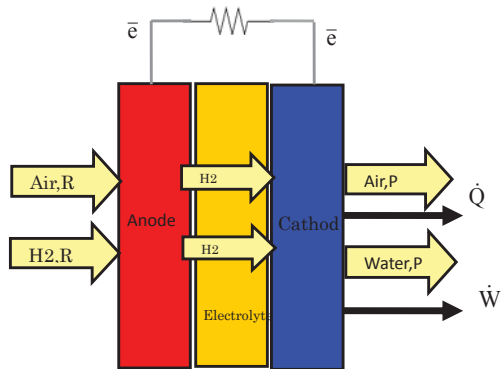


Figure 1. Proton Exchange Membrane Fuel cell (PEMFC)

CASE STUDY: THE FUEL CELL SYSTEM IN A MINI VEHICLE SYSTEM

The exergy analysis of a PEM fuel cell system is defined on the 1 kW XP PEM fuel cell power taken from Horizon. This stack is capable of providing 1 kW of unregulated DC output. The output voltage level can vary from 43V at no load to about 26V at the full load. The designed operating temperature in the stack is around 65°C at the full load. There are totally 50 cells connected in series in the stack. An individual fuel cell element consists of two electrodes, the anode and the cathode sides separated with a thin material called platinum catalysts layer. The assembly of electrodes, catalysts and membrane together form the membrane electrode assembly (MEA). A single fuel cell element produces about 1V at open circuit and about 0.6V at full current output. The geometric area of the fuel cell is 61 cm². The fuels is 99.99% hydrogen with no humidification and the hydrogen pressure to the stack is normally maintained at 0.5 bar. Oxygen comes from the ambient air. The stack is air-cooled; the cooling fan draws air from the ambient surroundings in order to cool the fuel cell stack and regulate the operating temperature.

The Fig 2 illustrates the schematic diagram of Horizon-1000 XP PEM fuel cell system on mini hybrid PEM fuel cell urban car. Hydrogen, oxidant air and cooling air must be supplied to the stack system. Exhaust air, product water and heat is emitted. The fuel supply system sources from compressed hydrogen tank. The fuel cell stack is pressurized with hydrogen during operation. Nitrogen and product water in the air stream slowly migrates across the fuel cell membranes and gradually accumulates in the

hydrogen stream. The accumulation of nitrogen and water in the anode results in the steady decrease in performance of certain key fuel cells which are termed purge cell. In response to the purge cell voltage, a hydrogen purge valve at the stack outlet is periodically opened to flush out inert constituents in the anode and restore performance. Only a small amount of hydrogen purges from the system less than one percent of the overall fuel consumption rate.

In order to determine the thermodynamic characteristics of the system, some general assumptions considered in the analysis. The PEM fuel cell as the engine sources are assumed to be at steady state. The gasses are assumed as an ideal gas and the environmental state is at STP conditions; 298 K and 1 atm.

RESULT AND DISCUSSION

In this paper, sensitivity analysis was carried at different operating temperatures and pressures. Fig 3 shows that the physical exergy of air entering the fuel cell engine ranges from zero at the respective temperature of 298 K and pressure of 1 atm to 95 KJ/kg at 298 K and 3 atm. Besides, as the temperature increase from 298 K to 373 K the physical exergy of the reactant air increase by about 15 %. As in the equation (5), air reactant was treated as an ideal gas to determine the physical of exergy. It was also observed that the physical exergy of the reactant air increase sturdily by a small amount for all the three pressure conditions.

CONCLUSIONS

A thermodynamic model in terms of exergy efficiency analysis of a PEM fuel cell mini urban car has been carried out. A parametric study is performed to investigate the performance of the system depending on varying operating parameters such as temperature ratios and pressure ratio.

ACKNOWLEDGEMENTS

The authors would like to acknowledge and thank all the authors used as reference in this work.

References

- [1] S. Campanari, G. Manzonini, F. Garcia de la Iglesia. "Energy analysis of electric vehicles using batteries or fuel cells through wheel-to-wheel driving cycle simulations". *J. Power Source*. **186**, 2009, pp. 464-477.
- [2] E. Arcaklioglu, A. Çavus oğlu and A. Erisen. "An algorithmic approach towards finding better refrigerant substitutes of CFCs in terms of the second law of thermodynamics". *Energy Conv. Manage.* **46**, 2005, pp. 1595-1611.

THE POTENTIAL OF DELIVERING CLEAN LOCALLY AVAILABLE LIMITLESS RICE HUSK ENERGY IN THE CELEBES ISLAND INDONESIA

Aditya Rachman¹, Usman Rianse², Mustarum Musaruddin³ and Yulius Pasolon⁴

¹Mechanical Engineering Department of Halu Oleo, University Andounohu Kendari, Indonesia

²Agricultural Department of Halu Oleo, University Andounohu Kendari, Indonesia

³Electrical Engineering Department of Halu Oleo, University Andounohu Kendari, Indonesia

SUMMARY: For the Celebes Island, the world's eleventh-largest island laying in the eastern part of Indonesia, consisting of six developing provinces, inhabited by around 19 million populations, the energy availability seems still to be a challenge. Depending merely on the conventional fossil sources, to cope with this challenge, should be less appropriate as their limitation and detrimental environmental impacts. The role of these unclean conventional limit power sources can be potentially shifted into an alternative clean sustainable energy generation based on locally available rice husk. The aim of this study is to assess the potential, the environmental aspect and the economical attractiveness on the application of rice husk as the electricity generation in the Celebes Island. It proposes a model of a direct boiler combustion power plant model based on the rice husk biomass, combined with the statistical data on the annual paddy production obtained from the Department of Agriculture to assess the energy potential. The environmental assessment is conducted by calculating the lifecycle carbon-dioxide equivalent and the economical assessment is performed by employing the model of the Levelised Cost of Energy (LCOE). The result shows that the potential of the rice husk energy in this island is around 815 GWH annually under the proposed power plants, around ten percent of the current electricity use. The potential of the carbon dioxide emission generated by the proposed biomass power plants is less than five-percent of the total carbon dioxide emitted by current power plants installed. At a low feedstock cost, a low installation costs and a low discount rate, it is possible to obtain the LCOE of the biomass lower than the electricity production costs of some existing power sources, the electricity price under subsidy and the biomass purchased price under a government regulatory (Feed-in-Tariff (FIT)).

Keywords: Celebes Island, rice husk, energy, potential, economic, environment

INTRODUCTION

For the Celebes Island, the world's eleventh-largest island, located in the eastern part of Indonesia, covering the area around 170 thousand kilometer-square, and comprising of six developing provinces with around 19 million populations, the energy availability for its communities seems still to be a challenge. The average electricity ratio and the average electricity per-capita in this province are still relatively lower than those of the averages in Indonesia. However, the existence of the paddy commodities, also dominating in its annual agricultural food crop production, seems potentially to deliver optimistic on reducing the pressure on the present energy challenges.



Figure 1. Celebes Island : Economy & Electricity

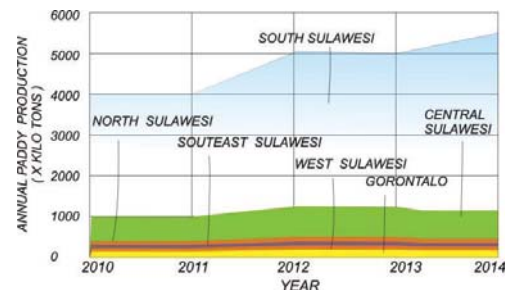


Figure 2. Celebes Island : Annual Paddy Production

The aim of this study is to assess the potential, the environmental and the economic aspects on the application of rice husk as the electricity source in the Celebes Island.

METHODOLOGY

In present study, it determines the potential annual rice husk energy by using a proposed model of a biomass power plant based on the direct combustion boiler, being combined with the data of the annual paddy production and the heating value of the rice husk. The proposed power plant model follows the ideal Rankine cycle, with steam as the working fluid. It is assumed that the amount of rice husk is a twenty percent of the paddy production. It employs the average paddy production from 2010 to 2014 in the six provinces, obtained from the data of the Agriculture Department of Indonesia.

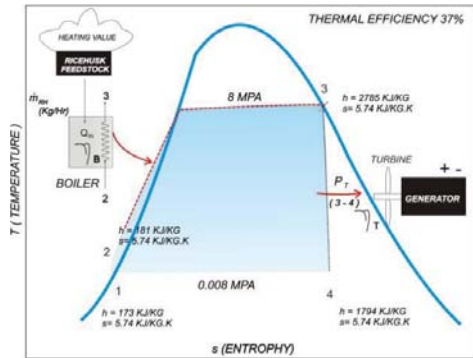


Figure 3. The proposed biomass power plant Rankine cycle model

In the economical assessment, it uses the LCOE model, one of the analytical tools to compare various alternative energy technologies when different scales of operation, investment or operating time period exist. In the environmental assessment, it calculates the greenhouse gas emission from the proposed biomass power plant by utilizing the lifecycle carbon-dioxide equivalent.

RESULTS

The potential of the rice husk energy is around 815 GWH annually, around 10 percent total current electricity use in this island (see figure 4). The province of South Sulawesi dominates the biomass potential energy (515 GWH annually), followed by the Central Sulawesi (107 GWH annually) and the North Sulawesi (65 GWH annually), while the West Sulawesi and Gorontalo provinces have the lowest potential husk energy, accounting less than 30 GWH annually. This phenomenon is related to the availability of the paddy production in each province. The more paddy production, the more potential biomass energy generated is.

The potential of the installed biomass power plant is around 94 Mega-Watt (MW). South Sulawesi has the highest potential biomass power capacity (around 70 MW), followed by Central Sulawesi (14MW), and North Sulawesi (9 MW), while Gorontalo and West Sulawesi have the lowest potential biomass power plant capacity (less than 6 MW).

The total potential greenhouse gas emission by the proposed biomass power plants is around 182 kilo-tons annually, less than five-percent to the total predicted current undesirable gas emitted by the power generation in this island (total around 4660 kilo-tons annually) (see figure 4). Generally, the high lifecycle carbon emission equivalent is dominated by the fossil sources, such as coal, oil and gas, while that of the biomass is relatively lower than those previous ones. This contributes in making the annual greenhouse gas emission by the biomass

energy relatively lower than those of the fossil energies.

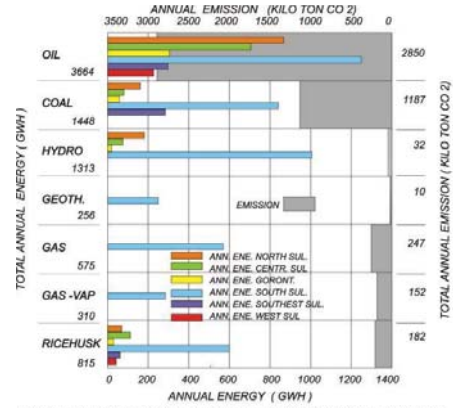


Figure 4. The annual energy production and carbon emission

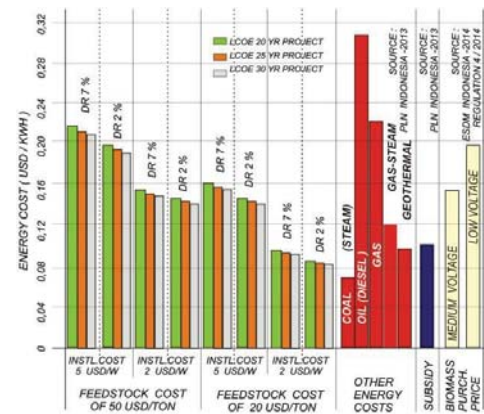


Figure 5. LCOE and its comparison to other energy costs

In comparison of the biomass LCOEs to the other energy costs, it is only that of the power based on coal seemingly difficult to compete. In comparison to the power price under the subsidy and to the biomass purchased price (Feed-in Tariff (FIT)) under the government regulation no 4 year 2012, on the connection into the medium voltage, it is only the LCOEs at the feedstock cost of 20 USD per ton at the installation cost of 2 USD-per watt seem able to compete well. In comparison to the biomass purchased prices (FIT) under connection into the low voltage, almost all LCOEs are able to compete well, except for those with the feedstock cost of 50 USD per ton at the installation cost of 5 USD per watt.

ANALYSES OF ENERGY USE AND CO₂ EMISSIONS IN RESIDENTIAL SECTOR. CASE STUDY: THAILAND AND VIETNAM

Vu Thi Hong Thuy¹ and Bundit Limmeechokchai¹

¹Sirinhorn International Institute of Technology, Thammasat University, Thailand

SUMMARY: This paper presents the energy consumption and CO₂ emission in the residential sector for both Thailand and Vietnam. The Long-range Energy Alternatives Planning (LEAP) is employed for analysis under three scenarios. The business-as-usual (BAU) scenario, which represents the residential sector without any policy intervention. The energy system of the base year 2010 is modeled using the reported data and then exiting energy consumption trends will be projected till to the end of the time plan which is 2030. The demand side management (DSM) scenario focussed on the efficiency improvement of four electric appliances: lighting, air-conditioning, cooking, and refrigeration to reduce the energy intensity in the residential sector. The promotion of renewable energy is also used to analysis the energy use and CO₂ emission in the residential sector in both countries. The result will compare for both countries to find which scenario is suitable to save the energy and reduce the CO₂ emission as much as possible.

Keywords: Residential sector, CO₂ emission, Energy use, LEAP model.

INTRODUCTION

With the recent rapid development of population and economic, the issue of energy demand and CO₂ emission has become an area of intense research. In the report of “World Energy outlook 2010” [1] published by IEA, it have clearly highlighted that how important the modern energy to achieve each of Millennium Development Goals. Especially in the Residential sector, improvements in living standards have caused a high growth of household related CO₂ emission. To cope with this issue, it is necessary to set reduction targets and promote efficiency policies.

THAILAND RESIDENTIAL SECTOR

In Thailand the total energy consumption in the residential sector is reported as 11,040 ktoe which is 15.6% of the final energy consumption in Thailand in 2011 [2]. Out of three demographic divisions, rural households have consumed 8,467 ktoe which is about 76.7% of final energy consumption in the sector. Remainder was shared by greater Bangkok area and municipal area with about 14.1% and 9.2%, respectively. Change in energy consumption by fuel type in residential sector from 1995-2011 is given in Figure 1 [3]. Similar to previous years, in 2011 also, traditional renewable energies (fuel wood, charcoal and paddy husk) have been consumed mostly. It accounted about 56% of the total consumption followed by electricity with 25.4% and petroleum products (mainly LPD) with 18.3%.

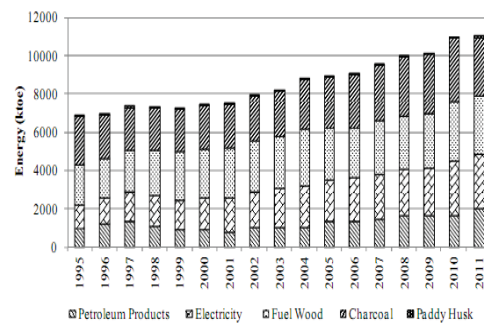


Figure 1. Energy consumption in Thai Residential Sector by fuel type

VIETNAM RESIDENTIAL SECTOR

Total energy consumption in the residential sector is reported as 48,597 ktoe which is 36.2% of the final energy consumption in Vietnam in 2010 [4]. The most energy efficient households have shared dwellings and large households. The least efficient have small households and air conditioning [5]. All the households covered by the survey had mains electricity, lighting and at least one electric fan. There are around 130 million lamps installed in homes in Vietnam; 60 million of these are compact fluorescent lamps (CELs) and 54 million are fluorescent tubes. Most of the rest are incandescent bulbs (16 million) [6]. Most of the electricity consumption in residential sector is represented by five end uses; lighting, air conditioning, rice cookers, refrigeration, and television. The percentage of household electricity consumption by different services is presented by the figure 2.

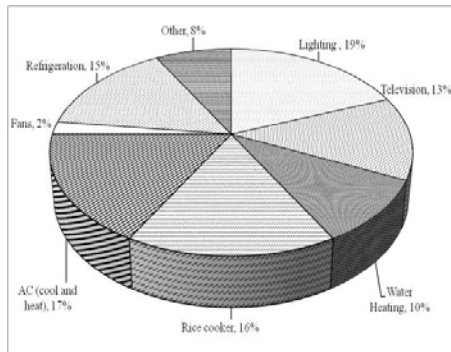


Figure 2. The household energy consumption of services

METHODOLOGY

The Long-range Energy Alternatives Planning System (LEAP) model was developed by the Stockholm Environmental Institute (SEI) to analyze energy policy and climate change. It is a tool for creating models of different energy systems with a specific structure.

The flow diagram of LEAP model is shown in Figure 3. Three scenarios are modeled by taking 2010 as the base year and projected the future energy demand within the time horizon 2010-2030 for both Thailand and Vietnam. Results will present of change in energy demand, in the fuel mix and in CO₂ emission.

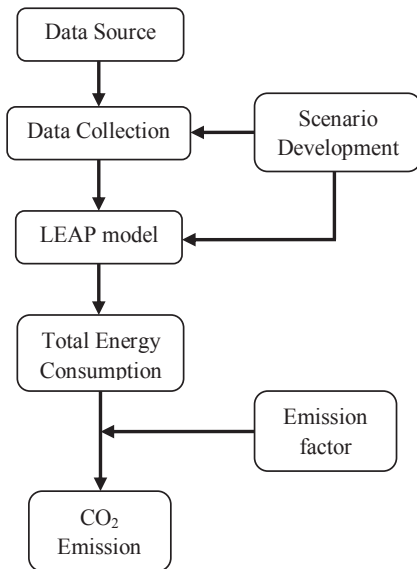


Figure 3. Flow diagram of LEAP model

EXPERTED RESULTS

Change in total energy consumption of residential sectors for both Thailand and Vietnam will be obtained under a BAU scenario and reference scenarios, it will be presented for the time period 2010-2030.

Energy saving and CO₂ emission mitigation potential of each modeled policy and action will be examined.

Technologies suitable to be included in promotion policies are established and their cost effectiveness and Greenhouse Gas reduction capacity are assessed.

ACKNOWLEDGMENT

The authors would like to thank Sirindhorn International Institute of Technology, Thammasat University for the scholarship provided, and the Stockholm Environment Institute (SEI) for the academic license of the LEAP model.

References

- [1] IEA, "World Energy Outlook-2010", International Energy Agency, Paris, 2010.
- [2] DEDE, "Annual Report: Thailand Energy Situation 2011", Department of Alternative Energy Development Efficiency, Ministry of Energy Bangkok, 2011.
- [3] DEDE, "Energy Consumption of Residential Sector by Fuel Type", 2014
- [4] IEA, "Vietnam: Electricity and Heat", International Energy Agency, 2010.
- [5] R. B. Matt Parkes, "Vietnam Residential Energy Use," Cimigo, Sustainable Futures Asia 2013.
- [6] "Vietnam Energy Efficiency Standards and Labelling Program: Australian Government support project," Australian Government, Department of Climate Change and Energy Efficiency 2012.

Bio Fuel Production Technology

REMOVAL OF COLOR AND CHEMICAL OXIGEN DEMAND FROM LANDFILL LEACHATE BY PHOTOCATALYTIC PROCESS WITH AC/TiO₂

Orawan Rojviroon¹, Thammasak Rojviroon¹ and Sanya Sirivithayapakorn²

¹ Department of Civil Engineering, Faculty of Engineering,
Rajamangala University of Technology Thanyaburi, Thailand

² Department of Environmental Engineering, Faculty of Engineering, Kasetsart University, Thailand

SUMMARY: A simplified sol-gel preparation method was developed to prepare hybrid AC/TiO₂ photocatalyst. The surface properties of the photocatalysts have been investigated by scanning electron microscopy (SEM), X-ray diffraction (XRD) and Brunauer–Emmett–Teller (BET) analysis. The results confirmed the existence of anatase phase TiO₂ particle on the AC surface. All of the surface properties including surface area, pore volume, and pore size tended to decrease in comparison to the uncoated AC. The photocatalytic performances of the AC/TiO₂ photocatalyst have been evaluated for the color and COD removal under simulated sunlight (UVA irradiation). The results showed the overall color and COD removal efficiencies were apparently increased when the TiO₂ was coated onto AC. In addition, the photoactivity performance showed a significant relationship with the increasing UVA intensity. Thus, the hybrid AC/TiO₂ photocatalyst is suitable as photocatalyst with high photoactivity under UVA irradiation.

Keywords: COD removal, decolorization, photooxidation, sol-gel, composite materials

INTRODUCTION

In spite of the implementation of waste reduction, reuse, recycling, and waste transformation, landfill still remained an unavoidable component of integrated solid waste management [1]. Therefore, landfill leachate continues causing environmental impacts.

Photocatalytic process using titanium dioxide (TiO₂) as photocatalyst has been considered an effective technology to treat the mature landfill leachates [2]. The main mechanism of reaction in photocatalytic process comprised of adsorption and photocatalytic reaction [3]. Therefore, the enhancement of surface area to increase the adsorption rate is beneficial to the overall photocatalytic process.

Activated carbon (AC) has suitable surface properties including high specific surface area and great pore volume [4]. In this research, a hybrid AC with TiO₂ coating on the surface (AC/TiO₂) has been prepared. The objectives of this research were to study the efficiencies and kinetics of color and chemical oxygen demand (COD) removal using the prepared AC/TiO₂ using UVA as the light source for solar simulation.

METHODOLOGY

Preparation of AC/TiO₂ photocatalyst

The AC used in this experiment was produced from coconut shell. Size selection of activated carbon were passed through 8 mesh sieve (2.36 mm) and retained on 10 mesh sieve (2.00 mm). The sieved AC was dip coating with TiO₂ sol-gel according to the methods defined by Rojviroon and Sirivithayapakorn [5].

Characteristic of AC/TiO₂ photocatalyst

The surface morphologies of AC/TiO₂ photocatalysts were analyzed by scanning electron microscopy (JEOL JSM-35 CF model). The

crystalline phase was identified by X-ray diffraction (Siemens D5000 diffractometer). The surface properties including specific surface area, pore size and pore volume were measured from Brunauer Emmet Teller (BELSORP-max; Bel Japan Inc.).

Photocatalytic activities test

The photocatalytic activity of AC/TiO₂ photocatalysts were evaluated by monitoring the degradation of color and COD from mature landfill leachate in a photoreactor (Fig.1). AC/TiO₂ (3g) was added to 250 mL erlenmeyer flask with 200 mL working volume and the initial concentration of COD was around 1,000 mg/L. Erlenmeyer flasks were mixed continuously by shaker placing in the photoreactor at room temperature equipped with UVA light bulb whereat the light intensity in the photoreactor was set at 27 and 32 $\mu\text{W}/\text{cm}^2$ (Figure 1). The concentrations of color and COD were recorded with the reaction time.

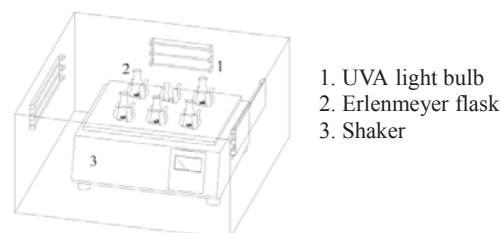


Figure 1. Photoreactor

RESULTS AND DISCUSSION

Characteristic of AC/TiO₂ photocatalyst

The strong XRD peak with diffraction angles at $2\theta = 25.2^\circ$ indicated the existence of anatase phase TiO₂ (Fig.2). The comparison of SEM images between AC and AC/TiO₂ clearly showed the TiO₂ particle on the AC surface (Fig.3). The surface properties results showed that all of surface

properties including surface area, pore volume and pore size tended to decrease (Table 1) due to the TiO₂ particle that coating on the AC surface filling the pore gaps of AC [6].

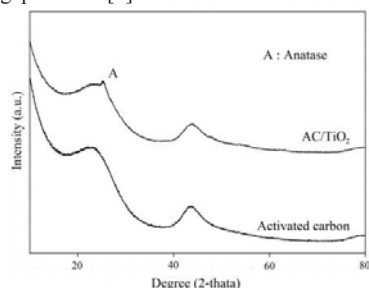
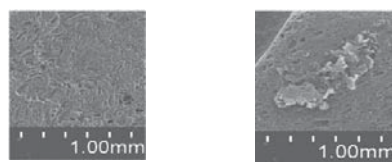


Figure 2. XRD pattern of AC/TiO₂



(a) AC (b) AC/TiO₂
Figure 3. SEM image of AC/TiO₂

Table 1. Results of the surface properties

Catalyst	Surface area (m ² /g)	Pore volume (mL/g)	Pore size (Å)
AC	981	6.323×10^{-1}	62.35
AC/TiO ₂	8.79	1.257×10^{-2}	20.67

Photocatalytic activities test

The experimental data showed that, as opposite to the COD degradation, the color degradation efficiencies of AC/TiO₂ was higher during the first 30 minutes in comparison to the COD removal efficiencies. This could be due to the fast adsorption of color to the surface and the slow degradation of complex compounds in the leachate [7]. Overall, with the increasing UVA intensity, the degradation efficiency of color and COD also increased. This could be explained by the increasing photon and high •OH production [8]. The results indicated that the AC/TiO₂ photocatalyst was suitable for treatment of complex and non-biodegradable organic compounds in photocatalytic process.

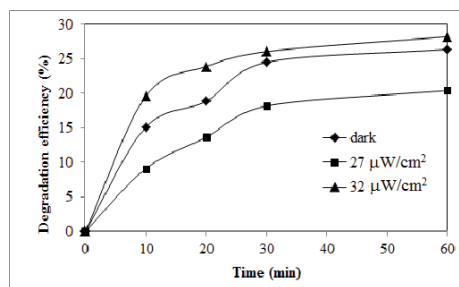


Figure 4. Color degradation efficiency of leachate

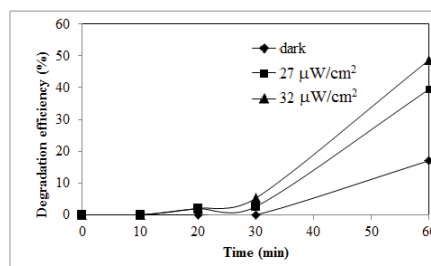


Figure 5. COD degradation efficiency of leachate

CONCLUSION

In this study, AC/TiO₂ photocatalyst was successfully prepared by sol-gel technique. Result from surface property testing indicated that the surface area, pore volume, and pore size tended to decrease in comparison to the pure AC. For the photocatalytic activities, the composite AC/TiO₂ materials exhibited photocatalytic activity for the degradation of color and COD.

References

- [1] J. Chung, S. Kim, S. Baek, N.H. Lee, S. Park, J. Lee, H. Lee, and W. Bae, "Acceleration of aged-landfill stabilization by combining partial nitrification and leachate recirculation: A field-scale study", *Journal of Hazardous Materials*. **285**, 2015, pp. 436-444.
- [2] R. Poblete, L.P. Rodriguez, I. Oller, M.I. Maldonado, S. Malato, E. Otal, L.F. Vilches and C.F. Pereira, "Solar photocatalytic treatment of landfill leachate using a solid mineral by-product as a catalyst", *Chemosphere*. **88**, 2012, pp. 1090-1096.
- [3] J. Mo, Y. Zhang, Q. Xu, J.J. Lamson and R. Zhao, "Photocatalytic purification of volatile organic compounds in indoor air: A literature review", *Atmospheric Environment*. **43**, 2009, pp. 2229-2246.
- [4] R. Wang, Y. Amano and M. Machida, "Surface properties and water vapor adsorption-desorption characteristics of bamboo-based activated carbon", *Journal of Analytical and Applied Pyrolysis*. **104**, 2013, pp. 667-674.
- [5] T. Rojviroon and S. Sirivithayapakorn, "Properties of TiO₂ Thin Films Prepared using the Sol-gel Process", *Surface Engineering*. 2012, pp.
- [6] Y. Li, X. Li, J. Li and J. Yin, "Photocatalytic degradation of methyl orange by TiO₂-coated activated carbon and kinetic study", *Water Research*. **40**, 2006, pp. 1119-1126.
- [7] C. Tan, G. Zhu, M. Hojamberdiev, K.S. Lokesh, X. Luo, L. Jin, J. Zhou and P. Liu, "Adsorption and enhanced photocatalytic activity of the {0 0 0 1} faceted Sm-doped ZnIn₂S₄ microspheres", *Journal of Hazardous Materials*. **278**, 2014, pp. 572-583.
- [8] A. Rezaee, Gh.H. Pourtaghi, A. Khavanin, R.S. Mamoory, M.T. Ghaneian and H. Godini, "Photocatalytic decomposition of gaseous toluene by TiO₂ nanoparticles coated on activated carbon", *Iranian Journal of Environmental Health Science & Engineering*. **5**, 2008, pp. 305-310.

FUEL PROPERTIES OF BIO-PELLETS PRODUCED FROM SELECTED MATERIALS UNDER VARIOUS COMPACTING PRESSURE

Tanakorn Unpinit¹, Thanaporn Poblarp¹, Narongrit Sailoon¹, Prasong Wongwicha¹ and Mallika Thabuot^{1,2}

¹Department of Chemical Engineering, Faculty of Engineering, KhonKaen University, Thailand.

²Center of Knowledge Development of Rubber Tree in Northeast group (KDRN), KhonKaen University, Thailand.

SUMMARY: The purpose of this study is to investigate the fuel properties of biomass pellets prepared from six different biomasses: bamboo sawdust, eucalyptus sawdust, corn cob, rubber tree branches, palm fibre and lippia grass. These materials were milled into the small particle less than 5mm before binderless pelletized by using the lab-scale hydraulic press under force of 56-166 MPa for 20 seconds into the pellets with 15 mm diameter. Thermal degradation of each biomass was analyzed by TGA. The increase in compaction pressure make the L/D ratio of pellet decreased and the pellet density increased, and rather maintained the constant value after 139 MPa was applied. Moreover, higher applied pressure also gave the pellets with higher tensile strength and less water impermeability.

Keywords: Biomass, solid fuel pellets, calorific value, densification, tensile strength

INTRODUCTION

Since the energy demand has been increased with the population growth, fossil fuels are depleted very fast. Alternative energy is gained more interested to replace this non-renewable energy to improve the environment. Biomass is converted into the green energy as it is the carbon-neutral material, cheap and abundant available. Compared to the fossil fuel, biomass is the sustainable energy feedstock and supports the reduction of greenhouse gas (GHG) emission. Agricultural lignocellulosic wastes have been paid high attentions to be converted into the bio-fuel in different states; liquid, gas and solid. Pyrolysis and gasification processes are investigated on the purpose to obtain the two former, however, high investment is needed. Densification is the promising technology to be applied for solid-fuel production from these wastes because it is the simply technology which can be adjusted for the local area. The bulk volume of the material can be reduced by mechanical compaction for easy handling, transportation and storage [1]. High density pellets is environmentally friendly solid bio-fuel, very comfortable in use for both households and industrial plants. In this study, the pelletization of selected biomass wastes without binder using were investigated under different compacting pressures in order to obtain pellet with the satisfied fuel properties.

METHODOLOGY

Six types of biomass wastes; bamboo sawdust, eucalyptus sawdust, corn cob, rubber tree branches, palm fibre and lippia grass; were achieved from the local area of Khon Kaen Province, Thailand. The materials were sundried for 3 days to reduce the moisture content, afterward they were milled using hammer mill. The ground materials with the particle size less than 2 mm were sieved and collected. The sieved samples were compressed into the pellets at ambient temperature using a laboratory scale Specac

hydraulic press with the maximum load of 555 MPa. A steel cylindrical die of dimension 1.3 cm diameter was used. Each sample was weighed about 1.5 g before applied into the die, the compaction was help for 20 seconds under the applied pressure of 56-166 MPa. The prepared pellets were kept for 3 weeks before analysis. Bulk density of the starting materials was found out by weighing sample in a known volume. The energy content was determined using bomb calorimeter. Thermal degradations of these materials under nitrogen atmosphere were investigated using Thermo gravimetric analyzer (TGA50, Shimadzu). The condition was swept from 30°C to 700°C at 10°C/min, and 10 minutes of the holding time at the final temperature. The moisture content and volatile mater were estimated from the temperature degradation curve. The ash content (ASTM-E80) was determined in the muffle furnace at 750°C for 2 h. The fixed carbon content was calculated from the weight difference. Elemental compositions were estimated using the same equations as provided in the other study [2]. The heating value was determined using Gallenkamp Adiabatic Bomb Calorimeters. The pellet density was determined from dividing the mass by the volume of compressed product. A digital weighing scale and a standard vernier caliper were used for checking the mass and dimensions of the pellets. The compressive strength of produced pellet was determined using the universal testing machine (LAX-Plus, Lloyd Instrument). A pelletised sample was placed horizontally in the compression test fixture and the load cell of 1 kN was applied at a constant cross-head speed of 2 mm/min until the pellet was cracked. To estimate the water impermeability, pellets were placed in the 27°C water for 30 second and then the ratio of amount of absorbed water to original weight was calculated.

RESULTS AND DISCUSSION

The thermal degradation behaviors in the

nitrogen atmosphere of all selected biomass are shown in the similar trends as seen in Figure 1. Water was evaporated from the material surface at 110°C, and the decomposition of hemicelluloses occurred between 200-260°C. Cellulose polymer was destroyed from 260°C to get water, CO₂, CO and char. These decomposed gases and liquids in the form of volatiles were released increasingly with the temperature increased up to 600°C. Corn cob, rubber wood and lippia grass were easier to be broken at the low temperature than bamboo sawdust and eucalyptus sawdust.

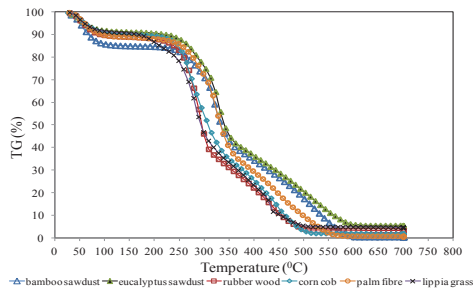


Figure 1. TGA curves of selected biomass

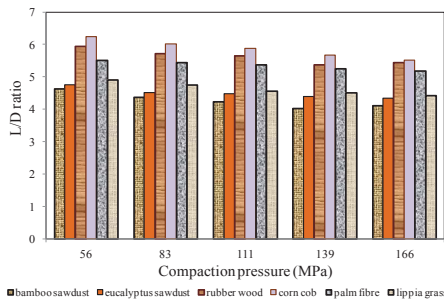


Figure 2. Effect of compaction pressure on the L/D ratios of bio-pellet

Among these materials, bamboo sawdust has the highest moisture content which effected on low heating value. From the pelletization, dimension measurement shows that the height of produced pellet decreased with the increase of compaction pressure and material types (Figure 2). Bamboo sawdust was the easiest material to be pressed while corn cob gave lowest densified pellet under the same press. This might be caused by high adhesion between individual molecular in the material structure. After 139 MPa, higher compaction pressure gave the slightly reduction of density. The relationship between pressure and pellet density were suggested as a simple exponential [3]. Figure 3 shows two groups of materials were classified; easy press and difficultly press. Herein, bamboo sawdust was the easiest pressed while corn cob was the most difficult one. Figure 3 shows the increase of applied pressure can improve the strength of obtained pellets. Herein,

pellet produced from rubber wood was the strongest product while corn cob pellet was the weakest one. With increasing the pressure level from 56 to 139 MPa, water impermeability of pellet decreased to the minimum value and then slightly increased at the higher pressure.

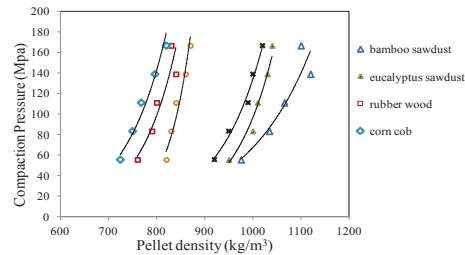


Figure 3. Relationship between compaction pressure and pellet density

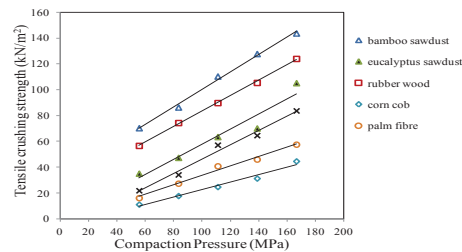


Figure 4. Effect of compaction pressure on the tensile crushing strength

These results could be suggested that the pellet production using die diameter of 1.3 cm should be done under the press of 139 MPa to get the densified product with high energy density. Bamboo sawdust, eucalyptus sawdust and lippia grass are the interesting bio-waste feedstocks to be promoted for the commercial pellets.

ACKNOWLEDGMENT

We would like to thank Center of Knowledge Development of Rubber Tree in Northeast group (KDRN), KhonKaen University (Thailand) for the fully funded support to conduct this research.

References

- [1] K. Theerarattananoon, F. Xu, J. Wilson, R. Ballard, L. Mckinney, S. Stagenborg, P. Vadlani, Z.J. Pei and D. Wang, "Physical properties of pellets made from sorghum stalk, corn stover, wheat straw, and big bluestem". *Industrial Crops and Products*. **33(2)**, 2011, pp.325-332.
- [2] R. Mythili and P.Venkatachalam, "Briquetting of Agro-residues". *Carbon*. **42(41.80)**, 2013, pp.42-08.
- [3] R. Razuan, K.N. Finney, Q. Chen, V.N. Sharifi and J. Swithenbank, "Pelletised fuel production from palm kernel cake". *Fuel Processing Technology*. **92(3)**, 2011, pp.609-615.

PREPARED OF ACTIVATED CARBON FROM MACADAMIA SHELL BY MICROWAVE IRRADIATION ACTIVATION EE

N. Dejang¹, O. Somprasit¹ and Sirinuch Chindaruksa¹

¹ Physics Department, Faculty of Science, Naresuan University, Thailand

SUMMARY: Activated carbon was prepared by carbonaceous material with difference condition activation process. The macadamia shell was wasted agriculturist from Doi Tung, Chiang Rai located in northeast of Thailand, and changed structure to carbon by confine space process in 500°C holding time 1 h. The physical properties of macadamia shell carbon were presented the yield produced 31.88% and moisture of wet 12.25% and dry 10.92% of carbon. The carbon was activated with water and ZnCl₂ combined microwave irradiation. After that, the carbon was crushed and sieved the particles size in the range less than 2 mm. The activated carbon process started by using physical (water) and chemical (ZnCl₂) activation with combined microwave power 90 and 360 W, time reaction during 1 to 5 min. It was found that the moisture all of activated conditions were presented less than 5%. The adsorptive capacity activated carbon was performed on iodine adsorption. There was the average value 680.87 and 672.38 mg/g of activation with water and ZnCl₂, respectively for microwave power 90 W. Then, activation of activation with water and ZnCl₂ for microwave power 360 W was appeared the iodine adsorption of average value 678.73 and 716.31 mg/g, following. It was similarly increased the value iodine adsorption number with increasing microwave power and time. The both microwave power condition of activation process were clearly permitted AWWA B 604 standard. From this results, we can activated the carbon within 1 min by microwave irradiation. Finally, it could be applied the microwave irradiation for activation process.

Keywords: activated carbon, iodine number, macadamia shell

INTRODUCTION

Today, macadamia nut has commercial importance for hill tribe Doi Tung, Chiang Rai. It was improved life quality and money income. It was improved life quality and money income for local people. The agricultural waste in macadamia industry is macadamia shell. Normally, it was deposited by heating furnace. In the other hand, carbons were able to produce from agricultural waste using carbonization method for improved producing. The raw materials carried of activated carbons on waste natural agriculture or minerals. The microstructure of carbons have depended the porosity, surface area and adsorption capacity in natural texture of raw materials. The method commonly used for activation of the carbon properties with two methods that were physical and chemical activation. Activated carbons were widely produced by carbonization and activation treatment for improved surface areas and porous. The advantage of activated carbon was used for removal toxic in waste water, gas and pollutions etc. However, the activated carbon properties were designed the modification to activation method. It has many methods for modification carbonization at high temperature example enrichment carbonization in nitrogen or carbon dioxide atmosphere for improve porosity or adsorption properties [1, 2]. The activated process was depended the comfortable preparation and economic. The pyrolysis typical process widely prepares charcoal and required gas feeding and high performance furnace. The production is likely complicated process and requirement complex condition.

In this work, the prepared activated carbon from

macadamia shell was investigated in fabrication of activated carbon by confine space. The carbon was activated using chemical and physical method with combined microwave irradiation during different time process. The chemical composition and microstructure of activated carbon were investigated. The physical properties were estimated using yield, moisture and iodine adsorption.

EXPERIMENTAL PRODEDURE

Prepared Activated Carbon

Macadamia shell was carbonized in confine space process temperature 500 °C, within 1 h. The carbon samples were crushed and collected sieve size in the range 0.5- 1.5 mm. The carbons in solution were activated with different time (1 to 5 min) and microwave irradiation power (90 and 360 Watt of condition parameters. The two methods activation was consisted the ZnCl₂ and water activation. The preparation ZnCl₂ concentration 25% mol solution was mixed with carbon by weight ration 3:1. The carbon was soaked all of particles in the solution. The activation step was carried out fixed the microwave power of 90 and 360 Watt with vary irradiation time of 1 to 5 min. The final products were washed with deionized water until the pH value reached about 7.0 and then dried at 100 °C. The water physical activation was implemented the carbon with ration water pre carbon 3:1 by weight.

Characterization method

The adsorptive capacity experiments were performed on iodine adsorption. The chemical composition of carbon was investigated using X-ray diffraction (X-Pert 100, Phillip Ltd.). The

morphologies of the activated carbons were characterized by scanning electron microscopy (SEM, LEO 1455VP, LEO Ltd.). Finally, the results were compared with Thai Industrial Standards Institute (No. 900 – 2532).

RESULTS AND DISCUSSION

The macadamia shell was transferred the carbon structure by temperature 500 °C with holding time 1 hr condition. The yield of carbon production was value 31.88%. The XRD resulted (in Fig. 1), the chemical composition of carbon of macadamia shell has composited the amorphous, carbon and graphite. The initial phase of carbon powder has highest intensity at 22.78° that it correspond carbon (JCPDF- 500926) and graphite (JCPDF- 020456) at 26.76°. The XRD intensity was high broad peak in diffraction pattern that it has the amorphous carbon.

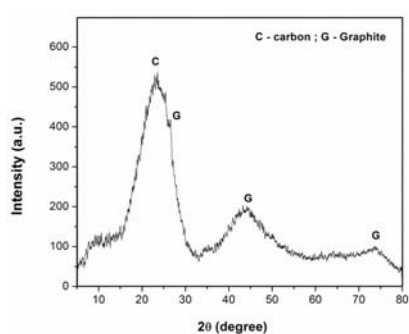


Figure 1. XRD pattern of macadamia shell carbon

Activated carbon was prepared using different method exhibited different adsorption properties by iodine adsorption number, as shown Fig. 2.

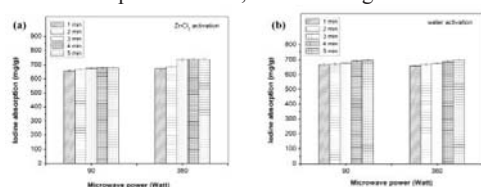


Figure 2. Iodine adsorption from the activated process

In Fig. 3, it was shown the morphology of some activated carbon by $ZnCl_2$ and water activation in 360 Watt. The girt activated carbon formed irregular granules.

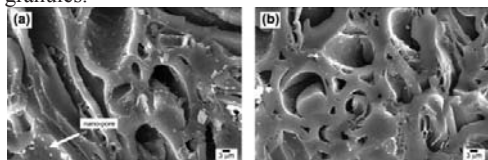


Figure 3. The morphology of activated carbon from different parameter (a) $ZnCl_2$ and water combined microwave during 5 min process

CONCLUSION

From the result, it was able to accept that the activated carbon from combined microwave irradiation activation has high quality activated carbon and following standard. The temperature 500 °C sufficiently produced carbon by confine heating. The precursor was able to absorb microwave energy and quickly treatment time. The less energy and time which 90 watt and 1 min activation can produce the activated carbon from macadamia shell that it passes the activated carbon standard.

ACKNOWLEDGMENT

The author would like to thank Naresuan university of financial support under project No. R2558B089

References

- [1] T. Badosz and J. Editor, "Activated carbon surfaces in environmental remediation" U.S.: Elsevier Ltd.; 2006.
- [2] Y. Guo, Y. Shofeng, K. Yu, J. Zhao, Z. Wang and H. Xu. "The preparation and mechanism studies of rich husk based porous carbon" *Mater. Chem. Phys.*, **74**, 2002, pp. 320-323.
- [3] C. Saka, BET, TG-DTG, FT-IR and SEM, "Iodine number analysis and preparation of activated carbon from acorn shell by chemical activation with $ZnCl_2$ " *J. Anal. Applied Pyrolysis*, **95**, 2002, pp. 21–24.
- [4] M.I. Yusufu, C.C. Ariaahu and B.D. Igbabul, "Production and characterization of activated carbon from selected local raw materials", *African J. Pure Applied Chem*, **6(9)**, 2012, pp. 123-131.
- [5] Rufford T.E., Hulicava-Jurcakova D., Huz J., Green carbon materials; Advances and applications, U.S.: Taylor&Francis group Ltd.: 2013.
- [6] Y. Gua and D.A. Rockstraw, "Activated carbons prepared form rice hull by one-step phosphoric acid activation", *Microporous and Mesoporous Mater*, **100**, 2007, pp. 12-19.

THERMOGRAVIMETRIC STUDIES ON OIL PALM EMPTY FRUIT BUNCH AND PALM KERNEL SHELL: TG/DTG ANALYSIS AND MODELING

Pichet Ninduangdee¹, Vladimir I. Kuprianov¹, Eui Young Cha¹, Rujira Kaewrath¹,
Wanwattana Athhawethworawuth¹ and Pattrapon Youngyuen¹

¹School of Manufacturing Systems and Mechanical Engineering, Sirindhorn International Institute of Technology, Thammasat University, Thailand

SUMMARY: In this study, combustion behavior and characteristics of oil palm residues, empty fruit bunch (EFB) and palm kernel shell (PKS), were investigated in a thermogravimetric analyzer. A 15-mg sample of each residue was heated from 30 °C to 900 °C at a rate of 20 °C/min in a dry airflow of 50 ml/min. TG/DTG curves, showing the sample degradation behavior, and combustion characteristics (including the ignition and burnout temperatures) were obtained and compared between the two biomasses. Kinetic parameters, such as the activation energy (E), the pre-exponential factor (A), and the reaction order (n), were determined for each biomass according to the Coats-Redfern method. The findings revealed excellent combustion properties of both palm oil residues. However, EFB exhibited higher thermal and combustion reactivity compared to PKS.

Keywords: Thermogravimetric analysis (TGA), oil palm residues, kinetic analysis, Coats-Redfern method

INTRODUCTION

In Thailand, oil palm residues are important and promising biomass resources with a significant, about 166 PJ/year, total energy potential [1]. Like any other lignocellulosic biomasses, these residues consist mainly of hemicellulose, cellulose, and lignin, and may also contain some biopolymer extractives [2]. The contents of these components affects the texture, physical properties, as well as thermal and combustion reactivity of a feedstock.

A thermogravimetric analysis (TGA) is reported to be an advanced tool to investigate and compare the thermal and combustion reactivity of different biomasses. TG/DTG tests provide important data on devolatilization and combustion behavior, as well as on combustion characteristics (such as the ignition burnout temperatures), of a biomass fuel. In addition, experimental data from a thermogravimetric study gives an information for determining some kinetic characteristics of a biomass during its degradation, such as the reaction order and the kinetic constants.

This study was aimed at investigating of the thermogravimetric characteristics of empty fruit bunch (EFB) and palm kernel shell (PKS) to assess thermal and combustion reactivity of these oil palm residues fuels. Characteristic temperatures, such as the ignition, peak and burnout temperatures, were determined and compared between the biomass fuels. The kinetic parameters for the combustion of the two residues were determined as well.

MATERIALS AND METHODS

Table 1 shows the chemical structure of EFB and PKS used in this study. With 56.4 wt.% in this composition, EFB seems to be more reactive compared to PKS.

A Mettler-Toledo TGA/DSC1 system was

employed to obtain the TG/DTG curves of the selected biomasses. Prior to testing, both EFB and

Table 1. Structural analysis of the selected biomasses

Chemical structure (on dry ash-free basis, wt.%)	EFB	PKS
Hemi-cellulose	16.3	14.4
Cellulose	56.4	33.4
Lignin	17.9	46.3

PKS were ground and sieved to produce fine particles with a particle size less than 200 μm . During each thermogravimetric test, a sample with the initial weight of 15 mg was heated from room temperature to 900 °C at heating rate $\beta = 20$ °C/min. Dry air was used as the furnace medium and supplied into the analyzer furnace at a flowrate of 50 ml/min. Experimental tests for selected conditions were performed three times for repeatability.

In this study, Coats-Redfern method [3] was applied to quantify major kinetic parameters, such as the activation energy (E), the pre-exponential factor (A), and the reaction order (n). In the kinetic analysis, the biomass decomposition rate (α) is determined as a function of time (τ):

$$\frac{d\alpha}{d\tau} = \frac{A}{\beta} \exp\left(-\frac{E}{RT}\right) (1-\alpha)^n \quad (1)$$

where n is an empirical factor, and R is the universal gas constant.

Eq. (1) can be integrated and approximated using the Taylor's series expansion. The final form of this takes the form:

$$\text{for } n = 1: \ln\left[-\frac{\ln(1-\alpha)}{T^2}\right] = \ln\left[\frac{AR}{qE}\right] - \frac{E}{RT} \quad (2)$$

$$\text{for } n \neq 1: \ln\left[\frac{1-(1-\alpha)^{1-n}}{T^2(1-n)}\right] = \ln\left[\frac{AR}{qE}\right] - \frac{E}{RT} \quad (3)$$

The left-hand side of Eq. (2) and Eq. (3) can be designated as y . Then for the selected temperature range and properly selected n , experimental data from a thermogravimetric test can be fitted by a first-order function:

$$y = a + bx \quad (4)$$

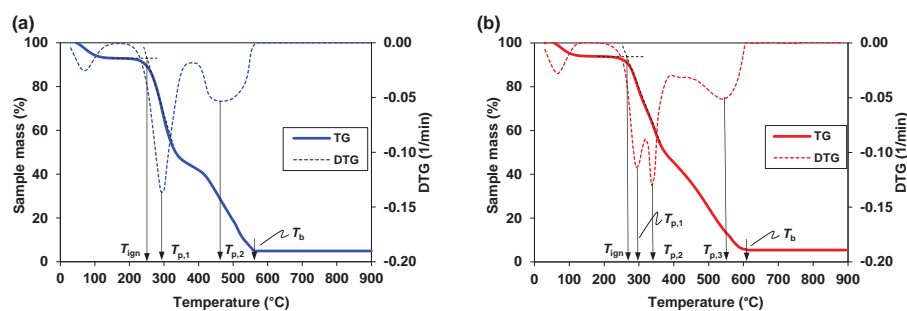


Figure 1. TG and DTG curves of (a) EFB and (b) PKS samples

Table 2. Fitting equations and kinetic parameters of EFB and PKS for different temperature range

Biomass	Temperature range (°C)	Fitting equation	Correlation coefficient, r	Activation energy, E (kJ/mol)	Pre-exponential factor, A (1/min)	Reaction order, n
EFB	183–381	$y = -12.28 + 14.83x$	0.9970	123	6.00×10^{10}	4.5
	390–588	$y = 6.139 + 4.829x$	0.9471	40.2	208	1.1
PKS	183–381	$y = -13.49 + 16.27x$	0.9975	135	2.93×10^{11}	5.5
	327–390	$y = -7.926 + 12.46x$	0.9945	104	6.90×10^8	5.8
	399–624	$y = 3.783 + 3.254x$	0.9370	27.1	10.43	0.8

where $x = 1/T$, and a designates the first term on the right-hand side of Eq. (2) and Eq. (3).

For variable x (or T), the curve $y = f(x)$ for the selected n can be then plotted on a semi-logarithmic graph to quantify the kinetic constants: E (by using the fit slope b) and A (from the expression for a).

RESULTS AND DISCUSSION

Figure 1 depicts the TG/DTG curves of EFB and PKS. Within the temperature range of 160–400 °C (associated with decomposition of hemicellulose and cellulose), the DTG profile of EFB exhibited only peak temperature (295 °C), while the DTG profile of PKS within the same temperature range exhibited two regions, and accordingly two peak temperatures: 300 °C and 345 °C. Within this temperature range (160–400 °C), some amount of lignin of both biomasses was apparently subject to a thermal degradation.

At the final stage (i.e., at temperatures higher than 400 °C), the mass loss was mainly caused by (i) decomposition of the remained lignin (accompanied by its conversion into char), and (ii) further oxidation (combustion) of the char. The maximum rate of biomass degradation at the final stage indicated another specific characteristic of the DTG curve: 471 °C (the second peak temperature) for EFB, and 543 °C (the third peak temperature) for PKS, associated with lignin decomposition.

Based on the combined analysis of both TG and DTG curves, the ignition temperature and the burnout temperature of the selected biomasses were determined to be, respectively: 267 °C and 557 °C for EFB, whereas 270 °C and 586 °C for PKS.

It can be generally concluded from the thermogravimetric study that with lower T_{ign} , $T_{p,1}$, and T_b , EFB can be basically characterized as a biomass with higher thermal/combustion reactivity compared to PKS.

Table 2 shows the kinetic characteristics (E , A , and n) of EFB and PKS. As seen in Table 2, at relatively low temperatures (the first stage of decomposition), the value of E for EFB was found to be 123 kJ/mol, which was substantially lower than that for PKS (135 kJ/mol), so EFB can be ignited much easier than PKS. This result explains the above-mentioned difference in T_{ign} between the two biomasses.

CONCLUSIONS

Empty fruit bunch and palm kernel shell, the major residues from the palm oil production, are lignocellulosic biomasses, both showing excellent combustion properties and great potential as biomass fuels for heat and power generation. From the thermogravimetric study, empty fruit bunch exhibits higher thermal and combustion reactivity compared to palm kernel shells. This fact is confirmed by the lower ignition temperature, the burnout temperature, and the activation energy of empty fruit bunch than those of palm kernel shell.

ACKNOWLEDGEMENT

The financial support from the Thailand Research Fund (Contract No. BRG5680014) is greatly acknowledged.

References

- [1] Department of Alternative Energy Development and Efficiency, "Thailand Alternative Energy Situation 2012", <http://www.dede.go.th> [accessed 01.01.15].
- [2] P. McKendry, "Energy production from biomass (part 1): overview of biomass", *Bioresource Technology*, **83**, 2002, pp. 37–46.
- [3] A.W. Coats and J.P. Redfern, "Kinetic parameters from thermogravimetric data", *Nature*, **201**, 1964, pp. 68–69.

ANAEROBIC CO-DIGESTION BIOMETHANATION OF CANNERY SEAFOOD WASTEWATER WITH *MICROCYSTIS SP*; BLUE GREEN ALGAE WITH/WIHOOUT GLYCEROL WASTE

Kiattisak Panpong^{1,2}, Kamchai Nuithitikul³, Sompong O-thong^{4,5}, Prawit Kongjan^{6,7}

¹Songkhla Rajabhat University (Satun Campus) and ²Department of Engineering, Faculty of Industrial Technology, Songkhla Rajabhat University, Thailand

³School of Engineering and Resources, Walailak University, Thailand

⁴Department of Biology, Faculty of Science, Thaksin University, Thailand

⁵Microbial Resource Management Research Unit, Faculty of Science, Thailand

⁶Chemistry Division and ⁷Bio-Mass Conversion to Energy and Chemicals (Bio-MEC) Research Unit, Department of Science, Faculty of Science and Technology, Prince of Songkla University (PSU), Thailand

SUMMARY: We investigated the feasibility of using *Microcystis sp*; blue green algae (MB) as a co-substrate to improve the mesophilic anaerobic digestion of cannery seafood wastewater (CSW) supplemented with 1% (v/v) glycerol waste (GW), to maximize bio-methane production. The MB content was set at 5, 10 and 15% (v/v) to find a near optimal methane yield. The maximum 291 mL CH₄/g VS-added methane yield, corresponding to 4.4 m³-CH₄/m³ - mixed wastewater, was achieved with a CSW: GW: MB mixture at the volumetric 94:1:5 ratio. The methane yield of CSW digested alone was 278 mL CH₄/g VS-added (2.2 m³ CH₄/ m³ of wastewater). The yields from our other experiments ranged within 81– 150 mLCH₄/g VS-added. Ratios of MB: CSW exceeding 5 % (v/v) gave lower than optimal methane yields. The energy content of methane from 1 m³ of mixed wastewater, with the near optimal mixture ratio 94:1:5, was 157 MJ or equivalently 44 kWh.

Keywords: Co-digestion, Biogas production, Cannery seafood wastewater, Glycerol waste, Blue green algae

INTRODUCTION

Seafood cannery processing requires large amounts of water and consequently, factories of tuna and sardine canning discharges about 14 to 22 m³-wastewater/ton-raw fish [1]. Anaerobic treatment is suggested for cannery seafood wastewater due to less energy consumption, low sludge production and gaining energy carrier in a form of biogas. However, cannery seafood wastewater contains generally high content of protein and fat, which are the most difficult to be anaerobically degraded [2]. Protein-rich wastewater tends to be biodegraded rapidly to large amount of ammonium that directly inhibits methanogens in the methanogenesis stage of anaerobic digestion process [3]. The CH₄ production from single anaerobic digestion process could be enhanced by a strategy of simultaneous digestion of two or more organic waste feedstock called co-digestion. Anaerobic co-digestion allows for increasing the external carbon source, COD concentration to feedstock by co-digesting nutrient-rich and improving the yields of methane production due to the positive synergisms in the anaerobic digestion [4].

Glycerol waste is a by-product of biodiesel production and is generated approximately 10% of oil material used. Its global production is currently more than 3,000,000 tons and is expected to be around 4,600,000 tons by 2020 due to increasing in demand of using biodiesel [5]. Low price glycerol waste having high COD content is easily digested anaerobically and can be stored at room temperature over a long time [6].

Eutrophication usually promotes excessive

cyanobacteria or blue green algae growth (algal bloom) and subsequent decay in natural lakes and reservoirs, which causes serious water toxicity problems, including N, P, and S pollution as well as bad smells. Energy recovery from the algal bloom biomass is potentially possible by anaerobic digestion (AD) that could produce in the form of methane rich biogas. Algal compositions are highly varied for 6–52% proteins, 7–23% lipids, and 5–23% carbohydrates by weight, depending on algal species [7].

METHODOLOGY

Batch biomethane production was performed in 1,000 ml serum bottles, with a 900 ml working volume. The volume of active granular sludge was held constant at 125 ml in all serum bottles. Each serum bottle was gassed with N₂ for a few minutes, then immediately sealed with a rubber septum and an aluminum crimp cap. All filled bottles were incubated in the incubator controlled at 35 ±1°C. The experimental tests were designed to assess the influence of the mixture ratio of CSW and 1%GW, and to select an MB concentration from 5, 10 and 15% (v/v), in order to maximize the methane production. The collected biogas quantities were determined daily by water displacement. The biogas composition was analyzed periodically by GC-TCD. The methane yield was defined as the total volume (STP reference conditions) of methane produced during the digestion period per amount of substrate initially added (mLCH₄/g VS added). Thus as yield we use the observed conversion relative to what idealized reactions could possible produce from the

feedstock.

RESULTS AND DISCUSSION

Table 1 showed the physical-chemical characteristics of Cannery seafood wastewater (CSW), Glycerol waste (GW) and *Microcystis* sp; blue green algae (MB). Prior to use as a co-substrate, the MB were centrifuged at 12,000 rpm for 15 minutes (Figure 1A) and GW was presented in Figure 1B. The *Microcystis* spp. was the dominant species in these sample mixtures (>99%) as shown in Figure 2. The results of cumulative methane production from various fractions of mixed substrate are shown in Figure 3.

Table 1 Physical-chemical characteristics of CSW, GW and MB

Parameter	CSW	GW	MB
pH	6.3	8.8	7.8
Chemical Oxygen Demand: COD (g/L)	10.4	1,760	85.28
Volatile fatty acid: VFA (mg-acetate/L)	2,230	6,650	*ND
Total alkalinity (mg-CaCO ₃ /L)	2,560	35,050	*ND
Total Kjeldahl Nitrogen: TKN (mg/L)	870	1,670	10,938
Total phosphorus: TP (mg/L)	53.6	71,500	*ND
Total Solid: TS (g/L)	9.37	969	84.85
Volatile solid (VS: g/L)	7.76	910	69.55
Sulfate (g/L)	*ND	15.58	*ND
*Protein (g/L)	3.9	1.28	35.60
Carbohydrate (g/L)	1.91	845	21.20
Fat (g/L)	0.13	63.76	4.73
C/N ratio	11	949	7

* ND. = Not determined, [†] Multiplying the organic nitrogen (TKN minus TAN) by 6.25



Figure 1. The co-substrates were used in experiment; (A) *Microcystis* sp; blue green algae (MB) and (B)



Figure 2. The dominant species of microalgae in the waste mixture was assessed by light microscopy

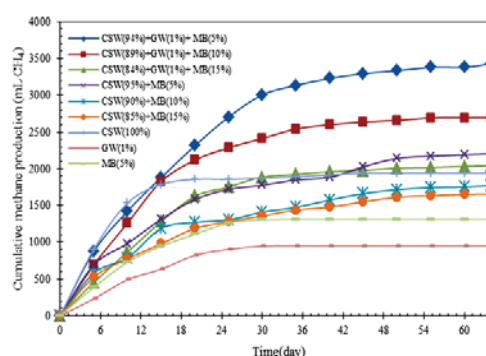


Figure 3. Cumulative methane production for each co-digested mixture of CSW, GW and MB

ACKNOWLEDGEMENT

The authors would like to thank the Office of Higher Education Commission (OHEC) for funding this research. This research project would not have been possible without extensive assistance of the staff from the Microbial Management Research Unit (MRM-TSU), Faculty of Science, Thaksin University, Thailand.

References

- [1] A. Palenzuela-Rollon. "Anaerobic Digestion of Fish Processing Wastewater with Special Emphasis on Hydrolysis of Suspended Solids", *Taylor and Francis*, London, 1999.
- [2] D. Batstone, J. Keller, I. Angelidaki, S. Kalyuzhny, S. Pavlostathis, A. Rozzi, W. Sanders, H. Siegrist and V. Vavilin. "Anaerobic digestion model no. 1 (ADM1)", *IWA publishing*, London, UK, 2002.
- [3] Y. Chen, J.J. Cheng and K.S. Creamer. "Inhibition of anaerobic digestion process: A review", *Bioresource Technology*, **99(10)**, 2008, pp. 4044-4064.
- [4] K.M. Kangle, S.V. Kore, V.S. Kore and G.S. Kulkarni. "Recent trends in anaerobic co-digestion: a review", *Universal Journal of Environmental Research and Technology*, **2(4)**, 2012, pp. 210-219.
- [5] M.M. Viana, A.V. Freitasb, R.C. Leitaoc, G.A.S. Pintoc and S.T. Santaellad. "Anaerobic digestion of crude glycerol: a review", *Environmental Technology Reviews*, **1(1)**, 2012, pp. 81-92.
- [6] M. Jingxing, V.W. Mariane, C. Marta and V. Willy. "Improvement of the anaerobic treatment of potato processing wastewater in a UASB reactor by co-digestion with glycerol", *Biotechnology Letter*, **30**, 2008, pp. 861-867.
- [7] W. Zhong, L. Chi, Y. Luo, Z. Zhang and W.M. Wu. "Enhanced methane production from Taihu Lake blue algae by anaerobic co-digestion with corn straw in continuous feed digesters", *Bioresource Technology*, **134**, 2013, pp. 264-270.

Wind, Wave and Tidal Resource Assessment
and Conversion Technology

DEVELOPMENT AND DESIGN OF PIC CONTROLLED FLOAT BUOY WAVE ENERGY CONVERTER SYSTEM

Rommel Anacan^{1,2} and Ramon Garcia²

¹Electronics Engineering Department,
Technological Institute of the Philippines, Manila, Philippines

²School of Graduate Studies,
Mapua Institute of Technology, Manila, Philippines

SUMMARY: The paper is entitled Development and Design of PIC Controlled Float Buoy Wave Energy Converter System is conceptualized to generate electricity as an alternative due to increasing oil prices and as a possible solution to energy crisis in the incoming years. Even though, unpopular type of renewable energy, wave energy is seen as a potential source that could be used to generate amount of power. Electricity can be generated by the mechanical force collected from the movement of waves in the oceans. Electricity will be stored to a 12 Volts Lead Acid Battery and monitored using a microcontroller. A prototype was built for testing the thesis in Pagudpod, Ilocos Norte. A 12- Volt battery is charge by mechanical force acting to the alternator due to the movement of floating buoy in the surface because of the waves. The PIC microcontroller with the CPLD module will monitor the charging and automatically switch to charge another stand by battery if the latter is full. The prototype was tested and proven to be functional. Another paper goal is to analyze the relationship of the wind speed and water depth to the power produced by the prototype. A regression equation was also develop for the prototype. It has proved that the water depth and wind speed has a direct relationship with the time of charging the batteries and the power produced.

Keywords: Float Buoy; Wave Energy Converter; PIC, Lead Acid Battery; CPLD

INTRODUCTION

Energy plays an indispensable role in a modern society. We all depend on a constant and reliable supply of energy – for our homes, business, and for transport. The current situation of power shortage in the country is alarming with continuous negative effects in many Small-Medium Enterprises (SME) and Multi-National Companies. The world suffers from the effects of climate change mostly coming on burning fossil fuels from electricity generation. Those events continue to recur until a definite solution has been defined. The joint effort conducted by different sectors and government agencies to formulate plans and programs to annihilate these tribulations.

The primary objective of the project is to promote renewable energy to generate electricity with the use of wave power. Therefore, Development and Design of PIC controlled Float Buoy Wave Energy Converter System is an applicable project to conduct. The second objective of the project is to produce a device using water wave energy from the seas and oceans as renewable source to generate electricity in Pagudpod, Ilocos Norte. Furthermore, the project aims to determine the optimal values of the parameters to generate electricity. The parameters to be measured with respect to the charging speed of the batteries are the depth of water and the wind speed. The third objective is to configure and program the PIC microcontroller with CPLD as a controlling and monitoring module. The PIC microcontroller is an additional technology in need to monitor, detect and switch a dry cell to another if in case it was already fully charged. The addition of PIC microcontroller will serve as a charge controller

that will ensure that the batteries will not be overcharge. The fourth objective is to prove if the water depth and wind speed have a relationship on the charging speed of the batteries. The last objective is to generate a regression equation that will predict the charging time of the batteries.

The focus of the design was limited to charging two dry cells. The things that are not included in the study are the effects of the buoy design, frictional losses and duration of the wind blowing in the rate of charging the battery. It was also not included in the study in situ and remote wave measuring systems which record various parameters. The study focused and limited only to evaluating the wave power data to see if Pagudpod is a suitable wave site.

METHODOLOGY

Project Flow

The first side of the flowchart is about wave power. The first thing to be considered was the design of buoy. The application of concepts in electrical machineries on how to generate electricity was applied in choosing the best alternator. The buoy is connected to a reel by a tether cable. As the wave passes over the device, the buoy rises and pulls up the cable thus rotating the cable reel. As the buoy passes over the wave crest and begins to descend the reel rewinds the cable thereby returning again to its original length. The mechanical movement of the generator as the cable reel rotates and returns is converted to electrical power which is transferred to the shores using an underwater transmission line and stored in dry cell batteries. The electricity produced in the generator is AC so

therefore this needs to be rectified to become DC.

The next side of the flowchart depicts the use of the PIC microcontroller with CPLD. A charged battery will be used as the source for the PIC microcontroller and CPLD module. Voltage regulation is required in order to provide good charging supply passed on to the Microcontroller - CPLD.

After configuring the generator and the Microcontroller-CPLD, the device was ready to use. The next step was to combine the two important parts of the prototype. The dry cell batteries to be charged were interfaced with the generator. These dry cell batteries were then connected to the PIC-CPLD. The PIC-CPLD then monitored the batteries. The PIC-CPLD would switch to another battery if in case the previous battery was fully charged.

RESULTS AND DISCUSSION

Table 1. Data of Time Charging of two batteries with water depth and average wind speed as regressor variables

Time of Charging of the two batteries (y) (s)	Water Depth (m) (x ₁)	Average Wind Speed (m/s) (x ₂)
3540	0.6096	1.12
2760	0.7620	1.13
2640	0.9144	1.21
1620	1.0668	1.31
1380	1.2192	1.54

To analyze the data above all the units were converted. The time of charging had an original unit of minutes converted to seconds. The water depth in feet was converted to meters and the average wind speed which was in km/hr was converted to m/s.

A. Statistical Analysis for Time of Charging vs. Water Depth vs. Wind Speed

	Coefficients
Intercept	5087.863636
Water Depth (m)	-4175.91267
Average Wind Speed (m/s)	886.3636364

The regression equation for the charging time of the batteries (y) is

$$y = 5087.863636 - 4175.91267x_1 + 886.3636364x_2$$

Table 3. Excel’s ANOVA table for Time of Charging vs. Water Depth vs. Wind Speed

ANOVA				
	df	SS	MS	F
Model	2	2993604.545	1496802	21.18984
Error	2	141275.4545	70637.73	
Total	4	3134880		

A. Statistical Analysis for Power vs. Water Depth vs. Wind Speed

Table 4. Data of the power produced at different depths with the wave height and wave cycle as regressor variables

Water Depth (m)	Average Windspeed (m/s)	Power (kW/m)	Wave Height (m)	Wave Cycle (s)
0.6096	1.12	0.32	0.35	5.21
0.7620	1.13	0.38	0.40	4.78
0.9144	1.21	0.43	0.50	3.43
1.0668	1.31	0.48	0.55	3.21
1.2192	1.54	0.54	0.60	2.98

Table 5. Data of the Power produced versus water depth and wind speed

Power (kW/m)	Water Depth (m)	Average Windspeed (m/s)
0.32	0.6096	1.12
0.38	0.762	1.13
0.43	0.9144	1.21
0.48	1.0668	1.31
0.54	1.2192	1.54

Table 6. Microsoft Excel’s result for the three unknowns in the multiple regression equation of power vs. other variables

Coefficients	
Intercept	0.101075758
Water Depth (m)	0.34926032
Average Wind speed (m/s)	0.007575758

The regression equation for the power (y) is $y = 0.101075758 + 0.34926032x_1 + 0.007575758x_2$

Table 7. Excel’s ANOVA table for Power vs. Water Depth vs. Wind Speed

ANOVA				
	df	SS	MS	F
Model	2	0.029160909	0.01458	745.977
Error	2	3.90909E-05	2E-05	
Total	4	0.0292		

CONCLUSION

It can be concluded from the study that the deeper the water depth and the faster the wind speed the better it is. The testing of the prototype was able to prove that water depth and wind speed have a direct relationship on charging time. The testing of the prototype was able also to prove that water depth and the wind speed have a direct relationship on power. The regression equation for the charging time of the batteries (y) is $y = 5087.863636 - 4175.91267x_1 + 886.3636364x_2$ while the regression equation for power (y) is $y = 0.101075758 + 0.34926032x_1 + 0.007575758x_2$.

EXPERIMENTAL INVESTIGATION OF HELICAL TIDAL TURBINE CHARACTERISTICS WITH DIFFERENT TWIST

Sathit Pongdoang¹, Chaiwat Kayankannavee² and Yodchai Tiaple¹

¹Department of Maritime Engineering, International Maritime Studies, Kasetsart University, Sriracha Campus, Thailand

²Water Resources Engineering, Faculty of Engineering, Kasetsart University, Thailand

SUMMARY: The helical tidal current turbine was studied and reported its performance and characteristics for free water flow electric turbine development. The scale model of tidal turbine was built in dimension as: 0.5m and 0.6m of diameters and 1.25m in length; the turbine cross section blade was symmetry foil NACA0020 with 0.07m chord length, and there were 3 blades with the helical angle of 120°, 135°, and 150°. The model was tested in towing tank (1.46m width, 3m depth and 45m length). The rotation and torque of the turbine was measured under various tow velocity setting, while power and power efficiencies under various tip speed ratio and helical angle velocities were presented. The characteristics obtained from this experiment provide useful for design and development of helical tidal current electrical turbine.

Keywords: hydrokinetic turbine, helical tidal turbine, Gorlov turbine, ocean energy, renewable energy

INTRODUCTION

Helical turbine was firstly developed by Prof. Alexander M. Gorlov from Northeastern University, called GHT [1]; such turbine was designed based on the Darrieus's type and composed of: symmetry foil and using the helix shape in length direction of the blade to increase turbine torque. The GHT can perform high rpm under low current velocity without shifting and cavitation; moreover, the overall efficiency is also higher than normal Darrieus's turbine [2]. Therefore, this turbine is always used for current electric turbine. The major advantage of such turbine is installation benefits such as simple mechanical coupling, shallow water installation ability, and it can be installed wherever the water current direction leads. These pros makes such turbine can be placed where the horizontal turbine cannot [3].

This article presents the characterization of helical current turbine at different turbine diameter and blade helix angle. The scaled model is towed at various speeds, while all parameters such as rpm and torque is recorded.

THEORY

Current energy is expressed in the form of kinetic energy (*KE*). Since the mass *m* kg is moved by velocity *V* m/s, the kinetic energy can be displayed as equation 1.

$$KE = \frac{1}{2}mV^2 \quad (1)$$

Since the current velocity has unit as mass per time, one can replace *m* in equation 1 by \dot{m} the kinetic energy of current will transform to hydrokinetics (*P*) as shown in equation 2

$$P = \frac{1}{2}\dot{m}V^2 \quad (2)$$

The ratio between current velocity *V* and cross section area *A* can be expressed as water mass velocity per time (equation 3).

$$\dot{m} = \rho VA \quad (3)$$

where ρ is the water density kg/m³. Replacing \dot{m} in equation 3 into equation 2, the maximum of water flow power is obtained as shown in equation 4

$$P_w = \frac{1}{2}(\rho AV^3) \quad (4)$$

The main purpose of such turbine is converting kinetic energy to mechanical energy which is similar to wind turbine concept [4]. The converting formula is shown in equation 5

$$P = \frac{1}{2}C_p\rho AV^3 \quad (5)$$

where ρ is the water density, *A* is the turbine swept area, *V* is the current velocity, and *C_p* is the turbine power efficient. In theory, the maximum of efficiency is not over 59.3% according to Betz limit [5]; however, the power efficient is directly proportion to the tip speed ratio (TSR): the ratio between tip speed and current velocity as shown in equation 6. The TSR also depends on blade shape and number of blade [4].

$$TSR = \frac{\Omega R}{V} \quad (6)$$

The Ω is angular velocity (rev/s), and R is the turbine radius. The power coefficient of turbine can also calculated by ratio between mechanical and kinetic energy as shown in equation 7

$$C_p = \frac{2Q\Omega}{\rho AV^3} \quad (7)$$

,where Q is the torque (N-m).

EXPERIMENT SETUP

The experiment setup consisted of: towing tank in 43m length, 1.46m width, and the water depth was 3m. There was the incline plan at the end of tank served as wave crumbling. The scaled model was composed of: 3 symmetry foils, no. NACA0020, and the dimension of turbine was included 0.07m chord (c), 0.5m and 0.6m of diameter (D), and 1.25m length. There were 3 different helical angle (δ) designs of blade which were 120°, 135°, and 150° as shown in figure 1

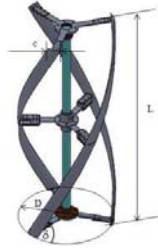


Figure 1. The schematic of helical current turbine

RESULT AND DISCUSSION

The towing speed was set from 0.9 – 1.655 m/s for each angle set of blades. Firstly, the helical angle of 120° were attached to the turbine and tested. The power coefficient derived from equation 7 was plotted against tip speed ration (TSR) as shown in figure 3. The same procedure was also carried out for the angle 135° and 150° helical angle blade as shown in figure 4 and 5 respectively.

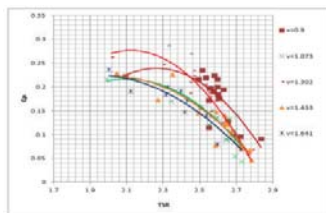


Figure 2. The experiment at $\delta = 120^\circ$

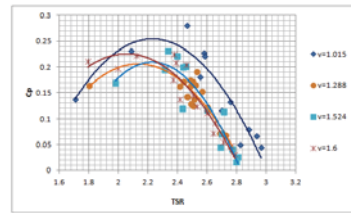


Figure 3. The experiment at $\delta = 135^\circ$

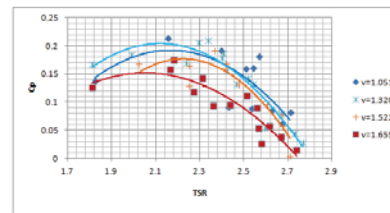


Figure 4. The experiment at $\delta = 150^\circ$

The results indicated that helical angle has influence to turbine efficiency, while the turbine solidity had effect only to TSR. At helical angle was $\delta = 135^\circ$, the system showed better efficiency for $\sigma = 0.134$ at $TSR \approx 2.2$ and for $\sigma = 0.111$ at $TSR \approx 2.5$. The experimental results suggested useful design information for tidal current electrical turbine development.

ACKNOWLEDGMENT

The authors would like to thank department of research and develop of irrigation department of Thailand for supporting the equipment and advises.

References

[1] http://en.wikipedia.org/wiki/Gorlov_helical_turbine
 [2] A.M. Gorlov, “Development of the helical reaction hydraulic turbine. Final Technical Report”, The US Department of Energy, August 1998, The Department of Energy's (DOE).
 [3] Edinburgh Designs Ltd. (2006) Variable Pitch Foil Vertical Axis Tidal Turbine, pp. 8-10. [Online]. Available: <http://www.dti.gov.uk>.
 [4] Burton T, Sharpe D, Jenkins N, Bossanyi E. Wind energy handbook. Chichester: Wiley; 2000
 [5] <http://windturbine-analysis.com/index-intro.htm>

DESIGN, DEVELOPMENT AND EXPERIMENTATION OF DEEP OCEAN WAVE ENERGY CONVERTER SYSTEM

Srinivasan Chandrasekaran¹ and Raghavi Bhoopathy²

¹Professor, Dept. of Ocean Engineering, Indian Institute of Technology Madras, India

²Research Scholar, Dept. of Ocean Engineering, Indian Institute of Technology Madras, India

SUMMARY: Energy from ocean waves remains largely a untapped resource, which is also highly consistent in comparison to other alternate sources of energy such as wind and solar. Present study deals with design and development of innovative wave energy converter (WEC) that uses a buoy-type point absorber. The device is proposed to be mounted on an offshore platform and be used to produce electric output for meeting the operational energy demands, partially. The device employs lever arm and gear boxes to obtain the mechanical work from the heave energy of the floating buoy. Subsequently, electric energy is generated from the mechanical work harnessed from the waves by deploying a generator. Design Failure Mode and Effect Analysis (FMEA) carried out on the system shows all the components except buoy have less risk of failure.

Keywords: renewable energy, wave energy, point absorber, wave power, energy converter

INTRODUCTION

Existing traditional methods of energy production are contributing to serious environmental problems. So there is an urgent need for pollution-free green power generation and hence the focus of present research and development in renewable energy is redirected towards viable and sustainable energy resources. Compared to other forms of alternate sources of energy, wave energy is more consistent and predictable [1]. Energy density is the highest amongst the renewable energy sources [2,3]. Ocean wave power can be converted into electrical energy by different methods [4-7] namely: (i) Oscillating water columns [8,9]; ii) Oscillating bodies [10,11]; and (iii) Overtopping devices [12]. In the resent study, point absorber type of oscillating bodies is used to harness wave power [13-17].

METHODOLOGY

Fig.1 shows the experimental setup of the proposed device. Horizontal cylindrical buoy with an extended fin is connected to an oscillating arm through the connector. This buoy is used for capturing wave energy in the heave mode. In order to convert the reciprocating vertical motion of the buoy to rotary motion, unidirectional gear assembly is deployed. A flywheel is also used to rectify the discontinuous flow of power. A permanent magnet DC generator is used to generate electric power by the principle of electromagnetic induction.



Figure 1. Experimental setup of the proposed device

DISCUSSION OF RESULTS

A 1:6 scaled model of the proposed wave energy converter is designed, fabricated and tested in 2m deep wave flume at Indian Institute of Technology Madras, India. Buoy of length 1.6 m and weight 165 kg is used for the experimental analysis. Counter weight of 45 kg is used to activate the reciprocating motion of the rotating arm. An 8-pole permanent magnet DC generator unit is used as the electricity generating unit and electrical bulbs are used as loading units. Generated electrical power is recorded using a power analyzer. Experiments are conducted for varying parameters of the device. Responses under the encountered waves for different degrees of rotation of the buoy are recorded. The responses for two different length of lever arm of 1m and 1.7m are also summarized. Mechanical and electrical outputs of the system are recorded for different wave heights varying from 0.24-0.30m and with the time period of 3s. Fig. 2 shows the comparison of mechanical power output for different wave heights and buoy position (0° , 16° , 32° and 48°) with respect to the wave approach angle, respectively. It is seen from the figure that there is an increase in the power output for increase in wave heights. Fig. 3 compares the electrical power output of the system for varying lengths of lever arms of 1m and 1.7m under 0.30m wave height, 3 s period. It is seen that output of the system is maximum for the lever arm of 1.7 m. Fig. 4 displays the average mechanical power produced for different angles of rotations of the buoy for 0.30m wave height, 3s wave period and 1.7m arm length. It is seen that the proposed wave energy converter produces maximum average power at 32° compared to that of 0° , 16° and 48° . Maximum mechanical power produced by the system is about 127.08 watts, as measured on the scaled model. Overall mechanical efficiency of the device is found to be 23.47%. Design FMEA shows floating buoy as the most vulnerable part with the RPN of 84. Recommended actions focus on the rigorous testing of the buoy in lab for robust design of the buoy.

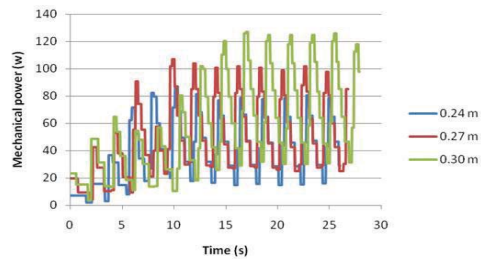


Figure 2. Variation of mechanical power output for different wave heights

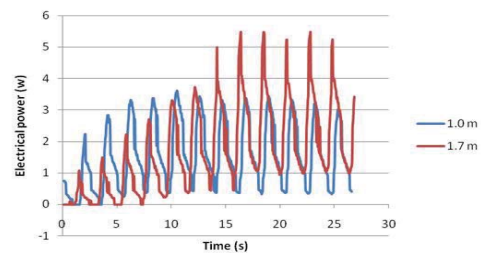


Figure 3. Variation of electrical power for lever arm

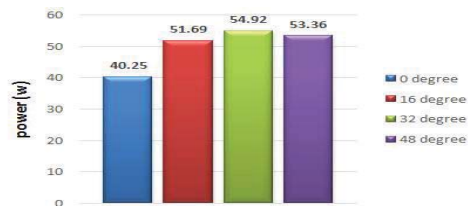


Figure 4. Variation of mechanical power for angle of rotation of the buoy.

ACKNOWLEDGMENTS

Authors sincerely thank the Earth System Science Organization, Ministry of Earth Sciences, Government of India for extending the financial support to conduct this research.

References

- [1] R. Pelc and R. M. Fujita. "Renewable energy from the ocean". *Marine Policy*, **26**, 2002, pp. 471–479.
- [2] A. Cle'ment, P. McCullen, A. Falca'õ. "Wave energy in Europe: current status and perspectives". *Renewable and Sustainable Energy Reviews*, **6(5)**, 2002, pp. 405–431.
- [3] T. W. Thorpe. "A brief review of wave energy, Technical report no" R120, Energy Technology Support Unit (ETSU), A report produced for the UK Department of Trade and Industry 1999.
- [4] B. Drew, A.R. Plummer and M.N. Sahinkaya. "A review of wave energy converter technology". *Proceedings of the Institution of Mechanical Engineers, Part A. Journal of Power and Energy* **223(8)**, 2009, pp. 887-902.
- [5] J. Falnes. "A review of wave-energy extraction". *Marine Structures*, **20(4)**, 2007, pp. 185–201.
- [6] Falca, F.De.O. "Wave energy utilization: A review of the technologies". *Renewable and Sustainable Energy Reviews*, **14(3)**, 2009, pp. 899-918.
- [7] T. Brekker, A. Joanne and H. Han. "Ocean wave energy overview and research at Oregon State University". *Power Electron. Mach. Wind Appl., Lincoln, NE, USA* 2009.
- [8] H. Martins-rivas and C.C. Mei. "Wave power extraction from an oscillating water column along a straight coast". *Ocean Engineering*, **36(6-7)**, 2009, pp. 426–433.
- [9] O. Malmo and A. Reitan. "Wave-power absorption by an oscillating water column in a channel". *Journal of Fluid Mechanics*, **158**, 1985, pp. 153- 175.
- [10] D.J Pizer. "Maximum wave-power absorption of point absorbers under motion constraints". *Applied Ocean Research*, **15(4)**, 1993, pp. 227-234.
- [11] M. Vantorre, R. Banasiak and R. Verhoeven. "Modelling of hydraulic performance and water energy extraction by a point absorber in heave". *Applied Ocean Research*, **26**, 2004, pp. 61–72.
- [12] L. Margheritinia, D. Vicinanzab and P. Frigaarda. "SSG wave energy converter: Design, reliability and hydraulic performance of an innovative overtopping device". *Renewable Energy*, **34(5)**, 2009, pp. 1371-1380.
- [13] A. Amarkarthik, S. Chandrasekaran, K. Sivakumar, and H. Sinhmar. "Laboratory experiment using non-floating body to generate electrical energy from water waves". *Frontier in Energy*, **6(4)**, 2012, pp. 361-365.
- [14] S. Chandrasekaran and H. Sinhmar. "Power generation using Mechanical wave energy converter". *Intl. J. Ocean Climate and Systems*, **3(1)**, 2012, pp. 57-70.
- [15] N.S. Tito. "Deep Ocean Wave Energy Converter". *M.Tech. Thesis, Department of Ocean Engineering, IIT Madras, India*, 2011.
- [16] H. Sinhmar. "Power Generation using Mechanical Wave Energy Converter". *Ph.D. Thesis, Department of Ocean Engineering, IIT Madras, India*, 2012.
- [17] S. Chandrasekaran and H. Manki. "Mechanical wave energy converter". *Report to Human Resource Development in Offshore and Plant Engg*, HOPE, Changwon National University, Republic of South Korea 2010.
- [18] B. Skelton. "Process safety Analysis-an Introduction". *Institution of chemical engineers, UK* 1997.
- [19] Potential failure mode and effect analysis reference manual. *Automotive Industry Action Group (AIAG)* 1995.

EVALUATION OF WIND RESOURCE IN SELECTED LOCATION IN GUJARAT

Garlapati Nagababu¹, Dharmil Bavishi¹, Surendra Singh Kachhwaha¹ and Vimal Savsani¹

¹ Pandit Deendayal Petroleum University, Gandhinagar, Gujarat, India

SUMMARY: This paper presents an assessment of wind energy potentials of six selected locations in the Gujarat, India, by using a 19-year (1995-2013) ERA-interim wind speed data subjected to two parameter Weibull distribution function. The results showed that the annual wind speed at Okha and Motisindhohli is having an average of 7.1 m/s and 7.0 m/s respectively, and Sanodar has lowest annual wind speed of 3.8 m/s. The maximum and minimum average wind power density and energy are 280.55 W/m², 2469.0026 kWh/m²/year at Okha and 54.51 W/m², 479.3827 kWh/m²/year at Sanodar respectively. Furthermore, Okha and Motisindhohli are suitable for the wind turbine applications where as Jafrabad, Veraval and Dandi can be considered for marginal wind power development based on their respective annual mean wind speeds and power densities.

Keywords: Wind energy, ERA-interim, Wind power density, Gujarat

INTRODUCTION

India, with its economy growing at more than 6.5 % and likely to grow around 8 % continues face shortage of power and energy. The shortages are assessed to be in the range of 7% - 12% in energy and from 8 % to 21 % of peak demand capacity [1]. The total electricity generation capacity in India as on March 2013 is 223 GW [1] and per capita consumption is 917 kWh in 2012-13 [1]. At present, nearly 68% of the energy generated from the thermal and based on fossil fuels [1]. The installed capacity of wind power in India was 22,644.63 MW on March 2015 [1]. Tamil Nadu and Gujarat are the leading states in terms of wind farm installation with a capacity of 7,253 MW and 3,093 MW [1]. With growing technological advancements the usage of fossil fuel energy resources has increased tenfold, which ultimately gives rise to concerns regarding global warming, depletion of resources, and increase in carbon footprints and rise in pollution levels. It's the need of the present hour to shift the focus of energy resources from fossil fuels to renewable energy sources, which not only create a good impact on the planet, but also will push the human race forward.

The present study evaluates wind resource characteristics among the selected locations in Gujarat by considering long range ERA-interim wind data from the European Centre of Weather for Medium Range (ECMWF) [2]. Gujarat is a state of India is located in North of the equator between 20° N to 25° N latitude and 68° E to 74° E longitude. The selection of various locations in our region of study depends on two major criteria, first is the site is located at the meteorological station near the sea shore and the other is the position of our location has been chosen nearer to the grid point provided under the ERA-interim data. A 19-year (1995-2013) monthly wind data were obtained from the European Centre of Weather for Medium Range (ECMWF) for Dandi, Sanodar, Veraval, Jafrabad, Okha and Motisindhohli. The main focus of this study includes calculating required power potential capacity, which will be acquired through rigorous analysis of wind

speed data.

MATHEMATICAL MODEL

Weibull distribution function

On the basis of the data generated the probability density function encompassing wind speed frequency curve and wind power density function estimation with the help of expressions [3]

$$f(v) = \left(\frac{k}{c}\right) \left(\frac{v}{c}\right)^{k-1} \exp\left[-\left(\frac{v}{c}\right)^k\right] \quad (1)$$

While the corresponding cumulative probability function is given by [3]

$$F(v) = \left[1 - \exp\left[-\left(\frac{v}{c}\right)^k\right]\right] \quad (2)$$

Where k and c are the Weibull shape and scale parameter respectively, the parameters are calculated on the basis of various approaches, in this paper Weibull parameters are calculated on the basis of the standard deviation method, but before that variance and mean of wind speeds are calculated and then the Weibull parameters are calculated on the basis of following approximations [3]

$$k = \left(\frac{\delta}{v_m}\right)^{-1.086} \quad (1 \leq k \leq 10); \quad c = \frac{v_m}{\Gamma\left(1 + \frac{1}{k}\right)} \quad (3)$$

Wind power density and wind energy

Wind power density (WPD) is a true indicator of a site's wind energy potential than wind power alone; it takes into consideration the wind speed, wind speed distribution, and air density. The wind power density can be expressed as

$$p(v) = \frac{1}{2} \rho v_m^3 \quad (5)$$

With the help of Eq. (5) the net power potential can be estimated and it is noted that with a slight increase in wind speed your power density increases rapidly, such is the power potential of wind compared to other renewable resources.

The above equation is dependent on the frequency of each velocity; hence, based on the Weibull probability density function, wind power density (wind power per unit area) can be calculated as [3]

$$p(v) = \frac{P(v)}{A} = \frac{1}{2} \rho c^3 \Gamma \left(1 + \frac{3}{k} \right) \quad (6)$$

The annual energy is defined by the relationship given by [3]

$$\bar{E}_a = \sum_{n=1}^{12} \bar{E}_{jm} \quad (kWh / m^2 / year) \quad (7)$$

Where \bar{E}_{jm} the extractible mean monthly energy is given by $24 \times 10^{-3} d \bar{P}$, \bar{P} is mean wind power density in (W/m^2) and d is the number of days in the month considered.

Wind speed extrapolation

Reanalysis numerical data has been extensively used and validated in prior studies. However, in this study, wind speeds are collected from the latest reanalysis data set from ECMWF, the ERA-Interim data [2]. The wind speeds data provided by ECMWF are calculated at 10 meter height about U (10U) and V (10V) direction with the magnitude $\sqrt{(10U)^2 + (10V)^2}$ and the extrapolation from a height of 10 m to the required hub height, i.e., 120 m was performed using the log-law which states that velocity V at a given height z is

$$\frac{V(z)}{V(z_{ref})} = \frac{\ln(z/z_o)}{\ln(z_{ref}/z_o)} \quad (8)$$

Neutral stability of the atmosphere and a surface roughness of $z_o = 0.2 mm$ have been assumed, which is recommended as an average value for calm and open seas [4].

In Fig. 1 illustrates the variations of wind speeds and wind power density in different months at different locations. It clearly shows that may, June, July, august accounts the maximum wind speed in all the locations, particularly it has been studied that July dominates having a maximum speed of 9.49 m/s in Okha and minimum 5.41 m/s in Sanodar.

Also one should account that Okha and Motisindhohli are having maximum wind power potential with having mean wind speed of 7.07 m/s and 7.02 m/s respectively, while Veraval and Sanodar account 5.09 m/s and 3.81 m/s respectively.

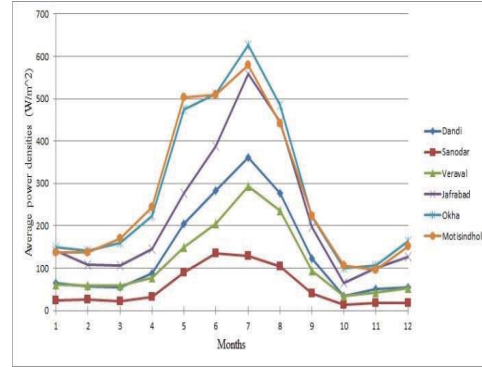


Figure 1. Monthly variations of average power densities for the selected locations

The average power density was maximum at Okha accounting around $280.55 W/m^2$ which leads to associate maximum power potential of $2469.00 kWh/m^2$ while Motisindhohli is having a maximum average power density of $275.32 W/m^2$ and having an average energy accounting $2421.67 kWh/m^2$ so as per wind speed data it suggests that Okha and Motisindhohli are the paragon locations for setting offshore wind farm to generating enough energy sufficing the needs of the region.

References

- [1] "Growth of electricity sector in India from 1947-2013," July 2013.
- [2] D. P. Dee, S. M. Uppala, A. J. Simmons and P. Berrisford. "The ERA-Interim reanalysis: configuration and performance of the data assimilation system". *Quarterly journal of the royal meteorological society*, **137**, 2011, pp. 553-597.
- [3] O. Ohunakin. "Wind resource evaluation in six selected high altitude locations in Nigeria". *Renewable Energy*, **36**, 2011, pp. 3273-3281.
- [4] J. Manwell, J. McGowan and A. Rogers. "Wind energy explained: theory, design, and application" *West Sussex: John Wiley*, 2009.

ECONOMIC EVALUATION OF OFFSHORE WIND POTENTIAL IN WESTERN COAST OF GUJARAT

Garlapati Nagababu¹, Dharmil Bavishi¹ and Surendra Singh Kachhwaha¹

¹Pandit Deendayal Petroleum University, Gandhinagar, Gujarat, India

SUMMARY: Wind energy has always been a prime sector to invest for the investors all over the world. The major reason for being a hot spot and center of investment is its feasibility, availability, high speed at strategically chosen locations, and alternative source of energy competing with the fossil fuels. As far as sustainability of energy security is concerned investment in wind energy portrays high potential and effective utilization of resources. In this paper an attempt has been made to carry out feasibility study on development of offshore wind energy in the western coast of Gujarat, India. Later a rigorous economic evaluation was performed over these regions and finally it has been concluded that the western offshore coast of Gujarat has a very high potential to generate energy at 4.5 rupees per kWh at a hub height of 80 m.

Keywords: Economics, wind speed, clean energy, western coast of Gujarat, energy security

INTRODUCTION

Power generation from non-conventional sources of energy have been always a fascinating and emerging sector to invest throughout the world. The potential of generating power from renewable energy sources like solar, wind, biogas etc. if utilized to its maximum level the issues regarding the imbalance of power supply in the country like India can be resolved and channelized to attain energy security to its peak level [1].

Wind energy has various advantages such as availability for 24*7, less floor space, high energy yield as for a country like India where wind speed is quite high. India has already seen the potential of onshore wind energy [2] and the investment pertaining to onshore has quite been challenging in the initial years, but the return on investment after a span of 6-15 years was quite acceptable and gave a boost to promote wind energy to offshore which will yield high revenues and can resolve the energy crisis over the different parts of the country.

Offshore wind is still around 50 percent more expensive than onshore wind. However, due to the expected benefits of more wind and the lower visual impact of the larger turbines, several countries now have very ambitious goals concerning offshore wind [3].

The feasibility of constructing the wind farm requires the rigorous cost analysis dealing with various factors associated with the generation of power cost [4].

Wind turbines include machines, together with their electrical and mechanical equipments. Also the cost associated with the transportation of components from onshore to offshore is included in the overall cost of the wind turbines. It has been estimated that Wind turbine installation accounts maximum cost. Optimising the cost of wind turbine is the major challenge for the investors.

Another factor associating with the cost is the foundation technology installation. The turbine foundation depends on the depth corresponding to installing the turbine. Example monopile foundation

technology is used up to the depth of 35 m.

Grid interface cost includes electrical equipment to realize the interconnections with the transmission network. Regulation of operating devices incurs cost. But the cost is minimal compared to cost associated to wind turbine installations and foundation technology.

The electrical system costs consist of mainly integrating the various electrical components to the wind turbine. It also accounts minimal cost compared to the cost of installation of the turbines.

In this paper, three major factors associated with the overall construction cost of the wind farm have been taken into consideration. They are wind turbines installation cost, foundation technology installation cost, grid cost, electrical system.

OFFSHORE WIND FARM INVESTMENT COSTS

Turbine cost

The turbine chosen for study has the capacity of 3.6MW. The well-equipped turbine installation cost can be evaluated by the means of the following expression [4]:

$$C_{wt} = 2.95 \cdot 10^3 \cdot \ln(P_{WT}) - 375.2 \text{ [k€]} \quad (1)$$

Where P_{WT} is the rated power [MW] of a single wind generator. The transportation cost has to be added to costs expressed in the above equation. Generally the transportation cost can be evaluated as 10% of the total turbine installation cost.

Foundation cost

Foundation costs include two components viz. manufacturing cost and cost of transportation and installations. The foundation cost is dependent on the depth of the sea in which the foundation technology needs to be installed and the hub height. In this paper monopile foundation technology has been incorporated at maximum depth of 35 m at a hub

height of 80 m and the rotor diameter of the turbine is 120 m. The cost can be evaluated as per the following equation [4]:

$$C_f = 320P_{WT}(1 + 0.02(D - 8)) \left(1 + 0.8 \cdot 10^{-6} \left(h \left(\frac{d}{2} \right) - 10^5 \right) \right) \quad (2)$$

[k€/turbine]

Where D is depth of sea in meters; h [m] is the hub height and d [m] is rotor diameter.

Electric system cost

Major factor responsible for the offshore wind farm cost is the cost associated with MV cable. The cost depends on transmission wire over the distance from the shore and also depends on the cross section of the cable wire. The cost can be evaluated on the basis of the following expression [4]

$$C_{c,MV} = 0.4818S + 99.153 \text{ [k€/km]} \quad (3)$$

Where S is the function of the cable section [mm²]

Grid integration cost

The main cost for substation electrical equipment comes from MV/HV transformer. For MV/HV transformers with HV level up to 165 kV, a cost of 9.8 k€/MVA. In this paper the HV level is 135 kV according to the national grid of India.

Investment cost

The total investment cost C_I of an offshore wind farm is given by the following expression

$$Total \ Investment \ cost [C_I] = C_{WT} + C_f + C_{c,MV} + C_{Gt} \quad (4)$$

Table 1. Investment cost of wind farm.

C _{WT}	C _f	C _{c,mv}	C _{Gt}	C _I
3803755	1378271	365000	250000	5797026
3928955	1643323	365000	270000	6207278
4003755	2040902	365000	270000	6709656

From the Table 1, the maximum cost is allocated to wind turbine installation at different sea depth level of 10 m, 20 m, 35 m respectively followed by the foundation technology cost. Overall cost associated at 35 m depth is 6709656 € while at a depth of 10 m cost is less comparatively viz. 5797026 €

Calculation of power generation cost

The economics of wind power, electricity production costs are evaluated. In general, the generation cost is calculated in annual energy production by annual recurring costs. In this paper the depreciation period is considered to be 20 years and the rate of interest is 9%. The annual expense ratio is calculated by using Eq. (6). So the net generation cost is evaluated as per the following

expression [5]

$$G_{cost} = \frac{C_I \times A + O}{kWh / year} \quad (5)$$

Where G_{cost}: Generation Cost
 C_I: Investment cost
 A: Annual expense ratio
 O: Operation and maintenance cost

$$A = \frac{r}{1 - (1 + r)^{-n}} \quad (6)$$

Where r=Interest rate
 n=Service life

Cost evaluation is performed at three depths of these level viz. 0-10 m, 10-20 m, 20-35 m. The capacity of the turbine is 3.6 MW installed at a hub height of 80 m with rotor diameter 120 m. The estimated cost of generation mention in the table is in rupee.

It can be well analysed from the main table that cost of installations of turbine accounts maximum cost followed by foundation cost and grid integration cost accounts less compared to the turbine installation cost. Also from the table cost associated with depth of 10-20 m accounts 3.5 rupees per kWh, while that corresponding to 0-10 m and 2-35 m accounts 4.62 and 5.67 per kWh.

Table 2. Offshore wind power generation cost in the western coast of India

Depth [m]	10	20	35
No.of turbines	20308	20853	48931
Power generation [Kwh/year (10 ⁶)]	210240	297840	499320
Investment cost [C _I]	5797026	6207278	6709656
O&M [Rs in crore]	8828	9706	24619
Generation cost [Rs/kWh]	4.62	3.58	5.42

References

[1] M. Esteban et al., "Why offshore wind energy?," *Renewable Energy*, **36**, 2011, pp. 444-450.
 [2] Jami Hossain et al., "A GIS based assessment of potential for wind farms in India", *Renewable Energy*, **36**, 2011, pp. 3257-3267.
 [3] Asifujiang Abudureyimu et al. "Analyzing the Economy of Offshore Wind Energy using GIS Technique", *APCBEE Procedia* **1**, 2012, pp. 182-186.
 [4] M. Dicorato et al., "Guidelines for assessment of investment cost for offshore wind generation", *Renewable Energy*, **36**, 2011, pp.2043-2051.
 [5] J. Earnest and T. Wizelius. "Wind power plants and project development" PHI learning Privite Limited, New Delhi, 2011.

HYDRO POWER POTENTIAL IN MOZAMBIQUE. “CHUA-MANICA”

Miguel M. Uamusse¹, Dinis Juízo², and Kenneth M. Person¹

¹Department of Water Resources Engineering, Lund University, Lund, Sweden

²Faculty of Engineering, Eduardo Mondlane University, Maputo, Mozambique

SUMMARY: Energy is an essential need for stimulating social and economic development of a society in any country. In Mozambique access to conversional energy in form of electricity has been limited to most of the rural population. Continuing to use wood fuel as a source of energy has a number of negative consequences with respect to the environment and human health. The objective of this investigation research is to analyze the Small Hydropower Plant exploration in Manica district. The current total installed power generation capacity in Mozambique is about 939MW. Hydropower contributes 561 MW, making a contribution of 61%, oil contributes 27%, and natural gas 12% of the total electric grid generation in Mozambique.

Keywords: Hydro, power, Energy, Mozambique, Manica

INTRODUCTION

Mozambique is a country with much of the population living in rural areas of difficult access and low population density on the other hand Mozambique country which most of population a poor see, in Figure 1.1. The government can get difficulty to distribute electricity from the national grid in all rural areas. Small hydropower can be one of the solutions to increase electrification in Mozambique and combat poverty in rural areas, can develop small industries from electrification through small hydropower [1][2].

Mozambique has vast amounts of energy resources which include solar, wind, biogas, coal, natural gas, hydropower, biomass and geothermal power. Biomass related type of fuel is considered both cheap and more accessible to the poor majority in rural and urban areas, thus becoming the most exploited source of energy[3][4]. Biomass energy resource, which are in the form of fuel-wood and charcoal derived from natural forest and plantations, accounts for over 90 percent of the total energy consumption in Mozambique[5][6].

THE STUDY AREA

Mozambique occupies a territory located on the south-eastern coast of Africa, between the latitudes 10 and 27 south and longitudes 30 and 41 east. Chua is located in Chua located in Manica District in Mavonde at Manica province. Manica is a district of Mozambique in the Manica *Province with a population of 215275* people and an area of 4.391Km². Manica District borders with the Republic of Zimbabwe in the west, the District of Gondola in the east, the District of Barué to the north through the Pungué River, and the District of Sussundenga in the south, which is bounded by the Revué and Zonué Rivers.

The climate in the district of Manica, according to Koppen climate classification is the moist temperate type. The rainy season starts in November and its end, in April and that the average annual is about 1220-1290 mm evapotranspiration.

MATERIAL AND METHODS

For the purpose of this research and to achieve the above research objectives the following activities were carried out, literature search, materials and technology survey, and to do assessment of old hydropower potential at Chua in Manica district requires the following:

- 1.1. Literature Review.
- 1.2. Net Available Head

$$H = H_g - \sum h \quad (1)$$

- 1.3. Power Generation

$$P = \frac{\eta \cdot \rho \cdot g \cdot H \cdot Q}{1000} [\text{kW}] \quad (2)$$

Where; P = Power estimate (kW), η = Efficiency of the turbine, ρ = Density of the water (kg/m³)

g = gravitational constant (m/s²).

- 1.4. Selection Of Turbines

CONCLUSIONS

The Chua village in Manica, the presence of electricity will be a major drive towards contributing to economic and social sustainability of the village. The power availability will change the livelihood of the villagers, resulting into creation of jobs such as small business enterprises. This will add some income to the village community.

The estimate power demand of Chua I, Chua II and Chua III is about 20kW(Chua I), 80kW(Chua II) and 52kW(chua III) and total Annual energy demand in Chua 4730,3MW is It was seen that from this power

will accommodate only few households including the village dispensary.

The all schemes in Chua have more than 50 m head with Pelton turbine. The net head in Chua stream is about 50 m and design flow is 0.2 m³/s. Therefore, from the turbine chart, Figure 3.4, the appropriate turbine type for this project is Pelton turbine.

References

- [1] L. Hammar, H. Ahlborg and S. Molander. Power sectors actors' views on productive use, private sector involvement, and renewable energy in rural electrification of Mozambique and Tanzania; 2011, Manuscript.
- [2].Project paper on a proposed restructuring of the energy reform and access project for the republic of Mozambique; Energy Team, Infrastructure Group, Africa Region, The World Bank; 2007
- [3] M. Uamusse, K. Persson, and A. Tsamba. "Gasification of Cashew Nut Shell Using Gasifier Stove in Mozambique". *Journal of Power and Energy Engineering*, **2**, 2014, pp. 11-18.
- [4] H. Ahlborg, J. Ehnberg, L. Hammar, S.C. Jagers and S Molander, "A background on social context and renewable energy sources in Mozambique and Tanzania: an initial report from the STEEP-RES project", *Chalmers University of Technology, in ESA Report 2008*, **21**, 2008, Göteborg .
- [5] S. Mishra, S.K. Singal and D.K. Khatod, "Optimal installation of small hydropower plant-A review", *Renewable and Sustainable Energy Reviews*, **15**, 2011, pp. 3862–3869.
- [6] O. Paish, "Small hydro power: technology and current status", *Journal of Renewable and Sustainable Energy Reviews*, **6**, 2002, pp. 537–556

Sustainable Architecture and Building Technology

THE DEVELOPMENT OF ENERGY EFFICIENCY ESTIMATION SYSTEM (EEES) FOR SUSTAINABLE DEVELOPMENT: A PROPOSED STUDY

Khairunnisa A.R¹, M.Z.M Yusof¹, M.N.M Salleh² and A.M Leman³

¹Faculty of Mechanical & Manufacturing Engineering, Universiti Tun Hussein Onn Malaysia, Malaysia

²Faculty of Computer Science and Information Technology, Universiti Tun Hussein Onn Malaysia, Malaysia

³Faculty of Engineering Technology, Universiti Tun Hussein Onn Malaysia, Malaysia

SUMMARY: In the modern era of globalization, energy can be regarded as something precious. Thus, energy efficiency (EE) and cost effectiveness is a key factor in maintaining economic growth. EE also can educate the consumers to use energy efficiently and help reducing energy consumption. Domestic sector is the third largest contributor of energy usage in Malaysia. The purpose of this study is to review EE practices and applications in residential buildings to raise awareness of energy consumption. In the preliminary stage of this study, the response from consumers about the electrical (home appliances) used the energy consumption (electricity bill) monthly will be determined by using Quality Function Deployment (QFD) Approach. QFD approach focus on consumer's opinion about electrical appliances used and function. Selection of residential was based on medium and affordable cost residential area in Johor. Databases for energy related to electrical appliances will be developed based on the data obtained from the relevant ministry/agencies such as KeTTHA, Energy Commission and TNB. Energy efficiency Estimation System (EEES) will be developed to help consumers to estimate the amount of energy that is used daily and indirectly this will help users to save energy and reducing the cost of living. EE indirectly will help reduce the effects of environmental pollution chain such as global warming phenomenon and the weakening of the power supply. The promotion of EE and independent of the energy source is important to ensure that sustainable development can be implemented and it helps to conserve the environment for future generations.

Keywords: Energy Efficiency (EE), Energy Consumption, Home Appliances, Sustainable Development.

INTRODUCTION

Our planet is facing an unprecedented energy challenge: even assuming that all recently introduced energy efficiency policies are implemented with full success, global primary energy demand is still expected to increase to 35% by 2035. This would have a dramatic impact on energy costs and energy security, competition for resources, access to energy for societies' poorest people, economic growth and of course climate change [1]. The global expansion of renewable and the future of electricity generation were much in the centre of the energy discussion. Improving EE and redesigning power generation must go hand in hand. According to the International Energy Agency (IEA), the share of global electricity supply provided by renewable could reach 30% by 2035. The remaining 70% will have to be met by conventional sources of energy. However, their supplies are finite, their costs are to rise and the impact of their use is climate-damaging.

MALAYSIAN SCENARIO ON ENERGY ISSUES

Shortage in the hydrocarbon fuel sources, energy preservation and the future stringent emission regulations have been a formidable challenge to the worldwide industry. However, petroleum is a finite source was identified as major source pollution in the worldwide ecosystem, particularly Carbon Dioxide (CO₂). This gas creates an atmospheric greenhouse effect linked to the global warming and climate change. In Malaysia, the Ministry of Energy, Green Technology and Water (KeTTHA) involved in reducing the CO₂ emissions up to 40% between 2005 and 2020 [2]. Green Technology and The Climate Change Council (MTHPI) is adopting implementation of green

technology on the reduction an atmospheric greenhouse linked to the global warming and climate change.

Although Malaysian economic growths are rapid and their expansions are fast, they still face challenges that influence their competitiveness. The current scenario, depicts the Malaysian energy are now facing challenges of supply and demand [3]. This could be evidenced from Department of Statistics (DoS) and Economic Transformation Program (ETP), 2010 and 2011 annual report. Malaysia's economy is expected to grow strongly over the outlook period with an annual average growth rate projected at 4.8%. The strongest growth will be from the industry (the manufacturing sector) and the services sectors, attributing shares of 54 and 46% of total Gross Domestic Product (GDP) in 2030 respectively [4,5]. This will naturally cause a substantial growth in energy demand for the transport, commercial and residential sectors. Figure 1 Show the Gross domestic Product and Population and figure 2 show final energy demand

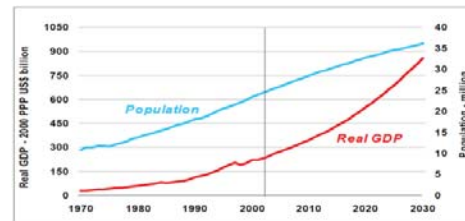


Figure 1. Gross Domestic Product & Population

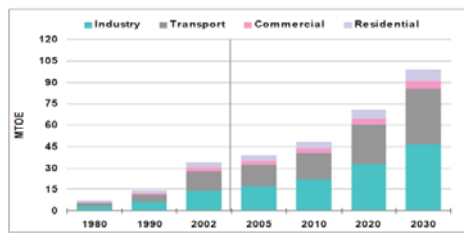


Figure 2. Final Energy Demand

The electricity demand of Malaysia will increase by 4.7% per year over the outlook period, to reach 274 TWh in 2030. Electricity demand for the residential sector will also experience strong growth of 4.9 % per year due to improving living standards. Per capita electricity demand is projected to more than double from 2002 to reach 7,571 kWh/person in 2030, higher than APEC region average at 6,833 kWh/person. So Malaysia has put their new economic development by introducing the ETP, which consist of 12 areas. Oil, gas and energy are one of the NKEA key areas. Under the Entry Point Project (EPP) of oil, gas and energy sector, EPP 9 is Energy efficiency under the sub cluster of building a sustainable energy platform for growth. The industry is governed by KeTTHA and is regulated by the Energy Commission (EC) [6].

METHODOLOGY

The research design of this study was formulated by several components which is that are the key point of the whole study. The study looks into Malaysian Economic Development and the Malaysian history on energy demand and consumption. For a certain reason (case reported by Energy Commission, KeTTHA and TNB) the EE issues was chosen as the theme of study. Figure 3 highlighted the research framework and the expected outcome of the research

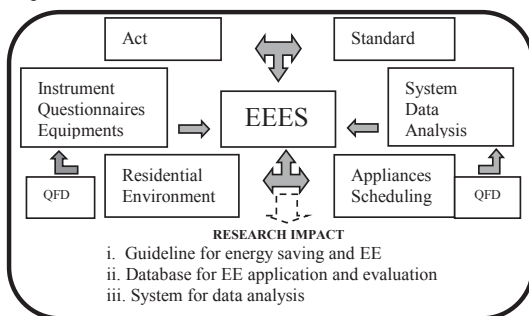


Figure 3. Proposed Research Framework

Two types of data collection were involved in this study are as follows;

- i. Questionnaires
 - a. Energy efficiency practice and application in residential (use QFD approach) [7,8].
 - b. Energy consumption by consumers

- (Energy bills and form) [9]
- c. System development (use System Development Life Cycle, SDLC approach) [10]
- ii. Data on energy related-appliances for residential building by using green technology approach.

EXPECTED RESULT

It is expected that the energy issues, especially in reducing energy bills (electricity bills) will be obtained in order to promote EE behaviour. Thus, the EE related data will be enhanced. The consumer can estimate their energy consumption and the new paradigm of attitude will help the consumer regarding the EE approach. It will help the country to achieve a growth economy towards developed countries. That is why EE as a key element to ensure energy use and stable rates of domestic trade. Other than that, the government's aim to make green technology as a catalyst for sustainable development will be achieved.

ACKNOWLEDGEMENT

The authors would like to express thanks to Universiti Tun Hussein Onn Malaysia (UTHM) and Ministry of Education Malaysia for Hadiah Latihan Persekutuan (HLP) Scholarship for the study.

References

[1] J.-P. Tricoire. "Visualizing The Hidden Fuel of Energy Efficiency". *The Journal of The International Energy Agency*. 4, 2013, 24–25.
 [2] KeTTHA, National Energy Efficiency Action Plan 2014, pp. 14–25.
 [3] The Economic Planning Unit. Tenth Malaysia Plan 2011-2015, 2010, pp. 1–451.
 [4] Prime Minister Department of Malaysia. Economic Transformation Program: Annual Report 2011.
 [5] Prime Minister Department of Malaysia. Economic Transformation Program: Annual Report 2011.
 [6] Energy Commission. Annual Report for 2013,2013.
 [7] Akao, Y. Quality Function Deployment (QFD): Integrating Customer Requirements into Product Design (1990) 1–24.
 [8] A. Lockamy and A. Khurana. "Quality Function Deployment: Total Quality Management For New Product Design". *International Journal of Quality & Reliability Management*, 12(6), 1995, pp. 73–84.
 [9] V.P. Borin, C.H Barriquello, R.A. Pinto, and S. Maria. (2013). An Improved Technique for Load Identification in Residential Buildings.
 [10] B.S. Blanchard, W.J, Fabrycky. Systems engineering and analysis (4th ed.) New Jersey: Prentice Hall, 2006. p.3

THE ENERGY SAVING CALCULATION FOR A RESIDENTIAL SECTOR IN THAILAND WITH TOP-DOWN METHODOLOGY

Anucha Tiangket¹, Bunyongvut Chullabodhi¹ and Sarawoot Watechagit¹

¹Department of Mechanical Engineering, Faculty of Engineering, Mahidol University, Thailand

SUMMARY: This paper presents the calculation to estimate the energy saving for the residential sector in Thailand, in order to investigate the impact from energy saving interventions according to the 20-year Energy Efficiency Development Plan (2011-2030). The proposed calculation method adopted from the top-down energy saving calculation standard BS EN 16212:2012 developed by British Standard Institution (BSI). The generalized standards of calculations proposed by BSI are modified to reflect only the energy saving for the residential sector. The modifications of the methods also to ensure that all data input for all calculations can be easily found from reliable or nationally accepted sources. The outputs, or indicators, include the overall energy saving per dwelling, the electricity per dwelling, the fuel consumption per dwelling, or the electricity per appliance, etc. Using the year 2005 as a base year according the 20-year plan, the calculation results show that the impact from energy 2 years of efficiency interventions is not yet shown in 2013. The overall energy consumption in 2013 is 1,432.27 ktoe higher than that is of 2005. Other indicators also show similar results. The causes of higher energy consumption, along with the validity of the calculation results is discussed.

Keywords: energy efficiency and saving calculation, top down method, residential sector

INTRODUCTION

In 2007, the Asia-Pacific Economic Cooperation (APEC) Leaders declared an agreement to collaborate in energy conservation promotion to achieve the agreed target in 2030. Consequently, the government of Thailand has developed the 20-year Energy Efficiency Development Plan (2011-2030) [1] in order to support this agreement. The energy saving target proposed in this plan is to reduce the national's energy intensity by 25% in 2013 as compared to that of in 2005. This amount of energy saving is equivalent to the reduction of final energy consumption by 20% in 2030, which is about 30,000 thousand tons of crude oil equivalent (ktoe). The aforementioned 20-year plan has suggested implementations of policies, campaigns, programs, or interventions in transportation, industry, buildings (commercial) and residential sectors. And while many parts of the plan have been implemented, the successfulness of those implemented policies, campaigns, programs, or interventions are subjected to an evaluation. A common question to be asked is whether or not the amount of energy saving resulting from the implementations is as close as what is expected according to the 20-year plan. With this regard, this research focuses on estimating the amount of energy saving in residential sector. According to the 20-year plan, the saving target for the residential sector is 3,700 ktoe in 2030.

To estimate the energy saving from the implementation of energy efficiency programs or interventions, there are two groups of methods to be used. Those are generally known as top-down and bottom-up methods. This paper presents the top-down calculation results adopted from the calculation framework developed by British Standard Institution (BSI).

METHODOLOGY

The top-down calculation method used here adopted from the international standard for energy saving calculation BS EN 16212:2012 by BSI [2]. Since the methods suggested in the calculation standard are of general, they are modified to reflect only the energy saving for the residential sector. The modifications of the methods also to ensure that all data input for the calculation can be easily found from reliable or nationally accepted sources. All indicators which are the outputs from the proposed calculation are shown in table 1.

Table 1. List of Indicators

No.	Indicator	Unit
1	Energy consumption per dwelling	ktoe/dwelling
2	Electricity per dwelling	ktoe/dwelling
3	Fuel consumption per dwelling	ktoe/dwelling
4	Electricity per refrigeration	ktoe/refrigeration
5	Electricity per large appliance	ktoe/large appliance
6	Electricity per cooling space	ktoe/cooling space
7	Electricity per cooking	ktoe/cooking
8	Electricity per other appliances	ktoe/other
9	Fuel consumption per cooking	ktoe/cooking

RESULT AND DISCUSSION

All indicators are calculated using data during 2005-2013. Here, the year 2005 is used as a base year for comparison. The results show energy saving for each type of commercial energy, as well as the overall saving. Specifically, Figure 1 to Figure 4 show the estimated energy saving represented by the indicator 1, indicators 4 to 8, indicator 9, and indicator 2 to 3, respectively. It is noting that in all figures shown, positive result means the energy saving for a particular indicator, vice versa. Base on all figures, considering the year 2013, all indicators indicate that the energy consumption is higher than those of in year 2005. The overall energy consumption in 2013 is 1,432.27 ktoe higher than that is of 2005. Similarly, the electricity sub-section consumption is higher by 324.30 ktoe. The LPG consumption is higher by 96.86 ktoe, and the total electricity and fuel consumption is higher by 1,241.96 ktoe. Therefore, while the results of higher energy consumption, along with the validity of the calculation results will be discussed at length in the full paper, the preliminary investigations here show that, even though there have been quite a number of interventions to promote the energy saving and energy efficiency in the residential sector according to the existing of 20-year plan, they might not have much impact on the energy conservation in the residential sector up to now.

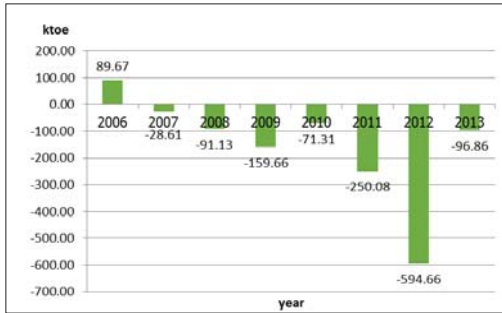


Figure 3. Energy saving in fuel (LPG) sub-section

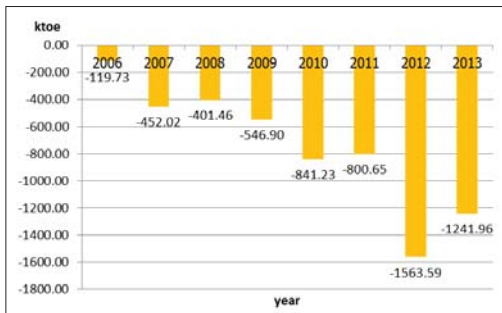


Figure 4. Energy saving in sum of electricity and fuel section

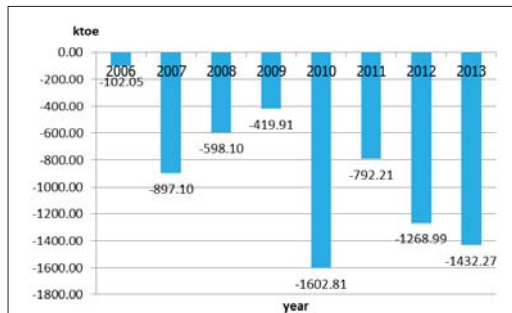


Figure 1. Overall energy saving of residential sector.

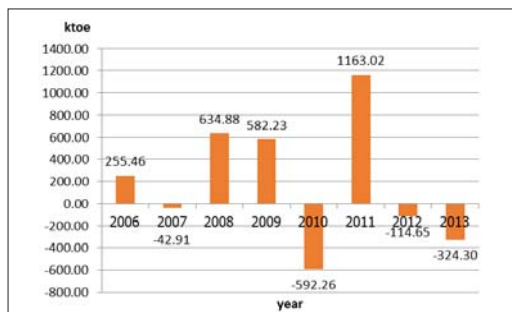


Figure 2. Energy saving of electricity sub-section

References

- [1] Ministry of energy, “Thailand 20-Year Energy Efficiency Development Plan”, 2011.
- [2] BSI Standard Publication, “Energy Efficiency and Saving Calculation, Top-down and Bottom-up Methods”, *BS EN 16212*, 2012.

STUDY OF OPTIMUM INWARD GLASS TILT ANGLE FOR WINDOW GLASS IN DIFFERENT INDIAN LATITUDES TO MINIMUM HEAT GAIN INTO BUILDINGS

Kiran kumar Gorantla¹ and Ashok Babu Talanki Puttaranga setty¹

¹National Institute of Technology Karnataka,
Mechanical Engineering Department, Karnataka, India

SUMMARY: Modern construction of Building material consists of glass. But using more glass as building material increases the heat gain and thus air conditioning requirement. Hence more energy demand to maintain the building conditions. This paper investigates the effect of inward glass tilt to gain minimum heat in to buildings for different latitudes of India with four different glass materials for energy efficient glass window design. The four glass materials considered for the study are clear, bronze, green and reflective glasses. The spectral optical properties of four glass materials were measured. Using measured spectral properties, solar optical properties have been calculated. In April month at 9^o, 13^o Latitudes, In May month 17^o, 21^o latitudes and in June month 25^o and 29^o Latitudes heat gain is maximum. Hence the optimum glass tilt for different Indian latitudes 9^o, 13^o, 17^o, 21^o, 25^o and 29^o in all orientations of the window glass (E, W, N, S, NE, NW, SE and SW) were calculated. From the results it is observed that at 9^o and 17^o N latitudes minimum heat gain is found to be in south direction for vertical position for all the glasses. For 13^o N latitude, 4^o inward tilt of the glass is found to be optimum in south direction. For latitudes 21^o and 25^o N. 2^o inward tilt of the glass is efficient in south orientation. 29^o N latitude requires an inward tilt of 6^o for glass materials to eliminate solar radiation passing through all the glasses studied.

Keywords: green glass, optimum glass tilt, solar optical properties, spectral optical properties

INTRODUCTION

Buildings are responsible for about 40% of total energy use in the world [1]. Glazing is the opening to provide visual interaction between outdoor and indoor environment. Glass is used in buildings envelopes to provide day lighting either side lighting using windows or top lighting using sky lights. Earlier, radiation passing through clear glass for Delhi climatic conditions was reported [2]. Glass window affects the building not only in terms of heat transmission but also in terms of thermal comfort. Most of the solar radiation enter in to the buildings through windows only. Solar radiation through windows depend upon solar optical properties of the glass materials used for the window. So it is necessary to reduce this radiation as much as possible to maintain the thermal comfort levels in the buildings. Earlier, researchers have also concentrated on numerical computations of design of windows to reduce solar radiation into the buildings with clear and brown glass materials [3]. The present study focuses on the effect of inward glass tilt on direct solar radiation passing through the four glass materials (Clear, Bronze, Green and Reflective).

EXPERIMENTAL METHODOLOGY

The Perkin Elmer Lambda 950 Spectrometer experimental set up was used to find the spectral optical properties of different glass materials [4]. The experiments were conducted with different glass materials and varying the angle of tilt of glasses from 0^o to 80^o to change the angle of incidence for the wavelength range 300-2500 nm. The spectral optical properties such as Transmittance, Absorbance and Reflectance of clear,

bronze, green and reflective glass materials were measured using Perkin-Elmer Lambda 950 Spectrometer shown in Fig.1, UGC DAE Consortium at Indore. These spectral optical properties were used to evaluate the solar optical properties. A computer program was developed for trapezoidal method and used to calculate solar optical properties such as, transmittance and absorbance from the spectral optical properties. Solar optical properties were used in computation of solar radiation passing through the glass materials.



Figure 1. Perkin-Elmer Lambda 950 Spectrometer

RESULTS AND CONCLUSIONS

Fig. 2 shows the Solar radiation through clear glass at 2^o tilt from vertical position for all indian latitudes in the all orientations.

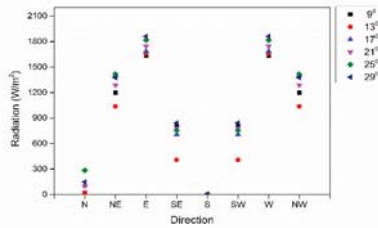


Figure 2. Solar radiation through clear glass at 2° tilt from vertical

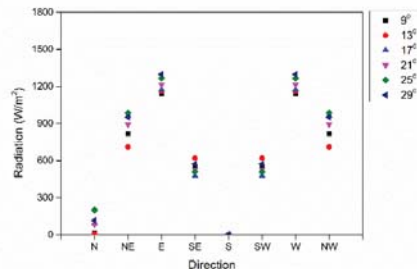


Figure 3. Solar radiation through bronze glass at 2° tilt from vertical

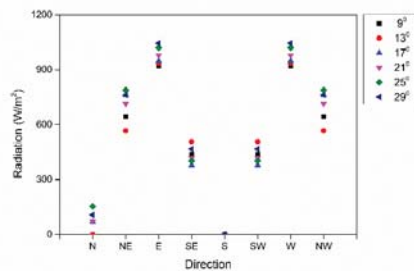


Figure 4. Solar radiation through green glass at 2° tilt from vertical

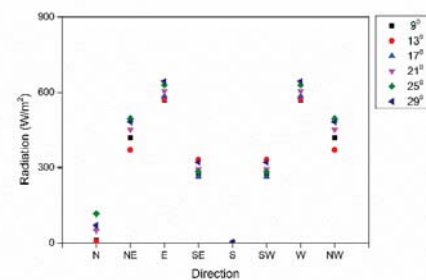


Figure 5. Solar radiation through reflective glass at 2° tilt from vertical

Fig. 3 and Fig. 4 show the Solar radiation through bronze and green glasses, respectively, at 2° tilt from vertical position for all indian latitudes in the all eight orientations (N, NE, E, SE, S, SW, W, and NW).

For vertical position (0° tilt) of all glass

materials at 9° and 17° N latitudes in the south direction, the radiation through glass is 0 W/m². This is due to higher angle of incidence. Hence vertical window glass location (0° tilt) is highly recommended in the south direction for latitudes 9° and 17°.

For 13° N latitude, the optimum tilt of the glass in south orientation was found to be 4° due to the 0 W/m² radiation through glass at 4° tilt of the glass. For N latitudes 21° and 25°, the recommended glass tilt angle is 2° in the south orientation and the radiation through the glass at 2° tilt of the glass is observed to be 0 W/m². For higher latitude of 29° N, 6° glass tilt is the best for 0 W/m² radiation in south orientation.

From the results, it is concluded that south direction is the optimum orientation for all the glass materials to gain minimum heat in to the buildings in all the Latitudes considered.

In case of any obstruction in South direction, then it is recommended North, South east and south west orientations for minimum heat gain through glass for all latitudes from 9° to 29° N and for all the glass materials. And it is suggested to avoid placing window glasses in East, West, North East and North West due to higher radiation through glass.

Among four studied glass materials (Clear, Bronze, Green and Reflective), the reflective glass material is found to be energy efficient due to its minimum heat gain through the glass. This is because of it's lowest transmissivity and absorptivity. Fig. 5 shows the solar radiation through reflective glass at 2° tilt from vertical.

ACKNOWLEDGMENT

I acknowledge my sincere thanks to UGC DAE consortium scientific research INDORE for providing the necessary facilities to carry out experimental work at their research center.

References

[1] ECBC, Energy conservation uilding code, Bureau of energy efficiency, 2009, pp. 1-2.
 [2] C. Ishwar, and K. Shree. "Curtaiment of Intensity of Solar Radiation Transmission through Glazing in Buildings at Delhi". *Architectural Science Review* **46(2)**, 2011, pp.167-174.
 [3] A.M. Taleb, and A.J.H. Alwattar. "Design of windows to reduce solar radiation transmittance into buildings." *Solar & Wind Technology* **5**, 1988, pp. 503-515.
 [4] ASTM E424 "Test for Solar energy Transmittance and Reflectance (terrestrial) of sheet materials." WashingtonDc, London, USA, 1320-1326.

RAY TRACING METHOD OF LIGHT THROUGH RECTANGULAR LIGHT PIPE WITH BENDS

Thanyalak Taengchum¹ and Surapong Chirarattananon¹

¹The Joint Graduate School of Energy and Environment, King Mongkut's University of Technology Thonburi, Bangkok, Thailand

SUMMARY: Light pipes can bring daylight from the sky into deep interior spaces of a building. A pipe is often connected with a bend so as to capture more light. Another bend is connected before the exit port to optimize delivery of light into a room. This paper presents results of modeling, experiment, and simulation of transmission of light through rectangular light pipes. Analytic method of forward raytracing is used for tracing light rays from the source into the bend through to the straight section and through to the bend and then the exit port into the room. The curve surface of the entry bend is modeled as a circular bend section. The interior surface of each section is specular but may have different reflectances. The algorithms of calculation are coded in MATLAB scripts and functions. The interior surfaces of the rectangular light pipe and bends are lined with a film of reflectance of 99.5%. A set of experiments was conducted indoor using an LED lamp as a point source. Results of calculation using the method match closely with those from experiments.

Keywords: light pipe, daylighting, ray tracing, bended pipes.

INTRODUCTION

Daylight in the tropical sky is voluminous and daylighting is attractive. One way of bringing daylight into the deep interior space of a building is to use light pipe, with highly specular and reflective interior surface.

Zastrow and Wittwer considered transmission of light beam across cylindrical light pipes and offers a simple relationship for light transmission as a function of the length and diameter of the pipe, and the entry angle of the light beam, [1]. Swift et al. developed theoretical model of transmission of light through rectangular pipe for collimated rays and reported that results from the model agree well with experimental results, [2]. Kocifaj et al. developed a method called HOLIGILM for calculation of illuminance on an incremental area at the exit port of a circular light pipe by considering backward tracing of a light ray through the entry dome or port to a sky zone, [3]. Kocifaj et al., [4] and Kocifaj and Kundacik, [5] extended the HOLIGILM method to the case where two straight pipes are connected to form a bend and consider the spread of light as it transmit through a pipe. Darula et al. applied the HOLIGILM method to study daylight transmission through a bended pipe on a roof. The authors concluded that effective design of bended tubular light pipe requires a study of interrelation between tube azimuth orientation and the angle of incidence of the sun beam [6]. Samuhatananon et al. used forward raytracing in a study on daylight transmission through cylindrical pipes with and without torus bends, [7]. This paper reports a study on the application of raytracing to trace ray transmission through rectangular light pipe that brings light to illuminate a space. The rectangular light pipe consists of 3 sections as shown in Fig.1. There are pie bend sections as entry and exit section and straight pipe.

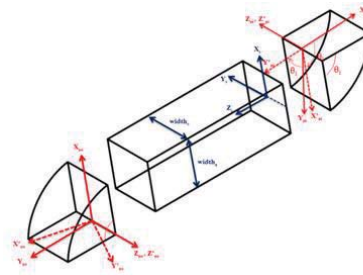


Figure 1. The three components of the light pipe

METHODOLOGY

In the method of forward raytracing, each individual ray is traced along its path of travel from a light source, where it is specularly reflected when it encounters a specular surface. At the point of interception with a surface, a part of radiative power in the ray is absorbed, and the other part is specularly reflected. For the present work, the glazing elements at the entry and exit ports of a pipe are omitted in order to elucidate the mechanism of transmission of light rays through the pipe and to distinguish its features from the effects of transmission by the port elements.

A ray with a given direction of travel is tested if it will intersect the exit or entry ports of a given section. If not, then it must intersect the bend or the pipe surface. The locations of the intersection and reflection vectors are then computed, and the ray continues to travel. This is repeated until the ray intersects an entry or exit port of the given section. A counter is used to count the number of times a ray intersects the surface of each section. A coordinate transformation is required when the coordinates between adjacent sections differ. When a ray leaves the exit port of the pipe, its position on the port and the direction of travel are recorded. After A ray

leave the pipe exit then it continues to travel into a room. A rectangular room is located at the exit port as illustrated in Fig 2. The walls, ceiling, and floors can be each divided conceptually into many sections. MATLAB functions were developed to calculate form factors and configuration factors between sections and location of sections. Specular rays and diffuse flux from the exit port reaching a section contribute as direct illuminance on the section. The specularly reflected light ray continues to travel to other section surfaces until its flux becomes too small to trace. With given diffuse reflectance of each section, flux transfer method is then used to calculate illuminance on all sections in the room.



Figure 2. Experiments under artificial lamp

COMPUTATIONAL RESULT

Figure 3 show ray trajectories in the rectangular pipe with pie bend at entry and exit section and travelling into a room.

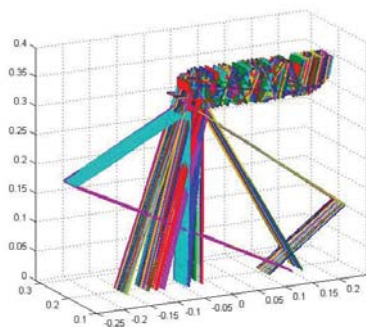


Figure 3. Rays travelling in rectangular pipe with pie bend at entry

CONCLUSION

The results from calculation agree well with those from experiments. This shows that the analytic method of raytracing and algorithms used not only give accurate results, but also lead to insight on the mechanisms of light transmission through each section of the pipe with bends.

ACKNOWLEDGMENT

The research work reported in this paper is funded by the Joint Graduate School of Energy and Environment (JGSEE). King Mongkut's University of Technology Thonburi.

References

- [1] A. Zastrow and V. Wittwer. "Daylighting with Mirror Light Pipes and with Fluorescent Planar Concentrator" *Results from the Demonstration Project Stuttgart-Hohenheim International Society for Optical Engine*, **69**, 1986, pp. 227-234.
- [2] PD. Swift, R. Lawlor, GB. Smith, and A. Gentle, "Rectangular-section mirror light pipes. *Solar Energy Materials and Solar Cells*, **92**, 2008, pp. 969-975.
- [3] M. Kocifaj, S. Darula, and R. Kittler. "HOLIGILM: Hollow Light Guide Interior Illumination Method An Analytic Calculation Approach for Cylindrical Light-Tubes". *Solar Energy* **82**, 2008, pp. 247-259.
- [4] M. Kocifaj, F. Kundracik, S. Durula, and R. Kittler "Theoretical Solution for Light Transmission of a Bended Hollow Light Guide" *Solar Energy* **84**, 2010, pp. 1422-1432.
- [5] M. Kocifaj and F. Kundracik "Luminous intensity solid of tubular light guide and its characterization using asymmetry parameter". *Solar Energy* **85**, 2011, pp. 2003-2010.
- [6] S. Darula, M. Kocifaj, R. Kittler and F. Kundracik. "Illumination of Interior Spaces by Bended Hollow Light Guides: Application of the Theoretical Light Propagation Method". *Solar Energy*, **84**, 2010, pp. 2112-2119.
- [7] S. Samuhatananon, S. Chirattananon and P. Chirattananon, "An Experimental and Analytical Study of Transmission of Daylight through Circular Light pipes". *Leukos*. **7** (4), 2011, pp. 203-219.
- [8] J.L. Scartezini and G. Courret. "Anidolic daylighting systems". *Solar Energy* **73** (2), 2002, pp. 123-135.
- [9] S.K. Wittkopf. "Daylight performance of anidolic ceiling under different sky conditions". *Solar Energy* **81**, 2006, pp. 151-161.
- [10] F. Linhart, S.K. Wittkopf and J.L. Scartezini. "Performance of anidolic daylighting system in tropical climates- Parametric studies for identification of main influencing factors". *Solar Energy* **84**, 2010, pp. 1085-1094.

ENERGY CONSUMPTION AND MANAGEMENT IN SUB-URBAN AREA

A.M Leman¹, Khairunnisa A.R², M.N.M Salleh³ M.Firdaus Zakaria² and M.Z.M Yusof²

¹Faculty of Engineering Technology, Universiti Tun Hussein Onn Malaysia (UTHM), Malaysia

²Faculty of Mechanical & Manufacturing Engineering, Universiti Tun Hussein Onn Malaysia (UTHM), Malaysia

³Faculty of Computer Science and Information Technology, Universiti Tun Hussein Onn Malaysia (UTHM), Malaysia

SUMMARY: Recently, energy can be considered as important and world issues. Thus, the cost of energy, energy efficiency, and operating is the key factor in maintaining good economy. In Malaysia, domestic sector users are the third largest of the energy usage. The purpose of this study is to find out about the electricity usage, to raise awareness of the saving measures in energy consumption, and to give an idea how to reduce electricity bill and energy consumption at 30 houses in Kampung Parit Raja Laut, Parit Raja, Batu Pahat, Johor. The observation for this case study is made in three months period includes electricity bill collection and proposed suggestion of improvement, discussion, analysis and calculation of potential saving which will stated in result of the study. This research approach is direct communication with the community to know the actual situation faced in energy management and energy conservation. Results show that the reduction percentage of the highest energy consumption was 32% for the January to February, while 7% for the month of February to March. The total decrease obtained at one home which has been selected as the best of reduction in electricity consumption for this study. Results from the study contribute a significantly awareness program towards sustainable development by the community and the responsible agency for determine the effectiveness of energy efficiency and opportunities to save energy in home.

Keywords: Energy Efficiency, Energy Consumption, Household Appliances, Sustainable Development.

INTRODUCTION

In 21st century, the world is confronted with many issues such as global warming, rising of crude oil prices in the world market, and issue of energy (green technology) sources to replace the existing energy. As petroleum is one of the main energy sources in the world, increasing petroleum price gives a major impact to energy industries. The utilities company who provide electrical energy to the market now faces an increase in their production and operating cost [1]. The increases were affect the consumer through the electricity tariff and their monthly utility bills. This increasing caused problem for energy end-use in all sectors including commercial, industrial and residential [2]. Thus, increasing cost of living. Consumer from domestic sector is the third largest consumer in Malaysia after the commercial sector and industrial sectors [3], if the energy consumption for this sector can be reduced. It provides many benefits to the nation and society.

RELATED WORKS

Energy plays a fundamental role in our lives. Most of this energy is generated by burning fossil fuels, coal, natural gas and oil which results in greenhouse gas emissions, also contributes of the nation's annual carbon dioxide emissions. Suburban mostly refers to a residential area, either existing as part of a city or as a separate residential. Generally people use energy for heating, cooling, lighting, heating water, and operating appliances. With the growth of urbanization and increase of household expenditure, household energy consumption

dramatically increases. The consumption style of consumers will greatly influence industries in the upstream and markets in the downstream. Therefore, it is crucial to assess household energy consumption systemically [4-6]

A study on a preliminary analysis on household energy consumption of shanghai had been done by Gua et al. They employing input-output analysis model, carries out an empirical study on household energy consumption. The results show that, more than 80% of household energy consumption was indirect. And the direct and indirect household energy consumption rose by 82.9% and 87.1% from 1992 to 2002, showing a fast upward trend. The indirect household energy consumption in each sector also shows a rapid increase[3]. Meanwhile Chung et al. done a study of residential energy use in Hong Kong by decomposition analysis from 1990-2007. This study was performed to analyse the end-use energy to all sectors. The division decomposition analysis is used to evaluate the respective contributions of changes in the number of households, share of different types of residential households, efficiency gains, and climate condition to the energy use increase. The analysis reveals that the major contributor was the increase of the number of households, and the second major contributor was the intensity effect [2]. The decomposition results for the residential sector composed of four segments. The energy consumption of the residential sector increased by 62.92% above the 1990 level and resulted in an increase of 20,340 TJ in 2007. So from the previous

study of other country also show the increase on the energy usage.

METHODOLOGY

For this study, the qualitative and quantitative method has been used to get the appropriate date. The flow of the study start with Select the sub urban area and ask the Head (30 homes were selected) and proper appointment has been made with electricity provider (TNB). Pilot study has been done in university to dry run the questionnaire before distribute to the villagers. At the same time montly electricity bill will be collected. Data collected from TNB and villagers will be analyze to ensure the strategy of solution could be made. Than conduct the community program and teach them how to save energy with a proper technique (Including measurement). After that monthly bill will be collected and analyze again and the recommendation will be given based on the saving. Figure 1 below show the methodology flow chart.

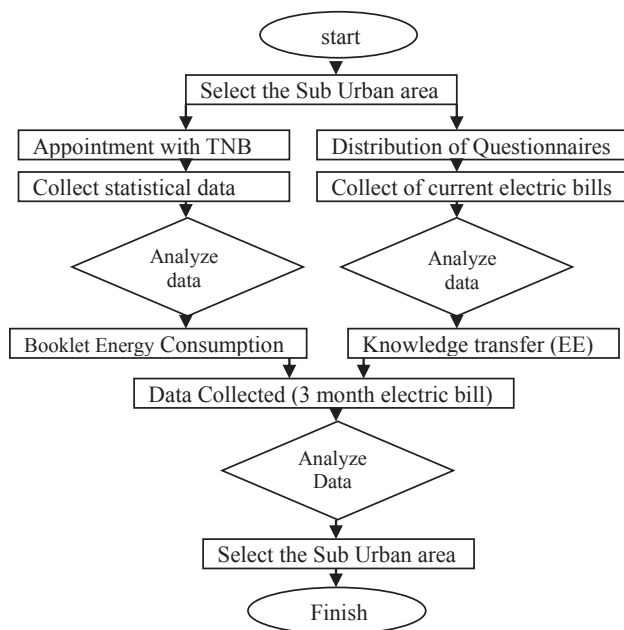


Figure 1. Methodology Flow Chart

RESULT AND DISCUSSION

Data from 30 homes in Kampung Parit Raja Laut were taken in the first month in which the energy management are not recognize by the user. User were asked to cooperate by providing their electricity bills, then explanation usings booklet were given for their understanding the importance and need for energy efficiency in their home. Next, practice the step of energy savings. Electricity bill for second month was collected to get the required data. Observation and data collection was carried out for three months. Data were collected, analyzed

and compare the percentage energy consumption (decrease).Result shows that 50% of the participants in this study was reduce their consumption.

ENERGY MANAGEMENT CAMPAIGN

Energy Management Campaign was held on 5th May 2012. The agenda is knowledge sharing from the speaker and the participants. Head of the University-Community Office of UTHM, give closing remarks for this community service and present a token to the winners of the campaign.

CONCLUSION

Generally, two main goals for this study was accomplished. First goal is to raise the awareness of the importance of saving measure in energy consumption. Second is to give an idea how to reduce electricity and energy consumption. In achieving the desired goal, 30 homes owner were participate. The authors also deliver the knowledge and understanding of the importance and need for energy efficiency. The reduction in energy consumption through electric bill data analysis show that 50% of reduction on achievement. Awareness program (Talk & practical session) with the community through campaign of energy management is the key element of this study.

ACKNOWLEDGMENT

The authors need to express thank you UTHM for funding this project through University and Community Relations Office

References

- [1] T.N. Berhad. Anuual Report. (2011).
- [2] W. Chung, M.S. Kam and C.Y. Ip, "A Study of Residential Energy Use In Hong Kong by Decomposition Analysis". *Elsevier*. **88(12)**, 2011, pp. 5180 – 5187.
- [3] R. Guo, Z. Ren and F. Li. "A Preliminary Analysis on Household Energy Consumption of Shanghai. Tongji University", *Shanghai, China. Retrieve from IEEE*, 2011.
- [4] Ministry of Energy, Green Technology and water Green Practices. KETTHA. Putrajaya. 2010.
- [5] K.R. Tremblay and L. Walker. "Energy Conservation in the Home". Colorado State University. 2009
- [6] U.S. Department of Energy EnergySavers Booklet: Tips on Saving Energy and Money at Home. Retrieve, 2009, from www.eere.energy.gov

THE ENERGY SAVING IN AIR CONDITION SYSTEM OF THAILAND'S BUILDING AND FACTORIES

Wutthisak Thanuanram¹, Narongrit Auppapong¹, Pruschapong Nupteotrong¹ and Damrong Buayorm²

¹Energy Technology Division, Thatphanom College
Nakhonphanom University, Thailand

²Energy Conservation Laboratory
King Mongkut's Institute of Technology Thonburi, Thailand

SUMMARY: The Air condition system in the industry and commercial sector is the large proportion of energy consumption in Thailand. Thus, the energy conservation in the air condition system is very important for decrease the capital of goods production or service. This research is the summarize of the 79 buildings and factories was accompany with the energy ministry in energy conservation project (include the air condition). Every case was managed and evaluates the energy conservation measure. The result showed that the measure was manage 101 times, the total energy saving about 9,830,655 kWh/year include the not investment 70 measure and investment 31 measure, it's can saving 6,938,135 kWh/year and 2,892,520 kWh/year respectively. The most of measure is demand side. The most of energy saving measure is the high efficiency chiller management to the main of machine run.

Keywords: commercial building, factory, Air condition system, energy saving, measure

INTRODUCTION

In 2013, Thailand has the energy consumption about 2,001 KTOE/day, the proportion of energy consumption in the industry sector is 36% and 7% for the commercial building. Thailand's government aim to energy saving by decrease the Energy Intensity; EI about 25% in 2030. Thus, the Government have to promote campaign and enforce measure for achieve to energy saving. The almost of energy consumption in the commercial building and factory is usage by air condition system. From this reason, the establishment will manage to save energy by individual or join with the government project. The result of the government project affects to widely of the factory and commercial building to energy saving measure manage. This research is the summarize of the 79 buildings and factories was accompany with the energy conservation air condition project from energy ministry. The project will energy saving measure created and measure verification. This study is the result of the manage follow the energy saving measure, problem's cause, problem solve and reward from energy saving in air condition measure.

METHODOLOGY

This study is the summary of the energy conservation in air condition system measure and usage in the establishment. The methodology of this study as follow;

Take the energy conservation report and choose the air condition measure, then divide the measure to many groups and study in each group about measure, result, problem's cause, problem solve and frequency of manage. Then conclude the result by groups, group 1 is the chiller's measure, group 2 is water pump's measure, group 3 is heat removal system's measure and group 4 is usage and small air condition's measure.

RESULT AND DISCUSSION

The 79 establishment has 101 of the air condition system measure, the total energy saving about 9,830,655 kWh/year include the not investment 70 measure and investment measure 31 measure the energy saving 6,938,135 kWh/year and 2,892,520 kWh/year respectively.

Table 1. Group 1's result of the energy saving in air condition system

Measure	Times	Saving (kWh/year)
Set point chill water temperature.	11	771,247
Reduce machine runtime	9	950,543
Chiller management	10	2,189,974
Crowd load	4	612,766

Group 1 is the chiller's measure about working control, the frequency of measure show as below;

The measure about set point of cool water temperature to higher, at first the cool water temperature was setting in the low temperature but we increase the temperature to higher.

The measure about reduce the run times of chiller by late to start up the chiller and quickly to shut down the chiller from as before and no effect to production or air condition.

The measure about chiller management, the establishment has many chillers and alternate running but the chiller has the difference efficiency thus we choose the best of efficiency to main chiller for running and decrease the low efficiency chiller running.

The measure about the condenser cleaning, when the dust stick on the heat transfer area it's affect to decrease heat transfer efficiency, thus will be more frequency to cleaning condenser 2-3 times/day.

Table 2. Group 2's result of the energy saving in air condition system

Measure	Times	Saving (kWh/year)
Pump management	7	309,281
Stop pump	5	857,331
VSD pump	1	57,024
Pump sizing	1	26,208

The measure in Group 2 is about the conservation in pump system consist of Chill water pump and Condenser pump, the measure as below;

Pump management measure, in the chill water and condenser pump has many set of pumps but in the process will running some pump set, thus this measure is choose the height efficiency pump to main running.

Stop pump measure, when the goods demand was decrease, the chill water demand for heat removal will decrease too, thus it's can stop running.

VSD pump measure, this measure is the invest measure for VSD to control the condenser pump, at first they control flow rate by narrow valve but VSD will control flow rate be appropriate with load.

Sizing pump measure, the large pump and oversize to use, will consider the narrow valve for control flow rate, thus it's should be to change the pump sizing but we will know the flow rate and head for used.

The measure in Group 3 is the heat removal by cooling tower or air cool chiller

Table 3. Group 3's result of the energy saving in air condition system

Measure	Times	Saving (kWh/year)
Heat removal improvement	4	394,403
Cooling tower control	2	418,622
VSD cooling tower fan	3	270,100

The improvement of heat removal measure consist of reduce the air cool chiller's surrounding temperature by install awning, change the new filler of cooling tower. The measure consist of cooling tower's fan control, when the water temperature is low the controller will command to fan stop working, cooling tower's fan control by VSD.

Table 4. Group 4's result of the energy saving in air condition system.

Measure	Times	Saving (kWh/year)
Set point Temperature	4	423,786
Management	27	1,332,052
Reduce Load	9	169,239
VSD AHU fan	4	271,914
Change chiller to evaporative	1	776,165

The measure in Group 4 is Demand side, the measure is below;

The management measure is reducing the run times and late to start up system and quickly to shut down. The decrease air condition load is reduce the leak point in the condition room for decrease the heat gain into the room. The set point measure is increase temperature to higher, install VSD at AHU fan. The change system measure is change air condition system from chiller to evaporative cooling system.

CONCLUSION

The most of energy conservation in air condition system of commercial building and factory is manage in demand side and not investment measure but the good worth measure is the chiller's measure is choose the best performance chiller to the main running, increase the chill water temperature and manage the run times.

ACKNOWLEDGMENT

The author would like to thank you the Energy Conservation Laboratory (EnConLab) for the support data

References

- [1] Energy Conservation Laboratory, King Mongkut's Institute of Technology Thonburi. The Operating Result of Energy Conservation Report in 2006 and 2008. Department of Alternative Energy Development and Efficiency, Ministry of Energy, Thailand.
- [2] Energy Conservation Laboratory, King Mongkut's Institute of Technology Thonburi. The energy consumption analysis report. The Energy Conservation in Commercial Building and Factory in 2009 and 2011. Metropolitan Electricity Authority, Thailand.

Eco-Friendly Community and Renewable Energy

INTEGRATED COMMUNITIES FOR THE SUSTAINABILITY OF RENEWABLE ENERGY APPLICATION: SOLAR WATER PUMPING SYSTEM IN BANYUMENENG VILLAGE GUNUNG KIDUL D.I. YOGYAKARTA

Nur Setyo Wahyuni¹, Suci Wulandari², Ellena Wulandari² and Didit Setyo Pamuji²

¹EnerBI (*Energi Bersih Indonesia* – Indonesian Clean Energy Foundation), Tangerang Selatan, Indonesia

²Kamase (*Komunitas Mahasiswa Sentra Energi* – Student Community of Energy), Department of Physics Engineering, Faculty of Engineering, Universitas Gadjah Mada, Indonesia

SUMMARY: Hamlet of Banyumeneng in Giriharjo Village, District of Panggang, is a region with severely limited access to water supply in Gunung Kidul Regency – D.I. Yogyakarta because of karst structure. People always have to face problem of water scarcity in the whole year. An international competition named Mondialogo Engineering Award (MEA) 2007 became an opening pathway to finance mitigation project of drought problem. This project is called Solar Water Pumping System (SWPS) which was started and initiated by Kamase (*Komunitas Mahasiswa Sentra Energi* – Student Community of Energy) together with Student Community Services program so-called KKN-PPM UGM. The problem faces is the sustainability of the plan. This paper shows a new integration concept of communities to keep it sustain for the late 5 years. The communities are Kamase, EnerBI (*Energi Bersih Indonesia* – Indonesian Clean Energy Foundation) and OPAK (*Organisasi Pengelola Air Kaligede* – Kaligede Water Management Organization) as a local community.

Keywords: renewable energy, solar water pumping system, sustainability, integrated communities

INTRODUCTION

Hamlet of Banyumeneng in Giriharjo Village, District of Panggang, is a region with severely limited access to water supply in Gunung Kidul Regency – Yogyakarta. People always have to face problem of water scarcity in the whole year, particularly during dry season. Its topography dominated by karst structure which is cannot reserve water. The local community have to struggle to obtain water by walking about 3.2 km/day, or spending at least IDR 150,000.00/month to buy while their income is just around IDR 400,000.00/month in average.

The local people are settled in a certain location approximately of 1.6 km in distance from the water source. Most of them are working as farmer and labor. The existing households had been electrified by state-owned electricity company (PLN) but there is no power grid of electricity nearby the water source. Before this project began, diesel pump had been installed close to the water source in order to meet the requirement of water supply for hamlet of Banyumeneng I, Banyumeneng II and Banyumeneng III. However, due to the operation and maintenance cost rising, more than 50 households in Banyumeneng I had been abandoned with no feasible access to clean water for many years.

An international competition named Mondialogo Engineering Award (MEA) 2007 became an opening pathway to finance mitigation project of drought problem. Kamase (*Komunitas Mahasiswa Sentra Energi* – Student Community of Energy) from Department of Engineering Physics, Universitas Gadjah Mada (UGM) in collaboration with Curtin University, Australia won the proposal competition and awarded 20,000 Euros by sponsor to develop the project as proposed. From that

moment, Solar Water Pumping System (SWPS) Program in Banyumeneng was started and initiated by Kamase together with Student Community Services program so-called KKN-PPM UGM. By available funding, the joint collaboration team had succeeded installing the system but unfortunately, it only coverage 30 households from total of 90 households. The SWPS remains sustain from the first start-up in August 2009 to recent day. The system running well and only minor impairment has been occurred for the last 4 years, such as leakage of main pipe or distribution pipe.

SWPS

Present status water production is about 6m³/day for 30 households (@200 liters) with system specification: direct use 1200 WP PV to 600 watts Submersible Pump Lorentz HR600.

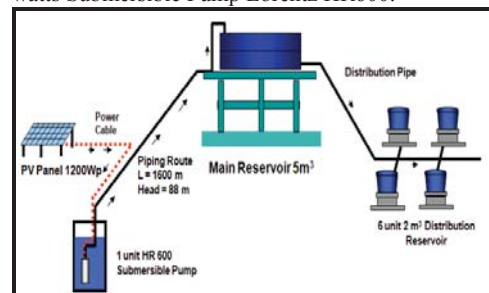


Figure 1. Existing Solar Water Pumping System (SWPS)

COMMUNITIES

Kamase

Kamase is an independent student organization that was established in the Department of Physics, Faculty of Engineering, Universitas Gadjah Mada

who concern in the field of renewable energy implementation in any scale.

EnerBI

EnerBI is a non-profit organization which engaged in research, consultancy in the field of renewable energy and helping people to fulfill their need corresponding with energy consumption. In Banyumeneng case the energy from Solar Panel were converted to water pump. This foundation was founded by alumni of Kamase.

OPAKg

OPAKg is local community which established to manage SWPS in Banyumeneng. This organization was initiated by Kamase and KKN PPL UGM. The sustainability is depends on this organization existence.



Figure 2. Logos of three communities

RESULT AND DISCUSSION

The detailed chronology of SWPS project in Banyumeneng started from 2007 until now is shown in Figure 3.

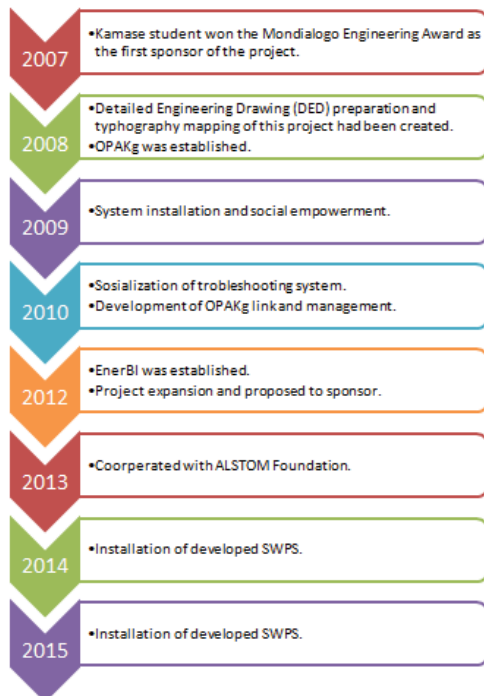


Figure 3. The chronology of SWPS project the work and coordination of three communities to reach the

sustainability of this project is shown in Figure 4.

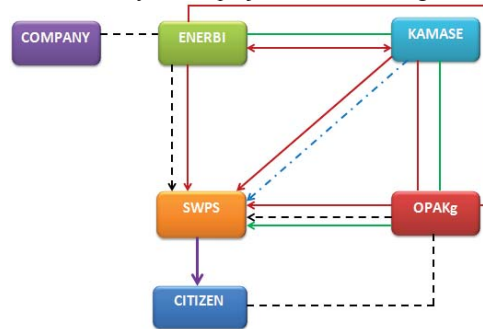


Figure 4. Work and coordination illustration of three communities

Note.

- - - - -> Funding
- > Installation
- > Monitoring & Controlling
- - - - -> Research
- > Receiver

CONCLUSION

The integration of three communities – Kamase, EnerBI, and OPAKg – gives a new integration concept of communities to keep the SWPS project in Banyumeneng sustain for the late 5 years.

ACKNOWLEDGMENT

Thank you to Kamase and EnerBI as a project initiator and very welcome to share the information and the data, local community at Banyumeneng village, and Mondialogo Engineering Award and ALSTOM Foundation as sponsors in this project.

References

[1] G. Liu, “Development of a General Sustainability Indicator for Renewable Energy Systems: A Review”, *Journal of Renewable and Sustainable Energy Reviews*, **31**, 2013, pp. 611-621.
 [2] R. Budiarto, M. K. Ridwan, A. Haryoko, Y. S. Anwar, Suhono, and K. Suryopranoto, “Sustainability Challenge for Small Scale Renewable Energy Use in Yogyakarta”, *Journal of The 3rd International Conference on Sustainable Future for Human Security SUSTAIN*, 2012.

ECONOMICAL BIODIESEL FUEL SYNTHESIS FROM CASTOR OIL USING MUSSEL SHELL-BASE CATALYST (MS-BC)

Said Nurdin¹, Nurul A. Rosnan¹, Nur S. Ghazali¹, Jolius Gimbun¹, Abdurahman H. Nour¹ and Siti F. Haron¹

¹Faculty of Chemical and Natural Resources Engineering, University of Malaysia Pahang (UMP), Malaysia

SUMMARY: Non-homogenous catalyst has been being developing for beneficial biodiesel synthesis. Formulation of mussel shell-base catalyst (MS-BC) for biofuel synthesis from castor oil could reduce production cost and environmental impacts. A transesterification of castor oil as non-edible feedstock to biodiesel was conducted in a flask reactor. Two catalysts were examined, where the calcined mussel shell and the impregnated calcium oxide with the potassium hydroxide were run by batch system. The catalysts and formed biodiesel were characterized and analyzed by Scanning Electron Microscopy (SEM), X-Ray Diffraction (XRD), Brunauer-Emmett-Teller (BET), Thermal Gravimetric Analysis (TGA), X-Ray Fluorescence (XRF) and Gas Chromatography (GC). The highest biodiesel yield (91.17%) was found by the catalyst of 2 wt/wt%, time of 3 h, temperature of 60°C and methanol oil ratio of 6:1. The impregnated catalyst provided magnificent results compared non-impregnated, and the reusable catalyst can be considered for economical biodiesel fuel synthesis.

Keywords: mussel shell, impregnated catalyst, transesterification, castor oil, economical biodiesel

INTRODUCTION

Development of bioenergy, like biodiesel as alternative fuel, environmental friendly, biodegradable properties has been becoming interesting issues. The biodiesel can be produced from edible, non-edible oils, etc. [1]. The castor oil as non-edible has high potential to be used as raw material. This vegetable oil contains high unsaturated fatty acid, it can be realized in the transesterification process for biodiesel synthesis, and it has been shown a significant reduction in particulate emission compared petroleum diesel [2], [3]. Next, the shell wastes of mussel were commonly deserted from the restaurants, food and canneries industry in Malaysia without any distinguished employment for precious products. Otherwise, the use of metal catalysts for biodiesel synthesis from edible sources like palm oil, soybean, etc. which are consumed as food creates versus fuel dilemma and expensive, thus this work aims to solve this issues by using the mussel shell-base catalyst (MS-BC) for biodiesel fuel synthesis. Biodiesel synthesis using calcium oxide base catalyst has some advantages such as higher activity, mild reaction condition, simple recycling, shorter time, low cost, and easy in separation process. Beside that, it is much cheaper than enzyme or other offered biochemical catalysts [4], [5].

METHODOLOGY

The mussel shell waste was collected from the sea food restaurants in Kuantan, Pahang, Malaysia. The potassium hydroxide, castor oil, etc. were ordered by the Permula Sdn Bhd, Kuala Lumpur, Malaysia. The mussel shell was crushed, activated and impregnated. This experiment examines the ability of mussel shell-base catalyst (MS-BC) to synthesize biodiesel from castor oil. The effects of catalyst amount (1 wt/wt%-5 wt/wt%), catalyst recyclability (1 cycle-5 cycles), time (1 h-5 h) and

temperature (40°C-80 °C) on the biodiesel yield were observed. The transesterification of castor oil were carried out under batch condition over activated solid catalyst. The activation of calcium oxide as the first catalyst derived from mussel shell was calcined at 1000 °C with heating rate of 10°C for 1 h. The second catalyst of calcium oxide was impregnated by potassium hydroxide for 2 h at 80°C. The characterization, transesterification, synthesis and analysis were conducted gradually. Analysis of castor seeds oil, catalyst and biodiesel were done by XRD, FESEM, BET, TGA, XRF and GC. The properties and performance of synthesized biodiesel were approved based on the proposed standard such as flash point, viscosity index, acid value etc. The characterization and analysis of activated and impregnated solid catalyst were compared with non-impregnated performance. The obtained castor oil biodiesel yields were interpreted based on the variation of process parameter. The synthesized biodiesels were approved by GC-MS, and its properties would be compared to the limitation of specification described by ASTM D6751.

RESULTS & DISCUSSION

The characterization and analysis results of activated catalyst shown a large surface area compared non-activated catalyst. The activated catalyst gave the maximum calcium oxide of 97.72%, and it is higher than clam shell (86.2%) [6]. This calcined catalyst reflected a great accomplishment of the catalyst. The catalyst weight lost post-calcination process. Next, the impregnated catalyst gave the outstanding results compared with non-impregnated performance. The maximum catalyst weight loss (11.33%) was recorded at the temperature range of 350°C – 450°C. The highest biodiesel fuel yield (91.17%) was found at temperature of 60°C, impregnated catalyst loading

of 2 wt/wt%, methanol oil ratio of 6 : 1 and reaction time of 3 h. The obtained yield is better than *Rubber* and waste frying biodiesel (75.93% and 87.28%) using clam and snail shell [6], [7]. Then, the biodiesel can be resulted after the catalyst was being reused 5 cycles, and it had the biodiesel yield of 79.72 % for 4 cycles. The yield of biodiesel dropped post 5 cycles of reused catalyst.

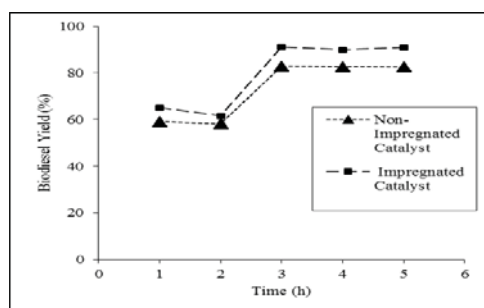


Figure 1. Biodiesel yield vs reaction time

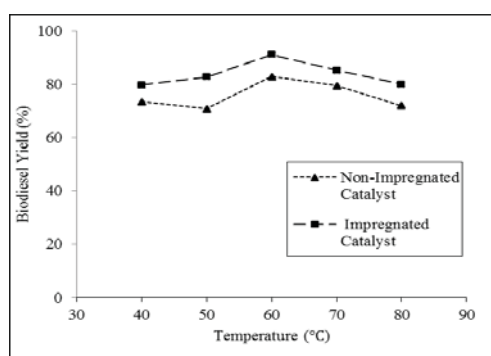


Figure 2. Biodiesel yield vs temperature

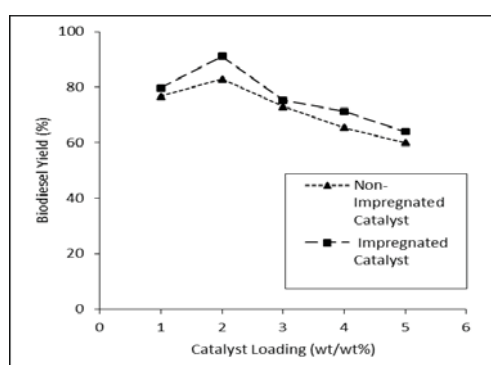


Figure 3. Biodiesel yield vs catalyst loading

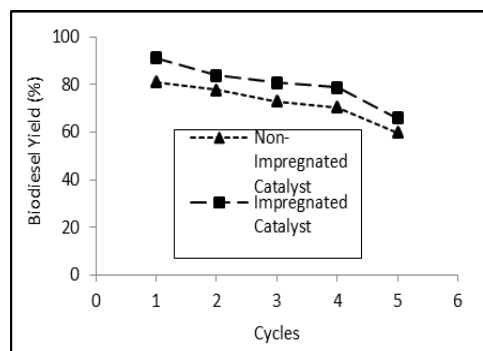


Figure 4. Biodiesel yield vs catalyst recyclability

ACKNOWLEDGMENT

We acknowledge the research funding from Ministry of Malaysia Education via RACE Grant-RDU 141303.

References

- [1] P. Sreenivas, V.R. Mamilla and K.C. Sekhar, "Development of biodiesel from castor oil", *I. J. of Energy Science*. **1** (3), 2011, pp. 192-197.
- [2] F. Halek, A. Delavari and A.K. Rahim, "Production of biodiesel as renewable energy source from castor oil". *J. of Clean Tech. Environ. Policy*. **15**, 2013, pp. 1063-1068.
- [3] J. Ahmad, S. Yusup, A Bokhari and R.N.M. Kamil, "Study of fuel properties of rubber seed oil based biodiesel", *Energy Conversion and Management*. **78**, 2014, pp. 266-275.
- [4] S. Semwal, A.K. Arorab, R.P. Badonia and D.K. Tulib., "Biodiesel production using heterogenous catalyst". *J. of Bioresource Technology*. **102** (3), 2011, pp. 2151-2161.
- [5] B. Shah, S. Sarina, J. Parveen and A.Md. Zahangir, "Production of heterogenous catalyst for biodiesel synthesis", *I. J. of Chemical and Environmental Engineering*. **5** (2), 2014, pp. 73-75.
- [6] A. Birla, B. Singh, S.N. Upadhyay and Y.C. Sharma, "Kinetics studies of synthesis of biodiesel from waste frying oil using a heterogeneous catalyst derived from snail shell". *J. of Bioresource Technology*. **106**, 2012, pp. 95-100.
- [7] S. Nurdin, F.A. Misebah, S.F. Haron, N.S. Ghazali, R.M. Yunus, and J. Gimibun, "Activated *Paphia undulate* shell waste (APSW): A cost effective catalyst for biodiesel synthesis from *Rubber* and *Jatropha curcas* seeds oil (RSOME&JSOME)", *I. J. of Chemical Engineering and Applications*. **5** (6), 2014, pp. 483-488.

SUSTAINABLE DEVELOPMENT AND ECO-FRIENDLY WASTE MANAGEMENT MODELLING FOR LOCAL COMMUNITY

Krongkaew Laohalidanond¹, Woranuch Jangsawang² and Somrat Kerdsuwan¹

¹ The Waste Incineration Research Centre,
Department of Mechanical and Aerospace Engineering, Faculty of Engineering,
King Mongkut's University Technology North Bangkok, Thailand

²Sustainable Energy Research Center, Faculty of Industrial Technology,
Phranakorn Rajabhat University, Thailand

SUMMARY: This study focuses on the sustainable development and eco-friendly waste management concept within local communities in developing countries with MSW generation less than 5 ton per day. For sustainable development and eco-friendly waste management, the public participation campaigns with 3R's concept (Reduced, Reuse and Recycle) must firstly be launched to reduce and separate waste from households to be mix combustible waste, organic waste and recycle waste. Biological-Mechanical-Treatment (BMT) is the most suitable technology for local community with MSW generation less than 5 ton daily, which can contribute to the sustainable development in rural areas, since the products of the process, e.g. organic fertilizer and Refuse Derived Fuel (RDF), can be used or sold. The waste management centre should be established as community enterprise. The community is the owner of the centre and can request for the financial support from central government. This sustainable and eco-friendly model of waste management can be used as prototype model for others rural areas in low or low-middle income countries.

Keywords: Municipal Solid Waste, Sustainable Development, MSW Management, Low Income Countries

INTRODUCTION

As an exponential growth in world population and an improvement of living standard, the amount of Municipal Solid Waste (MSW) which is the residues from human's routine activities generated from residential areas and commercial sectors is continuously increased. The proliferation of MSW worldwide can cause the environmental problems, particularly in developing countries or low-income countries where the governmental budget is scant. Although landfilling is the main MSW disposal method worldwide in both developed countries and developing countries, the utilization of sanitary landfill tends to be declined in developed countries due to the scarcity of landfill site and public's environmental concerns. In contrast to developed countries, many rural areas in developing countries are still using non-sanitary and uncontrolled landfill, in this case open dumping, as the MSW disposal method, which leads to negative effects to environment and human health.

There are two main factors which are still the challenge of MSW management in developing countries: the MSW characteristics and the regulations for MSW management. Compared to MSW generated in developed countries which contains less than 20-30%-wt. of organic waste, MSW produced from developing countries has a high organic waste of more than 60%-wt. [1]. The high portion of organic waste results in the extreme moisture content and low heating value. Considering the regulations for MSW management most of all developing countries do not separate, the regulation for separation of MSW from household is in force in many developed countries, whereas in developing countries, most of MSW is not separated at sources.

These two key factors play an important role on the decision making for MSW disposal technology in developing countries.

This study focuses on the sustainable development and eco-friendly waste management concept within local communities with the MSW generation of less than 5 ton per day in developing countries. Local Administrative Organization (LAO) which has MSW approximately 2.5 ton per day is the representative modelling as case study. Currently, MSW is generated in LAO which consists mostly of organic waste and plastic waste. This waste is collected from households by trucks without any source separations and disposed by non-sanitary landfill at dumpsite. As MSW quantification and characterization is the criterion to the selection of MSW disposal technology, this study will start with the prediction of the amount of MSW generation, followed by the MSW characterization and the conceptual design of MSW disposal technology for local community. Finally the MSW management model will be set up as the prototype for others rural areas in low or low-middle income countries.

METHODOLOGY

MSW Quantification

The amount of waste generated in LAO has been investigated followed by the waste generation rate using Eq. 1.

$$W_{gen} = \frac{W_{total}}{P_0} \quad (1)$$

W_{gen} is the waste generation rate per capita, W_{total} represents the total amount of waste generation and P_0 is the population in the current year. The

growth in population can be determined by the geometric curve based on the statistical data in last 10 year, as shown in Eq. 2 and the amount of waste generation in next 20 years was also calculated by Eq. 3 [2].

$$P_n = P_0 (1+r)^n \quad (2)$$

$$W_{\text{total},n} = P_n \times W_{\text{gen}} \quad (3)$$

P_n is the population in n^{th} -year; r is the population increasing rate per year.

Waste Characterization

Approximately 1 m³ of waste at dumpsite was taken as a sample for determination of physical and chemical composition. The physical composition of waste which is the main criteria for selecting the appropriate technology was investigated by quartering method and type separation. The physical and chemical properties which are necessary for design of selected technology were determined according to ASTM [3].

MSW Management Model

In order to develop the MSW manage model for LAO, approximately 120 questionnaires were given to people from 12 villages in LAO. Furthermore, 4 main criterions were taken into consideration for selection of proper technology, as in the following [4]:

- Practicability and performance, including efficiency, reliable, safety, operator-skill and environmental impact
- Economics, including investment and operation cost
- Maturity of technology
- Technological self-reliance, describing the potential of technology implementation and developing locally

After the technology selection, the conceptual design of selected technology was performed. This covers the process description and mass balance for the whole process. Finally the economic and ecological points of view were concerned.

RESULTS AND DISCUSSION

MSW Quantification

From the statistical data of population, the increasing rate in population of 0.27 % is obtained and with this increasing rate and constant waste generation rate of 0.49 kilogram per day per capita, LAO will have 12,049 populations in 2030 which will lead to the amount of waste generated of 5.90 ton per day. The amount of waste will be increase from 5.56 ton per day in 2010 to 5.90 ton per day in 2030.

MSW Characterization

The physical composition of waste consists mainly of organic waste (more than 40 %) which is combustible waste and can be referred as wet garbage and the other are plastic waste, paper, cloth, metal, glass, etc. Moisture content (as received) and heating value (dry basis) of waste range from 49-73 %-wt. and 15-30 MJ/kg, respectively.

MSW Management Model

Biological Mechanical Treatment (BMT) is considered to be the suitable technology for mix waste fraction, as its operation principle is quite the same as sanitary landfill technology which is widespread used in local community for MSW disposal. Because this technology works based on sanitary landfill concept but needs shorter time for decomposition, it can effectively reduce the volume of waste (in term of organic waste). Figure 1 illustrates the MSW management model for small community.

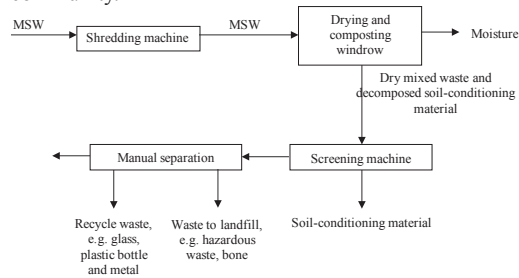


Figure 1. MSW management model

Meanwhile, 3R-concept (Reduce, Reuse and Recycle) should be promoted in all levels from home and school for children to policy and strategy for LAO.

ACKNOWLEDGMENT

The authors would like to thanks the National Research Council of Thailand (NRCT) for financial support, the Waste Incineration Research Center (WIRC) as well as Department of Mechanical and Aerospace Engineering (MAE), King Mongkut's University of Technology North Bangkok for any kinds of cooperation.

References

- [1] T. Karak, R.M. Bhagat, and P. Bhattacharyya, "Municipal Solid Waste Generation, Composition, and Management: The World Scenario", *Environmental Science and Technology*, **42**, 2012, pp. 1509-1630.
- [2] A. Thongkaimuk et al., "Waste Management", *Ministry of Science and Technology*, Thailand.

EFFECT OF APPLIED PRESSURE AND BINDER PROPORTION ON THE FUEL PROPERTIES OF HOLEY BIO-BRIQUETTES

Mallika Thabuot^{1,2}, Thanchanok Pagketanang¹, Kasidet Panyacharoen¹, Pisit Mongkut¹ and Prasong Wongwicha¹

¹Department of Chemical Engineering, Faculty of Engineering, KhonKaen University, Thailand

² Alternative Energy Research and Development, KhonKaen University, Thailand

SUMMARY: The manual hydraulic press was designed to prepare the holey briquettes from selected biomass wastes. Each biomass was sun dried and milled into the smaller particle size before mixing with 20wt.% of palm fiber, and molasse was used as the binder. The effects of applied pressure levels of 40, 50, 60 and 70 kg/cm² and of the binder amount on the density, calorific heating value and burning rate of the prepared briquettes were investigated. Results showed that briquettes have the average inside diameter, average outside diameter and height of 12, 38 and 25-30 mm, respectively. The density of the briquettes increased with the increasing of applied pressure, was in the range of 260-416 kg/m³. The most densified briquettes were obtained from bamboo sawdust at the use of 20wt.% molasse and pressure of 70 kg/cm². The heating value of bamboo briquette reached up to 21.26 MJ/kg, and rubber wood residue briquette obtained the slowest burning rate of 2.01 g/min.

Keywords: Biomass, Briquette, Calorific Value, Burning rate

INTRODUCTION

Biomass fuels are long term potential sources of renewable energy because of its abundant availability and CO₂ neutral. Depends on the technology selection, biomass can be utilized as fuel in different forms. Most of lignocellulosic agricultural residue is composed of the big molecular and complex structure, so the utilization of these materials has a few weak points of low energy density, less heating value, difficulties in transportation and storage [1-2]. Physical method is simply applied on the conversion of these materials into alternative fuel. Thailand has many agricultural crops which can be used as the renewable energy source. To meet the national energy policy which taking into account the energy demands, economic and environmental impact, the agro-residues are the potential energy feedstocks, Briquetting process is the most promising way to compress biomass residues into the solid biofuels. However, this technology should be cheap, simple and easy maintain. For this work, the hydraulic press machine was designed to prepare briquettes, and the fuel properties of solid fuel were investigated. The influences of applied pressure and amount of used binder on briquette properties are discussed here.

METHODOLOGY

Bamboo sawdust, eucalyptus sawdust, corn cob and palm fibre were collected from the local area of Khon Kaen Province, Thailand. All materials were sundried for 3 days before milling to get the particle size less than 5mm. The sieved material was mixed with 20wt.% of palm fibre and 15, 20, 25 and 30 wt.% of molasse. Compaction test on the blended samples was carried out using the hydraulic press machine with maximum capacity of 100 kg/cm² (see Figure 1). The mixture was fulfilled into each dies, the briquettes were produced under the applied pressures of 40, 50, 60 and 70 kg/cm² at the holding time of 1 minute. Then the products were kept for 2

two weeks in the ambient condition before subjected to analysis.

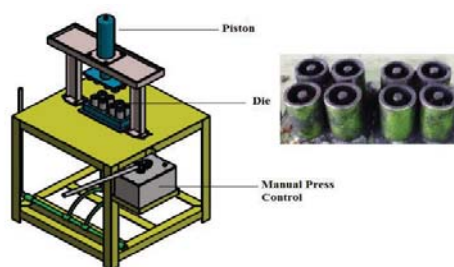


Figure 1. Briquetting hydraulic press machine

Properties of bulk materials were determined for the percentage of volatile matter, fixed carbon and ash content on the dried basis. The volatile matter (ASTM D3175-11) was carried out. The ash content (ASTM-E830) of the material was determined. The amount of fixed carbon was obtained from weight difference. Elemental compositions were estimated using the equations provided in the other study [2]. The calorific heating value of materials was determined using Gallenkamp Adiabatic Bomb Calorimeters. The bulk densities of each biomass species were determined from dividing the packed material mass by the known volume of cylinder. Briquette size was measured with a standard vernier caliper. The individual briquette density was determined from dividing the mass by the volume of briquette. Burning rate was then calculated from the subtraction of ignition time from the ashing time as reported [3].

RESULTS AND DISCUSSION

As the volatile matter contains combustible gases such as methane and other hydrocarbons, biomass with larger amount of volatile matter is

lower in fixed carbon content, easier for ignition and higher heating value. Selected biomass wastes have high amount of volatile matter between 93.44-99.57%. Low ash content might results to the high heating value of material. In this study, the heating value of bamboo sawdust is higher than the others. That means bamboo sawdust generated more energy with the same amount of other materials. The molar ratio of carbon to hydrogen and carbon to oxygen was about 0.61-0.63 and 1.28-1.34, respectively. Produced briquette was cylindrical shape with one vertical holes run through, height of holey briquette depends on the bulk density of biomass wastes and the applied pressure using in the process.

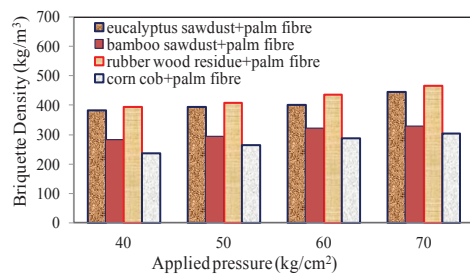


Figure 2. Briquettes prepared at 15wt. % molasse

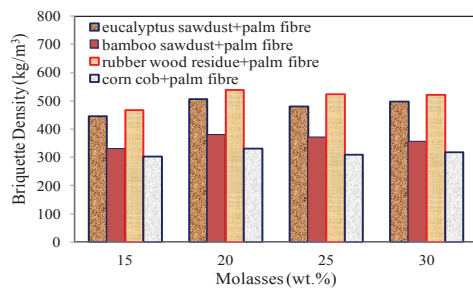


Figure 3. Briquettes prepared under 70 kg/cm²

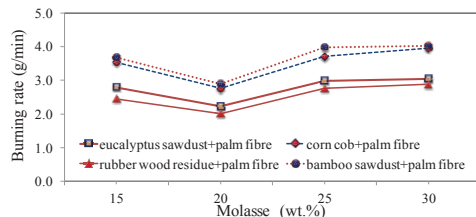


Figure 4. Briquettes prepared under 70 kg/cm²

From Figure 2, by using 15wt.% molasse, the increase of pressure induced the briquette density. Compared to briquetting production at the low pressure of 40 kg/cm², all produced briquettes have gained density about 1.1-1.3 times when high pressure of 70 kg/cm² was used. Rubber wood residue can be easily pressed under every pressure. At 70 kg/cm², its briquette had the highest density (468.34 kg/cm²) than the others, whereas corn cob

gave the most loosen briquette (304.23 kg/cm²). Figure 3 shows that too much proportion of binder is not recommended at all applied pressure. To obtain the densified briquette, 20wt.% molasse was suggested. Density of briquettes prepared from rubber sawdust increased to 540.76 kg/cm², also corn cob briquette had the increasing density of 332.54 kg/cm². From the heating value analysis, increasing amount of binder decreases the calorific heating value of briquette. Bamboo sawdust has the larger heating value than others, so high heating value briquette among the group was obtained from mixing 15wt.% of molasse with bamboo sawdust which was about 21.26 MJ/kg. It means more energy can be released from this kind of briquette than of the others. This study presented the same relationship of burning rate of briquettes prepared at different applied pressures which was also reported [3]. Burning rate increased with the increasing of applied pressure for briquette production. Eucalyptus sawdust-briquette and rubber wood residue-briquette have the slightly larger burning rate than the others at the low pressure, but the high compacted briquette gave the apparently low burning rate. From these results, applied pressure of 70 kg/cm² was selected to produce the briquettes at different proportions of molasse. Briquette with slower burning rate was given by using less molasse as seen in Figure 4. Briquettes prepared with 20wt.% of molasse have the slowest burning time, especially rubber wood-briquette. This might be caused by its high proportion of volatile matter and fixed carbon.

The study results presented briquette with high density, high heating value and slow burning rate can be produced depends on the material variables and process factors. Therefore, the briquetting process with economically, simply and cheap technology should be supported to the rural and small community in Thailand.

ACKNOWLEDGMENT

The authors are grateful of Alternative Energy Research and Development, KhonKaen University (Thailand) for the financial support carrying out the research work.

References

- [1] F. Zannikos, S. Kalligeros, G. Anastopoulos, and E. Lois, "Converting biomass and waste plastic to solid fuel briquettes", *Journal of Renewable Energy*. 2013, Article ID 360368.
- [2] R. Mythili and P. Venkatachalam, "Briquetting of Agro-residues", *Carbon*. **42**(41.80), 2013, pp.42-08.
- [3] A. Talukdar, D. Das, M. Saikia, "Study of Combustion Characteristics of Fuel Briquettes", *International Journal of Computational Engineering Research*. **4**(3), 2014, pp. 2250-3005.

AN INVESTIGATION OF FUEL ECONOMY POTENTIAL OF HYBRID VEHICLE UNDER REAL-WORLD DRIVING CONDITIONS IN BANGKOK

Siriorn Pitanuwat^{1,2} and Angkee Sripakagorn^{1,2}

¹Department of Mechanical Engineering, Faculty of Engineering, Chulalongkorn University, Thailand

²Smart Mobility Research Center, Faculty of Engineering, Chulalongkorn University, Thailand

SUMMARY: This study attempts to investigate fuel economy performance of hybrid vehicles (HVs) under real-world driving conditions in Bangkok. The effect of traffic conditions and driving styles are taken into account. To cover the variations in traffic conditions, city, suburban and highway traffics are selected to represent the variety of traffic flow. For the effect of driving styles, the experiment is conducted by four experienced drivers which consist of two-aggressive and two normal-to-calm drivers. This study employed the microtrip approach in order to quantify the impact of Bangkok traffic conditions and driving styles on both vehicles' fuel consumption. Statistical parameters, average speed and acceleration noise, are used to classify and analyze the microtrip data. Experimental results illustrate that HVs are capable of reducing fuel consumption in all traffic conditions and driving styles, covered by this study, compared to CVs. Particularly in the congested traffic condition of Bangkok, HVs potentially decrease the fuel consumption, by a maximum of 70%. More importantly, HVs can mitigate the effect of aggressiveness on excessive fuel consumption in practical driving habits.

Keywords: hybrid vehicle, conventional vehicle, fuel consumption reduction, traffic condition, driving style

INTRODUCTION

Globally, transportation sector has contributed to one-third of overall energy consumption; however, in metropolitan areas, the transportation energy consumption has critically increased due to large amount of car intensity [1]. In Bangkok metropolitan, the statistics from the pass five years show that the consumption level has dramatically risen approximately to 70%, which subjects to more than 90% of the overall city's Greenhouse gas (GHG) emissions. Over the past decades, automotive and transportation fields have been devoting to reduce on-road energy consumption and emissions. Several academia studies showed that powertrain technologies, traffic conditions, and driving styles are the fundamental causes of the excessive fuel consumption and emissions. [2]

Recently, A number of papers has consistently shown that fuel economy and GHG emission reduction of those electrified vehicles are more efficient than fuel economy and GHG emission reduction of internal combustion engine vehicles (ICEVs), especially in city drives [3]

Nevertheless, the energy consumption reduction potential of these vehicles significantly depends on local traffic conditions and driving styles Therefore, this study attempts to stimulate the perception toward HVs in Bangkok areas and provides an essential database for in policies development level.

METHODOLOGY

Route and driver selection

To capture the variety of driving incidents in Bangkok, average speed, number of vehicles at the peak hours, and locations were taken into account. All the major routes in Bangkok were clustered into

three traffic conditions; city, suburban and highway,

by the average speed. [4] The routes of which the average speeds were less than 20 km/h, between 20-50 km/h, and above 50km/h are clustered in city, suburban and highway traffic conditions respectively. Then, in each traffic condition, the routes that had the highest utilization were selected. In figure 1, the representative routes were Silom and Sathon Nuea, Vibhavadi Rangsit, and Motorway 7 of which the orientations covered three representing different areas which the red and blue areas indicated the inner city and downtown business zone. The brown, orange and yellow classified the density of inhabited areas from densely to sparsely, respectively. [5] Furthermore, four experienced drivers were employed to the experiment, two aggressive drivers and another two normal-calm drivers, in order to extend the range and capture the impact of aggressiveness and eco-driving on fuel consumption.

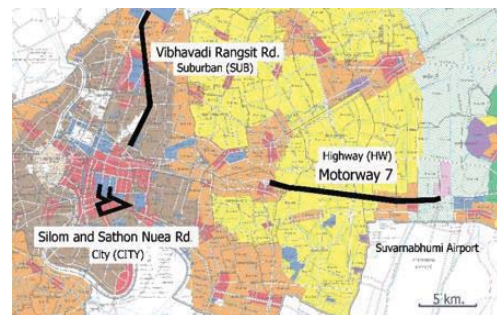


Figure 1. Representative route's orientation. [5]

Experiment set up

For the test vehicles, 2014 Toyota Prius and 2015 Toyota Corolla Altis were selected to represent HVs and CVs respectively. Both vehicles had engine size at 1,789 cc ,and were the dominant vehicle size

in Bangkok. The Prius weight was 480kg higher than the Altis weight due to the additional 60kW electric motor, 1.31kW Ni-MH battery. [6]

For data acquisition, Vehicle Interface Module (VIM) and Global Tech Stream (GTS) software were installed to record basic vehicle data, such as vehicle speed, engine revolution, fuel injected amount, and engine on-off conditions. The data recorder is connected via on-board diagnostics (OBD) port with sample rate at 8.5 Hz. [6]

Data interpretation

To understand HVs and CVs' fuel consumption characteristic due to the local traffic conditions and driving styles in bangkok, all the driving data were sectioned into microtrips.[7] Then, average speed and acceleration noise parameters were calculated to identify the microtrip's traffic conditions and driving styles. The congestion level of traffic conditions was indicated by average speed. [8] For driving styles, this study focused on driving aggressiveness which quantified by acceleration noise as shown in equation 1. [9]

$$A_{noise} = \sqrt{\frac{\sum_{i=0}^n a(t_i)^2 v(t_i)}{\sum_{i=0}^n v(t_i)}} \quad (1)$$

Where A_{noise} and $a(t_i)$ are acceleration noise and instantaneous acceleration in a unit of m/s^2 , $v(t_i)$ is instantaneous speed in a unit of km/h.

RESULTS AND DISCUSSION

HVs and CVs fuel consumption characteristics

According to the results from Fig.2. and Fig.3., traffic condition tended to dominate fuel consumption on both vehicles. As the average speed decreased, the fuel consumption gradually increased. However, there were some evidences showed that driving styles also had a significant impact on vehicle fuel consumption. In Fig.2. and Fig.3., HVs with CVs, the aggressiveness levels of both vehicles were apparently different. The microtrips of CVs reached the higher level of acceleration noise in all microtrips' average speed ranges compared to the microtrips of HVs at normal driving mode. However, the overall fuel consumption of HVs at the same average speed and acceleration noise levels appeared to be lower than fuel consumption of CVs. Especially at the speed below 15 km/h, HVs tended to operate frequently in pure-electric drives. The percentage of pure-electric drives at the average speed less than 5km/h, between 5-10 km/h, and between 10-20 km/h were found at 59%, 49%, and 14% respectively. As a result, more than half of HVs' fuel consumption data points in Fig.3. dropped down to zeros during low-speed drives and left some minor scattered data points above. On the other hand, CVs data points in Fig.2. aligned densely in the each average speed ranges with

inclining trends. As the average speed increased, the fuel consumption steadily increases. This characteristic also occurred with HVs at the average speed higher than 15 km/h. Nevertheless, the CVs tended to be more sensitive to aggressive driving styles compared with HVs.

HVs are capable of reducing fuel consumption compared to CVs. Particularly in the congested traffics, HVs potentially decrease the fuel consumption. More importantly, HVs can also mitigate the effect of aggressiveness on excessive fuel consumption in practical driving habits.

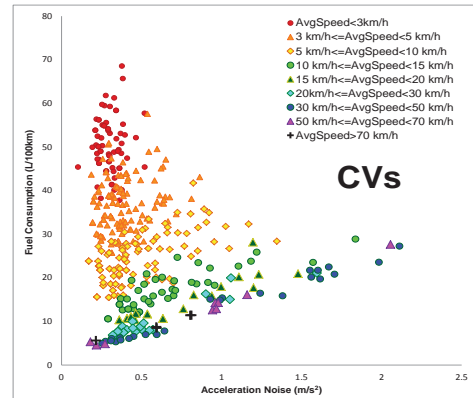


Figure 2. CVs fuel consumption characteristics

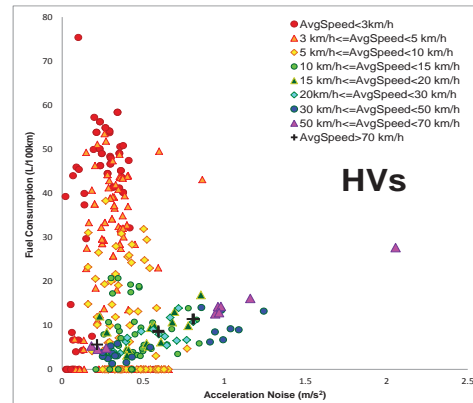


Figure 3. HVs fuel consumption characteristics

ACKNOWLEDGMENT

This study has been supported by Mechanical Engineering, Faculty of Engineering, Chulalongkorn University, and Toyota Motor Thailand Co., Ltd.

Reference

- [1] V. Franco, M. Kousoulidou, M. Muntean, L. Ntziachristos, S. Hausberger, and P. Dilara, "Road vehicle emission factors development: A review", *Atmospheric Environment*, **70**, 2013, pp. 84-97.

A FIELD STUDY OF THE THERMAL COMFORT IN UNIVERSITY BUILDINGS IN THAILAND UNDER AIR CONDITION ROOM

Noppanuch Puangmalee^{1,2}, Vorakamol Boonyayothin³

¹ Rattanakosin College for Sustainable Energy and Environment (RCSEE),
Rajamangala University of Technology Rattanakosin, Thailand.

² Department of Industrials Management and Technology, Faculty of Science and Technology,
Bansomdejchaopraya Rajabhat University, Thailand.

³ Department of Occupational Health and Safety, Faculty of Public Health, Mahidol University, Thailand

SUMMARY: The purpose of the present work was to determine the thermal comfort in university building in Thailand under air condition room. Students were tested in a 8x9x3 m³ test room set up with a 40,000 Btu/h 2 unit split type air conditioner. The room air temperature was varied from 25, 26, 27 and 28 °C and in each temperature, was varied air speed 3 levels (low, medium and high). Thermal comfort survey using questionnaire base on ASHRAE thermal sensation scale and indoor environment monitoring i.e., temperature, relative humidity and air velocity were conducted in varied condition. The results showed that the temperature of the Predicted Mean Vote (PMV=0) was increased with increasing of air speed. In addition, both in room air temperature (t_a) and air speed (v) affect to PMV as shown equation $PMV = 0.471t_a - 1.060v - 12.460$. The results of this research can apply to conditioning systems design and control for comfortable feeling of student.

Keywords: thermal comfort, predicted mean vote (PMV), actual sensation vote (ASV), air condition room,

INTRODUCTION

Thermal comfort has been defined by Hensen as “a state in which there are no driving impulses to correct the environment by the behavior” [1]. The American Society of Heating, Refrigerating and Air-Conditioning Engineers (ASHRAE) defined it as “the condition of the mind in which satisfaction is expressed with the thermal environment” [2]. As such, it will be influenced by personal differences in mood, culture and other individual, organizational and social factors. Based on the above definitions, comfort is not a state condition, but rather a state of mind. The definition of thermal comfort leaves open as to what is meant by condition of mind or satisfaction, but it correctly emphasizes that the judgment of comfort is a cognitive process involving many inputs influenced by physical, physiological, psychological, and other factors[3].

Indoor thermal environments can significantly influence human health and comfort. In addition, thermal comfort is very important for architects and engineers to ensure comfort and health of occupant in the building [4]. Since the late 20th century, the PMV (Predicted Mean Vote) model developed by Fanger has been widely used throughout the world. Although the PMV model is based on the database of European and North American subjects, many researchers around the world have conducted experiments in climate chambers and have demonstrated its validity [5]. However, many researchers have not been applied in sub-tropical climates such as Thailand. Thailand is located in sub-tropical zone at latitude 13°18'N and longitude 100°27'E, according to the climatological method of classification, the weather of Thailand is classified as “Humid Subtropical Climate”. For university

buildings, indoor thermal environments influence on learning of students. In addition, comfortable of student will be able to increase learning. Thus, this work was to study of thermal comfort in university buildings in Thailand under air condition room.

MATERIALS AND METHOD

The field measurements were performed in a room of size 8x9x3 m³ and set up split type air conditioner with a 40,000 Btu/h 2 unit. The room air temperature was varied from 25±0.5, 26±0.5, 27±0.5 and 28±0.5 °C and in each temperature, was varied air speed 3 levels (low, medium and high). The questionnaire addressed the following areas: (i) background and personal information; (ii) current clothing garments; (iii) subjective thermal sensation vote (the Actual Sensation Vote, or ASV) based on the ASHRAE sensation scale, the evaluation had seven levels, from -3 to +3 (table 1). The total number of subjects was 660 persons, 424 males and 236 females. The classroom was collected the indoor environment, i.e. temperature, relative humidity and air velocity.

Table 1. ASHRAE sensation scale [2]

Level	Thermal sensation
- 3	Cold
- 2	Cool
- 1	Slightly cool
0	Neutral
+1	Slightly warm
+2	Warm
+3	Hot

RESULT AND DISCUSSION

The general data

The general data of subjects, it found that, The total numbers of test subjects were 660 (424 males and 236 females). Average age of subjects was 22 years, average weight was 64 kg. for male and 59 kg. for female, average height was 1.73 m. for male and 1.63 m. for female. The subjects have an average thermal resistance of clothing was 0.909 clo for male and 0.959 clo for female.

Actual sensation vote (ASV)

The percentages of actual sensation vote under room temperature and air speed are shown in Table 2. It found that when the air speed at the same room air temperature was higher, the percent of actual sensation vote moved to the cool sensation vote side. While as the room air temperature was increased at the same air velocity, the percent of sensation vote tends to move to the hot sensation vote side. Therefore, thermal comfort can be provided by increasing the air velocity to compensate for the higher temperature.

Table 2. Percentage of actual sensation vote.

T (°C)	Air speed (m/s)	Percentage of actual sensation vote						
		-3	-2	-1	0	+1	+2	+3
25±0.5	0.5	7	20	40	33			
	0.7	20	13	47	20			
	0.9	27	20	47	7			
26±0.5	0.5		7	47	33	13		
	0.7		13	40	40	7		
	0.9		13	54	33			
27±0.5	0.5		7	40	33	20		
	0.7		7	36	34	13		
	0.9		13	53	27	7		
28±0.5	0.5			7	27	66		
	0.7				27	33	50	
	0.9		7	53	20	20		

Predicted mean vote (PMV)

Relation of predicted mean vote (PMV) and temperatur, air speed are shown in Fig. 1. It found that the temperature of the Predicted Mean Vote (PMV=0) was increased with increasing of air speed. One can say that as the air velocity increases, the neutral vote (PMV=0) shifts to higher air temperature are shown in Table 3.

Linear regression with the least square technique [6] was applied to construct the PMV equation. The obtained equation showed the relation between PMV and air temperature and air speed as shown in Eq. (1)

$$PMV = 0.471t_a - 1.060v - 12.460 \quad (1)$$

when t_a is room air temperature (°C) and v is air speed (m/s).

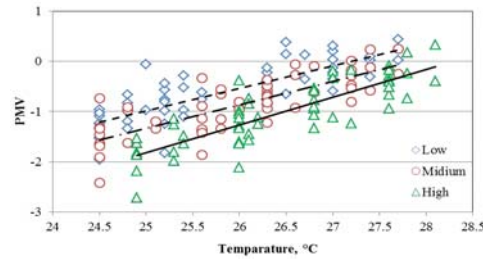


Figure 1. PMV vs. room air temperature under various air speed.

Table 3. Neutral temperature (PMV=0) for different air speed.

Air speed (m/s)	Neutral temperature, °C
0.5	27.20
0.7	27.85
0.9	28.30

CONCLUSION

The study of thermal comfort in school buildings in Thailand air condition room was found that:

The air speed at the same room air temperature was higher, affect to actual sensation to the more comfortable. While as the room air temperature is increase at the same air velocity, the actual sensation tends to the more hot sensation. Therefore, thermal comfort can be provided by increasing the air velocity to compensate for the higher temperature.

The temperature of the Predicted Mean Vote (PMV=0) increase with increasing of air speed. One can say that as the air velocity increases, the neutral vote shifts to higher air temperature

References

- [1] Hensen JLM., "On the thermal interaction of building structure and heating and ventilating system", PhD thesis, Technische Universiteit Eindhoven; 1991.
- [2] ASHRAE Standard 55. Thermal Environment Conditions for Human Occupancy; 2004.
- [3] Lin Z, Deng S. "A study on the thermal comfort in sleeping environments in the subtropics -developing a thermal comfort model for sleeping environments", Building and Environment, 2008, pp. 70-80.
- [4] Anh Tuan Nguyen, et al., "An adaptive thermal comfort model for hot humid South-East Asia", Building and Environment 56 (2012), pp. 291-300.
- [5] Bin Cao, Yingxin Zhu, et al., "Field study of human thermal comfort and thermal adaptability during the summer and winter in Beijing", Energy and Buildings 43 (2011), pp. 1051-1056.
- [6] Surat Atthajariyakul, et al., "Small fan assisted air conditioner for thermal comfort and energy saving in Thailand", Energy Conversion and Management 49 (2008), pp. 2499-2504.

Energy Efficiency

IDENTIFICATION OF DESIGN CRITERIA FOR DISTRICT COOLING DISTRIBUTION NETWORK WITH ICE THERMAL ENERGY STORAGE SYSTEM

Gerardo L. Augusto^{1,2}, Alvin B. Culaba¹ and Archie B. Maglaya¹

¹Department of Mechanical Engineering, De La Salle University Manila, Philippines

²Fluidnovation Research, Co., Quezon City, Philippines

SUMMARY: Two (2) distribution network models of district cooling system with ice thermal energy storage system are presented in which the theoretical system pressure drop, system flow rate and flow rate requirements in each energy transfer station were determined. The hydraulic calculation and system simulation of distribution networks with and without secondary lines are evaluated based on system temperature difference set-point of 11°C. Variable primary flow pumping system arrangement was used to improve energy usage and to eliminate the need for a distribution pump in the network. The system of nonlinear equations was solved using multivariable Newton-Raphson method. The linearized equations revealed that coefficient matrices formed between two networks were different from each other which suggested that different decomposition algorithms must be used to properly determine the solution vectors. Optimization technique such as exhaustive search method was adopted to identify the piping network design criteria that could yield minimum overall cost.

Keywords: district cooling system, ice thermal energy storage system, distribution network design criteria, multivariable newton-raphson method, exhaustive search method

INTRODUCTION

One of the largest contributors of electrical peak demand is to provide air conditioning of commercial buildings during summer daytime hours for comfort cooling. Other electrical loads include lighting, computers and operating equipment which allow additional electrical demand during peak hours. Commercial buildings are usually charged with higher energy charges which is based on their highest on-peak demand. To mitigate the increasing electrical costs, an ice thermal energy storage (Ice TES) system is needed which shifts electrical load during nighttime or off-peak periods. Such austerity measure significantly reduces energy and demand charges during summer and lower total energy usage as well. With the presence of ice thermal energy storage system, solid ice produces at night when the building electrical loads are at a minimum. Ice is stored in tanks to provide cooling and air conditioning requirement during daytime.

One of the advantages of Ice TES is to increase the building load factor which is the best alternative for increasing generating equipment and eliminating the costs of new generating plants. Although it requires higher overall costs for district cooling plants with Ice TES, it can reduce the initial investment costs of distribution network due to an increasing temperature difference set-point of 11°C. Allowable temperature difference set-point of district cooling plant with Ice TES system is around 13.3°C (Bahnfleth 2014). Nevertheless, it decreases the chilled water system flow rate requirement along the network by less than 18.2% as compared with district cooling plant without Ice TES system. As the distribution network is often the most expensive portion and requires large initial investment cost of the district cooling system, careful design is needed to optimize its use. It follows that appropriate piping network design criteria would be needed to properly

identify the minimum overall cost of construction and maintenance of distribution network.

MATERIALS AND METHODS

Ice TES system with temperature limits

In this study, the district cooling plant with Ice TES system discharges during daytime with partial load condition through temperature modulating valve set at 4.5°C. The bypass loop around the tank allows sufficient quantity of chilled water less than 11.1°C to mix with colder fluid from Ice TES system at 1.11°C and to achieve the desired supply temperature of 4.5°C. The chilled water return temperature leaves the energy transfer station at 15.5°C.

District cooling distribution network models

To compare the piping network design criteria of two distribution network models, the schematic diagrams DNModel-01_12 and DNModel-03_12 were used as shown in Figure 1 and Figure 2, respectively. Figure 2 shows the presence of secondary lines in the network. In both cases, twelve energy transfer stations in each network were used with total pipe length of approximately 5.2 km. The nominated cooling loads are listed in Table 1 with total cooling load capacity of 24,000 ton of refrigeration considering a diversity factor of 80%.

RESULTS AND DISCUSSION

Hydraulic calculation

The governing equations consisted of mass conservation and energy equations in the form of pump characteristic curve and distribution network characteristics. The system of nonlinear equations was solved using multivariable Newton-Raphson method in which the linearized equations formed require singular-value decomposition and LU decomposition methods for piping networks with

and without secondary lines, respectively. The results of system simulation revealed the best efficiency points during selected part load and full load conditions. When the nominated loads downstream of network reduced to 72%, a pump curve denoted as PC_{Mod} was generated located between upper and lower pump curve limits with six (6) and five (5) number of pumps operating at rated speed, respectively. At full load, higher pump head of 35.5 m for DNModel-01_12 is needed as compared with DNModel-03_12 which requires 23.8 m only. However, the system flow rates reduced to 12.70% and 15.05% for respective distribution network models with and without secondary lines as compared with district cooling plant without Ice TES system [1].

Optimization method

An optimization technique commonly known as exhaustive search method was used to determine the design criteria of district cooling distribution network with Ice TES system by examining a number of combinations of independent variables such as velocity and pressure drop limits that would give minimum overall cost. The objective function is a cost function derived from engineering economics in which comparative cost analyses such as present worth and annual cost pattern methods were used. The cost function variables are the following: (a) initial investment costs for pumps, plate-type heat exchangers, and distribution network, (b) installation costs for item (a), (c) excavation cost for distribution network including backfill and surface restoration, (d) operation and maintenance costs, (e) payroll taxes including taxes for property and insurance, and (f) depreciation cost.

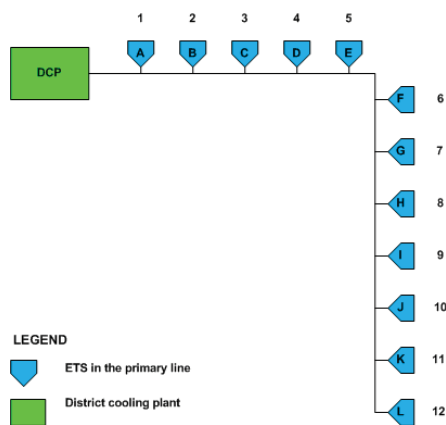


Figure 1. Schematic diagram of distribution network DNModel-01_12

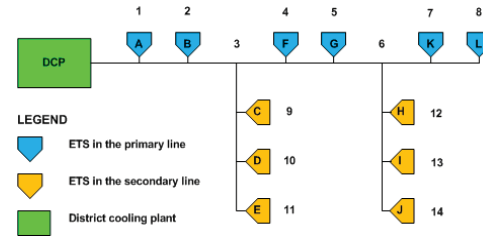


Figure 2. Schematic diagram of distribution network DNModel-03_12

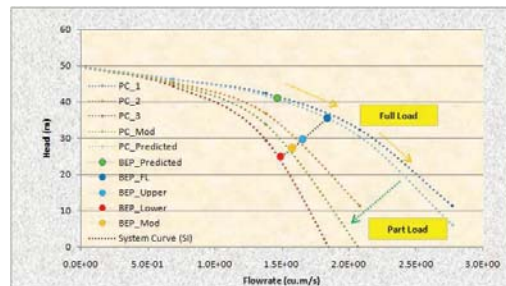


Figure 3. BEPs at part load and full load conditions for DNModel-01_12 with Ice TES system

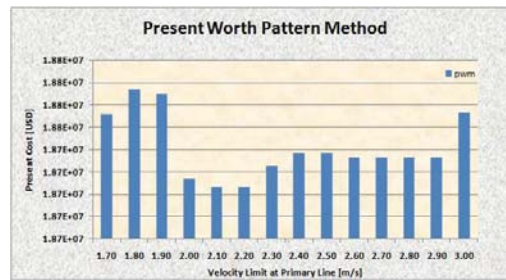


Figure 4. Optimization based on present worth pattern method for DNModel-03_12

Table 1. Nominated cooling loads in each building.

Building ID	Cooling Load (RT)	Building ID	Cooling Load (RT)
Tower A	3,000	Tower G	1,500
Tower B	2,800	Tower H	1,800
Tower C	2,500	Tower I	1,800
Tower D	2,500	Tower J	1,500
Tower E	2,000	Tower K	1,400
Tower F	1,800	Tower L	1,400

References

[1] G.L. Augusto, A.B. Culaba and R.R. Tan, "Identification of design criteria for district cooling distribution network", *Philippine Science Letters*. 6(2), 2013, pp.182-197.

IDENTIFICATION OF DESIGN CRITERIA FOR CHILLER PLANTS DISTRIBUTION NETWORK IN ALABANG TOWN CENTER

Gerardo L. Augusto^{1,2} and Alvin B. Culaba¹

¹Department of Mechanical Engineering, De La Salle University Manila, Philippines

² Fluidnovation Research, Co., Quezon City, Philippines

SUMMARY: The applicability and limitations of the method in identifying the design criteria for chiller plant distribution network in Alabang Town Center (ATC) were investigated. The hydraulic calculation technique, chilled water system simulation and optimization methods developed from previous studies were applied to validate the theoretical results from actual pipe dimensions of the combined Chiller Plant No.1 and Chiller Plant No.2 of ATC. The piping network has constant-volume primary and variable-flow secondary pumping arrangement with temperature difference set-point of 5.56°C. Optimization results for piping network design criteria revealed that minimum overall cost occurred when the velocity limit at primary line was 1.85 m/s and the velocity limits at secondary line and plot take-off both at 3.00 m/s considering a pressure drop limit of 100 Pa/m. Hydraulic calculation results also indicate that it has good agreement with the current piping dimensions of primary and secondary lines of chiller plants entry points in the Existing wing, Cinema area and Entertainment area.

Keywords: Alabang Town Center chiller plants, primary-secondary pumping arrangement, distribution network design criteria, multivariable newton-raphson method, exhaustive search method

INTRODUCTION

In order to validate the results of hydraulic calculation including system simulation and optimization methods developed from previous studies in an actual district cooling system, the distribution network of chiller plants in Alabang Town Center was used as benchmark for fluid flow analysis. Its applicability and limitations when actual chiller plants are analyzed have still to be verified. Hence, an actual investigation is conducted and discussed in this study.

The authors visited the chiller plants in Alabang Town Center in 2013 through the help of Philippine Integrated Energy Solutions, Inc. (PhilEnergy). PhilEnergy is a subsidiary of Ayala Land Inc. which manages the district cooling plants covering the needs of the Ayala Center redevelopment in Makati City, Trinoma and Alabang Town Center. PhilEnergy provided the site development plan including schematic diagram and layouts of chiller plants in ATC. The actual cooling loads, pump curves, pipe lengths and fittings were used as input parameters for the purpose of identifying the piping network design criteria of two (2) chiller plants in Alabang Town Center. Instead of using plate-type heat exchangers, the distribution network is directly connected to air handling units. Calculation results show that it has good agreement with the current piping dimensions of primary and secondary lines of chiller plants entry points in the Existing wing, the Cinema area and the Entertainment area.

MATERIALS AND METHODS

Chiller plants in Alabang Town Center

Alabang Town Center is a shopping mall owned by Ayala Malls located in Muntinlupa, Metro Manila. It has three (3) chiller plants which provide

air conditioning for the Entertainment area, Cinema area, Existing wing, the Garden and Expansion wing of the shopping mall with total chiller capacity of 4,375 ton of refrigeration. Chiller Plant No.1 and Chiller Plant No.3 are located at the ground floor, which serve the Entertainment area and Expansion wing including the Garden, respectively. Chiller Plant No.2 is located on the roof deck in the eastern side of Alabang Town Center, which provides air conditioning for Existing wing and Cinema area. The actual cooling load is approximately 3,050 ton of refrigeration with chilled water supply temperature of 6.7°C and temperature difference set-point of 5.56°C.

Chiller plants distribution network arrangement

Figure 1 illustrates the block diagram of main distribution network of three (3) chiller plants in ATC. The chiller plants are interconnected by a main header which provides chilled water for the Entertainment area, Existing wing including the Cinemas, the Garden and Expansion wing. Chiller Plant No.1 has a constant-volume primary pump which circulates chilled water between the chiller and air handling units. Although, the chiller capacity is 375 ton of refrigeration it operates at part load because the actual cooling load is less than 50%. As it is not practical to operate Chiller Plant No.1 at part load, either Chiller Plant No.2 or Chiller Plant No.3 supplies chilled water in the Entertainment area and the primary pump in Chiller Plant No.1 is used as transfer pump. However, both Chiller Plant No.2 and Chiller Plant No.3 operate at constant-volume primary and variable-flow secondary pumping system with actual cooling loads of 732.88 and 2,156.19 ton of refrigeration, respectively. As it requires larger matrix to solve the system of nonlinear equations, the distribution network for

Chiller Plant No.1 and Chiller Plant No.2 was used as basis for fluid flow analysis.

RESULTS AND DISCUSSION

Hydraulic calculation

The results of system simulation revealed the best efficiency points during selected part load and full load conditions. When the cooling loads downstream of network reduced to 60% with diversity factor of 90%, a pump curve denoted as PC_{Mod} was generated located between upper and lower pump curve limits with two (2) and one (1) number of secondary pumps operating at rated speed, respectively. At full load, the system pump head of Chiller Plant No.2 is 25.4 m only. As expected this value is lower than the overall system pressure drop of all pumps operating at full load in ATC which is ranging from 38.65 m to 42.17 m because Chiller Plant No.3 operation was neglected in the calculation.

Optimization method

Exhaustive search method was used in determining the design criteria of chiller plants distribution network by examining a number of combinations of values of independent variables such as pressure drop and velocity limits at primary line, secondary line and plot take-off that would give minimum overall cost. The objective function is a cost function derived from engineering economics in which comparative cost analyses such as present worth and annual cost pattern methods were used. The cost function variables are the following: (a) initial investment costs for pumps, air-handling units, and distribution network, (b) installation costs for item (a), (c) excavation and surface restoration costs for distribution network if any, (d) operation and maintenance costs, (e) payroll taxes including taxes for property and insurance, and (f) depreciation cost.

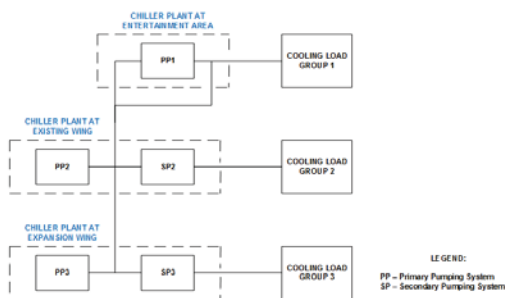


Figure 1. Block diagram of three chiller plants in Alabang Town Center with main header.

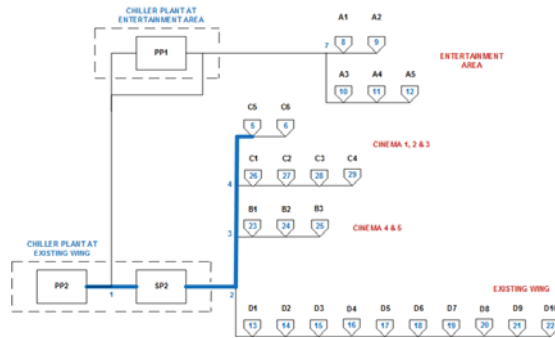


Figure 2. Predicted schematic diagram of the combined Chiller Plant No.1 and Chiller Plant No.2 serving the Existing wing and Entertainment area

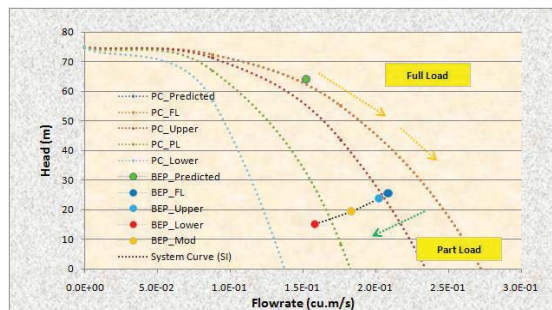


Figure 3. BEPs at part load and full load conditions for Chiller Plant No.2 in Alabang Town Center

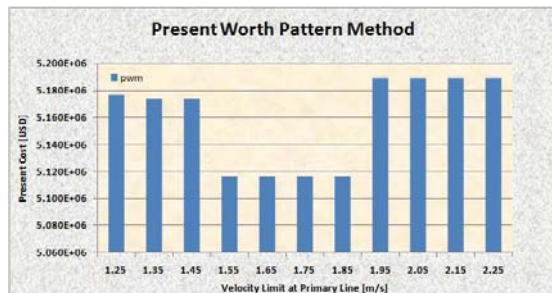


Figure 4. Optimization based on present worth pattern method for Chiller Plants No.1 and No.2 in Alabang Town Center

References

[1] G.L. Augusto, A.B. Culaba and R.R. Tan, "Identification of design criteria for district cooling distribution network", Philippine Science Letters. 6(2), 2013, pp.182-197.

ORGANIC BULK HETEROJUNCTION SOLAR CELLS: PERFORMANCE AND DEGRADATION ANALYSIS

R. P. Tandon¹

¹ Department of Physics & Astrophysics, University of Delhi, Delhi 110007, India

SUMMARY: Remarkable efforts are being made to improve the efficiency and lifetime of organic solar cells. Degradation in organic solar cells still remains a challenging field of research. The present work elaborates on the degradation behavior of solar cells fabricated in the following configuration: ITO/ hole extracting layer /active layer/Al. The cell performance of various device architectures showed lowering of V_{OC} and J_{SC} with time which could be co-related with the shift in energy levels of active layer and work function of Al and ITO electrodes. Theoretical comparison of the experimental results suggested that as time passes, the interfaces start playing a dominant role leading to creation of new interface states, increase in thickness of interface layer, and change in HOMO-LUMO levels of active layer. The conductivity of HEL, PEDOT:PSS, was improved using ethylene glycol and multi walled carbon nanotubes (MWCNT). Though the solar cell efficiency increased due to modified PEDOT:PSS, but similar degradation patterns were observed as compared to pristine solar cell. Degradation of PEDOT:PSS is mainly due to hygroscopic PSS. Therefore, the devices kept in vacuum and nitrogen gas environment showed better stability, i.e., approximately 80%, 50% and 40% fall in initial efficiency, respectively for devices kept in air, vacuum and nitrogen gas. Role of MWCNT in the active layer (P3HT:PCBM) was also studied and it was observed that the cell performance stabilizes in comparison to pristine cell by $\sim 20\%$. Organic solar cells using PEDOT:PSS have shown to degrade at an elevated rate due to the hygroscopic and acidic nature of PEDOT:PSS. Therefore, PEDOT:PSS layer was replaced by V_2O_5 film, grown by thermal evaporation technique. Open circuit voltage as high as 0.8 V was achieved, which is higher than PEDOT:PSS based solar cells.

Keywords: organic solar cells, efficiency, degradation

INTRODUCTION

Photovoltaic devices have been considered as promising technology for energy harvesting [1]. The need of the hour is to increase its efficiency and lifetime for commercial viability [2]. The advantages of organic solar cells (OSC) have triggered interest in developing more efficient and stable devices. Some of these advantages are: their cost effectiveness, ease of fabrication, low processing temperatures, can be deposited onto large flexible substrates, are light weight, and can be modified chemically [3]. Although, a tremendous improvement in power conversion efficiencies has been achieved in the last few years [4], the life time of these devices still remains a challenge.

In the present work, attempts have been made to understand the degradation mechanism in OSC. Focus has been on both increasing the efficiency and lifetime of the devices. The degradation behaviour of six different solar cell device configurations was studied and the performance was strongly found to depend of the device layers. Next, the theoretical analysis showed that the density of states, thickness of layer, mobility and lifetime of charge carriers plays vital role degradation. In order to increase the efficiency, MWCNT was used as an additive separately in the hole extracting layer (HEL) and in the active layer. The degradation of these cells was also studied. Finally, V_2O_5 was used as the HEL to fabricate stable solar cells. Open circuit voltage as high as 0.8 V was achieved, which is higher than PEDOT:PSS based solar cells.

EXPERIMENTAL DETAILS

Typical OSCs of configuration ITO/HEL/P3HT:PCBM/Al were fabricated onto ITO coated glass substrates by spin coating PEDOT:PSS and P3HT:PCBM. For V_2O_5 as the HEL, thermal evaporation in vacuum was used. The aluminum contacts were also deposited using thermal evaporation in vacuum. The PEDOT:PSS layer was annealed for 20 minutes at 120 C. The various MWCNT concentrations used will be subsequently mentioned in the text. Figure 1 shows the schematic diagram of a typical OSC.

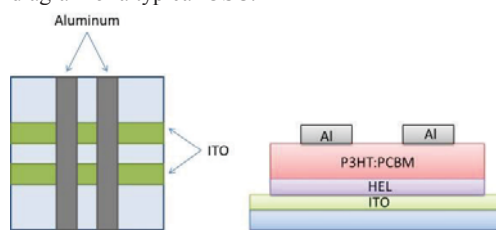


Figure 1. Schematic diagram of an OSC.

The I - V measurements were recorded with Keithley 2400 interfaced with a computer. The devices were illuminated at 100 mW/cm^2 using Photoemission Tech. SS50AAA.

RESULTS AND DISCUSSION

The degradation behaviour of six different solar cell device configurations was investigated. The degradation in these cells was studied up to 300 hours to analyze the effect of different layers on

their performance. It was observed that the deterioration of the cell parameters varied depending upon the architecture of the devices. Various degradation mechanisms are responsible for lowering of V_{OC} and J_{SC} leading to change in polarity with time and their net effect was to change the energy levels of the donor-acceptor composites and to shift the work functions of Al and ITO electrodes. As the device degrades, a situation comes when the direction of carrier collection probability reverses.

The theoretical analysis incorporated the changes taking place at the various interfaces of the solar cell layers. It was found that as time passes the activity at the electrode/polymer junctions become prominent, electrode interfaces deteriorate and interface states start affecting the device performance. Factors such as creation of interface states, increase in their density, increase in thickness of interface layer and change in HOMO-LUMO level of the active layer taken together with time greatly influence the solar cell characteristics and explain aging both for dark and illuminated conditions. The effect of degradation on the mobility and carrier lifetime showed that both mobility and lifetime decrease explaining the degradation behaviour of photovoltaic devices to a large extent.

The MWCNTs dispersed in ethylene glycol have been doped in the hole extracting layer (HEL), i.e. PEDOT:PSS. Doping PEDOT:PSS with ethylene glycol and MWCNT resulted in enhanced conductivity of the hole extracting layer. The efficiency of the cell also increased, however, the degradation mechanism does not change with doping of PEDOT:PSS.

Further investigations were carried out by using MWCNT in the active layer. Enhanced efficiencies were obtained at a concentration of 30 mg/ml of the active layer in chlorobenzene. The active layer, P3HT:PCBM with MWCNT, were studied for degradation and it was found that use of MWCNT stabilizes the cell performance in contrast to pristine solar cells.

Organic solar cells using PEDOT:PSS have shown to degrade at an elevated rate due to the hygroscopic and acidic nature of PEDOT:PSS. Therefore, PEDOT:PSS layer was replaced by V_2O_5 film, grown by thermal evaporation technique. Figure 2 shows the IV characteristics of V_2O_5 based organic solar cells at different thicknesses of the HEL. Open circuit voltage as high as 0.8 V was achieved, which is higher than PEDOT:PSS based solar cells.

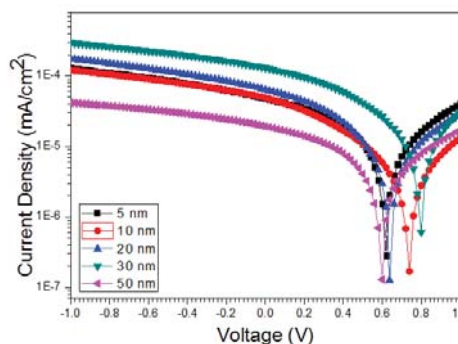


Figure 2. IV characteristics of V_2O_5 based organic solar cells at different thicknesses of the HEL.

CONCLUSION

In order to develop successful technology out of organic semiconductors, it is crucially important to study the stability of these materials and devices. Therefore, the present work gave insight into the degradation mechanisms of organic solar cells. From the studies, it was concluded that the behavior of solar cells is highly dependent on the device architecture. Doping the HEL and active layer increased the efficiency. However, an increased stability was obtained only in the devices with doped active layer. Furthermore, V_2O_5 was studied as a potential replacement to PEDOT:PSS.

ACKNOWLEDGMENT

Author wish to thank Delhi University Research and Development Scheme 2014–2015 for providing financial support (RC/2014/6820).

References

- [1] A. J. Ferguson, J. L. Blackburn, N. Kopidakis, *Materials Letters*, **90**, 115 (2013).
- [2] S. Saleh Ardestani, R. Ajeian, M. N. Badrabadi, M. Tavakkoli, *Solar Energy Materials and Solar Cells*, **111**, 107 (2013).
- [3] O. A. Abdulrazzaq, V. Saini, S. Bourdo, E. Dervishi, S. A. Biris, *Particul. Sci. Technol.* **31**(5) 427-442 (2013).
- [4] T. Kietzke, *Adv. Opt. Electron.* Article ID 40285 15 pages (2007).

INFLUENCING FACTORS OF ENERGY USE OF LOW AND MEDIUM INCOME HOUSEHOLDS IN THAILAND

Preecha Tumm¹, Surapong Chirattananon^{1,2}, Pattana Rakkwamsuk³, Pipat Chaiwiwatworakul^{1,2},
Surawut Chuangchote¹ and Siriluk Chiarakorn³

¹Joint Graduate School of Energy and Environment, King Monkut's University of Technology Thonburi

²Science and Technology Postgraduate Education and Research Development Office, Ministry of Education

³School of Energy Environment and Materials, King Monkut's University of Technology Thonburi

SUMMARY: Energy uses in household sectors of Thailand are great and increasing continuously. Most energy uses are from electricity for lightings, entertainments, amenity categories and other fuels for cooking category such as LPG or charcoal. This research aims to study on housing features, living styles, material uses, lighting conditions, interior thermal environment, and energy uses due to the use of houses of low and middle income earners in Thailand. Household surveys were conducted for the study and preliminary results of the surveys are reported in this study. The survey results show that the change of housing features, and living styles of low income earners from the past lead to increase the use of energy (especially electricity) hugely in the future due to the trends of air conditioner and water heater uses are increasing.

Keywords: household survey, low income housing, tropical housing

INTRODUCTION

Thai vernacular house designs are influenced by local cultures, living styles, climates and local climatological events such as storms and floods. T.Ramasoot and P. Nimsamer (2013) studied on vernacular house designs of riparian community of the central Thailand. A part of the report shows that house designs of the community which usually encounter the flood situation, always design their houses to settle with the situation by constructing a 2-storey houses with durable materials and easy to be repaired such as wood (old houses) or concrete walls (new houses). S. Chirattananon and V. D. Hien (2011) studied on thermal performance of light and massive walls of commercial and residential function of uses. The results indicate that light wall is proper for Thai houses because of absorbed solar radiation during daytime of the light wall is lower, the heat release into the spaces during night time is also lower. Due to such reason, most traditional houses in Thailand were constructed by low mass materials such as wood. The roof is a high pitched roof, rain can flow down faster and also helps on reducing radiant heat through the roof. In the past, basements was raised around 1 m for keeping their agricultural tools and to avoid inundated water in the rainy season. For Thai modern house, configurations of houses and materials of walls are changed because of differences of living styles and local construction materials in local area; family size of Thai people is continuously smaller than the past as reported in [National Statistical Office (2010)], a number of family size is reduced from 3.8 members to 3.1 members from year 2000 to year 2010 while number of households is increased from 15,937,804 to 20,523,470 households respectively. The uses of wooden materials for Thai house construction seem to be very difficult for low and middle income earners because of high prices and legal requirements not to cut them while the concrete

materials are cheaper and easier for finding in the local areas.

The surveys aim to study on design features, living styles, material uses, lighting conditions, interior thermal environment, and energy uses due to the use of houses of low and middle income earners in Thailand. Preliminary results of the surveys are reported in this study.

METHODOLOGY

A field surveys were conducted in 4 main regions of Thailand. Chiang mai, Supan buri, Ubon Ratchathani, and Phuket were selected to be a sample of northern, central, north- eastern and southern Thailand. There were 2 types of the survey sites of this study, NHA houses (houses which were built under a project of National Housing Authority of Thailand and other regional detached houses were selected for field surveys. The duration of the surveys are 2 days for each region, the surveys were conducted and finished in September 2014. A questionnaire and measuring instruments (Figure 1) were prepared to collect design features, living styles, material uses, lighting conditions, energy uses, and interior thermal environment of houses of low and middle income earners in Thailand. The required parameters for thermal comfort assessment were also measured during interviewing; DB temp, Globe temp, Wind velocity, %RH, Light illuminance.



Figure 1. Preparation of instruments of the survey team before conducting the surveys

RESULT AND DISCUSSION

The survey results show that housing features of current houses were changed from the past due to the change of their living style, occupation, family size, and habits. Family size of people was smaller, young people migrated to work in municipal area or other regions while elderly people were left alone in the local area with children. Concrete walls were used to replace wooden walls due to cheaper cost, faster construction, and available in the local market. The trend of electricity use is likely to be continuously increased due to increasing of the demand of air conditioning use which is influenced by poor housing designs and material selections. This situation lead to increase electricity consumption and CO₂ emission from energy uses from this sector and need to be focus as soon as possible.

ACKNOWLEDGMENT

The research work reported in this paper is funded by the Energy and Low Income Tropical Housing project (Grant Ref: EP/L002604/1) and financial support from the Thailand Research Fund through the Royal Golden Jubilee Ph.D. Program (Grant No. PHD/0327/2551) to student's name Mr. Preecha Tammu and advisor's name Prof. Dr. Surapong Chirarattananon is acknowledged.

References

- [1] T. Ramasoot and P. Nimsamer. "Vernacular Houses and Coping Capacity to Impact of Climate Change: A Case Study of Riparian Community in Sena District, Phranakhon Si Ayutthaya Province" 2013.
- [2] S. Chirarattananon and V.D. Hien. "Thermal performance and cost effectiveness of massive walls under Thai climate", *Energy and Buildings*, **43**, 2011, pp. 1655–1662.
- [3] National Statistical Office. Report on the population and household surveys of year 2000 and 2010.

THE ANALYSIS OF THE CYCLICAL IMPACT CHANGES IN THE WORLD, CHINA AND INDIA

Jarmo Vehmas¹, Jari Kaivo-oja¹ and Jyrki Luukkanen¹

¹Finland Futures Research Centre, Turku School of Economics, University of Turku, Finland

SUMMARY: In the paper the authors study key variables of the so-called ImPACT identity, which include four drivers of environmental impact (Im): population (P), affluence (A), intensity of consumption (C), and technology (T). In the empirical analysis, carbon dioxide emissions from fuel combustion (CO₂) represents the environmental impact, and the influencing factors are represented by the amount of population (POP), gross domestic capita per capita (GDP/POP), energy intensity of the national economy (TPES/GDP), and carbon intensity of energy supply (CO₂/TPES), respectively. The authors present annual changes in the ImPACT variables and their comparative analysis in the World, China and India during the time period 1971-2009. They also identify the cyclical nature of annual changes in the ImPACT variables, similar to the Goodwin growth cycle model. In the formation of green growth strategies this kind of empirical finding must be taken seriously into consideration.

Keywords: ImPACT analysis, China, India, the world, global sustainable development

INTRODUCTION

We have known a long time that economic growth, population and technological development are crucial variables when we discuss about sustainability of the world development. The nature of these interactions is highly complex and environmental problems cannot be ascribed to any single cause, such as “growth mania” or “careless technology” or “population explosion” [1]. There are many dynamic interactions between these key variables. An empirical study of these variables of sustainable development can provide some useful information for the planning of sustainable development in the world. In the article we analyze changes in sustainability towards less or more sustainable direction. There are many uncertainties related to climate change and socio-economic dynamics of climate change. Such uncertainties are linked to monitoring system of climate change, cost estimates, ecosystem services and impacts.

METHODOLOGY

In the article one scientific challenge is to analyse these basic issues with empirical basic data. The dynamic relationships of IPAT variables (Impact, Population, Affluence and Technology) is surely a relevant policy issue for global decision-makers and other stakeholders. We can expect that better understanding of the IPAT dynamics can help us to reflect precautionary principle in a better way.

On the basis of our IPAT analysis it is possible to identify extreme economic conditions (zones) and turning points of sustainable development in the global setting and in the country level and inform decision-makers in a better way. We can also note that historically the socio-economic needs to use precautionary principle vary. These equations constitute the basic methodological framework of

our analysis. This kind of methodological approach is very generic and allows comparative sustainability analyses in the global setting. Climate change mitigation may have to focus on greenhouse gases like CO₂ emissions and on the potential role of biomass as a carbon sink, among others. Today the global population is still growing in many developing countries and scaling up the environmental impact. Population issues and growing affluence must be considered when we are discussing about emission reductions.

Climate policy has only very recently had an influence on emissions, and strong political actions like changing energy mix and economic structures are now called for climate change mitigation. Environmental policies in general must cover all the regions and countries related to production and environmental impacts in order to avoid outsourcing of emissions and harmful leakage effects. The key idea of our analysis is that the macro-level drivers affecting changes in emissions can be identified with the ImPACT framework. Statistics for generally known macro-indicators are currently relatively well available for different countries and regions, and the method is extremely transparent, which increases the usability of the methodological framework. Using transparent macro-level figures and a simple top-down approach are also appropriate in evaluating and setting international emission reduction targets. In the basic form of the ImPACT model, the economic intensity of consumption and emission intensity of use are both included in the model. Similar kind of methodological framework has seen to be useful in many other studies [3].

The article is focused on global trends of sustainability in relative terms. We focus at the global level on the world, China and India. So our analysis covers the whole world with these three

major regions. We have selected these regions, because they are going to be in key strategic role in the global climate policy in the future. This kind of global analysis helps us to understand where world development is going nowadays. Our approach can provide realistic situation analyses for global decision-makers.

The analysis we provide in this article is also relevant for sustainable development policy, energy policy and global climate change policy. Our empirical analysis covers the years from 1971-2009, due to some data limitations. This means that we mostly analyze global developments after the first oil crisis period. In this article we shall use a method which is widely used for scientific analyses. The method is based on the IPAT identity. In IPAT identity, the forces of population (P), affluence (A), and technology (T) cause an impact (I). A developed version of IPAT model is the ImPACT model, which we use as a methodological starting point in this article [2].

As we have noted ImPACT model refers to a formula developed to describe the impact of human activity on the environment. This model describes how growing population, affluence, and technology contribute toward our environmental impact. This article is based on this basic ImPACT approach and framework. The classical Kaya identity approach is closely related to this approach [4].

CONCLUSIONS

Our new contribution to previous literature is to present the ImPACT model in such form that we can observe dynamics of sustainability in 4-space mapping framework, which helps us to identify “danger zones” of unsustainable development from less dangerous sustainability zones. In this article we are able to present some interesting observations about “extreme situations” and turning points in the history. Our world scale and country analyses of China and India reveal that historically sometimes they have been close to unsustainability zone (zone D), sometimes they have been in the unsustainability zone/zone C). We can also note that historically the socio-economic conditions of sustainability policy vary in time.

In the article we have studied key variables of the ImPACT identity and annual changes in the logarithmic values of $a + p$ variables and $c + t$ variables. The four ImPACT drivers are population, affluence (economic growth), intensity of use (consumption) and technologist's intensity of emissions. For global policy developments and changes in these critical key variables are very important. In this paper we present key changes in the variables of the ImPACT identity in the world, China and India. We have also presented a comparative regional analysis (China, India and the rest of the world) of the ImPACT variables. Finally, we report identified long-run ImPACT cycles in the

World, in China and in India. In the study various empirical findings concerning global sustainable development processes are presented and reported. Novel results in cycles between affluence-population dimension and consumption-technology dimension are reported. This empirical analysis reveals that the volatility of logarithmic $a + p$ variable is stronger than the volatility of logarithmic $c + t$ variable in the world, China and India. In this paper we have identified *global world scale sustainability cycle, sustainability cycle of China and sustainability cycle of India*. These cycles are having similar kind of logic with Goodwin's growth cycle model but with conventional ImPACT variables. This finding is quite interesting for further scientific research of sustainability challenge [see e.g. 5].

The issue of *sustainability cycle* needs more scientific attention in world politics and development policy. Because we identified very different kinds of cyclical sustainability cycles in the study, our conclusion is that there probably is not linear or simple sustainability path (or so called “sustainability tunnel”) for big countries like China and India. This means that the challenges of global governance include also sustainability management of giant economies like China and India.

Our ImPACT study serves such political needs and the smart shaping of sustainability strategies. Development towards low carbon economy is not linear but cyclical due to the system dynamics and time lags in the global economic system.

ACKNOWLEDGMENT

Funding from the Academy of Finland for the CHEC project is acknowledged by the authors.

References

- [1] P.E. Waggoner and J.H. Ausubel (2002). A framework for sustainability science: A renovated IPAT Identity, *Proceedings of the National Academy of Sciences*, **99**(12), pp. 7860-7865.
- [2] P.C. Schulze, “I = PBAT”. *Ecological Economics*, **40**, 2002, pp. 149–150.
- [3] L. Saikku, “Consumers and macro-level forces behind CO₂ emission development”, *Progress in Industrial Ecology*, **6**(4), 2009, pp. 371–386.
- [4] F.A.B. Meyerson, “Population, carbon emissions, and global warming: the forgotten relationship at Kyoto”, *Population and Development Review*, **24**, 1998, pp. 115–130.
- [5] P. Skott, “Effective demand, class struggle and cyclical growth”, *International Economic Review*, **30**(1), 1989, pp. 231-247.

Posters

OPTIMIZATION OF FACTORS AFFECTING ACID HYDROLYSIS OF WATER-HYACINTH STEM (EICHHORNIA)

Sakchai Pattra¹ and Sureewan Sittijunda²

¹Community Public Health Program, Faculty of Arts and Science, Chaiyaphum Rajabhat University, Thailand

²Biotechnology Program, Faculty of Technology, Udon Thani Rajabhat University, Thailand

SUMMARY: Response surface methodology (RSM) with central composite design (CCD) was applied to optimize hydrolysis conditions of water-hyacinth stem (WHS). Firstly, the effects of reaction time (h), % diluted H₂SO₄ concentration (v/v) and shaking speed (rpm) for hydrolyze WHS were investigated. The optimum condition for WHS hydrolysis was reaction time of 7.73 h, H₂SO₄ concentration of 1.31 % (v/v) and stirring speed of 264.41 rpm in which a maximum total sugar of 13 g/L was obtained. Secondly, the hydrolysate WHS obtained from the optimum hydrolysis condition was further used as the substrate for hydrogen production by heat-treated anaerobic sludge. Results showed that the maximum HP of 182.7 mmol H₂/L was obtained.

Keywords: dilute acid hydrolysis; hydrogen production; water-hyacinth; response surface methodology (RSM); central composite design (CCD)

INTRODUCTION

Biohydrogen is promising alternative fuel to replace fossil fuels due to the increasing of renewable energy, damaging of climate and environmental, depletion of fossil or petroleum fuel. Dark fermentative of hydrogen production process is more attractive due to its sustainable and less energy intensive compared to thermo-chemical and electro-chemical processes [1]. Biohydrogen is conventionally produced from substrate containing high amount of carbohydrates such as sugarcane, starch, corn, etc [1, 2]. However, use of these substrates significantly increases the cost of biohydrogen. Therefore, interest in second generation processes, i.e. processes utilizing lignocellulosic materials such as sugarcane bagasse, straw and corn stover has emerged.

Water-hyacinth (*Eichhornia crassipes*), is a free floating aquatic weed, which is a widely prevalent aquatic weed in Thailand [3, 4], constitutes a potential biomass resource for various uses [5]. Daily average water-hyacinth biomass productivity is 0.26 ton of dry biomass per hectare in all seasons [5]. Due to its fast growth and the robustness of its seeds, water-hyacinth has caused many problems in the whole river area, i.e. a reduction of fish [6], physical interference with fishing. The most common use of water-hyacinth is raw material for composting and substrate for biogas [7] and bioethanol production [5, 8]. Water-hyacinth consists of three main fractions i.e., cellulose, hemicellulose and lignin. It has a high content of hemicellulose (30-55% of dry weight), which further pretreated and obtained hemicellulosic sugars as a by-product [9]. Dilute acid treatment of hemicellulose fraction in water-hyacinth yields a solution containing mainly xylose and glucose [10]. Glucose and xylose were reported as a substrate for producing hydrogen by various types of microorganisms [10,11] and mixed culture [12,13], respectively.

In this study, RSM with CCD was used to optimization of hydrolysis condition of WHS at

room temperature in order to obtain a suitable WHS hydrolysate for producing hydrogen. The secondly, hydrogen production from WHS was investigate.

MATERIALS AND METHODS

Anaerobic seed sludge and inoculum preparation

The anaerobic granules obtained from upflow anaerobic sludge blanket (UASB) reactor were used as seed inoculum for hydrogen production. This UASB reactor was used to produce biogas from wastewater of cassava starch production process (Kalasin province, Thailand). The UASB granules were boiled at 100 °C for 2 h to inactivate the hydrogenotrophic methanogens. The hydrogen producing bacteria in UASB granules were enriched.

Water-hyacinth pretreatment

Fresh WHS was collected from Lopburi River (Lopburi province, Thailand) and washed with tap water to remove adhering dirt. Prior to use, WHS was chopped in small pieces, air dried and milled before storing at room temperature. WHS consists of (all in % (w/ wet weight)): cellulose, 27.55±0.81; hemicelluloses, 39.83±2.04; lignin, and 14.96±0.17.

Optimization dilute acid hydrolysis of WHS for total sugar production

The dried powder of WHS approximately 15 g dry weight were added into the 250 ml flask containing 150 ml of dilute H₂SO₄ (solid (g dry weight) to liquid (mL) ratio of 1:10) and incubated in the incubator shaker at room temperature. CCD was applied to find out the effects of these variables. Investigated variables were reaction time (h), H₂SO₄ concentration (v/v) and shaking speed (rpm). After hydrolysis, a solid residue was separated from the liquid phase (hydrolysate) by filtration through a thin layer cloth. Prior to being used as the substrate for hydrogen production, the hydrolysate was inhibitor removal was conducted as previous described in Pattra et al [14].

Analytical method

Hydrogen content in biogas compositions were determined by GC (Shimadzu 2014, Japan) equipped with a thermal conductivity detector (TCD) and a 2 m stainless column packed with Unibeads C (60/80 mesh). The GC-TCD condition was set according to Saraphirom and Reungsang [15].

RESULTS AND DISCUSSION

Optimization of hydrolysis reaction time (h), % of diluted H₂SO₄ concentration (v/v) and shaking speed (rpm) for hydrolyze of WHS on total sugar and inhibitor concentration

RSM with CCD was used to optimize the hydrolysis condition of WHS. Our results showed that the increase in H₂SO₄ concentration, reaction time and the shaking speed to the optimum level increased the total sugar concentration. An increase in acid concentration, reaction time and shaking speed in the acid pretreatment provides strong or complete reaction for the solubilization of the lignocellulosic material components leading to an increase in the total sugar concentration in the hydrolysate [4–6, 16]. However, a further increase in the H₂SO₄ concentration and reaction time resulted in a decrease in total sugar concentration. A long reaction time and high acid concentration might result in the secondary decomposition of the sugars to other derivatives such as hydroxymethyl furfural, formic acid, and levulinic acid [4–6, 16]. It's could result in the reduction of sugar concentrations in the hydrolysate.

Results from regression analysis indicated that the optimum acid hydrolysis condition was 7.73 h of reaction time, 1.31 % (v/v) of H₂SO₄ concentration and 264.41 rpm of stirring speed. The maximum total sugar of 13 g-total sugar/L was obtained at these conditions. At these conditions, the inhibitors include furfural and acetic acid was quite low (data not show). Then the hydrolysate obtained from these optimize conditions was further used as the substrate in the biohydrogen production experiment.

CONCLUSIONS

The optimum condition for WHS hydrolysis was reaction time of 7.73 h, H₂SO₄ concentration of 1.31 % (v/v) and stirring speed of 264.41 rpm in which a maximum total sugar of 13 g/L was obtained. A maximum HP of 182.7 mmol H₂/L was obtained from hydrolyzed of WHS. The total energy generated from the fermentative of WHS hydrolysate was 51 kJ.

ACKNOWLEDGEMENT

Authors would like to express their sincere gratitude to the Research Group for Development of Microbial Hydrogen Production Process from Biomass for the financial support of this work.

References

[1] LK. Kapdan and F. Kargi, "Bio-hydrogen

production from waste materials." *Enzyme Microbial Technol.* **38**, 2006, pp.569–582.

[2] DB. Levin, L. Pitt and M. Love, "Biohydrogen production: prospects and limitations to practical application." *Int. J Hydrogen Energy.* **29**(2), 2004, pp.173–185.

[3] C. Polprasert, N. Kongsricharoern and W. Kanjanaprapin, "Production of Feed and Fertilizer From Water Hyacinth Plants in the Tropics." *Waste Manag Res.* **12**, 1994, pp. 3–11.

[4] J. Mahujchariyawong and S. Ikeda. "Modelling of environmental phytoremediation in eutrophic river-the case of water hyacinth harvest in Tha-chin River, Thailand." *Ecol. Model.* **142**, 2001, pp.121–134.

[5] JN. Nigam. "Bioconversion of water-hyacinth (*Eichhornia crassipes*) hemicellulose acid hydrolysate to motor fuel ethanol by xylose-fermenting yeast." *J Biotechnol.* **97**, 2002, pp. 107–116.

[6] CC. Gunnarsson and CM. Petersen. "Water hyacinths as a resource in agriculture and energy production: A literature review." *Waste Management.* **27**, 2007, pp.117–129.

[7] AM. Abdelhamid and AA. Gabr. "Evaluation of water hyacinth as feed for ruminants". *Archives of Animal Nutrition.* **41**, 1991, pp. 754–756.

[8] HL. Chin, ZS. Chen and CP Chou, "Fed-batch operation using *Clostridium acetobutylicum* suspension cultures as biocatalyst for enhancing hydrogen production." *Biotechnol Prog.* **19**, 2003, pp. 383–388.

[9] A. Kumar, LK. Singh and S. Ghosh, "Bioconversion of lignocellulosic fraction of water-hyacinth (*Eichhornia crassipes*) hemicellulose acid hydrolysate to ethanol by *Pichia stipitis*." *Bioresour Technol.* **100**, 2009, pp. 3293–3297.

[10] H. Yokoi, Y. Maeda, J. Hirose, S. Hayashi and Y. Takasaki. "Hydrogen production by immobilized cell of *Clostridium butyricum* on porous glass beads." *Biotechnol Techniques.* **11**, 1997, pp. 431–433.

[11] Y. Mu, X.J. Zheng and H.Q. Yu. "Determining optimum conditions for hydrogen production from glucose by an anaerobic culture using response surface methodology (RSM)." *Int. J Hydrogen Energy.* **34**, 2009, pp. 7959–7963.

[12] Y. Mu, X.J. Zheng, H.Q. Yu and R.F. Zhu, "Biological hydrogen production by anaerobic sludge at various temperature." *Int. J Hydrogen Energy.* **31**, 2006, pp. 780–785.

[13] CC. Gunnarsson and CM. Petersen. "Water hyacinths as a resource in agriculture and energy production: A literature review." *Waste Management.* **27**, 2007, pp. 117–129.

[14] S. Pattra, S. Sangyoka, M. Boonmee and A. Reungsang, "Bio-hydrogen production from the fermentation of sugarcane bagasse hydrolysate by *Clostridium butyricum*." *Int J Hydrogen Energy.* **33**, 2008, pp. 5256–5265.

[15] P. Saraphirom and A. Reungsang. "Optimization of biohydrogen production from sweet sorghum syrup using statistical methods." *Int J Hydrogen Energy.* **34**, 2010, pp. 3435–3444.

[16] C. Xiong, W. Jinhua and L. Dongsheng, "Optimization of solid-state medium for the production of inulinase by *Cluyveromyces S120* using response surface methodology." *Biochem Eng J.* **34**, 2007, pp. 179–184.

BIOHYDROGEN AND BIOMETHANE PRODUCTION FROM CO-DIGESTION OF PALM OIL MILL EFFLUENT WITH SOLID RESIDUES BY TWO-STAGE SOLID STAGE ANAEROBIC DIGESTION PROCESS

Wantanasak Suksong¹, Prawit Kongjan² and Sompong O-Thong^{1,3}.

¹Biotechnology Program, Faculty of Science, Thaksin University, Thailand

²Department of Science, Faculty of Science and Technology, Thailand

³Microbial Resource Management Research Unit, Faculty of Science, Thaksin University, Thailand

SUMMARY: Hydrogen and methane production from co-digestion of palm oil mill effluent (POME) with empty fruit bunches (EFB) and decanter cake (DC) by two-stage solid stage anaerobic digestion process. The first stage co-digestion of DC 1:5POME and EFB1:5POME could generate a high hydrogen production 16.52, 16.26 ml H₂/gVS respectively. The effluent from the hydrogen production was further converted to methane in the second stage. The methane production of DC 1:5POME 391.62 mlCH₄/gVS and EFB1:5POME 240.65 mlCH₄/gVS. The hydrogen and methane content in biogas was 25.33% and 65.21% respectively. The two-stage solid stage anaerobic digestion process can be removal efficiently of cellulose 57-59%, hemicelluloses 35-40% and lignin 16-27%. Result obtained make practical use for the development of two-stage anaerobic digestion process providing hydrogen and methane co-production from palm oil waste residues.

Keywords: Hydrogen, methane, palm oil mill effluent, empty fruit bunches, decanter cake

INTRODUCTION

Palm oil mills produce significant quantities of wastes such as palm oil mill effluent (POME), empty fruit bunches (EFB) and decanter cake (DC). These wastes could cause environmental impact and lifestyle qualities in nearby communities[1]. Currently, most of palm oil mill plants use POME as feedstock for biogas production. DC and EFB has high content of organic matter and has potential to be used for biogas production. However, for high solid content wastes, such as agricultural crop straws and municipal solid wastes, liquid AD is not suitable solid biomass due to the high consumption of water and large volume of digesters required to treat certain amount of feedstock [2]. Two-stage anaerobic digestion for hydrogen and methane production has now emerged as an attractive and promising process. In this process, two separate conditions are connected in series, separating acidogenesis and methanogenesis [3]. Therefore, this study aimed to determine the biohydrogen and biomethane potential from solid state anaerobic co-digestion of POME with DC and EFB for two-stage hydrogen and methane.

MATERIAL AND METHOD

Hydrogen and methane co-production from solid state co-digestion of palm oil mill effluent with industrial residues was examined using a two-stage process of anaerobic digestion. The hydrogen stage was operated in batch test under a initial pH 5.5 and a temperature of (60°C). Subsequently, hydrogen effluent was investigated for methane production in second under initial pH at 7 and a temperature of (60°C).The two stage batch fermentation system including H₂ fermentation in the first stage and CH₄ fermentation in the second stage was set up in 500 mL serum bottles with a working volume of 200 mL. The solid-state anaerobic digestion tests were

conducted at 12-30% total solids (TS) content using F/M ratio of H₂ was 4.0 and 1.5 for CH₄ fermentation volatile suspended solid (VSS) of the H₂ and CH₄ inoculums were 0.25, 3.21(% of VSS) respectively. The system was flushed with nitrogen gas to generate anaerobic conditions. During the fermentation experiment, total gas volume and composition were periodically monitored by gas counters and gas chromatography, respectively. EFB and DC were ground in a blender to particles sizes of 0.5 mm and drying at 90 °c for 24 h. The characteristics and concentration of tested substrates are shown in table 1.

Table 1. The chemical characteristics of POME, EFB and DC

Characteristics	Characteristics		
	POME	EFB	DC
Total solid %(w/w)	58.79	97.48	99.16
Volatile solid %(w/w)	48.9	83.06	80.74
Cellulose%	4.2	49.65	32.78
COD (g/L)	44.72	-	-
TKN (mg/kg)	20.77	8.18	31.30
TVFA(g/L)	3.66	-	-
Carbohydrates(g/kg)	50.00	29.67	8.00
Fat Oil and Grease(mg/L)	1154.50	-	-

RESULT AND DISCUSSION

In the first stage, the maximum hydrogen yield was 16.26-16.52 ml H₂/gVS achieved from co-digestion DC with POME at mixing ratio of 1:5 and co-digestion of EFB with POME at mixing ratio of 1:5 (Table 2). The maximum methane yield in the second stage was 391.62 ml CH₄/gVS from co-digestion of DC with POME at mixing ratio of 1:5. The maximum methane yield in the second

stage was 240.65 ml CH₄/gVS from co-digestion of EFB with POME at mixing ratio of 1:5. The cumulative of hydrogen and methane are shown in Fig 1. The hydrogen and methane content in biogas was 25.33% and 65.21%, respectively. The celluloses, hemicelluloses and lignin removal efficiency are summarized in Table 2, 3. The effluent characteristics in the two stage anaerobic digestion process are shown in Table 4. Result obtained make practical use for the development of two-stage anaerobic digestion process providing hydrogen and methane co-production from palm oil waste residues. This technology can be implemented at large scale biogas plants improving economical and ecological characteristics of the overall process.

Table 2. The yield of hydrogen and methane

Ratio	Initial VS (g/L)	Yield	
		H ₂ (mLH ₂ /gVS)	CH ₄ (mLCH ₄ /gVS)
EFB 1:5 POME	60	16.26	240.65
EFB 1:2 POME	90	14.08	132.62
EFB 1:1 POME	125	3.62	126.97
EFB 2:1 POME	150	1.26	95.95
DC 1:5 POME	60	16.52	391.62
DC 1:2 POME	90	15.56	233.05
DC 1:1 POME	125	8.57	210.14
DC 2:1 POME	150	5.22	173.82

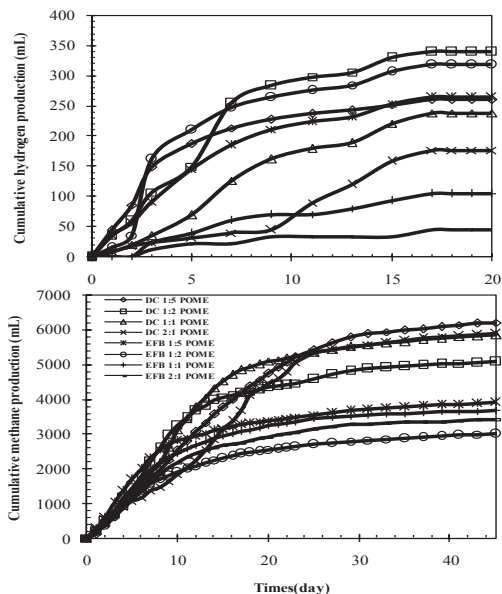


Figure 1. The cumulative of hydrogen and methane in two-stage solid stage anaerobic digestion process

Table 3. The removal efficiency of celluloses, hemicelluloses and lignin.

Ratio	% Removal efficiency		
	celluloses	hemicelluloses	lignin
EFB 1:5 POME	59.47	35.64	16.25
EFB 1:2 POME	51.66	32.53	18.66
EFB 1:1 POME	12.13	31.97	29.7
EFB 2:1 POME	0.61	23.18	14.79
DC 1:5 POME	57.60	40.98	27.21
DC 1:2 POME	41.17	39.72	22.86
DC 1:1 POME	39.12	23.88	10.7
DC 2:1 POME	22.42	12.57	3.98

Table 4. The effluent characteristics in the two stage anaerobic digestion process.

Characteristics	DC1:5POME	EFB1:5POME
pH	8.09	7.96
Total solid %(w/v)	5.43	6.1
Volatile solid%(w/v)	2.07	2.4
Alkalinity(CaCO ₃ :g/L)	28.5	13.8
COD (g/L)	3.79	2.18
TVFA (mg/L)	1,000	900
Carbohydrates (g/L)	1.3	2.13

ACKNOWLEDGMENT

We would like to thank the Microbial Resource Management Research Unit, Faculty of Science, Thaksin University.

References

- [1] A. Yahya, P.C. Sye, T.A. Ishola and H. Suryanto. "Effect of adding palm oil mill decanter cake slurry with regular turning operation on the composting process and quality of compost from oil palm empty fruit bunches", *Bioresource Technology*, **101**, 2010, pp.8736-8741.
- [2] S. O-Thong, K. Boe and I. Angelidaki. "Thermophilic anaerobic co-digestion of oil palm empty fruit bunches with palm oil mill effluent for efficient biogas production", *Applied Energy*, **93**, 2012, pp.648-654.
- [3] P. Kongjan, S. O-Thong and I. Angelidaki. "Hydrogen and methane production from desugared molasses using a two-stage thermophilic anaerobic process", *Engineering in Life Sciences*, **13**, 2013, pp.118-125.

HYDROGEN AND METHANE PRODUCTION FROM STARCH PROCESSING WASTEWATER BY THERMOPHILIC TWO-STAGE ANAEROBIC DIGESTION

Peerawat Khongkliang¹, Prawit Kongjan² and Sompong O-Thong^{1,3}

¹Biotechnology Program, Faculty of Science, Thaksin University, Thailand

²Microbial Resource Management Research Unit, Faculty of Science, Thaksin University, Thailand

³Department of Biology, Faculty of Science, Thaksin University, Thailand

SUMMARY: This two-stage thermophilic fermentation and mesophilic methanogenic process for hydrogen and methane production from wastewater of Cassava Rice and Corn starch at different concentration (5, 10 and 15 g/L). The hydrogen production from cassava starch at concentration of 5 g/L gave the highest hydrogen yield and followed by cassava starch at a concentration 10 g/L, rice starch at concentrations of 15 g/L. The hydrogen and methane yields from cassava starch processing wastewater by two-stage was 81.5 L H₂ kgCOD⁻¹ and 310.5 L CH₄ kgCOD⁻¹, respectively with total energy yield of 13363 kJ kgCOD⁻¹. Mixed hydrogen and methane (biohythane) production was 9.51 L biogas l⁻¹ with containing of 55% CH₄, 11% H₂ and 34% CO₂.

Keywords: biohydrogen, biomethane, biohythane

INTRODUCTION

Renewable and clean energy sources have been sought to be a substitute for fossil fuels that pose environmentally negative impacts. In the other hand, the two-stage anaerobic digestion (AD) process has often been reported as a viable way to produce biohydrogen and biomethane from a wide range of organic materials. [1] Much of the waste is carried in water and is a product of food processing usually having high chemical oxygen demand (COD) values. Food processing wastewater mostly contained starch because starch is one of the major components in many agricultural products and biopolymer as well as the most abundant energy storage reserve carbohydrate in plants. This work aims to investigate hydrogen production and methane of cassava, rice cone starch and energy recovery from thermophilic two-stage anaerobic digestion

MATERIAL AND METHODS

The BHP and BMP of POME were identified in batch assays under thermophilic conditions and mesophilic conditions, as described previously by Giordano et al. (2011). [2] The synthetic wastewater from Cassava, Rice and Corn starch was prepared according to O-Thong et al. (2011) [3] with different concentrations (5, 10 and 15 g/L). The two-stage batch thermophilic fermentation of starch processing wastewater was carried out in 500 mL serum bottle with a working volume of 200 mL. 160 mL of wastewater and 40 mL of inoculums was added into serum bottles in hydrogen fermentation in the first stage. The headspace was replaced with nitrogen gas and incubated for 4 days. When the biological hydrogen production ceased, 80 mL of methane inoculum was added into 120 mL hydrogen effluent and incubated at mesophilic condition for 45 days in order to evaluate the CH₄ production in the second stage. The reactors were manually mixed every day during the first 7 days and every 2 days for the rest of the experimental duration and then maintained at static conditions. Biogas production was determined

through the use of the water replacement method. [4] Biogas composition in the headspace of the vials was monitored by GC-TCD. The gas produced by the negative control bottles with inoculum was subtracted from the actual gas produced of each treatment. Polymerase chain reaction-denaturing gradient gel electrophoresis (PCR-DGGE) [5] was used to study microbial community structure in the hydrogen production stage methane production stage as pervious described by Kongjan et al. (2010). [6] Most of the bands were excised from the gel and re-amplified. After re-amplification, PCR products were purified and sequenced by Macrogen Inc. (Seoul, Korea). Closest matches for partial 16S rRNA gene sequences were identified by database searches in Gene Bank using BLAST. [7]

RESULTS AND DISCUSSION

A two-stage thermophilic fermentation and mesophilic methanogenic process for hydrogen and methane production from starch processing wastewater was investigated. The biohydrogen and biomethane potential from cassava starch processing wastewater were 68.3-81.5 L H₂ kgCOD⁻¹ and 250.3-310.5 L CH₄ kgCOD⁻¹, respectively. The biohydrogen and biomethane potential from corn starch processing wastewater were 64.2-72.8 L H₂ kgCOD⁻¹ and 261.4-289.9 L CH₄ kgCOD⁻¹, respectively. The biohydrogen and biomethane potential from rice starch processing wastewater were 48.2-79.8 L H₂ kgCOD⁻¹ and 280-288 L CH₄ kgCOD⁻¹, respectively. The hydrogen production from cassava starch at concentration of 5 g/L gave the highest hydrogen yield and followed by cassava starch at a concentration 10 g/L, rice starch at concentrations of 15 g/L (Table 1,2). The COD removal of starch processing wastewater from two-stage hydrogen and methane production was 46.7-88.3%. Cassava starch processing wastewater shown the best hydrogen and methane production. The hydrogen and methane yields from cassava

starch processing wastewater by two-stage was 81.5 L H₂ kgCOD⁻¹ and 310.5 L CH₄ kgCOD⁻¹, respectively with total energy yield of 13363 kJ kgCOD⁻¹. Mixed hydrogen and methane (biohythane) production was 9.51 L biogas l⁻¹ with containing of 55% CH₄, 10% H₂ and 35% CO₂. Hydrogen reactor

was dominated with hydrogen producing bacteria of *Thermoanaerobacterium thermosaccharolyticum*, while acetoclastic *Methanoculleus* sp. was the dominant methanogen in methane reactor. Two-stage process for biohythane production could be efficiently for energy recovery from starch processing wastewater.

Table1. Hydrogen production from cassava corn rice processing wastewater at difference starch concentration

Starch concentration (g/L)	Input (gCOD)	Remain (gCOD)	Consumed (gCOD)	Removal (%)	H ₂ yield (LH ₂ kgCOD ⁻¹)	Initial pH	Final pH	H ₂ production (LH ₂ L _{substrate} ⁻¹)	
Cassava	5	34.5	9.4	25.1	72.8	81.5	6.48	6.15	0.4
	10	39.7	11.8	27.9	70.3	81.2	6.32	5.74	0.9
	15	44.9	15.9	29.0	64.6	68.3	6.33	5.85	1.1
Corn	5	34.5	9.4	25.1	72.8	74.3	6.32	5.83	0.4
	10	39.3	11.9	27.4	69.7	69.2	6.42	5.83	0.7
	15	44.4	15.9	28.5	64.2	48.8	6.30	5.78	0.7
Rice	5	34.0	9.8	24.2	71.2	79.8	6.41	5.68	0.4
	10	38.7	12.3	26.4	68.2	48.2	6.31	5.91	0.5
	15	30.6	16.3	14.3	46.7	72.0	6.28	5.25	1.1

Table 2. Methane production from hydrogen effluent of cassava corn rice processing wastewater at difference starch concentration

Starch concentration (g/L)	Input (gCOD)	Remain (gCOD)	Consumed (gCOD)	Removal (%)	CH ₄ yield (LCH ₄ KgCOD ⁻¹)	Initial pH	Final pH	CH ₄ production (LCH ₄ L _{substrate} ⁻¹)	
Cassava	5	9.4	2.3	7.1	75.5	310.5	7.44	7.58	2.7
	10	11.8	2.4	9.4	79.7	303.7	7.33	7.62	3.4
	15	15.9	2.4	13.1	84.9	250.3	7.47	7.65	3.9
Corn	5	9.4	2.4	7.0	74.5	289.9	7.40	7.60	2.6
	10	11.9	2.5	9.4	78.9	308.0	7.34	7.64	3.4
	15	15.9	2.4	13.5	84.9	261.4	7.46	7.62	4.2
Rice	5	9.8	2.2	7.6	77.6	280.3	7.52	7.60	2.6
	10	12.3	2.0	10.3	83.7	288.7	7.53	7.63	3.6
	15	16.3	1.9	14.4	88.3	287.2	7.10	7.66	4.2

ACKNOWLEDGEMENT

I would like to thank Research and Development Institute Thaksin University (RDITSU) for financial supports.

Reference

- [1] A. Schievano, A. Tenca, S. Lonati, E. Manzini and F. Adan. "Can two-stage instead of one-stage anaerobic digestion really increase energy recovery from biomass". *Applied Energy*. **124**, 2014, pp.335-342.
- [2] A. Giordano, C. Cantu and A. Spagni. "Monitoring the biochemical hydrogen and methane potential of the two-stage dark-fermentative process". *Bioresource Technol.* **102**, 2011, pp.4474-79.
- [3] S. O-Thong, A. Hniman, P. Prasertsan and T. Imai. "Biohydrogen production from cassava starch processing wastewater by thermophilic mixed cultures". *International Journal of Hydrogen Energy*, **36(5)**, 2011, pp.3409-3416.

- [4] WF. Owen, DC. Struckey, JB. Healy and PL. Mccarty. "Bioassay for monitoring bio- chemical methane potential and anaerobic toxicity". *Water Research*, **13**, 1979, pp.485-92.
- [5] G. Muyzer and K. Smalla. "Application of denaturing gradient gel electrophoresis (DGGE) and temperature gradient gel electrophoresis (TGGE) in microbial ecology". *Antonie Van Leeuwenhoek*, **73**, 1998, pp.127-41.
- [6] P. Kongjan, S. O-Thong and I. Angelidaki. "Performance and microbial community analysis of two-stage process with extreme thermophilic hydrogen and thermophilic methane production from wheat straw hydrolysate". *Bioresource technology*. 102(5), 2011, pp. 4028-4035.
- [7] SF. Altschul, TL. Madden, AA. Schffer, J. Zhang, Z. Zhang, W. Miller, J. David and DJ. Lipman. "Gapped BLAST and PSI-BLAST: a new generation of protein database search programs". *Nucleic Acids Res.* **25**, 1997, pp. 389-402.

FACTORS AFFECTING ON PROCESS STABILITY OF CONTINUOUS HYDROGEN PRODUCTION FROM PALM OIL MILL EFFLUENT UNDER THERMOPHILIC CONDITION

Chonticha Mamimin^{1,2}, Suwarin Senbat³, Chaisit Niyasom³ and Sompong O-Thong^{2,3}

¹Biotechnology Program, Faculty of Science, Thaksin University, Thailand

²Microbial Resource Management Research Unit, Faculty of Science, Thaksin University, Thailand

³Department of Biology, Faculty of Science, Thaksin University, Thailand

SUMMARY: This study examined the effect of organic loading rate (OLR) temperature and continuous feeding of continuous hydrogen production from palm oil mill effluent (POME). Modified POME was supplemented with sugar at concentration of 5, 10 and 15 g l⁻¹ corresponding to OLR of 58, 63, 68 and 73 g l⁻¹. The hydrogen production at steady state were 241 ± 20, 3431 ± 52, 4138 ± 51 and 3712 ± 52 ml-H₂ l-POME⁻¹, respectively. The feed of continuous hydrogen production reactor were very from 1, 0.5 and 0 l d⁻¹ with hydrogen production at steady state of 1941 ± 107, 808 ± 78 and 0 ml-H₂ l-POME⁻¹, respectively. The hydrogen can be produce to stable within 12 day after feeding POME in to the reactor. Effect of temperature on continuous hydrogen production were study under thermophilic (60 °C) and mesophilic condition (room temperature) with hydrogen production of 2494 ± 196 and 15 ± 3 ml-H₂ l-POME⁻¹, respectively. Hydrogen production at 60 °C was stable within 8 day.

Keywords: continuous hydrogen, POME, thermophilic and mesophilic hydrogen, factor affecting on hydrogen

INTRODUCTION

Currently, development of biofuels as replacements for non-renewable fossil fuels by biological process is more intensive study. Among the various processes, hydrogen is an promising future energy carrier due to its potentially higher efficiency of conversion to usable power, low generation of pollutants and high energy density. There are a variety of technologies for biological hydrogen production, dark fermentation from organic waste has been attracting attention as environmentally friendly process and high production rate. The microbial fermentation process can utilize carbohydrate-rich materials from industry waste such as palm oil mill effluent (POME) for hydrogen gas production. High carbohydrate content in form of simple sugars, starch and cellulose makes the POME a potential feedstock for hydrogen production. Hydrogen yield from microbial fermentation of palm oil mill effluent was 115 ml H₂ gCOD⁻¹ [1].

The anaerobic sequencing batch reactor (ASBR), were developed to better handle high-suspended solids in wastewater. ASBRs are particularly useful for high solid slurry like POME. O-Thong et al. [2] obtained the hydrogen production rate of 12.12 mmol-H₂ l⁻¹h⁻¹ by *Thermoanaerobacterium thermosaccharolyticum* PSU-2 under thermophilic condition (60°C) at optimal values of OLR of 60 gCOD l⁻¹d⁻¹ in ASBR reactor. However, if the reactor is overloaded, the performance of the reactor turns down. Optimization of the operational conditions of biological reactors could also help improve hydrogen production. The following factors; organic loading rate (OLR) temperature and continuous feeding should be considered to achieve successful hydrogen production from POME.

Therefore, the main objective of this

investigation is to assess the effects of organic loading rate (OLR) temperature and continuous feeding on process stability of continuous hydrogen production from POME in ASBR reactors.

METHODOLOGY

Sludge from palm oil mill wastewater treatment plant was enriched in basal anaerobic (BA) medium with sucrose as carbon source. The enriched sludge was incubated at 60 °C and then centrifuged and re-suspend in POME for use as hydrogen inoculum. Modified POME was supplemented with iron, nitrogen and phosphorus and used as substrate. The pH was adjusted to 5.5 by NaHCO₃ before being fed to the ASBR reactor. Experimental setup consists of feed bottle, feed pump, reactor, effluent bottle and gas meter. The 2.0 l ASBR reactor was operating at 60 °C, pH of 5.5, 2 day of HRT and 58 g l⁻¹ of OLR.

The first part is the effect of OLR on process stability of hydrogen production, modified POME was supplemented with sugar at concentration of 5, 10 and 15 g l⁻¹ corresponding to OLR of 58, 63, 68 and 73 g l⁻¹. The steady-state condition was reach when hydrogen gas content, biogas volume and the volatile fatty acids (VFA) concentration in the effluent are stable (less than 10% variation) for a week. The second part is the effect of continuous feeding on process stability of hydrogen production and strategy of ASBR operation. The reactor was operate under thermophilic condition (60 °C) at mean OLR of 1 and 0.5 l until a steady state was reach at every OLR test. The modifild POME was stop after OLR of 0.5 l into the steady state and operating process until the biogas volume stable decreas. After that modifild POME was feedind to ASBR reactor. The last experiment, the hydrogen production was operate at room temperature until stady state and chage to thermophilic (60 °C)

condition again. The ASBR was routinely monitored for pH, gas production and composition, total carbohydrate utilization, total alkalinity, chemical oxygen demand (COD) and VFA.

RESULTS AND DISCUSSION

The hydrogen production by thermophilic mixed culture from modified POME supplemented with sugar at concentration of 5, 10 and 15 g l⁻¹ corresponding to OLR of 58, 63, 68 and 73 g l⁻¹ were 241 ± 20, 3431 ± 52, 4138 ± 51 and 3712 ± 52 ml-H₂ l-POME⁻¹, respectively. Hydrogen is very sensitive to organic overload. As seen from figure 1 the hydrogen production declined after increased organic loading to 73 g l⁻¹ at day of 42, indicating that 73 g l⁻¹ OLR is the maximum OLR for hydrogen production. The optimum OLR is 68 73 g l⁻¹ was hydrogen production of 4138 ± 51 ml-H₂ l-POME⁻¹ higher than modified POME without supplement (241 ± 20 ml-H₂ l-POME⁻¹).

Substrate compositions is important to achieve successful hydrogen production from POME. Palm oil mill industry has different initial substrate concentrations was feed into the reactor each day depend on volume of oil palm input to process. The OLR were very from 1, 0.5 and 0 l d⁻¹ with hydrogen production at steady state of 1941 ± 107, 808 ± 78 and 0 ml-H₂ l-POME⁻¹, respectively (Figure 2). At a OLR of 1 l was used at start process, the hydrogen was high due to sugar from the modified POME supplemented with sugar still remain in the process. When decreases substrate concentration hydrogen productions have a tendency to decrease and stable at day of 12-15. If not feeding POME into process hydrogen not produces. Recover process by 1 l OLR, the hydrogen production was stable within 12 days.

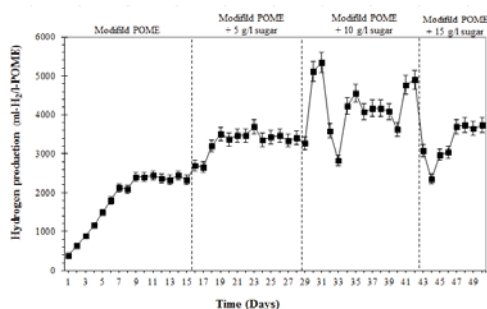


Figure 1. Hydrogen production at difference sugar concentration of 5, 10 and 15 g l⁻¹.

The optimal temperature for hydrogen production from POME varies because of complex microbial communities and the constituent materials. With operation at 60 °C, the high hydrogen productions (2494 ± 196 ml-H₂ l-POME⁻¹) were obtained, with was higher than that at room temperature (15 ± 3 ml-H₂ l-POME⁻¹). The hydrogen production was increase again after

increase temperature to 60 °C within 12 days. Thermophilic fermentation was demonstrated to be favorable for hydrogen production from POME, indicating that the mixed inoculum contained thermophilic microbial.

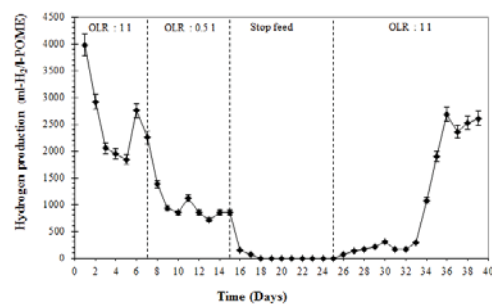


Figure 2. Hydrogen production at difference OLR of 1, 0.5 and 0 l-POME

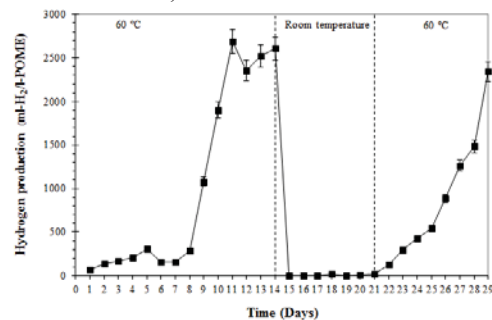


Figure 3. Effect of temperature on process stability of cotinuous hydrogen production from POME

ACKNOWLEDGMENT

The authors would like to thank Department of Biology Faculty of Science Thaksin University for financially supported this research.

References

- [1] S. O-Thong, P. Prasertsan, N. Intrasingkha, S. Dhamwichukorn and NK. Birkeland. "Improvement of biohydrogen production and treatment efficiency on palm oil mill effluent with nutrient supplementation at thermophilic condition using an anaerobic sequencing batch reactor", *Enzyme and Microbial Technology*. **41**, 2007, pp. 583-590.
- [2] S. O-Thong, P. Prasertsan, D. Karakashev and I. Angelidaki. "Thermophilic fermentative hydrogen production by the newly isolated *Thermoanaerobacterium thermosaccharolyticum* PSU-2", *International Journal of Hydrogen Energy*. **33**, 2008, pp. 1204-1214.

BIOGAS PRODUCTION FROM BIOMASS RESIDUES OF PALM OIL MILL BY SOLID STATE ANAEROBIC DIGESTION

Srisuda Chaikitkeaw¹, Prawit Kongjan² and Sompong O-Thong^{1,3}.

¹Biotechnology Program, Faculty of Science, Thaksin University, Thailand

²Department of Science, Faculty of Science and Technology, Prince of Songkla University, Thailand

³Microbial Resource Management Research Unit, Faculty of Science, Thaksin University, Thailand

SUMMARY: Three biomass residues from palm oil mill plant including empty fruit bunches (EFB), palm press fiber (PPF) and decanter cake (DC) were evaluated for methane production by solid-state anaerobic digestion. Oil palm biomass was mixed with inoculum at F/I ratio of 2:1, 3:1, 4:1, 5:1 and 6:1 based on the volatile solid (VS). Results shown that among the five F/I ratios tested, the F/I ratio of 2:1 gave the highest methane yield and methane production. The highest cumulative methane production of 2180 mLCH₄ was obtained from empty fruit bunches followed by palm press fiber (1964 mL CH₄) and decanter cake (1827 mL CH₄). The highest methane yield of 144 mL CH₄/gVS was obtained from EFB followed by PPF (140 mL CH₄/gVS) and DC (130 mL CH₄/gVS) at F/I ratios of 2:1. Methane production of 55 m³CH₄/ton was obtained from EFB followed by PPF (47 m³CH₄/ton) and DC (41 m³CH₄/ton).

Keywords: Palm oil biomass, biogas production, solid-state anaerobic digestion

INTRODUCTION

Oil palm is vastly cultivated as a source of oil in Malaysia, Indonesia and Thailand. In Southern Thailand, oil palm is one of the most important commercial crops. Oil palm mill plant also generates large amount of solids wastes such as empty fruit bunch (EFB) (23%), mesocarp fiber (12%) and shell (5%) for every ton of fresh fruit bunches (FFBs) processed in the mills [1]. Raw material supplied to the mills consists of fresh fruit bunches. In 2014 the yield of fresh fruit bunches was 1.127 million tons to year and the crude palm oil production was 0.192 million tons [2]. The oil extraction rate is about 10% from the palm oil biomass with the majority 90% left as residues biomass [1]. There are various forms of solid and liquid wastes from the mills. 60% of biomass residues from oil palm mills is a solid waste, while the rest is a liquid waste. Solid oil palm biomass residues are generated throughout the year include empty fruit bunches (EFB), palm press fiber (PPF), palm kernel cake (PKC), palm kernel shell (PKS), decanter cake (DC) in palm oil mills and liquid waste as palm oil mill effluent (POME) [3]. Liquid waste could be easily convert to value as products such as hydrogen and methane gas [4]. While, solid waste are not utilize, due to its composition are difficult to degrade by microorganisms. Oil palm biomass residues composed of cellulose, hemicelluloses that could be used as substrate for methane production by anaerobic digestion.

The anaerobic digestion (AD) process can operate in both liquid and solid states in terms of total solid (TS) content. In general, the TS content of liquid AD systems ranges from 0.5 to 15%, while solid-state AD (SS-AD) systems usually operate at TS contents of higher than 15% [5]. SS-AD can address several problems encountered in L-AD, such as floating and stratification of fibers, that

make it well suited to handle lignocellulosic biomass [6] like EFB, PPF and DC. Methane production from four lignocellulosic biomass feedstocks including corn stover, wheat straw, yard waste and leaves by solid-state anaerobic digestion was investigated by Cui et al. [6]. Results showed that the highest methane yield was attained for corn stover (81.2 L kg⁻¹ VS), followed by wheat straw (66.9 L kg⁻¹ VS), leaves (55.4 L kg⁻¹ VS) and yard waste (40.8 L kg⁻¹ VS). Methane production from EFB, PPF and DC by SS-AD are still not investigated. Therefore, this work aim to determine the methane potential from EFB, PPF and DC by SS-AD.

MATERIALS AND METHODS

EFB, PPF and DC used in this study were collected from a palm oil mill plant (Southern palm oil Co, Ltd. in Thailand). The biochemical methane potential assays of EFB, PPF and DC were evaluated for methane production via solid-state anaerobic digestion according to Angelidaki et al., [7]. The solid-state anaerobic digestion tests were conducted at 25% total solids (TS) content at feedstocks to inoculums (F/I) ratios of 2:1, 3:1, 4:1, 5:1 and 6:1. All tests were carried out in duplicate in a thermostat incubation room at 37°C for 45 days. The assay was conducted as batch cultivations in 500 mL serum bottles. Methane production was measured by water replacement method. The methane content was analyzed by a gas chromatograph (GC) equipped with a flame ionization detector [3]. Gas measurement was reported in STP conditions (standard temperature and pressure, 273 K, 1.01325 Pa). Theoretical methane potential was calculated according Bushwell's formula which is derived by stoichiometric conversion of the compound to CH₄, CO₂ and NH₃ [8].

RESULTS AND DISCUSSION

The total methane yields and methane production of EFB, PPF and DC at F:I ratios from 2:1-6:1 by SS-AD are shown in Fig. 1. Methane production decreased when increased F:I ratios. The F/I ratio of 2:1 gave the highest methane yield and methane production for all the feedstocks tested (EFB, PPF and DC). SS-AD of EFB at F:I ratio of 2:1 gave the highest methane yield of 144 mLCH₄/gVS followed by PPF (140 mLCH₄/gVS) and DC (130 mLCH₄/gVS). The highest methane production of 55 m³CH₄/ton was obtained from EFB. Methane production of 55 m³CH₄/ton was obtained from EFB followed by PPF (47 m³CH₄/ton) and DC (41 m³CH₄/ton) as show Fig.2. Final volatile fatty acid (VFA) at F:I 2:1 of EFB, PPF and DC was low, while high concentration of VFA was found at high F:I ratio (3:1-6:1) as shown in Fig.3.

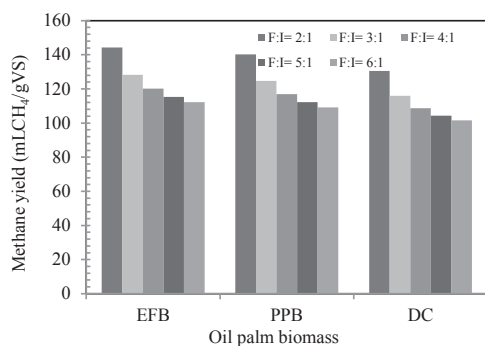


Figure 1. Methane yield from EFB, PPF and DC by SS-AD at different F:I ratios

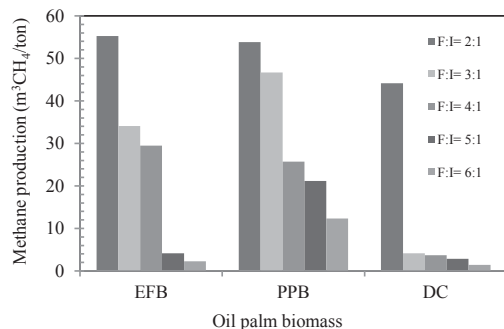


Figure 2. Methane production from EFB, PPF and DC by SS-AD at different F:I ratios

CONCLUSIONS

F/I ratio of 2:1 was suitable for methane production from EFB, PPF and DC by SS-AD.

The biochemical methane potential of EFB, PPF and DC by solid-state anaerobic digestion was 55, 47 and 41 m³CH₄/ton, respectively.

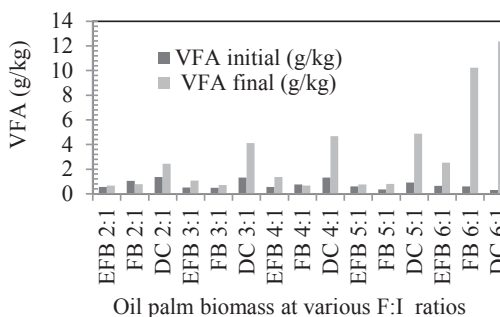


Figure 3. VFA concentration from EFB, PPF and DC by SS-AD at different F:I ratios

ACKNOWLEDGEMENT

I would like to thank Energy Policy and Planning Office (EPPO) and Higher Education Commission (CHE) for financial supports of this project.

References

- [1] Department of Agricultural Economics. Statistics oil palm. from <http://www.arda.or.th>
- [2] Y. Basiron and K.W. Chan. "The oil palm and its sustainability". *J Oil Palm Res.* **16**, 2004, pp.1-10.
- [3] S. Yusoff. "Renewable energy from palm oil innovation on effective utilization of waste". *J Clean Prod* **14**, 2006, pp.87-93.
- [4] S. O-Thong, K. Boe and I. Angelidaki. "Thermophilic anaerobic co-digestion of oil palm empty fruit bunches with palm oil mill effluent for efficient biogas production". *Applied Energy.* **93**, 2012, pp.648-654.
- [5] J. Guendouz, P. Buffiere, J. Cacho, M. Carrere, J.P. Delgenes. "Dry anaerobic digestion in batch mode: design and operation of a laboratory-scale completely mixed reactor". *Waste Manag.* **30**, 2010, pp.1768-1771.
- [6] Z. Cui, J. Shi and Y. Li. "Solid-state anaerobic digestion of spent wheat straw from horse stall". *Bioresour Technol.* **102**, 2011, pp.9432-9437.
- [7] I. Angelidaki, M. Alves, D. Bolzonella, L. Borzacconi, J.L. Campos and A.J. Guwy. "Defining the biomethane potential (BMP) of solid organic wastes and energy crops: a proposed protocol for batch assays". *Water Sci Technol.* **59**, 2009, pp.927-34.
- [8] G.E. Symons and A.M. Bushwell. "The methane fermentation of carbohydrate". *J Am Chem Soc.* **55**, 1933 pp.2028-39.

ETHANOL PRODUCTION FROM DESIZING WASTEWATER USING CO-CULTURE OF *BACILLUS SUBTILIS* AND *SACCHAROMYCES CEREVISIAE*

Sukon Tantipaibulvut¹, Anawat Pinisakul², Phannee Rattanachaisit², Kadsarin Klatin¹, Benjaporn Onsrirai¹ and Kanokwan Boonyaratsiri¹

¹Department of Microbiology and ²Department of Chemistry, Faculty of Science, King Mongkut's University of Technology Thonburi, Thailand

SUMMARY: This research studied about the production of ethanol from desizing wastewater of dye bleaching industry by using the co-culture of *Bacillus subtilis* (*B*) and *Saccharomyces cerevisiae* TISTR 5160 (*S*). The order of yeast inoculation, the inoculum ratio of *B* to *S*, shaking speed and incubation temperature after the addition of yeast were studied. The effect of nitrogen sources was also investigated. It was found that the optimum condition for growth and ethanol production of co-culture was shaking at 150 rpm and temperature of 37°C with the inoculation of *B* 1 day before *S* and the inoculum ratio of *B* to *S* was 5:10. This gave the ethanol concentration of 5.8 g/L after 48 h. Addition of nitrogen source prolonged the period the ethanol production going to the maximum.

Keywords: ethanol; dye-bleaching industry; *Bacillus subtilis*; *Saccharomyces cerevisiae*

INTRODUCTION

Textile plants, particularly those involve in dyeing and finishing process, consist of numerous wastewater streams from various operations. Among those wastewater streams, the one from the sizing and desizing operations was the main sources of pollution. In the sizing operation, the fibers are coated with a layer of sizing agents, mainly consisting of biopolymers like starch and other polysaccharides. After a weaving operation, the sizing agents are removed by washing with hot water. This washing step is called the desizing step. Desizing wastewater makes up approximately 50% of the organic load in wastewater discharged from the textile finishing industry.

Bioethanol is currently considered as one of the best substitutes for petroleum-derived fuels in many countries to solve their energy requirements in an environmentally friendly way. It can be produced from sugar, starch or lignocellulosic material. The production of ethanol from starch requiring two-step process where the starch is first converted to glucose by hydrolysis; the resulting sugar can in turn be converted to ethanol by fermentation.

Considering the substantial availability of high content of readily biodegradable matter at very low price by local dye-bleaching processing plants, the use of desizing wastewater as a low cost substrate for ethanol production could provide a benefit for the cost reduction. However, there is few information available on the use of desizing wastewater for the production of ethanol.

The aim of this study was to use *B. subtilis* which produces α -amylase to hydrolyze starch in desizing wastewater and co-cultivate it with *Saccharomyces cerevisiae* TISTR 5160 to study the effect of yeast inoculation at different time point, shaking condition, fermentation temperature and the addition of nitrogen sources on the ethanol production.

MATERIALS AND METHODS

Bacillus subtilis and *Saccharomyces cerevisiae* TISTR 5160 was maintained at 4°C on a nutrient agar slant and an YM slant, respectively.

The desizing wastewater, provided by a dye-bleaching plant in Samutprakarn Province, was kept at 4°C not more than 20 days. The composition and characteristics of the effluent are indicated in Table 1.

Table 1. Composition and characteristic of the desizing effluent from dye-bleaching industry.

Parameter	Unit	Value range
pH		4.7 – 6.5
Temperature	°C	26 – 31
Total solids	mg/L	15,800 – 34,800
Total suspended solids	mg/L	1,620 – 2,180
Total dissolved solids	mg/L	13,620 – 33,260
BOD	mg/L	7,160 – 8,954
COD	mg/L	73,260 – 79,540
Starch	µg/ml	573 – 1881
Reducing sugar	µg/ml	1,700 – 10,325

Coculture Ethanol Fermentation

For ethanol production by coculture of *B. subtilis* and *S. cerevisiae*, cells from nutrient slant of *B. subtilis* and from YM slant of *S. cerevisiae* were inoculated into 100 ml of nutrient broth and YM broth; shaking at 150 rpm for 24 h at 37°C and 30°C, respectively.

The amount of bacterial cell suspension and of *S. cerevisiae* culture were varied in both the order of inoculation and the ratio of each culture and inoculated into 100-ml desizing wastewater. Cocultures were incubated under stationary condition at either room temperature (23-26°C) or 37°C for ethanol fermentation. At intervals of 24 h, culture broths were analysed for ethanol content.

Fermentations were also carried out at stationary or shaking condition with the addition of various nitrogen sources (ammonium nitrate (NH_4NO_3), sodium nitrate (NaNO_3), peptone and yeast extract) at 2% final concentration and incubated at 37°C.

Analytical Methods

Reducing sugar was estimated by a 3,5-dinitrosalicylic acid reaction with glucose as standard and measuring the absorbance at 540 nm [1]. Residual starch was determined by measuring the blue colour of starch-iodine complex at 620 nm [2].

Total solids, total suspended solids, total dissolved solids, COD and BOD were measured according to procedures described in Standard Methods for the Examination of Water and Wastewater [3].

Ethanol concentration in fermented desizing wastewater was analysed by a gas chromatograph.

RESULTS AND DISCUSSION

Effect of Culture Ratio and Yeast Inoculation at Various Time Points on Ethanol Production

Simultaneous saccharification and fermentation of unhydrolysed starch involves the enzymatic hydrolysis of starch to fermentable sugars and their conversion to ethanol in the same fermenter, thereby preventing the inhibitory effect of sugars on amylase activity [4]. As shown in Figure 1, the production of ethanol can be investigated only in the mixed culture that bacillus was inoculated one day (B1S) or two days (B2S) before *S. cerevisiae*. The ethanol concentration of B1S was higher than that of B2S and it was highest at the inoculum ratio of 5% bacillus to 10% yeast (B5 S10).

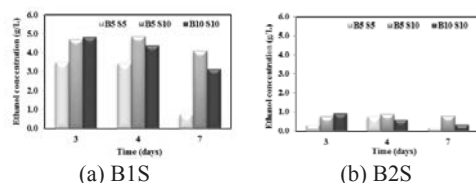


Figure 1. Ethanol production from desizing wastewater in B1S (a) and B2S (b) at 150 rpm, 37°C.

Effect of Temperature after Yeast Inoculation against Ethanol Production in Static Condition

B. subtilis (5%) was grown in desizing wastewater for one day in shaking condition of 150 rpm at 37°C. Then, *S. cerevisiae* (10%) was inoculated in this wastewater and incubated at either room temperature (23-26°C) or 37°C statically. As can be seen from Figure 2, when the temperature increased, the time the ethanol concentration going to maximum was shortened.

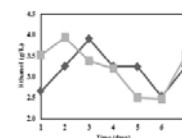


Figure 2. Ethanol production in wastewater (B1S) with the incubation temperature after yeast addition, either at room temperature (23-26°C, \blacklozenge) or 37°C (\blacksquare) in static condition.

Effect of Nitrogen Sources and Shaking Condition after Yeast Inoculation on Ethanol Production

Figure 3 shows the data for static and shaking conditions at 37°C for different time periods and different nitrogen sources. It can be seen that the concentration of ethanol reached up to the maximum level of 5.8 g/L after 2 days in shaking conditions compared to the maximum production of 4.9 g/L at the 5th day in static conditions. Furthermore, the addition of nitrogen sources in the desizing wastewater caused the reduction in ethanol concentration for approximately 33%, compared to those of the unsupplemented one, especially in shaking condition for the first two days after fermentation. It also prolonged the period the ethanol production going to the maximum.

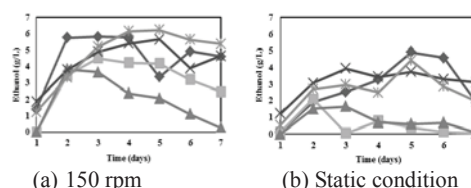


Figure 3. Ethanol production from desizing wastewater in different N-sources with shaking (a) and static condition (b), No nitrogen-source addition \blacklozenge , ammonium nitrate \blacksquare , sodium nitrate \blacktriangle , peptone \times , yeast extract $*$

ACKNOWLEDGMENT

The authors gratefully acknowledge the contribution of Thailand Research Fund.

References

- [1] G.L. Miller, "Use of dinitrosalicylic acid for determining reducing sugars", *Analytical Chemistry*, **31**, 1959, pp. 426-428.
- [2] L.C. Thomas and G.J. Chamberlin, *Colorimetric Chemical Methods*, 1980, pp. 234-236. Tintometer Ltd, Salisbury, UK.
- [3] American Public Health Association (APHA) 2005, *Standard Methods for Examination of Water and Wastewater*, 16th ed., American Public Health Association, Washington, DC.
- [4] M.M. Abouzied and C.A. Reddy, "Direct fermentation of potato starch to ethanol by cocultures of *Aspergillus niger* and *Saccharomyces cerevisiae*". *Applied and Environmental Microbiology*, **52**, 1986, pp. 1055-1059.

LANTHANUM-DOPED STRONTIUM TITANATES FOR TRANSESTERIFICATION OF PALM OIL TO FATTY ACID METHYL ESTERS

Polthep Sukpanish^{1,2} and Chawalit Ngamcharussrivichai^{1,2}

¹Department of Chemical Technology, Faculty of Science, Chulalongkorn University, Thailand

²Center of Excellence on Petrochemical and Materials Technology (PETROMAT), Chulalongkorn University, Thailand

SUMMARY: Perovskite-type strontium titanate (SrTiO₃) has been widely used in industrial applications due to its structural, chemical and thermal stability. In this work, a series of La-doped SrTiO₃ were synthesized via a sol-gel combustion method using citric acid as complexing agent in the presence of triblock copolymer, Pluronic P123, as structure directing agent. The mixed metal oxides attained were characterized for their physicochemical properties using various techniques. The X-ray diffraction confirmed a homogenous substitution of La³⁺ for Sr²⁺ in the perovskite lattice up to the La/Sr atomic ratio of 1:1. The specific surface area of the materials was higher than that of conventional SrTiO₃ due to the presence of mesoporosity. The incorporation of La into SrTiO₃ also enhanced basic properties. The La-doped SrTiO₃ with different La/Sr ratios were tested as heterogeneous base catalysts in the transesterification of palm oil with methanol to fatty acid methyl esters (FAME). A correlation between the FAME yield and the La content of the catalysts was found.

Keywords: Strontium titanate, Mesoporous mixed oxides, Sol-gel combustion, Lanthanum, Transesterification

INTRODUCTION

The current technologies for production of fatty acid methyl esters (FAME), as basic oleochemicals, are based on homogeneously catalyzed transesterification under basic conditions. Although the soluble bases gain the reaction rate under mild conditions, the process is environmentally unfriendly due to a massive wastewater discharged from biodiesel washing step. Heterogeneous catalysis is a promising technology for greener process in which the solid catalysts are easily separated from the product mixture and reused. Moreover, the washing step is no longer required [1].

Various alkaline earth metal oxides were investigated as solid base catalysts in transesterification of vegetable oils with methanol to FAME [2]. Their basic strength is ranged in the following order: BaO > SrO > CaO > MgO, which agree with an increasing trend in their electronegativity [3]. Strontium oxide (SrO) is an active catalyst in the transesterification of vegetable oil under reflux methanol, giving the FAME yield of 95% in 30 min. However, the leaching of active sites from SrO was problematic [4].

Perovskite-type strontium titanate (SrTiO₃) has been widely used in industrial and advanced applications due to its advantageous properties, such as structural, chemical and thermal stability. SrTiO₃ is typically synthesized by solid-state reaction of strontium carbonate (SrCO₃) and titanium dioxide (TiO₂) at high temperatures (>1000 °C), resulting in non-uniformity of particle size distribution and low degree of compositional homogeneity [5]. Sol-gel combustion is an alternative method, in which an organic acid is used as a complexing agent, to synthesize the mixed oxides with high purity and homogeneity at lower temperatures [6]. The fabrication of mixed oxides with mesostructure assisted by molecular self-assembly of block copolymer was a key to enhance the textural

properties of perovskite-type materials [7].

Lanthanum oxide is a rare earth metal oxide used as either an active component or a dopant in different types of heterogeneous catalysts. Its basicity has attracted much attention for heterogeneously catalyzed transesterification to produce high purity biodiesel and glycerol. Furthermore, the metal oxides doped with rare earth metals of lower electronegativity exhibited enhanced basicity and catalytic activity [8].

The present work has been aimed to synthesize La-doped perovskite SrTiO₃ with mesoporosity as heterogeneous base catalysts for production of FAME via the transesterification of palm oil with methanol. The effects of La/Sr atomic ratio on the physicochemical and catalytic properties of the resulting catalysts were reported.

METHODOLOGY

Catalysts preparation

A series of La-doped SrTiO₃ with different La/Sr atomic ratios were synthesized under acidic conditions via the sol-gel combustion method using citric acid as a complexing agent, triblock copolymer Pluronic P123 as a structure-directing agent, tetrabutyl titanate as a Ti source, Sr(NO₃)₂ as a Sr source, and La(NO₃)₃·6H₂O as a La source.

The precursor solutions were homogeneously mixed under vigorous stirring at room temperature for 3 h. The synthesis mixture was dried at 100 °C overnight, and then calcined in a muffle furnace at 600 °C for 4 h. The resulting mixed oxides were designated as LMST-*x*, where *x* denotes the La/Sr atomic ratio.

Catalysts characterization

The physicochemical properties of the catalysts were characterized using powder X-ray diffraction (XRD), N₂ adsorption-desorption measurement, scanning electron microscope (SEM), temperature-

programmed desorption of CO₂ (CO₂-TPD) and Hammett titration.

Transesterification procedure

Transesterification of palm oil with methanol was carried out in an 80-mL autoclave reactor equipped a magnetic stirrer. The temperature was controlled by an oil bath. The typical reaction conditions were the methanol/oil molar ratio = 20, catalyst amount = 10 wt%, temperature = 150 °C and reaction time = 3 h. The solid catalyst was separated by centrifugation and excess methanol was recovered using rotary evaporator. The FAME composition of reaction product was analyzed with a Shimadzu 14A gas chromatograph equipped with a 30-m DB-Wax capillary column and a flame ionization detector (FID).

Results and Discussion

Figure 1 shows the XRD patterns of SrTiO₃ without and with La doping at the La/Sr atomic ratios of 0.1:1 and 1:1. All samples showed mainly perovskite SrTiO₃ phase with a cubic structure. A trace amount of SrCl₂·2H₂O was found in all cases. The characteristic peaks of SrTiO₃ decreased in their intensity with increasing the La doping amount. There was no any La oxide phase detected even though the La/Sr ratio was increased up to 1:1. This result indicated that La³⁺ was homogeneously incorporated into the lattice of SrTiO₃. Since the ionic radii of La³⁺ (103 pm) is smaller than that of Sr²⁺ (118 pm), the substitution of La³⁺ for Sr²⁺ distorted the perovskite lattice. Accordingly, the lattice parameter was systematically decreased from 3.905 to 3.901 nm when the La/Sr atomic ratio was increased from 0:1 to 1:1 (Table 1).

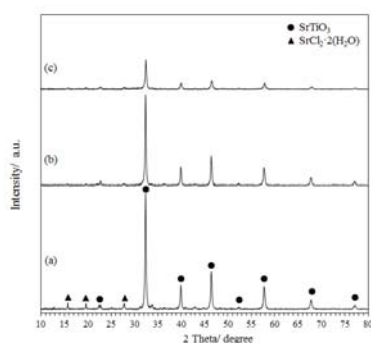


Figure 1. XRD patterns of (a) pristine SrTiO₃ (MST), (b) LMST-0.1:1 and (c) LMST-1:1.

As shown in Table 1, the total basicity of La-doped SrTiO₃ was increased with increasing the atomic ratio of La/Sr from 0.1:1 to 1:1. It should be due to a synergetic effect between Sr and La species. All samples showed the N₂ physisorption isotherms of type IV, which is typical for mesoporous materials. The BET surface area of the materials was increased with the La content in the range of 23.4–37.3 m²/g.

Table 1 compares the FAME yield attained from different catalysts. The FAME yield increased from 60.2 to 72.8 wt% when the atomic ratio of La/Sr was increased from 0.1:1 to 1:1, which follow the trend of catalyst basicity.

Table 1. Some physicochemical and catalytic properties of MST and LMSTs.

Catalyst	Lattice parameter ^a (Å)	Total basicity ^b (mmol/g)	FAME yield (wt%)
MST	3.905	0.19	60.2
LMST-0.1:1	3.904	0.23	61.3
LMST-1:1	3.901	0.58	72.8

^a Calculated from XRD data.

^b Measured by Hammett titration.

ACKNOWLEDGMENT

The authors are grateful to the Chumporn Palm Oil Industry Co., Ltd. for donating vegetable oil samples. The financial support from the Center of Excellence on Petrochemical and Materials Technology (PETROMAT) and the Ratchadaphiseksomphot Endowment Fund 2014 (CU-56-430-EN), Chulalongkorn University is also acknowledged.

References

- [1] S. Semwal, A.K. Arora, R.P. Badoni and D.K. Tuli, "Biodiesel production using heterogeneous catalysts", *Bioresource Technology*. **102**, 2011, pp.2151–2161.
- [2] A.P. Singh and A.K. Sarma, "Modern heterogeneous catalysts for biodiesel production: A comprehensive review", *Renewable and Sustainable Energy Reviews*. **15**, 2011, pp.4378–4399.
- [3] M. Kouzu and J. Hidaka, "Transesterification of vegetable oil into biodiesel catalyzed by CaO: A review", *Fuel*. **93**, 2012, pp.1–12.
- [4] X. Liu, H. He, Y. Wang and S. Zhu, "Transesterification of soybean oil to biodiesel using SrO as a solid base catalyst", *Catalysis Communications*. **8**, 2007, pp.1107–1111.
- [5] V. Berbenni, A. Marini and G. Bruni, "Effect of mechanical activation on the preparation of SrTiO₃ and Sr₂TiO₄ ceramics from the solid state system SrCO₃–TiO₂", *Journal of Alloys and Compounds*. **329**, 2001, pp.230–238.
- [6] T. Klaytae, P. Panthong and S. Thoutom, "Preparation of nano-crystalline SrTiO₃ powder by sol-gel combustion method", *Ceramics International*. **39**, 2013, pp.S405–S408.
- [7] D. Grosso, C. Boissière, B. Smarsly, T. Brezesinski, N. Pinna, P.A. Albouy, H. Amenitsch, M. Antonietti and C. Sanchez, "Periodically ordered nanoscale islands and mesoporous films composed of nanocrystalline multimetallic oxides", *Nature Materials*. **3**, 2004, pp.787–792.
- [8] Q. Liu, L. Wang, C. Wang, W. Qu, Z. Tian, H. Ma, D. Wang, B. Wang, and Z. Xu, "The effect of lanthanum doping on activity of Zn-Al spinel for transesterification", *Applied Catalysis B: Environmental*. **136**, 2013, pp.210–217.

UTILIZATION OF DENDROCALAMUS ASPER BACKER BAMBOO CHARCOAL AND PYROLIGNEOUS ACID

Panita Sumanatrakul¹, Panita Kongsune¹, Lakana Chotitham¹ and Aunwena Sukto¹

¹Department of Chemistry, Faculty of Science, Thaksin University, Thailand

SUMMARY: The purpose of this study was to assign the utilization of *Asper Backer* bamboo charcoal as activated carbon and pyroligneous acid as an alternative coagulating and antifungal agents for natural rubber sheet production. The effect of chemical activation process of bamboo charcoal was investigated. The physical properties like iodine number, moisture, ash, volatile and fixed carbon contents were measured. The results were found that the bamboo activated carbon has the highest iodine number value of 1398 mg/g which indicating a large of adsorption capacity at the optimum conditions as microwave power of 360 watts, activation time of 15 mins and the ratio of charcoal : phosphoric acid as 1 : 4. In addition, the effect of coagulating and anti-fungal activities of pyroligneous acid that is a by-product of *Dendrocalamus Asper Backer* bamboo charcoal burning was also observed. The comparison properties of pyroligneous acid with the commercial wood vinegar, formic and acetic acids have been measured. The coagulating efficiency of pyroligneous acid exhibited the shortest possible coagulation time at 18.30 mins between acids and latex. Herein, the antifungal efficiency was determined from a fungi growth area only 5% on air dried sheet rubber surfaces. The results were found that the coagulating and anti-fungal properties showed in the following order of commercial wood vinegar > bamboo pyroligneous acid > formic acid > acetic acid according to their acidic and phenolic compound contents.

Keywords: bamboo activated carbon, pyroligneous acid, coagulating agent, anti-fungal activities

INTRODUCTION

Dendrocalamus Asper Backer bamboo is encouraged to plant in Patthalung, Thailand due to it is renewable, fast-growing, and economic friendly. It has been used for housing, wood-composite products, and fuel energy [1-2]. To utilize the growing bamboo, pyrolysis which is a promising technology for exceeding disposal can be employed. There are several studies were focused on the production of bamboo charcoal with high adsorption capacity and modified to activated carbon [3-4]. Activated carbon is the most popular adsorbent for the removal of pollutants. However, its widespread use is restricted due to high cost. Therefore, low-cost precursors such as agricultural products have been searched for the production of activated carbon [5].

On the other hand, pyroligneous acid or wood vinegar is a by-product of charcoal burning that is the crude condensate of smoke generated during the process of making wood charcoal. It consists of more than 200 water soluble compounds comprising organic acids, phenolic, alkane, alcohol and ester compounds. Pyroligneous acid has widely uses as antimicrobial and growth-promoting agent [6-7]. Several authors reported that the strong antimicrobial activity of pyroligneous acid was correlated to its high contents of organic acids and phenolic compounds [8]. There are several researches have been presented the use of wood vinegar as coagulating and antifungal agents for natural rubber sheet production [9]. However, pyroligneous acid from *Dendrocalamus Asper Backer* bamboo has not been reported. Therefore, the objectives of this study were to investigate the utilizations of *Asper Backer* bamboo charcoal as activated carbon and pyroligneous acid as an

alternative coagulating and antifungal agents for natural rubber sheet production which compared with marketing wood vinegar and organic acids.

MATERIALS AND METHODS

Activated carbon preparation

The bamboo charcoal 100 grams were first soaked phosphoric acid at room temperature for 24 h with the ratio of charcoal : phosphoric acid as 1 : 4. The microwave-induced activation treatments were conducted in a modified microwave at microwave power of 360 watts and varied the activation time of 5, 10, 15, and 20 minutes, respectively. After microwave activation, the samples were cooled to room temperature under nitrogen flow, washed repeatedly with distilled water until pH 7, dried at 105°C for 12 h and stored in desiccators.

Natural rubber sheet production

Natural rubber sheets were prepared using different acid solutions as coagulating agents; commercial wood vinegar, pyroligneous acid, formic and acetic acids. The latex was filtered and the coagulation was carried out in individual pans; latex, water, and acid solutions were mixed and counted time until coagulation was completed. The slabs were compressed between two steel rolls and left on a drying ground until a constant weight. Finally, slabs were dried in rubber housing for 20 days. Rubber sheets were determined for antifungal efficiency comparison. The average pH value of all coagulant aqueous solutions was 3.

Characterizations

The average proximate analyses of the bamboo activated carbon were measured as moisture content, volatile matters, fixed carbon and ash on dry basis, respectively. Degree of activation is a measure of

the iodine adsorbed in the pores that defined as iodine number.

The antifungal efficiency of the coagulants was determined from a fungi growth area on the drying NR sheet surfaces after leaving them for 20 days. Percentage of the fungi growth area was calculated the fungi growth area on NR sheet surface per total area of NR sheet surface. Analysis of pyrolygneous acid components were achieved by gas chromatography mass spectrometry.

RESULTS AND DISCUSSIONS

The effect of chemical activation process on physical properties of *Dendrocalamus Asper Backer* bamboo activated carbon

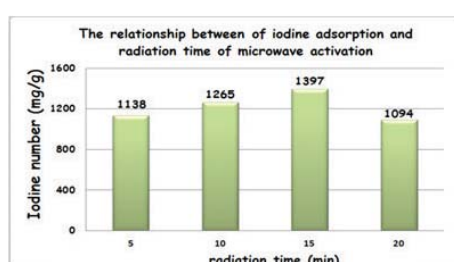


Figure 1. Effects of radiation time on iodine adsorption of bamboo activated carbon.

From Figure 1, the activation time had great influence on the development of pore structure at radiation time of 15 mins.

The effect of coagulating and anti-fungal activities of *Dendrocalamus Asper Backer* bamboo pyrolygneous acid

Table 1. Counting time and fungi growth area of natural rubber sheet

Coagulants	Agglomeration time (mins)	Fungi growth area (%)	rubber sheet appearance
Commercial wood vinegar	14.30	3.5	Dark brown
Bamboo pyrolygneous acid	18.30	5.0	Red brown
Acetic acid	25.00	13.3	Light yellow
Formic acid	39.00	17.6	Light yellow

From Table 1, the results were found that the anti-fungal properties showed in the following order of commercial wood vinegar > bamboo pyrolygneous acid > formic acid > acetic acid according to their phenolic compound contents. The phenolic compound contents of commercial wood vinegar are predominated more than the phenolic compound contents of the bamboo pyrolygneous acid as 21.84 % and 11.97 %, respectively.

These results are agreeable with Baimark and Niamsa (2009) verified that the antifungal efficiency of the wood vinegars was strongly depended upon their phenolic compound contents and confirmed through the inhibitory growth of the main fungi,

Penicillium griseofulvum [9].

CONCLUSIONS

The optimal activation conditions were determined as: microwave power 360W, radiation time 15 min and phosphoric acid/carbon ratio 4:1, under which an iodine number of 1398 mg/g and ash, moisture content, volatile matters, and fixed carbon on dry basis were 2.0, 2.4, 3.6, and 94.0, respectively. It is indicating that, this bamboo activated carbon has a large of adsorption capacity.

In addition, the results suggested that all wood vinegars had higher coagulating and antifungal efficiency than both formic and acetic acids because of the pyrolygneous acids contained several acidic and phenolic compounds whereas formic and acetic acids did not. Therefore, pyrolygneous acids from bamboo can be used as coagulating and antifungal agents to replace on organic acids.

ACKNOWLEDGMENT

The authors would like to thank the Research and Development Institute Thaksin University (RDITSU) for their financial support. Thanks are also given to the Department of Chemistry and Faculty of Science, Thaksin University for providing a scholarship to study and pursue this paper.

References

- [1] A. Darabant, M. Haruthaithanasan, W. Atkla, T. Phudphong, E. Thanavat and K. Haruthaithanasan, "Bamboo biomass yield and feedstock characteristics of energy plantations in Thailand", *Energy Procedia*. **59**, 2014, pp. 134 – 141.
- [2] P. Chaowana, "Bamboo: An Alternative Raw Material for Wood and Wood-Based Composites", *Journal of Materials Science Research*. **2**, 2013, pp. 90-102.
- [3] A.O. Oyedun, T. Gebreegziabher and C.W. Hui, "Mechanism and modelling of bamboo pyrolysis", *Fuel Processing Technology*. **106**, 2013, pp. 595–604.
- [4] S.H. Lin, L. Y. Hsu, C.S. Chou, J.W. Jhang and P. Wu, "Carbonization process of Moso bamboo (*Phyllostachys pubescens*) charcoal and its governing thermodynamics", *Journal of Analytical and Applied Pyrolysis*. **107**, 2014, pp. 9–16.
- [5] Q. Dong and Y. Xiong, "Kinetics study on conventional and microwave pyrolysis of moso bamboo", *Bioresource Technology*. **171**, 2014, pp. 127–131.
- [6] Q. Wu, S. Zhang, B. Hou, H. Zheng, W. Deng, D. Liu and W. Tang, "Study on the preparation of wood vinegar from biomass residues by carbonization process", *Bioresource Technology*. **179**, 2015, pp. 98–103.
- [7] H.A. Oramahi and F. Diba, "Maximizing the Production of Liquid Smoke from Bark of Durio by Studying Its Potential Compounds", *Procedia Environmental Sciences*. **17**, 2013, pp. 60-69.
- [8] V.S. Ferreira, I.N.C. Rego, F. Pastore, M.M. Mandai, L.S. Mendes, K.A.M. Santos, J.C. Rubim and P.A.Z. Suarez, "The use of smoke acid as an alternative coagulating agent for natural rubber sheets' production", *Bioresource Technology*. **96**, 2005, pp. 605–609.
- [9] Y. Baimark and N. Niamsa, "Study on wood vinegars for use as coagulating and antifungal agents on the production of natural rubber sheets", *Biomass and Bioenergy*. **33**, 2009, pp. 994–998.

FORECASTING OF CRUDE PALM OIL DEMAND TOWARDS FOOD AND ENERGY SECURITY IN THAILAND

Pranee Nutongkaew¹, Jompob Waewsak^{1,2}, Warangkhan Keerativibool^{1,3}, Chuleerat Kongruang⁴,
Tanate Chaichana^{1,2} and Yves Gagnon⁵

¹Research Center in Energy and Environment

²Department of Physics, Faculty of Science, Thaksin University (Phatthalung Campus)

³Department of Mathematics and Statistics, Faculty of Science, Thaksin University (Phatthalung Campus)

⁴School of Management, Walailak University

⁵Université de Moncton, Edmundston (NB), Canada

SUMMARY: According to the Alternative Energy Development Plan (AEDP) for Thailand, a biodiesel production of 4.5 million liters/day and 5.97 million liters/day is targeted in 2016 and 2021, respectively. The production of biodiesel requires crude palm oil (CPO) as a main mixture in the chemical processes. Consequently, the CPO available is shared between the production of cooking palm oil and the production of biodiesel. The objective of this paper is to forecast the demand of cooking palm oil for Thailand beyond 2021, towards food and energy security. The cooking palm oil consumption is predicted based on statistical models. The price of the palm oil bottle (PPO), the price of the soybean oil bottle (PSOY) and the average revenue per capita (GDP per Capita: PERCAP) are used as model inputs. The results forecasted show that Thailand's consumption for cooking palm oil is 1.02 million tons in 2021.

Keywords: Oil palm, cooking palm oil, energy security, food security, forecasting

INTRODUCTION

The Royal Thai Government, through the Department of Alternative Energy Development and Efficiency (DEDE), has launched the 15-year Alternative Energy Development Plan (AEDP) (2008-2021) [1]. The Plan aims to increase the share of renewable and alternative energy consumption to 25% by 2021. The main objective of the AEDP is to reduce oil imports, which account for approximately 80% of the total oil consumption in the country. With a current production capacity of 1.62 million liters/day, the biodiesel (B100) production target, based on a supply and demand analysis, for 2021 increases from 1.62 million liters/day to 5.97 million liters/day. On the supply side, the Royal Thai Government will promote the expansion of oil palm plantations to 5.5 million rai (880,000 hectares), with an oil palm harvesting area estimated at 5.3 million rai (848,000 hectares). With an average yield target of 3.2 tons/rai/year and a crushing rate of 18% for the crude palm oil, the production of CPO will be in the order of 3 million tons/year in 2021 [1].

In this context, the main objective of this research is to devise a strategy to manage and to achieve the goal of producing 5.97 million liters/day of biodiesel by 2021, without affecting any other parts of the supply chain for crude palm oil, including for the production of various types of food. The strategy adopted will need to achieve a balance between the plantation area available for harvesting and the increasing demand of palm oil to produce biodiesel. This paper concentrates on the forecasting of the consumption of cooking palm oil in 2021, in Thailand.

METHODOLOGY

Modeling Prediction

Various databases from the Government of Thailand are used to access data needed for the modeling, notably data on the climate, soil resources, water resources, forest resources and land use are used in this study.

(1) Multiple Regression Analysis

This study is conducted to generate a forecast of cooking palm oil bottle (PPO) consumption in Thailand. Using SPSS (Statistical Package for Social Sciences) version 17 and the SAS (Statistical Analysis System) version 9, the data used in this study is a time series of monthly cooking PPO consumption.

The dependent variable is the total demand for cooking palm oil and the independent variables are population, Gross Domestic Product per capita and household income. Time series data, with 28 observations per year, from 1985 to 2012, are used to construct the multiple regression analysis [2].

(2) Holt's Exponential Smoothing Method

The Holt's exponential smoothing method is also used in this study [3].

(3) Combined Forecasting Method

A combined forecasting method between multiple regression analysis and Holt's exponent smoothing method is also used to reduce the error from the forecast.

Forecast Performance Measure

Two criteria, i.e. the mean absolute percentage error (MAPE) and the root mean square error (RMSE), are used to compare the performance of the forecast values obtained from the multiple regression analysis, the Holt's exponential smoothing method and the combined forecasting

method.

RESULTS AND DISCUSSION

The demand for cooking palm oil has been steadily increasing in Thailand over the period of 1985-2012. Using a multiple regression analysis, the smoothing with an exponential curve of Holt and the Combined Forecasting Method (CFM), the model predictions are shown on Figure 1 and Table 1. The MAPE and RMSE criteria for the CFM are less than for the other methods, thus indicating that it is the most accurate in forecasting.

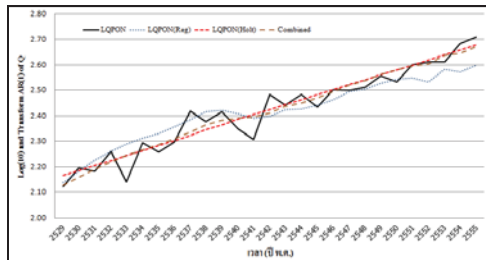


Figure 1. Comparison of the predicted cooking palm oil using three different models.

Results show that the most appropriate model is the CFM, namely,

$$\hat{Y}_3 = \hat{LQN}(\text{Combined}) \tag{1}$$

$$= -0.247239 + 0.407325\hat{Y}_1 + 0.694065\hat{Y}_2$$

The combined forecasting method is thus used to forecast the demand for cooking palm oil (Q) during the period 2013-2021. The demand for cooking palm oil (Q), in tons, follows the following regression:

$$\hat{Y}_t = \text{Log } Y_t - 0.529683 \text{Log } Y_{t-1} \tag{2}$$

$$Y_t = 10^{\hat{Y}_t + 0.529683 \text{Log } Y_{t-1}}$$

Therefore, the forecast demand for cooking palm oil can be calculated by the following equation:

$$\hat{Y}_t = 10^{\hat{Y}_{t-3} + 0.529683 \text{Log } \hat{Y}_{t-1,3}} \tag{3}$$

Finally, the demand for cooking palm oil in Thailand is forecasted to be the 1.02 million tons in 2021. The forecasting results from the CFM are shown in Table 2.

Table 1. Forecasting of the demand for cooking palm oil for the period 2013-2021.

Year	Forecasting (log base) of the demand for cooking palm oil (LQN)	
	Multiple Regression	CFM (Y ₃)
2013	2.61	2.69
2014	2.63	2.71
2015	2.64	2.73
2016	2.66	2.75
2017	2.67	2.77
2018	2.68	2.79
2019	2.70	2.81
2020	2.71	2.83
2021	2.73	2.85

Table 2. Forecasting of the demand for cooking palm oil in Thailand for the period 2013-2021 using the Combined Forecasting Method.

Year	Demand of cooking palm oil in Thailand (million tons)
2013	0.50
2014	0.54
2015	0.58
2016	0.64
2017	0.70
2018	0.77
2019	0.84
2020	0.93
2021	1.02

ACKNOWLEDGMENT

The authors would like to thank the Agricultural Research Development (Public Organization) for the financial support and the Research Center in Energy and Environment of Thaksin University for providing the research facility.

References

- [1] Department of Alternative Energy Development and Efficiency. Alternative Energy Development Plan (AEDP), Government of Thailand, 2012.
- [2] Montgomery, D.C., Peck, E.A. and Vining, G.G. 2006. Introduction to Linear Regression Analysis. 4th edition. New York. Wiley.
- [3] IBM Corporation. 2013. IBM SPSS Statistics Information Center. Available from <http://publib.boulder.ibm.com/infocenter/spsstat/v20r0m0/index.jsp?>

IDENTIFICATION OF POTENTIAL AREAS FOR THE EXPANSION OF OIL PALM PRODUCTION IN THAILAND

Pranee Nutongkaew¹, Jompob Waewsak^{1,2}, Chalong Kaewprasert³ and Yves Gagnon⁴

¹Research Center in Energy and Environment

²Department of Physics, Faculty of Science, Thaksin University (Phatthalung Campus), Thailand

³Faculty of Humanities and Social Sciences, Thaksin University (Songkhla Campus), Thailand

⁴Université de Moncton, Edmundston (NB), Canada

SUMMARY: The latest policy on biodiesel for Thailand plans a production of 4.5 million and 5.97 million liters/day in 2016 and 2021, respectively. Consequently, a land-use policy to promote oil palm plantations is needed to achieve the national alternative energy goals set by the Royal Thai Government. The objective of this paper is to identify and analyze suitable areas for oil palm plantations in Thailand using multi-criteria site selection techniques in a spatial analysis extension of Arc GIS 10.2. Topography, climate and soil conditions are the three main criteria used in the analysis. Results show that the central part of Thailand has the most suitable areas for the expansion of oil palm plantations. With 966,500 hectares of suitable areas throughout the country, there appears to be enough to meet the targets for biodiesel production set in the national Alternative Energy Development Plan 2021.

Keywords: spatial analysis, oil palm plantation, geographic information system (GIS), land-use, biodiesel

INTRODUCTION

Oil palm has high oil content and the highest potential of yield per unit area when compared to other oil crops [1]. Palm oil is also a major source of sustainable and renewable raw material for food, and for energy.

In Thailand, the current surface area covered by oil palm plantations is 7,175 km², mainly in the southern and central parts of the country, with 6,194 km² and 708 km², respectively. Building on a current capacity of 1.62 million liters/day of biodiesel production, the Thai Ministry of Energy recently launched the Alternative Energy Development Plan (AEDP), with a new target of 5.97 million liters/day of biodiesel production by 2021 [3]. To achieve the AEDP objectives, the oil palm plantations in Thailand will need to increase from the current 720,000 hectares to 880,000 hectares, with a total oil palm yielding of 848,000 hectares, by 2021. In parallel, the oil palm production is expected to increase from 20 tons/ha to 21.87 tons/ha. The strategy also seeks to promote domestic palm oil for consumption and for usage as an alternative source of energy, thus the need to set goals in regards to the domestic production and consumption. This will be achieved by assuring a balance between demand and supply, creating zoning policies for oil palm plantations, as well as developing new products to increase the value of the product.

Increasing demand for agricultural commodities is one of the major drivers of land use change and deforestation [2, 3]. In accordance with the policies of Thailand, the land use planning and expansion of oil palm plantations is intended to take place mainly on waste land, degraded land, acid soils, as well as land used for rubber and rice plantations. In this context, the main objective of this paper is to identify and assess potential land

areas that could be used in the expansion of the oil palm plantations in Thailand.

METHODOLOGY

To identify suitable areas for new oil palm plantations, a multi-criteria decision making analysis is applied. The criteria used to identify the biophysical suitability of production stem from the scientific literature on oil palm [4] and include:

1. Topography suitable for the target crop
2. Climate suitable for the target crop
3. Soil suitable for the target crop

Areas where all these principles are satisfied can be considered suitable for the sustainable agricultural production, to which are added indicators related to rainfall, slope, elevation, drainage and soil texture.

A GIS-based approach, using Arc GIS 10.2 Extension Spatial Analyst, is used for the site selection. The criteria used for the analysis are classified in three main classes, as shown in Table 1.

The data related to the climate of the country are from the Thai Department of Meteorology and Climatology over the 10-year period of 2001-2010. Data related to the soil resources of Thailand are obtained from the Office of Soil and Land Use Planning, Thai Land Development Department, with a map scale of 1: 50,000.

Suitable oil palm plantation areas are assessed on the basis of a scale with three levels, namely:

- Score 8-10: Suitable area
- Score 4-7: Moderately suitable area
- Score 0-3: Less suitable area

Table 1. Criteria used for the analysis of potential sites for the expansion of oil palm production.

Criteria	Weighting
Topography	30%
- Slope - Mean sea level	
Climate	35%
- Monthly mean rainfall	
- Monthly mean temperature	
- Monthly sunshine hours - Orientation	
Soil	35%
- Clay loam (CL) and clay (C) - Depth of soil layer over 75 cm	

RESULTS AND DISCUSSION

Along with the criteria used for the analysis of potential sites for oil palm production, other constraints are also taken into consideration, notably exclusion zones (including forests) where the transformation of the usage of the land into oil palm agricultural land would not be possible.

Further, once the potential areas for new oil palm plantations are identified, they are overlaid with the existing economic crops, i.e., cassava, sugar cane, oil palm, etc., in order to assess the added-value that would be achieved with the transformation of the land usage.

Results show that the suitable locations for new oil palm plantations reach a total area 9,665 km², corresponding to 966,500 hectares, which is enough to meet the targets of the Alternative Energy Development Plan by 2021. These findings suggest that Thailand has sufficient land areas for the production of oil palm, and thus for achieving its national goals towards food and energy security. The map of the suitable areas for the expansion of oil palm production is shown in Figure 1, while Table 2 classifies the new suitable areas in each region of the country.

Table 2. Classification of the suitable areas of Thailand for the expansion of oil palm plantations by region.

Region	Suitable	Moderately Suitable
Central	6,363	3,124
North	410	222
South	51	38
East	212	124
West	204	110
Northeast	2,425	1,357
Total (km²)	9,665	4,975
Total (ha)	966,500	497,500

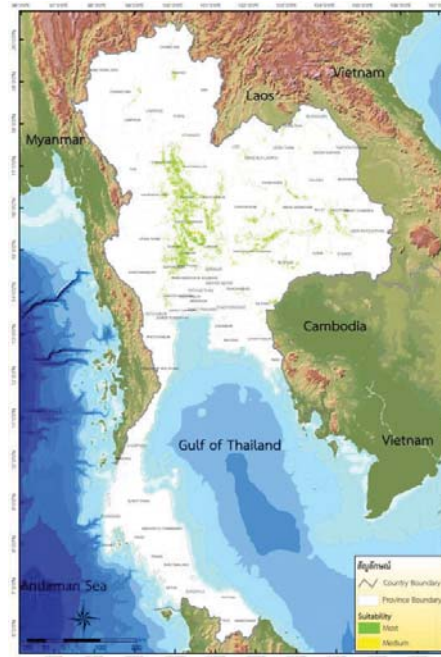


Figure 1. Map of the suitable areas of Thailand for the expansion of oil palm plantations.

Results from the spatial analysis show that the central part of Thailand has the most new suitable areas for oil palm plantations, while the southern part of Thailand has the least suitability for the expansion of oil palm production. This is due to the existing oil palm plantations in the southern region of the country, since approximately 86% of the total planted areas in this part of the country are already oil palm.

ACKNOWLEDGMENT

The authors thank the Agricultural Research Development Agency of Thailand (Public Organization) for its financial support, and the Research Center in Energy and Environment of Thaksin University for providing the research facilities.

References

- [1] B. Mattsson, C. Cederberg and L. Blix, "Agricultural land use in life cycle assessment (LCA): case studies of three vegetable oil crops" *Journal of Cleaner Production*, **8**, 2000, pp. 283-292.
- [2] R. Butler and W. Laurance, "New strategies for conserving tropical forests" *Trends in Ecology and Evolution*, **23** (9), 2008, pp. 469-472.
- [3] D. Pimentel, A. Marklein, M.A. Toth, M.N. Karpoff, G.S. Paul, R. McCormack, J. Kyriazis and T. Krueger, "Food versus biofuels: environmental and economic costs". *Human Ecology*, **37** (1), 2009, pp. 1-12.

CHARACTERISTICS OF REFUSED DERIVED FUEL-5 FROM THREE SITES IN SOUTHERN THAILAND

Pranee Nutongkaew¹ Jompob Waewsak^{1,2} and Yves Gagnon³

¹Research Center in Energy and Environment, Thaksin University, Thailand

²Department of Physics, Faculty of Science, Thaksin University (Phatthalung Campus), Thailand

³Université de Moncton, Edmundston (NB), Canada

SUMMARY: This paper presents the characteristics of the refused derived fuel-5 (RDF-5) obtained from three sites in southern Thailand. The RDF-5 was prepared from the municipal solid waste (MSW) in Phatthalung, Satun and Songkhla provinces. The MSW were randomly sampled based on the quartering method. Ultimate and proximate analyses were done based on the ASTM standard. The high heating value (HHV) of the RDF-5 was also investigated under the ASTM D4170 standard. Results show that the RDF-5 analyzed is composed of 48.5 - 54.5% carbon (C), 7.0 - 8.3% hydrogen (H), 13.7 - 18.4% oxygen (O) and 0.65 - 0.75% nitrogen (N), while it consists of approximately 6.5 - 8.6% of fixed carbon (FC), 72 - 78% of volatile matter content (VC), 3.7 - 4.7% of moisture content (MC), and 10 - 15% of ash content (AC). The HHV of the RDF-5 analyzed is in the range of 5,178 to 5,567 kcal/kg, indicating a good potential for the pre-processing of the MSW, which could be used as a fuel for power generation.

Keywords: municipal solid waste, refused derived fuel, heating value, quartering method

INTRODUCTION

In general, the generation of municipal solid waste (MSW) increases due to the socio-economic growth, both in urban and rural environments. In Thailand, the MSW generated in urban areas is predominantly disposed in landfills or accumulated in heaps situated on open land. Landfills are usually the lowest cost option in MSW management; therefore, it is the most popular means used in MSW elimination. However, this method of MSW management in developing country, such as Thailand, is usually not properly managed, while opportunities for adding value to the waste, such as for energy generation, are seldom implemented.

Three main technologies are used for energy recovery from MSW, i.e. refused derived fuel (RDF), incineration, and biomethanation. The RDF, produced by shredding or dehydrating MSW, is an efficient fuel due to its high calorific value; a recent study has shown that the energy content can reach values of 0.145 kW/kg [1]. Furthermore, it is a clean, energy efficient, eco-friendly alternative fuel for combustion in power generation plants.

According to its Alternative Energy Development Plan (AEDP), the Ministry of Energy of the Royal Thai Government promotes power generation by direct combustion of MSW. A target of 400 MW has been set for the country before 2021, which includes an Adder subsidy of 3.5 THB/kWh for the first 10 years of operation of the power plants. However, test results indicate that the mass direct combustion of MSW may result in a lower average heating value of the waste stream and a high possibility of toxic substance emissions due to incomplete combustion. Thus, the mass direct combustion process leads to a lower energy recovery potential compared to the usage of better quality RDF [2].

In this context, the objective of this paper is to

investigate the characteristics of the refused derived fuel-5 (RDF-5) from three landfill sites in southern Thailand in order to study the potential of using RDF-5 as a main fuel for power generation from a very small power producer (VSPP), with a capacity of less than 10 MW.

METHODOLOGY

Quartering, random sampling, stratified sampling and cluster sampling methods are evaluated for accuracy and efficiency in the analysis of MSW [1]. An optimum method for sampling MSW is proposed in relations to the object of the sampling, as per the MSW Management and Handling Rules [2].

The method used, i.e. the quartering method, reduces a sample by successively mixing and dividing a quantity of waste into quarters, and by keeping two opposite quarters of the sample, as shown schematically on Figure 1.

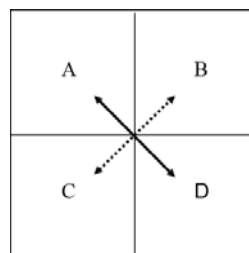


Figure 1. Sampling waste by the quartering method.

This method involves the following steps:

- The sample is placed on the floor and thoroughly mixed.
- The sample is then placed in a uniform pile covering a surface area of approximately 1 m².
- The sample is divided into four quarters using rope lines.

- The pair of opposite quarters are removed to leave half the original sample.
- The process is repeated until a sample size of 40 to 45 kg is obtained.

The samples were prepared into refused derived fuel-5 (RDF-5) for ultimate and proximate analyses, and for heating value testing. The ultimate analysis includes carbon, hydrogen, nitrogen, oxygen and sulfur-based tests. The ultimate and proximate analyses are done using the WI-RES-CHNS-O-001 by CHNS-O analyzer and an N/Protein analyzer. The calorific value was determined from the amount of heat in an Oxygen Bomb Calorimeter, as referred by the ASTM standard.

RESULTS AND DISCUSSION

The study areas consist of municipal waste landfill sites in Thepa (Songkhla province), Lampam (Phatthalung province) and Langu (Satun province) of Thailand. The MSW in the three study areas are shown in Figures 2 to 4, respectively.



Figure 2. Landfill in Thepa, Songkhla province.



Figure 3. Landfill in Lampam, Phatthalung province.



Figure 3. Landfill in Langu, Satun province.

For each of the three landfill sites studied, a sample of MSW is collected by the quartering method and an estimation of the weight compositions are shown in Table 1.

The ultimate analysis and the proximate analysis of the RDF-5 sampled are given in Tables 2 and 3, respectively.

The study found that the MSW composition for each site has different elements, and thus have site specific characteristics. However, there are some common waste elements. Indeed, the most common

waste elements found in the three sites are plastics, wood and biomass, and organic waste.

The analysis of the heating value revealed that the average heating values of each site are as follow: Thepa is 5,178 kcal/kg; Lampam is 5,422 kcal/kg; and Langu is 5,567 kcal/kg. These values are very much similar from one site to another. Further, they indicate a good potential for the pre-processing of the MSW, which could be used as a fuel for power generation.

Table 1. Estimation of the weight composition of the MSW in the three sites studied.

Composition	% by weight		
	Thepa	Lampam	Langu
Paper	4.92	10.47	9.94
Plastic	29.10	23.69	22.52
Cloth	2.38	3.49	2.95
Plastic foams	1.48	0.58	0.78
Wood and Biomass	22.21	24.13	28.57
Organic waste	10.33	19.48	16.93
Metal	6.89	5.67	5.75
Others	22.70	12.50	12.58

Table 2. Ultimate Analysis of the RDF-5 sampled.

Site	N (%)	C (%)	H (%)	S (%)	O (%)
Thepa	0.68	48.46	7.00	0	18.37
Lampam	0.65	54.44	8.29	0	17.45
Langu	0.75	52.97	7.85	0	13.74

Table 3. Proximate Analysis of the RDF-5 sampled.

Site	MC (%)	VC (%)	FC (%)	AC (%)
Thepa	4.46	71.99	8.59	14.96
Lampam	4.72	77.75	6.55	10.99
Langu	3.65	77.93	8.63	9.80

ACKNOWLEDGMENT

The authors would like to thank Sakol Energy Co. Ltd. and the Research Center in Energy and Environment for their financial support.

References

- [1] Monojit Chakraborty, Chhemendar Sharma, Jitendra Pandey and Prabhat K. Gupta, "Assessment of energy generation potentials of MSW in Delhi," *Energy Conversion and Management*, **75**, 2013, 249-255.
- [2] Ying-His Chang, W.C. Chen and Ni-Bin Chang, "Comparative evaluation of RDF and MSW incineration," *Journal of Hazardous Materials*, **58**, 1998, 33-45.

LIFE CYCLE GHG EMISSIONS OF UTILIZING PALM EMPTY FRUIT BUNCH AS FEEDSTOCK FOR ELECTRICITY PRODUCTION

Sarunya Chanlongphitak¹, Seksan Papong², Pomthong Malakul^{2,3}, Thumrongrut Mungcharoen¹

¹Faculty of Engineering, Kasetsart University, Thailand

²Life Cycle Assessment Laboratory of National Metal and Materials Technology Center (MTEC), Thailand

³The Petroleum and Petrochemical College, Chulalongkorn University, Thailand

SUMMARY: The environmental impacts of used palm empty fruit bunch as feedstock for electricity production in southern Thailand based on a life cycle approach is studied focusing on. The scope of this study includes the oil palm plantation and harvesting, crude palm oil and derivative production, electricity production and all transportation activities throughout its life cycle from cradle-to-gate. It is found that the greenhouse gas (GHG) emissions of utilizing palm empty fruit bunch as fuel for 1 kWh of electricity is 0.0201 kg CO₂ equivalent. From the literature review [1], the GHG emissions from fossil fuel, coal or natural gas are 2.6441, 3.0026 and 0.0554 kg CO₂ equivalent/kWh, respectively.

Keywords: Life Cycle Assessment, Greenhouse Gas, Palm Empty Fruit Bunch, Electricity

INTRODUCTION

Thailand is an agricultural country. Biomass is the waste from agricultural after harvesting and industrial, that large amount in Thailand. In any one year, a lot of agricultural residues can be applied as biomass energy. Currently, Thailand requires more energy to produce electricity, which is not sufficient and the fuel used in the production of a higher price. Thus, biomass energy plays a role in the production of renewable energy. One of them is the palm empty fruit bunch. It is a palm solid residue from palm oil production which is prevalent in Southern.

Thailand is the top palm oil producer, is ranked third in the world after Indonesia and Malaysia, respectively, with a total area of 654,400 ha of oil palm plantation and the yield about 18956.25 kg of palm oil per hectare (1ha = 6.25 rai)[2].

Nowadays, palm oil industry in Thailand has grown significantly. The process of palm oil is a waste of fiber, shell and palm empty fruit bunch is extracted oil out, which can be used as another beneficial. Especially, empty fruit bunch which is a biomass material can be used as fuel to generate electricity.

During 2013, 2385765.05 ton of EFB was generated as waste in Thailand. 97049 tons was still left unusefully. This can be a potential for generate electricity up to 46.47 MW per year [3].

The research aimed to evaluate and compare the life cycle environmental impacts of palm empty fruit bunches utilization for electricity production. Functional unit of this study is 1 kWh of electricity production. The impact assessment is assessed throughout its life cycle from cradle-to-gate.

METHODOLOGY

Functional unit and system boundary

The functional unit of this study is 1kWh of electricity generation from use palm empty fruit bunch as feedstock. In this study, the primary data were collected from the site at southern of Thailand including, crude palm oil and derivative production, electricity production and all transportation activities throughout its life cycle from cradle-to-gate. For allocation, the emissions were allocated by energy.

Data source

In this study, the data source is from primary and secondary data. Primary data is all stage of production except plantation and harvesting.

We are collected the primary data from field surveys. Secondary data is use in plantation and harvesting. It is almost use from literature review and the National Metal and Materials Technology Center that for calculating in this research. Land use changes and land management impacts are excluded.

Description of plant areas

Table1 is shown overall stage of electricity plantation case in southern of Thailand.

Table1. Overall Stage of Electricity Plantation

Stage of Production	Type of data
Demineralization Production	Primary
Steam Production	Primary
Electricity Production	Primary

RESULTS AND DISCUSSION

The GHG emissions contribution for demineralization, steam and electricity production stage of 1kWh is 18%, 23% and 59% are shows in Figure 1. The results show GHG emissions of the product will be lower emission than production of electricity by using

fossil fuel, coal or natural gas. The GHG emission from use empty fruit bunch as feedstock for electricity is 0.0201 kg CO₂ equivalent/kWh. For the literature, the difference sources such as natural gas, bunker and diesel are 0.0554, 3.0026 and 2.6441, respectively that shown in Figure 2. For calculation of GHG emissions, utilization of biomass for fuel is environmental friendly more than another fuel. In case study, figure3 shows the biomass as energy source in electricity production is 0.021, while the literature reviews are 0.045 and 0.035. From the results, use of palm empty fruit bunch as feedstock for electricity production could be environmental friendly more than other fuel sources.

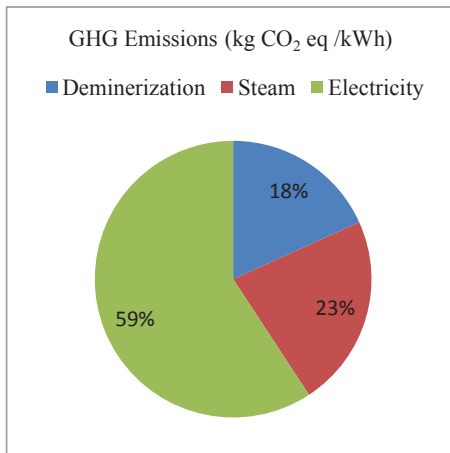


Figure 1. GHG emissions contribution for each stage of 1kWh electricity production

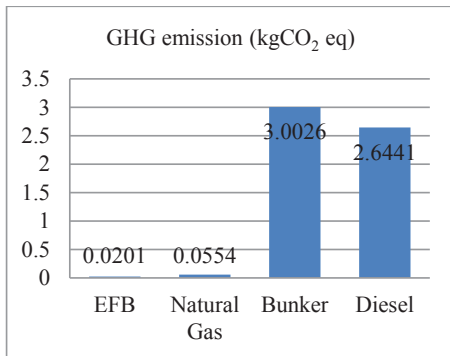


Figure 2. Comparison of GHG emissions for 1kWh electricity production from different fuel sources

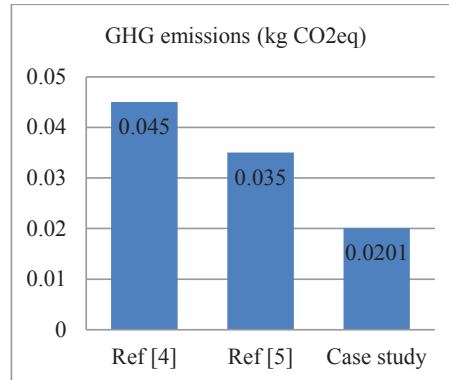


Figure 3. Comparison using biomass as energy source in electricity production

ACKNOWLEDGMENT

This research is supported by the National Metal and Materials Technology Center under National Science and Technology Development Agency, Ministry of Science and Technology. The authors would like to thank all factories, which support valuable data.

References

- [1] Thailand Greenhouse Gas Management Organization) (2010). CDM Project in Thailand.
- [2] Office of Agricultural economics (2014). Palm oil in Thailand.
- [3] Department of Alternatives Energy Development and Efficiency (2013). Biomass Potentials in Thailand. Ministry of Energy, Bangkok.
- [4] World Nuclear Association (2010). WNA Report Comparison of Lifecycle Greenhouse Gas Emissions of Various Electricity Generation Sources
- [5] D. Weisser. "A guide to life-cycle greenhouse gas (GHG) emissions from electric supply technologies". *Energy*, 32(9), 2007, pp. 1543-1559.

LIFE-CYCLE GHG EMISSION OF CASSAVA-BASED BIOETHANOL PRODUCTION

Tapanee Namjuncharoen¹, Seksan Papong²,
Pomthong Malakul^{2,3} and Thumrongrat Mungcharoen¹

¹Faculty of Engineering, Kasetsart University, Thailand

²National Metal and Materials Technology Center, Thailand

³The Petroleum and Petrochemical College, Chulalongkorn University, Thailand

SUMMARY: This study aims to assess the life-cycle GHG emissions of cassava ethanol production system focusing on utilization of biomass and biogas as energy source in the steam production process. Scope of life cycle assessment is “cradle to gate” approach by evaluating all stages of product’s life including cultivation and harvesting of feedstock, feedstock transport, feedstock processing, ethanol conversion, by products processing and on-site waste management. The functional unit of this study is 1 liter of anhydrous ethanol produced. The use of biogas from wastewater for steam production greatly affects the GHG emissions. The GHG emission of bioethanol plant that uses biogas from wastewater for steam production is 0.55 kg-CO₂-eq/L-ethanol, while the bioethanol plant without biogas utilization is 1.05 kg-CO₂-eq/L-ethanol.

Keywords: lifecycle assessment, Greenhouse gas, cassava, bioethanol

INTRODUCTION

From the sudden increase of energy consumption in the world and the depletion of fossil fuel reserves, has encouraged researches on renewable and sustainable resources. Bio-ethanol is one of significant role in renewable energy for transport since the price of oil has been growing at the rapid rate. Thailand is an agriculture based country, the government support to use bio-ethanol in order to reduce oil import.

The life-cycle greenhouse gas emissions of cassava-based bioethanol have been estimated in several studies [1,2,3]. Most of these studies suggested that using bioethanol from cassava as a fuel results in higher net GHG emissions than using gasoline. The most of GHG emission from the using coal as steam energy source. At present in Thailand, most the cassava based bioethanol plants have use biogas utilization as steam energy source and substituted biomass for coal.

The aim of this study is to assess the life-cycle GHG emissions of cassava-based ethanol production system focusing on utilization of biomass and biogas as energy source in the steam production process.

METHODOLOGY

Functional unit and system boundary

The scope of the study is “cradle to gate” approach by evaluating all stages of product’s life including cultivation and harvesting of feedstock, feedstock transport, feedstock processing, ethanol conversion, by products processing and on-site waste management. The functional unit for this study is 1 liter of anhydrous ethanol derived from cassava. Data included the transportation of cassava from the plantation to the factory, the production of electricity and water, and the air emissions from combustion process in boiler. If biomass was fuel that used in the boiler to produce steam from waste,

it gave no environmental burden but the data of biomass production was included. CO₂ emission from combustion process was excluded according to carbon neutral rule.

Data source

In this study, most of input–output data were collected as primary data at the actual sites in northeastern Thailand including cassava plantation, cassava chip production, and bioethanol production plants as well as the air emissions from combustion process in boiler. The secondary data were used in this study as necessary from literatures and calculation.

Description of plant cases

Table 1 summarizes the three actual cases of cassava ethanol plants in Thailand that were selected on the basis of information obtained from a field survey.

Table 1. Cases of each plant

	Wastewater treatment	Biogas	Steam energy source
Case 1	✗	✗	Biomass
Case 2	✓	Utilizing	Biomass + Biogas
Case 3	✓	✗	Biomass

RESULTS AND DISCUSSION

The GHG emissions for the three plant cases comparing with the results from literature [1] are shown in Figure 1. GHG emission for plant cases 1, 2 and 3 are 1.026, 0.548, and 0.613 kg-CO₂-eq/L-ethanol, respectively. Focusing on the ethanol conversion stage, the GHG emission contribution could be shown in Figure 2. The results showed that major emission caused from feedstock

cultivation & processing. While the major GHG emission of bioethanol plant that has no wastewater treatment system is CH₄ emission from wastewater treatment. The reason for GHG emission reduced of case 1 and 2 ethanol plant is mainly from steam production using biomass substituted for coal as energy source of the steam. From the literature review [1], the GHG emission of steam production is 0.872 kg-CO₂-eq/L-ethanol and GHG emission of using biomass in steam production in this study is 0.029 kg-CO₂-eq/L-ethanol (approximately 96% reduction) as shown in Figure 3. Result from this study indicate that using biomass and biogas as energy source in the steam production process could reduce GHG emission of cassava-based bioethanol more than 50%.

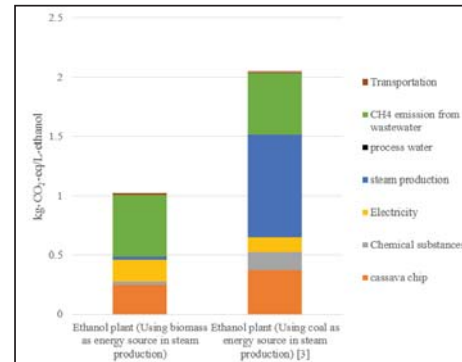


Figure 3. Comparison using biomass and coal as energy source in steam production

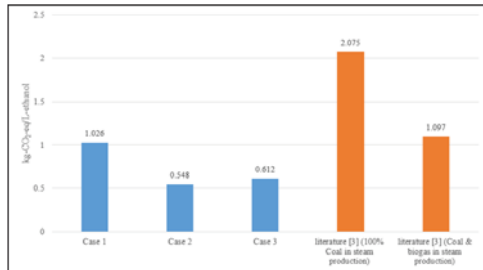


Figure 1. GHG emission for three bioethanol plants cases

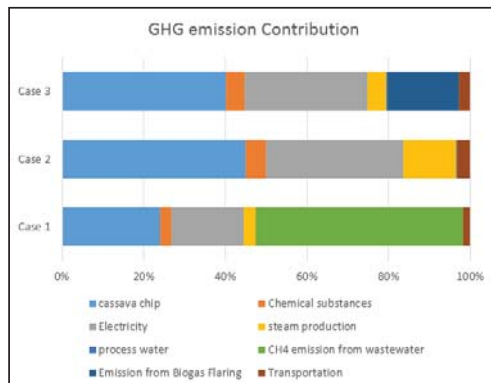


Figure 2. GHG emission contribution for three bioethanol plants cases

ACKNOWLEDGMENT

This research is supported by the National Metal and Materials Technology Center under National Science and Technology Development Agency, Ministry of Science and Technology. The authors would like to thank all data providers for this study.

References

- [1] Y. Moriizumi, P. Suksri, H. Hondo, and Y. Wake, "Effect of Biogas Utilization and Plant Co-Location on Life-Cycle Greenhouse Gas Emissions of Cassava Ethanol Production", *Journal of Cleaner Production*, **37**, 2012, pp. 326-334.
- [2] S. Papong, and P. Malakul, "Life-Cycle Energy and Environmental Analysis of Bioethanol Production from Cassava in Thailand", *Bioresource Technol*, **101(1)**, 2010, pp. S112-S118.
- [3] T. Silalertruksa, and S.H. Gheewala, "Environmental Sustainability Assessment of Bio-Ethanol Production in Thailand", *Energy*, **34**, 2009, pp. 1933-1946.

SCIENCE TECHNOLOGY AND INNOVATION CHALLENGES OF BIOMASS IMPLEMENTATIONS

Srichattra Chaivongvilan¹

¹Department of Social Development, National Science Technology and Innovation Policy Office, Thailand

SUMMARY: This paper provides an in-depth review and analysis on the science technology and innovation (STI) barriers in order to achieve bioenergy implementations in Thailand. Though, Thailand appears to have clear targets on alternative energy in the next 10 years according to the master plan formulated by Ministry of Energy but these ambitious-bioenergy targets are based solely on the potential of resources existing and planned planting in the country. In order to transform biomass to end-used consumption, it is a need to define the STI platform for actions. However, there is no study on the STI policy for bioenergy implementations. Yet, there are several concepts of best-practices in difference prospects but there is no integration of science technology and innovation policy as a whole. This paper utilized the qualitative method, the research data sources, and the industrial interviews in person. This paper contends the STI roles currently accorded to biomass to energy supply chain in Thailand and an early attempt at developing policy recommendations.

Keywords: STI policy, biomass, energy, research, implementation

INTRODUCTION

Thailand located in the tropical region with warm-humid climate. This geography, therefore, suited for agricultural sector and other land-use activities. With scarcity of domestic energy, the country has been faced with high import dependency for energy satisfaction. The Ministry of Energy, then, announced the *Alternative Energy Development Plan (AEDP) for the years 2012 to 2021* in order to set the renewable targets for assuring increasing-energy demand. Bioenergy, which consists of biomass for heat and power, biogas for heat and power, and biofuels in transportation, are shared about 80% of the plan. This is undoubted according to the prosperity of biobased resource for producing bioenergy. Several policies and mechanisms are formulated to support the consumption of bioenergy – such feed-in-tariff and research fund support. This paper reviews and analyses the science technology and innovation (STI) barriers in order to achieve bioenergy implementations in Thailand.

METHODOLOGY

The qualitative method is used in this paper. The unstructured interviewing and case studies are decidedly utilised in this study due to the dissemination of information. The series of reports and related works are examined with precise consideration on science, technology and innovation policies and their implementations.

Energy data

The data for energy policy in order to determine of STI policy are based on the master plan provided by the Ministry of Energy, Thailand. Thus, Ministry of Energy produce important data for the share of energy consumption per annum, the share of renewable energy per year and other energy related information such economic and environment.

Technology data

The basis for the technology data is from several studies and reports collected from diverse sources both academic and governance data. The technology status analysis has been made and conclude in *Thailand Bioenergy Technology Status Report 2013* as part of the results in this paper.

Economic data

The economic data based on the number in the white paper studied by the National Science Technology and Innovation Policy Office (STI) in year 2012 and updated in 2015.

TECHNICAL STATUS RESULTS

Biomass supply chain

According to supply chain of biomass to energy as shown below. Four sections are separated from this supply chain, namely, feedstock supply, biomass conversion, bioenergy distribution and energy endues. This study focuses solely on the feedstock supply and biomass conversion.



Figure 1. Biomass to energy supply chain

Biomass potential

The data in 2012, shown that Thailand' potentiality represented at 16,812.88 ktOE, in which 9,231.82 ktOE were form utilization as solid biofuel (agricultural residues), 6,560.82 ktOE from biogas production and 1,020.24 ktOE from biofuel production. The data, however, calculated by the estimation of total crops and divided by ratio of collection efficiency and wasted production during the transformation of food industry. The potential shown the calculation of full potential if the

collection and transformation technology is extremely applied for producing each type of bioenergy.

Table 1. Thailand biomass potential 2012

Type of Bioenergy	Quantity for biomass feedstock production	Energy potential (ktoe)
Agricultural waste	24.25 Million tons /year	9,231.82
Field based	17.23	6,570.54
Process based	5.77	2,196.70
Agro-based	1.15	464.57
Biogas	11,749.02 Million m3/year	6,560.82
Animal manure	733.68	364.72
Municipal solid waste	582.25	268.77
Industrial wastewater	10,433.09	5,927.33
Biofuels	1,525.70 Million litres/year	1,020.24
Bio-ethanol	642.40	323.52
Bio-diesel	883.30	696.72
Total		16,812.88

Technology status

Thermochemical conversion technology

Thermochemical conversion is one of processes that transform biomass into energy. The thermochemical conversion technologies include pretreatment, combustion, gasification, municipal solid waste, and pyrolysis. The status of each technology is varied according to the development of research and development in each section.

Biogas technology

Thailand has utilized biogas technologies for waste treatment and energy production since 1960s. There are four major types of biomass using to produce biogas, namely, industrial wastewater, farm wastes, bio crops, and municipal waste. Biogas technology is the success case of commercialized technology in Thailand. There are lots of local technology that can be commercialized successfully. However, there are still technologies need to be developed in further.

Liquid biofuel production technology

The current commercialised liquid biofuels in Thailand are ethanol and biodiesel. Majority of ethanol production is produced by the fermentation of molasses, a by-product of sugar manufacture. While biodiesel is produced from the transesterification of palm oil. The status of liquid biofuel production technology in Thailand are mostly in the commercialisation stage and in operation. The future technology, such lignocellulose and algae are under development or

only still at early stage.

POLICY RESULTS

The science, technology and innovation (STI) system is to apply the technical data and economic data. The knowledge integration covers the barriers and opportunities of bioenergy in Thailand. The definitions of science, technology and innovation in terms of policies are listed as follow;

Science: The definition of science in terms of policies in this paper is education, knowledge of science, research and development, and skills in academia

Technology: The definition of technology in terms of policies in this paper is practical activities of science, such engineering, technician, standard and technology transfer.

Innovation: The definition of innovation in terms of policies in this paper is marketing, business model of technology, innovative thinking, and creating idea.

In order to be able to represent the STI policies of bioenergy, it is necessary to apply the STI matrix to the bioenergy supply chain. What is important in this instance is that the overview of STI in each section of supply chain must be cleared with the evidences of technical data, economic data and research and development status. The evaluation of STI in bioenergy supply chain represented in this paper is shown in the overall of supply chain not in each technology section.

STI matrix of bioenergy supply chain

Table 1. Bioenergy supply chain and STI barriers

	Feedstock	Conversion	End-use
Science (S)	R&D , Knowledge, Skill improving course, Lab, etc.		
Technology (T)	Standard, Technology, Engineering, Technology transfer, etc.		
Innovation (I)	Innovative, Marketing, Business model, Tax, etc.		

CONCLUSIONS

This paper presents the suited STI ways of actions in order to implement bioenergy in Thailand with barriers and opportunities.

ACKNOWLEDGMENT

The author would like to thank Dr.Suneerat Fukuda from Joint Graduate School of Energy and Environment (JGSEE) and Miss Supatchaya Konsomboon for her supports on the technical contents and working partners.

ATTENUATION OF SOLAR RADIATION DUE TO AEROSOLS IN THE ATMOSPHERE OF THAILAND

Sayan Phokate¹

¹Department of Applied Physics, Faculty of Engineering,
Rajamangala University of Technology Isan, Khon Kaen Campus, Thailand

SUMMARY: This research aims to calculate the attenuation of solar radiation due to aerosols in the atmosphere of Thailand. Based on the solar radiation data derived from the measured and calculated by theoretical models on the cloudless sky. Then the relationship in a mathematical model for calculating the attenuation of solar radiation due to aerosols from visibility data, and use such models to calculate the attenuation of solar radiation due to aerosols of 85 meteorological stations nationwide. The results showed that the attenuation of solar radiation due to aerosols varies by time of year. In the dry season is high and in the rainy season is low. The average for the year was 0.1673 ± 0.0022 .

Keywords: solar radiation, attenuation, aerosols, visibility, cloudless sky

INTRODUCTION

Aerosol refers to particles small solid or liquid suspended in the air and moves according to the movement of air, the density, size, shape and distribution of the various elements [1,2]. Aerosols may be of natural origin such as forest fires, desert storms and volcanic eruptions, etc. Some aerosols resulting from human activities such as industrial aerosols and the vehicles. Generally, the amount properties and distribution of aerosols also depends on the area and time of year [3]. In creating the model for predicting climate (climate model) need to know the properties and distribution of aerosols which affect the reduction of solar radiation enter the Earth's surface [4,5].

RESEARCH METHODS

Determining the solar radiation from model

We can calculate the solar radiation at the Earth's surface on a cloudless sky using the different models that are accurate and difficulty [6]. Considering the weather in Thailand in various regions, which are different. Researchers use physical model of Nunez [1]. Because the model is generally applicable and easy to calculate. It also has a relatively high accuracy model does not consider the reduction of aerosols.

$$H_{\text{model}} = H_{sc} \frac{(1 - \alpha_A)(1 - \phi_o - \phi_w)}{1 - \alpha_A \alpha_G} \quad (1)$$

where H_{model} is solar radiation calculated at the Earth's surface; H_{sc} is solar radiation outside the Earth's atmosphere; α_G is reflection coefficient of the Earth's surface; α_A is scattering coefficient of air molecules and ϕ_w, ϕ_o are absorption coefficient of water vapor, and ozone, respectively.

Attenuation of solar radiation due to aerosols

Finding a attenuation of solar radiation due to aerosols required solar radiation on a cloudless sky. The data of solar radiation is measured by the Department of Alternative Energy Development and Efficiency of the 38 stations between the years 2000 to 2011. The difference between the solar radiation calculated from the model to the measured result from the aerosols in the atmosphere [1,7,8]. This can be written in the form of aerosol attenuation (A_{att}). Find the attenuation of solar radiation can only point to measure the solar radiation, which in Thailand is limited. Therefore, the values A_{att} correlated with visibility data from the same station. Which will have a relationship in empirical equation for the calculation A_{att} of the station without measuring the solar radiation.

RESULTS AND DISCUSSION

When calculating the intensity of solar radiation in cloudless sky using equation (1). The difference between the solar radiation measured with the calculated values. Using data in the day and the same time calculate the attenuation of solar radiation due to aerosols in the cloudless sky. Because finding the A_{att} by the above method do only for points the measured solar radiation. Therefore, finding the A_{att} at another location in Thailand, the researcher will use the visibility data. The relation of A_{att} with visibility data from the same station results are shown in Figure 1. The attenuation of solar radiation due to aerosols decreased when visibility is very valuable. Which is correlated with reliability a relatively high correlation coefficient (R^2) was 0.92. The relationship can be written in the following equation.

$$A_{\text{att}} = 0.0021(\text{vis})^2 - 0.058(\text{vis}) + 0.513 \quad (2)$$

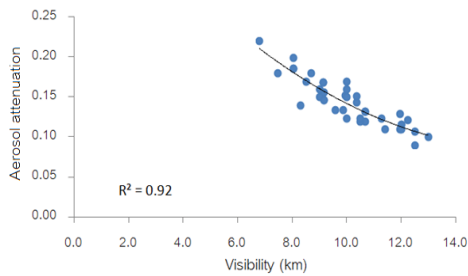


Figure 1. Show the relationship between the attenuation of solar radiation due to aerosols (A_{att}) with visibility data in the cloudless sky.

In this research, the data is divided into six regions for Thailand. The relationship of the attenuation of solar radiation due to aerosols with time of the year is shown in Figure 2. Found that, the North region is higher than all regions during the months of January to April. The most valuable in March, which is consistent with Chantraket et al., [5]. That is, during the month of March with the burning of agricultural waste materials to provide farmland including fog and forest fires which are a major source of aerosols. During January to March, the South was lower than all regions and was relatively constant throughout the year by aerosols mainly originate from the sea. In the whole of the country has changed by the time of year during January to March, it is very valuable. And then gradually reduced to a minimum in June. Then, there is an increasing trend. That is, the attenuation of solar radiation due to aerosols during the dry season (December to April) is very valuable with the most average in February equal to 0.2183 ± 0.0042 . During the rainy season (May to October) is less by the lowest average in June equal to 0.1314 ± 0.0007 . The annual average is 0.1673 ± 0.0022 with standard error of the mean equal to 0.00114 . Consistent with Esposito et al. [3] and Utrillas et al. [9] found that the attenuation of solar radiation due to aerosols is less in the rainy season and very valuable in the dry season, with an average during the 0.02 to 0.6. Which is constantly changing according to season and geography.

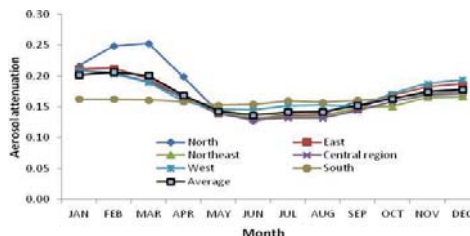


Figure 2. Changes by the time of year in each region of attenuation of solar radiation due to aerosols calculated using the average visibility data, which is the average monthly during 1983 to 2011

CONCLUSION

This research aims to calculate the attenuation of solar radiation due to aerosols in the atmosphere. The solar radiation data will be used to determine in conjunction with the ground data on the dates cloudless sky. Using the model for the solar radiation at ground level compared with the solar radiation is measured. Found that the attenuation of solar radiation is correlated with visibility data. That is, when the visibility is decreased attenuation of solar radiation is less. The attenuation of solar radiation due to aerosols has changed the time of year. The very valuable during the months of December to April and will be less in the months of June to November. The average maximum in February and average minimum in June with the average annual equal to 0.1673 ± 0.002 .

References

- [1] M. Nunez, "The development of a satellite-based insolation model for the Tropical Pacific Ocean", *Journal of Climatology*. **13**, 1993, pp.607-627.
- [2] M. Iqbal, "An Introduction to Solar Radiation", New York, *Academic Press*, 1983.
- [3] F. Esposito, L. Leone, G. Pavese, R. Restieri and C. Serio, "Seasonal variation of aerosols properties in South Italy: a study on aerosol optical depths, Angstrom turbidity parameters and aerosol size distributions", *Atmospheric Environment*. **38**, 2004, pp.1605-1614.
- [4] M.G. Iziomon, and H. Mayer, "Assessment of some global solar radiation parameterizations", *Solar Energy*. **64**, 2002, pp.1631-1643.
- [5] P. Chantraket, N. antiplubthong and T. Chanyatham. "Aersol and cloud condensation nuclei distribution during summer season over Northern region of Thailand", *J. Environ. Res.* **35**, 2013, pp. 87-120.
- [6] S. Izquierdo, M. Rodrigues and N. Fueyo "A method for estimating the geographical distribution of the available roof surface area for large-scale photovoltaic energy- potential evaluations", *Solar Energy*. **82**, 2008, pp. 929-39.
- [7] C.A. Gueymard, "Parametrized transmittance model for direct beam and circumsolar spectral irradiance", *Solar Energy*. **71**, 2001, pp.325-346.
- [8] P. Ineichen, "Comperison of eight clear sky broadband models against 16 independent data banks", *Solar Energy*. **80**, 2006, pp.468-478.
- [9] M.P. Utrillas, J.A. M a r t í n e z -Lozano, V.E. Cachorro, F. Tena and S. Hernandez, "Comparison of aerosol optical thickness retrieval from spectroradiometer measurement and from two radiative transfer mode", *Solar Energy*. **68**, 2000, pp.197-205.

EFFICIENCY ENHANCEMENT OF ZNO DYE-SENSITIZED SOLAR CELLS BY MODIFYING PHOTOELECTRODE AND COUNTERELECTRODE

Kritsada Hongsith^{1,2}, Niyom Hongsith^{2,3}, Duangmanee Wongratanaphisan^{1,2}, Atcharawon Gardchareon^{1,2}, Surachet Phadungthitidhada^{1,2} and Supab Choopun^{1,2}

¹Department of Physics and Materials Science, Faculty of Science, Chiang Mai University, Thailand

²Thailand Center of Excellence in Physics (ThEP center), CHE, Thailand

³School of Science, University of Phayao, Thailand

SUMMARY: In this research, ZnO photoelectrode and Platinum counterelectrode in dye-sensitized solar cells (DSSCs) were modified by sparking technique and investigated photoconversion properties. The ZnO photoelectrode was adjusted by using double-layered technique. Here, the DSSC structures were FTO/double-layered ZnO/N719/electrolyte/Pt counterelectrode. The efficiency characteristics for DSSCs were measured under illumination of simulated sunlight with the radiant power of 100 mW/cm². It was found that the best results of DSSCs were observed with power conversion efficiency of 2.53% at 250 sparking cycles for ZnO nanopowder over-layered which was significantly higher than 1.83% of the reference cell. The efficiency enhancement can be explained by the arising of short-circuit photocurrent due to increasing of light scattering and dye adsorption for double-layered photoelectrode and the increasing of the active surface area of Platinum nanoparticles in counterelectrode.

Keywords: Dye-sensitized solar cells, ZnO, Platinum, Nanoparticles, Sparking technique

INTRODUCTION

The structure of a dye sensitized solar cell (DSSC) consist photoelectrode, electrolyte and counterelectrode. The significant advancement has made by the work of Grätzel group [1]. Recently, ZnO semiconductors were widely used as photoelectrode in DSSCs. However, the energy conversion efficiency of DSSCs based on ZnO is relatively too low because it is affected by many factors depending on the structure of DSSCs especially, the limit of short circuit current density on the morphologies of photo- and counterelectrode. Thus, there are many techniques to improve the efficiency by improvement of photoelectrode and counterelectrode by mainly increasing of short circuit current density. One of interesting technique was used by using the double-layered of semiconductor in photoelectrode [2,3] and Platinum nanoparticles in counterelectrode [4]. To prepared ZnO and Platinum nanoparticles, a new technique was the sparking process [5]. The sparking process is used high voltage to apply between metal tips and resulting to melting. Therefore, nanoparticles moved towards the substrate by the high kinetic energy and oxidized in atmospheric air.

In this work, the double-layer in photoelectrode and Platinum nanoparticle in counterelectrode by sparking process were prepared for DSSC application. The enhancement of efficiency in term of an increase of thickness, surface area and decrease charge transfer resistance (R_{ct}) were explained.

METHODOLOGY

The ZnO nanoparticle thin films were obtained by sparking the zinc wire with high voltage on the

fluorine-doped tin oxide (FTO) glass substrate. The experiment was repeatedly done at 100, 150, 200, 250 and 300 cycles in ambient air under atmospheric pressure. Then, screened ZnO nanopowder on to ZnO nanoparticle to form double-layered photoelectrode. The ZnO photoelectrodes were prepared by soaking in an N719 dye solution and the platinum counterelectrode was prepared by sparking Platinum wire onto FTO and thickness of Platinum nanoparticles film controlled by number of sparking cycles for 15 cycles, schematic diagram of Photo- and Counter electrode showed in Fig. 1. The dye-loading ZnO photoelectrode and counterelectrode were assembled into a sealed cell with parafilm spacer. In the sealed cell, I⁻/I₃⁻ acetonitrile electrolyte was injected from the edges into the open cell and the cell was tested immediately by using simulated AM 1.5 sunlight illumination with 100 mW/cm² light output.

RESULTS AND DISCUSSION

The surface morphologies of ZnO and Platinum films in photoelectrode and counterelectrode were showed in Fig. 2. The photovoltaic performances of DSSCs with the different films ZnO of single layer (SL) and double layer (DL) based on reference platinum and sparking platinum was shown in Fig. 3. The photovoltaic performances of DSSCs with the different films thickness of ZnO nanoparticle by sparking with ZnO nanopowder as double layer based on sparking platinum counterelectrode and the electrochemical impedance of DSSCs was measured the Nyquist plots were showed in Fig. 4. The result showed that the efficiency increases when the

number of sparking cycles increased and the best results of DSSCs were observed with J_{sc} of 8.57 mA/cm² and power conversion efficiency of 2.53% at 250 sparking cycles for ZnO nanopowder overlayers which was significantly higher than 1.83% of the reference cell. The semicircle in the Nyquist plot indicated that the charge transfer resistance (R_{ct}) of the DSSCs with sparking 250 cycles as photoelectrodes had the smallest value of the charge transfer resistance and another results were summarized in Table 1.

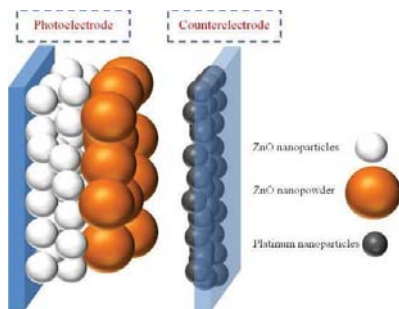


Figure 1. Schematic diagram of Photo electrode and Counterelectrode.

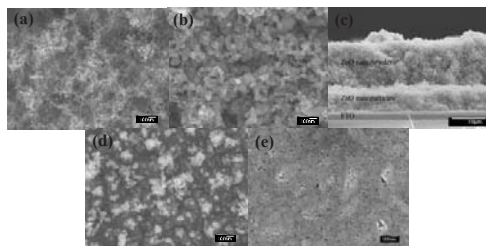


Figure 2. Surface morphology of the as-deposited films of (a) ZnO nanoparticles by sparking process, (b) ZnO nanopowder, (c) cross-section of a double layered of ZnO photoelectrode film, (d) Platinum films by sparking process and (e) Platinum films by thermal deposited

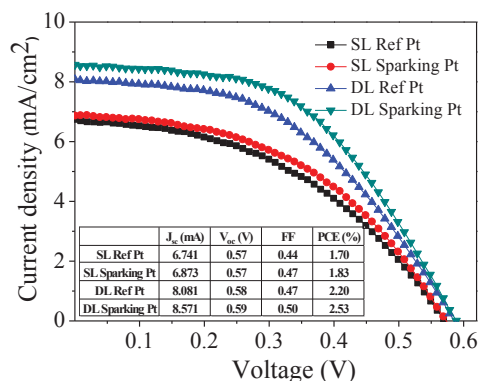


Figure 3. Photovoltaic performance of the DSSCs fabricated with different film of ZnO single layer

(SL) and double layer (DL) based on reference platinum and sparking platinum and Photovoltaic performance parameters of DSSCs (inset)

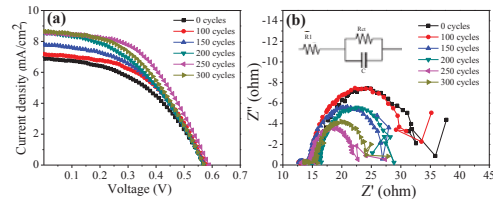


Figure 4. Photovoltaic performance and Nyquist plots of the DSSCs fabricated with different film thickness of ZnO nanoparticle by sparking to double-layered

Table 1. Photovoltaic performance parameters of DSSCs fabricated with different number of sparking cycle of ZnO nanoparticle by sparking process.

Sparking cycles (cycle)	V_{oc} (V)	J_{sc} (mA)	FF	PCE (%)	R_{ct} (Ω)
0	0.57	6.873	0.47	1.83	16.26
DL100	0.58	7.179	0.49	2.04	15.92
DL150	0.57	7.793	0.47	2.09	11.92
DL200	0.57	8.576	0.44	2.15	11.37
DL250	0.59	8.571	0.50	2.53	7.896
DL300	0.57	8.646	0.47	2.29	8.963

ACKNOWLEDGMENT

Kritsada Hongsith would like to acknowledge a financial support from the Graduate School, Chiang Mai University and 50th CMU Anniversary-Ph.D. Scholarship.

References

- [1] B. O'Regan and M. Grätzel, "A low-cost, high efficiency solar cell based on dye-sensitized colloidal TiO₂ films," *Nature*, **353**, 1991, pp. 737-740.
- [2] G. Dai, L. Zhao, J. Li, L. Wan, F. Hu, Z. Xu, B. Dong, H. Lu, S. Wang, J. Yu. "A novel photoanode architecture of dye-sensitized solar cells based on TiO₂ hollow sphere/nanorod array double-layer film". *J. Colloid Interface Sci.* **365**, 2012, pp.46-52.
- [3] J. Tae Park, D. Kyu Roh, W. Seok Chi, R. Patel and J. Hak Kim. "Fabrication of double layer photoelectrodes using hierarchical TiO₂ nanospheres for dye-sensitized solar cells". *J. Ind. Eng. Chem.* **18**, 2012, pp. 449-455.
- [4] C. H. Yoon, R. Vittal, J. Lee, W. S. Chae and K. J. Kim. Enhanced performance of a dye-sensitized solar cell with an electrodeposited-platinum counter electrode. *Electrochimica Acta.* **53**, 2008, 2890-2896.
- [5] K. Hongsith, N. Hongsith, D. Wongratnanaphisan, A. Gardchareon, S. Phadungthitidhada, P. Singjai and S. Choopun, "Sparking deposited ZnO nanoparticles as double-layered photoelectrode in ZnO dye-sensitized solar cell," *Thin Solid Films*, **539**, 2013, pp. 260-266.

EFFECT OF ZNO DOUBLE LAYER AS ANTI-REFLECTION COATING LAYER ON DYE-SENSITIZED SOLAR CELLS

Ekkachai Chanta^{1,3}, Duangmanee Wongratanaphisan^{1,2}, Atcharawon Gardchareon^{1,2},
Surachet Phadungdhitidhada^{1,2}, Pipat Ruankham¹ and Supab Choopun^{1,2}

¹Department of Physics and Materials Science, Faculty of Science, Chiang Mai University, Thailand

²Thailand Center of Excellence in Physics (ThEP center), CHE, Thailand

³Energy Policy and Planning Office, Ministry of Energy, Thailand

SUMMARY: Dye-sensitized solar cells based on ZnO double layer anti-reflection coating (DLARC) thin films are investigated. The ZnO DLARCs were prepared by stacking two different ZnO morphologies prepared by two different techniques including RF-magnetron sputtering (rf-ZnO) and sparking technique (sp-ZnO). The device using rf-ZnO as the bottom layer and sp-ZnO (3 cycles) as the top one exhibits short circuit current density (J_{sc}) of 5.80 mA/cm² and the maximum power conversion efficiency (PCE) of 1.88 %, which is higher than that of the device stacking in a reverse order and the device using ZnO single layer anti-reflection coating (SLARC). The main enhancement of PCE is attributed to the reduction of light reflection at the substrate surface. This leads to increase of J_{sc} for efficiency improvement of DSSCs.

Keywords: ZnO, dye-sensitized solar cells, Double layer anti-reflection coating, Sputtering process, Sparking technique.

INTRODUCTION

Dye-sensitized solar cells (DSSCs) have been widely paid attention due to their great potential for low cost energy conversion devices. However, DSSCs show low power conversion efficiency (PCE) because of some efficiency losses, such as reflection of light by a substrate, charge recombination and carrier trapping in a material and surface, power dispersion due to the resistance of cell (material, metal, electrode, etc). Approached to improve the power conversion efficiency of DSSCs are to reduce these losses. Reduction of light reflection by using double layer anti-reflection coatings (DLARCs) is one of the effective approaches. [1]. DLARCs are expected to reduce the reflection and increase the transmission of light at the glass surface. These lead to an increase of the total flux of photons to photocurrent through the electrode and short circuit current density (J_{sc}), as shown in equation (1) [2].

$$J_{sc} = \int_{\lambda_1}^{\lambda_2} qF(\lambda)[1 - R(\lambda) + S(\lambda)]Q_i(\lambda)d\lambda \quad (1)$$

where q is elementary charge, λ_1 and λ_2 are the wavelength limits, $F(\lambda)$ is spectral solar flux (flux of the solar spectrum), $R(\lambda)$ is reflection of light, $S(\lambda)$ is scattering factor and $Q_i(\lambda)$ is internal quantum efficiency.

In this work, two size-different ZnO thin films were prepared by two different techniques including rf-magnetron sputtering process and sparking technique. Two of them were stacked onto each other and used as DLARCs in DSSCs.

EXPERIMENTAL

Two size-different ZnO thin films were prepared by two different techniques including RF-magnetron sputtering and sparking technique. RF-

magnetron sputtering (rf-ZnO) was performed for 60 minute under an atmosphere of Ar at 2.5×10^{-2} torr and sputtering power of 150 watts. Sparking technique apply high voltage when the 25 nF capacitor was changed to 10 kV for two Zn wires sharp and connected it by rotating control switch with 1 (sp1-ZnO), 3 (sp3-ZnO), 5 (sp5-ZnO) sparking cycles. One sample was prepared by using NP as the bottom layer and TF as the top one. The other sample was prepared in a reverse order. Subsequently, the samples were annealed at 450°C for 1 hr in the air. Surface and cross-sectional morphologies were characterized by field emission scanning electron microscopy (FE-SEM). Also, optical properties were studied by measurement of transmittance and reflectance via UV-vis spectroscopy. In addition, refractive index was obtained via ellipsometry. Finally, photoelectrochemical characteristics of the DSSCs were tested under stimulated sunlight AM 1.5 with the radiant power of 100 mW/cm².

RESULTS AND DISCUSSION

Figure 1. (a) shows FE-SEM image of ZnO prepared by sparking method with diameter of about 20 nm. The topography surface roughness and grain size of the ZnO prepared by sparking technique are smaller than those of the one prepared by sputtering method (Figure 1 (b)).

Reflectance and transmittance of the samples are show in Figure 2. It is seen that reflectance of all ZnO DLARCs are lower than that of the ZnO single layer anti-reflection coating (SLARC) and the reference (glass). Figure 2. (b) shows that transmittance of ZnO DLARCs using ZnO prepared by sputtering method as the bottom layer are higher than that the one using ZnO prepared by sparking method as the bottom layer. Especially, the rf-

ZnO/sp3-ZnO is highest transmittance value at 89.17% because the refractive index of the rf-ZnO/sp3-ZnO are lower than that of sp3-ZnO/rf-ZnO as shown in Figure 3. Therefore, light travels through the films prepared by rf-ZnO/sp3-ZnO was faster than the other conditions.

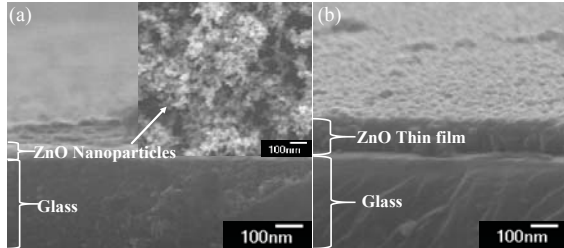


Figure 1. FE-SEM image and cross section thickness of (a) ZnO Nanoparticles prepared by sparking process and (b) ZnO thin films prepared by rf-magnetron sputtering at 60 min

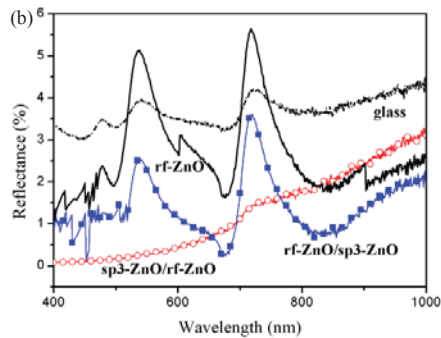
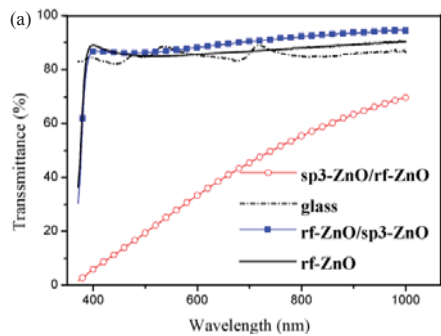


Figure 2. (a) the optical transmittance and (b) the optical reflectance spectra ZnO DLARCs prepared by rf-magnetron sputtering and sparking process

Moreover, Figure 4. shows photovoltaic performances of the DSSCs. The device with the rf-ZnO/sp3-ZnO exhibited J_{sc} of 5.80 mA/cm² and the maximum PCE of 1.88 %, which is higher than that of the reference cell (4.07 mA/cm², 1.53%).

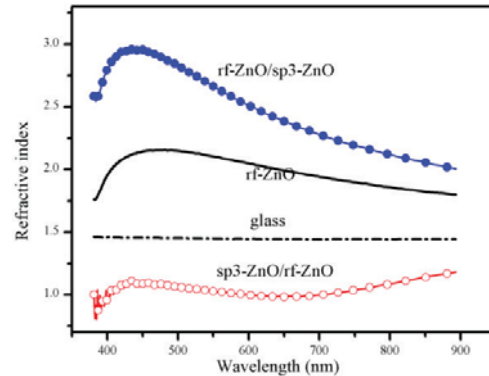


Figure 3. Total refractive index of ZnO double layer anti-reflection coatings (DLARCs)

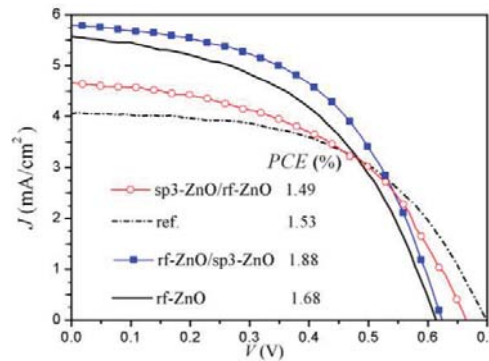


Figure 4. Photovoltaic performances of the DSSCs fabricated with ZnO DLARCs

ACKNOWLEDGEMENT

This research was supported by Energy Policy and Planning Office, Ministry of Energy, and the Graduate School, Chiang Mai University, Thailand.

References

- [1] D. Zhang, I.A. Digdaya, R. Santbergen, A.W. Weeber, "Design and fabrication of a SiO_x/ITO double-layer anti-reflective coating for heterojunction silicon solar cells", *Solar Energy Materials and Solar Cells*. **117**, 2013, pp.132–138.
- [2] E. Chanta, C. Bhoonanee, A. Gardchareon, D. Wongratanaphisan, S. Phadungdhithidhada and S. Choopun, "Development of Anti-Reflection Coating Layer for Efficiency Enhancement of ZnO Dye-Sensitized Solar Cells", *Journal of Nanoscience and Nanotechnology*. 2015, Article inpress.
- [3] K. Hongsith, N. Hongsith, D. Wongratanaphisan, A. Gardchareon, S. Phadungdhithidhada, P. Singjai and S. Choopun, "Sparking deposited ZnO nanoparticles as double-layered photoelectrode in ZnO dye-sensitized solar cell", *Thin Solid Films*. **539**, 2013, pp. 260–266.

ENHANCEMENT OF ZNO DYE-SENSITIZED SOLAR CELL PERFORMANCE BY MODIFYING PHOTOELECTRODE USING TWO-STEPS COATING-ETCHING PROCESS

Sutthipoj Sutthana¹, Duangmanee Wongratanaphisan^{1,2}, Atcharawon Gardchareon^{1,2},
Surachet Phadungthitidhada^{1,2}, Pipat Ruankham^{1,2} and Supab Choopun^{1,2}

¹Department of Physics and Materials Science, Faculty of Science, Chiang Mai University, Thailand

²Thailand Center of Excellence in Physics (ThEP center), CHE, Bangkok, Thailand

SUMMARY: ZnO photoelectrodes modified by two-steps coating-etching process with chemical wet etchants for dye-sensitized solar cell were investigated. The ZnO films were coated on a fluorine-doped tin oxide glass substrate and etched by mixed acid solution of HCl:HNO₃:distilled water, washed, and thermally treated for the first step. The second step, films coating process was repeated and etched by base solution of diluted NH₄OH in distilled water. Surface morphologies of unmodified and modified ZnO films look similar. DSSCs with modified photoelectrodes showed efficiency enhancement with maximum power conversion efficiency of 2.29%. From EIS analysis, it was suggested that the fill factor plays an important role on enhancement of power conversion efficiency. The fill factor increased due to the formation of pores structure in the photoelectrodes during etching process.

Keywords: ZnO, dye-sensitized solar cell, performance, two-steps coating-etching process.

INTRODUCTION

Solar cell factors included short-circuit current density (J_{sc}), open-circuit voltage (V_{oc}) and fill factor (FF) are long time investigated to enhance power conversion efficiency (PCE). The J_{sc} is directly related to amount of dye adsorption which can be increased by simple method such as increase thickness of photoelectrode or increase porosity [1]. V_{oc} can be improved by modify energy difference between Fermi level (E_F) of metal oxide and redox potential (Eredox) of electrolyte. FF can be improved by enhancing the rate of charge transport and regeneration. The increased J_{sc} is expected by increase dye adsorption supported by thick photoelectrode. However, the thicker photoelectrode will derogate carrier mobility affecting electron scattering and slow down regeneration due to aggregate particles. These effects lead to reduction of FF . To solve this effect, aggregate particles will be removed to form as porous photoelectrode. The pores structure will make single pathway direction for faster electron transport. Moreover, the increased ZnO/dye/electrolyte interfaces due to the pores will encourage faster electron regeneration [2].

In this work, ZnO photoelectrodes modified by two-steps coating-etching process with chemical etchants for DSSCs and their photoconversion properties were investigated. The two-steps coating-etching process include two-steps coating process and two-steps etching process. DSSCs with modified photoelectrode showed efficiency enhancement by increasing of FF and can be attributed to formation of pores structure in ZnO films during etching process.

EXPERIMENTAL

ZnO bottom films (ZBF) was coated on fluorine-doped tin oxide (FTO) glass substrates,

annealed at 400 °C for 1 h. The films were textured by mixed HCl:HNO₃:distilled water in volumetric ratio of 0.7:0.3:44 (acid solutions) for 10 s, rinsed by flow distilled water and annealed at 120 °C for 30 min. The second step, ZnO past was repeated coated on ZBF and annealed form as ZnO top films (ZTF) and etched by diluted NH₄OH (base solution) for 1, 2 and 3 min form as modified photoelectrode. Photoelectrodes were immersed in dye solution (N719) for 1 h and fabricated DSSCs.

Surface morphology was observed by field emission scanning electron microscopy (FE-SEM). Photovoltaic characteristics were measured under standard illumination (AM1.5) from solar simulator. Internal properties were investigated by electrochemical impedance spectroscopy (EIS)

RESULTS AND DISCUSSION

Surface morphologies of unmodified and modified films with acid solution for 10 s and base solution for 1, 2 and 3 min are shown in Fig. 1. The microstructures with some pores are observed and they look similar. However, from Image-J software analysis it was found that calculated pores area (A_p) of ZnO films is the minimum value of 45.6%. After surface modification, the areas are increased in ranks of 50.5-51.7%.

Current density-voltage (J - V) characteristic is measured as shown in Fig. 2, and parameters are summarized in table 1. The two-steps coated films showed greater J_{sc} than one-step coated films as expectation due to thicker films. However, there is poor in FF because aggregation of ZnO particles might derogate electron transport and regeneration. After modify by two-steps coating-etching process, J_{sc} showed small decreased because thickness is decreased during etching process.

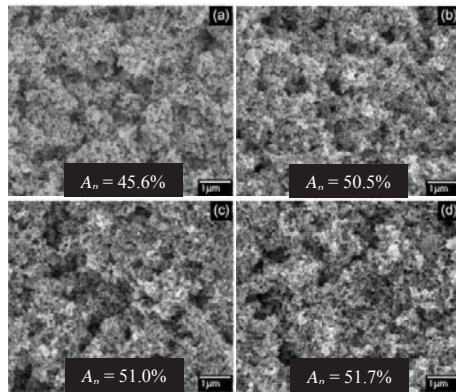


Figure 1. FE-SEM images of (a) ZnO films, and modified photoelectrodes with acid solution for 10 s and base solution for (b) 1 min, (c) 2 min and (d) 3 min.

FF showed rapidly increased and reached maximum value of 0.52 for base solution etching time of 1 min and enhance maximum PCE of 2.29%. The increase in FF can be attributed to the faster electron transport and regeneration. These results suggested that J_{sc} and FF can be improved by two-steps coating-etching process.

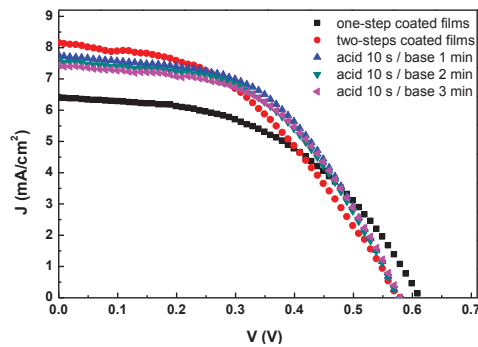


Figure 2. J-V characteristics of DSSCs fabricated on unmodified and modified photoelectrodes

Table 1. Photovoltaic parameters.

Films	J_{sc} (mA/cm^2)	V_{oc} (V)	FF	PCE (%)
one-step coated films	6.40	0.61	0.49	1.91
two-steps coated films	8.16	0.58	0.43	2.05
acid 10s/ base 1 min	7.75	0.57	0.52	2.29
acid 10s/ base 2 min	7.57	0.57	0.51	2.20
acid 10s/ base 3 min	7.43	0.58	0.51	2.21

Nyquist plots and Bode-phase plots of EIS spectra showed in Fig. 3, and the parameters were summarized in table 2. Recombination is slightly increased for DSSCs fabricated on modified photoelectrodes according to decreased R_{CT} which is not good for DSSC. The increased recombination in can be described as increased interfacial contact and surface defect due to etching process [3]. However,

small increased recombination is not much affecting to internal electron transport because the calculated τ is not changed. Decrease in R_{Pt} indicated faster charge migration across Pt-electrolyte interfaces and through to regenerate with oxidized dye. Regeneration may be occurred immediately after charge migrated to oxidized dye. Moreover, the increased pores area from morphologies results suggested that regeneration rate may be faster due to increased ZnO/dye/electrolyte interfaces. The pores position will reduce the pathway for electron scattering and increase probability of forward electron transport. These results can lead to an improvement in the FF and exhibits a good agreement with photovoltaic characteristics results.

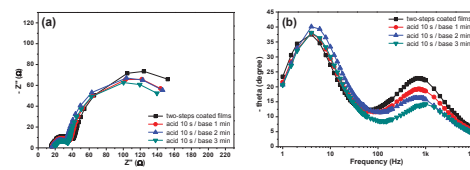


Figure 3. (a) Nyquist plots and (b) Bode-phase plots.

Table 2. EIS parameters of fabricated DSSCs.

Films	R_s (Ω)	R_{CT} (Ω)	R_{Pt} (Ω)	f_{peak} (Hz)	τ (ms)
two-steps coated films	15.4	150.7	26.9	4	39.8
acid 10s/ base 1 min	16.4	138.4	21.8	4	39.8
acid 10s/ base 2 min	16.5	139.7	17.5	4	39.8
acid 10s/ base 3 min	19.8	131.3	16.5	4	39.8

ACKNOWLEDGEMENT

This work was supported by CMU Mid-Career Research Fellowship program. Sutthipoj Sutthana would like to acknowledge for financial support from Energy Policy and Planning Office, Ministry of Energy; and Graduate School, Chiang Mai University.

References

- [1] H. Krysova, J. Trckova-Barakova, J. Prochazka, A. Zukal, J. Maixner, L. Kavan, "Titania nanofiber photoanodes for dye-sensitized solar cells" *Catalysis Today*, **230**, 2014, pp. 234-239.
- [2] S. Yang, H. Kim, S.-H. Ahn, C.S. Lee, "The effect of the agglomerated microstructure of dry-deposited TiO_2 electrodes on the performance of dye-sensitized solar cells", *Electrochimica Acta*, **166**, 2015, pp. 117-123.
- [3] C. Fei, J. Tian, Y. Wang, X. Liu, L. Lv, Z. Zhao and G. Cao, "Improved charge generation and collection in dye-sensitized solar cells with modified photoanode surface", *Nano Energy*, **10**, 2014, pp. 353-362.

AN EXPERIMENTAL STUDY OF THERMO-SYPHON SOLAR WATER HEATER IN THAILAND

Promparn Sae-Jung¹, Tanaporn Krittayanawatch¹, Phichamon Deedom¹ and Bundit Limmeechokchai¹

¹Research Center in Sirindhorn International Institute of Technology
Department of Mechanical, Faculty of Engineering, Thammasat University, Thailand

SUMMARY: The most widespread application of solar thermal energy is the thermo-syphon solar water heater (TSSWH). This paper presents the mathematical models and the experimental study for prediction the temperature of hot water produced from TSSWH. Results are presented of storage temperature, collector temperature and thermal efficiency of the TSSWH. From the experimental study during 7 days, average thermal efficiency was found about 46%, average temperature of hot water in the storage tank is 55.23°C and average collector temperature is 59.08°C. Finally, the results of TSSWH economic analysis revealed is competitive to the conventional electric heaters, especially when utilization factor is high and electricity price is high, used to access the cost effectiveness under conditions in Thailand.

Keywords: Thermo-syphon solar water heater, thermal efficiency, collector temperature, storage tank temperature

INTRODUCTION

The sun is an important power resource in the world and solar energy is heat and light that emitting from the sun and it is an important source of the renewable energy in the world. The technologies of the solar energy are broadly divide in passive solar and active solar depending on the method that use for capture and distribute the solar energy or the way its convert the solar energy into solar power.

In this experiment will focus on Passive system is the type of solar energy that uses indirect advantage from solar energy such as designing the roof of house in some country to fully capture the sunlight. They are two type, Integral collector-storage passive systems and Thermo-syphon system which using in this experiment. Thermo-syphon solar water heater is one of equipment that uses the advantage from natural convection. The Solar Water Heater is come with thermometer installed at the top, middle and the bottom of the tank, and also the inlet and outlet of the solar panel

METHODOLOGY

The solar water heater consists of storage tank with capacity 150 liters, the flat plate solar collector with area 2.16m², cover with double glasses for prevent heat losses. Connecting the systems with the pipe. The pipes are made from coppers, which copper can transfer heat better than other type of materials cover with insulator and aluminum tape. Before start the experiment, clean the system by release the water inside the system out completely; includes the tank storage that placed under the solar collector, and also removes unwanted lichen. Refill the water in the tank and pump it up to tank storage that setting above the solar.

Record the temperature of the water at different locations (T₁, T₂, T₃, T₄, T₅, T₆) also measured solar intensity by using a hand pyrometer and calculate the efficiency, pipe loss, and storage tank loss of the system.

ANALYSIS

This research has related to the experiment and could be calculated the efficiency and the necessary parameters.

RESULT AND DISCUSSION

This experiment determines the efficiency of the thermo-syphon solar water heater system with bimetal thermometer and compare to the original system which use thermo-couple type K to measure water temperature also predicts the temperature of hot water that will produce from this system. The setup was exposed to the solar radiation in one week, 8 hours per day by record all temperature in every 15 minutes at the same storage tank volume which is 150 liters and use the same condition with the original experiment. This experiment was conducted on 13-19 January 2015. The collector was exposed to the solar intensity from 9:00 a.m. to 5:00 p.m. The maximum water temperature was found to be 99 C around 1:00 p.m. with solar intensity 972 mV. It was observed from the collector outlet temperature (T₂) that heat up to the water storage. In the end of the day, the collector outlet temperature is lower than the storage water temperature due to the solar intensity in that time. The initial water which entering the collector (T₁) or drain from the storage tank give a lower temperature than the other temperature.

ACKNOWLEDGMENT

The team would like to thank Dr. Bundit Limmeechokchai, Mr. Nikhom Meedet, Mr. Natthawut Ruangtrakoonand, and Mr. Tongchana Thongtip for comments and help us to set up the experiment and Sirindhorn International Institute of Technology Thammasat University for the partial financial support to this study.

References

- [1] Wikipedia the Free Encyclopedia, (2014) Solar Energy, Energy from the Sun, URL: <http://en.wikipedia.org>
- [2] Wikipedia the Free Encyclopedia, (2014) Thermosiphon, Simple thermosiphon, URL: <http://en.wikipedia.org>
- [3] Wikipedia the Free Encyclopedia, (2014) Solar thermal collector, Flat plate collectors, URL: <http://en.wikipedia.org>
- [4] R. Shukla, K. Sumathy, P. Erickson and J. Gong. "Renewable and Sustainable Energy Reviews", *Solar water heating systems*, 2013, pp. 174-177.
- [5] M. and N.R. Ismail. "Collectors Innovation to Increase Performance Solar Water Heater" Literature Review, *Older Studies*, 2013, pp. 465-466.
- [6] M. Duff and J. Towey. "Two Ways to Measure Temperature Using Thermocouples Feature Simplicity, Accuracy, and Flexibility, Introduction, Thermocouple Theory" Why Use a thermocouple?, *disadvantage*, **44**, 2010, pp. 1.
- [7] Sirindhorn International Institute of Technology Thammasat University, Mechanical Engineering Faculty (2009), mechanical engineering Laboratory II Solar Water Heater.

TECHNO-ECONOMIC ASSESSMENT OF 3-5 kW_p SOLAR PHOTOVOLTAIC RESIDENTIAL ROOFTOP SYSTEMS IN SOUTHERN THAILAND

Mongkol Kuasakul¹, Jompob Waewsak¹, Chuleerat Kongruang² and Yves Gagnon³

¹Research Center in Energy and Environment
Department of Physics, Faculty of Science, Thaksin University (Phatthalung Campus)

²School of Management, Walailak University

³Université de Moncton, Edmundston (NB), Canada

SUMMARY: This paper presents a techno-economic assessment of 3, 4, and 5 kW_p solar photovoltaic (PV) residential rooftop systems in southern Thailand, a region where the rainy season is longer than other parts of the country. The systems consist mainly of a PV array, a grid connected inverter and a meter. The solar energy resources in 14 provinces were classified into 3 classes: low, medium and high solar radiation intensity. The system studied had a roof tilt angle of 30°, 8 major orientations and 6 different PV technologies: silicon-based technology; m-Si, p-Si, and hybrid heterojunction with intrinsic (HIT) and thin film-based technology; a-Si, CdTe, and CIS using PVSyst 6.3.2. The maximum annual energy yield was used for the economic analysis. Results show that the a-Si thin film and the CIS technology are the best technologies for the climatic conditions of southern Thailand, with an annual energy yield reaching a maximum of 7,635 kWh/year, with a system efficiency of 17% and a performance ratio (PR) of 84%. The economic analysis revealed that, under the current system cost and Feed-in-Tariff (FiT) incentive, solar PV residential rooftop systems are feasible in southern Thailand.

Keywords: feed-in-tariff, photovoltaic technology, rooftop systems, solar energy

INTRODUCTION

Recently, the Royal Thai Government launched its latest policy to increase the share of renewable energy in the country by utilizing Thailand's abundant solar energy resource potential. In 2013, the National Energy Policy Commission (NEPC) approved two policy packages increasing Thailand's target installed photovoltaic (PV) capacity by 1,000 MW to a total of 3,000 MW. One of the two packages is a solar PV rooftop program, with the power purchased under a feed-in-tariff (FiT). This program promotes the installation of up to 200 MW of PV systems on rooftops or other parts of buildings. Within the 200 MW, 15 MW is reserved for residential units with a capacity not exceeding 10 kW_p. The FiT incentive will be the same throughout the country, i.e. 6.85 THB/kW, including in the 14 provinces of southern Thailand.

Regarding the climatic conditions of southern Thailand, where the rainy season is longer than other regions of the country, the solar radiation intensity is in the range of 17.6-20.3 MJ/m²/day, while the average solar radiation intensity for Thailand is 19-20 MJ/m²/day. Figure 1 shows the solar energy resource for the whole territory of Thailand.

Figure 1 shows that the solar resource in Southern Thailand is less than in other regions of the country, mainly due to the longer rainy season affected by the Northeast and Southwest monsoons. In this context, the objective of this paper is to perform a techno-economic assessment of 3, 4, and 5 kW_p solar PV residential rooftop systems under the climatic conditions of southern Thailand and under the latest FiT incentive. This will assist in

making informed decisions on energy investments, while contributing to the mitigation of global warming.



Figure 1. Solar energy resource of Thailand [1].

METHODS

Solar energy resource in southern Thailand

The solar energy resources in 14 provinces of southern Thailand were classified into 3 classes: low, medium and high solar radiation intensity, in the range of 17.6-18.5, 18.5-19.4, and 19.4-20.3 MJ/m²/day, respectively. Songkla province, Ranong

province, and Satun province are indicative provinces for low, medium, and high solar radiation intensity, respectively.

Simulation of a 3-5 kWp PV rooftop system

A 3, 4, or 5 kWp solar PV rooftop system consists mainly of PV panels connected in series and parallel to an array junction box, a DC panel, a grid inverter, an AC panel with an AC surge protector, and a meter. The systems were simulated using the PVSyst 6.32 computer software with six different PV technologies: m-Si, p-Si, and the hybrid heterojunction with intrinsic (HIT) for the silicon-based technology and a-Si, CdTe, and CIS, for thin film technology. The effect of the orientation of the sun was investigated. The annual energy yield was evaluated and the maximum energy yield (in kWh/year) was used for the economic analysis.

Technical and economic analysis

The technical performances of 3, 4, and 5 kWp solar PV rooftop systems, the system efficiencies, and the performance ratios [2] were evaluated under the solar energy resource of Songkhla, Ranong, and Satun provinces.

Using a cost benefit analysis (CBA), the maximum yield was chosen for the economic analysis. The four main financial indicators, i.e., benefit cost ratio (BCR), net present value (NPV), internal rate of return (IRR), and payback period (PBP) were analyzed using the cost provided by the Solar Thai Future Company Limited and the latest FiT of 6.85 THB/kWh over a period of 25 years. The assumptions used for the economic analysis are given in Table 1.

Table 1. Assumptions for the economic analysis.

Parameters	Value
Project Lifetime	25 years
Inverter Replacement@10 th Year	75,000 THB
PV Module Efficiency Degradation	5% each year
Dust Effect	5%
System Cost (before VAT)	
3 kWp	280,000 THB
4 kWp	350,000 THB
5 kWp	420,000 THB
VAT	7%
Transportation to Site	20,000 THB
FiT for 25 years	6.85 THB/kWh

RESULTS AND DISCUSSION

Results show that the SW, S, and SE directions are the three main orientations where solar PV rooftop 3-5 kWp systems can generate the most energy in Songkhla, Ranong and Satun provinces.

For the 3 kWp and 5 kWp systems, it was found that the CIS technology could generate an additional 4,793 kWh and 7,635 kWh, respectively, of energy per year in comparison to the other technologies. However, the a-Si appears to be the best technology for 4 kWp solar PV rooftop systems,

with a generation of 6,344 kWh/year

The module efficiencies were in the range of 4.5% for the a-S, while it was up to 15.7% for the HIT PV technology. On the other hand, the system efficiency was in the range of 4.3% for the a-Si while it was in the range of 15.3% for the HIT PV technology.

For all systems, the performance ratios (PR) were in the range of 77 to 84%.

Results from the economic analysis, Tables 2 to 4, reveal that four main financial indicators meet the financial requirements. The payback period is in the range of 5-6 years. The IRR is in the range of 13-17%. Thus, the results demonstrate that solar PV rooftop projects in southern Thailand are feasible

In the implementation of the policy, an important challenge will be the promotion of such systems in southern Thailand, notably due to the lack of mechanisms for knowledge and technology transfer to the target groups who can afford this kind of technology.

Table 2. Main financial indices for a 3 kWp solar rooftop PV project in southern Thailand.

Indices	Songkhla	Ranong	Satun
BCR	1.99	2.25	2.09
NPV (THB)	217,721.51	274,380.92	238,910.27
IRR (%)	14.32	17.44	15.49
PBP (Year)	6	5	5

Table 3. Main financial indices for a 4 kWp solar rooftop PV project in southern Thailand.

Indices	Songkhla	Ranong	Satun
BCR	1.91	2.16	2.01
NPV (THB)	260,497.85	331,391.37	287,007.69
IRR (%)	13.54	16.62	14.71
PBP (Year)	6	5	6

Table 4. Main financial indices for a 5 kWp solar rooftop PV project in southern Thailand.

Indices	Songkhla	Ranong	Satun
BCR	1.98	2.23	2.07
NPV (THB)	344,113.67	434,122.93	377,769.23
IRR (%)	14.52	17.69	15.72
PBP (Year)	6	5	5

References

- [1] <http://weben.dede.go.th/webmax/content/areas-solar-power-potential>
- [2] Jompob Waewsak, Samphan Seinksanor, Wanchi Chimchawee and Sirinuch Chindaruksa, "Field comparative study of monocrystalline Si, CdTe thin film, and a-Si thin film grid connected in Thailand", *Proceeding of 1st ICCEP 07 Conference on Clean Energy and Power*, 2007, pp. 389-396.

FEASIBILITY OF A 3.5 kWp ROOFTOP RESIDENTIAL SOLAR PHOTOVOLTAIC INSTALLATION IN NAKHON SI THAMMARAT PROVINCE, THAILAND

Jompob Waewsak¹, Mongkol Kuasakul¹, Chuleerat Kongruang² and Yves Gagnon³

¹Research Center in Energy and Environment

Department of Physics, Faculty of Science, Thaksin University, Thailand

²School of Management, Walailak University, Thailand

³Université de Moncton, Edmundston (NB), Canada

SUMMARY: This paper presents the feasibility of a 3.5 kWp rooftop residential solar photovoltaic (PV) installation in Nakhon Si Thammarat province, southern Thailand. The installation consists mainly of a PV array, a grid connected inverter and a power meter. The system was simulated with six different PV technologies: silicon-based technology; m-Si, p-Si, and hybrid heterojunction with intrinsic (HIT) and thin film-based technologies; a-Si, CdTe, and CIS using PVSyst 6.3.2. The maximum annual energy yield was assumed for the economic analysis of the system. Results show that the a-Si thin film is the best technology, which is best suited to the climatic conditions of Nakhon Si Thammarat province, southern Thailand. The annual energy yield of the system reaches a maximum of 3,700 kWh/year, with a system efficiency of 18% and a performance ratio (PR) of 89%. The economic analysis reveals that, under current system costs and Feed-in-Tariff (FIT) incentives, the benefit cost ratio (BCR) is 1.03, the net present value (NPV) is 75,000 THB, the internal rate of return (IRR) is 6.5% and the payback period (PBP) is 13 years.

Keywords: Feed-in-Tariff, performance ratio, photovoltaic technology, system efficiency, solar energy

INTRODUCTION

The Royal Thai Government is moving forward to increase the share of renewable energy in the country by capitalizing on Thailand's abundant solar energy resource potential. In 2013, the National Energy Policy Commission (NEPC) approved two policy packages to increase Thailand's target installed photovoltaic (PV) capacity by 1,000 MW, to a total 3,000 MW. One of the two packages is a rooftop solar PV program with a Feed-in-Tariff (FIT) for power purchases. This program promotes the installation of 200 MW of PV systems on roofs or on parts of buildings (Table 1), while providing the same financial incentive FIT throughout the country. Table 2 shows the parameters for the installed capacity and the FIT as a function of the building.

Table 1. Objectives for the 200 MW target for rooftop solar PV systems in Thailand.

Jurisdiction	Residences	Small Enterprises, Medium-Large Enterprise/ Industries
PEA	40 MWp	40 MWp
MEA	60 MWp	60 MWp

PEA: Provincial Electricity Authority (Provinces of Thailand)
MEA: Metropolitan Electricity Authority (Bangkok area)

However, the solar resource in Southern Thailand is less than in other regions of the country, mainly due to the longer rainy seasons affected by the Northeast and Southwest monsoons. Consequently, the main objective of this paper is to investigate the feasibility of a 3.5 kWp rooftop residential solar PV installation under the climatic conditions of Nakhon Si Thammarat province and the national FIT incentive. Along with providing

metrics for investment decisions, the results will contribute to the development of national policies, as well as to share the mitigation of global warming.

Table 2. Parameters for the rooftop solar PV installed capacity and the FIT as a function of the building type.

Building Type	Installed Capacity (kWp)	FIT (THB/kWh)
Residences	Not Exceeding 10	6.96
Small Enterprises	10 – 250	6.55
Medium-Large Enterprises/Industries	> 250 – 1,000	6.16

METHODOLOGY

Solar energy resource in Nakhon Si Thammarat

The project site is in Muang District, Nakhon Si Thammarat province, with a GPS location of 8°26'41.87" N and 99°58'45.36" E. The existing residence in this study is a two story building with 325 m² space area and 100 m² of available roof area. The residence is facing North, while the orientation of the roof is East-West. The slope of the roof is 35°.

The solar energy resource in Muang District is evaluated using the database provided by the Department of Alternative Energy, Development and Efficiency (DEDE) of Thailand, along with the NASA database in PVSyst 6.3.2. The variation of the monthly mean global solar radiation is shown in Figure 1, where the monthly mean global solar radiation varies in the range of 13-21 MJ/m²/day.

Simulation of a 3.5 kWp rooftop solar PV system

The 3.5 kWp rooftop solar PV system consists mainly of PV panels connected in series and in parallel to an array junction box, a DC panel, a grid inverter, an AC panel with an AC surge protector,

and a power meter, as shown in Figure 2. The system is simulated using the PVSyst 6.32 computer software with six different PV technologies: m-Si, p-Si, and hybrid heterojunction with intrinsic (HIT) for the silicon-based technology and a-Si, CdTe, and CIS, for the thin film technology [1]. The annual energy yield is evaluated and the maximum yield is chosen for the economic analysis.

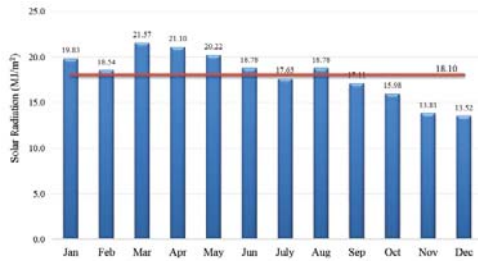


Figure 2. Variation of the monthly mean global solar radiation in Nakhon Si Thammarat province.

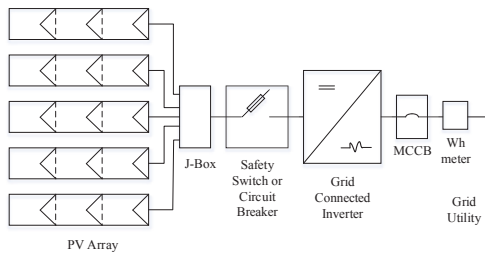


Figure 3. Diagram of the rooftop solar PV system.

Technical and economic analyses

In order to analyze the technical performance of a 3.5 kWp rooftop solar PV installation in Nakhon Si Thammarat province, southern Thailand, the system efficiency and the performance ratio (PR) [2] are evaluated.

The maximum annual energy yield is assumed for the economic analysis of the system, which is based on a cost benefit analysis (CBA). The four main financial indicators, i.e., benefit cost ratio (BCR), net present value (NPV), internal rate of return (IRR), and payback period (PBP), are analyzed using the cost provided by the Solar Thai Future Company Limited and a FIT of 6.85 THB/kWh for 25 years. The assumptions used in the economic analysis are given in Table 3, while the research methodology for this work is summarized in Figure 4.

RESULTS AND DISCUSSION

Results show that the a-Si thin film technology is the best technology suited to the climatic conditions of Nakhon Si Thammarat province, southern Thailand. The annual energy yield of the system reaches a maximum of 3,700 kWh/year, with

a system efficiency of 18% and a PR of 89%. Results from the economic analysis reveal that, under current system costs, the BCR is 1.03; the NPV is 75,000 THB; the IRR is 6.5%; and the PBP is 13 years. Finally, it appears that the installation of a 3.5 kWp rooftop solar PV system in Nakhon Si Thammarat is feasible, albeit with a longer PBP.

Table 3. Assumptions used in the economic analysis.

Parameters	Value
Project lifetime	25 years
Inverter replacement@10 th year	75,000 THB
PV module efficiency degradation	5% per year
Dust effect (losses)	5%
System cost (before VAT)	280,000 THB
VAT	7%
Transportation to site	20,000 THB
FIT for 25 years	6.85 THB/kWh

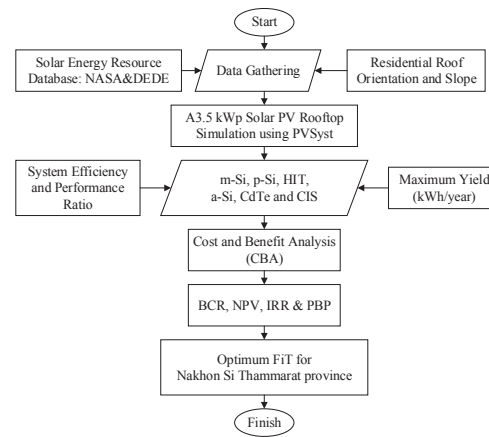


Figure 4. Methodology for the technical and economic analyses of a 3.5 kWp rooftop solar PV installation.

ACKNOWLEDGMENT

The authors would like to thank the Solar and Wind Energy Research Laboratory (SWERL) for providing the research facility and the financial support for this research.

References

[1] T.D. Atmaja, “Façade and rooftop PV installation strategy for building integrated photovoltaic application”, *Energy Procedia*, **32**, 2013, pp. 105-114.
 [2] J. Waewsak, S. Seinksanor, W. Chimchawee and S. Chindaruksa., “Field comparative study of monocrystalline Si, CdTe thin film, and a-Si thin film grid connected in Thailand”, *Proceeding of 1st ICCEP 07 Conference on Clean Energy and Power*, 2007, pp. 389-396.

WIND SPEED PROJECTIONS FOR ELECTRICITY APPLICATION OVER THAILAND

Sujittra Ratjiranukool¹ and Pakpoom Ratjiranukool²

¹Department of Physics and Materials Science, Faculty of Science, Chiang Mai University

²Department of Physics and General Sciences, Faculty of Science and Technology, Chiang Mai Rajabhat University, Thailand

SUMMARY: One of alternative renewable energy in Thailand has rapidly grown is wind energy for electricity generation. Investigation to identify the region of high potential electricity generation and possibility in decision making for locating new wind turbines is needed. Investment risks in wind speed variability influenced by climate change during the life span of wind turbine. The typical height of wind turbine is 80 m which requires wind speed at least 6 m/s for generating electricity. In this study, wind magnitudes are simulated by a regional climate model, PRECIS, Providing REgional Climate for Impact Studies, driven by two different general climate models (GCMs). The control runs (1961-1990) are forced by two boundary conditions, HadAM3P and ECHAM4. The future projections (2071-2100) are undertaken based on higher (SRES-A2) and lower (SRES-B2) emission scenarios. Wind speeds at 80 m wind turbine were analyzed to identify potential of wind power during 2071-2100 compared with 1960-1991. Assessments of wind speed indicated that the sufficient regions located the southern and northeastern Thailand. The result shows that seasonal mean wind speeds in DJF associated with northeast monsoon active are strongest among other seasons. Surface and higher altitude wind changes with increases are also founded in southwest monsoon period which agree with likely-strengthen monsoon systems.

Keywords: wind speed projection, regional climate model, Thailand

INTRODUCTION

Renewable energy resources, for example, solar power, wind power, have rapidly grown in the world. One of alternative renewable in Thailand is also wind energy. However, confidence in surface and lower troposphere wind speed change is relatively low in global scale. Climate pattern in the future are likely to change because the impacts of greenhouse gas increasing. Many studies indicate that surface wind speeds in tropics and mid-latitudes shows small negative trend with -0.1 to -0.14 m/s per decade (McVicar et al., 2012). Regional wind speed should be investigated for identify potential and possibility of harvesting wind power before wind farm construction. For Thailand wind speed during monsoon season is higher than other seasons. And the observations show southern Thailand.

Objective of this study is to determine area in Thailand which provides wind speed of 6m/s onwards at 80m for wind power application and how much changes in wind speed between control (1961-1990) and projection period (2071-2100).

DATA AND TOOLS

The simulated near surface wind speeds were conducted by a regional climate model called PRECIS, Providing REgional Climate for Impact Studies, with boundary conditions forced by ECHAM4 and the atmosphere-only HadAM3P. The projections for the end of this century being undertaken based on high (SRES-A2) and low (SRES-B2) emission scenarios. The horizontal resolution in this study is 0.22°x 0.22° (25 x 25 km) and model timestep is 5 minutes. PRECIS is land surface and atmospheric model with limited area.

METHODS

Wind speed at the height of 80 m (u_{80}) can be calculated from power-law profile (Holt and Wang, 2012)

$$\frac{u_{80}}{u_{10}} = \left(\frac{z_{80}}{z_{10}}\right)^\alpha \quad (1)$$

Where u_{80} and u_{10} is wind speed at altitude of z_{80} and z_{10} . And α is friction coefficient as

$$\alpha = \frac{\ln \frac{u_{b80}}{u_{a80}}}{\ln \frac{z_{b80}}{z_{a80}}} \quad (2)$$

Where u_{b80} and u_{a80} are horizontal wind speeds at 1000mb and 850 mb with the height of z_{b80} and z_{a80} . A constant value of $\alpha = 0.2$ has been used in this study.

Seasonal average wind speeds were calculated for every grid cell in time period of 30 year simulation to determine wind speed change.

RESULTS

Control runs

Seasonal mean wind speeds during control runs implied that wind speeds during DJF associating with northeast monsoon active is the strongest. Region that have sufficient wind power for supporting wind turbine (with 6 m/s onwards) appears over part of northeastern, eastern and southern Thailand (Fig 1).

Climate projections

Preliminary results for 4 future projections in the end of this century forced by 2 GCM under high (SRES-A2) and low (SRES-B2) emission scenarios

briefly indicated that wind speed changes have insignificant difference. The resulting maps (Fig. 2) projected generally increase in seasonal average wind speed during DJF and JJA which are in dry and wet monsoon periods which agree with likely-strengthen monsoon systems. Percent of day with wind speed 6m/s onwards at the height of 80m during 30 years are compared between 1961-1990 and 2071-2100. (Table 1)

Table 1. Percent of day with 80m wind speed 6m/s onwards during 30 years.

City	Lat (°)	Lon (°)	Percent	
			Control	projection
Mukdahan	17.53	104.72	27.0	30.8
Roiet	16.05	103.68	36.1	41.5
Chanthaburi	12.62	102.11	15.1	34.5
Phatthalung	7.58	100.17	34.4	52.2
Phuket	7.88	98.40	34.1	53.3

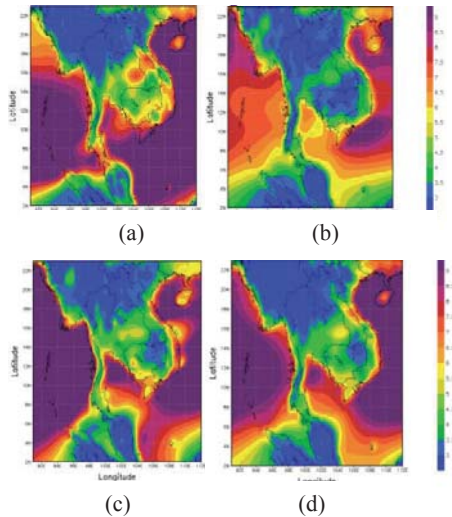


Figure 1. seasonal mean wind speed (m/s) for control runs driven by HadAM3 during (a) DJF (b) MAM (c) JJA (d) SON

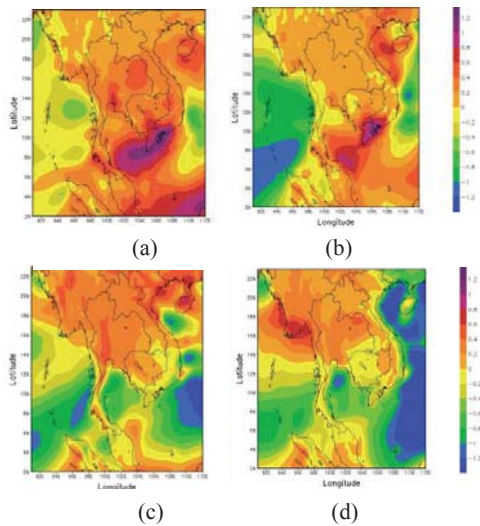


Figure 2. seasonal mean wind speed difference (m/s) for projection driven by (a) DJF (b) MAM (c) JJA (d) SON

ACKNOWLEDGMENT

Thank UK Met Office for PRECIS code and for boundary condition data.

References

[1] E. Holt and J. Wang, "Trends in Wind Speed at Wind Turbine Height of 80 m over the Contiguous United States Using the North American Regional Reanalysis (NARR)", *J. of Applied met and clim*, **51**, 2012, pp 2188- 2202.

[2] T.R. McVicar, M.L. Roderickb, R.J. Donohuea, L.Tao Lia, T.G. V. Nielc, A. Thomasd, J. Griesere, D. Jhahariaf, Y. Himrig, N.M. Mahowaldh, A.V. Mescherskayai, A.C. Krugerj, S. Rehman and Y. Dinpashoh "Global review and synthesis of trends in observed terrestrial near-surface wind speeds Implications for evaporation", *J. Hydrol.*, **416**, 2012, pp 182–205.

[3] S. C. Pryor, R. J. Barthelmie and E. Kjellstrom. "Potential climate change impact on wind energy resources in northern Europe: analyses using a regional climate model Climate Dynamics", *Climate Dyn.*, **25**, 2005, pp 815–835.

GENERATION OF SYNTHETIC WIND SPEEDS USING THE MARKOV ALGORITHM

Jompob Waewsak¹, Somphol Chewamongkolkarn¹ and Yves Gagnon²

¹Research Center in Energy and Environment
Department of Physics, Faculty of Science, Thaksin University (Phattalung Campus), Thailand
²Université de Moncton, Edmundston (NB), Canada

SUMMARY: Long term statistical measured wind speeds and directions over a period of time are essential data and information for the design of wind farms and for the estimation of the energy production. In a wind measurement campaign, measured wind speeds are often missing from the time series, notably due to sensor or data logger failures, such as malfunctions, icing events, lightning, etc. Therefore, the aim of this paper is to evaluate the performance of the Markov algorithm to generate synthetic wind speeds. The 1-year (2014) measured wind speeds of a 120 m agl met mast installed at Pakphanang district, Nakhon Si Thammarat province, Thailand is used to test the performance of the algorithm. In the assessment of the performance of the algorithm, presumed missing wind speed data for low (0-3 m/s), medium (4-7 m/s), and high (8-11 m/s) speeds which cover a significant portion of the power curve (i.e. cut-in to nominal wind speeds) of megawatt class modern wind turbine generators are randomly selected from the measured data. Daily and weekly periods of missing data are specifically evaluated. The synthetic wind speed data are compared to the measured data. Results show that the synthetic wind speed data approximate adequately the measured data, particularly for medium and high wind speed regimes, but with a more important error in low wind speed regimes. As the period of missing data increases in time, the RMSE also increases. Thus, the accuracy of the synthetic wind speed data appears to be at acceptable levels for daily periods of missing data, especially for medium to high wind speeds.

Keywords: synthetic wind speed, Markov algorithm, gap filling, synthetic data

INTRODUCTION

In the investigation of the wind energy potential for wind farm development, wind speeds and directions are essential variables to assess potential sites. Long-term statistical measured wind speeds and directions over a period of time are essential data and information for the design of wind farms and the estimation of the energy production. In normal conditions, the characteristics of the wind resource on a target site are determined using at least one year of measured data for the wind speeds and directions. However, wind speed and direction data are often missing from the time series, notably due to sensor or data logger failures, such as malfunctions, icing events, lightning, etc. Tower shadowing also degrades the quality of the wind data, particularly when a redundant wind speed measurement campaign is applied. It is general practice that the missing data should not exceed 10% of the time series [1].

The stochastic behavior is the most important property of the wind speed. Therefore, synthesizing missing data is a challenge to achieve accurate wind resource assessments in the presence of missing data. The Markov chain is an innovative model to synthesize stochastically wind data as it is able to exhibit strong congruency between synthetic and measured data [2]. The objective of this paper is to evaluate the performance of the generation of synthetic wind speeds using the Markov algorithm for wind energy applications.

METHODOLOGY

The Markov algorithm replicates the observed distribution, diurnal pattern, autocorrelation, and wind shear pattern in synthesizing wind speed and direction data. It is applied to synthesize wind speeds in a commercial computer software, namely, Windographer [3].

In order to evaluate the performance of synthetic wind speeds, 1-year (2014) measured wind speed and direction data obtained from a 120 m agl met mast installed at Pakphanang district, Nakhon Si Thammarat province, Thailand is used. The data recovery rate for the whole year is 91%. However, there are significant periods of missing data in May and June due to a data logger problem. In the assessment of the performance of the algorithm, presumed missing wind speed data for low (0-3 m/s), medium (4-7 m/s), and high (8-11 m/s) speeds which cover a significant portion of the power curve (i.e. cut-in to nominal wind speeds) of megawatt class modern wind turbine generators are randomly selected from the measured data. Daily and weekly periods of missing data are also evaluated. The synthetic wind speed data are compared to the measured data. The mean absolute error, percent relative error, and root mean square error (RMSE) are analyzed to assess the performance of the algorithm. The annual mean speed, power density and Weibull distribution, with and without using synthetic data, are compared.

RESULTS AND DISCUSSION

The comparison between measured and synthetic wind speed data for low, medium, and high

wind speeds are shown in Figures 1 and 2, respectively on a daily and weekly basis. The mean absolute error, the percent relative error and the root mean square error are presented in Table 1. It can be seen that the synthetic wind speed data approximate adequately the measured data, particularly for medium and high wind speed regimes. Regarding low wind speed regimes, the error is quite large, with RMSE of 17.4 and 28.8% for low wind speed regimes on a daily and weekly basis, respectively.

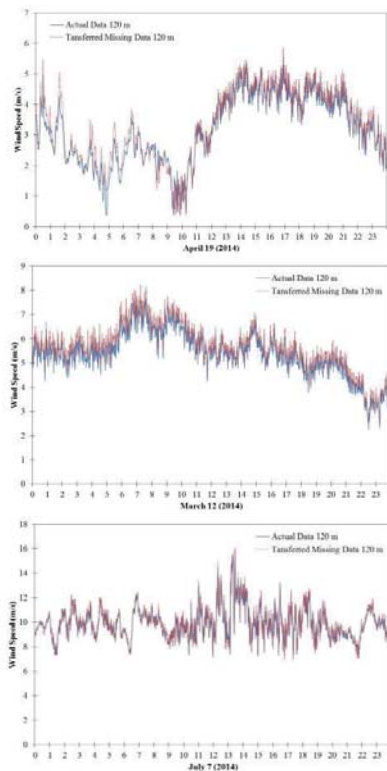


Figure 1. Comparison of the synthetic wind speed data and the measured data, on a daily basis, during low (top), medium (middle) and high (low) wind speed regimes.

Table 1. Mean absolute, relative and root mean square errors for the comparisons.

Data Missing	Mean Absolute Error	Relative Error (%)	RMSE (%)
Daily - Low	0.15	4.6	17.4
Daily - Medium	0.29	5.4	5.8
Daily - High	0.09	0.9	2.2
Weekly - Low	0.19	5.9	28.8
Weekly - Medium	0.30	4.9	9.5
Weekly - High	0.32	3.5	6.5

CONCLUSION

Results from the evaluation of the Markov algorithm in wind speed data synthesizing reveals that the temporal scale of the missing data plays a significant role in its performance. Specifically, the algorithm performs well for medium to high wind speed regimes, with an RMSE between 2.2 and 9.5%. However, an RMSE between 17.4 and 28.8% is quite high for low wind speed regimes.

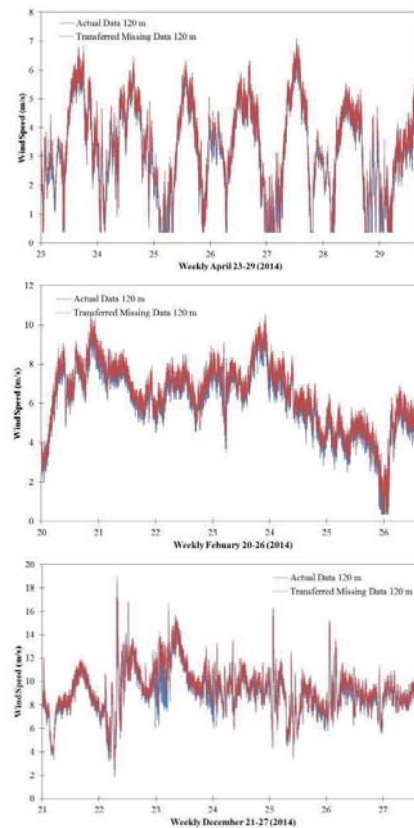


Figure 2. Comparison of the synthetic wind speed data and measured data, on a weekly basis, during low (top), medium (middle) and high (low) wind speed regimes.

References

- [1] N. Masseran, "Markov chain model for the stochastic behaviors of wind-direction data" *Energy Conversion and Management*, **92**, 2015, pp. 266-274.
- [2] F.O. Hocaoglu and M. Kurban, "The effect of missing wind speed data on wind power estimation," *Lecture Notes in Computer Science*, **4881**, 2007, pp.107-114.
- [3] <http://www.windographer.com/>

ENERGY YIELD ASSESSMENT OF A PROPOSED 45 MW WIND POWER PLANT IN SOUTHERN THAILAND

Jompob Waewsak¹, Somphol Chewamongkolkarn¹ and Yves Gagnon²

¹Research Center in Energy and Environment
Department of Physics, Faculty of Science, Thaksin University (Phatthalung Campus), Thailand
²Université de Moncton, Edmundston (NB), Canada

SUMMARY: The objective of this paper is to present the yield assessment of a proposed 45 MW onshore wind power plant in southern Thailand. The energy yield assessment is executed using one year of measured wind data, and the topography and the roughness of the terrain, along with the power curve of 13 potential wind turbine generator models. A microscale wind resource map, with a resolution of 90 m, is developed based on computational fluid dynamics (CFD) wind flow modeling. The Annual Energy Production (AEP) is estimated, while wake losses and other losses are included in the analysis of the capacity factor. The results show that the maximum AEP is in the order of 140 GWh/year, corresponding to a 35% capacity factor with wake losses of 18 GWh/year.

Keywords: wind farm, yield assessment, capacity factor, annual energy production, wind turbine generator

INTRODUCTION

In wind power development, the energy yield assessment is a critical step in the selection of a wind turbine generator. Accurate assessments require relevant wind measurements, temperature and air pressure data at hub height, accurate wind flow and wake modeling, the power curve and thrust curve of potential wind turbine generators (WTG), and digital terrain and roughness information for the target area.

The objective of this paper is to present the energy yield assessment of a proposed 45 MW onshore wind power plant in southern Thailand.

METHODOLOGY

In order to assess the energy yield of a wind power plant, the Annual Energy Production (AEP) is estimated using the power curve and the thrust curve of the potential utility-scale WTG, along with 1-year of continuous measured wind data. Further, the WindSim 7.0 computational fluid dynamics wind flow modeling is applied under the following conditions: resolution of 90 m, standard k-epsilon turbulence model and wake model No. 1. The wind speeds and directions at 120 m above ground level (agl) were measured in 2013 using calibrated industry grade three-cup anemometers and wind vanes. The Weibull distribution and the wind rose of the measured winds are displayed in Figure 1.

For this investigation, 13 potential three blade horizontal axis, utility-scale WTG are analyzed, with their characteristics shown in Table 1. The nominal capacity of these potential WTG ranges from 1.8 to 3.3 MW, with hub heights ranging from 85 to 137 m.

In the analysis of the AEP, the wake effects and the main assumptions are considered as follows: the wake losses are site specific and are related to the dimensions of the turbines and the layout of the power plant; wind speed and direction availability of

97%; electrical loss of 2%; turbine availability of 96%; and environmental losses of 0.5%. The net AEP for P50, P75, and P90 are summarized for each model of WTG, while the capacity factor is computed in order to display the efficiency of the proposed wind power plants.

The gross AEP, in GWh/year, at P50, P75, and P90 for each model of a WTG are presented in Table 2. For its part, Table 3 shows the losses due to wake effects, availability, electrical, environmental, and WTG performances. The total losses are also given in Table 3, while the capacity factors of the modeled wind power plants are displayed in Table 4.

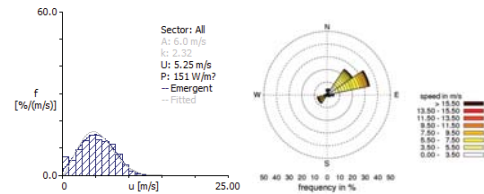


Figure 1. Weibull distribution and wind rose of 1-year measured wind data in 2013.

Table 1. Characteristics of the 13 potential utility-scale wind turbine generators.

WTG Option	Hub Height (m)	Rotor Diameter (m)	Rated Capacity (MW)	Peak Power Coefficient (Cp)
I	85	100	1.8	0.48
II	120	120	1.8	0.48
III	125	114	1.8	0.47
IV	93	114	2.0	0.47
V	120	121.5	1.8	0.44
VI	120	121.5	2.5	0.44
VII	90	111	2.1	0.44
VIII	120	111	1.8	0.44
IX	120	110	2.1	0.44
X	125	110	1.8	0.46
XI	125	110	2.0	0.46
XII	137	126	1.8	0.46
XIII	137	126	3.3	0.44

RESULTS AND DISCUSSION

Figure 1 shows the microscale wind resource map, at a resolution of 90 m, for the site considered. It can be seen that the annual average wind speeds are in the range of 5.2 to 5.3 m/s, which corresponds to a low to moderate wind regime for commercial wind power developments.

Results show that the gross AEP (P50) is in the range of 94 to 175 GWh/year, as shown in Table 2. WTG XIII could generate a much higher AEP since it has a nominal capacity of 3.3 MW. Wake losses are in the range of 0.35 to 4.5 GWh/year, as shown in Table 3. WTG VI has the highest wake losses, mainly due to the fact that it has the largest rotor diameter of the potential WTG. In this regards, the WTG with the large rotor diameters exhibit higher wake losses. The total losses are in the range of 9.6 to 19 GWh/year, as shown in Table 3. Finally, the capacity factors for the modeled 45 MW wind power plant are in the range of 24 to 35%, as shown in Table 4. It can be seen that WTG II has the highest capacity factor. Therefore, WTG II is appears to be the best turbine for this site.

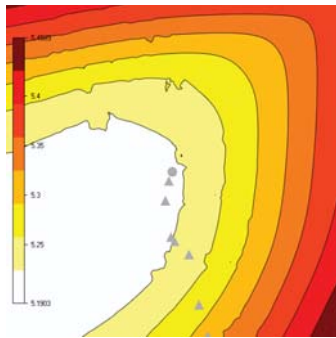


Figure 2. Microscale wind resource map at 137 m agl (CFD modeling at a resolution of 90 m).

Table 2. Gross AEP in GWh/year.

WTG/AEP	P50	P75	P90
I	139.60	131.56	126.76
II	139.77	130.25	125.45
III	122.02	113.30	108.50
IV	126.80	117.92	113.12
V	107.06	98.52	93.73
VI	148.70	138.91	134.11
VII	117.60	108.74	103.95
VIII	108.43	99.95	95.16
IX	126.50	117.50	112.70
X	114.66	106.23	101.44
XI	127.40	118.63	113.83
XII	94.98	89.46	84.66
XIII	174.73	168.45	163.65

Table 3. Wake losses and other losses for the modeled 45 MW wind power plant.

WTG/Losses	Wake	Avail.	Elec	Env.	WTG Perf.	Total
I	2.71	4.19	2.79	0.66	6.34	16.68
II	4.19	4.19	2.80	0.65	6.27	18.11
III	3.39	3.66	2.44	0.57	5.43	15.48
IV	3.55	3.80	2.54	0.59	5.66	16.14
V	3.21	3.21	2.14	0.49	4.69	13.74
VI	4.46	4.46	2.97	0.69	6.71	19.30
VII	3.53	3.53	2.35	0.54	5.20	15.15
VIII	3.14	3.25	3.17	0.50	4.76	13.82
IX	3.67	3.80	2.53	0.59	5.64	16.22
X	3.10	3.44	2.29	0.53	5.07	14.43
XI	3.44	3.82	2.55	0.59	5.69	16.09
XII	0.19	2.85	1.90	0.45	4.23	9.62
XIII	0.35	5.22	3.48	0.84	8.18	18.08

Table 4. Capacity factors for the modeled 45 MW wind power plant.

WTG/CF	P50	P75	P90
I	35.41	33.37	32.16
II	35.46	33.04	31.82
III	30.95	28.74	27.52
IV	28.95	26.92	25.83
V	27.16	24.99	23.78
VI	27.16	25.37	24.50
VII	25.57	23.64	22.60
VIII	27.51	25.36	24.14
IX	27.51	25.55	24.51
X	29.09	26.95	25.73
XI	29.09	27.08	25.99
XII	24.09	22.69	21.48
XIII	24.09	23.31	22.64

CONCLUSION

Using the optimum WTG, the gross AEP (P50) of the proposed 45 MW wind power plant is in the order of 140 GWh/year. The wake losses are in the order of 4 GWh/year, while the total losses are 18 GWh/year. The corresponding capacity factor is 35%.

ACKNOWLEDGMENT

The authors would like to thank Energy Absolute PLC and Thaksin University for providing financial support for this research.

References

[1] Nurulkamal Masseran, "Comparative analysis on power curve models of wind turbine generator in estimating capacity factor", Energy, 73, 2014, 88-95.

ENVIRONMENTAL IMPACT ASSESSMENT OF A WIND POWER PLANT: A CASE STUDY FOR NAKHON SI THAMMARAT PROVINCE, THAILAND

Jompob Waewsak¹, Chana Chancham¹ and Yves Gagnon²

¹Research Center in Energy and Environment
Department of Physics, Faculty of Science, Thaksin University, Thailand
²Université de Moncton, Edmundston (NB), Canada

SUMMARY: This paper presents the environmental impact assessment of a proposed wind power plant in Nakhon Si Thammarat province, in southern Thailand. The noise emission, the shadow flicker and the zone of visual influence (ZVI) are three key environmental impacts of operating wind power plants. The noise emission and propagation model is simulated using noise emission information from the wind turbine manufacturer, the topography of the terrain and its roughness, as well as the local wind speeds measured over a 1-year period. For their parts, the shadow flicker and the ZVI are simulated using the solar geometry and the topography of the terrain, along with the GPS locations and the dimensions of each wind turbine in the wind power plant. A proposed 45 MW wind power plant in Pakphanang district in Nakhon Si Thammarat province, southern Thailand is simulated and presented in this paper.

Keywords: wind power plant, noise emission, shadow flicker, zone of visual influence, environmental impact

INTRODUCTION

The Ministry of Energy of Thailand launched its latest policy to promote wind power, with an objective of 1,800 MW of installed capacity before 2021. The policy calls for an Adder subsidy scheme in the form of a feed-in-tariff program. In Thailand, the current 214.5 MW wind power installed capacity consists of one Small Power Producer (SPP) project in Nakhon Ratchasima province, with an installed capacity of 207 MW, and a Very Small Power Producer (VSPP) project with an installed capacity of 7.5 MW in Chaiyabhum province.

Wind data information obtained from a met tower measurement campaign and a wind atlas indicate that the area along the coastal line of Nakhon Si Thammarat and Songkla provinces has high potential for a utility-scale wind power plant. The average annual wind speed is in the range of 5.0 to 5.5 m/s. Consequently, with a Power Purchase Agreement (PPA) of 126 MW, a private sector company intends to develop three distinct wind power plants in Pakphanang (45 MW) and Huasai districts (45 MW) in Nakhon Si Thammarat province, as well as in Ranot district (36 MW) in Songkhla province.

Prior to installing a wind power plant in a target area [1] in Thailand, an Initial Environment Examination (IEE) should be accomplished and the information be disseminated to the communities and stakeholders of the project located within a 3 km radius of the project. The objective of this paper addresses the IEE by presenting the noise emission, the shadow flicker and the ZVI of a 45 MW wind power plant operating under the wind conditions of Pakphanang district, Nakhon Si Thammarat province.

METHODOLOGY

The project site is the coastal area located in Pakphanang district in Nakhon Si Thammarat

province, Thailand. The proposed wind power plant consists of 25 wind turbine generators, as shown in Figure 1. The physical characteristics of the wind turbine generators are as follows: three blades, 1.8 MW generator, hub height of 137 m, rotor diameter of 110 m, cut in wind speed of 3.0 m/s, rated wind speed of 10.5 m/s, and cut-out wind speed of 20 m/s.

The noise emission, the shadow flicker and the ZVI are simulated using WindFarmer 5.3. The modeling input consists of the digital terrain map (GDEM, resolution of 5 m), a roughness map interpreted from land-use data obtained from the Department of Land Development, the 1-year wind speeds and directions measured in 2013 using a 120 m met tower, and the physical characteristics of the wind turbine generator. The noise emission and propagation modeling is based on the physical model of noise absorption, propagation and reflection under realistic conditions, and the wind turbine noise information from the manufacturer. The results of the simulations are exported into data files for mapping using Arc GIS 10.2.



Figure 1. Location of the 25 wind turbine generators of the 45 MW wind power plant analyzed.

RESULTS AND DISCUSSION

The noise emission map, the shadow flicker map expressed in hours per year, and the ZVI map are shown in Figures 2 to 4, respectively.

From Figure 2, it can be seen that the noise emission at ground level from the wind power plant, operating under the measured wind speed conditions, is in the range of 40 to 45 dB(A) at a distance of 50 m around each wind turbine generator. The noise level decreases with the distance from a wind turbine generator; at 100 m from each wind turbine generator, the noise emission is in the range of 35 to 40 dB(A). These results of noise emission confirm that the wind power plant will be operating within the Thai regulations issued by the Department of Pollution Control.

However, as part of the IEE investigation, a field measurement campaign should be executed in order to measure the background noise in order to analyze the degree of disturbance, which should not exceed 10 dB(A) to comply with the Thai regulations.

The shadow flicker map, Figure 3, shows that the number of hours per year for shadow flickering reaches a maximum in the order of 400 to 500 hours, corresponding to a proportion of 4.6 to 5.7% for the whole year and 9.1 to 11.4% of the daytime. However, this shadow flickering affects limited areas in the 50 m vicinity of the turbines in the East-West direction.

The zone of visual influence, Figure 4, shows that the number of wind turbine generators with a high level of impact is limited to six turbines.

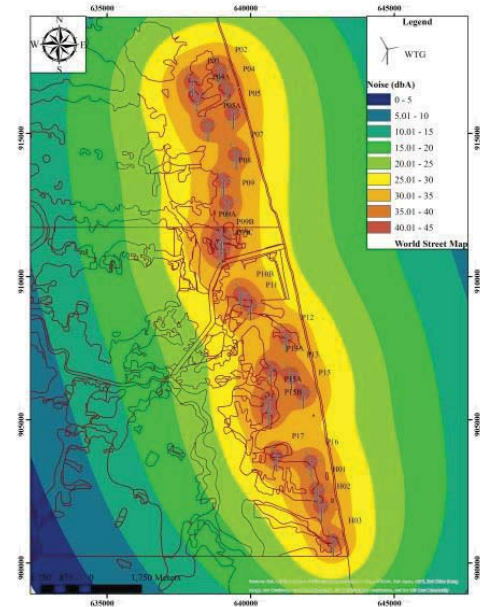


Figure 2. The contour map of the noise emission for the proposed 45 MW wind power plant.

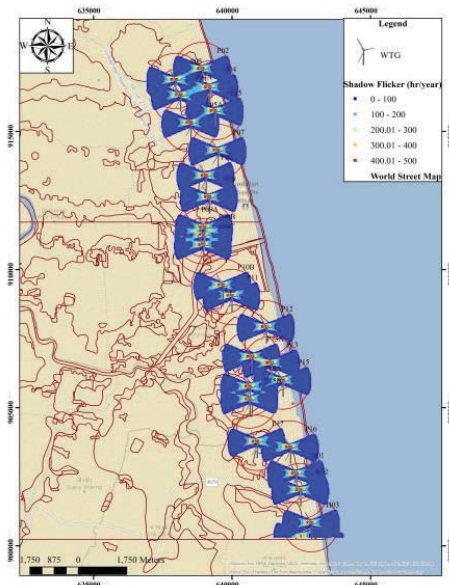


Figure 3. The shadow flicker map for the proposed 45 MW wind power plant.

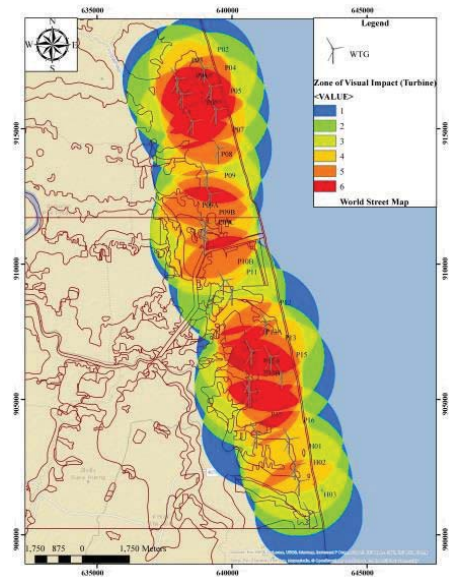


Figure 4. The zone of visual influence (ZVI) for the proposed 45 MW wind power plant.

ACKNOWLEDGMENT

The authors would like to thank Energy Absolute PLC and Thaksin University for their financial support in this work.

Reference

- [1] T. Abbasi, M. Premalatha, T. Abbasi and S.A. Abbasi, "Wind Energy: Increasing Deployment, Rising Environmental Concerns", *Renewable and Sustainable Energy Reviews*, 31, 2014, 270-288.

ON THE ASSESSMENT OF TURBULENCE MODELS FOR WIND FLOW MODELING OVER FLAT, SEMI-COMPLEX, AND COMPLEX TERRAINS

Arom Puteh¹, Jompob Waewsak¹, Tanate Chaichana¹, Nattawoot Dusadee², Warit Werapun³ and Yves Gagnon⁴

¹Research Center in Energy and Environment

Department of Physics, Faculty of Science, Thaksin University (Phatthalung Campus), Thailand

²Research Center in Energy, Maejo University, Thailand

³Faculty of Science and Industrial Technology, Prince of Songkla University (Suratthani Campus), Thailand

⁴Université de Moncton, Edmundston (NB), Canada

SUMMARY: The objective of this paper is to assess the performance of turbulence models in CFD-based (Computational Fluid Dynamics) wind flow modeling over flat, semi-complex, and complex terrains, with test sites in a coastal area of Nakhon Si Thammarat province, a mountainous area in Phangan Island and a high-land and mountainous area in Chiang Mai province, respectively, in Thailand. An 80 m met mast, with wind data at heights of 80 m, 40 m, and 20 m and recordings performed in 2009, was installed on the complex terrain site, while 120 m agl met masts, with wind data at heights ranging from 50 m to 120 m and recordings in 2012, were installed on both the flat and the semi-complex terrain sites. The digital elevation model (DEM) and the digital roughness data, along with 1-year wind speed data at 80 m and 120 m, were the input for the CFD-based wind flow modeling, which included different turbulence and wake models. Wind profiles obtained from measurements and predictions under several turbulence models are compared in order to find the most appropriate turbulence model as a function of the terrain type. The root mean square error (RMSE) is the main criteria to assess the performance of the turbulence models. While further work is still needed to fully assess the models, the initial results from this work show that most turbulence models are promising for flat terrains, while the standard k-epsilon and k-epsilon with YAP turbulence models appear to be the most promising for semi-complex and complex terrains. These findings could be used as initial guidelines for wind resource predictions using CFD modeling.

Keywords: wind energy, computational fluid dynamics, turbulence model, complex terrain, wind flow modeling

INTRODUCTION

Wind farm siting and optimum layout in wind project development require accurate predictions of the annual energy production (AEP), which depends on having an accurate and detailed understanding of the spatial distribution of the wind resource across the area of interest. The wind profile is also important since the wind speeds at hub height are needed for the AEP estimations, along with having an impact on the fatigue loads on the blades.

Currently, numerical wind flow modeling, along with on-site meteorological measurements, is the preferred approach to estimate the AEP produced by a wind farm. However, while providing valuable information, numerical wind flow modeling is still being improved in terms of accuracy and robustness.

Linear wind flow models based on the theory of Jackson and Hunt (1975) [1], such as WASP, are widely used to predict the spatial wind resource over a territory. In the early stage of development of these models, since the computing resources were relatively limited, the wind resources simulated were not affected by complex flow phenomena such as flow on slopes, flow separation, thermally driven flows, low-level jets, and other dynamic and non-linear phenomena.

Models based on Computational Fluid Dynamics (CFD) are considered as the next generation wind flow models for wind resource predictions. They are developed based on the mass

and momentum conservation components of the non-linear Navier-Stokes equations, and they run until convergence is reached while applying a constant inlet wind profile. Research work has revealed that, for 2-D or 3-D wind flows over escarpments and hills, such steady-state CFD models perform well and they give details on the turbulence characteristics of the flow [2]. From several research works, it could be concluded that CFD models perform better than the industry standard WASP model in many cases, but not all cases [3-4].

Consequently, the objective of this paper is to assess the performance of turbulence models in wind flow modeling over flat, semi-complex, and complex terrains.

METHODOLOGY

The CFD wind flow modeling studied in this work solve the non-linear Reynolds Average Navier-Stokes (RANS) equations to obtain steady solution on different direction sectors using the General Collocated Velocity (GCV) solver with the commercial software package WindSim.

The RANS equations are closed with different versions of turbulence models, including the standard k-epsilon model, modified k-epsilon model, RNG k-epsilon model, k-epsilon with YAP correction model, and k-omega model.

In this paper, WindSim is tested with several

combinations of conditions, i.e., terrains, turbulence models and wake models. The input of the CFD-based wind flow simulations, with 90 m resolution and neutral air stability, consist of 10x10 km² digital elevation models (DEM) and digital roughness heights, and 1-year observed wind data. Wind speeds and directions were measured using calibrated three cup NRG #40C anemometers and a Nomad II Wind data logger with a sampling interval of 1 sec and a logging interval of 10 min.

In order to simulate the wind flow over different terrains, the wind speed and wind direction data at 120 m agl, obtained in 2012 from met masts in Pakphanang District, Nakhon Si Thammarat province and Koh Phangan, Suratthani province, Thailand, were used to test WindSim over flat and semi-complex terrains, whereas wind speed and wind direction data at 80 m agl, obtained in 2009 at Maejaem District, Chiang Mai province, Thailand were used to test the CFD-based wind flow modeling over complex terrain.

The conditions for the CFD-based wind flow modeling are taken from several combinations of terrains (flat, semi-complex and complex), closure modeling (standard, modified, and RNG k-epsilon; k-epsilon with YAP correction; and k-omega), and wake models (identified as 1, 2, and 3).

The simulated wind speeds at heights of 120, 110, 100, 90, 80, 65 and 50 m at Pakphanang, and at height of 110, 100, 90, 80 and 65 m at Koh Phangan were compared to the wind speeds measured on these sites. For Maejaem, the simulated wind speeds at heights of 80, 40 and 20 m were compared to the measured wind speeds. The root mean square error (RMSE) is the criteria used to assess the performance of the turbulence models.

RESULTS AND DISCUSSION

The wind profiles over flat, semi-complex and complex terrain, with different turbulent models and wake model 1, are shown in Figures 1-3, respectively. The initial results from this work show that most turbulence models are promising for flat terrains, while the standard k-epsilon and k-epsilon with YAP turbulence model appear to be the most promising for semi-complex and complex terrains. While further work needs to be performed to fully assess the accuracy and the robustness of the models, these findings could be used as initial guidelines for wind resource predictions using CFD modeling. In future work, the condition of air stability should also be investigated further.

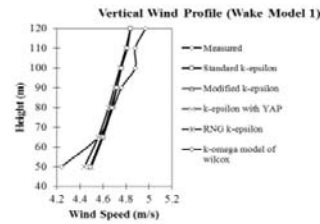


Figure 1. Comparison of the wind profile obtained from measurements and different turbulence models over a flat terrain at Pakphanang District, Nakhon Si Thammarat province, Thailand.

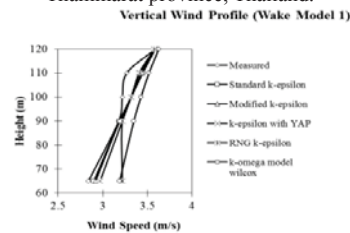


Figure 2. Comparison of the wind profile obtained from measurements and different turbulence models over a semi-complex terrain at Koh Phangan, Suratthani province, Thailand.

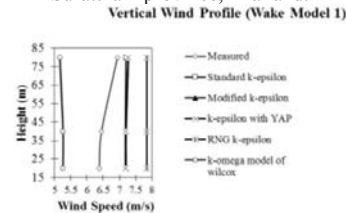


Figure 3. Comparison of the wind profile obtained from measurements and different turbulence models over a complex terrain at Maejaem District, Chiang Mai province, Thailand.

ACKNOWLEDGMENT

The authors would like to thank the Research and Development Institute (RDI), Thaksin University for their financial support. The authors extend their appreciation to the National Research Council of Thailand (NRCT) and the Solar and Wind Energy Research Laboratory (SWERL) for providing the research facility and financial support.

References

- [1] WAsP Manual: Wind Analysis and Application Program (WAsP), Vol. 2: User Guide, Riso, National Laboratory, Roskilde, Denmark, ISBN 87-550-178, 1993.
- [2] E. Berge, F.K. Nyhamme, L. Tallhaug and O. Jacobsen, "An Evolution of the WAsP Model at a Coastal Mountainous Site in Norway", *Wind Energy*, **9**, 2006, pp. 131-140.
- [3] O. Undheim. "The Non-Linear Microscale Flow Solver 3-D Wind", Development and Validation. Ph.D. Thesis at the Norwegian Technical University, Trondheim, Norway, 2005.
- [4] K.J. Eidsvik, "A System for Wind Power Estimation in Mountainous Terrain, Prediction of Askervein Hill Data", *Wind Energy*, **8**, 2005, pp. 237-249.

PERFORMANCE EVALUATION OF CO-AXIS COUNTER-ROTATION WIND TURBINE

Tanate Chaichana¹ and Sumpun Chaitep²

¹Research Center in Energy and Environment Department of Physics, Faculty of Science, Thaksin University

²Retired, Department of Mechanical, Faculty of Engineering, Chiang Mai University, Thailand

SUMMARY: The present work was studied the effect of the tip speed ratio to the starting rotation, rev up rotation, power and torque coefficients of a two-shaft co-axis counter-rotating wind turbine (CR-WT). The prototype of CR-WT was tested in the open type wind tunnel with the velocities of 1.5, 2.0, 3.0, 4.0 and 5.0 m/s. CR-WT consisted of 8 blades. The blade is made of wood. It consists of 2 hubs 2 axis and 4 arms. The inner axis are clockwise rotation and outer axis is anticlockwise rotation. The inner and outer are in the identical axis. Both axes are driven the pulley by using the counter rotating gear. The analysis of the experimental results showed that the cut in wind speed of CR-WT was 1.744 m/s and it is increasing when the tangential force ratio increasing. Rev up rotation period depends on wind speed and tangential force ratio. The most affected of angle of attack to power output is very small. The average of power coefficient of CR-WT was 14.89%.

Keywords: vertical axis wind turbine, power coefficient, cut-in wind speed, tip speed ratio,

INTRODUCTION

Wind is a natural resource and it can use as an alternative energy. Wind energy is a one of the better choices to compensate fossil energy and solve a problem about the energy situation in Thailand. Other Moreover, wind energy is clean, abundant and it can reduce the global warming problem. There are 2 kinds of wind in Thailand [1], seasonal and local wind. The seasonal (monsoon) wind is consisting of northeastern wind and southwest wind. Local wind is a wind system that's expected change in direction every such as mountain-valley breezes, land-sea breezes. Wind power is the conversion of wind energy into a useful form, such as electricity with wind turbines.

Generally, wind turbines can be divided into two types based on the axis in which the turbine rotates. There are horizontal axis wind turbine (HAWT) and Vertical-axis wind turbines (VAWT), but HAWT is more popular than the other one. VAWT have the main rotor shaft arranged vertically. Key advantages of this arrangement are that the turbine does not need to be pointed into the wind to be effective. VAWT can work in all directions and it requires low wind speed (2 m/s) [2]. However, the VAWT has lower rotational speed and efficiency than HAWT in which a maximum tip speed is not over double of wind speed and 17 – 30 % of efficiency [3]. Nevertheless, the efficiency of VAWT will be increased by adding some equipment, such as Savonius type of main turbine, resulting in the cut in wind speed is reduced [4].

The development of the vertical axis wind turbine has been explored over 30 years [5-8]. Recently, the vertical axis wind turbines are more on attentiveness in term of optimization of power generation and cost effective. Ever since 1925 – 1926, the initial result was shown the various experimental work out how they design [9]. However, the Horizontal Axis Wind Turbines

(HAWT) are still the favorite configuration of turbine for electrical generation. Many types of rotor have designed and tested for evaluating the behavior and efficiency. Additional of Savonius to Darrieus type vertical wind turbine can increase the efficiency and decreased the wind speeds essentially required for starting rotation [10].

The present work studied the effect of the operating conditions to the starting rotation, rev up rotation, power and torque coefficients of a two-shaft co-axis counter-rotating wind turbine (CR-VAWT).

THE EXPERIMENT SETUP

The model of two-shaft co-axis counter-rotating wind turbine (CR-VAWT) was tested in the open flow wind tunnel. To measure the power delivered by the rotor, a pony brake dynamometer principle is used. The difference between the dead weight and load cell readings produces the tangential force action on the pulley. Time and value were recorded and process by computer. The rotational speed was measured by a laser sensor tachometer. Wind speed in wind tunnel was control of fan with inverter and measure by a hot wire type anemometer. 3 testing methods were used in this research;

Test 1 Vary wind speed and Dead load

1. Blade type; symmetrical curved with 150 mm of high, 150 mm of width and 75 mm of thickness-curved.
2. Number of blades: 8 (4 for clockwise rotation and 4 for counterclockwise)
3. Swept plan was set to parallel with the radiance line and fix all the time of the test
4. Blade pitch angle fixes at 0°
5. Wind speed 1.0 – 5.0 m/s
6. Dead weight rang; 0 - 1 kg

Test 2 Vary Blade pitch angle (Dead load constant)

1. Dead weight was constant at 100 g

2. Blade type; symmetrical curved with 150 mm of high, 150 mm of width and 75 mm of thickness-curved.
3. Number of blades: 8 (4 for clockwise rotation and 4 for counterclockwise)
4. Blade pitch angle, γ , 0, 15, 30, 45, 60 and 75 degree.
5. The wind speed of tested; 1 – 10 m/s

Test 3 Vary formats of blade (Fix dead load and blade pitch angle)

1. Dead weight was constant at 100 g
2. Number of blades: 8 (4 for clockwise rotation and 4 for counterclockwise)
3. Blade pitch angle; 0°

RESULTS AND DISCUSSION

The cut in wind speed increase when the X_F Increase and it's become constant about 5.0 m/s. The cut in wind speed is a logarithm function of X_F (N/m^2) as expressed by Eqn 1 with the coefficient of determination (R^2) of 99.64%. At no load the cut in wind speed were 1.74 m/s. It is the wind speed that can exert force to overcome all frictional losses of the CB-VAWT.

$$V_{cut-in} = (1.20(\ln X_F)) - 1.74 \tag{1}$$

When

$$X_F = \frac{\text{tangential force he pulley}}{\text{swept area of CB-VAWT}} = \frac{[mg - F_{loadcell}]}{R \times span}$$

At lower wind speed the starting time sequences (T_s , s) go up more rapidly with respect to the increasing rate of X_F . Conversely, at higher wind speed T_s go up with less responsive to the increasing rate of tangential force.

$$T_s = (-1.01(\ln V) + 1.55)X_F + 0.05V^{3.20} \tag{2}$$

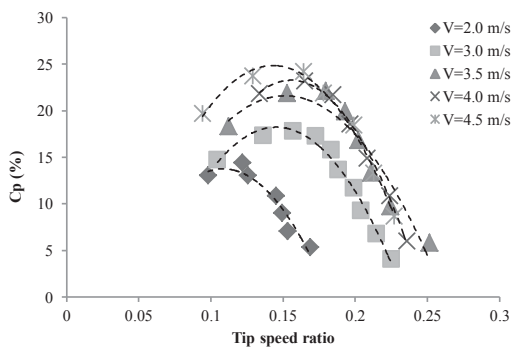


Figure 1 power coefficient of CR-VAWT

The rated rotational speed, N_r (RPM), was a direct variation with wind speed and inverse variation with tangential force

$$N_r = (23.12)V + (-0.31X_F) + 25.60 \tag{3}$$

Figure 1 and 2 shows the power coefficient and the Torque coefficient of CR-VAWT at tip speed ratio. Power coefficient was increased to a maximum value and then diminishes with further increasing of tip speed ratio. The maximum value of power coefficient was occurring in a range of tip speed ratio 0.1- 0.2. Torque coefficient was decreased with an increase in the tip speed ratio corresponding to the increasing wind speed.

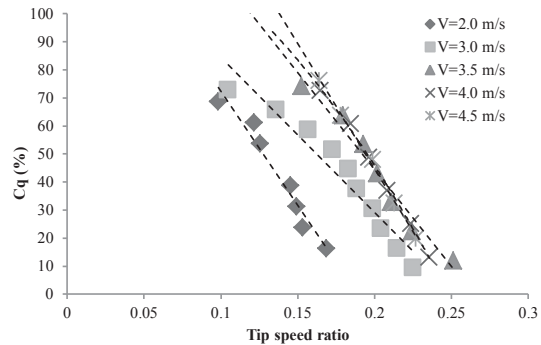


Figure 2 Torque Coefficient of CR-VAWT

References

- [1] Rangsap Apakupakul. (2004). *Introduction to Meteorology*. Chulalongkorn University Press. ISBN 974-13-2752-8, Thailand.
- [2] J. F. Manwell., J. G. McGowan., and A. L. Rogers. (2002). *Wind Energy Explained*. John Wiley & Sons; Baffins Lane, Chic Hester, West Sussex PO19 1UD, England.
- [3] J.-L. Menet, 2004. A double-step Savonius rotor for local production of electricity: a design study. *Renewable Energy*, V 29, 843–1862.
- [4] Jack Park. (1975). *Simplified Wind Power System for Experimenters*. 2nd edition: Helion
- [5] V.H.Morcós and O.M.E. Abdel-Hafez, (1996). “Testing of an arrow-head vertical axis wind turbine model”. *Renewable energy*, Vol. 7, No 3, pp. 223-231
- [6] I. P. Ficenc, (1987). “ The VAWT and its power train design”, *CME*, April, 34-39
- [7] P. J. Musgrove, (1976). “The variable geometry vertical axis windmill”. *Int. Symp. On Wind Energy System*, 7-9 September
- [8] I. D. Mays and H. Rhodes, (1984). “Progress with the UK vertical axis wind turbine programme”. *Proc. European wind Energy Conf.*, Hamburg, 22-26 October
- [9] Esmail Ajdehak, (2008). “Analyzing power generation in Vertical Axis Wind Turbine (VAWT)” [online] <http://www.scribd.com/doc/8015472/VAWT>
- [10] Smarn Sen-Ngam, (1998). “Windmill for Electrical Generation in the Rural Area” Final Research Report, Faculty of Engineering Prince of Songkla University (PSU.), Hat Yai, Songkla, THAILAND

THE POSSIBILITY OF USING ELECTRICAL MOTOR FOR BOAT PROPULSION SYSTEM

Rattakrit Reabroy¹, Yodchai Tiaple¹, Sathit Pongduang¹, Tewarat Nantawong¹ and Phansak Iamraksa¹

¹Faculty of International Maritime Studies, Kasetsart University, Sriracha Campus, Thailand

SUMMARY: This research was intended to use electric motor in order to replace fuel consumption engine. By focusing on the development of electrical propulsion system (EPS), one had to find the motor which was compatible with 4 m length boat model. The target of this development was attempting to design the electric drive which could reach up to 5 knots. The electricity of EPS was supplied by 4 batteries providing 24 volts of direct current, while thrust of the vessel was delivered by 3-phases 2.2 kW squirrel cage induction motor. The in-house designed inverter, converting from direct current system to 3-phase system, was coupled between batteries. The onsite experiment was carried out in the open-sea at Sriracha bay west of the campus. The result indicated that the maximum speed of the system could reach 5 knots within 1 kilometer distance.

Keywords: electrical propulsion, electric boat, inverter, electric drive, thrush

INTRODUCTION

Alternative energy becomes more interesting topics for researchers and engineers since 21st century. High price of fossil fuel urges not only government but also academic and private to find another source of energy which is sustainable. Among various forms of human used energy, electricity is the major usable energy source which is utilized in many applications from lighting to driving a vehicle, and it can be derived by different nature renewable energy such as wind, ocean wave or even sunlight.

Several attempts to replace normal outboard engine to electrical motor had been developed by various groups [1-3]. Normal electric motors which were available in the market such as permanent synchronous motors, squirrel cage induction motors and direct current motors were tested and reported [1-3]. Unlike diesel or petrol engine, the performance of electric propulsion were limited due to small power output of electric motor; however, different ship designs resulted slight improvement for instance catamaran vessel could perform better than mono-hull vessel when it used electric propulsion system [2-3]. In this article, squirrel cage induction motor with designed inverter/controller was used into small fishing boat.

EXPERIMENT SETUP

The experimented boat for this report was mono hull, and it was manufactured by fiberglass material. The principle dimension of boat was shown in table 1.

Table 1. The boat dimension.

Length Overall (L _{OA})	4m.
Beam Overall (B _{OA})	1.235m.
Length on waterline (L _{WL})	3.214m.
Draft	0.417m.
Displacement Volume	0.77m ³

The outboard electrical propulsion system (EPS) consisted of 3-phases 2.2kW squirrel cage induction motor coupling with space vector pulse width modulation (SVPWM) inverter. The battery bank consisted of 4 12V deep cycle batteries which can provide constant current up to 120Ah. Speed of the EPS could be controlled by width of the signal generated from SVPWM; additionally, the propeller could be rotated in both clockwise and counter clockwise by this inverter too.

RESULT AND DISCUSSION

The performance test was carried out at Sriracha bay locating at 10km west from campus as shown in figure 1. The testing included nautical velocity, acceleration and usage power of electric motor test at different speed setting: 10% 50%, 70% and 100%. The velocity was investigated by averaging speed recorded at forward and return trips, while the electrical measurement was also carried out during the speed-run trip, and the results from onsite test were shown in table 2. Note that the velocity and time were determined by GPS module, while the electrical measurement was determined by using clamp multimeter.



Figure 1. Open sea performance test.

Table 2. Recorded speed at different power setting.

Power Setting (%)	Recorded average speed (knots)
10	1.9
50	3.58
70	4
100	5.02

From the table 2, it indicated that the highest velocity achieved by this EPS was surprisingly close to the objective; however, the maximum speed might occur higher or lower than expecting because of various reasons such as size of the boat, weight of pay loads and propeller diameter. These parameters had to be brought to consideration when the engine was selected to fit into the given boat. The resistance analysis, computed from the boat dimension and geometry, was one of the major concerning for choosing right engine; the mechanical power of the engine should be close to the resistance in order to obtain the given speed. Let consider the electrical investigation at maximum speed as shown in table 3.

Table 3. The electrical parameter at maximum speed.

No. run	Velocity (knot)	Power (kW)	Distance (km)	Time (S)
1	5.1	1.72	0.075	68
2	5.05	1.68	0.07	62
3	4.9	1.73	0.065	55.5

The electrical power at 5knots was close to the calculated resistance of the boat at the same speed regime which was 1.8kW. This indicated that the thrust power, provided by electrical motor was matched to the boat resistance.

CONCLUSION

General electric motor is capable to modify into outboard engine for small boat with several concerns. Firstly, the given boat have to be studied its hydrodynamic parameters such as resistance in order to find the thrust power requirement. Secondly, several type of electric motor may need to be tested for its thrust power because it is difficult to predict and convert its electrical power into nautical velocity. This process may cause complication for boat builders when they want to replace fuel engine into electric. However, the normal estimation can be used in the electric mode as well as fuel mode for instance the horse power of electric motor can be considered as the same horse power of fuel engine. Another issue for EPS implementation is matching the propeller with the round speed of electric motor. Additionally, since the EPS needs battery, it would require many batteries for the boat to cover the travelling distance for each trip, and it causes added weight larger than normal fuel engine.

ACKNOWLEDGMENT

The authors would like to thank Research Identity program of faculty of International Maritime Study and The research committee of Kasetsart University Siracha campus for funding and supports.

References

- [1] G.S. Spagnolo, D. Papalillo, A. Martocchia and G. Makary, "Solar-Electric Boat", *Journal of Transportation Technologies*, 2, 2012, pp.144-149.
- [2] I. Utama, P.I. Santosa, R.M. Chao and A. Nasiruddin. "New Concept of Solar-Powered Catamaran Fishing Vessel", *Proceedings of 7th international Conference on Asian and Pacific Coasts*, 2013, pp. 903-909.
- [3] M. Ferry, W.B.W. Nik, A. Fitriadhy, S. Amahek and A.M. Muzathik "Efficient and Pollution Free Electric Catamaran Ferry For Kuala Terengganu River", *Proceedings of international Conference on Marine Technology*, 2012, pp.1-7.

THE STUDY OF POWER SYSTEM IN PHOENIX BY LOAD SHEDDING SYSTEM

Krit Rattanapanyapan¹ and Arkom Kaewrawang²

¹Energy Engineering, Faculty of Engineering, Khon Kaen University, Thailand

²Department of Electrical Engineering, Faculty of Engineering, Khon Kaen University, Thailand

SAMMARY: At present, the reliable of electrical power is very important for the distribution and electrical systems in the plant. Phoenix Pulp & Paper PCL (PPPC) generates electrical power about 95% and buys from Provincial Electricity Authority (PEA) of 5%. The protection system should be installed to protect the electrical bus when the machines are break down. It causes electrical system failure and machines stop the operation. Consequently, the productions will be loss. Therefore, PPPC must use load shedding system for cutting the connection of the machines to stop in a few minutes for protection of electrical system. Power flow of electrical power from 115 kV PEA to 11 kV via 2 transformers of 115 kV/11 kV and PPPC's 3 generators is studied. The real electrical power (P), reactive electrical power (Q), current (I) and voltage (V) used to set in the protection relay of load shedding system of 11 kV switchboards and motor control panel simulated by SKM Power Tools program is investigated in this research work. The simulation results: P, Q, I and V are divided in 4 cases: the trip from TG-PUC, TG2, TG3 and PEA. In the PEA trip case, P generated from 3 generators is insufficient about 6,512 kW that the machines have to stop the operation. In case of each generator trip, some P is received from PEA. Therefore, the load shedding scheme is important to protect the blackout system from distribution generator trip problem.

Key word: Power Flow, Load Shedding, Gauss-Seidel method, Electronic stability, Power fault

INTRODUCTION

Phoenix Pulp & Paper PCL (PPPC) is manufacturer of paper productions for pulp from Eucalyptus. The bark used in the process will be taken to the boiler for the electricity process for its own usage. Currently, the plant has the 3 generators: Generator 1 (TG-PUC), Generator 2 (TG-2) and Generator 3 (TG-3) that generate the apparent electrical power of 12.025, 26.50 and 36.71 MVA, respectively. In addition, it is from Provincial Electricity Authority (PEA) at 115 kV converted to 11 kV via the two of 25 MVA transformers connected in parallel.

In the record, three generators of the plant stopped occasionally suddenly (or breakdown) and maintenance. In 2013, there are the breakdowns for TG-PUC, TG-2, TG-3 and PEA of 6, 18, 12 and 9 times, respectively. In 2014, there are the breakdowns for TG-PUC, TG-2, TG-3 and PEA of 5, 12, 10 and 11 times, respectively. As a result, the machine was severely damaged due to a breakdown and it affects to the damage of pulp and paper production that causes loss money to resume the production and time for maintenance machine.

PPPC is finding a way to block off bus power system by installing the load shedding system [1], [2] by calculating the flow of electrical current and load flow in the system [3], [4]. SKM Power Tools program was used to calculate the values that have to be set up with power protection system (relay protection system) [5] by cutting the electricity to the machine that can stop and wait or other less important in the production process to prevent the

breakdown for all power systems along the way and to stabilize the electricity to the plant.

POWER FLOW EQUATION

Power flow in bus loop - real power electrical (P), reactive power electrical (Q) and voltage (V) in each bus and 3 generators connected to bus is calculated by Gauss-Seidel theory. At beginning of method, choose and set the unknown quantity values. Then, set each iterative. The solution continues until those quantities in accept range.

The voltage of i^{th} bus is

$$(V_i)^{(k+1)} = \frac{P_i^{sch} - jQ_i^{sch}}{V_i^{*(k)}} + \sum Y_{ij} V_j^{(k)} \\ \sum y_{ij}$$

where $i \neq j$

The real power of i^{th} bus is

$$P_i^{(k+1)} = \text{RE} \left\{ V_i^{*(k)} \left[V_i^{(k)} \sum_{j=0}^n Y_{ij} - \sum_{j=1}^n Y_{ij} V_j^{(k)} \right] \right\}$$

where $i \neq j$

The reactive power of i^{th} bus is

$$Q_i^{(k+1)} = -\text{Im} \left\{ V_i^{*(k)} \left[V_i^{(k)} \sum_{j=0}^n y_{ij} - \sum_{j=1}^n y_{ij} V_j^{(k)} \right] \right\}$$

where $i \neq j$

V_i is the voltage of i^{th} bus, Q_i is the reactive power of i^{th} bus, P_i is the real power of i^{th} bus, y_{ij} is the admittance between i^{th} bus and j^{th} , P_i^{sch} is the real power net of i^{th} bus and Q_i^{sch} is the reactive power

SIMULATIONS

The real power, reactive power, current and voltage of the bus loop are analyzed by SKM Power Tools program. Power and current should not be over the limitation of each device as shown in table 1. PPPC's transformers are connected with PEA electrical distribution and the bus loop is connected to each bus by cable tie as shown in Fig.1.

Table 1 Power (in MW) and current (in A) limit in each electrical device.

Device	Load (MW)	Current (A)
TR101	22.0	1,725
TR102	22.0	1,725
TG-PUC	7.756	1,016
TG-2	15.50	1,600
TG-3	23.34	2,000
Bus tie A-E	17.5	1,200
Bus tie B-C, D	21.5	1,650
Bus tie C, D-G	16.2	1,240
Bus tie A-B	21.5	1,650
Bus tie A-B	26.0	2,000

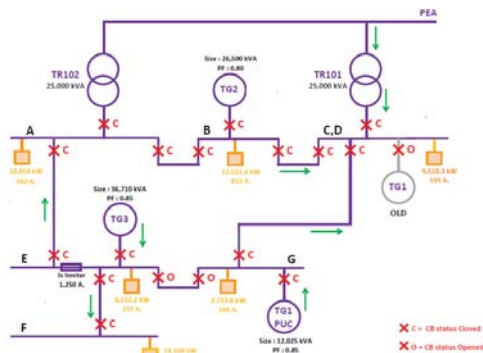


Figure 1. Electrical bus loop

RESULTS AND DISCUSSIONS

Table 2 shows the load loss in each bus from the normal case: bus A, B, C-D, E, F and G about 10,654.0, 12,521.6, 9,510.3, 4,232.2, 14,500.0 and 2,772.6 kW, respectively. In PEA trip case, three generators cannot generate P enough. So, load shedding must cut the load in bus A, B and C-D out about 1,478, 450 and 4,585 kW, respectively to protect the electrical power system blackout. In each three generator trip cases, the load in each bus is enough from PEA and running generators.

Table 2 Total loss load (in kW) in each case.

BUS	Load Normal (kW)	PEA TRIP		EACH TG TRIP	
		Load (kW)	Load loss (kW)	Load (kW)	Load loss (kW)
A	10,654.0	9,176.0	1,478.0	10,654.0	0.0
B	12,521.6	12,071.6	450.0	12,521.6	0.0
C,D	9,510.3	4,926.3	4,584.0	9,510.3	0.0
E	4,232.2	4,232.2	0.0	4,232.2	0.0
F	14,500.0	14,500.0	0.0	14,500.0	0.0
G	2,772.6	2,772.6	0.0	2,772.6	0.0

CONCLUSION

The load shedding of PPPC simulated by SKM Power Tools program is investigated to protect the blackout of electrical system. There are 4 cases: 3 cases of generator trip and 1 case of PEA trip. In the normal case, load power is about 54,190 kW. In PEA trip case, three generators cannot generate enough P, so load shedding must cut load in bus A, B and C-D out of 1,478, 450 and 4,584 kW, respectively. In case of each generator trip, the P will be compensated by PEA. The PPPC needs the electricity from PEA and losses the money as well. PPPC must have load shedding scheme when main transformer (TR101 and TR102) or PEA cannot supply electrical power to load for protection of the electrical system blackout. Therefore, the method of load shedding is an appropriate method for power management on all electrical systems.

References

- [1] C.H. Fujisawa, M.F. Carvalho, A.T. Azevedo, S. Soares, E.P. Santos and T. Ohishi, Load Shedding in a Distribution Network, 978-1-4673-2673-5/12, Brazil, 2012
- [2] B.Fox, J.G. Thompson and C.E. Tindall, *Adaptive Control of Load Shedding Relays Under Generation Loss Conditions*, The Queen's University of Belfast, UK
- [3] J.A. Treece, "Bootstrap Gauss-Seidel load flow", *PROC. IEE*, **116(5)**, 1969, pp. 866 – 870
- [4] Raed O. Abdelqader, *Method to model Active Harmonic Filter in Harmonic Simulation Packages*, 978-1-4244-1770-4/08, Australia, 2008
- [5] S. Hirodantis, H. Li and P.A. Crossley, Load Shedding in a Distribution Network, IEEE, 2009

THE STUDY OF THE EFFECT OF TDeq AND ΔT ON OTTV (CASE STUDY 6th FLOOR PIENVICHITR BUILDING)

Chutinan Singhpoo¹, Nattadon Pannucharoenwong¹ and Chatchai Benjapiyaporn¹

¹Department of Mechanical Engineering, faculty of Engineering,
Khon Kaen University, Thailand

SUMMARY: This study was conducted to search for the relationship to predict values of Overall Thermal Transfer Value (OTTV) of the building at different time in one day to determine the effects of temperature difference equivalent for wall (TDeq), and temperature difference for window glass (ΔT) affecting OTTV value: A case study of the sixth floor of Pienvichitr Building, Faculty of Engineering, Khon Kaen University, where the TDeq and ΔT values obtained from the calculation using the data of the temperature and the solar radiation in Khon Kaen Province. It is based on the reference direction of the building from 06.00 a.m. - 06.00 p.m. The results showed that the OTTV value with the highest value was at 02.00 p.m., and the minimum was at 06.00 a.m. The equation used to predict the OTTV with high accuracy compared to the TDeq and ΔT according to the rules of the Ministry of Energy used. This is approximately 1.5% of the error, but the OTTV can be taken to improve energy efficiency in the building further.

Keywords: Overall Thermal Transfer Value (OTTV), Temperature difference equivalent (TDeq), Temperature difference (ΔT), Solar radiation, Direction

INTRODUCTION

Since Thailand is located in the tropical zone, the energy consumption is considerably high and is not efficiently utilized. Therefore, energy saving in air conditioning system is very important because it can significantly reduce total energy consumption. Electricity consumption in air conditioning system can be reduced by an appropriate ventilation system [2]. Although amount of heat generated in buildings cannot be reduced, external heat which transferred through building perimeters can be reduced and is adjustable by improving OTTV [1]. Nevertheless, the latest update of the temperature and the solar radiation constant value are not used to calculate the OTTV. Consequently, the result from calculation is not consistent with the actual current condition [3]. The research aims to for the relationship to predict values of Overall Thermal Transfer Value (OTTV) of the building at different time in one day to determine the effects of temperature difference equivalent for wall (TDeq), and temperature difference for window glass (ΔT) affecting OTTV value, the OTTV can be taken to improve energy efficiency in the building further.

OTTV CALCULATION

The OTTV is total average heat gain through building as calculated from 3 parts of equation:

- Heat from heat conduction through wall
- Heat from heat conduction through window glass
- Radiation from window glass

OTTV each side can be calculated from

$$OTTV_i = \frac{(A_w \times U_w \times TDeq) + (A_f \times U_f \times \Delta T) + (A_f \times SC \times SF)}{A_i}$$

OTTV can be calculated from

$$OTTV = \frac{\sum(OTTV_i \times A_i)}{\sum A_i}$$

A case study of the sixth floor of Pienvichitr Building, where the TDeq and ΔT values obtained from the calculation using the data of the temperature and the solar radiation in Khon Kaen Province. It is based on the reference direction of the building from 06.00 a.m. - 06.00 p.m.

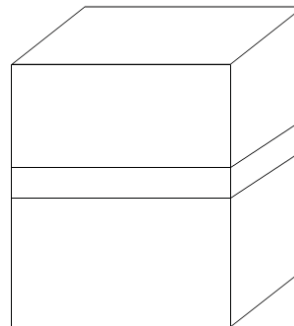


Figure 1. 6th floor of Pienvichitr Building

RESULT

The results showed that the OTTV value with the highest value was at 02.00 p.m., and the minimum was at 06.00 a.m. The equation used to predict the OTTV with high accuracy compared to the TDeq and ΔT according to the rules of the Ministry of Energy used. This is approximately 1.5% of the error.

Table 1. Minimum and Maximum OTTV

Time	direc	TDeq	ΔT	OTTVi	OTTV
6 a.m.	N	1.3	1.025	29.48	36.75
6 a.m.	S	0.4	1.025	32.37	
6 a.m.	E	3.9	1.025	62.79	
6 a.m.	W	0.4	1.025	22.36	
2 p.m.	N	11.0	6.875	45.10	53.06
2 p.m.	S	10.2	6.875	50.36	
2 p.m.	E	10.2	6.875	71.77	
2 p.m.	W	11.8	6.875	45.02	

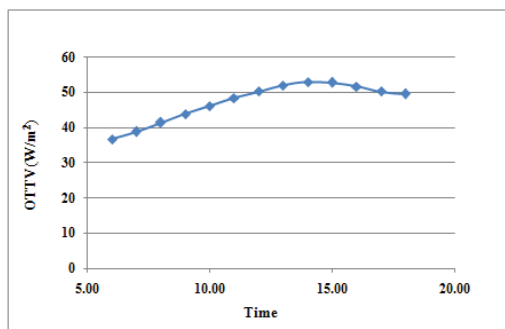


Figure 2. Time and OTTV

References

[1] A. Kunchornrat. "Study to review and purpose new parameters for OTTV calculation in existing building in Thailand". Ph.D. Dissertation, Department of Energy Technology, School of Energy and Mateials, KingMongkut's University of technology Thonburi. 2005.

[2] P. Prakongjai. "A comparison of heat gain calculation by transfer function method with OTTV and RTTV calculation". A thesis for the degree of master Engineering in Mechanical Engineering Graduate School Khon Kaen University. 2004.

[3] K. Sittikorn. "A support system for classroom scheduling to minimize energy utilization index". A thesis for the degree of master of Engineering in Industrial Engineering Graduate School Khon Kaen University. 2009.

EFFECT OF CALCINATION TEMPERATURE ON MICROSTRUCTURE AND PHASE FORMATION OF CaCO_3 PREPARED FROM DONAX SCORTUM SHELL

Suthasinee Kheawmaneechai¹ and Chontira Sangsubun¹

¹Department of Physics, Faculty of Science, Thaksin University, Thailand

SUMMARY: This research aims to fabricate calcium carbonate (CaCO_3) powder from *Donax scortum* shell using high-energy ball milling followed by calcination processing. *Donax scortum* shell powders were characterized using X-ray diffraction (XRD), scanning electron microscopy (SEM) and energy dispersive X-ray analysis (EDX). It was found that the CaCO_3 phase occurred after the calcinations temperature exceeded 600 °C. The particle size of CaCO_3 powder is in the range of 1-3 μm . The results of energy dispersive x-ray analysis found that the powder of *Donax scortum* shell that calcined at 600 °C contained mainly Ca, C and O.

Keywords: Calcium carbonate, calcination, *Donax scortum*, microstructure

INTRODUCTION

CaCO_3 has three polymorphs such as aragonite and vaterite [1]. In recent years, many research studies have been interested in aragonite because of its biocompatible properties [2-3]. Moreover, the CaCO_3 has a wide variety of industrial and commercial applications, such as plants, inks, paper, plastics, medicines and rubbers because it can be resolved and replaced by bone [4]. The aragonite is also being used to produce advanced drug delivery systems [7] and scaffolds for bone repair [4, 8].

The aim of this experiment was to synthesize calcium carbonate from *Donax scortum* shell by calcination at different temperatures. The structure of powders was investigated by X-ray diffractometer. The microstructure was investigated by SEM. Also, the chemical structure of powders was investigated by EDX.

PREPARATION OF MANUSCRIPT

The *Donax scortum* shells were washed. Then, the shells were ground using mortar before reducing their diameter in micrometer using high energy ball milling for 40 min. The powders were dried in an oven for 25 h at 90 °C. Then, approximately 20 g of *Donax scortum* shells were calcined at 500-700°C for 2 h. The microstructure of shells powders were analyzed by SEM. The element analysis was carried out using an energy dispersive X-ray analyzer. The structure of the powders was investigated by an X-ray diffraction.

RESULTS AND DISCUSSION

The surface morphologies of *Donax scortum* shell powders as obtained by SEM after dried in an oven for 90 °C are shown in Fig.1(a). The powders were agglomerated with the particles size ranges between 0.5-2 μm . The SEM images of shell powders after calcination at 500°C are shown in Fig.1(b). The powders were agglomerate. The particle sizes of powders are in the range of 0.5-2.5 μm . After calcined at 600 °C of *Donax scortum* shell powders, the SEM shows the powders of diameter 1-3 μm is present at Fig.3. While the microsize of *Donax scortum* shell

powders of diameter 15-40 μm were observed in powders calcined at 700°C. Table 1 shows the different elements after calcination at various temperatures and dried at 90°C as determined by EDX. The results show that the powder after 600°C contained calcium, carbon and oxygen.

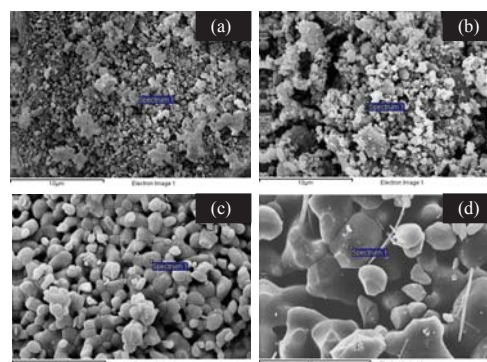


Figure 1. The surface morphology of (a) dried Venus shell at 90°C (b) *Donax scortum* shells at 500°C (c) calcined *Donax scortum* shells at 600°C (d) calcined *Donax scortum* shells at 700°C.

Table 1. Different element of (a) dried *Donax scortum* shells at 90°C (b) calcined *Donax scortum* shells at 500°C (c) calcined Venus shell at 600°C (d) calcined *Donax scortum* shells at 700°C determined by EDX. All results in atomic percent

Sample	C	O	Ca	Cu	Zn	Na	Cl	K
a	28	52	16	3.7	0.3			
b	32	50	15			1.4	1	0.6
c	10	39	51					
d	33	46	21					

ACKNOWLEDGMENT

The authors would like to thank Thaksin University for financial support. The authors also thank the Research Center in Energy and Environment for providing the research facilities and financial support.

References

- [1] H. Bala, W. Fu, J. Zhao, X. Ding, Y. Jing, K. Yu and Z. Wang, "Preparation of BaSO₄ nanoparticles with self dispersing properties", *Colloids and Surfaces A: Physicochemical and Engineering Aspects*. **252**, 2005, pp. 129-134.
- [2] J. Chen and L. Xiang, "Controllable synthesis of calcium carbonate polymorphs at different Temperatures", *Powder Technology*. **189**, 2009, pp. 64-69.
- [3] F. Guo, Y. Li, H. Xu, G. Zhao and X. He, "Size-controllable synthesis of calcium carbonate nanoparticles using aqueous foam films as templates", *Materials Letters*. **61**, 2007, pp. 4937-4939.
- [4] K.N. Islam, M.Z.B.A. Bakar, M.M. Noordin, M.Z.B. Hussein, N.S.S.B.A. Rahman and M.E. Ali, "Characterisation of calcium carbonate and its polymorphs from cockle shells (*Anadara granosa*)", *Powtec*. **213**, 2011, pp. 188-191.
- [5] C.Wang, J. Zhao, Xu. Zhao, H. Bala and Z.Wang, "Synthesis of nanosized calcium carbonate (aragonite) via a polyacrylamide inducing process", *Powder Technology*. **163**, 2006, pp. 134-138.
- [6] S.I. Stupp and P.V. Braun, "Molecular manipulations of materials: biomaterials", *Ceramics and Semiconductors Science*. **277**, 1997, pp. 1242-1248.
- [7] Z.P. Xu, Q.H. Zeng, G.Q. Lu, and A.B. Yu, "Inorganic nanoparticles as carriers for efficient cellular delivery", *Chemical Engineering Science*. **61**, 2006, pp.1027-1040.
- [8] K.N. Islam, M.Z. Bin Abu Bakar, M.E. Ali, M.Z. Bin Hussein, M.M. Noordin, M.Y. Loqman, G. Miah, H. Wahid and U. Hashim, "A novel method for the synthesis of calcium carbonate (aragonite) nanoparticles from cockle shells", *Powder Technology*. **235**, 2013, pp.70-75.

UNDERSHOT WATER WHEEL FOR A SMALL HYDRO-POWER SYSTEM

Songchai Wiriyaumpaiwong¹ and Jindaporn Jamradloedluk¹

¹Thermal process research unit, Faculty of Engineering, Mahasarakham University, Thailand

SUMMARY: This work aims to develop and test a small undershot water wheel for the final purpose of electricity generation. The micro-hydroelectric power system is installed on an irrigation canal with trapezoid flume. Slope of the irrigation canal is 0.0005. The undershot water wheel was tested at different levels of water in the canal and levels of paddle immersion (depth of paddle in the water). The mechanical, electrical, and overall efficiencies were calculated in each test. It was found that all efficiencies increased with increasing immersion paddle level. The water level in the canal also affected the system efficiencies. The higher water level resulted in the higher efficiencies of the system. Mechanical efficiency, electrical efficiency, and overall efficiency were maximized at the 0.6 m water level and the 28.5 cm immersion paddle level corresponding to the highest efficiencies of 0.82, 0.29, and 0.24, respectively.

Keywords: electrical efficiency, irrigation canal, paddle immersion level, water level

INTRODUCTION

Due to its high investment cost, environmental impact and insufficient public acceptance, large scale hydroelectric power plant, by means of massive dam, has a tendency to be replaced by micro-hydroelectric power system.

A simple design traditional water wheel and water mill have a low cost of operation and maintenance which is suitable in rural area [1]. The latter modern system must be designed to ease for portage [2]. Much attention has been paid on development of the high efficiency water wheels for the low flow rate and high head water resources [3 & 4]. Water wheel was generally rotated in perpendicular to the river flow. River flow spins water wheel, which could directly drive an electrical generator via chain mechanism. For instance, the Pelton turbine was found to provide a maximum mechanical efficiency of 0.47 ± 0.02 for a water flow rate of 0.17 l/s [3]. This study aims to develop and test a small undershot water wheel with trapezoid flume which is installed on an irrigation canal. Effects of paddle immersion level and water level on the mechanical, electrical, and overall efficiencies were also investigated.

METHODOLOGY

Undershot water wheel development

The micro-hydroelectric power system (Figure 1) consisted of 5 main components: undershot water wheel, increasing gear speed sets, DC generator, frame structure, and flume. The 1 m diameter undershot water wheel consists of 12 paddles made from 10 cm diameter PVC ducts (cutting in half), 24 PVC paddle arms and 5 mm thickness hubs. 4 sets of transmission that included 52 and 14 teeth's sprockets and chains were used to increase gear speed which connect to a DC generator. A frame structure supported water wheel and flume is made of 5 cm hollow square steel. A flume for increasing velocity of the water flow at the front of water wheel inlet is made of galvanized iron with 2 m long.



Figure 1. Micro-hydroelectric power field test

Stream flow measurement

Generally, the irrigation canal is lining with ordinary concrete. Water flow is based on gravitational force between high and low energy regions. The average water flow velocity (U , m/s) related to water level, dimension, and slope of the irrigation canal can be calculated as follows [5].

$$U = (n^{-1}) R^{2/3} S^{1/2} \quad (1)$$

$$A = y (L_1 + L_2) / 2 \quad (2)$$

$$P = L_2 + 2(0.5625 + y^2)^{1/2} \quad (3)$$

where

n = roughness coefficient ($0.013 \text{ m}^{1/3}\text{s}^{-1}$)

$R = A / P$ = hydraulic radius, m

A = cross-sectional area of irrigation canal, m^2

P = wet perimeter of irrigation canal, m

S = slope of irrigation canal, -

y = water level, m

L_1 = irrigation canal wide at the top level, m

L_2 = irrigation canal wide at the bottom level, m

To confirm the average water flow velocity, the average value of water flow velocities in different depths from water surface were measured by a current meter (General Oceanics Inc. model 2030R).

Undershot water wheel field test

The micro-hydroelectric power system was installed on top of the irrigation canal and set up at 3 different levels of water in the canal (0.5-0.6 m) and 3 levels of paddle immersion (19.0-28.5 cm). The water velocities at the flume inlet and the undershot water wheel inlet at the same level of paddle immersion were measured by the current meter.

Speeds (rpm) of the undershot water wheel and the DC generator were measured by a tachometer (Testo 470). Water power due to kinetic energy (P_w), mechanical power of water wheel (P_s), and electrical power produced from DC generator (P_e) are determined using the following equations.

$$P_w = (1/2)\dot{m} U^2 \quad (4)$$

$$P_s = 2\pi r l F \quad (5)$$

$$P_e = IV \quad (6)$$

where

\dot{m} = mass flow rate, kg/s

r = water wheel speed, rps

l = arm radius of water wheel, m

F = resultant force from water flow force minus drag and gravity forces, N

I = electric current, A

V = electric voltage, V

Performance of the system was expressed in terms of mechanical (η_m), electrical (η_e), and overall (η_o) efficiencies.

$$\eta_m = P_s / P_w \quad (7)$$

$$\eta_e = P_e / P_s \quad (8)$$

$$\eta_o = P_e / P_w \quad (9)$$

RESULTS AND DISCUSSION

Velocity profile in irrigation canal

Primarily, velocity of the water flow through the flume was measured and it was found that flume can increase water velocity from 0.375 to 0.480 m/s for the water level, of the canal, at 0.58 m. In such a condition, velocity profile of the water flow at different depths of the water was shown in Figure 2. From surface of the water, flow velocity started to increase with the water depth and then it provided a slight change (almost constant) at the depth of 0.20-0.35 m. The flow velocity was finally reduced as the increasing depth due to frictions of canal wall and bottom. The highest velocity ranging on 0.842 – 0.943 m/s was found at the water depth of 0.15 – 0.30 m.

Micro-hydroelectric power system test

Since water level in the irrigation canal depended on the upstream water level and water demand, it varied in each day. The variations of water levels in canal were in a range of 0.5 – 0.6 m during the field tests. Different paddle immersion depths (19 – 28.5 cm) were also tested in a day. Experimental data from field test are depicted in Table 1.

An increase of paddle immersion depth led to the increasing water flow velocity and water wheel speed. Consequently, mechanical and electrical powers and all efficiencies became higher. Similarly, the higher water level caused the higher water flow velocity and water wheel speed. Finally, water, mechanical, and electrical powers increased.

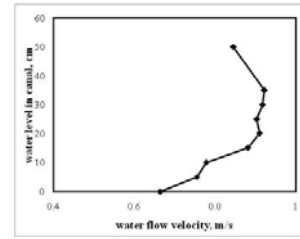


Figure 2. Velocity profile in irrigation canal

Table 1 Micro-hydroelectric power field test

water level (m)	paddle immersion depth (cm)	water flow velocity (m/s)	water wheel speed (rpm)	P_w (W)	P_s (W)	P_e (W)	η_m (-)	η_e (-)	η_o (-)
0.50	19	0.76	5.2	62.4	22.1	8.4	0.35	0.38	0.13
	23	0.78	5.6	62.4	22.3	9.7	0.36	0.43	0.15
	27	0.83	6.2	62.4	26.2	12.0	0.42	0.45	0.19
0.55	20	0.81	7.1	79.8	43.7	12.0	0.54	0.27	0.15
	24	0.87	7.8	79.8	52.3	15.6	0.65	0.29	0.19
	28	0.91	8.2	79.8	53.2	16.2	0.66	0.30	0.20
0.60	20.5	0.85	8.3	98.9	68.4	18.0	0.69	0.26	0.18
	24.5	0.89	9.3	98.9	75.8	21.2	0.76	0.27	0.21
	28.5	0.96	9.6	98.9	81.4	24.0	0.82	0.29	0.24

Considering performance of the hydro-power system, mechanical and overall efficiencies were similarly increased with their electrical powers. However, it was found that electrical efficiency decreased as the electrical power increased. This was probably because conversion of mechanical power to electrical power was less than conversion of water power to mechanical power.

ACKNOWLEDGEMENT

Authors would like to thank Faculty of Engineering, Mahasarakham University for financial support.

References

- [1] G.A. Ibrahim, C.H.C. Haron and C. Husna Azhari, "Traditional water wheels as a renewable rural energy", *The Online Journal on Power and Energy Engineering (OJPEE)*. **1(2)**, Reference Number: W09-0014, pp. 62-66.
- [2] P. Yelguntwar, P. Bhange, Y. Lilhare and A. Bahadure, "Design, fabrication & testing of a waterwheel for power generation in an open channel flow", *IJREAT International Journal of Research in Engineering & Advanced Technology*. **2(1)**, 2014, pp. 1-6.
- [3] D. Agar and M. Rasi, "On the use of a laboratory-scale Pelton wheel water turbine in renewable energy education", *Renewable Energy*. **33**, 2008, pp. 1517-1522.
- [4] R. Clifford and T. Roberts, "Round and round with paddle wheel propulsion", *Third International Symposium on Marine Propulsors*, 2013, pp. 279-282.
- [5] B. R. Munson, D. F. Young, T.H. Okiishi, "Fundamentals of Fluid Mechanics." 5th ed. Danvers, MA, 2006.

IMPROVING A GRID-BASED ENERGY EFFICIENCY BY USING SERVICE SHARING STRATEGIES

Boonyong Punantapong¹, Panit Punantapong² and Itthidech Punantapong³

¹King Mongkut's University of Technology North Bangkok, Thailand

²Electricity Generating Authority of Thailand, Thailand

³Provincial Electricity Authority, Bangkok, Thailand

SUMMARY: One of most important concerns in electrical power markets and distribution network is supplying the customer demands. It is necessary to forecast the usage of electrical power in distribution network. The pattern of electrical power usage depends on many different parameters such as the density of population in those areas, the week days, weather condition and etc. However, the electric utilities and regulators face difficult challenges evaluating new energy efficiency and smart grid programs prompted by recent state. In this paper, it is tried to forecast the electrical power usage according to above parameters by using artificial neural network base on service sharing strategies regarding that can help meet their energy efficiency policy goals. It is tried to find out the pattern of electrical power usage with the dataset which is prepared by real data. Therefore, it has been used here is useful in all kind of power forecasting such as short term, middle term, and long term. It can be helpful to manage the distributed generators production schedule and also correction of electrical power usage.

Keywords: renewable energy, energy efficiency, power distribution, service provider, smart grid

INTRODUCTION

The term "smart grid" refers to a reworking of electricity infrastructures encompassing technology, policy, and business models. Substantial amounts of government investment in several countries and regions have been devoted to smart grid research, development, and deployment. Smart grids are being pursued in order to address several challenges associated with today's power and energy systems, notably the following:

- **Economics:** Utilities and service providers today are sometimes forced to pay high prices for electricity that is import from grid connected neighbors at times of shortage or transmission congestion.
- **Reliability:** In developed economies, transmission infrastructure is aging and new infrastructure investment is lagging the increase in consumption and the addition of new generation. As a consequence, grid reliability is worsening.
- **Energy security:** The electrification of road transportation is seen as a strategy to reduce imports of foreign oil and gas. The additional load on the grid required, the individual loads are created additional challenges for today's power systems.

At the same time, smart grid investments and developments are covering the entire electricity value chain: generation, transmission, distribution, markets, and increasingly, consumers. The role of the end-use customer is in particular focus, primarily because the increasing penetration of wind and solar power is necessitating a more active role for energy management in homes, buildings and industries. The intermittency and unpredictability of renewable generation sources is in sharp contrast to traditional power generation. However, an often stated objective of the smart grid is to enable

building and/or industries demands to be more responsive to utility and grid system loads [1]. By potentially providing utility capability for direct load control, measurement in support for dynamic pricing, and as well the granular data needed for energy use to be more precisely targeted to consumer needs, the smart grid may enable significant electric energy savings as well as peak demand savings.

This paper considers these questions, and proposes architectural directions for the smart grid that compare utility-controlled and consumer-controlled energy networks. With utility control, the intelligence of devices is derived from a central control point via a private utility network. With consumer control, these devices use a control system that is located in the home or business, or on the internet but ultimately managed by the needs of the consumer.

METHODS

Smart grid is a broad objective, addressing opportunities for enhanced communications and control in transmission and distribution of electricity. Within distribution, a key component under consideration is Advanced Meter Infrastructure (AMI), which is usually defined as measuring energy use at the meter at hour intervals or less and communicating these reads at least daily to utility. However, it remains ambiguous as to whether the deployments will include the elements needs for efficiency and demand response. Some parameters such as reliability, power loss, voltage profile and etc are more important in this part of power system and this is all because of being the large number of customer in distribution networks and load profile. These parameters can be used in forecasting the electrical load which is classified in four classes:

- Very short term load forecasting: The load

forecasting for 1 minute to few hours.

- Short term load forecasting: The load forecasting for 1 day to 1 week.
- Medium term load forecasting: The load forecasting from several weeks to one or several years.
- Long term load forecasting: The load forecasting up to 20 years.

The condition and necessity one of these classes is used in load forecasting such as reference [2] introduces a brief overview in long term forecasting methods. Reference [3] multi-layer perceptions network is used to estimate the load in short term by using 2 variables; the historical load demand and time. Reference [4] used the Artificial Neural Network (ANN) to forecast electrical power load according to hours in short term. In this paper is tried to find out the way to forecast the electrical power load in power distribution network by using artificial neural network with the help of Matlab software. The input is involved 3 features; historical load demand, weather, and time. Mean square error is used as performance measure. The method of learning in ANN which is used in this study is back propagation.

RESULTS

The dataset is 580 samples of three elements so the dataset is matrix that has 580 rows and three columns which its 1st column is time, the 2nd column is weather, and the last column is customers' electrical power usage. In this paper is tried to find the way to forecast the power usage. The network setting is original back propagation 4 inputs and 1 output. The hidden layers, the learning rate setting, momentum and number of Epoch changes in the cases while stopping criteria is 0.008 and the performance measure is MSE (Mean Square Error).

Table 1: Result of training in different cases

Case	No. Iteration	Performance	Gradient	MU	Reason of Stopping
1	15	$2.88*10^9$	$7.33*10^{-5}$	$1*10^{11}$	Max MU reached
2	2510	0.180	$9.98*10^{-6}$	0.01	Min gradient reached
3	26	$2.81*10^9$	$3.06*10^{-5}$	$1*10^{11}$	Max Mu reached
4	6224	0.0235	$9.76*10^{-6}$	$1*10^{-8}$	Min gradient reached
5	28000	0.0211	$5.01*10^{-5}$	1	Max epoch reached
6	658	0.0140	$9.54*10^{-6}$	0.01	Min gradient reached
7	28000	0.0184	0.000598	0.1	Max epoch reached
8	655	0.0148	$9.87*10^{-6}$	0.01	Min gradient reached
9	662	0.0158	$9.96*10^{-6}$	0.1	Min gradient reached
10	28000	0.0103	0.000241	0.1	Max epoch reached
11	160	0.0065	0.00185	0.01	Performance goal met
12	66	0.0066	0.00821	0.001	Performance goal met
13	76	0.0082	0.00121	0.01	Performance goal met
14	45	0.0076	0.12500	0.01	Performance goal met
15	32	0.0074	0.05821	0.01	Performance goal met

CONCLUSION

The result of this simulation shows the high efficiency of the neural network in forecasting the electrical power load. So it can be said that this method is not limited to any of the classes that described before because if we have the weather parameters it is possible to forecast the load. This research about load forecasting can be helpful for scheduling on requirement on developing electrical distribution network, selling energy, maintenance and also standby the sources.

References

- [1] L. Edward, "Strategies and Policies for improving energy efficiency programs: closing the loop between evaluation and implementation", *Energy Policy*. **36(10)**, 2008, pp.3872-3881.
- [2] L. Ghods and M. Kalantar, "Different methods of long-term electric load demand forecasting; A comprehensive review", *Iranian Journal of Electrical & Electronic Engineering*. **7(4)**, 2011, pp.249-259.
- [3] S.K. Sheikh and M.G. Unde, "Short-term load forecasting using ANN technique", *International Journal of Engineering Sciences & Emerging Technologies*. **1(2)**, 2012, pp.97-107.
- [4] K. Geetha and S.K. Mohiddin, "Short-term load forecasting using generalized neuron model with error gradient functions", *International Journal of Advanced Research in Computer Science and Software Engineering*. **3(4)**, 2013, pp.357-360.

EFFECT OF CHANNEL DESIGN AND OPERATING PARAMETERS ON OPEN-CATHODE PEM FUEL CELL PERFORMANCE: A COMPUTATIONAL STUDY

Suchart Kreesaeng¹, Benjapon Chalermisinsuwan^{1,2} and Pornpote Piumsomboon^{1,2}

¹Fuels Research Center, Department of Chemical Technology, Faculty of Science, Chulalongkorn University, Thailand

²Center of Excellence on Petrochemical and Materials Technology, Chulalongkorn University, Thailand

SUMMARY: This paper presents the effect of cathode channel design with vary cross-sectional area and aspect ratio. Three dimensional, steady state and single phase model was developed to investigate the effect of cross-sectional area and aspect ratio of cathode flow channel on the cell performance for open-cathode PEM fuel cell. The result shows that increasing of cross-sectional area lead to decreasing of pressure drop in channel and decreasing of molar concentration of oxygen at the interface of catalyst layer and membrane. The result of increasing aspect ratio shows that the pressure drop was decreased and the molar concentration of oxygen was increased.

Keywords: PEMFC, open-cathode, cathode channel aspect ratio, cell performance, CFD

INTRODUCTION

Today social awareness about global warming caused by carbon dioxide due to the burning of carbon fuels is recognized. Therefore, finding new alternative to reduce carbon dioxide emission has got more attention. Hydrogen gas is one of alternatives since when hydrogen is burnt, it does not emit carbon dioxide. One of the engines using hydrogen to produce power efficiently is fuel cells.

A fuel cell is an energy conversion process that can convert chemical energy directly into electrical energy by electrochemical reaction. There are many types of fuel cells. Proton exchange membrane (PEM) fuel cell is one type that is widely used because it operates at low pressure and temperature. Reactants for PEM fuel cell are hydrogen and oxygen and its products are water and heat.

To operate a typical fuel cell system, there are a number of components, such as reactant feeding system, humidifier, cooling fan, air compressor and control components, connecting with each other to support the system. To reduce the number of components, an open-cathode PEM fuel cell is recently developed by inducing ambient air to the cathode as a reactant and cooling media. Its main disadvantage is that air feeding into cathode side is by natural convection causing lower cell performance than those by compressed air. However, the disadvantage of using compressed air is the non-uniform oxygen mass transport. Sasmito et al. [1] showed that for open-cathode PEM fuel cell, the increasing of channel height increased the air flow rate and consequently increased current density. Wang et al. [2] studied a PEM fuel cell with serpentine flow field. They found that decreasing of the flow channel size increased the reactant inlet velocity, which transported more oxygen to the cathode catalyst layer. Thus, the cell performance was improved. Nevertheless their smallest unit did not give the best performance because of the power lost due to high pressure drop.

From the literatures, one of the solutions for the mass transport problem could be solved by appropriate cathode flow field design. In this study, the effect of cross-sectional area and aspect ratio on the cell performance for open-cathode PEM fuel cell was investigated.

MODEL DESCRIPTION

In this study, the three dimensional, single phase model was developed for open-cathode PEM fuel cell. The governing equations including mass, momentum, and species conservations were solved. The assumptions in this model were ideal gas, steady state and isothermal system.

Flow field design

Cathode channels were designed by varying channel aspect ratio (Width/Depth) and cross-sectional area (Width*Depth) with 6 different configurations as shown in Table 1 and Figure 1.

Table 1. Detail of cathode channel designs.

Design No.	Cross-sectional area (mm ²)	Aspect ratio	Width (mm)	Depth (mm)	No. of channels
1	2.0	0.8	1.26	1.58	40
2		1.25	1.58	1.26	40
3	5.0	0.8	2.00	2.50	25
4		1.25	2.50	2.00	25
5	8.0	0.8	2.53	3.16	20
6		1.25	3.16	2.53	20

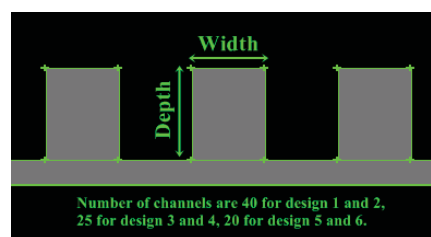


Figure 1. Cathode channels.

Numerical method

The computational domains were created and meshed using the commercial software, Gambit 2.2.30. The governing equations were discretized using first-order upwind scheme and solved by commercial CFD software FLUENT 6.3 with the SIMPLE algorithm. The convergence criteria for all relative residuals were 10^{-6} .

RESULTS AND DISCUSSION

The effect of cross-sectional area and aspect ratio

The results of pressure drop are shown in Figure 2. The lower aspect ratio induced slightly higher pressure drop while the larger cross sectional area caused lower pressure drop. The increasing of flow channel cross-sectional area is the main reason why the reactant velocity and system pressure drop decrease.

Figures 3, 4 and 5 demonstrate the molar concentration of oxygen at interface of catalyst layer and membrane for design 1, 3 and 4 respectively. When the effect of cross-sectional area is considered, comparing 2 mm^2 to 5 mm^2 , the lower cross-sectional area made the molar concentration of oxygen to be higher. These lead to the increasing of current density and lessening of mass transport problem.

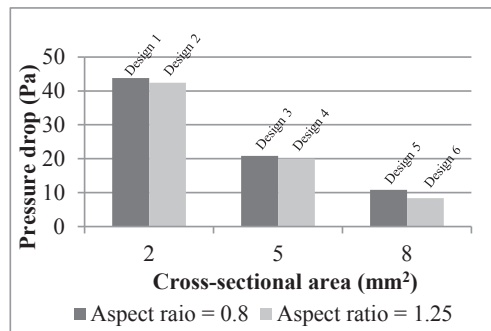


Figure 2. Pressure drop with different designs.

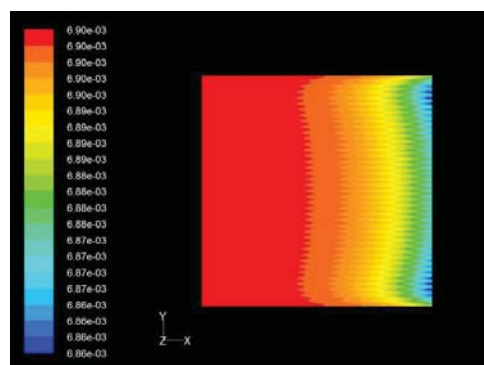


Figure 3. Molar concentration of oxygen gas at interface of catalyst layer and membrane for design 1

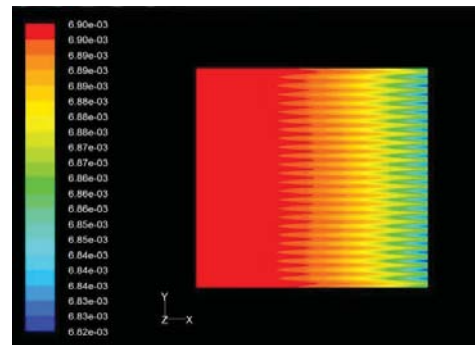


Figure 4. Molar concentration of oxygen gas at interface of catalyst layer and membrane for design 3

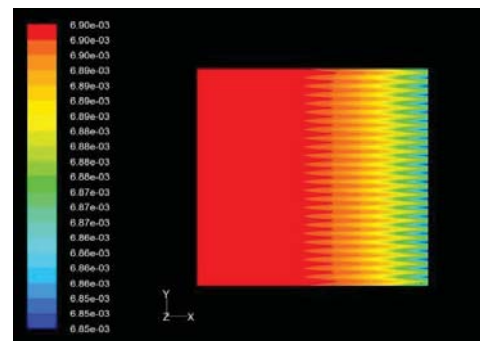


Figure 5. Molar concentration of oxygen gas at interface of catalyst layer and membrane for design 4

When comparing the effect of aspect ratio in case of 5 mm^2 cross-sectional area, the larger aspect ratio increases molar concentration of oxygen and also leads to the increase of current density. The higher aspect ratio has increased the diffusing area between the flow channel and gas diffusion layer.

ACKNOWLEDGEMENT

The author would like to thank Fuels Research Center, Department of Chemical Technology, Faculty of Science, Chulalongkorn University and Department of Mechanical Engineering, Faculty of Engineering, Chulalongkorn University

References

[1] A.P. Sasmito, K.W. Lum, E. Birgersson and A.S. Mujumdar, "Computational study of forced air-convection in open-cathode polymer electrolyte fuel cell stacks", *Journal of Power Sources*. **195**, 2010, pp. 5550–5563.
 [2] A.P. Manso, F.F. Marzo, M. Garmendia Mujika, J. Barranco and A. Lorenzo, "Numerical analysis of the influence of the channel cross-section aspect ratio on the performance of a PEM fuel cell with serpentine flow field design", *International Journal of Hydrogen Energy*. **36**, 2011, pp. 6795 – 6808.

A STUDY OF FINISHED PRODUCT TOM YUM GOONG BY FREEZE-DRYING PROCESS

Sateeruj Srisantisuk¹, Piyachart Thateenaranon² and Vinai Pimpinit³

^{1,3}Faculty of Technology and Innovation, Bangkokthonbury University, Thailand

²Department of Mechanical Engineering, Faculty of Industrial Education, Rajamangara University of Technology Suvarnabhumi, Thailand

SUMMARY: This research aims to study the physical properties of the nutritional content of moisture. And calculate the percentage weight balance, subject to drying Freeze Standard is a -100 liter having wide a 1.5m long 1.5m and high 2m. To get 10kg of water, which process drying, freezing. The drying process, which relies on the sublimation of the water out of the product, so the product will not be destroyed by overheating. Products smell and taste. Including the structure and texture of the product will remain unchanged, no shrinking or sagging. Also, the product is also convenient to the consumer because of a good recovery and wire speed. This research is the moisture content before %79.69 and after %3.32, Protein before 16.90g and after 62.4g, Fat before 1.30g and after 3.50 g, Carbohydrate before 1.30g and after 15.6g.

Keywords: drying Freeze, Tom Yum Goong, protein, carbohydrate

INTRODUCTION

Nowadays consumers play an important role to determine quality of the food products. They require high nutrition, food safety and long shelf life. A freeze-drying process is the most famous method to reduce moisture of the fresh products or transform liquid food into powder to extend the shelf life, and conveniently store and transfer. Also it increases product choices and convenience to comfort present rush life of the people such as a semi-instant dry food that requires a little water to add and ready to serve. However the products have to be with quality, safety and acceptable appearance to the consumers.

There are many drying methods and each method has different pros and cons such as natural air drying, solar cooking and other applications of hot air (convective) including tray dryer, tube dryer, fluidized bed dryer, spray dryer or solar dryer. All these machines can dry food which is in form of lump, chunk, powder, fiber, semi-liquid and grain. However, this method consumes too much energy and can destroy nutrition because of the overheating. Therefore evaporation of the moisture at a very low temperature such as vacuum drying process which will increase drying ratio in a very short time and that remains aroma, flavor, physical appearance (color, shape) in the good condition. Such a drying process requires vacuum room, heating generator, vacuum generator. Fruits and vegetables, meat, herbs, spices, and mushrooms are normally dried by this process. However, the most efficient vacuum generator costs a lot. Some food products have limitation; it can be depreciated when it has emerged to heat and low temperature. Therefore the freezing process could be an alternative in cooperation with reducing the pressure to the point that the products can sublimate. The freezing drying is suitable for the food products that are sensitive to the heat such as expensive products, ginseng coffee, fruit juice powder, strawberry, high grade dried shrimps, dried mushrooms. The freeze drying process can keep

major properties of the food that can be easily destroyed in the heat such as vitamin, aroma, color, appearance, and texture as the fresh one. However, it requires high investment and takes a long time to dry.

METHODS

Type of Shrimps

Shrimps are generally found in both fresh water and sea water. Especially sea water shrimps are caught. There are 2 families of shrimps that are most caught, Penaidae Family and Palaemonidae Family and each family can be categorized as follows:

1. Penaidae Family can be divided into 2 species
 - 1.1 Peaneus eg. Pacific white shrimp (*P. Iadicus*), Banana shrimp (*P. Margiuensis*), Tiger Prawn (*P. Monodon*)
 - 1.2 Metapenaeus eg. Jinga shrimp (*Metapenaons mononeron*)
2. Palaemonidae Family eg. Dwarf prawn (*Palaemon sp*), River Shrimp (*Leander sp*). Shrimp is traded by size, mixed types, not by same types.

RESULT AND DISCUSSION

The analysis of Fresh Shrimp characteristics

The analysis resulted from the experiment, and compared to the standard characteristics.

Table 3 Nutrition facts from the edible part 100 grams of shrimp meat.

Description	Standard	Shrimp Sample
Moisture	73 %	79.69 %
Protein	21 g	19.85 g
Fat	2 g	1.67 g
Carbohydrate	1 g	1.19 g
Energy	106 Kcal	101 Kcal

From table 3 the fresh shrimps contained 16.9 grams/100 grams of protein, 1.3 grams/100grams of fat, 1.3 grams/100 grams of carbohydrate and 99.00 Kcal. The analytical result varied to the source of the fresh shrimps, the cultivated area, the method of raising the shrimps and the analytic method used.

The analysis of the shrimp characteristics after freeze-drying process.

The results of the study showed in the table below.

Table 4. Nutrition contents after freeze drying process

Description	Fresh shrimps	Fz.D1	Fz.D2	Fz.D3	Average
Weight	100g	19.40 g	20.22 g	19.56 g	19.73 g
Moisture	79.69 %	3.68 %	3.32 %	3.24 %	3.41 %
Protein	19.85 g	19.56 g	19.53g	19.62g	19.57 g
Fat	1.67 g	1.64 g	1.63 g	1.65 g	1.64 g
Carbohydrate	1.19 g	1.0g	1.1g	0.98 g	1.03g
Energy	101 Kcal	96 Kcal	98 Kcal	95 Kcal	96.33 Kcal

From table 4 the products after drying process were analyzed to check the quality of the products to maintain shape, color, aroma, flavor as they were, which affected to shelf life storage with the average weight at 19.73 grams/100 grams. The moisture measurement average moistures at 3.41% or 4.27% yield based on the weight before storing in a proof package to prevent sun, air and moisture.

CONCLUSION

Although freeze drying process is a drying process that requires tools and complex steps, there are still benefits in terms of preservation and storage to last longer, but is still nutritious. This study could be a guideline for further methods in the future.

ACKNOWLEDGEMENT

The authors would like to thank Rajamangala University of Technology Suvarnabhumi (Suphanburi Campus) and Bangkokthonburi University for providing partially financial support to this research work, and to our research center.

References

- [1] B.K Bala. "Drying and storage of cereal grains". Oxford and IBH Publishing Co. PVT. Ltd., New Delhi, India, 302 pages. 1997.
- [2] B.K Bala and S. Janjai. "Solar drying of fruits, vegetables, spices, medicinal plants and fish: Developments and Potentials", *International Solar Food Processing Conference*, 2009, pp. 1-24
- [3] K. Kathiravan, K.K. Harpreet, J. Soojin, I. Joseph and D. Ali, D. "Infrared heating in food processing: an overview". *Comprehensive Reviews in Food Science and Food Safety*, **7**, 2008, pp. 2-13.
- [4] G.P. Sharma, R.C. Verma and P.B. Pathare. "Thin-layer infrared radiation drying of onion slices". *Journal of Food Engineering*, **67**, 2005, pp. 361-366.
- [5] T. N. Tulasidas, G.S.V. Raghavan and A.S. Mujumdar, "Microwave drying of grapes in a single mode at 2450 MHz-II and energy aspect" *Drying Technology*, **13**, 1995, pp. 1973-1992.

THE CONSTRUCTION OF CHARGING BATTERY FOR SMALL ELECTRIC CAR THREE-WHEELER

Sateeruj Srisantisuk¹, Popong Anudit¹ and Saichol Wangsang¹

¹Faculty of Technology and Innovation, Bangkokthonbury University, Thailand

SUMMARY: This research aims to construction of charging battery for small electric car three-wheeler from the results showed that the pressure of the best in the generator to recharge the battery pack hydroelectric tricycles that the pressure at 1.25 bar. the test used in this nozzle diameter of 0.1 mm, and when you open it up. Valve will open and propeller starts. Cause voltage starting at 8.08 volts, then turn off the water at low pressure to 0 volts and the voltage before closing at 38.80 volt, rechargeable battery.small electric car three-wheeler used for 3 hr. At 7 km / hr.

Keywords: battery, generator, valve

INTRODUCTION

According current energy crisis, energy consumption is a big problem in the world. It continuously affects to human living. Several agencies try to find good solutions by doing researches, surveys and trails of new technologies seriously. For the reason is to bring renewable energies and new technologies to replace the current energies in Thailand as well as it still concerns about resources and environment.

A bicycle is a kind of vehicles that was built for a long time. In the past, we used manpower to ride but nowadays we learn to control and produce electricity to move the bicycle. Generator is an electrical equipment changing electrical energy to mechanical energy which is applied to an ordinary bicycle. It is transformed to an electric bicycle afterwards. Generator is installed on the electric bicycle as an electrical device and uses a battery as a power source. Currently a lot of exercise bicycles are built to comfort human by equipping with Generator. Its function is to produce electricity stored in a battery to recycle use in electrical devices. Generator acts as a source of electricity and the battery plays an important role of energy storage to propel the bicycle.

The research members are interested in collecting data related to the creation of the battery. The research is to study process and invent a rechargeable battery used for a small electric car 3 wheeler. The purpose of using water energy is to compensate electrical energy.

METHODS

Theoretical orientation

Water flow is a result of the different level of the area. For this reason, Potential energy will change to Kinetic energy. The use of various mechanical parts transforms latent Kinetic energy which comes from water into electricity. This technic is already available but it needs design of that equipment to be suitable for a work terrain. It is also easy use and has most efficiency as possible. From Bernoulli's Equation,

$$\frac{P}{\rho g} + \frac{V^2}{2g} + z = \text{constant}$$

It shows that the energy per unit weight of fluid contains kinetic energy ($V^2/2g$), potential energy (z) and the energy in terms of pressure ($P/\rho g$). All three energies can converse among them. As the above equation, if the fluid velocity or fluid pressure is higher than atmospheric pressure or the fluid level is higher than the reference level, that fluid is able to change energy into work, for example, the production of electricity from water stored above a dam. It converts potential energy into electrical energy. It found that current in a river or a stream during flood tide has high speed velocity. That is kinetic energy ($V^2/2g$) which can swop to electrical energy by using a turbine and a hydro generator. The more speed of water velocity has, the more electricity it produces.

However, potential energy is converted into kinetic energy in a hydroelectric power plant. Before water enters the turbine, water will have a very high speed in case of water in a river. Nevertheless its speed is low when energy per unit weight is low too. If the electric power gets to the design target, the turbine must be larger to allow more water flow through a propeller as the equation below.

$$\text{Power} = \frac{\eta \rho g Q v^2}{2}$$

When η is turbine efficiency
 ρ is water density (kg/m^3)
 Q is water flow rate through the turbine (m^3/s)
 v is water velocity before entering the turbine (m/s)
 g is acceleration due to gravity (m/s^2)

RESULT AND DISCUSSION

Creation of the rechargeable battery with a small electric car 3 wheeler

1. Built the steel case to place the pressure tank.

2. Drilled the tank to fill the pressure control equipment.
3. Set pipeline and pump water to the pressure tank. Glued the pipe with a motor tightly to prevent vacuum in the pipeline.
4. Set circuit for the motor. Used Flasher switches and relays to control motor pumping.
5. Installed a pressure gauge on the tank to check internal pressure
6. Installed a safety valve to prevent a broken tank and vacuum inside the tank.
7. Kept various water pressure of 0.5 bars, 1 bar, 1.25 bars as details below

Results showed that the pressure of the best in the generator to recharge the battery pack hydro electric tricycles that the pressure at 1.25 bar. the test used in this nozzle diameter of 0.1 mm, and when you open it up. Valve will open and propeller starts. Cause voltage starting at 8.08 volts, then turn off the water at low pressure to 0 volts and the voltage before closing at 38.80 volt, rechargeable battery, small electric car three-wheeler used for 3 hr. At 7 km/hr.

CONCLUSION

It could summarize the test which was used 0.1 mm. nozzle diameter and water pressure of 1.25 bars. The result showed that when the machine was turned on, valve would open up and the propeller started working. The electrical voltage occurred at 8.08 volts on the 5th test. When water was turned off at a zero pressure, the voltage was at 38.80 volts before closing the valve on the 44th test.

Referring the pressure range from 0.5 – 1.25 bars with 1 mm. nozzle diameter, it concluded that the pressure of 0.5 bars was the lowest pressure to open up valve and then water flowed down through the propeller. When the machine started working, the electrical voltage would appear at 6.33 volts on the 2nd test. In addition, the pressure of 1.25 bars was the highest pressure which could open valve and then water flowed down through the blade. When the machine started working, the electrical voltage was at 8.08 volts on the 5th test.

ACKNOWLEDGEMENT

The authors would like to thank Bangkokthonburi University for providing partially financial support to this research work, and to our research center.

References

- [1] A.T. Saylor, "Hydraulic and Compressible Flow Turbomachines", *McGraw -Hill (UK) Company Ltd.* 1990.
- [2] R.K. Turton. "Principle of Turbomachinery, 2 nd ed. Chapman and Hall", London , 1995.
- [3] A.R. Robert and J. K. Jack. "Energy and the Environment. New York" *John Wiley and Sons.* 1999.
- [4] W. Shepherd and D.W. Shepherd. "Energy Studies. Singapore" *World Scientific.* 1998.

THE STUDY OF TEST NOZZLE FOR INDUSTRIAL APPLICATIONS

Sateeruj Srisantisuk¹, Pairat Promma² and Pranot Yooi³

^{1,3}Faculty of Technology and Innovation, Bangkokthonbury University, Thailand

²Nakornluang Polytechnic College, Thailand

SUMMARY: This research aims to create test nozzles of different sizes for select charters bindings for which tests were used nozzle size 2 mm, 3 mm, 4 mm, 5 mm and 6 mm with open impeller turbine at different materials are plastic, brass and stainless steel. The results of 1.25 psi pressure turbine blade plastic type better speed blade brass type and blade stainless steel type

Keywords: nozzles, turbine

INTRODUCTION

Development of renewable energy to research, test, development and demonstration, as well as promote renewable energy. The clean energy No environmental impact and as a source of energy available in the wind, solar, biomass, such as local and more to be produced. And commonly exploited Effective and are suitable both technical, economic and social for users in rural and urban areas, in which the research and development of renewable energy will also include the development of tools and equipment to use the most effective jobs and education. Renewable Energy As part of the plan to develop renewable energy. The research projects that are directly under the plan. Energy Research and are linked to rural development programs in the establishment of a power generation system.

Current plans for rural development projects in established power generation system. Charge the battery with solar panels for villages without electricity. The study and develop renewable energy by providing a permanent job the implementation of the activities. The objective to support the development of renewable energy technologies. Both academic theory and laboratory and testing equipment, including the promotion and dissemination. This will support and supports the availability of establishing new projects. In research on energy and other projects. The related preliminary study. Track progress and cooperation with other agencies involved in the development, test, analyze and evaluate primary and is actively promoting the development of projects that are working to make a more complete. As well as support for projects already completed have taken action to promote and exploit optimally the next (Source: Strategic Energy Plan).

Researchers have been interested in collecting information related to the nozzle is used to generate electricity. In order to study the procedure and test generator nozzle size 20 liter tank.

METHODS

Significant theories related with this study was the rules. The rolling waves and the variable gain dimensions of the turbine and the turbine is the basic

equation Pelton (Pelton Wheel Turbine) which a turbine that generates up the test in this research. And will reflect equations used to analyze capacity and efficiency of the turbine.

Rules flexibility the roll and variable gain dimensions of the turbine.

As a rule, similar the analogy of fluid machinery has line graph for the machines that are designed to transactions of large amounts and uses graph these of this Office. For design options Using the machine as task that to which the design is the single point on the graph line the highest performance. For the turbine. To determine the speed, power jobs exports and the flow rate under head power one of the a valuable efficiency fixed point the Czech when tested turbines subject under the power of the H1 and N1 in which the speed of the roll rule flexibility for the turbine at the under the the head H2 power and speed N2 will

$$\frac{H_1}{N_1^2} = \frac{H_2}{N_2^2} \quad \text{Hence} \quad N_2 = N_1 \left(\frac{H_2}{H_1} \right)^{1/2}$$

H₂ = 1 will be

$$N_2 = \frac{N_1}{H_1^{1/2}} = N_u \quad (1)$$

And similar will the flow rate and capacity. The task for the head the first power unit.

$$Q_u = \frac{Q}{H^{1/2}} \quad (2)$$

$$\dot{W}_u = \frac{\dot{W}}{H^{3/2}} \quad (3)$$

However, the coefficient of dimension called the coefficient of head Energy and Power coefficient.

$$\bar{W} = \frac{\dot{W}}{\rho N^3 D^5} = \frac{\dot{W} N^5 \psi^{5/2}}{\rho N^3 (gH)^{5/2}} = \frac{\dot{W} N^2 \psi^{5/2}}{\rho (gH)^{5/2}}$$

$$\text{หรือ} \left(\frac{\bar{W}}{\psi^{5/2}} \right)^{1/2} = \frac{N \dot{W}^{1/2}}{\rho^{1/2} (gH)^{5/4}} = \text{ค่าคงที่} \quad (6)$$

And by substituting the Power, $W = \rho g QH$ into the equation (6) will be

$$\frac{NQ^{1/2}}{(gH)^{3/4}} = \frac{\phi_D^{1/2}}{\psi_D^{3/4}} = \text{ค่าคงที่} \quad (7)$$

The second law of motion at Newton

This rule the sum of all the force of the fluid only to the rate of change of momentum of the fluid Written the following equation

$$\sum F_x = \dot{m} (C_{2x} - C_{1x}) = \rho Q (C_{2x} - C_{1x}) \quad (8)$$

Mining turbines, which have blades that rotate around a central axis motion shows are the only works if between the fluid and the form. Multiplier effect between the torque to the angular velocity (in with rad / s) in Figure 2 shows the motion of the particles of the fluid from the first to the radius r1 to the second place. radius r2, C1x and C2x is the organization consists of speed in the direction of flow. The tangential entry and exit respectively. It will be the sum. All of torque acting on the system.

$$= \sum (\tau \omega) = \dot{m} \omega (r_2 C_{2x} - r_1 C_{1x}) \quad (10)$$

$$\dot{W} = \dot{m} (U_1 C_{1x} - U_2 C_{2x}) \quad (11)$$

The equation is called the Euler’s equation

RESULT AND DISCUSSION

Education nozzle generator tank size of 20 liters

Nozzles are used in generators of various sizes are available. Who will be deployed to study the data that nozzles that are appropriate to the task

Education Equipment used to test generators

- Nozzle size 20 liter tank.
- Water tank
- Meter Revolutions
- Batteries
- Propeller

This research aims to create test nozzles of different sizes for select charters bindings for which tests were used nozzle size 2 mm, 3 mm, 4 mm, 5 mm and 6 mm with open impeller turbine at different materials are plastic, brass and stainless steel. The results of 1.25 psi pressure turbine blade plastic type better speed blade brass type and blade stainless steel type

CONCLUSION

A comparison of different nozzles in each voltage value. The best of the pressure 0.25 bar is a test nozzle size 5 mm Minimum value was 527.5 in the fourth maximum is 999.9 in the 29 and had an average of 845.858 good value. The pressure is 0.50 bar is a test nozzle size 6 mm Minimum value was 541.1 in the second maximum is 987.6 in the 19 and the mean value of 785.46 the best of force. Pressure of 0.75 bar is a test nozzle size 5 mm Minimum value is 513.3 in the 37 maximum is 992.3 in the 49 and had an average of 863.106, the best value of the pressure first. bar is a test nozzle size 5 mm Minimum value is 513.1 in the 23 maximum is 989.2 in the 47th and had an average of 850.92 is the best of the pressure 1.25 bar is. Test nozzle size 2mm Minimum value was 620.2 in the eighth maximum is 1618 in the No. 47 and the mean value of 1094.932.

ACKNOWLEDGEMENT

The authors would like to thank Bangkokthonburi University and Nakornluang Polytechnic College for providing partially financial support to this research work, and to our research center.

References

- [1] A.J Wood and B.F. Wollenberg, “Power generation operation and control”, *John Wiley and Sons, New York*, 1984
- [2] A.T. Saylor. “Hydraulic and Compressible Flow Turbomachines” *McGraw-Hill (UK) Company Ltd.* 1990.
- [3] R.K. Turton, “Principle of Turbomachinery, 2 nd ed” *Chapman and Hall , London ,* 1995.
- [4] A.R. Robert and J.K. Jack. “Energy and the Environment. New York” *John Wiley & Sons.* 1999.
- [5] W. Shepherd and D.W. Shepherd, D.W. “Energy Studies. Singapore” *World Scientific.* 1998.

THE APPLICATION OF NATURAL DOLOMITIC ROCK AS A HETEROGENEOUS CATALYST IN TRANSESTERIFICATION FOR BIODIESEL SYNTHESIS

Achanai Buasri^{1,2}, Kanokphol Rochanakit¹, Wasupon Wongvitvichot¹, Uraiporn Masa-ard¹
and Vorrada Loryuenyong^{1,2}

¹Department of Materials Science and Engineering, Faculty of Engineering and Industrial Technology,
Silpakorn University, Thailand

²National Center of Excellence for Petroleum, Petrochemicals and Advanced Materials,
Chulalongkorn University, Thailand

SUMMARY: The aim of this study was to analyze the catalytic performance of natural dolomitic rock as an environmentally friendly catalyst in the reaction of *Jatropha Curcas* oil with methanol under microwave-assisted transesterification. The dolomite was utilized as a source of calcium oxide (CaO) and magnesium oxide (MgO). The main characteristic of this rock is the high content of $\text{CaMg}(\text{CO}_3)_2$ which was transformed into CaO-MgO mixed oxide by calcination. The activation method to improve the activity, basicity and stability of CaO as the catalyst has been investigated. The CaO was turned into calcium glyceroxide complex, by combining with glycerol of the by-product. It was determined that calcium glyceroxide ($\text{Ca}[\text{O}(\text{OH})_2\text{C}_3\text{H}_5]_2$) is formed during the transesterification and acts as the most active phase. The catalyst was characterized by X-ray diffraction (XRD), X-ray fluorescence (XRF), scanning electron microscope (SEM) and nitrogen adsorption/desorption (BET) method. The effects of reaction variables such as reaction time, microwave power, methanol/oil molar ratio, and catalyst loading on the yield of biodiesel were investigated by gas chromatograph-mass spectrometry (GC-MS). The results indicated that the developed catalyst could also be reused feasibly up to three consecutive cycles. Overall, the potential of this low-cost heterogeneous base catalyst has been demonstrated for transesterification applications.

Keywords: biodiesel, natural dolomitic rock, CaO-MgO mixed oxide, calcium glyceroxide, *Jatropha Curcas* oil

INTRODUCTION

Biodiesel is renewable and environmentally friendly fuel which can be obtained by transesterification of vegetable oils or animal fats with methanol in the presence of both homogeneous and heterogeneous catalysts [1]. In the primary stage, the homogeneous catalysts were mentioned, where the high conversion of triglycerides (TG) into fat acid methyl esters (FAME) was achieved, but the post-treatment process to purify biodiesel was energy guzzling for the solubility of the homogeneous catalysts in the products. Then, the heterogeneous catalyst was developed, which simplified the transesterification by facilitating the separation and the purification, and it has been demonstrated to be more environmental [2].

Based-catalyzed transesterification reaction has been claimed to provide better conversion of vegetable oil to biodiesel compared with acid-catalyzed reaction. Dolomite is a type rock that can be found around the world which can be used as non-toxic base catalyst. Chemically, it consists of calcium carbonate (CaCO_3), magnesium carbonate (MgCO_3) and very small percentages of other compounds [3]. A review of temperature controlled experiments using fresh dolomite shows that basic calcium oxide (CaO) and magnesium oxide (MgO) are formed after the carbonate groups have decomposed. Dolomite is mainly used in agriculture and cement manufacturing. Its use as a catalyst in many processes such as gasification and reforming has attracted much attention, as it is cheap, has high basicity, and is environmentally friendly [4].

In this work, we have carried out transesterification using the natural dolomitic rock as an inexpensive and environment-friendly catalyst. The objective was to optimize the process for biodiesel production from *Jatropha Curcas* oil using renewable catalyst. A microwave-assisted production of biodiesel was applied in this research to expedite the chemical reaction and give a high product yields in a short time. The effects of reaction time, microwave power, methanol/oil molar ratio, and catalyst loading were systematically investigated.

MATERIALS AND METHODS

Jatropha Curcas oil was purchased from Thai Physic Nut Oil Company Limited. The natural dolomitic rock was obtained from L.S.M. (1999) Company Limited. All chemicals were analytical-grade reagents (Merck).

Calcium glyceroxide ($\text{Ca}[\text{O}(\text{OH})_2\text{C}_3\text{H}_5]_2$) was synthesized as follows: the reactor was charged with 90 ml of methanol, 30 ml of glycerol and 2 g natural dolomitic rock calcined at 900 °C for 2 h. The resulting mixture was vigorously stirred at 60 °C for 8 h. The mixture was cooled and centrifuged. The obtained precipitate was thoroughly washed with distilled water and dried at 100 °C for 12 h. The catalysts samples were stored under vacuum in a desiccator that contains silica gel to remove the humidity and carbon dioxide (CO_2) of the residual desiccator atmosphere [5]. The derived catalyst was characterized using X-ray diffraction (XRD), X-ray

fluorescence (XRF), scanning electron microscope (SEM) and nitrogen adsorption/desorption (BET) method.

The reactions were carried out in a 500 ml glass reactor equipped with condenser and mechanical stirrer at atmospheric pressure, placed inside a household microwave oven. The fixed 100 g of *Jatropha Curcas* oil and the desired amount of the derived catalysts were added to the reactor, and then the methanol was introduced to the oil at various methanol/oil molar ratios. The transesterification was operated with varied reaction time under microwave irradiation, and it was instantly stopped by rapid cooling in an ice bath. Composition of the FAME was analyzed with gas chromatograph-mass spectrometry (GC-MS) equipped with a flame ionization detector (FID).

RESULTS AND DISCUSSION

The dolomitic material is a double calcium and magnesium carbonate ($\text{CaMg}(\text{CO}_3)_2$), which when calcinated decomposes into CaO and MgO that are highly basic. The catalytic tests showed that during the induction period the formed glycerol reacts with basic sites of CaO to form calcium-glycerol complex [5]. The materials were characterized by XRD, XRF, SEM, and N_2 adsorption/desorption. The raw material was activated and used as a catalyst for the transesterification of *Jatropha Curcas* oil with methanol. The conversion of oil to FAME was optimized, under different reaction time, microwave power, methanol/oil molar ratio, and catalyst loading. The optimum conditions, which yielded a conversion of oil of nearly 95% for activated dolomitic catalyst, were reaction time 4 min, microwave power 800 W, methanol/oil molar ratio 18:1, and catalyst loading 4 wt%.

SUMMARY

The natural dolomitic rock has been successfully utilized as a renewable catalyst in the transesterification reaction of *Jatropha Curcas* oil with methanol. The experimental results show that derived catalyst had excellent activity and stability during reaction. The catalyst was used for 3 cycles and apparent low activity loss was observed. The physical and chemical properties of biodiesel produced conform to the available standards.

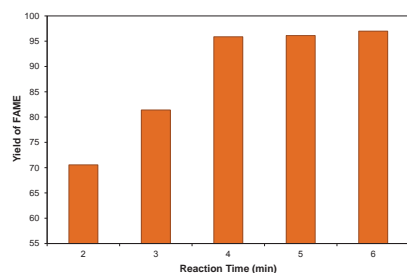


Figure 1. Effect of reaction time.

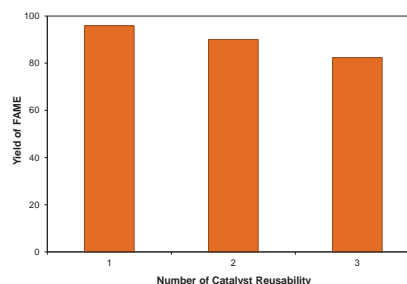


Figure 2. Effect of catalyst reusability.

ACKNOWLEDGMENT

The authors acknowledge sincerely the Department of Materials Science and Engineering, Faculty of Engineering and Industrial Technology, Silpakorn University and National Center of Excellence for Petroleum, Petrochemicals, and Advanced Materials, Chulalongkorn University for supporting and encouraging this investigation.

References

- [1] O. Ilgen, "Reaction kinetics of dolomite catalyzed transesterification of canola oil and methanol", *Fuel Processing Technology*. **95**, 2012, pp.62-66.
- [2] S.L. Niu, M.J. Huo, C.M. Lu, M.Q. Liu and H. Li, "An investigation on the catalytic capacity of dolomite in transesterification and the calculation of kinetic parameters", *Bioresource Technology*. **158**, 2014, pp.74-80.
- [3] Z.A.S. Nur, Y.H. Taufiq-Yap, M.F.R. Nizah, S.H. Teo, O.N. Syazwani and A. Islam, "Production of biodiesel from palm oil using modified Malaysian natural dolomites", *Energy Conversion and Management*. **78**, 2014, pp.738-744.
- [4] B. Yoosuk, P. Udomsap and B. Puttasawat, "Hydration-dehydration technique for property and activity improvement of calcined natural dolomite in heterogeneous biodiesel production: Structural transformation aspect", *Applied Catalysis A: General*. **395**, 2011, pp.87-94.
- [5] A. Esipovich, S. Danov, A. Belousov and A. Rogozhin, "Improving methods of CaO transesterification activity", *Journal of Molecular Catalysis A: Chemical*. **395**, 2014, pp.225-233.

BIOGAS PRODUCTION FROM VEGETABLE WASTE BY USING DOG AND CATTLE MANURE

Natacha Phetyim¹, Tawanna Wanthong¹, Phijittra kannika¹ and Anuwat Supngam¹

¹Department of Chemical and Materials Faculty of Engineering, Rajamangala University of Technology, Thanyaburi, Thailand

SUMMARY: This research investigates the effect of ratios between dog and cattle manures on anaerobic digestion in batch digesters under mesophilic conditions. The batch test was conducted for 28 days. Mixed Chinese cabbages and cabbages as the major wastes have been filled up in 200-liter digester. The vegetable wastes per day were studied under the specific increasing loaded weight as 0.5 kg and 1.0 kg each week. The additional waste load of 1.0 kg showed the optimum condition with the high biogas yield. The biogas accumulated from dog manure 10 wt% and 20 wt% were calculated using total amount of biogas produced per day, the results were 0.602 m³ and 0.711 m³, respectively. The methane content increased by used higher percentage of dog manure.

Keywords: biogas, anaerobic digestion, dog manure, vegetable waste, methane content

INTRODUCTION

Recently, the problem of municipal solid waste (MSW) disposal has been critical situation in Thailand, as the rapid urbanization and economic growth. The department of Pollution Control reported that huge amount of MSW, approximate 26.17×10⁶ tons per year was collected each year. However, in the year of 2014 the amount of disposal was approximate 14.81×10⁶ tons. Organic wastes have been treated by composting, landfill and incineration together with other MSW. Energy production from biomass or organic wastes considered as a renewable energy source, because the methane-rich biogas produced is suitable for fuel gas. It can replace liquid petroleum gas (LPG) in household uses. Due to its nature and composition, it can be deteriorated easily and cause bad smell. In the traditional system for MSW treatment, the spread of odor during composting produce serious greenhouse gas, and huge leachate discharges during landfill, with unsteady burning, resulting in dioxin production during incineration [1]. Considering the high moisture and organic content, these wastes should better be treated in biological treatment like anaerobic digestion than other techniques such as incineration and composting [2].

The aims of this research were to determine the effects of vegetable loading rate of 0.5 kg and 1.0 kg per week on biogas production under mesophilic conditions. Then the most applicable loading rate was studied by considering the effect yield from alter percentages of dog manure to cattle manure at 10 wt% and 20 wt%.

MATERIALS AND METHODS

Feedstock

The feed consisted of mixed vegetable wastes between Chinese cabbages and cabbages were collected from traditional market nearby Rajamangala University of Technology Thanyaburi

(RMUTT), grinding as feedstock for municipal anaerobic digester. The starter used in the research was mixed dog manure with cattle manure. The dog manure were collected from Phasukmaneejak Temple and cattle manure were collected from farm located in Agricultural Faculty of RMUTT. Both manures were unscreen.

Experimental design and biogas measurement

The digestion tests were performed on a single stage fed-batch anaerobic digester with total volume of 200 liters. It was operated at ambient temperature in mesophilic conditions for 28 days (4 weeks). The First part of this research studied additional of vegetable waste loaded by started addition 0.5 kg for the first week and then increased 0.5 kg per week (0.5, 1, 1.5 and 2 kg). The second batch test increased waste loading 1.0 kg per week (0.5, 1.5, 2.5 and 3.5 kg) with only cattle manure was the starter. The temperature and pH were monitored daily used thermometer and pH meter. The daily biogas production of each digester was determined by the volume of biogas produced, that was calculated from the height of collected gas tank and diameter of the tank. The biogas samples were collected by Tedlar sample bags from digesting tank and determinate amount of biogas by Geotech Biogas check analyzer. The composition of biogas (concentration of methane, carbon dioxide, oxygen, hydrogen sulfide and the others) in digester was monitored weekly. The second part studies mixing of starter between dog manure at 10 wt% and 20 wt% in cattle manure.

RESULT AND DISCUSSION

Biogas yield at different substrates loading rate

Substrates from vegetable wastes were fed to the digester by increased addition rate as 0.5 and 1.0 kg per week. The effects of additional vegetable waste loaded with biogas yields were showed in Figure 1. After 5 days, biogas produced and

increased until 28 days. The results were shown biogas accumulated as 0.5202 m³ for additional waste load of 0.5 kg per week. The biogas yield as additional waste load of 1.0 kg per week was 0.6689 m³. Therefore, additional waste load at 1.0 kg per week was selected for digestion of mixed dog and cattle manure. Figure 2. showed biogas produced as first day of digestion that faster than digestion by used only cattle manure The digestion of 20 wt% of dog manure was produced biogas yield more than digestion test of 10 wt%. The biogas accumulation of dog manure at 10 wt% and 20 wt% were calculated from biogas production per day, the results were 0.602 m³ and 0.711 m³ respectively.

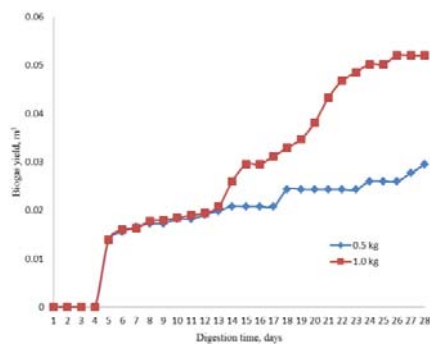


Figure 1. Biogas yield between substrates loadingrate at 0.5 kg and 1.0 kg.

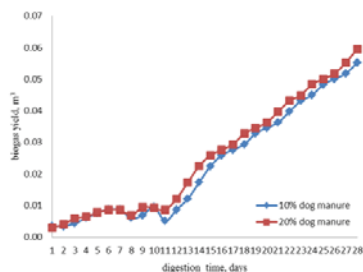


Figure 2. Biogas yield at different percentage of dog manure

Biogas composition and methane yield

The composition of biogas produced from digestion test (4th week) used only cattle manure consist of methane 44.6%, carbon dioxide 19.3%, oxygen 5.0 %, other 31.1 % and hydrogen sulfide 1,318.0 ppm. The 10 wt% and 20 wt% of dog manure are shown in table 1. and table 2., respectively. The methane content of biogas at 20 wt% of dog manure higher than at 10 wt% of dog manure mixed with cattle manure. Hydrogen sulfide concentration of biogas from digestion used only cattle manure showed higher concentration than co-starter between dog and cattle manure.

Table 1. Biogas composition at 10 wt% of dog manure

composition	Digestion time, weekly			
	1 st	2 nd	3 rd	4 th
% CH ₄	30.6	40.3	54.0	62.7
% CO ₂	10.6	21.5	25.1	21.3
% O ₂	7.8	3.4	1.4	1.1
% other	51.0	34.8	19.5	14.9
H ₂ S (ppm)	7.0	104.0	219.0	11.0

Table 2. Biogas composition at 20 wt% of dog manure

composition	Digestion time, weekly			
	1 st	2 nd	3 rd	4 th
% CH ₄	42.3	65.1	65.3	69.3
% CO ₂	23.2	28.8	29.9	26.6
% O ₂	3.8	0.4	0.4	0.3
% other	30.7	5.7	4.4	3.8
H ₂ S (ppm)	1,957.0	618.0	505.0	367.0

CONCLUSION

The anaerobic digestion by used dog manure mixed with cattle manure is an appropriate the quality and quantity of biogas. The methane content of more percentage of dog manure was increased and showed low hydrogen sulfide concentration compared with digestion used only cattle manure.

ACKNOWLEDGMENT

The research was financially supported by Faculty of Engineering Rajamangala University of Technology Thanyaburi. We would like to Thank the National Metal and Materials Technology Center (MTEC) for providing Biogas check analyzer.

References

- [1] H. Hartmann and B.K. Ahring, "Strategies for the anaerobic digestion of the organic fraction of municipal solid waste: an overview". *Water Sci. Technol.*, **53**, 2006, pp. 7-22.
- [2] B. Velmurugan, R.A. Ramaujam, "Anaerobic digestion of vegetable wastes for biogas production in a fed-batch reactor". *Int.J. Energy. Sci.* **1**, 2011, pp.478-486.

PHYSICAL AND THERMAL PROPERTIES OF BRIQUETTE FUELS FROM RICE STRAW AND SUGARCANE LEAVES BY MIXING MOLASSES GUIDELINES

Pongsak Jittabut¹

¹Physics and General Science Program, Faculty of Science and Technology,
Nakhon Ratchasima Rajabhat University, Thailand

SUMMARY: The physical and thermal properties of the briquette were determined by varying rice straw and sugarcane leaves ratios of 100:0, 80:20, 50:50, 20:80 and 0:100 using molasses as the binding agent. The briquette-molasses to binder ratio of 100:50 was used. Ultimate and proximate analyses were carried out to determine the average composition of their constituents. The physical properties studied included species density, compressive strength and moisture content. Fuel properties were determined using standard laboratory methods. The result was indicated that the density, high heating value, and compressive strength were also tested. Results showed that fixed carbon was 9.06-13.63%, volatile matter was 68.14-74.67%, ash content was 7.84-12.85%, and moisture content was 4.2-6.2%. Results from ultimate analysis showed that the content of C H O N S was follows; 38.6-43.2%, 5.4-6.2%, 34.5-36.4%, 0.27-0.44% and 0.02-0.04%. The high heating value was in the range of 16.3-17.83MJ/kg. The density was in the range of 0.53-0.58kg/m³. The compressive strength was in the range of 32.4-44.7 kg/cm². The Briquette from rice straw: sugarcane leaves had optimum ratio at the ratio (50:50). The thermal properties and physicochemical characteristics of these wastes demonstrated that they are potential candidates to produce briquettes as fuel in several applications.

Keywords: physical/thermal properties, briquette fuels, rice straw, sugarcane leaves, molasses

INTRODUCTION

Energy resources are classified into two, namely renewable and non-renewable. The renewable are thought to be a better option since the non-renewable such as kerosene, diesel, gasoline etc have the capability not to be replenished and would be exhausted [1]. More so, the environmental impacts as a result of emissions of CO₂, SO₂, NO_x etc during combustion of the non-renewable resources, prompted the use of renewable for cooking and heating purposes. Out of the renewable sources of energy, agricultural waste is one of the most versatile. Energy from biomass which includes agricultural waste, has made the greatest contribution to national energy consumption in both developed and developing countries [2].

The burning of the agricultural waste in loose form results in loss of fuel and widespread air pollution. However, briquetting the agricultural waste forestall the aforementioned problems. Agricultural waste briquettes have the following advantages over the loose ones, there is increase in the net calorific value per unit volume, the fuel is easy to transport and store, uniform in size and quality.

Biomass energy in Thailand is mainly consumed in 2 economic sectors: residential and commercial sector and manufacturing sector. In 2002, total final energy demand of charcoal and fuel wood was about 11.94 million tons equivalent to 5.64 mtoe with an increasing rate of 1.8% from the past year. Residential and commercial sector consumed about 4.99 mtoe (about 88.48% of total charcoal and fuel wood demand) and the rest was fuel wood was consumed in manufacturing sector [3].

The aim of the present study was to determine

to rice straw and sugarcane leaves ratios of 100:0, 80:20, 50:50, 20:80 and 0:100 using molasses as the binding agent and to identify the briquetting properties, such as physical properties, ultimate analyses, proximate analyses, density, compressive strength and high heating value.

EXPERIMENTAL DETAILS

The raw biomass rice straw and sugarcane leaves was dried for 3 days in open sunshine, and then it was used for briquetting. Particle sizes of rice straw and sugarcane leaves used for the study were 1 mm or less. Suitable raw material combinations were made for briquetting process by manually. Then it is used as a input for briquetting machine to produce briquetted sample. Briquettes were prepared by adding molasses binder ratio of 100:50 in each selected biomass sample. The materials were combined at mixing proportions: 100:0, 80:20, 60:40, 50:50, 40:60, 20:80 and 0:100 (Rice straw: Sugarcane leaves). The ultimate analysis or the determination of their percentage compositions were carried out using standard methods. Thus, ASTM D5373-02 method was used for the determination of percentage composition of carbon, hydrogen and nitrogen, ASTM D4239-02 method was used for the determination of percentage composition of sulphur and ASTM D5142-02 method was used for the determination of percentage ash content of individual composite briquette samples. The percentage oxygen content of the individual composite agricultural waste briquette was determined by difference. The higher heating value of material was determined by using of bomb calorimeter (ASTME-711). The moisture content, ash content, volatile matter and the fixed carbon of

the plant material and coal were determined in line with the ASTM D-3173.

RESULTS AND DISCUSSION

Bulk density

It was observed from the Figure 1 that the maximum bulk density was found 0.59 g/cm³ in rice straw: sugarcane leaves (50:50). The lowest bulk density was found 0.54 g/cm³ in rice straw: sugarcane leaves (80:20). The density of briquette fuels are increasing with the increase for containing rice straw and sugarcane leaves. Briquette fuels are replaced by sugarcane leaf to compression of density higher than replaced by rice straw.

Moisture Content

The Figure 1 shows that the moisture content of mixed raw biomass was found to be in the range of 4.42 to 8.14%wb. The lowest moisture content was found 4.42 %wb. in rice straw: sugarcane leaves (50:50). The maximum moisture content was found 8.14%wb. in rice straw: sugarcane leaves (100:0). The moisture content of briquette fuels are decreasing with the increase for containing rice straw and sugarcane leaves.

Compressive strength

The Fig. 1 shows that the compressive strength of mixed raw biomass was found to be in the range of 32.4 to 44.7 kg/cm². The lowest compressive strength was found 32.4 kg/cm² in rice straw: sugarcane leaves (100:0). The maximum compressive strength was found 44.7 kg/cm² in rice straw: sugarcane leaves (50:50). Briquette fuels are replaced by sugarcane leaf to compression of compressive strength higher than replaced by rice straw.

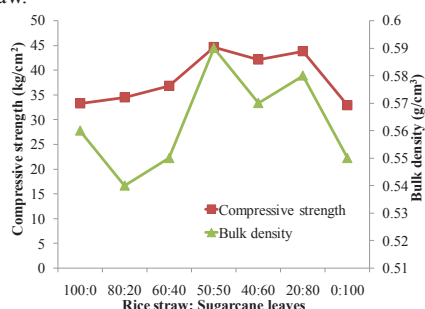


Figure 1. The compressive strength and bulk density of briquette fuels from rice straw and sugarcane leaves by mixing molasses

PROXIMATE ANALYSIS

The Figure 2 shows that the volatile matter of mixed raw biomass material was found to be in the range of 68.18 to 74.67% and ash content was found to be in the range of 7.84 to 12.85%. The fixed carbon was found to be in the range of 9.06 to 13.63%. Maximum fixed carbon was found 13.63 in rice straw: sugarcane leaves (50:50), volatile matter was found 74.67% in rice straw: sugarcane leaves

(50:50) and ash content was found 12.85% in rice straw: sugarcane leaves (50:50) respectively.

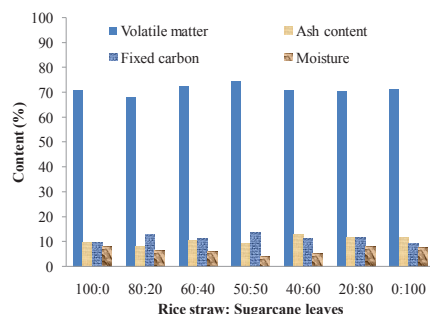


Figure 2. Proximate analysis of the briquettes in weight percentage

ULTIMATE ANALYSIS AND GROSS CALORIFIC VALUE

The gross calorific value of mixed raw biomass was found to be in the range of 16.33 to 17.83 MJ/kg. The maximum calorific value was found 17.83 MJ/kg in rice straw: sugarcane leaves (50:50) combination. The lowest calorific value (LCV) was found 16.33 MJ/kg in rice straw: sugarcane leaves (100:0) combination.

The resulting composition of biomass affects its combustion characteristics as the total overall mass of the fuel decreases during the volatile combustion phase of the combustion process, as the hydrogen to carbon ratio of the fuel increases and, to a lesser extent, as the oxygen to carbon ratio increases. Nitrogen and Sulphur are significant in the formation of harmful emissions and have an effect on reactions forming ash. The Sulphur and Nitrogen contents reported which are below 1% is a welcome development as there will be minimal release of sulphur and nitrogen oxides into the atmosphere, thereby limiting the polluting effect of the briquettes.

ACKNOWLEDGMENT

The authors would like to acknowledge the Faculty of Science and Technology, Nakhon Ratchasima Rajabhat University, Thailand, for financial support of this work.

References

- [1] O. A. Kuti. "Impact of charred palm kernel shell on the calorific value of composite sawdust briquette". *Journal of Engineering and Applied Sciences*. **2**, 2007, pp. 62-65.
- [2]. A. N Anozie, O.J Odejobi and E. E Alozie. "Estimation of carbon emission reduction in a cogeneration system using sawdust, energy sources". *Part A: Recovery Utilization and Environmental effects*. **31(9)**, 2009, pp. 711-721.
- [3] Department of Alternative Energy Development and Efficiency. Biomass Database Potential in Thailand. Available from <http://weben.dede.go.th/webmax/content/biomass-databas-e-potential-thailand> (12 May 2015)

EFFECT OF NANOSILICA ON MECHANICAL AND THERMAL PROPERTIES OF CEMENT COMPOSITE FOR THERMAL ENERGY STORAGE MATERIALS

Pongsak Jittabut¹

¹Physics and General Science Program, Faculty of Science and Technology,
Nakhon Ratchasima Rajabhat University, Thailand

SUMMARY: This research was presented the mechanical and thermal properties of cement-based composite for thermal energy storage materials. The effects of nanosilica particle size and concentration determined by mixing three nanosilica particle sizes of 12, 50 and 150 nm, using nanosilica were of 1-5 wt%. Thermal properties coefficients were tested using a direct measuring instrument with surface probe (ISOMET2114). The influence of nanosilica on the performance, such as compressive strength, bulk density, thermal conductivity, volume heat capacity and thermal diffusivity of hardened composite cement pastes were studied for future solar thermal energy materials with better performance. According to the development of thermal storage materials and their application environment requirement in solar thermal power, the specimens were subjected to heat at 350°C and 900°C. There were observed that, before heating, the compressive strength is optimized at nanosilica amount of 4wt% with nanosilica particle size of 50 nm at the age of 28 days. Moreover, after heating at 350°C and 900°C, the thermal conductivity and volume heat capacity of the cement paste enriched with nanosilica were significantly lesser than that of the before heating one.

Keywords: thermal properties, mechanical properties, cement composites, thermal energy storage, nanosilica

INTRODUCTION

Solar thermal power is being attractive to many researchers around the world because of its clean energy. Four main sections are required in the solar thermal power plant: concentrator, receiver, transport-storage media system and power conversion device. There is no sunshine at night and limitation of solar energy available on cloudy days. So thermal energy storage (TES) systems balancing energy supply are designed to collect more solar energy during a sunny day, which is necessary component of four sections. Typical storage media for sensible heat consists of molten nitrate salt, rocks and pebbles or concrete [1, 2]. Thermal energy storage systems of four main sections can facilitate the integration of solar thermal power plants into the electrical grids by smoothing out fluctuations, thus avoiding instability problems and increasing electricity production [3]. Solid sensible materials store thermal energy through inherent characteristics with the change of temperature, and exhibit non-toxicity and non-corrosiveness. Cementitious materials have been extensively studied as a promising type of sensible energy storage materials due to abundant source, good thermal stability, and good thermal properties. Some efforts are made to further optimize cementitious thermal storage materials and improve the storage efficient. The use of nanoparticles in cementitious-concretes materials significantly modifies their behavior not only in the fresh but also in the hardened conditions as well as the physical, mechanical and microstructure development. So, we introduced nanosilica into cement composites materials and prepared solar thermal storage composite materials. The mixtures of nanosilica were prepared with the cement replacement of 1-5wt%. by mixing three nanosilica particle with average particle sizes of 12, 50 and 150

nm, respectively. As well, they were heated at 350°C and 900°C respectively. Todate, few studies have been reported on thermal and mechanical properties in assessment of cement composites for thermal energy materials.

EXPERIMENTAL DETAILS

Ordinary Portland Cement (OPC) which obtained from SCG Experience Company Limited of Thailand conforming to ASTM C150 standard was used. The mixtures of nanosilica were prepared with the cement replacement of 1%, 2%, 3%, 4% and 5% by weight. The water-cementitious ratio (W/C) was 0.5 and three contents of nanosilica particle with average particle sizes of 12, 50 and 150 nm, respectively. The paste samples of 10cm×10cm×10cm were prepared, cured and their thermal property measured at the curing ages of 28 days. In addition, three specimens were tested for bulk density in accordance with the standard of ASTM B962-08 and thermal property coefficients were tested using a direct measuring instrument with surface probe (ISOMET2114, Applied Precision Ltd.). The compressive strength of three specimens were tested in accordance with the standard of ASTM C109. All paste samples of 10cm×10cm×10cm were prepared, cured and their compressive strength measured at the curing ages of 28 days. Furthermore, the selection of heat treatment temperature depends strongly on the actual operation conditions in solar energy application. In this paper, we mainly chose two heat treatment temperatures of 350°C and 900°C respectively. The heat treatment time is 6 hours.

RESULTS AND DISCUSSION

Bulk density of the pastes

It can be clearly seen that for all nanosilica sizes, the addition of nanosilica reduced the sample density in comparison to the control cement paste. For the cement pastes with 12 nm nanosilica, the density monotonously decreases with increasing amount of nanosilica. On the other hand, the cement pastes with 50 nm and 150 nm nanosilica showed a drop in density for the nanosilica addition of 1-2% and a slightly increase for 3-4% and a drop again at 5%. Overall, it can be concluded that the density has a tendency to decrease with an addition of nanosilica.

Compressive strength of the pastes

There are many interesting points regarding this plot. Firstly, the compressive strength increases to the maximum point with the addition of certain amount of nanosilica and then drops when excessive nanosilica is introduced. For 12 nm nanosilica, the pastes show the maximum strength at 1% addition while for 50 and 150 nm sizes, the strength is maximized at 4% nanosilica. Secondly, the size of nanosilica has a significant effect on the strength. The cement paste with 50 nm nanosilica shows the higher strength than the others, with the maximum strength of >50% higher than the control cement paste.

THERMAL CONDUCTIVITY OF THE PASTES

The thermal conductivity of pastes with different quantity of nanosilica before and after heatings were shown in Figure 1. The result was shown that the thermal conductivity of cement pastes slightly decrease with the increment of quantity. However, after heating both at 350 and 900°C for 6 hours the thermal conductivities reduce approximately 38%.

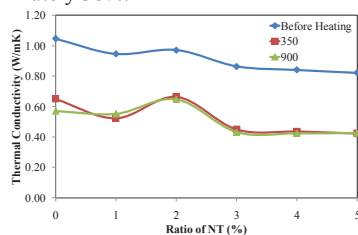


Figure 1. Thermal conductivity of pastes with different quantity of nanosilica before and after heating

VOLUME HEAT CAPACITY OF THE PASTES

Figure 2 has shown that, before heating the cement paste, the volume heat capacity of every ratio of nanosilica particle admixed into cement paste remained constant at 1.7 MJ/m³K. Whereas, after heating them at 350°C and 900°C for 6 hours, the volume heat capacity of them reached to the

maximum volume at 1.34 and 1.028 MJ/m³K (at the ratios of NT particle between 2-3 wt.%) respectively.

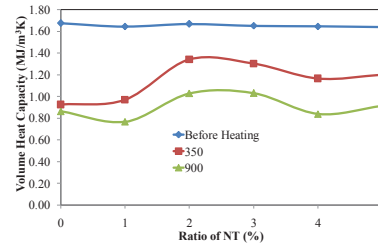


Figure 2. Volume heat capacity of pastes with different quantity of nanosilica before and after heating

THERMAL DIFFUSIVITY OF THE PASTES

Figure 3 has shown that, before heating the cement paste, the thermal diffusivity of every ratio of nanosilica particle admixed into cement paste remained constant around 0.9-1 μm²/s. While, after heating them at 350°C and 900°C for 6 hours, the thermal diffusivity remained constant around 0.5-0.6 μm²/s. The addition of nanosilica was beneficial to the composite pastes.

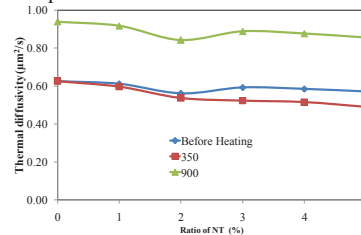


Figure 3. Thermal diffusivity of pastes with different quantity of nanosilica before and after heating

ACKNOWLEDGMENT

The authors would like to acknowledge the Faculty of Science and Technology, Nakhon Ratchasima Rajabhat University, Thailand, for financial support of this work.

References

- [1] G. Antoni, M. Medrano, I. Martorell, A. Lázaro, P. Dolado, B. Zalba and L.F. Cabeza, "State of the art on high temperature thermal energy storage for power generation. Part 1-Concepts, materials and modellization", *Sustainable Energy Rev.* **14**, 2010, pp. 31-55.
- [2] D. Laing, W.D. Steinmann, P. Viebahn, F. Gräter and C. Bahl, "Economic Analysis and Life Cycle Assessment of Concrete Thermal Energy Storage for Parabolic Trough Power Plants", *J. Sol. Energy Eng.* **132**(4), 2010, pp. 041013-410136.
- [3] D. Laing, W.D. Steinmann, M. Fiß, R. Tamme, Thomas Brand and C. Bahl, "Solid Media Thermal Storage Development and Analysis of Modular Storage Operation Concepts for Parabolic Trough Power Plants", *J. Sol. Energy Eng.* **130**(1), 2007, pp. 011006.

WAVE ENERGY POTENTIAL IN THE GULF OF THAILAND

Kanchana Noojeensang¹, Jompob Waewsak¹, and Yves Gagnon²

¹Research Center in Energy and Environment
Department of Physics, Faculty of Science, Thaksin University, Thailand
²Université de Moncton, Edmundston (NB), Canada

SUMMARY: This paper presents an investigation of the wave energy potential in the Gulf of Thailand. The Simulating Wave Nearshore (SWAN) model is used to generate the significant wave height (SH). The input to the SWAN model consists in the NCEP global reanalysis wind database, the ETOPO1 bathymetry and the physical boundaries of the Gulf of Thailand. Each 3-hr NCEP wind database is run with the SWAN model under the principle of wind induced wave in order to generate the 1-hr SH over a full year. It is found that the SH in the Gulf of Thailand is in the range of 1.1-1.3 m in November-February during the Northeast monsoon period, while being in the range of 1.1-1.2 m in May-August during the Southwest monsoon period. Results show that the wave energy is in the range of 123-830 W/m.

Keywords: Simulating Wave Nearshore (SWAN) model, wave, wave energy, significant wave height

INTRODUCTION

Among alternative energy sources, wave power is one of the most abundant sources on Earth. Ocean energy is exhibited in many forms: tides, surface waves, ocean circulation, salinity and thermal gradients. The worldwide wave power resource potential is enormous and global power potential has been estimated to be 17.5 PWh/year [1]. This is comparable to the annual worldwide electricity energy consumption. Thus, wave power has the potential to provide a large portion of the world's electricity energy demand if it can be utilized efficiently.

The best wave climates, with annual average power between 20-70 kW/m of wave front, are found in the mid-latitudes where strong storms occur. However, attractive wave climates are also found within the 30° latitude where regular trade winds blow [2]. In addition, some specific areas where monsoons affect the waves show high potential for wave energy conversion into electricity.

In Thailand, the latest policy, namely the Alternative Energy Development Plan (AEDP), was launched to promote the deployment of renewable energy to achieve 25% of power generation from renewable sources by 2025 [3]. Under the AEDP, power generation using wave and tidal energy is targeted at 2 MW.

Wave energy refers to the kinetic energy and the potential energy in waves on the ocean surface. According to the linear wave theory, the wave energy flux P is proportional to the wave period of motion T and to the square of its height H , as shown in Eq. 1:

$$P = \frac{\rho g^2}{64\pi} H^2 T \quad (1)$$

where ρ is the density and g is the gravitational acceleration.

In order to achieve the objectives of the AEDP, the first key step of deployment is the resource assessment. Consequently, the objective of this

paper is to investigate the significant wave height (SH) and wave energy in the Gulf of Thailand.

METHODOLOGY

The Simulating Wave Nearshore (SWAN) model, with source code 44.01, is used together with the 3-hr NCEP global reanalysis wind database for 2013, the EOTPO1 bathymetry and the physical boundaries of the Gulf of Thailand in order to generate the 1-hr SH. SWAN is the third generation model developed by Delft University of Technology to compute the random short-crested wind generated waves in coastal regions [4]. It mainly accounts for the following physics: wave propagation in time and space, shoaling, refraction due to current and depth, frequency shifting due to currents and non-stationary depth, wave generation by wind, three and four wave interactions, bottom friction and depth-induced breaking, dissipation due to aquatic vegetation, turbulent flow and viscous fluid mud, transmission through and reflection against obstacles, and diffraction. The extreme condition of SH in the spatial domain for every month of the year is displayed using the PanoplyWin64 computer software. Finally, the wave energy is calculated in order to investigate the power potential of the wave resource in the Gulf of Thailand.

RESULTS AND DISCUSSION

The spatial distribution of the extreme SH for every month of the year is shown in Figures 1 to 6. The extreme SH is in the range of 0.5-1.3 m. The maximum extreme SH occurs during the period of November to January, which is the period of the Northeast monsoon. A high extreme SH also occurs during the month of May to August, due to the effect of Southwest monsoon. The details of the extreme SH for every month is as follows: January, 1.3 m; February, 1.1 m; March, 0.5 m; April, 0.5 m; May, 1.1 m; June, 1.2 m; July, 1.0 m; August, 1.3 m; September, 0.7 m; October, 0.7 m; November and December, 1.3 m. The maximum wave energy is

estimated to be in the range of 123-830 W/m, with an assumption of sea water density of 1.025 g/ml and a period of 1 s.

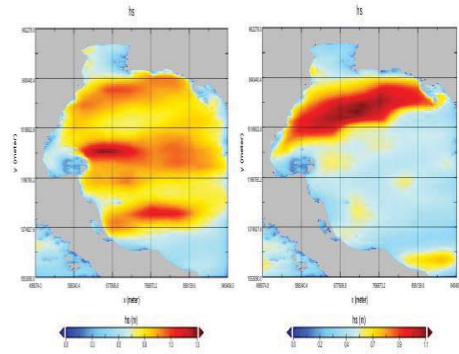


Figure 1. SH in January 2014 (02:00) and in February 2013 (20:00).

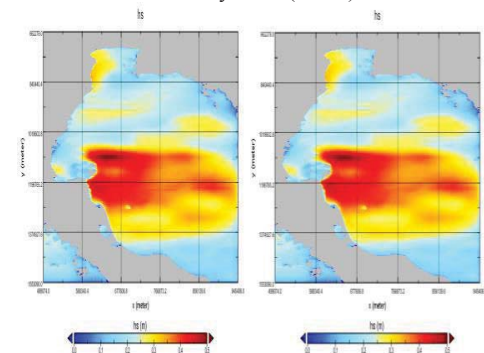


Figure 2. SH in March 2013 (02:00) and in April 2013 (14:00).

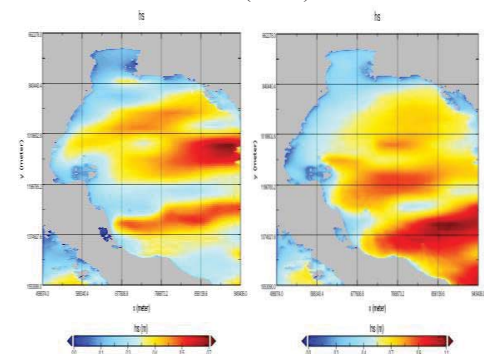


Figure 3. SH in May 2013 (09:00) and in June 2013 (07:00).

ACKNOWLEDGMENT

The authors would like to thank the National Research Council of Thailand (NRCT) for providing the financial support for this research project.

References

[1] S.G. Seigel, T. Jeans, T.E. McLaughlin, “Deep ocean wave energy conversion using a cycloidal

turbine”, *Applied Ocean Research*, 33 (2011) 110-119.

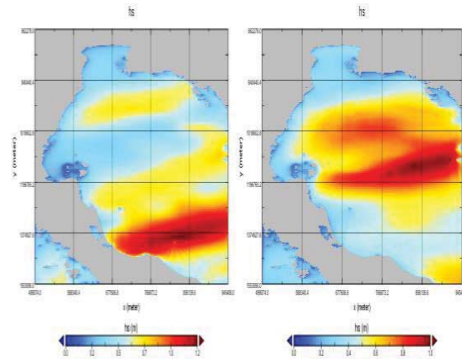


Figure 4. SH in July 2013 (24:00) and in August 2013 (18:00).

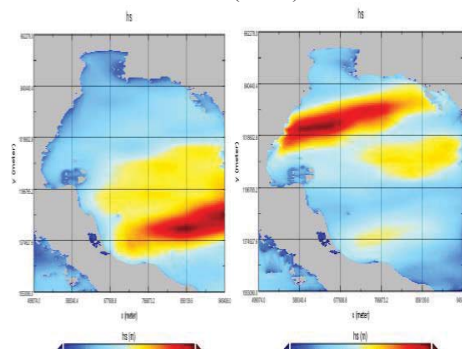


Figure 5. SH in September 2013 (08:00) and in October 2013 (23:00).

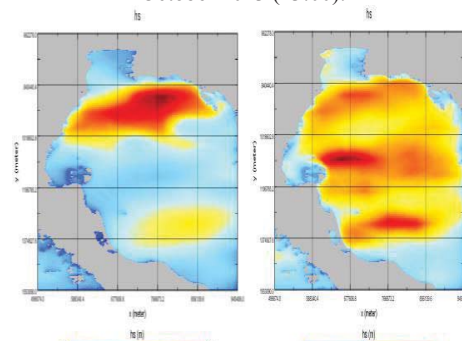


Figure 6. SH in November 2013 (02:00) and in December 2013 (18:00).

[2] L. D. Fresco and A. Traverso, “Energy conversion of orbital motions in gravitational waves: simulation and test of seaspoon wave energy converter”, *Energy Conversion and Management*, 86 (2014) 1164-1172.

[3] <http://www.dede.go.th/>

[4] <http://www.swan.tudelft.nl/>

THERMAL EFFECT OF THERMAL ENERGY STORAGE (TES) TANK FOR SOLAR ENERGY APPLICATION DURING CHARGING CYCLE BASED ON THE GRID SENSITIVITY ANALYSIS

Tanti Ali¹, Norfadzilah Jusoh¹, Rosli Abu Bakar¹, Kumaran Kadirgama¹

¹Faculty of Mechanical Engineering, Universiti Malaysia, Malaysia

SUMMARY: Present design and engineering processes often rely on the simulation tools as the preliminary assessment or verification process of development. This is due to computational tools are naturally augmented by the sensitivity and uncertainty. As from the incomplete understanding of the input parameters, it is important and necessary to judge the reliability of the results. This is where the grid sensitivity play the role as the point of reference, verification and evaluation data. In this paper investigate the effect of grid sensitivity analysis based on level of mesh to the thermal effect of thermal energy storage (TES) tank for solar energy application during charging cycle. The experiment was performed with TES tank is using water as the working fluid and operated for 9 hours from 9 am to 6 pm with the volume flow rate of 13.2 L/min. The experiment resulted the temperature TES outlet is in the range of 45 to 65 °C. The experimental data is used in the simulation and the results is compared and discussed. The grid sensitivity analysis based on different level of mesh is simulated using CFD flow simulation. The simulation resulted the best initial mesh level to compare with experimental results is mesh level 5. The comparison of experimental and simulation using initial mesh level 5 resulted the percentage difference of 9.67%. In conclusion, the grid sensitivity analysis not only affect the thermal behavior of the TES tank but also the computational time.

Keywords: thermal energy storage; charging cycle; grid sensitivity analysis.

INTRODUCTION

Reviews of sensitivity analysis methods have been conducted in variation of methods due to quantitative uncertainty analysis is currently prominent [1,2,3]. Some of the studies explicitly highlight the advantages and disadvantages of various methods and provide very good summaries of the topic. This analysis understanding is studied further, instead of only based on the simple evaluation of influence factors of an experimental [4].

These influence of different uncertainties of model factors on the modelling outcome, has become a key question [5]. Therefore, the source of uncertainties including parameters, boundary conditions, model structure, etc can be varied in the modelling process. This is very important if the aim is to minimize the uncertainties of a model when the resources and collecting data are limited [4].

This paper describes the purpose of grid sensitivity analysis has the affect the flow pattern and the temperature distribution of TES tank [4].

The experimental is setup as in Figure 1.

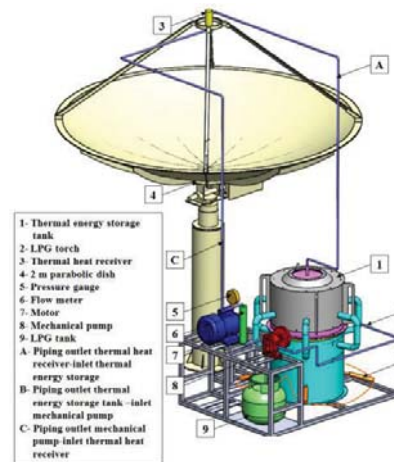


Figure 1. Apparatus arrangement for experiment testing.

The results of simulation is compared with the experimental results during charging cycle. The comparison of both results expected the temperature difference percentage as in Figure 2.

Temperature difference percentage is calculated as in Eq (1):

$$\left(\frac{T_1 - T_2}{\frac{T_1 + T_2}{2}} \right) \times 100 \quad (1)$$

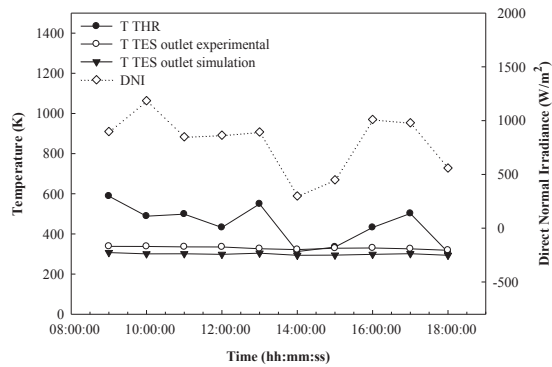


Figure 2. Comparison of experimental and simulation results

References

- [1] D. Coyle, M.J Buxton and B.J. O'Brien. "Measure of importance for economic analysis based on decision modeling". *J Clin Epidemiol*, **56**, 2003, pp. 989-97.
- [2] H.C.Frey and SR. Patil "Identification and review of sensitivity analysis method". *Risk Anal* , **22**, 2002, pp. .553-78.
- [3] J.C. Helton, R.M. Cooke, M.D. McKay and A. Saltelli. "Sensitivity of model output: SAMO 2004 – editorial special issue". *Reliab Eng Syst Safety* , **91**, 2006, pp. 1105-8.
- [4] F. Pappenberger, B. KJ, M. Ratto and P. Ma. "Multi-method global sensitivity analysis of flood inundation models". *J Advances in Water Resources*, **31**, 2008, pp. 1-14

LIFE CYCLE ASSESSMENT OF BIODIESEL PRODUCTION FROM USED COOKING OIL BY PYROLYSIS PROCESS

Supanit Tritanate¹ and Prasert Reubroycharoen²

¹Interdisciplinary Program of Energy Technology and Management
Graduate School, Chulalongkorn University, Thailand

²Department of Chemical Technology
Faculty of Science, Chulalongkorn University, Thailand

SUMMARY: This study focused on life cycle assessment of biodiesel production from used cooking oil by pyrolysis process. The scope of this study focused on production process at 430 °C, 101 KPa for input, output and energy calculation on the HYSYS simulation program. Then, the data from HYSYS simulation program will be prepare for life cycle assessment by using SimaPro simulation program. It's the simulation program for calculation the environment impact. Comparing the environment impact result with tranesterification, the pyrolysis process has the lower fossil fuels. Because the pyrolysis process used the lower stream process than tranesterification and don't have methanol in the production process.

Keywords: life cycle assessment, biodiesel, used cooking oil, pyrolysis, HYSYS

INTRODUCTION

Due to the problem of demand of oil and rising the oil price that will be increase every year, and many people interested in environmental and human health. Then, alternative energy will be the most important for sustainable and replacement the fossil fuels. Especially, biodiesel is the most famous for alternative energy. Because it is renewable, environmental friendly and has the same properties as diesel.

The most process for produced biodiesel is tranesterification, which is derived from vegetable oil, animal fats or used cooking with alcohol group (methanol or ethanol) by using catalyzed chemical reaction (acid, base or enzyme). The product from tranesterification process is fatty acid methyl ester (FAME) or biodiesel and byproduct is glycerol. Another one is micro emulsion, dilute with diesel and pyrolysis process.

Pyrolysis is the thermochemical of triglyceride with metal catalyst under the high temperature 450-600 °C. [1] The main product from pyrolysis is hydrocarbon (diesel range) and byproduct is carbon dioxide. The characteristics of main product will be same as diesel that comes from fossil fuels.

However, biodiesel process that is industrialized (tranesterification) effect with environmental issue. Such as water that come from the wet washing process, the excess methanol on the process. One of the tooling for analysis the environmental impact is life cycle assessment.

Life cycle assessment (LCA) is the technique for calculation the environmental impact each step of product life. The steps for analysis LCA have 4 steps. [2]

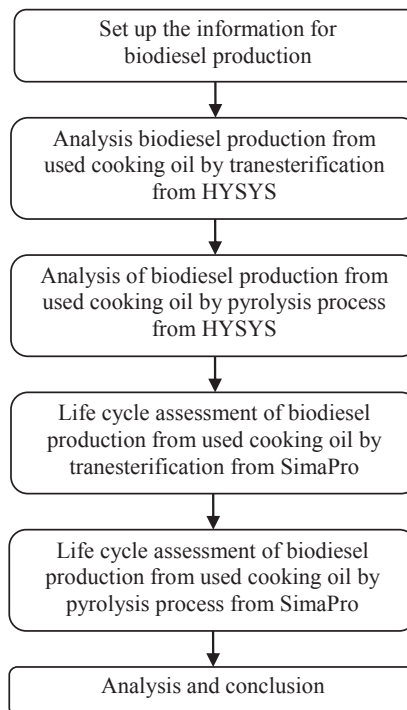
1. Definition and boundary: The functional unit is 1 kg of biodiesel. The system boundary focused on biodiesel production.

2. Life cycle inventory analysis: Input, Output and energy used for each steps will be estimated from HYSYS simulation.

3. Life cycle impact assessment: In this study used SimaPro and Eco indicator 99 for environmental impact analysis with 11 categories. (carcinogen, respiratory organics, respiratory inorganics, climate change, radiation, ozone layer, ecotoxicity, acidification/eutrophication, land use, minerals and fossil fuels)

4. Interpretation: The result will be evaluated each steps.

METHODOLOGY



The work focused on life cycle assessment of

biodiesel production from used cooking oil by pyrolysis process comparing with transesterification.

RESULTS AND DISCUSSION

The HYSYS simulations for transesterification and pyrolysis process are shown in figure 1 and 2 respectively.

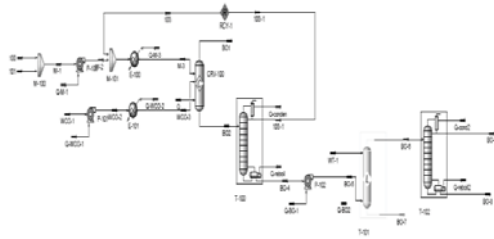


Figure 1. The transesterification process for biodiesel production from used cooking oil

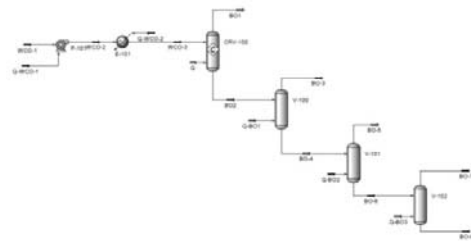


Figure 2. The pyrolysis process for biodiesel production from used cooking oil

Table 1 Single score of environmental impact each process by using Eco indicator99

Impact category	Transesterification	Pyrolysis
Carcinogen	-0.00453	-0.00662
Respiratory organics	7.89E-6	-0.000202
Respiratory inorganics	0.0076	0.0036
Climate change	-0.0102	-0.012
Radiation	5.68E-5	2.5E-5
Ozone layer	8.13E-7	-1.84E-6
Ecotoxicity	0.000613	-0.000214
Acidification/ Eutrophication	0.00259	0.00248
Land use	0.09	0.114
Minerals	0.000522	-0.00047
Fossil fuels	0.0261	-0.392

Unit : Pt

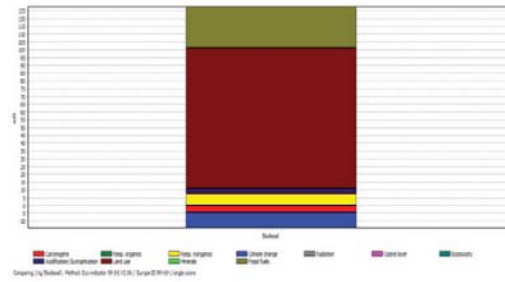


Figure 3. The single score of transesterification, as indicated by Eco-indicator 99

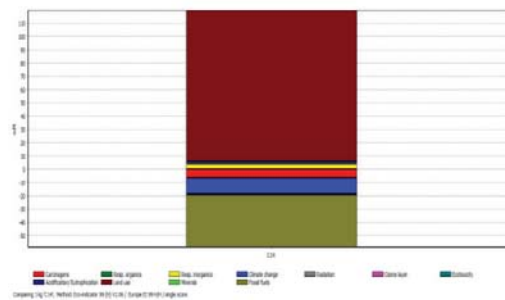


Figure 4. The single score of pyrolysis process, as indicated by Eco-indicator 99

ACKNOWLEDGMENT

The author would like to acknowledge the Chemical Technology, Faculty of Science, Chulalongkorn University.

References

[1] K. D. Marher and D.C. Bressler “Pyrolysis of triglyceride materials for the production of renewable fuels and chemicals” *Bioresource Technology*, **98**, 2007, pp.2351-2368
 [2] K. Choosak, T. Chanporn and P. Pornpote “LCA studies comparing biodiesel synthesized by conventional and supercritical methanol methods” *Journal of Cleaner Production*, **17**, 2009, pp.143-153

LIQUID PHASE PYROLYSIS OF GIANT LEUCAENA WOOD TO BIO-OIL OVER NiMo/Al₂O₃ CATALYST

P. Wattanapaphawong¹, N. Khuhaudomlap¹, N. Hinchiranan¹, P. Kuchontara¹,
K. Kangwansaichol³ and P. Reubroycharoen^{1,2}

¹Department of Chemical Technology, Faculty of Science, Chulalongkorn University, Thailand

²Center for Petroleum, Petrochemicals and Advanced Materials, Chulalongkorn University, Thailand

³PTT Research and Technology Institute, PTT (PLC), Ayutthaya, Thailand

SUMMARY: Renewable fuels are major alternatives to fossil fuels. Biomass was considered as raw materials and renewable energy sources. Pyrolysis process is one of the efficient methods for converting biomass in bio-oil. This work investigates the pyrolysis of Giant Leucaena wood in liquid phase by various conditions. The experiments were conducted in an autoclave at following conditions; temperature of 325-400 °C, holding time of 0.5 - 2 hour, biomass 500 g, catalysts (0-20 %by mass) such as Ni/Mo FCC and MgO by using hexane as a solvent. Bio-oils were analyzed by GC-MS to identify the structure and chemical compounds, also by CHNO analyzer and other instrument such as Karl Fischer titration, total acid number titration bomb calorimeter. The results showed that the liquid products were phenolic compounds, cyclic compounds, furans determined by GC-MS.

Keywords: Giant Leucaena wood; pyrolysis; bio-oil

INTRODUCTION

The current petroleum prices are high and increasing day by day. Effective use of renewable energy sources is necessary for sustainable energy and society. Biomass is a promising alternative and sustainable energy source, as it is renewable, CO₂ neutral. When compared to other renewable sources, biomass has been receiving considerable attention lately because it is a very attractive feedstock due to its abundance, low price and non-competitiveness with the food chain.

Pyrolysis is a thermochemical processes that convert the biomass to a liquid fuel commonly referred to as "bio-oil". Generally, bio-oil product from conventional pyrolysis cannot be used directly. This is due to its high oxygen contents around 35-40% by weight [1], resulting in low heating value and high acidity. Thus, deoxygenation of bio-oil has been interested to improve quality of bio-oil. Bio-oil products were upgraded by pyrolysis in the liquid phase with using a suitable catalysts.

In this work, pyrolysis in liquid phase or thermochemical liquefaction was mainly aimed at obtaining bio-oil by conversion of giant leucaena wood in hexane as solvent at moderate temperature and nitrogen pressure in the presence of Ni-Mo/Al₂O₃, MgO, and FCC as catalyst for deoxygenation.

EXPERIMENTAL

The experimental runs were performed using 250 g of dried giant leucaena wood, 1000 g of hexane as solvent (the ratio of biomass to solvent is 1 : 4), and by varying temperature between 325 and 400 °C, holding time between 0 and 90 minute. Experiments were carried out in a 20 L (Fig. 1) high-pressure autoclave reactor and the autoclave was stirred with a magnetically driven impeller and can be operated at a maximum pressure of 210 bar.

The autoclave was heated with an external electrical furnace. The air inside the autoclave was purged by nitrogen gas for three times, then pressure in the autoclave was raised to 10 bar with nitrogen gas to avoid solvent vaporization. The reactor was heated from ambient temperature to the desired temperature. After reaction finished, all products were separation and the reaction was cooled to room temperature quickly by cool water.

The bio-oil and solid residue characterization were performed using CHN analyzer and GC-MS. The gaseous product was obtained via mass balance by subtracting the bio-oil portion and solid product, which analyzed for its composition by GC-TCD

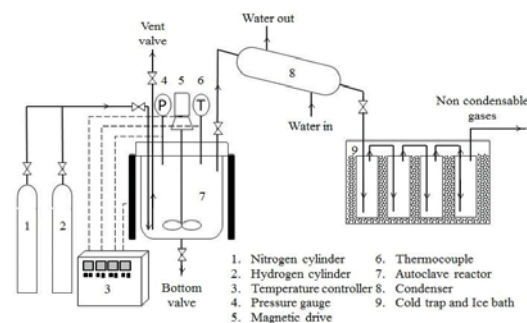


Figure 1. Schematic of the autoclave reactor for pyrolysis of giant leucaena wood to bio-oil.

RESULTS AND DISCUSSION

Effect of operating temperature on products distribution

The effects of temperature on the product yield can be explained by Fig. 2, which presents the results obtained at 325-400°C for holding time 0 min. The yield of bio-oil increased with increase in temperature reaching a maximum of 22.55% at 375°C and the dropped down to 9.51% at 400°C. The

decrease in to the bio-oil yield at higher temperature can be attributed by when the temperature is larger than the activation energies for the bond breaking, the extensive biomass repolymerization, fragmentation, condensation and isomerization occur [2], resulting in lower amounts of bio-oil. Therefore, intermediate temperature usually yields higher amounts of bio-oil [3].

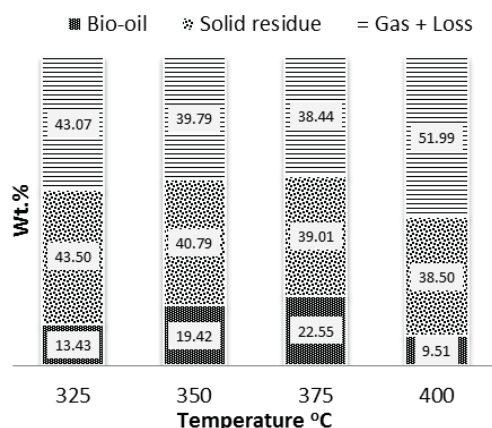


Figure 2. Effect of temperature on products distribution in liquid phase pyrolysis

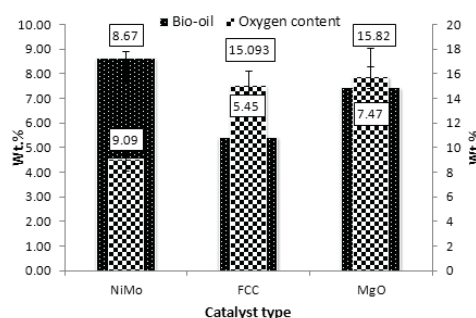
Table 2. Properties of raw feedstock and bio-oil obtained from liquid phase pyrolysis at different conditions

Conditions	Elemental analysis (wt.%)				HHV. (MJ kg ⁻¹)
	C	H	N	O*	
Giant leucaena wood	49.99	6.19	0.80	43.02	18.9
Temperature, °C					
325	58.17	8.42	0.38	33.42	25.81
350	67.51	9.40	0.52	23.09	32.22
375	70.77	10.74	0.60	18.50	36.05
400	80.07	10.41	0.79	9.53	40.31

*by difference

Table 2 shows the elemental compositions and the HHVs of biooil and solid residue obtained from hydrothermal liquefaction at 325-400°C. The elemental analysis showed that both the bio-oil contained more carbon and less oxygen with the increasing in temperature. Heating values of the bio-oil was found to be higher than that of the raw material. Heating values of the bio-oil was found in range of 25.81 – 40.31 MJ kg⁻¹. HHVs of bio-oil obtained in this study were in good agreement with earlier studies reported in the literature [4-6].

Among all catalysts, NiMo/Al₂O₃ with 20 wt%, at pyrolysis condition of initial hydrogen pressure of 20 bar, 375°C, and holding time for 60 minutes was the optimum condition to produce bio-oil with lowest oxygen content at 9.09 wt% and the oil yield at 8.67 wt%.



CONCLUSIONS

Bio-oil could be produced at 375 °C for higher yield via liquid phase pyrolysis of giant leucaena wood. The heating values of bio-oil increased with the increase of temperature.

References

- [1] Z. Qi, C. Jie, W. Tiejun and X. Ying, *Energy Conversion and Management*, **48**, (2007), pp. 87-92.
- [2] P. Sun, M. Heng, S. Sun and J Chen, *Energy*, **35**, (2010), pp. 5421-5429.
- [3] J. Akhtar and N. S. Amin, *Renewable and Sustainable Energy Reviews*. **15**, (2011), pp. 1615-1624.
- [4] K. Akalin, *Bioresource Technology*, **110**, (2012), pp. 682-687.
- [5] U, Jena, *Energy Fuels* **25**, (2011), pp. 5472-5482.
- [6] U, Jena, *Bioresource Technology*, **102**, (2011), pp. 6221-6229.

List of First Authors

Abdol Rahima A. H.	287, 289
Akkaravathasinp S.	153
Al-Doghachi F. J.	57
Al-Hadhrami L. M.	267
Ali T.	501
Alom F.	137
Amanul Alam K. C.	313
Amelia A. R.	123, 127
Anacan R. M.	363
Ankawattan P.	295
Anudit P.	487
Appamana W.	341
Archewarahuprok B.	259
Ardissone G.	31
Ariful kabir K. M.	313
Arifwidodo S. D.	207
Arinal M.	323
Ariyavongvivat E.	231
Artnaseaw A.	255
Assabumrungrat S.	59
Atilgan B.	205
Attanatho L.	57
Atthawethworawuth W.	357
Augusto G. L.	407
Auppapong N.	387
Azapagic A.	205
Azmi W. H.	155, 163, 165, 173, 245
Baba I.	117
Bakar R. A.	501
Banerji S.	133, 135, 329
Barra D.	287
Bavishi D.	369, 371
Benjapiyaporn C.	475
Bin Mamat A. M. I.	169
Boonkum P.	115
Boonmak J.	211
Boonmeemak W.	249
Boonrod Y.	315
Boonvithaya N.	43
Boonyaratsiri K.	427
Boonyayothin V.	401
Buasri A.	491
Buayorm D.	387
Cao N. D.T.	253

Cha E. Y. _____	357
Chaichana T. _____	433, 467, 469
Chaikitkeaw S. _____	425
Chaiprasert P. _____	231
Chaitep S. _____	469
Chaivongvilan S. _____	443
Chaiwiwatworakul P. _____	93, 95, 411
Chaiyawong P. _____	33
Chaiyawong P. _____	35
Chakraborty R. _____	109
Chalermcharoenrat S. _____	223
Chalermkinsuwan B. _____	483
Chalermyanont K. _____	185
Chancham C. _____	259, 465
Chandrasekaran S. _____	367
Chandrasiri O. _____	207
Chanlongphitak S. _____	439
Chanta E. _____	449
Chantharasenawong C. _____	183
Chewamongkolkarn S. _____	461, 463
Chiarakorn S. _____	283, 411
Chiemchaisri C. _____	335
Chindaruksa S. _____	355
Chirarattananon S. _____	93, 383, 411
Chitapornpan S. _____	335
Choonut A. _____	49
Choonut O. _____	113
Choopun S. _____	447, 449, 451
Chotitham L. _____	431
Chuangchote S. _____	93, 129, 411
Chulaluksananukul W. _____	43
Chullabodhi B. _____	379
Chunark P. _____	279
Chungpaibulpatana S. _____	79
Chuvaree R. _____	247
Comwien J. _____	43
Culaba A. B. _____	405, 407
Darawun W. _____	171, 319
Deb S. K. _____	317
Deedom P. _____	453
Dejang N. _____	355
den Poel D. V. _____	133, 135
Devabalaji K. R. _____	191, 193
Dewsbury J. _____	81
Duangwang S. _____	47
Estel L. _____	29
Fadhlullah M. _____	289
Fareq M. _____	73, 75, 123, 125, 127, 323

Ferreira P.	133, 329
Fitra M.	323
Fongsamut C.	249
Gagnon Y.	259, 331, 435, 437, 443, 455, 461, 463, 465, 467, 457, 499
Garcia R. G.	363
Gardchareon A.	451, 447, 449
Garo A.	29
Ghazali N. S.	393
Gimbun J.	393
Glinwong C.	43
Gomesh N.	73, 75, 123, 125, 127, 323
Goodwin V.	303
Gorantla K. K.	381
Gréhan G.	29
Hamid K. A.	155, 163, 165
Hanapi S.	289, 339, 434
Haron S. F.	393
Hashim U.	73, 75
Haziah A. H.	125
Himmler R.	93
Hinchiranan N.	505
Hirota M.	167
Hongsith K.	447
Hongsith N.	447
Hussain T.	323
Iamraksa P.	471
Ibrahim S.	127
Inklab N.	93
Irwan M.	323
Irwan Y. M.	73, 75, 123, 125, 127
Irwanto M.	73, 75, 123, 125, 127, 323
Ismail H.	173
Ismaile N.	233
J. Jamradloedluk	479
Jangsawang W.	227
Janjai S.	315
Jansri S.	111
Jaroenkhaseemmesuk C.	151
Jash T.	195
Jayatilaka P. R.	281
Jermkwan N.	149
Jijai S.	233
Jindapeng C.	91
Jittabut P.	495, 497
Jusoh N.	501
Kachhwaha S. S.	369, 371
Kadirgama K.	501
Kaewprasert C.	435

Kaewrath R. _____	357
Kaewrawang A. _____	473
Kaivo-oja J. _____	413
Kanan S. _____	81
Kandpal T. C. _____	71, 121
Kangwansaicho K. _____	505
Kannika P. _____	493
Kaosol T. _____	225, 239
Kayankannavee C. _____	365
Keerativibool W. _____	433
Kerdsuwan S. _____	33, 35, 39, 221, 223, 227, 395
Keson J. _____	333
Ketsamee P. _____	185
Khairunnisa A.R. _____	377, 385
Khalid A. _____	117
Khanam T. _____	187
Kheawmaneenail S. _____	477
Khedari J. _____	401
Khongkliang P. _____	421
Khuhaudomlap N. _____	505
Kiattamrong S. _____	251
kimtun P. _____	113
Kirtikara K. _____	129
Kitaide Y. _____	167
Kittipoomwong P. _____	299
Klatin K. _____	427
Klomkloa S. _____	113
Kollasuta D. _____	183
Kongjan P. _____	359
Kongjan P. _____	45, 105, 419, 421, 425
Kongkaew N. _____	309
Kongruang C. _____	433, 455, 457
Kongsune P. _____	431
Korprasertsak N. _____	177, 179
Krittayanawatch T. _____	453
Kuasakul M. _____	455, 457
Kuchontara P. _____	505
Kullack T. _____	79
Kumar M. _____	133
Kumaresan C.A. _____	405
Kumneadklang S. _____	51
Kungkajit C. _____	225
Kuprianov V. I. _____	217, 219, 357
Kusumadewi T. V. _____	277
Landry M. _____	331
Lane-Serff G. _____	81
Laohalidanond K. _____	33, 35, 39, 221, 223, 227, 395
Laosiripojana N. _____	235

Le D. T. H. _____	101
Leephakpreeda T. _____	87, 177, 179, 263, 269
Leman A. M. _____	117, 377, 385
Leow W.Z. _____	123, 127
Lerdratranataywee W. _____	239
Limmeechockchai B. _____	77, 139, 141, 197, 209, 273, 275, 277, 279, 281, 347
Limpitipanich P. _____	139, 241
Loryuenyong V. _____	491
Luukkanen J. _____	413
Maglaya A. B. _____	405
Majumdar D. _____	195
Malakul P. _____	441, 439
Mamat A. M. I. B. _____	173
Mamat R. _____	155, 163, 165, 173
Mamimin C. _____	423
Manorach K. _____	235
Marsitah S. _____	323
Maruyama N. _____	167
Masa-ard U. _____	491
Mathenge S. _____	321
Mathew S. A. _____	181, 265
Meenaroch P. _____	221
Meepoh M. _____	295
Mettanant V. _____	95
Minmunin J. _____	241
Misila P. _____	141
Mohamed W. A. N. W. _____	173, 169, 245, 339, 343
Mongkut P. _____	397
Monyakul V. _____	171, 319
Mukhopadhyay P. _____	109
Mullick S. C. _____	71, 121
Mungcharoen T. _____	439, 441
Mungkalasiri J. _____	115, 211
Musaruddin M. _____	345
N. Dusadee _____	467
Nagababu G. _____	369, 371
Najafi G. _____	155, 163, 165
Nakhshinieva B. _____	37
Namjuncharoen T. _____	441
Nantawong T. _____	471
Narasingha M. _____	299
Narataruksa P. _____	147, 149, 153
Nathakaranakule A. _____	209
Nenkaew P. _____	157
Ngamcharussrivichai C. _____	429
Ngamlarp S. _____	179
Ngaotrakanwiwat P. _____	85, 249
Ngetha H. _____	321

Ninduangdee P. _____	217, 357
Nithitsuttibuta C. _____	273
Nitorisravut R. _____	101, 253
Niyasom C. _____	51, 423
Noojeensang K. _____	499
Noparata P. _____	103
Nour A. H. _____	307, 393
Novianti S. _____	37
Nuithitikul K. _____	45, 359
Nupteotrong P. _____	387
Nurdiawati A. _____	37
Nurdin S. _____	307, 393
Nutongkaew P. _____	433, 435, 437
Onsriprai B. _____	427
O-Thong S. _____	45, 51, 103, 105, 233, 359, 419, 421, 423, 425
Ouboukhlik M. _____	29
P. Aryal P. _____	87
Paengjuntuek W. _____	211
Pagketanang T. _____	397
Paichid N. _____	113
Paketanang T. _____	255
Pamuji D. S. _____	391
Pan X. _____	103
Pankeaw P. _____	315
Pannucharoenwong N. _____	475
Panpong K. _____	45, 359
Panrare A. _____	199
Panyacharoen K. _____	397
Papong S. _____	439, 441
Pasolon Y. _____	345
Pasom W. _____	209
Patanasemakul N. _____	129
Pattra S. _____	417
Patumsawad S. _____	309
Peerapong P. _____	77
Persson K. M. _____	373
Phadungdhitidhada S. _____	449, 451, 447
Phdungsilp A. _____	327
Phetyim N. _____	493
Phokate S. _____	445
Phongaksorn M. _____	145, 147, 247, 301
Phoualavand S. _____	197
Pichid N. _____	49
Pimpinit V. _____	485
Pinisakul A. _____	427
Pisutpaisal N. _____	61, 63, 65, 67, 99, 237
Pita P. _____	139
Pitanuwat S. _____	399

Piumsomboon P. _____	483
Poblarp T. _____	353
Pongdoang S. _____	365, 471
Poonsrisawat A. _____	235
Prapainainar C. _____	153, 149, 209
Prasad R. _____	329
Praserthdam P. _____	59, 103
Prasertsit A. _____	185
Prateepchaikul G. _____	225
Promma P. _____	489
Promvongsa J. _____	29
Promwungkwa A. _____	241
Pruksakit W. _____	309
Puangmalee N. _____	401
Punantapong B. _____	481
Punantapong I. _____	481
Punantapong P. _____	481
Puteh A. _____	467
Puttaranga Setty A. B. T. _____	89, 381
Quan P. _____	263, 269
Rachman A. _____	345
Raghavi B. _____	367
Rahim A. H. A. _____	339, 343
Rahman M. K. _____	267
Rakkwamsuk P. _____	93, 129, 411
Ramdas B. _____	181
Rashedi A. _____	187
Ratana T. _____	145, 301, 303
Ratanapisit J. _____	341
Ratanawilai S. _____	305
Ratchaniphont A. _____	333
Ratjiranukool P. _____	459
Ratjiranukool S. _____	459
Rattana T. _____	147
Rattanachaisit P. _____	427
Rattanapanyapan K. _____	473
Ravi K. _____	191, 193
Reabroy R. _____	471
Reubroycharoen P. _____	53, 503, 505
Rianse U. _____	345
Riyakad P. _____	283
Rochanakit K. _____	491
Rodseanglung T. _____	301
Rojviroon O. _____	351
Rojviroon T. _____	351
Rosnan N. A. _____	393
Rouf R. A. _____	313
Ruankham P. _____	449, 451

S. Kreesaeng	483
Saad A.	305
Sae-Jung P.	453
Saengkaew S.	29
Safwati I.	123
Saha B.B.	313
Sahay M.	135
Saidur R.	169, 173
Sailoon N.	353
Saiman M. I.	57
Sainan K. I.	173, 287, 289
Saisirirat P.	293
Saito M.	167
Salleh M. N. M	117, 377, 385
Sangcharean A.	315
Sangkharak K.	49, 113
Sangsong S.	247
Sangsubun C.	477
Sangwichien C.	47
Sani W.	117
Saravanan M.	265
Sarkar M. M. A.	313
Sarma B. C.	317
Sasaki M.	321
Savsani V.	369
Sawasdee V.	61, 65
Selvakkumaran S.	273, 275
Senbat S.	423
Shaahid S. M.	267
Shaik S.	89
Sharma A. K.	71, 121
Sharma C.	71, 121
Shukri E. S.	159, 161
Singhpoo C.	475
Siripatana C.	233
Sirivithayapakorn S.	351
Sisodia G. S.	133, 135, 329
Sittijunda S.	417
Siwarasak P.	341
Smith D. R.	203
Smith R. B.	203
Soares I.	133, 135, 329
Sohsalam P.	199
Soisuwan S.	59
Somprasit O.	355
Songprakorp R.	129, 171, 319
Sootchiewcharn N.	53
Sornchamni T.	145, 247

Srimachai T.	45
Sripakagorn A.	251, 399
Srisantisuk S.	485, 487, 489
Srisuwan A.	291
Srisuwan G.	233
Steurer E.	31
Suheri P.	219
Sukawat D.	183
Sukkathanyawat H.	145, 147
Sukpanish P.	429
Suksong W.	419
Suksuntornsiri P.	139
Sukto A.	431
Sumanatrakul P.	431
Sumida H.	37
Supngam A.	493
Suraraksa B.	231
Sutthana S.	451
Suwarno	323
Syafinar R.	73, 75
Syafruddin H. S.	323
Tachajapong W.	215
Taengchum T.	383
Taheri M.	321
Talib S. F. A.	169, 245
Tandon R. P.	409
Tangthieng C.	157
Tanikkul P.	63, 67
Tantipaibulvut S.	427
Tasaso A.	85
Taufiq-Yap Y. H.	57
Thabuot M.	255, 353, 397
Thanuanram W.	387
Thanungkano W.	115
Thateenaranon P.	485
Thepa S.	171, 319
Therdyothin A.	209
Thongwic S.	341
Thuy V. T. H.	347
Tia W.	139
Tiangket A.	379
Tiapple Y.	471
Tiapple Y.	365
Tijani A. S.	287, 289, 339, 343
Tippayawong N.	151
Tirawanichakul Y.	261
Tohsing K.	315
Tondee T.	199

Tongurai C.	305
Tritanate S.	503
Tummu P.	411
Tungkamani S.	145, 147, 247, 301, 303
Uamusse M. M.	373
Unpinit T.	353
Usri N. A.	155, 163, 165
Vehmas J.	413
Vikromvarasiri N.	99, 235, 237
Waewsak J.	259, 261, 433, 437, 455, 457, 461, 463, 499, 435, 465, 467
Wahyuni N. S.	391
Wangsang S.	487
Wanthong T.	493
Warayanon W.	145
Watechagit S.	379
Wattan R.	315
Wattanapaphawong P.	505
Wattanasiriwech D.	291, 295
Wattanasiriwech S.	291, 295
Werapun W.	261, 467
Winyuchakrit P.	141
Wiriyampaiwong S.	479
Wisaijorn W.	59
Wisarnsuwannakorn R.	115
Wisnoe W.	159, 161
Wongchai P.	215
Wongfhad N.	105
Wongratanaphisan D.	447, 449, 451
Wongsai N.	333
Wongsai S.	333
Wongvitvichot W.	491
Wongwicha P.	255, 353, 397
Wulandari E.	391
Wulandari S.	391
Yamamoto M.	167
Yooin P.	489
Yoosuk B.	147, 303
Yoshikawa K.	37
Youngyuen P.	357
Yunu T.	49, 113
Yusof M. Z. M.	377, 385
Yuvaraj T.	191, 193
Zailani R.	161
Zainal Z.	57
Zaini I. N.	37
Zakaria I.	169, 173, 245
Zakaria M. F.	385
Zhafarina M.	125